THE
PHYSICAL REVIEW
A journal of experimental and theoretical physics established by E. L. Nichols in 1893

SECOND SERIES, VOL. 98, NO. 4 MAY 15, 1955

Comparison of the Energy Excitations in Liquid He^3 and He^4*

O. K. RICE
Department of Chemistry, University of North Carolina, Chapel Hill, North Carolina
(Received February 2, 1955)

In both He^3 and He^4 there are two types of excitation, a Debye type involving large numbers of molecules, and a localized type of excitation. The latter type is considered in this paper. In the case of He^3 the localized excitations of lowest energy can be discussed rather successfully by means of a pair-rotator model, with hindered rotation in a plane. The pair-rotator model breaks down in the case of the next higher group of excited levels; their energy is about right but there are more such levels than would be expected on the pair-rotator model. The reason for this is considered. In the case of He^4 the so-called roton excitations are of much higher energy than the excited levels in He^3, on account of the statistics and also on account of the effect of the higher density on the hindering of the rotation. These effects can be understood with the aid of the pair-rotator model. The model, itself, however, breaks down for these levels, and the nature of the break-down and the probable character of the rotons are discussed. The results are also of interest in connection with mixtures of He^3 and He^4. Some remarks are appended on the possibility of a λ transition in He^3.

SUFFICIENT is now known about the excitations in liquid He^3 and He^4 so that a comparison of the two cases should lead to new insights. In some respects they are quite similar. In each case the thermodynamic properties can be accounted for by assuming that there are two types of excitation; first, a Debye or phonon type involving simultaneous vibration of large numbers of atoms, and, secondly, a localized type of excitation involving only a small number of atoms (but in general at least two, and partaking of some of the character of a rotation—localized vibrational excitations would involve higher energies than need to be considered at low temperatures). It is the latter with which we wish to deal in this paper. The localized excitations in He^4 (rotons) involve much more energy than is the case with He^3. This difference is due principally to the difference in statistics, but, as we shall see, there is also an indirect effect arising from the difference in mass, which is sufficient to give He^3 a considerably higher zero-point energy than He^4 for any predetermined density and which consequently results in a much lower equilibrium value of the density for He^3.

Liquid He^3 has recently been treated with some success by means of what may be called a pair-rotator model,[1] in which N atoms are considered to form $N/2$ pairs which can undergo rotation, among other types of motion. If the pair-rotator model is to have validity, the cells in which the pairs are to rotate will be fixed by the surrounding molecules. Thus a molecule does not, at a particular instant, have a choice as to which other molecule it will pair with, but on the average is much more likely to exchange places with some one of its neighbors than with the others, this exchange being associated with a certain average energy [0.4° times the Boltzmann constant, according to Eq. (1)]. Although the pairing will change from moment to moment, this may be considered to be a part of the zero-point fluctuation and does not contribute to the entropy. If this were not the case, the pair-approximation would not give good results.

Temperley[1] has proposed a partition function for a pair whose logarithm is given by

$$\ln(1+3e^{-0.4/T}+8e^{-2.7/T}),$$

so that the partition function of He^3 *per atom* is given (after a Debye term is added) by

$$\ln(\text{p.f.})_{He^3}=\tfrac{1}{2}\ln(1+3e^{-0.4/T}+8e^{-2.7/T})+0.0108T^3. \quad (1)$$

The data on the nuclear paramagnetism, the specific heat, and the entropy can be reproduced by this partition function (and apparently only by one whose form is close to this). The weight, 3, of the energy level at $0.4k$ (about 0.8 cal per pair-mole) arises from the

* Work supported by the Office of Naval Research.
[1] P. J. Price, Phys. Rev. **97**, 259 (1955); O. K. Rice, Phys. Rev. **97**, 263 (1955); H. N. V. Temperley, Phys. Rev. **97**, 835 (1955); and (unpublished work).

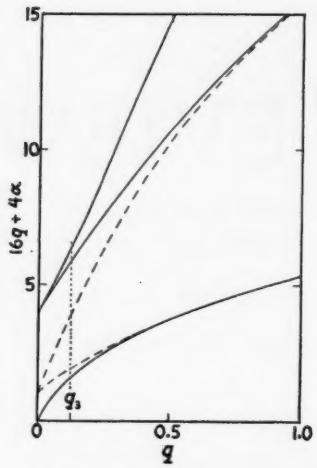

FIG. 1. The five lowest energy levels for the restricted rotator as functions of q. Solid curves, symmetrical rotational states; broken curves, antisymmetrical states. q_0 is the estimated value of q for He^3.

fact that this state is a triplet state with respect to the nuclear spin of He^3 (hence, also, it contributes to the paramagnetism). This state, then, has no spatial degeneracy.

We have pointed out[2] that the weight of three is exactly what would be expected on the pair-rotator model if the pair-rotator acts as a hindered plane rotator. The lowest state of rotational oscillation is symmetrical in the space coordinates, hence antisymmetric in the spin coordinates and a singlet, while the next excited state is antisymmetrical in the space coordinates and hence a triplet. The normal twofold spatial degeneracy of the plane rotator (due to clockwise and counterclockwise rotation) is lifted in the hindered rotator. The existence of a hindering potential is of course to be ascribed to the interactions of neighboring molecules.

In treating the problem of hindered rotation it is commonly assumed that the potential energy is given as a function of the angle θ of rotation by an expression of the form[3] $V_0-V_0\cos 2\theta$, where V_0 is a constant parameter. This leads to the wave equation

$$d^2\psi/d\theta^2+(8\pi^2\mu r_0^2/h^2)(W-V_0+V_0\cos 2\theta)\psi=0, \quad (2)$$

where μ is the reduced mass, r_0 the interatomic distance for the rotator, and W is the value of the energy. This is Mathieu's equation, and can be written

$$d^2\psi/d\theta^2+(4\alpha+16q\cos 2\theta)\psi=0, \quad (3)$$

where

$$\alpha=(2\pi^2\mu r_0^2/h^2)(W-V_0)$$

and

$$q=\pi^2\mu r_0^2 V_0/2h^2.$$

[2] O. K. Rice, Phys. Rev. **97**, 1176 (1955).
[3] See L. Pauling, Phys. Rev. **36**, 430 (1930).

If V_0 is zero, Eq. (2) reduces to the equation for the plane rotator with energy levels given by

$$W=j^2h^2/8\pi^2\mu r_0^2, \quad (4)$$

where j is an integer. The quantity $16q+4\alpha$ is the energy expressed in terms of the unit $h^2/8\pi^2\mu r_0^2$. By finding the characteristic values of Mathieu's equation for periodic solutions, the allowed values of $16q+4\alpha$ can be determined[4] as functions of q. These values are shown in Fig. 1.

In attempting to apply these results to the pair-rotator model, we assume that r_0 is equal to the average interatomic distance in He^3, which we estimate[5] to be 3.46 A. Then $h^2/8\pi^2\mu r_0^2=2.68$ cal per pair-mole. However, according to Temperley's equation [Eq. (1)], which also agrees roughly with our own conclusions, the actual energy gap between the lowest singlet and the next triplet state is about 0.8 cal per pair-mole. Using the hindered plane-rotator model, we conclude from Fig. 1 that q must be about 0.145 ($V_0=6.2$ cal per pair-mole), as indicated on Fig. 1. With this value of q we see that there is a triplet level at an energy of roughly 7 cal per pair-mole above the ground state. This is close to the average energy of Temperley's suggested second group of excited energy levels, namely 5.4 cal per pair-mole. At first glance, however, the expected multiplicity is three, which contrasts with Temperley's multiplicity of eight. Temperley suggested that his eightfold level consisted of two triplets and two singlets. Exactly this composition is not required, however, and if the hindered pair-rotator picture has validity, it appears from Fig. 1 that the singlet states are rather high to be included.[6] On the other hand, it seems possible that some spatial degeneracy might appear in the higher energy levels. As mentioned above, the pair-rotator model implies that an atom pairs with a particular neighbor, determined by the instantaneous configuration of the system as a whole. It seems likely that this restriction would break down for excitations involving higher energies, so that an atom would select its partner at random regardless of the configuration, implying at least the possibility of several distinct, geometrically distinguishable states with comparable energy.[7] If there are not too many of these excitations they will not, furthermore, interfere with each other.

[4] S. Goldstein, Trans. Cambridge Phil. Soc. **23**, 303 (1927).
[5] This estimate is obtained from the average distance, 3.15 A, in He^4 [J. Reekie and T. S. Hutchison, Phys. Rev. **92**, 827 (1953)] and the cube root of the ratio of the density of He^4 [W. H. Keesom, *Helium* (Elsevier Publishing Company, Inc., Amsterdam, 1942), p. 207] to that of He^3 [E. C. Kerr, Phys. Rev. **96**, 551 (1954)].
[6] It should be stated that the term "degeneracy" should not be given too literal an interpretation. As Temperley quite explicitly mentions, it is not to be supposed that all the energy levels in a group coincide exactly. It is merely supposed that they constitute a fairly closely-spaced group, which can be considered as a group in which the degeneracy has been lifted by the perturbations only to a relatively small extent. The singlet states do appear too high to be included with the second triplet.
[7] This difference in the degeneracies of the various energy levels is discussed in an Addendum.

It seems probable from the case of He^4 (see Reekie and Hutchison[5]), that each atom has on the average four nearest neighbors with which it could pair. Such a pair, however, would involve two atoms. Therefore, the effect of random pairing would be to introduce a degeneracy of 4/2 per atom into the corresponding term of the partition function, or a degeneracy of 4 per pair. Taking into account the fact that we are dealing with a triplet state, the total possible degeneracy becomes 12, whereas the observed degeneracy is about 8. It appears, thus, that the random-pairing degeneracy is not fully developed, but the order of magnitude observed appears to be about right. With this amendment, the hindered pair-rotator model seems not to do badly in the case of He^3. It is not to be denied that, in spite of this apparent success, it is a highly idealized model, and must be accepted with some reserve. Indeed, we have already mentioned certain effects which may result from interactions between the pair-rotators, or from cooperative effects involving all the atoms.[1] However, the usefulness of the hindered plane pair-rotator in the case of He^3 tempts us to accept it tentatively as an aid in the comparison of He^3 with He^4.

Since He^4 obeys the Bose-Einstein statistics and has no spin, we need to consider only symmetrical, singlet states, represented by the solid curves in Fig. 1. Since the interatomic distance is so much less in He^4 we may expect the potential barrier against free rotation of a pair to be much greater than in He^3. Just how much greater is of course difficult to say. If we suppose q to be 0.5 for He^4, then we see from Fig. 1 that the energy gap between the ground state and the next singlet state is something like 17 cal per pair-mole, since the value of $\hbar^2/8\pi^2\mu r_0^2$ for He^4 is 2.45, taking[5] r_0 as 3.15; if q should be 1.0, then the energy gap would be about 25 cal per pair-mole. These energies are just of the order of magnitude of the excitation for rotons. (Only the order of magnitude and the fact that this level is higher than the second group of excitations for He^3 can be of importance—in view of the complications to be considered the rather close agreement with the roton excitation energy must be a coincidence.) An important difference between He^3 and He^4 lies in the degeneracy of the excited state. The degeneracy in He^4 is much greater, despite the fact that a singlet rather than a triplet state is involved. We have estimated[8] from specific heat data that the degeneracy is about 9; this however, is based on atoms, not pairs of atoms, and the pair model would require that the degeneracy of pairs be 18.

In estimating the degeneracy, we assumed that rotons were groups of atoms which formed an ideal solution with the single atoms of superfluid. This, of course, is an approximation at best, but it means essentially that the groups of atoms can be definitely located with relation to the single atoms of the superfluid. This localization might be to some extent blurred by the zero-point motion. This would mean that the entropy of mixing was overestimated; if it had to be lowered, it would have to be compensated by increasing the estimate of the degeneracy. However, it seems probable that *groups* of atoms can be better localized among the other atoms than these atoms can be localized with respect to each other.

The high degeneracy probably arises from the fact that a number of atoms (perhaps six or eight) seem to be involved in the roton excitations. With the large amount of energy required it appears likely that a pair would have reached, so to speak, its "dissociation energy," it being held in its cell essentially only by the repulsion of the surrounding atoms. In other words, the individuality of the pairs would break down, and we could expect some cooperative effects in which a number of atoms are involved; coordinated rotations of several neighboring pairs could conceivably effect a lowering of the hindering potential, and such coordinated rotations could occur in a variety of ways. Of course considerable lowering of the effective hindering potential would be required in order for the total excitation of a whole group of six or eight atoms to be no higher, or only a little higher, than that expected for a pair. It is also possible that rotations of the group of atoms as a whole might contribute to the degeneracy. This possibility was mentioned by Feynman,[9] who, however, carefully refrained from any categorical statement that the roton excitations were necessarily of this nature.

We think that there may be some experimental evidence that the roton excitations are more likely to involve mutual rotations of individual pairs than rotation of the whole group. If rotation of the whole group is involved it is not clear that the spacing of the atoms within the group should be much affected; so it is not too easy to see why the rotons are denser than the residual fluid, i.e., the superfluid, as they presumably are, in view of the negative coefficient of expansion of helium II. If, however, the individual excited atoms move more freely through longer distances (i.e., have greater "mean free paths," as would be expected from individual or pairwise excitation) than the atoms of superfluid, then, as we have remarked before,[8] the excited energy levels should depend less strongly on interatomic distances than is the case in the ground state. This permits the roton atoms to lower their potential energy by decreasing their average interatomic distance. This may, in fact, be one of the ways that cooperative effects in the excitation can lower the total energy, and so make such excitations more probable, though this effect is undoubtedly small.

The nature of the roton excitations and the smaller volume of rotons as compared to superfluid are, of course, intimately connected with the behavior of He^4

[8] O. K. Rice, Phys. Rev. **96**, 1460 (1954).

[9] R. P. Feynman, Phys. Rev. **94**, 262 (1954).

at elevated pressures. It is found that the specific heat at constant volume increases with increasing pressure.[10] This means greater ease of excitation, hence relative lowering of the energy of excitation. What we really should conclude is that the rotons are less affected by pressure than the superfluid. In the superfluid the zero-point energy is raised by pressure more than the energy of the rotons is raised, since the energy levels of rotons depend less strongly on the density, as noted in the preceding paragraph. Of course, the potential barrier to rotation should increase with increasing density, and if the hindered rotator model (and this may apply not only to a pair-rotator model but to any model involving rotation of groups of atoms as a whole) had not broken down in the case of He^4, we should expect enhanced pressure to have the opposite effect (i.e., more effect on the roton energy than on the zero-point energy). But if what happens involves "dissociation by rotation" of the pair-rotator, then the observed effect is easily understood if the zero-point energy of the superfluid is raised more than the dissociation energy. In the light of these remarks, a study of the effect of pressure on the thermodynamic properties of He^3 would be extremely interesting.

If a roton is a group of atoms having excitations internal to the group and having a number of energy levels (the excitation energy is, of course, an average only, and we may expect in actuality a range of energies, as with He^3), it should behave rather similarly to a classical liquid. Liquid He^3 is certainly sufficiently highly excited around 1°K to behave like a classical liquid. There is, therefore, some basis for the belief that rotons and He^3 would mix and to a reasonable approximation form an ideal solution, even at this low a temperature. The deviation of He^3-He^4 mixtures from ideality, according to Taconis' hypothesis,[11] arises in large part from insolubility of He^3 in superfluid He^4, which may be caused by effects on the zero-point energy.[12] We have recently shown[13] that Taconis' hypothesis, together with the assumed ideality of a mixture of He^3 and excited He^4 and the perhaps somewhat questionable assumption that the average number of atoms involved in a roton is not affected by the presence of He^3, gives a reasonably good account of the experiment of Sommers, Keller, and Dash[14] on the heat and entropy of mixing at 1°K.

The picture of liquid He^3 and He^4, which emerges from the present considerations, requires some modifications in the suggestion which we have previously made[12] concerning the apparent lack of a λ transition in He^3. We had proposed earlier[15] that the λ transition in He^4 is connected with the appearance of clusters of superfluid. In the later work we considered a possible mechanism for the formation of such clusters, and pointed out that the formation of clusters of appreciable numbers of atoms of superfluid might be expected to result, in He^4, in a lowering of the zero-point energy. We explained the lack of such clusters in He^3 on the grounds that an He^3 atom would always have some neighbors in a spin state such that their relative angular momentum could not be zero, at least if there was any exchange at all. However, the pair-rotator model represents a situation in which the lowest energy of a pair is attained, there being no exchange involving separate pairs. If this picture is correct, it is quite possible that clusters of "superfluid" He^3 (i.e., liquid He^3 without excitations) might appear as the temperature was lowered; in this case, also, there might be an energetic advantage in clusters of appreciable magnitude. This might then result in a λ transition in He^3 at sufficiently low temperatures. On the other hand, since the formation of large clusters of He^3 with all pairs of atoms in their lowest states of restricted rotation would require some special arrangement of atoms in order to keep the atoms of a pair which had a mutually symmetrical spin wave function relatively far away from each other,[1] this might *not* be energetically favorable. The situation in this case does not seem to be nearly as clear cut as with He^4. Temperley[1] has suggested that the alignment of spins may involve a Curie-type transition, but without suggesting clusters and without using the word "superfluid."

In conclusion, we think it may be said that despite the fact that it represents a highly idealized picture, the hindered plane pair-rotator model seems to be surprisingly successful in facilitating the discussion of the properties of He^3, with due regard for its limitations, and it appears also to give a semiquantitative understanding of the differences between He^3 and He^4. The differences, of course, arise principally from the much higher excitations required in He^4, a property which is to be traced to the fact that He^4 lacks antisymmetrical states. The differences are, however, enhanced by the resistance to relative motion of the atoms caused by the smaller interatomic distance in He^4. It is very interesting that it appears to be possible to treat the lowest excited energy level of He^3 very well by means of the pair-rotator model with hindered rotation, but that this model appears to begin to break down for the next series of excited states. In He^4, on account of the considerable hindrance to rotation, the lowest excited states have a higher energy even than the second set of excited states in He^3, and for them the pair-rotator model breaks down even more completely. The nature of these excited states can, however, be tentatively inferred, and in making this inference the model is of considerable assistance.

[10] See W. H. Keesom, *Helium* (Elsevier Publishing Company, Inc., Amsterdam, 1942), p. 219.
[11] Taconis, Beenakker, Nier, and Aldrich, Phys. Rev. **75**, 1966 (1949).
[12] O. K. Rice, Phys. Rev. **93**, 1161 (1954), Sec. 4.
[13] O. K. Rice, Phys. Rev. **96**, 1464 (1954).
[14] Sommers, Keller, and Dash, Phys. Rev. **92**, 1345 (1953).
[15] O. K. Rice, Phys. Rev. **76**, 1701 (1949).

ADDENDUM: DISCUSSION OF THE DEGENERACY OF THE ENERGY LEVELS IN He³

Referring to Fig. 1, it is seen that in the case of $V_0=0$, i.e., pure rotation, the lowest energy level is single and symmetrical in the rotational coordinates, while all the other levels are double. As V_0 increases, and we approach the condition of pure oscillation, each level is double, there being one symmetrical singlet state and one antisymmetrical triplet state. One of these states connects with the rotational level just above that with which the other connects. The multiplicity of the energy levels is most readily understood by considering the case of V_0 large. Let us consider all the energy levels which can arise from the lowest pair of symmetrical and antisymmetrical states, that is, from the lowest vibrational state with V_0 large. If V_0 is large we can consider that each particular position A in space has a wave function ψ_A (excluding spin). Taking a particular pair of atoms, if atom 1 is at position A and atom 2 at position B the wave function is $\psi_A(1)\psi_B(2)$, while if they have changed position the wave function is $\psi_B(1)\psi_A(2)$. Of course, the wave function must be properly symmetrized; the two energy levels, lowest solid and lowest broken line in Fig. 1 correspond to $\psi_A(1)\psi_B(2)+\psi_B(1)\psi_A(2)$ and $\psi_A(1)\psi_B(2)-\psi_B(1)\psi_A(2)$, respectively, provided ψ_A and ψ_B are the lowest wave functions for their particular positions, and therefore identical except that one is centered at A and the other at B.

Now consider the whole assembly of N atoms, each having the wave function corresponding to the lowest energy state. Each of these N wave functions, ψ_A, ψ_B, ψ_C, $\cdots$, has a particular spin function, either α, corresponding to spin in one direction, or β, corresponding to spin in the other direction, associated with it. Since there are two spin possibilities for each atom, there are altogether 2^N possibilities. Since these wave functions contain both spatial coordinates and spin, each must be made antisymmetrical to exchange of atoms. There will be 2^N independent wave functions built up from the set of lowest wave functions, ψ_A, ψ_B, ψ_C, $\cdots$, and the spin functions. These, of course, do not all have to have the same energy.

We turn now to the case of $N/2$ pair-rotators, rotating in a plane. Each one of these pairs can have a singlet and a triplet state built up out of the proper combination of, e.g., ψ_A and ψ_B, and the spin functions. Thus each pair has four states; altogether the $N/2$ pairs will have $4^{N/2}=2^N$ states. Thus the hindered-plane-rotator model, when its two lowest energy levels are considered, gives exactly the correct number of states built up from the lowest eigenfunctions of individual atoms; and presumably it is the only rotator model which will do this. Further, it can give some idea of what the energies involved are.

A higher oscillational level of the hindered rotator with large V_0 corresponds to higher individual energy levels, with wave function ϕ, let us say. If an atom has wave function ϕ it must, if the pair rotator model is reasonably correct, have one nearest neighbor with a similar function. If there are two atoms among the N atoms which have a wave function ϕ, and if each atom in the system has on the average four nearest neighbors, then there are $2N$ distinct ways in which two of the N functions, ψ_A, ψ_B, ψ_C, $\cdots$, can be replaced by ϕ's. Once this replacement is made, then the possible number of states, including spin, can be found just as before. However, it is seen that it is not sufficient to say that any one of $N/2$ pairs can have its wave functions replaced by ϕ's. This gives only one-fourth the total number of possibilities. We thus see how it comes about that the hindered-plane-rotator model can give a reasonable account of the energies of the three lowest sets of energy levels in He³, and how it can give the correct multiplicity for the lowest and next lowest set of levels, yet may be expected to break down in giving the multiplicity for the third set of levels. Of course, strictly speaking, this means that the partition function no longer has the form given by Eq. (1), but if not too many ψ's are replaced by ϕ's this should not cause serious error.

Stability of a Phase Boundary Inside a Superconductor

F. BECK*
Fritz Haber-Institut der Max-Planck-Gesellschaft, Berlin-Dahlem, Germany
(Received September 17, 1954)

According to the London–von Laue theory a phase boundary between superconducting and normal-conducting phases inside a superconductor can exist in a stationary state in the presence of a critical magnetic field. It is shown here explicitly that such a boundary is not in stable equilibrium against variations which lead to a periodic perturbation of the shape of this boundary. In connection with Pippard's idea of a finite transition region the discussion gives an outline of the meaning of this instability for the breakdown of superconductivity in the critical field.

I.

THE London–von Laue electrodynamics of the superconducting state leads, as is well known, to a thermodynamics which gives the breakdown of superconductivity in a sufficiently strong magnetic field H_c. This was first shown by London,[1] for the general case by von Laue.[2] This thermodynamics, however, leads also to a conclusion never confirmed by experiments, namely that superconducting kernels surrounded by normal-conducting material could exist in arbitrarily high magnetic fields if the size of these kernels is sufficiently small. Thus, for a cylindrical kernel with radius R the equilibrium longitudinal field strength comes out to be

$$H_c(R)=H_{c\infty}[J_0(i\beta R)]/[-iJ_1(i\beta R)]. \quad (1)$$

(J_0, J_1 are the Bessel functions; $\beta^{-1}=c\Delta^{\frac{1}{2}}$ is the penetration depth; $H_{c\infty}=[2(f_n-f_s)]^{\frac{1}{2}}$, where f_n, f_s are the Helmholtz free energies of the normal and superconducting phases, respectively.) In an increasing external field H_0 there is always an equilibrium radius, R_0, for which $H_c(R_0)=H_0$ holds. If therefore the magnetic field exceeds the threshold value of the whole specimen, penetrating into the superconductor by a radial contraction of the superconducting region, then only the region $R>R_0$ undergoes the transition and, since $R_0>0$ for finite fields, the whole specimen never undergoes the transition. It can also easily be shown that this equilibrium is stable with respect to *radial* contractions or expansions of the superconducting region.

On the other hand, experiments show in specimens of almost vanishing demagnetizing factors (long thin cylinders or thin laminae in longitudinal fields) an entire breakdown of the whole superconducting phase, if the magnetic field exceeds its critical value on the surface of the specimen. These experiments show a different behavior of the phase boundary according to whether it is inside or on the surface of the superconducting material.

To explain this, different authors[3] introduced a positive surface energy α_{ns} between the two phases of the same material. (α_{ns} is mentioned here as a surface energy *additional* to the electromagnetic energy in the penetration layer which, in some cases, can also be treated as a surface energy.) It has to be of the order of magnitude[4] $H_{c\infty}^2/2\beta$ to explain the completeness of the transition, in a field which exceeds the critical value on the surface of the specimen. But such a hypothesis was never without objections.[5] Furthermore, from experimental results, Pippard[6] derived that α_{ns}, if present at all, should be smaller than the above-mentioned value by at least a factor of 10. Also, von Laue[7] pointed out that the consideration of *radial* displacements alone is not sufficient to draw thermodynamic conclusions about what is really happening, and so does not give a sufficient reason for introducing the interphase surface energy. After this, Koppe[8] made the suggestion that the above-mentioned stability of the equilibrium against radial displacements does not hold in considering displacements which lead to a periodically perturbed boundary. This suggestion has support from the fact that the field energy, contained in the penetration layer, enters the electrodynamic potential[9] with a negative sign, and acts, as is well known, for thick (in comparison to the penetration depth) superconductors as a kind of negative surface energy. By increasing the surface one can probably come to a state of lower potential, which would indicate the instability of the equilibrium. However, this suggestion has to be proved in detail. For the perturbation also affects the field distribution in the penetration layer and this effect has the same magnitude as the effect of increasing the surface.† In two mathematically simple examples we calculate, in the following, the values of the potential

* Present address: Massachusetts Institute of Technology, Department of Physics, Cambridge, Massachusetts.

[1] H. London, Proc. Roy. Soc. (London) **A152**, 650 (1935).

[2] M. von Laue, Ann. Physik **32**, 71 (1938); also *Superconductivity* (Academic Press, Inc., New York, 1952) quoted in the following as "Sc."

[3] First mentioned by H. London, reference 1.

[4] We use Lorentzian units. In Gaussian units there would occur a factor 4π in the denominator.

[5] M. von Laue, Sc, pp. 98, 99.

[6] A. B. Pippard, Proc. Cambridge Phil. Soc. **47**, 617 (1951).

[7] M. von Laue, Z. angew. Phys. **4**, 458 (1952).

[8] H. Koppe (private communication).

[9] M. von Laue, Z. Physik **125**, 517 (1949); also Sc, Sec. 14.

† *Note added in proof.*—In the meantime Koppe published a paper [Z. Naturforsch. **9a**, 724 (1954)] where he calculates the potential neglecting the change in the field distribution. His result differs from that given in this paper.

in the initial and the varied state. The calculation establishes the instability of a phase boundary inside the superconductor.

II.

In the first case, we examine the phase boundary for a semi-infinite superconductor. This problem is equivalent to that of an infinite plate in a longitudinal field since the character of the solution remains unchanged with finite thickness. The phase boundary in the semi-infinite superconductor is in neutral equilibrium with respect to displacements parallel to itself. We choose $z=0$ for the undisturbed boundary, with the positive z-axis pointing into the superconductor. (The boundary of the material is necessarily located at an unimportant value $z=a<0$.) For the magnetic field we choose the x-direction. Let the variation be the periodic perturbation $\delta z=z_0(y)$ (Fig. 1). Then the field-variables also depend periodically on y. The differential equation, valid for each field-component in the stationary state,[10] is

$$\Delta u-\beta^2 u=0. \tag{2}$$

With respect to H_x it has the solution (vanishing at $z=\infty$)

$$H_x(z,y)=H_0\{\exp(-\beta z)+\sum_{n=1}^{\infty}\epsilon_n \exp[-(1+(2\pi n/l\beta)^2)^{\frac{1}{2}}\beta z]\times\sin[(2\pi n/l)y+\varphi_n]\}. \tag{3}$$

This solution is allowable for every arbitrary periodical displacement $z_0(y)$ of the phase boundary. But the shape of this perturbation is unimportant, so we use in (3) only the term $n=1$ and determine $z_0(y)$ from the boundary condition

$$H_x(z_0)=H_0=H_{c\infty}. \tag{4}$$

We introduce dimensionless units:

$$\beta x=\xi,\quad \beta y=\eta,\quad \beta z=\zeta,\quad 2\pi/l\beta=\omega, \tag{5}$$

and get, by using the Maxwell equation $\mathbf{I}^s=c\ \mathrm{curl}\ \mathbf{H}$,

$$H_z(\zeta,\eta)=H_0\{\exp(-\zeta)+\epsilon\exp[-(1+\omega^2)^{\frac{1}{2}}\zeta]\sin\omega\eta\}, \tag{6}$$

$$I_y^s(\zeta,\eta)=-\beta cH_0\{\exp(-\zeta)+\epsilon(1+\omega^2)^{\frac{1}{2}}\exp[-(1+\omega^2)^{\frac{1}{2}}\zeta]\sin\omega\eta\}, \tag{7}$$

$$I_z^s(\zeta,\eta)=-\epsilon\beta cH_0\omega\exp[-(1+\omega^2)^{\frac{1}{2}}\zeta]\cos\omega\eta. \tag{8}$$

To solve the boundary condition (4) with respect to $\zeta_0(\equiv\beta z_0)$, we have to expand (6) in a power series in ζ_0. Here we must take into account at least terms of the second order in ζ_0, for we know from the equilibrium condition that the potential is unaffected by first-order terms of the displacements. Realizing that ζ_0 is small, of the same order as ϵ, we drop, in all following expansions, terms of higher than second or bilinear order in ζ_0 and ϵ.

[10] See, e.g., Sc, Sec. 6.

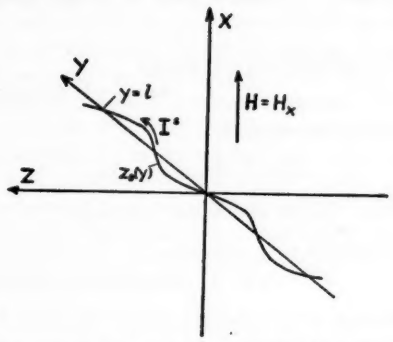

FIG. 1. The phase boundary in the semi-infinite superconductor.

By expanding (6), we get from (4) the quadratic equation

$$\zeta_0^2-2(1+\epsilon\kappa\sin\omega\eta)\zeta_0+2\epsilon\sin\omega\eta=0;\quad \kappa=(1+\omega^2)^{\frac{1}{2}}. \tag{9}$$

The solution which vanishes together with ϵ is

$$\zeta_0=\epsilon\sin\omega\eta\{1-\epsilon(\kappa-\tfrac{1}{2})\sin\omega\eta\}. \tag{10}$$

To investigate the stability, we use the electrodynamic potential[9] which has, in the absence of a superconducting ring, the form

$$V=-\int_V\{\tfrac{1}{2}\mu\mathbf{H}^2+\mathbf{M}\cdot\mathbf{H}+\tfrac{1}{2}\Lambda\mathbf{I}^{s2}\}d\tau.$$

Since in our case the work done by the field is used to transfer the superconducting into the normal-conducting phase, it follows from thermodynamics that in a stable equilibrium the free enthalpy $G=V+F$ (where F is the free energy of the phases per cm^3) has a minimum compared to all states which are producible by isothermal, small and continuous changes in the system:

$$\delta G\geq 0 \text{ in stable equilibrium.} \tag{11}$$

The electrodynamic potential V contains additively a part which comes from the field inside the superconducting phase, V_s, and a part V_n from the outside. We calculate V_s from[11]

$$V_s=-(1/2\beta^2 c)\int_s(\mathbf{I}^s\times\mathbf{H})_n d\sigma. \tag{12}$$

The integrand is, in our case, since on the surface $\mathbf{H}=H_x=H_0$ (see Fig. 1),

$$(\mathbf{I}^s\times\mathbf{H})_n=-H_0 I_{\tan}{}^s(\zeta_0,\eta) \tag{13}$$

with

$$I_{\tan}{}^s=I_y{}^s(\zeta_0,\eta)[1+\tfrac{1}{2}(I_z{}^s/I_y{}^s)^2]. \tag{14}$$

[11] This equation comes from the fact that in our case V_s equals the negative free field energy and by using the identity [Eq. (7-4)] in M. von Laue (reference 10),

$$\int_s\{\Lambda\mathbf{I}^{s2}+\mathbf{H}^2\}d\tau=c\Lambda\int_s(\mathbf{I}^s\times\mathbf{H})_n d\sigma.$$

By expanding (7) with respect to ζ_0 and using (10), we get

$$I_y^s(\eta)=-\beta cH_0\{1+\epsilon(\kappa-1)\sin\omega\eta - \epsilon^2\kappa(\kappa-1)\sin^2\omega\eta\}; \quad (15)$$

and, in a similar manner,

$$(I_x^s/I_y^s)^2=\epsilon^2\omega^2\cos^2\omega\eta. \quad (16)$$

Then from (14) we obtain the following:

$$I_{\tan}{}^s=-\beta cH_0\{1+\epsilon(\kappa-1)\sin\omega\eta - \epsilon^2\kappa(\kappa-1)\sin^2\omega\eta+\tfrac{1}{2}\epsilon^2\omega^2\cos^2\omega\eta\}. \quad (17)$$

We integrate over a surface region of width l in the x-direction and length L in the y-direction (where L has to be an integer multiple of l). Then the surface-element becomes

$$d\sigma=l\cdot ds=(d\eta/\beta)[1+(d\zeta_0/d\eta)^2]^{\frac{1}{2}} =(d\eta/\beta)[1+\tfrac{1}{2}\epsilon^2\omega^2\cos^2\omega\eta]. \quad (18)$$

Finally V_s becomes, after performing the η-integration,

$$V_s=-\pi H_0^2/\beta^2\omega-(\epsilon^2H_0^2L/4\beta)[(1+\omega^2)^{\frac{1}{2}}-1]. \quad (19)$$

The corresponding expression V_s^0 for the plane boundary $z_0=0$ comes from (19) with $\epsilon=0$. So we get, for the change produced by the perturbation of the boundary,

$$\Delta V_s=V_s-V_s^0=-(\epsilon^2H_0^2L/4\beta)[(1+\omega^2)^{\frac{1}{2}}-1]. \quad (20)$$

Because of the condition of equilibrium,

$$\tfrac{1}{2}H_0^2=f_n-f_s, \quad (21)$$

ΔV_n and ΔF cancel each other. Since in the normal phase we have the constant field $H_z=H_0$, the change in the potential is

$$\Delta V_n=-\tfrac{1}{2}H_0^2\Delta v_n \quad (22)$$

(where v_n is the volume of the normal phase). Further, since $\Delta v_s=-\Delta v_n$,

$$\Delta F=(f_n-f_s)\Delta v_n, \quad (23)$$

and hence

$$\Delta V_n+\Delta F=0. \quad (24)$$

So we arrive at

$$\Delta G=\Delta V_s=-(\epsilon^2H_0^2L/4\beta)[(1+\omega^2)^{\frac{1}{2}}-1]\leq 0. \quad (25)$$

The plane phase boundary inside a superconductor is not in stable equilibrium. For a given amplitude ϵ of the perturbation, $|G|$ increases with increasing ω. Then, according to (5) the "wavelength" l goes to zero and the surface splits up entirely. In Sec. IV, we shall give a qualitative reason for a lower limit of this quantity l and discuss the meaning of Eq. (25) for the breakdown of superconductivity in the critical field.

The instability can also be exhibited by using the rigid condition of equilibrium, valid for arbitrary shape of the boundary[2]:

$$\tfrac{1}{2}\Delta I^{s2}=f_n-f_s. \quad (26)$$

In equilibrium the London stress $\frac{1}{2}\Delta I^{s2}$, which points into the superconductor, equals the "pressure" f_n-f_s of the superconducting phase. If the stress at the points $z_0=(z_0)_{\max}$ is larger and at the points $z_0=(z_0)_{\min}$ is smaller than the pressure f_n-f_s, then the deviations from the plane boundary do not lead back to the previous equilibrium. From (17) it follows that

$$\tfrac{1}{2}\Delta I_{\tan}{}^{s2}=\tfrac{1}{2}H_0^2\{1+2\epsilon(\kappa-1)\sin\omega\eta\}. \quad (27)$$

[Here it is only necessary to proceed to the order ϵ. Since the potential corresponds to the work done by the force-density (27) in making the small displacement z_0, we need the force only to the first order, if we keep the potential to second order.] The tension (27) is indeed larger at the maxima of ζ_0 ($\sin\omega\eta=1$) and smaller at the minima ($\sin\omega\eta=-1$), than the equilibrium value $\frac{1}{2}H_0^2$.

III.

For the second case we take a curved boundary, forming a circular cylinder with radius R which may be contained in a cylindrical specimen with radius $R_0>R$. We take the magnetic field parallel to the axis. The critical value H_c is, according to (1), dependent on the radius. The equilibrium is stable with respect to radial displacements of the boundary. We perform a displacement corresponding to that in II (see Fig. 2). The steps of the calculation are also the same.

The equation $\Delta u-\beta^2u=0$ for the field components leads in cylindrical coordinates (for z-independence) to the Bessel differential equation with the solution (single-valued in ϑ)

$$u=C_0J_0(i\beta r)+\sum_{n=1}^{\infty}C_nJ_n(i\beta r)\sin(n\vartheta+\varphi_n). \quad (28)$$

With $\rho=\beta r$, $\mathrm{P}=\beta R$, and again taking only one term of the sum, we get for $H_z(\rho,\vartheta)$:

$$H_z(\rho,\vartheta)=(H_0/J_0(i\mathrm{P}))\{J_0(i\rho)+\epsilon J_n(i\rho)\sin n\vartheta\}. \quad (29)$$

[$H_0=H_c(R)$ is the critical field in accordance with (1).] Since H_z is real, ϵ must, in view of the properties of the

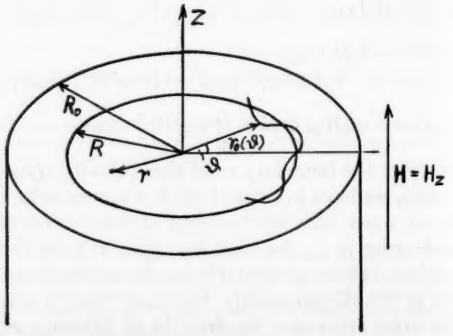

FIG. 2. Variation of the cylindrical phase boundary.

Bessel functions ($J_n \sim i^n$), be of the form

$$\epsilon = i^{-n}\tilde{\epsilon}, \tag{30}$$

with $\tilde{\epsilon}$ real.

For the current density we get

$$I_\vartheta^s(\rho,\vartheta) = -(\beta c H_0/J_0(i\mathrm{P}))\{J_0'(i\rho) + \epsilon J_n'(i\rho)\sin n\vartheta\}, \tag{31}$$

$$I_r^s(\rho,\vartheta) = \epsilon(\beta c H_0/J_0(i\mathrm{P}))(nJ_n(i\rho)/\rho)\cos n\vartheta. \tag{32}$$

($J_n' = dJ_n/d\rho$.) The boundary condition is now

$$H_z(\rho_0,\vartheta) = H_0; \quad \rho_0 = \mathrm{P} + \delta\rho. \tag{33}$$

From this we can again obtain a quadratic equation for $\delta\rho$ and proceed in the same manner as in II. After some laborious but straightforward calculations, one reaches finally the result

$$\Delta G = \tilde{\epsilon}^2(\pi H_0^2\mathrm{P}/2\beta^2)[(16-11n^2)/32]\mathrm{P}^{-2}, \tag{34}$$

where we have used an asymptotic representation for the Bessel functions up to the order P^{-2}. ΔG in this case is also negative for $n \geq 2$. This shows that the cylindrical phase boundary, $R = \text{const}$, inside a superconductor is unstable with respect to a periodic perturbation.

It is also easy, from (31) and (32), to prove that here, too, the stress $\frac{1}{2}\Delta I^{s2}$ is larger in the minima and smaller in the maxima of $\rho_0(\vartheta)$ than the equilibrium value for $\rho_0 = \mathrm{P}$ and so the deviation does not lead back to equilibrium.

IV.

We wish to discuss the instability of the phase boundary (which we have shown here) in view of the phase transition in the critical field. This discussion is more or less qualitative, for to be more rigorous we would have to know more about the intermediate state. First of all, the present calculation shows that it is probably necessary to introduce into the phenomenological theory of superconductivity, besides the penetration depth β^{-1}, a further characteristic length Δ, as was first suggested by Landau[12] and Ginsburg[13] in connection with the theory of the intermediate state. This quantity recently was given more importance by investigations of Pippard[6,14] who connected it with a spread-out boundary between the superconducting and the normal phase instead of the geometrical sharp boundary hitherto assumed. This suggestion has some support from the fact that the wave packets associated with the superconducting electrons have a finite extension. From experimental data Pippard derived for Δ the order of magnitude $\Delta \approx 10^{-5}$ cm. In the transition region of the thickness Δ, the "order" of the superconducting phase decreases continuously to the "disorder" of the normal phase. Equation (25) and the following text show that, without introducing a lower limit for the period of the perturbation l, this quantity goes to zero in order to give the potential its smallest value. So, by exceeding the critical field on its surface, the superconductor would decay into small superconducting and normal-conducting strings, similar to London's "layer-structure".[15] That is quite natural, for the field energy in the penetration layer which one can regard as a "negative surface energy" tends to make the interphase surface as large as possible.[16]

Since we have performed our calculations by assuming a sharp boundary, we impose on the period of the perturbation the condition

$$l \gtrsim \Delta \approx 10^{-5} \text{ cm}. \tag{35}$$

With this condition it is easy to see qualitatively what happens inside the superconductor after exceeding the critical field on its surface. After the first creation of normal phase the phase boundary (which we can imagine in the beginning as plane) will go out of its unstable equilibrium and form waves with the smallest possible period $l \approx \Delta$. Since by doing this the equilibrium condition (26) is violated, the amplitudes of the waves tend to larger and larger values. The end of this development is an intermediate state of alternating superconducting and normal-conducting regions of linear dimension Δ. But, by this process, we have a state which, by assuming a finite transition region between the two phases, can be entirely brought over into normal phase without the assumption of an additional surface energy.[17]

To show how this transition from the above-described intermediate state to the entirely normal-conducting state can occur, we make more detailed assumptions about the finite transition region. The idea is to investigate the influence of the gradual transition on the critical field H_c. If there exists a point where H_c decreases with decreasing diameter of the superconducting region, then this region collapses entirely into normal-conducting material. We take as the "ordering-parameter," which describes the superconducting phase, the London constant Λ. Then, in a superconductor which is thick compared to the transition region, Λ decreases

[12] L. Landau, J. Phys. (U.S.S.R.) **7**, 99 (1943).
[13] V. Ginsburg, J. Phys. (U.S.S.R.) **9**, 305 (1945).
[14] A. B. Pippard, Proc. Roy. Soc. (London) **A216**, 547 (1953).

[15] F. London, *Macroscopic Theory of Superconductivity* (John Wiley and Sons, Inc., New York, 1950), pp. 125–128.

[16] However, in our case, contrary to London, the layer structure can only occur if the magnetic field exceeds its critical value. This comes from the fact that we consider continuous variations (in the beginning of the transition the field has to press in the superconducting phase in order to establish the phase boundary *inside* the superconductor; this is, without increasing the enthalpy G, only possible if $H \geq H_c$), whereas London compares two states which can not be brought over into each other by continuous variations. They are probably divided from each other by a potential barrier [compare also P. M. Marcus, Phys. Rev. **88**, 373 (1952)].

[17] One can of course relate Δ to a surface energy, as Pippard does. This is, however, only possible as long as the linear dimensions of the superconducting regions are large compared to Δ. In our case, one should not work in terms of a surface energy, just as one does not regard the electromagnetic energy contained in the penetration layer as a surface energy if the dimension of the superconductor is comparable to the penetration depth λ.

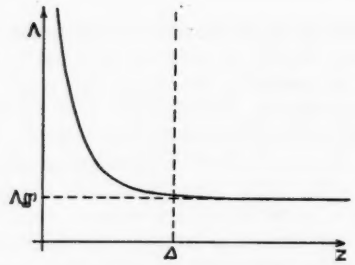

FIG. 3. Variation of the London constant Λ in the transition region $0 \leq z \leq \Delta$ in the case of a thick superconductor.

in this region from infinity (normal phase) to its very small value $\Lambda_\infty(T) \approx 10^{-31}$ sec^2 inside the superconductor (see Fig. 3). In the other case, if one dimension of the superconductor is comparable with Δ, the undisturbed value Λ_∞ can no longer be reached. The effective value Λ_{eff} in such a superconductor depends on its size (see Fig. 4). Then $H_{c\infty}$ of Eq. (1) also depends on the smallest linear dimension of the superconducting region, since for superconductors which have a high value of Λ, the critical field strength is smaller. To get the function $H_{c\infty}(\Lambda)$, we eliminate the temperature from the functions which give the temperature dependence (according to the Casimir-Gorter model)

$$H_{c\infty}(T) = H_{c\infty}{}^0[1-(T/T_s)^2] \tag{36}$$

and

$$\Lambda(T) = \Lambda^0[1-(T/T_s)^4]^{-1}, \tag{37}$$

and get

$$H_{c\infty}(\Lambda) = H_{c\infty}(\Lambda^0)[1-(1-\Lambda_0/\Lambda)^{\frac{1}{2}}]. \tag{38}$$

Now we regard H_c from Eq. (1) as a function of R and Λ_{eff}, which itself is a function of R, and calculate

$$dH_c/dR = H_{c\infty}\{\partial f(R,\Lambda_{eff})/\partial R + [\partial f(R,\Lambda_{eff})/\partial\Lambda_{eff}](d\Lambda_{eff}/dR)\} + f(R,\Lambda_{eff})(dH_{c\infty}/d\Lambda_{eff})(d\Lambda_{eff}/dR), \tag{39}$$

$$f(R,\Lambda_{eff}) = J_0(i\beta R)/[-iJ_1(i\beta R)]; \quad \beta = (c\Lambda_{eff}{}^{\frac{1}{2}})^{-1}. \tag{39a}$$

A negative value of dH_c/dR indicates stability of the superconducting region against variations of R. A positive value, on the contrary, shows that by diminishing the radius R by $-\delta R$ one comes into regions where the equilibrium field strength is lowered by $-(dH_c/dR)\delta R$. In a constant magnetic field such a region collapses by radial contraction. In Eq. (39) the expression in the curly brackets is negative because $f(\beta R)$ decreases for increasing argument βR. But the second term is positive since $dH_{c\infty}/d\Lambda_{eff}$ and $d\Lambda_{eff}/dR$ are both negative. Now there may exist a point $R = R_{min}$ such that the second term equals the absolute value of the bracket term at $R = R_{min}$ and exceeds this value for $R < R_{min}$. This means that for $R < R_{min}$ a superconducting cylinder in the critical field $H_c(R_{min})$ is unstable and undergoes the complete transition into the normal phase.

To show this explicitly, we specialize to the case $\beta R \ll 1$. Then

$$H_c(R) = 2H_{c\infty}/\beta R = 2H_{c\infty}c\Lambda^{\frac{1}{2}}/R, \tag{40}$$

and

$$dH_c/dR = -2H_{c\infty}c\Lambda^{\frac{1}{2}}R^{-2} + H_{c\infty}(\Lambda^0)c\Lambda^{-\frac{1}{2}}(d\Lambda/dR)R^{-1} \times[1-(1-\Lambda^0/\Lambda)^{\frac{1}{2}} - (1-\Lambda^0/\Lambda)^{-\frac{1}{2}}\Lambda^0/\Lambda] \tag{41}$$

holds. In expanding the bracket and $H_{c\infty}$ from (38) for $\Lambda \gg \Lambda^0$, one gets

$$dH_c/dR = cH_{c\infty}(\Lambda^0)R^{-2}\Lambda^0\Lambda^{-\frac{1}{2}} \times[-1+\tfrac{1}{2}|d\Lambda/dR|\Lambda^{-1}R]. \tag{42}$$

If one chooses for $\Lambda(R)$ a sufficiently strongly decreasing function, e.g.,

$$\Lambda = \Lambda_\infty \exp(\Delta/R), \tag{43}$$

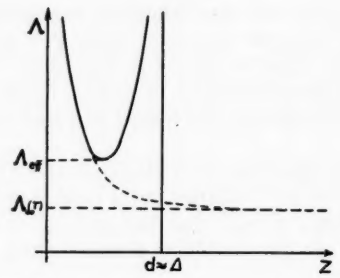

FIG. 4. Variation of Λ in a thin superconductor $0 \leq z \leq d$.

then it leads to

$$dH_c/dR = \text{const}[-1+\tfrac{1}{2}\Delta/R]. \tag{44}$$

This is positive for $R < \Delta/2$. Of course, the approximation $\beta R \ll 1$ may not be adequate, since Δ and β^{-1} are of the same order of magnitude.‡

Thus we have shown that the instability of a phase boundary inside a superconductor, together with the assumption of a finite transition region between the phases may lead to an explanation of the complete breakdown of superconductivity in the critical field. A detailed elaboration of these points could probably throw some light on the intermediate state as well as on hysteresis phenomena.

ACKNOWLEDGMENTS

I wish to express my deep gratitude to Professor M. von Laue for stimulating this work and for many valuable discussions. I would also like to thank Dr. J. Nitsche for his help in evaluating Eq. (34).

‡ *Note added in proof.*—A more vigorous calculation performed meanwhile yields a similar result.

PHYSICAL REVIEW VOLUME 98, NUMBER 4 MAY 15, 1955

Spatial Distribution of Atoms in Liquid He⁴

LOUIS GOLDSTEIN, *University of California, Los Alamos Scientific Laboratory, Los Alamos, New Mexico*

AND

JAMES REEKIE, *Physical Metallurgy Division, Department of Mines, Ottawa, Ontario, Canada*

(Received December 22, 1954)

The x-ray scattering diagrams of liquid helium, obtained by one of the authors, have been analyzed in this paper using the Los Alamos "701" IBM Electronic Calculator. The liquid He⁴ atomic correlation and pair distribution functions have thus been obtained over a wide range of interatomic separations and at a number of liquid temperatures between 1.25 and 4.20°K.

The limitations in the experimental scattering structure factors give rise, among others, to two types of limitations in the correlation functions. One of these concerns their behavior at small atomic separations; this limitation could be compensated for without difficulties. The second limitation, of more elusive character, appears to be connected with the lack in these functions of any manifest tendency toward their asymptotic behavior at large atomic separations. The here derived correlation or pair distribution functions should, nevertheless, be good approximations to their correct values at medium and intermediate separations extending to about fifteen angstroms, whereby the relevant range extends to 10–15 A. This could be verified using two types of integral checks on the correlation functions. In one of these, their space integrals, out to relevant distances, turned out to be quite close to their expected values determined only by the macroscopic properties of the liquid. In the second series of integral checks, they reproduced closely the original experimental structure factors. This verified the internal consistency of the calculations and indicated that the results should be correct at the relevant interatomic separations.

At all the liquid temperatures here investigated, in any sphere of given radius, around an origin atom, or in any spherical shell of given thickness, the computed number of atoms was always less than what one would compute neglecting the interatomic correlations.

An application, of major physical significance, of the correlation or pair distribution functions obtained in this work was made by deriving the approximate mean potential energies per liquid He⁴ atom at the various temperatures. The mean potential energy, as a function of the liquid temperature, has a cusp at the lambda point. Its temperature derivative, which is the configurational heat capacity, is thus discontinuous at the transition point with an inverted lambda type of discontinuity. The knowledge of this qualitative behavior of the configurational heat capacity was sufficient to prove, on quite general grounds, that the lambda transition of liquid He⁴ is of kinetic energy origin, i.e., it is connected with the momentum space behavior of the liquid atoms.

I. INTRODUCTION

AN analysis of the atomic distribution in liquid He⁴ has been first performed by one of us[1] using x-ray scattering data obtained recently.[1,2] The x-ray scattering data communicated to Los Alamos have there been analyzed using the "701" IBM Electronic Calculator. Some of the results obtained in these machine calculations have already proved to be of great value in the interpretation[3] of the Los Alamos slow-neutron total scattering cross-section measurements[4] in liquid He⁴. While the machine calculations have fully confirmed the results derived by hand calculations,[1] they originated in that the necessarily slow hand calculations could not really fully exploit the available x-ray scattering data. These hand calculations succeeded in analyzing the spatial distribution of the helium atoms, around one chosen to be at the origin of the coordinate system, up to separations r of about 6 A. This distance is only some 1.5 times the mean separation of the atoms resulting from the mean liquid concentration. Clearly, for purposes of deriving the neighborhood picture within the liquid, that is the number of first, second, and even third, neighbors of a given atom, the previous analysis[1] was satisfactory. However, as recognized at Los Alamos, the restriction on the linear extension r of the region explored, resulting inevitably from the time-consuming hand calculations, could not lead to an entirely satisfactory picture of the interatomic correlations in liquid helium whose analytical description defines the liquid correlation function or correlation concentration. Indeed, the investigation of the space integral of the correlation function of restricted range showed its failure to satisfy the all-important statistical thermodynamic test requiring it to yield a quantity directly connected with the mean square fluctuation of the number of atoms, per atom, under isothermal conditions.[5] It was then decided to reanalyze the x-ray scattering data with the Los Alamos "701" IBM Electronic Calculator. In so doing, however, it was fully realized that the results to be derived would be affected, inevitably, by limitations arising from various causes.

One of these was experimental and was associated with the restricted response of the measurements to temperature variations of the liquid. An attempt to compensate for this lack of sensitivity of the data, at small scattering angles, was made using a method of extrapolation of the scattering diagrams toward small angles, where the liquid temperature has a critical effect on the scattering. The method of extrapolation is based on the rigorous theory of small angle radiation scat-

[1] J. Reekie and T. S. Hutchison, Phys. Rev. **92**, 827 (1953); C. F. A. Beaumont and J. Reekie, Proc. Roy. Soc. (London) **A228**, 363 (1955).

[2] Reekie, Hutchison, and Beaumont, Proc. Phys. Soc. London **A66**, 409 (1953).

[3] L. Goldstein and H. S. Sommers, Jr. (to be published).

[4] Sommers, Dash, and Goldstein, Phys. Rev. **97**, 855 (1955).

[5] L. S. Ornstein and F. Zernike, Proc. Roy. Soc. (Amsterdam) **17**, 793 (1914).

tering.[6] The liquid correlation functions could thus be investigated here over a wide temperature interval, extending from 1.25 to 4.20°K. However, the correlation functions here derived are found to be better approximations at the low and the high temperatures, than at intermediate ones, such that

$$2.50-2.75 \leqslant T \leqslant 3.0-3.25°\text{K}.$$

While a method of analysis exists for a fairly well approximated evaluation of the number of first-, second- and higher-order neighbors of the atom at the origin of the coordinate system within the liquid, this method is far from being simple in its applications at medium and larger separations. It has been used by one of us[1] to derive both the low- and high-temperature neighborhood picture in liquid helium. In the present work, we limited ourselves to a rigorous evaluation of the number of neighbors of the origin atom filling spheres of given radii, which in turn determine the number of atoms in spherical shells of any thickness. This method seems to be the only practical method of deriving a fair picture of the atomic distribution beyond the shells of neighbors of the first few orders.

The correlation functions will be seen to satisfy with good approximation their test relation based on their space integral, with the latter extended to the range of r at which they were evaluated, or r equal to 15–20 A. Nevertheless, the experimental x-ray scattering data failed to yield the correct limit of these functions at vanishing separations[6] $r \to 0$. While this appears to be a serious failure of local character, it could be obviated without too much difficulty. Another shortcoming of these functions appeared in that they did not exhibit any definite tendency to approximate their expected asymptotic large distance behavior.[6,7]

A major application, along a line conjectured previously,[3] was finally made of the correlation functions obtained in the present work, through the two-atom or pair distribution functions which they define. This consisted in a rigorous proof of the kinetic energy origin of the lambda transition in liquid helium. The proof could be based on quite general grounds and involved mainly the qualitative temperature behavior of the pair distribution function. This result, while justifying the current theoretical trends attempting to explain the lambda transition, should help to provide a solid guidepost for the establishment of an improved theory of liquid helium.

II. INTERATOMIC CORRELATION FUNCTION IN LIQUID He⁴

The coherent scattering cross section for radiation of wavelength λ, per liquid atom, and per unit solid angle whose axis is at an angle 2θ to the direction of incidence, can be shown to yield, with

$$\Delta k = |\Delta \mathbf{k}| = 2|\mathbf{k}| \sin\theta = 4\pi(\sin\theta)/\lambda, \quad (1)$$

the momentum change, in units of $h/2\pi$, of the incident radiation on scattering in the direction 2θ, $\mathbf{k}$ being its propagation vector, $F_L^2(\Delta k,T)$ standing for the experimentally derived scattering intensity structure factor per atom, and by the Fourier integral theorem, the correlation function[8]

$$g(r,T) = (1/2\pi^2 r)\int_0^\infty [F_L^2(\Delta k,T)-1] \times (\sin r\Delta k)(\Delta k)d(\Delta k). \quad (2)$$

In the limit of vanishing separations r, one obtains

$$\lim_{r\to 0} g(r,T) = (1/2\pi^2)\int_0^\infty [F_L^2(\Delta k,T)-1](\Delta k)^2 d(\Delta k) = -n(T), \quad (3)$$

because in this limit the two-atom distribution function $n(r,T)$ or $dN(r,T)/dv(r)$, the latter including the quantum-mechanical exchange effects,

$$dN(r,T) = n(r,T)dv(r) = [n(T)+g(r,T)]dv(r), \quad (4)$$

has to vanish; no two atoms being able to approach each other too closely, with finite probability, under equilibrium conditions of the liquid. Equation (3) constitutes a rigorous normalization or check relation for the experimental structure factors F_L^2. It will, however, be seen below that this relation is not critical, in the sense that if it is not strictly satisfied, the empirically derived structure factors may still be fair approximations to the actual ones.

In the present work the portions of the structure factor functions $F_L^2(\Delta k,T)$ above $\Delta k \sim 0.9$ A^{-1} belonged to either the low- or high-temperature liquid. They have been obtained experimentally[2] from 0.9 to about 6 A^{-1} and they are given in Fig. 1. The regions $\Delta k < 0.9$ A^{-1} will be fully discussed below. The preceding Δk range is equivalent, for the Cu K_α radiation used in the scattering experiments,[2] to a scattering angular range $12° \leqslant 2\theta \leqslant 100°$. Limitations inherent in the very low scattering cross section of liquid helium and the experimental technique have prevented the effective exploration of a larger Δk or θ interval. It may, however, be expected that techniques with increased detection sensitivities should help to widen the explorable Δk range and to increase the over-all precision of the scattering structure factors. The estimated average relative error will be seen on Fig. 1 to be about 5 to 7 percent.

The first exploratory x-ray scattering experiments[9] have already demonstrated the absence of any major change in the scattering diagram of liquid He⁴ over a

[6] L. Goldstein, Phys. Rev. 84, 466 (1951).
[7] F. Zernike, Proc. Roy. Soc. (Amsterdam) 19, 1520 (1916).
[8] F. Zernike and J. A. Prins, Z. Physik 41, 148 (1927).
[9] W. H. Keesom and K. W. Taconis, Physica 5, 270 (1938); J. Reekie, Proc. Cambridge Phil. Soc. 36, 236 (1941); 43, 262 (1947).

temperature range extending from well below to somewhat above the lambda point. The more recent data[1,2] fully confirm the above results and tend to indicate that in the explored Δk-range the scattering structure factor does not change, within experimental errors, up to temperatures approaching the normal boiling point. The total liquid density change in the temperature range 1.25–4.2°K, with the apparent density cusp at the lambda point, is relatively small. The interference factor in the integrand appearing in the scattering cross section[6] will tend to minimize the expected changes in the correlation function $g(r,T)$ over this temperature interval. This then is probably the main cause of the absence of any easily detectable variation in the structure factor F_L^2 over a relatively wide temperature interval and for Δk-values larger than 0.9 or 1.0 A^{-1}.

The structure factors should exhibit, however, considerable temperature variations at small momentum changes or small scattering angles[6] or precisely in a Δk range which remained unexplored in the experiments.[2] At $\Delta k \lesssim 0.5$ A^{-1} or so, it should be possible to observe the relatively large variations of the structure factor as shown in the rather difficult experiments of Tweet[10] on the very small angle x-ray scattering as well as in the small angle slow neutron scattering work of London and Egelstaff[11] in liquid He⁴. More recent x-ray scattering work, using counter detection techniques, by Gordon *et al.*[12] where the explored scattering angular range extended from 1.5 to 90°, again confirms at small angles the expected large variations of the structure factor with liquid temperature. The small angle scattering structure factors are determined essentially by the macroscopic concentration fluctuations of the liquid,

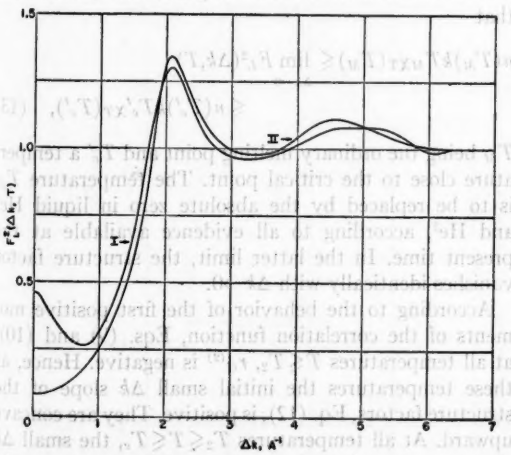

FIG. 1. The experimental structure factors $F_L^2(\Delta k,T)$ *vs* Δk, at two liquid temperatures I(4.20°K); II(2.06°K). For the extrapolated portions of these graphs at $\Delta k < 0.9$ A^{-1} see the text.

[10] A. G. Tweet, Phys. Rev. **93**, 15 (1954).
[11] H. London and P. A. Egelstaff, Proceedings of the Third International Conference on Low Temperature Physics and Chemistry (Rice Institute, Houston, 1953).
[12] Gordon, Shaw, and Daunt, Phys. Rev. **96**, 1444 (1954).

under isothermal conditions.[6] The simple physical basis of the following rigorous result has been discussed previously[13] and need not be considered here,

$$\lim_{\Delta k \text{ small}} F_L^2(\Delta k,T) = n(T)kT\chi_T - r_G^{(2)}\frac{(\Delta k)^2}{6}, \quad (5)$$

where

$$r_G^{(2)} = 4\pi \int r^4 g(r,T)dr, \quad (6)$$

is the second moment of the correlation function.

In the present analysis of the atomic distribution in liquid He⁴, the low-temperature structure factor, the one at 2.06°K, where $\Delta k \gtrsim 0.9-1.0$ A^{-1}, was taken to be the same, approximately, at all temperatures $T < 3$°K. The observed structure factor at the normal boiling point was taken to be the same, approximately, in the above mentioned Δk-range, at the temperatures $3 \lesssim T \lesssim 4.2$°K. In spite of the rather large experimental errors, the structure factor curves of Fig. 1 suggest that there should be a rather smooth change-over from the low- to the high-temperature structure factors at $\Delta k \gtrsim 0.9-1.0$ A^{-1}. It is thus expected, as a consequence of the above-mentioned approximate groupings of the structure factors, that the results obtained in the present analysis, with the low- and high-temperature structure factors, will not join smoothly. They will thus be affected with greater errors in the transition region $2.50-2.75 \lesssim T \lesssim 3-3.25$°K than at the other temperatures.

The structure factors at the different temperatures and at $0 \lesssim \Delta k \lesssim 0.9$ A^{-1} have been obtained by interpolation between their rigorous value at vanishing Δk, where they reduce to $n(T)kT\chi_T$, Eq. (5), and the measured value of $F_L^2(\Delta k,T)$ at the smallest Δk-value of about 0.9 A^{-1}. The interpolation was facilitated by the somewhat rough knowledge of the second moments $r_G^{(2)}(T)$ of the correlation function $g(r,T)$. These moments became available through the analysis of the small angle x-ray[10] and slow neutron[11] scattering experiments, to a rather limited degree of approximation. The parabolic behavior at small Δk, as shown by (5), tended to simplify considerably the interpolation procedure at these small Δk-values. It should be noted that in considering $F_L^2(\Delta k,T)$ as a function of $(\Delta k)^2$ rather than Δk, a change in independent variable evidently justified by the even character of F_L^2 in Δk, the structure factor has a small linear region in $(\Delta k)^2$. It becomes parabolic through the term in $(\Delta k)^4$ which follows the quadratic term in the expansion of $F_L^2(k,T)$.[6] The interpolation procedure out to $\Delta k \sim 0.9$ A^{-1} entailed, inevitably, a good many uncertainties. These, however, are minimized in the Fourier integral (2) in this same range of small Δk values. We give in Fig. 2 a series of the interpolated approximate small Δk structure factors at various temperatures. The behavior of the small Δk

[13] L. Goldstein, Phys. Rev. **83**, 289 (1951).

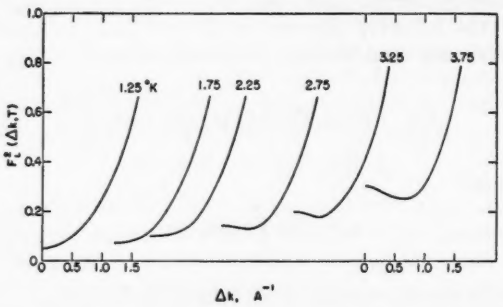

FIG. 2. The extrapolated small Δk structure factors at various liquid temperatures. The origin and the common abscissa scales are given only for the first and last curves. All structure factors start at vanishing Δk.

structure factors has been discussed previously in various connections.[6,13,14]

It does not seem superfluous to restate here briefly some general properties of the correlation functions valid in all liquids. Physically the correlations cannot but vanish at large separations r, or, we have at both limits of r, with (3),

$$\lim_{r\to 0} g(r,T) = -n(T); \quad \lim_{r\to\infty} g(r,T) = 0. \tag{7}$$

At small separations, around the atom chosen to be at the origin of the coordinate system, there is a very large density defect as a result of the interatomic repulsion at such separations. Actually, at vanishing separations $g(r,T)$ reaches its minimum minimorum. This largest density defect is then followed by a large density excess at increasing separations, with a damped oscillatory behavior at larger distances. It is easy to see that the zero order moment of the correlation function, which is the fluctuation integral $G(T)$,

$$\begin{aligned} r_G^{(0)}(T) &= \int g(r,T)dv(r) \\ &= G(T) \\ &= n(T)kT\chi_T - 1, \end{aligned} \tag{8}$$

is such that there is a single characteristic temperature[15] T_0, in any liquid, whereby, T_c being the critical temperature,

$$\begin{aligned} r_G^{(0)}(T \leqslant T_0) &= G(T \leqslant T_0) \leqslant 0; \\ r_G^{(0)}(T_0 \leqslant T \leqslant T_c) &= G(T_0 \leqslant T \leqslant T_c) \geqslant 0. \end{aligned} \tag{9}$$

Similarly, if T_n denotes that liquid temperature at which the n'th moment, of the correlation function, $r_G^{(n)}$, n even, vanishes, one has

$$r_G^{(n)}(T \leqslant T_n) \leqslant 0; \quad r_G^{(n)}(T \geqslant T_n) \geqslant 0. \tag{10}$$

It can be shown that the characteristic temperatures T_n form the sequence

$$\cdots < T_{n+2} < T_n < T_{n-2} < \cdots < T_4 < T_2 < T_0 < T_c. \tag{11}$$

Indeed, a moment $r_G^{(n)}$ which is negative at some low temperature will increase faster with liquid temperature the higher is its order, because the negative contributions to the moment integrals decrease with decreasing density. The higher the order of the moment the faster the decrease,[14] because the negative contributions are due predominantly to regions of $g(r,T)$ at small r or $r < z_1$, z_1 being the first zero of $g(r,T)$. It will be seen that the sequence (11) is finite, since, if n is large enough there is no liquid temperature at which the corresponding moment can become negative.

The small angle scattering structure factors of liquids can be at once understood on the basis of the preceding results which are rigorous. These structure factors are defined by their limiting $\Delta k \to 0$ value, that is $[1+G(T)]$ or $n(T)kT\chi_T$ and by their slope at Δk small, or, by (5),

$$\lim_{\Delta k \text{ small}} \frac{dF_L^2(\Delta k,T)}{d(\Delta k)} = -(r_G^{(2)}/3)(\Delta k). \tag{12}$$

The mean square fluctuation in the number of atoms, per atom, $n(T)kT\chi_T$, is a monotonically increasing function of the temperature. Even in liquid helium where the compressibility might have a very slight discontinuity and where $n(T)$ has a cusp at the lambda point, the over-all behavior of $n(T)kT\chi_T$ in the liquid in equilibrium with its vapor is a monotonic increase. Hence the family of structure factor curves represented as a function of Δk, the temperature being a parameter, reaches the ordinate at vanishing Δk, with values such that

$$\begin{aligned} n(T_M)kT_M\chi_T(T_M) \leqslant \lim_{\Delta k\to 0} F_L^2(\Delta k,T) \\ \leqslant n(T_c')kT_c'\chi_T(T_c'), \end{aligned} \tag{13}$$

T_M being the ordinary melting point and T_c' a temperature close to the critical point. The temperature T_M is to be replaced by the absolute zero in liquid He^4 and He^3, according to all evidence available at the present time. In the latter limit, the structure factor vanishes identically with $\Delta k \to 0$.

According to the behavior of the first positive moments of the correlation function, Eqs. (9) and (10), at all temperatures $T \leqslant T_2$, $r_G^{(2)}$ is negative. Hence, at these temperatures the initial small Δk slope of the structure factors, Eq. (12), is positive. They are concave upward. At all temperatures $T_2 \leqslant T \leqslant T_c$, the small Δk slopes are negative, the structure factors start to decrease from their limiting values, the vertices of the osculating parabolas (5). At small Δk-values, at these higher temperatures, the structure factors are convex upward.[16] These results have the strength of a rigorous

[14] L. Goldstein, Phys. Rev. **85**, 35 (1952).
[15] In reference 6 this was denoted by T_i.
[16] The discussion of the small Δk structure factors in reference 14 was led with the characteristic temperature T_0 allowing only the use of the inequalities $T < T_0$ and $T > T_0$.

theorem and are valid in all liquids.[14] The proof given above is based on monatomic liquids. It should, however, remain valid in molecular liquids also, provided one considers only that part of their structure factor which is determined by the intermolecular interference effects. The wide generality of the preceding results stems from the following facts: their derivation assumes only the existence of a correlation function which is used in a rigorous theory of radiation scattering phenomena by a collection of scattering atoms with the assumed spatial correlations.

The structure factor F_L^2 is an even function of Δk, while $g(r,T)$ is an even function of r. Since an extremely general argument based on the repulsion of two atoms at close distances yields the rigorous result (3), the latter may be used to obtain semi-quantitatively the very large Δk-behavior of the structure factor. Equation (3) requires that

$$\lim_{\Delta k \text{ large}} [F_L^2(\Delta k,T)-1] \leqslant \varphi(T)/(\Delta k)^n; \quad n>3. \quad (14)$$

Here $\varphi(T)$ is some function of the temperature only. The structure factor of liquids has to tend toward unity, at very large Δk, faster then $(\Delta k)^{-3}$.

We are now prepared to discuss the various details of the results obtained in the present analysis of the liquid He⁴ structure factors. As previously intimated, the Fourier integrals (2) have been obtained as sums of two integrals, namely,

$$g(r,T)=g_1(r,T)+g_2(r,T)$$
$$=(1/2\pi^2 r)\left\{\int_0^{\Delta k}[F_L^2(\Delta k,T)-1][\sin r(\Delta k)]\right.$$
$$\times(\Delta k)d(\Delta k)+\int_{\Delta k}^{\infty}[F_L^2(\Delta k,T)-1]$$
$$\left.\times[\sin r(\Delta k)](\Delta k)d(\Delta k)\right\}, \quad (15)$$

where Δk was 1.0 A^{-1}. The upper limit in the second integral $g_2(r,T)$ is only symbolic, inasmuch as the integrand vanishes at a finite Δk-value. The approximate experimental structure factors reach unity at a finite Δk; the data used here suggested that, within experimental errors, F_L^2 was unity beyond about 6 A^{-1}.

We have to consider now the limiting $r\to 0$ value of $g(r,T)$ or $[-n(T)]$, by Eq. (3). The latter rigorous relation was not found to be satisfied by the experimental structure factors. This indicates, of course, the complete deficiency of the data as far as the important and rigorous relation (3) is concerned. The $g(r,T)$ functions had thus to be cut-off at small separations r. The following cut-off procedure has been used here:

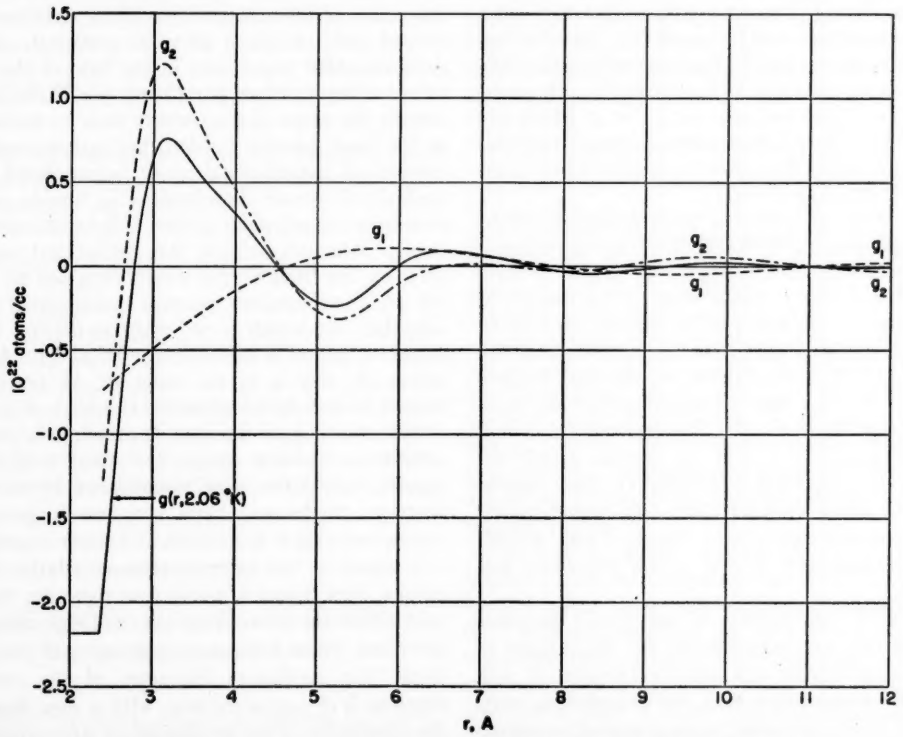

FIG. 3. Partial, $g_1(r)$, $g_2(r)$, and total correlation functions $g(r,T)$ as a function of the interatomic separation at 2.06°K.

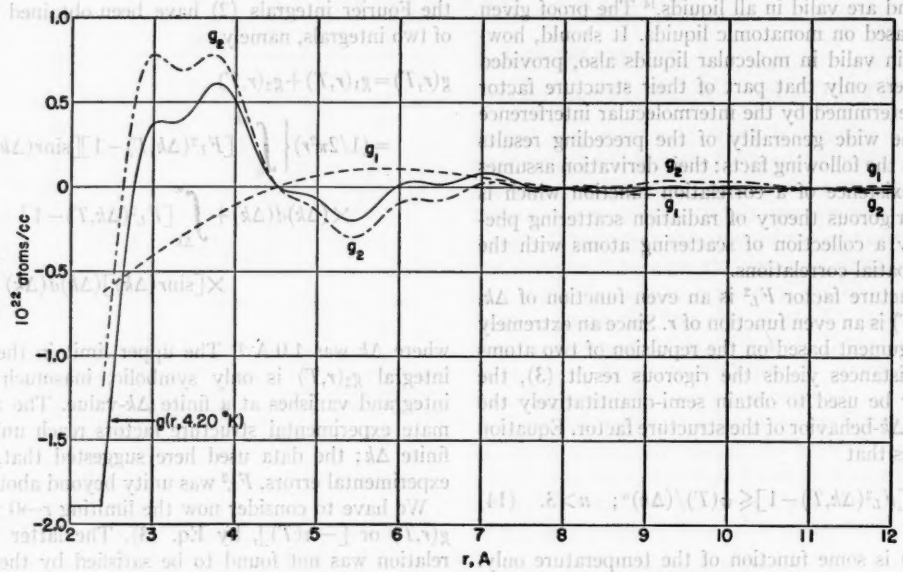

FIG. 4. Partial, $g_1(r)$, $g_2(r)$, and total correlation functions $g(r,T)$ as a function of the interatomic separation at 4.20°K.

the correlation functions had their first zero at about 2.8 A. At $r<2.8$ A, they fell toward increasingly large negative values, as they should. When they reached the value of $[-n(T)]$ at some value a of r, they were taken to be equal to $[-n(T)]$ at all $r\leqslant a$. At $r\geqslant a$ they were of course determined by the Fourier integrals (15). This procedure appears to be reasonable in spite of the angular point introduced into $g(r,T)$ at a. Physically this cut-off procedure is equivalent to postulating that the minimum closest distance of approach of two atoms is $a(T)$; this is a function of T.

We should like to give now some numerical results on the correlation functions resulting from the integrals (15). These results are presented in graphical form through Figs. 3 and 4. These refer to the two liquid temperatures of 2.06 and 4.20°K and are thus representative of the low- and high-temperature correlation functions. At both temperatures, we give the functions $g_1(r,T)$, $g_2(r,T)$, and their algebraic sum or the correlation function itself, $g(r,T)$. These results show that the contributions to $g(r,T)$ of the function $g_1(r,T)$ are of considerable importance not only at larger separations, as one might have expected, but throughout the whole r-range investigated here. Figures 3 and 4 exhibit clearly the application of the cut-off procedure just discussed.

A superficial examination of the $g(r,T)$ functions might lead one to underestimate the importance of these functions beyond the third extremum. It will, however, be shown below that this procedure is quite unjustified, unless, of course, one is prepared to analyze only the very close neighborhood picture.

It is believed that the results based on the evaluations of the component functions $g_1(r,T)$ and $g_2(r,T)$ are of interest for the whole field of the determination of atomic distributions in liquids. It is thus realized that the procedure of the extrapolation of the structure factors toward their vanishing Δk-value previously discussed acquires added importance in the light of the relative values of the functions $g_1(r,T)$ and $g_2(r,T)$. It is entirely outside the scope of the present work to review, even in the most cursory fashion, the rather considerable amount of experimental work accumulated on the analysis of atomic distributions in liquids, and this even from the sole point of view of the small momentum change structure factors. We cannot but emphasize here, on the basis of the results obtained by us over the whole temperature interval investigated, the considerable care which is necessary in dealing with the structure factors in the Δk-range $0\leqslant\Delta k\leqslant 1.0$ A^{-1}, or at values of $(\sin\theta)/\lambda$ in the range $0\leqslant\Delta k/4\pi\leqslant 0.08$ A^{-1}. Failure to include the structure factors over all or part of the preceding Δk-intervals in attempts to derive the correlation function cannot but yield results which, though, may have some resemblance to the correct function, might not have very much quantitative connection with it at medium and larger separations.

A glance at the representative correlation function graphs, Figs. 3 and 4, shows that there are characteristic differences between the low- and high-temperature functions. These differences originate with the g_2 functions. The oscillatory character of the correlation function is of course evident, with a slow damping of the amplitudes of the oscillations at large separations.

It is to be noted here that the evaluations of the Fourier integrals (15) were made with the help of the

experimental structure factors, Figs. 1 and 2, at every 0.025 A^{-1} interval in Δk. The $g(r,T)$ functions have been obtained at every 0.05 A in r, out to r equal to 20 A. The necessity of obtaining $g(r,T)$ at such close intervals was imposed by their future use which involved their integration. Since the Δk-intervals of integration were kept constant, it was of course realized that at increasing r-values, the integrand was approximated with a polygon of decreasing number of sides. Hence, at increasing r, the functions $g(r,T)$ tended to become less accurate. However, even at the largest separation of 20 A, the number of integration intervals per half cycle of the sine function in the integrands of (15) was never less than six. Indeed, with the Δk-interval of 0.025 A^{-1}, $r\Delta k$ is 0.5 radian at r equal to 20 A, and, hence, per half-cycle of the sine function, there were 2π integration intervals.

It is entirely outside the scope of the present work to investigate methods of evaluating numerically Fourier integrals. Nevertheless, an independent evaluation of $g(r,T)$ was made at 2.06°K liquid He temperature using a method[17] which did not have the limitations arising from the decreasing accuracy of integrations at large separations. In this method no approximations have been made at all in the integration of the sine function of the integrand of $g(r,T)$.

Let us, indeed, define the function $f(\Delta k,T)$ by

$$f(\Delta k,T)=[F_L^2(\Delta k,T)-1](\Delta k), \tag{16}$$

and rewrite (15) as

$$g(r,T)=(1/2\pi^2 r)\int_0^\infty f(\Delta k,T)\sin(r\Delta k)d(\Delta k), \tag{17}$$

the interval of integration is finite and extends from zero to ΔK. Assume that this finite interval has been divided into equal segments ϵ. Then,

$$g(r,T)=(1/2\pi^2 r)\left[\int_0^\epsilon f(\Delta k,T)\sin(r\Delta k)d(\Delta k) + \int_\epsilon^{2\epsilon} f(\Delta k,T)\sin(r\Delta k)d(\Delta k)+\cdots\right]. \tag{18}$$

The function $f(\Delta k,T)$, varying slowly in any small interval, may be replaced by $\bar{f}(\Delta k,T)$ its value in the middle of the small interval ϵ and we may thus write, with good approximation, integrating the sine function,

$$\begin{aligned} g(r,T)&\cong(1/2\pi^2 r^2)[-\bar{f}(0,\epsilon)\cos r\Delta k|_0^\epsilon - \bar{f}(\epsilon,2\epsilon)\cos r\Delta k|_\epsilon^{2\epsilon}-\cdots] \\ &=(1/2\pi^2 r^2)[\bar{f}(0,\epsilon)+[\bar{f}(\epsilon,2\epsilon)-\bar{f}(0,\epsilon)]\cos r\epsilon \\ &\quad+[\bar{f}(2\epsilon,3\epsilon)-\bar{f}(\epsilon,2\epsilon)]\cos 2r\epsilon+\cdots] \\ &=(1/2\pi^2 r^2)\left[f_1+\sum_{n=1}^{N}(f_{n+1}-f_n)\cos(nr\epsilon)\right]. \end{aligned} \tag{19}$$

[17] This was suggested by Mr. Bengt Carlson who is in charge of the Numerical Analysis Group.

Here, the range of integration has been divided into N equal intervals, and

$$f_n=\bar{f}((n-1)\epsilon, n\epsilon),$$

denotes the value of the function $f(\Delta k,T)$ in the center of the nth interval.

Using the preceding method at 2.06°K, the results of the direct method of integration have been fully checked. An advantage of this last method lies in the possibility of extending the evaluation of $g(r,T)$ over much wider separations r without loss of accuracy, in contrast with the more primitive method of direct integration, whose accuracy decreases at $r>15$ A.

The correlation function at 2.06°K has been studied with the help of Eq. (19) to rather large r-values. The function was found to be oscillatory and relatively slowly damped. But apart from the very large r-behavior of $g(r,T)$, one might have expected to find some tendency of these functions toward an asymptotic type of behavior below 20 A. This was not observed. It is true that the characteristic asymptotic expression of $g(r,T)$,[6]

$$\lim_{r\gg\rho} g(r,T)\cong(G(T)/4\pi\rho^2)\exp(-r/\rho)/r, \tag{20}$$

is derived[6] from considerations which do not involve scattering theory. But the scattering structure factors $F_L^2(\Delta k,T)$ determine uniquely the correlation functions $g(r,T)$ over their whole range and, in particular, at very large r, where the asymptotic expression (20) should result from the straightforward analysis of the structure factors. The range $\rho(T)$ of $g(r,T)$ or its square is given[6] by

$$[\rho(T)]^2=r_G^{(2)}(T)/[6n(T)kT\chi_T], \tag{21}$$

where, on the right-hand side the absolute value is to be taken if $r_G^{(2)}(T)$ is negative at $T<T_2$. Numerically, $\rho(T)$ could have been expected to be moderate at all the liquid temperatures investigated here. Hence, the appearance of the asymptotic form (20) at the larger separations r studied by us seems to be possible. No attempt will be made here to supply an explanation for the absence, at large r, of any tendency of the $g(r,T)$ functions toward their asymptotic form (20). It is, however, clear that, as a result, the correlation functions here derived cannot be used safely in integrals over monotonically increasing functions of r. It should be noted that (20) and (21) lose their precise meaning at the temperature T_2.

The problem of the convergence of the correlation functions may be considered also from the point of view of rather simple physical arguments. These functions give, by definition, the local excess or defect of the atomic concentrations from their mean value. Since the mean values $n(T)$ are not known to better than about a fraction of a percent, it would be somewhat illusory to use the correlation functions in regions of r where their extrema, positive of negative, reached values of, say, $\pm[n(T)/500]$, approximately. We give

TABLE I. Extrema of $g(r,T)$ and of the ratios $g(r,T)/n(T)$ at two liquid temperatures ($r>10$ A).

r A	$g(r,2.06°K)$ 10^{22} atoms/cc	$\frac{g(r,2.06°K)}{n(2.06°K)}$%	r A	$g(r,4.20°K)$ 10^{22} atoms/cc	$\frac{g(r,4.2°K)}{n(4.2°K)}$%
11.65	−0.00921	−0.420	10.10	0.00983	0.520
13.05	0.00841	0.383	10.70	−0.00210	−0.111
14.70	−0.00423	−0.193	11.10	0.00181	0.0959
15.75	0.00231	0.105	11.65	−0.00522	−0.276
17.05	−0.00156	−0.0711	12.25	0.00488	0.258
17.65	−0.00479	−0.0218	12.80	0.00105	0.0553
18.15	−0.00102	−0.0466	13.05	0.00169	0.0896
19.45	0.00213	0.0970	13.65	−0.00305	−0.161
			14.20	0.00108	0.0571

in Table I, the positions and values of the positive and negative extrema of $g(r,T)$, $r>10$ A, as well as the ratios g/n, at the two liquid temperatures of 2.06 and 4.20°K, with $n(2.06°K)$ and $n(4.20°K)$ equal, respectively, to 2.194 and 1.892×10^{22} atoms/cc. This Table I indicates that with the just-mentioned limitation of the physical significance of the values of $g(r,T)$, the latter would be well determined to separations $r\lesssim10-15$ A. One would thus expect that all those physical properties of the liquid which are evaluated as integrals with the correlation functions should be, in turn, determined by integrations extending to 10−15 A. Any extension of these integrals beyond these separations should not modify sensibly their values obtained at the limits of 10−15 A. It will be seen below that this is generally the case. It is to be remembered, however, that the preceding situation will be realized actually only if the integrands in question are sufficiently convergent. With fast monotonically increasing functions, as mentioned already, the preceding integration procedure with the $g(r,T)$ functions here derived cannot lead to the desired result.

In order to achieve a more rapid convergence of the $g(r,T)$ functions, a rather customary method could have been used, in principle. Namely, the direct method of evaluation of the integrals (15) could have been followed up to say 10−15 A. Beyond these separations, one might start integrating by parts the sine function in the Fourier integrals. This yields integrals which fall as r^{-2}, r^{-3}, ⋯, etc. However, this necessitates the numerical evaluation of the successive derivatives, with respect to Δk, of the structure factors $F_L^2(\Delta k,T)$, an operation fraught with considerable difficulties and uncertainties. This method did not appear to be usable here.

In concluding the study of the liquid helium correlation functions, we cannot but state that neither the expected very small r nor the possible very large r behavior of these functions have been verified. It is to be expected, however, that at the intermediate separations, $a\lesssim r\lesssim15$ A, the directly evaluated $g(r,T)$ functions should be good approximations to the presently unknown correct correlation functions of this liquid. That this is the case, essentially, will be shown below by investigating some integral properties of these functions.

An interesting method has been worked out[18] for the determination of the numbers of these first, second, ⋯, neighbors with the help of the surface concentrations $4\pi rn(r,T)$, and it has been used by one of us[1] to separations $r\sim6$ A. This method, though somewhat laborious at even relatively small separations, becomes quite difficult to use at larger separations where the peaks of the distributions $n(r,T)$ or $4\pi rn(r,T)$ become more and more smeared and less pronounced.

We have here obtained the function

$$N(r,T)=\int_0^r 4\pi r^2 n(r,T)dr, \tag{22}$$

which gives the number of atoms surrounding the origin atom in any sphere of radius r, complete isotropy being assumed throughout in the spatial distribution of the atoms. Clearly, the number of atoms in the spherical shell of thickness $(r'-r)$, is

$$N(r'-r,T)=N(r',T)-N(r,T). \tag{23}$$

If the function $N(r,T)$ is known for all relevant r-values, it becomes a relatively easy matter to locate the approximate positions of the successive spherical shells with their number of atoms in conjunction with the peaks in $g(r,T)$, $n(r,T)$, $4\pi rn(r,T)$, and $4\pi r^2n(r,T)$. Such an analysis of the spatial distribution of atoms and molecules in liquids has been made use of by Hildebrand.[19]

As an illustration of the spatial distribution of atoms in liquid helium we give in Fig. 5, the functions $N(r,2.06°K)$ and $N(r,4.20°K)$. To distances $r\simeq6$ A, these distribution numbers will be seen to be the same as those given before by one of us.[1] A comparison of these numbers with the limiting numbers

$$\bar{N}(r,T)=(4\pi r^3/3)n(T), \tag{24}$$

shows that the correct distribution (22) is always smaller than the limiting distribution (24). This is, of course, always the case at the temperatures $T<T_0$, T_0 being the intermediate temperature defined above, Eq. (9), at which $G(T)$ vanishes or at which the mean square isothermal fluctuation of the number of liquid atoms per atom is unity as in an ideal classical gas.[6] At temperatures $T_0<T<T_c$, the opposite situation prevails, insofar as the correct distributions $N(r,T)$ are in excess of the limiting distributions (24). In liquid He^4, the intermediate temperature T_0 was found to be[6] about 4.6°K.

Since, in the liquid He II region, the liquid contracts with increasing temperature at $1.25\leqslant T\leqslant2.18$°K, the

[18] G. S. Rushbrooke and C. A. Coulson, Phys. Rev. **56**, 1216 (1939).

[19] See the book of J. H. Hildebrand and R. L. Scott, *Solubility of Nonelectrolytes* (Reinhold Publishing Corporation, New York, 1950), third edition, pp. 62–105. See also, Henshaw, Hurst, and Pope, Phys. Rev. **92**, 1229 (1953).

pair distribution functions $n(r,T)$ automatically exhibit a parallel behavior insofar as their space integrals are increasing functions of the temperature. The liquid contraction also manifests itself somewhat through the slight decrease of the values of the cut-off separations $a(T)$, at and below which $n(r,T)$ vanishes. In the He II region, one finds that $da(T)/dT<0$, while $da(T)/dT>0$ in the He I region.

For the sake of completeness, we give in Table II a series of values, at $r\gtrsim 6$ A, of the pair distribution functions $n(r,T)$ at the two temperatures of 2.06 and 4.20°K, respectively.[20] While these functions have been calculated at many temperatures and close r-intervals, we give only these two distributions, representatives of the low- and high-temperature groups, at intervals of 0.2 A.

The limitations in the pair distribution functions are, of course, similar to those of the correlation functions. These concern their precise meaning at large separation, $r>15-20$ A, as well as their relative poorness at intermediate temperatures $2.50\lesssim T\lesssim 3.00-3.25$°K, as discussed above and in Sec. III.

TABLE II. The pair distribution functions $n(r,T)$ at two temperatures, in units of 10^{22} atoms/cc.

r A	$n(r,2.06°K)$ [$a=2.360$ A]	$n(r,4.20°K)$ [$a=2.384$ A]
6.0	2.20	1.90
6.2	2.25	1.92
6.4	2.277	1.910
6.6	2.283	1.913
6.8	2.277	1.95
7.0	2.26	1.974
7.2	2.24	1.966
7.4	2.22	1.93
7.6	2.20	1.89
7.8	2.18	1.879
8.0	2.16	1.883
8.2	2.15	1.882
8.4	2.15	1.87
8.6	2.16	1.864
8.8	2.17	1.87
9.0	2.18	1.88
9.2	2.19	1.894
9.4	2.20	1.894
9.6	2.209	1.893
9.8	2.214	1.896
10.0	2.214	1.90
	$\lim_{r\text{ large}} n(r,T)\to 2.194$	$\lim_{r\text{ large}} n(r,T)\to 1.892$

III. THE FLUCTUATION INTEGRAL. THE DEGREE OF APPROXIMATION ACHIEVED IN THE DERIVATION OF THE CORRELATION FUNCTIONS

We have seen in the preceding section that at one and only one of its points the value of the structure factor $F_L^2(\Delta k,T)$ is determined by purely macroscopic properties of the liquid. This is the value of F_L^2 at vanishing Δk, where Eq. (5) reduces strictly to

$$\lim_{\Delta k\to 0} F_L^2(\Delta k,T)=1+G(T)$$
$$=n(T)kT\chi_T. \qquad (25)$$

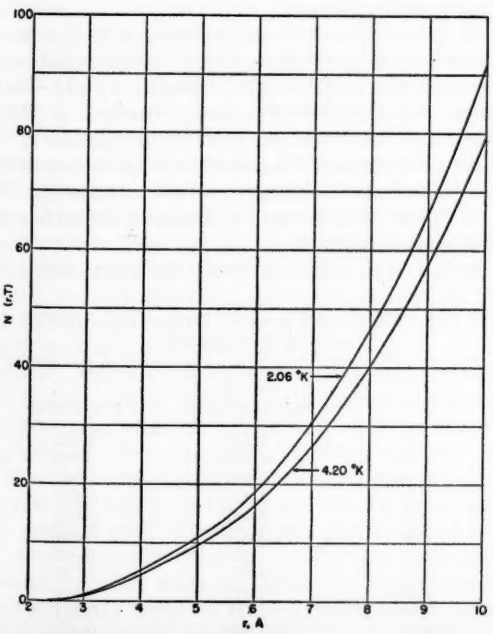

FIG. 5. The total number of liquid atoms $N(r,T)$ in spheres of radius r, around the central atom, at 2.06 and 4.20°K.

[20] For $r\lesssim 6$ A, see reference 1.

The space integral of the correlation function, the fluctuation integral, is $[n(T)kT\chi_T-1]$. This quantity is actually independent of the scattering data. It appears thus reasonable to state that the evaluation of the fluctuation integral $G(T)$ constitutes, at the present time, a method of checking the correlation functions $g(r,T)$ derived from the scattering data. It is to be remembered here that by the use of the rigorous limiting relation (3), which was adapted to our evaluation of the $g(r,T)$ functions through a cut-off method described in Sec. II, we have, strictly speaking, modified the experimental structure factor functions $F_L^2(\Delta k,T)$. It is, of course, expected that this modification should affect predominantly the F_L^2 functions at larger Δk values. One should also expect, nevertheless, that the F_L^2 functions derived from the correlation functions, modified in the sense of Eq. (3), should not be too different from the experimental structure factor functions.

The present attempt at assessing the degree of approximation achieved in the $g(r,T)$ functions, derived in the preceding section, is thus two-fold. On the one hand, the space or fluctuation integrals $G(T)$ have been obtained over the whole liquid He⁴ temperature interval explored. On the other hand, the $F_L^2(\Delta k,T)$ functions have been evaluated with the here-derived $g(r,T)$ functions at two representative temperatures, 2.06 and 4.20°K. These two types of checking of the correlation functions will now be discussed.

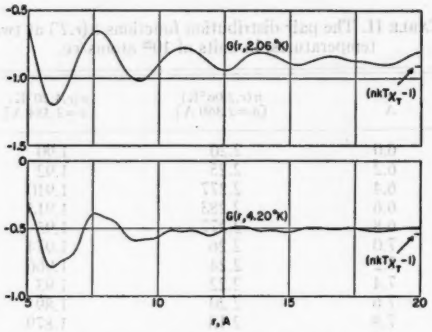

FIG. 6. The fluctuation integrals $G(r,T)$ as a function of r, at 2.06 and 4.20°K.

As far as the fluctuation integral $G(T)$ is concerned, it is being calculated with a function $g(r,T)$ which is known only to a finite though relatively large value of r, $r\simeq 20$ A. Hence we can obtain only

$$G(r,T)=\int_0^r 4\pi r^2 g(r,T)dr, \tag{26}$$

and we have to study this integral $G(r,T)$ as a function of its upper limit r. This was done at all the liquid temperatures investigated here. We give in Fig. 6 the $G(r,2.06°\text{K})$ and $G(r,4.20°\text{K})$ functions. The values of $\lim_{r\to\infty} G(r,T)$ or $[n(T)kT\chi_T-1]$ are also indicated in these graphs. It will be observed that beyond about $r\simeq 10-12$ A, the $G(r,T)$ functions closely approximate their limiting values $G(T)$ or $[n(T)kT\chi_T-1]$. Clearly, the $g(r,T)$ functions being oscillatory over their whole range at which they are available, the $G(r,T)$ functions, being negative at all the temperature $T\leqslant 4.20°\text{K}$, exhibit a series of extrema.

We give in Table III the last minima of the $G(r,T)$ functions. These are all negative, but their sign has been changed in the table. The third column gives the limiting $r\to\infty$ value of $[-G(r,T)]$ or $[1-n(T)kT\chi_T]$. An examination of the $G(r,T)$'s shows that beyond about 10−12 A they closely approximate their experimental values of $[n(T)kT\chi_T-1]$. One may thus feel justified in stating that *as far as their fluctuation integral test is concerned, the $g(r,T)$ functions obtained in the present work are satisfactory*. Clearly, there being no direct elementary test on the point behavior of the $g(r,T)$ functions themselves, the fact that they satisfy the integral test appears to be a justification for their use as representing at the present time the best available correlation functions of liquid He^4 in the temperature interval investigated.

The use of the minima of the $G(r,T)$ functions as the best representative of the $G(T)$ integrals originates in the following property of the correlation functions. The asymptotic behavior of the $g(r,T)$'s at the temperatures $T\leqslant 4.20°\text{K}$ requires that they tend toward the r-axis from below. This is apparent from the permanently negative values of $G(T)$ or $[n(T)kT\chi_T-1]$ at $T\leqslant 4.20°\text{K}$. This is interpreted by saying that the oscillatory functions $G(r,T)$ are better approximated at some finite r, if this r-value coincides with such a zero of this function which was reached from the negative side. The minima of the $G(r,T)$ integrals correspond precisely to these zeros r_0 of the $g(r,T)$'s at which $g(r_0-\epsilon, T)<0$, $\epsilon/r_0\ll 1$.

That the $G(r,T)$ values do not join smoothly in going from $T\leqslant 2.75$ to $T\geqslant 3.01°\text{K}$ was expected on the basis of the approximated structure factors, which are poorer in the transition region $2.50\leqslant T\leqslant 3.25°\text{K}$ than outside of it. This was briefly discussed in Sec. II.

In the evaluation of those properties of liquid helium which involve an integration of some function of the atomic separation r, with the correlation functions $g(r,T)$ as weight functions, one may expect that the so calculated quantity would be as well approximated as the approximation achieved by the $G(r,T)$ functions on their limit $G(T)$. The latter may be said, according to the present work, to amount to a few percent, at worst, in the relevant range of r, that is $r\simeq 15$ A. This will hold, provided that the quantity calculated is associated with a rigorous analytical expression of r. If, however, the analytical expression in question is only an approximation itself, then the accuracy with which this physical quantity has been obtained, after integration with $g(r,T)$, will be determined essentially by the over-all precision with which the analytical expression used in the calculations approximates the actual and correct expression of the physical property under consideration.

As discussed briefly in the preceding section, in those calculations of quantities which involve integration of the correlation function out to separations $r>15-20$ A, where the representation here obtained is either deficient or not available, as would be the case in the direct calculation of the positive even moments of the $g(r,T)$'s, one could not expect satisfactory results. This is, of course, an important limitation of the correlation functions here derived.

A method to obtain indirectly the lower order even

TABLE III. The last computed extrema of $[-G(r,T)]$ at various temperatures.

T°K	$-G(r,T)$ $18.55\leqslant r\leqslant 18.65$ A	$1-n(T)kT\chi_T$
1.25	0.922	0.953
1.50	0.913	0.942
1.75	0.900	0.931
2.06	0.901	0.915
2.25	0.886	0.902
2.50	0.860	0.884
2.75	0.827	0.860
3.01	0.887	0.830
3.25	0.845	0.802
3.50	0.784	0.757
3.75	0.689	0.697
3.97	0.624	0.628
4.20	0.520	0.542

positive moments of the correlation functions $g(r,T)$ has been discussed previously[6] and there is no need to consider it here again. A second indirect method exists also and we shall briefly describe it here. This consists in the fitting, by the method of least squares, for instance, the experimental structure factors or the difference,

$$F_L^2(\Delta k,T)-F_L^2(0,T)$$
$$=F_L^2(\Delta k,T)-n(T)kT\chi_T$$
$$=\sum_1^\infty(-)^n(\Delta k)^{2n}[r_G^{(2n)}/(2n+1)!], \quad (27)$$

where use was made of the definition of the moments (6), (8), and (10). A relatively low-order polynomial in $(\Delta k)^2$ should yield, in principle, with a fair degree of approximation the moments $r_G^{(2n)}$.

We should like to turn now to the second type of control of the correlation functions mentioned above. This concerns the numerical evaluation of the generalized structure factors, or

$$F_L^2(\Delta k,T,r)=1+\int_0^r\frac{\sin(r\Delta k)}{r\Delta k}4\pi r^2g(r,T)dr, \quad (28)$$

with the correlation function obtained here and modified at small separations r as discussed in Sec. II. These generalized structure factors depend on the upper limit r of the integral through which they are defined. The actual structure factors at liquid temperatures T not too close to the critical temperature, are the limits $r\to\infty$ of the $F_L^2(\Delta k,T,r)$ functions. The latter have been calculated at two liquid temperatures, 2.06 and 4.20°K, at intervals of Δk of 0.25 A^{-1}, and at intervals of 0.05 A in r, from the origin to 20.0 A. These integrals do not change practically beyond about 12 A and evidently belong to that class which should be fairly well approximated by the correlation functions derived here. We give in Table IV the values of $F_L^2(\Delta k,T,20\text{ A})$ and compare these calculated structure factors with the original experimental ones $(F_L^2)_{\text{exp}}$ given in Fig. 1. It will be seen that the agreement, in spite of the modification of the $g(r,T)$ functions, is satisfactory and these calculations provide us with a control of the internal consistency of the method of derivation of the $g(r,T)$ functions as well as of the numerical methods used in obtaining the generalized structure factors $F_L^2(\Delta k,T,r)$. The values at vanishing Δk are the arithmetic means at the three largest r-values of $G(r,T)$ at 2.06 and 4.20°K. A glance at Table IV shows that the modified $g(r,T)$ functions give rise, at $\Delta k>3$ A^{-1}, to structure factors which are smaller than the experimental ones. Still these calculated structure factors lie well within the estimated $\pm(5-7)$ percent mean errors given on the experimental values. At the smaller Δk-values the calculated structure factors $F_L^2(\Delta k,T,r)$ are larger than the experimental ones. It is to be remembered here that the uncertainties on the experimental structure factors are the largest at small and large Δk-values.

TABLE IV. The experimental $(F^2)_{\text{exp}}(\Delta k)$ and the calculated $F_L^2(\Delta k,T,20\text{ Å})$ structure factors at 2.06 and 4.2°K.

Δk A^{-1}	$(F_L^2)_{\text{exp}}(\Delta k,$ 2.06°K)	$F_L^2(\Delta k,$ 2.06°K,20 A)	$(F_L^2)_{\text{exp}}(\Delta k,$ 4.2°K)	$F_L^2(\Delta k,$ 4.2°K,20 A)
0.0	0.0820	0.089	0.458	0.478
0.25	0.0875	0.128	0.381	0.429
0.50	0.116	0.157	0.300	0.337
0.75	0.172	0.208	0.265	0.284
1.00	0.255	0.277	0.313	0.317
1.25	0.383	0.392	0.448	0.431
1.50	0.575	0.565	0.665	0.639
1.75	0.909	0.891	1.02	0.990
2.00	1.32	1.28	1.28	1.25
2.25	1.27	1.26	1.23	1.21
2.50	1.13	1.12	1.09	1.07
2.75	1.04	1.02	1.01	1.00
3.00	1.00	0.974	0.970	0.972
3.25	0.978	0.946	0.959	0.961
3.50	0.979	0.938	0.970	0.964
3.75	0.999	0.947	0.990	0.974
4.00	1.04	0.984	1.01	0.984
4.25	1.09	1.02	1.05	1.00
4.50	1.11	1.04	1.07	1.01
4.75	1.10	1.03	1.08	1.02
5.00	1.08	1.02	1.08	1.02
5.25	1.06	1.00	1.07	1.02
5.50	1.04	0.990	1.06	1.01
5.75	1.02	0.985	1.02	0.987
6.00	1.00	0.986	0.990	0.970

In closing this section on the verification of the correlation functions derived in Sec. II, it appears reasonable to say that, on the whole, the analysis performed in this work on the basis of the data of one of us[1,2] has led to a picture of the indirect atomic correlations, expressed by the $g(r,T)$'s, which should be rather good approximations to the actual correlations, at least out to separations $r\simeq 15$ A. It is, indeed, felt that the checking of the limiting large r-values of the $G(r,T)$'s at all the liquid temperatures here investigated, as well as the structure factors, Tables III and IV, constitute reasonable grounds for this belief. Clearly, the preceding method of checking does not provide us with a proof for the completely correct character of the correlation functions derived above. We are unaware of any existing methods of supplying for these functions a closer check than the one used by us.

IV. THE MEAN POTENTIAL ENERGY PER LIQUID He⁴ ATOM, CONFIGURATIONAL HEAT CAPACITIES. A PROOF OF THE KINETIC ENERGY ORIGIN OF THE LAMBDA TRANSITION

In any applications of the atomic distributions derived from x-ray scattering data in liquids, one has to keep in mind the inevitable limitations of the correlation functions $g(r,T)$ or the pair distribution functions $n(r,T)$. In addition, the physical property of the liquid under consideration, which is to be evaluated, has its own limitations. Such evaluations of elementary physical properties involve functions depending on interatomic or intermolecular separations r, their spatial

isotropy being actually realized or assumed. Here one has to face, in general, the contingency that the elementary physical property in question has only a more or less well justified analytical form, the latter being an approximation of its unknown correct analytical expression. In spite of these limitations which cannot but decrease the degree of quantitative or numerical approximations achieved on any elementary or atomic property in liquids, it is felt that unless the distribution functions derived are made use of in furthering the knowledge of elementary physical quantities in liquids, the derivation of the distribution functions *per se*, or for the sole purpose of comparison with distributions in the solid phase, tends to lead to some kind of a scientific impasse.

The first important application of the distribution function data has been made by Hildebrand and his collaborators.[21] They first used the distribution functions determined by them in liquid mercury for an investigation of the classical potential energy of this liquid. Subsequently, Hildebrand studied the potential energy in different liquids.

In these studies it is assumed that the total potential energy of the liquid formed by N atoms, or molecules, is the sum of the spatially isotropic potential energies of all its $N(N-1)/2$ pairs. In the present work on liquid He^4 this assumption will be retained. We have defined by Eq. (4), $dN(r,T)$ as the differential probability to find an atom in the volume element $dv(r)$, whose center is at a distance r from the origin atom. The differential potential energy, per atom, of the pair of atoms at the origin and at r, is

$$d\Phi(r,T)=\tfrac{1}{2}\varphi(r)dN(r,T)$$
$$=2\pi\varphi(r)n(r,T)r^2dr, \qquad (29)$$

where $\varphi(r)$ is the isotropic mutual potential energy of two stationary atoms in the system, separated by the distance r. The total potential energy, per atom, in the whose system is thus, exchange energy included,

$$\Phi(T)=2\pi\int_V \varphi(r)n(r,T)r^2dr, \qquad (30)$$

where the integral extends over the volume V of the system. At liquid temperatures $T<T_c$, T_c being its critical temperature, the integration may be extended over the whole space. The remarkable and simple formula due to Hildebrand[21] is rigorous within the limitations of the above mentioned assumption on the representation of the total potential energy of the liquid. At any rate, it seems reasonable to say that (30) is expected to be at least a first approximation to the classical potential energy, per atom, of the system in the case where the linear superposition of the pair potential energies turned out to be only the first term of a possible series expansion representation of the total potential energy of the liquid.

One of the major obstacles in the path of the extensive use of Eq. (30) is the general unavailability of the mutual potential energy function $\varphi(r)$ of two stationary atoms or molecules of the liquid under study.

In our case of liquid He^4, two approximate analytical expressions are available[22,23] for the total mutual potential energy of two stationary He^4 atoms. These two differ only in their attractive parts, the one including the mutual induced dipole-quadrupole interaction,[23] beside the dipole-dipole one, leads to a distinctly lower total potential energy. These two potential energy expressions are, respectively,

$$\varphi_{\rm I}(r)=Ae^{-\alpha r}-B_{\rm I}r^{-6},$$
$$\varphi_{\rm II}(r)=Ae^{-\alpha r}-B_{\rm II}r^{-6}-C_{\rm II}r^{-8}. \qquad (31)$$

The approximate range is $(1/\alpha)$, with α equal to $4.60\ A^{-1}$, r is in angstrom units, and the various constants are the following, in units of 10^{-11} ergs:

A	$B_{\rm I}$	$B_{\rm II}$	$C_{\rm II}$
77	0.149	0.139	0.370

Using the forms (31), we have calculated $\Phi_{\rm I}(T)$ and $\Phi_{\rm II}(T)$ at the various liquid temperatures at which the pair distribution functions $n(r,T)$ have been obtained. The mean potential energies per atom $\Phi(T)$ had, of course, to be studied as a function of the upper limit r of the integral in their definition of Eq. (30). In view of the rapid convergence of the potential energy inte-

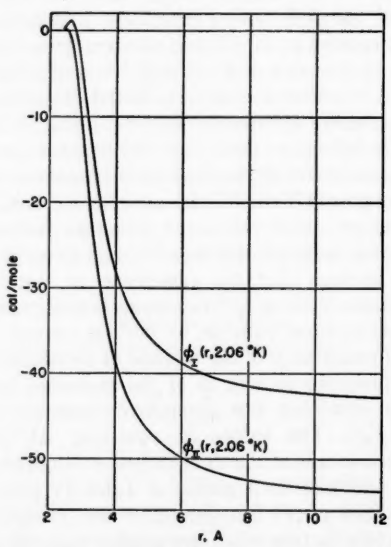

FIG. 7. The mean potential energies per liquid He^4 atom $\Phi_{\rm I}(r,T)$ and $\Phi_{\rm II}(r,T)$, at 2.06°K, as a function of r, for the two analytical approximations of the mutual potential energy of two stationary isolated He^4 atoms.

[21] J. H. Hildebrand and S. E. Wood, J. Chem. Phys. **1**, 817 (1933). For the literature of the work of the Berkeley group see the book quoted in reference 19.

[22] J. C. Slater and J. G. Kirkwood, Phys. Rev. **37**, 682 (1931).

[23] H. Margenau, Phys. Rev. **56**, 1000 (1939).

grals (30), the limiting large r values of the potential energies are reached already at the relevant separations $r \simeq 10-12$ A. This is seen in Fig. 7 which gives $\Phi_{\rm I}(r,2.06°{\rm K})$ and $\Phi_{\rm II}(r,2.06°{\rm K})$. We give in Table V the values of $\Phi_{\rm I}(T)$ and $\Phi_{\rm II}(T)$ at the various liquid temperatures at the extreme separation of 20 A. It will be seen that $\Phi_{\rm II}(T)$ is about $(5/4)\Phi_{\rm I}(T)$. In part of the present investigation, however, the actual numerical values of the mean potential energies are of no importance. What is, however, of major qualitative significance is their decreasing trend with increasing liquid temperature in the He II region, and their increasing trend with increasing temperature in the He I region. The potential energy functions $\Phi_{\rm I}(T)$ and $\Phi_{\rm II}(T)$ have a cusp at the lambda point. This result is in agreement with what one might have expected on the basis of the observed peculiar contraction of liquid He II, at $T \gtrsim 1.25°$K, with increasing temperature and the normal expansion of liquid He I with increasing temperatures.

In order to fully exploit the numerical results in Table V, it is necessary to write down formally the expression of the total energy of the liquid. In so doing, we shall still be on very general grounds. Indeed a rigorous quantum mechanical solution of the liquid He⁴ problem is expected to yield, after ensemble averaging, an expression of the type

$$E_{\rm tot}(T)=E_{\rm kin}(T)+\Phi(T). \tag{32}$$

The total energy of the liquid at temperature T, $E_{\rm tot}(T)$ is the sum of the classical kinetic, $E_{\rm kin}$, and potential plus quantum-mechanical exchange, $\Phi(T)$, energies. In forming the ensemble average of the energies in (32), the term $E_{\rm kin}$ will depend critically on the momentum space distribution of the system. Let us now define the configurational heat capacity of our system by

$$\Gamma(T)=d\Phi(T)/dT. \tag{33}$$

All heat capacities to be considered will be associated with the saturated liquid. With (32) and (33), we obtain

$$C_{\rm tot}(T)=[dE_{\rm kin}/dT]+\Gamma(T), \tag{34}$$

for the total calorimetrically measurable heat capacity of the liquid. Experimentally, $C_{\rm tot}(T)$ is a rapidly increasing function of the temperature below the lambda point and a decreasing function above the lambda point, over some small temperature interval.[24] The characteristic lambda anomaly is expressed by

$$\Delta C_{\rm tot}=C_{\rm tot+}-C_{\rm tot-}<0, \quad (T=T_\lambda), \tag{35}$$

the + and − subscripts referring to the high- and low-temperature sides of the transition temperature T_λ. In contrast with the lambda anomaly of the total heat capacity, the configurational heat capacity has an inverted lambda anomaly. Since $\Phi(T)$ has a cusp at the lambda point, one finds Γ_- or $\Gamma(T<T_\lambda)<0$, and Γ_+ or $\Gamma(T>T_\lambda)>0$, as shown by the potential energies $\Phi(T)$ of Table V. This was the behavior of major qualitative significance pointed out in the aforementioned. The discontinuity of the configurational heat capacity is

$$\Delta\Gamma(T_\lambda)=\Gamma_+(T_\lambda)-\Gamma_-(T_\lambda)>0. \tag{36}$$

Its sign is opposite to that of the total heat capacity (35). Hence, independently of the actual numerical values of the configurational heat capacity $\Gamma(T)$, one has to conclude that the observed lambda anomaly of the total liquid helium heat capacity is strictly of kinetic energy origin. It is thus connected with the temperature variation of the distribution of the liquid He⁴ atoms in momentum space.

With the aforementioned behavior of $\Gamma(T)$, it will be seen that at $1.25°{\rm K}<T<T_\lambda$, the kinetic heat capacity is larger than the total heat capacity. Also, in a limited temperature range beyond T_λ, the decreasing kinetic heat capacity is still larger than the increasing positive configurational heat capacity.

The proof given here of the kinetic energy origin of the lambda anomaly in liquid helium appears to be quite general though involving the derived pair distribution functions and the use of the approximate mutual potential energies of a pair of stationary He⁴ atoms. The proof obtained seems to provide a solid foundation for the development of the theory of liquid helium concerning its momentum space behavior.

It is also of interest to consider the approximate numerical values of the configurational heat capacity $\Gamma(T)$ resulting from the approximate potential energies $\Phi_{\rm I}(T)$ and $\Phi_{\rm II}(T)$. In order to obtain $\Gamma_{\rm I}(T)$ and $\Gamma_{\rm II}(T)$ associated with the potential energies $\Phi_{\rm I}$ and $\Phi_{\rm II}$, we have fitted these with parabolae of the form

$$\Phi_\sigma(T)=a_\sigma+b_\sigma T+c_\sigma T^2. \quad \sigma={\rm I, II}. \tag{37}$$

These yielded at once the heat capacities:

$$\Gamma_\sigma(T)=d\Phi_\sigma/dT =b_\sigma+2c_\sigma T, \tag{38}$$

linear in T over the restricted temperature ranges where the parabolic fits have been obtained. The various constants of the parabolas (37) are given in Table VI

TABLE V. Mean potential energies $\Phi_{\rm I}(T)$ and $\Phi_{\rm II}(T)$ per atom in liquid helium at various temperatures.

T°K	$\Phi_{\rm I}(T)$ cal/mole	$\Phi_{\rm II}(T)$ cal/mole
1.25	−43.04	−53 95
1.50	−43.08	−54.00
1.75	−43.10	−54.03
2.06	−43.25	−54.29
2.25	−43.30	−54.34
2.50	−43.08	−54.02
2.75	−42.77	−53.58
3.01	−40.15	−50.69
3.25	−39.71	−50.07
3.50	−39.18	−49.33
3.75	−38.55	−48.48
3.97	−37.91	−47.58
4.20	−37.12	−46.47

[24] See the monograph of W. H. Keesom, *Helium* (Elsevier Publishing Company, Inc., Amsterdam, 1942), pp. 211–226.

TABLE VI. Coefficients of the parabolic fits of the mean potential energies per atom in liquid helium.

Temperature range	a_I cal/mole	a_{II}	b_I cal/mole×deg	b_{II}	c_I cal/mole×(deg)^2	c_{II}
$1.25 \leqslant T \leqslant 2.10$°K	−43.17	−54.39	0.3192	0.8234	−0.1710	−0.3765
$3.05 \leqslant T \leqslant 4.20$°K	−36.77	−46.33	−3.711	−4.957	0.8635	1.1705

in the two temperature intervals $1.25 \leqslant T \leqslant 2.10$°K and $3.05 \leqslant T \leqslant 4.20$°K. The parabolas in the liquid He II range actually extend up to 2.25°K, which is the "apparent" lambda temperature in these calculations. Actually, if we had performed the calculation of the correlation function at the empirical lambda point of about 2.18°K, the pair distribution functions in Eq. (35) would have led to the inverted cusp of the $\Phi(T)$ functions at this correct lambda temperature. We give in Table VII the configurational heat capacities $\Gamma_\sigma(T)/R$, in molar units. The heat capacities at $T < 2.25$°K, refer to the decreasing negative branches of the discontinuous functions $\Gamma_I(T)$ and $\Gamma_{II}(T)$. It is expected that the potential energy function $\Phi_{II}(T)$, which is likely to overestimate the actual mean potential energy, in absolute value, should give rise to configurational heat capacities $\Gamma_{II}(T)$ in excess of their actual values. A glance at Table VII shows that, in the liquid He II range, $1.25°K < T < T_\lambda$, the $\Gamma(T)$ values are quite small in comparison to the total heat capacities.[25] In the vicinity of the lambda point, on its low temperature side, Γ_I and Γ_{II} amount, respectively, to about 3 and 6 percent of the total heat capacity. While in the He II region, the Γ's are small fractions of the total heat capacity, they tend to become dominant at high temperatures, in the He I region. At $T > 3$°K, $\Gamma_I(T)$ seems to have plausible values, while Γ_{II} is quite large, and at $T > 3.5$°K it turns out to be larger than the total heat capacity, whose experimental accuracy may be low here. This indicates that $\Phi_{II}(T)$ is likely to be in excess, in absolute value, of the actual mean potential energy per atom at these temperatures. At any rate, there is a qualitative change in the roles played by the configurational heat capacity in the He II and He I regions, respectively, when compared to the total heat capacity.

The anomalous behavior of $\Gamma(T)$ in the He II region appears to be the manifestation of some elementary property of this liquid, wherein this potential part of the heat capacity tends to oppose the extreme anomaly exhibited by the kinetic heat capacity. In terms of a more elementary picture, not involving directly temperature derivatives, the peculiar behavior of the liquid density in the He II region seems to correspond to some kind of defense mechanism tending to counteract the dominating anomaly which originates in the momentum space properties of the liquid. It is noteworthy that the late F. London[25] has emphasized, through qualitative considerations, that the peculiar behavior of the density of liquid He II is a manifestation of the opposition by the liquid to its assumed Bose-Einstein condensation process. This opposition was presumed to originate in the classical mutual atomic interactions.

The quantitative results obtained in the present work which led to the picture just discussed by us, are based on quite general grounds. In particular the details of the mechanism of the dominant lambda phenomenon were not needed at all, while a proof could be given of its momentum space origin.

Finally, a few remarks may be of interest here concerning the expected behavior of $\Gamma(T)$ below 1.25°K. It is seen on Table VII that $\Gamma(T)$ increases with decreasing temperatures. It may be expected that $\Gamma(T)$ will vanish at some temperature below 1.25°K to reach a positive maximum and to remain positive at low temperatures, tending to vanish there, from positive values, at the approach of the absolute zero. This behavior would be similar to that of the expansion coefficient of liquid He II which, as predicted,[26] became positive at low enough temperatures.[27] This expansion coefficient should also have a positive maximum before tending to vanish, from the positive side, at the approach of the absolute zero.

TABLE VII. Configurational heat capacities $\Gamma_I(T)$ and $\Gamma_{II}(T)$ in units of R at various temperatures.

T	$\Gamma_I(T)/R$	$\Gamma_{II}(T)/R$
1.25	−0.055	−0.059
1.50	−0.098	−0.154
1.75	−0.141	−0.249
2.10	−0.201	−0.381
2.25	−0.227	−0.428
3.05	0.784	1.10
3.25	0.958	1.33
3.50	1.17	1.63
3.75	1.39	1.92
4.00	1.61	2.22
4.20	1.78	2.45

ACKNOWLEDGMENTS

We wish to thank Mr. Bengt Carlson for his cooperation in the planning of the numerical calculations. We are indebted to Mr. Max Goldstein both for planning and coordinating the numerical work. His independent studies on a number of problems raised in the course of the numerical analysis were of great help in the present work.

The major part of the machine calculations has been performed by Mr. P. E. Harper. Mr. Chester S. Kazek, Jr., has also lent his collaboration in this work. We deeply appreciate their cooperation. Our thanks are equally due to Miss M. L. Johnson and Mrs. J. E. Powers for numerous hand calculations, and to Mrs. A. M. Snowden and Mrs. L. E. Moss for various calculations and the preparation of the graphs.

[25] F. London, J. Chem. Phys. 11, 203 (1943).

[26] L. Goldstein, Phys. Rev. 89, 597 (1953).

[27] K. R. Atkins and M. H. Edwards, Phys. Rev. 93, 1416 (1954).

Results of Limitations on Space Current Densities in Galactic and Intergalactic Space*

W. F. G. SWANN
Bartol Research Foundation of The Franklin Institute, Swarthmore, Pennsylvania, and
The Franklin Institute Laboratories for Research and Development, Philadelphia, Pennsylvania
(Received January 25, 1955)

The accepted view as to the very high electrical conductivity of space has raised difficulties in mechanisms concerning the production of cosmic-ray energies. It is to be observed that high conductivity does not avoid the existence of a saturation on current density, i, which is equal to nec, where n is the sum of the numbers of positive and negative ions per cc. Thus for $n=1$, the saturation current density is of the order 5×10^{-9} ampere/cm². The effect of saturation is illustrated by the following idealized conditions.

Consider two coplanar rings of gas A and B, A being the smaller. Under conditions of very high conductivity, it would be impossible for the magnetic flux through either circuit to change and the electric field would be zero. If B expands, the flux through A due to B will change, but the total flux through A will not change if A has high conductivity. A will acquire induced current to compensate the change of flux arising from B. However, as time proceeds, and if the ionic density in A is small, a stage will be reached at which A can no longer develop the current necessary for magnetic flux compensation. An electric field will now arise in A and the ions will become accelerated to cosmic-ray energies, not by appreciable alteration of velocity which has already attained its maximum c, but by alteration of relativistic mass.

INTRODUCTION

THE fact that the conductivity of interstellar space is, to a first approximation, independent of the density and is comparable with that of a completely ionized gas at atmospheric pressure, amounting in fact to 2 percent of the conductivity of copper, has played an important role in cosmological considerations pertaining to cosmic-ray phenomena. It is to be observed, however, that in spite of the large conductivity for small fields, an upper limit depending upon the absolute number of ions per cc is placed upon the attainable current density. The current density, i, cannot, in fact, exceed the value given by

$$i=nec,$$

where n is the sum of the numbers of positive and negative ions per cc, so that, in the truly rather extreme case where $n=1$, we have

$$i\sim5\times10^{-10}\times3\times10^{10}/3\times10^{9}\sim5\times10^{-9}\text{ ampere/cm}^2.$$

It is interesting to trace the implications of the above matter. Problems of a cosmological nature are apt to assume forms in which the relevant matters, sometimes of a simple nature, tend to become obscured by more or less irrelevant matters of a complex nature. For this reason, it becomes desirable to discuss more or less idealized problems in which an attempt is made to avoid the difficulties involved in the complexities without destroying the content of the fundamentals. In what follows, this policy should be borne in mind.

AN IDEALIZED PROBLEM

A problem illustrating the significance of the role played by limitation of the current density is the following (see Fig. 1).

We envisage a large ring of gas B, with ample ionic content, so that it never runs the danger of approaching a saturation current density. In the plane of this ring is another smaller ring of gas A which has a small ionic content and which, as a consequence, will, under suitable circumstances, approach a saturation current density.[1]

We shall suppose that initially B carries a current I_{20} which diminishes with time increase, so that a current is induced in A. It will be convenient to endow B with an ohmic resistance R, so as to provide for the decay of I_{20}, but the essential elements of the problem will best be illustrated by assuming that A has no resistance.[2]

We shall first study the case where there is no current density limitation in either A or B. Subscript (1) shall apply to A and subscript (2) to B. The simple Lagrangian function for the system, with the current in

FIG. 1. Two concentric rings of gas. The current in B decays, generating induced current in A.

* Assisted in part by the joint program of the Office of Naval Research and the U. S. Atomic Energy Commission.

[1] We choose the rings coplanar so as to insure that the mechanical forces of electromagnetic origin shall not complicate the considerations by demanding relative motions of the rings.

[2] The problem is, of course, greatly idealized. Thus, we are imagining that there are some kinds of constraints which cause the currents to be confined to the rings and not wander off into space. We can hardly suppose R to arise from the elementary kinetic theory of resistance as in such a case its effect would, in the case of dimensions of large scale, be insignificant in relation to the inertia of self-induction. The resistance R simply symbolizes a mechanism by which we can, with consistency, *allow* the current in B to decay.

electrostatic units, will be $\mathfrak{L}$, where

$$\mathfrak{L}=\frac{1}{c^2}(\tfrac{1}{2}L_{11}I_1^2+L_{12}I_1I_2+\tfrac{1}{2}L_{22}I_2^2) \quad (1)$$

the L's being the coefficients of self- and mutual-inductance. The dissipation function F is

$$F=\tfrac{1}{2}RI_2^2.$$

The application of Lagrange's equations yields

$$\frac{d}{dt}(L_{11}I_1+L_{12}I_2)=0, \quad (2)$$

$$\frac{d}{dt}(L_{12}I_1+L_{22}I_2)+Rc^2I_2=0. \quad (3)$$

Equation (2) yields

$$L_{11}I_1+L_{12}I_2=N_1, \quad (4)$$

where N_1 is a constant.

Equations (3) and (4) then readily yield

$$I_2=I_{20}\epsilon^{-\alpha t},$$

where

$$\alpha=Rc^2L_{11}/(L_{11}L_{22}-L_{12}^2),$$

and I_{20} is the value of I_2 at $t=0$. The time constant of B is $\tau=1/\alpha$.

Suppose that, at $t=0$, we start with a condition in which there is no current in A, so that the flux through A is $L_{12}I_{20}=N_1$.

As I_2 diminishes, the flux $L_{12}I_2$, contributed by B through A, diminishes, so that A has to acquire an induced current I_1 to keep the flux N_1 constant.

Provided that there is a plentiful supply of ions in A, the current which it is called upon to acquire will be a current composed of a large number of ions moving with a relatively small velocity. If, however, the ionic density in A is small, the current developed in it will be composed of a small number of ions moving with a high velocity. When the current density demanded in A exceeds the value nec, the demands for increase of current will fail to be met, and the magnetic flux through A will cease to remain constant.[3] There will be a net rate of increase of flux through A and a *resultant* electromotive force, and so an electric field, which field never exists so long as A can increase its current without limit. The field will continue to give energy to the ions, not by increasing their velocities appreciably, since the velocity has already reached a value nearly equal to c, but by increasing the relativistic mass of the ions. In other words, by drawing upon the importance of a very slight difference between v and c in the expression for the mass m $[=m_0(1-v^2/c^2)^{-\frac{1}{2}}]$, the field, so long as it exists, is able to pump energy without limit into A. In this way cosmic-ray energies may be acquired by A.

If one asks what explanation is to be given of the invalidity of (4) for this case, the answer is that our original Lagrangian must be regarded as in error in a manner which will be clear from the following:

We shall simplify the discussion by confining ourselves to ions of one sign. This is not necessary, but will avoid algebraical complexity which tends to obscure the essentials. In a more complete presentation we, of course, include charges of both signs.

For ions of one sign, our Lagrangian assumes the form

$$\mathfrak{L}=-\sum m_0c^2(1-\beta_1^2)^{\frac{1}{2}}-\sum m_0c^2(1-\beta_2^2)^{\frac{1}{2}}+\frac{L_{11}}{2c^2}I_1^2+\frac{L_{22}}{2c^2}I_2^2+\frac{L_{12}}{c^2}I_1I_2, \quad (5)$$

where β_1 and β_2 are equal to v_1/c and v_2/c respectively. The summations are for all of the ions concerned. We shall suppose m_0 to correspond to the mass of a *proton*.

If, for simplicity, we suppose that β_1 is the same for all the ions in A and β_2 is the same for all the ions in B, and if V_1 and V_2 are the volumes of the rings A and B respectively, and n_1 and n_2 the ionic densities,

$$\sum m_0c^2(1-\beta_1^2)^{\frac{1}{2}}=m_0c^2n_1V_1(1-\beta_1^2)^{\frac{1}{2}},$$
$$\sum m_0c^2(1-\beta_2^2)^{\frac{1}{2}}=m_0c^2n_2V_2(1-\beta_2^2)^{\frac{1}{2}}.$$

If, further, we write $I_1=n_1ec\beta_1a_1$ and $I_2=n_2ec\beta_2a_2$, where the a's are the cross-sectional areas of the rings,

$$\mathfrak{L}=-m_0c^2n_1V_1(1-\beta_1^2)^{\frac{1}{2}}-m_0c^2n_2V_2(1-\beta_2^2)^{\frac{1}{2}}+(L_{11}/2c^2)(n_1ec\beta_1a_1)^2+(L_{22}/2c^2)(n_2ec\beta_2a_2)^2+(L_{12}/c^2)(n_1ec\beta_1a_1)(n_2ec\beta_2a_2).$$

The dissipational function is, as before, RI_2^2 $=R(n_2ec\beta_2a_2).^2$

If we take v_1 and v_2 as our velocity variables, Lagrange's equations now yield

$$n_1v_1\frac{d}{dt}\frac{m_0v_1}{(1-\beta_1^2)^{\frac{1}{2}}}+\frac{1}{c^2}\frac{d}{dt}\times[L_{11}n_1ea_1(n_1ec\beta_1a_1)+L_{12}(n_1ea_1)(n_2ec\beta_2a_2)]=0,$$

[3] It is of interest to observe that in a practical case the potentiality of A to keep the flux through itself constant is very limited if n is small, so that in the problem under consideration, for example, the stage at which this limitation sets in may occur before the flux through A due to B has changed by more than a very small amount; and, of course, the attainment of this stage marks the time when the particles have attained a velocity nearly equal to c and are on their way to cosmic-ray energies. It is of interest to consider a few reasonable orders of magnitude.

Consider, for example, the case where A has a mean radius R, and a radius r for the cross section of the ring itself. The maximum field H_m which it can produce at its center is given by $H_m=(2\pi/Rc)(\pi r^2)(nec)\sim(10^{-8}r^2/R)n$. If $2r/R=0.1$, $H_m\sim2\times10^{-11}Rn$. If $R=10^8$, then, in order to have $H_m=1000$, we must have $n=5\times10^5$, which corresponds to about 2×10^{-11} mm of mercury pressure.

$$\frac{d}{dt}\frac{m_0v_2}{(1-\beta_2^2)^{\frac{1}{2}}}+\frac{1}{c^2}\frac{d}{dt}$$

$$\times[L_{22}n_2ea_2(n_2ec\beta_2a_2)+L_{12}(n_2ea_2)(n_1ec\beta_1a_1)]$$

$$+n_2ea_2R(n_2ec\beta_2a_2)=0.$$

If l_1 and l_2 are the mean circumferences of the rings,

$$\frac{l_1c^2}{e}\frac{m_0v_2}{(1-\beta_1^2)^{\frac{1}{2}}}+L_{11}I_1+L_{12}I_2=N_1=\text{const}, \quad (6)$$

$$\frac{l_2c^2}{e}\frac{m_0v_2}{(1-\beta_2^2)^{\frac{1}{2}}}+L_{22}I_2+L_{12}I_1+Rc^2\int_0^t I_2dt$$

$$=N_2=\text{const}. \quad (7)$$

To crystallize the problem further, let us suppose that circuit B has a mean radius R_2 equal to 2×10^9 cm, and a radius of cross section r_2 equal to 10^8 cm, so that $l_2=2\pi R_2$ and $a_2=\pi r_2^2$. Suppose that the initial value I_{20} of I is such as to produce a field H_2 equal to 1000 gauss at the center of B. Then

$$H_2=2\pi I_2/R_2c,$$

$$I_{20}=R_2cH_2/2\pi=2\times10^9\times3\times10^{10}\times1000/2\pi\sim10^{22}\text{ esu},$$

$$\pi r_2^2n_2v_2e=10^{22},$$

$$n_2v_2=\frac{10^{22}}{\pi\times10^{16}\times4.8\times10^{-10}}\sim7\times10^{13}.$$

Thus, if $n_2=3\times10^{13}$, which corresponds to about 10^{-6} atmosphere, we can have v_2 as low as 2 cm/sec. For this value, β_2 in (7) is negligible, and the ratio of the term containing m_0 to $L_{22}I_2$ is η, where

$$\eta=\frac{2\pi R_2c^2m_0v_2}{L_{22}eI_2}\sim\frac{2\pi R_2c^2m_0v_2}{L_{22}e^2\pi r_2^2n_2v_2}\sim\frac{2\pi R_2c^2m_0}{L_{22}e^2\pi r_2^2n_2}.$$

Since $2\pi^2R_2\sim L$ and $n_2\sim3\times10^{13}$, $\eta\sim2\times10^{-15}$. This conclusion as to the smallness of η holds, of course, for a wide range of the parameters assumed. Thus, we may neglect the term containing m_0 in Eq. (7).

The maximum value of I_1 is $\pi r_1^2n_1ce$, i.e.,

$$(I_1)_{\max}\sim3\times10^{14}\times3\times10^{10}\times4.8$$

$$\times10^{-10}n_1\sim0.5\times10^{16}n_1\text{ esu}.$$

Even if n_1 is as large as 10^4 ions per cc, this is small compared with I_{20} as calculated above, and since $L_{12}<L_{22}$, the term $L_{12}I_1$ is negligible compared with $L_{22}I_2$. Thus, Eq. (7) may be written

$$L_{22}I_2+Rc^2\int_0^t I_2dt=\text{const}, \quad (8)$$

$$L_{22}dI_2/dt+Rc^2I_2=0. \quad (9)$$

This tells us, as we might have guessed intuitively, that the equation for the circuit B (with its plentiful supply of ions) is unaffected to a first approximation by the term containing m_0, and is also unaffected by the inductive action of the current limited circuit A.

From (9),

$$I_2=I_{20}e^{-t/\tau}, \quad (10)$$

where τ is the time constant L_2/Rc^2 of the circuit B.

Substituting this value of I_2 in (6) and (7), we obtain, neglecting the term involving v_2 and β_2, for the reasons stated,

$$\frac{l_1c^2}{e}\frac{m_0v_1}{(1-\beta_1^2)^{\frac{1}{2}}}+L_{11}I_1+L_{12}I_{20}e^{-t/\tau}=N_1, \quad (11)$$

$$L_{12}I_1+L_{22}I_{20}e^{-t/\tau}+L_{22}I_{20}[1-e^{-t/\tau}]=N_2. \quad (12)$$

Multiplying (12) by L_{11}/L_{12} and subtracting from (11), we get

$$\frac{l_1c^2}{e}\frac{m_0v_1}{(1-\beta_1^2)^{\frac{1}{2}}}+\left(L_{12}e^{-t/\tau}-\frac{L_{11}L_{22}}{L_{12}}\right)I_{20}-N_1-\frac{L_{11}}{L_{12}}N_2=0.$$

Hence

$$\frac{l_1c^2}{e}\left[\frac{m_0v_1}{(1-\beta_1^2)^{\frac{1}{2}}}-\frac{m_0v_{10}}{(1-\beta_{10}^2)^{\frac{1}{2}}}\right]=L_{12}I_{20}(1-e^{-t/\tau}),$$

where v_{10} and β_{10} refer to $t=0$.

Hence, if $v_{10}=0$, the momentum of the particle by the time I_2 has fallen by $1/e$ of its original value is

$$M=\frac{m_0v_1}{(1-\beta_1^2)^{\frac{1}{2}}}=\frac{eL_{12}}{l_1c^2}\left(1-\frac{1}{e}\right)I_{20}.$$

If v_1 is nearly equal to c, as will presently appear to be the case, we may write for the energy W

$$W=Mc=\frac{eL_{12}}{l_1c}\left(1-\frac{1}{e}\right)I_{20},$$

or, in electron volts,

$$W\sim300\frac{L_{12}}{l_1c}(\tfrac{2}{3})I_{20}.$$

Since $l_1=2\pi R_1$, and $L_{12}I_{20}/c=\pi R_1^2H_{20}$, where H_{20} is the initial field at the center of B at $t=0$, with $R_1=2\times10^8$ cm, and $H_{20}=1000$ gauss,

$$W\sim100R_1H_{20}=2\times10^{13}\text{ ev}.$$

This, of course, carries with it the conclusion that $v_1\sim c$ and justifies the approximate assumption to that effect.

COMMENTS ON THE SPECIALIZATION OF THE PROBLEM

The foregoing problem is specialized in the sense that the *reason* for the rate of change of the magnetic field of B has not been defined. We are relying on the fact that the magnetic fields of large cosmical entities *do* change with time. We have symbolized the reason for this change through the assumption of a resistance R for B as a whole. However, this resistance must not be associated with the ordinary resistance to be expected of the ring regarded as a completely ionized gas. Such a resistance would be so small that the time constant τ would be enormous.

A more physically understandable process by which the field due to B at its center can change rapidly with time is one in which the ring B expands under the influence of the currents on it. An illustration of such a problem has been given by the present writer.[4] By such processes, reasonably rapid decay of the field at the center of B can occur.

We have arbitrarily supposed that the currents are confined to the rings A and B as though these were solid conductors. Such a process can only be justified for a gas if the ionic orbits themselves validate the perpetuation of the ring structure. It is felt, nevertheless, that something is to be gained by considering the problem in the light in which it has been presented, in the general belief that the essentials would perpetuate themselves into a more exact solution of the whole problem if such could be presented. The lines which such a solution would take are indicated in another paper by the present writer.[5] However, the line of discussion as presented in the present paper serves to emphasize, in a form fairly easily manipulatable through Lagrange's equations, the role played by the equivalent self-inductances of the circuits and the "situation" phenomenon resulting from the small density of ions in the ring A.

[4] W. F. G. Swann, J. Franklin Inst. **251**, 120 (1951). See in particular pp. 153–155. Note that in the line $d^2r/dt^2 > N^2/nr_0^2M$, the quantity n should be replaced by n^2. The slip is typographical and does not carry through.

[5] W. F. G. Swann, J. Franklin Inst. **258**, 383 (1954).

Quantum Effects in the Interaction between Electrons and High-Frequency Fields. II

I. R. SENITZKY
Signal Corps Engineering Laboratories, Fort Monmouth, New Jersey

(Received November 12, 1954)

The study of the appearance of quantum effects in an essentially classical experiment—involving the passage of an electron through a resonant cavity—as the frequency of the electromagnetic field increases, was begun in a previous paper, in which the electron velocity was examined. In the present paper, an analysis is made of the electric field in the same experiment. Both the expectation value of the field, and the expectation value of the square of the deviation from the expectation value (the dispersion) of the field are calculated to the lowest order in the electron charge. The expectation value of the field is seen to differ from the classical value by a small amount, the difference being due to the wave properties of the electron. The dispersion in the field is shown to consist of three parts: one due to the quantum-mechanical properties of the field alone, the second due to the wave properties of the electron, and the third due to the interaction between the quantum-mechanical properties of the field and the classical properties of the electron. The orders of magnitude of the three terms are shown to decrease in the order in which they are enumerated. A calculation is then made of the effect on the field of a number of electrons passing through the cavity, the interaction between the electrons being neglected. The number of electrons required in a "bunch" to produce a field comparable to the dispersion in the field is calculated, and, for a typical set of experimental conditions, it is seen that the highest frequency at which this requirement can be met is of the order of 3×10^{12}/sec.

IN a previous paper,[1] a study was made of the appearance of certain quantum-mechanical effects in an essentially classical experiment involving the interaction between an electron and the electromagnetic field as the frequency of the field becomes high. The particular experiment considered was the passage of an electron through a resonant cavity, and the effects studied were those pertaining to the motion of the electron. An analysis was made of the velocity of the electron, treating the system of electron and field quantum-mechanically, and the departures from classically predicted behavior were noted. In order to obtain a better understanding of the quantum effects involved, however, the behavior of the field should also be studied. The purpose of the present paper, therefore, is to examine the behavior of the field in the same experiment and to find out how it differs from the classical behavior.

In (I) it was shown that the state of a system in a classical experiment must correspond to reasonably narrow wave packets for all the dynamical variables. Without going again into the reasons for the choice of initial conditions, we reformulate them here briefly. Let the electric and magnetic fields of the cavity be given respectively, by

$$\mathbf{E}=-4\pi c\mathbf{P}, \quad \mathbf{H}=\nabla\times\mathbf{A}.$$

We then expand

$$\mathbf{A}=\sum_j Q_j\mathbf{u}_j(\mathbf{r}), \quad \mathbf{P}=\sum_j P_j\mathbf{u}_j(\mathbf{r}), \tag{1}$$

and set

$$\mathbf{E}_j=-4\pi c\mathbf{u}_j(\mathbf{r})P_j, \tag{2}$$

where the subscript j refers to the jth normal mode of the cavity, $\mathbf{u}_j(\mathbf{r})$ is a normalized function describing the spatial dependence of the field,[2] and Q_j and P_j are the coordinate and momentum operators of the radiation oscillators, satisfying the commutation relationships $[Q_j,P_j]=i\hbar$, all other pairs commuting.[3] The initial state of the system is specified by the wave function,

$$\varphi(\mathbf{r}_e,P_j,0)=\varphi(\mathbf{r}_e,0)\textstyle\prod_j\varphi_j(P_j,0), \tag{3}$$

with

$$\varphi(\mathbf{r}_e,0)=b^{-\frac{1}{2}}\pi^{-\frac{1}{4}}\exp\left(-\frac{r_e^2}{2b^2}+ik_0x_e\right), \tag{4}$$

and

$$\varphi(P_j,0)=\left(\frac{4c^2}{\hbar\omega_j}\right)^{\frac{1}{4}}\exp\left[-\frac{4\pi c^2}{\hbar\omega_j}\left(\tfrac{1}{2}P_j^2-\frac{i\delta_{js}}{4\pi c}E_0P_j\right)\right], \tag{5}$$

where $\mathbf{r}_e$ is the coordinate of the electron, $\omega_j/2\pi$ is the frequency of the jth mode, the sth mode is the oscillating one, and b and k_0 are constants determining the initial width and velocity of the electron wave packet, re-

[1] I. R. Senitzky, Phys. Rev. **95**, 904 (1954) hereafter referred to as (I).

[2] The function $\mathbf{u}_j(\mathbf{r})$ is a solution of the equation $\nabla^2\mathbf{u}+(\omega_j/c)^2\mathbf{u}=0$, subject to the conditions $\mathbf{n}\times\mathbf{u}=0$ at the boundary of the cavity, $\int u^2d^3\mathbf{r}=1$, and $\operatorname{div}\mathbf{u}=0$. We neglect resistive losses. These conditions are sufficient to prescribe an orthonormal set of functions $\mathbf{u}_j(\mathbf{r})$ corresponding to a discrete frequency spectrum ω_j inside a closed cavity. Our cavity is not completely closed, however, since it must have openings for the electron to enter and leave. We assume the apertures to be such that those possible fields in the cavity which are of interest to us decay rapidly as a function of distance out of the cavity through the apertures. (The apertures might be, for instance, wave guides well below cutoff at the frequency in which we are interested.) Without attempting to prescribe conditions explicitly over a complete boundary, we assume that such a prescription is possible for a region that includes the inside of the cavity, the apertures, and a sufficiently large neighborhood of the electron path outside of the cavity. This yields a spectrum and the corresponding mode functions. The only modes which concern us are those for which nearly all of the contribution to $\int u^2(\mathbf{r})d^3\mathbf{r}$ comes from inside the cavity. Except in the immediate neighborhood of the aperture, then, $\mathbf{u}(\mathbf{r})$ is vanishingly small outside of the cavity for these modes. The origin of the coordinate system is taken to be outside of the cavity, and further from the fringing field than the width of the electron wave packet.

[3] Note the slight change in notation from that of (I). Capital Q's and P's are used for the modes of the electromagnetic field in the present paper, while small q's and p's were used in (I).

spectively. It should be noted that $\mathbf{r}_e$ in Eq. (3) is different from $\mathbf{r}$ in Eqs. (1) and (2). The former refers to the position of the electron and is a dynamical variable, while the latter is merely a parameter indicating where, in the cavity, the field is being evaluated. The significance of these initial conditions has already been discussed.

We now inquire about the behavior of the field of a given mode. The same assumptions will be made which were made in (I); namely, that the interaction between electron and field produces only a small perturbation, and that the quantum-mechanical correction terms are small compared to the classical terms, the justification for the latter assumption being that we are interested in the situation in which quantum effects first begin to arise. We will calculate the expectation value of the electric field and the expectation value of the square of the deviation from the expectation value (mean square deviation) of the electric field. Only terms with the lowest power of electron charge, e, will be retained,[4] and the analysis will be nonrelativistic.

The Hamiltonian for the system of electron and radiation field is[5]

$$H=\sum_j[2\pi c^2P_j^2+(\omega_j^2/8\pi c^2)Q_j^2] +(1/2m)[\mathbf{p}+(e/c)\sum_j Q_j\mathbf{u}_j(\mathbf{r}_e)]^2.$$

In order to obtain the equations of motion for the field of a particular mode in operator form in the Heisenberg picture, we first differentiate Eq. (2),

$$d\mathbf{E}_j/dt=-4\pi c\mathbf{u}_j(\mathbf{r})(dP_j/dt).$$

Using the relationship

$$dP_j/dt=(1/i\hbar)[P_j,H], \tag{6}$$

and a similar one for Q_j, we obtain

$$\frac{dP_j}{dt}=-\frac{\omega^2}{4\pi c^2}Q_j-\frac{e}{mc}\mathbf{u}_j(t)\cdot\mathbf{p}(t) -\frac{e^2}{mc^2}(u_j^2Q_j+\tfrac{1}{2}\sum_{i\neq j}\mathbf{u}_j\cdot\mathbf{u}_iQ_i),$$

$$\frac{dQ_j}{dt}=4\pi c^2P_j,$$

where $\mathbf{u}_j(t)$ stands for $\mathbf{u}_j(\mathbf{r}_e(t))$. We can replace these differential equations by integral equations containing the initial operators $P_j(0)$, $Q_j(0)$.

$$P_j(t)=P_j(0)\cos\omega_jt-\frac{\omega_j}{4\pi c^2}Q_j(0)\sin\omega_jt -\frac{e}{mc}\int_0^t dt_1\mathbf{u}_j(t_1)\cdot\mathbf{p}(t_1)\cos\omega_j(t-t_1) -\frac{e^2}{mc^2}\int_0^t dt_1[u_j^2(t_1)Q_j(t_1)+\tfrac{1}{2}\sum_{i\neq j}\mathbf{u}_j(t_1) \cdot\mathbf{u}_i(t_1)Q_i(t_1)]\cos\omega_j(t-t_1), \tag{7}$$

$$Q_j(t)=Q_j(0)+\int_0^t dt_1P_j(t_1).$$

We will use these integral equations to obtain a solution for $P(t)$ up to the second power in e.

Let us expand each of the operators which are functions of t as a sum of terms in the following manner:

$$P_j(t)=P_j^{(0)}(t)+P_j^{(1)}(t)+P_j^{(2)}(t)+\cdots, \tag{8}$$

and similarly for $Q_j(t)$, $\mathbf{u}_j(t)$, $\mathbf{p}(t)$, and $\mathbf{r}_e(t)$, where the superscript of each term indicates the power of e contained in that term. It is evident, then, that

$$P_j^{(0)}(t)=P_j(0)\cos\omega_jt-(\omega_j/4\pi c^2)Q_j(0)\sin\omega_jt, \tag{9}$$

$$P_j^{(1)}(t)=-(e/mc)\int_0^t dt_1\mathbf{u}_j^{(0)}(t_1) \cdot\mathbf{p}^{(0)}(t_1)\cos\omega_j(t-t_1), \tag{10}$$

$$P_j^{(2)}(t)=-\frac{e}{mc}\int_0^t dt_1[\mathbf{u}_j^{(0)}(t_1)\cdot\mathbf{p}^{(1)}(t_1) +\mathbf{u}_j^{(1)}(t_1)\cdot\mathbf{p}^{(0)}(t_1)]\cos\omega_j(t-t_1) -\frac{e^2}{mc^2}\int_0^t dt_1[u_j^{(0)2}(t_1)Q_j^{(0)}(t_1)+\tfrac{1}{2}\sum_{i\neq j}\mathbf{u}_j^{(0)}(t_1) \cdot\mathbf{u}_i^{(0)}(t_1)Q_i^{(0)}(t_1)]\cos\omega_j(t-t_1). \tag{11}$$

Also,

$$Q_j^{(0)}=Q_j(0)\cos\omega_jt+(4\pi c^2/\omega_j)P_j(0)\sin\omega_jt. \tag{12}$$

In order to obtain P up to the second power in e, we need expressions for $\mathbf{u}_j(t)$ and $\mathbf{p}(t)$ up to the first power in e.

Now, $\mathbf{u}_j$ is a known function of a dynamical variable (or operator), namely, the position of the electron, $\mathbf{r}_e(t)$. It is obvious that[6]

$$\mathbf{u}_j^{(0)}(t)=\mathbf{u}_j(\mathbf{r}^{(0)}(t)).$$

[4] In those calculations in which the terms linear in e vanish, the quadratic terms will be obtained. That is the reason for retaining the e^2 term in the Hamiltonian.

[5] Electrostatic effects in the interaction between the electron and cavity are neglected.

[6] Since there is little possibility of confusion, we drop the subscript e for simplicity of notation.

Also,

$$\mathbf{u}_j^{(1)}(t)=[\mathbf{u}_j(\mathbf{r}^{(0)}(t)+\mathbf{r}^{(1)}(t))]_1-\mathbf{u}_j^{(0)}(t), \quad (13)$$

where the notation $[\ ]_1$ indicates that terms inside the bracket containing powers of e higher than the first are neglected. Using relationships of the type of Eq. (6) for $\mathbf{r}(t)$ and $\mathbf{p}(t)$, we obtain

$$\frac{d\mathbf{r}(t)}{dt}=\frac{1}{m}\mathbf{p}(t)+\frac{e}{mc}\sum_i Q_j(t)\mathbf{u}_j(t),$$

and

$$\frac{d\mathbf{p}(t)}{dt}=-\frac{e}{mc}\sum_i Q_i(t)\nabla[\mathbf{u}_i(t)\cdot\mathbf{p}(t)]$$

$$-\frac{e^2}{2mc^2}\sum_{i,j} Q_i(t)Q_j(t)\nabla[\mathbf{u}_i(t)\cdot\mathbf{u}_j(t)].$$

An integration yields

$$\mathbf{p}^{(0)}(t)=\mathbf{p}(0), \quad (14)$$

$$\mathbf{p}^{(1)}(t)=-\frac{e}{mc}\int_0^t dt_1\sum_i Q_i^{(0)}(t_1)\nabla[\mathbf{u}_i^{(0)}(t_1)\cdot\mathbf{p}^{(0)}], \quad (15)$$

$$\mathbf{r}^{(0)}(t)=\mathbf{r}(0)+(t/m)\mathbf{p}^{(0)}, \quad (16)$$

$$\mathbf{r}^{(1)}(t)=\frac{1}{m}\int_0^t \mathbf{p}^{(1)}(t_1)dt_1$$

$$+\frac{e}{mc}\int_0^t dt_1\sum_i Q_i^{(0)}(t_1)\mathbf{u}_i^{(0)}(t_1). \quad (17)$$

We can now write

$$\mathbf{u}_j^{(0)}(t)=\mathbf{u}_j[\mathbf{r}(0)+(t/m)\mathbf{p}(0)]. \quad (18)$$

We will need to know the result of the operation of $\mathbf{u}_j^{(0)}(t)$ on functions of $\mathbf{r}(0)$. With $\mathbf{u}_j^{(0)}(t)$ as given in (18) and without specifying the function $\mathbf{u}_j(\mathbf{r})$ explicitly, this will be possible only if the functions on which $\mathbf{u}_j^{(0)}(t)$ operates are eigenfunction of its argument $\mathbf{r}(0)+(t/m)\mathbf{p}(0)$. In order to achieve greater versatility for $\mathbf{u}_j^{(0)}(t)$, we cast it into a different form. Using the Fourier integral representation for $\mathbf{u}_j(\mathbf{r})$, we have

$$\mathbf{u}_j(\mathbf{r})=\int d^3\mathbf{k}\mathbf{U}_j(\mathbf{k})\exp(i\mathbf{k}\cdot\mathbf{r}).$$

Therefore,

$$\mathbf{u}_j^{(0)}(t)=\int d^3\mathbf{k}\mathbf{U}_j(\mathbf{k})\exp\{i\mathbf{k}\cdot[\mathbf{r}(0)+(t/m)\mathbf{p}(0)]\}.$$

Now, if A and B are two noncommuting quantities the commutator of which commutes with both A and B, we have the identity

$$e^{A+B}=e^{-\frac{1}{2}[A,B]}e^Ae^B.$$

Applying this to the foregoing expression for $\mathbf{u}_j^{(0)}(t)$, we obtain

$$\mathbf{u}_j^{(0)}(t)=\int d^3\mathbf{k}\mathbf{U}_j(\mathbf{k})\exp\left(\frac{it\hbar k^2}{2m}\right)$$

$$\times\exp(i\mathbf{k}\cdot\mathbf{r})\exp\left(\frac{it\mathbf{k}\cdot\mathbf{p}}{m}\right), \quad (19)$$

where $\mathbf{r}$ and $\mathbf{p}$ stand for $\mathbf{r}(0)$ and $\mathbf{p}(0)$. With this form, the result of the operation of $\mathbf{u}^{(0)}(t)$ on any eigenfunction of $\mathbf{p}(0)$ can be written down immediately. Since any function which can be expressed by a Fourier representation is a combination of such eigenfunctions, the form (19) will be very useful. It was derived in (I) from other considerations.

We now have enough information to calculate the expectation value of the electric field, $\langle\mathbf{E}_j\rangle$, up to the first power in e. From Eqs. (2) and (8),

$$\langle\mathbf{E}_j\rangle=-4\pi c\mathbf{u}(\mathbf{r})(\langle P_j^{(0)}\rangle+\langle P_j^{(1)}\rangle), \quad (20)$$

where, in view of Eqs. (9) and (10),

$$\langle P_j^{(0)}\rangle=\langle P_j(0)\rangle\cos\omega_j t-(\omega_j/4\pi c^2)\langle Q_j(0)\rangle\sin\omega_j t, \quad (21)$$

and

$$\langle P_j^{(1)}\rangle=-\frac{e}{mc}\int^t dt_1\langle\mathbf{u}_j^{(0)}(t_1)\cdot\mathbf{p}^{(0)}(t_1)\rangle\cos\omega_j(t-t_1). \quad (22)$$

The values of $\langle P_j(0)\rangle$ and $\langle Q_j(0)\rangle$ can be obtained very simply in the P representation by means of Eq. (5), when one uses $i\hbar\partial/\partial P_j$ for Q_j. We have

$$\langle P_j(0)\rangle=0, \quad \langle Q_j(0)\rangle=\delta_{js}E_0c/\omega_j. \quad (23)$$

In order to evaluate $\langle\mathbf{u}_j^{(0)}(t_1)\cdot\mathbf{p}^{(0)}(t_1)\rangle$, we make use of Eqs. (14) and (19), obtaining[7]

$$\langle\mathbf{u}_j^{(0)}(t)\cdot\mathbf{p}\rangle=b^{-3}\pi^{-\frac{3}{2}}\int d^3\mathbf{r}\int d^3\mathbf{k}$$

$$\times\exp\left[-\frac{r^2}{2b^2}-ik_0x+\frac{it\hbar k^2}{2m}+i\mathbf{k}\cdot\mathbf{r}\right]U_j(\mathbf{k})\cdot\mathbf{p}$$

$$\times\exp\left(\frac{it\mathbf{k}\cdot\mathbf{p}}{m}\right)\exp\left[-\frac{r^2}{2b^2}+ik_0x\right],$$

[7] The electron wave function is defined for all of space, and the integration in this equation is likewise over all of space. However, $\mathbf{u}(\mathbf{r})$ is defined only in a restricted region. The walls of the cavity, for instance, are excluded from this region. In order to avoid the necessity of setting up $\mathbf{u}(\mathbf{r})$ outside of this region, we consider only those electron wave packets for which b is sufficiently small, so that $\exp(-r^2/2b^2)$ is vanishingly small outside of the region. Physically, this means that our wave packet is sufficiently well localized so as to be able to travel through the apertures of the cavity without being intercepted by the walls. We thus avoid diffraction and reflection effects, and are able to study only those quantum effects involved in the interaction between the electron and the radiation field.

where $\mathbf{p}$ stands for $\mathbf{p}(0)$. If we replace the function $\exp(-r^2/2b^2)$ on which $\mathbf{p}$ operates by its Fourier integral representation,

$$\exp\left(-\frac{r^2}{2b^2}\right)=\frac{b^3}{(2\pi)^{\frac{3}{2}}}\int d^3\mathbf{k}_1 \exp(-\tfrac{1}{2}k_1^2b^2+i\mathbf{k}_1\cdot\mathbf{r}), \quad (24)$$

the result of the two $\mathbf{p}$ operations may be written down immediately, since the $\mathbf{p}$ operators are now followed by eigenfunctions of $\mathbf{p}$. Integrating then with respect to $\mathbf{r}$ and $\mathbf{k}_1$, we obtain

$$\langle \mathbf{u}_j^{(0)}(t)\cdot\mathbf{p}\rangle=\hbar\int d^3\mathbf{k}\exp[i\mathbf{k}\cdot\mathbf{v}_0t-k^2\delta^2(t)] \times\mathbf{U}_j(\mathbf{k})\cdot\left(\mathbf{k}_0-\tfrac{1}{2}\mathbf{k}+\frac{i\hbar t}{2mb^2}\mathbf{k}\right),$$

where $\mathbf{k}_0$ is the vector $(k_0,0,0)$, $\mathbf{v}_0=\hbar\mathbf{k}_0/m$, and

$$\delta^2(t)=(b/2)^2+(\hbar t/2mb)^2. \quad (25)$$

In view of the fact that $\operatorname{div}\mathbf{u}(\mathbf{r})$ vanishes, it is easily seen that $\mathbf{U}(\mathbf{k})\cdot\mathbf{k}$ also vanishes. Therefore, we obtain

$$\langle \mathbf{u}^{(0)}(t)\cdot\mathbf{p}\rangle=\hbar\mathbf{k}_0\cdot\int d^3\mathbf{k}\mathbf{U}(\mathbf{k})\exp(i\mathbf{k}\cdot\mathbf{v}_0t) \times\exp[-k^2\delta^2(t)]. \quad (26)$$

If the last factor in the integrand were missing, we would have just the classical value $m\mathbf{v}_0\cdot\mathbf{u}(\mathbf{v}_0t)$. This last factor in the integrand provides the quantum-mechanical correction to the classical value. We can write

$$\begin{aligned}&\langle \mathbf{u}_j^{(0)}(t)\cdot\mathbf{p}^{(0)}\rangle\\ &=m\mathbf{v}_0\cdot\int d^3\mathbf{k}\mathbf{U}_j(\mathbf{k})\exp[-k^2\delta^2(t)]\exp(i\mathbf{k}\cdot\mathbf{r})\,|_{\mathbf{r}=\mathbf{v}_0t}\\ &=m\mathbf{v}_0\cdot\int d^3\mathbf{k}\mathbf{U}_j(\mathbf{k})\exp[\delta^2(t)\nabla^2]\exp(i\mathbf{k}\cdot\mathbf{r})\,|_{\mathbf{r}=\mathbf{v}_0t}\\ &=m\mathbf{v}_0\cdot\exp[\delta^2(t)\nabla^2]\mathbf{u}_j(\mathbf{r})\,|_{\mathbf{r}=\mathbf{v}_0t}\\ &=m\mathbf{v}_0\cdot\exp[-(\omega^2/c^2)\delta^2(t)]\mathbf{u}_j(\mathbf{v}_0t), \end{aligned} \quad (27)$$

where use has been made of the properties of $\mathbf{u}(\mathbf{r})$ described in footnote 2. Combining Eqs. (20), (21), (22), (23), and (27), we obtain

$$\langle \mathbf{E}_j(\mathbf{r},t)\rangle=E_0\delta_{js}\mathbf{u}_j(\mathbf{r})\sin\omega_jt+4\pi e\mathbf{u}_j(\mathbf{r})\int_0^t dt_1\mathbf{v}_0 \cdot\mathbf{u}_j(\mathbf{v}_0t_1)\cos\omega_j(t-t_1)\exp(-4\pi^2\delta^2(t_1)/\lambda^2). \quad (28)$$

The exponential factor produces the quantum-mechanical effect in the expectation value of the electric field strength to the extent that it is different from unity. We see that this effect is always such as to reduce the increment of field due to the electron. This is to be expected, since the electron is essentially no longer a point, but is "smeared out" over the wave packet, and therefore has less net effect on the field of any particular mode. Our interest lies in the case $\delta(t_1)\ll\lambda$, since we are studying small quantum effects. It is to be noted that the quantization of the field does not affect its expectation value, to the degree of approximation we have used.

As was pointed out in (I) with respect to the electron velocity, the quantum mechanical effect represented by the change in the expectation value of the field is of less significance (for small changes) than the quantum-mechanical effect represented by the dispersion in strength of the field, since, when applied to a microwave device, the former is merely a small attenuation in signal, while the latter produces noise. We therefore proceed to calculate the mean square deviation from the mean of electric field strength for a given mode.

From Eq. (2), we have

$$\langle(E_j-\langle E_j\rangle)^2\rangle=16\pi^2c^2u_j^2(r)[\langle P_j^2\rangle-\langle P_j\rangle^2]. \quad (29)$$

Now, up to the second power in e,

$$\begin{aligned}\langle P_j^2\rangle-\langle P_j\rangle^2&=[\langle P_j^{(0)2}\rangle-\langle P_j^{(0)}\rangle^2]+\langle P_j^{(0)},P_j^{(1)}\rangle\\ &\quad+[\langle P_j^{(1)2}\rangle-\langle P_j^{(1)}\rangle^2]+\langle P_j^{(0)},P_j^{(2)}\rangle, \end{aligned} \quad (30)$$

where for conciseness, we use the notation

$$\langle A,B\rangle=\langle AB\rangle+\langle BA\rangle-2\langle A\rangle\langle B\rangle.$$

The first bracket on the right side of Eq. (30) is independent of the presence of the electron and is due to the field only. The other terms involve the electron. It can be seen without difficulty that $\langle P_j^{(0)},P_j^{(1)}\rangle=0$, since $P^{(0)}$ contains only field variables $(P(0),Q(0))$ while $P^{(1)}$ contains only electron variables $(r(0),p(0))$. The lowest order terms in Eq. (30) due to the electron, therefore, are the ones in e^2. We proceed to calculate these, as well as the term due to the field alone. The latter may be evaluated easily by means of Eq. (5) to be

$$\langle P_j^{(0)2}\rangle-\langle P_j^{(0)}\rangle^2=\hbar\omega_j/8\pi c^2. \quad (31)$$

In the calculation of $[\langle P_j^{(1)2}\rangle-\langle P_j^{(1)}\rangle^2]$, we interchange the expectation value operation with the time integration to obtain from Eq. (19)

$$\langle P_j^{(1)2}\rangle=\left(\frac{e}{mc}\right)^2\int_0^t dt_1\int_0^t dt_2\cos\omega_j(t-t_1) \times\cos\omega_j(t-t_2)\langle \mathbf{u}_j(t_1)\cdot\mathbf{p}\mathbf{u}_j(t_2)\cdot\mathbf{p}\rangle. \quad (32)$$

Writing

$$\langle \mathbf{u}_j(t_1)\cdot\mathbf{p}\mathbf{u}_j(t_2)\cdot\mathbf{p}\rangle=\sum_{a,b=1}^{3}\langle u_j^a(t_1)p^au_j^b(t_2)p^b\rangle,$$

making use of Eqs. (10) and (24), and carrying through

all the $\mathbf{p}$ operations, we have

$$\langle u_j{}^a(t_1)p^a u_j{}^b(t_2)p^b\rangle$$
$$=\frac{\hbar}{4\pi^4}\int d^3\mathbf{r}\int d^3\mathbf{k}_1\int d^3\mathbf{k}_2\int d^3\mathbf{k}_3 U_j{}^a(\mathbf{k}_1)U_j{}^b(\mathbf{k}_2)$$
$$\times(k_2{}^a+k_3{}^a+k_0{}^a)(k_3{}^b+k_0{}^b)\exp\{-r^2/2b^2$$
$$+i\mathbf{r}\cdot(\mathbf{k}_1+\mathbf{k}_2+\mathbf{k}_3)+it_1(\hbar/m)[\tfrac{1}{2}k_1{}^2$$
$$+\mathbf{k}_1\cdot(\mathbf{k}_2+\mathbf{k}_3+\mathbf{k}_0)]+it_2(\hbar/m)[\tfrac{1}{2}k_2{}^2$$
$$+\mathbf{k}_2\cdot(\mathbf{k}_3+\mathbf{k}_0)]-\tfrac{1}{2}k_3{}^2b^2\}. \quad (33)$$

We integrate the right side of Eq. (33) first with respect to $\mathbf{r}$ and then with respect to $\mathbf{k}_3$. Then, when we consider the summation with respect to a and b, several terms in the above expression vanish, some due to cancellation when a is interchanged with b and k_1 with k_2, others due to the fact that $\sum_a U_j{}^a k_{1,2}{}^a$ equals zero, as was pointed out in the derivation of Eq. (26). We have, dropping these terms,

$$\langle u_j{}^a(t_1)p^a u_j{}^b(t_2)p^b\rangle$$
$$=\hbar^2\int d^3\mathbf{k}_1\int d^3\mathbf{k}_2 U_j{}^a(\mathbf{k}_1)U_j{}^b(\mathbf{k}_2)\exp(i\mathbf{k}_1\cdot\mathbf{v}_0t_1)$$
$$\times\exp(i\mathbf{k}_2\cdot\mathbf{v}_0t_2)\exp[-k_1{}^2\delta^2(t_1)-k_2{}^2\delta^2(t_2)$$
$$-2\mathbf{k}_1\cdot\mathbf{k}_2\delta^2((t_1t_2)^{\frac{1}{2}})+i\hbar\mathbf{k}_1\cdot\mathbf{k}_2(t_1-t_2)/2m]$$
$$\times\{k_0{}^ak_0{}^b-\tfrac{1}{4}k_2{}^ak_1{}^b-(1/b^2)(\hbar/2mb)^2t_2k_2{}^at_1k_1{}^b$$
$$+\delta_{ab}/2b^2+(i/b)(\hbar/2mb)[(k_0{}^b-\tfrac{1}{2}k_1{}^b)t_2k_2{}^a$$
$$+(k_0{}^a+\tfrac{1}{2}k_2{}^a)t_1k_1{}^b]. \quad (34)$$

The analysis of Eq. (34) is similar to that of Eq. (26). The first four factors of the integrand and the $k_0{}^ak_0{}^b$ term of the curly bracket constitute the classical value, namely $m^2v_0{}^av_0{}^bu_j{}^a(\mathbf{v}_0t_1)u_j{}^b(\mathbf{v}_0t_2)$. All the other terms are quantum-mechanical corrections, and therefore, in accordance with our previously stated program, we assume that they are small compared to the classical terms. This means that

$$(kb/2)^2\ll 1, \quad (\hbar kt/2mb)^2\ll 1, \quad k/k_0\ll 1,$$

where k stands for either $|\mathbf{k}_1|$ or $|\mathbf{k}_2|$ and has a value in the range for which $\mathbf{U}_j(\mathbf{k})$ is substantially different from zero. The first two inequalities imply that both the initial and final widths of the wave packet are small compared to the dimensions of the cavity.[8] The last inequality is implied by the first two, as can be seen from the following consideration. The time which occurs in the second inequality is the time taken by the electron to traverse a distance of the order of, or larger than, the dimensions of the cavity. Calling this distance D, we have $t\sim D/\hbar k_0m^{-1}$. Therefore,

$$(kD/2bk_0)\sim(\hbar kt/2mb)<1, \quad \text{and} \quad k/k_0<b/D\ll 1.$$

As in (I), we also assume that

$$(\hbar kt/2mb)\sim kb/2, \quad \text{so that} \quad (1/b)(\hbar t/2mb)\sim 1.$$

The terms in (34) (except for the δ_{ab} term) can now be classified according to the decreasing orders of magnitude of $k_0{}^2$, k_0k, and k^2. Since we are interested only in first-order quantum-mechanical effects, we neglect the k^2 terms. Likewise, we expand the third exponential factor in the integrand of Eq. (34), and neglect higher powers of the exponent than the first. Carrying through the indicated multiplication and dropping products of small order terms, we obtain

$$\langle\mathbf{u}_j(t_1)\cdot\mathbf{p}\mathbf{u}_j(t_2)\cdot\mathbf{p}\rangle$$
$$=\sum_{a,b}\hbar^2\int d^3\mathbf{k}_1\int d^3\mathbf{k}_2 U_j{}^a(\mathbf{k}_1)U_j{}^b(\mathbf{k}_2)$$
$$\times\exp(i\mathbf{k}_1\cdot\mathbf{v}_0t_1)\exp(i\mathbf{k}_2\cdot\mathbf{v}_0t_2)$$
$$\times\{k_0{}^ak_0{}^b-k_0{}^ak_0{}^b[k_1{}^2\delta^2(t_1)+k_2{}^2\delta^2(t_2)$$
$$+2\mathbf{k}_1\cdot\mathbf{k}_2\delta^2((t_1t_2)^{\frac{1}{2}})-i\hbar\mathbf{k}_1\cdot\mathbf{k}_2(t_1-t_2)/2m]+\delta_{ab}/2b^2$$
$$+(i/b)(\hbar/2mb)(t_2k_0{}^bk_2{}^a+t_1k_0{}^ak_1{}^b)\}. \quad (35)$$

After we substitute this expression into Eq. (32), an interchange of t_1 and t_2 becomes possible, so that the t_1-t_2 term vanishes, and the $t_2k_0{}^bk_2{}^a$ term combines with the $t_1k_0{}^ak_1{}^b$ term. Furthermore, if we expand the quantum-mechanical correction factor in Eq. (26), namely, $\exp[-k^2\delta^2(t)]$, and again neglect powers of the exponent higher than the first, we note that the subtraction of $\langle P^{(1)}\rangle^2$ will cancel the $k_0{}^ak_0{}^b$, $k_1{}^2\delta^2(t_1)$, and $k_2{}^2\delta^2(t_2)$ terms. We are thus left with

$$\langle P_j{}^{(1)2}\rangle-\langle P_j{}^{(1)}\rangle^2$$
$$=\left(\frac{e}{mc}\right)^2\int_0^t dt_1\int_0^t dt_2\cos\omega_j(t-t_1)\cos\omega_j(t-t_2)$$
$$\times\sum_{a,b=1}^{3}\hbar^2\int d^3\mathbf{k}_1\int d^3\mathbf{k}_2 U_j{}^a(\mathbf{k}_1)U_j{}^b(\mathbf{k}_2)$$
$$\times\exp(i\mathbf{k}_1\cdot\mathbf{v}_0t_1)\exp(i\mathbf{k}_2\cdot\mathbf{v}_0t_2)$$
$$\times\{-2k_0{}^ak_0{}^b\mathbf{k}_1\cdot\mathbf{k}_2\delta^2((t_1t_2)^{\frac{1}{2}})+\delta_{ab}/2b^2$$
$$+(2i/b)(\hbar/2mb)t_2k_0{}^bk_2{}^a\}. \quad (36)$$

The right side may be rewritten as

$$\left(\frac{e\hbar}{mc}\right)^2\int_0^t dt_1\int_0^t dt_2\cos\omega_j(t-t_1)\cos\omega_j(t-t_2)$$
$$\times\sum_{a,b}\left\{2k_0{}^ak_0{}^b\nabla_1\cdot\nabla_2\delta^2((t_1t_2)^{\frac{1}{2}})+\frac{2}{b}\frac{\hbar t_2}{2mb}k_0{}^b\frac{\partial}{\partial r_2{}^a}+\frac{\delta_{ab}}{2b^2}\right\}$$
$$\times u_j{}^a(\mathbf{r}_1)u_j{}^b(\mathbf{r}_2)\big|_{\mathbf{r}_1=\mathbf{v}_0t_1,\mathbf{r}_2=\mathbf{v}_0t_2}.$$

[8] Actually, these inequalities imply even more than that; namely, that the width of the wave packet is small compared to distances over which there are large changes in $\mathbf{u}(\mathbf{r})$.

Recalling that

$$\delta^2((t_1t_2)^{\frac{1}{2}})=(b/2)^2+(\hbar/2mb)^2t_1t_2,$$

and that $\mathbf{k}_0$ has a nonvanishing component only in the x-direction, it can be seen without much difficulty that

$$\langle P_j^{(1)2}\rangle-\langle P_j^{(1)}\rangle^2=(e\hbar/mc)^2$$
$$\times\left\{\left(\frac{b}{2}\right)^2k_0^2\left[\int_0^t dt_1\cos\omega_j(t-t_1)\nabla u_j^x(\mathbf{r}_1)\,|_{\mathbf{r}_1=\mathbf{v}_0t_1}\right]^2\right.$$
$$+2\left[\frac{\hbar}{2mb}k_0\int_0^t dt_1t_1\cos\omega_j(t-t_1)\nabla u_j^x(\mathbf{r}_1)\,|_{\mathbf{r}_1=\mathbf{v}_0t_1}\right.$$
$$\left.\left.+\frac{1}{2b}\int_0^t dt_1\mathbf{u}_j(\mathbf{v}_0t_1)\cos\omega_j(t-t_1)\right]^2\right\}. \quad (37)$$

In order to simplify this expression further, we assume that

$$\frac{\partial}{\partial y}u_j^x(x,0,0)=\frac{\partial}{\partial z}u_j^x(x,0,0)=0.$$

Then the first and second integrals may be integrated by parts. We also assume that $u_j^x(x,0,0)=u_j^y(x,0,0)=0$.[9] If we set $\omega_jt=\theta_j$ and $u_j^x(v_0t,0,0)=V^{-\frac{1}{2}}f_j(\theta_j)$, where V is the volume of the cavity, we obtain after integration by parts[10]:

$$\langle P_j^{(1)2}\rangle-\langle P_j^{(1)}\rangle^2=\frac{2e^2}{c^2V}\left\{\left(\frac{b}{2}\right)^2A^2+\left(\frac{\hbar}{2mb}\right)^2\frac{1}{\omega^2}B^2\right\}, \quad (38)$$

with

$$A=\int_{\theta_j^-}^{\theta_j^+}d\theta' f_j(\theta')\sin(\theta_j-\theta'),$$

and

$$B=\int_{\theta_j^-}^{\theta_j^+}d\theta' f_j(\theta')\theta'\sin(\theta_j-\theta'),$$

where θ^- and θ^+ are the entrance and exit angles, respectively.

In order to complete the evaluation of $(\langle P_j^2\rangle-\langle P_j\rangle^2)$ up to the second power in e, we must yet calculate the last bracket on the right side of Eq. (23), namely, the quantity

$$\langle P_j^{(0)},P_j^{(2)}\rangle\equiv\langle P_j^{(0)}P_j^{(2)}\rangle+\langle P_j^{(2)}P_j^{(0)}\rangle-2\langle P_j^{(0)}\rangle\langle P_j^{(2)}\rangle. \quad (39)$$

The nonvanishing of this quantity is a purely quantum-mechanical effect, since the classical equivalent of it is obviously zero. Now, $P_j^{(0)}$ contains only the initial field variables and not the electron variables, as has been pointed out previously. On the other hand, $P_j^{(2)}$ contains both the field variables and the electron variables. It follows from Eqs. (11), (13), (15), and (17), that $P_j^{(2)}$ is a linear function of the $Q^{(0)}$'s. We can therefore write

$$P_j^{(2)}(t)=\int_0^t dt_1\sum_l a_l(t,t_1)Q_l^{(0)}(t_1)F_l(\mathbf{p}(0),\mathbf{r}(0),t_1).$$

We have, thus,

$$\langle P_j^{(0)}(t),P_j^{(2)}(t)\rangle=\int_0^t dt_1\sum_l a_l\langle P_j^{(0)}(t),Q_l^{(0)}(t_1)\rangle\langle F_l\rangle,$$

since $Q_l^{(0)}$, also, is a function only of the initial field variables and not the electron variables. Now $\langle P_j^{(0)}(t),Q_l^{(0)}(t_1)\rangle$ will be different from zero only if $j=l$. We can therefore drop, as far as our present purpose is concerned, all terms in $P^{(2)}$ which do not contain the field variables of the jth mode. Also, in accordance with our previous considerations, the expectation value of F_n will differ by only a small amount from the classical value of F_n. Since we are evaluating a small-order (quantum-mechanical) term, and are interested only in the first-order quantum-mechanical effect, we can replace the expectation value of F_n by its classical value. Thus $\mathbf{p}(0)$ and $\mathbf{r}(0)$ can be regarded, in the calculation of $\langle F_n\rangle$, as commuting numbers, having the magnitudes of their respective expectation values, and purely quantum-mechanical correction terms may be dropped in this case. (This means we are treating the electron classically and the field quantum mechanically in this particular instance.) We go back to Eq. (13) and make use of the simplifications just introduced. From Eqs. (16) and (17), it is clear that $\mathbf{r}^{(0)}(t)$ and $\mathbf{r}^{(1)}(t)$ commute in the case where the electron variables commute with each other, since $\mathbf{r}^{(0)}(t)$ does not involve the field operators. We can therefore expand $\mathbf{u}(\mathbf{r}^{(0)}+\mathbf{r}^{(1)})$ in a Taylor's series about $\mathbf{r}^{(0)}$. We thus have

$$u_j^{(1)}(t)=\mathbf{r}^{(1)}(t)\cdot\nabla u_j(\mathbf{r})\,|_{\mathbf{r}=\mathbf{r}^{(0)}t},$$

where u stands for any component of $\mathbf{u}$. Making use of Eqs. (14) through (17), and dropping all terms for which $i\neq j$, in accordance with the aforementioned considerations, we obtain

$$u_j^{(1)}(t)=\frac{e}{mc}\nabla u_j(\mathbf{r})\cdot\int_0^t dt_1Q_j^{(0)}(t_1)$$
$$\times\{\mathbf{u}_j(\mathbf{r}_1)+(t_1-t)\nabla[\mathbf{u}_j(\mathbf{r}_1)\cdot\mathbf{v}_0]\}\,|_{\mathbf{r}=\mathbf{v}_0t,\,\mathbf{r}_1=\mathbf{v}_0t_1}.$$

[9] These assumptions correspond to the situation in most experimental arrangements for the production of velocity modulation. The field components perpendicular to the electron path would cause deflection of the electron beam, and are therefore undesirable. On the other hand the field component along the electron path produces the desired effect and should be a maximum.

[10] In arriving at Eq. (38), use is made of the conditions $u^x(0)=0$ and $u^x(t)=0$. The first condition follows from the fact that the origin of the coordinate system is well outside of the cavity. The second condition holds only for those values of t such that the electron has already left the cavity (or more accurately, has left the fringing field of the cavity). Equation (38) therefore holds only for t greater than exit time. The preceding equations, however, hold for all t.

Substituting in Eq. (11), bearing in mind that $\mathbf{v}_0$ is in the x-direction, and again dropping terms for which $i \neq j$, we have

$$P_j^{(2)}(t)=\frac{e^2v}{m^2c^2}\int_0^t dt_1 \cos\omega_j(t-t_1)\Big\{\mathbf{u}_j^{(0)}(t_1)\cdot\int_0^{t_1}dt_2 \times Q_j^{(0)}(t_2)\nabla_2 u_j^x(\mathbf{r}_2)-\nabla_1 u_j^x(\mathbf{r}_1)\cdot\int_0^{t_1}dt_2 Q_j^{(0)}(t_2) \times[\mathbf{u}_j^{(0)}(t_2)+v_0(t_2-t_1)\nabla u_j^x(\mathbf{r}_2)]\Big\}\Big|_{\mathbf{r}_1=\mathbf{v}_0t_1,\,\mathbf{r}_2=\mathbf{v}_0t_2} -\frac{e^2}{mc^2}\int_0^t dt_1 u_j^{(0)2}(t_1)Q_j^{(0)}(t_1)\cos\omega_j(t-t_1).$$

Using the relationship

$$\langle P_j^{(0)}(t), Q_j^{(0)}(t')\rangle=\hbar\sin\omega_j(t'-t),$$

which may be obtained easily in the P representation from Eqs. (5), (9), and (12), we obtain

$$\langle P_j^{(0)}(t),P_j^{(2)}(t)\rangle=\frac{e^2\hbar}{mc^2}\int_0^t dt_1\cos\omega_j(t-t_1) \times\Big\{v_0\mathbf{u}_j^{(0)}(t_1)\cdot\int_0^{t_1}dt_2\sin\omega_j(t_2-t)\nabla u_j^x(\mathbf{r}_2) -v_0\nabla u_j^x(\mathbf{r}_1)\cdot\int_0^t dt_2\sin\omega_j(t_2-t) \times[\mathbf{u}_j^{(0)}(t_2)+v_0(t_2-t_1)\Delta u_j^x(\mathbf{r}_2)] -u_j^{(0)2}(t_1)\sin\omega_j(t_1-t)\Big\}\Big|_{\mathbf{r}_1=\mathbf{v}_0t_1,\,\mathbf{r}_2=\mathbf{v}_0t_2}.$$

For simplicity, we make the same assumption which was made in going from Eq. (37) to Eq. (38). We then obtain, after integration by parts and some transformation,

$$\langle P_j^{(0)}(t),P_j^{(2)}(t)\rangle=\frac{e^2\hbar}{mc^2\omega_jV}G, \tag{40}$$

where

$$G=\int_{\theta_j^-}^{\theta_j^+}d\theta_1\int_{\theta_j^-}^{\theta_1}d\theta_2 f_j(\theta_1)f_j(\theta_2)(\theta_1-\theta_2)\sin(\theta_j-\theta_1) \times\cos(\theta_j-\theta_2).$$

We have now evaluated all terms up to the second power in e which contribute toward $(\langle P_j^2\rangle-\langle P_j\rangle^2)$ and obtain, by combining Eq. (30), (31), (38), and (40)

$$\langle P_j^2\rangle-\langle P_j\rangle^2=\frac{\hbar\omega_j}{8\pi c^2}+\frac{2e^2}{c^2V}\left[\left(\frac{b}{2}\right)^2A^2+\left(\frac{\hbar}{2mb}\right)^2\frac{1}{\omega_j^2}B^2\right] +(e^2\hbar/mc^2\omega_jV)G. \tag{41}$$

It is interesting to note the physical origin of the three terms on the right side of Eq. (41), which account for the uncertainty in the field. As mentioned previously, the first term is due only to quantization of the field and has no connection with the electron. It indicates the uncertainty in the undisturbed field resulting from its quantum-mechanical properties. The second term is due only to the wave properties of the electron; that is, the initial wave packet width and the subsequent spreading of the wave packet both produce an uncertainty in the field radiated by the electron. The last term comes from the interaction between the quantum-mechanical uncertainty in the field and the electron, the behavior of the latter being treated classically. We can explain this last effect in the following way: the uncertainty in the initial field produces, in a classical manner, an uncertainty in the motion of the electron, which, in turn, produces, again in a classical manner, an uncertainty in the field which the electron radiates.

It is instructive to compare the orders of magnitude of the two terms in Eq. (41) containing e^2, that is, the two terms due the electron. Since $\mathbf{u}_j(\mathbf{r})$ is normalized over the volume of the cavity, $f_j(\theta)$ is of the order of unity. If $f_j(\theta)$ does not contain a sinusoidal variation with the periodicity 2π, A and G are also of the order of unity. On the other hand, the integral B is of the order of $\frac{1}{2}(\theta^-+\theta^+)$. Now, θ/ω is just the time t required by the electron to travel from the origin to x. We therefore have for the second term on the right side of Eq. (41)

$$\langle P_j^{(1)2}\rangle-\langle P_j^{(1)}\rangle^2\sim(2e^2/c^2V)\delta^2(\tau),$$

where

$$\tau=\tfrac{1}{2}(t^-+t^+),$$

and for the third term,

$$\langle P_j^{(0)}(t),P_j^{(2)}(t)\rangle\sim e^2\hbar/mc^2\omega_jV.$$

The ratio of the last two expressions is

$$\frac{\langle P_j^{(0)}(t),P_j^{(2)}(t)\rangle}{\langle P_j^{(1)2}\rangle-\langle P_j^{(1)}\rangle^2}=\frac{1}{2\pi}\frac{\lambda_0\lambda_j}{\delta^2(\tau)},$$

where λ_0 is the Compton wavelength, $\hbar/mc=4\times10^{-11}$ cm. Now, $\delta^2(\tau)$ cannot be made arbitrarily small for a given τ. It is a function of b, and the minimum possible value it may assume, as is easily seen from Eq. (25), is $\frac{1}{4}\hbar\tau/m$, which can also be written as $\frac{1}{4}\lambda_0(c/v_0)(x^-+x^+)$. Thus,

$$\frac{1}{2\pi}\frac{\lambda_0\lambda_j}{\delta^2(\tau)}\leqslant\frac{2}{\pi}\frac{v_0}{c}\frac{\lambda_j}{x^-+x^+}.$$

In any reasonable experimental arrangement, the right hand side of this inequality is much smaller than unity.[11]

[11] We have not previously said anything about the distance of the origin from the cavity except to require that the origin be outside the fringing field of the cavity at a distance greater than the initial width of the electron wave packet. Now, the origin is

Of the two terms in e^2 (which are the two terms arising from the electron) on the right side of Eq. (41), therefore, the second one is much smaller than the first, and we will neglect it in our further considerations. Making use of Eq. (29), we obtain, finally

$$\langle(\mathbf{E}_j-\langle\mathbf{E}_j\rangle)^2\rangle\cong 2\pi u_j^2(\mathbf{r})\hbar\omega_j + 32\pi^2e^2\frac{u_j^2(\mathbf{r})}{V}\left[\left(\frac{b}{2}\right)^2A^2+\left(\frac{\hbar}{2mb}\right)^2\frac{1}{\omega_j^2}B^2\right]. \quad (42)$$

It is readily seen that application of the preceding analysis to a specific experiment requires detailed consideration of the parameters of the experiment, which is outside the scope of the present paper. The significance of the analysis may be illustrated, however, by performing a few order-of-magnitude calculations. We will now calculate the relative magnitudes of the first and second terms with respect to each other and with respect to the square of the expectation value of field increment. From Eq. (42), and the preceding order-of-magnitude calculations, we have

$$\langle(\mathbf{E}_j-\langle\mathbf{E}_j\rangle)^2\rangle\sim 2\pi u_j^2(\mathbf{r})\hbar\omega_j+32\pi^2e^2u_j^2(\mathbf{r})\delta^2(\tau)/V. \quad (43)$$

The ratio of the second to the first term on the right side of Eq. (43) is

$$\frac{16\pi}{137}\frac{\lambda_j\delta^2(\tau)}{V}.$$

If we take $V\sim\lambda_j^3$, then this ratio is of the order of $\delta^2(\tau)/\lambda_j^2$. For the case in which we are interested, as has been pointed out previously, this is much smaller than unity, so that the uncertainty in field of a particular mode produced by a single electron is much smaller than the uncertainty which exists initially in the field. If $f(\theta)$ contains a sinusoidal variation with a periodicity of 2π, then the previously estimated orders of magnitude of A and B may have to be multiplied by $(\theta^+-\theta^-)$, which could be large. This is a case of resonance between the electron and field, or a "traveling wave" effect. We will not consider this case. In order to calculate the ratio of each of the terms in Eq. (43) to the square of the expectation value of the increment in field due to the electron, we obtain from Eq. (28)

$$\Delta\langle\mathbf{E}_j\rangle\cong 4\pi e\mathbf{u}_j(\mathbf{r})v_0V^{-\frac{1}{2}}\omega_j^{-1}C, \quad (44)$$

where

$$C=\int_{\theta_j^-}^{\theta_j^+}d\theta' f_j(\theta')\cos(\theta_j-\theta').$$

In accordance with the previous discussion, therefore,

$$\Delta\langle\mathbf{E}_j\rangle\sim 4\pi e\mathbf{u}_j(\mathbf{r})v_0V^{-\frac{1}{2}}\omega_j^{-1},$$

and we have

$$\frac{\langle(\mathbf{E}_j-\langle\mathbf{E}_j\rangle)^2\rangle}{(\Delta\langle\mathbf{E}_j\rangle)^2}\sim 137\pi^2\frac{c^2}{v_0^2}\frac{V}{\lambda_j^3}+2\frac{c^2}{v_0^2}\frac{\delta^2(\tau)}{\lambda_j^2}. \quad (45)$$

The first term on the right is the square of the ratio of the uncertainty due to field quantization to the field increment, and the second term is the square of the ratio of the uncertainty due to electron quantization to the field increment. We note that the first term is always large. This means that the increment in field due to a *single* electron is much smaller than the initial uncertainty in the field, and shows that a large number of electrons are needed to produce a change in field comparable to its uncertainty. The second term is, of course, much smaller than the first.

It is seen that one electron cannot affect the field significantly. It would therefore be interesting to study the effect of the passage of many electrons. We consider a simplified situation in which the interactions between the electrons may be neglected. Use can then be made of the above analysis. For simplicity of notation, we omit the mode subscript on the right side of the following equations. We drop the second-order term in Eq. (8) since, as has been shown, its contribution to the dispersion in field is much smaller than that of the first order term, and we have already neglected this contribution in writing down Eq. (42).[12] It is evident that the suitable modification for Eq. (7) in the case of a number of electrons is then

$$P_j(t)=P(0)\cos\omega t-\frac{\omega}{4\pi c^2}Q(0)\sin\omega t - \frac{e}{mc}\sum_\alpha\int_0^t dt_1\mathbf{u}_\alpha^{(0)}(t_1)\cdot\mathbf{p}_\alpha^{(0)}(t_1)\cos\omega(t-t_1), \quad (46)$$

where $\mathbf{u}_\alpha(t_1)$ stands for $\mathbf{u}(\mathbf{r}_\alpha(t_1))$, and the index α refers to the αth electron. We consider a group of n electrons, the initial wave packet of each being the same as the initial wave packet for the single electron we have considered, except that it is displaced by an amount ϵ_α along the x-axis. Rather than using a different analytical form for each of these wave packets in making calculations with the interaction term in Eq. (46), we can make use of the results already obtained by considering a different coordinate system for each electron, the αth coordinate system for the αth electron having its origin at ϵ_α. Of particular interest are the modifications in

the place where the electron wave packet has its minimum uncertainty product, $\Delta x\Delta p_x=\hbar/2$, and likewise for the other coordinates. As the electron proceeds from the origin, the uncertainty product becomes greater. In an experimental arrangement, the electron has to be "prepared," that is, endowed with its initial properties, before it is sent through the cavity. After its preparation, the wave packet will spread and its uncertainty product increase. If the preparation is an ideal one, resulting in the minimum uncertainty product, the place where the electron was prepared corresponds to the origin of the coordinate system in our analysis. If the preparation was not an ideal one, we can still regard the place of preparation of the electron as the origin, but now, the experimental quantum effects will be larger than those calculated.

[12] The contributions of both terms are of second order.

Eqs. (42) and (45) which must be made in order to account for more than one electron. It is evident that Eq. (42) becomes

$$\langle(\mathbf{E}_j-\langle\mathbf{E}_j\rangle)^2\rangle=2\pi u^2(\mathbf{r})\hbar\omega$$
$$+32\pi^2e^2\frac{u^2(\mathbf{r})}{V}\sum_\alpha\left[\left(\frac{b}{2}\right)^2A_\alpha^2+\left(\frac{\hbar}{2mb}\right)^2\frac{1}{\omega^2}B_\alpha^2\right], \quad (47)$$

where

$$A_\alpha=\int_{\theta_\alpha^-}^{\theta_\alpha^+}d\theta' f_\alpha(\theta')\sin(\theta-\theta'),$$

and

$$B_\alpha=\int_{\theta_\alpha^-}^{\theta_\alpha^+}d\theta' f_\alpha(\theta')\theta'\sin(\theta-\theta').$$

It is equally evident that

$$\theta_\alpha^-=(\omega/v_0)x_\alpha^-=(\omega/v_0)(x^--\epsilon_\alpha)=\theta^--(\omega/v_0)\epsilon_\alpha,$$
$$\theta_\alpha^+=\theta^+-(\omega/v_0)\epsilon_\alpha,$$

and

$$f_\alpha(\theta)=V^{\frac{1}{2}}u_\alpha(x)=V^{\frac{1}{2}}u(x+\epsilon_\alpha)=f(\theta+\epsilon_\alpha\omega/v_0).$$

We can therefore write A_α and B_α as

$$A_\alpha=\int_{\theta^-}^{\theta^+}d\theta' f(\theta')\sin\left(\theta-\theta'+\frac{\omega}{v_0}\epsilon_\alpha\right),$$

and

$$B_\alpha=\int_{\theta^-}^{\theta^+}d\theta' f(\theta')\left(\theta'-\frac{\omega}{v_0}\epsilon_\alpha\right)\sin\left(\theta-\theta'+\frac{\omega}{v_0}\epsilon_\alpha\right).$$

By the same reasoning, we obtain, as the modification of Eq. (44),

$$\Delta\langle\mathbf{E}_j\rangle\cong 4\pi e\mathbf{u}(\mathbf{r})v_0V^{-\frac{1}{2}}\omega^{-1}\textstyle\sum_\alpha C_\alpha, \quad (48)$$

where

$$C_\alpha=\int_{\theta^-}^{\theta^+}d\theta' f(\theta')\cos\left(\theta-\theta'+\frac{\omega}{v_0}\epsilon_\alpha\right).$$

Equations (47) and (48) can be simplified considerably if we assume that ϵ_α is sufficiently small so as not to change appreciably the value of the sine or the cosine of which it is part of the argument. This means that we are considering what is known as a "bunch." Then we have

$$\Delta\langle\mathbf{E}_j\rangle\cong 4\pi e\mathbf{u}(\mathbf{r})v_0V^{-\frac{1}{2}}\omega^{-1}nC,$$

and

$$\langle(\mathbf{E}_j-\langle\mathbf{E}_j\rangle)^2\rangle\cong 2\pi u^2(\mathbf{r})\hbar\omega$$
$$+32\pi^2e^2\frac{u^2(\mathbf{r})}{V}n\left[\left(\frac{b}{2}\right)^2A^2+\left(\frac{\hbar}{2mb}\right)^2\frac{1}{\omega^2}B^2\right].$$

We now see that if we have a large number of electrons, the second term will become larger than the first, and is equal to the first when the number of electrons is given by

$$n=137V/8\lambda\delta^2(\tau)\sim 17\lambda^2/\delta^2(\tau). \quad (49)$$

The equation corresponding to (45) is

$$\frac{\langle(\mathbf{E}_j-\langle\mathbf{E}_j\rangle)^2\rangle}{(\Delta\langle\mathbf{E}_j\rangle)^2}\sim\frac{137\pi^2}{n^2}\frac{c^2}{v_0^2}\frac{V}{\lambda^3}+\frac{2}{n}\frac{c^2}{v_0^2}\frac{\delta^2(\tau)}{\lambda^2}. \quad (50)$$

It is interesting to note the number of electrons needed to produce a field equal to the uncertainty in the field, which is obtained by setting the right side of Eq. (50) equal to unity. Assuming, for the moment, that the second term is much smaller than the first, we obtain

$$n^2\sim 137\pi^2(c^2/v_0^2)V/\lambda^3.$$

If we consider a case where $v_0=10^{-1}c$, and $V\sim\lambda^3$, then the number of electrons needed (in a bunch) is of the order of 400. If we have $\delta(\tau)\ll\lambda$, which is the case we have considered all along, then it is easily seen that the second term on the right side of Eq. (50) is much smaller than unity for $n\sim 400$, so that our assumption was justified. We see, thus, that this second term becomes the dominant term (for increasing n) only when n is very large [larger than the value given by Eq. (49)], and then the ratio of uncertainty in field to field increment is much smaller than unity. The first term is the dominant one in the cases which are of main interest to us, namely, those in which the above ratio is of the order of unity.

One may ask how the ratio of Eq. (50), the nonvanishing of which is a purely quantum-mechanical effect, depends on the frequency. The answer lies in the fact that, even if V/λ^3 is maintained constant, n will become smaller at higher frequencies, and the ratio will increase. Firstly, if the dimensions of the cavity become small, the cross section of the electron beam must become small.[13] Secondly, the n electrons must all be, as we have seen, within a distance ϵ along the x-axis such that

$$(\omega/v_0)\epsilon=2\pi(c/v_0)(\epsilon/\lambda)\ll 2\pi. \quad (51)$$

As the wavelength becomes short, therefore, n must become small, and the ratio of uncertainty in field to field increment will become large.

It is of interest to perform a numerical order-of-magnitude calculation to see how n is limited by the frequency. We will consider a dense electron beam passing through the cavity and determine the number of electrons in a segment of beam having the length of a bunch. If I_0 is the beam current, then

$$n=I_0\epsilon/ev_0.$$

[13] Although we have assumed in our analysis that all the electrons lie along the x-axis, this is obviously an idealization, and, in practice, the electron beam has a macroscopic cross section.

A dense electron beam can be taken to be $I_0 \sim 10^5 A$, where I_0 is in amperes and A, the cross-sectional area of the beam, is in square meters.[14] If, in accordance with Eq. (51), we take $\epsilon \sim 10^{-1}\lambda v_0/c$, and if we consider $A \sim \lambda^2$, then $n \sim 2\times 10^{16}\lambda^3$, where λ is in meters. It is thus evident that n becomes small with the wavelength. If we want to know at what wavelength n is just large enough to produce an increment in field equal to the initial uncertainty in field, we set n equal to 400 and find that the wavelength is of the order of a tenth of a millimeter.

The author wishes to thank Professor Julian Schwinger for very helpful discussions of the foregoing subject matter and for his reading of the manuscript.

[14] This is the order of magnitude of the current in the densest beams used in microwave tubes.

PHYSICAL REVIEW VOLUME 98, NUMBER 4 MAY 15, 1955

Freundlich Red-Shift Formula

M. A. MELVIN
Department of Physics, Florida State University, Tallahassee, Florida

(Received November 17, 1954)

Freundlich has attempted to explain various anomalous observations by suggesting that the red shift be reinterpreted as an effect proportional to radiation density and length along the path of a photon. For a star of radius R the contribution of the outside radiation field exceeds that within the atmosphere (thickness l_0) by a factor of the order of $R/l_0 = 1000$ for average stars; this makes Freundlich's original formula untenable. The question is here examined whether the objections to Freundlich's conception can be removed if one reduces his constant of proportionality by 10^{-3}. To give the conception a full trial the calculations are made realistically, taking into account the extension of the star, and the deviations from Lambert's law of emission which result from the radiative transfer conditions in the photosphere. The resultant formula for the radiation shift gives an approximate fit with solar observations out to near the limb without retaining, as Freundlich does, an additional relativity shift equal to one fifth of the expected value. However, the rise of the observed shift at the limb to the gravitational value (and even higher) is unaccounted for. The serious objections to Freundlich's interpretation from other astronomical evidence still stand, though the order of magnitude of the discrepancies is in some instances considerably reduced.

THERE are systematic anomalies, as compared with the expected gravitational values, in the red shifts of the sun,[1] of many of the hotter stars,[2] and of the cool supergiant M stars.[3] The situation with the white dwarfs is not altogether clear: there is some doubt about the consistency of the observations on Sirius B with proposed models; on the other hand Popper[4] has recently found a fairly good verification of the gravitational shift in 40 Eridani B.

In an attempt to correlate the various anomalous red shifts Freundlich[5] has suggested that there is a red shift $\Delta\lambda/\lambda$ proportional to the radiation density U in the path of a photon and to the path length. Presumably such a shift, if it exists, is due to some as yet unformalized action of a radiation field upon a photon; none of the accepted processes for light scattering have anywhere near the size of cross section required to produce such an effect.[6] Thus, there is a natural reserve about accepting Freundlich's interpretation. A preliminary question to be settled before one even considers interpretation is whether the suggested proportionality of shift to U and path length really is valid.

For paths of length l along which U is constant, the

[1] C. E. St. John, Astrophys. J. **67**, 195 (1928); Freundlich, Brunn, and Bruck, Z. Astrophys. **1**, 43 (1930); M. G. Adam, Monthly Notices Roy. Astron. Soc. **108**, 446 (1948); L. Spitzer, Monthly Notices Roy. Astron. Soc. **110**, 216 (1950). Spitzer finds reasons why the collisional shifts are likely to be to the violet rather than the red, helping to explain the observed defect from the gravitational values. The articles by L. Goldberg and C. E. Moore, in *The Sun*, edited by G. P. Kuiper (University of Chicago Press, Chicago, 1953), contain useful bibliographies on the line shift problem.

[2] This is shown by the dependence of the K-term on spectral class of stars: R. J. Trumpler and H. F. Weaver, *Statistical Astronomy* (University of California, Berkeley, 1953), pp. 291, 354, 566; H. F. Weaver, *Vistas in Astronomy* (Pergamon Press, London, 1954). Even after Weaver's recent reanalysis of the data, and correcting for the gravitational effect, there seems to be a residual shift of 1–2 km/sec for O and B stars. Also in some Wolf-Rayet stars, which are much hotter yet, extraordinary red shifts have been demonstrated: O. C. Wilson, Astrophys. J. **91**, 394 (1940); **109**, 76 (1949).

[3] W. S. Adams and E. MacCormack, Astrophys. J. **81**, 119 (1935). These, like the solar discrepancies, have been ascribed to large systematic motions in the atmospheres; however various investigators do not agree about the likelihood of such large motions.

[4] D. M. Popper, Astrophys. J. **120**, 316 (1954).

[5] E. F. Freundlich, Proc. Phys. Soc. (London) **A67**, 192 (1954); Phil. Mag. **45**, 303 (1954).

[6] D. Ter Haar, Phil. Mag. **45**, 320 (1954). It should be remarked however that, in a recent analysis, T. Neugebauer, Acta Phys. Acad. Sci. Hung. **IV**, 31 (1954) has pointed out the enormous preponderance, under certain conditions, of small-angle forward scattering (the "Mie effect") such as would be requisite to produce red shift phenomena; he has suggested that neutrino-photon scattering may occur with sufficient probability to serve as an alternative to the relativistic explanation of the Hubble (cosmic) shift.

suggested shift may be written

$$\Delta\lambda/\lambda = BU\int dl = BUl = AT^4 l, \qquad (1)$$

where A and B are constants, and T is the cavity-radiation temperature along the path. Freundlich evaluates A empirically, from data on B-type stars, to be 2×10^{-29} deg^{-4} cm^{-1}.

In analyzing the red shift across the solar disk, Freundlich assumes that the length of path l through the atmosphere is equal to $l_0 \sec\Theta$, l_0 being the thickness of the atmosphere and Θ the angle between the outward solar radius and the line to the observer (Fig. 1). The formula (1) then gives

$$(\Delta\lambda/\lambda)_{\text{inside}} = BUl_0 \sec\Theta. \qquad (1')$$

This expression, corrected by an added adjusted constant, is represented by the dashed curve in Fig. 2. (Freundlich interprets the added constant, *ad hoc*, as a relativity shift equal to $\frac{1}{5}$ the expected value.)

Freundlich's basic conception was not applied consistently by him, since, except in one case, he considered only the effect of the radiation field in the atmosphere of the star. Several people have since made calculations including the effect of the radiation field outside a star both on one of its own photons and on that of another star passing near it. The conclusions seem incompatible with observational data both from individual[6] and binary stars,[7] because the outside contribution (see below) turns out to be a thousand times greater than the contribution (1).

In view of the peristent anomalies, however, it is worth while to ask whether it is possible to salvage Freundlich's attempted correlation by analyzing the data on the basis of an outside shift instead, and revaluating his constant A accordingly. That this might possibly yield the center-limb increase in shift across the solar disk is suggested by the fact that a photon coming from near the limb has a longer path in the vicinity of the sun than a photon coming straight away from the center. The M-supergaint and cosmic shift evidence cited by Freundlich is of course not compatible with attributing the bulk of the shift to an outside effect, and their reinterpretation would have to be dropped.

For generality, we consider the shift in λ for a photon originating at any point P in the neighborhood of a principal star ☉, which we shall refer to conveniently as "solar" (Fig. 1). With suitable reinterpretation this may be applied to a stellar photon nearly grazing the sun at time of total eclipse, or to a photon originating in the companion of the principal star in a binary system. Let the angle between the outward solar radius vector and the line of sight at P be Θ. Let ρ be the variable radial distance given as a fraction of the solar

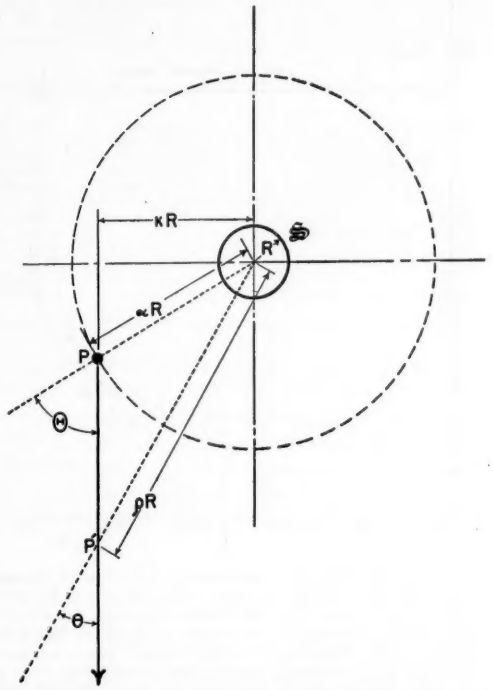

FIG. 1. Variables involved in the calculation of the effect of the radiation density around a primary star ☉ upon a photon originating at P and moving along the path PP'.

radius; α is the value of ρ where the photon originates and κ is the component of α normal to the photon path. If P' is any point on the line of sight, and θ the corresponding angle, the following relations hold:

$$\kappa/\rho = \sin\theta, \quad d\rho/d(l/R) = \cos\theta. \qquad (2)$$

The fractional red shift in the light on the path from P to E (the observer) is then

$$(\Delta\lambda/\lambda)_{\text{outside}} = B\int_P^E U(P')dl$$

$$= BR\int_\alpha^\infty U(\rho)(1/\cos\theta)d\rho, \qquad (3)$$

where the distance to the observer is set equal to infinity. On the point-source model used by Ter Haar[6] and Helfer,[7]

$$U = u_1/\rho^2, \qquad (4)$$

one finds

$$(\Delta\lambda/\lambda)_{\text{outside}} = Bu_1R\Theta/\kappa = Bu_1(R/\alpha)\Theta/\sin\Theta. \qquad (4')$$

The proper value to be given to the constant u_1 will be indicated below. At the surface of the sun $\alpha=1$ and the contribution (4′) would certainly far outweigh (1′) since $R/l \gtrsim 10^3$. The dependence on Θ in (4′) is too

[7] H. L. Helfer, Phys. Rev. **96**, 224 (1954).

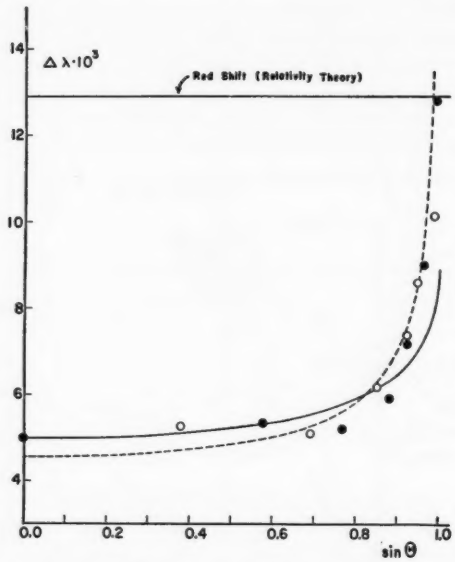

FIG. 2. The red shift $\Delta\lambda$ of solar lines as a function of the angle Θ between the solar radius to a point on its surface and the line of sight from that point. The full circles represent Adam's data (Oxford, 1948) (reference 1), the open circles Freundlich's data (Potsdam, 1930) (reference 1). The dashed curve represents Freundlich's secant formula based upon considering only the atmospheric contribution to the radiation shift. The full curve represents the outside contribution according to Eq. (5″) with Freundlich's constant reduced to 10^{-3} of his value.

gradual to represent the observed variation across the sun (Fig. 2) since (with a suitably adjusted B) it rises from the initial value of 5×10^{-3} to only $7.8\times10^{-3}A$ at $\Theta=\pi/2$, whereas the observed rise is quite steep near the limb. One may not reject (3) outright on this basis, however, since (4) has been derived assuming the point source model of the radiation field, which can lead to appreciable error near a star where the shift effect is greatest.

A more careful calculation,[8] taking into account the extension of the (spherical) source and the proper angular distribution of intensity emitted from the photosphere, shows that the radiation field near a star can be fairly well represented by

$$U(\rho)=U_1[1-(1-1/\rho^2)^{\frac{1}{2}}],$$
$$[U_1=(7/4)\text{Emittance}/c]. \quad (5)$$

The difference in general form between $U(\rho)$ in (5), and the point-source expression (4) takes account of the extension of the source. On the other hand the numerical factor (7/4 rather than 2, as it would be with Lambert's law) in the expression for U_1 represents approximately the effect of the law of radiance from the outer boundary of the photosphere resulting from radiative transfer conditions within. [We note that for (4) to be an approximation to (5) u_1 must be taken *one-half* as large as U_1.]

Using (2), setting $1/\rho\equiv\sin\varphi$ and $1/\alpha\equiv\sin\Phi$, and substituting (5) in (3) we find

$$\left(\frac{\Delta\lambda}{\lambda}\right)_{\text{outside}}=BU_1R\int_0^{\Phi}\frac{1-\cos\varphi}{\sin^2\varphi\Delta(\varphi)}\cos\varphi d\varphi,$$
$$[\Delta(\varphi)\equiv(1-\kappa^2\sin^2\varphi)^{\frac{1}{2}}].$$

The integral may be expressed in terms of elliptic integrals of the first and second kind, and gives

$$\left(\frac{\Delta\lambda}{\lambda}\right)_{\text{outside}}=BU_1R\left[\mathcal{E}_\alpha(\Theta)-\frac{1-\cos\Phi}{\sin\Phi}\cos\Theta\right], \quad (5')$$

where we have introduced the function

$$\mathcal{E}_\alpha(\Theta)=E(\Phi,\kappa), \qquad (\kappa\equiv\alpha\sin\Theta\leq1)$$
$$\mathcal{E}_\alpha(\Theta)=\kappa[E(\Theta,1/\kappa)-(1-1/\kappa^2)F(\Theta,1/\kappa)]. \qquad (\kappa\equiv\alpha\sin\Theta\geq1)$$

(The second argument in E and F is the modulus.) At the surface of the sun $\alpha=1$ and $\Phi=\pi/2$. We then have

$$(\Delta\lambda/\lambda)_{\text{outside}}=BU_1R[\mathcal{E}_1(\Theta)-\cos\Theta]. \quad (5'')$$

This formula, adjusted to coincide with the observational point at $\Theta=0$, is shown by the full curve in Fig. 2. As we see, it is an improvement on the point-source representation (4′). However, it still falls appreciably short of the full limb value, rising only to about 8.8×10^{-3} A. Thus (5′) cannot be regarded as very satisfactory.

From the respective calculated and observed quantities at $\Theta=0$:

$$\mathcal{E}_1(0)-\cos0=\pi/2-1, \quad (\Delta\lambda/\lambda)_{\text{obs}}=5\times10^{-3}/6100,$$

and the known values of the radius and emittance for the sun, we find

$$U_1=(7/4c)\times6.25\times10^{10}\text{ erg cm}^{-3},$$
$$B=5.7\times10^{-18}\text{ cm}^2\text{ erg}^{-1},$$

which corresponds to an approximate value

$$A=(7\sigma/4c)B=2\times10^{-32}\text{ deg}^{-4}\text{ cm}^{-1}, \quad (6)$$

one thousand times smaller than Freundlich's value.

The counter-evidence to Freundlich's hypothesis, assembled by Helfer from binary star data, is still decisive. In Table I we have listed again the double-star systems selected by Helfer, where both components are of the same type. Assuming rough equality in the radii, we have first calculated on the basis of (5′), using A as given in (6), the fixed shift in the light of each component due to its own radiation field (column 6). In the last column of Table I we have calculated the minimum, middle, and maximum observable radiation shifts over a half-period of revolution [at $\Theta=\sin^{-1}(1/\alpha)$,

[8] A calculation of the radiation flux field outside a radiatively transferring spherical source has been made [M. A. Melvin (to be published)].

TABLE I. A reanalysis of Helfer's data from five binary star systems by which Freundlich's red-shift interpretation was tested. The results in column 7 are obtained upon the basis of formula (5′). For the minimum and middle shifts the values obtained by means of the point-source model do not differ appreciably from the more exact values given in column 7; for the maximum shift the difference is appreciable and is indicated in parentheses.

1 Star name	2 Eff. temp. °K	3 Mean radius in units of the solar radius	4 Radial distance between stars in units of their radius	5 Observed semi-amplitudes expressed in km/sec	6 Calculated fixed shift of each star due to own radiation field, km/sec	7 Calculated min middle and max shift in a half-period, due to radiation field of companion km/sec
TT Aur.	18 000	4.3	2.7	197; 246	188	36 ; 55 ; 102 (259)
WW Aur.	8000	2.1	6.0	116; 135	3.6	0.3; 0.5; 0.9 (5.3)
TX Her.	10 000	1.6	6.7	121; 140	6.7	0.5; 0.8; 1.3 (10)
Z Vul.	18 000	4.3	3.5	96; 214	188	28 ; 42 ; 81 (268)
Y Cyg.	25 000	5.9	4.8	245; 241	960	101 ; 156 ; 304 (1405)

$\pi/2$, and $\pi-\sin^{-1}(1/\alpha)$], in the light of one component due to the radiation field of its companion. It is seen that, while the variations in shift are now within the semiamplitudes of the radial velocity curves, they are still, except for two of the systems, considerably outside of observational error.

In view of the reduced magnitude of the stellar-statistical K-term which emerges from Weaver's recent analysis,[1] there is no longer any possibility of correlating the solar shift values with those found in *O* and *B* stars—that is if one adheres to the temperature fourth power (radiation density) dependence, or any reasonable modification thereof. This is illustrated forcibly again by the large values in column 6 of Table I.

PHYSICAL REVIEW VOLUME 98, NUMBER 4 MAY 15, 1955

Entropy of Radiation

AADNE ORE
Physics Institute, University of Oslo, Oslo, Norway
(Received January 7, 1955)

In view of the recent publication of a derivation of the expression for the entropy flux of radiation, in terms of its spectral specific intensity, a brief comparative study of various known methods for obtaining the entropy formula is presented.

IN a recent article P. Rosen presents an interesting discussion of the question of how to obtain an expression for the entropy flux of electromagnetic radiation of specified intensity.[1] The very problem itself implies, in its general formulation, a well-defined entropy concept for nonequilibrium radiation. Rosen's derivation of the above-mentioned expression starts with the ordinary statistical definition of entropy, in this case for a system of photons (bosons) in terms of their density in phase space, followed by the substitution of this density by the equivalent expression in terms of the specific intensity of the corresponding radiation.

The explicit solution to the problem may be expressed in "differential" form as a relation connecting K_ν, the specific radiation (energy) intensity of linearly polarized light of frequency ν, and L_ν, the corresponding specific entropy intensity. K_ν is defined in such a manner that $K_\nu d\nu d\sigma \cos\theta d\Omega$ represents radiation energy pr. sec (power) in the frequency band $d\nu$ which passes through an element of area, $d\sigma$, and inside an element of solid angle, $d\Omega$, in a direction which makes an angle θ with the normal to the area. L_ν is defined correspondingly. The desired relation turns out to be the following:

$$L_\nu=(k\nu^2/c^2)[(1+x)\ln(1+x)-x\ln x],\quad x\equiv c^2K_\nu/h\nu^3, \quad (1)$$

where k=Boltzmann's constant, h=Planck's constant, and c=velocity of light.

In passing to present his elegant derivation of what amounts to this formula, Rosen makes a statement to the effect that while Planck has previously derived a functional relation, $L_\nu=\nu^2 f(K_\nu/\nu^3)$, no explicit expression was given by the latter[2] for $f(K_\nu/\nu^3)$.

In the opinion of the present author, however, the explicit relationship for L_ν in terms of K_ν was indeed known to Planck, even prior to the advent of the Bose-Einstein statistics proper.[3] It seems worth while, therefore, to present a brief comparison of various methods of proving the entropy formula (1).

As previously mentioned, Rosen bases his method on

[1] P. Rosen, Phys. Rev. **96**, 555 (1954).

[2] M. Planck, *The Theory of Heat* (The MacMillan Company, New York, 1949).

[3] Bose, Z. Physik **26**, 178 (1924).

the statistical extension of the entropy concept to non-equilibrium states of a system of bosons. Long ago Planck[4] derived formula (1) by an admittedly less satisfactory method which, on the other hand, in part bears a formal resemblance to the more modern one based on Bose-Einstein statistics. The introduction of the concept of entropy of radiation dates back toWien.[5] Planck has shown, furthermore, that reasoning along the lines of ordinary thermodynamics and classical electrodynamics leads, firstly, to what is a generalized form of Wien's displacement law, namely, the functional relation previously indicated:

$$L_\nu=(\nu^2/c^2)F(c^2K_\nu/\nu^3), \tag{2}$$

and, secondly, to the following relations connecting, in the stationary state for oscillators exposed to radiation, the mean vibrational energy, U, and the mean entropy, S, of a linear, harmonic oscillator (resonator) of frequency ν, with the field quantities K_ν and L_ν:

$$U=(c^2/\nu^2)K_\nu, \quad S=(c^2/\nu^2)L_\nu. \tag{3}$$

Equations (2) and (3) imply

$$S=F(U/\nu). \tag{4}$$

The statistical definition of entropy is then introduced in order to obtain Eq. (4), and thereby Eq. (2), in explicit form. In distributing a given amount of energy on a system of identical resonators Planck[4] actually introduces energy quanta, $h\nu$. The statistical problem is then mathematically equivalent to that for bosons, a fact which is also apparent from the resultant expression:

$$S=k\left[\left(1+\frac{U}{h\nu}\right)\ln\left(1+\frac{U}{h\nu}\right)-\frac{U}{h\nu}\ln\frac{U}{h\nu}\right], \tag{5}$$

when this is being compared with the statistical expression for the entropy of a system of bosons.[1] It is readily seen, furthermore, that the formula (5) renders Eq. (2) identical with Eq. (1). It may, perhaps, be considered a matter of convenience whether the explicit form of the function F be derived in this way rather than by considering directly the relation (2) for the radiation itself.

A different method of deducing the entropy formula (1) is one which makes explicit use of the extension of the temperature concept. The first attempt to assign a definite temperature to monochromatic radiation seems to have been made by Wiedemann,[6] but in a rather limited way. More generally, the temperature may be defined thermodynamically, i.e., by putting

$$dL_\nu=dK_\nu/T, \quad \text{or} \quad \partial L_\nu/\partial K_\nu=1/T. \tag{6}$$

Again, T and K_ν are interlinked through the celebrated Planck formula:

$$K_\nu=\frac{h\nu^3}{c^2}\frac{1}{e^{h\nu/kT}-1}, \tag{7}$$

which has been derived in a variety of more or less satisfactory ways during the first quarter of this century. This is the general relation between K_ν and T because in the equilibrium state (cavity radiation of temperature T) radiation of each frequency must be thought of as having the same temperature, equal to that of the cavity wall, as there is no internal or external dissipation of energy.

When Eq. (7) is solved with respect to $1/T$, and the result inserted in Eq. (6), integration of the latter leads once more to the same (absolute) entropy formula (1).[7]

[4] See M. Planck, *Theorie der Wärmestrahlung* (Johann Ambrosius Barth, Leipzig, 1906), first edition, p. 148ff.
[5] W. Wien, Ann. Physik **52**, 132 (1894).
[6] E. Wiedemann, Ann. Physik **34**, 446 (1888).
[7] M. Planck, *Theorie der Wärmestrahlung* (Johann Ambrosius Barth, Leipzig, 1913), second and subsequent editions. See also R. Clark Jones, J. Opt. Soc. Am. **43**, 138 (1953).

Velocity Analysis of Thermionic Emission from Single-Crystal Tungsten*†

ANDREW R. HUTSON‡
Research Laboratory of Electronics, Massachusetts Institute of Technology, Cambridge, Massachusetts
(Received January 13, 1955)

A 180° magnetic velocity analyzer tube has been used to observe the energy distributions of the thermionic emission from various crystallographic directions of a single-crystal tungsten filament. The distributions were the same in all of the directions and were not Maxwellian. An energy-dependent reflection coefficient for the tungsten surface, previously proposed by Nottingham, is capable of explaining the shape of the distributions quite well. The tube permitted measurements of the differences between the true work functions of the various directions. The changes of true work functions with temperature between 1700°K and 2000°K were also measured for all directions except the (110). The non-Maxwellian character of the energy distributions and the temperature variations of the work functions can largely explain the discrepancy between the emission constant, $A=120$, of Richardson's equation and the Richardson-plot emission constants obtained for the various directions of a tungsten crystal by Nichols and by Smith.

I. INTRODUCTION

At the present time, knowledge of the phenomenon of thermionic emission is still incomplete. Thermodynamics and the Fermi-Dirac statistics yield the well-known Richardson equation, $j=AT^2(1-\bar{R})\exp(-e\phi/kT)$, when applied to an electron gas in equilibrium with a metal of work function ϕ at a temperature T. The emission constant, A, is made up of well-known physical constants and is 120 amperes/cm² deg², and $\bar{R}$ is an average reflection coefficient for the metal surface. However, this equation, without the factor $(1-\bar{R})$, is usually applied empirically to the situation in which saturation current is being drawn from the metal surface. A Richardson plot of the variation of emission current with temperature is used to obtain empirical values of the work function and emission constant. These values may differ from the true work function and the A of 120 because of "patchiness" of the surface, temperature variation of the true work function, and reflection at the metal surface. The review article by Herring and Nichols[1] treats both the thermodynamic aspects of the Richardson equation and these difficulties in its application.

Nichols[2] was the first to make quantitative measurements of the emission from a single crystal of tungsten in the crystallographic directions of maximum and minimum emission. He obtained Richardson plot values for the work functions and emission constants in the various directions. Smith[3] has recently repeated this experiment with some refinements in technique, and his results are in substantial agreement with those of Nichols. The empirical emission "A" constants obtained in the different directions differ from one another, and with the exception of the (112) direction they are all less than 120. From the results of this experiment, one cannot distinguish between the effects of patchiness, temperature variation of the work function, and reflection.

Both patchiness and reflection, if it is energy-dependent, would result in an anomalous energy distribution of the emitted electrons. If there were no patchiness or reflection, one should observe an energy distribution characteristic of the particle current of a Maxwell-Boltzmann gas, since the density of the electron gas in equilibrium with the metal is low enough for the Fermi-Dirac distribution to be well represented by the classical distribution. (The principle of detailed balance requires that the energy distribution of the particle current from the metal surface be the same as that of the particle current in the gas provided that there is no reflection at the metal surface.) The only observations of energy distribution have been made in terms of retarding-potential data in which one obtains the integral under the energy distribution curve from a variable lower limit to infinity instead of the curve itself. Nottingham[4] found that his careful retarding-potential measurements on tungsten and thoriated tungsten could be best represented by an empirical reflection coefficient, which was an exponential function of the energy associated with motion perpendicular to the surface. The fact that all of Nottingham's retarding-potential curves for tungsten and thoriated tungsten in all states of activation could be represented accurately by a single reflection coefficient is significant, in that it tends to support the view that one is dealing with a fundamental reflection effect rather than patchiness.

A previous measurement of the temperature coefficient of the work function of polycrystalline tungsten at thermionic temperatures has been made by Krüger and Stabenow.[5] They obtained an average value of $+6\times10^{-5}$

* This work was supported in part by the Signal Corps; the Office of Scientific Research, Air Research and Development Command; and the Office of Naval Research.

† This paper is based on a thesis submitted by Andrew R. Hutson in partial fulfillment of the requirements for the degree of Doctor of Philosophy in the Department of Physics of the Massachusetts Institute of Technology.

‡ Now at Bell Telephone Laboratories, Murray Hill, New Jersey.

[1] C. Herring and M. H. Nichols, Revs. Modern Phys. **21**, 185 (1949).

[2] Myron H. Nichols, Phys. Rev. **57**, 297 (1940).

[3] George F. Smith, Phys. Rev. **94**, 295 (1954).

[4] W. B. Nottingham, Phys. Rev. **49**, 78 (1936).

[5] F. Krüger and G. Stabenow, Ann. Physik **22**, 713 (1935).

Stabenow.[5] They obtained an average value of $+6\times10^{-5}$ ev/deg in the temperature range 2100°K to 2700°K by a calorimetric method. They claimed an accuracy of 20–30 percent for this result, however, their vacuum conditions were poor by modern standards. Langmuir[6] and Potter[7] have obtained values for the temperature coefficient of polycrystalline tungsten between room temperature and 1000°K. Their results are in disagreement, being of opposite sign, and in any case an extrapolation to thermionic temperatures would not be warranted.

In the present experiment, magnetic velocity analysis of the thermionic emission from a single-crystal tungsten filament has yielded: (1) the energy distributions of the emission in the various crystal directions, (2) the temperature coefficients of the work functions in the various directions, and (3) the actual differences in work function between the different directions at thermionic temperatures. The results of the first two measurements can satisfactorily explain the A values obtained by Nichols and by Smith. The third measurement serves as a check on the self-consistency of the interpretation.

II. FILAMENT PREPARATION

The growth of single crystals in G.E. "218" tungsten wire (of the pre-World War II variety) occupying the entire cross section and extending over several centimeters of length is now a well-known art. Robinson[8] has shown that one need only hold the temperature of the wire in the recrystallization range (about 2000°K) for a few hours to obtain large single crystals. There appears to be an optimum temperature for the process, above which many small crystals are produced because of the increased rate of formation of seed crystals, and below which the linear growth from a given seed crystal becomes impractically slow. The crystals grow with a face diagonal (110) direction, in the axis of the wire as a result of strains imparted to the wire in the drawing process. The crystal faces which can then be exposed on the surface must have as their normals the directions (*hhk*). Martin's[9] study of the emission from a single-crystal tungsten sphere showed that the principal maxima and minima of emission occurred on just these planes, though recent field-emission work[10] has also included a minor maximum in the (310) direction.

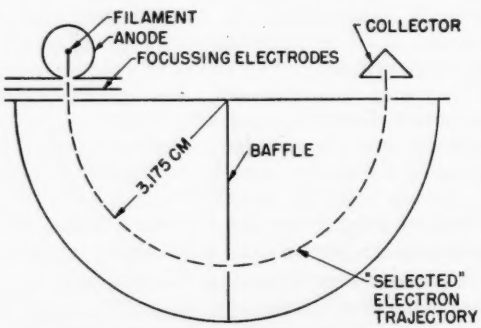

FIG. 1. Cross section of the analyzer tube.

The "dopes" which are added to the tungsten in fabrication to catalyze this growth of large crystals are largely driven out in the sintering and swaging processes. Nichols[11] gives the results of spectroscopic analyses of doped and undoped tungsten as well as their average Richardson plot emission constants and work-functions. He shows that the lower values of A^{**} and ϕ^{**} for the doped wire are merely due to the higher degree of preferred orientation, and that the crystals in "218" wire should be characteristic of pure tungsten.

As it comes from the manufacturer, the surface of the tungsten wire contains many deep longitudinal die scratches and therefore must be ground and polished smooth since accurate knowledge of the applied field demands a smooth surface. The grinding and polishing was carried out on a specially constructed wire polisher[12] which rotates the wire between a pair of laps, coated with abrasive, that traverse the length of the wire on a carriage driven by a lead screw.

The filament used for the present experiment was ground and polished from an initial diameter of 0.003 inch to about 0.002 inch as read on a micrometer caliper. After polishing, the wire appeared to have a mirror surface with just the faintest indication of abrasive scratch under observation with a 400× optical microscope. Johnson[13] has shown that these light scratches disappear during subsequent ac heating, and his observation has been verified for a number of filaments.

The diameter of the filament was measured by an interferometric technique with the 5461 A mercury line. The average of several readings along its length yielded a value of 5.16×10^{-3} cm.

The filament was given its recrystallization heat treatment in a cylindrical electron projection tube[14] in which the pattern of the intensity of thermionic emission may be observed directly. In this manner, the growth and quality of the large single crystals growing in the filament were easily monitored. Alternating current was used for filament heating in order to avoid dc etch, a peculiar type of surface roughening believed to be due to the effect of a longitudinal electric field upon the surface migration of the tungsten atoms.[15]

One interesting peculiarity was observed in the

[5] David B. Langmuir, Phys. Rev. **49**, 428 (1936).
[7] James G. Potter, Phys. Rev. **58**, 623 (1940).
[8] C. S. Robinson, Jr., J. Appl. Phys. **13**, 647 (1942).
[9] Stuart T. Martin, Phys. Rev. **56**, 947 (1939).
[10] M. K. Wilkinson, J. Appl. Phys. **24**, 1203 (1953).
[11] M. H. Nichols, Phys. Rev. **78**, 158 (1950).
[12] Johnson, White, and Nelson, Rev. Sci. Instr. **9**, 253 (1938).
[13] R. P. Johnson, Phys. Rev. **56**, 947 (1939).
[14] R. P. Johnson and W. Shockley, Phys. Rev. **49**, 436 (1936).
[15] R. P. Johnson, Phys. Rev. **54**, 459 (1938); R. W. Schmidt, Z. Physik **120**, 69 (1943); D. B. Langmuir, Phys. Rev. **89**, 911(A) (1953).

projection-tube patterns of all of the recrystallized filaments. When the filament temperature was held at 2000°K or lower, the (100) direction appeared as a narrow minimum between two broad (116) maxima, in agreement with previous observations. However, at a filament temperature of 2300°K, the (100) direction appeared as a narrow maximum separated from the (116) maxima by narrow minima. The explanation of this effect is found in the measurements of the temperature variations of the work functions.

III. VELOCITY ANALYZER TUBE

The principal elements of the velocity analyzer tube are shown in cross section in Fig. 1. The single-crystal filament was located coaxially within the cylindrical anode, and was supported in such a manner that it could be rotated about this common axis. Electrons emitted by the filament were accelerated in the radial direction by a positive potential applied to the anode. Those originating from a narrow sector of the filament passed through a slit in the anode and were focused into the entrance slit of the 180° analyzer chamber. The analyzer was a semicircular tantalum box whose faceplate (the diameter of the semicircle) contained the entrance and exit slits which were each 0.026 cm wide and 1.0 cm long. The analyzer chamber was partitioned by a baffle containing a slit of width 0.2 cm. An externally imposed uniform magnetic field, perpendicular to the plane of Fig. 1, caused the electrons to move in circular paths so that those electrons with precisely the right kinetic energy of motion in the plane of the diagram traversed all of the slits and were recorded as collector current.

The focusing electrodes modified the electric fields between the anode slit and analyzer entrance slit in a manner such that this region acted as a doubly convergent lens. This design feature resulted from the conflicting requirements of high angular resolution for the anode slit and sufficient resolution in energy within the analyzer. The anode slit, of width 0.026 cm, defined an angular sector of about three degrees in the one-centimeter diameter anode. However, unless there was a large radial accelerating field at the filament, there would have been a considerable number of electrons originating on either side of this three-degree sector which would have been able to pass through the anode slit by virtue of their initial tangential velocities. Numerical integration of electron trajectories within the anode indicated that an anode potential of about 1000 volts (radial field at the filament $\approx 75\,000$ volts/cm) would yield satisfactory angular resolution even in the crystallographic directions of lowest emission. This radial field is also much larger than the fields resulting from the differences of work function around the single-crystal filament.

The resolution in energy of this type of analyzer, $\Delta V/V$, is the ratio of slit width to analyzer radius which was 1/125. Thus, to obtain a "slice" of the energy distribution only a few hundredths of an electron volt wide, the electrons had to proceed through the analyzer with an energy of only a few electron volts. For most of the operation of the tube, the electrons were retarded from about 1000 ev to about 3 ev between the anode slit and the analyzer entrance slit ($\Delta V = 0.024$ v).

The action of the focusing electrodes upon the ribbon-like beam in the region between the anode and the analyzer is shown in an enlarged cross section in Fig. 2. If the anode slit and analyzer slit had been merely placed face-to-face without the focusing electrodes, the beam would have been divergent in the retarding field between the slits so that only a small fraction of the beam would have entered the analyzer. Also, the analyzer slit itself would have acted as an extremely short focal-length lens so that those electrons which did enter the analyzer would be fanned out and only a few would have been able to pass through the angle-limiting slit in the baffle.

The lens properties of this arrangement of slits were investigated on paper before the tube was finally designed. Solutions of LaPlace's equation in the region shown in Fig. 2 were obtained for a variety of focusing slit potentials by tracing the equipotentials on a large sheet of conducting paper[16] upon which the electrodes had been painted with silver, printed-circuit paint. The paraxial ray equation was integrated point-by-point making use of the values of the potential and the radius of curvature of the equipotentials at the lens axis. After the desired trajectory had been "bracketed" by trajectories obtained with various values of focusing voltage, it was concluded that the optimum focusing potential could best be obtained experimentally.

The structure of the analyzer tube is illustrated in Fig. 3 in which a number of the design features are apparent. With the exception of the collector, all of

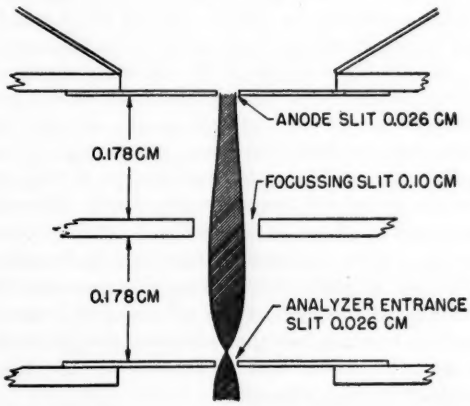

FIG. 2. Enlarged cross section of region between anode and analyzer. The electron trajectories lie within the shaded area.

[16] Manufactured for recording purposes by the Western Union Company under the trade name "Tele-Deltos."

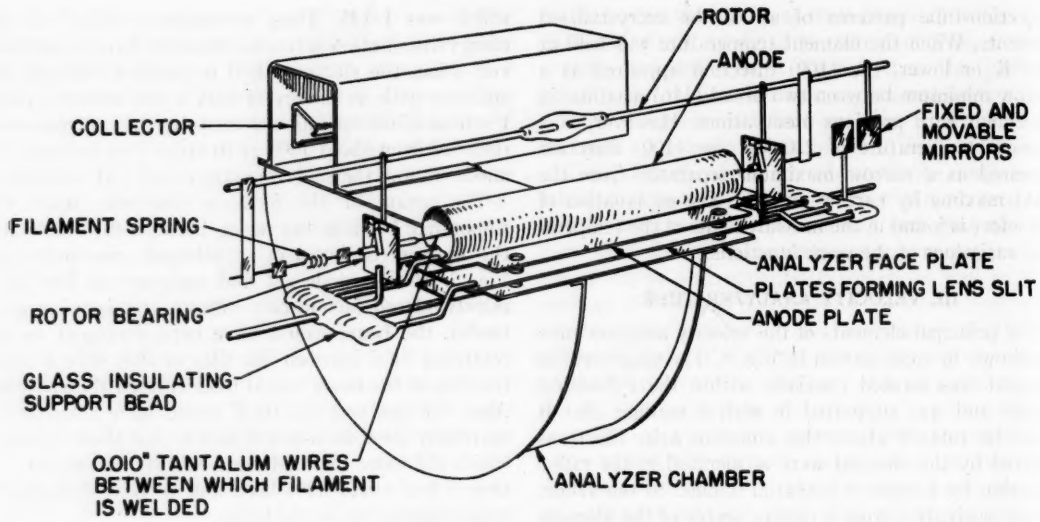

FIG. 3. Illustration of the analyzer structure.

the elements of the structure were mechanically supported by the analyzer face-plate. The face-plate was fabricated from accurately flat 0.020-inch tantalum sheet, and in order that the entrance and exit slits would not appear to be "corridors" they were sawed in a 0.003-inch tantalum sheet which had been welded over rectangular cut-outs in the face-plate. The same technique was used for the anode slit in the 0.010-inch tantalum anode plate. The anode itself was a cylinder, 1.0 cm in diameter, formed from 0.003-inch tantalum sheet. It contained a cut-out, larger than the slit in the anode plate, which fitted over the anode slit when the cylinder was welded tangent to the plate. The lens, or focusing slit, consisted of a gap between two coplanar, insulated 0.010-inch tantalum plates. Insulation of the two sides of the focusing slit allowed the application of a transverse electric field in the lens which could be used to compensate for small errors in the alignment of the slit and filament. All of the slits were sawed on a milling machine. After pre-outgassing the various parts, final assembly of the analyzer, anode, focusing electrodes, and the tantalum plates containing the holes for the rotor shafts was accomplished by flowing glass over the prebeaded tungsten support rods. The alignment holes which can be seen in Fig. 3 were used to hold the parts rigidly in a carefully machined jig (machining tolerances ± 0.0005 inch) during this operation. The advantage of this method of final assembly is that the structure is strain-free after removing the jig, thus all of the slits and the axis of rotation of the filament remained accurately parallel.

The 6-cm length of 0.002-inch recrystallized filament, containing the large single crystal was held on the axis of rotation of the rotor by tantalum wires which passed through guide holes accurately drilled along the axes of the rotor shafts. A tungsten helical spring maintained the proper tension in the filament.[17]

The structure of Fig. 3 was supported with the filament axis vertical by a single re-entrant press in a five-inch diameter pyrex envelope. The collector was supported independently by its own shielded re-entrant press. In order to rotate the filament, the entire tube was tipped so that the rotor would swing under the influence of gravity. (Rotation schemes involving a permanent magnet within the tube could not be used because of possible distortion of the analyzing field.)

The evacuation schedule of the tube, involving repeated cycles of baking and outgassing of the structure, conformed with modern high-vacuum technique. A Bayard-Alpert ionization gauge of our own design[18] was attached to a sidearm of the main envelope and sealed off with the tube. Immediately after seal-off, the gauge recorded a pressure of 9×10^{-10} mm which slowly rose to 1.5×10^{-9} mm, due largely to the diffusion of atmospheric helium through the Pyrex walls. The gauge remained in continuous operation after seal-off, and the pressure remained at 1.5×10^{-9} mm. The vacuum conditions in the tube proved satisfactory for the performance of the experiment. No change of the total emission of the filament was ever observed. There was only one observable change in the analyzer work-function. It occurred when a measurement was being attempted at a filament temperature of 2100°K and an anode potential of 1000 v. Enough gas was driven from the anode by electron bombardment to raise the pressure in the tube to 4×10^{-9} mm. Subsequently, the

[17] K. B. Blodgett and I. Langmuir, Rev. Sci. Instr. **5**, 321 (1934).
[18] R. T. Bayard and D. Alpert, Rev. Sci. Instr. **21**, 571 (1950); Research Laboratory of Electronics, Massachusetts Institute of Technology, Quarterly Progress Report, Jan. 15, 1952, p. 1 (unpublished).

operation of the ionization gauge served to reduce the pressure once again to 1.5×10^{-9} mm, and no further changes in the analyzer work function were observed.

IV. ELECTRICAL CIRCUITS

A block diagram of the circuit is shown in Fig. 4. The filament was pulse-heated by conduction. Each pulse provided a positive bias voltage across R_b so that electrons could only reach the analyzer when there was no potential drop along the filament due to heating current. The pulse-heater, utilizing a pair of *FG–67* mercury thyratrons in an inverter circuit, was devised by Nottingham, and has previously been described by him.[19] The temperature of the filament was monitored during pulse-heating by a photoelectric ammeter consisting of a series-connected auxiliary filament which illuminated a phototube whose output was measured by a null method with an *FP–54* electrometer circuit. Calibration of the photoammeter was accomplished by heating the filament by direct current measured with a 1-ohm standard resistor and a Leeds and Northrup type-*K* potentiometer. The dc heating current corresponding to the desired operating temperature was obtained from the Forsythe-Watson tables[20] of resistivity and emissivity of tungsten and the interferometrically determined diameter of the filament. With the aid of some feedback and the continuous operation of the photoammeter, changes of emission due to changes of filament temperature could be held to less than 1 percent. The correction to the temperature at the center of the filament due to the cooling of its ends was negligible. During the course of the experiment, the filament was operated at 2000°K on pulse-heating for long periods of time. In order to avoid dc etch, the direction of flow of heating current was reversed every ten minutes, and the filament was heated to 2400°K on 60-cycle ac every two or three hours of operation.

The filament bias, which served as the variable in taking energy distributions, was supplied by storage batteries and measured with the type-*K* potentiometer. The anode and lens supplies were electronically regulated, and the anode potential was potentiometered. A Compton quadrant electrometer was used as a null indicator to measure the collector current.

The analyzing magnetic field was produced by a large pair of Helmholtz coils. Since the field necessary for analysis was only a few gauss, the earth's magnetic field was canceled in the region of the analyzer to better than 1 percent by a second pair of Helmholtz coils. The current in each set of coils was obtained from storage batteries and could be potentiometered. An oscilloscope with a high-gain vertical amplifier was connected across the Helmholtz coils in order to detect

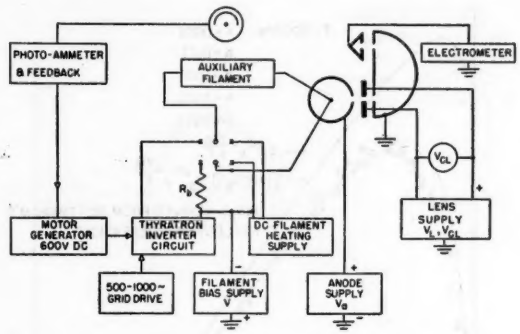

FIG. 4. Block diagram of the circuits used with the analyzer tube.

the presence of any stray, time-varying magnetic fields. No fields were found to have sufficient magnitude to lower the analyzer resolution.

The alignment of the tube in the magnetic field was checked by measuring the slope of a plot of the filament bias, V, necessary to observe either the peak or a half-maximum current point of the thermal energy distribution from a single direction as a function of the square of the Helmholtz coil current, I. This slope is a function of only the dimensions of the Helmholtz coils, the analyzer radius, and e/m for an electron. The analyzer radius calculated from the measured slopes agreed with the designed radius to within one-half the entrance slit-width. When a half-maximum current point was taken as the reference point on the distribution, least-squares analyses of the V *vs* I^2 data indicated a slight curvature which could be ascribed to loss of resolution in the analyzer with increasing electron energy within the analyzer.

V. ENERGY DISTRIBUTIONS AND WORK-FUNCTION DIFFERENCES

The energy distributions of the electrons as obtained in this experiment are expressed in terms of a variable which we have chosen to call V_p. Thus, eV_p is the kinetic energy (expressed in electron volts) associated with two components of the electron's momentum as it crosses the image barrier: p_x, the momentum perpendicular to the filament surface, and p_y, the tangential component perpendicular to the magnetic field. The other component of momentum, p_z, remains unaffected by any field in the tube and need not be considered. The kinetic energy of the electron within the analyzer associated with its motion in the plane perpendicular to the magnetic field is then eV_p plus the difference in potential energy between the point of emission (at the top of the image barrier) and the inside of the analyzer chamber. This change of potential is $(V+\phi_f-\phi_a)$, where $-V$ is the filament bias potential, ϕ_f is the true work function of that part of the crystal from which the electron was emitted, and ϕ_a is the average work function of the inside of the analyzer chamber. The condition that must be satisfied

[19] W. B. Nottingham, Phys. Rev. 41, 793 (1932); W. B. Nottingham, Phys. Rev. 55, 203 (1939).

[20] W. E. Forsythe and E. M. Watson, J. Opt. Soc. Am. 24, 114 (1934).

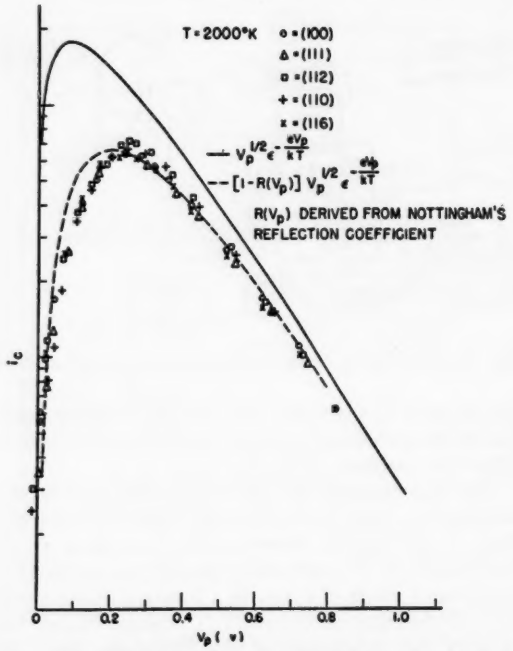

FIG. 5. Superposition of the energy distributions obtained from the directions of maximum and minimum emission with an anode potential of 1000 v. The Maxwellian distribution, and the Maxwellian distribution modified by Nottingham's reflection coefficient are shown for comparison.

in order that the electron may reach the collector is then

$$V+\phi_f-\phi_a+V_p=\tfrac{1}{2}(e/m)B^2R_0^2, \qquad (1)$$

where B is the magnetic field and R_0 is the analyzer radius.

The energy distribution of the electrons in the variable V_p is obtained directly by plotting collector current, i_c, as a function of filament bias, V, at constant magnetic field. This method of taking the distributions has two desirable features: the "slice" of the energy distribution remains the same in scanning the distribution, and the only field change within the tube is a change of 0.1 percent in the radial accelerating field within the anode.

The focusing fields between the anode and analyzer do not differentiate between electrons whose initial energy was largely associated with p_x or with p_y upon emission. The reason for this may be seen in the expression for the radial component of momentum at the anode slit,

$$p_r^2=2meV_a+p_x^2+p_y^2[1-(r_0/r_1)^2], \qquad (2)$$

and the very small ratio of filament radius to anode radius, $r_0/r_1=0.005$. The lack of dependence of the energy distribution shapes upon the exact conditions of focussing was experimentally verified by defocussing the lens. The beam cross-over (see Fig. 2) was moved backwards and fowards and from side to side with no change in distribution shape, although collector currents were drastically reduced.

A superposition of the experimental energy distributions at 2000°K for the important crystallographic directions is shown in Fig. 5. The data identified as (116) were actually taken in a direction between the (114) and (116) where the emission has a maximum, which therefore corresponds with the direction for which Nichols[2] and Smith[3] made Richardson plots. Note that in Fig. 5 the collector current is plotted on a logarithmic scale, allowing the distributions to be superposed without the use of scale factors. The horizontal shifts along the V axis which are necessary in order to superpose the distributions taken in different crystallographic directions yield the differences between the work functions in these directions [see Eq. (1)]. The work-function differences obtained from the distributions of Fig. 5 are shown in Table I. These are true work-function differences at 2000°K and should not be confused with the differences between Richardson plot work functions. The very high work function in the (110) direction seems to bear out, at least qualitatively, field emission work[21] and the estimates made by Smith.[3]

The shape of the energy distribution is of particular interest. In Fig. 5 one can see that the energy distribu-

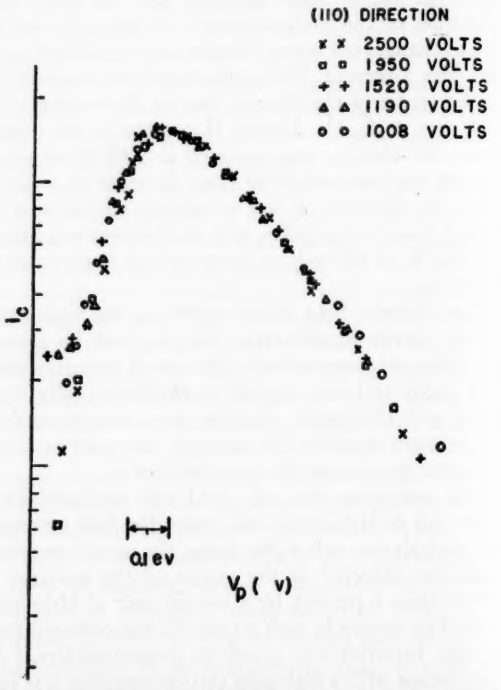

FIG. 6. Superposition of energy distributions obtained at 2000°K in the (110) direction at different anode potentials.

[21] M. Drechsler and E. W. Müller, Z. Physik **134**, 208 (1953); Dyke, Trolan, Dolan, and Grundhauser, J. Appl. Phys. **25**, 106 (1954).

tions from the different directions are identical to within experimental accuracy. The Maxwellian distribution, $V_p^{\frac{1}{2}} \exp(-eV_p/kT)$, lies above the experimental points for low energies indicating a deficiency of slow electrons for "saturation" emission. Such a deficiency of slow electrons may be described by an energy-dependent reflection coefficient for the emitting surface. (In fitting experimental distributions to the Maxwellian distribution, the experimental points on the high-energy side of the distribution are assumed to approach the Maxwellian curve asymptotically, and $V_p=0$ is determined as the point on the low side of the distribution where the slope is characteristic of the resolution of the analyzer. This procedure amounts to finding the smallest possible reflection coefficient which will explain the data.) Nottingham[4] observed a similar dearth of slow electrons in carefully taken retarding-potential data. He developed a reflection coefficient which is an exponential function of the momentum in the direction perpendicular to the surface at the top of the image barrier, $R(p_x)=\exp(-p_x^2/2me\omega)$, in which he determined the parameter $\omega=0.191$ ev from his data. In order to apply this reflection coefficient to distributions in V_p it is necessary to convert $R(p_x)$ to $R(V_p)$. This can be accomplished by multiplying the Maxwellian distribution, written in terms of $p_r=(p_x^2+p_y^2)^{\frac{1}{2}}$ and $\theta=\tan^{-1}(p_y/p_x)$, by the transmission coefficient $[1-\exp(-p_r^2\cos^2\theta/2me\omega)]$, and integrating

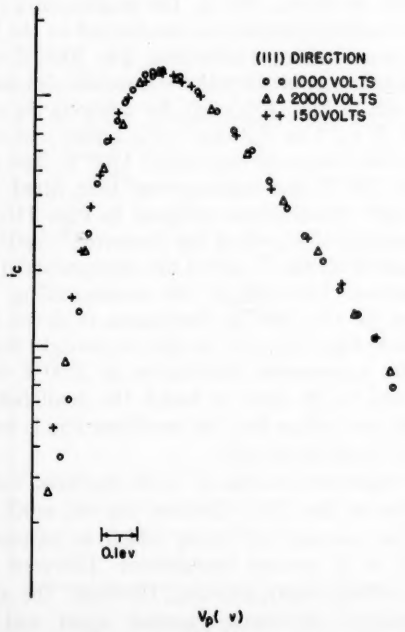

FIG. 7. Superposition of energy distributions obtained at 2000°K in the (111) direction at different anode potentials.

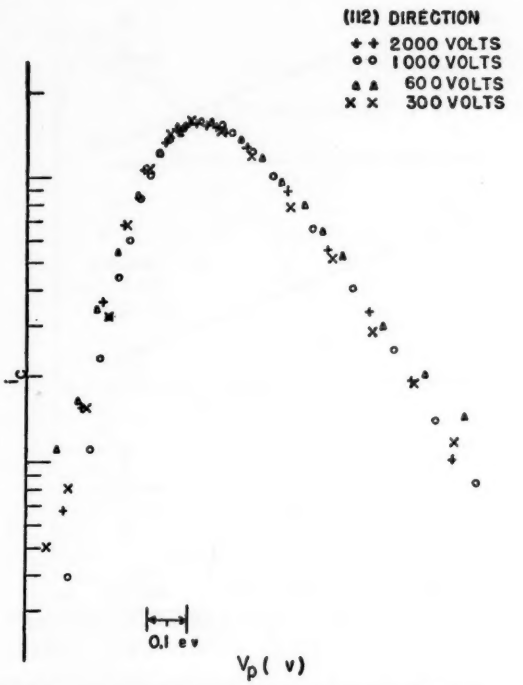

FIG. 8. Superposition of energy distributions obtained at 2000°K in the (112) direction at different anode potentials.

over θ. The result is

$$R(V_p)=x^{-1}\exp(-x^2)\int_0^x \exp(y^2)dy=x^{-1}F(x), \quad (3)$$

where $x=(V_p/\omega)^{\frac{1}{2}}$, and $F(x)$ has been tabulated by Miller and Gordon[22] for values of the argument between 0 and 12.

The dashed curve in Fig. 5 is the Maxwellian distribution modified by this reflection coefficient using the value of ω determined by Nottingham. The fit to the experimental points is remarkably close.

These distributions were obtained with a magnetic field corresponding to an electron energy within the analyzer of 3 ev. Distributions obtained at 5 ev in the analyzer were similar, indicating that the distribution shape did not depend upon analyzer resolution as long as the resolution was high.

VI. FIELD EFFECTS

Energy distribution data were taken at a variety of different anode potentials in the (110), (111), and (112) directions in attempts to observe any dependence of the reflection effect on applied field. Figures 6–8 are superpositions of the data taken in these three directions. Although the data in the (110) direction and the energy distribution for $V_a=600$ v in the (112) direction

[22] W. Larsh Miller and A. R. Gordon, J. Phys. Chem. 35, 2785 (1931), see Table XXVIII.

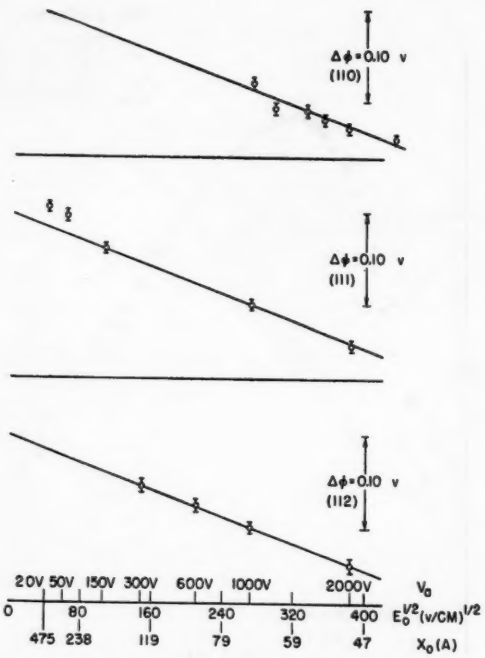

FIG. 9. The change of work function with applied field (Schottky effect) as obtained from the shifts along the voltage axis necessary to superpose the distributions of Figs. 6–8. The solid lines are plotted with the theoretical slope.

show the effects of a small background current, there appears to be *no* significant variation in the shape of the energy distribution with applied field. The changes in reflection coefficient which are responsible for the periodic deviations from Schottky plots are probably too small to be observed in these distributions which are characterized by a reflection coefficient which is appreciable over tenths of volts of energy.

By plotting the change in work function, as obtained from the shifts along the voltage axis required for superposition of the distributions, as a function of the square root of the applied field in Fig. 9, "direct" Schottky plots are obtained. The lines have the theoretical slope, the field being determined from the anode potential, anode radius, and the interferometrically determined filament radius. The probable errors indicated on the experimental points are those associated with uncertainty in the position of "best match" of two distributions. This uncertainty of ±0.005 v in work-function difference measurement is better than one might assume on the basis of the resolution, $\Delta V/V$, because the transmission of the analyzer is a peaked function of electron energy.

TABLE I. True work function differences (in volts) between crystal faces of tungsten at 2000°K.

$(\varphi_{116}-\varphi_{111})$	−0.01
$(\varphi_{100}-\varphi_{111})$	+0.02
$(\varphi_{112}-\varphi_{111})$	+0.12
$(\varphi_{110}-\varphi_{111})$	+0.71

The two points which lie above the theoretical line in the (111) direction represent distributions taken at extremely low anode voltage where there has undoubtedly been a loss of resolution in azimuth within the anode. As might be expected, since the (111) direction is one of minimum work function, these two points indicate that the work function appears to rise as electrons from higher work-function regions neighboring the (111) direction become part of the measured current. Sizable contributions from neighboring directions of lower work function were apparent in the (110) direction for $V_a<1000$ v, and therefore no measurements at lower fields were attempted in this direction.

VII. TEMPERATURE DEPENDENCE OF WORK FUNCTIONS

The rates of change of work function with temperature in the various directions were derived from shifts along the V axis between distributions for the same direction at different temperatures. The change of distribution shape with temperature required the following technique:

Energy distributions were taken at 2000°K and 1700°K in all of the important directions except the (110) by varying V at constant magnetic field. Logarithmic plots of the 2000°K distributions were then fitted to the Maxwellian distribution, $V_p^{\frac{1}{2}}\exp(-eV_p/2000k)$, in such a manner as to yield an experimental reflection coefficient, $R(V_p)$. The position of $V_p=0$ of the Maxwellian distribution was marked on the V axis of the experimental distribution. The 2000°K experimental points as fitted to the Maxwellian distributions are shown in Figs. 10(a)–(d). By applying the experimental $R(V_p)$'s to $V_p^{\frac{1}{2}}\exp(-eV_p/1700k)$ one obtains the distributions to be expected at 1700°K. The experimental 1700°K distributions were then fitted to the "expected" distributions as shown in Figs. 11(a)–(d). The position of $V_p=0$ of the "expected" distribution was marked on the V axis of the experimental 1700°K distribution. The shift of the corresponding $V_p=0$ position for the 2000°K distribution is shown at the bottom of Figs. 11(a)–(d). A shift to the right indicates that the *experimental* distribution at 1700°K had to be moved to the right to match the prediction from 2000°K, and means that the work function is lower at 1700°K (positive $d\phi/dT$).

The observed changes of work function, with the exception of the (112) direction, are not much larger than the accuracy of fitting which is estimated as ±0.005 v. A greater temperature difference would have yielded larger changes. However, the present experimental techniques imposed upper and lower bounds upon the filament temperature. It was found that if the filament were held at 2100°K the current of

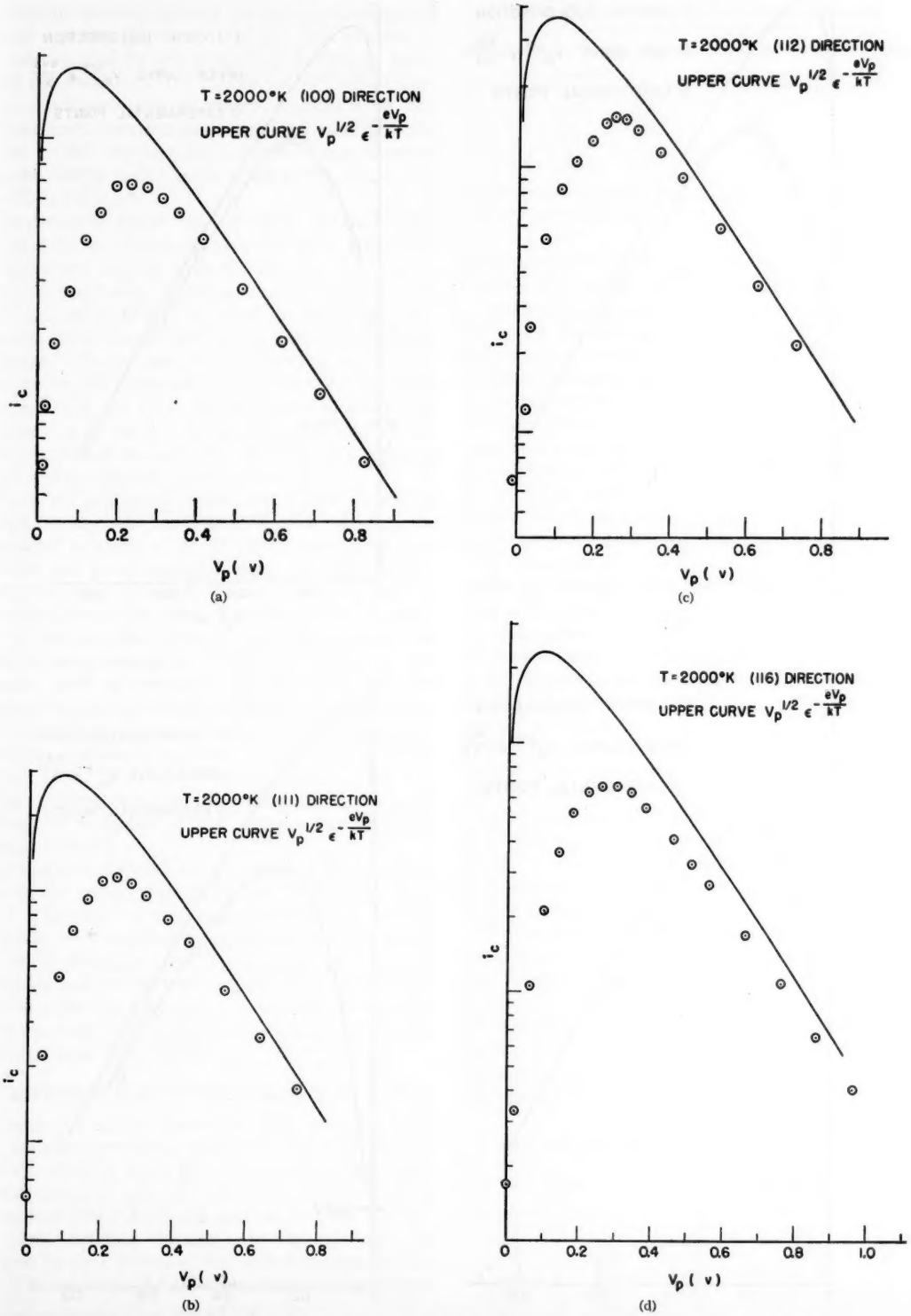

FIG. 10. 2000°K distributions as fitted to the Maxwellian distribution for the determination of experimental $R(V_p)$'s.

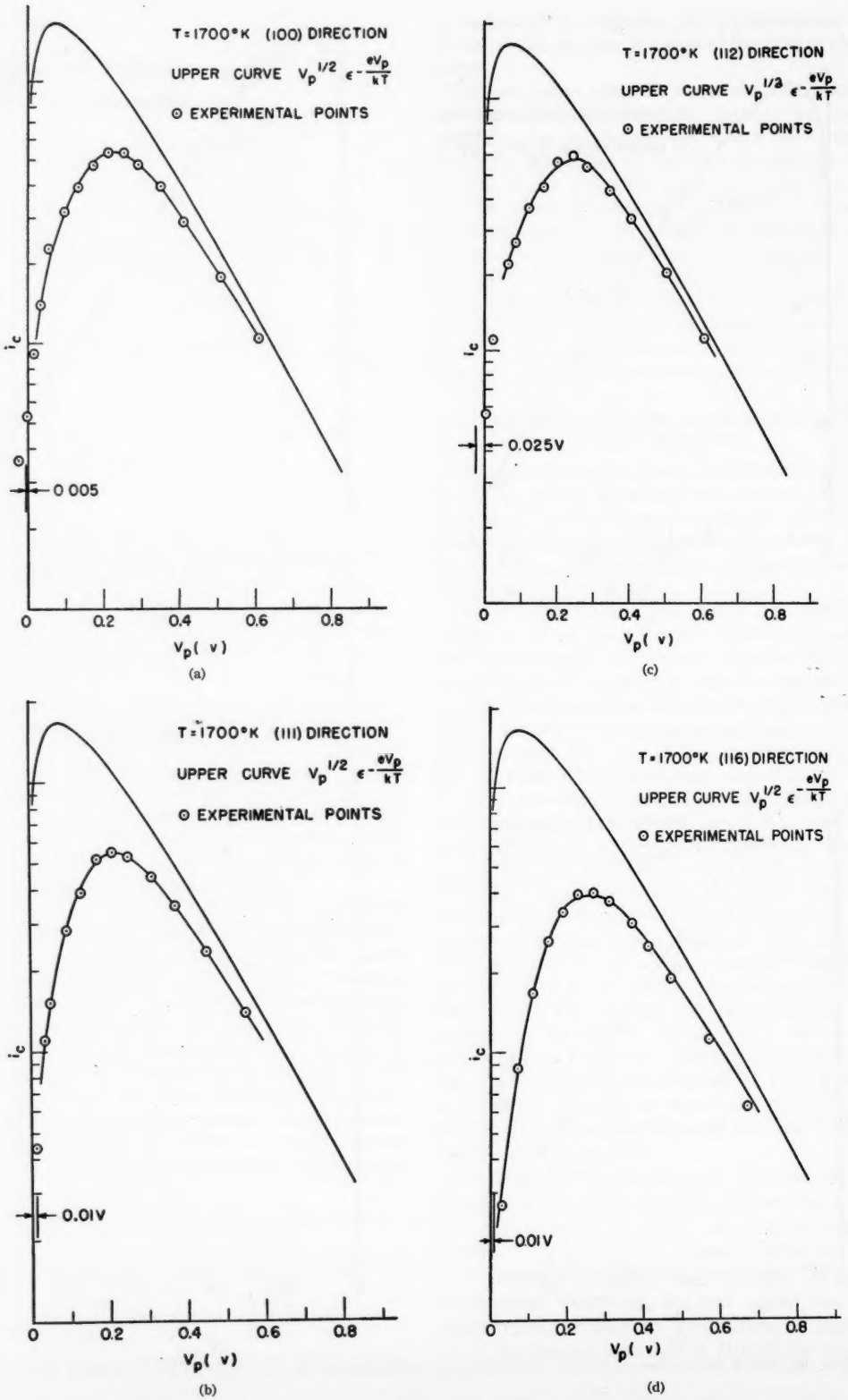

FIG. 11. 1700°K distributions fitted to the distributions expected on the basis of the $R(V_p)$'s observed at 2000°K.

high-energy electrons striking the anode was enough to liberate a perceptible amount of gas. The pressure in the tube as read by the monitoring ionization gauge would rise from 1.5×10^{-9} mm to 4×10^{-9} mm. Under these conditions, the necessary constancy of the analyzer work function could not be guaranteed. No change in the analyzer work function was observed between 2000°K distributions taken before and after a 1700°K distribution.

Temperatures lower than 1700°K did not yield enough collector current for accurate work. Since high resolution was used for these distributions, the fraction of the current finally reaching the collector was quite small, and at 1700°K each point on the energy distribution curve was obtained by the method of "capture of charge." No low-temperature distribution could be taken in the (110) direction. Even at 1800°K the energy distribution in the (110) direction showed distortions in shape due to small, varying leakage currents to the collector, though no shift was observed in comparing it with the distribution taken at 2000°K.

There are two small corrections which should be applied to the observed shifts in V before they can be interpreted in terms of $d\phi/dT$. Both corrections arise from the fact that the applied potential difference between the filament and the analyzer chamber is measured outside the tube. The first is the iR drop, due to the emission current, occurring between the point of measurement of V and the center of the filament, and the second is the thermoelectric emf generated by the temperature difference between these two points.[23] It turned out that the thermoelectric correction cancelled that due to the iR drop to within 10^{-3} v.

The resulting temperature coefficients of the work function of tungsten in the various directions are given in Table II.

Herring and Nichols have summarized the contributions to the temperature derivative of the work function.[24] The sum of the contributions from volume properties such as thermal expansion, internal effects of atomic vibrations upon the electrical and chemical potentials, and the electronic specific heat can be of the order of a few times k/e and of either sign. The magnitudes observed in the present experiment are not inconsistent with this estimate.

VIII. INTERPRETATION OF RICHARDSON PLOT DATA

A summary of the Richardson plot work functions and emission constants published by Nichols[2] and Smith[3] is given in Table III. (The asterisk will be used to distinguish a quantity obtained directly from a Richardson plot.) As Smith pointed out, the data for the (110) direction do not correctly represent the emission in that direction, but rather the sum of the true (110) emission and a spurious current of secondary electrons originating on the inner walls of the anode in the tube used by both Nichols and himself.

[23] Conyers Herring, Phys. Rev. **59**, 889 (1941).
[24] See Table VII on page 244 of reference 1.

TABLE II. Temperature coefficients of work function for crystal faces of tungsten.

Direction	$d\varphi/dT$ (volts/degree)[a]
(100)	-1.7×10^{-5}
(111)	$+3.3$
(112)	-8.3
(116)	$+3.3$
(110)	$<5\times10^{-5}$(?)

[a] Estimated error less than 1.6×10^{-5}.

In the present experiment, secondary electrons from the anode do not have enough energy to reach the analyzer. Nor were any significant currents of reflected primaries observed. Reflected primaries from regions of the anode receiving copious emission from one of the low-work-function directions might be expected to have shown themselves as a spurious energy distribution peak when the crystal was oriented for observation of the (110) emission. However, such reflected primaries would be defocused by the lens since their trajectories would not be radial at the anode slit.

In connection with the data in Table III, Smith also points out that his work functions are slightly lower than those obtained originally by Nichols because of the elimination of a small spurious current of photoelectrons leaving the collector. He ascribed the larger discrepancy in measured work functions in the (116) direction to the violent heat treatment given to his crystal in which its diameter decreased 4 percent through evaporation, and "plateaus" developed on the surface of the crystal normal to the (110), (112), and (100) directions.

The crystal used in the present experiment had only mild heat treatment, similar to that given Nichols' original crystal. Therefore, Nichols' original Richardson plot constants in the (116) direction should probably be used for purposes of comparison.

The nonideality of the energy distribution of the thermionic current may be represented by a transmission coefficient $\alpha[1-R(V_p)]$. In this expression, $R(V_p)$ is the reflection coefficient obtained from fitting the experimental distribution to the ideal distribution, and α is a constant, less than or equal to unity, which can take account of a reflection which varies so slowly with energy that it cannot be detected in the fitting

TABLE III. Summary of Richardson-plot work functions and emission constants.

Direction	Nichols φ^*	Nichols A^*	Smith φ^*	Smith A^*
(111)	4.39	35	4.38	52
(112)	4.69	125	4.65	120
(116)	4.39	53	4.29	40
(100)	4.56	117	4.52	105
(110)	4.68	15	4.58	8

TABLE IV. Compatibility of the data on differences between true work functions, temperature variations of true work functions, and differences between Richardson-plot work functions.

Direction "a"	$(\varphi_a-\varphi_{111})$	$(\varphi_a^*-\varphi_{111}^*)$	$\frac{(\varphi_a-\varphi_{111})-(\varphi_a^*-\varphi_{111}^*)}{T}$	$\left(\frac{d\varphi_a}{dT}-\frac{d\varphi_{111}}{dT}\right)$[a]
(116)	−0.01	0[b]	-0.5×10^{-5}	0
(100)	+0.02	+0.14	-6.0×10^{-5}	-5.0×10^{-5}
(112)	+0.12	+0.27	-7.5×10^{-5}	-11.6×10^{-5}
(110)	+0.71	?	?	?

[a] The error in the observed differences may be as large as 3×10^{-5} v deg^{-1}. See Table II.
[b] The old Nichols values of $\varphi_{116}^*=\varphi_{111}^*=4.39$ v were used.

process. Richardson's equation for the saturation emission current density may then be written as

$$j=\alpha A(1-\bar{R})T^2\exp(-e\varphi/kT), \tag{4}$$

where $\bar{R}$ is the average of $R(V_p)$ over the Maxwellian distribution. The quantities derived from a Richardson plot are then[25]

$$\varphi^*=\varphi-T\frac{d\varphi}{dT}-\frac{kT^2}{e(1-\bar{R})}\frac{d\bar{R}}{dT}, \tag{5}$$

$$A^*=\alpha A(1-\bar{R})\exp\left[-\frac{e}{k}\frac{d\varphi}{dT}-\frac{T}{(1-\bar{R})}\frac{d\bar{R}}{dT}\right]. \tag{6}$$

A check on the self-consistency of the present data on work-function differences and $d\phi/dT$, and the Nichols-Smith values of ϕ^* can be made. From the direct comparison of the energy distributions (Fig. 5) it can be inferred that $\bar{R}$ and $d\bar{R}/dT$ are very much the same for all of the surfaces. Therefore, if Eq. (5) is considered for two surfaces, "a" and "b," we may write

$$\frac{(\varphi_a-\varphi_b)-(\varphi_a^*-\varphi_b^*)}{T}=\left(\frac{d\varphi_a}{dT}-\frac{d\varphi_b}{dT}\right). \tag{7}$$

The compatibility of the data in terms of Eq. (7) at 2000°K is shown in Table IV. The only discrepancy is in the (112) direction. The assumption that the term involving $\bar{R}$ in Eq. (5) cancels out in taking the differences between the (112) and (111) directions was found to be satisfactory by numerical integration of the experimental $R(V_p)$'s for these directions. It is felt that the contact potential measurements between the surfaces are sufficiently accurate to rule out an error in $(\phi_{112}-\phi_{111})$ which could cause the discrepancy. The remaining possibilities are that the negative temperature coefficient of the (112) work function is not as large as the present measurements indicate or that ϕ_{112}^* is about 0.09 v too low.

It is interesting to compute the quantity $A\alpha$ from Eq. (6) using the measured values of $d\phi/dT$, the Nichols-Smith A^*'s, and Nottingham's reflection coefficient for $\bar{R}$ and $d\bar{R}/dT$. The Nottingham reflection coefficient is a good representation of the observed reflection, and integrates to the simple form $\bar{R}=(1+kT/\omega)^{-1}$. Table V shows the calculated values of $A\alpha$ for the different directions. For the (100), (111), and (116) directions, the values are the same to within the experimental uncertainties of 10 percent in A^* and 20 percent in $\exp[(e/k)(d\phi/dT)]$. A reasonable value of $\alpha=0.9$ seems to be indicated. The discrepancy appearing here in the (112) direction is of the same nature as that found in Table IV. In fact, if the temperature coefficient in the (112) direction is assumed to be -4.2×10^{-5} v/deg instead of the -8.3×10^{-5} v/deg which was measured, the discrepancy is completely removed from both tables. However, if the measured temperature coefficient in the (112) direction is presumed correct, then it must be assumed that the Richardson plot measurement of ϕ_{112}^* is low by roughly 0.08 v and that A_{112}^* should have been about 190. This sort of error in the Richardson plot values could

TABLE V. Emission constants $A\alpha$(amperes/cm^2 deg^2) obtained by correcting the Richardson-plot A^* values for the observed temperature variation of the work functions and the non-Maxwellian character of the energy distributions.

Direction	A^*	$A\alpha$
(111)	52	101
(112)	120	61
(116)	53[a]	103
(100)	105	113

[a] The old Nichols value.

[25] See Sec. I.5 of reference 1.

TABLE VI. Best estimates of the true work functions for a tungsten crystal in the temperature range 1700°K to 2000°K utilizing measured temperature variations and Nottingham's reflection coefficient.

Direction	φ in volts
(111)	$4.30+(3\times10^{-5})T$
(112)[a]	$4.57-(5\times10^{-5})T$ or $4.66-(8\times10^{-5})T$
(116)[b]	4.20 to $4.31+(3\times10^{-5})T$
(100)	$4.44-(2\times10^{-5})T$
(110)	5.09 at $T=2000°$

[a] The first value corresponds to the assumption that the Richardson plot data were not affected by a spurious current and the second is based upon the observed temperature coefficient.
[b] The spread in work function is assumed to be due to differences in heat treatments of the crystals.

have been due to a small amount of the same type of background current that invalidated the (110) Richardson plots.[3]

Table VI shows the best estimates of true work function for the various directions in the thermionic temperature range obtained from Eq. (5) [and the measured work-function differences for the (110) direction]. It should be pointed out that an extrapolation of the values of Table VI to room temperature would be of doubtful validity since $d\phi/dT$ cannot be expected to remain constant over large ranges of temperature.

Since the experimental Richardson plots cover the temperature range from 1500°K to 2000°K, the effect of reflection was calculated at 1700°K for Tables V and VI. This procedure amounts to finding the slope and intercept of the straight line which would be tangent to the Richardson plot points at 1700°K.

IX. CONCLUDING REMARKS

The energy distributions observed in this experiment have, as yet, no satisfactory theoretical explanation. It would seem extremely unlikely that the various surfaces of a single crystal of tungsten would be patchy in just such a manner as to yield identical energy distributions. The possibility that the observed reflection could be due to the band structure of tungsten seems to be ruled out by the consideration that the emission in the (110) direction must originate at a point 0.7 ev higher in energy than the emission in the (111) direction.

The author would like to express his gratitude to Professor W. B. Nottingham for suggesting this problem and for his advice and encouragement while the research was in progress. He is also grateful to the Radio Corporation of America for the RCA Fellowship in Electronics which he held during part of this work.

PHYSICAL REVIEW VOLUME 98, NUMBER 4 MAY 15, 1955

Density of States Curve for Nickel*

G. F. KOSTER†
Massachusetts Institute of Technology, Cambridge, Massachusetts
(Received December 24, 1954)

A density of states curve for the d bands in nickel is presented. This curve is an extension over the entire energy range of the d bands of the density of states curve for nickel already computed by Fletcher and Wohlfarth. The matrix of the interaction of the d states with the periodic potential is exactly the same as was used by Fletcher and Wohlfarth.

IN a recent paper[1] by Slater and the author, a density of states curve for the d electrons in the body-centered structure was calculated using the tight-binding approximation. In this approximation, the solution for the energies of the periodic potential problem is assumed to consist of linear combinations of Bloch functions made out of atomic orbitals. For the d electrons, the solution is assumed to consist of a linear combination of Bloch sums made out of the five d atomic orbitals. The matrix of the Hamiltonian when formed between these Bloch sums involves parameters which represent the interaction between a d atomic orbital located at the central lattice site in the crystal with d atomic orbitals located at neighboring lattice sites. In the aforementioned paper, the values of these parameters were taken from a paper by Fletcher and Wohlfarth[2] who had calculated the band structure of face-centered nickel. From the band structure obtained in this way a density of states, representing the number of energy levels in a given energy range, was obtained. The striking feature of the density of states curve obtained in this way for the d electrons in the body-centered structure is a pronounced dip at center of the density of states. Since the shape of the density of states curve for the transition metals is important in problems of magnetism and electronic

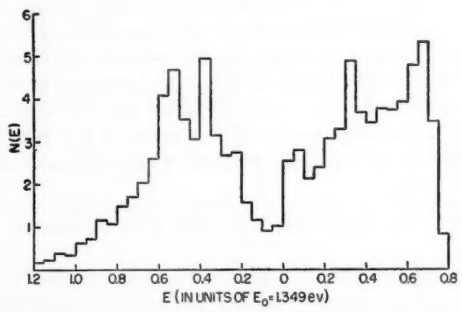

FIG. 1. Density of states $N(E)$ as a function of energy for the d bands in nickel.

* The research in this paper was supported jointly by the Army, Navy, and Air Force under contract with the Massachusetts Institute of Technology.
† Staff Member, Lincoln Laboratory, Massachusetts Institute of Technology, Cambridge, Massachusetts.
[1] J. C. Slater and G. F. Koster, Phys. Rev. 94, 1498 (1954).
[2] G. C. Fletcher and E. P. Wohlfarth, Phil. Mag. 42, 106 (1951); G. C. Fletcher, Proc. Phys. Soc. (London) A65, 192 (1952).

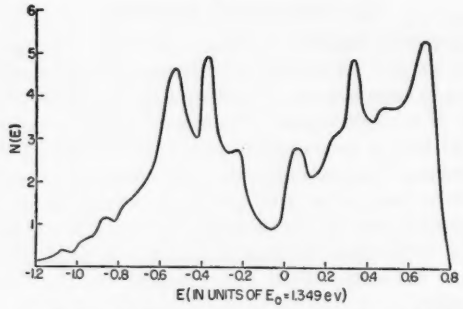

FIG. 2(a). Smoothed out density of states $N(E)$ as a function of energy for the d bands in nickel.

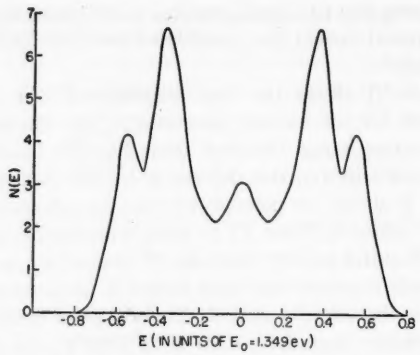

FIG. 2(b). Smoothed out density of states $N(E)$ as a function of energy for the d bands in a body-centered structure.

specific heat it would be interesting to have a complete density of states curve for the face-centered as well as for the body-centered transition metals.

Fletcher and Wohlfarth in their papers have calculated the density of states for face-centered nickel but, unfortunately, because of the computational difficulties involved, have only extended their calculation of the density of states over part of the region in energy over which the d bands extend. In their paper, they have set up the matrix of the Hamiltonian for the interaction of the d electrons in nickel, and it was decided to solve for the roots of this Hamiltonian matrix throughout the first Brillouin zone of reciprocal space and calculate the density of states over the entire range of energies of the d bands.

The availability of a high-speed computer makes the solution of this five-by-five secular equation quite simple. The calculation of the matrix of interaction as well as the diagonalization of the matrix was carried out on the Whirlwind computer at M.I.T.[3] Because of the symmetry of the energy bands in reciprocal space it is only necessary to compute the roots of the five-by-five secular equation throughout one forty-eighth of the first Brillouin zone. The mesh which was chosen in reciprocal space for which the matrix was diagonalized was the same as that used in reference 1. This is a mesh of 10° in the three directions of reciprocal space. This gave a total of 680 points on one forty-eighth of the first Brillouin zone at which the five-by-five secular equation must be diagonalized. The roots of the secular equation were calculated and from them a density of states by the method described in reference 1. The results of this calculation are given in the density of states curve for nickel which is shown in Fig. 1. The step nature of this curve is not real but merely indicative of the method of calculation. In Fig. 2(a), we show a smoothed out density of states curve for the face-centered and for comparison, in Fig. 2(b), the corresponding density of states curve for the body-centered structure.[1] (All the density of states curves in this paper are normalized to have a total area of five corresponding to five states per atom.)

We notice that the curve for the face-centered structure shows a dip just as the density of states curve for the body-centered structure does. This dip in the density of states curve was predicted many years ago in the work of Krutter[4] and Slater.[5] Their calculation of the density of states was based on a cellular calculation. More recent cellular calculations by Howarth[6] on copper which agree qualitatively with the tight-binding calculations of Fletcher and Wohlfarth disagree in the details of the energy bands with the older calculations of Krutter and Slater. Even though there is this disagreement as to the precise form of the energy bands in nickel between Krutter and the calculation of Fletcher and Wohlfarth, it is interesting to note that the density of states curves which results from these two calculations are quite similar. This is rather comforting since it means that many of the conclusions which were based on the dip in the density of states curve as calculated by Krutter and Slater still remain valid even though we cannot trust the details of this earlier calculation.

ACKNOWLEDGMENTS

The author wishes to express his gratitude to Dr. Alvin Meckler who provided the routine for diagonalizing the Hamiltonian matrix and to Inderjit Prakash who aided in the computations.

[3] Availability of Digital Computer Laboratory time (for this problem) was made possible by the Office of Naval Research.

[4] H. M. Krutter, Phys. Rev. **48**, 664 (1935).
[5] J. C. Slater, Phys. Rev. **49**, 537, 931 (1936).
[6] D. J. Howarth, Proc. Roy. Soc. (London) **A220**, 513 (1953).

Dielectric, X-Ray, and Optical Study of Ferroelectric $Cd_2Nb_2O_7$ and Related Compounds*

F. JONA, G. SHIRANE, AND R. PEPINSKY
Department of Physics, The Pennsylvania State University, State College, Pennsylvania

(Received January 13, 1955)

Single crystals of $Cd_2Nb_2O_7$ have been grown, and dielectric, x-ray, and optical studies have been carried out on these above and below the ferroelectric Curie point. The x-ray analysis confirms the pyrochlore structure, and gives the oxygen parameter $x=0.305$ at room temperature. The symmetry below the Curie point, −85°C, is uncertain, due to the very slight lattice distortion: c/a is about 1.0005 if the ferroelectric phase is tetragonal. The spontaneous polarization along the cubic (111) axis is 6 microcoulombs/cm² at −180°C.

Partial replacement of Cd by Pb or Ca, or of Nb by Ta, decreases the Curie temperature of $Cd_2Nb_2O_7$. Dielectric measurements revealed no anomaly in several other $A_2B_2O_7$ compounds. Lattice parameters are reported for $Pb_2Ta_2O_7$, $Y_2Ti_2O_7$, and $Cd_2Nb_2O_6$.

I. INTRODUCTION

THE discovery of ferroelectricity in cadmium niobate, $Cd_2Nb_2O_7$, by Cook and Jaffe,[1,2] introduced a new member into the family of ferroelectric compounds.

Dielectrically, the behavior of $Cd_2Nb_2O_7$ shows characteristics common to all ferroelectrics. The dielectric constant has quite a high value, and increases hyperbolically upon approaching the Curie point from the paraelectric side; thus the Curie-Weiss law is satisfied. The Curie point was first reported to lie at 170°K.[1] Further measurements by Shirane and Pepinsky,[3] and independently by Hulm,[4] established the Curie point at 185±3°K. The fluctuations are the result of different firing temperatures of the ceramic specimens and thus apparently to partial evaporation of CdO. Shirane and Pepinsky[3] and Hulm[4] also discovered a second anomaly in the dielectric constant *versus* temperature curve, at 85°K, which suggests the existence of a second phase change at this temperature (see Fig. 1). Ferroelectric hysteresis loops were observed from the Curie point at 185°K down to 4°K; the value of the spontaneous polarization is about 1.8 microcoulomb/cm² at 100°K. All the above measurements were carried out on ceramic specimens.

Structurally, $Cd_2Nb_2O_7$ represents a new type of ferroelectric. The crystal structure was examined by Bystroem[5] by means of x-ray powder patterns, as were related substances $Cd_2Ta_2O_7$, $Ca_2Ta_2O_7$, and $Pb_2Sb_2O_7$. Bystroem found that all four compounds belong to the cubic $E8_1$ structure type,[6,7] first known as the *koppite* type but more properly called the *pyrochlore* type (since koppite is now discredited as a mineral species[8]).

The $E8_1$ structure type can be viewed as having a resemblance to a distorted fluorite (Cl) structure. However, instead of having the composition $(A,B)_4X_8$, which would correspond to the AX_2 ratio in fluorite, the formula is $(A,B)_4X_7$; thus one of the eight anions in the fluorite-type structure is missing, and the remaining oxygens are considerably shifted.[2] The space group is $Fd3m$, and there are 8 "molecules" per cell. The structural framework is a three-dimensional array of BO_6 octahedra, all sharing corners, and the framework thus has the composition $(B_2O_6)_\infty$. One parameter, x, determined the shape of the octahedra; the condition for regular octahedra is $x=\frac{5}{16}=0.312$. The seventh set of oxygens and the A ions occupy open spaces in the framework. A projection of the unit cell on (110) is shown in Fig. 2.

The existence of three-dimensionally directly-linked oxygen octahedra which encase highly polarizable ions relates $Cd_2Nb_2O_7$ to the perovskite ferroelectrics of the general formula ABO_3. In both cases the BO_6 octahedra

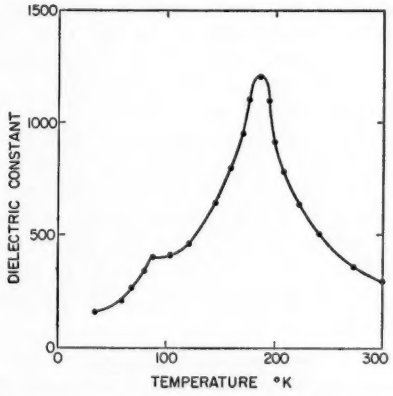

FIG. 1. Dielectric constant of ceramic $Cd_2Nb_2O_7$ *vs* temperature.

* Investigation supported by a contract with Wright Air Development Center.

[1] W. R. Cook, Jr. and H. Jaffe, Phys. Rev. **88**, 1426 (1952).
[2] W. R. Cook, Jr. and H. Jaffe, Phys. Rev. **89**, 1297 (1953).
[3] G. Shirane and R. Pepinsky, Phys. Rev. **92**, 504 (1953).
[4] J. K. Hulm, Phys. Rev. **92**, 504 (1953).
[5] A. Bystroem, Arkiv Kemi, Mineral. Geol. **18A**, No. 21 (1944).
[6] Hermann, Lohrmann, and Philipp, *Strukturbericht II* (reprinted by Edwards Brothers, Inc., Ann Arbor, 1943); K. Hermann, *Strukturbericht VII* (reprinted by Edwards Brothers, Inc., Ann Arbor, 1943).
[7] A. J. C. Wilson, editor, *Structure Reports X* (Oosthoek, Utrecht, 1953).
[8] Palache, Berman, and Frondel, *Dana's System of Mineralogy* (John Wiley and Sons, Inc., New York, 1944), seventh edition, Part I.

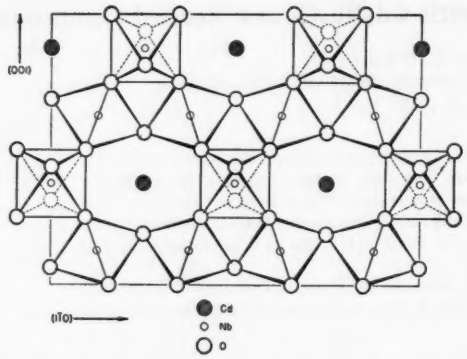

FIG. 2. NbO_6 octahedra configuration in $Cd_2Nb_2O_7$, projected on (110) plane. (The Cd ions, which overlap with the Nb ions at $(\frac{1}{8}, \frac{1}{8})$, etc., and the seventh set of oxygens, which are located above and below the Cd ions, are not shown.)

share corners only. There are essential differences between the two structure types, however. In the ABO_3 perovskites the O-*B*-O chains lie on straight lines which are parallel to the cubic axis; and this arrangement has been shown to be favorable for the occurrence of ferroelectricity because of the large internal field along this chain.[9] In the pyrochlore structure the configuration of the BO_6 octahedra is much more complicated, the O-*B*-O chains lying on zig-zag lines along the ⟨110⟩ directions. Furthermore, in the perovskite structure the *A* ion only can be absent, if charge neutrality obtains as in WO_3 or Na_xWO_3. In the pyrochlore structure, on the other hand, the *A* ions and the seventh oxygens are essential neither to the stability of the network of octahedra nor to the charge neutrality. It appears that the number of oxygen ions can vary from 6 to 7, if the number of the *A* ions varies accordingly, resulting in a general formula $A_{1+x}B_2O_{6+x}$. It is also possible partially to replace the *A*O group with other combinations *A'X*, according to the general formula $A_{1+x}A_{1-x}'B_2O_{6+x}X_{1-x}$. An example of the second case is pyrochlore itself, $CaNaNb_2O_6F$; an example of the first case, reported by Cook and Jaffe,[2] seems to be $Pb_{1.5}Nb_2O_{6.5}$. This point will be discussed in more detail below.

The ultimate aim of our investigation is an understanding of the structural mechanism leading to ferroelectricity within crystals of the pyrochlore type. To date our attention has been devoted exclusively to the phase change at 185°K. Single crystals of $Cd_2Nb_2O_7$ were first grown, and these were then studied dielectrically, optically, and by x-rays. A series of other compounds with the general formula $A_2B_2O_7$ has also been investigated.

II. CRYSTAL GROWTH

The melting point of $Cd_2Nb_2O_7$ was determined by means of an optical pyrometer as approximately 1450°C. Near 1200°C, and above, a strong smoke is developed, very probably due to the evaporation of CdO. In attempting to grow single crystals of $Cd_2Nb_2O_7$ one must therefore take the following possibilities into account: (a) if growth can be accomplished at temperatures lower than 1200°C, no noticeable loss of CdO is to be expected; (b) if, however, the starting material must be heated above 1200°C for a considerable period, then an excess of CdO must be provided in the crucible (depending in amount on the heating time and maximum temperature) in order to compensate for CdO evaporation.

The first of these possibilities can be realized by using a suitable flux. Many different substances were tried as fluxes; the most successful among these turned out to be NaF and KF. Good results are obtained by mixing NaF and $Cd_2Nb_2O_7$ in molar ratio 10:1 (for example, 4.2 g of NaF and 5.2 g of $Cd_2Nb_2O_7$). The mixture is heated within a covered Pt crucible up to 1050°C, kept at this temperature for about 1 hour, and cooled down to 700°C at a rate of about 40 degrees/hour. With this procedure one obtains small plate-like crystals of hexagonal or triangular shape, with areas ranging between 2 and 6 mm^2. If the molar ratio of flux to $Cd_2Nb_2O_7$ is changed to 20:1, only very few octahedron-shaped crystals are produced.

$Cd_2Nb_2O_7$ crystals are colored light yellow. X-ray studies show that the plate surfaces are {111} planes. Figure 3 shows the relative orientation of the crystal plates with respect to the common octahedral habit.

The $Cd_2Nb_2O_7$ crystals obtained with NaF as a flux (in the following these are referred to as *N*-crystals) contain Na as an impurity; the ionic radii of Na^{+1} and Cd^{+2} are close enough for the first to substitute partially for the second. A qualitative spectroscopical analysis revealed the presence of Na in an amount roughly two percent by weight. An analysis for F has not been carried out, but the most probable composition of the *N* crystals appears to be $Cd_{1.6}Na_{0.4}Nb_2O_{6.6}F_{0.4}$. The

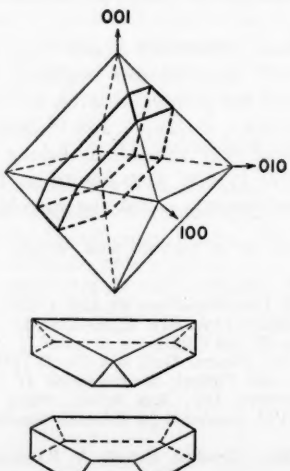

FIG. 3. Morphology of $Cd_2Nb_2O_7$.

[9] J. C. Slater, Phys. Rev. 78, 748 (1950).

lattice constant of $Cd_2Nb_2O_7$ was determined from the lines 10,6,6 and 12,4,4 of a powder diagram taken with a Norelco camera ($R=11.4$ cm) and Cu $K\alpha$ radiation. $Cd_2Nb_2O_7$ ceramic shows $a=10.372\pm0.001$ A, in agreement with previous data,[5] whereas the lattice constant of the N crystals is slightly larger, being 10.386 ±0.001 A.

Crystals with the same morphology as that indicated in Fig. 3 are obtained from a binary melt of KF and $Cd_2Nb_2O_7$ in molar ratio 3.5:1 (for example, 2.0 grams of KF and 5.2 grams of $Cd_2Nb_2O_7$). The lattice constant of these (indicated as K crystals in the following) is $a=10.384\pm0.001$ A. The advantage of KF over NaF is that the former is very soluble in water, thus facilitating the recovering of the crystals from the melt after the growing process. No chemical or spectroscopical analysis has been carried out on the K crystals.

During the process of finding a suitable flux for the growth of $Cd_2Nb_2O_7$ crystals, the following observation was made. A mixture of B_2O_3 and $Cd_2Nb_2O_7$ in molar ratios 5:1, 2:1, or 1:1, heated to about 1200°C and cooled at a rate of 80 degrees/hour, produces perfectly transparent, colorless, needle-shaped crystals with orthorhombic habit. Under the polarizing microscope the crystals show extinction at 90°. c-axis rotation and Weissenberg photographs of these crystals gave the following values for the lattice dimensions: $a=5.85$ A, $b=14.8$ A, $c=5.15$ A. The chemical composition of these crystals has not yet been directly explored; but comparison of their powder pattern with that of ceramic $CdNb_2O_6$ led us to assume the formula $CdNb_2O_6$ as the most probable one. The ($hk0$) reflections on the Weissenberg satisfy the conditions given for the columbite structure[10] (space group *Pbcn*), which include such compounds as $MnSb_2O_6$, $MgNb_2O_6$, and $ZnTa_2O_6$.

In order to obtain pure $Cd_2Nb_2O_7$ crystals, the second of the two possibilities listed above had to be considered, i.e., growth from the pure melt. In addition to the already mentioned evaporation of CdO, another practical difficulty, in this case, is represented by the fact that it is impossible to extract the solidified mass from the Pt crucible without peeling off the latter. The best results were obtained from the following procedure: a basket of Pt foil, containing pure $Cd_2Nb_2O_7$ powder, is introduced into a larger Pt crucible containing a proper amount of CdO. The crucible, with its cover, is sealed as tightly as possible with alundum cement. The whole is heated to 1470°C, cooled to 1420°C in one hour, and further cooled very quickly. If the excess CdO is not enough to maintain a saturated CdO atmosphere within the crucible during the heating and cooling process, two types of crystals are produced in the basket; one is $Cd_2Nb_2O_7$, and the other is an orthorhombic crystal showing the same powder pattern as ceramic $CdNb_2O_6$ and as the crystals obtained from B_2O_3 as a flux. This latter is again very probably $CdNb_2O_6$.

[10] A. F. Wells, *Structural Inorganic Chemistry* (Oxford University Press, London, 1950), p. 504.

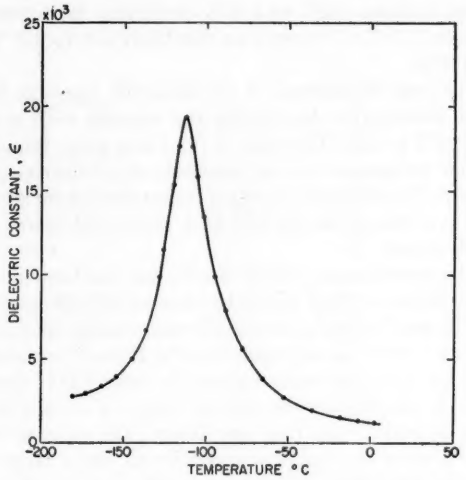

FIG. 4. Dielectric constant of $Cd_2Nb_2O_7$ crystals, grown with NaF as flux *vs* temperature.

The lattice constant of the $Cd_2Nb_2O_7$ crystals thus obtained is the same as for ceramic $Cd_2Nb_2O_7$: $a=10.372$ ±0.001 A. The crystals are too small for dielectric measurements, however, and can only be used for x-rays and optical investigations.

III. DIELECTRIC MEASUREMENTS

The study of the dielectric properties has been carried out exclusively on the N and K crystals, since crystals of pure $Cd_2Nb_2O_7$ of required size were not obtained. Unless otherwise stated, the results quoted below are those obtained with N crystals.

The crystal plates (areas ranging between 2.5 and 6 mm², and thicknesses between 0.1 and 0.3 mm) were selected under the microscope for homogeneity and absence of defects. The two larger surfaces, perpendicular to the cubic [111] direction, were ground parallel to each other and provided with evaporated silver electrodes.

Figure 4 shows the behavior of the dielectric constant *versus* temperature for a field applied along the cubic [111] direction. The room temperature value is 850; the peak value, at the Curie point, is about 20 000. The measurement was made by varying the temperature slowly and continuously (about 40 degrees/hour), with a field of 50 v/cm and a frequency of 10 kc/sec. The Curie temperature is −120°C upon cooling, −112°C upon heating—showing a remarkable decrease with respect to the ceramic $Cd_2Nb_2O_7$. This decrease is no doubt due to the impurities contained in the single crystals. The dielectric constant shows the hyperbolic behavior characteristic of ferroelectric crystals above the Curie point, according to the Curie-Weiss law $\cong C/(T-\theta)$. For ceramics the values of the Curie constant ranges from 4×10^4 to 10×10^4 °K, and θ

varies between 145° to 175°K according to different authors. For the N crystals we obtained $C=1.1\times10^5$ °K, $\theta=177$°K.

The field dependence of the dielectric constant has been investigated by biasing the crystals with a dc field of 5 kv/cm. The shift of the Curie point towards higher temperatures is of the order of 1.5 degrees per kv/cm. The dielectric constant is decreased upon application of the dc biasing field both above and below the Curie points.

The spontaneous polarization P_s has also been measured. Because of lack of precise dimensional information for the small crystals, the value found, 6 microcoulombs/cm² at −185°C, is only approximate. It must be noticed that the field was applied along the cubic [111] direction. If the ferroelectric axis is along the cubic [100] axis, as may be the case (see below), the value of the spontaneous polarization would be $\sqrt{3}$ times larger—that is, about 10 microcoulombs/cm².

IV. X-RAY ANALYSIS OF N, K, AND PURE $Cd_2Nb_2O_7$ CRYSTALS AT ROOM TEMPERATURE

The single crystal used for the x-ray study was a parallelopiped with the dimensions 0.03×0.03×0.10 mm, grown from pure $Cd_2Nb_2O_7$ melt. As already mentioned, this type of crystal always has its [110] axis along a long edge, and (111) planes as surfaces. It was very difficult to pick up a crystal with [100] along the edge. It appeared, however, that the [110] zone is preferable for the structural study.

Weissenberg diagrams were taken for several layers of the [110] crystal, using Cu $K\alpha$ radiation; and absent reflections confirmed the space group as $Fd3m$. General intensity relations can be explained very well by Cd and Nb positions as given by Bystroem. The intensity data for (hhl) reflections were collected using Mo $K\alpha$ radiation filtered through Zr foil. The multifilm technique with a calibrated intensity scale was used to obtain intensities, using visual estimation. Since the crystal is very small, no absorption correction was necessary; but five-day exposures were needed to obtain sufficient spot densities.

With heavy Cd and Nb atoms in a crystal, it is generally difficult to determine the exact positions of oxygen atoms. In $Cd_2Nb_2O_7$, however, the intensities of one group of reflections, of type ($4n+2$, $4n+2$, $4m$), depend only upon oxygen atoms; and intensities of another group, of type ($2n+1$, $2n+1$, $2m+1$), depend only on oxygens and *differences* between Cd and Nb structure factors ($f_{Cd}-f_{Nb}$), the difference being of the same order of magnitude as the factor for oxygen. From these, the oxygen parameter x was found to be $x=0.305\pm(0.003)$. This value is very close to the condition for regular NbO_6 octahedra. The remaining reflections are chiefly determined by $f_{Cd}+f_{Nb}$.

All structure factors were calculated with this oxygen parameter, and extinction effects observed in the strong reflections at low angles were corrected by a method recently described by Vand.[11] The over-all agreement is very good, the discrepancy factor $R=(\sum||F_o|-|F_c||)/\sum|F_o|$ being 0.06 for all reflections, and 0.11 for the two groups of reflections which were used for oxygen parameter determination only.

One of the N crystals was also studied. The crystal was ground along [110] to cylindrical form, with a diameter of 0.14 mm. Intensity data for (hhl) reflections were taken with Cu $K\alpha$ radiation. The same oxygen parameter as for pure $Cd_2Nb_2O_7$ explain intensities of the ($4n+2$, $4n+2$, $4m$) reflections, but do not account for those of ($2n+1$, $2n+1$, $2m+1$) type. The latter can be explained qualitatively if we assume that in the N crystal approximately 30 mole percent of total Cd is replaced by Na. Probably the same amount of seventh oxygen may be replaced by F, although this is difficult to establish by x-rays. The N crystal may perhaps be written as $Cd_{1.4}Na_{0.6}Nb_2O_{6.4}F_{0.6}$. The agreement of this formula with one estimated from spectroscopic analysis is as good as can be expected.

V. OPTICAL STUDY OF THE TRANSITION

The phase change in $Cd_2Nb_2O_7$ at the Curie point has also been examined by means of a new type of low-temperature stage[12] on a polarizing microscope. For pure $Cd_2Nb_2O_7$ the cubic to noncubic change occurs at 182°K, in good agreement with dielectric observations on ceramic specimens; it appears at about −123°C for the N-type crystals, and at about −133°C for the K-type—also in agreement with dielectric measurements.

Below the Curie point no definite extinction positions are detectable optically, nor are definite domain walls visible. This is in contrast with the case of ferroelectric $BaTiO_3$ and closely-related crystals, which reveal well-defined domain configurations with distinguishable extinction positions. Upon rotation of the $Cd_2Nb_2O_7$ plates between crossed nicols, a thin curved shadowy line rotates within the crystals; the border between light and dark regions is always diffuse and irregular. Under high magnification a fine structural pattern is visible at the surface. Near the crystal edges many small parallel wedges appear. These are elongated along the ⟨211⟩ directions, and are about 1μ wide. In the central region of the plate surface a very fine two-dimensional grid is apparent. The grid lines are probably walls of domains, the dimensions of which are very small.

The actual symmetry below the Curie point cannot be established from these observations, but a qualitative explanation can be given for them. The light travels in the cubic ⟨111⟩ direction. If the crystals become tetragonal or orthorhombic below the transition, one of

[11] V. Vand, "Methods for the Correction of X-Ray Intensities for Primary and Secondary Extinction in Crystal Structure Analysis," Technical Report to Office of Naval Research, July 1, 1954 (unpublished).

[12] Jona, Shirane, and Pepinsky (unpublished).

the cubic ⟨100⟩ directions will become a polar axis (see Sec. VI, below). If the domains are polarized at about 90° to each other and the walls lie at 45° to the cube edges, as in tetragonal $BaTiO_3$, a (111) plate comprised of only two domains would show extinction positions at 30° and 60° from one or the other domain. The trace of the domain wall (110) on the (111) surface is parallel to the ⟨211⟩ direction. It is in this direction that the very fine wedge-shaped domains appear elongated.

A macroscopic crystal plate contains a very large number of these domains. Some of these will always be in extinction position, regardless of the rotation of the plate (about ⟨111⟩) with respect to the vibration directions of the nicols. This probably accounts for the "rotating" extinction observed upon rotation of the crystal.

A (111) plate of $Cd_2Nb_2O_7$ about 100μ thick has a light yellow color of first-order. The birefringence must therefore be very small—of the order of 0.004.

VI. LOW-TEMPERATURE X-RAY STUDY

Powder patterns of a ceramic (pure) $Cd_2Nb_2O_7$ specimen at −140°C revealed no line-splitting, even at high scattering angles, due to distortion from the former cubic lattice. A single-crystal examination of a pure $Cd_2Nb_2O_7$ crystal was then initiated at −150°C, by means of our low-temperature Weissenberg camera,[13] with radius=11.4 cm and using Cu $K\alpha$ radiation. Zero-layer patterns from a crystal rotating about [110] showed very slight splitting in a few high-angle reflections; but a study of these did not permit any decision concerning the new crystal system. Some very remarkable intensity changes were apparent in reflections of the $(2n+1,\ 2n+1,\ 2m+1)$ class, however. These reflections involve structure factors f_0 and $f_{Cd}-f_{Nb}$ only. Thus shifts of Cd ions with respect to Nb ions must occur; shifts in oxygens may or may not accompany these.

One of the *N*-type crystals was also examined at −140°C. The splitting of high-angle reflections is larger than in pure $Cd_2Nb_2O_7$. Splitting is significant for reflections such as 4,4,12 and 9,9,3, but not detectable for 7,7,9 or 8,8,8. This suggests that the lattice is probably *not* rhombohedral, with a former cubic [111] axis as the polar axis. We can account for the separations by assuming a tetragonal lattice with $a=10.378$ A, and $c/a=1.0011$; but it is not possible to exclude an alternative orthorhombic distortion. A comparison with pure $Cd_2Nb_2O_7$ at −150°C suggests a possible tetragonal cell for it also, with $a=10.364$ A, $c/a=1.0005$.

Why pure $Cd_2Nb_2O_7$ shows a smaller distortion than *N*-type crystals is not clear.

VII. STUDY OF OTHER $A_2B_2O_7$ TYPE COMPOUNDS

Besides $Cd_2Nb_2O_7$, a good number of other crystals have been reported as pyrochlore types.[6,7] These are discussed exhaustively in reference 8, under the pyrochlore-microlite classification. There it is reported that, in the $A_2B_2O_6$(O, OH, F) formula, *A* can include Na, Ca, K, Mg, Fe^{+2}, Fe^{+3}, Mn^{+2}, Sb^{+3}, Pb(?), Ce, La, Di, Eu, Y, Th, Zr, and U; and *B* includes Nb, Ta, Ti, Sn(?), Fe^{+3}, and W(?). The number of mixed crystals which might be examined in a complete investigation of the pyrochlore-type structure is thus enormous. Bystroem[5] prepared $Cd_2Ta_2O_7$, $Ca_2Ta_2O_7$, and $Pb_2Sb_2O_7$ artificially, and others of the species have also been prepared.[8] Recently, $Pb_2Nb_2O_7$ was reported to have a rhombohedral lattice slightly distorted from the cubic pyrochlore lattice.[1] It is also known that although $Ca_2Sb_2O_7$, $Sr_2Sb_2O_7$, and $Cd_2Sb_2O_7$ have the same $A_2B_2O_7$ formula, they belong to the weberite species,[5] which has an interrupted octahedra network which would presumably not be favorable for ferroelectricity.

A modest beginning has been made on a study of the dielectric and structural properties of some solid solution systems related to $Cd_2Nb_2O_7$. The ceramic specimens were prepared by firing the appropriate mixtures at temperatures listed in Table I. All of the dielectric measurements were carried out at 10 kc/sec and a field strength of about 5 v/cm. The lattice parameters were determined using the 11.4-cm diameter Norelco powder camera and Cu $K\alpha$ radiation.

From considerations of ionic size, the following systems were considered likely to form solid solution readily: $Cd_2Nb_2O_7$-$Pb_2Nb_2O_7$, $Cd_2Nb_2O_7$-$Ca_2Nb_2O_7$, and $Cd_2Nb_2O_7$-$Cd_2Ta_2O_7$. The lattice constant of these compositions are shown in Fig. 5 and Table I.

All compositions of the $Cd_2(Nb, Ta)_2O_7$ system show the cubic powder patterns of pyrochlore type with little change of lattice constant, as expected from the similarity of ionic radii of Nb and Ta. The $(Cd, Pb)_2Nb_2O_7$ system also shows the pyrochlore

TABLE I. Cell and dielectric constants for some $A_2B_2O_7$ crystals.

Composition	a (A)[a]	Firing temperature (°C)	Dielectric constant at room temperature
$Cd_2Nb_2O_7$	10.372	1200	310
$(Cd_{0.9}, Pb_{0.1})_2Nb_2O_7$	10.407	1150	460
$(Cd_{0.8}, Pb_{0.2})_2Nb_2O_7$	10.443	1150	300
$(Cd_{0.4}, Pb_{0.6})_2Nb_2O_7$	10.550	1100	...
$(Cd_{0.2}, Pb_{0.8})_2Nb_2O_7$	10.596	1100	...
$(Cd_{0.1}, Pb_{0.9})_2Nb_2O_7$	10.615	1100	165
$Pb_2Nb_2O_7$	10.675	1050	190
	($\alpha=88°\ 50'$)		
$(Cd_{0.95}, Ca_{0.05})_2Nb_2O_7$	10.376	1200	600
$(Cd_{0.9}, Ca_{0.1})_2Nb_2O_7$	10.382	1200	540
$(Cd_{0.8}, Ca_{0.2})_2Nb_2O_7$	10.392	1200	380
$Cd_2(Nb_{0.95}, Ta_{0.05})_2O_7$	10.372	1200	570
$Cd_2(Nb_{0.9}, Ta_{0.1})_2O_7$	10.370	1200	380
$Cd_2(Nb_{0.8}, Ta_{0.2})_2O_7$	10.372	1200	200
$Cd_2Ta_2O_7$	10.376	1200	35
$Pb_2Ta_2O_7$	10.700	1050	51
	($\alpha=88°\ 25'$)		
$Y_2Ti_2O_7$	10.095	1200	65

[a] All lattices are cubic except for the two for which values of α are given; the latter are rhombohedral.

[13] Keeling, Frazer, and Pepinsky, Rev. Sci. Instr. **24**, 1087 (1953).

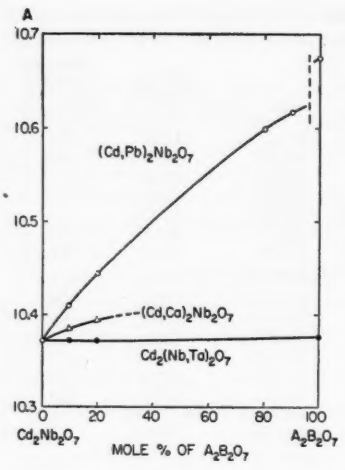

FIG. 5. Lattice parameters of solid solutions involving $Cd_2Nb_2O_7$.

lattice, except for a narrow range on the $Pb_2Nb_2O_7$ side which shows a rhombohedral lattice. This point will be discussed later.

In the $(Cd, Ca)_2Nb_2O_7$ system, on the other hand, a pyrochlore-type solid solution is formed only for some compositions on the pure $Cd_2Nb_2O_7$ side. $(Cd_{0.8}, Ca_{0.2})_2Nb_2O_7$ shows, in addition to the main cubic patterns of pyrochlore type, some additional weak lines which suggest that this composition may be a mixture. Pure $Ca_2Nb_2O_7$ shows a quite different powder pattern from that of $Cd_2Nb_2O_7$, indicating that the structure is not of the pyrochlore type.

The Curie temperature of these solid solution systems were determined by dielectric measurements, as shown in Fig. 6. The results for $Cd_2(Nb, Ta)_2O_7$ are not shown in the figure because they very nearly coincide with the curve for $(Cd, Pb)_2Nb_2O_7$. The important result is that the Curie temperature of pure $Cd_2Nb_2O_7$ is always decreased by the replacement of Cd or Nb by other ions. The behavior of the second phase transitions in $Cd_2Nb_2O_7$ at 85°K was studied only for the system $(Cd, Pb)_2Nb_2O_7$. This transition temperature was also decreased with increasing Pb concentration. It is 60°K for $(Cd_{0.95}, Pb_{0.05})_2Nb_2O_7$, and it was not observed above 10°K for $(Cd_{0.9}, Pb_{0.1})_2Nb_2O_7$.

$Pb_2Nb_2O_7$ presents an interesting problem. This compound was first studied by Cook and Jaffe,[1] and the structure was reported as a rhombohedral distortion of the pyrochlore-type structure with $a=10.570$ A and $\alpha=89°\,15'$.[14] The dielectric measurements[3,4] have revealed that the compound shows a flat maximum of the dielectric constant to 14°K. However, the polarization *vs* field relation is quite linear even below 14°K under a field strength of 10 kv/cm. This leads us to the conclusion that $Pb_2Nb_2O_7$ is probably not ferroelectric.

The powder lines of $Pb_2Nb_2O_7$ can be explained very well by assuming a rhombohedral lattice; and a comparison with the powder lines of $Cd_2Nb_2O_7$ shows that this rhombohedral lattice may be formed by a slight distortion from the cubic pyrochlore lattice. Accurate lattice constant were calculated from high angle lines 10,6,6 and 12,4,4, yielding $a=10.674$ A, $\alpha=88°\,50'$. These values are somewhat different from the constants reported by Cook and Jaffe.[15]

Figure 5 shows that the phase boundary of rhombohedral $Pb_2Nb_2O_7$, and the cubic phase of $Cd_2Nb_2O_7$ lies somewhere between $(Cd_{0.1}, Pb_{0.9})_2Nb_2O_7$ and pure $Pb_2Nb_2O_7$. To explore this phase line, dielectric measurements were carried out on $Pb_2Nb_2O_7$ between 20°C and 500°C and on $(Cd_{0.1}, Pb_{0.9})_2Nb_2O_7$ between 20°C and −180°C. No anomaly indicating a phase transition was observed. Goodman also carried out dilatometric measurements of pure $Pb_2Nb_2O_7$ up to 1000°C without observing any anomaly.[16]

Two more compositions were studied in this range. $(Cd_{0.025}, Pb_{0.975})_2Nb_2O_7$ showed strong rhombohedral lines and some weak cubic lines; and $(Cd_{0.05}, Pb_{0.95})_2Nb_2O_7$, on the other hand, showed strong cubic lines and some weak rhombohedral lines. Although this seems to establish the existence of the mixed phase, it must be mentioned that the results immediately above might be due to nonuniformity of composition in the specimen, since the composition is very critical.

It is certain, in any case, that this rhombohedral phase is limited to the narrow range near pure $Pb_2Nb_2O_7$. In this connection it is of interest that Cook and Jaffe reported a cubic lead niobate with the approximate composition $Pb_{1.5}Nb_2O_{6.5}$ ($a=10.561$ A). This seems to provide an example of a general formula of pyrochlore type $A_{1+x}B_2O_{6+x}$. A further investigation of this problem is in progress.

In addition to the above-mentioned compounds, the following were prepared: $Pb_2Ta_2O_7$, $Y_2Ti_2O_7$, $Sr_2Nb_2O_7$, $Y_2Zr_2O_7$, $La_2Ti_2O_7$, $La_2Zr_2O_7$. From powder photographs,

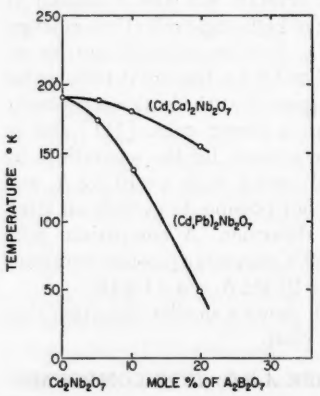

FIG. 6. Curie temperatures of solid solutions involving $Cd_2Nb_2O_7$.

[14] Originally, the value $a=5.285$ A was published, (see reference 1) but later it was implied that the true cell dimension is twice as large (see reference 2).

[15] The lattice parameters of $Pb_2Nb_2O_7$ can be calculated from the d spacings given in Goodman's paper (see reference 16). $a=10.64$ A and $\alpha=88°\,50'$ were obtained from 2,2,0 and 3,1,1 line groups.

[16] G. Goodman, J. Am. Ceram. Soc. 36, 368 (1953).

only the first two compounds were found to have pyrochlore-type structures. The other four compounds show complicated powder patterns, and no effort was made further to interpret them. $Pb_2Ta_2O_7$ shows, as does $Pb_2Nb_2O_7$, a rhombohedral lattice; and $Y_2Ti_2O_7$ shows a cubic lattice. No dielectric anomaly was found for $Pb_2Ta_2O_7$ or $Y_2Ti_2O_7$ between 20°C and −180°C. The dielectric constants of these pyrochlore types are relatively high in general, which fact renders them worth examining. Hulm[4] reported no anomaly in $Cd_2Ta_2O_7$, $Pb_2Ta_2O_7$, $In_2Ti_2O_7$, or $In_2Zr_2O_7$. The structure of the last two compounds is unknown.

To date, no rules are known according to which one can judge whether or not a compound of constitution $A_2B_2O_7$ is likely to have a pyrochlore structure. However, the following may be said upon consideration of the ionic radii of the involved ions. It does seem that a pyrochlore structure can be realized for only a narrow range of ionic radii: 0.95 to 1.15 A for ion A and 0.60 to 0.70 A for ion B. (It should of course be possible to include small amounts of other ions in the network, thus accounting for the large number of mineral varieties in this species.) $Cd_2Nb_2O_7$ has the smallest A ion and the largest B ion in this range, and this might be related to the fact that the Curie temperature of $Cd_2Nb_2O_7$ is always shifted downward upon replacement of Cd or Nb by other ions. This critical condition on ion size is in contrast with the case of the perovskite-type structure of composition ABO_3. A large number of crystals have been reported as members of this group, with a relatively wide range of ionic radii for A and B; and several of the members have been found to be ferroelectric. A good number of other types of multiple oxides containing Nb, Ta, and/or Ti deserve examination, and some of them are under study in our laboratory.

ACKNOWLEDGMENTS

The authors are greatly indebted to Dr. H. L. Lovell for the spectroscopic analyses, to Professor R. Roy for illuminating discussions, and to Mr. J. L. McLaughlin for assistance in crystal growth and dielectric measurements.

PHYSICAL REVIEW VOLUME 98, NUMBER 4 MAY 15, 1955

Model for Luminescence and Photoconductivity in the Sulfides

JOHN LAMBE AND CLIFFORD C. KLICK
U. S. Naval Research Laboratory, Washington, D. C.

(Received January 10, 1955)

A model for sulfides activated by monovalent metals is discussed which differs in several important respects from that usually employed. Because of the net negative charge of the lattice volume surrounding the activator there is a large cross section for trapping of holes which may be accompanied by release of a large amount of energy. This is presumed to be the transition leading to luminescence. A subsequent trapping of an electron returns the center to its original condition. For the electron trapping there is no Coulomb field and both the capture cross section and energy released would be expected to be small compared with the case of hole trapping. On the basis of this model, there is a simple explanation of the fast luminescence decay associated with hole capture and the slow conductivity decay associated with that of free electrons. Other well-known phenomena in the sulfides are examined on the basis of this model. In addition, predictions of this model concerning the infrared photoconductivity and infrared stimulation of luminescence have been verified by experiment on silver-activated cadmium sulfide.

I. INTRODUCTION

THERE exists an extensive literature on both the luminescence and conductivity properties of the sulfide phosphors. Impurity-activated sulfides have been among the earliest materials studied, and in recent years have been the subjects of intensive investigations, stimulated in part by their many practical applications. A recent paper by Klasens[1] summarizes much of the current theory of luminescence for sulfides. Similarly a large amount of work has been done on the conductivity of sulfides, particularly on cadmium sulfide which can be prepared in the form of fairly large crystals by the method of Frerichs,[2] and which is of special practical interest because of its unusually high photosensitivity. An introduction to the literature on the conductivity of cadmium sulfide may be found in a paper by Rose.[3] Schön[4] and Klasens and his associates[5] have proposed a "hole migration" theory of luminescence of sulfides activated with monovalent impurities such as Ag^+. This theory is illustrated in Fig. 1 for the case where excitation of luminescence is by absorption of light in the fundamental band of the host lattice. The sequence of events is as follows:

[1] H. A. Klasens, J. Electrochem. Soc. **100**, 72 (1953).
[2] R. Frerichs, Naturwiss. **33**, 381 (1946).
[3] A. Rose, RCA Rev. **12**, 362 (1951).
[4] M. Schön, Z. Physik **119**, 463 (1942).
[5] H. A. Klasens, Nature **158**, 306 (1946); Klasens, Ramsen, and Quantie, J. Opt. Soc. Am. **38**, 60 (1948).

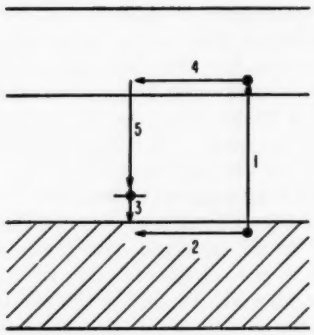

FIG. 1. Conventional model for sulfides with monovalent activator (1) excitation; (2) hole migration; (3) hole capture (nonradiative); (4) electron migration; (5) electron capture resulting in luminescence.

(1) Light is absorbed in the fundamental absorption band producing a free electron and hole and leading to photoconductivity.

(2) The hole may migrate toward the impurity center. If, for example, the center is due to Ag^{+} substituted for Cd^{++} in CdS, then the center has a net negative charge and attracts the hole with a Coulomb-like attraction.

(3) The hole is captured by the impurity center, giving off a small amount of energy as infrared radiation or as vibrational quanta.

(4) The electron wanders through the lattice until it finally comes near the center.

(5) The electron is captured by the center. It recombines with the captured hole and gives off energy as luminescent emission. The electronic transition may be directly from the conduction band to the ground state of the center, or may be by way of an intermediate excited state of the center. After luminescence the cycle is complete and the process may again be repeated.

By extending this model to include two impurity atoms, Schön and Klasens are able to account for the effect of poisons, variations of luminescence color with temperature of some phosphors, the nonlinear relationship between luminescent output and the exciting intensity, and other similar phenomena in the sulfides.

Another important development in the theory of the sulfides has been the work of Kröger and his associates,[6] who showed that in zinc sulfide it is necessary to balance each monovalent positive ion introduced by a monovalent negative ion or a trivalent positive ion. This "charge compensation" principle serves to explain the role of fluxes normally used to prepare these phosphors. In addition it emphasizes the essentially ionic nature of the impurity center. Thus even if the sulfide lattice is primarily covalent in character, it appears that in the vicinity of most impurities the ionic character of the impurity is decisive. Recently Klasens[1] has suggested that the luminescent center is actually a sulfide ion perturbed by the presence of the activator ion, rather than the activator ion itself. This modification of the theory does not essentially alter the sequence of events previously described in the luminescent process.

While a major part of the work on sulfides has dealt either with the luminescence or conduction properties separately, some investigations have been made on both properties simultaneously. One very striking fact which emerges from such investigations is that the decay of luminescence is much more rapid than the decay of photoconductivity. On the basis of the model of Fig. 1, it would be expected that the decay times of luminescence and photoconductivity would be approximately alike since the capture of the electron in step 5 leads to both luminescence and to a decrease in conductivity. Several attempts have been made to explain this phenomenon. Bube[7] has suggested that in ZnS the luminescence might be typical of the crystal and that the conductivity is characteristic of a small surface layer. Kallman and Kramer[8] postulate that electron transfer occurs in the crystal in some cases without having electrons enter the conduction band. McKay[9] has investigated the conductivity of *n-p-n* junctions and inferred that the slow current decay may be characteristic of such junctions. Each of these suggestions involves the assumption that the crystal has regions in which the properties are different from those of the bulk of the crystal.

The band picture of Fig. 1 is oversimplified in that a variety of other levels may enter and be of importance. One set of levels is due to the "quenching" centers which have been investigated by Hardy[10] and Taft and Hebb.[11] If a small current is drawn from the crystal by applying an electric field and irradiating in the fundamental absorption band, additional irradiation in the quenching bands first causes a transient increase and then a steady decrease in current flow. For CdS, the edge of the fundamental absorption band is at about 5000 A and the quenching bands are about 10 000 A. Rose[8] and Taft and Hebb[11] interpret absorption in these centers as excitation of a hole from an acceptor level to the valence band. The free holes which are produced in this process first add to the number of charge carriers and the conductivity is increased. In the steady state condition, however, these holes recombine with electrons resulting in a decreased concentration in the conduction band and, since Hall effect measurements indicate that electrons are the principal charge carriers, the conductivity is observed to decrease.

[6] F. A. Kröger and J. F. Hellingman, J. Electrochem. Soc. **93**, 156 (1948); **95**, 68 (1949); F. A. Kröger and J. Dikhoff, Physica **16**, 297 (1950).

[7] R. H. Bube, Phys. Rev. **83**, 393 (1951).
[8] H. Kallman and B. Kramer, Phys. Rev. **87**, 91 (1951).
[9] K. G. McKay, Phys. Rev. **84**, 833 (1951).
[10] A. E. Hardy, J. Electrochem. Soc. **87**, 355 (1945).
[11] E. A. Taft and M. H. Hebb, J. Opt. Soc. Am. **42**, 249 (1952).

Another set of fairly deep electron traps is introduced by the charge compensation centers when a monovalent metal substitutes for a divalent positive ion of the host lattice. There is evidence that these centers can consist of trivalent positive ions substituted at divalent positive ion sites, monovalent negative ions substituted at divalent negative ion sites, or negative ion vacancies. In each case a deep electron trap should be formed involving a Coulomb attraction for the electron.

In addition to these centers, there appear to be a variety of traps of varying depths which are less well understood but which may, in practice, determine some of the properties of materials used experimentally.

II. PROPOSED MODEL

In this section a somewhat different model is proposed. The model is illustrated in Fig. 2 and differs from Schön's and Klasen's model in that the trapping of the hole by the center is considered to be a large energy transition and is assumed to give rise to luminescence. On an ionic picture of the center, the substitution of a monovalent positive ion for a divalent one leaves the volume around the center with a net negative charge. This has two effects: first, the cross section for trapping of a hole becomes large because of the Coulomb attraction; and second, the energy released in the capture of a hole may be large. The proposed cycle is then as follows:

(1) Light is absorbed producing a free hole and electron leading to conductivity.

(2) The hole and electron move in their respective bands, and eventually the hole migrates near the impurity center.

(3) The hole is captured by the impurity center and luminescent emission occurs leaving the center now neutral in charge.

(4) The electron wanders through the lattice until it finally comes near the center.

(5) The electron is finally captured by the center, and in the capture only a small amount of energy is given off as infrared radiation or as vibrational quanta.

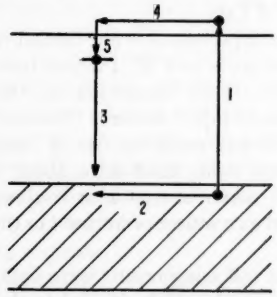

FIG. 2. Proposed model for sulfides with monovalent activator: (1) excitation; (2) hole migration; (3) hole capture resulting in luminescence; (4) electron migration; (5) electron capture (nonradiative).

The center is now returned to its initial condition and the cycle can be repeated.

The essential difference between the conventional model and the model presented here is that the former assumes that luminescence results from the capture and subsequent recombination of a conduction electron, whereas the latter assumes that luminescence results from the capture and subsequent recombination of a free hole. As has been assumed by Klasens,[1] the levels involved here arise from sulfur ions adjacent to the monovalent activator. On the basis of the model proposed here, however, it is assumed that the energy required to free an electron from one of these sulfur ions is small. There is a long-wavelength extension of the fundamental absorption band which arises when monovalent activator ions are introduced into sulfides. This would be interpreted as arising not from sulfur ions immediately adjacent to the monovalent activator, but from sulfur ions further removed. These levels would be shifted slightly above the valence band due to the negatively charged luminescent center.

The luminescence of "self-activated" sulfides may be considered as similar to that due to monovalent metals both on Klasen's model and that proposed here if the center is that proposed by Kröger and Vink[12]: a positive-ion vacancy whose nearest surroundings have lost one electron.

The difficulty of choosing a model for sulfides on the basis of a limited variety of experiments is emphasized by Duboc[13] who has shown that the nonlinearity of luminescence and photoconductivity with exciting intensity in photoconducting phosphors can be explained with at least sixteen different two-center models. It appears, therefore, that only by examining a variety of experimental data is it possible to reach conclusions concerning the correctness of a model.

III. COMPARISON WITH EXPERIMENT

An attempt will be made to relate the model proposed here to various phenomena in sulfides. In addition, several experiments have been performed involving luminescence and photoconducting properties of sulfides at low temperatures under infrared excitation in order to check the predictions of this model.

Mention has already been made of the fact that, typically, the decay time of photoconductivity is two orders of magnitude larger than the decay time of luminescence. While the explanations which have been advanced involve the assumption that there are special regions of the crystal with properties different from the main crystal, it is also possible to invent a scheme, based on the Schön-Klasens model (Fig. 1), to explain this effect. We may postulate that killer centers exist in addition to luminescent centers. The killer centers should have the property that recombination of

[12] F. A. Kröger and H. J. Vink, J. Chem. Phys. **22**, 250 (1954).
[13] C. A. Duboc, Brit. J. Appl. Phys. **107**, Suppl. No. 4 (1955).

electrons and holes at the center does not result in visible luminescence. Also the centers should have levels high enough above the top of the filled band so that thermal release of trapped holes does not occur to an appreciable extent at ordinary temperatures. Finally, the killer center should have a large cross section for trapping of holes but only a small cross section for trapping of an electron once the hole has been captured. On illumination in the fundamental absorption band, then, free electrons and holes are released and the holes are first trapped at killer centers until these are filled leaving a number of free electrons in the conduction band. As excitation proceeds, holes are trapped at the luminescent centers and electrons quickly combine with these holes to give off luminescence. When the exciting light is removed the luminescent process quickly ceases, but because of the low cross section for capture of electrons by the killer centers, the electrons which will recombine with holes at these centers remain in the conduction band for a long time. In this way long-decay photoconductivity and short-decay luminescence could occur without seriously impairing the high luminescence efficiency under steady excitation.

The same results are obtained from the model proposed in this paper without using centers other than the luminescent centers. In Fig. 2 the hole-trapping process of step 3 is one for which there is presumed to be a large cross section due to Coulomb attraction, and this leads to luminescence. The subsequent trapping of an electron in step 5 may have a very small cross section and lead to the slow photoconductive response.

The change of luminescent color with temperature of doubly activated phosphors has been adequately explained on the Schön-Klasens model. On the basis of the model proposed here, this phenomena would be interpreted as follows. We suppose the electron in one center lies closer to the conduction band than the electron in the other center (Fig. 3). As the phosphor is warmed up from low temperatures, the electron in the shallower center will be thermally ejected into the conduction band and the center will become inactive as far as luminescence is concerned. The observed luminescence would then tend to become more and more characteristic of the deeper-lying center. Such behavior could thus give rise to the well-known blue to green color shift of ZnS:Ag,Cu for example.

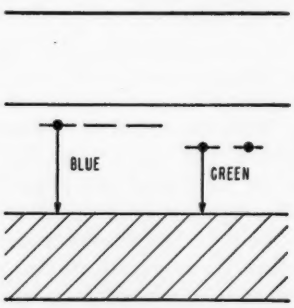

FIG. 3. Explanation of color change in luminescence on the basis of proposed model. The blue levels are thermally emptied as the temperature is raised.

It is evident that on the basis of the above qualitative arguments, both the conventional model and the model proposed here are capable of explaining many of the observed properties of photoconducting phosphors. Although the proposed model does seem to afford a simpler interpetation of luminescent and photoconductive decay times, there is in the above discussion no overriding evidence favoring one or the other. Therefore, in order to clarify some of the issues raised here, an experimental investigation of silver-activated CdS crystals was undertaken on the properties of these phosphors under infrared excitation.

When measured at 77°K, silver-activated CdS shows a broad emission band centering at about 6100 A.[14] A study of the decay times of this luminescence and the associated photoconductivity at 77°K shows that the decay time of the luminescence is about one-hundredth the decay time of the photoconductivity.[15] A number of experiments in the infrared region were performed on this phosphor to discover whether silver activation introduced an electronic level lying just below the conduction band as suggested by the new model. The crystals used in this work were activated with silver by introducing silver vapor into the vapor phase growth of CdS.

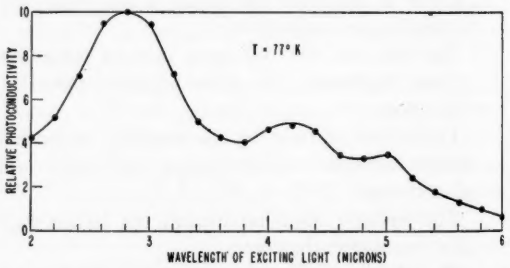

FIG. 4. Infrared photoconductive response of CdS(Ag) at 77°K for equal number of incident quanta.

Most of the experiments were carried out at 77°K, but a few were made at 4°K. Temperature control was maintained by direct immersion of the sample in liquid nitrogen or liquid helium. Electrical connection to the crystals was made by use of indium contacts and the electric fields used were about 50 v/cm. A rocksalt prism monochromator in conjunction with a glowbar served as a source of infrared in the range from 1 to 10μ.

At 77°K the following results were obtained. Radiation in the 1μ wavelength region led to the well-known quenching of conductivity[10,11] produced by simultaneous

[14] C. C. Klick, J. Opt. Soc. Am. 41, 816 (1951).
[15] J. J. Lambe (to be published).

irradiation with light in the fundamental band. If the crystal was cooled to 77°K in the dark, no photoconductive response was observed on irradiation with infrared at wavelengths longer than 1μ. However, if the crystal was first illuminated with light in the fundamental absorption band and this visible illumination was then removed, infrared response was found in a region beginning about 1.8μ and extending out to about 6μ. The details of this are shown in Fig. 4. This band was determined to be the result of silver activation by performing similar experiments on unactivated CdS. It was noted that if the infrared was left on the crystal, the response gradually diminished. At 4°K this infrared

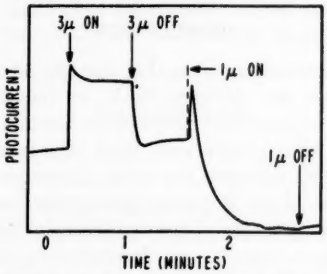

FIG. 5. Comparison of the action of 3μ irradiation and 1μ irradiation on photoconductivity of CdS(Ag) at 77°K.

response was not found, indicating, possibly, that these transitions are to excited states of the center from which thermal energy frees the charge carrier.

The next step was to determine whether the infrared response was due to freeing of holes or electrons. In order to do this the following approach was followed. As previously mentioned, the well-known quenching action of 1μ irradiation has been ascribed to the liberation of holes. It is assumed that these holes then recombine with electrons in some manner, thus reducing the number of conduction electrons. It was decided, therefore, to compare the action of 1μ irradiation and 3μ irradiation on an existing photocurrent at 77°K. To do this a small amount of visible light was allowed to fall on the crystal and the crystal was irradiated first at 3μ and then at 1μ. The results of this experiment are shown in Fig. 5. It is seen that the 3μ irradiation produces a steady stimulation, while the 1μ irradiation brings about a complete quenching of the photocurrent. This indicates that the 3μ irradiation raises electrons into the conduction band rather than producing free holes. Moreover, it was noted that by irradiating at 1μ the 3μ response could be completely removed. It required re-exposure to visible light to restore the 3μ response.

More evidence will be presented in subsequent paragraphs regarding the difference in the effects of 1μ and 3μ irradiation, but at this point it may be well to summarize these experimental results in terms of the present model as is illustrated in Fig. 6. At 77°K,

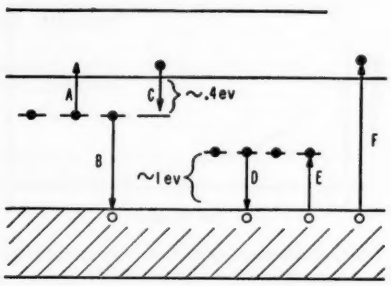

FIG. 6. Specific model proposed for CdS(Ag). Levels ~0.4 ev below conduction band result from silver activation. Levels 1 ev above valence band are normally present in CdS. *A:* Infrared excitation of trapped electrons (3μ region). *B:* Luminescent recombination of trapped electrons and free holes. *C:* Trapping of electrons. *D:* Trapping of holes. *E:* Freeing of trapped holes by excitation in 1μ region. *F:* Excitation.

if the crystal has been exposed to light in the fundamental absorption band, there are filled electron levels about 0.4 ev below the conduction band due to silver activation. If the crystal has been cooled in the dark, these levels are empty; this will be discussed in more detail at the end of this section. In addition, there are the usual quenching levels the order of 1 ev above the valence band. If the crystal in this state were illuminated with infrared, no response should be observed, which is in agreement with experiment. If the crystal is illuminated with light of wavelength less than 5000 A, electrons will be raised into the conduction band, and many of them may be trapped at the luminescent centers. In addition, electrons in the quenching levels can combine with free holes in the valence band and thus the holes can be "trapped." Let the exciting illumination now be removed. Many of the electrons will remain in traps and also trapped holes will remain. If we now illuminate with 3μ infrared radiation, we can eject electrons from the luminescent centers and this will give rise to an infrared photoconductive response. If we illuminate with 1μ irradiation, this will free holes from the quenching centers which can then empty electrons from the Ag activator levels or recombine with free electrons. This should cause both the 3μ infrared photoconductive response to disappear as well as lower the conductivity due to irradiation in the fundamental band. Both these effects are observed. If the action of the quenching centers is due to the release of free holes, then the opposite effects, observed with the infrared centers introduced by the activator, should be due to the release of free electrons. It would appear extremely difficult to fit this conclusion into the Schön-Klasens model.

In the model proposed here, it is assumed that the luminescent transition associated with the silver activation is due to the recombination of a hole in the valence band with an electron in the shallow activator level. It is clear then that irradiation in the quenching centers, which is believed to release free holes, should stimulate

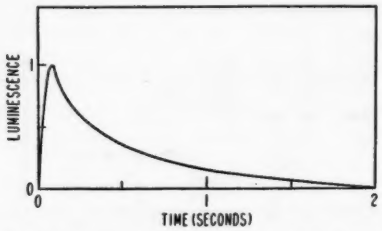

FIG. 7. Stimulation of luminescence in CdS(Ag) produced by 1μ irradiation.

luminescence if this model is to be consistent. To test this point the following experiment was carried out. A CdS(Ag) crystal was cooled to 77°K and irradiated with blue light. The light was removed and then the crystal was irradiated at 1μ. This caused a burst of orange luminescence which could be observed visually. A photomultiplier was used to record this burst and the result is shown in Fig. 7. Irradiation at 3μ did not produce any observable effect which is also in agreement with the model presented here.

Finally, it may also be noted that the bottom of the silver activation level is approximately 0.4 ev below the conduction band. The observed silver emission centers at about 2 ev so that these values are at least consistent with a total forbidden gap of 2.5 ev. The value of 0.4 ev from these infrared measurements is also in good agreement with the value of 0.5 ev obtained by Kröger, Vink, and van de Boomgaard[16] for silver activated cadmium sulfide from luminescence and absorption measurements.

The question arises as to why the silver activation levels should be normally empty as the crystal is cooled in the dark. The reason may be that on the basis of charge compensation, the introduction of silver without a coactivator should lead to missing sulfur ions at other parts of the crystal. These sulfur ion vacancies or other positively charged centers would form deep electron traps which may be filled by electrons from the shallow silver levels. This results in the behavior of silver activator levels as empty rather than as filled donor levels as the crystal is cooled in the dark to low temperature. In this case, irradiation in the fundamental band would first allow the shallow activator levels to be filled with electrons while the corresponding holes also become localized. After equilibrium has been reached, the luminescence mechanism would proceed as previously described. Before equilibrium can be reached, silver activator levels must be filled. This fact causes certain transient effects in luminescence and photoconductivity. These effects have been studied and are reported elsewhere.[15]

[16] Kröger, Vink, and van de Boomgaard, Z. physik Chem. **203**, 1 (1954).

CONCLUSION

A model which assumes that the trapping of a hole, rather than an electron, leads to luminescence in sulfides activated by monovalent metals has been compared with experiment. Both this model and an older model account for such phenomena as the appearance of an impurity absorption band on the long-wavelength side of the fundamental band, effects of poisons, variation of luminescence color with temperature of doubly activated phosphors, and nonlinear effects in luminescence and conductivity. The explanation of the different decay times for luminescence and photoconductivity appears to be simpler on the new model. Finally, the observed stimulation of activator luminescence by irradiation in the quenching band and the increase in photoconductivity (rather than quenching) on irradiation in the 2–6μ infrared band were predicted on the basis of the present model; it would appear to be difficult to explain these experiments with the older model.

ACKNOWLEDGMENTS

We should like to thank M. E. Bishop and David Patterson for their assistance in various aspects of this work.

Theory of Donor States in Silicon*

W. KOHN, *Department of Physics, Carnegie Institute of Technology, Pittsburgh, Pennsylvania and Bell Telephone Laboratories, Murray Hill, New Jersey*

AND

J. M. LUTTINGER, *Department of Physics, University of Michigan, Ann Arbor, Michigan and Bell Telephone Laboratories, Murray Hill, New Jersey*

(Received February 2, 1955)

By using the recently measured effective masses for n-type Si, $m_1=0.98\ m$ and $m_2=0.19$ m, approximate solutions of the resulting effective mass Schroedinger equation are obtained. The accuracy of the solutions was tested in the limiting cases where $m_2/m_1=1$ and 0 respectively. The nature of the resulting states and their degeneracy is discussed in some detail, taking into account the fact that the conduction band of Si has six equivalent minima. Experimentally measured ionization energies show that the effective mass theory is seriously in error in the case of the ground state. This error is attributed to failure of the effective mass theory near the donor nucleus, and allowance for this failure is made in the case of higher states. This leads finally to a theoretical spectrum for the electrons bound by P, As, or Sb donors.

1. INTRODUCTION

IT is well known that P, As, or Sb—all Group V atoms—when added to Si, act as so-called electron donors. The following qualitative picture has been well confirmed by experiment[1]: The donor atom has five electrons outside of closed shells. Four of these serve to complete bonds with neighboring atoms. The fifth finds itself in the Coulomb field of the remaining charge (reduced by the dielectric constant of the medium). In this field there exist bound states, with ionization energies of a few hundredths of a volt. The purpose of this paper is to examine these states theoretically in the light of existing experimental information.

This investigation was stimulated by the spin resonance experiments of Fletcher *et al.*[2] on n-type Si, and we have examined only donor states in Si in some detail. However, most of our considerations apply *mutatis mutandis* also to n-type Ge. On the other hand, acceptor states in Si and Ge represent a rather different situation, because of the special structure of the top of the valence band, to which we hope to come back in a later publication.

2. EXPERIMENTAL SITUATION

The following experimental data are of special significance for our purposes:

(a) Ionization Energies

These have been determined from the temperature dependence of the Hall coefficient. The results are given in Table I. We have included in this table results for Li donors which very likely occupy interstitial positions in the lattice.

(b) Band Structure

Recent measurements of piezo-resistance,[3] magneto-resistance[4] and cyclotron resonances[5] lead conclusively to the following picture. The conduction band of Si has six minima located on the (1,0,0) and equivalent axes. If the minimum on the (1,0,0) axis is denoted by $\mathbf{k}^{(1)}=(k_0,0,0)$, the energy near this point is given by

$$E=E_0+(\hbar^2/2m_1)(k_x-k_0)^2+(\hbar^2/2m_2)(k_y^2+k_z^2), \quad (2.1)$$

where

$$m_1=0.98m, \quad m_2=0.19m, \quad (2.2)$$

m being the free electron mass.

3. EFFECTIVE MASS THEORY

The donor state wave functions satisfy a Schrödinger equation of the form

$$\left(-\frac{\hbar^2}{2m}\nabla^2+V(\mathbf{r})+U(\mathbf{r})\right)\psi(\mathbf{r})=E\psi(\mathbf{r}), \quad (3.1)$$

where $V(\mathbf{r})$ is the periodic potential of an electron in a perfect Si lattice, and $U(\mathbf{r})$ is the additional potential due to the replacement of a Si atom by a donor ion. We choose the donor nucleus as coordinate origin. Then, for large r,

$$U(\mathbf{r})=-e^2/\kappa r, \quad (3.2)$$

TABLE I. Experimental ionization energies of donor states.

Donor	Ionization energy (ev)
P	0.044[a]
As	0.049[a,b]
Sb	0.039[a]
Li	0.033[a,c]

[a] F. J. Morin *et al.*, Phys. Rev. **96**, 833 (A) (1954).
[b] E. Burstein *et al.*, J. Phys. Chem. **57**, 849 (1953).
[c] C. S. Fuller and J. A. Ditzenberger, Phys. Rev. **91**, 193 (1953).

* Supported in part by the Office of Naval Research. Preliminary reports have appeared in Bull. Am. Phys. Soc. **30**, No. 2, 38 (1955) and Phys. Rev. **97**, 1721 (1955).

[1] E.g., G. L. Pearson and J. Bardeen, Phys. Rev. **75**, 865 (1949).
[2] R. C. Fletcher *et al.*, Phys. Rev. **94**, 1392 (1954); **95**, 844 (1954).
[3] C. Smith, Phys. Rev. **94**, 42 (1954).
[4] G. L. Pearson and C. Herring, Physica (to be published).
[5] R. N. Dexter *et al.*, Phys. Rev. **96**, 222 (1954).

where κ is the dielectric constant of Si, having the value 12.0. Because of this large reduction of the Coulomb field of the donor ion, one expects bound states around the donor having dimensions large compared to the lattice spacing. In this limit it can be shown[6] that (3.1) has solutions of the form

$$\psi^{(i)}(\mathbf{r})=F^{(i)}(\mathbf{r})\psi(\mathbf{k}^{(i)},\mathbf{r}), \quad i=1, 2, \cdots 6, \quad (3.3)$$

where $\psi(\mathbf{k}^{(i)},\mathbf{r})$ is the Bloch wave at the minimum $\mathbf{k}^{(i)}$ assumed to be nondegenerate. The $F^{(i)}(\mathbf{r})$ satisfy the effective mass equations,

$$\left[-\frac{\hbar^2}{2m_1}\frac{\partial^2}{\partial z_i^2}-\frac{\hbar^2}{2m_2}\left(\frac{\partial^2}{\partial x_i^2}+\frac{\partial^2}{\partial y_i}\right)-\frac{e^2}{\kappa r}-\epsilon\right]F^{(i)}(\mathbf{r})=0, \quad (3.4)$$

where m_1 and m_2 are defined in (2.1) and z_i lies along the direction of $\mathbf{k}^{(i)}$. The function $\psi^{(i)}(\mathbf{r})$ is normalized, provided we set

$$\int_{\text{unit cell}}|\psi(\mathbf{k}^{(i)},\mathbf{r}|^2 d\mathbf{r}=\Omega, \quad (3.5)$$

Ω being the volume of the unit cell, and

$$\int_{\text{all space}}|F^{(i)}(\mathbf{r})|^2 d\mathbf{r}=1. \quad (3.6)$$

Finally it is convenient to choose the phases of the $\psi(\mathbf{k}^{(i)},\mathbf{r})$ such that the $\psi(\mathbf{k}^{(i)},0)$ are all real. The eigenvalue ϵ of (3.4) represents the energy of the state (3.3) relative to the bottom of the conduction band.

In the following two sections we shall study the solutions (3.3) and their energy spectrum. Actually, however, the assumption of a sufficiently large orbit—which leads to (3.3)—is not always too well satisfied and we shall come back to this difficulty in Sec. 6.

4. GROUND STATE

We begin by examining the lowest lying solution of (3.4). We introduce

$$a_B=\hbar^2\kappa/m_2e^2, \quad \epsilon_0=m_2e^4/2\hbar^2\kappa^2, \quad (4.1)$$

as units of length and energy respectively, and write

$$\gamma\equiv m_2/m_1(<1). \quad (4.2)$$

This leads to the equation

$$\left[-\left(\gamma\frac{\partial^2}{\partial z^2}+\frac{\partial^2}{\partial x^2}+\frac{\partial^2}{\partial y^2}\right)-\frac{2}{r}-\epsilon\right]F(\mathbf{r})=0, \quad (4.3)$$

where we have dropped the subscripts and superscripts i. For $\gamma<1$ this equation does not completely separate and no exact solutions have been found. It is therefore of interest to consider two limiting cases:

[6] J. M. Luttinger and W. Kohn, Phys. Rev. **97**, 869 (1955).

(i) $m_1=m_2$ (or $\gamma=1$)

This is the hydrogenic case, leading to the following normalized solution:

$$F(r)=\pi^{-\frac{1}{2}}e^{-r}, \quad (4.4)$$

with an energy

$$\epsilon=-1. \quad (4.5)$$

(ii) $m_1\gg m_2$ (or $\gamma\ll 1$)

This we call the adiabatic limit for the following reason. Equation (4.3) may be regarded as the Schrödinger equation describing three one-dimensional particles of masses $1/\gamma(\gg 1)$, 1, and 1, respectively, interacting through the potential $-2/(x^2+y^2+z^2)^{\frac{1}{2}}$. Since one of these masses is much larger than the other two, we follow the well known adiabatic procedure of first solving the equation

$$\left[-\left(\frac{\partial^2}{\partial x^2}+\frac{\partial^2}{\partial y^2}\right)-\frac{2}{(x^2+y^2+z^2)^{\frac{1}{2}}}-\lambda(z)\right]\Phi(x,y;z)=0, \quad (4.6)$$

where z is treated as parameter (*cf.* electronic motion for fixed nuclear position in molecular problems), and then

$$[-\gamma d^2/dz^2+\lambda(z)-\epsilon]u(z)=0 \quad (4.7)$$

(*cf.* nuclear motion in molecular problems). Let us now introduce

$$\rho=(x^2+y^2)^{\frac{1}{2}}, \quad \varphi=\tan^{-1}(y/x). \quad (4.8)$$

Then (4.6) becomes

$$\left[-\frac{1}{\rho}\frac{\partial}{\partial\rho}\rho\frac{\partial}{\partial\rho}-\frac{1}{\rho^2}\frac{\partial^2}{\partial\varphi^2}-\frac{2}{(\rho^2+z^2)^{\frac{1}{2}}}-\lambda(z)\right]\Phi(\rho,\varphi;z)=0. \quad (4.9)$$

The ground state is of course independent of φ.

In the extreme adiabatic limit ($\gamma\ll 1$), the lowest eigenvalue of (4.9) is

$$\lim_{\gamma\to 0}\epsilon=\lambda(0), \quad (4.10)$$

where $\lambda(0)$ is the lowest eigenvalue of Eq. (4.9) with $z=0$. The corresponding solution is

$$\Phi=e^{-2\rho}; \quad \lambda(0)=-4. \quad (4.11)$$

Thus we see that if m_2 is kept fixed while m_1 increases from m_2 to ∞, the ionization energy changes from $-\epsilon_0$ to $-4\epsilon_0$.

It is also of interest to calculate $u(z)$ in the extreme adiabatic limit. For this purpose we require $\lambda(z)$, Eq. (3.13), for small z. A simple perturbation calculation gives

$$\lambda(z)=-4+32|z|+\cdots. \quad (4.12)$$

Substituting into (4.7) leads to

$$\left[-\frac{d^2}{dz^2}+\frac{32}{\gamma}|z|-\left(\frac{4+\epsilon}{\gamma}\right)\right]u(z)=0. \quad (4.13)$$

By changing the variable to

$$\xi \equiv z(32/\gamma)^{\frac{1}{3}}, \quad u(z)=v(\xi), \tag{4.14}$$

Eq. (4.13) becomes

$$[-d^2/d\xi^2+|\xi|-\eta]v(\xi)=0, \tag{4.15}$$

where

$$\eta=\frac{1}{(32)^{\frac{1}{3}}\gamma^{\frac{1}{3}}}(4+\epsilon). \tag{4.16}$$

Equation (4.10) can be solved in terms of Bessel functions. The lowest solution is symmetric in ξ and is given by

$$\eta=1.02,$$

$$v(\xi)=C(\eta-\xi)^{\frac{1}{2}}J_{-1/3}[\tfrac{2}{3}(\eta-\xi)^{\frac{3}{2}}]+J_{1/3}[\tfrac{2}{3}(\eta-\xi)^{\frac{3}{2}}], \quad 0\leq\xi\leq\eta, \tag{4.17}$$

$$v(\xi)=C(\sqrt{3}/\pi)(\xi-\eta)^{1/2}K_{1/3}[\tfrac{2}{3}(\xi-\eta)^{\frac{3}{2}}], \quad \eta\leq\xi\leq\infty, \tag{4.18}$$

where

$$C^2\approx 5.3, \tag{4.19}$$

when v is normalized such that

$$\int_{-\infty}^{\infty}[v(\xi)]^2 d\xi=1. \tag{4.20}$$

From (4.16) and (4.17) we obtain the following refinement of (4.11):

$$\gamma\to 0: \epsilon=-4+10.3\gamma^{1/3}, \tag{4.21}$$

$$F=[(8/\pi)^{1/2}(32)^{1/6}\gamma^{-1/6}]e^{-2\rho}v[(32/\gamma)^{\frac{1}{3}}z]. \tag{4.22}$$

The qualitative aspect of this function is of interest: As $\gamma\to 0$ (i.e., $m_1\to\infty$) the dependence on y and z tends to a constant function, $e^{-2\rho}$, which extends over dimensions of the order of a_B, the Bohr radius associated with m_2. On the other hand the extent of the wavefunction in the x-direction is of the order of $(m_2/m_1)^{1/3}a_B$, i.e., the function becomes pancake-like as $m_1/m_2\to\infty$. At the origin we have from (4.22), (4.17), and (4.19):

$$\gamma\to 0: F(0)\to A\gamma^{-1/6}, \tag{4.23}$$

$$A\cong 1.98. \tag{4.24}$$

Variational Method

Neither the hydrogenic nor the adiabatic case are of much direct practical value for the actual case $m_2/m_1=0.19$, which lies in between. However a simple variational function, namely,

$$F^{(v)}=(\pi a^2 b)^{-\frac{1}{2}}\exp[-(\rho^2/a^2+z^2/b^2)^{\frac{1}{2}}],^{13} \tag{4.25}$$

represents, with a suitable choice of a and b, a very good approximation to the actual situation for all $\gamma\leq 1$. [We use again (4.3) and (4.2) as units of length and energy.] Its accuracy can be nicely tested in both limiting cases. $F^{(v)}$ is evidently exact for $\gamma=1$. For $\gamma\to 0$, one finds, by minimizing the energy,

$$a\to 4/3\pi=0.424, \quad b\to\tfrac{1}{3}(4/\pi)^{2/3}\gamma^{1/3},$$
$$\epsilon\to-\tfrac{2}{3}(3\pi/4)^2=-3.701, \tag{4.26}$$
$$F^{(v)}(0)\to 2.12\gamma^{-1/6}.$$

The agreement with the true limiting function (4.23) and (4.24) and energy (4.11) is remarkably good. Figure 1 shows a plot of the energy as a function of $\gamma=m_2/m_1$; as calculated with the variational function (4.25). The error is only 7.5 percent at $\gamma=0$ and no doubt smaller for all intermediate γ. For Si, with $\gamma=0.19$ we find

$$\epsilon=-0.029 \text{ ev}. \tag{4.27}$$

Degeneracy

We remarked in Sec. 3 that in the effective-mass approximation, the Schrödinger equation has six equivalent and evidently degenerate solutions of the form (3.3). These functions must form a basis for a representation of the symmetry group of our system, *viz.*, the tetrahedral group T_d[14] about the donor atom. The six functions (3.3) behave under operation of T_d like $x, -x; y, -y; z, -z$ respectively. T_d has five classes and we list in Table II the characters of the present representation, $\{1s\}$, as well as of the 5 irreducible representations of T_d:

TABLE II. Characters of tetrahedral point-group representations.

Representation \ Group element	E	$8C_3$	$3C_2$	$6\sigma_d$	$6S_4$
A_1	1	1	1	1	1
A_2	1	1	1	−1	−1
E	2	−1	2	0	0
T_1	3	0	−1	1	−1
T_2	3	0	−1	−1	1
$1s$	6	0	2	2	0

Comparison with the characters of the irreducible representations shows that $\{1s\}$ decomposes into

$$\{1s\}=A_1+E+T_1, \tag{4.28}$$

which are one-, two-, and three-dimensional respectively. The degeneracy of the six functions (3.3) obtains of course only in our effective mass approximation. In reality this degeneracy will be partially lifted according to (4.28) and one singly-, one doubly-, and one triply-degenerate level will be produced. If we number the minima in the (1,0,0), (−1,0,0), (0,1,0), (0,−1,0), (0,0,1), (0,0,−1) directions by 1, 2, ⋯, 6, respectively, the correct linear combinations are given by

$$\Psi_i=\sum_{j=1}^{6}\alpha_i^{(j)}\psi^{(j)}, \quad i=1, 2, \cdots, 6, \tag{4.29}$$

[13] This function was independently introduced by M. Lampert, and by G. Mitchell and C. Kittel (to be published).

[14] See, e.g., Eyring, Walter, and Kimball, *Quantum Chemistry* (Jonn Wiley and Sons, Inc., New York, 1944), p. 388.

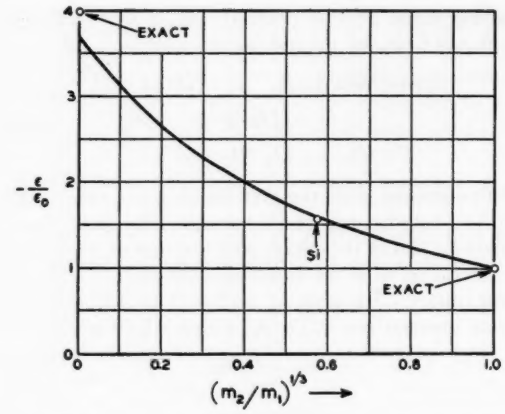

FIG. 1. Energy of ground state as function of mass ratio, $\gamma=m_2/m_1$, calculated with the trial function (4.25); $\epsilon_0=m_2e^4/2\hbar^2\kappa^2$.

where

$$\left.\begin{aligned}\alpha_1^{(j)}&=(1/\sqrt{6})(1,1,1,1,1,1), \quad (A_1)\\ \alpha_2^{(j)}&=\tfrac{1}{2}(1,1,-1,-1,0,0),\\ \alpha_3^{(j)}&=\tfrac{1}{2}(1,1,0,0,-1,-1),\end{aligned}\right\}(E)$$

$$\left.\begin{aligned}\alpha_4^{(j)}&=(1/\sqrt{2})(1,-1,0,0,0,0),\\ \alpha_5^{(j)}&=(1/\sqrt{2})(0,0,1,-1,0,0),\\ \alpha_6^{(j)}&=(1/\sqrt{2})(0,0,0,0,1,-1).\end{aligned}\right\}(T_1) \qquad (4.30)$$

Since all $\psi^{(j)}(0)$ are equal (see Sec. 3), we notice that only the nondegenerate function Ψ_1 has a finite value at the donor nucleus. It therefore will have a much larger hyperfine structure than the other states. The experiments of Fletcher *et al.*,[2] who have measured the hyperfine splitting of electron spin resonances in donor-doped Si at liquid helium temperatures, show that in fact Ψ_1 must be the ground state. Other considerations which will be discussed in Sec. 6 support the same conclusion.

5. EXCITED STATES

We now wish to obtain some orientation concerning the excited solutions of Eq. (4.3). This equation is invariant under rotations about the z axis and under inversion through the origin. Hence the solutions of (4.3) may be labelled by an integral magnetic quantum number m $[F(\mathbf{r})\sim e^{im\varphi}]$ and a parity $P=\pm1$.

It is of interest to trace, qualitatively, the spectrum of (3.4) as we pass from the hydrogenic case to the adiabatic limit.

(a) Hydrogenic Limit

For $\gamma=1$, the spectrum is given:

$$\epsilon=-1/n^2, \quad n=1,2,\cdots, \qquad (5.1)$$

where n is the principal quantum number. The states of even and odd l have $P=\pm1$, respectively.

The case where γ is just less than one, $\gamma=1-\delta$, must be treated by degenerate perturbation theory, the perturbation being $\delta\partial^2/\partial z^2$ [see Eq. (4.3)]. This mixes states of given n and m and all l of a given parity, e.g., the states $n=2$, $m=0$, $l=0$ and 2, and the accidental degeneracy due to different l and m will be lifted. (The double degeneracy corresponding to $\pm m$ remains of course.)

(b) Adiabatic Limit

Proceeding as in the last section, we first solve (4.9), obtaining, for $z=0$,

$$\Phi_{m,t}(\rho,\varphi)=\rho^{|m|}L_{|2m|+t}^{|2m|}\left(\frac{4}{|2m|+2t+1}\rho\right)e^{im\varphi},$$
$$\lambda_{m,t}(0)=-4/(|2m|+2t+1)^2, \qquad (5.2)$$
$$m=0,\pm1,\pm2,\cdots, \quad t=0,1,2,\cdots,$$

where $L_\alpha^\beta(x)$ denotes an associated Laguerre polynomial.

In principle, $\lambda(z)$ for $z\neq0$ can be similarly found and used to solve (4.7). Since $\lambda(z)$ is a symmetric function of z the solutions of (4.7) will be either even or odd. They may be labeled by a quantum number q representing the number of nodes. Thus the total wave function becomes, in the adiabatic limit,

$$F_{m,t;q}(\mathbf{r})=\Phi_{m,t}(\rho,\varphi)u_{m,t;q}(z), \qquad (5.3)$$

and

$$\epsilon_{m,t;q}=\lambda_{m,t}(0)+\mu_{m,t;q}, \qquad (5.4)$$

where $\mu_{m,t;q}$ is defined by the above equation. Evidently

$$\lim_{\gamma\to0}\mu_{m,t;q}=0. \qquad (5.5)$$

The parity of $F_{m,t;q}$ is given by

$$P=(-1)^{m+q}. \qquad (5.6)$$

(c) Connection Between Hydrogenic and Adiabatic Limit

We now raise the following question: What happens to the hydrogenic level scheme as γ decreases from 1 to 0. This change to γ may be considered as the gradual appearance of a perturbation, $\partial^2/\partial z^2$. Since this perturbation commutes with rotations about the z-axis and inversion, m and P are conserved. However, all states with the same m and P are mixed. In Table III we list, for $\gamma=1$, the states corresponding to given m and P in order of increasing energy. We shall use the symbol R_i to denote a set of states with given m and P. The R_i

TABLE III. Hydrogenic levels grouped according to values of m and P.

R_1 $m=0, P=1$	R_2 $m=0, P=-1$	R_3 $m=1, P=-1$	R_4 $m=1, P=1$
1s	2p	2p	3d
2s	3p	3p	4d
3s, 3d	4p, 4f	4p, 4f	5d, 5g
4s, 4d	5p, 5f	5p, 5f	6d, 6g

belong to different representations of the symmetry group of the Hamiltonian in (4.3). As the perturbation $\partial^2/\partial z^2$ comes into play, two levels belonging to different R_i may cross freely but those in the same R_i "interact" and hence cannot cross.

Let us begin by considering R_1. For $\gamma=1-\delta$ (δ being a small positive number), its levels are all discreet and in a definite order

$$R_1: \quad 1s,\ 2s,\ (3s,d)^{(1)},\ (3s,d)^{(2)},\ \cdots, \qquad (5.7)$$

where the superscripts (1) and (2) indicate certain linear combinations. These levels represent the lowest, second lowest, etc., level corresponding to $m=0$, $P=1$. As γ approaches zero, they remain the lowest, second etc. level corresponding to $m=0$, $P=1$, as a result of the noncrossing principle; i.e., they go over into the adiabatic levels, $m=0$, $l=0$ and $q=0, 2, 4, \cdots$. [In the adiabatic limit these all lie lower than the levels $m=0$, $l>0$, $q=0, 2, 4, \cdots$, which belong to the same representation, see (5.2) and (5.5)]. Thus we have the following correspondences:

$$\begin{array}{lll} & m\ \ l\ \ q \\ R_1: \ 1s,\ m=0 & \rightarrow 0\ \ 0\ \ 0 \\ \quad 2s,\ m=0 & \rightarrow 0\ \ 0\ \ 2 \\ \quad (3s,d)^{(1)},\ m=0 & \rightarrow 0\ \ 0\ \ 4 \\ \quad (3s,d)^{(2)},\ m=0 & \rightarrow 0\ \ 0\ \ 6. \end{array} \qquad (5.8)$$

Similarly for the other groups:

$$\begin{array}{lll} & m\ \ l\ \ q \\ R_2: \ 2p,\ m=0 & \rightarrow 0\ \ 0\ \ 1 \\ \quad 3p,\ m=0 & \rightarrow 0\ \ 0\ \ 3 \\ R_3: \ 2p,\ m=1 & \rightarrow 1\ \ 0\ \ 0 \\ \quad 3p,\ m=1 & \rightarrow 1\ \ 0\ \ 2 \\ R_4: \ 3d,\ m=1 & \rightarrow 1\ \ 0\ \ 1 \\ \quad 4d,\ m=1 & \rightarrow 1\ \ 0\ \ 3. \end{array} \qquad (5.9)$$

We see then that all hydrogenic levels go over, in the adiabatic limit, into adiabatic levels with the same m, and $l=0$.[15] Therefore, as γ diminishes from 1 to 0, the energy of a hydrogenic level n, l, m changes from $\epsilon=-1/n^2$ to $\epsilon=-4/(2|m|+1)^2$ [see Eq. (5.2)]. Figure 2 illustrates the correspondence for the first few hydrogenic levels.

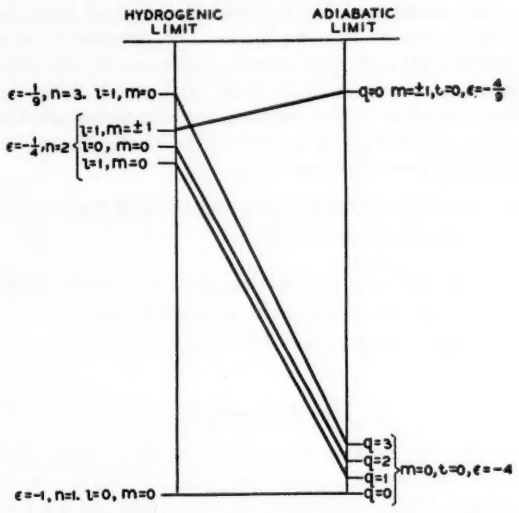

FIG. 2. Correspondence between energy levels in the hydrogenic limit, $m_2/m_1=1$, and the adiabatic limit, $m_2/m_1=0$ (schematic). ϵ is in units of $\epsilon_0=m_2e^4/2\hbar^2\kappa^2$. Note that ϵ is drawn on different scales in the two limits.

(d) Variational Calculations

To determine the energies of the first few excited states of donors in Si, we have made variational calculations which we have tested in the limits $\gamma=1$ and 0. This comparison enabled us to make slight corrections and to estimate the error of our calculation.

TABLE IV. Energies in the effective mass approximations.[a]

State	Trial function	γ	E_{var}	E_{ex}	E_I
$1s$ (0,0,0)	$C\exp[-(\rho^2/a^2+z^2/b^2)^{\frac{1}{2}}]$	0	−3.70	−4.00	
		0.19	−1.60		−1.63±0.03
		1.00	−1.00	−1.00	
$2p$, $m=0$ (0,0,1)	$Cz\exp[-(\rho^2/a^2+z^2/b^2)^{\frac{1}{2}}]$	0	−3.47	−4.00	
		0.19	−0.597		−0.63±0.03
		1.00	−0.250	−0.250	
$2s$, $m=0$ (0,0,2)	$(C_1+C_2\rho^2+C_3z^2)\exp[-(\rho^2/a^2+z^2/b^2)^{\frac{1}{2}}]$	0	−3.34	−4.00	
		0.19	−0.456		−0.49±0.03
		1.00	−0.245	−0.250	
$3p$, $m=0$ (0,0,3)	$(C_1+C_2\rho^2+C_3z^2)z\exp[-(\rho^2/a^2+z^2/b^2)^{\frac{1}{2}}]$	0	−3.22	−4.00	
		0.19	−0.288		−0.32±0.03
		1.00	−0.111	−0.111	
$2p$, $m=1$ (1,0,0)	$Cx\exp[-(\rho^2/a^2+z^2/b^2)^{\frac{1}{2}}]$	0	−0.434	−0.444	
		0.19	−0.324		−0.33±0.005
		1.00	−0.250	−0.250	

[a] All energies are expressed in units of ϵ_0, Eq. (4.1), which for Si has the value 0.0179 ev.

[15] The adiabatic levels with $l>0$ have no counterpart in the hydrogenic spectrum.

The results are listed in Table IV, together with the exact results in the two limits. The description of a state by, say, $2p$, $m=1$ means that as $\gamma\to 1$, the state becomes a hydrogenic $2p$ state, with $m=1$ along the direction of $\mathbf{k}^{(i)}$. The numbers in parentheses are the quantum numbers m, l, q in the adiabatic limit. The following notation is used:

$$\begin{aligned} &E_{\text{var}} = \text{energy calculated variationally with the indicated trial function;}\\ &E_{\text{ex}} = \text{exact energy;}\\ &E_f = \text{final energy, i.e., variational energy, corrected by comparison with exact energies, including an error estimate;}\\ &\gamma = m_2/m_1. \end{aligned} \tag{5.10}$$

(e) Degeneracy

Considerations similar to those of Sec. 4 show that each effective mass wave function $F^{(i)}(\mathbf{r})\psi(\mathbf{k}^{(i)},\mathbf{r})$ is one of a 12-fold degenerate set for $m\neq 0$, and a 6-fold degenerate set for $m=0$. It is of interest to find the linear combinations of these functions which transform according to the irreducible representations of the tetrahedral group. For this purpose we given in Table V the characters of the tetrahedral point group for the representations corresponding to different m values.

Comparison with Table II gives the following decomposition:

$$\begin{aligned} &|m|=0: && A_1+E+T_1,\\ &|m| \text{ even } (\neq 0): && A_1+A_2+2E+T_1+T_2,\\ &|m| \text{ odd}: && 2T_1+2T_2. \end{aligned} \tag{5.11}$$

Thus deviations from the effective mass model will split each degenerate set into groups according to the following scheme:

$$\begin{aligned} &m=0: && 6=1+2+3,\\ &m \text{ even } (\neq 0): && 12=1+1+2+2+3+3,\\ &m \text{ odd}: && 12=3+3+3+3. \end{aligned} \tag{5.12}$$

6. DEVIATIONS FROM THE EFFECTIVE-MASS FORMALISM

The shortcomings of the effective-mass formalism are best seen from the following comparisons with experiment. The effective-mass theory predicts an ionization energy of 0.029 ev for all donors, whereas the experimental values for P, As, and Sb range from 0.039 to 0.049 ev (see Table I). The discrepancies undoubtedly arise largely due to the breakdown of our assumptions in the immediate vicinity of the donor atom, for the following two reasons: (1) The perturbing potential $U(\mathbf{r})$ changes from $-e^2/\kappa r$ to $-\Delta Ze^2/\kappa r$ near $r=0$, where ΔZ is the excess charge of the donor nucleus over that of Si. (2) The effective-mass formalism does not apply in this region since the fractional change of $U(\mathbf{r})$ in a typical lattice distance, a, is large.

We do not have a good quantitative theory to take these effects into account. But it is clear that they will be largest for the states of greatest amplitude near the donor nucleus. In the remainder of this section we shall discuss the effect of deviations from the effective mass formalism on the most important low-lying levels.

TABLE V. Characters of tetrahedral point group representations.

$\lvert m\rvert$ \ Group element	E	$8C_3$	$3C_2$	$6\sigma_d$	$6S_4$
0	6	0	2	2	0
even, $\neq 0$	12	0	4	0	0
odd	12	0	−4	0	0

"1s"-states

We begin by considering the six states (4.29), (4.30), whose modulating functions $F^{(i)}(\mathbf{r})$ becomes "1s"-like when $m_2/m_1\to 1$. The lowest of these is almost certainly Ψ_1 corresponding to the identity representation. Since all $\Psi^{(j)}(0)$ are equal, the 6 terms in the sum (4.29) are all in phase at $r=0$ so that $\Psi_1(0)$ would be expected to be quite large. This is borne out by the observed large hyperfine splitting of the lowest donor state.[2] It is therefore not surprising that the energy of this state, as calculated by the effective mass approximation is substantially in error. As was noted previously, the observed ionization energies for group V donors are from 35 to 70 percent greater than the effective mass energy. We have discussed this state in some detail elsewhere.[16] The other five "1s"-states evidently vanish at $r=0$ [see Eq. (4.30)].

For orientation let us study these six 1s-states in the tight binding approximation. In this case, in the vicinity of the donor nucleus,

$$\psi^{(j)}=\alpha R_s(r)+\beta\frac{\mathbf{k}^{(j)}\cdot\mathbf{r}}{k^{(j)}r}R_p(r), \tag{6.1}$$

where $R_s(r)$ and $R_p(r)$ are the normalized radial atomic $3s$ and $3p$ functions, and α and β are numerical constants of comparable order of magnitude. The p-part of this function contains the factor $\mathbf{k}^{(j)}\cdot\mathbf{r}$, because it must be invariant under rotations which leave $\mathbf{k}^{(j)}$ invariant.

With the help of (6.1), we can make a plausible guess as to the positions of the 1s-levels belonging to the representations A_1, E, and T_1. By (4.29) and (4.30), we see that in the vicinity of the donor nucleus (and extending over about one atomic volume), we have:

$$A_1:\quad \Psi_1(\mathbf{r})=\sqrt{6}\alpha R_s(r), \tag{6.2}$$

$$E:\begin{cases}\Psi_2(\mathbf{r})=0,\\ \Psi_3(\mathbf{r})=0,\end{cases} \tag{6.3}$$

$$T_1:\begin{cases}\Psi_4(\mathbf{r})=\sqrt{2}\beta(x/r)R_p(r),\\ \Psi_5(\mathbf{r})=\sqrt{2}\beta(y/r)R_p(r),\\ \Psi_6(\mathbf{r})=\sqrt{2}\beta(z/r)R_p(r).\end{cases} \tag{6.4}$$

[16] W. Kohn and J. M. Luttinger, Phys. Rev. 97, 883 (1955).

Therefore we would expect Ψ_1 to be lowest because the electron spends a relatively larger time near the nucleus, where the attraction is greater. Similarly we would expect the states belonging to T_1 to have somewhat lower energies than the effective-mass energy, but because of their p-nature to lie substantially above Ψ_1. Finally the energy of the two states belonging to E should be rather accurately described by the effective-mass energy.

"2s"-states

Among the excited levels, we expect the greatest deviation from the effective-mass energy in the case of that $2s$-state which belongs to the identical representation A_1 of T_d (see Table II). Since the energy difference ΔE between this state and the corresponding $1s$-state is small ($\sim$0.03 ev), their wave functions will be practically identical in the vicinity of the donor atom.[17] It is therefore possible to estimate the shift of this level relative to its effective mass value from the experimentally observed shift of the corresponding $1s$-level.

To make the analysis manageable let us replace the two different masses m_1 and m_2 by a single mean mass m^*. A reasonable choice is to take

$$m^*=0.31\, m, \tag{6.5}$$

which in the effective-mass approximation gives the same ground-state energy as the measured masses. Now for $r \geq a$, where a is a typical lattice distance, the wave functions $\Psi_{n,s}$ for both the $1s$- and $2s$-states, belonging to the identity representation, will be given by the effective-mass expressions

$$\Psi_{ns}=F_{ns}(r)\sum_{i=1}^{6}\psi(\mathbf{k}^{(i)},\mathbf{r}); \quad n=1, 2, \quad r\geq a. \tag{6.6}$$

where because of the single mass m^* all $F^{(i)}(\mathbf{r})$ are identical for $i=1, \cdots 6$ [see Eqs. (3.3), (3.4), and (4.29)]. The functions $F_{ns}(\mathbf{r})$ satisfy equations of the hydrogenic form

$$\left(-\frac{\hbar^2}{2m^*}\nabla^2-\frac{e^2}{\kappa r}-\epsilon_{ns}\right)F_{ns}(\mathbf{r})=0, \tag{6.7}$$

where ϵ_{ns} is the actual energy of the ns-state. Since the ϵ_{ns} do not exactly coincide with the hydrogenic levels, $-m^*e^4/2\hbar^2\kappa^2n^2$, the F_{ns} which vanish at $r=\infty$ would become infinite if continued to $r=0$. However, for $r<a$ the effective-mass function (6.6) no longer is reliable. On the other hand, in view of the negligible value of $\Delta\epsilon(\equiv\epsilon_{2s}-\epsilon_{1s})$ we have in this region

$$\Psi_{1s}=\Psi_{2s}, \quad r\leq a. \tag{6.8}$$

[17] It can be easily seen that the relevant criterion is $\Delta E \ll(\hbar^2/2m)a_s^2$, where a_s is the radius of the Wigner-Seitz sphere. In the present case $\Delta E\approx 0.02(\hbar^2/2m)a_s^2$.

TABLE VI. Correction of $2s$-energy.

Element	$1s$-energy[a] Eff. mass	$1s$-energy[a] Observed	δ	$\frac{1}{(1-\delta/2)^2}$	$2s$-energy[a] Eff. mass	$2s$-energy[a] Corrected
P	−1.0	−1.52	0.18	1.21	−0.30	−0.36
As	−1.0	−1.69	0.23	1.27	−0.30	−0.38
Sb	−1.0	−1.35	0.14	1.16	−0.30	−0.35
Li	−1.0	−1.14	0.07	1.07	−0.30	−0.32

[a] All energies are in units of $\bar{\epsilon}=-0.029$ ev.

By combining (6.6) and (6.8), we find

$$\left[\frac{\partial F_{2s}/\partial r}{F_{2s}}\right]_{r=a}=\left[\frac{\partial F_{1s}/\partial r}{F_{1s}}\right]_{r=a}. \tag{6.9}$$

Since a is much smaller than the "Bohr" radius a^* of this problem ($a^*=\kappa\hbar^2/m^*e^2\approx 20$A), the situation is entirely analogous to that encountered in the optical spectrum of the alkalies. One finds therefore in the same way that

$$\epsilon_{ns}=-\bar{\epsilon}/(n-\delta)^2, \tag{6.8}$$

where $\bar{\epsilon}$ is the "Rydberg" ($=m^*e^4/2\hbar^2\kappa^2$) and δ is the quantum defect which is independent of n. (6.8) may also be written as

$$\epsilon_{ns}=-\frac{\bar{\epsilon}}{n^2}\frac{1}{(1-\delta/n)^2}, \tag{6.7}$$

the last factor being the correction factor due to departures from a simple Coulomb law in the interior region. Thus δ may be determined from a comparison of $\bar{\epsilon}$ ($=-0.029$ ev) and the observed ground-state energy, and the correction factor for the $2s$-state can then be calculated from (6.7), and applied to the effective-mass value of the $2s$-energy, -0.0088 ev (see Table IV). The results are listed in Table VI.

We see that in all cases the correction of the $2s$-level is fairly small.

It can be shown that the replacement of m_1 and m_2 by m^* does not materially affect the correction we have just calculated.

The remaining five $2s$-states are expected to be much less shifted (see the discussion of the $1s$-levels), presumably slightly downward.

"p"-states

These states have the property that the modulating functions $F^{(i)}(\mathbf{r})$ vanish at the donor nucleus. Since the relevant length in these functions is of the order a_B (which is about 20 A), their amplitude will be completely negligible in that region near the donor nucleus where the effective mass theory breaks down. Therefore we would expect the effective mass theory to be excellent for "p"-states.†

† See note added in proof at the end of the paper.

TABLE VII. Level scheme of donor states in silicon.

State	Representations of T_d [a]	Number of degenerate [b] states	Eff. mass theory	(Energy in ev) $\times 10^2$ [c] P	As	Sb
$1s, m=0$	A_1	1	-2.9 ± 0.1	-4.4 [d]	-4.9 [d]	-3.9 [d]
$1s, m=0$	$E+T_1$	5	-2.9 ± 0.1	-3.2 ± 0.3	-3.3 ± 0.4	-3.1 ± 0.2
$2p, m=0$	A_1+E+T_1	6	-1.13 ± 0.06	-1.13 ± 0.06	-1.13 ± 0.06	-1.13 ± 0.06
$2s, m=0$	A_1	1	-0.88 ± 0.06	-1.06 ± 0.10	-1.11 ± 0.10	-0.94 ± 0.08
$2s, m=0$	$E+T_1$	5	-0.88 ± 0.06	-0.93 ± 0.11	-0.95 ± 0.13	-0.90 ± 0.08
$2p, m=+1$	$2T_1+2T_2$	12	-0.59 ± 0.01	-0.59 ± 0.01	-0.59 ± 0.01	-0.59 ± 0.01
$3p, m=0$	A_1+E+T_1	6	-0.57 ± 0.06	-0.57 ± 0.06	-0.57 ± 0.06	-0.57 ± 0.06

[a] See reference 14.
[b] These states are only approximately degenerate, consisting in general of several strictly degenerate sets, as appears from the second column. Spin degeneracy is not included.
[c] The indicated errors represent estimated uncertainties within the framework of the present model.
[d] Experimental.

7. SUMMARY AND DISCUSSION

On the basis of the previous sections, our picture of the donor levels in Si is represented in Table VII and Fig. 3, which latter shows graphically the level scheme for one of the donors. In summary we may recall that this picture is based on the following model:

(1) The conduction band of Si has six minima in the (1,0,0) and equivalent directions. At each minimum the band is nondegenerate. The minima are not too close to $k=0$.

(2) The effective masses are $m_1=0.98\ m$, $m_2=0.19\ m$ (twice).

(3) Except in the immediate vicinity of the donor atom, the donor states are described by functions of the form

$$\Psi=\sum_{j=1}^{6}\alpha^{(j)}F^{(j)}(\mathbf{r})\psi(\mathbf{k}^{(j)},\mathbf{r}), \tag{7.1}$$

where the $F^{(j)}(\mathbf{r})$ are modulating functions satisfying the effective-mass equations (3.4), the $\psi(\mathbf{k}^{(j)},\mathbf{r})$ are the Bloch functions at the minima $\mathbf{k}^{(j)}$ of the conduction band, and the $\alpha^{(j)}$ are constants obeying the requirements of tetrahedral symmetry.

(4) Shifts of the energy levels relative to their values in the effective-mass theory are attributed to failure of the effective-mass formalism in the vicinity of the donor atom. From the known shift of the ground state, the shifts of other levels are estimated.

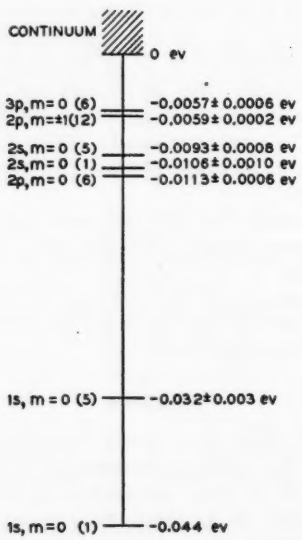

FIG. 3. Spectrum of bound states around a phosphorus-donor. Numbers in parentheses indicate number of approximately degenerate states; spin degeneracy is not included. See Table VII.

We should like to mention explicitly that the effects of lattice vibrations on the position and width of the levels has not been considered.

All the states can be excited thermally. However, only the p-states are expected to play a major role in the optical transitions from the ground state. Oscillator strengths for these transitions will be published shortly.

There exist as yet no experimental data with which our results can be quantitatively compared. It is hoped that when such data become available their agreement or disagreement with our results will throw some light on the nature of donor states.

This work was begun at the Bell Telephone Laboratories in the summer of 1954. It is a great pleasure to thank their staff for the hospitality they extended to us. We are grateful to Dr. R. C. Fletcher, Dr. C. Herring, and Dr. G. Wannier for many stimulating and helpful conversations.

Note added in proof.—Since this paper was submitted we have learned of experimental work by Burstein, Picus, and Henvis (to be published) who have observed optical transitions from the ground state to various excited states of donor electrons. These measurements are in excellent agreement with the theoretical positions of the excited "p"-states reported in the present paper. A discussion of the experimental results in the light of the theory is in press.

Electron Capture Probability of the Upper Copper Acceptor Level in Germanium

R. M. Baum and J. F. Battey
Electronics Division, Sylvania Electric Products, Ipswich, Massachusetts

(Received December 23, 1954)

The doping of a germanium sample is arranged so that the minority carrier lifetime is inversely proportional to the electron capture probability of the upper acceptor level introduced by copper atoms. It is found that the lifetime decreases exponentially with increasing temperature. A suggested interpretation is that only electrons of energy greater than 0.22 ev above the bottom of the conduction band can enter the second copper acceptor level.

It is generally believed that the recombination of minority carriers in the bulk of presently produced single crystal germanium proceeds by transitions to and from intermediate energy levels in the forbidden energy gap. The statistics of the process have been described by Hall[1] and by Shockley and Read.[2] For low levels of minority carrier injection in a nondegenerate semiconductor where the charge in the recombination traps is neglected and a steady state with respect to injection and recombination is achieved, the lifetime, τ, of the injected carriers is given by

$$\tau=(1/C_p)(n_0+n_1)/(n_0+p_0)+(1/C_n)(p_0+p_1)/(n_0+p_0). \quad (1)$$

C_p is the product of the trap density and the probability per unit time of an individual trap capturing a hole, averaged over the holes in the valence band. C_n is the product of the trap density and the probability of an individual trap capturing an electron, averaged over the electrons in the conduction band. n_0 and p_0 are the equilibrium electron and hole densities, and n_1 and p_1 are the values the equilibrium electron and hole densities would have if the Fermi level were located at the same position in energy as the recombination traps.

The bulk lifetime of most germanium samples thus far investigated increases exponentially with increasing temperature in the range where the sample is extrinsic. This is presumed to be due to the exponential variation of the carrier density in the dominant term in the numerator of (1), the denominator being virtually constant in the extrinsic range. An example of this behavior has been reported by Hall,[1] and some further illustrations of this behavior due to recombination levels of an undetermined origin are shown in Fig. 1. It is the purpose of this article to report that there is a method of preparing germanium samples so that the bulk lifetime decreases exponentially with increasing temperature. This is done by diffusing copper into an originally n-type semiconductor to such an extent that the upper acceptor levels introduced by the copper are approximately half populated. Details of sample preparation are described in a previous letter by the authors.[3]

It has been shown by Burton *et al.*[4] that the upper copper levels in germanium act as recombination levels for which at room temperature $10/C_p \simeq 1/C_n$ and the diffusing in of the copper served to reduce the room temperature bulk lifetime of the samples investigated here by several orders of magnitude. For such samples as this the charge in the traps cannot be neglected, and the deviations in electron and hole densities from the equilibrium values as well as the associated lifetimes are no longer equal. Under these circumstances the steady-state electron lifetime is given as[2]

$$\tau_n=\frac{(1/C_p)(n_0+n_1)+(1/C_n)[p_0+p_1+N_t(1+p_0/p_1)^{-1}]}{n_0+p_0+N_t(1+p_0/p_1)^{-1}(1+p_1/p_0)^{-1}}, \quad (2)$$

where N_t is the density of recombination centers. For the sample preparation described $(1/C_p)(n_0+n_1)$ is negligible compared to the remainder of the numerator around room temperature, and n_0 is negligible compared

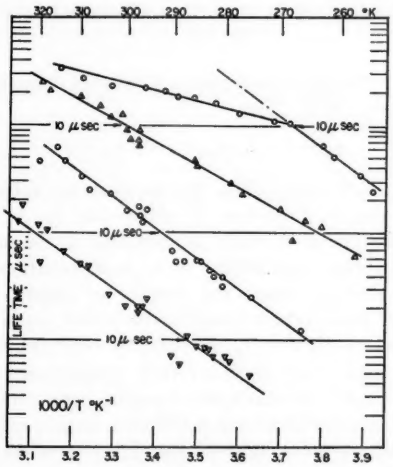

Fig. 1. Variation of bulk lifetime with temperature in n-type germanium due to recombination levels of undetermined origin. It is interesting to note that the sum of the activation energies derived from the two sections of the upper curve is approximately equal to the energy gap. This is to be anticipated if there is a transfer in dominance of the numerator of Eq. (1) from the term involving n_1, to that involving p_1, or vice versa.

[1] R. N. Hall, Phys. Rev. **87**, 387 (1952).
[2] W. Shockley and W. T. Read, Jr., Phys. Rev. **87**, 835 (1952).
[3] J. F. Battey and R. M. Baum, Phys. Rev. **94**, 1393 (1954).
[4] J. A. Burton *et al.*, J. Phys. Chem. **57**, 853 (1953).

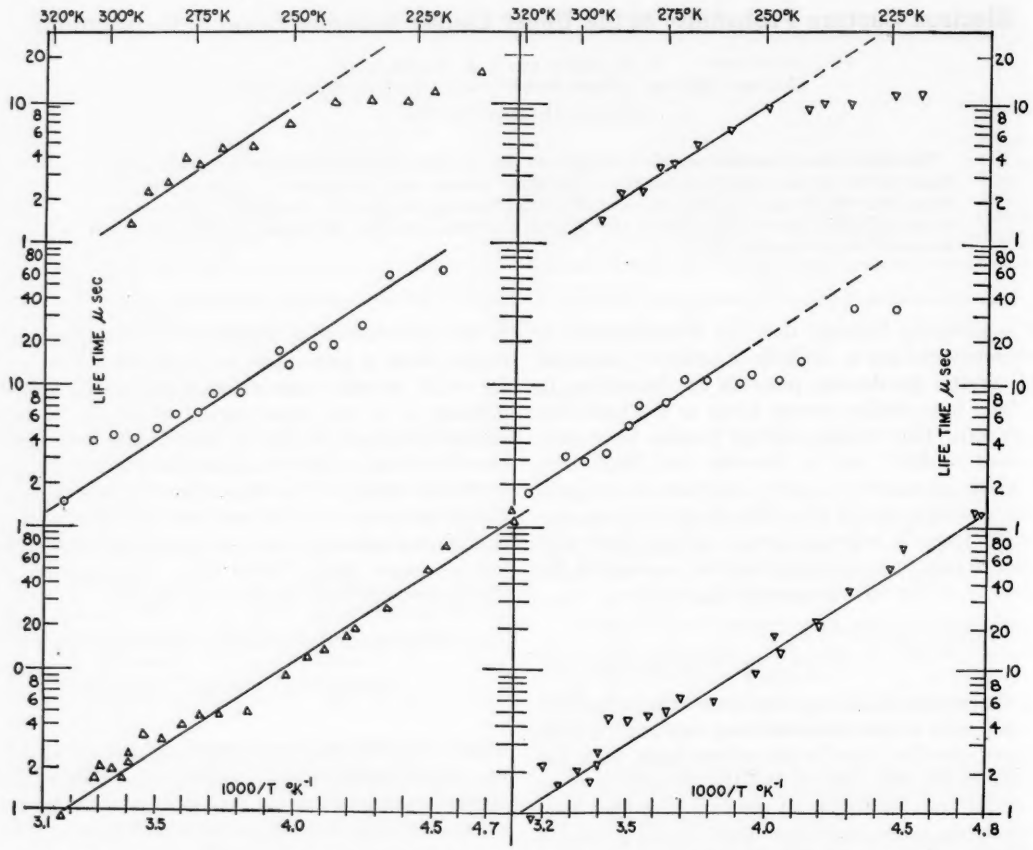

FIG. 2. Lifetime *versus* temperature in different parts of a high-resistivity copper-doped sample, wherein the lifetime is inversely proportional to the capture probability of the upper copper acceptor level for electrons.

to the other terms in the denominator for all temperatures below about 50°C. Then

$$\tau_n \simeq (1+p_1/p_0)/C_n = 1/C_n f_{pt}, \qquad (3)$$

where f_{pt} is the probability that a copper recombination level be empty. Equation (3) states that the minority carrier lifetime is inversely proportional to the product of the capture probability of a recombination level for an electron times the density of empty levels. Over the temperature range investigated, p_0 is small compared to N_t and f_{pt} is virtually constant for the samples used. Thus, τ_n is inversely proportional to C_n.

The lifetime measurements reported here were made at low injection levels by a diffusion length measurement using a point light source. They were corrected for surface recombination in a manner previously described by one of the authors.[5] As might be expected for etched samples and the low values of bulk lifetime encountered, the corrections were negligible except at low temperatures, where they were still small. The data are shown in Fig. 2 in a semilogarithmic plot, which seems to be the most significant way to display it. The data exhibited were taken on the previously described[3] sample for which carrier concentrations are calculated under the tacit assumption that the traps are not degenerate. It will be noticed that within the accuracy of the data, the runs on several parts of the sample are straight lines. It is presumed that the failure of the lifetime to increase as rapidly as exponentially with decreasing temperature in other parts of the sample is due to competition from other recombination processes which become of comparable importance at lower temperatures.

In calculating the lifetime from the measured diffusion length, the presumption is made that the minority carrier diffusion length varies as $T^{-0.6}$,[6] which is a weak dependence compared to that of the lifetime itself. It is felt that trapping by the upper copper levels has a small effect on the diffusion coefficient, inasmuch as the relative sizes of $1/C_p$ and $1/C_n$ at room temperature indicate that once an electron is captured in the

[5] S. Visvanathan and J. F. Battey, J. Appl. Phys. **25**, 99 (1954).

[6] M. B. Prince, Phys. Rev. **92**, 681 (1953).

recombination level, it has a much greater probability of going to the valence band (p_0C_p/N_t) than returning to the conduction band (n_1C_n/N_t). Nevertheless to check against any possible unforeseen variations with temperature in the diffusion coefficient, the lifetime was also measured by a conductivity modulation technique, with substantially the same results. The conductivity modulation decays due to recombination of both electrons and holes, which do not necessarily have the same steady-state lifetime if the charge in the traps cannot be neglected. However, if it is presumed that the holes in the traps rapidly come to equilibrium with the holes in the valence band, as seems to be the case for the upper copper level, then both electrons and holes subsequently decay with the lifetime of the electrons.

The apparent exponential increase of C_n with increasing temperature is regarded as somewhat surprising. It is the result that would be anticipated if only the electrons of energy greater than a certain critical energy above the bottom of the conduction band were allowed to enter the upper copper levels. This energy as obtained from the slopes of Fig. 2 is approximately 0.22 ev.

ACKNOWLEDGMENTS

The authors wish to give thanks to Robert Carye and George Servente for assistance with the experimental work.

PHYSICAL REVIEW VOLUME 98, NUMBER 4 MAY 15, 1955

Ferromagnetic Resonance in Ferroxdure

M. T. WEISS AND P. W. ANDERSON
Bell Telephone Laboratories, Holmdel, New Jersey
(Received January 28, 1955)

Ferromagnetic resonance experiments have been performed on Ferroxdure at various microwave frequencies from 9000 Mc/sec to 50 000 Mc/sec. With no externally applied field a natural resonance occurs near 50 000 Mc/sec. With magnetic field applied perpendicular to the hexagonal axis, a double resonance occurs for frequencies below 50 000 Mc/sec, while with a field applied along the hexagonal axis a single resonance occurs above 50 000 Mc/sec. A theory is developed to explain the above results.

FERROMAGNETIC resonance experiments have been performed on Ferroxdure at various microwave frequencies. Ferroxdure[1] is a ceramic permanent magnet material with high anisotropy having a hexagonal crystal structure and having essentially the composition $BaFe_{12}O_{19}$.

THEORY

The ferromagnetic resonance frequencies of a hexagonal crystal with high anisotropy along the hexagonal axis can be calculated as follows:

The anisotropy energy is given by $U=K\sin^2\theta$, where θ is the angle of the magnetization with respect to the hexagonal axis. Higher order terms in $\sin\theta$ as well as anisotropy within the basal plane can be neglected for Ferroxdure at room temperature. The torque due to the anisotropy is given by

$$T=-\frac{\partial U}{\partial\theta}=-\frac{\partial U}{\partial M_{xy}}\frac{\partial M_{xy}}{\partial\theta}=-\frac{2K}{M^2}M_{xy}M_z, \qquad (1)$$

or vectorially

$$\mathbf{T}=+(2K/M^2)\mathbf{M}\times\mathbf{M}_z=\mathbf{M}\times\mathbf{H}_A,$$

where $\mathbf{M}$ is the magnetization vector, $\mathbf{M}_z$ and $\mathbf{M}_{xy}$ are evident from Fig. 1, and $\mathbf{H}_A$ is an equivalent anisotropy field which would produce the same torque. Evidently,

$$\mathbf{H}_A=(2K/M^2)\mathbf{M}_z=A\mathbf{M}_z, \qquad (2)$$

so that the equivalent anisotropy field is along the hexagonal axis and is proportional to the magnetization along that axis.

In the standard equation of motion[2] for the magnetization $d\mathbf{M}/dt=\gamma\mathbf{M}\times\mathbf{H}$, one must take into account

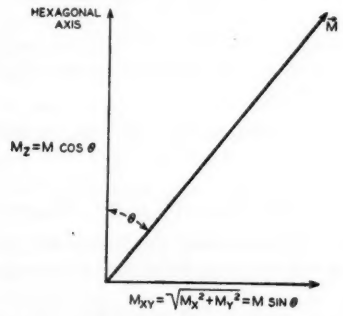

FIG. 1. Vectors used in calculating ferromagnetic resonance frequencies of Ferroxdure.

[1] Went, Rathenau, Gorter, and Van Oosterhaut, Philips Tech. Rev. 13, 194–208 (1952).

[2] C. Kittel, *Introduction to Solid State Physics* (John Wiley and Sons, Inc., New York, 1953), p. 155.

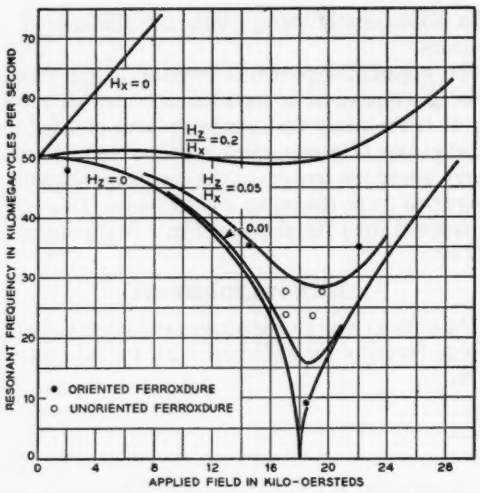

FIG. 2. Theoretical curves and experimental results of ferromagnetic resonance frequency *versus* applied field for Ferroxdure.

both the aforementioned equivalent anisotropy field as well as the externally applied field. Thus, for small variations of **M** about its equilibrium position, assumed to be in the xz plane, one obtains

$$\begin{aligned} j\omega\delta M_x &= \gamma[\delta M_y(H_z+AM_z)], \\ j\omega\delta M_y &= \gamma[-\delta M_x(H_z+AM_z)+\delta M_z(H_x-AM_x)], \\ j\omega\delta M_z &= -\gamma\delta M_y H_x, \end{aligned} \tag{3}$$

where δM_i indicates a small variation in M_i about its equilibrium value. It should be noted from the second of the above Eqs. (3), that although the anisotropy field is in the z direction, the equivalent field along the x axis is affected by the anisotropy for variations in M_z. Solving the secular determinant of the above equations one obtains the resonant frequencies given by

$$(\omega/\gamma)^2=H_x(H_x-AM_x)+(H_z+AM_z)^2. \tag{4}$$

The equilibrium values of M_x and M_z are determined from

$$(H_z+AM_z)/H_z=M_z/M_x. \tag{5}$$

For the special case where the applied magnetic field is perpendicular to the hexagonal axis so that $H_z=0$, Eq. (4) reduces to

$$(\omega/\gamma)^2=A^2M^2-H_{\rm app}^2 \quad \text{for} \quad H_{\rm app}<AM,$$

and

$$(\omega/\gamma)^2=H_{\rm app}[H_{\rm app}-AM] \quad \text{for} \quad H_{\rm app}>AM. \tag{6}$$

If the applied field is along the hexagonal axis so that $H_x=0$, then the resonant frequency is given by

$$(\omega/\gamma)=H_{\rm app}+AM. \tag{7}$$

If neither H_x nor H_z is equal to zero, one must combine Eqs. (4) and (5) in order to obtain the resonant frequencies as a function of applied field. In the previous discussion, demagnetizing factors due to sample shape or poles formed at domain walls have been neglected.[3]

Figure 2 shows the theoretical curves of resonant frequency *versus* applied field for the applied field along the hexagonal axis, perpendicular to the hexagonal axis, and for $H_z/H_x=0.01$, 0.05, and 0.2. These curves are drawn for a material whose maximum anisotropy field, AM, is equal to 18 000 oersteds. It is to be noted that with magnetic field applied perpendicular to the hexagonal axis a double resonance is predicted for frequencies below 50 000 Mc/sec, while no resonance is to be observed for fields along the hexagonal axis at frequencies below 50 000 Mc/sec. If the field is not applied exactly perpendicular to the hexagonal axis, the resonant frequencies are substantially affected at fields near 18 000 oersteds, as seen from the curves for $H_z/H_x=0.05$ and 0.01.

EXPERIMENTAL RESULTS

The above theory is directly applicable to single crystal material. Since single crystal Ferroxdure was not available to us, our experiments at 9200 Mc/sec and at 35 300 Mc/sec were performed with oriented polycrystalline Ferroxdure, having the hexagonal axis of the crystallites oriented along one direction. The results were in agreement with theory in that no resonances at these frequencies were observed with field applied along the hexagonal axis, double resonances were observed with field applied perpendicular to the hexagonal axis, while with zero applied field a resonance near 50 000 Mc/sec was observed. The results obtained with the oriented material, as well as those obtained at 23 600 Mc/sec and 27 800 Mc/sec with unoriented material are shown in Fig. 2 and are to be compared with the theoretical curves. The above theory cannot, of course, be expected to apply to the experiments with unoriented material since for this material the magnetic field is automatically applied in all directions with respect to the hexagonal axis. Therefore, some sort of averaging process is required in order to determine the resonant fields. Even for the oriented sample an averaging process is required since uniform orientation of the crystallites over the spherical sample was impossible to obtain. Within these experimental limitations our results are in fair agreement with the theory.

We wish to thank F. J. Schnettler for preparing the oriented samples, J. H. Rowen for his help in making the 9000-Mc/sec measurements, and A. G. Fox and H. Suhl for many helpful discussions.

[3] These corrections were discussed by J. Smit at the Conference on Ferrimagnetism held at the U. S. Naval Ordnance Laboratory on October 11–12, 1954.

Magnetic Resonance for Arbitrary Field Strengths

ROALD K. WANGSNESS
United States Naval Ordnance Laboratory, White Oak, Maryland
(Received February 1, 1955)

Starting from a microscopic viewpoint, the steady-state value of the magnetization of a system of moments has been calculated semiclassically and quantum mechanically when the external field has a circularly polarized component perpendicular to the constant component. It is assumed that the only other processes which can change the orientation of the individual moments are strong collisions, and that their average tendency is to produce equilibrium with respect to the instantaneous value of the field. The solutions thus obtained predict a nonzero absorption in zero constant field, and that there is no dependence of g-values on frequency. Further properties of the solutions are discussed. It is also shown that the solutions for the circularly polarized case, as well as Garstens' expression for the absorption coefficient for the linearly polarized case, can be obtained as steady-state solutions of the macroscopic equation

$$d\mathbf{M}/dt=\gamma\mathbf{M}\times\mathbf{H}+\tau^{-1}[\chi_0\mathbf{H}-\mathbf{M}].$$

This equation is a special case of an equation in which longitudina relaxation is assumed to be along and transverse relaxation perpendicular to the instantaneous field. The relation of these results to the question of the general validity of this modified form of Bloch's equation is discussed.

INTRODUCTION

THE phenomenological equations of motion for the magnetization which were devised by Bloch[1] for the description of nuclear magnetic resonance have also been widely used in the analysis of magnetic resonance experiments on paramagnetic, ferromagnetic, and ferrimagnetic materials. In this way, many results of interest concerning the interactions affecting the spin systems have been inferred from the comparison of experimental line shapes with those given by the solutions of Bloch's equations, since the latter depend upon the values of the longitudinal and transverse relaxation times.

Recent measurements of electronic magnetic resonance at low dc fields[2,3] have shown that the experimental results no longer agree even qualitatively with the predictions of Bloch's equations. In particular, the Bloch formula predicts zero absorption at zero field in contrast to the finite absorption found experimentally; this point has been recently emphasized by Garstens.[4] This general failure of Bloch's equations at zero field is not too surprising, since the detailed analysis[5] of the conditions required for the validity of Bloch's equations showed that it is necessary that the applied field be large compared to the line width.

The question then naturally arises as to the proper mode of description of magnetic resonance for arbitrary values of the fields, and, in particular, for very small fields. In general, there are several approaches one can use in attempting to solve this problem. For specific cases, one can start with the microscopic situation and make a direct calculation of the average value of the magnetization in the steady state which results from the final macroscopic balance between the effect of the applied field and the interactions affecting the system which tend to restore the system to a state of thermodynamic equilibrium. Garstens' calculation is essentially of this kind; he considered specifically the role of strong collisions in a paramagnetic gas. The principal disadvantage of this procedure is that it cannot be carried through except for extremely simple cases, and even then, the precise relation of the specific results thus obtained to the general problem is usually not at all clear. On the other hand, one can modify the macroscopic phenomenological equations in some plausible way and then proceed by comparing the predictions of the modified equations with experiment. The suggestions of Codrington, Olds, and Torrey[2] fall into this category; this procedure has the advantage of apparent generality but the principal disadvantage here is that one has no firm basis on which to predict the applicability of these equations to a new set of experimental conditions. Perhaps the most satisfactory, but also the most difficult, procedure would be to follow the general ideas of the treatment used by Wangsness and Bloch for strong fields in that one tries to obtain a general description of the phenomena by a suitable method of averaging the microscopic behavior of the system over all the degrees of freedom which are not of direct interest.

In the present paper, we shall not discuss the problem in its full generality, but rather from a point of view which is a combination of the first two discussed above. First, we shall discuss the case of a paramagnetic gas for which we assume that strong collisions are the only important factors to be considered in addition to the applied field. We shall assume the applied field to consist of a circularly polarized component in the plane perpendicular to the constant component. This problem will be treated both semiclassically and quantum mechanically. After considering some of the specific properties of the solutions obtained in this way, we shall discuss the relation of these and Garstens' results to each other and to the solutions of a more general differential equation. Finally, we shall give a brief discussion of the possibility of extending the treatment

[1] F. Bloch, Phys. Rev. **70**, 460 (1946).
[2] Codrington, Olds, and Torrey, Phys. Rev. **95**, 607 (1954).
[3] Garstens, Singer, and Ryan, Phys. Rev. **96**, 53 (1954).
[4] M. A. Garstens, Phys. Rev. **93**, 1228 (1954).
[5] R. K. Wangsness and F. Bloch, Phys. Rev. **89**, 728 (1953).

of Wangsness and Bloch to the case of arbitrary field strengths by using some of the methods used here.

SEMICLASSICAL GAS MODEL: CIRCULARLY POLARIZED FIELD

The general philosophy of calculations based on a strong-collision gas model, and which we shall adopt, is essentially the following: we assume that between collisions only the external field has any effect on the orientation of the magnetic moment associated with a given molecule so that we can follow its changes in orientation exactly between collisions, provided that we can solve the appropriate equation of motion; the collisions are assumed to be so strong and to last such a short time that during a collision the change in orientation produced by the external field can be neglected as compared to that effected by the collision; and that, immediately after a collision, the moment has an orientation completely determined by this last collision. An average over the ensemble representing our gas thus requires an average over the varying times between collisions, and over the orientations of the moments immediately after the last collision. Collisions are therefore the only mechanism we have provided to enable the system of moments to come into thermal equilibrium with its surroundings. If the external field were constant, the average over last collisions must reflect the fact that for the equilibrium state the moments have a Boltzmann distribution with respect to the external field, and thus that the parallel component of the magnetization is given by the classical Langevin function while the transverse components are zero. If we now assume an additional time-varying field to be present, whose period is long compared to the duration of a collision, then the instantaneous field seen by the molecule after collision is the same as that before collision. Therefore, it is reasonable to assume in this case that an average over the orientations after the last collision should correspond to an equilibrium state with respect to the *instantaneous* field at the last collision.

We shall carry this program out only for the case in which the external field $\mathbf{H}$ consists of a constant plus a rotating component perpendicular to it, i.e., we assume that

$$H_z=H_0, \quad H_+=H_x+iH_y=H_1e^{-i\omega t}. \tag{1}$$

The advantage of discussing this case is that the solutions of the equation of motion $d\mathbf{M}/dt=\gamma\mathbf{M}\times\mathbf{H}$ can be obtained exactly[6]; thus we can avoid the difficulties encountered by Garstens for both the circularly and linearly polarized case which resulted from not using an exact description of the motion of the moment between collisions.

If $\boldsymbol{\mu}$ is an individual moment whose last collision occurred at a time t', the values of its components at the time t are given by[6]

$$\mu_+(t)=\mu e^{-i\omega t}\{\cos\phi\,\sin\theta+\tfrac{1}{2}\sin\phi[(\cos\theta-1)e^{i(\alpha\tau'+\eta)} +(\cos\theta+1)e^{-i(\alpha\tau'+\eta)}\}. \tag{2}$$

$$\mu_z(t)=\mu[\cos\phi\,\cos\theta-\sin\phi\,\sin\theta\,\cos(\alpha\tau'+\eta)], \tag{3}$$

where

$$\mu_+=\mu_x+i\mu_y, \tag{4}$$

$$\alpha^2=\Delta^2+\omega_1^2, \quad \tan\theta=\omega_1/\Delta, \tag{5}$$

$$\Delta=\gamma H_0-\omega=\omega_0-\omega, \quad \omega_1=\gamma H_1. \tag{6}$$

In (2) and (3), the time which has elapsed since the last collision is $\tau'=t-t'$, and ϕ and η give the orientation of $\boldsymbol{\mu}$ for $\tau'=0$ in the primed coordinate system of reference 6, i.e., a coordinate system rotating with angular velocity $-\omega\mathbf{k}$, so that the components of the effective field in this system are given by

$$H_{x'}=H_1, \quad H_{y'}=0, \quad H_{z'}=\Delta/\gamma.$$

The situation for $\tau'=0$ is illustrated in Fig. 1(a).

We must, however, perform our averaging over orientations at the last collision in the laboratory system where we have assumed that the collisions tend to result in equilibrium with respect to the instantaneous value of the actual field. We can choose the axes of our laboratory system to coincide with the primed axes at t', and we let φ and ξ give the orientation of $\boldsymbol{\mu}$ with respect to the resultant field $H=(H_0^2+H_1^2)^{\frac{1}{2}}$. This situation is illustrated in Fig. 1(b); we note that $\tan\vartheta=H_1/H_0=\omega_1/\omega_0$. Since both sets of angles give the orientation of the same moment at the same time, we can equate the expressions for $\mu_{z'}$, $\mu_{y'}$, and $\mu_{z'}$ obtained from the two parts of Fig. 1 to get the following relations:

$$\begin{aligned}\cos\varphi\,\sin\vartheta+\sin\varphi\,\cos\xi\,\cos\vartheta &=\cos\phi\,\sin\theta+\sin\phi\,\cos\eta\,\cos\theta,\\ \sin\varphi\,\sin\xi&=\sin\phi\,\sin\eta,\\ \cos\varphi\,\cos\vartheta-\sin\varphi\,\cos\xi\,\sin\vartheta &=\cos\phi\,\cos\theta-\sin\phi\,\cos\eta\,\sin\theta.\end{aligned} \tag{7}$$

From these, we easily find that

$$\begin{aligned}\cos\phi&=\cos\varphi\,\cos(\theta-\vartheta)+\sin\varphi\,\cos\xi\,\sin(\theta-\vartheta);\\ \sin\phi\,\cos\eta&=-\cos\varphi\,\sin(\theta-\vartheta)\\ &\quad+\sin\varphi\,\cos\xi\,\cos(\theta-\vartheta),\\ \sin\phi\,\sin\eta&=\sin\varphi\,\sin\xi.\end{aligned} \tag{8}$$

Results which represent averages only over orientations in the laboratory system will be represented by $\langle\ \rangle$; in accordance with our assumption of equilibrium with respect to the instantaneous field, we can now assume that: φ and ξ are independent with respect to averaging; ξ has a random distribution; and, φ is described by a Boltzmann distribution with respect to the resultant field H.

[6] R. K. Wangsness, Am. J. Phys. **21**, 274 (1953). The right side of the expression for μ_y in Eq. (9) of this paper should have a minus sign before it.

Thus, we have

$$\langle \sin\varphi \cos\xi\rangle = \langle \sin\varphi \sin\xi\rangle = 0,$$

and

$$\langle \cos\varphi\rangle = L(\mu H/kT) \simeq \mu H/3kT, \tag{9}$$

where L is the Langevin function. Averaging over Eqs. (8), and using these results, we find that

$$\begin{aligned} \langle \cos\phi\rangle &= \langle \cos\varphi\rangle \cos(\theta-\vartheta), \\ \langle \sin\phi \cos\eta\rangle &= -\langle \cos\varphi\rangle \sin(\theta-\vartheta), \\ \langle \sin\phi \sin\eta\rangle &= 0, \end{aligned} \tag{10}$$

so that

$$\langle \sin\phi e^{\pm i\eta}\rangle = -\langle \cos\varphi\rangle \sin(\theta-\vartheta). \tag{11}$$

Therefore, we see that (2) and (3) become

$$\langle \mu_+(t)\rangle = \mu\langle \cos\varphi\rangle e^{-i\omega t}\{\sin\theta \cos(\theta-\vartheta) + \tfrac{1}{2}\sin(\theta-\vartheta) \times [(1-\cos\theta)e^{i\alpha\tau'} - (1+\cos\theta)e^{-i\alpha\tau'}]\}, \tag{12}$$

$$\langle \mu_z(t)\rangle = \mu\langle \cos\varphi\rangle[\cos\theta \cos(\theta-\vartheta) + \sin\theta \sin(\theta-\vartheta) \cos\alpha\tau']. \tag{13}$$

The second part of our averaging process now involves the average over the intervals τ' using the distribution function $e^{-\tau'/\tau}(d\tau'/\tau)$, where τ is the mean time between collisions. Representing our final averages by $\langle\ \rangle_{Av}$, we find from (12) and (13) that

$$\langle \mu_+(t)\rangle_{Av} = \mu\langle \cos\varphi\rangle e^{-i\omega t}\{\sin\theta \cos(\theta-\vartheta) - [\sin(\theta-\vartheta)(\cos\theta - i\alpha\tau)/(1+\alpha^2\tau^2)]\}, \tag{14}$$

$$\langle \mu_z(t)\rangle_{Av} = \mu\langle \cos\varphi\rangle\{\cos\theta \cos(\theta-\vartheta) + [\sin\theta \sin(\theta-\vartheta)]/(1+\alpha^2\tau^2)\}. \tag{15}$$

If we now multiply these equations by the number of moments per unit volume, N, we will obtain the values of the magnetization components at the time t. From (9), we have $N\mu\langle \cos\varphi\rangle = N\mu^2 H/3kT = \chi_0 H$, where χ_0 is the static susceptibility. From (5), (6), and Fig. 1(b), we also find that

$$\begin{aligned} \cos(\theta-\vartheta) &= (\alpha^2+\omega\Delta)/\gamma\alpha H, \\ \sin(\theta-\vartheta) &= \omega H_1/\alpha H. \end{aligned}$$

Substituting these into (14) and (15), we get

$$M_+(t) = \chi_0 H_1 e^{-i\omega t}\{1+[(\omega\Delta\tau^2 + i\omega\tau)/(1+\alpha^2\tau^2)]\}, \tag{16}$$

$$M_z(t) = (\chi_0/\gamma)\{\omega_0 - (\omega\omega_1^2\tau^2)/(1+\alpha^2\tau^2)\}. \tag{17}$$

We can also obtain expressions for the in- and out-of-phase components of the susceptibility, for, if we write

$$M_+(t) = (\chi' + i\chi'')H_+ = (\chi' + i\chi'')H_1 e^{-i\omega t} \tag{18}$$

we find from (16) that

$$\frac{\chi'}{\chi_0} = 1 + \frac{\omega\Delta\tau^2}{1+\Delta^2\tau^2+\omega_1^2\tau^2}, \tag{19}$$

$$\frac{\chi''}{\chi_0} = \frac{\omega\tau}{1+\Delta^2\tau^2+\omega_1^2\tau^2}. \tag{20}$$

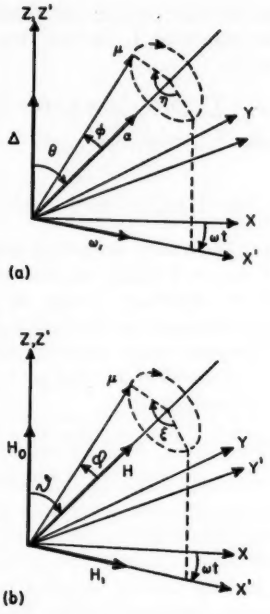

FIG. 1. Orientation of the moment and the field components at the time of the last collision in the coordinate systems used in the text. (*a*) Rotating system. (*b*) Laboratory system.

We shall defer a detailed discussion of these results until a later section, but for the present we can note that they reduce to the correct values for the static case, for when $\omega=0$, $\chi'=\chi_0$, $\chi''=0$, and $M_z=\chi_0 H_0$. As Garstens noted, his results for the circularly polarized case, which can be obtained from the above by dropping the one in (19) and replacing ω by ω_0 in the numerators of (19) and (20), are incorrect in that they do not reduce to the proper values for the static case.

We can also point out here that the maximum value of χ'' occurs when $\Delta=0$, i.e., $\omega_0=\omega$. Thus, for the circularly polarized case, there is no change in g-value with frequency.

QUANTUM-MECHANICAL DERIVATION

In the previous section, we considered the effect of the external field and of collisions upon the magnetization components. In this section, we shall instead consider the effect upon the distribution function, i.e., the density matrix for the spins.

As before,[5] we shall use a representation in which the z component of the spin, I_z, is diagonal with eigenvalues m. In terms of the spin probability amplitudes $a_m(t)$, the components of the density matrix ρ are given by

$$(m|\rho(t)|m') = a_m(t)a_{m'}{}^*(t). \tag{21}$$

We also have the relation

$$\boldsymbol{\mu} = \gamma\hbar\mathbf{I}, \tag{22}$$

so that we can initially confine our considerations to the expectation values of **I**. In fact, the expectation values are given by

$$\begin{aligned}\langle I_+\rangle&=\mathrm{Tr}(I_+\rho)=\textstyle\sum_m(m|I_+|m-1)(m-1|\rho|m),\\ \langle I_z\rangle&=\mathrm{Tr}(I_z\rho)=\textstyle\sum_m m(m|\rho|m),\end{aligned}\tag{23}$$

where

$$(m|I_+|m-1)=[(I+m)(I-m+1)]^{\frac{1}{2}}.$$

Although all of the results describing the effect of the external field alone on ρ which we shall be using have been obtained for arbitrary values of I,[7] we shall restrict our considerations to the case that $I=\frac{1}{2}$ since the formulas become quite cumbersome otherwise. Since then $m=\pm\frac{1}{2}$, we shall let $(+\frac{1}{2}|\rho|+\frac{1}{2})=\rho_{++}$, etc., so that Eqs. (23) simplify to

$$\langle I_+\rangle=\rho_{-+}\quad\text{and}\quad\langle I_z\rangle=\tfrac{1}{2}(\rho_{++}-\rho_{--}).\tag{24}$$

If we now transform from the laboratory system to the primed coordinate system which is rotating so as to keep the resultant field H in the $x'z'$ plane, it is convenient to express everything in terms of the probability amplitudes b_m and the density matrix ρ' in the rotating system. Using the results quoted by Bloch and Rabi[7] for the transformation of the probability amplitudes,

$$b_+=e^{-i\frac{1}{2}\omega t}a_+\quad\text{and}\quad b_-=e^{i\frac{1}{2}\omega t}a_-,$$

we find that

$$\rho_{++}=\rho_{++}',\quad\rho_{--}=\rho_{--}',\quad\rho_{-+}=e^{-i\omega t}\rho_{-+}',$$

so that the expectation values in the laboratory system given by (24) becomes

$$\langle I_+\rangle=\rho_{-+}'e^{-i\omega t}\quad\text{and}\quad\langle I_z\rangle=\tfrac{1}{2}(\rho_{++}'-\rho_{--}').\tag{25}$$

In the primed coordinate system, the probability amplitudes at the time t in terms of their values at the time t' are given by[7]

$$b_+(t)=Ab_+{}^0+Bb_-{}^0,\quad b_-(t)=Bb_+{}^0+A^*b_-{}^0,\tag{26}$$

where

$$\begin{aligned}A&=\cos(\tfrac{1}{2}\alpha\tau')+i\cos\theta\sin(\tfrac{1}{2}\alpha\tau'),\\ B&=i\sin\theta\sin(\tfrac{1}{2}\alpha\tau'),\end{aligned}\tag{27}$$

and where, as before, $\tau'=t-t'$ is the interval since the last collision. Therefore, we find for the elements of ρ' the following:

$$\begin{aligned}\rho_{-+}'&=(A^*)^2\rho_{-+}{}'{}^0-B^2\rho_{+-}{}'{}^0\\&\quad+A^*B(\rho_{++}{}'{}^0-\rho_{--}{}'{}^0),\\ \rho_{++}'-\rho_{--}'&=(AA^*+B^2)(\rho_{++}{}'{}^0-\rho_{--}{}'{}^0)\\&\quad+2B(A^*\rho_{-+}{}'{}^0-A\rho_{+-}{}'{}^0),\end{aligned}\tag{28}$$

where $\rho_{++}{}'{}^0=b_+{}^0b_+{}^{0*}$, etc. These results must now be averaged over the state at the last collision and then over the intervals since the last collision.

According to our basic assumption, the average over the states at the last collision should correspond to an equilibrium distribution with respect to the instantaneous resultant field H of Fig. 1(b). If we use c_+ and c_- as the probability amplitudes in the system whose z'' axis lies along H and whose y'' axis coincides with y', we can therefore assume that there exists complete incoherence in the relative phases of c_+ and c_-. If we let averages over the states at last collision be represented by $(\ )_c$, our basic assumption therefore is equivalent to the relations

$$\begin{aligned}(c_+c_-)_c&=(c_+{}^*c_-)_c=(c_+{}^*c_-{}^*)_c=(c_+c_-{}^*)_c=0,\\ (c_+c_+{}^*-c_-c_-{}^*)_c&=\tanh(\mu H/kT)\simeq\mu H/kT=\kappa.\end{aligned}\tag{29}$$

Since the systems in which the b's and c's are used differ by a rotation about the y' axis by the angle ϑ, the relation between the amplitudes is given by[7]

$$b_+{}^0=c_+\cos\tfrac{1}{2}\vartheta-c_-\sin\tfrac{1}{2}\vartheta,\quad b_-{}^0=c_+\sin\tfrac{1}{2}\vartheta+c_1\cos\tfrac{1}{2}\vartheta,$$

and therefore, we find that

$$(\rho_{-+}{}'{}^0)_c=(\rho_{+-}{}'{}^0)_c=\tfrac{1}{2}\kappa\sin\vartheta,\quad(\rho_{++}{}'{}^0-\rho_{--}{}'{}^0)_c=\kappa\cos\vartheta,$$

so that (28) becomes:

$$\begin{aligned}(\rho_{-+}')_c&=\kappa[\tfrac{1}{2}\sin\vartheta((A^*)^2-B^2)+\cos\vartheta A^*B]\\&=\tfrac{1}{2}\kappa\{\sin\theta\cos(\theta-\vartheta)+\tfrac{1}{2}\sin(\theta-\vartheta)\\&\quad\times[(1-\cos\theta)e^{i\alpha\tau'}-(1+\cos\theta)e^{-i\alpha\tau'}]\},\end{aligned}\tag{30}$$

$$\begin{aligned}&(\rho_{++}'-\rho_{--}')_c\\&=\kappa[\cos\vartheta(AA^*+B^2)+\sin\vartheta B(A^*-A)]\\&=\kappa[\cos\theta\cos(\theta-\vartheta)+\sin\theta\sin(\theta-\vartheta)\cos\alpha\tau'].\end{aligned}\tag{31}$$

The next step would now be to average these results over the intervals since the last collision. We do not, however, have to carry this through as we can now easily see that we will get the same results as before. For, if we now wanted to get a result to compare with that of the last section at an equivalent stage such as (12), we see from (22) and (25), we can get $\langle\mu_+(t)\rangle$ by multiplying (30) by $\gamma\hbar e^{-i\omega t}$. Then the factor in front of the braces of (30) becomes, except for $e^{-i\omega t}$, $\frac{1}{2}\gamma\hbar\kappa=\mu\kappa=\mu^2H/kT=\chi_0H/N$ where χ_0 is the static susceptibility appropriate to spin $\frac{1}{2}$. Since we showed in the last section that $\mu\langle\cos\varphi\rangle=\chi_0H/N$, if we now compare the form of (30) and (12) we see that we will be led to exactly the same final result upon averaging (30) over τ' as we were from (12). Similarly, since the terms in the brackets of (31) are the same as (13), an average of (31) over τ' will lead to the same final results as did (13). Thus, we see that Eqs. (16)–(20) will also be obtained by this quantum-mechanical calculation.

PROPERTIES OF THE RESULTS FOR THE CIRCULARLY POLARIZED CASE

The quantities of principal interest to us in this section are the susceptibilities

$$\frac{\chi'}{\chi_0}=1+\frac{\omega\Delta\tau^2}{1+\alpha^2\tau^2},\quad\frac{\chi''}{\chi_0}=\frac{\omega\tau}{1+\alpha^2\tau^2}.\tag{32}$$

[7] F. Bloch and I. I. Rabi, Revs. Modern Phys. **17**, 237 (1945).

We note first of all that for zero constant field ($\omega_0=0$) they become

$$\frac{\chi'}{\chi_0}=\frac{1+(\omega_1\tau)^2}{1+(\omega\tau)^2+(\omega_1\tau)^2},\quad \frac{\chi''}{\chi_0}=\frac{\omega\tau}{1+(\omega\tau)^2+(\omega_1\tau)^2}. \tag{33}$$

We see that $\chi''\neq 0$ so that there is an absorption at zero field as there should be and, in fact, if the rotating field is sufficiently weak, i.e., $(\omega_1\tau)^2\ll 1$, χ'' reduces correctly to the Debye formula $\chi_0\omega\tau/(1+\omega^2\tau^2)$.

For extremely large fields ($\Delta\to\infty$), we also find that these formulas reduce to the reasonable values $\chi'\to\chi_0$ and $\chi''\to 0$.

As mentioned before, χ'' has its maximum value for $\Delta=0$ (resonance), and we have

$$\chi'_{\text{res}}=\chi_0,\quad \chi''_{\text{res}}=\chi_0\omega\tau/(1+\omega_1^2\tau^2).$$

It is interesting to see that χ' is not zero when χ'' is a maximum, but rather is equal to the static value of the susceptibility.

For more detailed discussion, it is convenient to write (32) in terms of a set of dimensionless variables

$$x=\omega\tau,\quad x_0=\omega_0\tau,\quad x_1=\omega_1\tau, \tag{34}$$

$$r=x_0/x=\omega_0/\omega, \tag{35}$$

so that resonance corresponds to $r=1$. In addition, we introduce a parameter ϵ, which is a convenient measure of the combined effect of the frequency and amplitude of the rotating field, and which is defined by

$$\epsilon=[(1+x_1^2)/x^2]^{\frac{1}{2}}. \tag{36}$$

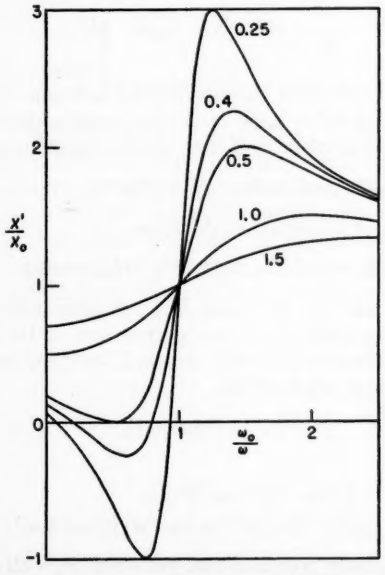

FIG. 2. Real part of susceptibility *vs* applied field when transverse field is circularly polarized. The numbers near the peaks are the values of the parameter ϵ which measures the combined effect of frequency and amplitude.

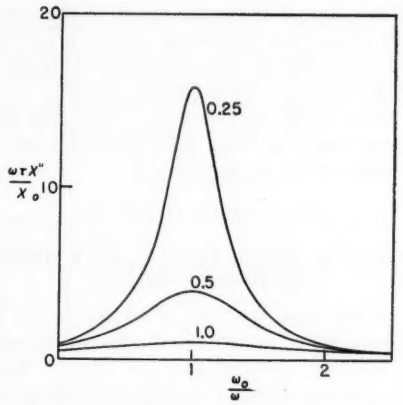

FIG. 3. Imaginary part of susceptibility *vs* applied field when transverse field is circularly polarized. The numbers near the peaks are the values of the parameter ϵ which measures the combined effect of frequency and amplitude.

In this notation, $1+\alpha^2\tau^2=x^2[(r-1)^2+\epsilon^2]$, and (32) becomes

$$\frac{\chi'}{\chi_0}=1+\frac{(r-1)}{(r-1)^2+\epsilon^2},\quad x\left(\frac{\chi''}{\chi_0}\right)=\frac{1}{(r-1)^2+\epsilon^2}. \tag{37}$$

These forms are more useful in performing numerical calculations.

One easily finds that the points at which χ'' is equal to half its maximum value are $r=1\pm\epsilon$, or $(\omega_0)_{\frac{1}{2}}=\omega(1\pm\epsilon)$. It also turns out that these are the same as the points at which χ' has its maximum and minimum values. In fact, we have, for $(\omega_0)_{\max}=\omega(1+\epsilon)$,

$$(\chi'/\chi_0)_{\max}=1+1/2\epsilon$$

and for $(\omega_0)_{\min}=\omega(1-\epsilon)$,

$$(\chi'/\chi_0)_{\min}=1-1/2\epsilon.$$

Thus, except for the case discussed below, the maximum and minimum values of χ' are equally above and below χ_0. If $\epsilon<\frac{1}{2}$, $(\chi')_{\min}$ is negative; if $\epsilon>\frac{1}{2}$, $(\chi')_{\min}$ is positive, while for $\epsilon=\frac{1}{2}$, $(\chi')_{\min}=0$, $(\chi')_{\max}=2\chi_0$, $(\omega_0)_{\min}=\frac{1}{2}\omega$, and $(\omega_0)_{\max}=\frac{3}{2}\omega$. If $\epsilon>1$, however, the above formula would indicate that $(\omega_0)_{\min}$ is negative; this means, of course, that for $\epsilon>1$, the minimum value of χ' corresponds to the value for $\omega_0=0$ and is greater than the value $1-(1/2\epsilon)$ given by the above formula.

It is possible for χ' to go through or become zero, but only if $\epsilon\leqslant\frac{1}{2}$. If $\epsilon<\frac{1}{2}$, χ' is zero at the frequencies given by

$$\omega_{0z}^{\pm}=\tfrac{1}{2}\omega[1\pm(1-4\epsilon^2)^{\frac{1}{2}}],$$

while if $\epsilon=\frac{1}{2}$, the two zeros coincide and equal the value $\omega/2$ found above for $(\omega_0)_{\min}$. On the other hand, if $\epsilon>\frac{1}{2}$, χ' is always positive.

Figures 2 and 3 show calculated curves of (χ'/χ_0) and $x(\chi''/\chi_0)$ as functions of r for various values of ϵ. They clearly show the existence of absorption for zero

H_0 and the change in the character of the curves as discussed above for increasing values of ϵ. Experimentally, this could be obtained under suitable conditions by increasing ω_1 for a fixed value of ω.

The value of M_z as given by (17) never changes appreciably from the value $\chi_0 H_0$ except for very large ω_1. The value of M_z at resonance is

$$(M_z)_{\text{res}}=\chi_0 H_0/(1+\omega_1^2\tau^2).$$

RELATION OF THESE RESULTS TO A GENERAL EQUATION OF MOTION

As was discussed, it would be of interest to have a general equation of motion for the magnetization, possibly a suitably modified form of Bloch's equation, which is a more accurate description of resonance phenomena for arbitrary fields, particularly at low fields. In the previous sections we derived expressions for the susceptibilities which do reduce to what are felt to be the correct forms at low fields. If we could now show that these susceptibilities can also be derived from a general equation under the same conditions as used in the previous sections rather than necessitating the type of detailed calculation we have actually used, this would furnish a limited theoretical support from the microscopic point of view for the validity of the macroscopic equation.

Briefly stated, the basic assumption in our derivation was that the effect of the strong collisions was the tendency to establish equilibrium with respect to the instantaneous value of the field. This is similar to the suggestion of Codrington, Olds, and Torrey[2] that Bloch's equation be altered by assuming that longitudinal relaxation takes place along the instantaneous field while transverse relaxation is perpendicular to it. We shall now show that our specific results can be obtained from an equation of this type.

If we let T_1 and T_2 be the usual longitudinal and transverse relaxation times, respectively, then the equation of motion suggested by Codrington, Olds, and Torrey would have the form

$$\frac{d\mathbf{M}}{dt}=\gamma\mathbf{M}\times\mathbf{H}+\frac{1}{T_1}\left[\chi_0\mathbf{H}-\frac{(\mathbf{M}\cdot\mathbf{H})}{H^2}\mathbf{H}\right]-\frac{1}{T_2}\left[\mathbf{M}-\frac{(\mathbf{M}\cdot\mathbf{H})}{H^2}\mathbf{H}\right]$$

or

$$\frac{d\mathbf{M}}{dt}=\gamma\mathbf{M}\times\mathbf{H}+\frac{\chi_0\mathbf{H}}{T_1}-\frac{\mathbf{M}}{T_2}+\left(\frac{1}{T_2}-\frac{1}{T_1}\right)\frac{(\mathbf{M}\cdot\mathbf{H})}{H^2}\mathbf{H}. \quad (38)$$

If we let $M_+=M_x+iM_y$ then (38) is equivalent to

$$\dot{M}_+=-\left(i\gamma H_z+\frac{1}{T_2}\right)M_++\left[i\gamma M_z+\frac{\chi_0}{T_1}+\left(\frac{1}{T_2}-\frac{1}{T_1}\right)\frac{\mathbf{M}\cdot\mathbf{H}}{H^2}\right]H_+, \quad (39)$$

$$\dot{M}_z=\frac{\gamma}{i2}(M_+H_+^*-M_+^*H_+)-\frac{M_z}{T_2}+\left[\frac{\chi_0}{T_1}+\left(\frac{1}{T_2}-\frac{1}{T_1}\right)\frac{\mathbf{M}\cdot\mathbf{H}}{H^2}\right]H_z. \quad (40)$$

If we now assume that $\mathbf{H}$ has the constant and circularly polarized components given by (1), we can find a steady state solution of (39) and (40) of the form

$$M_+=(\chi_-'+i\chi_-'')H_1e^{-i\omega t}, \quad M_{z-}=\text{const.} \quad (41)$$

When (41) is substituted in (39) and (40), we find that

$$\chi_-'=\chi_0 D_-[1+(\alpha^2+\omega\Delta)T_2^2], \quad (42)$$

$$\chi_-''=\chi_0 D_-\omega T_2, \quad (43)$$

$$M_{z-}=(\chi_0/\gamma)D_-[\omega_0(1+\alpha^2T_2^2)-\omega\omega_1^2T_2^2], \quad (44)$$

where

$$(1/D_-)=1+\alpha^2T_1T_2-T_2(T_1-T_2)(\omega_1^2+\omega_0\Delta)^2/(\omega_0^2+\omega_1^2). \quad (45)$$

Now in the case of gases, where strong collisions provide the relaxation mechanism, it is known[5] that there is no longer any real distinction between T_1 and T_2. In order to compare these results with those of previous sections, therefore, we should consider the case that $T_1=T_2=\tau$; then we see at once that (42)–(44) reduce exactly to the corresponding expressions in (17), (19), and (20). In other words, the results obtained by the earlier detailed calculations can most simply be obtained as the steady-state solution of the equation to which (38) reduces when $T_1=T_2=\tau$; namely,

$$\frac{d\mathbf{M}}{dt}=\gamma\mathbf{M}\times\mathbf{H}+\frac{1}{\tau}[\chi_0\mathbf{H}-\mathbf{M}]. \quad (46)$$

We can also find the steady-state solution of (39)–(40) for the other sense of circular polarization. If we assume the external field now has the components

$$H_z=H_0, \quad H_+=H_1e^{i\omega t}, \quad (47)$$

and assume a solution of the form

$$M_+=(\chi_+'+i\chi_+'')H_1e^{i\omega t}, \quad M_{z+}=\text{const.}$$

we find that χ_+', χ_+'', and M_{z+} are given exactly by simply replacing ω by $-\omega$ everywhere in the corresponding results (42)–(45) obtained for the other case. For example, we find that

$$\chi_+''=-\chi_0 D_+\omega T_2, \quad (48)$$

where

$$(1/D_+)=1+[(\omega_0+\omega)^2+\omega_1^2]T_1T_2-T_2(T_1-T_2)[\omega_1^2+\omega_0(\omega_0+\omega)]^2/(\omega_0^2+\omega_1^2). \quad (49)$$

The linearly polarized case for which $H_x=2H_1\cos\omega t$, $H_y=0$ is very difficult to solve exactly. For our present purposes, it will be sufficient to restrict our considerations of the linearly polarized case to the simpler

equation (46). We can get an approximate steady-state solution if we assume H_1 to be small enough so that we can neglect the product M_xH_x. We then find that a solution of the equation corresponding to (40) is

$$M_{zl}=\chi_0 H_0=\text{const.}$$

The corresponding equation (39) then becomes simply

$$\dot{M}_{+l}=-\left(i\omega_0+\frac{1}{\tau}\right)M_{+l}+\chi_0\left(i\omega_0+\frac{1}{\tau}\right)\times H_1(e^{i\omega t}+e^{-i\omega t}) \quad (50)$$

since $H_+=2H_1\cos\omega t$.

Equation (50) can be easily integrated directly to find the steady-state value of M_{+l} which we see will be proportional to H_1. But the linear form of (50) suggests that we should be able to write M_{+l} as the sum of the solutions we found for the two circularly polarized cases when $T_1=T_2=\tau$, provided that we neglect the quantity $(\omega_1\tau)^2$. This can be verified directly to be the case and therefore we can write

$$M_{+l}=(\chi_-'+i\chi_-'')H_1e^{-i\omega t}+(\chi_+'+i\chi_+'')H_1e^{i\omega t},$$

or

$$M_{xl}=2H_1[\tfrac{1}{2}(\chi_-'+\chi_+')\cos\omega t+\tfrac{1}{2}(\chi_-''-\chi_+'')\sin\omega t],$$

$$M_{yl}=2H_1[\tfrac{1}{2}(\chi_-''+\chi_+'')\cos\omega t-\tfrac{1}{2}(\chi_-'-\chi_+')\sin\omega t]. \quad (51)$$

The only term which will contribute to the energy absorption is the coefficient of $2H_1\sin\omega t$ in the expression for M_{xl}, and this can be written in the normal manner as χ_l''. Thus, from (51), (43), and (48), we get

$$\chi_l''=\tfrac{1}{2}(\chi_-''-\chi_+'')=\tfrac{1}{2}\chi_0\omega\tau\left[\frac{1}{1+(\omega_0-\omega)^2\tau^2}+\frac{1}{1+(\omega_0+\omega)^2\tau^2}\right], \quad (52)$$

which is exactly the expression obtained by Garstens for the linearly polarized case[4] and is known to agree well with experiment.[3] Since Garstens, Singer, and Ryan always used extremely small amplitudes for their oscillating field, one could not expect their experiments to show the effects of the additional terms $(\omega_1\tau)^2$ which will likely appear in a less approximate solution of (46).

The general origin of Garstens' expression for χ_l'' is now less obscure since we have just shown it to be obtainable from an approximate steady-state solution of the general equation of motion (46) in which both relaxation times are taken to be equal.

DISCUSSION

In general, the fact that our results for the circularly polarized case and that of Garstens for the linearly polarized case, which were derived by suitable averaging over the microscopic states, can be obtained as solutions of the macroscopic equation (46) provide support for the feeling that (46) and hence the more general equation (38) will provide a valid description of magnetic resonance phenomena for a wide range of experimental conditions. In order to specify these conditions in detail, we would obviously require a more elaborate analysis than given here. It seems likely that this task could be carried through, at least for the circularly polarized case, by transforming to a properly chosen rotating coordinate system in which the external field has effectively been eliminated, as we did in previous sections by means of the simple transformation equations for spin $\frac{1}{2}$, and then by proceeding along lines similar to those used before.[5]

It has been common practice to use equations of the Bloch form as a basis of discussion of line shapes and relaxation times in ferromagnetic and ferrimagnetic resonance experiments. One of the qualitative results obtained here is the definite indication that g-values obtained by the usual method of finding the field at which the peak of the absorption curve occurs should depend on whether one is using a linearly or circularly polarized field, and it would be interesting if this should also be the case for ferromagnetic and ferrimagnetic materials. This point is currently being investigated experimentally by Dr. T. R. McGuire of this Laboratory.

Note added in proof.—Since this article was submitted, I have learned from private communications that similar conclusions about the necessity of considering the interactions as tending to produce equilibrium with respect to the instantaneous field have been independently arrived at by E. P. Gross, J. Kaplan, and P. Weiss.

Change in KCl Lattice by Soft X-Rays*

CHESTER R. BERRY
Research Laboratories, Eastman Kodak Company, Rochester, New York
(Received December 31, 1954)

The lattice dimensions of powdered specimens of annealed and unannealed KCl were measured during irradiation by soft x-rays. One set of specimens was allowed to color during irradiation and another group was prevented from coloring by simultaneous white-light illumination. The following observations were made: There was an increase in lattice dimension during exposure for every specimen. No difference existed for specimens which were colored or not colored. Saturation in the change in lattice dimension occurred at a lower exposure for the unannealed specimens than for the annealed specimens. The total increase in lattice dimension was about $\Delta a/a=1\times10^{-5}$ for all specimens, compared with values given in the literature for maximum changes in length of approximately $\Delta l/l=20\times10^{-5}$. The difference indicates production of void volume, presumably Schottky defects. The failure to observe a difference between colored and uncolored specimens may be caused by a considerably larger production of Schottky defects than of color centers.

THE lattice dimensions of powdered specimens of KCl were measured during irradiation by soft x-rays. One group of measurements was made with light excluded from the KCl so that the crystals became colored, and another group was made with white-light illumination which prevented coloration. Analytical-grade KCl from Baker and Adamson was ground to produce a fine powder and three kinds of specimens were made from the powder: an unannealed specimen, and specimens annealed at about 500° and 600°C. The annealing was accomplished by keeping the powder at the elevated temperatures for about 16 hours and then cooling it to room temperature in about 24 hours.

The powdered KCl was packed lightly in a cavity in a metal block with no binder except diluted petroleum jelly, which also acted as a lubricant and tended to prevent changes in lattice dimension owing to pressure effects which have been reported earlier.[1] The flat specimens produced in this way were placed inside a constant-temperature jacket at about 25°C. The temperature of the air near the surface of the specimen was known to within 0.03°C and lattice dimensions were corrected to 25.00°C.

The lattice dimensions were calculated by determining the values, using Ni $K_{\alpha 1}$ radiation, at diffraction angles of about 161 and 122 degrees and extrapolating to the value at 180 degrees, using the function proposed by Nelson and Riley.[2] Although this function was derived for a cylindrical specimen, analytical treatment shows that errors in the flat-specimen technique arising from such sources as incorrect positioning of the specimen or incorrect zero-angle adjustment may be greatly reduced by the extrapolation. The two diffraction peaks were read to the nearest 0.002 degree from a chart recording the rate of pulse generation in a Geiger counter detector as a function of angle. Corrections for refraction of the x-rays were made.[3] The two diffraction peaks were recorded in about 10 minutes and seven successive measurements were obtained from each specimen, the same source of radiation both coloring the crystals and producing the diffraction pattern. The radiation was from a nickel-target tube operating at 50 kvp and 8 ma.

Measurements of absolute intensity of the beam at the specimen were made with a calibrated ionization chamber described by Seemann.[4] To permit readings of relatively high intensity, a small lead diaphragm was placed over the window of the chamber. The effective wavelength of the incident radiation determined by using aluminum absorbers was about 1.58 A, not very different from 1.66 A, the characteristic radiation. The intensity at the center of the incident beam was 19.0 R/sec. This was converted to absolute intensity with the relationship of Seemann,[5] giving 160 ergs/cm² sec. If Harten's[6] value of 120 ev for the average energy of F-center formation in KCl at room temperature is applicable to our specimens, the rate of F-center production at the center of the surface may be estimated as

$$-(dI/dz)_{z=0}/120=\mu I_0/120=2.2\times10^{14}/\text{cm}^3\ \text{sec}.$$

The results of the measurements are shown in Fig. 1. Each point on the plot represents the average from

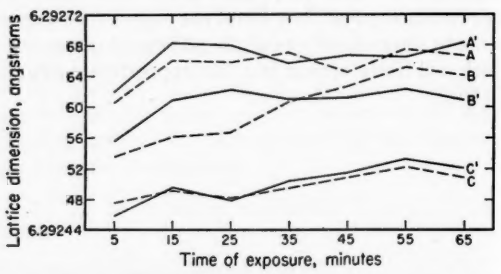

FIG. 1. Lattice dimension of KCl during x-ray exposure. A and A', unannealed specimens; colored by x-rays and prevented from coloring, respectively. B and B', annealed at 500°C; colored and not colored. C and C', annealed at 600°C; colored and not colored.

* Communication No. 1707 from the Kodak Research Laboratories.

[1] Berry, VanHorn, and Griffith, Acta Cryst. **7**, 135 (1954).

[2] J. B. Nelson and D. P. Riley, Proc. Phys. Soc. (London) **57**, 160 (1945).

[3] A. J. C. Wilson, Proc. Cambridge Phil. Soc. **36**, 485 (1940).

[4] H. E. Seemann, Rev. Sci. Instr. **20**, 903 (1949).

[5] H. E. Seemann, Rev. Sci. Instr. **21**, 314 (1950).

[6] H. U. Harten, Z. Physik **126**, 619 (1949).

about twenty separate specimens and has a standard error of 0.000015 A to 0.000020 A, as determined from the statistics. This error refers to the precision of the data, and the error in the absolute lattice dimension of pure KCl may be somewhat larger. The following conclusions appear from the figure: There is an increase in lattice dimension during exposure for every specimen. No significant difference exists between specimens which were colored and those which were prevented from coloring during irradiation. The lattice dimension of the unannealed specimens seems to rise more rapidly than the annealed specimens and then levels off. Since the difference in level of lattice dimension of the three sets of specimens may persist even at zero exposure, it may be attributed to changes produced during the annealing process or to certain systematic differences which we suspect, rather than to differences occurring during irradiation. Some additional measurements which were made following prolonged irradiation of the specimens for about 20 hours indicated that no significant change in lattice dimension occurred between 1 and 20 hours. The total increase in lattice dimensions is approximately $\Delta a/a=1\times10^{-5}$ for all specimens.

Since the x-ray beam was not of uniform intensity over the surface or in the depth of the specimen, the concentration of color centers and the change in lattice dimension were also not uniform. In addition, the various parts of the specimen are not weighted equally in a diffraction pattern. So it is of interest to determine how the measured change in lattice dimension is related to the value at the surface of the specimen in the most intense part of the beam. If it is assumed that the change in lattice dimension of an element in the specimen is proportional to the x-ray intensity incident on it, then

$$\Delta a(x,y,z)=KI_i(x,y,z)=KI_0(x,y)e^{-\mu_i z}.$$

The weight assigned to this element is proportional to the intensity in the reflected beam and is $I_r(x,y,z)\Delta x,\ \Delta y,\ \Delta z=I_{0\alpha}(x,y)\exp(-2\mu_\alpha z)\Delta x,\ \Delta y,\ \Delta z$. Averaging the contribution over the entire specimen gives the measured change in lattice dimension as

$$\langle\Delta a\rangle_{Av}=K\frac{\int\int\int I_0(x,y)I_{0\alpha}(x,y)\exp(-2\mu_\alpha z-\mu_i z)dxdydz}{\int\int\int I_{0\alpha}(x,y)\exp(-2\mu_\alpha z)dxdydz}.$$

Integration with respect to z in numerator and denominator gives the value $2\mu_\alpha/(2\mu_\alpha+\mu_i)$, which is very nearly $\frac{2}{3}$. Substituting this value and assuming that the total incident intensity $I_0(x,y)$ is proportional to the characteristic intensity, $I_{0\alpha}(x,y)$ gives

$$\langle\Delta a\rangle_{Av}=\frac{2K}{3}\frac{\int\int I_0^2(x,y)dxdy}{\int\int I_0(x,y)dxdy}.$$

These integrals were evaluated numerically from the map of intensity and gave a value in terms of the maximum intensity, such that

$$\langle\Delta a\rangle_{Av}\cong\tfrac{1}{2}KI_{\max}=\tfrac{1}{2}\Delta a_{\max}.$$

If the change in lattice dimension saturates at some exposure, the measured change will approach the saturation value. Thus, the change in lattice dimension measured in the diffraction experiment will correspond remarkably closely to the change produced in the most intensely irradiated portion of the specimen. This is a different situation from that in many other types of measurement, which weight the effect of all elements of the specimen equally, although the specimen is not saturated through the entire depth.

It is interesting to compare the maximum change in lattice dimension of KCl with related measurements discussed in the literature. Sakaguchi and Suita[7] determined that the increase in thickness of KCl saturated at a value, $\Delta l/l=5.7\times10^{-5}$. Estermann, Leivo, and Stern[8] found that the density decreased to a minimum such that $\Delta\rho/\rho=-7\times10^{-5}=-3\Delta l/l$. However, in both these cases, it was stated that the coloration decreased with depth such that the surface saturation values of $\Delta l/l$ were many times greater than those given above, possibly $\Delta l/l=20\times10^{-5}$. In any case, the surface saturation value for $\Delta l/l$ is many times greater than the saturation x-ray value of $\Delta a/a$. Then the density decrease and external expansion must be attributed primarily to an increase in void volume in the specimens, presumably Schottky defects, rather than to lattice expansion. If the saturation values for $\Delta l/l$ and $\Delta a/a$ are presumed to be about 20×10^{-5} and 1×10^{-5}, respectively, then the fraction of Schottky defects in the length of the specimen is almost 20×10^{-5}, or 6×10^{-4} in the volume. On this basis, the change of lattice dimension associated with formation of Schottky defects is $\Delta a=0.05a$ per defect. This is in a reasonable range to agree with the calculation of Mott and Littleton[9] that the nearest neighbors at a vacancy in NaCl are displaced outward by about $0.07a$.

It is rather puzzling that no difference was observed between the colored and uncolored specimens. A de-

[7] K. Sakaguchi and T. Suita, Technol. Repts. Osaka Univ. 2, 177 (1952).
[8] Estermann, Leivo, and Stern, Phys. Rev. 75, 627 (1949).
[9] N. F. Mott and M. J. Littleton, Trans. Faraday Soc. 34, 485 (1938).

crease of about $0.15a$ in Δa per defect in the colored specimens was expected, owing to the reduction in Coulomb repulsion, which would occur on trapping an electron at a negative-ion vacancy. This estimate is suggested by the observation that a 15 percent decrease in lattice dimension occurs when a chloride ion is replaced by a fluoride ion in KCl. The observed result could occur in such a case only if the concentration of F-centers were many times smaller than the concentration of Schottky defects.

ACKNOWLEDGMENT

The assistance of S. J. Marino in making the measurements is greatly appreciated.

PHYSICAL REVIEW VOLUME 98, NUMBER 4 MAY 15, 1955

Magnetic Susceptibility of Hafnium and Manganese

C. J. KRIESSMAN* AND T. R. MCGUIRE
U. S. Naval Ordnance Laboratory, White Oak, Maryland
(Received February 1, 1955)

The magnetic susceptibility of hafnium, which has been measured from 4.2°K to 1670°K, increases with increasing temperature above 77°K. At room temperature, the susceptibility is $(0.42\pm0.01)\times10^{-6}$ emu/g. The susceptibility of manganese between 77°K and room temperature shows a maximum at 125°K. This can be identified with antiferromagnetism by a correlation with neutron diffraction data. In the temperature region below 77°K the susceptibility increases again quite rapidly.

INTRODUCTION

THERE has been recent interest in the magnetic susceptibility of transition metals. On the basis of data recently obtained, Kriessman and Callen[1] have proposed a qualitative band theory interpretation of the temperature dependence of the susceptibility. We have extended this work by measuring the magnetic susceptibility of hafnium and manganese by the body-force method described in a previous paper.[2] The susceptibility of hafnium has not previously been measured while no data exist for manganese at low temperatures.

Manganese is of interest because Shull[3] has found evidence from neutron diffraction that it is antiferromagnetic with a Curie temperature at about 100°K. The only previous measurements on manganese in this temperature range are those of Serres.[4] They were limited to points at 80°K, 170°K, and room temperature, which gave some indication of a maximum in the susceptibility, an important characteristic of antiferromagnetism. It appeared that this feature needed further investigation to fix the exact location of the maximum value. No previous magnetic susceptibility data exist below 77°K, but it has been established by Goodman[5] using magnetic methods that manganese is not a superconductor down to 0.14°K. In all probability, Goodman's method would also have indicated a transition to ferromagnetism if it existed.

EXPERIMENTAL RESULTS

Hafnium

Our sample was obtained from H. K. Adenstedt of the Materials Laboratory, Air Materials Command, Wright-Patterson Air Force Base. Bommer[6] estimated from periodic table considerations that the susceptibility of hafnium should be about 0.5×10^{-6}. We find that the room-temperature value is $(0.42\pm0.01)\times10^{-6}$ and that the susceptibility increases regularly with temperature up to 1670°K, as shown in Fig. 1. The two upper curves (B and C) are from a series which one obtains from successive high-temperature runs. Curve A is the one finally reached, and, since it is reproducible and without field dependence, we assume it is the true behavior of the metal. The other curves evidently represent a ferromagnetic impurity whose effect slowly decreases on heat treatment. Measurements were also made at 77°K giving a value of 0.40

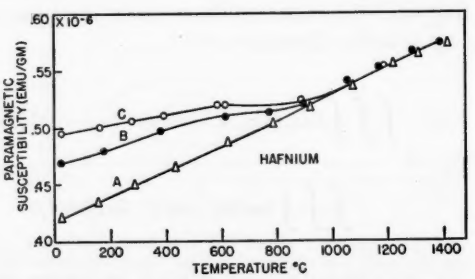

FIG. 1. Magnetic susceptibility of hafnium as a function of temperature. Upper curves (B and C) represent effects of ferromagnetic impurity.

* Now at Remington Rand, Philadelphia, Pennsylvania.
[1] C. J. Kriessman, Revs. Modern Phys. **25**, 122 (1953); C. J. Kriessman and H. B. Callen, Phys. Rev. **94**, 837 (1954).
[2] T. R. McGuire and C. T. Lane, Rev. Sci. Instr. **20**, 489 (1949).
[3] C. G. Shull and M. K. Wilkinson, Revs. Modern Phys. **25**, 100 (1953).
[4] A. Serres, J. phys. radium **9**, 377 (1938).
[5] B. Goodman, Nature **167**, 111 (1951).
[6] H. Bommer, Z. anorg. u. allgem. Chem. **247**, 249 (1941).

$\times 10^{-6}$ and at 4.2°K with a higher value of 0.46×10^{-6} emu/g.

Manganese

The sample of Mn came from Shull[3] and had been used in his neutron diffraction experiments. It had been heated by him in vacuo and then washed in acid. He gives its purity as 99.98 percent. The susceptibility measurements are illustrated in Fig. 2. There is a broad maximum at 125°K, and a large increase in susceptibility at liquid hydrogen and helium temperatures. This particular sample was analyzed by J. V. Gilfrich and E. D. Adams of the Naval Ordnance Laboratory for gas content, using vacuum fusion methods, with the following results: 0.00016 percent hydrogen, 0.0014 percent nitrogen, and 0.0011 percent oxygen by weight. The gas measured is from all sources, whether free or combined in chemical compounds such as MnO and MnO_2. It is believed that these quantities of gas are so small that they would not influence the susceptibility measurements.†

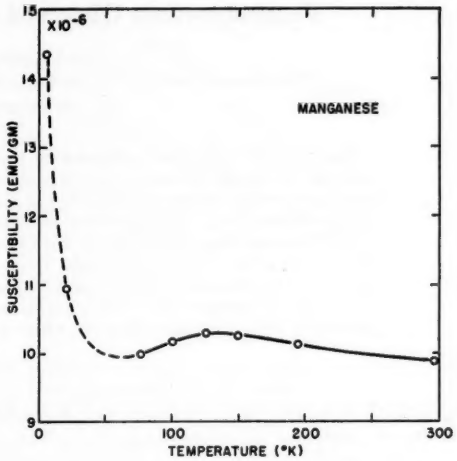

FIG. 2. Magnetic susceptibility of manganese as a function of temperature.

DISCUSSION

The behavior of hafnium is less complicated than that of manganese. The increase in susceptibility (χ) with temperature exhibited by this element is also found in other metals, such as tungsten, molybdenum[1] and chromium.[7] This temperature dependence can be qualitatively accounted for by the band theory of metals.[1,8,9] In general, the temperature coefficient depends critically on the shape of the density-of-states curve. An increase or decrease of χ with T depends on the position of the Fermi limit with respect to a maximum or minimum in the band form. Presumably, a more complicated temperature dependence of χ can be accounted for by assuming a more complicated band structure. The fact that the susceptibility of hafnium increases with temperature fits in with the band theory interpretation given by Kriessman and Callen,[1] which predicts that the temperature dependence of the susceptibility of the transition elements should be periodic with the columns in the periodic table.

The existence of ferromagnetic impurities that disappear with heat treatment as found in hafnium is not unusual. Evidently, iron impurities in uranium[7] have the same effect. It is believed that at the higher temperatures the ferromagnetic impurities are converted to paramagnetic compounds. If, now, this paramagnetism has a Curie law behavior, one would expect a slight increase to occur in the susceptibility at very low temperatures. Therefore, the increase in the χ of hafnium observed at 4.2°K might be due to this type of impurity.

The maximum in the susceptibility of manganese is almost certainly identified with antiferromagnetism. These measurements would place the Curie temperature at 125°K. Comparing the behavior of metallic manganese to antiferromagnetic compounds such as MnO and Cr_2O_3, one finds the same general features in the shape of the susceptibility curve. Shull[3] estimates the antiferromagnetic moment of the manganese atom as a few tenths of a Bohr magneton. With such a small moment, it is believed that the antiferromagnetism has only a small effect on the over-all susceptibility.

If the antiferromagnetism is ignored, then manganese shows a decreasing susceptibility from 4.2°K up to almost 1000°K, where a crystal structure transition occurs. This behavior is in qualitative agreement with the band theory treatment[1] mentioned above.

Palladium,[10] which also has a maximum at low temperatures, seems to exhibit the beginnings of a new susceptibility rise at 20°K, so that its over-all behavior may be analogous to that of manganese. There are also examples of antiferromagnetic compounds such as CoF_2 and NiF_2,[11] in which, below the Curie temperature, there is an increase in the susceptibility suggestive of the behavior of manganese.

ACKNOWLEDGMENTS

We wish to thank the personnel of the Cryogenics Section of the National Bureau of Standards for their cooperation in supplying the liquid helium used in this work.

† *Note added in proof.*—Recent work by Arrott, Coles, and Goldman indicates the low-temperature susceptibility of manganese may be very sensitive to small amounts of impurities, and that the increase below 77°K is due to impurities (private communication from J. E. Goldman, to be published).

[7] T. R. McGuire and C. J. Kriessman, Phys. Rev. **85**, 452 (1954) and **85**, 71 (1952).

[8] E. C. Stoner, Proc. Roy. Soc. (London) **A154**, 656 (1936); E. C. Stoner, Acta Metallurgica **2**, 259 (1954).

[9] E. P. Wohlfarth, Phil. Mag. **40**, 1095 (1949); Proc. Roy. Soc. (London) **A195**, 434 (1949).

[10] F. E. Hoare and J. C. Mathews, Proc. Roy. Soc. (London) **A212**, 137 (1952).

[11] W. J. deHaas and B. H. Schultz, Physica **6**, 481 (1939).

Paramagnetism Observed at the Superconducting Transition

YOSHIO SHIBUYA AND SEIICHI TANUMA
The Research Institute for Iron, Steel, and Other Metals, Tohoku University, Sendai, Japan
(Received December 17, 1954)

Measurements have been performed on the paramagnetic effect in superconducting tin. The current minimum, I_0, for the appearance of the paramagnetic effect is represented in the $(I-H-T)$ space by the simultaneous equations $I_0=\xi\gamma d(T_c-T)$ and $H_0=\xi(T_c-T)-I_g/\gamma d$. Here I_g, γ, T_c, and ξ are the characteristic constants of the superconductor and have the values 1.2 amp, 0.23 amp/mm oersted, 3.73°K and 1.1×10^2 oersteds/deg respectively for the case of tin. H_0 and d are the magnetic field in oersteds and the specimen diameter in mm respectively. It has been shown that the formula $I_0=I_g+\gamma dH$ hitherto accepted for the minimum current requirement is the one for the orthogonal projection of the critical line in the $(I-H-T)$ space on the $(I-H)$ plane. It seems that there is a lower limit of specimen diameter for the appearance of the paramagnetic effect, which is 1.3×10^{-2} mm for the case of tin.

MEISSNER *et al.*[1,2] and Teasdale and Rorschach[3] have confirmed the paramagnetic effect first discovered by Steiner and Schoeneck.[4,5] We also investigated the paramagnetic effect, and in particular the question of the existence of hysteresis phenomena in the effect.

Two cylindrical specimens were prepared from Johnson-Matthey spectroscopically pure tin; one specimen is a single crystal of diameter 2.4 mm and length 70 mm, and the other specimen is a polycrystalline specimen of diameter 1.5 mm and length 86 mm.

We employed first the static method, similar to that used by Mendelssohn *et al.*,[6] of dropping an induction coil in a uniform magnetic field from a position 7 cm above the specimen to the center portion. We measured the deflection of a ballistic galvanometer connected to the coil. The deflection is proportional to the change of total flux through the coil. For the study of the intrinsic nature of the paramagnetism, measurements were carried out in such a way that two variables, the longitudinal magnetic field H and the temperature T, were held constant throughout, while the third variable, the current I through the specimen, was changed in small steps. The coil was dropped at each step. The hysteresis measurement consisted in holding I and T constant throughout and reducing H in small steps from the value above H_c to zero, followed by a similar increase in H. At the present stage of the investigation, we can conclude that there is no hysteresis and the effect is quite reversible.

The formula for the minimum current requirement proposed by Steiner[4] and extended by Meissner *et al.*[1] is

$$I_0=I_g+\gamma dH. \tag{1}$$

Here I_g and γ, which are characteristic constants of the superconductor, are 1.2 amp and 0.17 amp/mm oersted respectively for tin, when the specimen diameter d and the magnetic field H are measured in mm and in oersted respectively. According to this formula it seems always possible, irrespective of temperature, to observe the paramagnetism with a current larger than I_0 for a fixed value of H. Actually, however, there is a one-to-one correspondence between H in Eq. (1) and the temperature T. Therefore, the current minimum required for the paramagnetism should be determined as a curve in three-dimensional $(I-H-T)$ space, instead of by Eq. (1). The determination of the current minimum referred to above was carried out by holding T constant throughout, taking I as a parameter, and reversing H; the latter was changed in small steps. In this determination the induction coil was fixed around the center of the specimen, and a compensating coil connected in opposition to the induction coil was placed above the specimen in the region of uniform field. Figure 1 is a typical example of the results; a/b shown in the inset gives the apparent permeability μ, which is a function of H provided I and T are constant. μ^*, which designates the maximum of μ for the fixed values of I and T, has a meaning similar to that of $\tilde{\mu}$ defined by Meissner *et al.*[1] μ^* was plotted against I, and the extrapolation to the abscissa for which $\mu^*=1$ defines the current minimum I_0 at that temperature. In this way the I_0-T relation was obtained. This gives the orthogonal projection of the critical line characterizing the current minimum on the $(I-T)$ plane. In a similar way, we plot μ^* against H to obtain H_0, the magnetic field over which we cannot observe the paramagnetism at a given temperature, by the extrapolation to the abscissa. In this way we obtain the H_0-T relation, which is the projection of the critical line on the $(H-T)$ plane. The critical line was determined as a straight line in the $(I-H-T)$ space from two projections obtained. Figure 2 shows schematically the relations between I_0, H_0, and T for two specimens. The critical lines terminate at the points (I_g, T_g) on the $(I-T)$ plane. Though T_g depends on the specimen diameter, I_g is constant, irrespective

[1] Meissner, Schmeissner, and Meissner, Z. Physik **130**, 521, 529 (1951); Z. Physik **132**, 529 (1952).
[2] Meissner, Schmeissner, and Meissner, Phys. Rev. **90**, 709 (1953).
[3] T. S. Teasdale and H. E. Rorschach, Jr., Phys. Rev. **90**, 709 (1953).
[4] K. Steiner and H. Schoeneck, Physik Z. **44**, 346 (1943).
[5] K. Steiner, Z. Naturforsch. **4a**, 271 (1949).
[6] Mendelssohn, Squire, and Teasdale, Phys. Rev. **87**, 589 (1952).

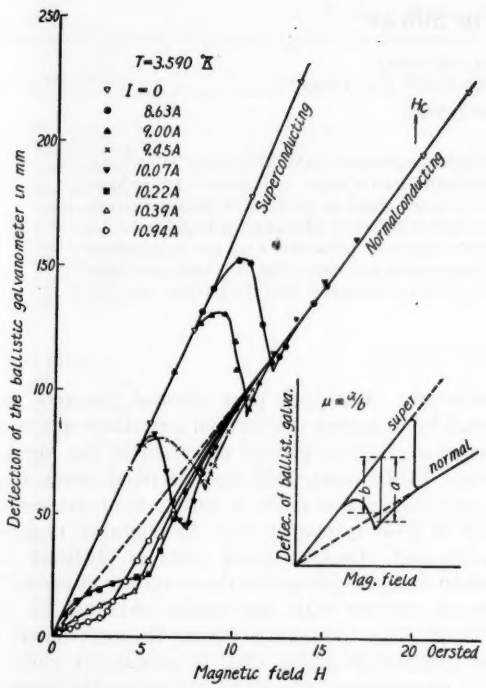

FIG. 1. The deflections of a ballistic galvanometer when the external magnetic field was reversed. a/b shown in the inset gives the apparent permeability μ.

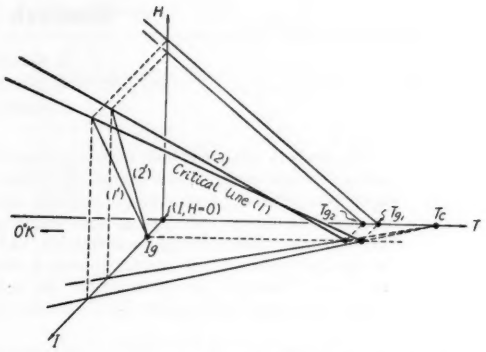

FIG. 2. The minimum of current necessary for the appearance of the paramagnetic effect for two specimens in the three dimensional space. The critical lines (1) and (2) belong to the specimens of diameter 2.4 mm and 1.5 mm respectively. The $(I-H)$ projections (1') and (2') of the critical lines are represented well by Eq. (1) in the text.

of the diameter. All the $(I-T)$ projections of the critical lines point to the transition temperature T_c. The $(H-T)$ projections are parallel to each other and T_c-T_g is inversely proportional to d. The critical line is represented in the three-dimensional space by the following simultaneous equations:

$$I_0=\xi\gamma d(T_c-T), \quad H_0=\xi(T_c-T)-I_g/\gamma d. \qquad (2)$$

I_g, γ, T_c, and ξ are the characteristic constants of the superconductor and have the values 1.2 amp, 0.23 amp/mm oersted, 3.73°K, and 1.1×10^2 oersteds/deg respectively for the case of tin. The relation found by Meissner *et al.* corresponds to the one concerning the $(I-H)$ projection of the critical line. Indeed, the projection is represented by Eq. (1) which can be drived from Eq. (2). Though we obtained $\gamma=0.23$ amp/mm oersted instead of 0.17 amp/mm oersted, we verified in the $(I-H-T)$ space that I_g, the minimum current for zero field, was 1.2 amp.

We observed, moreover, the approximately periodic dependence of μ on the magnetic field, apparently similar to the de Haas-van Alphen effect, when measurements were performed in such a way that the magnetic field was changed in smaller steps than usual; for instance, at $I=4.50$ amp and $T=3.697$°K for the case of the specimen of 2.4 mm diameter.

We plotted contour lines for which $\mu=$const in the $(I-H)$ planes at the temperatures studied in order to determine the paramagnetic region in the $(I-H-T)$ space and we obtained closed contour lines at temperatures near T_g. The lines converge with increasing values of μ to the point of finite maximum at finite values of I and H. Finally, although the extension of the I_0-T relation to the absolute zero of temperature would not be permissible, it seems from this extension that there is a lower limit of specimen diameter, d_0, for the appearance of a paramagnetic effect. The limit can be deduced from the equation $I_g=\xi\gamma d_0 T_c$. For the case of tin d_0 is 1.3×10^{-2} mm.

Experiments on other superconductors such as mercury and indium are in progress. A detailed report on the experiment described here will appear in a forthcoming issue of Science Report, Research Institute Tohoku University. We would like to express our thanks to Professor T. Fukuroi who gave us facilities for experiments and helpful suggestions.

Seebeck Effect in Silicon

T. H. GEBALLE AND G. W. HULL
Bell Telephone Laboratories, Murray Hill, New Jersey
(Received February 3, 1955)

The Seebeck effect has been measured from liquid hydrogen temperatures into the intrinsic range for a series of single-crystal silicon samples in which varying concentrations of donor and acceptor atoms have been incorporated. Large values of Seebeck voltage believed to be caused by the type of phonon-electron coupling previously postulated as occurring in germanium have been found. This effect is found to be dependent upon charge carrier concentration, and upon sample dimension below 100°K. A low-temperature reversal of the sign of the Seebeck voltage is observed for large carrier concentrations. It is understandable in terms of impurity band conduction. The behavior above room temperature into the intrinsic range is found to be consistent with electrical conductivity data.

INTRODUCTION

THE previously reported investigations of the Seebeck effect in germanium[1,2] have proved to be understandable in terms of the band structure of germanium and have also indicated an interesting type of interaction between mobile charge carriers and phonons. We have therefore been led to extend this type of study to silicon, where considerable knowledge of the band structure has recently been obtained from cyclotron resonance experiments.[3] Good single crystals of silicon are now available in which a type of mobile charge carrier-phonon interaction similar to that found in germanium should be likely to exist. There have been no recent investigations reported in the literature other than on a few samples of polycrystalline material.[4,5]

EXPERIMENTAL PROCEDURE

We are indebted to Morin and Maita for making available the same set of silicon samples containing boron and arsenic used in their investigation of the electrical properties of silicon.[6] These samples were measured in the apparatus previously described.[1] The following method was adopted in order to make low-impedance ohmic electrical contacts as well as good thermal contacts between the thermocouple blocks and the sample. First a small region of high electrical conductivity was produced on the surface. This was accomplished by alloying a small amount of gold, containing a few percent antimony (for *n*-type) or aluminum (for *p*-type), to the surface of the sample directly under the thermocouple. A thin layer of silver paste was fired on to this region at 550°C for 10 minutes. This provided a surface which could be wet easily with solder but was omitted for high-resistivity samples where heat treatment might affect the carrier concentration. Occasional poor thermal contacts were noted by observing the thermal impedance across the copper-silicon junctions as described in the previous paper. In all cases, Hall and electrical conductivity measurements were made at various temperatures and were in good agreement with the published results of Morin and Maita.[6] Seebeck voltages obtained with helium or hydrogen gas in the container disagreed by several percent with the results obtained in high vacuum. This indicates a poorer thermal contact at the junctions in silicon than in germanium where no such disagreement was found. This made it necessary to make all measurements in high vacuum.

The very high thermal conductivity of the purer silicon samples in the low-temperature range made it appear likely that end effects in the flow of heat could complicate the measurement of the temperature difference between the junctions. We were led therefore to measure a few samples with a geometry designed to minimize end effects. This was accomplished by measuring some long (about 10 cm) filaments of rectangular cross section. The thermocouples were secured in the central portion away from boundaries. The heater was constructed from No. 40 manganin wire wrapped directly onto the filament. Short lengths of No. 28 copper wire were wrapped and soldered around the filament at each thermocouple-silicon junction and used to minimize temperature gradients along the thermocouple leads near the junction. The region between the thermocouples was electrically probed at room temperature and in the samples used was uniform to 20 percent. The sample was mounted in a conventional apparatus consisting of a radiation shield inside an evacuated container. The bottom of the sample was soldered to the radiation shield which was in thermal contact with the bath. The lead wires were brought to the temperature of the radiation shield and were sufficiently long to insure a negligible heat leak along the wires and thus making thermal conductivity measurements possible.[7] Lead wires for electrical conductivity measurements were attached at the filament ends and in some

[1] T. H. Geballe and G. W. Hull, Phys. Rev. **94**, 1134 (1954).
[2] H. P. R. Frederikse, Phys. Rev. **92**, 248 (1953).
[3] Dexter, Lax, Kip, and Dresselhaus, Phys. Rev. **96**, 222 (1954); R. N. Dexter and B. Lax, Phys. Rev. **96**, 223 (1954).
[4] A. E. Middleton and W. W. Scanlon, Phys. Rev. **92**, 219 (1953).
[5] J. Savornin and F. Savornin, Compt. rend **235**, 465 (1952); **236**, 898 (1953); B. I. Boltaks, J. Tech. Phys. (U.S.S.R.) **20**, 3 (1950).
[6] F. J. Morin and J. P. Maita, Phys. Rev. **96**, 28 (1954).
[7] These results have been summarized: G. W. Hull and T. H. Geballe, Phys. Rev. **96**, 846 (1954).

TABLE I. Dimensions and composition of samples.

Sample No.	Area, cm²	Distance between thermocouples, cm	Donor concentration, cm⁻³	Acceptor concentration, cm⁻³
		n-type		
131 bridge[a]	0.086×0.16	1.1	2.75×10^{14} arsenic	1.0×10^{14}
537 filament	0.47 ×0.47	3.8	3.7×10^{14} phosphorous	9×10^{13}
566 filament	0.12 ×0.47	3.8	similar to 537	
565 filament	0.078×0.087	1.7	similar to 537	
130 bridge[a]	0.093×0.16	1.2	2.6×10^{15} arsenic	5×10^{14}
129 bridge[a]	0.084×0.16	1.2	2.2×10^{16} arsenic	1.5×10^{15}
139 bridge[a]	0.12 ×0.16	1.2	1.3×10^{17} arsenic	2.2×10^{15}
563 bridge[b]	0.12 ×0.16	1.1	1.1×10^{18} arsenic	1.0×10^{18} boron
126 bridge[a]	0.085×0.16	1.2	2.2×10^{18} arsenic	
140 bridge[a]	0.12 ×0.16	1.2	2.7×10^{19} arsenic	
		p-type		
127 bridge[a]	0.12 ×0.16	1.2	2.2×10^{14}	9.2×10^{14} boron
552 filament	0.50 ×0.50	4.3	1.9×10^{14}	1.0×10^{15} boron
559 filament	0.25 ×0.18	2.75	similar to 552	
117 bridge[a]	0.085×0.16	1.1	2.3×10^{16}	2.6×10^{16} boron
119 bridge[a]	0.086×0.16	1.2	4.9×10^{15}	2.0×10^{17} boron
141 bridge[a]	0.12 ×0.16	1.1		1.0×10^{18} boron
125 bridge[a]	0.084×0.16	1.0		1.5×10^{19} boron
		Measured in intrinsic range		
554 (b)	0.040×0.67	1.5	similar to 537	
562 filament	0.078×0.25	5.0	similar to 537	
561 filament	0.058×0.25	5.0	similar to 552	
561 (a)			filament 561, second series of measurements	

[a] Concentration data for these samples taken from reference 6.
[b] Concentration data for all samples except 563 estimated from curve fitting of Hall data as described in reference 5. Data for sample 563 estimated from growth conditions as indicated in text.

cases Hall leads were attached midway between the thermocouples. Samples measured in this apparatus are referred to as "filaments" and in the previous apparatus as "bridges." Bridges and filaments were lightly sandblasted with 180 mesh silicon carbide powder on all surfaces.

EXPERIMENTAL RESULTS AND ANALYSIS

In this section, we shall consider the experimental data obtained for the 20 samples characterized in Table I. The data for samples measured in the extrinsic range are presented in Figs. 1 and 2. The QT product, where Q is the thermoelectric power, is plotted as a function of the absolute temperature T for n-type samples in Fig. 1, and for p-type samples in Fig. 2. It can be seen that there are certain common types of behavior and also some strikingly different types; these are discussed in detail in the following sections.

1. Dependence of Q upon Carrier Concentration near Room Temperature

It can be seen from Figs. 1 and 2 and Table I that the samples with the highest value of QT around room temperature are those with the smallest concentration difference between the donor and acceptor atoms, that is, those with the smallest density of mobile charge carriers. This is the same type of behavior observed for germanium and is to be expected for any model in which the thermoelectric energy is transported by mobile charge carriers. In fact for any two samples in Fig. 1, or any two samples in Fig. 2, other than the degenerate samples No. 125 and 140, $(Q_2-Q_1)=\log(n_1/n_2)$ near room temperature, where n is the charge carrier density. This probably means that the activity coefficients of the mobile carriers and the kinetic energy transported by them [ΔE_T of Eq. (1), reference 1] are constant over the concentration range 10^{-6} to 10^{-2} mole percent.

2. The Contribution Due to Phonon-Electron Scattering

It is evident from the marked rise in Q at low temperatures that the phonon-electron coupling mechanism invoked by Herring[8] and Frederikse[2] to explain the germanium data must also be present in silicon. Using Eqs. (4) and (5) of the previous paper,[1] assuming a density of states mass, $N_v^{\frac{2}{3}}m^*/m$, equal to unity we have calculated values of Q_p. Q_p is the contribution to Q arising from the anisotropic phonon-electron scattering. The values are plotted for the nondegenerate n-type samples in Fig. 3 and for the nondegenerate p-type samples in Fig. 4. Values for samples 127 and 130 have been omitted. Inspection of curves for those samples in Figs. 2 and 1, respectively, shows a discontinuity at low temperatures. In both cases, the discontinuity was observed upon warming from liquid hydrogen to liquid nitrogen temperatures and was accompanied by an

[8] C. Herring, Phys. Rev. 96, 1163 (1954).

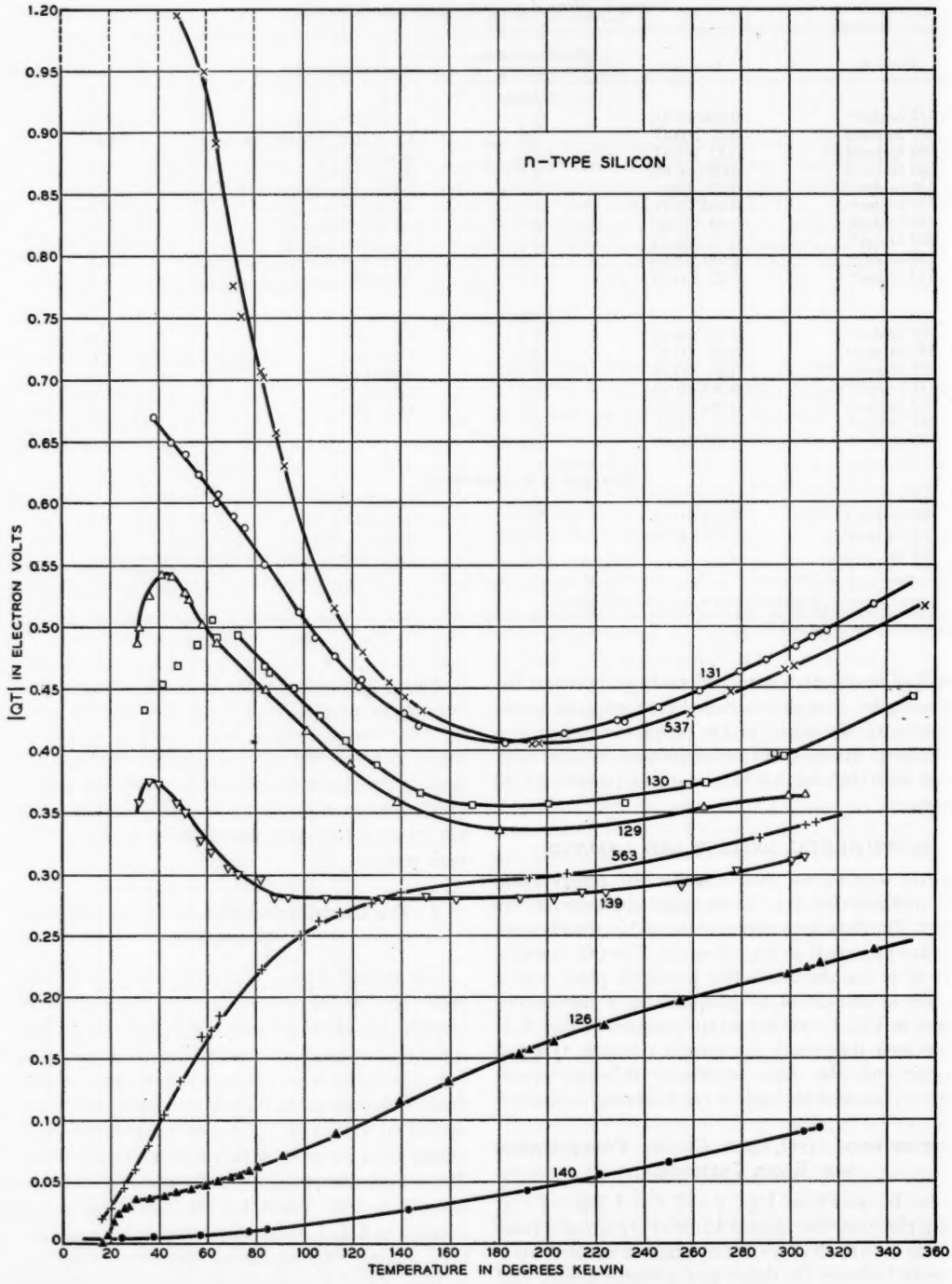

FIG. 1. Measured values of the QT product for eight n-type samples listed in Table I.

increased thermal gradient across the thermocouple-silicon junction. This was determined by the differential thermocouples shown in Fig. 1 of the previous paper. The other samples showed no such effects and therefore they are the ones considered here.

The pure n- and p-type filaments of large dimension

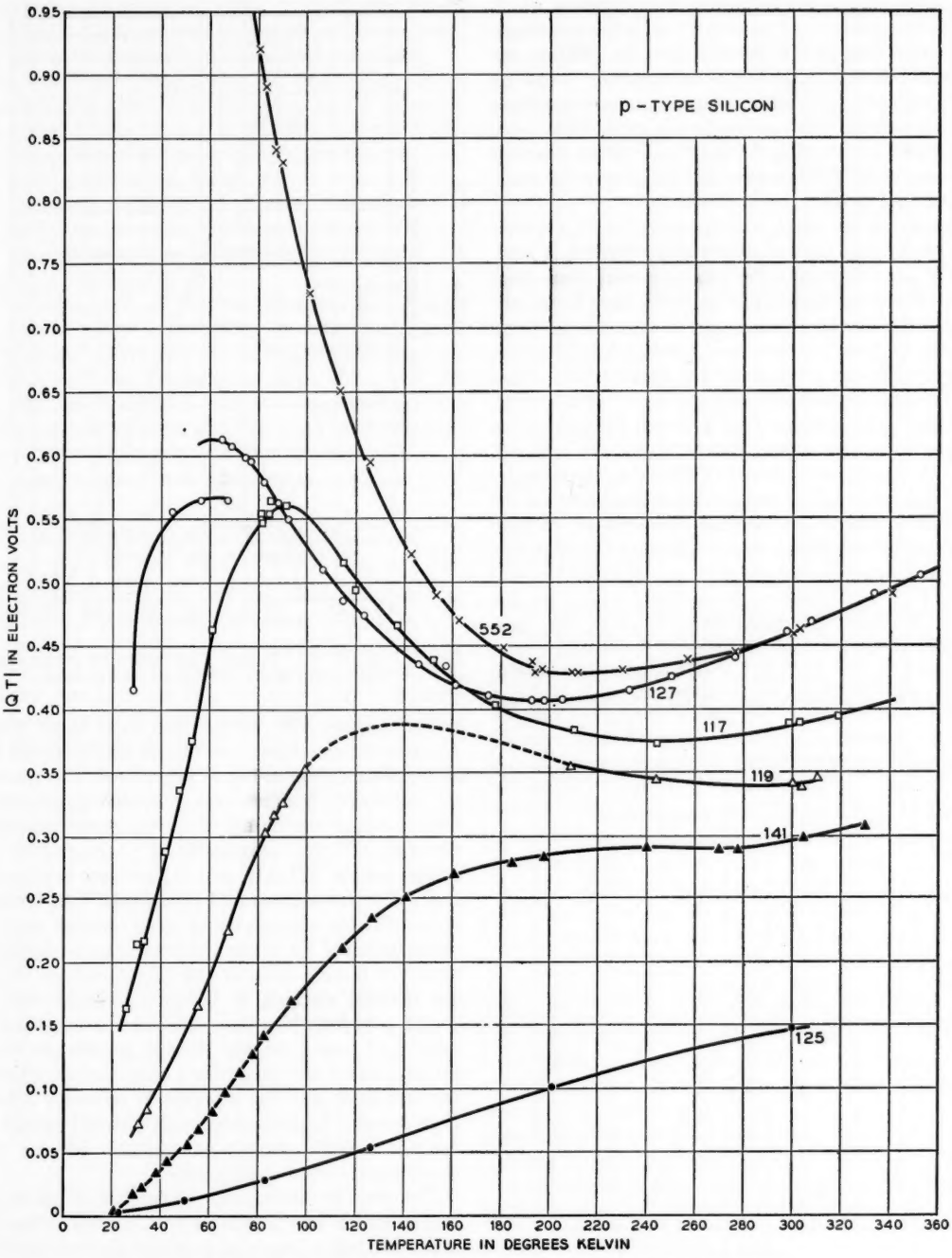

FIG. 2. Measured values of the QT product for six p-type samples listed in Table I.

(No. 537 and No. 552) have a value of Q_p proportional to $T^{-2.3}$ over a wide range of temperature. This is shown in Figs. 3 and 4. This is the general type of behavior predicted by Herring (reference 8, Sec. V) for the ideal case where the carrier concentration is small, where there is no boundary scattering and where the temperature is well below the Debye temperature. However, the magnitude of the exponent, 2.3, is much lower than the theoretical expectation for the ideal case which is from 3.5 to 4.0. The effect of the finite size of

the sample and of the saturation effect, both of which are discussed below, act so as to decrease the magnitude of the exponent at low temperatures. In addition the expected behavior as the Debye temperature (~650°K) is approached is also such as to reduce the magnitude of the exponent. The combination of these effects may be influential in causing the magnitude of the observed exponent to be less than the ideal value over the whole temperature range.

The saturation effect in reference 8, Sec. 7, becomes important when the concentration of carriers is sufficiently great to perturb the phonon system away from the steady state distribution it would have in the absence of the carriers and acts so as to decrease Q_p. There is evidence from thermal conductivity data that the bridge results are consistently low below 100°K where the thermal conductivity becomes high. This is probably due to nonuniform heat flow near the ends of the bridges where the thermocouple blocks are soldered. For this reason, we choose to compare bridge samples only with other bridge samples when analyzing for the saturation effects, but hesitate, for example, to infer anything by comparing bridge 131 with filament 565. The strikingly low values of Q_p for samples 126 and 141 in Figs. 3 and 4 are partly ascribed to the saturation effect. However, the rapid drop off of Q_p for these samples at the low temperature end is believed due to "impurity band" conduction and is discussed further below. The saturation effect is clearly evident in the

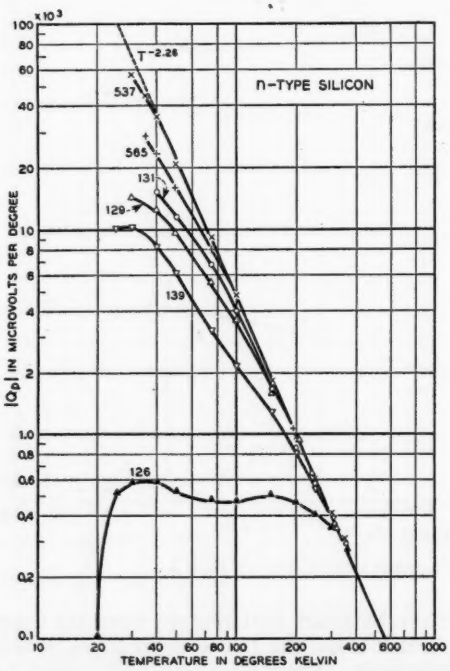

FIG. 3. Dependence of Q_p upon temperature for n-type samples which differ in size or donor concentration.

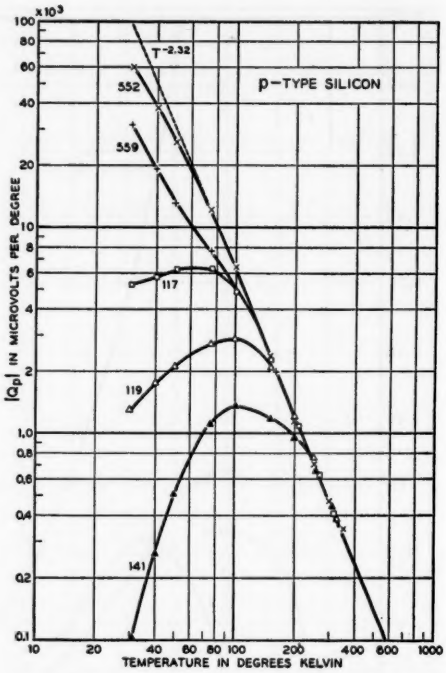

FIG. 4. Dependence of Q_p upon temperature for p-type samples which differ in size or acceptor concentration.

n-type samples, 126, 139 and 129, even above 100°K. At lower temperatures, the carrier concentration falls off rapidly as given in Fig. 6, reference 6. This prevents the values of Q_p from saturating out more rapidly except for the case of sample 126 where the carrier concentration falls off much less rapidly with temperature. The p-type samples 141, 119, and 117 saturate in a qualitatively different manner and at not such high temperatures. This is not surprising. It is evident that the perturbation of the phonon system must be dependent upon the inertial mass of the charge carriers. Indeed the detailed analysis of Herring indicates that the p-type samples which have the larger average inertial mass[2] and thus a smaller thermal wavelength should saturate to a lesser extent for a given concentration. If the spin-orbit splitting reported in reference 2 for p-type samples is comparable with thermal energy the analysis for the phonon contribution will be more complicated than our simple one.

The effect of the finite size of the sample can be seen in Fig. 5. The n-type sample No. 537 was reduced by approximately a factor of 4 in one cross-sectional dimension to make sample 566; sample 565 was prepared from an adjacent slice with each cross-sectional dimension reduced by a factor of 6. It can be seen from the figure that this caused a reduction of 18 percent and 32 percent respectively in the measured values of Q at 55°K. In terms of Q_p the reduction is almost the same since the electronic contribution, Q_e, amounts to only

5 percent of the measured value. At 30°K, the 36-fold reduction in the cross section of sample 565 has caused a 44 percent reduction in the measured value of Q.

For the p-type sample No. 552 a reduction of the cross-sectional area by a factor of 2×2.8 caused a decrease of 10 percent in Q at 55°. The lower-temperature values shown as dashed in the figure are uncertain to about ±10 percent because of an unaccountably low measured value of the thermal conductivity of sample 559. In all cases, the electrical conductivity of the reduced dimension samples checked that of the original sample.

The persistence of the size effect to an absolute temperature about 5 times that at which size effects are important in thermal conductivity measurements is similar to the case of germanium. Again this is evidence that the thermoelectric energy transported by the phonon system which is given by the Q_pT product resides largely in long-wavelength phonons. This is a basic assumption in Herring's theory.

3. Measurements at High Concentration of Donors and Acceptors[9]

It is evident from the mobility data of Morin and Maita, Figs. 8 and 9, reference 6, that there must be a different type of mechanism responsible for the low mobilities of samples 126 and 141. They suggest that impurity band conduction by low-mobility carriers may be occurring. We are able to offer further evidence that this indeed is the case.

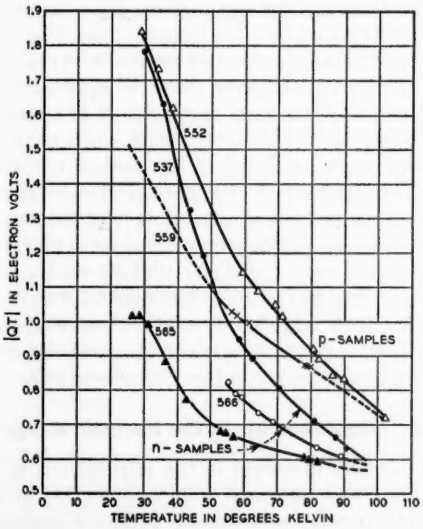

FIG. 5. Dependence of measured value of QT upon sample dimension for n-type and p-type samples. At higher temperatures the curves merge to within 1 percent of that shown for sample 537 in Fig. 1 or sample 552 in Fig. 2.

[9] The results given below were presented in part at the Seattle meeting of the Physical Society [Phys. Rev. 96, 847(A) (1954)].

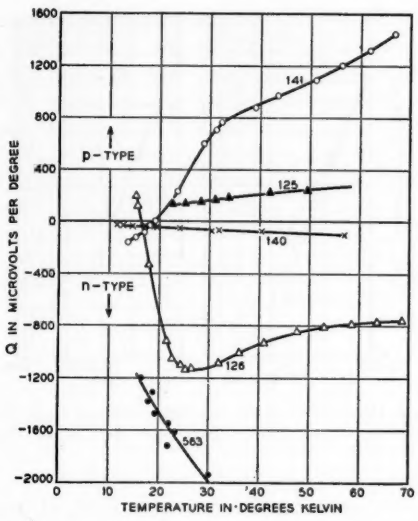

FIG. 6. Low-temperature results for samples with large donor or acceptor concentrations showing how the reversal of sign of the nondegenerate samples 126 and 141 differs from the degenerate samples 125 and 140.

By impurity band conduction is roughly meant the charge transfer between donor or acceptor atoms interacting directly.[10] In sample 126, there is approximately 1 arsenic atom per 2×10^4 silicon atoms and in sample 141 there is approximately one boron atom per 5×10^4 silicon atoms. Therefore, assuming a random distribution of donor and acceptor atoms, charge carriers must interact at the order of 10 to 20 lattice distances. The energy level associated with the isolated donor or acceptor atom is broadened into an energy band. This is the so-called impurity band. For sample 126 there are only 2×10^{15} electrons per cc in the conduction band at 25°K. In this sample the donor atoms greatly outnumber the acceptor atoms; that is, the sample is not highly compensated. This means that below 25°K most of the electrons are attached to arsenic atoms and are interacting to form the impurity band. If the impurity band is practically full, and if it does not overlap the conduction band, it should act like the valence band of a semiconductor and give rise to a positive Seebeck effect. This indeed we believe is the qualitative explanation of the reversal of sign shown in Fig. 6. The Seebeck voltage goes from negative to positive at 16°K. It becomes more positive as the temperature is lowered, perhaps roughly according to the equation

$$Q=(Q_e\sigma_e+Q_i\sigma_i)/\sigma, \qquad (1)$$

where σ is conductivity and the subscripts refer to conduction and impurity bands. This equation follows from the crude assumption that the impurity and

[10] This mechanism has been discussed recently by many authors, see footnote 11 of reference 8. See also C. Hung and J. R. Gliessman, Phys. Rev. 96, 1226 (1954).

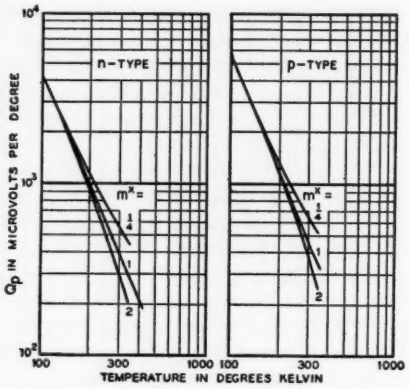

FIG. 7. Dependence of the calculated value of Q_p of the purer samples upon choice of mass parameter used in the density of states equation.

conduction bands are acting in parallel. Q_i must be essentially constant below 25°K. This is because the small percentage of compensation by the acceptor atoms present is now large with respect to the number of electrons in the conduction band, n_c; hence the number of holes in the impurity band is almost constant. Since σ_c varies directly as n_c while Q_c varies as $-\log n_c + dQ_p/dT$, σ_c is probably the dominant term in Eq. (1) for values of Q near 0. A value of Q_i would enable one to estimate the energy difference between the conduction band and the almost filled impurity band by a plot of $\log(Q_c - Q)$ against $1/T$. We are currently constructing apparatus that will extend the measurements to lower temperatures in order to provide an experimental estimate of Q_i.

The aforementioned model can equally well explain the reversal of the Seebeck voltage of the normally p-type sample No. 141 at 19°K.

In order to test this model further, a crystal was grown with both arsenic and boron present. From this crystal, sample 563 was prepared. From the growth

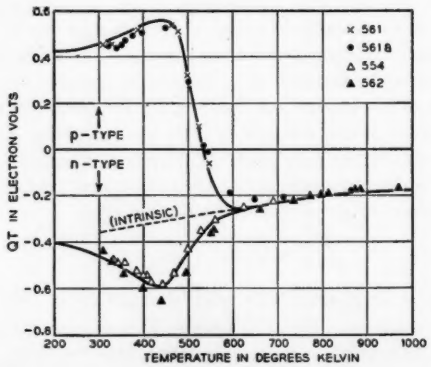

FIG. 8. Calculated values (curves) and measured values (points) for n-type and p-type samples measured into the intrinsic range.

conditions of the sample, and taking the distribution coefficient of boron in silicon as 1,[11] it is estimated that the concentration of boron in sample 563 is 1.0×10^{18}. The room-temperature Hall effect gives the concentration of arsenic as 1.25×10^{17} atoms per cc greater than the boron concentration. Thus sample 563 is about 90 percent compensated. At low temperatures, therefore, the impurity band must be only about 10 percent full. On the basis of the sample model described above, Q should not change sign. The low-temperature experimental points taken for the sample are also shown in Fig. 6. The general nature of the curve can be seen in Fig. 1. Because of the difficulty of measuring a small voltage over a high-impedance circuit, the low-temperature points scatter; however, they appear to extrapolate to 0 at $T=0$. This is the limit required by the third law. More conclusive evidence must await the extension of the measurements to lower temperatures.

4. The Effective Mass

The effective mass which enters into the density of states equation [Eq. (2), reference 1] can be determined by a comparison of charge carrier density with the electronic contribution to the thermoelectric power, Q_e. This is discussed in the previous paper.[1] In the present case it is difficult to obtain an accurate value of Q_e at room temperature because of the uncertainty in Q_p. Q_p in silicon does not extrapolate to a small value as it does in germanium. An uncertainty of 90 μv is equivalent to a factor of two in the mass parameter. We have chosen a mass parameter of unity since this minimizes the curvature in the $\log Q_p$ *versus* $\log T$ curves near room temperature. It can be seen from Fig. 7 that changing the mass parameter results in curvature. In this figure curves are given for Q_p of samples 537 and 552 calculated for a mass parameter of $\frac{1}{4}$, 1, and 2. It is seen that Herring's theory which predicts $Q_p \propto T^{-n}$ at temperatures well below the Debye temperature agrees with a choice of mass parameter close to unity. A value near unity is in agreement with the results of Dexter, Lax, Kip, and Dresselhaus[2] for n-type silicon which give a value $N_v^{\frac{2}{3}} m^*/m = 6^{\frac{2}{3}}(0.26) = 0.86$. A comparison of the p-type results is difficult due to spin-orbit splitting. The results in the following section, above room temperature, where Q_p is smaller are not accurate enough to use in this type of analysis.

5. Measurements in the Intrinsic Range

The samples measured in the intrinsic region listed in Table I were prepared from samples 537 and 552. The measurements were made in a conventional manner in a vertical furnace using platinum-platinum rhodium thermocouples. The Seebeck voltage was read across the Pt leads. Due to the high thermal conductivity of the silicon, it was necessary to reduce the cross section

[11] N. B. Hannay (personal communication).

of the samples between the thermocouples in order to avoid radial thermal discontinuities. The points shown in Fig. 8 are the measured values. The curves are calculated from the equation

$$QT=[(Q_+n_+\mu_+ + Q_-n_-\mu_-)T_+ + Q_{(Pt)}T]/(n_+\mu_+ + n_-\mu_-) \quad (2)$$

Q_+ and Q_- are the values either the holes or electrons would have in the absence of the other. The values include a phonon contribution estimated from Figs. 3 and 4. $Q_{(Pt)}$, the absolute thermoelectric power of platinum, is used in order to have the calculated value apply to the silicon-platinum couple. It is important only in the purely intrinsic range where it amounts to something less than a 10 percent correction. The concentrations of holes and electrons, n_+ and n_-, and their mobilities μ_+ and μ_-, have been taken from the data of Morin and Maita.[6] Values of $|n_+-n_-|$ are determined from resistivity measurements in the saturation region taken concurrently with the thermoelectric readings using the thermocouples as potential probes. These are combined with the values of $(n_+n_-)^{+\frac{1}{2}}$ given in Fig. 13 of Morin and Maita. The values of μ_+ and μ_- are taken from the extrapolated values given in their Fig. 12. These represent a major uncertainty. The reasonable agreement shown in Fig. 7 is significant in demonstrating the overall consistency of the data; however, it seems doubtful that the choice of different mass parameters to improve the fit would be meaningful.

ACKNOWLEDGMENTS

We are greatly indebted to C. Herring and F. J. Morin for many useful comments and discussions concerning the ideas presented here. We also wish to acknowledge the important contribution of E. Buehler and E. Kolb in preparing the single crystals of silicon from which our samples were prepared.

PHYSICAL REVIEW VOLUME 98, NUMBER 4 MAY 15, 1955

Plasma Oscillations in Metals

E. N. Adams
Institute for Nuclear Studies, University of Chicago, Chicago, Illinois
(Received July 26, 1954; revised manuscript received February 7, 1955)

The self-consistent field treatment of the electronic wave functions of a solid is used as a basis for a theory of plasma oscillations in a metal. Two procedures are used to calculate the plasma frequency, both being based on the Bohm and Pines method of introducing the plasma oscillators. It is found that band-to-band virtual transitions have a strong effect on the plasma oscillations in a metal. It is concluded that the effective mass treatments are not adequate to treat the electron-plasma interaction, except perhaps in certain semiconductors.

INTRODUCTION

In the last few years, several papers have appeared which discuss the theory of the formation of an electron plasma[1-5] in metals. In this paper we would like to treat an aspect of that problem which we believe has been given insufficient attention, *viz.*, the effect of the energy band structure on the plasma frequency.

The effect of the lattice potential on the plasma frequency has heretofore to our knowledge been treated only by Wolff,[5] who limited his explicit consideration to matrix elements of the electron-electron interaction leading to in-band scattering processes. Wolff estimated for a particular case the effects of interband scattering processes on the plasma frequency and found that they caused a large frequency shift. We will show in the following that for metals band-to-band processes are in general quite important, so that Wolff's quantitative results are probably limited in applicability to semiconductors.

Although previous work has sought to establish the dispersion relation for plasma waves, we have been content to calculate the plasma frequency for very long wavelength plasma waves. Our results indicate that this frequency is strongly affected by band-band virtual transitions, the effects of which are difficult to calculate accurately. We have not concerned ourselves, therefore, with extending the dispersion relation since we feel that this cannot be done correctly in a treatment which does not make an adequate treatment of band-band transitions.

In carrying out our calculations we have chosen to use the method of Bohm and Pines (BP)[2,3] for introducing the generalized coordinates of the plasma modes. We made this choice because we feel that their method is basically the simplest we know and leads most directly to the results we want. However, we suspect that certain aspects of their treatment of the auxiliary conditions are incorrect, and believe the problem of the auxiliary con-

[1] D. Bohm and E. P. Gross, Phys. Rev. **75**, 1851, 1854 (1949).
[2] D. Bohm and D. Pines, Phys. Rev. **85**, 338 (1952).
[3] D. Bohm and D. Pines, Phys. Rev. **92**, 609 (1953).
[4] D. Pines, Phys. Rev. **92**, 626 (1953).
[5] P. Wolff, Phys. Rev. **92**, 18 (1953).

ditions deserves further study. In the present work we do not solve the problem of satisfying the auxiliary conditions, so our treatment is on that score subject to the same criticism as is that of Bohm and Pines.

In the following sections, we will establish an "in principle" basis for treating the outer electrons of a metal as an electron gas, and then present two somewhat different procedures for calculating the plasma frequency. The first procedure is most easily applied to systems such as semiconductors in which the plasma frequency is small compared to the energy band spacing. It gives results which closely parallel those of Wolff. The second procedure is very much like the treatment of Bohm and Pines. It is most easily applied to systems for which the plasma frequency is large compared to the energy band spacing. Actually in many metals the energy band spacing is comparable to the plasma frequency. Unfortunately neither of our procedures affords an accurate way of calculating the frequency in this case, so we are unable to add very much to Wolff's qualitative discussion of the absorption of plasma quanta which takes place when two bands are in "resonance" via an absorption process. However, we have set the theory up in such a way as to make it clear that shifts in the plasma frequency due to band-band transitions can be large whether or not the exact resonance condition is satisfied.

Our chief qualitative conclusion is that even in a "free electron" metal-like sodium, the band-band transitions should affect the plasma frequency strongly, so it is not generally correct to apply to metals the results of Bohm and Pines obtained for a free electron gas.

1. REDUCTION OF OUTER ELECTRON PROBLEM

We want to begin by discussing in a formal way how we can reduce the Schrödinger equation for the outer electrons. Since we are interested in treating correctly the field of the atomic cores, we will need to make use of some kind of self-consistent field (SCF) method to get inner-shell wave functions. We will want to use the energy band type solutions since we are concerned here with typically metallic properties.

For the simple calculations we will do, it is immaterial whether we suppose the use of the Hartree (H), Hartree-Fock-Slater (HFS), or some other[6] SCF procedure. However, we wish to comment on those characteristics of the SCF wave functions which would be most desirable if we were carrying through a complete configuration interaction calculation. Feasibility of mathematical treatment requires two things. First our one-electron wave functions should form a complete orthonormal set; second our inner-core wave functions should be so good that we need consider only a single configuration for the inner shell. In most cases the simple Hartree SCF wave function satisfies only the first of these conditions, but the HFS wave functions satisfy both. Thus the HFS set of SCF wave functions would be suitable for providing a "frame of reference" in the function space.

It is possible to conceive that some SCF procedure other than the HFS procedure would be best[6] for determining the one-electron wave functions which define the "fixed frame." Certainly the simple HFS method has the disadvantage that the dependence of energy on wave number is peculiar at the Fermi surface,[7] and that feature would be objectionable in some parts of the calculation. We have not made a study to determine the best way of choosing a SCF principle in general, but will merely suggest one which satisfies the two requirements of orthonormality and of giving good inner shell wave functions and has in addition one other desirable feature which will be discussed below. The suggested principle uses the following one-electron Hamiltonian for determining the one-electron wave functions:

$$H\psi(x)=[p^2/2m+V(x)+A_e(x)]\psi(x). \qquad (1.1)$$

The Schrödinger type Eq. (1.1) describes the motion of an electron in the average field $V(x)$ of the nuclei and all the other electrons plus an exchange potential $A_e(x)$ due to the core alone. This exchange potential suffices to insure that the core wave functions are substantially the same as the HFS wave functions, since exchange with the outer electrons should not have much effect on the wave functions of the core electrons. At the same time it is easy to show that the eigensolutions of (1.1) have the desired orthogonality properties.

Equation (1.1) is just the HFS equation with exchange among the outer electrons removed. In the SCF approximation it will lead, therefore, to an estimate of the ground state energy which is poorer than that obtained by the more usual HFS procedure. Nevertheless, once committed to going beyond HFS, we would prefer to treat the exchange among the valence electrons explicitly. The reason for such a preference is that the HFS procedure introduces a strong correlation between positions of electrons of parallel spin and no correlation between positions of electrons of antiparallel spin, and thus introduces a preferential lowering of the energy of high spin states which is at least partly spurious. In a number of physical phenomena the crux of the problem is just to understand the competition between Coulomb correlation and exchange to lower the energy. In such cases we prefer to study the two effects on the same footing, somewhat in the manner of Pines,[4] rather than to start from wave functions which overestimate one effect and ignore the other.

So much for the starting wave functions. We now wish to see how to construct an approximation to the true ground state wave function which is better than the SCF ground-state wave function. The first step is to calculate the matrix of the energy in a representation

[6] J. C. Slater, Phys. Rev. **81**, 385 (1951).

[7] F. Seitz, *The Modern Theory of Solids* (McGraw-Hill Book Company, Inc., New York, 1940), p. 340.

using antisymmetrized products of the SCF wave functions. One must calculate the expectation value of the energy for each configuration which is to be included in the calculation. Having done so one can for each configuration write the diagonal matrix element as an expression consisting of (a) a sum of SCF parameters for the occupied states, (b) a sum of Coulomb and exchange integrals for the lowest SCF configuration, (c) a sum of Coulomb and exchange integrals which take account of the difference in charge distribution between the configuration of reference and the SCF ground-state configuration. We will neglect the terms (c) in our subsequent discussion, since the ground state should consist chiefly of configurations which are relatively low, and the terms (c) should be small for all these low configurations. In any case the terms we wish to take account of are very much larger than the terms (c).

Thus we see that for our purposes the energy of a configuration (c) will be of the form

$$E(c)=\sum_{\mu}{}^{(c)}\,\mathbf{E}_{\mu}+\sum_{\mu\nu}{}^{(c)}\,E_{\mu\nu}{}^{(x)}. \tag{1.2}$$

In (1.2) the configuration (c) refers only to the outer electrons; the inner shell configuration being always the same, we need not mention the inner electrons any more. The energy $E_{\mu\nu}{}^{(x)}$ is just the exchange energy between electrons μ and ν. The Coulomb and exchange interaction between outer and inner electrons and between inner and inner electrons is completely taken account of in the SCF parameters E_{μ}. The zero of energy in (1.2) has been chosen so as to get rid of the Coulomb and exchange integrals (b).

Having gotten the matrix elements of the energy which are diagonal in configurations, we next have to treat the matrix elements which lead to configuration interaction. These will have the property that, except for some small exchange terms, they connect only configurations which differ in the quantum numbers of just two electrons, and in fact, it is for this reason that we are able to replace the inner shells by an equivalent potential. Now the SCF energy eigenvalues take account of the matrix elements of the electron-electron interaction which are diagonal in the configuration. These matrix elements involve only the particular Fourier components of the interaction with wave vectors equal to the wave vectors $\mathbf{K}$ of the reciprocal lattice. No matrix elements which lead to scattering between configurations have been taken into account, of course. If we include the exchange energy in the SCF energy parameters (as would be done in the HFS procedure), we would have as our perturbation just those matrix elements of the electron-electron interaction which mix configurations.

If we do not include the exchange energy in the SCF eigenvalues, though, we must retain the diagonal matrix elements when computing exchange but not otherwise. The last case may be treated formally by simply using the electron-electron interaction with the Fourier components $\mathbf{K}$ removed. The deletion of this discrete set of Fourier components does not affect the calculated value of any quantity except the diagonal-in-configuration nonexchange matrix element of the Coulomb interaction, and it causes the value of this quantity to be zero. That is exactly what we want.

Making use of the "crystal momentum representation,"[8] we can now write down the configuration interaction problem in a Hamiltonian form with the simple Hamiltonian

$$H=\sum_{\mu}\mathbf{E}(p_{\mu})+\sum_{k\mu\nu}{}''(2\pi e^2/k^2)\times\mathbf{q}(p_{\mu},k)\mathbf{q}(p_{\nu},-k)e^{ik\cdot x_{\mu\nu}} \tag{1.3}$$

in which $\mathbf{q}$ denotes the effective charge. The first prime on the second summation in (1.3) refers to the fact that k does not take on the value zero nor that of any reciprocal lattice vector. The second prime is a reminder that $\mu\neq\nu$. Greek indices are used to denote electrons. p_{μ} denotes the "crystal momentum" of the μth electron, x_{μ} denotes the "crystal coordinate" which is conjugate to p_{μ}, $x_{\mu}\equiv i\hbar\partial/\partial p_{\mu}$, $x_{\mu\nu}$ denotes $x_{\mu}-x_{\nu}$. The quantity $\mathbf{q}(p,k)$ is a matrix in the bands. Its matrix elements are given in terms of the SCF wave functions by

$$\mathbf{q}_{nn'}(p,k)=(\psi_{np+\hbar k},e^{ik\cdot x}\psi_{n'p}). \tag{1.4}$$

The states we have to work with are those properly antisymmetrized eigenstates of (1.3) in which no electrons occupy the states which were previously assigned to the inner shell electrons. In the remainder of the paper we will omit the double prime on such summations as that in (1.3) since it plays no role in our considerations, which concern only scattering matrix elements.

2. PLASMA FREQUENCY: APPROXIMATION OF WOLFF

In the previous section we have described a certain Hamiltonian procedure for treating the electron-electron interaction problem in a representation based on SCF solutions of the many electron problem. In this section we will attempt to deduce the plasma frequency for very-long-wavelength plasma waves. We will use a mathematical method which is the exact analog of the BP method, except that we will use the language of perturbation theory to describe certain approximate stages of the calculation. Following BP, we introduce auxiliary quantized oscillators with the associated operators p_k, q_k which satisfy

$$\begin{aligned}&[p_k,q_{k'}]=(\hbar/i)\delta_{kk'},\\ &p_k{}^{+}=p_{-k},\quad q_k{}^{+}=q_{-k}.\end{aligned} \tag{2.1}$$

We will not be concerned with deciding just how many oscillators should be introduced, but will refer to BP for a discussion of that question. The treatment we will make will apply only to small k values in any case.

To introduce the oscillator coordinates into the

[8] E. N. Adams, J. Chem. Phys. 21, 2013 (1953).

Hamiltonian (1.3), we replace (1.3) by

$$H=\sum_\mu \mathbf{E}(p_\mu)+\sum_{k\mu\nu}{}^{(l)}(2\pi e^2/k^2)\mathbf{q}(p_\mu,k)\mathbf{q}(p_\nu,-k)e^{ik\cdot x_\mu} +\tfrac{1}{2}\sum_k{}^{(s)}\{p_k-(4\pi e^2/k^2)^{\frac{1}{2}}\sum_\mu \mathbf{q}(p_\mu,k)e^{ik\cdot x_\mu}\} \times\{p_k{}^+-(4\pi e^2/k^2)^{\frac{1}{2}}\sum_\nu \mathbf{q}(p_\nu,-k)e^{-ik\cdot x_\nu}\}. \quad (2.2)$$

The notation (l), (s) for the regions of summation of k is used to indicate that the wave numbers in the two regions are "large" and "small" respectively as discussed in BP. Clearly the Hamiltonian (2.2) has the same matrix elements as the Hamiltonian (1.3) between wave functions which satisfy the auxiliary conditions,

$$\Omega_k\psi\equiv p_k{}^+\psi=0. \quad (2.3)$$

We may therefore adopt for the Hamiltonian the expression given by (2.2) instead of (1.3), provided that we use it in a function space in which all functions satisfy (2.3).

We now make a unitary transformation in the manner of BP to a new representation in which we will be able to introduce the so-called "random phase approximation" (RPA). The desired transformation is made by means of the unitary operator

$$u_1=\exp(is_1/\hbar),\qquad s_1=-\sum_{k\mu}(4\pi e^2/k^2)^{\frac{1}{2}}q_k e^{ik\cdot x_\mu}. \quad (2.4)$$

Before writing down the results of the transformation (2.4) on H, we will describe the RPA briefly. The essence of the approximation is to say that for finite k such a sum of phase factors as $\sum_\mu e^{ik\cdot x_\mu}$ is small compared to n, the value of the sum when $k=0$. The BP assumptions imply that the value of such a sum should vanish essentially like k, so that for small k we may in certain cases neglect these sums. The basis for the approximation is the supposition that in the true wave function the only configurations which are very probable are those for which the electrons are rather evenly distributed. We will not go into the matter here since it is discussed thoroughly in BP.

For brevity we will call that term in the Hamiltonian involving the sum (l) over large values of k, H_{SR}. Further, in treating the sum (s) we will make use of the approximation, valid[8] for small k,

$$1-\mathbf{q}(p_\mu,k)\approx -ik\cdot\mathbf{X}(p_\mu), \quad (2.5)$$

where $\mathbf{X}(p)$ is a matrix in the bands. Its general matrix element can be expressed in terms of the modulating function of the Bloch wave by

$$X_{nn'}(p)\equiv(u_{np},\partial u_{n'p}/\partial p).$$

We will also use the following relations:

$$u_1\mathbf{E}[p_\mu]u_1{}^{-1}=\mathbf{E}[p_\mu+\sum_k(4\pi e^2/k^2)^{\frac{1}{2}}ikq_k e^{ik\cdot x_\mu}]. \quad (2.6)$$

$\mathbf{E}[p]_{nn}$ is the energy eigenvalue for a Bloch state of momentum p in the nth band.

$$u_1\Omega_k u_1{}^{-1}=p_k+(4\pi e^2/k^2)^{\frac{1}{2}}\sum_\mu e^{ik\cdot x_\mu}. \quad (2.7)$$

By means of the aforementioned equations we can now reexpress the Hamiltonian (2.2) in the new representation defined by the unitary transformation (2.4). We have, in the approximation to which we will work,

$$u_1Hu_1{}^{-1}=\sum_\mu[\mathbf{E}(p_\mu)+\sum_k{}^{(s)}(4\pi e^2/k^2)^{\frac{1}{2}} \times\{i\mathbf{k}\cdot\mathbf{v}(p_\mu)/2,e^{ik\cdot x_\mu}\}q_k+(1/2m)\sum_{kl}{}^{(s)} \times(4\pi e^2/k\cdot l)\boldsymbol{\alpha}(p_\mu):\mathbf{kl}e^{i(k-l)\cdot x_\mu}q_k q_l{}^+ +\cdots] +H_{SR}+\tfrac{1}{2}\sum_k{}^{(s)}[p_k-(4\pi e^2/k^2)^{\frac{1}{2}} \times\sum_\mu ik\cdot\mathbf{X}(p_\mu)e^{ik\cdot x_\mu}] \times[p_k{}^+ +(4\pi e^2/k^2)^{\frac{1}{2}}\sum_\nu ik\cdot\mathbf{X}(p_\nu)e^{ik\cdot x_\nu}]. \quad (2.8)$$

In (2.8) we have used the notation

$$\boldsymbol{\alpha}(p)=m\partial^2E(p)/\partial\mathbf{p}\partial\mathbf{p},\qquad \mathbf{v}(p_\mu)=\partial E(p_\mu)/\partial\mathbf{p}_\mu. \quad (2.9)$$

Using the RPA, we may neglect those terms in (2.8) which involve $q_kq_l{}^+(k\neq l)$. We will also neglect for the moment the terms involving $k\cdot\mathbf{X}$ and H_{SR} and look at the partial problem defined by the Hamiltonian,

$$H_0=\sum_\mu[\mathbf{E}(p_\mu)+\sum_k{}^{(s)}(4\pi e^2/k^2)^{\frac{1}{2}}\{\tfrac{1}{2}ik\cdot v(p_\mu),e^{ik\cdot x_\mu}\}q_k] +\tfrac{1}{2}\sum_k{}'[p_kp_k{}^+ +\omega_{0k}{}^2q_kq_k{}^+] \quad (2.10)$$

with auxiliary conditions $u_1\Omega_k u_1{}^{-1}\psi=0$. In (2.10) we have introduced the notation

$$\omega_{0k}{}^2=(4\pi e^2/m)\sum_\mu \boldsymbol{\alpha}(p_\mu):\mathbf{kk}/k^2, \quad (2.11)$$

and used curly brackets to denote the anticommutator.

For this partial problem we will go beyond our original program and derive the dispersion relation for the plasma waves. We want to show that the Hamiltonian (2.10) gives exactly the dispersion relation of Wolff,[5] so that effectively the approximation which he makes is to neglect the terms in $(k\cdot\mathbf{X})$. To get the dispersion relation for the plasma waves we first introduce the creation-destruction operators for the plasma waves through the usual type of relations:

$$q_k=(\hbar/2\omega_{0k})^{\frac{1}{2}}(a_k+a_{-k}{}^+),\qquad p_k=(\hbar\omega_{0k}/2)^{\frac{1}{2}}(a_{-k}-a_k{}^+)/i. \quad (2.12)$$

Using (2.12) we rewrite (2.10).

$$H_0=\sum_\mu E(p_\mu)+\sum_{\mu k}{}^{(s)}(2\pi e^2\hbar/\omega_{0k}k^2)^{\frac{1}{2}}\{i\mathbf{k}\cdot v(p_\mu)/2,e^{ik\cdot x_\mu}\} \times(a_k+a_{-k}{}^+)+\sum_k{}^{(s)}\hbar\omega_{0k}(N_k+\tfrac{1}{2}). \quad (2.13)$$

To get the dispersion relation of Wolff, we need only calculate the effect of the interaction term in the second order of perturbation theory, ignoring the Pauli principle in the intermediate states. Writing

$$\boldsymbol{\alpha}(p_\mu):\mathbf{kk}/k^2\equiv\alpha_k(\mu),\qquad [v(p_\mu)\cdot k]/k\equiv v_k(\mu), \quad (2.14)$$

we can write the second-order energy as

$$\Delta E=-\sum_\mu[\sum_k \tfrac{1}{2}mv_k{}^2(\mu)/\sum_\nu \alpha_k(\nu)]+\sum_k(N_R+\tfrac{1}{2}) \times\hbar\omega_{0k}[\sum_\mu k^2v_k(\mu)^2\alpha_k(\mu)/2\omega_{0k}{}^2\langle\alpha_k\rangle]. \quad (2.15)$$

The first of the terms in (2.15) represents an eigenvalue renormalization. If the energy surfaces are spheres ($\alpha_k(\mu)=\text{const}$) we get the BP result that the mass of the electron is reduced by the relative amount ($n'/3n$) with n' the number of oscillators per unit volume.

The second term of (2.15) represents a frequency shift. It agrees with the formula (21) of Wolff,[5] so we are justified in regarding our procedure as essentially the same as his. It is easily shown that (2.15) agrees with the BP formulas if the energy surfaces are spherical.

We will now return to (2.8) and re-examine the terms in the energy which we have not yet taken into account. These extra terms are given by

$$H_1=\sum'_{\mu k}{}^{(s)}(4\pi e^2/k^2)^{\frac{1}{2}}p_k ik\cdot\mathbf{X}(p_\mu)e^{-ik\cdot x_\mu}+\sum_{k\mu\nu}{}^{(s)} \times(2\pi e^2/k^2)[\mathbf{k}\cdot\mathbf{X}(p_\mu)][\mathbf{k}\cdot\mathbf{X}(k_\nu)]e^{ik\cdot x_{\mu\nu}}. \quad (2.16)$$

The second term in (2.16) is a residual long wavelength interaction between the electrons. If the bands are far apart so that $\mathbf{k}\cdot\mathbf{X}(p_\mu)$ are small, this last term represents an interaction very much weaker than the original Coulomb interaction, and may properly be ignored. Probably there are many cases in which it cannot be ignored. We will return to this question later.

The first term describes an interaction between electrons and plasma quanta which can cause the electrons to scatter from one band to the other. There will be a frequency shift due to this term and we will estimate the shift by means of perturbation theory also. We will here omit the eigenvalue renormalization term and give only the expression for the frequency shift. We assume notationally that only the n band is occupied with electrons.

$$\delta\omega/\omega=4\pi e^2\sum_{\mu,n'}|k\cdot\mathbf{X}_{nn'}(p_\mu)|^2E_{nn'}(p_\mu)/ k^2[E_{nn'}{}^2(p_\mu)-(\hbar\omega_k)^2]. \quad (2.17)$$

The sum over bands n' in (2.17) should be taken only over those bands which are unoccupied in order to be consistent with the "fixed frame" treatment of the inner shells.

It is not immediately obvious whether or not the shift given by (2.17) is significantly large in the general case. In order to get some basis for an opinion we can see what (2.17) gives in several limiting cases. The special cases we will discuss are those in which either (a) $\hbar\omega_k\gg|E_{nn'}|$ for those states n' which make an important contribution to the sum, or (b) $|E_{nn'}|\gg\hbar\omega_k$ for all important states, or (c) $E_{nn'}\sim\hbar\omega_k$ for some of the important states.

In case (a) we get

$$\delta\omega/\omega\approx-4\pi e^2\sum_{\mu n'}|k\cdot X_{nn'}|^2E_{nn'}/[k^2(\hbar\omega_k)^2]. \quad (2.18)$$

Using the commutation relation

$$X_{nn'}=(\hbar/mi)P_{nn'}/E_{nn'}, \quad (2.19)$$

we can write (2.18) in the form

$$\delta\omega/\omega\approx-(4\pi e^2/m)\sum_{\mu n'}|k\cdot P_{nn'}|^2/(k_m{}^2E_{nn'}\omega_k{}^2). \quad (2.20)$$

We could do such a sum over n' explicitly if the summation were over all bands ($n'\neq n$), since by the f sum rule

$$(2/m)\sum_{n'}|k\cdot P_{nn'}|^2/(k^2mE_{nn'})=\alpha_k-1. \quad (2.21)$$

Actually we are supposed to sum only over bands n' which are unoccupied, hence higher in energy than the band n which is of interest. Nevertheless, we may use (2.21) to get an estimate of the order of magnitude of the frequency shift (2.20). The estimate so obtained is

$$\delta\omega/\omega=\sum_\mu(\alpha_k(\mu)-1)/\sum_\mu 2\alpha_k. \quad (2.22)$$

The estimate (2.22) indicates that even when the plasma frequency is large there may be a substantial percentage shift as a result of the band-band interaction. According to (2.22) the shift is positive and amounts to just 50 percent when $|\alpha_k|\gg1$. When $|\alpha_k|$ is of the order of unity, the predicted shift may have any sign and size. This last feature of (2.22) must not be taken seriously, since it is clear from (2.20) that in perturbation approximation the frequency shift is always positive. The strongest statement we can make is that the shift is always positive as long as the assumption (a) is met, and (2.22) gives a lower limit on the amount of the shift.

In case (b) we assume that $\hbar\omega_k$ is small. Such a situation can be met, for example, in semiconductors. In such a case it is clear from (2.17) that the plasma frequency is always reduced by the band-band processes. The relative shift is obtained from the expression (2.20) by reducing each term in the sum by the factor $(\hbar\omega_k)^2/E_{nn'}{}^2$. But this factor is very small by assumption, so one can probably neglect the shift in most cases (b).

In case (c) we have the possibility of a sort of resonance behavior, so the shift cannot be accurately estimated by the formula (2.17) at all. There is no reason, however, to suppose that the shift is especially small, if the matrix elements $\mathbf{X}$ are large. We cannot tell what sign to expect for the shift in this case.

The band-band transitions will also affect the dispersion relation. Inasmuch as we have been unable to get a generally accurate formula for the frequency at long wavelength, it would be pointless to give our approximate formula for the correction to the dispersion relation.

To summarize the situation, we can say that there are several terms which can have a large effect on the plasma frequency but which were not explicitly treated by Wolff. (Wolff estimated the effect of these terms for certain of the transition metals and decided that it is large.) One of these terms gives the frequency shift which we have estimated crudely by (2.17) and found normally to be large in a metal. The other kind of term is the second term of (2.16) which we cannot readily treat using our present approach, but which is probably large in many cases. We conclude that Wolff's dispersion relation is probably not valid in metals because of the band-band interaction terms of the first sort.

In order to establish what the situation is as regards the terms (2.16), we will have to do another calculation.

3. PLASMA FREQUENCY: APPROXIMATION OF BOHN AND PINES

We will now do an analogous calculation to the one of Sec. 2, except that we will use the exact transformation of BP so that the terms (2.16) do not occur. Thus, starting with the Hamiltonian (2.2) we will make the unitary transformation generated by the unitary operator u_2 constructed in the usual way from $\mathbf{S}_2$:

$$\mathbf{S}_2=-\sum_{k\mu}(4\pi e^2/k^2)^{\frac{1}{4}}\mathbf{q}(p_\mu,k)e^{ik\cdot x_\mu}q_k. \quad (3.1)$$

It is straightforward to establish the following equations:

$$u_2\Omega_k u_2^{-1}=p_k{}^+ +(4\pi e^2/k^2)^{\frac{1}{4}}\sum_\mu \mathbf{q}(p_\mu,-k)e^{-ik\cdot x_\mu}, \quad (3.2)$$

$$\begin{aligned}u_2\mathbf{E}(p_\mu)u_2^{-1}=&\mathbf{E}(p_\mu)+(1/2m)\sum_k(4\pi e^2/k^2)^{\frac{1}{4}}\\&\times\{ik\cdot\mathbf{P}(p_\mu),\mathbf{q}(p_\mu,k)e^{ik\cdot x_\mu}\}q_k\\&+\sum_{\mu kl}(2\pi e^2/mkl)(k\cdot l)\mathbf{q}(p_\mu,k)\\&\times\mathbf{q}(p_\mu,-l)e^{i(k-l)\cdot x_\mu}q_k q_l{}^+. \quad (3.3)\end{aligned}$$

In (3.3), the operator $P(p)$ is a matrix in the bands. Its matrix elements are given in terms of the SCF functions by

$$P_{nn'}(p)=(mi/\hbar)X_{nn'}(p)[E_n(p)-E_{n'}(p)].$$

By means of Eqs. (3.2), (3.3), and the RPA we can get for the transformed Hamiltonian the form

$$H=\sum_\mu \mathbf{E}(p_\mu)+H_I+\tfrac{1}{2}\sum_k{}^{(a)}(p_k{}^2+\omega_0{}^2q_k{}^2)+H_{SR}. \quad (3.4)$$

In (3.4), $\omega_0{}^2\equiv(4\pi e^2/m)$ is the plasma frequency for a free electron gas having the same mean electron density as our metal, and H_I is given to sufficient approximation by

$$H_I\doteq(1/2m)\sum_{k\mu}{}'(4\pi e^2/k^2)^{\frac{1}{4}}\{ik\cdot\mathbf{P}(p_\mu),e^{ik\cdot x_\mu}\}q_k. \quad (3.5)$$

Besides the RPA we have made a further approximation and dropped all terms which would not affect the plasma frequency in lower order than order k^2.

The Hamiltonian (3.4) is just that of BP with the difference that we sum only over "outer" electrons, and we have been able to make a slight simplification in the matrix elements which occur in H_I. We will not be interested in calculating anything like the BP dispersion relation, however. We wish merely to estimate the effect of band-band transitions on the plasma frequency for long wavelength plasma waves.

We can again estimate the frequency shift by means of second-order perturbation theory. We obtain in the same manner as previously,

$$\delta\omega_k/\omega_0=(1/mn)\sum_{\mu n'}|k\cdot P_{nn'}(p_\mu)|^2E_{nn'}(p_\mu)/[E_{nn'}{}^2-\hbar^2\omega_0{}^2]k^2. \quad (3.6)$$

Formula (3.6) is, of course, unreliable unless the shift it gives is relatively small.

We will now examine as before the limiting cases (a) $\hbar\omega_0\gg|E_{nn'}|$, (b) $\hbar\omega_0\ll|E_{nn'}|$. We will begin with (b) this time and use the f sum rule just as we did in case (a) of Sec. 2. Such a procedure yields the formula,

$$\delta\omega_k/\omega_0\approx(1/2n)\sum_\mu[\alpha_k(p_\mu)-1]. \quad (3.7)$$

It is not immediately clear that (3.7) gives anything like the result that was obtained in Sec. 2. However, in view of the fact that (3.7) is a perturbation theory result, we are justified in rewriting (3.7) in the form

$$\begin{aligned}\omega_0+\delta\omega_k&=\{1+\sum_\mu[\alpha_k(p_\mu)-1]/n\}^{\frac{1}{2}}\omega_0\\&=\langle\alpha_k\rangle^{\frac{1}{2}}\omega_0. \quad (3.8)\end{aligned}$$

Equation (3.8) is identical with the zero-order result of Wolff. While it cannot be said that we have verified Wolff's result, the agreement of (3.8) with Wolff's result is not disappointing. It should be noted, however, that the agreement is not as complete as it appears at first sight. In the first place, to get (3.8) we have summed over all intermediate bands n' in contravention of the Pauli principle and in clear violation of the restrictions on our "fixed frame of reference" in the function space. In the second place, we obtain the result (3.7) taking all terms into account, while the result of Wolff was obtained with the neglect of the terms (2.16). If (3.8) were really a valid result, we might conclude that the agreement between (3.8) and Wolff's result (2.11) justifies the neglect of the terms (2.16). Although that interpretation of our results is not justified, we take the view that, while the terms (2.16) may not be insignificant, the procedure of Sec. 2 is the most satisfactory one to use when $\hbar\omega_0\ll|E_{nn'}|$. Thus we think Wolff's results may be useful in semiconductors.

We now return to case (a) $\hbar\omega_0\gg|E_{nn'}|$. We see that the shift predicted by (3.6) is relatively much smaller than that we found for case (b) and normally positive. Thus if the plasma frequency is very high the band-band transitions would not affect it very much and the frequency should be similar to what it would be if the electrons were free.

As in Sec. 2, we conclude that when $|E_{nn'}|\sim\hbar\omega_0$, the shift is difficult to predict and may be large.

4. SUMMARY AND CONCLUSIONS

We would like now to summarize the tentative conclusions which we draw from the calculations of Secs. 2 and 3. First we conclude that for the case that the plasma frequency is small the results of Wolff are probably valid. In that case the procedure of Sec. 2 is probably the simplest to follow in studying the plasma since it gives rather good results in zero order. In the case that the plasma frequency is larger, however, the procedure of Sec. 3 is probably the simplest to use, since the equations indicate that the behavior is much more free-electron-like.

The strength of the band-band interactions brings into question the adequacy of the "fixed frame" treat-

ment. In a metal for which ω_0 is large, the inner-shell electrons are capable of interacting strongly with the plasma waves and thus in turn perturbing them. We will discuss this question further below, but it should be said here that the whole matter could stand further examination.

The treatment that we have made is based in principle on a limited configuration interaction calculation according to which all inner-shell states are completely occupied. Strictly speaking, the prohibition against exciting electrons from inner shells must be maintained even in virtual processes if we are to justify the Hamiltonian formalism which we used. Actually, since the electron-electron interaction is so strong, it might be better to seek a procedure which treats the inner shells more accurately, but we have not been able to imagine one which does not have drawbacks. The difficulty which results when too many bands are brought into the purview of the calculation is somewhat obscured by our method of calculation, but it lies in the fact that the exclusion principle must eventually be satisfied. In the BP treatment, which we have followed, the problem of satisfying the Pauli principle cannot be separated from the problem of satisfying the auxiliary conditions. As we bring in more electrons it becomes harder to satisfy the auxiliary conditions, and at the same time more important to do so. We note that in the BP papers[3] the auxiliary conditions were simply ignored. That may well be the reason that BP failed to obtain the effect of exchange[5] on the plasma frequency.

The entire question of the correct way to treat the auxiliary conditions is too complicated for us to go into here, and we do not know the answer anyhow. However, if our practice of ignoring the Pauli principle and auxiliary conditions in intermediate states can be justified, we can see that the manner of treatment of inner shells is optional. Equation (2.11) shows that closed shell electrons contribute nothing to the plasma frequency since the sum of the $\boldsymbol{\alpha}\cdot(\boldsymbol{p}_\mu)$ over a band will vanish. Further, if the electrons are in bands lying so deep that the level spacing is large compared to $\hbar\omega$, then the argument of Sec. 2 shows that the band-band virtual transitions of the electrons will have only a small effect on the plasma frequency. On this basis we can say the results of our calculation are insensitive to the particular way in which we separate the electrons into "inner" and "outer" provided that all electrons which lie below the Fermi surface by not more than a small multiple of $\hbar\omega$ are treated as "outer" electrons.

As an application of our ideas we will comment on the plasma frequency in sodium, because we think it presents a particular point of interest. Since the effective mass of the sodium electrons is close to unity, the plasma frequency will be found to be the same, in the first approximation, whether one adopts the method of calculation of Sec. 2 or of Sec. 3. Indeed, the reputation of sodium as a "free electron" metal might lead us to expect that this first approximation value of the frequency should be close to the actual plasma frequency for sodium. Actually our theory suggests that such need not be the case. From the matrix point of view the small deviation of the effective mass from unity in sodium is a consequence of the cancellation between terms in the f sum going through higher bands and terms going through lower bands. Our rough estimate (3.6) shows that the dipole matrix elements are weighted differently in the formula for the frequency shift than in the f sum, so the rather complete cancellation found in the f sum is no longer to be expected. Since the dipole matrix elements in sodium are not abnormally small and since the plasma energy is comparable with the interband spacing the imbalance of cancellation in (3.6) should be substantial and the frequency shift large. Moreover, if we observe the Pauli principle in a manner consistent with our "fixed frame" treatment of the inner shells, the sum in (3.6) should be extended only over bands n' of higher energy, and the imbalance is complete. Thus we must be prepared to find that the observed plasma frequency differs substantially from that calculated on the free electron gas model. Unfortunately it is difficult to make an accurate estimate of the expected shift.

While the case of sodium is of special interest because it illustrates that even the best "free electron" metal cannot be treated as an electron gas for the purpose of forming a plasma, our conclusion is actually quite general that in metals the effective mass approximation is inadequate for treating the electron-plasma interaction. We think that semiconductors provide the only possibility of cases for which the effective mass treatment is adequate.

In our opinion the published theories of the electron plasma in metals are unsatisfactory as regards the treatment of the exclusion principle. However, it seems possible that the exclusion principle only affects the frequency of waves of finite wavelength since the effect of density waves of sufficiently long wavelength should be nearly equivalent to a static perturbation and the effect of a static perturbing potential on the one electron wave functions is not affected by the exclusion principle. For that reason, we believe that the considerations of this paper have some chance to be valid, even in view of their incompleteness.

While this manuscript was in preparation the writer has had the pleasure of a number of conversations on the subject with J. McClure, D. Pines, and M. Cohen.

Low-Temperature Luminescence and Absorption of CdS

L. R. Furlong and C. F. Ravilious
United States Naval Research Laboratory, Washington, D. C.
(Received December 10, 1954)

Measurements of the emission and absorption of CdS single crystals have been made at several temperatures. At 4°K a set of emission lines in the range 4850–5020 A has been found. A study of these lines together with observations at other temperatures suggests that they are emitted by a system consisting of the combination of a gas and CdS, the gas being adsorbed on the crystal.

INTRODUCTION

THE luminescence of CdS at low temperatures has been studied by several workers. At 93°K Kroeger[1] found several emission bands in the range 5100–5600 A and other bands at shorter wavelengths. At 77°K Klick[2] found several emission bands in the range 5000–5600 A and at 4°K he found a set of bands in the same region together with some diffuse structure at shorter wavelengths. At 4°K one of us[3] found three less intense bands lying among Klick's three most intense bands.

This paper is a result of further investigation of the luminescence and absorption of CdS single crystals. At 4°K we have found a set of emission lines, the half-width being of the order of 1 A, and some similarly narrow absorption lines. In connection with this we have investigated the emission and absorption at other temperatures. At 300°K our study of the single emission band leads us to suggest that it is associated with the line emission at 4°K.

The luminescence measurements were made by photographing the emission of a single crystal with a Hilger medium glass spectrograph. The crystal was excited by ultraviolet radiation from a one-kilowatt Westinghouse mercury vapor lamp Type SAH 1000 A filtered with a Corning 7-54 filter. The absorption measurements were made by similarly photographing the light transmitted by a single crystal which was irradiated by a tungsten-filament lamp.

Table I. Low-temperature luminescence of CdS.

Green bands at 4°K λ(A)	Blue bands at 4°K λ(A)	Bands at 77°K λ(A)
5100	4853	4840
5133	4867	4870
5182	4886	4885
5212	4907	4946
5267	4913	5027
5290	4925	5129
5350	4940	5214
5445	4962	5300
5530	4990	5390
5630	5004	5478
	5020	5572

[1] F. A. Kroeger, Physica **7**, 1 (1940).
[2] C. C. Klick, Phys. Rev. **89**, 274 (1953).
[3] L. R. Furlong, Phys. Rev. **95**, 1086 (1954).

EXPERIMENTAL RESULTS

A. At 4°K

The emission of a CdS single crystal at 4°K is shown in the first two columns of Table I and in Fig. 1(a).

Two of the green bands listed in Table I, namely 5212 A and 5290 A, have been obscured in Fig. 1(a) by the over-exposure of the 5182, 5267, and 5350 A bands. The over-exposure of these green bands was necessary in order to detect the much less intense blue lines on the same plate. The half-width of these bands is of the order of 10 A, as reported in reference 2, and have fairly regular spacing.

The blue emission lines at 4°K have a half-width of the order of 1 A and lack the regular spacing characteristic of the green bands. They are also much less intense than the green bands. Furthermore, these lines can be restored to full intensity by means of a short exposure to air after their intensity has been reduced by simultaneously baking and pumping on the crystal.

The absorption spectrum at 4°K also has very interesting characteristics. Gross and Karryev[4] reported a narrow absorption line at 4869 A for a cadmium sulfide single crystal at 73°K. At 4°K we have found absorption lines, of approximately 1 A half-width, at 4825, 4852, and 4867 A. Of the three absorption lines the weakest is at 4825 A and there is a very weak emission corresponding to this at a slightly longer wavelength. The absorption line at 4852 A seems to correspond to the emission line at 4853 A. The most

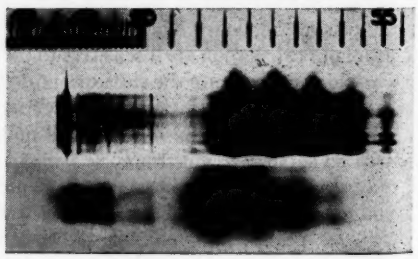

Fig. 1. Luminescence of CdS single crystal (a) at 4°K; (b) at 77°K. The scale at the top is the wavelength scale (in units of 100 A).

[4] E. F. Gross and N. A. Karryev, Doklady Akad. Nauk S.S.S.R. **84**, 471 (1952).

interesting and most intense of the absorption lines is at 4867 A. As shown in Table I and Fig. 1(a) this is also the wavelength of the most intense of the blue emission. This phenomenon is reminiscent of resonance radiation, characteristic of gases. However, this suggestion is made with reservations because of the possibility of a 1 A error.

We found these three absorption lines to be superimposed on an absorption continuum which for unpolarized incident radiation is maximum and constant at wavelengths shorter than 4850 A and decreases rapidly at longer wavelengths. In connection with the absorption continuum, Gobrecht and Bartschat[5] observed that the position of the absorption edge of cadmium sulfide crystals at 293°K and at 93°K is a function of the direction of polarization of the incident light with respect to the *C*-axis of the crystal. We have observed the same behavior of the absorption edge at 4°K. When the incident light is linearly polarized with the electric vector parallel to the striations in the crystal platelet (and, therefore, parallel to the *C*-axis[5]) the absorption continuum is the same as when the incident radiation is unpolarized. However, when the incident light is polarized perpendicular to the striations the longest wavelength of maximum absorption moves from 4850 A to 4874 A.

B. At 77°K

The emission spectrum of a cadmium sulfide single crystal at 77°K is shown in the third column of Table I and in Fig. 1(b). For CdS:Ag at 77°K Klick[6] has obtained structure in the 4800–5000 A region and Kroeger[1] found some bands in this region at 93°K.

In this case we found absorption lines at about 4840 A and 4870 A. For the incident radiation unpolarized or polarized parallel to the *C*-axis the longest wavelength of maximum absorption is at 4880 A whereas this occurs at 4910 A for perpendicularly polarized incident radiation.

C. At 300°K

We found a single green emission band maximized at 5077 A with a half-width of 160 A. We also obtained the absorption continuum. The emission band lies within the absorption continuum except for a small portion of the long-wavelength tail. This fact might indicate that this emission is surface emission but not necessarily since the emission might originate within the crystal and be absorbed to a large extent before reaching the surface. However, other observations do indicate this to be surface emission. For example, gentle scraping of the crystal suppresses this emission as does ionizing the gas surrounding the crystal. Furthermore, microscopic examination of the emitting crystal indicates surface emission. We determined the position of the peak of this emission band as a function of temperature, with the results given in Table II. We have not included entries at 77°K and 4°K since at these temperatures we have structure rather than a single band. However, it is interesting that the trend of the peak is toward that portion of the spectrum occupied by the blue set of emission lines at 4°K and that the spread of the blue lines (that is, from 4853 A to 5020 A) is approximately the half-width of the single band at room temperature.

TABLE II. Position of maximum of the luminescence band as a function of temperature.

T(°K)	λ(A)
300	5077
273	5065
195	4980
147	4960
113	4895

DISCUSSION

The characteristics of the blue set of emission lines at 4°K are: (1) narrowness, the half-width being of the order of 1 A as compared to a half-width of the order of 10 A for the green band; (2) lack of regular spacing such as was found for the green bands; (3) a much lower intensity, in general, than that of the green bands; (4) an apparent connection with the green emission band at 300°K, which we have ascribed to the surface; (5) the restoration of these lines to full intensity by means of a short exposure to air after the intensity has been reduced by simultaneously baking and pumping on the crystal; (6) the appearance of an absorption line apparently at the position of the 4867 A emission line.

These characteristics suggest that one explanation for these emission lines is that they are representative of the combination of a gas and cadmium sulfide, the gas being adsorbed on the crystal. It is not unreasonable to suppose that the electronic states of a gaseous system might be modified by a dielectric on which it is adsorbed. The temperature shift of the emission may be associated with the same causes which account for the temperature variation of the forbidden energy gap in the crystal. The structure at 4°K, as contrasted with the single band at 300°K, could arise from less coupling with the lattice vibrations as the temperature is lowered.

[5] H. Gobrecht and A. Bartschat, Z. Physik **136**, 224 (1953).
[6] C. C. Klick, J. Opt. Soc. Am. **41**, 816 (1951).

Oscillatory Hall Effect, Magnetoresistance, and Magnetic Susceptibility of a Graphite Single Crystal

TED G. BERLINCOURT AND M. C. STEELE
United States Naval Research Laboratory, Washington, D. C.
(Received January 17, 1955)

The Hall coefficient, magnetoresistance, and magnetic susceptibility of a graphite single crystal have been measured at liquid helium temperatures and in magnetic fields up to 25 kilogauss. All three phenomena are periodic functions of reciprocal field and exhibit the same period for like orientations of the crystal axes with respect to the magnetic field. The phases however are different. Where possible, experiment and theory have been compared.

INTRODUCTION

THE low-temperature oscillatory dependence of magnetic susceptibility upon magnetic field characteristic of the de Haas-van Alphen effect is known to exist in 15 metal crystals (see Shoenberg's monograph[1] for an account of much of this work). Moreover, in bismuth, for the same orientation of the crystal with respect to the magnetic field, oscillations of the same period as the susceptibility oscillations have been observed in the magnetoresistance,[2] Hall coefficient,[3,4] thermoelectric effect,[5] and thermal conductivity.[6] The present work was undertaken in an effort to find and study some of the latter effects in graphite, which had already been shown by Shoenberg[1] to exhibit the susceptibility oscillations. Preliminary reports[7,8] on the discovery of magnetoresistance and Hall effect oscillations have already been given. The data to be reported here concern magnetoresistance, Hall effect, and magnetic susceptibility measurements on the same crystal for the same orientation of the crystal with respect to the field.

These magneto-oscillatory effects are of interest because they provide information regarding the effective masses and chemical potential of the pertinent electrons. Under presently attainable conditions of high magnetic field and low temperature they are observable only when the effective masses and chemical potential are small, *viz.*, when a very few electrons (of the order of 10^{-5} to 10^{-3} per atom) overlap a Brillouin zone boundary. In general the pertinent properties may be described to a fair approximation by an equation of the form

$$y=\sum_i\left[f_y(H,T,\beta_i,E_{0i})+a_y(H,T,\beta_i,E_{0i})\sin\left(\frac{2\pi E_{0i}}{\beta_i H}+\theta_i\right)\right], \tag{1}$$

where y is the quantity under consideration, H is the magnetic field, T is the temperature, and β is a double effective Bohr magneton involving an effective mass m^* and given by

$$\beta=e\hbar/m^*c. \tag{2}$$

E_0 is the energy at the surface of constant energy measured from the bottom of the relevant zone in the case of electrons or from the top in the case of holes, and θ gives the phase of the oscillations which are periodic (of period β/E_0) in H^{-1}. The summation appears in Eq. (1) because several groups of overlapping electrons (each group characterized by different parameters β and E_0) may coexist in a given crystal such that the observed oscillations exhibit beats among the various terms. Also, if the temperature is low enough and the field large enough, harmonics of each of these terms become important. $f_y(H,T,\beta,E_0)$ is in general a monotonic function upon which are superposed oscillations of amplitude determined by the function $a_y(H,T,\beta,E_0)$. The theoretical forms of these functions have been derived by Landau[9] for the magnetic susceptibility of a free electron gas, and reasonably good agreement between theory and experiment is obtained for this case provided the electronic mass is treated as an adjustable parameter, *viz.*, an anisotropic effective mass. A theory for the magnetoresistance oscillations has been developed by Davydov and Pomeranchuk.[10] A discussion of the applicability of these theories to the present work will be deferred until after the experimental results have been presented. No detailed theory exists as yet for the oscillations in the Hall effect, the thermoelectric effect, and the thermal conductivity.

[1] D. Shoenberg, Trans. Roy. Soc. (London) **245**, 1 (1952).
[2] P. B. Alers and R. T. Webber, Phys. Rev. **91**, 1060 (1953). See also Ted G. Berlincourt, Phys. Rev. **91**, 1277 (1953).
[3] Laird C. Brodie, Phys. Rev. **93**, 935(A) (1954).
[4] Reynolds, Leinhardt, and Hemstreet, Phys. Rev. **93**, 247 (1954); see also Phys. Rev. **96**, 1203 (1954).
[5] M. C. Steele and J. Babiskin, Phys. Rev. **94**, 1394 (1954).
[6] J. Babiskin and M. C. Steele, Phys. Rev. **96**, 822 (1954).
[7] T. G. Berlincourt and J. K. Logan, Phys. Rev. **93**, 348 (1954).
[8] T. G. Berlincourt and M. C. Steele, Phys. Rev. **98**, 227(A) (1955).
[9] L. D. Landau, see appendix to D. Shoenberg, Proc. Roy. Soc. (London) **A170**, 341 (1939).
[10] B. Davydov and J. Pomeranchuk, J. Phys. (U.S.S.R.) **2**, 147 (1940).

EXPERIMENTAL WORK

All of the measurements were carried out at liquid helium temperatures in the horizontal field of an Arthur D. Little electromagnet which was capable of rotation about a vertical axis and supplied a maximum field of about 25 kilogauss. The magnet was calibrated with a nuclear resonance fluxmeter to an accuracy of better than 0.02 percent, and time variations of the field were limited to less than 5 gauss during the course of a single measurement.

The graphite single crystal used throughout the investigation was carefully cut from a large crystal of natural graphite (Catalog number 48789, Essex County, New York) kindly loaned by Dr. George Switzer of the Smithsonian Institution. The crystal was a shiny well-formed hexagonal plate. Dilute hydrochloric acid was used to dissolve the calcite in which it was imbedded. Three sets of lines making angles of 60° with each other were just discernable on the crystal's surface indicating some twinning and permitting identification of the binary axes.[11] The experimental specimen was cut in the form of a rectangular plate 9.2 mm long (along a binary axis), 2.05 mm wide, and 0.36 mm thick (in the direction of the hexagonal axis). The long dimension, i.e., a binary axis, was vertical throughout the investigation.

For the Hall effect and magnetoresistance measurements, the ends of the crystal were thickly electroplated with copper for a distance of about 2 mm and were then clamped lightly to a Textolite holder with small copper bars which comprised the current leads. The Hall probes were located on the edges of the crystal as accurately as possible directly opposite each other and midway between the current leads. A potential probe was also placed on one edge 1 mm from one of the Hall probes permitting magnetoresistance measurements to be made. These three probes were of the spring contact type fashioned from phosphor bronze wire. The Hall effect measurements were carried out only with the field parallel to the hexagonal axis, which was located to better than 1/2° by means of magnetoresistance measurements. For this geometry, the expression

$$A = 10^8\, Vt/IH \qquad (3)$$

defines the Hall coefficient A in cm³/coulomb provided the Hall potential V is in volts, the measuring current I is in amperes, the magnetic field H is in gauss, and the crystal thickness t is in cm.

Over the range of fields investigated the Hall voltages fell between 25 and 75 microvolts for a sample current of 20 milliamperes and were measured with a six-dial potentiometer to an accuracy of about 0.2 microvolt. The usual practice of deducing the Hall voltage from two sets of measurements made with the magnetic field in directions differing by 180° was adopted in order to eliminate magnetoresistance components arising from inexact positioning of the Hall probes. The voltages arising from these magnetoresistance components proved to be comparable with the Hall voltages such that the magnetoresistance could be deduced from measurements on the Hall probes as well as from measurements on the magnetoresistance probes. Voltages on the magnetoresistance probes were large enough that they could be recorded as a function of magnet current directly on a 10-millivolt by 10-millivolt $X-Y$ recorder.

The magnetic susceptibility measurements were carried out by the torsion balance method[1] which yields the difference of susceptibility along two perpendicular directions in a single crystal as deduced from measurements of the vertical couple acting on the crystal placed in a homogeneous horizontal magnetic field. (Methods which utilize a field gradient are of course unsatisfactory for measurements of field dependent susceptibilities.) The graphite crystal was mounted on the torsion balance with its hexagonal axis horizontal and a binary axis (i.e., the long dimension) vertical as was the case for the Hall effect and magnetoresistance measurements. However, since the couple acting on an anisotropic crystal vanishes when the field coincides with a symmetry axis (such as the hexagonal axis in graphite) it was necessary to make the measurements with a small angle ϕ between the magnetic field and the hexagonal axis. $\phi = 10°$ was chosen for this investigation. Comparison with the Hall effect and magnetoresistance data (for which $\phi = 0$) is possible because, as Shoenberg[1] has shown, the *locations* in field of the susceptibility oscillations in graphite depend to considerable accuracy only upon the component of field parallel to the hexagonal axis although the *amplitude* of the susceptibility oscillations is of course slightly less for $\phi = 10°$ than for $\phi = 0°$.

EXPERIMENTAL RESULTS

The experimental results for the Hall coefficient, the magnetoresistance, and the magnetic susceptibility are presented for two different temperatures in Fig. 1. The data are plotted against reciprocal field in order to illustrate the periodicity in H^{-1}. The change of resistance ΔR in the magnetic field plotted in Fig. 1 was deduced from measurements on the Hall probes. The resistance measured on these probes increased by a factor of roughly 10^3 in going from zero field to 25 kilogauss, i.e., $\Delta R = 5 \times 10^{-3}$ ohm corresponds to $\Delta R/R_0 \cong 10^3$, where R_0 is the resistance in zero field. R_0 could not be measured accurately enough to ascertain whether $\Delta R/R_0$ increased or decreased with temperature in the liquid helium range.

A puzzling aspect of the magnetoresistance measurements is that the amplitude of the oscillations in the magnetoresistance as deduced from measurements on the Hall probes is much greater than the amplitude observed on the magnetoresistance probes. For example, at 20 kilogauss the envelope of the oscillations comprises about 14 percent of the monotonic magneto-

[11] For a discussion of the morphology of graphite crystals see C. Palache, Am. Mineralogist **26**, 709 (1941).

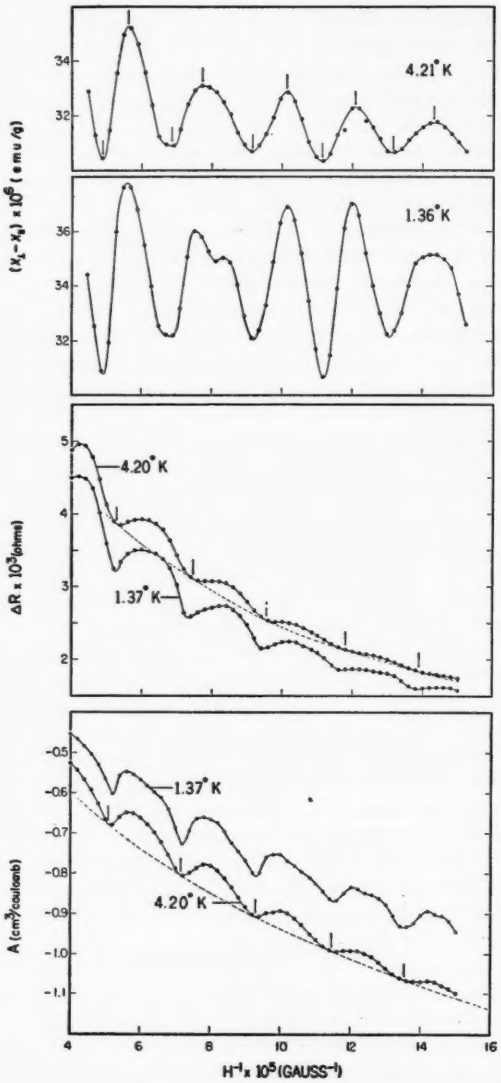

FIG. 1. The Hall coefficient A, the change of resistance ΔR in a magnetic field, and the difference in magnetic susceptibility parallel and perpendicular to the hexagonal axis of a graphite single crystal plotted as functions of the reciprocal of the component of magnetic field parallel to the hexagonal axis. The arrows indicate locations of maxima and minima in reciprocal field.

resistance for the former case but only 4 percent for the latter. The form of the magnetoresistance curve obtained using the potential probes was identical with the form of the curve reported earlier[7] which was obtained from measurements of the potential between the copper clamping bars at the ends of the crystal. This curve is presented again in Fig. 2. It should be pointed out that the locations in reciprocal field of the magnetoresistance minima as indicated by the arrows agree to better than 1 percent with those noted in Fig. 1 for the magnetoresistance measurements carried out on the Hall probes. A possible explanation for the discrepancy in amplitude is that the portion of the crystal embraced by the Hall probes might have been more perfect than the remainder thus giving rise over this portion to a larger relative amplitude. Such inhomogeneity in the basal plane of the crystal would however affect the potential distribution and lead to uncertainties in comparisons between theory and experiment.

The difference in magnetic susceptibility $\chi_\perp-\chi_\parallel$, where $\chi_\perp$ and $\chi_\parallel$ are the magnetic susceptibilities perpendicular and parallel, respectively, to the hexagonal axis, plotted at the top of Fig. 1 is that measured at $\phi=10°$ but plotted against the reciprocal of the component of the magnetic field parallel to the hexagonal axis thus permitting comparison for $\phi=0°$ of the locations in reciprocal field of the oscillations in the three oscillatory phenomena under investigation. Furthermore, since $|\chi_\parallel|\gg|\chi_\perp|$,[12] $(\chi_\perp-\chi_\parallel)_{\phi=10°}\cong-\chi_\parallel$. These susceptibility data are in excellent agreement with the earlier data of Shoenberg,[1] whose analysis indicated that the beats (which are most noticeable at the lower temperature) occur because of the coexistence of two oscillatory terms [as provided for in Eq. (1)], the weaker exhibiting a period in reciprocal field which is just $\frac{3}{4}$ that of the dominant term. The fact that the Hall effect and magnetoresistance oscillations are not pure sinusoids can most likely be attributed to this same cause. Fortunately, the 4.2°K data are not so badly distorted by the second term as to preclude comparison of phases and periods for the three effects. In Fig. 3, values of reciprocal field (as indicated by the arrows in Fig. 1) at which Hall coefficient minima, magnetoresistance minima, and susceptibility maxima and minima occur have been plotted against integers. The Hall coefficient and magnetoresistance minima were chosen as the points where the experimental curves are tangent to the monotonic (dashed) envelope curves. The strict linearity of the plots in Fig. 3 indicates that the oscillations are indeed periodic in reciprocal field. A least squares fit was used in drawing the line for the susceptibility data which show more scatter because of the greater relative strength of the subordinate term. The parallelism of the three lines indicates an identical period for all three phenomena which (calculated from the slope of these lines) is $\beta/E_0=2.15\times10^{-5}$ gauss^{-1}. This agrees well with Shoenberg's value $\beta/E_0=2.20\times10^{-5}$ gauss^{-1}. The separations of the lines provide measures of the relative phases of the various effects although the asymmetries of the oscillations prohibit very precise determinations. In any event, the data indicate that in reciprocal field, magnetoresistance minima lag minima in diamagnetism by approximately $\pi/2$, while Hall coefficient minima lag minima in diamagnetism by approximately $\pi/4$.

[12] N. Ganguli and K. S. Krishman, Proc. Roy. Soc. (London) A177, 168 (1941).

The field dependences of the dashed curves tangent to ΔR and A are presumably of some interest and are given approximately by

$$\Delta R \propto H^{0.80} \tag{4}$$

and

$$A \propto H^{-0.45} \tag{5}$$

over the range of fields investigated. It should also be mentioned that oscillations in ΔR were still readily discernable even when the angle between the hexagonal axis and the field was as great as 20°.

COMPARISON WITH THEORY

Comparisons between experiment and theory in the case of graphite are greatly complicated by the presence of the second term in the oscillatory phenomena. Nevertheless, Shoenberg[1] carried out a rather careful analysis of the susceptibility oscillations and concluded that according to Landau's theory[9] the pertinent electronic constant energy surfaces in graphite consist of two ellipsoids of revolution, the first or dominant ellipsoid with $E_0=2.3\times10^{-14}$ erg, $m_\perp=3.6\times10^{-2}\ m_0$, $m_\parallel=200\ m_0$, and $n=3.4\times10^{-5}$, where $m_\perp$ and $m_\parallel$ are the effective masses perpendicular and parallel, respectively, to the hexagonal axis, m_0 is the free electron mass, and n is the number of electrons per atom. For the subordinate ellipsoid, $E_0=1.6\times10^{-14}$ erg, $m_\perp=7\times10^{-2}\ m_0$, $m_\parallel=25$ to $700\ m_0$, and $n=1.4$ to 7×10^{-5}. In view of the good agreement between Shoenberg's susceptibility data and ours, no additional analysis of the susceptibility data was attempted. However, since the 4.2°K Hall effect and magnetoresistance data plotted in Fig. 1 appeared to consist almost entirely of the dominant term alone, an attempt to determine the empirical field dependences of the amplitudes of these effects seemed worthwhile. It was thought that a functional form resembling the susceptibility amplitude field dependence would serve as a starting point for such an analysis.

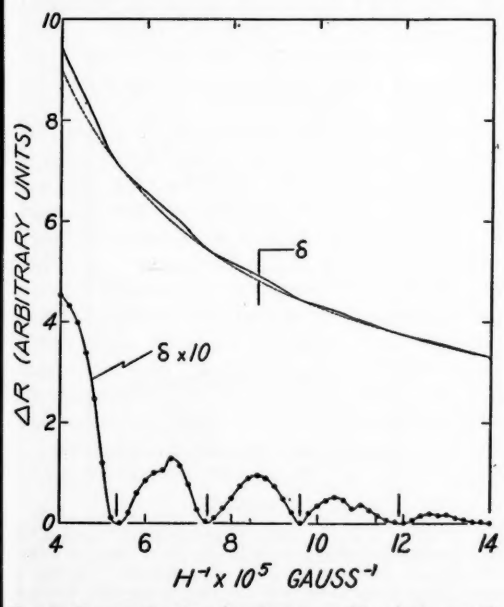

FIG. 2. Change of resistance ΔR of a graphite single crystal as a function of H^{-1} at 4.22°K (solid line). δ is the difference between the experimental values and the dashed envelope curve. These measurements (Berlincourt and Logan, reference 7) were carried out over a larger portion of the crystal than was utilized in obtaining the magnetoresistance data appearing in Fig. 1.

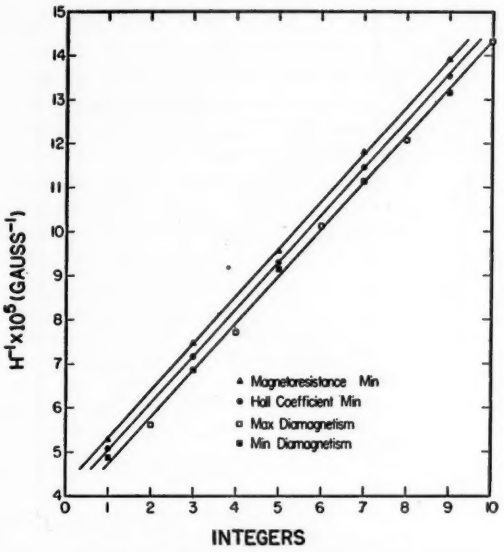

FIG. 3. Values of H^{-1} at which Hall coefficient, magnetoresistance, and susceptibility maxima and minima occur in a graphite single crystal plotted against integers. The linearity indicates strict periodicity in H^{-1}; the parallelism indicates the same period for all three phenomena; the separations indicate relative phases.

According to Landau's theory, the amplitude a of the susceptibility oscillations should depend upon field at a given temperature in the following way.

$$a \propto \frac{1}{H^r \sinh(2\pi^2 kT/\beta H)}, \tag{6}$$

where $r=3/2$. It can be shown that if this expression is applicable a plot of $\log_{10}\{aH^r[1-\exp(-4\pi^2kT/\beta H)]\}$ against H^{-1} should yield a straight line. The 4.2°K Hall effect data fit this same function quite well between 8 and 25 kilogauss provided Shoenberg's value $\beta=5.1\times10^{-19}$ erg gauss^{-1} as derived from magnetic susceptibility measurements is used in the factor $[1-\exp(-4\pi^2kT/\beta H)]$. An even better fit to the Hall effect data is obtained if $r=5/2$ as illustrated by the linearity of the lower plot in Fig. 4. Actually there is some evidence[13,14] that Eq. (6) with $r=5/2$ also describes the field dependence of the magnetic suscep-

[13] F. J. Donahoe and F. C. Nix, Phys. Rev. **95**, 1395 (1954).
[14] T. G. Berlincourt and M. C. Steele, Phys. Rev. **95**, 1421 (1954).

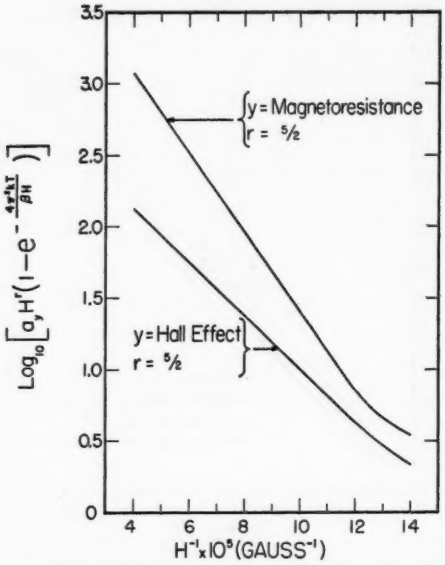

FIG. 4. The field dependence of the amplitude a (in arbitrary units) of the Hall coefficient and magnetoresistance oscillations of a graphite single crystal. The more linear the curve the better the fit of the indicated expression to the observed dependence.

tibility oscillations slightly better than it does with the theoretical $r=3/2$, but uncertainties regarding the strengths and phases of harmonic components preclude any clear-cut choice. It should be mentioned that unpublished data of Overton and Berlincourt on the Hall coefficient oscillations in bismuth also favor $r=5/2$ as against $r=3/2$, although the difference is not so marked as in the case of graphite, perhaps because the bismuth work was carried out in fields below 12 kilogauss where the power of H is not so important.

Equation (6) with $r=5/2$ also describes the 4.2°K magnetoresistance data of Fig. 1 quite well above 8 kilogauss as indicated by the linearity of the top curve in Fig. 4. This differs from the field dependence given by the theory of Davydov and Pomeranchuk,[10] but this comparison must be regarded with caution in view of the puzzling aspects of the magnetoresistance data already mentioned.

DISCUSSION

It is established that the Hall coefficient, the magnetoresistance, and the magnetic susceptibility of graphite single crystals are periodic functions of reciprocal magnetic field at low temperatures. Furthermore, for the same orientation of the crystal axes with respect to the magnetic field the periods are the same, but the phases are different. Magnetoresistance minima lag minima in diamagnetism by approximately $\pi/2$ in reciprocal field, while Hall coefficient minima lag minima in diamagnetism by roughly $\pi/4$, although the latter figure is less accurately determined.

With regard to the matter of relative phases it is worthy of note that unpublished data of Overton and Berlincourt on bismuth reveal zero phase difference between magnetoresistance and Hall coefficient minima. Furthermore, as noted earlier,[7] an examination of Nachimovich's magnetoresistance data[15] on a single crystal of zinc with its hexagonal axis parallel to the magnetic field reveals oscillations of the same period as the susceptibility oscillations for the same orientation, with magnetoresistance minima lagging minima in diamagnetism by $\pi/2$ in reciprocal field in agreement with our graphite results. This is illustrated in Fig. 5 where values of reciprocal field at which maxima and minima in the magnetoresistance and susceptibility of zinc occur are plotted against integers. The susceptibility data are those of Berlincourt and Steele[14] referred to the same orientation. Although this comparison has been made between results on two different crystals, its validity is supported by the excellent agreement between susceptibility measurements made on several different zinc crystals.[13,14,16] Thus, the $\pi/2$ phase difference between the magnetoresistance and susceptibility oscillations could hardly be in error by more than 20 percent.

The forms of the amplitude dependence upon field for the Hall coefficient, the magnetoresistance, and magnetic susceptibility oscillations are similar in some respects, but on the basis of the data set forth herein generalizations would be premature. In fact, it should be noted that the asymmetries in the Hall effect and magnetoresistance oscillations at 1.37°K (induced by

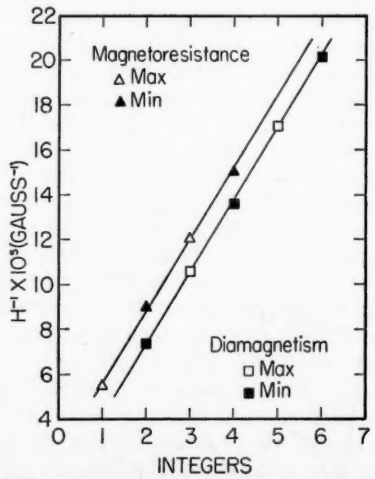

FIG. 5. Values of H^{-1} at which magnetoresistance and susceptibility maxima and minima occur in zinc plotted against integers for the magnetic field parallel to the hexagonal axis. Note that the relative phase is the same as in the case of graphite. The magnetoresistance data are those of Nachimovich (reference 15), and the susceptibility data are those of Berlincourt and Steele (reference 14).

[15] N. M. Nachimovich, J. Phys. (U.S.S.R.) **6**, 111 (1942).
[16] L. Mackinnon, Proc. Phys. Soc. (London) **B62**, 170 (1949).

the subordinate periodic term as well as harmonics of both terms) appear to be quite different from the asymmetries in the susceptibility oscillations suggesting that the relative strengths of the two periodic terms and their harmonics are probably quite different in the different effects studied.

The magnetoresistance and Hall effect data show reasonable agreement with the data of Kinchin[17] (whose measurements extended up to about 9 kilogauss), although his data were not sufficiently detailed to reveal the presence of oscillations. The magnetic susceptibility data are in excellent agreement with Shoenberg's data even with regard to the finer details. Indeed, it should be emphasized that the fundamental parameters β and E_0 derived from de Haas-van Alphen (susceptibility) measurements show remarkable reproducibility (within a few percent) from crystal to crystal of a given element despite relatively rough physical treatment and in some cases[1,13,18] alloying up to 0.5 atomic percent. Since relatively good agreement is obtained between theory and experiment in the case of magnetic susceptibility, values of these parameters so obtained are probably more reliable than values deduced from Hall effect and magnetoresistance data.

[17] G. H. Kinchin, Proc. Roy. Soc. (London) A217, 9 (1953).

[18] Croft, Love, and Nix, Phys. Rev. 95, 1403 (1954).

PHYSICAL REVIEW. VOLUME 98, NUMBER 4 MAY 15, 1955

Hall Mobility of Optically Excited Carriers in Germanium

W. W. Tyler and R. Newman
General Electric Research Laboratory, Schenectady, New York
(Received February 7, 1955)

Steady-state Hall coefficient measurements of optically excited carriers have been made for high-resistivity gold-, iron-, cobalt-, and nickel-doped germanium crystals in the temperature range from 200°K to 54°K. In the spectral region of impurity absorption, ($h\nu<0.7$ ev), carriers generated in p-type samples are holes; carriers generated in n-type samples are electrons. In the region of intrinsic absorption, ($h\nu>0.7$ ev), Hall coefficient measurements indicate that photoconduction is due primarily to mobile electrons in both p- and n-type high-resistivity samples. These observations suggest that, in the crystals studied, hole trapping is primarily responsible for the intrinsic photosensitivity in both n- and p-type samples. These results are qualitatively consistent with the double-acceptor model, proposed to account for the two impurity levels introduced into Ge by each of the aforementioned impurities.

I. INTRODUCTION

STUDIES of the properties of Ge crystals doped with Au,[1] Fe,[2,3] Co,[4] and Ni[4] indicate that each of these impurities introduce two deep energy levels, one above and one below the center of the forbidden band of Ge.[5] Thus for each of these doping elements it is possible to prepare both n- and p-type crystals whose extrinsic behavior is dominated by a specific deep impurity level. Resistivity values for such crystals rise to very high values in the region of liquid nitrogen temperature with the resistivity-temperature relationship characteristic of the specific impurity level. The low-temperature photoconductivity spectrum for each of these materials may be resolved into a region of intrinsic photoconduction, ($h\nu>0.7$ ev), and a region of extrinsic or impurity photoconduction, ($h\nu<0.7$ ev). For the intrinsic case the absorption is due to generation of electrons and holes.[6] For the extrinsic photoconduction, the absorption has been presumed to result from the direct excitation of a carrier from the impurity center to the appropriate band. The long-wavelength threshold for impurity photoconduction is related to the ionization energy of the specific impurity level.[7] Primarily because of the much higher value of absorption constant in the region of intrinsic absorption, intrinsic photosensitivity is considerably higher than is impurity photosensitivity. For all of the impurity elements studied, n-type samples show considerably higher intrinsic photosensitivity than p-type samples. They are slower in recovery and demonstrate quenching effects characteristic of hole trapping. Further evidence for hole trapping in n-type Fe-doped Ge has been obtained from studies of injection breakdown[8] and optical absorption of injected carriers.[9]

These observations have been explained by assuming that dissolved impurity atoms (Au, Fe, Co, Ni) each

[1] W. C. Dunlap, Jr., Phys. Rev. 91, 1282 (1953).
[2] W. W. Tyler and H. H. Woodbury, Phys. Rev. 96, 874 (1954).
[3] R. Newman and W. W. Tyler, Phys. Rev. 96, 882 (1954).
[4] Tyler, Newman, and Woodbury, Phys. Rev. 97, 669 (1955); 98, 461 (1955).
[5] Recently evidence has been presented indicating that Au also introduces a donor level at about 0.05 ev above the valence band. See Morton, Hahn, and Schulz, Proceedings of the Atlantic City Photoconductivity Conference, November, 1954 (unpublished). Also see W. C. Dunlap, Jr., Phys. Rev. 97, 614 (1955). Also Bull. Am. Phys. Soc. 30, No. 2, 12 (1955). We will not be concerned with the 0.05-ev level in this paper.

[6] Hall, Bardeen, and Blatt, Phys. Rev. 95, 559 (1954).
[7] R. Newman, Phys. Rev. 94, 278 (1954).
[8] W. W. Tyler, Phys. Rev. 96, 226 (1954).
[9] R. Newman, Phys. Rev. 96, 1188 (1954).

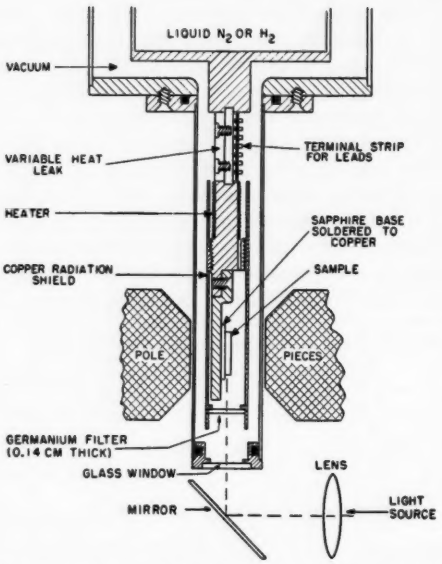

FIG. 1. Sample holder used for Hall measurements, indicating the method of focusing light on the sample.

introduce two acceptor states in Ge.[5] This assumption permits a reasonable model for hole trapping in *n*-type samples based on charge considerations.[2] If hole trapping is an important photoconductive process, giving rise to the high intrinsic photosensitivity, long decay times, quenching, and breakdown effects in *n*-type samples, intrinsic photoconduction in such samples should be due primarily to mobile electrons. In order to test this specific hypothesis and to gain general understanding of photoconduction in Ge, it seemed necessary to ascertain the type of carriers responsible for photoconduction in both *n*- and *p*-type samples in spectral regions of impurity and intrinsic absorption. To this end studies of steady-state Hall mobility of optically excited carriers were undertaken.

II. EXPERIMENTAL METHOD

Figure 1 shows the experimental arrangement. A cryostat described previously[2] was modified as shown to permit focusing light from the exit slit of a Gaertner spectrometer (crystal quartz optics) on the Ge sample. To excite intrinsic photoconduction light of 1.58 microns (0.78 ev) was used; for impurity photoconduction, light of 2.3 microns (0.54 ev) was used. Slit widths were normally set at 0.5 mm. The light source used was a tungsten ribbon lamp. Some measurements were also performed using a Perkin-Elmer Spectrometer, which provided greater resolution and freedom from stray light. The results were independent of the spectrometer used. For some high-light-level experiments in which spectral resolution was not important, (*n*-type samples), the W lamp was used directly without the spectrometer. For such experiments, the Ge filter, held at the temperature of the sample under study was particularly important in filtering short-wavelength radiation which would be surface-absorbed in the test sample. With the filter the effects of inhomogeneous absorption of intrinsic radiation were not serious.

Hall mobility measurements were made with the instrumentation which has been described.[2] The magnetic field used for all data to be reported was 4800 gauss. The preparation of samples has also been described. Fused Sn contacts were used for *n*-type samples and fused In contacts used for *p*-type samples. Applied voltages during measurement were held at less than one volt to minimize injection effects.

III. EXPERIMENTAL RESULTS

Although *p*- and *n*-type high-resistivity samples doped with Au, Fe, Co, and Ni have been studied, detailed data will be shown only for samples designated 55B, Au-doped, *p*-type; 1476, Au-doped, *n*-type[10]; 122B, Co-doped, *p*-type; and 124H, Co-doped, *n*-type. Qualitatively all high-resistivity samples of the same type behaved in the same manner. The Au- and Co-doped samples were chosen for detailed study because of their relatively high impurity photosensitivity and relatively low photovoltages.

Equilibrium mobility, resistivity and photoconductivity data have been published for Co-doped samples

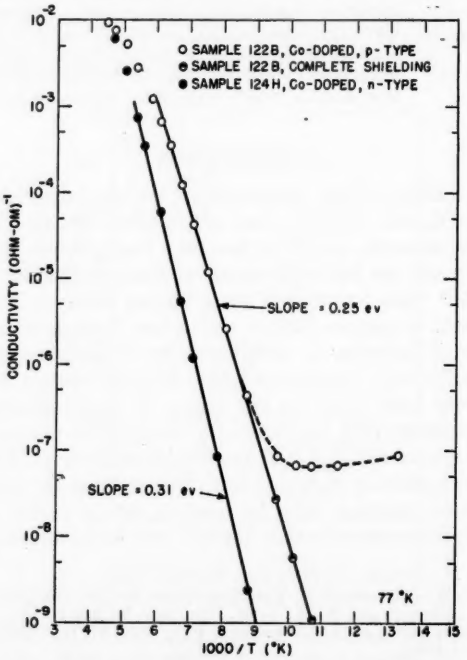

FIG. 2. Dark conductivity data for Co-doped Ge samples 122B and 124H taken with the arrangement shown in Fig. 1. For data indicated by half closed circles, the Ge filter was replaced by copper.

[10] We are indebted to W. C. Dunlap, Jr., for providing us with this sample.

122B and 124H.[4] Samples studied with the arrangement shown in Fig. 1 are continually exposed to the component of 300°K radiation which is not absorbed in the Ge filter. Consequently, values of resistivity and mobility designated as dark values in this paper are not necessarily true equilibrium values. Figure 2 shows the dependence of conductivity on temperature for the Co-doped samples, studied with the arrangement shown in Fig. 1. On replacing the Ge filter with an opaque shield, the conductivity of sample 122B follows the linear relationship to values $<10^{-9}$ (ohm-cm)$^{-1}$. On exchanging the 1.4-mm Ge filter for one five times as thick, the upper curve of Fig. 2 was reproduced exactly, indicating that the sensitivity of sample 122B to 300°K radiation is due almost entirely to the extrinsic component.[11] Figure 2 indicates that sample 122B is more sensitive to 300°K radiation than is 124H, which is consistent with the higher impurity photosensitivity reported for 122B.[4] Figures 3 and 4 show dark values of conductivity and mobility for Au-doped samples 55B and 1476 measured with the arrangement of Fig. 1. For these, the *n*-type sample is more sensitive to 300°K radiation, again consistent with impurity photoconductivity studies.[6]

Figures 5 and 6 illustrate experimental results characteristic of all high-resistivity *n*-type samples. Effective Hall mobility values are plotted as a function of conductivity. For a series of fixed temperatures, the

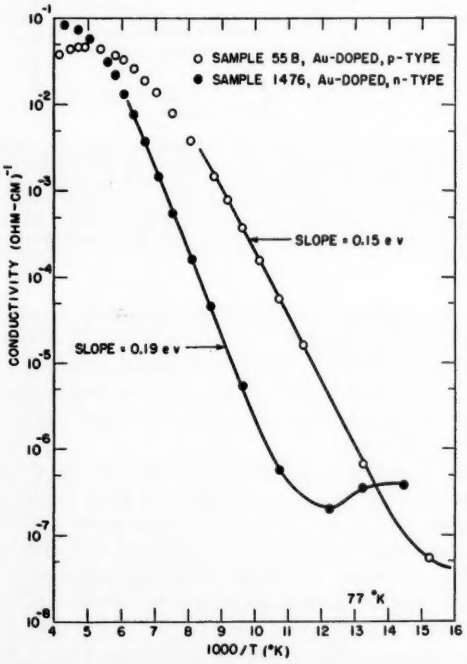

FIG. 3. Dark conductivity data for Au-doped Ge samples 55B and 1476, with the arrangement of Fig. 1.

[11] Similar results were reported for *n*-type Fe-doped samples in reference 2.

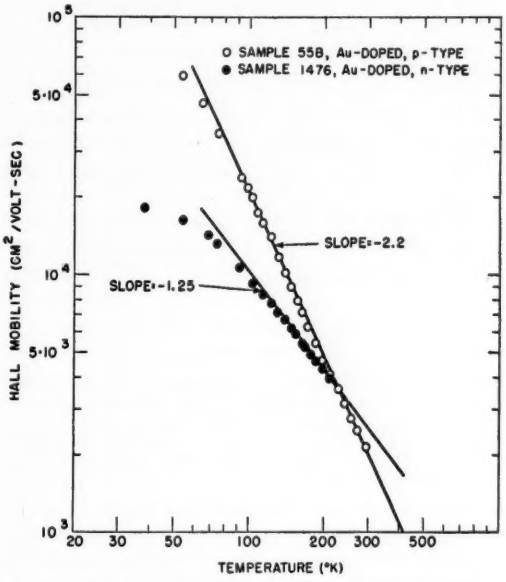

FIG. 4. Dark mobility data for the Au-doped samples 55B and 1476, with the arrangement of Fig. 1.

conductivity was increased from the dark value by increasing the light intensity. As monochromator experiments indicated no significant dependence of behavior (other than sensitivity) on wavelength of the light used, most of these data were taken using the W lamp directly, in order to obtain higher light levels. For both samples some data using monochromatic light are also shown. High-resistivity *n*-type samples show no appreciable change in effective Hall mobility whether excited by light in the region of intrinsic or impurity absorption. For samples of highest photosensitivity, the conductivity could be changed as much as six or seven factors of ten (primarily intrinsic response) without any appreciable drop in effective mobility. Throughout the temperature range studied, and particularly for the lowest temperatures where the change in conductivity is largest, hole mobility (measured in *p*-type samples) is higher than electron mobility (measured in *n*-type samples).[12] Thus the data indicate that holes do not contribute significantly to steady-state photoconduction in high-resistivity *n*-type samples.

For sample 124H, dark-mobility values at the lowest temperatures tend to fall somewhat below the approximate $\frac{3}{2}$ power temperature dependence observed at higher temperatures. Also at low temperature dark-mobility values show considerable scatter (± 10 percent). With light, effective mobility values rise to saturation values consistent with the $\frac{3}{2}$ power temperature dependence and less scatter is observed. These characteristics of *n*-type samples were also observed for *n*-type Fe- and Ni-doped samples. In some cases

[12] See references 2 and 4 for mobility data on Fe-, Co-, and Ni-doped samples and Fig. 4 for Au-doped samples studied.

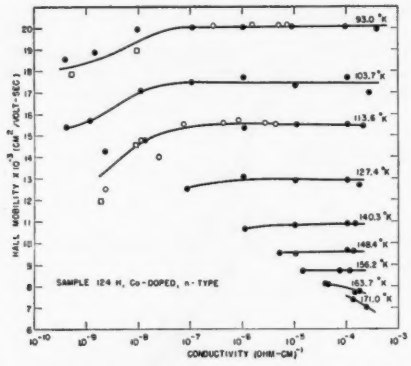

FIG. 5. Effective mobility plotted against optically excited conductivity for Co-doped, n-type sample 124H. Closed circles indicate response to radiation from the tungsten lamp. Squares indicate response to extrinsic radiation (2.3 microns), open circles indicate response to intrinsic radiation (1.58 microns). All Hall coefficients are negative.

samples with an anomalous dark mobility-temperature dependence[4] showed a linear $\frac{3}{2}$ power relationship using the photo-saturation values. At the highest temperatures for sample 124H where photosensitivity decreases, effective mobility values fall slightly with increase in conductivity, perhaps indicating that hole conduction is beginning to contribute in determining the Hall coefficient. For sample 1476, effective mobility values initially fall about 5 percent with increasing light level and rise slightly at the highest light levels. For both Figs. 5 and 6, for each temperature, data points to the far left represent dark values of mobility. Data points to the far right were taken at approximately the same light level.

Figures 7 and 8 illustrate behavior typical of high-resistivity p-type samples doped with Au, Fe, Co, and Ni. Square data points indicate values of effective mobility as a function of the conductivity change induced by impurity excitation (2.3 microns). Circles represent response to intrinsic excitation (1.58 microns);

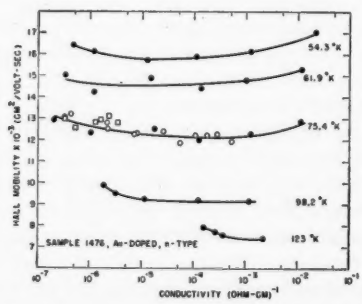

FIG. 6. Effective mobility plotted against optically excited conductivity for Au-doped n-type sample 1476. Closed circles indicate response to radiation from the tungsten lamp. Squares indicate response to extrinsic radiation (2.3 microns), open circles indicate response to intrinsic radiation (1.58 microns). All Hall coefficients are negative.

open circles indicate positive values of Hall coefficient, solid circles indicate negative values of Hall coefficient. The Hall inversion which was observed for all high-resistivity p-type samples studied, occurs for 122B after the conductivity had been increased by a factor between 3.5 and 4; for 55B the Hall inversion occurs after increasing the conductivity by a factor of about 2.

The data shown in Figs. 7 and 8 indicate that impurity photoconduction in high-resistivity p-type samples is due to an increase in the concentration of mobile holes. Conversely, intrinsic photoconduction is due primarily to an increase in the concentration of mobile electrons. Although it is expected that in this temperature range hole mobility is greater than electron mobility,[12] it is not clear exactly what ratio should be used in attempting to analyze the Hall inversion. The curves of Figs. 7 and 8 were repeated at about 10 different temperatures for each sample. The

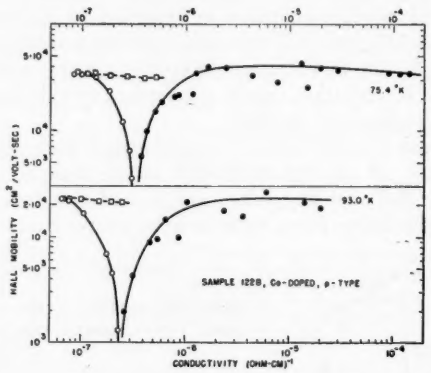

FIG. 7. Effective mobility plotted against optically excited conductivity for Co-doped p-type sample 122B. Squares indicate response to extrinsic light (2.3 microns). Both open and closed circles represent response to intrinsic radiation (1.58 microns). For data points indicated by squares and open circles, Hall coefficients are positive. For closed circles Hall coefficients are negative.

effective mobility after inversion saturates at values approximately equal in magnitude to the dark value. There is no evidence for any of the samples studied that the saturation values of mobility after the Hall inversion follow a temperature dependence characteristic of electron mobility.

Photovoltages were observed in many of the p-type samples studied but were negligible for all of the n-type samples. For sample 55B photovoltages were always less than several percent of the current and Hall potentials. However, for sample 122B photovoltages were in some cases as high as 20 percent of current and Hall potentials. The periodic rise and fall of effective mobility values after inversion shown in Fig. 7 was correlated with factor of 10 scale changes in the current source used in taking data; for the high data points probe potentials due to the current through the sample were appreciably larger than photovoltages, for the

lowest data points photovoltages were as high as 20 percent of probe potential. The spread in data points was considerably greater than shown in Fig. 7 before the potentials used in calculating the conductivity and Hall coefficient were corrected for photovoltages. As the magnitude of photovoltages remained small until the Hall inversion, the inversion point is not affected by photovoltage.

At 75.4°K the dark conductivity value for sample 122B is about 5 factors of ten higher than the true equilibrium value (see Fig. 2). However, the Hall inversion occurs after the same change in conductivity as that observed at 113°K, (not shown in Fig. 7), at which temperature the dark conductivity is approximately equal to the equilibrium value. This is consistent with the observation mentioned above, that the photoresponse of sample 122B to 300°K radiation is due to impurity photoconduction.

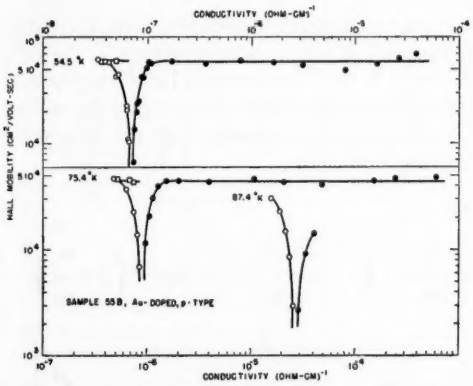

FIG. 8. Effective mobility plotted against optically excited conductivity for Au-doped p-type sample 55B. Squares indicate response to extrinsic light (2.3 microns). Both open and closed circles represent response to intrinsic radiation (1.58 microns). For data points indicated by squares and open circles, Hall coefficients are positive. For closed cirlces Hall coefficients are negative.

Efforts to compare these properties of high-resistivity samples doped with Au, Fe, Co, and Ni with normal Ge samples of high purity, met with little success because of the low photosensitivity of such samples. However, for one n-type sample containing about 2×10^{12}cm^{-3} low ionization energy donor impurities, with a pair lifetime of about 5 milliseconds, the following results were observed. At temperatures from 160°K to about 77°K, when the W lamp was used directly, conductivity increases of about 20 percent resulted in reproducible decreases in effective mobility of about 15 percent. This constitutes some evidence that in normal high-lifetime Ge under intrinsic excitation both electrons and holes contribute to photoconductivity.*

IV. SUMMARY AND DISCUSSION

A. Impurity Photoconduction

Impurity photoconduction in high-resistivity Ge crystals doped with Au, Fe, Co, and Ni is the result of an increase in the concentration of mobile holes in p-type samples and an increase in the concentration of mobile electrons in n-type samples. These results have been assumed heretofore on the basis of the spectral dependence of the impurity photoconduction.[6] The present results demonstrate this directly by Hall coefficient measurements.

In terms of the double-acceptor model which has been proposed to account for the two deep levels introduced in Ge by each of the impurities studied, the explanation of impurity photoconduction is direct. For p-type samples in thermal equilibrium, at least part of the lower acceptor levels are unoccupied. Electrons are excited from the valence bands to these levels, leaving mobile holes. In n-type material, all of the lower levels and at least part of the upper levels are occupied by by electrons. Light excites electrons from these levels directly to the conduction band.

B. Intrinsic Photoconduction

In the region of intrinsic absorption, it is assumed that the production of a free electron and free hole is the initial consequence of the absorption of a photon. To explain our experimental results we assume that, both in n- and p-type samples, the free electron lifetime is significantly larger than the free hole lifetime.[13] Hole trapping seems to be the important photoconductive process in both n- and p-type samples. Because of the higher photosensitivity, longer decay times and quenching effects observed in n-type samples it seems evident that hole trapping is more effective in n-type samples than in p-type samples, giving an appreciably longer free electron lifetime in n-type samples.

A hypothesis for hole trapping in n-type material based on considerations of charge distribution at a double-acceptor site has been proposed to explain high photosensitivity in n-type Fe-doped crystals.[2] It was postulated that hole trapping in such samples was due to the much larger capture cross section for holes by doubly charged negative sites than for electrons by singly charged negative sites. This hypothesis may be extended to explain hole trapping in p-type samples. It is now proposed that the capture cross section for holes by singly charged negative sites is sufficiently larger than the capture cross section for electrons by neutral sites, so that even in p-type material, free-electron lifetimes are appreciably larger than free-hole lifetimes.

* *Note added in proof.*—The cyclotron resonance measurements of optically excited carriers in germanium show that both holes and electrons are mobile in normal high-purity samples at 4°K [see A. F. Kip, Physica **20**, 813 (1955)]. It would be of interest to use the techniques of cyclotron resonance to study the class of phenomena described in this report.

[13] See A. Rose, Phys. Rev. **97**, 322 (1955), for a detailed account of the relationship of carrier lifetime to photoconductive behavior.

Infrared Absorption of Indium Antimonide*

W. KAISER† AND H. Y. FAN
Purdue University, Lafayette, Indiana

(Received January 17, 1955)

Indium antimonide samples of a wide range of carrier concentrations were measured from ~5°K to 500°K, over a wavelength region of 3 to 35 microns. Experimental results on the shift of the absorption edge in degenerate *n*-type samples are presented and discussed. Both *n*-type and *p*-type samples show the same absorption at long wavelengths, after becoming intrinsic at elevated temperatures. At lower temperatures, the absorption in *n*-type samples increases with wavelength, whereas in *p*-type samples it remains practically constant over a wide wavelength region. The absorption coefficient in different samples, *n*-type or *p*-type, does not increase proportionately with the carrier concentration. Possible mechanisms for the absorption are discussed.

OF the large group of intermetallic-compound semiconductors, indium antimonide is of particular interest. The material exhibits a very high electron mobility, up to 60 000 cm²/volt-sec, and a small energy gap, 0.18 ev at 300°K in samples of high purity.[1–5] Its optical properties have been reported by several investigators with emphasis on the absorption edge.[5–12] We present in the present paper some results obtained from transmission measurements at different temperatures on samples of various carrier concentrations.[8] Measurements were made not only near the absorption edge but also at longer wavelengths, up to 35 microns. The results show some interesting behaviors of the absorption coefficient, for which tentative explanations are suggested. The samples used are not single crystals but consisted of several large crystallites.

THE ABSORPTION EDGE

It has been found that absorption edges in *n*-type InSb samples of high carrier concentrations are at much shorter wavelengths than in purer specimens. Burstein[7] proposed that due to the small effective mass the conduction electrons become degenerate at high concentrations and the absorption edge should then shift with the Fermi level. The displacement of the absorption edge with increasing carrier concentration can be derived in the following way. The absorption coefficient α should be proportional to the probability of the excited state to be unoccupied

$$\alpha=\alpha_0\left(1-\frac{1}{\exp[(E-\zeta)/kT]+1}\right), \tag{1}$$

where α_0 is the absorption coefficient if the excited state is unoccupied, E is the electron energy in the excited state, and S is the Fermi energy. Let E_0 be the energy of the electron in the valence band before the excitation and let all energies be measured from the bottom of the conduction band. Then

$$h\nu=E-E_0$$
$$=\frac{h^2}{2m_e}k^2-\left(-E_G-\frac{h^2}{2m_h}k^2\right)=E_G+E\left(1+\frac{m_e}{m_h}\right), \tag{2}$$

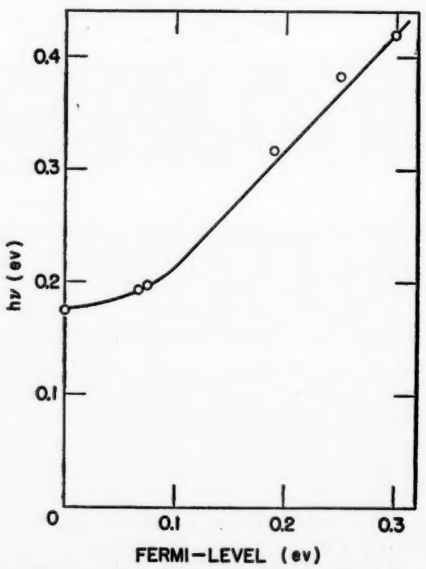

FIG. 1. The shift of the absorption edge. Photon-energy at an absorption coefficient of 300 cm^{-1} *versus* Fermi-level for various *n*-type samples with carrier concentrations up to 5×10^{18} cm^{-3}. Points are experimental results. The solid curve is calculated from Eq. (1).

* Work supported by a Signal Corps Contract.
† Now at Signal Corps Engineering Laboratories, Fort Monmouth, New Jersey.
[1] H. Welker, Z. Naturforsch. **7a**, 744 (1952).
[2] M. Tannenbaum and J. P. Maita, Phys. Rev. **91**, 1009 (1953).
[3] Cunnell, Saker, and Edmond, Proc. Phys. Soc. (London) **A66**, 1115 (1953).
[4] O. Madelung and H. Weiss, Z. Naturforsch. **9a**, 527 (1954).
[5] Breckenridge, Blunt, Hosler, Frederikse, Becker, and Oshinsky, Phys. Rev. **96**, 571 (1954).
[6] M. Tannenbaum and H. B. Briggs, Phys. Rev. **91**, 1561 (1953).
[7] E. Burstein, Phys. Rev. **93**, 632 (1954).
[8] W. Kaiser and H. Y. Fan, Phys. Rev. **94**, 1431 (1954). This abstract gives a brief account of the work reported here.
[9] Koch, Miller, and Goering, The Electrochemical Society Spring Meeting 1954 (unpublished).
[10] F. Oswald and R. Schade, Z. Naturforsch. **9a**, 611 (1954).
[11] Hrostowski, Wheatley, and Flood, Phys. Rev. **95**, 1683 (1954).
[12] T. S. Moss, Conference on Photoconductivity, Atlantic City, 1954, will appear in the Conference Proceedings to be published.

where E_G is the energy gap. The electron wave number k remains the same before and after the excitation due to the selection rule. Combining (1) and (2) we get

$$h\nu(\alpha)=E_G+\left[\zeta-kT\ln\left(\frac{\alpha_0}{\alpha}-1\right)\right]\left(1+\frac{m_e}{m_h}\right). \quad (3)$$

The second term gives the displacement of $h\nu$ for a given α with varying carrier concentration which is related to ζ. The solid curve in Fig. 1 is calculated according to (3), using the following values: $\alpha=300$ cm^{-1}, $T=295$°K, $m_e/m_h=0.15$, and $E_G=0.175$ ev. The value of E_G is taken from the absorption edge (at $\alpha=300$ cm^{-1}) of samples with small carrier concentrations. In our transmission measurements absorption coefficient was measured up to 10^3 cm^{-1} for samples of small carrier concentrations. From reflection measurements, Moss[12] has estimated higher absorption coefficients at shorter wavelengths. The values for α_0 to be used in (3) were obtained from these data. The experimental results are given by the points in Fig. 1. Values of $h\nu$ corresponding to $\alpha=300$ cm^{-1} were taken from the absorption coefficient curves measured for n-type samples with different carrier concentrations as given by Hall effect and resistivity measurements. The value of ζ corresponding to each carrier concentration is calculated assuming $m_e=0.03m$. The agreement between the points and the calculated curve seems to be quite satisfactory.

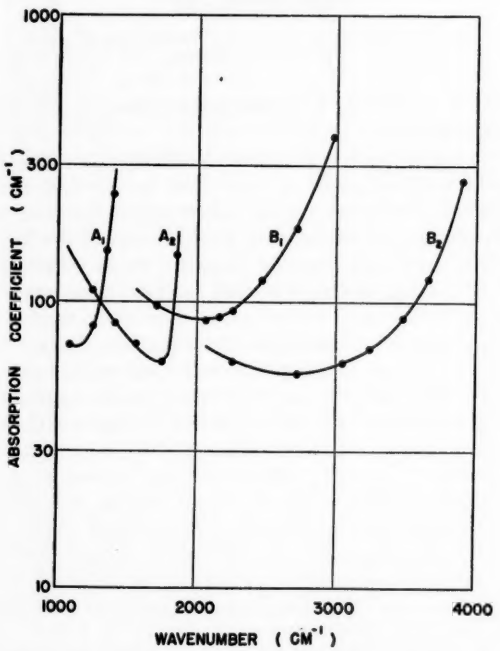

FIG. 2. The absorption edge of a nondegenerate InSb sample (p-type). Curve A_1 at 300°K, curve A_2 at ~5°K. Curves B_1 and B_2 show the absorption edge of a highly degenerate n-type specimen at 300°K and ~5°K, respectively.

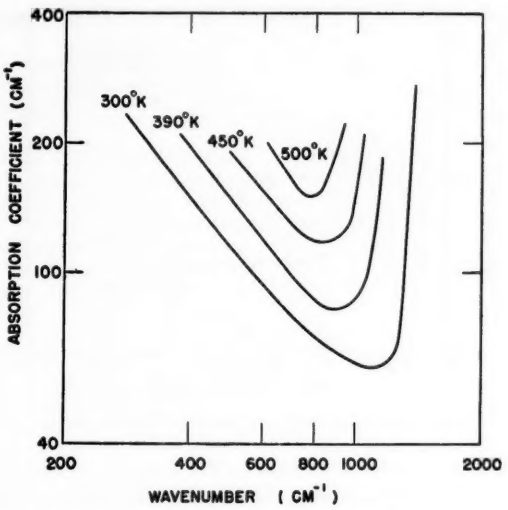

FIG. 3. Absorption of an n-type sample ($n=10^{17}$ cm^{-3}) at high temperatures.

Measurements at different temperatures show that the absorption edge shifts to shorter wavelengths with decreasing temperature. For samples of small carrier concentrations, this shift indicates a change of the energy gap amounting to -2.8×10^{-4} ev/°K, in the temperature range 5°K to 520°K. Figure 2 shows two curves A_1 and A_2 taken on such a sample at 300°K and ~5°K, respectively. The same figure shows also the curves B_1 and B_2 taken on a degenerate n-type sample at the same temperatures. These curves show a much larger shift, nearly all of which took place between 300°K and 77°K. According to (3), one might indeed expect that for a drop in temperature the increase in $h\nu$ will be larger than the increase in E_G on account of the term involving kT. However, this term comes from (1) and expresses the fall-off of the distribution function at the Fermi energy; with decreasing temperature the fall-off becomes sharper. According to (1), α at a given temperature should rise exponentially with increasing E or $h\nu$, so long as $\alpha\ll\alpha_0$, and $\ln\alpha$ plotted against $h\nu$ should have a slope $1/kT$, disregarding the variation of α_0 in the small interval of $h\nu$. Curves B_1 and B_2 in Fig. 2 have much smaller slopes than $1/kT$, especially curve B_2 for the lower temperature. In fact B_2 has about the same shape as B_1 instead of being much steeper, and both curves are much flatter than the curves A_1 and A_2 for the nondegenerate sample. It is possible that there is some broadening of the absorption edge in the low range of α covered by these curves, but it is not yet clear what is the most likely mechanism for such broadening.

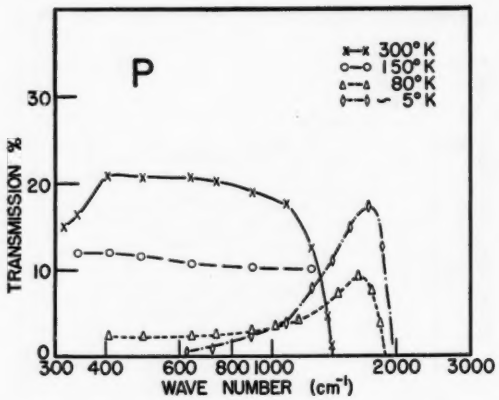

FIG. 4. Transmission of a p-type sample ($p=9\times10^{16}$ cm^{-3}) at low temperatures.

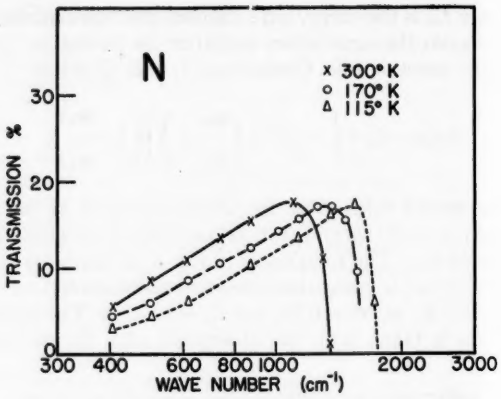

FIG. 5. Transmission of an n-type sample ($n=10^{17}$ cm^{-3}) at low temperatures.

LONG-WAVELENGTH ABSORPTION

Measurements were made up to 35 microns. Figure 3 shows a series of absorption curves at different elevated temperatures for an n-type sample. The absorption increases with wavelength and rises with increasing temperature. The sample is well in the intrinsic range at 500°K. The curves for the two higher temperatures agree with the results obtained on a p-type sample which becomes intrinsic above 400°K. Thus the long-wavelength absorption at high temperatures in the intrinsic range seem to be due to free carriers.

The situation is more involved at lower temperatures with samples in the extrinsic range. Typical transmission curves are given in Fig. 4 for a p-type sample and in Fig. 5 for an n-type sample. These curves show that the absorption in n-type samples increases with wavelength whereas it remains practically constant in p-type samples, begining to rise only beyond 25 microns (400 cm^{-1}) at room temperature. In contrast to germanium and silicon, the absorption coefficient for different samples is not proportional to the carrier concentration, e.g., at room temperature n-type samples with carrier concentrations ranging from 10^{17} cm^{-3} to 4.6×10^{18} cm^{-3} gave absorption coefficients varying by a factor of 6 only, and in p-type samples with hole concentrations varying from 3.5×10^{16} cm^{-3} to 10^{18} cm^{-3} the absorption coefficient varied only by a factor of 2.5. Furthermore, the variation of the absorption coefficient with temperature is interesting. For both n-type and p-type samples the absorption coefficient increases with decreasing temperature, very strongly in the p-type. On the other hand, Hall effect and resistivity measurements indicate that the carrier concentration in these samples remains practically constant between 77°K and 300°K and the mobility does not show much change. All these observations indicate that it is difficult to attribute the absorption to the free carriers.[13]

It might be suggested that the absorption is caused by optical ionization of impurities or localized electronic states in general. As the temperature decreases, the Fermi level approaches to either one of the band edges. In n-type material impurity levels very close to the conduction band become more occupied by electrons which can be excited to the conduction band giving absorption. Analogous effect can be obtained in p-type samples with impurity level close to the valence band. The absorption is proportional to the electron or hole population of these impurities. To agree with the electrical data, we have to assume that the concentration of such impurity states is sufficiently small so that changes in their electron population do not affect appreciably the concentration of free carriers. However, calculations show that it is difficult to account for the experimental observations using this model which confines the variation of the absorption coefficient to much smaller temperature ranges.

A possible mechanism is the excitation rather than ionization of electrons or holes in localized states. The probability for the carrier to be in the excited state having energy E above the ground state is given by the Boltzmann factor. For a constant number of electrons or holes, the absorption at a given wavelength will be proportional to $[1-\exp(-E/kT)]$. The experimentally observed temperature variations of α can be fitted by choosing a suitable value for E, e.g., for the p-type sample an approximate fit can be obtained with $E=0.006$ ev.

This work is a part of the investigations on intermetallic compounds initiated by Professor K. Lark-Horovitz and we wish to thank him for stimulating discussions.

[13] See H. Y. Fan and M. Becker, *Semiconducting Materials* (Butterworths Publications, London, 1951).

Temperature Variation of the Elastic Constants of Cubic Elements. I. Copper

W. C. Overton, Jr., and John Gaffney
United States Naval Research Laboratory, Washington 25, D. C.

(Received September 8, 1954)

The ultrasonic pulse technique has been used in conjunction with a specially devised cryogenic technique to measure the velocities of 10-Mc/sec acoustic waves in copper single crystals in the range from 4.2°K to 300°K. The values and the temperature variations of the elastic constants have been determined. The room temperature elastic constants were found to agree well with those of other experimental works. Fuchs' theoretical c_{44} at 0°K is 10 percent larger than our observed value but his theoretical c_{11}, c_{12}, K and $(c_{11}-c_{12})$ agree well with the observations. The isotropy, $(c_{11}-c_{12})/2c_{44}$, was observed to remain practically constant from 4.2°K to 180°K, then to diminish gradually at higher temperatures. Some general features of the temperature variations of elastic constants are discussed.

INTRODUCTION

ACCURATE experimental measurements of the elastic constants of single crystals of the metallic elements at temperatures low enough to permit reliable extrapolations to 0°K provide particularly important fundamental quantities. Such values at 0°K are needed in several areas of the solid state theory. They provide a check into the accuracy of the quantum mechanical calculations, such as those due to Fuchs,[1] of the elastic constants and the cohesive energy. They permit testing the equations relating the elastic constants at 0°K to the atomic force constants which are used in the calculation of the vibrational spectra and specific heats by the method of Born and von Karman.[2] If central forces are assumed in a theory of the elasticity of monatomic solids[3] the Cauchy relations result but these are not observed experimentally. The deviations from Cauchy relations can be studied in detail with elastic constants at 0°K in view of a recent hypothesis due to de Launay[4] which takes the electron gas elasticity into account. Both the values at 0°K and the details of the temperature variations of the isothermal elastic constants are needed to test the validity of the Born theory[5] for these temperature variations.

We are particularly interested in checking the validity of the Born-von Karman theory of specific heat in the case in which only nearest and next-nearest neighbor interactions are considered in the theory.[6] This requires both experimental elastic constants and experimental specific heat measurements. Calorimetric techniques have improved to the point that some relative experimental uncertainties in specific heats are as small as a few tenths of a percent[7] at low temperatures and it is expected that the absolute accuracies will ultimately improve to better than one percent. Thus these considerations demand as reasonably good accuracy of measurement of the elastic constants on good quality single crystals as can be obtained by conventional ultrasonic techniques in conjunction with a cryogenic technique suitable for such measurements at liquid helium temperatures.

The measurements on copper crystals reported herein are the first results of a program for the measurement of the elastic constants of crystals of the face-centered and body-centered cubic metallic elements in the range from room temperature to liquid helium temperatures. Because this is the first paper of a series some of the experimental details discussed here will be omitted from later papers. Copper is of interest because of Fuch's theoretical calculations,[1] because its specific heat is reliably known[8] down to 10°K and because Leighton's theoretical specific heat calculations[6] were in terms of parameters that differ but little from the experimental parameters for copper.

EXPERIMENTAL METHODS

Well-known results of the theory of plane elastic wave propagation in cubic crystals are the velocities of propagation of one longitudinal and two transverse plane waves in any crystallographic direction. These plane wave velocities, appearing in the elastic theory in the form ρv^2, are the solutions of a cubic secular determinantal equation. The elements of this determinant are defined by the elastic constants and the direction cosines of the direction of propagation. Thus if the cosines are known and the velocities are measured in a sufficient number of crystallographic directions (sometimes only one direction is required) this is equivalent to the measurement of the fundamental adiabatic elastic constants themselves. It may be shown that it is usually more reliable, from the experimental view-

[1] K. Fuchs, Proc. Roy. Soc. (London) **A151**, 585 (1935); **A153**, 622 (1936).
[2] M. Born and Th. von Karman, Physik. Z. **13**, 297 (1912); Physik. Z. **14**, 15 (1913).
[3] I. Stakgold, Quart. Appl. Math. **8**, 2 (1950).
[4] J. de Launay, J. Chem. Phys. **21**, 1975 (1953).
[5] M. Born, J. Chem. Phys. **7**, 591 (1939); Proc. Cambridge Phil. Soc. **36**, 160 (1940); M. Born, Proc. Cambridge Phil. Soc. **39–40**, 100 (1943–44); M. Born and M. Bradburn, Proc. Cambridge Phil. Soc. **39–40**, 104 (1943–44); M. M. Gow, Proc. Cambridge Phil. Soc. **39–40**, 151 (1943–44).
[6] R. B. Leighton, Revs. Modern Phys. **20**, 165 (1948).
[7] J. R. Clement and E. H. Quinnell, Phys. Rev. **92**, 258 (1953).
[8] W. F. Giauque and P. F. Meads, J. Am. Chem. Soc. **63**, 1897 (1941); S. M. Dockerty, Can. J. Research **15A**, 59 (1937); J. A. Kok and W. H. Keesom, Physica **3**, 1035 (1936).

point, to measure the plane wave velocities of waves propagating in crystallographic symmetry directions, such as the [001] and [011] directions. For these two special directions there are five distinct roots of the secular equations for cubic crystals as follows: $\rho v_1^2 = c_{11}$, a longitudinal wave propagating in the [001] direction; $\rho v_2^2 = c_{44}$, two identical roots, corresponding to transverse waves polarized in the [010] and [100] directions propagating in the [001] direction; $\rho v_3^2 = (c_{11}+c_{12}+2c_{44})/2$, a longitudinal wave propagating in the [011] direction; $\rho v_4^2 = c_{44}$, a transverse wave polarized in the [100] direction propagating in the [011] direction; $\rho v_5^2 = (c_{11}-c_{12})/2$, a transverse wave polarized in the [0$\bar{1}$1] direction propagating in the [011] direction.

The velocities, v_1 to v_5, may be determined directly by experiment by measuring the transit time of plane ultrasonic longitudinal or transverse waves in (001) and (011) crystal specimens. To assure that the waves are sufficiently plane it is considered necessary that the diameter of the radiating source be large compared to the wavelength of the sound waves and that the wave front should be small enough in diameter so that it does not suffer appreciable interaction with the walls of the specimen. We have satisfied these requirements sufficiently well in practice by using 2 cm diameter specimens and 2 cm diameter quartz crystals cemented directly to the specimen end faces and excited over 1.4 cm of their diameter at a frequency of 10 Mc/sec. In copper the wave fronts of the propagated waves of 1.4-cm wave-front diameter are about 30 wavelengths across for longitudinal waves and about 50 wavelengths across for transverse waves. It may be shown that these waves are "sufficiently plane" for accurate measurements of the elastic constants. Under these experimental conditions the ultrasonic beam width between half-intensity points is less than 1° in copper so that the wave does not suffer noticeable wall reflections during the time interval of measurement.

We use the following experimental methods for measuring these velocities as functions of temperature (1) the ultrasonic pulse-echo technique for measuring the round trip transit times of 10-Mc/sec longitudinal and transverse waves in the crystal specimens, (2) a cryogenic technique for controlling the temperature between room temperature and 4.2°K, and (3) techniques providing for acoustical coupling over this temperature range between the specimen and the thin wafer quartz crystal which serves as the ultrasonic transducer. All three of these techniques have been discussed previously in detail and so it is only necessary to discuss certain features pertinent to the copper measurements here.

Ultrasonic Technique

The ultrasonic pulse-echo technique as employed in the measurement of the elastic constants of solids has been described in several papers in the literature.[9] Our electronic equipment is similar to most of those previously described, in that the Du Mont A/R 256-D radar range oscilloscope is employed both for the purpose of triggering the ultrasonic cycle as well as serving as the precision time measuring instrument.

The velocities of longitudinal waves were measured in an (001) copper crystal of length 5.3622 cm at 27.4°C and in an (011) crystal whose length at 20°C was 5.7833 cm. These waves are generated by an X-cut quartz cemented directly to the specimen, the cement providing the acoustical coupling between quartz and specimen. The attenuation of the 10 Mc/sec ultrasonic waves was relatively small in these copper crystals and remained in the neighborhood of 10^{-3} neper per cm over the whole temperature range. Thus very little decay in the sharpness of the leading edges of the echos resulted from attenuation. These specimen lengths were short enough, for longitudinal waves, so that there were always 4 echos of the ultrasonic pulse train in the first 100 microseconds and long enough so that the various end effects, if any, would have a negligible effect on the over-all accuracy of measurement. The most accurate range of the 256-D scope is the delayed-sweep range from 0 to 100 microseconds. In this range the uncertainty in a measurement of the time of arrival of an echo having a rapid rise time can be made as low as about ±0.02 microsecond, when the manually controlled sweep-delay circuit is properly adjusted and calibrated against calibration markers derived from the 100-kc/sec crystal standard.

The time of arrival of each of the first 4 echos in the train was read 5 times and the 5 readings averaged. Immediately after measuring the arrival times of the echos at each temperature the arrival times of the calibration markers were read. Each calibration marker was also read 5 times to give the average arrival time of each of the 10 markers in the 100 microsecond sweep range. From the latter measurements a calibration correction curve was made by plotting the deviation of the sweep delay dial reading from the (true) time of arrival of the markers. These calibration correction curves always turned out to be smooth and the 256-D scope was adjusted so that the deviations from true time were small (usually less than 0.05 microsecond). Thus the corrections to be applied to the echo arrival times also were usually quite small (in the neighborhood of 0.05 microsecond) and the uncertainty of the corrections were estimated to be no greater than 0.01 to 0.02 microsecond. With this procedure we obtained the corrected time of arrival of each of the first 4 echos in the wave train at each temperature of observation.

To get the round-trip transit times at each temperature the corrected average arrival times were treated by

[9] D. L. Arenberg, Radiation Laboratory, Massachusetts Institute of Technology Report 932, 1946 (unpublished); H. B. Huntington, Phys. Rev. **72**, 321 (1947); D. Lazarus, Phys. Rev. **76**, 545 (1949).

least squares. The arrival time, τ, of any echo can be represented by the straight line function, $a+tn$, where the intercept, a, represents the total electronic delay time after the initiating trigger through the electronic circuits and the crystal transducer, the slope, t, represents the round-trip transit time through the ultrasonic specimen, and n is the integer representing the echo number. Because n is an integer the least-squares determination of the delay, a, and the round-trip transit time, t, from the observed times, τ's, is arithmetically simple. The delay, a, was about 0.7 microsecond while the desired transit times for both the (001) and (011) crystals ranged between 22 and 25 microseconds. Only the round-trip transit times, t's, are needed in the calculation of the elastic constants.

Transverse wave velocity measurements were made in the manner described above on the (001) copper crystal in the temperature ranges from 4.2°K to 90°K and from 140°K to 300°K. These measurements yielded the temperature variation of the shear elastic constant c_{44}. They were not made as functions of temperature in the (011) crystal because of the difficulty of properly orienting the Y-cut quartz crystal transducer to give the properly polarized shear waves. This difficulty arose because the cementing of the quartz to the specimen had to be done by remote control within the low temperature cryostat at a temperature of about 120°K. However checks at room temperature showed the internal consistency of the elastic constants of the two crystals.

In the transverse wave measurements on the (001) crystal only two echos could be read in the 100 microsecond sweep range of the 256-D scope because of the long round-trip transit time (about 36 microseconds) of the transverse waves. Thus least squares could not be used to adjust the two-echo data. About 75 different transverse wave measurements were taken in the range from 4.2°K to 300°K. A curve was smoothed through the plot of round-trip transit time *versus* temperature and the residuals, i.e., the deviations of the observed points from the smoothed curve were plotted on probability paper. The standard deviation resulting from this plot was less than ± 0.03 microsecond. This corresponds to a relative error of ± 0.08 percent in the velocity of transverse waves. However the over-all error in the elastic constant c_{44}, has been estimated to be about ± 0.25 percent when other possible sources of error are taken into account.

Transit-Time Correction

In pulse-echo ultrasonic measurements in solids the presence of the cement film bonding the quartz transducer to the specimen solid necessitates a small transit time correction to the observed round-trip transit time through specimen plus film plus quartz. This correction ought to be only the round-trip transit time through the thickness of the cement film only. However, consideration of the various physical factors involved (too detailed to discuss here) shows the possibility of interference among the high-frequency components comprising the leading edges of both the acoustic and electrical pulses impinging on the transducer. The cement film thickness affects the interference pattern and the combined electrical and acoustic effects explain the observed "apparent" delay in "expected" time of arrival of occasional pulses of the echo train.

The magnitudes of these small "apparent" delays (less than 0.1 microsecond at 10 Mc/sec) have been observed experimentally to be temperature dependent. The particular pulses for which the delays are most apparent has also been observed to be temperature dependent. The delays affect the measured average transit time but little while averages of data taken over a temperature range tends to wipe out the effect of the "apparent" delays altogether. On the other hand if the transit time correction is computed from sets of data taken at just one temperature it is likely to be far too large. Thus to get a correct value for the transit time correction by the usual method of measurement on several specimens of different lengths one should perform the measurements at several different specimen temperatures.

We measured transit times on four different specimen lengths [all painstakingly cut from the same (001) copper crystal] at 2°K intervals from 290°K to 310°K. These data were treated by least squares and the average correction, computed at 300°K was 0.01 microsecond. In another experiment the transit time through specimen only was measured directly using the liquid acoustic cell technique. Using these data together with the data for the same specimen cemented directly to quartz the computed correction was only about 0.005 microsecond at 300°K. Thus the small corrections which we might make to our copper data are within the usual reading errors (0.01 to 0.02 microsecond). Now the corrections determined, presumably at just one temperature, by Smith *et al.*[10] range from 0.03 to 0.10 microsecond while those reported by Lazarus[10] range from 0.10 to 0.15 microsecond. We feel that these corrections are too large because they were computed from data taken, presumably, at just one value of the temperature.

Cryogenic Technique

The cryogenic technique used in these experiments is similar to that reported previously.[11] The specimen is mounted in a metal holder which surrounds it and tends to maintain a uniform temperature over its length. The metal holder also contains a platinum

[10] D. Lazarus, Phys. Rev. **76**, 545 (1949); Neighbors, Bratten, and Smith, J. Appl. Phys. **23**, 389 (1952); T. R. Long and Charles S. Smith, Office of Naval Research Technical Report No. 12, NR 019201, July, 1953 (unpublished).

[11] W. C. Overton, Jr., J. Chem. Phys. **18**, 113 (1950); thesis, Rice Institute, 1950 (unpublished); W. C. Overton, Jr., and R. T. Swim, Phys. Rev. **84**, 758 (1951).

resistance thermometer for the temperature range above 20°K and a carbon composition thermometer for the range below 20°K. The temperature of the specimen can be measured to an accuracy of better than 0.1°K at all temperatures. This assembly is supported in the bottom of a Dewar flask by stainless steel support tubes. One of these tubes also serves as a coaxial line down which the 10-Mc/sec rf pulse is fed. The acoustical cement coupling between the quartz crystal and the specimen is made at a temperature of 125°K by using a low melting point cement (5 parts ether, 5 parts isopentane, two parts ethyl alcohol, this mixture abbreviated EPA). This cement is applied on the top face of the thin quartz crystal slab at 125°K as a single tiny drop. The specimen is then lowered onto the quartz thus spreading the drop of EPA into an extremely thin film. On further lowering the temperature to 100°K the EPA film solidifies into a glassy solid thus providing acoustical coupling between quartz and specimen for both longitudinal and transverse waves. It has been found experimentally that no cement applied at room temperature maintains proper acoustical coupling to temperatures below 120°K. Thus it is necessary to have some such technique as here described for cementing at low temperatures in order to attain the still lower temperatures without introducing excessive stresses across the specimen-quartz interface.

Three acoustical bonds were required in order that the whole temperature range below 300°K could be covered. Salol applied at 40°C has been used with success at room temperature as reported in several papers,[9,11] and we employed it successfully in the range from 300°K down to 210°K for cementing the quartz to copper. We used ordinary stop-cock grease as a cement to cover the range from about 250°K down to 130°K. Both the salol and stop-cock grease cements are applied at room temperature or slightly higher. The cementing technique in which the EPA mixture is used as just described provides acoustical coupling from 100°K to 4.2°K. Few measurements were made in the range from 130°K down to 100°K since a suitable stress-free cement for that range is not presently known.

Temperature control was accomplished by a closed system heat exchanger which could be inserted in the lower part of the cryostat. Liquid nitrogen fed into this heat exchanger provided the necessary refrigeration between 300°K and 90°K. To cool from 300°K to 90°K required a minimum time of 30 minutes but we purposely cooled very slowly to prevent thermal shock and so that the specimen crystal could attain a uniform temperature before taking the ultrasonic measurements. It usually required about 8 hours to cover the temperature range from 300°K to 210°K with a salol cement and a similar period to cover the range from 250°K to 130°K when using stop-cock grease as a binder. Constant attention was required during these periods so that when an equilibrium temperature was reached the ultrasonic measurements could be taken. It was necessary to take data on the "cool-down" so that the onset of excessive stress across the quartz-specimen interface could be detected.

PREPARATION OF SPECIMENS

Crucibles of high purity graphite were designed so that crystals 2 cm in diameter by 5 or 6 cm long of preferred orientation could be grown from 0.5-cm seeds of "nearly" preferred orientation by the Bridgman technique. The crucibles were made in two parts, the upper part being a sleeve to contain the melt, the lower part being a solid cylinder machined with a shoulder over which the upper part fits. The snug fit of the sleeve over the lower part prevents molten metal from leaking past the graphite-graphite joint. In order to obtain a crystal of some desired orientation a 0.5-cm diameter seed of nearly this orientation is selected and a hole to contain it is drilled in the lower part of the crucible at the proper angle. The angle may vary from 0 to 10 degrees, the maximum being determined by the one inch diameter of the crucible and the length of the seed crystal. The proper adjustment of the seed in its hole is facilitated by use of an optical goniometer designed to hold the entire crucible.

With the aforementioned arrangement two large single crystals of copper, 2 cm in diameter by 6 cm long, one with [001] cylinder axis within ½ degree and the other with [011] cylinder axis within one and one half degrees, were grown from seeds of nearly preferred orientation. Melts of Johnson, Matthey, and Company spectroscopic copper (Lab. No. 2804) were lowered through the gradient of a vertical tube furnace in an atmosphere of pure helium. After annealing, a crystal, with seed attached, could be removed from its crucible by simply disassembling the crucible.

A specimen crystal could be separated from its seed by first potting them in a wax matrix, then sawing away the seed with a jeweler's saw. Since the crystal structure is damaged only at the cut, the damage may be removed by acid and the seed may be reoriented in the crucible and used again to grow another large single crystal of preferred orientation.

To prepare a large crystal for ultrasonic measurements, it was waxed into a special thick walled hollow cylinder having flat and parallel end faces closely perpendicular to the cylinder axis. When waxed in, the "growth" and "meniscus" ends of the single crystal protrude beyond the end faces of this cylinder, so that when machined in a lathe these ends develop into flat faces. Care was taken to prevent damage to the crystal structure by machining only 0.002 inch per cut until the "growth" and "meniscus" ends of the crystal were removed and end faces developed. Several cuts of 0.001 inch, then several of 0.0005 inch were taken off these newly developed end faces. Finally about 30 cuts of 0.0001 inch were made so as to remove damage produced by the larger cuts. The crystals were then

carefully hand lapped, tested for parallelism with a Sheffield Style 1000 comparator gauge, and found to be parallel to about ±0.00005 inch across the 2 cm diameter of the face. The crystal lengths were determined at room temperature to about ±0.005 percent by comparing against Taft-Pierce gauge blocks.

A spectroscopic analysis of the crystal specimen showed the following impurities: Pb(TR); Fe(FTR); Ag, Ca, Mg(TR); Si(VW). Analysis of the original Johnson, Matthey, and Company copper rods showed: Fe, Ag(TR); Ca, Mg(FTR); Si(VW), Pb not detectable. The symbols denote as follows: (FTR) <0.0001 percent, 0.0001 percent < (TR) <0.001 percent, 0.001 percent < (VW) <0.01 percent. The Pb and slight increases in Ca and Mg impurities evidently were picked up from the low ash content of the graphite crucibles.

EXPERIMENTAL RESULTS

Some 55 measurements of the round-trip transit time for longitudinal waves in the (001) copper crystal were obtained in the manner described above. These constitute the data from which $c_{11}=\rho v_1^2$ *versus* temperature were calculated. If $t_1(T)$ is the measured transit time at temperature T, then the experimental value of c_{11} at T is obtained conveniently by

$$c_{11}(T)=\rho(T)[v_1(T)]^2 = \frac{\rho_0 l_{10}^2}{\left(1+\int_0^T \alpha dT\right)} \times \frac{1}{[t_1(T)]^2}, \quad (1)$$

where ρ_0 is the density at 0°K and l_{10} is the length of the (001) crystal at 0°K.

Nix and MacNair[12] have measured the linear expansion coefficient of pure copper by an interferometric method from 80°K to about 600°K. They found that the Grüneisen formula,

$$\alpha(T)=\frac{C_v/Q_0}{[1-\frac{1}{6}(m+n+3)U/Q_0]^2}, \quad (2)$$

fitted their experimental measurements very well with the following parameters: C_v and U determined from the Debye specific heat and energy functions with Debye $\Theta=325$°K, $Q_0=1.2\times10^5$ cal-mole^{-1} $(m+n+3)/6=2.8$. Using Eq. (2) and these parameters we calculated $\alpha(T)$, determined $\int_0^T \alpha dT$ by graphical integration and prepared a table of $(1+\int_0^T \alpha dT)$ at 10°K intervals from 0°K to 300°K. The measured values of the length l_1 at room temperature is then easily converted to l_{10} at 0°K.

For density, ρ_0, we took the product of the x-ray value[13] for copper at 20°C of 8.9366 g/cm^3 with the cube of $(1+\int_0^{293.2} \alpha dT)$ obtained by interpolation of the aforementioned table. Such interpolations also give the value of $(1+\int_0^T \alpha dT)$ to be used in Eq. (1) at each temperature of measurement.

[12] F. C. Nix and D. MacNair, Phys. Rev. **60**, 597 (1941).
[13] M. Straumanis and O. Mellis, Z. Physik **94**, 184 (1935); M. Straumanis, Z. Physik **126**, 49 (1949).

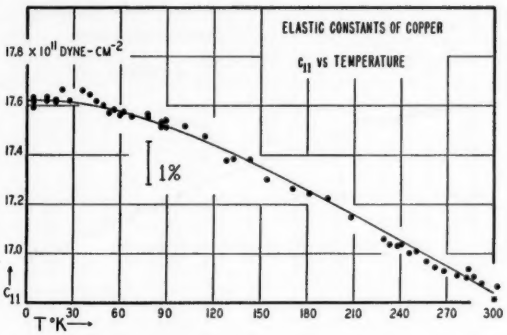

FIG. 1. The adiabatic elastic constant c_{11} of copper *versus* temperature. The points represented by the open circles have been calculated from the measured transit times (t_1's) by means of Eq. (1). The solid curve has been smoothed as described in the text.

In a similar manner the elastic constant c_{44} was computed by

$$c_{44}(T)=\frac{\rho_0 l_{10}^2}{\left(1+\int_0^T \alpha dT\right)} \times \frac{1}{[t_2(T)]^2}, \quad (3)$$

where t_2 is the experimental round-trip transit time for transverse waves in the (001) crystal.

Since the cylinder axis of the (001) crystal deviated by about ½° from the [001] direction the question of a minor correction of the observations to the true [001] direction was considered. The secular determinant was solved for this direction in order to determine this necessary small correction factor, which turned out to be too small, compared to experimental error, to take into account. Thus the actual experimental points of $c_{11}(T)$ and $c_{44}(T)$ shown in Figs. 1 and 2 may be considered as defining the true values and the temperature variation of these elastic constants.

In Fig. 1, in the range from 10°K to 50°K, several experimental points are seen to be higher than the smoothed curve by about 0.4 percent (note the 1 percent bracket). These experimental points were taken on the rapid "warm-up" from 4.2°K, during which time the temperature gradients over the length of the specimen crystal were fairly large. Experimental points taken in this same range on the "cool-down," during which the temperatures were fairly well controlled, are within ±0.15 percent of the curve. Although the mechanism is not understood it is believed that the deviations are caused by the large thermal gradient, for under isothermal conditions with the specimen in baths of liquid N_2, O_2, or He the deviations in the data usually did not exceed about ±0.1 percent.

The experimental deviations in c_{44} *versus* T in Fig. 2 average slightly larger than those of c_{11} as may be seen

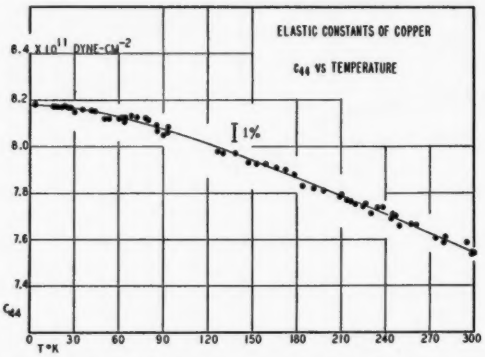

FIG. 2. The adiabatic elastic constant c_{44} of copper *versus* temperature. The points represented by the open circles have been calculated from the measured transit times (t_3's) by means of Eq. (3). The solid curve has been smoothed as described in the text.

by referring to the 1 percent brackets. As pointed out previously this is due to the fact that measurements could be made on only two echos in the more accurate 0–100 microsecond delayed sweep range of the 256-D measuring equipment. Nevertheless the standard deviation is still fairly small and the absolute error in c_{44} from all sources is estimated not to exceed ± 0.25 percent, while that for c_{11} is about ± 0.2 percent.

The most accurate measurements obtained were the longitudinal wave measurements on the (011) crystal. Earlier experience gained on the (001) crystal in regard to the preparation of flat and parallel end faces was put to use in preparing the (011) crystal with the result that the probable error of each measurement (based on the least-squares treatment at each experimental point as earlier described) was smaller than the similarly treated longitudinal measurements in the (001) crystal. This may be noted by comparing the spread in the experimental points in Fig. 3 with that in Fig. 1.

The orientation of the cylinder axis of the (011) copper crystal deviated from the true [011] direction by about 1.3°, the direction angles, expressed as spherical coordinates being about 46.2° and 88.7° instead of 45° and 90°. The secular equation solved for this direction of propagation showed that a correction of 1.27 parts in 10,000 should be added to ρv_3^2. This correction was made to each of the 40 experimental points although it, too, is small compared to the experimental error of ± 0.1 percent. Each experimental point was computed according to

$$\rho v_3^2 = \frac{\rho_0 l_{30}^2}{\left(1+\int_0^T \alpha dT\right)} \times \frac{1}{[t_3(T)]^2} \qquad (4)$$

$$= (c_{11}+c_{12}+2c_{44})/2,$$

where t_3 is the measured round-trip transit time in the [011] direction and l_{30} is the length of the (011) crystal at 0°K computed from the room-temperature length as previously described.

Because the temperatures of observation of the experimental points in Figs. 1, 2, and 3 do not coincide, except at some fixed bath temperatures, the calculation of c_{12}, the shear mode, $C'=(c_{11}-c_{12})/2$ and the adiabatic bulk modulus $K=(c_{11}+2c_{12})/3$ from linear combinations of the experimental results must be made from values picked off curves smoothed through the experimental results. Curves were drawn through the experimental points keeping in mind that the variation with temperature should be monotonic and have zero slope at 0°K. These curves were then slightly readjusted to minimize, particularly in those isothermal regions where the measurements are most reliable, the sum of squares of the residuals. From values picked off the smoothed curves of c_{11}, c_{44}, and ρv_3^2 the additional elastic constants were calculated.

Table I summarizes the adiabatic elastic constants c_{11}, c_{12}, the bulk modulus K, the shear mode C', and the crystalline isotropy factor $S=(c_{11}-c_{12})/2c_{44}$. The errors determined from the experimental measurements are c_{11}, ± 0.2 percent; c_{44}, ± 0.25 percent; ρv_3^2, ± 0.1 percent. Using the standard formulas for the propagation of errors the probable errors in the calculated constants are as follows: c_{12}, ± 0.44 percent; the bulk modulus K, ± 0.34 percent, the shear mode C', ± 1.8 percent; and the crystalline isotropy factor S, ± 1.8 percent.

The isothermal elastic constants, c_{11}^T, c_{12}^T and the isothermal bulk modulus K^T may be calculated from the adiabatic constants in Table I by the thermodynamic relationships,

$$c_{11}^T = c_{11} - K^s(\gamma-1)/\gamma,$$
$$c_{12}^T = c_{12} - K^s(\gamma-1)/\gamma, \qquad (5)$$
$$K^T = (1/\gamma)K^s,$$

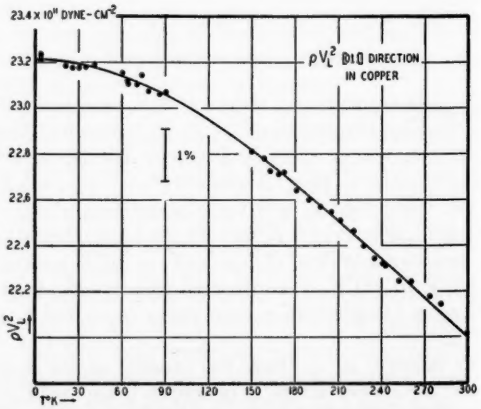

FIG. 3. The combination of adiabatic elastic constants $(c_{11}+c_{12}+2c_{44})/2=\rho v_3^2$ of copper *versus* temperature. The points represented by the open circles have been calculated from the measured transit times (t_3's) by means of Eq. (4). The solid curve has been smoothed as described in the text.

where $\gamma=C_p/C_v$. By using numerical values of the linear expansion coefficient, density, the adiabatic bulk modulus K^s in Table I and the smoothed values of the specific heat at constant pressure, C_p (Giauque and Meads[8]), in the thermodynamic relation,

$$(\gamma-1)=9T\alpha_1^2K^s/\rho c_p, \qquad (6)$$

the value of γ was determined at 10°K intervals below 300°K. These were then used in Eqs. (5) to calculate the isothermal elastic constants and the isothermal bulk modulus shown in Table II. It is to be noted that the thermodynamic formula, Eq. (6), requires the expansion coefficient, $\alpha_1=dL/LdT$ instead of the $\alpha=dL/L_0dT$ of Eq. (2). If α instead of α_1 is used to calculate first γ and then the elastic constants by Eqs. (5), the latter will sensibly be in error. In the case of copper at room temperature, the isothermal constants would be incorrect by about 0.03 percent.

The number of significant figures in Tables I and II is greater than is warranted by the accuracy of the absolute values. One additional significant figure has been retained for it indicates the smoothness of the elastic constants calculated from the curves smoothed through the experimental data as described previously and, moreover, the relative variations of the elastic constants are known to greater accuracy than the absolute values.

TABLE I. The adiabatic elastic constants, the $[0\bar{1}1](011)$ shear constant $C'=(c_{11}-c_{12})/2$, the reciprocal adiabatic compressibility $K^s=(c_{11}+2c_{12})/3$, and the isotropy $S=(c_{11}-c_{12})/2c_{44}$ of copper. The number of significant figures does not indicate the accuracy of the absolute value.

	Adiabatic constants $\times10^{-11}$ dyne-cm^{-2}					Isotropy
T°K	c_{11}	c_{12}	K^s	c_{44}	C'	S
0	17.620	12.494	14.203	8.177	2.564	0.314
10	17.620	12.494	14.203	8.176	2.564	0.314
20	17.618	12.492	14.201	8.173	2.563	0.314
30	17.613	12.488	14.196	8.168	2.563	0.314
40	17.605	12.482	14.190	8.160	2.561	0.314
50	17.593	12.475	14.181	8.149	2.559	0.314
60	17.578	12.467	14.170	8.135	2.556	0.314
70	17.560	12.457	14.158	8.118	2.551	0.314
80	17.540	12.447	14.145	8.100	2.546	0.314
90	17.517	12.437	14.130	8.080	2.540	0.314
100	17.493	12.425	14.115	8.059	2.534	0.314
110	17.467	12.414	14.098	8.036	2.527	0.314
120	17.441	12.402	14.081	8.013	2.519	0.314
130	17.412	12.389	14.064	7.990	2.512	0.314
140	17.383	12.377	14.045	7.966	2.503	0.314
150	17.353	12.364	14.027	7.942	2.495	0.314
160	17.322	12.350	14.008	7.917	2.486	0.314
170	17.290	12.337	13.988	7.892	2.477	0.314
180	17.258	12.323	13.968	7.867	2.468	0.314
190	17.225	12.309	13.948	7.841	2.458	0.314
200	17.192	12.295	13.927	7.816	2.448	0.313
210	17.158	12.280	13.906	7.790	2.439	0.313
220	17.123	12.266	13.885	7.763	2.429	0.313
230	17.088	12.251	13.863	7.736	2.419	0.313
240	17.053	12.236	13.842	7.709	2.409	0.313
250	17.018	12.220	13.820	7.681	2.399	0.312
260	16.982	12.205	13.797	7.654	2.389	0.312
270	16.947	12.189	13.775	7.626	2.379	0.312
280	16.911	12.174	13.753	7.597	2.368	0.312
290	16.875	12.158	13.730	7.568	2.358	0.312
300	16.839	12.142	13.708	7.539	2.348	0.312

TABLE II. The isothermal elastic constants and reciprocal isothermal compressibility of copper. The number of significant figures does not indicate the accuracy of the absolute value.

	Isothermal constants $\times10^{-11}$ dyne-cm^{-2}		
T°K	c_{11}^T	c_{12}^T	K^T
0	17.620	12.494	14.203
10	17.620	12.494	14.203
20	17.618	12.491	14.200
30	17.611	12.486	14.194
40	17.599	12.476	14.183
50	17.579	12.461	14.167
60	17.553	12.442	14.146
70	17.522	12.419	14.120
80	17.487	12.395	14.092
90	17.450	12.369	14.062
100	17.410	12.342	14.031
110	17.368	12.315	13.999
120	17.325	12.287	13.966
130	17.281	12.259	13.933
140	17.236	12.230	13.899
150	17.190	12.201	13.864
160	17.144	12.172	13.830
170	17.096	12.143	13.794
180	17.049	12.114	13.759
190	17.001	12.085	13.723
200	16.952	12.055	13.687
210	16.903	12.025	13.651
220	16.854	11.995	13.615
230	16.804	11.965	13.578
240	16.754	11.935	13.541
250	16.704	11.905	13.504
260	16.653	11.874	13.467
270	16.602	11.844	13.430
280	16.551	11.813	13.393
290	16.500	11.783	13.355
300	16.448	11.752	13.317

COMPARISON OF RESULTS

In Table III the present measurements on copper are compared with other measurements by the ultrasonic pulse-echo method and by the composite oscillator method. Recently Long[14] has measured the elastic constants of copper at room temperature and has made preliminary measurements of the temperature variation between 77°K and 300°K. His c_{11}, c_{12}, c_{44}, and K^s agree with the present work within 0.5 percent at 300°K but there is 1.7 percent difference between the $(c_{11}-c_{12})/2$ values. At 80°K the agreement is poorer but this is probably due to differences in cryogenic techniques. Our use of an acoustic cement having a low melting temperature (105°K) in the low-temperature range

[14] T. R. Long (unpublished). We are indebted to Professor C. S. Smith, Case Institute of Technology, and to Mr. Long for their kind permission to use their copper measurements in advance of publication.

TABLE III. Comparison of the present measurements (P) with those of Long (TRL), Goens and Weerts (GW), and with the theoretical calculations of Fuchs (KF). The present data (P) has also been recomputed and denoted by (PC) using Lazarus' large 0.10-microsecond transit-time correction in order to compare the present measurements on the same basis with those of Lazarus (LC).

Obs.	Temp.	c_{11}	c_{12}	c_{44}	$(c_{11}-c_{12})$	K^*
P	300°K	16.84	12.14	7.54	4.70	13.71
TRL	300°K	16.83	12.21	7.54	4.62	13.75
GW	room	16.98	12.26	7.53		
P	80°K	17.54	12.45	8.10	5.09	14.15
TRL	80°K	17.63	12.59	8.03	5.04	14.27
P	4.2°K	17.62	12.49	8.18	5.13	14.20
KF	0°K	17.5	12.4	8.9	5.1	14.1
PC	300°K	17.04	12.40	7.58		
LC	room	17.10	12.39	7.56		

below 100°K considerably minimizes stresses between the transducer and specimen. Such stresses would arise from differential thermal contraction if a cement having a high melting temperature were used at low temperatures. Excessive stresses cause distortion of the ultrasonic echos and associated transit time errors and because our cryogenic technique reduces these, we feel that our measurements are quite reliable at low temperatures.

Lazarus' c_{ij} values[10] are denoted in Table III by (LC) and he computed these presumably using 0.10 to 0.15 microsecond transit time connections which, our experiments have shown, are probably far too large. However, to compare our present elastic constants, denoted by (P), with those of Lazarus we have recomputed a set, denoted by (PC), for which we used Lazarus' value of 0.10 microseconds as the transit time correction. The good agreement of (PC) with (LC) (within 0.35 percent) and of (P) with Long's data, (TRL) in Table III, attests to the relative accuracy and reproducibility of the ultrasonic pulse technique. However to obtain reliable absolute values, such as we believe we have in Tables I and II and denoted by (P) in Table III, one must take considerable care in the experimental determinations of the transit time corrections.

The room temperature c_{11} and c_{12} values of Goens and Weerts[15] (GW) in Table III, determined from measurements by a composite oscillator technique, differ from the present data (P) at 300°K by only about 1 percent while the c_{44} values are in very good agreement. Elastic constants determined by this technique should be just as reliable as those obtained by plane wave ultrasonic methods provided the couplings between the various composite oscillator vibrational modes are properly accounted for and corrected.

Fuchs' quantum-mechanical treatment[1] of the copper lattice led to values of the elastic constants and compressibility that are in very good agreement with our present experimental results at 4.2°K except the theoretical c_{44} is about 10 percent larger than the observed value. Fuchs compares his theoretical c_{ij}'s with certain c_{ij} values at 0°K obtained from extrapolating experimental results at and above 80°K. The extrapolated values at 0°K are too large in comparison with our measured values at 4.2°K. At the present time such extrapolations from liquid air temperatures are to be considered unreliable for precision purposes and this lends further emphasis to the need and importance for extending the experimental measurements to liquid helium temperatures.

DISCUSSION

Previously reported linear variations of the elastic constants with temperature, for the temperature range above about Debye $\Theta/3$, are not very much in error because the observed nonlinear monotonic decreasing (or increasing in some cases) elastic constants deviate but little, above $\Theta/3$, from linearity. Below $\Theta/3$, however, the deviations from linearity become important since the c_{ij} *vs* T should approach 0°K with zero slope. Such is the case for the experimentally observed variations of the elastic constants of copper (Figs. 1, 2, and 3). To see any deviations from linearity above $\Theta/3$ requires accurate experimental observations indeed for in the present measurements one might easily fit the copper data above 110°K by a straight line. It is only the nature of the variation below $\Theta/3$ ($\Theta\approx 325$°K for copper) that requires the monotonic variations above this temperature to be nonlinear.

Lazarus[10] has established experimentally for copper, aluminum, and some other solids that the elastic constants must be explicit functions of both temperature and volume. This finding has been further substantiated, using Lazarus' data on the pressure variation of elastic constants, by Long and Smith[10] and independently by Sutton[16] for aluminum. A formula, in which the volume and temperature appear explicitly, for representing the variation of c_{44} of aluminum, used by Sutton is

$$c_{44}=Ae^{-B\beta T}R^{-2},$$

where β is the volume expansion coefficient and R is the ratio of volume at temperature T to that at some fixed temperature. We find that a similar relation,

$$c_{44}/c_{44}(0°\text{K})=e^{-B\alpha T}\Big/\left(1+\int_0^T \alpha dT\right)^9,$$

where α is the linear expansion coefficient, represents c_{44} of copper in Table I within 0.2 percent from 0°K to 300°K. In spite of the good fit, these formulas are purely empirical and have no fundamental theoretical basis.

The Born theory[5] on "The Thermodynamics of Crystal Lattices" provides for the explicit dependence of the elastic constants for face-centered cubic lattices,

[15] E. Goens and J. Weerts, Physik. Z. **37**, 321 (1936).

[16] P. M. Sutton, Phys. Rev. **91**, 816 (1953).

on both volume and temperature in the form,

$$c_{ij}(V,T)=(a_{ij}+b_{ij}T)/V,$$

where a_{ij} and b_{ij} are explicit functions of the volume, but leads to the Cauchy relations, $c_{12}=c_{44}$, at 0°K. Preliminary attempts to fit Gow's[5] theoretical calculations to the observed elastic constants of copper have not proved successful, primarily because of the observed deviations from the Cauchy relations.

It is surprising that the elastic constants may also be very closely represented as linear functions of the volume only in the temperature range below Debye Θ. Details of the correlation of the elastic constants of copper and aluminum with thermal expansion data will be discussed in a later paper.[17]

It is of interest to note that the isotropy, $S=(c_{11}-c_{12})/2c_{44}$, of copper is constant at 0.314 up to about 180°K, then it gradually decreases to 0.312 (about 1 percent lower) at 300°K (0.2 of the melting temperature). This means that the two shears, c_{44} and $(c_{11}-c_{12})/2$, have the same relative temperature variation up to about one-half Debye Θ, but at higher temperatures $(c_{11}-c_{12})/2$ decreases faster than c_{44}. We note from Sutton's[16] measurements that aluminum has the same behavior, for at 773°K (0.8 of the melting temperature), the isotropy has decreased to a value about 10 percent lower than the 0°K value. In the Born theory[5] on "The Stability of Crystal Lattices" the vanishing of the shear, c_{44}, is used as an approximate criterion for melting. In view of Sutton's aluminum measurements[16] and our copper data it would appear that $(c_{11}-c_{12})/2$ would disappear at a lower temperature than c_{44}, and so its earlier vanishing would seem to be a more suitable criterion for melting for the monatomic face-centered cubic lattices. Judging from the theoretical graphs of Gow,[5] however, it appears that the Born theory would have $(c_{11}-c_{12})/2$ and c_{44} vanish at the same temperature.

[17] de Launay, Clement, and Overton (to be published).

One of the fundamental problems for which the elastic constants at 0°K are required is the Born-von Karman theory of the lattice specific heat at constant volume. Here the assumed linear atomic restoring force constants needed in the vibrational spectrum calculations may be computed from linear combinations of the elastic constants. The relations used for the face-centered cubic lattice by Leighton[6] and determined by de Launay[4] by a phenomenological theory are here considered to be the correct ones. These are $\mu=ac_{44}$, $\sigma=a(c_{11}-c_{12}-c_{44})/4$, where μ is the force constant for nearest neighbor interaction, σ that for next-nearest neighbor interaction, and a is the lattice constant at 0°K.

Using the experimental values of the elastic constants in Table I at 0°K we compute respectively for μ and σ, 2.940×10^4 and 2.742×10^3 dyne-cm^{-1}. Then with the aid of de Launay's[18] theoretical specific heat calculations we find the theoretical Debye Θ of 340.1°K at 0°K. A novel correlation technique[19] for comparing Leighton's theoretical specific heat calculations with experimental specific heats has led to an empirically determined Θ at 0°K of 341±1°K, from raw experimental specific heats. This technique has also led to values of μ and σ which agree within a few percent with those calculated directly from the elastic constants and promises even closer agreement when more theoretical specific heat data become available for the correlation. Thus it appears that a two constant Born-von Karman theory represents fairly accurately the specific heat of copper over our present range (10°K to 100°K for copper) of comparison provided μ and σ are related by the above equations to the elastic constants.

ACKNOWLEDGMENT

The authors are indebted to Dr. J. de Launay and J. R. Clement for many fruitful discussions.

[18] J. de Launay, J. Chem. Phys. **22**, 1676 (1954).

[19] W. C. Overton, Jr., and J. R. Clement, Phys. Rev. **95**, 602 (1954) (to be published in further detail).

Dynamic Behavior of Domain Walls in Barium Titanate*

ELIZABETH A. LITTLE
Laboratory for Insulation Research, Massachusetts Institute of Technology, Cambridge, Massachusetts

(Received January 26, 1955)

The nucleation and growth of 90° and 180° domains in barium titanate single crystals have been measured with optical techniques. Both types of domains nucleate as long thin wedges with an initial velocity of the order of 10^4 cm/sec for a driving field of 5 kv/cm. For 90° domains, detailed measurements of the nucleation rate as a function of time and field strength are given. After domains have been introduced into a crystal, their growth may be described in terms of wall motion. The 90° wall displacement depends strongly on strains and clamping of the crystal; wall motion appears to cease for frequencies in the megacycle range, where the piezoelectric resonances of the crystal set in. The sideways growth of 180° wedges is affected by the availability of neutralizing electric charges. Interaction of 180° and 90° domains may lead to 90° wall configurations with head-to-head or tail-to-tail orientation of the polar axes.

THE investigation of ferroelectricity in barium titanate and its derivatives, is one of the long-range projects of the Laboratory for Insulation Research.[1] In the course of this work, a number of facts have been established concerning the existence and formation of domains in $BaTiO_3$ single crystals,[2] and a detailed domain analysis has been made by birefringence studies.[3] These investigations have been carried out mainly with static fields. To arrive at a better understanding of hysteresis loops, frequency response and aging characteristics of ferroelectrics requires dynamic studies with movie cameras, and transient or ac voltages. The present paper is a first contribution to the subject of "domain dynamics."

CRYSTALS AND METHODS OF INVESTIGATION

Crystals were grown from ternary melts according to the method developed by Matthias *et al.*[4] and the best "*a*" crystal plates (where the polar axis lies in the plane of the plate) were selected. These crystals, *ca* 10 μ thick, had an area of *ca* 400×400 μ^2. Electrodes were painted on two opposite edges by laying the crystal flat on a microscope slide and applying silver paint (Dupont 4548) with the help of a micromanipulator.

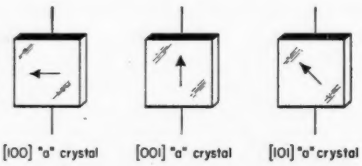

FIG. 1. Three different types of "*a*" crystals, distinguished by the edges to which electrodes are attached.

Depending on whether the electrodes were applied to the [100], [001], or [101] edges, i.e., parallel, perpendicular, or at 45° to the polar axis, we shall refer to them as [100], [001] or [101] "*a*" crystals (Fig. 1).

A polarizing microscope equipped with a micrometer eyepiece and a Land camera sufficed for most observations. Fast processes were photographed with a 16-mm movie camera (Cine-Kodak, 64 frames per sec). The wall displacements could be measured with a microfilm viewer to $\frac{1}{2}$ μ. The linear magnification in our birefringence studies ranged up to 1100×.

Electric fields applied to the crystals included short rectangular single pulses from $\frac{1}{4}$ to 200 μsec duration, sinusoidal signals from 20 to 3×10^5 cps, and dc fields. Voltages up to 500 v proved adequate for most experiments.

90° DOMAINS

A 90° wall is a {101} twin plane and readily visible in transmitted light as a dark line approximately 0.4 μ thick (Fig. 2). Ghosts appear at the edges of the line by optical diffraction and are also observed at the edges of the crystals at high magnification. At room temperature, the 90° wall stands at an angle of 44°15′ to the polar axis; this angle corresponds to the *a*/*c* ratio of the unit cell [Fig. 3(a)]. A 90° wall is therefore actually an 88°30′ wall, a concept of importance for the study of wall dynamics. The 1°30′ difference in orientation between the crystal axes across a 90° twin plane implies a slip of one domain with respect to its neighbor as the 90° wall moves [Fig. 3(b)]. In conse-

FIG. 2. A 90° wall (1000×).

* Sponsored by the Office of Naval Research, the Army Signal Corps, and the Air Force; it is based on a thesis submitted in partial fulfillment of the requirements for the degree of Doctor of Philosophy in Physics at the Massachusetts Institute of Technology.

[1] See A. von Hippel, Revs. Modern Phys. **22**, 221 (1950).
[2] B. Matthias and A. von Hippel, Phys. Rev. **73**, 1378 (1948).
[3] P. W. Forsbergh, Jr., Phys. Rev. **76**, 1187 (1949).
[4] Blattner, Matthias, and Merz, Helv. Phys. Acta **20**, 225 (1947); Blattner, Matthias, Merz, and Scherrer, Experientia **3**, 148 (1947).

quence, it is not astonishing that mechanical pressure can introduce and move 90° walls.

Figure 4 shows a group of wedge-shaped 90° domains as sometimes found in a crystal after cooling through the Curie point. Both the narrowness of the wedges and the fact that many wedges terminate along the same line, can be attributed to the mechanical distortions caused by 90° wedges.

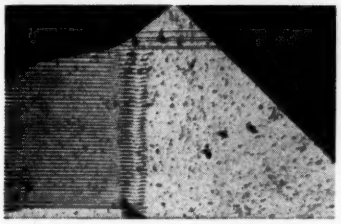

FIG. 4. A group of 90° wedges in an "a" crystal.

Nucleation of 90° Domains

To study 90° domains without interference by 180° domains, we selected a [100] crystal with the polar axis parallel to the electrodes. A good crystal of this kind is initially a single-domain crystal. A dc field exercises a strong torque tending to rotate the polar axis by 90°. If the field is increased slowly, 90° wedges are nucleated at the crystal boundaries [Fig. 5(a)] at

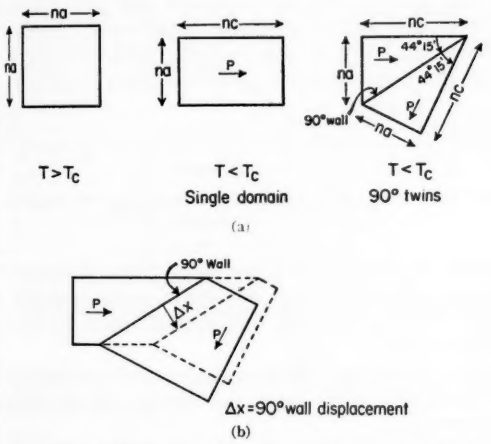

FIG. 3. 90° twinning: (a) distortion of square crystal due to phase change at Curie point (T_c) and 90° twinning (exaggerated); (b) change in shape of twinned crystal due to displacement of 90° wall by Δx (exaggerated).

a critical field strength E_c and extend, 2 to 10 μ wide, across the crystal (*ca* 0.05 cm) in less than 1/100 sec. When the field is removed, the stresses caused in the crystal by the presence of 90° domains frequently force the wedges out of the crystal. They shrink slowly at first, then disappear suddenly.

In a field of opposite polarity [Fig. 5(b)], 90° wedges will enter from the opposite side of the crystal, that is, they start normally at the cathode side. However, there are exceptions, particularly at high temperatures.

A special [100] crystal (crystal "A") was chosen for the following experiments because 90° wedges were always forced out of it by stresses when the field was removed. The field required to maintain wedges in the crystal (about 1 kv/cm) serves as a measure of the magnitude of the mechanical stresses involved. The critical dc field strength E_c of nucleation for crystal "A" is plotted against temperature in Fig. 6. The similarity of this curve with that of the spontaneous polarization and strain in a single-domain crystal[5] confirms that these quantities are related.

To determine the initial growth of 90° wedges as a function of time and field strength, a square pulse was applied to the single-domain crystal "A" and the number of wedges in the crystal immediately afterwards recorded. After a few minutes of rest, strain had forced the domains out and restored the single domain crystal. The number of wedges N was measured as a function of pulse height E and pulse time t (Fig. 7). Each measurement at a given E and t was repeated several times; the estimated accuracy is indicated. Above 10 kv/cm, N depends somewhat on prehistory.

No wedges were observed for $\frac{1}{4}$ μsec pulses and $E \leq 11$ kv/cm; for pulse times longer than 1 μsec, every observed domain extended across the crystal; for shorter times, some wedges did not reach the opposite side. Pulses longer than 10 μsec widen the wedges slightly after they have traversed the crystal. However, no wedges were wider than 20 μ for pulses of 200 μsec or less. The expansion normal to the wedge axis proceeds with a velocity of *ca* 100 cm/sec at 7.4 kv/cm.

Figure 7 shows that N increases with E and t. A threshold pulse length t_0 exists for a given field strength

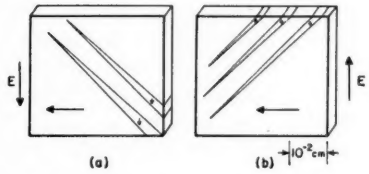

FIG. 5. 90° wedge nucleation in a [100] crystal: (a) positive field, and (b) negative field.

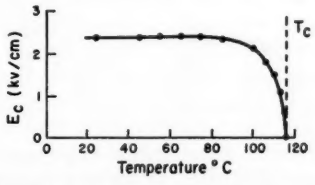

FIG. 6. Critical field for 90° wedge nucleation in crystal "A" as a function of temperature.

[5] W. J. Merz, Phys. Rev. **76**, 1221 (1949).

below which no wedges are formed. It appears (Fig. 8) that $t_0(E-E_c)^2$ is nearly a constant for low fields, while at high fields

$$t_0 = t_s e^{B/E}, \tag{1}$$

where $B=25$ kv/cm and $t_s=0.05$ μsec. If t_0 is interpreted as the minimum time required for 90° wedges to grow large enough to be observed, i.e., to about 500 μ the limiting velocity of a wedge at high fields would be *ca* 10^6 cm/sec, or of the order of sound velocity.

N proves for a given field strength to be about proportional to $\ln(t/t_0)$ as

$$N = 0.28 e^{\gamma E} \ln(t/t_0), \tag{2}$$

$$dN/dt = 0.28 e^{\gamma E}/t \quad (t \geq t_0), \tag{3}$$

where $\gamma = 0.36 \times 10^{-5}$ $(\text{v/m})^{-1}$. Thus the nucleation rate decreases with time and increases with E. This time dependence appears reasonable from the standpoint that, after nucleation has started, less material is available for new domains.

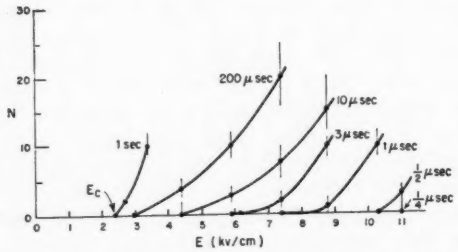

FIG. 7. Number N of 90° wedges nucleated by a square pulse as a function of pulse length and pulse height.

90° Wall Motion

After 90° wedges have been introduced into a crystal, domain growth can be described in terms of wall motion. Once a wedge has grown across a crystal, the two now-parallel walls separate and move sideways with decreasing velocity and some irregularity. We investigated this situation in a [100] crystal "B", which retained its domains when the field is removed. In other words, the mechanical restoring force in this crystal was small.

Application of a small field to this crystal made the parallel walls of a 90° domain oscillate. Since the wall velocity is zero at both extremes of an ac oscillation, the wall appeared to split in two at high frequencies. The distance $|x|$ between the two lines is designated as "wall amplitude" (Fig. 9) and plotted as a function of E and of frequency. At 20 cps the critical field for the onset of motion is small and the wall amplitude at low field strengths is approximately proportional to E^2. The minimum field strength for wall motion increases with frequency, hence the wall amplitude at constant field decreases.

At 300 kcps and fields above 3.5 kv/cm, crystal "B"

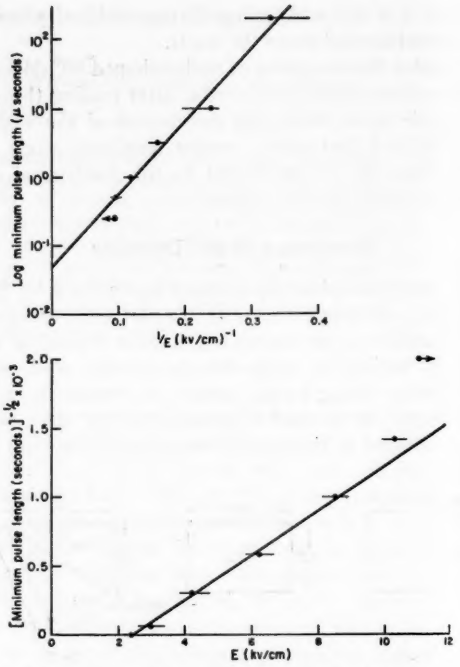

FIG. 8. Minimum pulse length t_0 for nucleation of 90° wedges as a function of pulse height E.

heated up beyond the Curie point. Since temperature change affects the wall amplitude, measurements at high frequency and high field strength must be viewed with caution.

No significant difference was found between the amplitude of oscillation at the edge and in the middle of a crystal.

A 90° wall seems to be thick and its motion not a process of discrete molecular steps. Significant is the low critical field strength at low-frequency oscillations. The trend of the critical field as a function of frequency, neglecting heating effects, suggests that the wall should

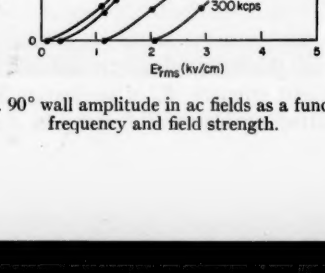

FIG. 9. 90° wall amplitude in ac fields as a function of frequency and field strength.

not be able to move at finite field strengths for frequencies much above about 3 Mc/sec. The lowest piezoelectric resonance of our crystals was about 5 Mc/sec. Since 90° wall motion is strongly affected by macroscopic mechanical distortions, it is not surprising to find that the wall motion is damped out as the acoustic resonance frequency is approached.

180° DOMAINS

Antiparallel domains are difficult to observe. Merz[6] first made 180° domains visible by applying an electric field normal to the c axis. The polar axes in adjacent domains are thus rotated in opposite directions and have different extinction positions (Fig. 10). For an optical study of the dynamic behavior of 180° walls, thin "a" crystals with {101} edges are therefore well suited. One component of the field makes the domains visible, the other forces them to grow. If not very large fields are applied, the formation of 90° domains can be avoided. Figure 11 shows such a [101] crystal with its antiparallel domains; the domains of one polarity are placed in extinction (black), those of opposite polarity

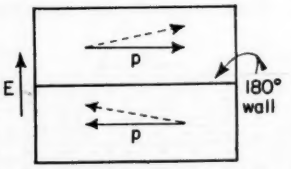

FIG. 10. Rotation of polar axes near a 180° wall in a field perpendicular to the wall.

transmit light. A transition region of about $\frac{1}{2}$ μ width at the wall does not rotate in the field.

Nucleation and Initial Motion

To study the initial growth of 180° domains, short rectangular pulses were applied to a single-domain [101] crystal. A negative[7] pulse of 7.5 kv/cm (10 μsec or longer) applied to a single-domain crystal orientated at extinction causes occasionally some thin spikes ($\frac{1}{2}$ to 5 μ at the widest part) to appear, extending from several edges nearly across the crystal (0.05 cm); they remain visible for as long as a second after pulsing. For as many as 50 subsequent pulses the same wedges have been observed; they do not appear to grow.

In an inverse experiment, some large (20 μ wide and 500 μ long) 180° wedges were introduced into the crystal by a dc field, and short positive pulses ($E=7.5$ kv/cm), spaced several seconds apart, applied to remove them. Each pulse makes the domains still present visible for about a second. With pulses of 10 μsec or longer, some domains are removed entirely by the first pulse; a bright region is left behind which fades out in

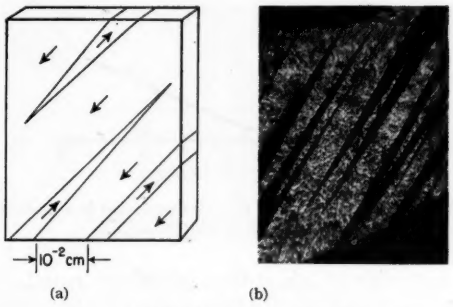

FIG. 11. 180° domains in a [101] crystal.

about a second. For pulses shorter than 1 μsec, each pulse narrows the domains significantly, and the wedge tip retreats slightly.

Two tentative conclusions can be drawn from these experiments: (1) an antiparallel domain is formed as a spike at the edge of the crystal and extends along the polar axis with a velocity between 5×10^3 and 5×10^4 cm/sec at 7.5 kv/cm; (2) space-charge effects associated with the wedges may cause the bright region; their relaxation time in our crystals is of the order of a second.

This second conclusion, based on the visible after-effects of pulses, requires closer scrutiny. If a 180° domain is wedge-shaped with a wedge angle θ, the spontaneous polarization P_s produces a large electric field ca $(P_s/\epsilon_0)\sin\theta$ at the walls. The spontaneous polarization[8] at room temperature is about 0.26 coul/m^2; hence $E\simeq10^5\sin\theta$ kv/cm. Such a field must create a large lattice distortion near the 180° wall, but quasi-stationary domains (wedge angle of 20° or more) do not show such distortions. This suggests that a compensating electric charge accumulates and neutralizes the ends of the dipole chains.

These experiments are in line with the concept of von Hippel[9] that the conductivity of $BaTiO_3$ crystals is of great importance for the dynamics of domain formation, and with observations by Mitsui and Furuichi[10] on the effect of charges on the domains in Rochelle salt crystals.

Growth of 180° Domains

The manner in which spikes grow in a negative dc field until the crystal polarization is reversed, is illustrated schematically in Fig. 12. The last domains to

FIG. 12. Schematic diagram of 180° domain switching process in a [101] crystal.

[6] W. J. Merz, Phys. Rev. **88**, 421 (1952).
[7] The field strength will be designated as negative when opposite to the initial polarization.
[8] W. J. Merz, Phys. Rev. **91**, 513 (1953).
[9] A. von Hippel, Z. Physik **133**, 158 (1952).
[10] T. Mitsui and J. Furuichi, Phys. Rev. **90**, 193 (1953).

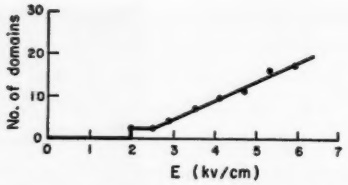

FIG. 13. Number of 180° domains nucleated in a dc field as a function of field strength.

leave are wide wedges at the edges of the crystal, often difficult to remove completely even with a high field.

To study these processes without interference by 90° wedges, the negative field is applied gradually, reaching its peak value in about ½ sec. Typical thin spikes starting from both directions extend across the crystal before this peak field is reached. The spikes tend to nucleate at identical places at the edge of the crystal when the experiment is repeated. Their number increases with E (Fig. 13) as well as with the time derivative of the field. For low field strengths, few new spikes appear after E is reached; for fields greater than 6 kv/cm, spikes tend to grow from existing walls and N continues to increase during the experiment. The times required to reach approximately 50 percent (a) or 90 percent reversal (b) were measured as a function of the peak field strength (areas of opposite polarity were estimated visually). Since $1/t$ describes the velocity of reversal, this parameter has been plotted in Fig. 14 in its dependence on E.

A minimum field strength of about 2 kv/cm is required for the nucleation of 180° wedges. For E smaller than about 2.4 kv/cm, the wedges did not grow for observation times as long as 12 hours. Both the number of domains and the growth velocity increases with E;

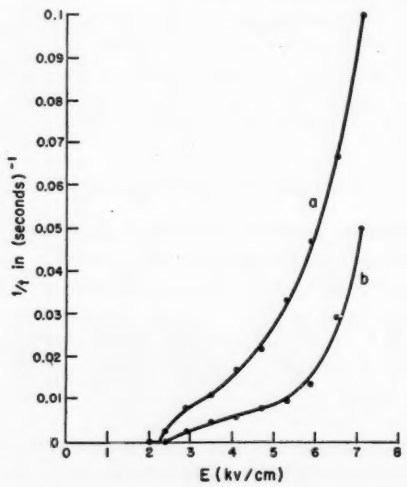

FIG. 14. Reciprocal of time required for 180° domains to reverse the polarization of a [101] crystal: (a) by 50 percent and (b) by 90 percent.

the growth is slowed down appreciably in the last stages of reversal.

This experiment leads again to the interpretation that, while the forward advance of spikes is initially fast, the sideways growth rate of 180° wedges is limited by the electrostatic energy of the depolarizing field. The large wedge angles observed towards the end of the process appear to require the accumulation of neutralizing charges on the domain walls. Since the walls of adjacent domains merge as growth proceeds, the velocity of polarization reversal decreases with time as the number of domains decreases.

The 180° walls are probably quite thin (possibly only one lattice distance) and the activation energy for motion perpendicular to the polar axis correspondingly very high. Such motion however is observed, and must therefore be explained by a sequence of dipole flips which propagate along the polar axis (Fig. 15). The fact that about the same limiting field is observed for nucleation and growth is in line with this observation, for both processes involve the reversal of individual dipole moments.

If one breathes on the crystal, the 180° domains move faster. This supports the idea that the con-

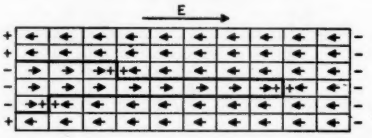

FIG. 15. Model for a 180° wedge.

ductivity of the crystals is of importance and that we have to consider surface as well as volume conductivity.

While the results reported (high initial forward velocity, slow sideways growth leading to saturation) are qualitatively the same for all crystals studied, there are quantitative differences from crystal to crystal, as would be expected when imperfections and conductivity vary from sample to sample. 180° domains in [001] "a" crystals appear to behave similarly to those in [101] "a" crystals.

Dielectric Measurements

Figure 16 shows the equivalent susceptibility[11] χ_{eq}' as a function of measuring field strength for a [001] "a" crystal with frequency as a parameter. χ_{eq}' approaches about 300 for low fields. The critical field for domain motion for the [001] crystal appears to be somewhat lower than observed visually for a [101] crystal, even when the different geometry is taken into account. This might imply that very thin and therefore

[11] $\chi_{eq}=A_1/\epsilon_0 E_0$, when A_1 is the coefficient of the first Fourier term, $E=E_0 \sin\omega t$ is the applied field and $P=\sum_{k=1}^{\infty} A_k \sin k\omega t$ is the polarization.

invisible spikes move at low fields. That the wall motion damps out at around 10^4 cps is consistent with our optical results. That χ_{eq}' increases rapidly with decreasing frequency is electrical evidence of the slow switching process. Hyde,[12] in this laboratory, found by tracing hysteresis loops that the slope $\Delta P/\Delta E$ continues to increase for frequencies as low as 10^{-1} cps. This would be expected from our domain observations with dc fields.

After this study was completed, the author received a prepublication copy of work by Merz[13] on the switching of 180° domains, observed electrically. The initial spike velocity determined from the switching time agrees well with our values measured optically. A significant difference is that we actually observed the 180° walls moving perpendicularly to the polar axis, an effect not perceived in Merz's electrical measurements.

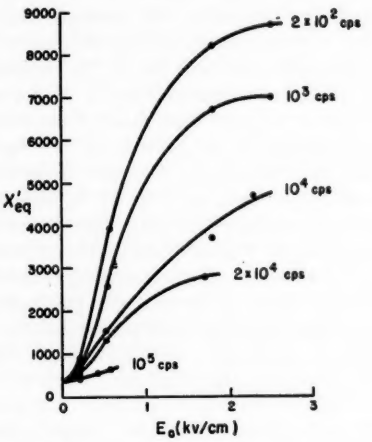

FIG. 16. Dependence of "equivalent" susceptibility on field strength and frequency in an [001] "*a*" crystal.

INTERACTIONS OF 90° AND 180° DOMAINS

When 90° and 180° domains are simultaneously active in a crystal, complicated interaction effects occur. The general behavior, however, may be predicted from a few rules which can be best demonstrated in a [101] crystal (Fig. 17). This is the type in which we studied the 180° domains, but now we make no effort to suppress 90° domains. Beginning the experiment with a single-domain crystal (a), we suddenly apply a negative dc field, and both 90° and 180° wedges form and grow (b). After a short time a 90° wall is in contact with 180° wedges and the motion is impeded (c). The antiparallel wedges penetrate into the adjacent area with a 90° turn (d), because otherwise the electric field concentration at the 90° wall becomes excessive. Finally, the antiparallel domains disappear and a

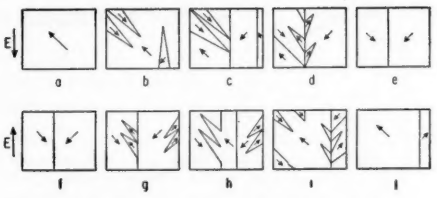

FIG. 17. Schematic diagram of 180° and 90° wall interactions in a [101] crystal.

head-to-head (or tail-to-tail) configuration of the 90° walls remains (e). This can be verified by measuring the rotation of the extinction axes of adjacent domains; these axes rotate in opposite directions. As the field gets larger, a region nearly 5 μ wide near the wall rotates so far that it appears bright yellow when the rest of the crystal is at extinction.

There is no observable optical difference between a head-to-head, tail-to-tail or head-to-tail 90° wall at magnifications up to 1100×. Obviously free charges at the 90° wall have neutralized the interfacial polarization that would otherwise produce a large field.

A domain configuration, as discussed above, may be called pseudo-saturated because, even though there exist 90° domains, they cannot be removed by a field as long as the energy barrier for rotation is too high.

If the field direction is now reversed [Fig. 17(*f*)], no net force acts on the 90° wall when the field is first applied. If the field is just greater than the critical field for nucleation of 180° domains (2 kv/cm), such domains will nucleate in spikes from the 90° wall and from the crystal edges and proceed slowly to invert the 90° domains (g). After 180° domains have nucleated at a 90° wall, a force acts through them on the 90° wall, and this wall may break away from its initial position and its space charge (h). It moves now freely and rapidly as a head-to-tail wall until running into another set of 180° domains (i). Where the 90° wall comes to a stop, depends on the growth rate of the 180° domains and on field strength. Strain may play a part in determining the final equilibrium configuration in the field, but the end result is again complete pseudo-saturation (j).

In order to measure these domain interactions, a negative square pulse with a rise time of <0.01 sec

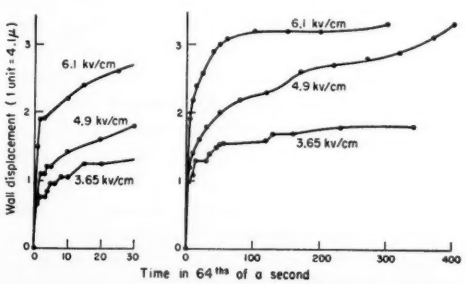

FIG. 18. 90° wall displacement in a [101] crystal as a function of time (two time scales) for several field strengths.

[12] J. Hyde, thesis, Massachusetts Institute of Technology, June, 1954 (unpublished).

[13] W. J. Merz (private communication, June, 1954); Phys. Rev. 95, 690 (1954).

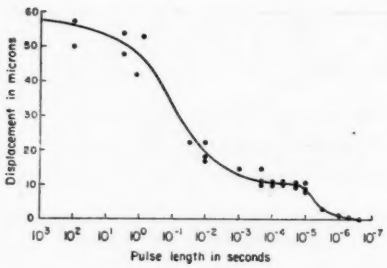

FIG. 19. 90° wall displacement in a [101] crystal caused by a square pulse of height 6.8 kv/cm as a function of pulse length.

and a duration of *ca* 6 sec was applied to the [101] crystal. A large positive field was applied previously for several minutes to insure that the crystal was initially pseudo-saturated. The motion of a typical 90° wall, as recorded by its position on movie film, is plotted for two different time scales in Fig. 18 with the pulse height as parameter.

The characteristics of typical 90° wall motion are here clearly evident. For the initial free motion the velocity is very high; next the wall velocity abruptly decreases as the wall collides with 180° domains. The slow process approximately fits an exponential relation with a time constant of about $\frac{1}{2}$ sec. There may be some additional motion for times as long as several minutes. Irregularities in the motion of the 90° wall reflect changes in the 180° domains affecting its progress. These jerky steps are prominently displayed in slow motion pictures and give rise to a ferroelectric Barkhausen effect.

Figure 19 shows the 90° wall displacement caused by a negative square pulse (height 6.8 kv/cm) as a function of pulse length. As the pulse shortens below 10 μsec, the wall displacement drops rapidly to zero. The free motion of the 90° wall takes place with a velocity of about 50 cm/sec. After intersecting the 180° domains it continues with much slower speed until the crystal is pseudo-saturated.

Naturally, there are many variations of the case here discussed. New 90° wedges may enter from an edge and extend rapidly across the crystal. After meeting 180° wedges, the 90° walls are slowed down, as shown previously. Since 180° domains can nucleate from any 90° wall on one or both sides of it, more complicated interactions are bound to arise.

ACKNOWLEDGMENTS

The author is greatly indebted to Professor A. R. von Hippel for suggesting the problem and for his advice and encouragement during the course of this research. She wishes to thank Dr. P. W. Forsbergh, Jr., for an introduction to the intricacies of domain patterns in barium titanate and many illuminating discussions; Professor F. R. Kotter for the use of his rectangular-pulse generator; Professor H. E. Edgerton for a stroboscopic light source; W. B. Westphal for assistance in obtaining the dielectric measurements; and L. E. Johnson, B. Frackiewicz, and Professor D. J. Epstein for help in the electrical instrumentation.

The author wishes to express her gratitude to the International Business Machines Corporation for support in the form of a fellowship, and to Dr. D. R. Young of I.B.M. for informative discussions.

Recombination Processes in Cadmium Sulfide*

JOHN LAMBE
United States Naval Research Laboratory, Washington, D. C.
(Received January 28, 1955)

An experimental study has been carried out on the photoconductivity and luminescence of cadmium sulfide. The two main properties investigated were the photoconductive spectral response, and the relationship between luminescence and photoconductivity. It is found that the observed spectral response can be explained in terms of the dependence of lifetime of conduction electrons on the wavelength of exciting light. The rise and decay of photoconductivity and luminescence have been examined for silver-activated CdS, and for the red and green luminescence of unactivated CdS. It is found that the decay of luminescence is much more rapid than the decay of photoconductivity. An explanation for this behavior is offered, based on the assumption that the luminescence results from the recombination of localized electrons and free holes.

I. INTRODUCTION

THE photoconductive process can be conveniently discussed in terms of three subprocesses. These are excitation, conduction, and recombination. In the present work we shall be primarily concerned with the recombination process as it occurs in cadmium sulfide. The experimental approach used in this study is based on observations of the transient response of photocurrent and luminescence to varying excitation.

The general considerations involved in the study of recombination are indicated in the following discussion which is essentially that given by Gildart and Ewald[1] in connection with their work on CdS. We consider a homogeneous photoconductor in which the photoconductivity arises primarily from the motion of electrons in the conduction band. Free holes and electrons are liberated by the absorption of light in the fundamental absorption band. The electrons move in the conduction band and may be trapped, and also of course electrons previously trapped may be thermally ejected from traps. Similar considerations apply to free holes. Finally electrons and holes recombine. If n_c represents the number of conduction electrons, then

$$dn_c/dt = L - R - T + U, \tag{1}$$

where L = number of electrons excited per unit time, R = number of electrons recombining per unit time, T = number of electrons trapped per unit time, and U = number of electrons released from traps per unit time. Under steady-state conditions, we have $dn_c/dt = 0$, $T = U$, so that $L = R$. If the excitation, L, is cut off at $t = 0$, then momentarily the rate of decay of conduction electrons is

$$dn_c/dt = -R, \quad (L = R,\ t \leqslant 0;\ L = 0,\ t > 0). \tag{2}$$

By measuring dn_c/dt at $t = 0$, one may thus obtain a measure of R. If one also measures n_c, then the ratio of n_c to dn_c/dt gives a quantity which may be termed the lifetime of the conduction electron. This is the average time that an electron, which has been excited, will spend in the conduction band. Experimentally, one actually measures the photocurrent I, and dI/dt, but if one assumes that photoconductivity arises primarily from the motion of conduction electrons then one has

$$I = en_c\mu E,$$

and one obtains

$$\tau = \frac{n_c}{dn_c/dt} = \frac{I}{dI/dt}$$

= average lifetime of the conduction electron.

In addition to this method, one can obtain information regarding the recombination process from a study of luminescence since it comprises part of the recombination mechanism. In the present work recombination has been studied in relation to two properties of CdS: the shape of the spectral response curve of photoconductivity in CdS, and the relationship between photoconductivity and luminescent decay.

II. EXPERIMENTAL METHOD

For the measurement of photoconductivity, an alternating current method was employed at a frequency of 100 kc/sec. This ac method was used in order to avoid some of the difficulties of direct current methods. By this method the necessity for direct metallic contact to the CdS crystal is eliminated, and also the effects of polarization can be minimized.

The crystals used in this method were plate-like in shape, and were mounted in the manner shown in Fig. 1. The crystals were thus capacitively coupled to metallic electrodes. The measurements were made at 100 kc/sec to insure that this capacitive coupling impedance was very small in comparison to the photoresistance of the crystal. The ac photoresistance was then measured by means of a bridge (Fig. 2). The ac field applied to the crystal was of the order of 10 volts per cm. The transient behavior of the ac photocurrent was observed by means of an oscilloscope. The oscilloscope trace was photographed and measurements were made on these photographs.

* A part of a dissertation submitted in partial fulfillment of the requirements for the Ph.D. degree at the University of Maryland.
[1] L. Gildart and A. W. Ewald, Phys. Rev. 83, 359 (1951).

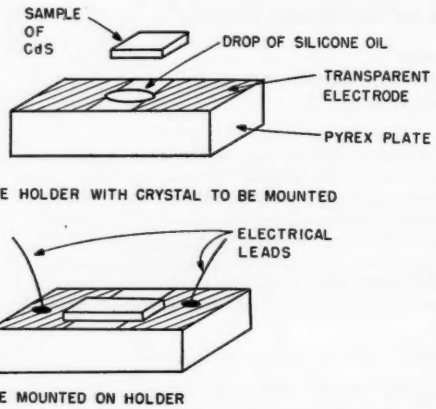

FIG. 1. Details of mounting of CdS crystals on sample holder.

The transient behavior of the luminescence was observed by means of a 6217 photomultiplier in conjunction with an appropriate filter for the color of luminescence being observed. The signal from the photomultiplier was also displayed on an oscilloscope and recorded photographically.

Temperature control was obtained as follows. For work at 300°K, samples were placed in a container which was then evacuated to about 10^{-5} mm of Hg and then filled with helium gas at 1 atmosphere pressure. At 4°K and 77°K the samples were immersed directly in liquid helium and liquid nitrogen respectively. Measurements at 200°K were made by suspending the samples above a bath of liquid nitrogen and determining the sample temperature by means of a copper-constantan thermocouple.

III. SPECTRAL RESPONSE OF PHOTOCONDUCTIVITY

The photoconductive spectral response of CdS is such that in most cases the peak in photoconductivity lies to the long wavelength side of the region of maximum optical absorption. This means that although the absorption decreases, the photoconductive response actually increases. Several explanations have been offered for this behavior. Leverenz[2] suggests that because the light in the fundamental absorption band is absorbed in a shallow surface layer ($\sim 10^{-5}$ cm), electrons liberated in this region move in a very imperfect surface region and have low mobility as compared with electrons excited by light which penetrates into the interior of the crystal. Another possibility is that electrons excited in the surface region have a shorter lifetime than electrons excited in the interior of the crystal.[3,4] This question has been investigated by several workers.[5–7]

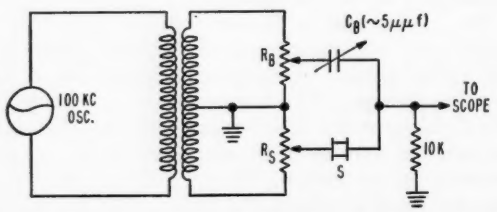

FIG. 2. Simplified diagram of bridge used in ac measurements. R_s varied the voltage applied to sample S. R_B and C_B were used to balance out any ac voltage across $10K$ resistor when sample (S) was in dark.

Fassbender and Seraphim[5] report no wavelength dependence of the photoconductive decay time on several crystals of CdS. They do not state whether or not these crystals show the usual peak in spectral response in the region of 5150 A. Gurevich, Tolstoi, and Feofilov[6] report finding a wavelength dependence of the photoconductive decay time in CdS crystals. Also Bube[7] has found wavelength-dependent effects in the decay time under the influence of water vapor. It appeared that a more thorough study of this matter would be useful in understanding the spectral response of CdS. Observations have been made on the optical absorption, the spectral response, and the decay rate of photoconductivity.

Consider a crystal being irradiated by L incident quanta per second at wavelength λ. Of these L quanta, AL will be absorbed by the crystal, where A is the absorptance of the crystal (i.e., fraction of incident light quanta which are absorbed). If we assume that each absorbed quanta gives rise to one conduction electron, then the number of conduction electrons under steady-state condition is

$$n_c(\lambda) = AL\tau, \tag{3}$$

where τ = lifetime of conduction electrons. If the mobility is not a function of the wavelength of exciting light, then we have for the photocurrent I as a function of wavelength:

$$I \propto AL\tau, \tag{4}$$

or

$$I(\lambda)/L(\lambda) \propto A\tau.$$

[$I(\lambda)/L(\lambda)$ is the photoconductive spectral response curve.]

Thus if the product $(A\tau)$ yields a curve which is in good agreement with the observed spectral response, the above assumption about mobility is valid, and the observed spectral response can be explained in terms of the wavelength dependence of τ and A alone. This is the proposition which was tested experimentally by measuring τ, A, and the spectral response.

The measurement of $\tau(\lambda)$ was made as follows. The crystal was illuminated using a tungsten lamp in con-

[2] H. W. Leverenz, *Introduction to Luminescence of Solids* (John Wiley and Sons, Inc., New York, 1950).

[3] J. Fassbender, Ann. Physik. **5**, 33 (1949).
[4] A. Rose, RCA Rev. 362 (September, 1951).
[5] J. Fassbender and B. Seraphim, Ann. Physik **10**, 374 (1952).
[6] Gurevich, Tolstoi, and Feofilov, Doklady Akad Nauk U.S.S.R. **71**, 29 (1950).
[7] R. H. Bube, J. Chem. Phys. **21**, 1409 (1953).

junction with a monochromator to obtain light of a given wavelength. By means of a rotating sector the light was interrupted for a short interval. A measurement was then made of the time interval required for the photocurrent to drop to 0.95 of its initial value. If Δt is this time interval, then

$$\tau(\lambda)=\frac{I}{dI/dt}=\frac{I}{(0.05\times I)/\Delta t}=20\Delta t.$$

This method is approximate, of course, and will yield a value slightly larger than if a true measure of the initial slope were made. However, the error will be small, and since we are mainly interested in the relative value of τ at different wavelengths, this method is satisfactory.

Lifetime measurements were carried out on two crystals of CdS, and they are shown in Fig. 3. Optical absorption measurements were made on these same

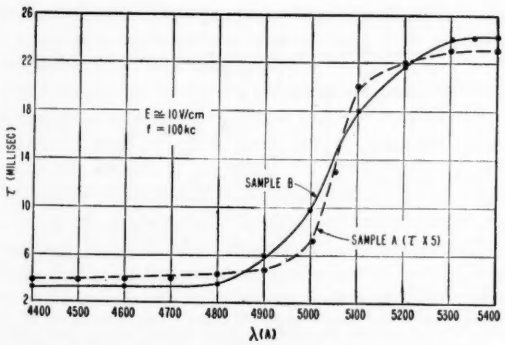

FIG. 3. Measurement of lifetime of conduction electrons as function of the waveleng th of exciting light.

crystals using a Beckman spectrophotometer. The product of the optical absorptance A and the lifetime τ was then plotted along with the measured spectral response as shown in Figs. 4 and 5 normalized to arbitrary scales. These curves indicate that a consideration of the lifetime as a function of wavelength can very nearly account for the observed spectral response, and therefore the wavelength dependence of mobility is not an important factor.

The cause of the wavelength dependence is not clearly understood, but it is of interest to point out some of the observations of others in this regard. Bube[6,8] has found that the presence of water vapor can reduce the photoconductivity in CdS. Moreover, he has found this effect to be wavelength dependent, being more pronounced at shorter wavelengths. He was able to show that the water vapor affected the recombination rate, and since light on the short wavelength side of the absorption edge is absorbed in a shallow surface layer, photoconductivity due to this light is quite dependent

[8] R. H. Bube, Phys. Rev. **83**, 393 (1951).

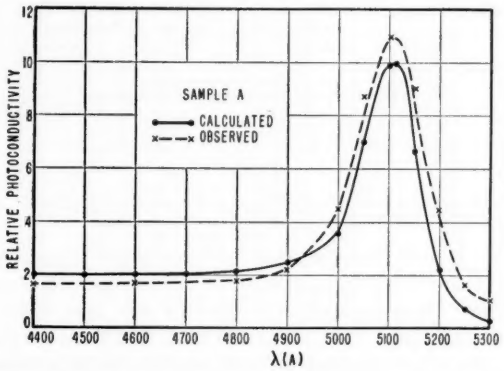

FIG. 4. Comparison of measured photoconductive response with the product $(A\tau)$ for sample A. Curves have been normalized to arbitrary scales.

on surface conditions. Liebson[9] has found similar effects due to electronegative vapors, and has interpreted these results in terms of surface recombination processes. It thus appears that the wavelength dependence of the lifetime of the conduction electrons is related to surface recombination effects, the precise nature of which are as yet undetermined.

The observation of Fassbender and Seraphim[5] indicating the absence of any wavelength dependence of the time constant is also of interest. Unfortunately, they do not state whether the crystals they used showed the usual spectral response peak at 5200 A. Observations have been made in the course of this work of crystals which showed no peak in photoconductivity, and which showed no wavelength dependence of the time constant. This is a further indication the spectral response peak is associated with the time constant behavior.

IV. LUMINESCENCE AND PHOTOCONDUCTIVITY

In this section we shall discuss the relation between the decay of luminescence and the decay of photoconductivity. On the basis of the model often used for photoconducting phosphors (Fig. 6), it is seen that one should expect the luminescence and photoconductivity

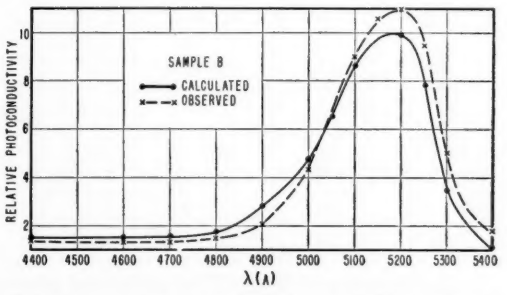

FIG. 5. Comparison of measured photoconductive response with the product $(A\tau)$ for sample B.

[9] S. H. Liebson, J. Electrochem. Soc. **101**, 359 (1954).

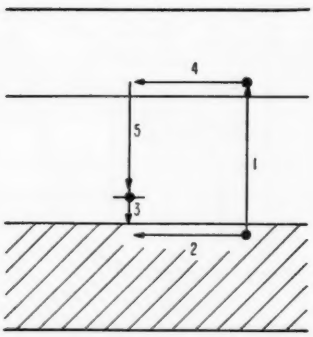

FIG. 6. Conventional model for photoconducting phosphor: (1) excitation; (2) hole migration; (3) capture of hole at luminescent center; (4) electron migration; (5) capture of electron leading to luminescent emission.

to have more or less equivalent decay times, or else the luminescence should persist longer than the photoconductivity. This is because luminescence is assumed to occur after the capture of a conduction electron by the luminescent center. In order to investigate this matter measurements were carried out on the decay of photoconductivity and the decay of the orange luminescence of silver-activated CdS, the green edge luminescence of CdS, and the red luminescence of "self-activated" CdS.

IV(a). Luminescence and Photoconductivity in CdS(Ag)

Silver-activated CdS shows a broad luminescence centered about 6100 A.[10] This luminescence can be observed at 77°K, but gradually disappears as the crystal is warmed to room temperature. The crystals used in this work were activated with silver by introducing silver vapor into the vapor phase growth of CdS crystals.

The first step in the present study was to observe the decay of photocurrent and luminescence at 77°K. The luminescence was observed by means of a 6217 photomultiplier in conjunction with a Corning 2-63 filter. The crystals were excited by light of 3650 A wavelength. This excitation was interrupted by means of a rotating sector, and the decay of luminescence and photoconductivity could then be observed by means of an oscilloscope.

The results of such observations are shown in Fig. 7(a). This shows clearly that the luminescence decay is much more rapid than the photoconductive decay. Further measurements indicated that the luminescence decay time (time required to drop to $\frac{1}{2}$ of initial value) is about 0.05 millisecond, while photoconductive decay time was about 5 milliseconds. The

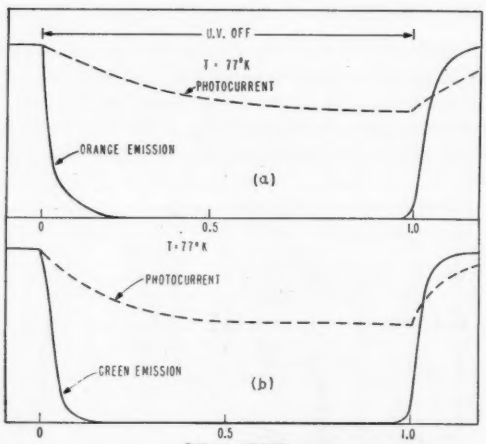

FIG. 7. Comparison of decay of luminescence and photoconductivity: (a) CdS(Ag) at 77°K, orange emission; (b) CdS at 77°K, green edge emission.

[10] C. C. Klick, J. Opt. Soc. Am. 41, 816 (1951).

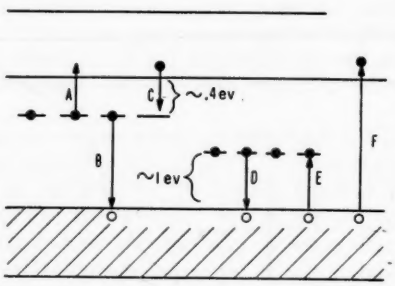

FIG. 8. Model proposed for CdS(Ag). (See reference 11.) The levels 0.4 ev below the conduction band result from silver activation. The levels 1 ev above the valence band are normally present in CdS. (*A*) infrared excitation of trapped electrons (3μ region); (*B*) luminescent recombination of trapped electron and free hole; (*C*) trapping of electrons; (*D*) trapping of holes; (*E*) freeing of trapped holes by excitation in 1μ region; (*F*) excitation.

simple model of Fig. 6 does not afford an explanation of such a result.

In order to explain this behavior we shall consider a model which has recently been proposed for the luminescence process in CdS(Ag).[11] This model is illustrated in Fig. 8. Silver activation results in the formation of electron traps about 0.4 ev below the conduction band. These are the luminescence centers. In addition there are hole traps about 1 ev above the valence band. Such hole traps have been posulated in connection with infrared quenching effects in CdS.[4,12] In the model proposed, the following processes occur: (1) Irradiation in the fundamental band produces free holes and electrons. Some of the free electrons are then trapped in the luminescent centers, while some free holes are trapped by the levels 1 ev above the valence band. (2) As excitation continues, electrons in the luminescent centers recombine with free holes, resulting in lumines-

[11] J. Lambe and C. C. Klick (to be published).
[12] E. A. Taft and M. H. Hebb, J. Opt. Soc. Am. 42, 249 (1952).

cence. (3) When the excitation is removed, luminescence continues until the number of free holes is exhausted. If free holes have a short lifetime, the luminescence decay will be very rapid. (4) Electrons remaining in the conduction band after excitation ceases will continue to be trapped by empty luminescent centers, and also they may recombine nonradiatively with trapped holes. The photoconductivity will persist until the number of free electrons is exhausted.

Such a model was found to be consistent with observations on infrared photoconductivity and stimulation of luminescence in CdS(Ag).[11]

The proposed model affords a simple explanation of the difference in decay time of luminescence and photoconductivity. If one assumes that the lifetime of free holes is much shorter than the lifetime of free electrons, it is clear that luminescence, which is associated with the capture of free holes, will decay much more rapidly than photoconductivity which is associated with the motion of free electrons. The difference between free hole and electron lifetimes is presumed to be due to the existence of a large number of hole traps or to a larger cross section for hole trapping.

Since the proposed model is consistent with observations of infrared effects,[11] and also with the measurement of decay times reported here, let us examine some further observations in regard to the nature of the build up of luminescence and photoconductivity when CdS(Ag) is illuminated. In the experiments to be described, the CdS(Ag) crystal was kept in darkness for the major part of the time and was irradiated every 100 milliseconds by two short pulses of ultraviolet (3650 A) 1 millisecond apart (Fig. 9). The pulses were 1 millisecond in duration. We consider first the behavior of the photoconductivity and luminescence after many excitation cycles have elapsed. From Fig. 10(a) it is seen that at 77°K the rise of the luminescence was much more rapid than the photoconductivity for both pulses. The decay of luminescence is of course more rapid than the decay of photoconductivity as noted previously. At 200°K, however, this behavior has changed considerably. In this case it is seen from Fig. 10(b) that the rise of luminescence is much slower, and actually the rise of luminescence now parallels the rise of photoconductivity for the first pulse of the pair on each cycle. The decay shows the usual behavior. The rise of the second luminescence pulse of the pair is considerably steeper than the first pulse. It should be emphasized that these patterns are observed after many excitation cycles have elapsed and they are observed for each pair of excitation pulses.

The aforementioned behavior can be explained directly in terms of the proposed model. At 77°K electrons can be "frozen" in the luminescent levels, so that luminescence can occur as soon as free holes are generated. Thus, once a substantial number of the luminescent centers are filled, the rise of luminescence will be very rapid. At 200°K, however, electrons are not retained in the

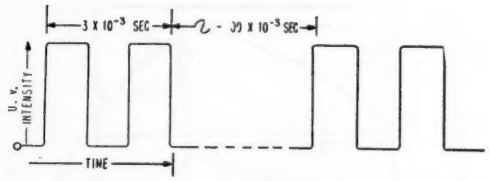

FIG. 9. Ultraviolet (3650 A) pulse pattern used in rise time studies.

luminescent levels for a long period of time. During the time when the crystal is in darkness these levels are emptied and the ejected electrons recombine with trapped holes in a nonradiative manner. When excitation is applied free holes and electrons are generated. The luminescent levels are empty, however, so that the free holes cannot recombine immediately with electrons in these levels. Thus, before luminescence can occur these levels must be filled. At 200°K, it appears that the number of electrons in luminescent levels is roughly proportional to the number of conduction electrons so that the rise of luminescence follows the rise of photoconductivity. The steeper rise of the second luminescence pulse in Fig. 10(b) is understandable since a substantial number of traps remain filled in the short period following the first excitation pulse.

In Fig. 11 a qualitative picture of the observed luminescence pulse pattern is derived as the product of the number of electrons trapped in luminescent levels (n_T), and the number of free holes (assuming n_T is proportional to n_C and that free holes have a short lifetime due to hole trapping).

Two further observations are of interest in this connection. Suppose that CdS(Ag) be cooled from 300°K

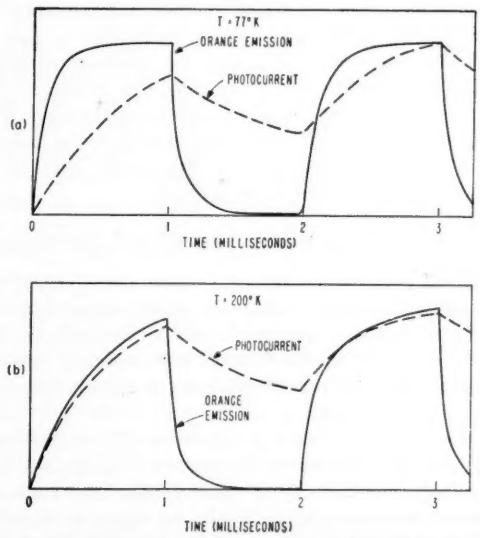

FIG. 10. Behavior of luminescence and photoconductivity at 77°K and 200°K under excitation by ultraviolet pulses (see Fig. 9 for ultraviolet pulse pattern) after many excitation cycles have elapsed.

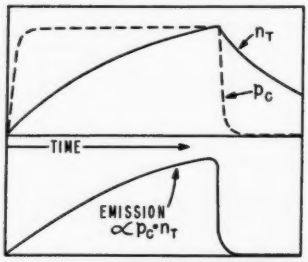

FIG. 11. Qualitative picture showing how the luminescence pulse observed in CdS(Ag) at 200°K can be derived as the product of n_t and p_c. n_t is the number of electrons localized in shallow luminescent levels and it is assumed that at 200°K, n_t is proportional to the number of conduction electrons. p_c is the number of free holes and it is assumed that free holes have short lifetimes.

down to 77°K in darkness. The luminescent levels would then be empty. If we then excite the crystal with ultraviolet, the rise of luminescence for the very first pulse should be slow since luminescence cannot occur until the luminescent levels are filled. Figure 12 shows what occurs on the very first excitation cycle under these conditions. The rise of luminescence is very slow compared to Fig. 10(a). After several excitation cycles, the luminescent levels become substantially filled (and remain filled at 77°K) and the rise of luminescence becomes very rapid [Fig. 10(a)]. Let the ultraviolet excitation now be removed, and let the crystal then be irradiated in the 1μ region. This radiation should liberate holes, and these free holes should then recombine with electrons in luminescent levels (giving rise to a burst of orange luminescence as has been reported[11]). The result of all this is to empty the luminescent levels. If we now remove the 1μ radiation and reapply the ultraviolet pulses, the rise of luminescence is again very slow for the initial pulses as shown in Fig. 12, just as was observed when the crystal was cooled in darkness from room temperature. Of course, after several excitation cycles, the rise of luminescence becomes rapid. This behavior is just what one should expect on the basis of the proposed model since a substantial number of luminescent levels will then be filled.

IV(b). Photoconductivity and Edge Luminescence

In this section experimental observations will be described on the relation between photoconductivity and the green edge luminescent band[13] of CdS at 77°K and 4°K. In these experiments the luminescence was observed with a 6217 photomultiplier in conjunction with a Corning 3-69 filter.

Figure 7(b) shows a comparison of the photoconductive and luminescent decay at 77°K. It is clear that the luminescent decay is much more rapid than the photoconductive decay. Again we have a situation which cannot be interpreted in terms of the simple model of Fig. 6. In order to clarify this matter, a study was carried out by means of the double-pulse method just as was done in the case of CdS(Ag). Let us first describe the series of observations which were made and then attempt to interpret them. Figure 13(a) shows the rise and decay of luminescence and photoconductivity at 77°K after many excitation pulses. The rise of photoconductivity and luminescence are nearly the same, while the decay of luminescence is much more rapid than the decay of photoconductivity. This is similar to what was observed at 200°K for CdS(Ag).

Figure 13(b) shows the behavior of green luminescence at 4°K. Here we see that the rise of luminescence has become quite rapid, and is now much faster than the rise of photoconductivity. At 4°K then, there is little apparent relation between photoconductivity and luminescence. This is very similar to what was observed for CdS(Ag) at 77°K.

In order to obtain more information on the slow rise of green luminescence at 77°K, the following experiment was carried out. Certain samples of CdS have been found to have very high dark conductivities. This conductivity is presumably due to a stoichiometric excess of cadmium. Such crystals have been studied by Kröger, Vink, and van den Boomgaard.[14] They find an activation energy of about 0.03 ev associated with this dark conductivity, and thus the number of conduction electrons can remain very large even at 77°K. In the samples used in these experiments the number of conduction electrons was roughly estimated at 10^{16}/cc at 77°K. Figure 13(c) shows the behavior of the green luminescence of such crystals under the double-pulse excitation after many excitation cycles have elapsed. It is to be noted in particular that the rise of luminescence is very rapid, and that the rise and decay times are equivalent.

Although the mechanism responsible for green luminescence is not yet clearly established, it is possible to give a phenomenological explanation of the foregoing observations based on a model similar to the one used for CdS(Ag). That is, let us assume the green luminescence arises from the recombination of trapped electrons and free holes just as was done for CdS(Ag). In the

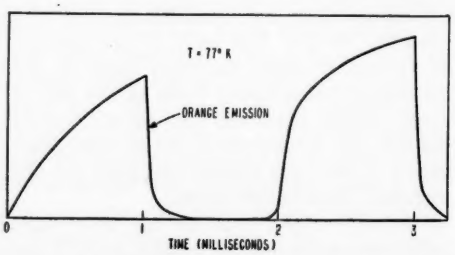

FIG. 12. Initial luminescence pulse for CdS(Ag) crystals at 77°K for a crystal cooled in darkness from room temperature or for a crystal pre-irradiated with 1μ infrared at 77°K.

[13] C. C. Klick, Phys. Rev. **89**, 274 (1953).

[14] Kröger, Vink, van den Boomgaard, Z. physik. Chem. **203**, 1 (1954).

green luminescence case the electron traps would not be as deep as in the CdS(Ag), since the green corresponds to a higher-energy transition than the orange luminescence of CdS(Ag).

The rapid decay of green luminescence would then be ascribed to a short lifetime for free holes, just as was discussed for CdS(Ag). The slower decay of photoconductivity is due to the longer lifetime of free electrons.

The results of the double-pulse observations can also be interpreted on the basis of the CdS(Ag) model. The electron traps responsible for green luminescence are such that at 77°K electrons are not "frozen" in for a long period of time. Thus before luminescence can occur, these traps must be filled. This is the reason for the slow rise of green luminescence at 77°K. This is analogous to the behavior of CdS(Ag) at 200°K.

At 4°K, electrons can be "frozen" in the traps responsible for green luminescence so that the rise of luminescence becomes quite rapid, once these traps have been filled by previous excitation pulses. This is just what occurred at 77°K in the case of CdS(Ag).

The behavior of high dark-conductivity crystals at 77°K can also be interpreted on the CdS(Ag) model. In high dark-conductivity crystals there are a large number of conduction electrons so that a substantial number of the trapping levels would be filled. This means that luminescence can occur as soon as free holes are generated, so that the rise of green luminescence is very rapid in these crystals even at 77°K.

It is clear that on the basis of a model similar to the one proposed for CdS(Ag) one can explain the behavior of green luminescence and photoconductivity under a variety of conditions. This explanation does not offer any description as to the details of the center or mechanism of the luminescence. It is of interest to note that Kröger[15] has offered arguments to support the view that the green luminescence results from the recombination of free holes and free electrons by means of the formation of excitons. On such a picture the green emission would be proportional to the product of the number of free electrons and the number of free holes. Such an exciton picture is consistent with the observations made here at 77°K. The relation between photoconductivity and luminescence and the effect of high dark conductivity could be explained on such a basis. However, the results at 4°K do not appear to be consistent with the exciton model.

Since the observations presented here can be interpreted on the basis of the recombination of a trapped electron and free hole, it may be worthwhile to speculate as to a possible center which could give rise to such behavior. Kröger and his co-workers[14] have indicated that sulfur vacancy which has trapped one electron, acts as a shallow trap for an additional electron. This additional electron, trapped at the sulfur defect, could then recombine with a free hole to give the observed

[15] F. A. Kröger (to be published).

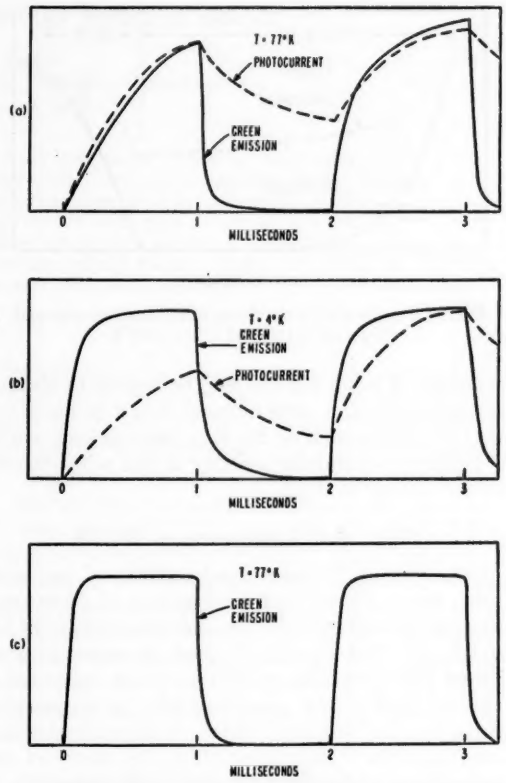

FIG. 13. Pulse patterns obtained for CdS at 77°K and 4°K under excitation by ultraviolet pulse pattern shown in Fig. 8. (a) for samples of CdS with low dark conductivity at 77°K; (b) for CdS crystals with low dark conductivity at 4°K; (c) for CdS crystals of high dark conductivity at 77°K.

luminescence. Kröger[15] has shown that the vibrational structure in the edge luminescence is associated with the longitudinal modes of vibration of the lattice. The theory of Huang and Rhys[16] indicates that in the *F* center for example, the electronic transitions are coupled to the longitudinal modes of vibration of the lattice. Further, the wave function of a weakly bound electron in a material of high dielectric constant may be expected to extend over several lattice spacings so that the vibrational modes with which it interacts could be characteristic of the lattice rather than the specific center to which the electron is bound. It would appear, therefore that the luminescent center proposed here could show the vibrational structure which is observed. Another interesting observation in this connection has been made by Bishop[17] at this laboratory. It was found that by firing CdS crystals in sulfur vapor at 800°C, the green edge luminescence can be removed. Similar treatment in cadmium vapor or in vacuum did not produce this effect, leading one to conclude that the

[16] K. Huang and A. Rhys, Proc. Roy. Soc. (London) **A204**, 406 (1950).

[17] M. E. Bishop (unpublished).

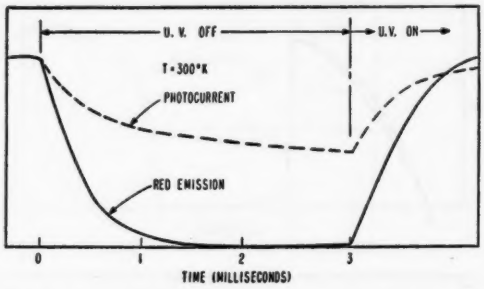

FIG. 14. Comparison of the decay of red luminescence and photoconductivity of CdS at 300°K.

formation of sulfur defects may be needed to observe the luminescence. A more thorough investigation of the effect of sulfurization on the edge luminescence would be useful in determining whether or not sulfur defects are the centers involved.

IV(c). Red Luminescence of CdS

CdS, without the intentional addition of any activator, shows a broad red luminescence at room temperature. This emission corresponds to an energy of 1.4 to 1.8 ev.[18] The crystals in these experiments were excited with ultraviolet at 3650 A and the red emission observed with a 6217 photomultiplier in conjunction with a Corning 2-64 filter. As before, the excitation was interrupted for a short interval and the decay of red luminescence and photoconductivity was observed.

Figure 14 shows the results of such observations. Here again, the luminescent decay is considerably faster than the photoconductive decay. Measurements made using the double pulse method showed that the rise and decay of red luminescence are equivalent, both being much more rapid than the photoconductivity.

This behavior can be interpreted in a rather simple manner if one assumes that the luminescence arises from the recombination of an electron in a donor level and a free hole. That is if we have a donor level ~1.5 ev above the valence band, an electron in such a level could recombine with a free hole in a radiative manner so that luminescence could terminate before photoconductivity. Conductivity would terminate when an electron was captured by the empty donor level. This is essentially the same type of model which is proposed for CdS(Ag).

Since little is known of the center responsible for red luminescence, the above picture is purely phenomenological. For the present, however, it does offer a simple explanation of the difference in decay times between red luminescence and photoconductivity.

[18] R. Frerichs, Phys. Rev. **72**, 594 (1947).

V. CONCLUSION

The measurements of the wavelength dependence of the recombination process show that the spectral response of the photoconductivity is clearly related to such a dependence. The reasons for this wavelength dependence have not been definitely established, but indications are that surface recombination effects may play an important role.

Measurements on the relation between photoconductivity and luminescence show that luminescence decay is much more rapid than the photoconductive decay in CdS. A detailed study of CdS(Ag) indicated that this result is explicable on the basis of a model in which luminescence results from the recombination of trapped electrons and free holes. Such a model could also explain the results obtained in the case of green edge luminescence, and the red luminescence of "pure" CdS.

ACKNOWLEDGMENT

I would like to thank M. E. Bishop, who grew the crystals used in this work, and other members of the Electromagnetics Branch of the Naval Research Laboratory for their advice and assistance on various aspects of this problem. I am also indebted to Professor R. D. Myers, Dr. Jules DeLaunay, and Dr. Clifford C. Klick for their helpful interest in the course of this work.

Interpolation Scheme for Energy Bands in Solids*

LELAND C. ALLEN
Massachusetts Institute of Technology, Cambridge, Massachusetts
(Received February 4, 1955)

The orthogonalized plane wave method is formulated as an interpolation scheme for use in conjunction with calculations made at symmetry points in the Brillouin zone. The Fourier coefficients of the crystal potential and the matrix components of the Hamiltonian between core functions are treated as parameters to be fitted to other calculations made at symmetry points by such methods as the cellular, orthogonalized plane wave, and augmented plane wave. The interpolation scheme then provides a method for making calculations at a general point in the Brillouin zone. The scheme is most useful for the case of valence and excited states where the wave function on one center overlaps many of its neighbors.

I. INTRODUCTION

BECAUSE of the computational difficulty in carrying out rigorous solutions most energy band calculations are made only at symmetry points in the Brillouin zone. It is therefore desirable to consider methods for interpolating between such symmetry points. In general, the requirement for a satisfactory interpolation scheme is the separation of spatial parts and $\mathbf{k}$ dependent parts in the relation determining E as a function of $\mathbf{k}$. Further, the $\mathbf{k}$ dependence should have a relatively simple analytic form so that, e.g., enough general points in the Brillouin zone can be calculated to get an adequate density of states curve. The cellular method[1,2] or procedures which utilize solutions for an atomic interior joined to exterior plane wave solutions on some arbitrary surface,[3–6] do not seem suited to this type of separation.[7]

However, Slater and Koster,[8] starting with the LCAO (linear combination of atomic orbitals) or tight binding approximation, have succeeded in making such a separation and have used the integrals involving the Hamiltonian between two atomic functions as parameters to be fitted to calculations made at symmetry points. The number of parameters to adequately represent strongly overlapping atomic functions may become very large, however, and this method seems best suited to the more tightly bound states.

Another method for which an analytic $\mathbf{k}$ dependence can be separated from the spatial parts in the matrix components of the Hamiltonian is the orthogonalized plane wave method.[9] As with the orthogonalized plane wave method in general this scheme: (a) does not depend on an assumption of a spherical potential for atomic interiors, (b) is most easily applied when the wave functions for an atom in the crystal can readily be separated into a set of core or highly localized functions not overlapping neighboring atoms and a set of valence and excited functions which have very strong overlapping, (c) requires special consideration at certain $\mathbf{k}$ values where the plane waves are orthogonal by reasons of symmetry to all core states. The scheme seems particularly useful for bands with large overlapping and as such may be used to supplement the method of Slater and Koster.

II. PARAMETERIZATION OF THE ORTHOGONALIZED PLANE WAVE METHOD

The orthogonalized plane wave method was developed by Herring.[10] Our treatment differs from that of Herring primarily in use and interpretation and in that we set up the method in terms of less restrictive core functions than free atom functions. We consider N identical unit cells, each of which has volume Ω_0, and for simplicity we assume one atom per unit cell. The orthogonalized plane wave corresponding to the lattice vector $\mathbf{K}_n$ in $\mathbf{k}$ space is defined by

$$N^{\frac{1}{2}}\psi_n=\frac{e^{i(\mathbf{k}+\mathbf{K}_n)\cdot\mathbf{r}}}{\Omega_0}-\sum_i^{(\text{core})}\mu_{in}b_i, \tag{1}$$

where the Bloch sums are

$$b_i(\mathbf{k},\mathbf{r})=\sum_{R_j}e^{i\mathbf{k}\cdot\mathbf{R}_j}\varphi_i(\mathbf{r}-\mathbf{R}_j). \tag{2}$$

The μ_{in}'s are determined from the orthogonality

* Supported in part by the Office of Naval Research.
[1] E. Wigner and F. Seitz, Phys. Rev. **43**, 804 (1933).
[2] J. C. Slater, Phys. Rev. **45**, 794 (1934).
[3] J. Korringa, Physica **13**, 392 (1947).
[4] J. C. Slater, Phys. Rev. **92**, 603 (1953); M. M. Saffren and J. C. Slater, Phys. Rev. **92**, 1126 (1953).
[5] W. Kohn and N. Rostoker, Phys. Rev. **94**, 1111 (1954).
[6] P. M. Morse, "Multiple scattering of waves from a spatial array of spherical scatters" (unpublished).
[7] For a spherically symmetrical potential inside a radius r_i and constant between spheres, the methods given by Kohn and Rostoker (reference 5) and Morse (reference 6) may lead to a practical scheme for getting general points in the Brillouin zone. However, at present no estimate is available as to whether it will be practical to calculate a sufficient number of points for, e.g., a density of states curve.
[8] J. C. Slater and G. F. Koster, Phys. Rev. **94**, 1498 (1954). A prior account of much of this work is given in J. C. Slater, Technical Report No. 4, Solid-State and Molecular Theory Group, MIT, July 15, 1953 (unpublished).
[9] This is also possible for the Fourier series or plane wave method, and a parameterization scheme could be set up using the Fourier coefficients of the potential as disposable parameters. However, the poor convergence of this method is well known and a rough estimate based on wave functions for sodium given by Slater [reference 2 and J. C. Slater, Revs. Modern Phys. **6**, 209 (1939)] show that for an adequate representation the resultant secular equation is well outside the range readily solvable by present high-speed digital computers.
[10] C. Herring, Phys. Rev. **57**, 1169 (1940).

condition

$$\int_\infty b_j^* \psi_n d\mathbf{r} = 0. \tag{3}$$

We assume that the b_i's are orthogonal:

$$\frac{1}{N}\int_\infty b_i^* b_j d\mathbf{r} = \delta_{ij}. \tag{4}$$

This implies that the core functions φ_i form an *orthonormal* set with respect to functions on neighboring centers as well as on the same center. Both this assumption and the choice of core functions will be considered later. The μ_{in}'s resulting from (3) and (4) are then Fourier transforms of the core functions:

$$\mu_{in} = \int_\infty \frac{e^{i(\mathbf{k}+\mathbf{K}_n)\cdot\mathbf{r}}}{\Omega_0^{\frac{1}{2}}} \varphi_i^*(\mathbf{r}) d\mathbf{r}. \tag{5}$$

Our one-electron energy band functions for a given $\mathbf{k}$ are now constructed from a linear combination of functions of the form (1):

$$\Psi(\mathbf{r},\mathbf{k}) = \sum_n A_n \psi_n. \tag{6}$$

Putting this in

$$H\Psi = E\Psi$$

yields the usual secular equation

$$\left| H_{mn} - E\int_\infty \psi_m^* \psi_n d\mathbf{r} \right| = 0, \tag{7}$$

where

$$\begin{aligned} H_{mn} = &\frac{1}{N}\int_\infty \frac{e^{-i(\mathbf{k}+\mathbf{K}_m)\cdot\mathbf{r}}}{\Omega_0^{\frac{1}{2}}} H \frac{e^{i(\mathbf{k}+\mathbf{K}_n)\cdot\mathbf{r}}}{\Omega_0^{\frac{1}{2}}} d\mathbf{r} \\ &- \frac{1}{N}\int_\infty \frac{e^{-i(\mathbf{k}+\mathbf{K}_m)\cdot\mathbf{r}}}{\Omega_0^{\frac{1}{2}}} H \sum_j \mu_{jn} b_j d\mathbf{r} \\ &- \frac{1}{N}\int_\infty \sum_i \mu_{im}^* b_i^* H \frac{e^{i(\mathbf{k}+\mathbf{K}_n)\cdot\mathbf{r}}}{\Omega_0^{\frac{1}{2}}} d\mathbf{r} \\ &+ \frac{1}{N}\int_\infty \sum_i \mu_{im}^* b_i^* H \sum_j \mu_{jn} b_j d\mathbf{r}. \end{aligned} \tag{8}$$

Let us consider the last term in (8). Defining

$$\int_\infty \varphi_i^*(\mathbf{r}) H \varphi_j(\mathbf{r}-\mathbf{R}_q) d\mathbf{r} = \mathcal{H}_{ij}(\mathbf{R}_q), \tag{9}$$

the last term becomes

$$\sum_i \sum_j \mu_{im}^* \mu_{jn} \sum_{R_q} e^{i\mathbf{k}\cdot\mathbf{R}_q} \mathcal{H}_{ij}(\mathbf{R}_q). \tag{10}$$

Next, we treat the two middle or cross terms in (8). For these, we first consider the expansion of Hb_j since b_j is not necessarily an eigenfunction of the crystal Hamiltonian. The set of functions in which it is convenient to make this expansion are the Bloch sums made up from our initially chosen core functions,[11] φ_i. Thus, using (4),

$$Hb_j = \sum_i c_{ij} b_i = \frac{1}{N}\sum_i \left(\int_\infty b_i^* H b_j d\mathbf{r} \right) b_i. \tag{11}$$

Putting (11) into the second term of (8) and using (5), (9) we have

$$\begin{aligned} &-\frac{1}{N}\int_\infty \frac{e^{-i(\mathbf{k}+\mathbf{K}_m)\cdot\mathbf{r}}}{\Omega_0^{\frac{1}{2}}} H \sum_j \mu_{jn} b_j d\mathbf{r} \\ &= -\frac{1}{N}\sum_j \mu_{jn} \left(\sum_i \int_\infty e^{-i(\mathbf{k}+\mathbf{K}_m)\cdot\mathbf{r}} b_i d\mathbf{r} \right) \left(\frac{1}{N}\int_\infty b_i^* H b_j d\mathbf{r} \right) \\ &= -\sum_i \sum_j \mu_{im}^* \mu_{jn} \sum_{R_q} e^{i\mathbf{k}\cdot\mathbf{R}_q} \mathcal{H}_{ij}(\mathbf{R}_q). \end{aligned} \tag{12}$$

This is the negative of (10). Because of the Hermitian property of H the other cross term is equal to (12). To investigate the first term in (8) we write out the one-electron crystal Hamiltonian as

$$H = -\nabla^2 + V(\mathbf{r}).$$

The first term then becomes

$$\begin{aligned} &|\mathbf{k}+\mathbf{K}_n|^2 \delta_{mn} + \frac{1}{\Omega_0}\int_{\Omega_0} e^{i(\mathbf{K}_n-\mathbf{K}_m)\cdot\mathbf{r}} V(\mathbf{r}) d\tau_c \\ &\equiv |\mathbf{k}+\mathbf{K}_n|^2 \delta_{mn} + V(\mathbf{n}-\mathbf{m}). \end{aligned}$$

Collecting the terms, Eq. (8) can thus be written

$$\begin{aligned} H_{mn} = &|\mathbf{k}+\mathbf{K}_n|^2 \delta_{mn} + V(\mathbf{n}-\mathbf{m}) \\ &- \sum_i \sum_j \mu_{im}^* \mu_{jn} \sum_{R_q} e^{i\mathbf{k}\cdot\mathbf{R}_q} \mathcal{H}_{ij}(\mathbf{R}_q). \end{aligned} \tag{8'}$$

Letting $H=1$ in (8), we also get

$$\int_\infty \psi_m^* \psi_n d\mathbf{r} = \delta_{mn} - \sum_i \mu_{im}^* \mu_{in}.$$

It is now the general method of our interpolation scheme to treat the integrals representing the Fourier coefficients of the potential $V(\mathbf{n}-\mathbf{m})$ and the matrix components $\mathcal{H}_{ij}(\mathbf{R}_q)$ as fitting parameters. The $V(\mathbf{n}-\mathbf{m})$ depend only on the differences of the sets of integers characterizing our initial choice of the vectors $\mathbf{K}_n$. The $\mathcal{H}_{ij}(\mathbf{R}_q)$ are the same parameters introduced by Slater and Koster[8] in their LCAO or tight binding approximation interpolation method. At symmetry points our secular Eq. (7) will factor, and we can determine the values of our integrals $V(\mathbf{n}-\mathbf{m})$

[11] In this expansion the b_i's do not form a complete set, and in particular we are omitting any plane wave contribution to the part of b_j which differs from a crystal eigenfunction. It is hoped that in most cases Eq. (11) will be adequate, but there may be instances where an appreciable plane wave contribution enters. In such circumstances it will probably be best to assume that b_j is an eigenfunction and thus use only diagonal $\mathcal{H}$'s in Eq. (8').

and $\mathcal{H}_{ij}(\mathbf{R}_q)$ by fitting to primary calculations made by other methods at these points. In the cases treated by Slater and Koster with the LCAO method, their secular equation factored to such an extent that they were able to fit integrals analytically and for approximately the same number of disposable constants we may also expect to accomplish our fitting analytically. However, for more complicated cases the fitting will probably be done most easily by a trial and error procedure.

III. DISCUSSION

A. Choice of Core Functions

In the formulation and use of the orthogonalized plane wave method, free atom wave functions have usually been assumed for the core functions φ_i.[10,12–15] Callaway[14] has found, however, that such an assumption may lead to considerable error. Since we are using a parameterization scheme and are thus not making extensive calculations with our core functions, we may use less restrictive functions.

If we assume the form

$$R(r)Y_l^m(\theta,\varphi), \tag{13}$$

where $R(r)$ may be a series of terms made up from polynomials in r times exponentials and the Y_l^m's are spherical harmonics, then the Fourier transforms which give the μ_{in}'s are spherical harmonics in $\mathbf{k}$ space times polynomials in $|\mathbf{k}+\mathbf{K}_n|$.[16,17] Further, we may use a technique suggested by Parmenter.[18] In his calculation for Li by the orthogonalized plane wave method, he assumed an exponential for the $1s$ core function and determined the coefficient in the exponent by a variation calculation using the crystal potential which he had constructed. It seems entirely feasible to introduce such variation parameters into $R(r)$ and, if desirable, to consider linear combination of terms of the form (13) determining such parameters and coefficients of the linear combinations by a variation calculation using the crystal potential constructed for the symmetry point solutions.

If a choice of core states is made which includes functions φ_i which overlap functions φ_j centered on neighboring sites, Eq. (4) is not satisfied and considerable additional effort is required to properly handle them. For this case it seems that the most satisfactory procedure for our interpolation scheme is to consider that set of functions on each center which overlap other centers and to construct from these a new orthogonal set. This can be carried out in a symmetrical manner by the method of Löwdin.[19] For example, in germanium, if we consider the core as those functions through $3d$, we could classify the functions through $3p$ as nonoverlapping and the $3d$ as overlapping nearest-neighbor $3s$, $3p$, and $3d$ functions. We would then orthogonalize the $3d$ to $3s$, $3p$, and $3d$ functions on nearest-neighbor sites.

B. Numerical Considerations

The basic problem is the solution of the secular equation, (7), at every value of $\mathbf{k}$ we wish to consider, and its order depends directly on the initial choice of the vectors $\mathbf{K}_n$. There is evidence that in using orthogonalized plane waves very few sets of neighboring $\mathbf{K}_n$ vectors in $\mathbf{k}$ space give a good representation of many of the valence and excited states.[12,14,18] If we consider the vectors $\mathbf{K}_n$ out through nearest neighbors in $\mathbf{k}$ space, the secular equations for the face-centered cubic structure are 9×9 and for the body-centered cubic are 13×13; through next to nearest neighbors these become 15×15 and 19×19, respectively. Solving such secular equations at a large number of points in the Brillouin zone is practicable on high-speed digital computers by a program like that developed by Dr. Alvin Meckler for Whirlwind I at M.I.T. This program has been successfully employed for 5×5 secular equations by Slater and Koster for the density of states curve computed using their LCAO interpolation method. It is worth noting that because of the large number of points involved, Slater and Koster also found it desirable to have the digital computer compute the matrix components even though these were expressed in a simple analytic form. It is expected that such a procedure would also be adopted for the present interpolation scheme.

The number of parameters $V(\mathbf{n}-\mathbf{m})$, of course, is governed by the choice of vectors $\mathbf{K}_n$; e.g., for the f.c.c. structure, going out to nearest neighbors yields four V's while if we go out to next to nearest neighbors we get a total of six V's (if it is convenient to take the average potential equal to zero we get one less in each case). The number of $\mathcal{H}_{ij}(\mathbf{R}_q)$ parameters arising from the matrix components of the Hamiltonian between core states depends on the particular solid and how many sets of neighboring atoms in real space are to be considered, and may be predicted directly from the tables given by Slater and Koster.[8] Since, in general, our core functions are chosen as those functions which do not overlap, we can use the much restricted set of $\mathcal{H}_{ij}(\mathbf{R}_q)$'s corresponding to $\mathbf{R}_q=0$. However, for those core functions which overlap to some extent (and have been made into an orthogonal set by the method given in the previous section), it is reasonable that only nearest neighbors will have to be considered.

C. Orthogonality by Virtue of Symmetry

It was originally pointed out by Herring[10] and also by others[12–14] that the plane wave parts of the wave func-

[12] C. Herring and A. G. Hill, Phys. Rev. **58**, 132 (1940).
[13] F. Herman, Phys. Rev. **93**, 1214 (1954).
[14] J. Callaway, Phys. Rev. **97**, 933 (1955). The author wishes to thank Dr. Callaway for being permitted to see his work before publication.
[15] F. Herman and J. Callaway, Phys. Rev. **89**, 518 (1953).
[16] B. Podolsky and L. Pauling, Phys. Rev. **34**, 109 (1929).
[17] R. McWeeny, Acta Cryst. **4**, 513 (1951).
[18] R. H. Parmenter, Phys. Rev. **86**, 552 (1952).
[19] P. -O. Löwdin, J. Chem. Phys. **18**, 365 (1950).

tions (6) at certain symmetry points (e.g., $\mathbf{k}=0$) form bases for irreducible representations of the crystal point group, some of which may be automatically orthogonal to core functions made from orbitals of the form (13). At such points we are left with the relatively poor convergence properties of the non-orthogonalized plane waves. For these circumstances Herring has suggested the addition of a Bloch sum of atomic-like functions of the expansion having the appropriate symmetry properties and the proper rapid variation near the nucleus. Callaway has constructed and successfully used such functions in his treatment of iron[14] (if we orthogonalize these functions to the core states as indicated in Part A they do not in principle have to be constructed so as to vanish at half the interatomic spacing as contemplated by Herring and used by Callaway). For our interpolation we first make an initial choice of the vectors $\mathbf{K}_n$ and then for a particular crystal investigate at which points the automatic orthogonality occurs. Then, in order to insure a good representation at and around these points, such atomic-like functions are to be included and treated in the same manner as the core functions.

IV. ACKNOWLEDGMENTS

The author wishes particularly to thank Dr. W. H. Kleiner of the Lincoln Laboratory for many helpful discussions and suggestions.

PHYSICAL REVIEW VOLUME 98, NUMBER 4 MAY 15, 1955

Response of Anthracene and Stilbene to Low-Energy Protons and X-Rays*

J. M. Fowler† and C. E. Roos‡
Department of Physics, The Johns Hopkins University, Baltimore, Maryland
(Received January 20, 1955)

The scintillation response of anthracene and stilbene to low-energy protons (170–570 kev) and x-rays (10–40 kev) has been investigated. In agreement with previous work at higher proton energies, the proton pulse height *vs* energy curves are quite nonlinear. The x-ray data are essentially linear down to 10 kev. This result is contrary to the reported response of these crystals to electron bombardment, but seems to be in agreement with the theory proposed by Birks. With the aid of this theory, proton response curves are obtained for stilbene and anthracene over an extended energy range.

INTRODUCTION

THE response of anthracene and stilbene to protons having energies greater than 500 kev has been extensively investigated.[1–3] Studies have been made of electron response below 500 kev,[4,5] but the response to protons in this energy range has not been reported. It is in this low-energy region that the nature of the scintillation response can be investigated in detail. The work of Hopkins[4] and Taylor *et al.*[3] shows that the response to electrons below 25 kev is nonlinear, and although the proton response is nonlinear above 500 kev, it becomes more pronounced at lower energies.

In the case of low-energy gamma rays or x-rays, the photoelectric process plays the major role. One might therefore expect gamma rays and electrons to have the same response. However, the nonlinearity observed for electrons[3,4] is not apparent in the curves presented here for x-rays which are linear within experimental error. An explanation of this discrepancy can be found in the relation developed by Birks,[6] between the luminescence S and the energy E of the ionizing particle:

$$dS/dr=\phi\frac{AdE/dr}{1+kBdE/dr}. \quad (1)$$

AdE/dr gives the number of "excitons" produced in the crystal by the incident particle. The term "exciton" refers to the quantity which links the energy of the incident particle to the fluorescence. Birks has given arguments which indicate that these "excitons" are photons of about 10-ev energy. The function ϕ is given by the expression

$$\phi=1-\tfrac{1}{2}[\exp(-r/a_0)-(r/a_0)E_i(r/a_0)],$$

where $E_i(r/a_0)$ is the exponential integral, a_0 is the mean free path of the "exciton" in the crystal, and r the range of the incident particle in the crystal. ϕ gives the probability of capture of an "exciton" before it escapes through a crystal surface. $kB\ dE/dr$ represents the quenching of these "excitons" by molecules damaged by the ionizing particle or by inactive impurity molecules.

* This research was supported in part by the U. S. Atomic Energy Commission.
† Now at Washington University, St. Louis, Missouri.
‡ Now at the University of California at Riverside, Riverside, California.
[1] Franzen, Peele, and Sherr, Phys. Rev. **79**, 742 (1950).
[2] Frey, Grim, Preston, and Gray, Phys. Rev. **82**, 372 (1951).
[3] Taylor, Jentschke, Remley, Eby, and Kruger, Phys. Rev. **84**, 1034 (1951).
[4] J. I. Hopkins, Rev. Sci. Instr. **22**, 29 (1951).
[5] J. B. Birks and F. D. Brooks, Phys. Rev. **94**, 1800 (1954).
[6] J. B. Birks, Proc. Phys. Soc. (London) **A64**, 874 (1951).

For photoelectrons produced deep within the crystal, such as is the case with x-rays or high-energy electrons, the probability of an "exciton" escaping is small and ϕ approaches unity. In addition, dE/dr is very small for electrons. For 20-kev electrons dE/dr is 1.70×10^{-2} Mev/cm-air-equivalent, and for 500-kev electrons it is 0.33×10^{-2} Mev/cm-air-equivalent, according to the data reported by Glendenin.[7] Since kB is found to be approximately 6 (see below), the term $kB\ dE/dr$ can be neglected for electrons of energy greater than 500 kev, and it makes only a 10 percent contribution to dS/dr at 20 kev. The formula (1) can therefore be approximated by

$$dS/dE=A, \tag{2}$$

and the curve of S *vs* E is substantially linear for x-rays and fast electrons, which penetrate an appreciable distance into the crystal. For low-energy electrons which do not penetrate very far below the surface, the quantity ϕ is a function of r and therefore of E, and this dependence combined with the $1+kB\ dE/dr$ contribution produces the nonlinear effect which is observed.

For heavy particles such as protons and alphas, where dE/dr is no longer small, there is a significant nonlinearity introduced by the $kB\ dE/dr$ term in (1). In fact, for very highly ionizing particles for which dE/dr is large, (1) approaches

$$dS/dr=(A/kB)\phi. \tag{3}$$

Birks[8] has given values of ϕ plotted against r/a_0. Therefore, using Eqs. (2) and (3), and knowing dS/dE for x-rays and dS/dr for alphas, one can determine A and kB. Then using these values in (1), one can construct curves for dS/dr which are correct for any incident particle. With dE/dr obtained from range-energy curves, this information can then be presented in the more useful form of curves of S *vs* E.

In the following sections, kB and A are calculated from data for low-energy protons and x-rays and the predicted curves of S *vs* E are then drawn for both anthracene and stilbene. The validity of these curves is tested by comparing them with high-energy proton data reported in the literature.

EXPERIMENTAL PROCEDURE

The anthracene and stilbene crystals used in the proton experiment were $1\times1\times0.2$ cm in size, and in the x-ray experiment they were $1\times2\times0.2$ cm. The scintillations were detected with an RCA 6199 photomultiplier tube to which the crystals were directly coupled with optically clear grease. After passing through a linear amplifier, the pulses were analyzed by a single-channel pulse-height discriminator.

The source of protons was an electrostatic accelerator. They were observed after being scattered from a thin (1000 A) nickel foil. A scattered beam was used in order to decrease the danger of radiation damage which is known to result from a high-intensity beam. The proton energy was measured by a generating voltmeter which was calibrated by observing the well-known resonance in the $Li^7(p,\gamma)Be^8$ reaction. The protons were observed at 90° and traveled in an evacuated path from scatterer to crystal. The lowest energies were obtained using the H_2^+ beam of the accelerator.

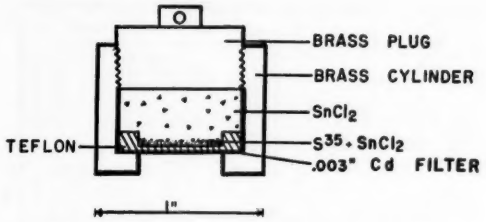

FIG. 1. S^{35}-Sn x-ray source used for calibrations.

In order to study the response of these crystals to electron excitation, monochromatic x-rays of the desired energies were isolated from the general radiation of a tungsten-target x-ray tube by means of a 1.5-meter Bragg single-crystal spectrometer. The regulated high-voltage power supply used in this work has been previously described.[9]

Since the x-ray source and the proton source were in different parts of the laboratory, it was desirable to use an x-ray line as a reference to insure equivalence of gain settings when the equipment was turned off and moved. Several low-energy x-ray sources were constructed by mixing 2 Mc of S^{35}, a pure beta emitter, with the salts of elements such as molybdenum and tin. The details of construction are shown in Fig. 1. The beta rays eject the K electrons from these elements and the characteristic K x-rays are produced. Zirconium and cadmium foils were used to filter out the K_β x-rays.

The S^{35}-Sn source is free of x-rays whose energy is greater than 150 kev and emits very few x-rays above 50 kev. With a filter, the tin K_α lines are approximately 5 times more intense than the general radiation. The peak of the pulse-height distribution obtained from the radiation of the S^{35}-Sn source was found to be the same as that of the monochromatic 25.5-kev radiation obtained from the crystal spectrometer.

RESULTS

Pulse-height distributions from protons incident upon anthracene and stilbene had the expected Gaussian shape with a full width at half-maximum of about 30 percent for 0.46-Mev protons. The pulse heights observed were reproducible to 1 volt, if gain, optics, etc., were kept constant. For a different crystal or a different optical coupling, a relative shift in pulse height was observed, and therefore all proton data reported are for the same anthracene and stilbene crystals.

[7] L. E. Glendenin, Nucleonics **2**, 12 (1948).
[8] J. B. Birks, *Scintillation Counters* (McGraw-Hill Book Company, Inc., New York, 1953), Chap. 6.5.
[9] G. Schwarz and E. H. Byerly, Rev. Sci. Instr. **19**, 273 (1948).

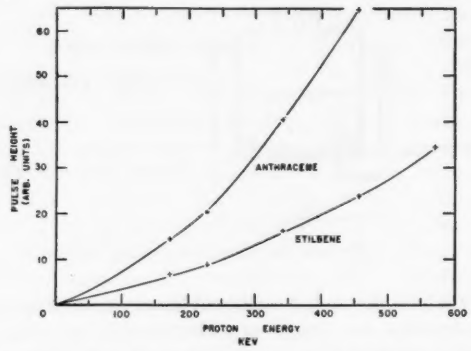

FIG. 2. Pulse heights from anthracene and stilbene as a function of proton energy.

In Fig. 2 is shown the variation of average pulse height with proton energy. The average stilbene to anthracene pulse-height ratio for a common proton energy was 0.41, in good agreement with the value of 0.40 reported elsewhere in the literature for protons of higher energy.[3] The ratio seemed higher at the very low energy points, but in this region the results are very dependent on surface structure, and so can vary from crystal to crystal. The curves are nonlinear in the entire region investigated, in agreement with the relation (1) discussed in the introduction.

The plot of average pulse height *vs* x-ray energy is shown in Fig. 3. With the exception of the 10-kev x-ray points, the mean of each distribution in the pulse height spectrum could be obtained from the axis of symmetry of the distribution. In the case of the 10-kev points, fluorescence pulses obscured the low end of the distributions, making it necessary to determine the mean solely from the location of the maxima of the curves. Wright[10] has recently pointed out that low-energy radiations may give asymmetric pulse-height distributions, making it difficult to assign meaning to the locations of their maxima.

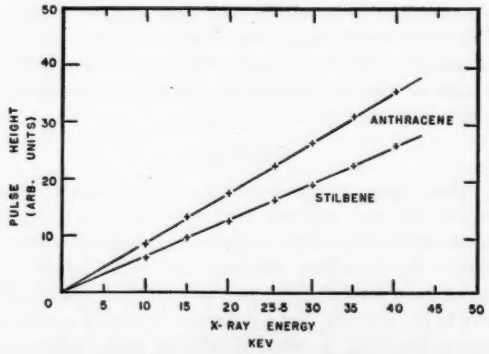

FIG. 3. Pulse heights from anthracene and stilbene as a function of x-ray energy.

[10] G. T. Wright, Phys. Rev. **96**, 569 (1954).

The pulse-height units on the curves in Fig. 3 are the same as those of the proton curves, and this conformity was insured by using the x-ray line from the S^{35}-Sn source as a common normalizing point. The curves are linear within experimental error, and intersect at the point of zero energy. That this point corresponds closely to the point of zero pulse height was confirmed by finding the true zero of the pulse-height analyzer. In terms of the units shown in Fig. 3, the point of intersection of the extrapolated linear curves was found to lie below the origin by 0.5+1.0 units. Hence a slight nonlinearity below 10 kev is not inconsistent with the data. The ratio of pulse height in stilbene to pulse height in anthracene was found to be 0.72. An examination of the data of Taylor *et al.*[3] shows their ratio to be 0.6 approximately.

In Fig. 4 the data are plotted in a manner which is useful in calibrating crystals with natural sources. The energy of the proton is plotted *vs* the energy of that x-ray which produces an equal pulse height. It is seen

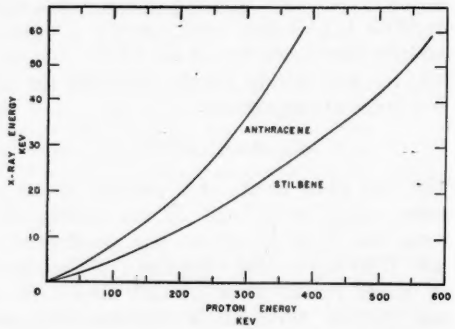

FIG. 4. X-ray energy *versus* proton energy for equal pulse heights.

that in anthracene an x-ray gives approximately the same light output as a proton with ten times its energy, while for stilbene this factor is 15. This factor is not constant, but is larger for the low energies and decreases for higher energies.

DISCUSSION

The relation between the average pulse height and energy observed for x-rays down to 10 kev is compatible with the linear relation (2). Birks and Brooks[9] have recently reported on experiments conducted on anthracene with soft x-rays from secondary radiators. They fitted the results to the theoretical curve predicted by (1) with experimentally determined values of A and kB. A slight nonlinearity is indicated by the theoretical curve but the data seem to be consistent also with a straight line within experimental error. Robinson and Jentschke[11] have also given data for the

[11] W. H. Robinson and W. Jentschke, Phys. Rev. **95**, 1412 (1954).

response of anthracene to x-rays with energies up to 30 kev. The major part of the nonlinearity of response which they reported occurs in extrapolating the measured points to zero energy and zero pulse height.

The quenching factor kB could be calculated directly from dS/dr if one had experimental data from highly ionizing particles such as alphas, where dE/dr is large enough to allow the approximation (3) to be made. For 2-Mev alphas, $dE/dr=1.8$ Mev/cm-air-equivalent[6] and ϕ is approximately one. Birks calculates $kB=7.15$ cm-air-equivalent/Mev on the basis of his experimental value of dS/dr.

The protons in our experiment have a dE/dr of only 0.80 Mev/cm-air-equivalent for the lowest energy (0.174 Mev) and are therefore not highly ionizing enough to use the approximation (3). For a value of $a_0=3$ mm-air-equivalent as given by Birks[5] it is found that ϕ varies from 0.91 to 0.98 in the energy range investigated, and so must be taken into account. kB is

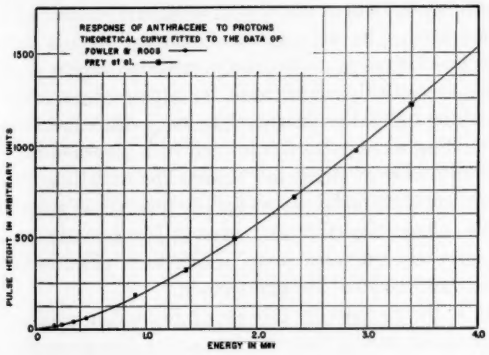
RESPONSE OF ANTHRACENE TO PROTONS
THEORETICAL CURVE FITTED TO THE DATA OF
FOWLER & ROOS
FREY et al.
PULSE HEIGHT IN ARBITRARY UNITS
ENERGY IN MEV

FIG. 5. Pulse heights *versus* proton energy for anthracene. Experimental data of Frey *et al.* (see reference 2) normalized to the curve at 3.4 Mev.

then calculated by using the value of A as determined from the x-ray data, the experimental values of dS/dE, and dE/dr from Bethe's[12] data. Equation (1) is re-

[12] H. A. Bethe, Revs. Modern Phys. **22**, 213 (1950).

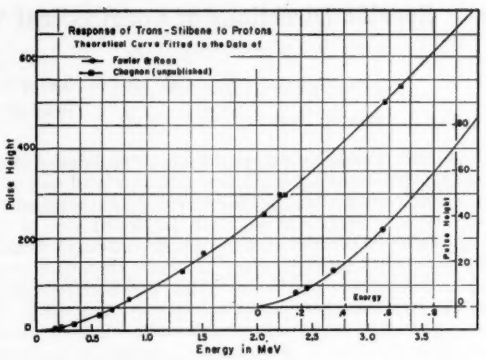

FIG. 6. Pulse heights *versus* proton energy for stilbene. Experimental data of Chagnon normalized to the curve at 3.3 Mev.

written in the form

$$kB=\frac{1}{dE/dr}\left[\frac{\phi A}{dS/dE}-1\right]. \tag{4}$$

The average of the values of kB calculated in this manner are for anthracene, $kB=6.3$ cm-air-equivalent/Mev, and for stilbene, $kB=13.7$ cm-air-equivalent/Mev. The anthracene value is to be compared with 7.15 cm-air-equivalent/Mev reported by Birks.[6] Since kB is the quenching factor which depends upon crystal damage and impurities, the agreement between our value and that of Birks is surprisingly good.

With values of kB and A empirically determined, a theoretical curve of dS/dE was drawn and then integrated to give S *vs* E. This curve is shown for anthracene in Fig. 5 and for stilbene in Fig. 6 for energies up to 4 Mev. To check its conformity with experiment, pulse height *vs* energy data from the literature were normalized at one point and plotted on the theoretical curves. The agreement between experiment and theory is excellent.

The authors would like to thank Dr. J. A. Bearden, Dr. S. S. Hanna, and Dr. G. E. Owen for many helpful discussions, and R. A. Slaven for assistance in the computations. We are also indebted to Paul Chagnon for the proton data above 0.6 Mev in Fig. 6 and the opportunity of using the data before publication.

Specific Directions of Longitudinal Wave Propagation in Anisotropic Media*

F. E. Borgnis†
California Institute of Technology, Pasadena, California
(Received January 4, 1955)

Plane elastic waves can be propagated in every direction of an unbounded elastic medium. It is known that associated with each direction there are three independent waves, the displacements of which form a mutually orthogonal set. In general none of the three displacement vectors coincides with the vector of the normal to the wave front, that is, in general the waves are neither longitudinal nor transverse. The purpose of this paper is to find specific directions in a medium of given anisotropy, along which the displacement of one of the three possible waves is exactly parallel to the direction of wave propagation. A method is developed which leads to the complete set of such "longitudinal" directions, if the matrix of the elastic coefficients is known.

The method is applied to several groups of crystal symmetry, namely to the trigonal, hexagonal, tetragonal, and cubic systems, and the general conditions are established under which pure longitudinal waves exist. For α quartz, for example, the numerical calculation shows that there are five such distinct directions, not counting the ones which are equivalent by symmetry properties.

As a by-product of the results, special conditions between the elastic constants are obtained under which longitudinal waves could be propagated in any direction in a hypothetical anisotropic medium fulfilling these conditions. Owing to their relation to an early investigation by G. Green in 1839, the latter are called specialized Green's conditions.

1. INTRODUCTION

THE general laws of elastic waves propagated in crystalline media are well known.[1] In an infinitely extended crystalline medium, plane elastic waves can be propagated along any direction. If ξ is the vector of particle displacement and $\mathbf{k}$ the wave-vector normal to planes of constant phase, the elastic wave motion is described by

$$\xi = \xi_0 e^{i(\omega t \mp \mathbf{k}\cdot\mathbf{r})}, \tag{1}$$

$\mathbf{r}$ being the position vector of any point P in the medium. The displacement vector ξ has certain specified directions, which, in general, are not parallel to the wave-vector $\mathbf{k}$.

The theory of wave propagation through infinitely extended anisotropic media reveals that for any chosen direction of the wave-normal, that is, of the vector $\mathbf{k}$, there are three possible displacement vectors ξ which are functions of the direction of $\mathbf{k}$. These three displacement vectors are independent of each other and form a mutually orthogonal set; they belong to three independent plane waves propagated, in general, with three different velocities in the direction of $\mathbf{k}$. If it happens that one of the three displacement vectors coincides with $\mathbf{k}$, the other two necessarily lie in a plane perpendicular to $\mathbf{k}$; in this case the wave-triplet consists of one purely longitudinal (i.e., compressional) and two purely transverse waves.[2]

For certain crystals, for example quartz, special directions of $\mathbf{k}$ are known, along each of which the direction of ξ coincides with that of $\mathbf{k}$, or, in other words, along each of which compressional waves can be propagated. The only strain connected with a compressional wave in an infinitely extended region is the one normal to the wave front. By superposition of two such longitudinal waves traveling in opposite directions, a standing wave pattern is formed with planes of nodes and antinodes of stress and strain. The nodal planes of strain are then nodal planes for the total set of stresses. These planes therefore can serve as free boundaries of an infinitely extended plate, which then vibrates in a pure compressional thickness mode.

It is the purpose of this paper to outline a general method for finding the complete set of directions along which compressional waves can be propagated in an anisotropic medium and to apply the method to a number of crystal classes.

In the general case, where the displacement vector is not parallel to the wave normal, it can also be shown easily that in an infinitely extended medium there exist equidistant planes parallel to the wave front, in which all strains, and therefore all stresses, disappear. Any two such planes can serve as the free boundaries of a plate, which then can be excited in thickness vibration.

In *finite* plates, however, such standing waves cannot exist except in very special cases, without being associated with parasitic vibrations. Owing to elastic cross-coupling, a special set of stresses exists throughout the vibrating plate. In order to enforce the boundary conditions of stress-free edges of the plate, other modes of vibration will be set up which are inseparably associated with the original one-dimensional standing wave pattern, thus destroying its purity.[3]

* This paper constitutes a technical report under a contract with the United States Air Force, monitored by the Office of Scientific Research, Air Research and Development Command.

† Now at Gordon MacKay Laboratory of Applied Science, Harvard University, Cambridge, Massachusetts.

[1] For a condensed treatment see A. E. H. Love, *The Mathematical Theory of Elasticity* (Cambridge University Press, London, 1934), p. 298; and W. G. Cady, *Piezoelectricity* (McGraw-Hill Book Company, Inc., New York and London, 1946), p. 104. The subject is dealt with in detail by R. Bechmann, Arch. d. elektr. Übertragung 6, 361 (1952).

[2] If ξ has any arbitrary direction, it can always be decomposed into a longitudinal and a transverse component, the components *not*, however, being independent of each other.

[3] A detailed physical outline of the mechanism of mode-coupling may be found in H. G. Baerwald, U. S. Patent No. 2,485,129, October 18, 1949.

2. PLANE ELASTIC WAVES IN ANISOTROPIC MEDIA

We now summarize in brief the pertinent features of the theory of propagation of plane elastic waves in anisotropic media. The theory was first worked out completely in 1839 by Green, although modern writers refer predominantly to a paper by Christoffel in 1877.[4] Green was interested in the mechanical theory of light propagated through crystalline media, and looked for the conditions under which transverse waves may exist. He found, between the 21 elastic coefficients needed for describing the most general stress-strain relations, 14 relations which must be fulfilled in order to ensure displacement vectors normal to any chosen direction of wave propagation. Besides the two transverse waves, according to Green's theory, there is always a third purely longitudinal wave possible. Green's problem, therefore, is closely related to the one treated here. Whereas Green derived certain relations between the elastic coefficients which must be satisfied in order to obtain transverse waves in any arbitrary direction, we assume those coefficients to be known and seek the set of special axes along which purely compressional waves may be propagated. These axes are necessarily associated with the two independent transverse waves in which Green was interested. We shall obtain conditions similar to those found by Green as a by-product of our results.

In a continuous anisotropic medium under adiabatic conditions the general stress-strain relation is[5]

$$T_i=\sum_k c_{ik}{}^D S_k-\sum_l h_{il}D_l, \qquad (i, k=1, 2\cdots 6;\ l=1, 2, 3), \quad (2)$$

where $c_{ik}{}^D=c_{ki}{}^D$. The D_l are the components of the electric displacement vector. We shall limit ourselves to purely mechanically excited waves and therefore shall assume that no external electric fields are applied to the medium. Then the vector $\mathbf{D}$ is necessarily constant in both space and time. Since we are interested only in harmonic wave motion, $\mathbf{D}$ can be assumed to be zero and Eq. (2) can be written

$$T_i=\sum_k c_{ik}{}^D S_k. \quad (i, k=1, 2\cdots 6). \qquad (3)$$

We choose a unit vector $\mathbf{s}$ with direction cosines l_1, l_2, l_3 as the direction of wave propagation. Any of the three independent and mutually orthogonal displacement vectors $\boldsymbol{\xi}$ associated with the three possible plane waves propagating along $\mathbf{s}$ may be characterized by its direction cosines m_1, m_2, m_3. Then Green's theory shows that for a given $\mathbf{s}$ the direction of any $\boldsymbol{\xi}$ can be found from the following set of equations:

$$\begin{aligned} m_1\Gamma_{11}+m_2\Gamma_{12}+m_3\Gamma_{13}&=m_1q,\\ m_1\Gamma_{12}+m_2\Gamma_{22}+m_3\Gamma_{23}&=m_2q,\\ m_1\Gamma_{13}+m_2\Gamma_{23}+m_3\Gamma_{33}&=m_3q. \end{aligned} \qquad (4)$$

The coefficients $\Gamma_{ik}=\Gamma_{ki}$ are given by

$$\begin{aligned} \Gamma_{11}&=l_1^2c_{11}+l_2^2c_{66}+l_3^2c_{55}+2l_2l_3c_{56}+2l_1l_3c_{15}+2l_1l_2c_{16},\\ \Gamma_{22}&=l_1^2c_{66}+l_2^2c_{22}+l_3^2c_{44}+2l_2l_3c_{24}+2l_1l_3c_{46}+2l_1l_2c_{26},\\ \Gamma_{33}&=l_1^2c_{55}+l_2^2c_{44}+l_3^2c_{33}+2l_2l_3c_{34}+2l_1l_3c_{35}+2l_1l_2c_{45},\\ \Gamma_{13}&=l_1^2c_{15}+l_2^2c_{46}+l_3^2c_{35}+l_2l_3(c_{45}+c_{36})\\ &\quad+l_1l_3(c_{13}+c_{55})+l_1l_2(c_{56}+c_{14}),\\ \Gamma_{23}&=l_1^2c_{56}+l_2^2c_{24}+l_3^2c_{34}+l_2l_3(c_{23}+c_{44})\\ &\quad+l_1l_3(c_{45}+c_{36})+l_1l_2(c_{46}+c_{25}),\\ \Gamma_{12}&=l_1^2c_{16}+l_2^2c_{26}+l_3^2c_{45}+l_2l_3(c_{46}+c_{25})\\ &\quad+l_1l_3(c_{56}+c_{14})+l_1l_2(c_{12}+c_{66}). \end{aligned} \qquad (5)$$

The three (real) values of q in Eq. (4) follow from the roots of a cubic equation, given in determinant form by

$$\begin{vmatrix} \Gamma_{11}-q & \Gamma_{12} & \Gamma_{13}\\ \Gamma_{12} & \Gamma_{22}-q & \Gamma_{23}\\ \Gamma_{13} & \Gamma_{23} & \Gamma_{33}-q \end{vmatrix}=0. \qquad (6)$$

With the values l_1, l_2, l_3 of $\mathbf{s}$ given, the Γ_{ik} can be computed from Eq. (5), and the three values of q are found from Eq. (6). Each value of q belongs to one set of direction cosines m_1, m_2, m_3, which are found by inserting q in Eq. (4). The three wave equations are

$$\partial^2\xi_\mu/\partial t^2=q_\mu\partial^2\xi_\mu/\partial s^2 \quad (\mu=1, 2, 3), \qquad (7)$$

the solution of which has been given in Eq. (1). The wave velocity is

$$v_\mu=\omega/k_\mu=(q_\mu/\rho)^{\frac{1}{2}}, \qquad (8)$$

ρ being the density of the medium. q_μ is therefore called the stiffness coefficient of the wave with the displacement $\boldsymbol{\xi}_\mu$.

3. CONDITIONS FOR PURELY COMPRESSIONAL WAVE MOTION

For longitudinal waves the direction of the displacement vector $\boldsymbol{\xi}$ with direction cosines m_1, m_2, m_3 is to be parallel to the unit vector in the direction of wave propagation $\mathbf{s}$ with the direction cosines l_1, l_2, l_3. Let us consider the values of m_iq in Eq. (4) as the components p_i of a vector $\mathbf{p}$ which lies in the direction of the displacement vector $\boldsymbol{\xi}$. Then $\mathbf{p}$ coincides with $\mathbf{s}$, if $\mathbf{p}\times\mathbf{s}=0$, that is, if

$$l_2p_3-l_3p_2=0, \quad l_1p_3-l_3p_1=0, \quad l_1p_2-l_2p_1=0, \qquad (9)$$

or,

$$l_1:l_2:l_3=p_1:p_2:p_3. \qquad (10)$$

Actually the systems (9) or (10) represent only two independent equations. The components of $\mathbf{p}$ follow from Eq. (4) upon replacing m_i by l_i, since $\mathbf{p}$ and $\mathbf{s}$

[4] G. Green, Trans. Cambridge Phil. Soc. **7**, 121 (1839); *Mathematical Papers* (Macmillan and Company, London, 1871), p. 307; E. W. Christoffel, Ann. di matematica pura ed applicata (2) **8**, 193 (1877). An excellent account of Green's work can be found in Lord Kelvin's *Baltimore Lectures* (Cambridge University Press, London, 1904), Lectures XI and XII.

[5] W. G. Cady, J. Acoust. Soc. Am. **22**, 579 (1950). For the notation see Proc. Inst. Radio Engrs. **37**, 1378 (1949).

are assumed to be parallel:

$$\begin{aligned} l_1 q &= p_1 = \Gamma_{11} l_1 + \Gamma_{12} l_2 + \Gamma_{13} l_3, \\ l_2 q &= p_2 = \Gamma_{12} l_1 + \Gamma_{22} l_2 + \Gamma_{23} l_3, \\ l_3 q &= p_3 = \Gamma_{13} l_1 + \Gamma_{23} l_2 + \Gamma_{33} l_3. \end{aligned} \tag{11}$$

When p_i and Γ_{ik} are substituted from Eqs. (11) and (5) into Eq. (9), the latter yields a set of three equations involving the elastic constants c_{ik}^D and the direction cosines l_1, l_2, l_3, which we wish to find. To each set of real values of the l_i satisfying simultaneously Eqs. (9), there belongs a direction of propagation of a longitudinal wave. By the method outlined we shall investigate now a number of crystal groups with respect to the existence of such directions.

4. GROUP OF TRIGONAL SYMMETRY, CLASSES D_3, C_{3v}, D_{3d}

This group includes α quartz. The elastic constants form the following matrix:

$$\begin{bmatrix} c_{11} & c_{12} & c_{13} & c_{14} & 0 & 0 \\ c_{12} & c_{11} & c_{13} & -c_{14} & 0 & 0 \\ c_{13} & c_{13} & c_{33} & 0 & 0 & 0 \\ c_{14} & -c_{14} & 0 & c_{44} & 0 & 0 \\ 0 & 0 & 0 & 0 & c_{44} & c_{14} \\ 0 & 0 & 0 & 0 & c_{14} & \tfrac{1}{2}(c_{11}-c_{12}) \end{bmatrix}. \tag{12}$$

Using this scheme we compute the Γ_{ik} from Eq. (5), then insert them in Eq. (11) and by using Eq. (9) arrive at the following set of equations:

$$\begin{aligned} l_2 l_3\{(l_1^2+l_2^2)(-c_{11}+c_{13}+2c_{44})+l_3^2(-c_{13}+c_{33}-2c_{44})\} \\ +c_{14}\{3(l_1^2 l_2^2+l_2^2 l_3^2-l_1^2 l_3^2)-l_2^4\}=0, \end{aligned} \tag{13}$$

$$\begin{aligned} l_1 l_3\{(l_1^2+l_2^2)(-c_{11}+c_{13}+2c_{44})+l_3^2(-c_{13}+c_{33}-2c_{44})\} \\ +c_{14}\{l_1 l_2(3l_1^2-l_2^2-6l_3^2)\}=0, \end{aligned} \tag{14}$$

$$3c_{14} l_1 l_3 (l_1^2-3l_2^2)=0. \tag{15}$$

The last equation yields immediately the three solutions

$$l_3=0, \tag{16}$$

$$l_1=0, \tag{17}$$

$$l_1/l_2=\pm\sqrt{3}. \tag{18}$$

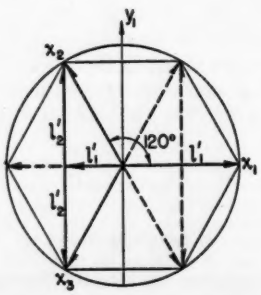

FIG. 1. Set of equivalent directions in a trigonal system with direction cosines $(\pm 1, 0, 0)$ and $(\pm 1/2, \pm\sqrt{3}/2, 0)$.

Putting each one of these solutions into Eq. (13) or (14) we have to investigate whether sets of real values l_1, l_2, l_3 exist that satisfy Eq. (13) or Eq. (14).[6]

Inserting the first value $l_3=0$ into Eq. (13), we obtain

$$c_{14} l_2^2 (3l_1^2-l_2^2)=0. \tag{19}$$

This equation, and therefore Eqs. (13), (14), and (15) are satisfied simultaneously by

$$l_2=0 \quad \text{and} \quad l_2/l_1=\pm\sqrt{3}. \quad [l_3=0] \tag{20}$$

Next, inserting $l_1=0$ from Eq. (17) into Eq. (13) yields either $l_2=0$ or the following cubic equation for the ratio l_3/l_2:

$$\begin{aligned} (-c_{13}+c_{33}-2c_{44})(l_3/l_2)^3+3c_{14}(l_3/l_2)^2 \\ +(-c_{11}+c_{13}+2c_{44})(l_3/l_2)-c_{14}=0. \quad [l_1=0] \end{aligned} \tag{21}$$

Finally, upon inserting $l_1'/l_2'=\pm\sqrt{3}$ from Eq. (18) into Eq. (13), we find that either $l_2=0$ again or that the following equation must hold:

$$\begin{aligned} (-c_{13}+c_{33}-2c_{44})(l_3'/l_2')^3-6c_{14}(l_3'/l_2')^2 \\ +4(-c_{11}+c_{13}+2c_{44})(l_3'/l_2')+8c_{14}=0. \\ [l_1'/l_2'=\pm\sqrt{3}] \end{aligned} \tag{22}$$

[The primes on l_2', l_3' are added to distinguish them from l_2, l_3 of Eq. (21).]

A brief calculation shows that Eq. (21) passes into Eq. (22) by the transformation

$$l_3/l_2=-l_3'/2l_2'. \tag{23}$$

At this point it is appropriate to take notice of the trigonal symmetry of the group under consideration. A rotation of the coordinate system in a medium of trigonal symmetry about the z-axis by $\pm 120°$ leads, as is well known, to an equivalent coordinate system. That is, any point $P'(x',y',z')$ with reference to the system so rotated is in every respect equivalent to the point $P(x,y,z)$ in the original system, if $x=x'$, $y=y'$, $z=z'$. The points P' and P pass into each other by a rotation of their position vectors by $\pm 120°$ around the z-axis. Consequently, associated with any direction in the trigonal group there are two more equivalent directions, all three directions being related, with respect to wave propagation, to each other by a 120° rotation about the z-axis. Each direction is also equivalent to its opposite direction.

Now, Eq. (20) contains a set of directions which lie in the xy-plane, as shown in Fig. 1. When $l_2=l_3=0$ we have $l_1=\pm 1$; when $l_2/l_1=\pm\sqrt{3}$, we have $l_1=\pm 1/2$, since $l_1^2+l_2^2+l_3^2=1$. The directions thus defined pass into each other by a rotation of $\pm 120°$ about the z-axis and are therefore equivalent. Hence it is sufficient to consider only one of them. Selecting the direction determined by $l_2=l_3=0$ we obtain the well-known result that in a medium of trigonal symmetry the x-axis allows the propagation of longitudinal waves.

[6] It may be noted that Eqs. (13) to (15) contain all elastic constants of the matrix (12) except c_{12}.

An infinitely extended plate with planes normal to the x-axis (X-cut) can be excited in purely longitudinal thickness vibration.

A second direction which we obtained from Eqs. (17) and (13) is the one corresponding to the direction cosines $l_1=l_2=0$, that is, $l_3=1$, or the z-axis, which consequently is also an axis allowing longitudinal waves.

Considering next $l_1=0$ according to Eq. (17), we found the corresponding values of l_3/l_2 to be determined by the cubic Eq. (21). When l_3/l_2 in this equation is replaced by $-l_3'/2l_2'$ according to Eq. (23), Eq. (21) passes into Eq. (22), which resulted from the condition $l_1'=\pm\sqrt{3}l_2'$ of Eq. (18).

It is easily seen that the conditions expressed by Eqs. (17) and (18) are equivalent through trigonal symmetry. Figure 2 shows the projection onto the xy-plane of unit vectors with components 0, l_2, l_3 corresponding to Eq. (17), and $l_1'=\pm l_2\sqrt{3}/2$, $l_2'=-l_2/2$, $l_3'=l_3$, which obviously have a 120° relation about the z-axis. Equations (18) and (22) therefore lead only to directions which by trigonal symmetry are equivalent to the directions determined by Eqs. (17) and (21), so that it will be sufficient to consider only the axes in the yz-plane ($l_1=0$) resulting from Eq. (21). From the directions thus found all other equivalent directions are obtained by applying the rules of trigonal symmetry. A cubic equation has either one or three real roots; hence, there are either one or three directions in the yz-plane resulting from Eq. (21).

Including the x- and z-axes already mentioned, we have altogether a set of three or five "longitudinal" directions in the trigonal group here considered. Counting also the equivalent directions resulting from trigonal symmetry, we have in all 7 or 13 "longitudinal" directions,[7] each of them allowing longitudinal wave propagation in either sense.

5. GROUP OF TRIGONAL SYMMETRY, CLASSES C_3, C_{3i}

There is another trigonal crystal group containing Class C_3 and C_{3i}, the elastic constants of which form the matrix

$$\begin{pmatrix} c_{11} & c_{12} & c_{13} & c_{14} & -c_{25} & 0 \\ c_{12} & c_{11} & c_{13} & -c_{14} & c_{25} & 0 \\ c_{13} & c_{13} & c_{33} & 0 & 0 & 0 \\ c_{14} & -c_{14} & 0 & c_{44} & 0 & c_{25} \\ -c_{25} & c_{25} & 0 & 0 & c_{44} & c_{14} \\ 0 & 0 & 0 & c_{25} & c_{14} & \tfrac{1}{2}(c_{11}-c_{12}) \end{pmatrix}. \quad (24)$$

This group evidently contains one more independent elastic constant than the group characterized by the matrix (12), namely c_{25}. Without going into a detailed discussion of the complete system of compressional axes of this group, we will treat briefly some properties of this group with respect to such axes.

[7] The z-axis is counted only once.

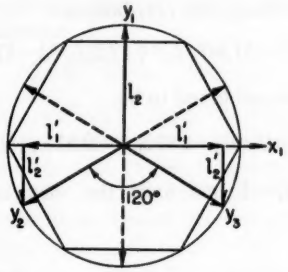

FIG. 2. Projection on the xy-plane of a second set of equivalent directions in a trigonal system.

Using the matrix (24) we find by Eqs. (5), (11), and the last equation of (9) the following condition for the direction cosines of compressional axes:

$$c_{14}l_1l_3(l_1^2-3l_2^2)+c_{25}l_2l_3(3l_1^2-l_2^2)=0. \quad (25)$$

One solution immediately found is $l_3=0$, which corresponds to directions of compressional wave propagation in the xy-plane. With $l_3=0$ one obtains from either of the other two equations in (9) the equation

$$(l_1/l_2)^3-3(c_{14}/c_{25})(l_1/l_2)^2-3(l_1/l_2)+(c_{14}/c_{25})=0. \quad (26)$$

This equation yields a set of three possible compressional axes in the xy-plane, the directions of which depend only on the ratio c_{14}/c_{25}. The three directions are mutually related by the 120° symmetry of the trigonal group.

If $c_{25}=0$, l_2 becomes zero in accordance with the result found in the previous section; in the group considered there the x-axis was found to be a possible compressional axis. This fact is due to the absence of c_{25} in the matrix (12). If $c_{14}=0$, l_1 becomes zero and the y-axis can propagate compressional waves.

If $c_{14}=-c_{25}$, it follows from Eq. (26) that $l_1=l_2=1$; in this case compressional waves may be propagated along the 45° direction in the x, y-plane.

6. COMPRESSIONAL WAVES IN α QUARTZ

As an example of the trigonal groups considered we study the complete set of longitudinal directions in α quartz. The elastic constants are assumed to have the following values[8] expressed in units of 10^{10} dyne cm^{-2}:

$$c_{11}=87.5,\quad c_{12}=7.62,\quad c_{13}=15.1,\quad c_{14}=17.2,\quad c_{33}=107.7,\quad c_{44}=57.3,\quad c_{66}=39.9. \quad (27)$$

[8] W. G. Cady, reference 1, p. 137. The values of c_{ik}, according to Eq. (3), should be those at constant dielectric displacement **D**. The values given here hold at constant electric field **E**. The difference between c_{ik}^E and c_{ik}^D for quartz, however, is small enough to be neglected here. For simplicity the superscript E or D is omitted. The coefficients in Eq. (27) are valid for both right quartz and left quartz, if the systems of coordinate axes are chosen according to p. 408, Fig. 76, of the reference given above, that is a right-handed system of axes for a right quartz and a left-handed system for a left quartz.

With these values, Eq. (21) becomes

$$-22(l_3/l_2)^3+51.6(l_3/l_2)^2+42.2(l_3/l_2)-17.2=0. \quad (28)$$

The solutions are found to be

$$l_3/l_2=0.307, \quad 2.912, \quad -0.874. \quad [l_1=0] \quad (29)$$

From $l_2^2+l_3^3=1$ one finds the following direction-cosines:

(a)	(b)	(c)
$l_3=0.294$	0.946	0.658,
$l_2=0.956$	0.325	−0.753,

(30)

corresponding to angles of about −73°, −19°, and 49° with respect to the z-axis, as indicated in Fig. 3.[9] Knowing the direction cosines we can compute the coefficients Γ_{ik} from Eq. (5) and find the stiffness coefficients q for the longitudinal waves along these directions by Eq. (4), where now $m_1=l_1$, $m_2=l_2$, $m_3=l_3$, since the wave-normal coincides with the direction of displacement. We can also use Eq. (6), which yields not only the q-values belonging to the longitudinal waves, but also the q-values of the two purely transverse waves associated with but independent of each one of the longitudinal waves.

The following values in units of 10^{10} dyne cm^{-2} have been found for the stiffness coefficients q_l of the longitudinal wave and the stiffness coefficients q_{t1} and q_{t2} for the associated transverse waves for the directions indicated by (a), (b), and (c) in Eq. (30) and Fig. 3:

$$\begin{aligned}
&\text{(a)}\ q_l=\ 76.65, \quad q_{t1}=51.09, \quad q_{t2}=60.24,\\
&\text{(b)}\ q_l=109.40, \quad q_{t1}=42.90, \quad q_{t2}=66.04, \quad (31)\\
&\text{(c)}\ q_l=131.34, \quad q_{t1}=29.25, \quad q_{t2}=30.41.
\end{aligned}$$

For the z-axis, which we found also to be a direction allowing longitudinal waves, q_l reduces to c_{33}, as is easily proved. The values q_t of the associated transverse waves with displacements lying in the xy-plane follow from Eq. (6). With the coefficients c_{ik} from Eq. (27) we obtain

$$\text{(d)}\ q_l=c_{33}=107.7, \quad q_{t1}=q_{t2}=c_{44}=57.3. \quad (32)$$

For transverse waves therefore rotational symmetry exists about the z-axis.

The x-axis, commonly used as a direction for pure longitudinal waves, has for the longitudinal waves $q_l=c_{11}$. The numerical values for the longitudinal and the associated transverse waves are[10]

$$\text{(e)}\ q_l=c_{11}=87.5, \quad q_{t1}=29.32, \quad q_{t2}=67.88. \quad (33)$$

To conclude the considerations of media of trigonal symmetry we may consider the special hypothetical relations between the elastic constants c_{ik} which would have to hold in order to ensure purely longitudinal wave propagation in *any* direction. These relations, which we will call "specialized Green conditions" follow immediately from Eqs. (13) to (15), which are fulfilled for *any* set of direction-cosines l_1, l_2, l_3, if

$$c_{11}=c_{33}, \quad 2c_{44}=c_{11}-c_{13}, \quad c_{14}=0. \quad (34)$$

If there were a medium of trigonal symmetry obeying these relations between its elastic constants, it could propagate both pure longitudinal and pure transverse waves in every direction. The condition $c_{14}=0$ would convert the trigonal symmetry into hexagonal symmetry. Upon computing the Γ_{ik} from Eq. (5) by the use of the relations (34) and inserting the Γ_{ik} thus found into Eq. (11), one finds that the stiffness coefficient q for the longitudinal waves becomes $q=c_{11}$ independent of the direction. For the associated transverse waves, however, velocity and polarization are not independent of the direction of wave propagation.

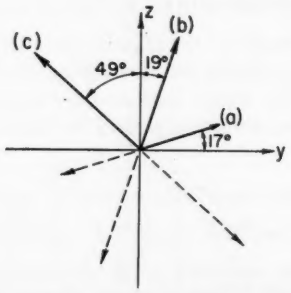

FIG. 3. Directions of longitudinal wave propagation in α quartz. The length of each arrow is proportional to the value of the corresponding stiffness-coefficient q.

[9] It will be noted that the directions (a) and (c) according to Fig. 3 are very close to the so-called 18.5° cut and BT-cut of α quartz. See, for example, W. G. Cady, reference 1, p. 459.

7. GROUP OF HEXAGONAL SYMMETRY

The matrix of elastic constants c_{ik} of the hexagonal system is obtained by setting $c_{14}=0$ in the matrix (12) of the trigonal system considered above. The possible directions of longitudinal wave propagation in a crystal of hexagonal symmetry are therefore determined by our former Eqs. (13) to (15) with $c_{14}=0$. Equation (15) is then fulfilled automatically and we are left with the equations

$$l_2l_3\{(l_1^2+l_2^2)(-c_{11}+c_{13}+2c_{44}) +l_3^2(-c_{13}+c_{33}-2c_{44})\}=0, \quad (35)$$

$$l_1l_3\{(l_1^2+l_2^2)(-c_{11}+c_{13}+2c_{44}) +l_3^2(-c_{13}+c_{33}-2c_{44})\}=0. \quad (36)$$

[10] I. Koga, Reports of Radio Researches and Works in Japan 2, No. 2, 157 (1932). Koga's values differ slightly from the ones given in Eq. (33), owing to the slight difference between Koga's values for the c_{ik} and the values used here from Eq. (27).

These equations are satisfied by

$$l_3=1, \quad l_1=l_2=0; \tag{37}$$

$$l_3=0, \quad l_1^2+l_2^2=1; \tag{38}$$

$$\frac{l_3^2}{l_1^2+l_2^2}=\frac{c_{11}-c_{13}-2c_{44}}{-c_{13}+c_{33}-2c_{44}}. \tag{39}$$

Equation (37) renders the z-axis, and Eq. (38) any axis in the x, y-plane, as possible directions of longitudinal wave propagation. Equation (39) gives another set of directions, all of which lie on a circular cone, the generating lines of which form an angle θ about the z-axis with

$$\tan\theta=\left[\frac{c_{33}-c_{13}-2c_{44}}{c_{11}-c_{13}-2c_{44}}\right]^{\frac{1}{2}}. \tag{40}$$

All compressional directions show rotational symmetry about the z-axis, that is the hexagonal character of the crystal-structure does not manifest itself with respect to such directions as it was the case in the trigonal classes considered.

As an example of the hexagonal group we consider β quartz, which is stable from 573° to 870°C. The elastic constants, in units of 10^{10} dynes cm^{-2}, at 600°C are taken as[11]

$$c_{11}=118.4, \quad c_{13}=32.0, \quad c_{33}=107.0, \quad c_{44}=35.8. \tag{41}$$

With these values, Eq. (40) gives $\tan\theta=0.479$, or $\theta=25.6°$, as the angle about the z-axis of the direction of propagation.

8. GROUP OF TETRAGONAL SYMMETRY, CLASSES V_d, D_4, C_{4v}, D_{4h}

The elastic constants of this group have the following matrix:

$$\begin{pmatrix} c_{11} & c_{12} & c_{13} & 0 & 0 & 0 \\ c_{12} & c_{11} & c_{13} & 0 & 0 & 0 \\ c_{13} & c_{13} & c_{33} & 0 & 0 & 0 \\ 0 & 0 & 0 & c_{44} & 0 & 0 \\ 0 & 0 & 0 & 0 & c_{44} & 0 \\ 0 & 0 & 0 & 0 & 0 & c_{66} \end{pmatrix}. \tag{42}$$

From this matrix we compute the Γ_{ik} from Eq. (5); from Eqs. (11) and (9) the following set of equations is then obtained:

$$l_2l_3\{l_1^2(-c_{12}+c_{13}+2c_{44}-2c_{66})+l_2^2(-c_{11}+c_{13}+2c_{44}) +l_3^2(-c_{13}+c_{33}-2c_{44})\}=0, \tag{43}$$

$$l_1l_3\{l_1^2(-c_{11}+c_{13}+2c_{44})+l_2^2(-c_{12}+c_{13}+2c_{44}-2c_{66}) +l_3^2(-c_{13}+c_{33}-2c_{44})\}=0, \tag{44}$$

$$l_1l_2(l_1^2-l_2^2)(c_{11}-c_{12}-2c_{66})=0. \tag{45}$$

[11] W. G. Cady, reference 1, p. 158. The difference between c_{ik}^D and c_{ik}^E can be assumed small enough to be neglected.

Unless $c_{11}-c_{12}-2c_{66}$ happens to be zero, Eq. (45) yields the solutions

$$l_1=0, \quad l_2=0, \quad l_1=\pm l_2. \tag{46}$$

Equations (43) and (44) express the tetragonal symmetry, since they pass into each other by interchanging l_1 and l_2. From Eqs. (43) to (46) it is seen immediately that the x-, y-, and z-axes are compressional directions. Further compressional axes are determined by

$$l_1=\pm l_2$$

and

$$\left[\frac{l_1}{l_3}\right]^2=\left[\frac{l_2}{l_3}\right]^2=\frac{c_{13}-c_{33}+2c_{44}}{-c_{11}-c_{12}+2c_{13}+4c_{44}-2c_{66}}, \tag{47}$$

$$l_1=0 \quad \text{and} \quad \left[\frac{l_2}{l_3}\right]^2=\frac{c_{13}-c_{33}+2c_{44}}{-c_{11}+c_{13}+2c_{44}}, \tag{48}$$

$$l_2=0 \quad \text{and} \quad \left[\frac{l_1}{l_3}\right]^2=\frac{c_{13}-c_{33}+2c_{44}}{-c_{11}+c_{13}+2c_{44}}. \tag{49}$$

Equations (47) to (49) show again the tetragonal symmetry about the z-axis, since l_1 and l_2 can be exchanged.

In the special case where $c_{11}-c_{12}-2c_{66}=0$, Eqs. (47) to (49) reduce themselves to

$$(l_1^2+l_2^2)/l_3^2=(c_{11}-c_{33}+2c_{44})/(-c_{11}+c_{13}+2c_{44}). \tag{50}$$

The compressional direction given by Eq. (50) therefore possesses rotational symmetry about the z-axis.

The specialized Green conditions for the tetragonal group under consideration follow from Eqs. (43) to (45) as

$$c_{11}=c_{33}=c_{13}+2c_{44}=c_{12}+2c_{66}. \tag{51}$$

If the elastic constants were mutually related in this way, Eqs. (43) to (45) would be satisfied for any values of l_1, l_2, l_3 and purely compressional waves therefore could be propagated in any direction in a medium of this tetragonal group.

9. GROUP OF CUBIC SYMMETRY

The matrix of the elastic constants c_{ik} for a medium of cubic symmetry is obtained from the matrix (42) by setting $c_{13}=c_{12}$, $c_{33}=c_{11}$, and $c_{66}=c_{44}$. Unless $c_{11}-c_{12}-2c_{44}=0$, it follows from Eqs. (43) to (45) that again the x-, y-, and z-axes are compressional directions. Another set of such directions is

$$\pm l_1=\pm l_2=\pm l_3=\pm 1/\sqrt{3}. \tag{52}$$

All the compressional directions in the cubic system are independent of the special values of the elastic constants.

If $c_{11}-c_{12}-2c_{44}=0$, the cubic system passes into an isotropic system and compressional waves can be propagated in every direction.

Electrical Resistance of Copper-Gold Alloys at Low Temperatures*

ELIO PASSAGLIA† AND WILLIAM F. LOVE‡
Randal Morgan Laboratory of Physics, University of Pennsylvania, Philadelphia, Pennsylvania
(Received October 26, 1954; revised copy received January 26, 1955)

The resistance of copper-gold alloys of composition 25, 37.5, 50, 62.5, and 75 atomic percent gold has been measured as a function of temperature from room temperature to 2°K in states slowly cooled and rapidly quenched from above the ordering temperatures. The room temperature resistivities agree with those previously obtained by Johanssen and Linde. The residual resistances are high in both the quenched and slowly-cooled states, but the ratio of residual resistance to the ice point resistance was found to be appreciably lower in the slowly-cooled states for the 25 and 50 atomic percent gold composition. The other compositions showed no such difference in the residual resistance ratio for the quenched and annealed states. Values of Debye temperature calculated by means of the Grüneisen function were found to be strongly temperature dependent, and no appreciable difference was found in the Debye temperatures of the quenched and slowly-cooled states. The Debye temperatures at 75°K were found to obey the equation: $1/\theta_{AB}^3 = x/\theta_A^3 + (1-x)/\theta_B^3$. Hysteresis anomalies of the order of 1 percent were found in the neighborhood of 225°K.

INTRODUCTION

ALTHOUGH the measurement of the electrical resistivity of copper-gold alloys at room temperature and above has yielded much valuable information about the ordering process,[1,2] very little work has been done on this property at low temperatures. Such information would appear to be valuable since it would separate the structural contributions to the change in resistivity on ordering[3] from the phonon contributions. The former would be expected to appear as change in the residual resistivity at absolute zero, whereas the latter would appear as changes in the Debye characteristic temperature. To determine how these two properties are affected, the electrical resistance of a series of five alloys in quenched and annealed states was studied from room temperature to about 2°K. The composition of the alloys was 25, 37.5, 50, 62.5, and 75 atomic percent gold.

EXPERIMENTAL

The metals for the alloys were of the highest purity. The copper was obtained from the Johnson-Mathey Corporation and had a stated purity of 99.999 percent. The gold was obtained from J. Bishop and Company and had a purity of 99.99 percent. Amounts of the components to make approximately five grams of alloy were carefully weighed on an analytical balance. They were then sealed in Vycor tubes under high vacuum (10^{-4} mm Hg). The evacuated tubes were heated in a gas-oxygen flame until the contents were molten and then shaken vigorously to provide a homogeneous melt. Further homogenization was achieved by annealing all the samples except the 75 atomic percent gold at 850°C for 48 hours. The 75 atomic percent gold sample was annealed 48 hours at 900°C. The resulting slugs were drawn into wires of two diameters (0.005 inch and 0.020 inch) by J. Bishop and Company of Philadelphia. The composition of the 0.020-inch wires was checked by x-ray determination of the lattice constant in the disordered state, and within the accuracy of the method (plus or minus 0.4 percent) was found to be as stated above.

To produce a state of high order, the wires were sealed in separate evacuated glass ampules, which were placed in a furnace simultaneously and the following program carried out: The temperature was held at 415°C for 48 hours to order the 50 atomic percent gold sample. The temperature was lowered in the space of eight hours to 385–390° and held at this temperature for 48 hours to order the 25 atomic percent gold sample. The temperature was then lowered to room temperature over a period of 14 days, with the daily increment increasing from 10 degrees at the start to approximately 50 degrees at the end.

To produce the disordered state, the samples were sealed in glass under vacuum, heated to 550°C for a few hours and rapidly quenched in water.

The wires were carefully mounted on a bakelite and brass device, which had bulbs for a constant volume thermometer and helium and hydrogen vapor pressure thermometers, and contained a Leeds and Northrup platinum resistance thermometer. The vapor pressure thermometers were used for the measurement of temperature in their respective range while the constant volume thermometer, which was calibrated against the vapor pressure thermometers, was used between liquid helium and liquid hydrogen temperatures. The platinum resistance thermometer was used above liquid hydrogen temperatures. The temperature of the samples was determined to an accuracy of at least 0.1°K over the whole temperature range. Current and potential contact to the samples was made mechanically. The whole apparatus was shielded by a heavy copper can and placed in the experimental chamber of the Collins

* This work was performed under a contract with the U. S. Atomic Energy Commission.
† Present address: Jackson Laboratory, E. I. Du Pont De Nemours and Company, Incorporated, Wilmington, Delaware.
‡ Present address: Physics Department, University of Colorado, Boulder, Colorado.
[1] C. H. Johanssen and J. C. Linde, Ann. Physik **25**, 1 (1936).
[2] F. W. Jones and C. Sykes, Proc. Roy. Soc. (London) **A166**, 376 (1938).
[3] M. Hirabayashi, J. Phys. Soc. (Japan) **6**, 129 (1951).

cryostat. Current and potential leads were brought out to an external measuring circuit. Potentials were measured by a Leeds and Northrup Type K potentiometer, and the current by the potential across a one-ohm standard resistor.

The current through the samples was kept constant to an accuracy of 0.02 percent. Readings were taken with and without current in order to compensate for small thermal emf's present in the circuit. The resistance was obtained to an accuracy of 0.02 percent in general but for some samples at the lowest temperatures the accuracy was only 0.1 percent. Measurements were taken as the cryostat cooled down, but when the cooling rate exceeded one degree per minute (about 170°K) it was felt the departure from thermal equi-

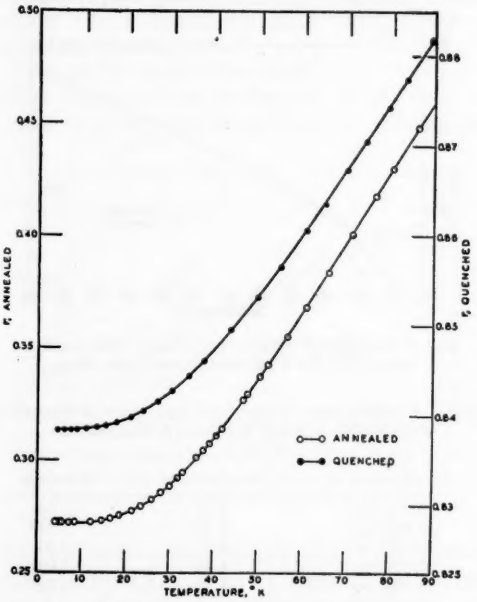

FIG. 1. Reduced resistance *vs* absolute temperature for 25 atomic percent gold alloy.

librium would be too great to give reliable data. After liquid helium temperatures had been reached, the cryostat was shut off and measurements were taken as it warmed up to room temperature, a process which took about 24 hours.

RESULTS AND DISCUSSION

The room-temperature resistivity in the quenched and annealed state calculated from the resistance of the 0.005-inch wire checked very closely with the results of Johanssen and Linde. At liquid helium temperature all the samples showed a high residual resistance in both the annealed and the quenched states. Typical results for the 25 and 50 atomic percent gold samples are shown in Figs. 1 and 2 where there is plotted the reduced resistance (R/R_i) against absolute temperature. These

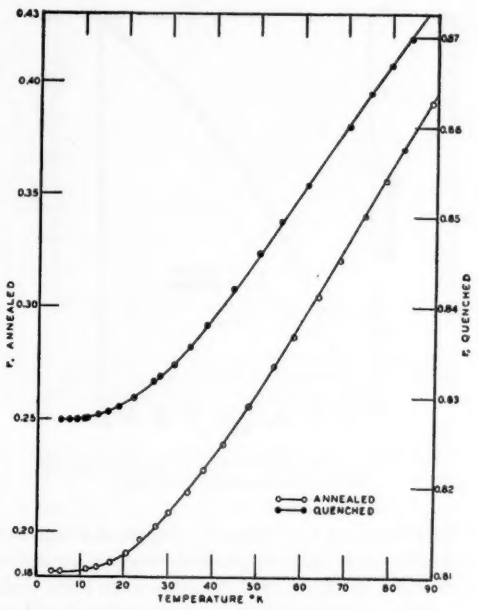

FIG. 2. Reduced resistance *vs* absolute temperature for 50 atomic percent gold alloy.

two samples showed an appreciably lower residual resistance in the annealed state. This was not the case with the other samples. The reduced residual resistances are given in Table I. It is seen that whereas the residual resistances are considerably lower in the annealed state for the 25 and 50 atomic percent gold samples, the change on annealing in the 37.5 and 62.5 atomic percent gold samples is much smaller, while in the 75 atomic percent gold sample there is no change at all. These results are qualitatively similar to the results of the Johanssen and Linde for the room temperature resistivity of ordered and disordered copper-gold.

It is interesting to speculate as to the reason for the high residual resistance in the ordered 25 and 50 atomic percent gold samples. A metal of the purity of the components used in preparing these alloys should show a reduced residual resistance ratio of about 0.001, whereas the ordered copper gold shows a reduced residual resistance ratio of approximately 0.2. Most of this can no doubt be explained on the basis of imperfect stoichiometry, but it is doubtful that if even with perfect stoichiometry a behavior analogous to that of a pure metal would be obtained. This is due to the fact that

TABLE I. Reduced residual resistance.

Sample	Quenched	Annealed
25 At. % Au	0.838	0.272
37.5 At. % Au	0.859	0.782
50 At. % Au	0.828	0.193
62.5 At. % Au	0.846	0.742
75 At. % Au	0.792	0.789

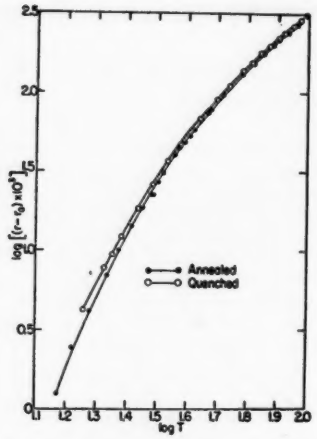

FIG. 3. Log resistance *vs* log absolute temperature for 25 atomic percent gold alloy.

it is doubtful that the necessary degree of order could be obtained with any reasonable ordering procedure. For example, if the ordered domains were 1000 atomic sites long, a situation roughly corresponding to 0.1 percent impurity would be achieved, and such an impurity content would have a large effect on the residual resistance.

As a further analysis, log-log plots of the temperature-dependent portion of the reduced resistance $[(R-R_0)/R_i]$ against the temperature were made to determine if a power law was followed at low temperature. Typical plots in the ordered and quenched states for the 25 and 50 atomic percent gold samples are shown in Figs. 3 and 4. The other samples showed similar behavior. It is to be noticed that there is no indication that a strict power law was followed at even the lowest temperatures, and the curves are very nearly parallel over the whole temperature range. The slope of these curves at the lowest temperatures is given in Table II. In all cases the power is lower than 5. However the slope of the curves in Figs. 3 and 4 is increasing, and if it were possible to resolve the temperature-dependent portion of the resistance more clearly at the lowest temperatures the theoretical value of 5 might be reached.

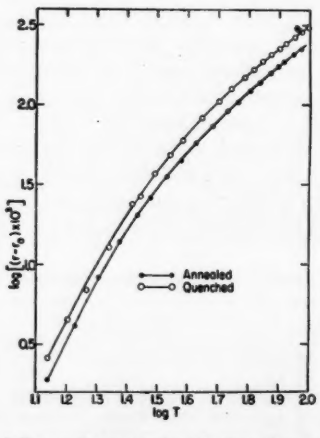

FIG. 4. Log resistance *vs* log absolute temperature for 50 atomic percent gold alloy.

Following Grüneisen,[4] Debye characteristic temperatures were calculated for each of the alloys in the quenched and annealed state. Grüneisen has provided tables of the function

$$\frac{\sigma}{\sigma_\infty}=\frac{4T^4}{\theta^4}\int_0^{\theta/T}\frac{x^5dx}{(e^x-1)(1-e^{-x})},$$

where $\sigma=\rho/T$, $\rho=$ temperature-dependent part of the resistivity, and $\sigma_\infty=\rho_\infty/T_\infty$. T_∞ is any temperature such

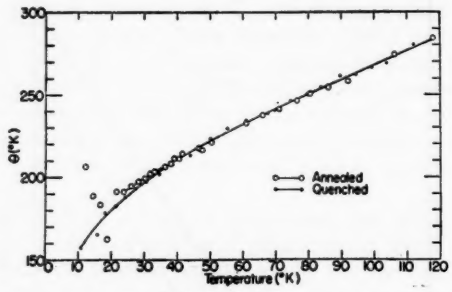

FIG. 5. Variation of Debye temperature with absolute temperature for 25 atomic percent gold alloy.

TABLE II. Limiting value of slope from log-log plot of temperature-dependent portion of resistance *vs* temperature.

Sample	Slope annealed	Quenched
25 % Au	4.33	3.70
37.5% Au	4.59	3.55
50 % Au	3.70	3.83
62.5% Au	4.46	3.09
75 % Au	3.50	3.62

that $T_\infty \gg \theta$. θ is the Debye temperature. In applying this formula to get θ, σ_∞ was obtained in a different fashion. Due to the anomalous behavior of the resistivity of these samples just below room temperature, it was felt that the σ_∞ obtained from the data at room temperature would not be reliable. However, all of the data were smooth and linear with temperature in the region around 100°K. Since σ_∞ is essentially the slope of the resistivity curve in the linear region, it was felt that the most reliable value of σ_∞ could be obtained from the slope of the resistance curves at 100°K. This also avoids any complications due to setting in of order as one goes to temperature higher than room temperature. On the basis of the accuracy of the resistance measurements, θ is determined to within 5°K for all temperatures above 20°K. Below 20°K the accuracy

[4] E. Grüneisen, Ann. Physik **16**, 530 (1933).

becomes very poor and unreliable because of the large residual resistance of the alloys. Typical results for the 25 and 50 atomic percent gold samples are shown in Figs. 5 and 6. In all cases it was impossible to fit Grüneisen's formula with a constant value of θ. These plots show that there is little if any difference in the Debye temperatures between the ordered and quenched states. The difference of about five degrees shown in the 50 atomic percent gold sample is the largest difference found in any of the samples. This contrasts with the results of Bowen[5] for 25 atomic percent gold, but is in agreement with the results of Nix and MacNair.[6]

The source of the disagreement with Bowen is difficult to ascertain since the accuracy quoted in his paper is the same as in the present work, but the method of obtaining θ is different in the two cases. Direct measurements of θ from specific heat data would provide the best answer to this question.

Although the values of θ obtained are of questionable validity because of the inadequacy of the Grüneisen formula, it is tempting to speculate on the change of

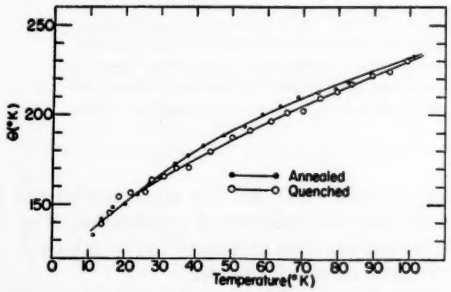

FIG. 6. Variation of Debye temperature with absolute temperature for 50 atomic percent gold alloy.

Debye temperature with composition. If we tentatively assume the additivity of specific heats at low temperatures where the specific heats follow a cubic temperature law, we can readily obtain

$$\frac{1}{\theta_{AB}{}^3}=\frac{x}{\theta_A{}^3}+\frac{1-x}{\theta_B{}^3}, \tag{1}$$

where θ_{AB}, θ_A, and θ_B are the Debye temperatures of the alloy, component A and component B respectively, and x is the atomic fraction of component A. In Fig. 7 we have plotted our results against Eq. (1). The values for pure copper and gold were those quoted in the literature from electrical resistance.[7] The value of Debye temperature used for the alloys was in all cases our value at 75°K. The fit is so good as to appear to some extent fortuitous. The applicability of Eq. (1) however,

[5] D. Bowen, Acta Meteorol. **2**, 573 (1954).
[6] F. C. Nix and D. MacNair, Phys. Rev. **60**, 320 (1941).
[7] D. K. C. MacDonald, Progr. Metal. Phys. **3**, 59 (1952).

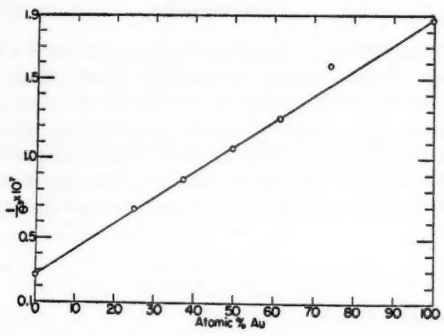

FIG. 7. Variation of Debye temperature at 75°K with composition. The line represents the variation calculated on the basis of additivity of specific heats at low temperatures.

merely demands that the temperature rate of change of the heat of solution be zero, which does not appear to be a completely unjustifiable assumption, since the third law of thermodynamics requires that it approach zero as the temperature approaches zero. Some such rule appears to be more valid than the practice of taking a weighted average of the Debye temperatures of the components as the Debye temperature of an alloy.

At a temperature of about 250°K, a certain amount of hysteresis was observed. An example is shown in Fig. 8. The resistance did not follow a smooth curve, and did not reproduce itself with increasing and decreasing temperature. As can be seen, the variations were far greater than experimental error. These effects were irreproducible and occurred more often in the quenched than in the annealed alloys, and more often in the 37.5 and 62.5 atomic percent gold samples than in the others. Whether this represents a transformation of the martensitic type, or some kind of internal strain changes, remains to be investigated.

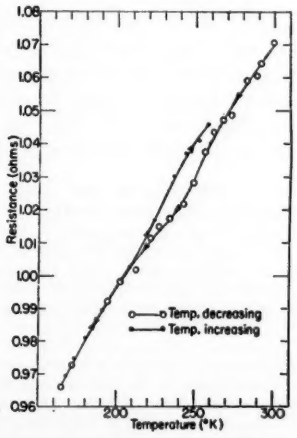

FIG. 8. Resistance *vs* absolute temperature for 62.5 atomic percent gold alloy. This type of behavior was irreproducible and was occasionally encountered in all of the alloys.

CONCLUSION

The annealing of copper-gold alloys produces a large change in the residual resistance in those alloys that show order, and little or no change in the other compositions. The values of Debye temperature obtained from the electrical resistance are strongly temperature-dependent, and show no appreciable difference between the quenched and annealed states. Most of the change in electrical resistance on annealing appears to be due to structural changes rather than to changes in the phonon spectrum.

ACKNOWLEDGMENT

The authors are indebted to Mr. W. B. Teutsch for valuable assistance in the design of the apparatus and taking of data.

PHYSICAL REVIEW VOLUME 98, NUMBER 4 MAY 15, 1955

Dielectric Behavior of Barium Titanate in the Paraelectric State

M. E. DROUGARD, R. LANDAUER, AND D. R. YOUNG
International Business Machines Corporation, Research Department, Poughkeepsie, New York
(Received January 19, 1955)

The coefficients in the equation of state of $BaTiO_3$ proposed by Devonshire can be considered as describing the polarization and temperature dependence of the dielectric constant. This dependence has been studied by a dynamic method. The polarization is developed by a large-amplitude af field and the dielectric constant is measured by means of a small rf signal.

This method provides an accurate measurement of the coefficient of the P^4 term in Devonshire's equation for the free energy of $BaTiO_3$. This coefficient has been studied as a function of temperature, and, contrary to previous assumptions, has been found to have a strong temperature dependence, decreasing linearly, with temperature. The fields which can be applied without breaking the samples are not high enough to detect any contribution due to the P^6 term at temperatures as low as only 4°C above the transition to the cubic state.

I. INTRODUCTION

IN a paper published in 1949,[1] Devonshire developed a phenomenological theory of ferroelectricity in barium titanate. He expanded the free energy of the unit volume[2] of a stress-free crystal as

$$\mathfrak{A}=A(P_x^2+P_y^2+P_z^2)+B(P_x^4+P_y^4+P_z^4)+B_1(P_y^2P_z^2+P_z^2P_x^2+P_x^2P_y^2)+C(P_x^6+P_y^6+P_z^6)+\cdots+\mathfrak{A}_0(T), \quad (1)$$

where P_x, P_y, and P_z are components of the polarization along the a, b, and c axes respectively, and computed the values of A, B, and C from the experimental data that were available to him. In order to account for the Curie-Weiss law behavior of the dielectric constant, A was taken to be a linear function of temperature, namely $A=\alpha(T-T_0)$. All the other coefficients were assumed to be independent of temperature. The three phase transitions were accounted for by taking B to be negative and B_1 and C positive.

More recently,[3] Merz has shown that the double hysteresis loop of barium titanate around 120° (the upper Curie point) can be easily explained by Devonshire's theory. Merz measured the values of the polarization as a function of field, obtained at different temperatures, and computed the coefficients A, B, and C. Merz found that B was actually negative, which means that the transition must be of the first order.

Several investigators[4–7] have also observed that the transition from the ferroelectric to the paraelectric state occurs at higher temperatures than the converse transition. Here again the thermodynamic theory[5] predicts the possibility of such a temperature hysteresis for a first-order transition. The agreement is only qualitative, however; the thermodynamic treatment leaves deliberately aside some factors (nucleation processes, particularly) that probably play an important part.

We have felt it would therefore be of interest to investigate the validity of Devonshire's treatment in a

[1] A. F. Devonshire, Phil. Mag. **40**, 1040 (1949), see also A. F. Devonshire, Advances in Phys. **3**, 85 (1954).

[2] Strictly speaking, we are not interested in the free energy of a unit volume, but in the free energy of a fixed amount of barium titanate. These are not the same, since the volume involved changes with polarization and temperature. Since it is the free energy $\mathfrak{A}$ of the whole crystal with which we are concerned, we have $\partial\mathfrak{A}/\partial Q=V$, where Q is the total charge on the electroded area and V is the applied voltage. Since Q and V rather than P and E are the fundamental variables, it is not necessary to correct for dimensional changes due to the polarization. For purposes of comparison, however, our values of charge have been divided by the approximate area of the crystal at room temperature and our values of voltage have been divided by the crystal thickness at room temperature. This point has been brought to our attention through a set of mimeographed lecture notes for which we are indebted to Conyers Herring.

[3] W. J. Merz, Phys. Rev. **91**, 513 (1953).

[4] L. E. Cross, Phil. Mag. **44**, 1161 (1953).

[5] P. W. Forsbergh, Phys. Rev. **93**, 686 (1954).

[6] S. Roberts, Phys. Rev. **85**, 925 (1952).

[7] W. Känzig and N. Maikoff, Helv. Phys. Acta **24**, 343 (1951).

wider range of temperature. In the ferroelectric state, however, the range of variation of polarization is quite narrow, and we have limited our work to the paraelectric state, from about 120°C to 150°C. We performed our experiments on single crystals of pure barium titanate grown in our laboratory by C. Karan and B. Skinner. The samples were very thin plates with gold electrodes evaporated on their faces. They were prepared by H. Dunn and E. Davin. They are characterized by a dielectric constant of about 200 at room temperature with a very high peak (16 000) at the Curie point.[8] The saturation polarization at room temperature is 0.26 coul/m².

II. METHODS

Above the Curie point, the only polarization that can exist is that developed by the field applied to the electrodes, perpendicular to the faces of the plate. We can then write

$$P_x=P_y=0, \quad P_z=P, \qquad \mathfrak{A}=AP^2+BP^4+CP^6+\cdots+\mathfrak{A}_0(T), \tag{2}$$

and by differentiating Devonshire's equation we obtain

$$\partial\mathfrak{A}/\partial P=E=2AP+4BP^3+6CP^5.$$

Above the Curie point, the dielectric constant is so large that we can neglect the term E in comparison to $4\pi P$. Hence

$$\partial E/\partial P\cong 4\pi/\epsilon=2A+12BP^2+30CP^4, \tag{3}$$

where E is the externally applied field and ϵ is the permittivity of the material (equal to the dielectric constant if we use the cgs system, which we will do from now on).

Since the dielectric constant is the physical variable that can be measured most accurately, our method consists of studying the polarization dependence of the capacitance of a sample. The polarization is developed by a low-frequency (60 cps) field of variable amplitude and a very-small-amplitude radio-frequency field is superposed on the low-frequency field to allow the measurement of the capacitance. Measurements taken at different temperatures will thus show the temperature dependence of the coefficients under study.

Merz[3] has already pointed out a slight difficulty due to the electrocaloric effect. Devonshire was primarily concerned with phase transitions and limited himself to equilibrium conditions, with no field applied. His work therefore involves the Helmholtz free energy $\mathfrak{A}$, the minimum of which determines the stable state. Since we are using an ac method, the conditions are much more nearly adiabatic. Therefore the temperature T is a function of the applied polarization P. Let T_i be the temperature at zero polarization. Then if $T-T_i=\Delta T$ is small,

$$E(P,T)=\left(\frac{\partial\mathfrak{A}}{\partial P}\right)_T=\left(\frac{\partial\mathfrak{A}}{\partial P}\right)_{T_i}+\frac{\partial^2\mathfrak{A}}{\partial P\partial T}\Delta T; \tag{4}$$

and since we are studying adiabatic phenomena,

$$dS=d\left(-\frac{\partial\mathfrak{A}}{\partial T}\right)=\frac{\partial S_0}{\partial T}dT-\left[2\frac{dA}{dT}P+4\frac{dB}{dT}P^3+6\frac{dC}{dT}P^5\right]dP=0.$$

S_0 is the entropy of the unpolarized state. This shows that the temperature of the crystal varies along the polarizing cycle according to the equation

$$\Delta T=\frac{T_i}{c_P\rho}\left[\frac{dA}{dT}P^2+\frac{dB}{dT}P^4+\frac{dC}{dT}P^6\right], \tag{5}$$

where T_i is the temperature of the crystal at zero polarization, c_P is the specific heat at constant polarization, and ρ is the density. Substituting this value of ΔT in Eq. (4) and differentiating, we find

$$\left(\frac{dE}{dP}\right)_S=\frac{4\pi}{\epsilon}=2A+12\left[B+\frac{T_i}{2c_P\rho}\left(\frac{dA}{dT}\right)^2\right]P^2+30\left[C+\frac{T_i}{c_P\rho}\frac{dA}{dT}\frac{dB}{dT}\right]P^4. \tag{6}$$

If we use the values $c_P=0.16$ cal/g deg, $\rho=6.04$ g/cm³, and $dA/dt=3.7\times10^{-5}$, the corrective term to B,

$$\tfrac{1}{2}(T_i/c_P\rho)(dA/dT)^2,$$

appears to be of the order of 5×10^{-15} cgs, which turns out to be negligible.

Above the Curie point, barium titanate crystals are electrostrictive and exhibit an induced piezo-effect which leads to a more serious difficulty. (The piezoelectric effect is induced by polarizing the crystal.)

In order to evaluate the importance of this effect, we can consider the two cases of a free crystal (denoted by the subscript F) and that of a crystal (denoted by the subscript LC) which is clamped in one direction parallel to the faces of the plates, and cannot change its dimensions in this particular direction. We have

$$4\pi/\epsilon_F=2A+12B_FP^2+\cdots,$$
$$4\pi/\epsilon_{LC}=2A+12B_{LC}P^2+\cdots.$$

If we now denote by $\epsilon_F{}^{LC}$ the longitudinally clamped dielectric constant of a free crystal (this is a crystal which is constrained only with respect to small dimensional changes in one direction, such as occur in a dielectric constant measurement; this crystal is not constrained for large and slow changes in polarization),

[8] M. E. Drougard and D. R. Young, Phys. Rev. 95, 1152 (1954).

it is shown in the Appendix that

$$B_{LC}-B_F=\frac{\pi}{3P^2}\left[\frac{1}{\epsilon_{LC}}-\frac{1}{\epsilon_F}\right]=\frac{\pi}{2P^2}\left[\frac{1}{\epsilon_F{}^{LC}}-\frac{1}{\epsilon_F}\right].$$

The quantity $\epsilon_F{}^{LC}$ can be calculated from piezoelectric measurements taken in our laboratory by E. J. Huibregtse. At 120°C, using a dc field of 12 cgs units, he found a longitudinal coupling coefficient[9] $k=0.54$. The corresponding dielectric constant was $\epsilon_F=3.3\times10^4$, while the zero field dielectric constant, ϵ_0, was 13 000. The polarization developed by the dc field is approximately

$$P\cong\epsilon_0E/4\pi E\cong1.3\times10^4 \text{ cgs units},$$

and the dielectric constant $\epsilon_F{}^{LC}$ is given by

$$\epsilon_F{}^{LC}=\epsilon_F(1-k^2)\cong23\,000,$$

and we can now compute the difference:

$$B_{LC}-B_F\cong\frac{\pi}{2(1.3)^2 10^8}\left[\frac{1}{13\,600}-\frac{1}{23\,000}\right]$$

$$\cong1.2\times10^{-13} \text{ cgs units}.$$

As will be seen later, this correction is about one-half of B, and this is in the case of a crystal clamped in only one direction perpendicular to the polarization. It is therefore quite likely that the free energy of a completely clamped crystal would have a positive P^4 term, leading to a second-order rather than a first-order transition, as has been predicted by Devonshire.

It is therefore necessary to avoid clamping the samples, which would happen to some extent if we were using a small electrode area evaporated on a much larger crystal. The best measurements should be obtained on plates having their faces entirely coated. We have used several such plates, of either a rectangular or a circular shape.

III. EXPERIMENTAL ARRANGEMENT

Temperature Regulation

The quite drastic temperature dependence of the dielectric constant in the paraelectric region, and especially near the Curie point, necessitates a very accurate stabilization of the temperature of the sample. Our system, shown in Fig. 1, is capable of holding the temperature constant to within 0.01°C for a period of 10 minutes or more.

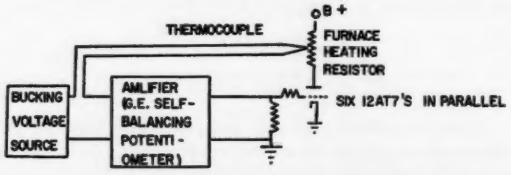

FIG. 1. Temperature stabilization arrangement.

The stabilization is accomplished by having the heating resistor in the plate circuit of a parallel arrangement of tubes. A control thermocouple in contact with the furnace is placed in series with an adjustable bucking voltage source, and the very small differential emf is, after amplification in a General Electric Self Balancing Potentiometer, applied to the grids of these tubes.

In order to measure the dielectric constant as a function of polarization we have used the same basic arrangement that was already described in an earlier paper.[10] This arrangement is shown in Fig. 2.

The very-small-amplitude radio-frequency field is added in a mixer to a large amplitude 60-cps driving sine wave, obtained from an ac regulator. The resulting wave is fed into the "Detector" terminals of a G.R. 716 bridge. The sample is housed in a very small furnace.

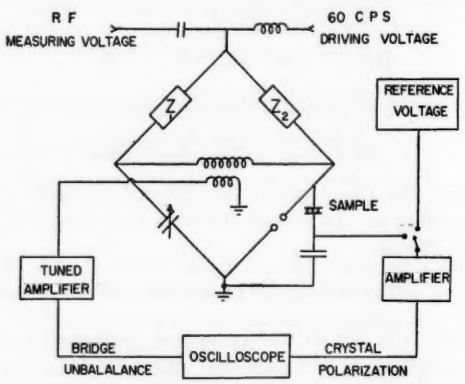

FIG. 2. The capacitor in series with the ferroelectric sample measures the polarization. The voltage developed across this series capacitor is applied to one axis of the oscilloscope. The bridge unbalance is applied to the other axis.

A large capacitor is in series with it, and the combination is connected to the "Unknown" terminals of the bridge, the output of which is taken at the "Generator" terminals. The voltage across the series capacitor, which is a measure of the polarization developed across the sample, is applied to the Y axis of the scope. The bridge output is applied to the other axis, so that the unbalance of the bridge is displayed against the polarization, and the bridge can thus be balanced for any value of polarization.

The measurement of the polarization itself is effected by bringing the reticle of a low-power microscope in coincidence with the chosen balance point. The Y input of the scope is then switched to a well-regulated adjustable ac source (60 cps) and the ends of the trace brought to coincidence with the microscope reticle. The measurements are accurate to a few parts in a thousand.

[9] For a definition of longitudinal coupling coefficient see W. P. Mason, *Piezoelectric Crystals and their Application to Ultrasonics* (D. Van Nostrand Company, Inc., New York, 1950), Chap. 5.

[10] Drougard, Funk, and Young, J. Appl. Phys. **25**, 9 (1954).

IV. RESULTS

From Eq. (1) it is seen that if $\epsilon_0(T)$ and $\epsilon_P(T)$ are the dielectric constants respectively of a nonpolarized sample and of the same sample having a polarization P, the difference,

$$\frac{4\pi}{\epsilon_P(T)}-\frac{4\pi}{\epsilon_0(T)}=12BP^2+30CP^4,$$

is, for small values of P, a linear function of P^2. This is what we experimentally observe, and the slope of the straight line gives the coefficient B.

In agreement with Devonshire's calculations and with Merz's earlier measurements, we find that the coefficient B is negative. Typical results obtained on entirely electroded samples and on samples having an electrode area much smaller than the area of the whole crystal are plotted in Fig. 3, as a function of temperature. For both crystals, the coefficient A can be expressed as

$$A=3.8\times10^{-5}(T-T_0)\text{ cgs units},\quad (T_0\cong105°\text{C})$$

in agreement with other authors.

The two kinds of samples differ most strikingly in the magnitude of B. The temperature dependence of B for the case of a free crystal is very nearly linear. If this linear law still holds at higher temperatures, the coefficient B should change sign in the vicinity of 175°C. This fact has not been checked experimentally.

No good data on the coefficient of the P^6 term can be presented as yet, because the accuracy of the measurements is slightly affected by a small frequency-independent hysteresis phenomenon which we have not been able to explain.

We have thought that it would be of interest to check our conclusions as to the variation of the temperature of the crystal during the polarizing cycle. The temperature of the crystal is as indicated by Eq. (5), an increasing function of P^2, and the average temperature of the crystal must, at equilibrium, be equal to the temperature of the furnace. Thus, if we vary the polarization at 60 cps, the zero-polarization temperature of the crystal should be slightly lower than the temperature of the furnace. Correspondingly, the dielectric constant at the zero-polarization point of the cycle should be larger than the dielectric constant we would find if only the small amplitude measuring field were applied to the crystal. This is actually what we observe on a completely electroded sample. From the capacitance readings we can compute the temperature difference due to the application of the driving field, and this turns out to be about one-half of the first term of our Eq. (5), which is the expected deviation.

V. DISCUSSION

We can compare our results to both Devonshire's and Merz's results. As pointed out by Merz,[2] the first comparison can only be fair if we replace the values of dielectric constant and polarization used by Devonshire, by those observed on our own crystals. According to the theory, our coefficient B should be given by

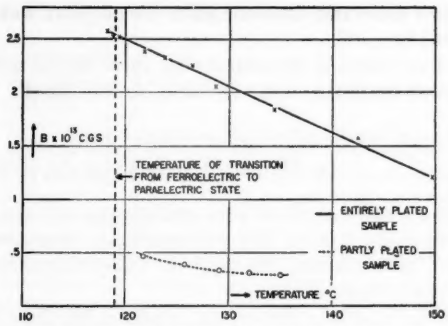

FIG. 3. Measured values of Devonshire's B coefficient *versus* temperature. The magnitude of B is larger for the entirely plated sample.

$$B=4\pi/\epsilon_c P_c^2,$$

where ϵ_c is the dielectric constant in the paraelectric state at what Devonshire calls the critical temperature (this is the temperature at which $\mathfrak{A}(P)$ has three equal minima), and P_c is the spontaneous polarization in the ferroelectric state at the same temperature, which is somewhere in the narrow temperature hysteresis range observed. As a good approximation, we can then take

$$\epsilon_c=16\,000,\quad P_c=0.18\text{ coul/m}^2=5.4\times10^4\text{ cgs units},$$

and therefore find $B=2.7\times10^{-13}$ cgs units, which is in much better agreement with our observed value of 2.5×10^{-13} cgs at the Curie point than Merz's value of 1.7×10^{-13}.

VI. SUMMARY

We have measured the coefficient of the P^4 term of the free-energy expansion for barium titanate single crystals. We find that our value near the 120° transition is in very good agreement with Devonshire's theory. Such an agreement can be obtained only if one uses samples which have their faces entirely covered by the electrodes. We show by calculations that this coefficient is extremely sensitive to clamping and we have verified this experimentally. The existence of a hysteresis phenomenon above the Curie point has prevented us from making any good measurements of the coefficient of the P^6 term.

VII. APPENDIX. RELATION BETWEEN THE CLAMPED AND FREE DIELECTRIC CONSTANTS OF A FREE CRYSTAL AND THE DIELECTRIC CONSTANT OF A LONGITUDINALLY CLAMPED CRYSTAL

The quantities corresponding to a free crystal will be denoted by the subscript F and those for a crystal which is clamped in one direction perpendicular to the polarization by the subscript LC. The longitudinally

clamped dielectric constant of a free crystal will be denoted by $\epsilon_F{}^{LC}$.

In both cases, if we assume that there are no shears and limit ourselves to the P^4 terms, we can write

$$\mathfrak{A}=\tfrac{1}{2}c_{11}(x_1^2+x_2^2+x_3^2)+c_{12}(x_1x_2+x_2x_3+x_3x_1)+AP^2+B_cP^4+g_{11}x_3P^2+g_{12}(x_1+x_2)P^2,$$

where c_{11} and c_{12} are stiffness coefficients, and the x's stand for the strains. The polarization is taken to be in the "3" direction. We explicity follow Devonshire[1] and ignore terms of the type x^2P^2.

For the case of a free crystal, we have $\partial\mathfrak{A}/\partial x_i=0$ or explicitly

$$\begin{aligned} c_{11}x_1+c_{12}x_2+c_{12}x_3&=-g_{12}P^2,\\ c_{12}x_1+c_{11}x_2+c_{12}x_3&=-g_{12}P^2,\\ c_{12}x_1+c_{12}x_2+c_{11}x_3&=-g_{11}P^2. \end{aligned} \tag{I}$$

Solving these equations gives x_1, x_2, and x_3 as a function of P^2 and we note that x_1, x_2, and x_3 are proportional to P^2.

The field is given as a function of polarization by

$$E=\frac{d\mathfrak{A}}{dP}=\frac{\partial\mathfrak{A}}{\partial x_i}\frac{\partial x_i}{\partial P}+\frac{\partial\mathfrak{A}}{\partial P}=\frac{\partial\mathfrak{A}}{\partial P},$$

since the $\partial\mathfrak{A}/\partial x_i$ are equal to zero, or

$$E=2AP+4B_cP^3+2g_{11}x_3P+2g_{12}(x_1+x_2)P. \tag{II}$$

The free dielectric is obtained by differentiating Eq. (II) with respect to P. Since the quantities x_1, x_2, and x_3 are proportional to P^2,

$$dx_1/dP=2x_1/P,\quad dx_2/dP=2x_2/P,\quad dx_3/dP=2x_3/P,$$

and we obtain

$$4\pi/\epsilon_F\cong dE/dP=2A+12B_cP^2+2g_{11}x_3+2g_{12}(x_1+x_2)+2g_{11}Pdx_3/dP+2g_{12}P(dx_1/dP+dx_2/dP).$$

That is,

$$4\pi/\epsilon_F=2A+12B_cP^2+6[g_{11}x_3+g_{12}(x_1+x_2)]. \tag{III}$$

In the case of a longitudinally clamped crystal, if the strains are now denoted by a prime superscript, we have

$$x_1'=0,\quad \partial\mathfrak{A}/\partial x_2'=0,\quad \partial\mathfrak{A}/\partial x_3'=0,$$

or explicitly

$$\begin{aligned} x_1'&=0,\\ c_{11}x_2'+c_{12}x_3'&=-g_{12}P^2,\\ c_{12}x_2'+c_{11}x_3'&=-g_{11}P^2, \end{aligned} \tag{IV}$$

and the field is

$$\frac{\partial\mathfrak{A}}{\partial P}=E=\frac{\partial\mathfrak{A}}{\partial x_i}\frac{dx_i}{dP}+\frac{\partial\mathfrak{A}}{\partial P}=\frac{\partial\mathfrak{A}}{\partial P},$$

$$E=2AP+12B_cP^3+2P(g_{12}x_2'+g_{11}x_3').$$

The dielectric constant of this crystal is obtained by differentiating this last equation, and taking for dx_1', dx_2', and dx_3' the differentials of x_1', x_2', and x_3' as given by Eq. (IV). As in the case of a free crystal, we have

$$dx_2'/dP=2x_2'/P,\quad dx_3'/dP=2x_3'/P,$$

and therefore

$$4\pi/\epsilon_{LC}=2A+12B_cP^2+6[g_{11}x_3'+g_{12}x_2']. \tag{V}$$

We wish now to compute the longitudinally clamped dielectric constant of a free crystal. This can be done by differentiating Eq. (II), and the corresponding dx's are obtained by differentiating Eqs. (I), but this time we keep x_1 constant, so that if we denote the corresponding differential strains by the symbols $d'x_1$, $d'x_2$, and $d'x_3$,

$$\begin{aligned} d'x_1&=0,\\ c_{11}d'x_2+c_{12}d'x_3&=-2g_{12}PdP,\\ c_{12}d'x_2+c_{11}d'x_3&=-2g_{11}PdP. \end{aligned} \tag{VI}$$

We note that we obtain the same expression by differentiating Eqs. (IV). Thus, if we forget the physical significance of the x_i''s and consider them as mere algebraic symbols,

$$d'x_2/dP=2x_2'/P,\quad d'x_3/P=2x_3'/P,$$

and the dielectric constant becomes

$$\begin{aligned} 4\pi/\epsilon_F{}^{LC}&=2A+12B_cP^2+2g_{11}x_3+2g_{12}(x_1+x_2)+2g_{11}Pd'x_3/dP+2g_{12}Pd'x_2/dP,\\ 4\pi/\epsilon_F{}^{LC}&=2A+12B_cP^2+2[g_{11}x_3+g_{12}(x_1+x_2)]+4[g_{11}x_3'+g_{12}x_2']. \end{aligned} \tag{VII}$$

We have verified that the coefficient of the P^2 term of the free energy is the same in the case of a free or longitudinally clamped crystal. Therefore the dielectric constant at zero polarization is unaffected by clamping. If we now compute the difference,

$$\begin{aligned} 4\pi/\epsilon_F{}^{LC}-4\pi/\epsilon_F&=4\{[g_{11}x_3'+g_{12}x_2']-[g_{11}x_3+g_{12}(x_1+x_2)]\},\\ 4\pi/\epsilon_C-4\pi/\epsilon_F&=6\{[g_{11}x_3'+g_{12}x_2']-[g_{11}x_3+g_{12}(x_1+x_2)]\}, \end{aligned}$$

we see that

$$1/\epsilon_C-1/\epsilon_F=\tfrac{2}{3}[1/\epsilon_F{}^{LC}-1/\epsilon_F],$$

which is the relation we used in the text.

Magnetic Properties of Zinc Sulfide and Cadmium Sulfide Phosphors*

SIMON LARACH AND JOHN TURKEVICH
RCA Laboratories and Princeton University, Princeton, New Jersey
(Received February 11, 1955)

Measurements of magnetic susceptibility were made of various preparations of zinc sulfide and cadmium sulfide by the Gouy method, from 77°K to 300°K. The materials differed in crystalline state and modification, type and content of impurities, methods of preparation, and neutron radiation treatment. No temperature-dependent paramagnetism was found for either the zinc sulfides or the cadmium sulfides. The diamagnetism was dependent on the variables cited above.

Uncrystallized zinc sulfide obtained by precipitation had a specific diamagnetic susceptibility of -0.36×10^{-6}, while that of cadmium sulfide was -0.268×10^{-6}. On crystallization, the susceptibility values obtained depended on whether air, nitrogen or hydrogen-sulfide atmospheres were used during the crystallization, and whether chloride or aluminum ion "flux" was used. Only small differences were found in the susceptibilities of the cubic and of the hexagonal forms of zinc sulfide.

It has been postulated that Cl^{-1} or Al^{+3} aided in the luminescence of zinc sulfide phosphors by allowing the formation of monovalent zinc, through charge compensation. It would be expected that this monovalent zinc would give rise to a temperature-dependent paramagnetic species. No such paramagnetism was found. Instead, the diamagnetism increases, suggesting that the role of the Cl^{-1} and Al^{+3} ions is to perturb the lattice. The radial extent of such a perturbed volume in a zinc sulfide phosphor, optimally activated with Ag or Cu, is calculated as approximately 50 A. The luminescence center in such phosphors is identified with the metallic activator surrounded by the perturbed volume.

High-intensity neutron bombardment of a zinc sulfide:Cu phosphor causes a marked increase in the value of the diamagnetic susceptibility.

INTRODUCTION

THE present investigation of magnetic properties of phosphors is part of a general program on the physico-chemical properties of inorganic luminescent materials. Although the luminescence properties of zinc sulfide phosphors have long been known and described, very little work has been reported on the magnetic properties of zinc or cadmium sulfides. Rupp[1] and Sibaiya and Venkataramiah[2] have reported on the magnetic properties of some sulfide-dominated phosphors, Zimens and Hedvall[3] have investigated magnetic susceptibility as a function of crystal structure of zinc sulfide, and Pacault[4] has investigated the susceptibilities of colloidal dispersions of several sulfides.

In the present investigation, the purity, crystal modification, and synthesis procedures were carefully controlled, and the effect of charge-compensating-agents ("fluxes") and activators on the magnetic properties were determined. In this fashion, it was hoped to gain further insight into the role of sulfide-phosphor-constituents.

EXPERIMENTAL METHODS

Magnetic

The Gouy equipment, described in a previous article,[5] was modified for the present study, in order to obtain greater sensitivity. An Ainsworth Type FDI micro-balance, capable of being read to two micrograms was used on a vibration-proof mounting. The sample tubes consisted of precision-bore Pyrex, 1.25 mm i.d.±0.01 mm, enabling density determinations to be carried out with a high degree of accuracy.

Figure 1 shows a circuit designed to measure and control the magnet current, as well as to protect the magnet from surge voltages. The power was obtained from a motor-generator, exclusively used with the magnet. The current was controlled by a pair of high-capacity, water-cooled rheostats, R7, R8, and was measured by the *IR* drop across a 0.0045-ohm resistor, R2. In order to provide surge protection for the magnet, a fuse delay-line was provided, F1-F4, R3-R5, in conjunction with a 1000 VDC capacitor, C1, and a General Electric Thyrite across the magnet coils. The magnet was calibrated with Mohr salt,[6] the field strength being obtained as a function of millivolts developed across the 0.0045-ohm resistor.

The simplified Gouy equation requires that the field be a maximum at one end of the sample, and negligible

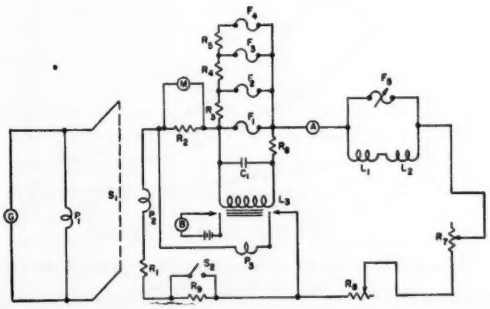

FIG. 1. Electromagnet control, measuring, and protective circuit.

* This article is based upon a dissertation submitted by Simon Larach in partial fulfillment of the requirements for the degree of Doctor of Philosophy at Princeton University.

[1] E. Rupp, Ann. Physik **78**, 505 (1925).
[2] L. Sibaiya and H. S. Venkataramiah, Current Sci. **9**, 224 (1940).
[3] K. E. Zimens and J. A. Hedvall, Svensk, Kem. Tidskr. **53**, 12 (1941); Trans. Chalmers Univ. Tech. **9**, 3 (1942).
[4] A. Pacault, J. Chim. Phys. **49**, 585 (1952).
[5] S. Larach and J. Turkevich, Phys. Rev. **89**, 1060 (1953).
[6] L. C. Jackson, Trans. Roy. Soc. (London) **A224**, 1 (1923).

at the other end. Field strength as a function of vertical distance was determined, and is shown in Fig. 2. As the squares of the field strengths are involved, it is seen that samples longer than 11 cm can be treated as having negligible field at the upper end.

Magnetic susceptibilities were determined from the weight change of the sample as a function of the field. In making measurements, the characteristics of the material were obtained by measuring the magnetic properties of the glass sample tube and of the tube filled with material.

Chemical

Phosphor Syntheses

Techniques for the preparation of sulfide phosphors have been given by Leverenz.[7] The precipitated, luminescence-pure zinc sulfide[8] that was used, showed no spectroscopically-detectable "poison" impurities, such as Fe, Co, Ni, or activator impurities, such as Ag, Cu, Mn.

The phosphors were synthesized from the base material by adding appropriate solutions of activator and flux materials in triple-distilled water. The mixtures were stirred well, dried at 110°C, and transferred to silica containers, for crystallization from 800°C to 1200°C in temperature-controlled, Vycor tube furnaces. Where an inert atmosphere was desired during crystallization, purified nitrogen was used. After crystallization, the preparations were washed free of water-soluble chlorides and were dried.

EXPERIMENTAL RESULTS

The results of the magnetic measurements are given below, and are summarized in Table I. Figure 3 is an example of a typical run.

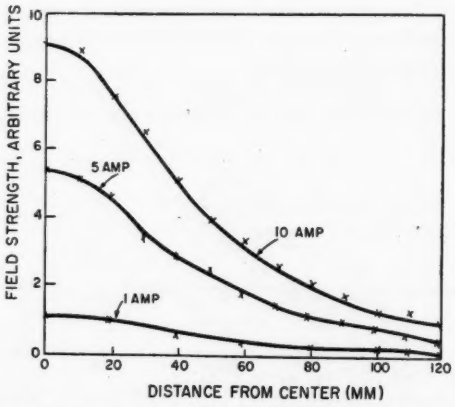

FIG. 2. Field strength as a function of vertical distance, for various magnet currents.

[7] H. W. Leverenz, *Introduction to Luminescence of Solids* (John Wiley and Sons, Inc., New York, 1950).

[8] Obtained as LM476, from the RCA Victor Division, Lancaster, Pennsylvania.

Diamagnetism of Zinc Sulfide Phosphors

Precipitated zinc sulfide.—The specific diamagnetic susceptibility of zinc sulfide (precipitated and dried) was determined as -0.36×10^{-6}. Other investigators[1,3,4] have reported -0.28×10^{-6}, -0.42×10^{-6}, and -0.33×10^{-6}, the last value being for a colloidal dispersion.

Effect of crystal modification and synthesis procedures.—On crystallization in a nitrogen atmosphere, the susceptibility dropped, being $(-0.262\pm0.009)\times10^{-6}$ for cubic-ZnS, and $(-0.290\pm0.003)\times10^{-6}$ for the hexagonal modification.[9] The values of the susceptibility were temperature independent in the range of 77°K–300°K.

If however the crystallization was carried out in a reactive atmosphere, the susceptibility increased. Thus, hexagonal-ZnS, crystallized in an atmosphere of hydrogen sulfide, had a specific diamagnetic susceptibility of $(-0.387\pm0.005)\times10^{-6}$. Cubic-ZnS, crystallized in air in a closed container, or essentially in an SO_2 atmosphere, had a specific diamagnetic susceptibility of $(-0.373\pm0.004)\times10^{-6}$.

TABLE I. Summary of sulfide magnetic properties.

Material	Crystal modification	Crystallization atmosphere	$-\chi\times10^6$
ZnS(pptd.)	cubic[a]	···	0.36
ZnS	cubic	N_2	0.262
ZnS	hexagonal	N_2	0.290
ZnS	cubic	air	0.373
ZnS	hexagonal	H_2S	0.387
ZnS:NaCl	cubic	air	0.402
ZnS:Ag:NaCl	cubic	air	0.406
ZnS:Al(0.01)	cubic	H_2S	0.357
ZnS:Al(0.1)	cubic	H_2S	0.409
CdS(pptd.)	[b]	···	0.268
CdS(650°C)	[b]	N_2	0.254
CdS(900°C)	[b]	N_2	0.158
CdS:Cl	···	N_2	0.253

[a] The precipitated (pptd.) zinc sulfide was found to be cubic, and of very poor crystallinity.

[b] W. O. Milligan, J. Phys. Chem. **38**, 798 (1934), has reported the existence of cubic and hexagonal forms of cadmium sulfide, depending on synthesis procedure. X-ray findings (unpublished) by Dr. J. A. Amick have confirmed this. Precipitated cadmium sulfide was found to be 30 percent cubic and 70 percent hexagonal. Co-crystallization with chloride yields materials with very high hexagonal content, which upon grinding, revert partially to the cubic modification. The materials were prepared by Dr. S. M. Thomsen of the RCA Laboratories.

Effect of "fluxes."—The use of chloride or aluminum ions as "fluxes" also increased the susceptibility. Cubic-ZnS was air-crystallized with two percent, by weight, of NaCl. The residual chloride was removed by washing, and the material was dried. The incorporated chloride for similar materials has been found to be approximately 130 microgram-atoms per mole of phosphor.[10] The specific diamagnetic susceptibility of this material was $(-0.402\pm0.017)\times10^{-6}$, an appreciable increase over the material with no chloride.

That the incorporated halide is responsible for the increased diamagnetic susceptibility rather than the

[9] W. Voigt and S. Kinoshita, Ann. phys. **24**, 492 (1907), obtained a value of -0.264×10^{-6} for a crystal of sphalerite (cubic-ZnS).

[10] R. H. Bube, J. Chem. Phys. **20**, 708 (1952).

activator is shown by the fact that additional incorporation of a metallic activator ion (silver) had no further effect. Thus, cubic-ZnS, air-co-crystallized with chloride and with 0.01 percent by weight of Ag, had a specific diamagnetic susceptibility of $(-0.406\pm0.008)\times10^{-6}$.

Trivalent charge-compensating additives have been reported by Kröger and Dikhoff[11] and by Bube and Larach.[12] To test the effect of such trivalent additives, the magnetic properties were determined of zinc sulfide: Al materials, crystallized in hydrogen sulfide. The specific diamagnetic susceptibility for the material to which 0.01 percent by weight of alumium ion had been added was $(-0.357\pm0.008)\times10^{-6}$, and for the material with 0.1 percent aluminum $(-0.409\pm0.003)\times10^{-6}$.

Neutron-irradiated ZnS.—Zinc sulfide: Cu, irradiated for approximately 32 hours in the Brookhaven National Laboratory nuclear reactor, had the extremely high diamagnetism of -0.59×10^{-6}.

Diamagnetism of Cadmium Sulfide

Uncrystallized CdS.—The specific diamagnetic susceptibility for precipitated, and dried CdS was found to be -0.268×10^{-6}. Pacault,[4] working with colloidal dispersions has reported a value of -0.394×10^{-6}.

Crystallized CdS.—Cadmium sulfide was fired at 650°C in an atmosphere of purified nitrogen. The resulting material was electrically insulating ($\sim10^{10}$ ohm cm), and its specific diamagnetic susceptibility was $(-0.254\pm0.015)\times10^{-6}$, again temperature-independent in the range of 77°–300°K.

A sample of CdS, fired at 900°C in a nitrogen atmosphere, was electrically conducting ($\sim10^{4}$ ohm cm). The specific susceptibility was $(-0.158\pm0.003)\times10^{-6}$. This decrease in diamagnetism is not associated with a temperature dependence of susceptibility, in the range of 77°K to 300°K.

CdS, with incorporated chloride, fired at 900°C in a nitrogen atmosphere, was conducting, and had a specific diamagnetic susceptibility of $(-0.253\pm0.004)\times10^{-6}$.

DISCUSSION

Effect of Crystallization

The value of the diamagnetic susceptibility of uncrystallized zinc sulfide found in the present investigation falls within the range of values previously reported by others.[1,3,4] The effect reported by Rupp[1] of a decrease in the diamagnetic susceptibility on crystallizing zinc sulfide has been corroborated. It has been found, however, that this effect occurs only when zinc sulfide is (1) pure, and (2) when it is crystallized under inert atmosphere conditions. This decrease in the absolute value of the diamagnetic susceptibility has no temperature coefficient, and consequently, the crystallization process does not involve the formation of

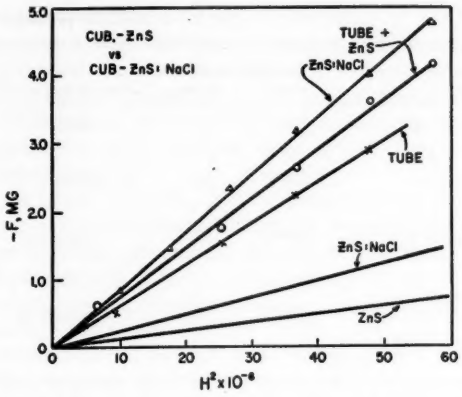

FIG. 3. Force on the sample as a function of the square of the field strength, for (a) cubic-ZnS, and (b) cubic-ZnS with chloride flux.

atomic or molecular species having normal temperature-dependent paramagnetism. The decrease in susceptibility must be ascribed to an actual decrease of diamagnetism, either on the surface or in the volume of the material. If this decrease in diamagnetism is ascribed to changes of bulk properties, defects of the order of 30 percent would have to be postulated, a value inconsistent with the constancy of position of the x-ray lines and their becoming sharper on crystallization, as shown in Table II.[13] For this reason, the decrease in diamagnetism is ascribed to a decrease in the surface, where the electrons must have a greater orbital radius and diamagnetism than in the bulk. This point of view is consistent with the high surface recombination effects often observed in semiconductors.

On the other hand, crystallization in a reactive atmosphere, such as air or H_2S, causes a slight increase in the diamagnetism. To account for this effect, it must be assumed that the decrease of surface diamagnetism is more than compensated for by the formation of Schottky defects, produced by the diffusion of zinc atoms from the interior to the surface layer of oxygen or sulfur, deposited by the reactive atmosphere. Since the half-width of the x-ray lines is not broadened, the defects are probably less than 1 percent, indicating that the diamagnetic contribution of these Schottky defects is very great.

Cadmium sulfide, like zinc sulfide, shows a decrease in the absolute value of diamagnetism on crystallization at a temperature of 900°C. No temperature-dependence of susceptibility was observed, and the susceptibility decrease is ascribed to a diminution of the surface area. It should be noted that this decrease in diamagnetism is associated with conversion of the cadmium sulfide from an insulator to a conductor, an effect which may be associated with the destruction of surface recombination sites.

[11] F. A. Kröger and J. Dikhoff, Physics **16**, 297 (1950).
[12] R. H. Bube and S. Larach, J. Chem. Phys. **21**, 5 (1953).

[13] X-ray data were obtained by Dr. J. A. Amick of the RCA Laboratories, with a Philips Norelco x-ray diffractometer.

TABLE II. X-ray data for several zinc sulfide materials.

Form of material	Crystallization Temp	Atmos	Crystal modification	Half-width of peak (*hkl*)	Intensity of peak (*hkl*)	a_0	c_0
Precipitated	···	···	cubic[a]	0.55°(331) 0.7°(422)		5.404	
Crystallized	800°C	N_2	cubic[a]	0.37°(331) 0.4°(422)		5.411	
Crystallized	1200°C	N_2	hexagonal	0.275°(203) 0.325°(210)	13.25(203) 6.5(210) 6.0(211)	3.822	6.257
Crystallized	1200°C	H_2S	hexagonal	0.25°(203) 0.325°(210)	13.5(203) 6.5(210) 5.5(211)	3.821	6.255

[a] The precipitated material was less crystalline than the 800°-N_2 material. The α_1 and α_2 peaks could not be resolved for the precipitated ZnS, but were resolvable for the 800°-N_2-crystallized ZnS.

Cubic and Hexagonal Zinc Sulfide

Zinc sulfide exists in two well-known crystal modifications, cubic (sphalerite) and hexagonal (wurzite), the transition temperature from the cubic to the hexagonal form being about 1020°C.

Very little work has been reported on the susceptibilities of these two crystalline forms of zinc sulfide. Zimens and Hedvall[3] have given the values of -0.38×10^{-6} for the cubic form, and -0.40×10^{-6} for the hexagonal form. However, their hexagonal zinc sulfide was a phosphor containing traces of copper, and synthesis procedures were not given.

In the present investigation, pure zinc sulfide was used, and crystallizations were carried out in an atmosphere of pure nitrogen. The phosphors were not ground, since the hexagonal modification can revert to the cubic form on grinding.[14,15] A value of $(-0.262\pm0.009)\times10^{-6}$ was obtained for the specific susceptibility of cubic zinc sulfide, and $(-0.290\pm0.003)\times10^{-6}$ for the hexagonal form.[16]

Chloride and Aluminum "Fluxes"

Zinc sulfide phosphors are usually prepared with the addition of an alkali halide, commonly referred to as a "flux." The proportion added is rarely critical. The functions of a flux have been thought to be mainly: (1) to provide a fluid phase for solvation and transport of ingredients, and (2) to increase surface reactivity and atomic mobility to facilitate crystal growth.[17] Recent investigators have assigned a greater role to halide than that of a mere chemical flux, by postulating that the presence of halide affects the luminescence properties of zinc sulfide phosphors by causing changes in the internal structure of the crystal.[12,18] Smith[19] has suggested that the halide is incorporated into the crystal and causes crystal defects, and Kröger and Hellingman[20,21] have reported a correlation between proportion of chloride incorporated and emission intensity. Kröger's recent theory assumes that the luminescence center involves monovalent zinc, whose formation is permitted by the incorporation of a halide anion, or by a trivalent cation, aluminum.

Cubic zinc sulfide, air-fired with chloride, was found to have a specific susceptibility of -0.402×10^{-6}, compared to -0.373×10^{-6} for the material prepared without chloride. The specific susceptibility of ZnS:Al is apparently dependent on the concentration of aluminum, going from -0.357×10^{-6} for 0.01 percent Al, to -0.409×10^{-6} for 0.1 percent Al.

No temperature dependence of susceptibility was found to 77°K, indicating the absence of a temperature-dependent paramagnetic species which could be attributed to monovalent zinc. The detection limit of the equipment for such a paramagnetic species is about 0.01 percent. Not only is a paramagnetic species absent, but the absolute value of diamagnetism is *increased* by the flux incorporation. As with zinc sulfide, the incorporation of chloride in cadmium sulfide acts to increase the diamagnetism.

A large *increase* in the absolute value of the diamagnetism is obtained when either chloride or aluminum ions are used as "fluxes." This increase, above that related to crystallization in an active atmosphere, is evidently due to the incorporation of the flux ions, with consequent perturbation of the lattice. The extent of the perturbation is discussed in a later paragraph.

[14] A. Schleede and H. Gantzckow, Z. Physik **15**, 184 (1923).
[15] J. S. Van Wieringen, Physica **19**, 397 (1953).
[16] The value given by Zimens and Hedvall for their cubic form (-0.38×10^{-6}) corresponds to that obtained in the present investigation for air-crystallized cubic material (-0.37×10^{-6}), indicating that their material was probably air-fired. Similarly, the Zimens and Hedvall value for hexagonal zinc sulfide (phosphor) is the same as obtained in the present investigation for phosphors crystallized with chloride flux, as is usually the case with copper-activated phosphors.
[17] Reference 7, p. 78.
[18] S. Rothchild, Trans. Faraday Soc. **42**, 635 (1946).
[19] A. L. Smith, J. Electrochem. Soc. **96**, 75 (1949).
[20] F. A. Kröger and J. E. Hellingman, J. Electrochem. Soc. **93**, 156 (1948); **95**, 68 (1949).
[21] More recently, F. A. Kröger and H. J. Vink [J. Chem. Phys. **22**, 250 (1954)] have proposed that the luminescent center in "self-activated" ZnS phosphors is associated with a cation vacancy whose environment has lost an electron.

Thus, in cadmium sulfide, as in zinc sulfide, the incorporation of chloride has a large effect on the crystal diamagnetism, presumably due to the large perturbation introduced by the chloride. As CdS:Cl is practically nonluminescent in the visible region of the spectrum, it might be expected that (1) an infrared emission band may occur,[22] or (2) conductivity, and possibly other electronic properties would be affected.

Composition and Extent of the Luminescence Center

The existence of large activator centers in phosphors has been postulated by various investigators. Lenard[23] proposed that the luminescence center consisted of an impurity atom linked with a number of host atoms. This view was further developed by Ewles,[24,25] who first attempted to explain luminescence efficiency as a function of activator concentration.

The diamagnetic data obtained in the present investigation of magnetic properties of solids can be used to calculate the size of a luminescence center in zinc sulfide.

The diamagnetism of zinc sulfide is increased from -0.373×10^{-6} to -0.402×10^{-6} when chloride is incorporated into the solid during crystallization, and to -0.406×10^{-6} when 0.01 percent Ag is also incorporated. From the susceptibility change and the amount of chloride which is incorporated, the radius of the electron orbit can be calculated from the well-known formula

$$\chi=\frac{-Ne^2}{6mc^2}\sum\langle r^2\rangle_{Av},$$

where N is the number of atoms, e, m, and c have their usual meanings, and $\langle r^2\rangle_{Av}$ is the mean square radius of the electron orbit. In the present case, the radius of the orbit is calculated as being approximately 50 A.

Mott and Gurney[26] and Mott[27] have pictured a foreign atom in a crystal as being in a continuum having a high dielectric constant, and having an associated electron traveling in a large orbit over a considerable number of lattice atoms. Simpson[28] has calculated for electrons trapped in defects, that the associated wave function may spread over several lattice spacings.

It is seen therefore, that the function of the halide in zinc sulfide is to perturb the lattice. The diameter of the perturbation sphere, extending over 26 zinc atoms, is approximately 100 A, compared to 115 A, for the chloride-to-chloride distance for a given chloride proportion calculated for zinc sulfide assuming random distribution. Leverenz[29] has calculated the average silver-to-silver distance for the optimum proportion of silver in cubic zinc sulfide as being 83 A. This would indicate that the optimum proportion of silver is obtained when one, and only one, silver lies within the perturbation volume produced by a given chloride atom.

The luminescence center in optimally activated (Ag or Cu) and fluxed zinc sulfide phosphors can thus be associated with a metallic activator ion with its immediate environment, and situated in a perturbed volume. This perturbed volume encompasses about 2×10^4 zinc atoms.

CONCLUSIONS

The role of chloride (flux) in zinc sulfide phosphors is to perturb the sulfide lattice. The luminescence center in activated and fluxed zinc sulfide consists of a metallic activator ion and its environment, situated in a perturbed volume of the crystal.

No evidence was found for the existence of a paramagnetic species, such as monovalent zinc, in phosphors to which halide or aluminum charge-compensating-agents had been added.

The diamagnetic susceptibilities of zinc sulfide as a function of impurity, crystal modification, and synthesis procedure were determined. Only small differences were found to exist in the susceptibilities of the cubic and hexagonal forms of zinc sulfide.

The effects of crystallization and chloride incorporation in cadmium sulfide were found to be similar to zinc sulfide.

An anomalously high diamagnetic susceptibility was found in a ZnS:Cu phosphor which had previously undergone neutron bombardment.

[22] An infrared emission band has recently been reported for CdS:Cu by Garlick and Dumbleton, Proc. Phys. Soc. (London) **B67**, 442 (1954).

[23] P. Lenard, *Handbuch der Physik* (Verlag Julius Springer, Berlin, Germany, 1926), Vol. 23, p. 569.

[24] J. Ewles, Proc. Roy. Soc. (London) **A129**, 509 (1930).

[25] J. Ewles, J. Electrochem. Soc. **100**, 392 (1953).

[26] N. F. Mott and R. W. Gurney, *Electronic Processes in Ionic Crystals* (Oxford University Press, London, 1948), second edition, p. 84.

[27] N. F. Mott, Proc. Inst. Elec. Eng. (London) **96**, 254 (1949).

[28] J. H. Simpson, Proc. Roy. Soc. (London) **A197**, 269 (1949).

[29] Reference 7, p. 480.

Computed Transition Probabilities for X-Ray Continua of Potassium*

MARGARET N. LEWIS,† LOUIS C. GREEN, MARJORIE M. MULDER,‡ PAUL C. MILNER,§ *Strawbridge Observatory, Haverford College, Haverford, Pennsylvania*

AND

ELEANOR K. KOLCHIN, *Watson Scientific Computing Laboratory, Columbia University, New York, New York*

(Received January 20, 1955)

The rate of change of the oscillator strength at the K-edge of ionized potassium has been computed in a number of ways and a few computations have been made on the L-edge. The work has been carried through by using both hydrogenic and Hartree wave functions at the level of the single-electron approximation and Hartree and Hartree-Fock wave functions when the single-electron approximation was not used. Calcium wave functions both with with and without exchange have also been employed. The moment, momentum, and acceleration matrix elements have been computed. The momentum matrix element gives values most closely in agreement with experiment and is most stable with respect to changes in the wave functions. It is followed by the acceleration and the moment in that order. The single electron approximation gives good results. If the single-electron approximation is not used, it is essential that exchange effects be included by employing the determinant form of the wave functions, and the Hartree-Fock one-electron wave functions then give considerably better results than the ordinary Hartree functions. It also proves to be possible to substitute the wave functions of the unexcited ion of next higher atomic number, calcium, for the wave functions of potassium excited in an x-ray level without noticeable deterioration in the results.

THE application of the various atomic fields in the range of optical energies and spectra has been the subject of numerous papers, but the corresponding x-ray phenomena have received less attention. In particular the calculations of x-ray photoelectric absorptions in the nonrelativistic energy region have customarily been made by scaling and extrapolating hydrogen transition probabilities.[1] In the present paper the rates of change of the oscillator strengths in certain x-ray continua of K^+ are calculated by several procedures of differing degrees of sophistication.

K^+ presents a particularly attractive case for investigation. On the theoretical side the wave functions for the ground state of singly ionized potassium have been given by the Hartrees, both without and with exchange.[2,3] Wave functions without exchange for $K^{++}(1s^{-1}4s^{-1})$ and $K^{++}(2p^{-1}4s^{-1})$ have been given by Thatcher.[4] It is also an advantage that the wave functions, both without and with exchange, are known for $Ca^{++}(4s^{-2})$[5,6] since, as Thatcher[4] has shown, there is considerable similarity between the Ca^{++} wave functions and those of K^{++} excited in an x-ray state. This means that in some cases where the excited K functions are not available, one may employ known Ca functions as an approximation. Moreover the atomic number for potassium is sufficiently low so that relativistic effects will be small near the absorption edges, but still sufficiently high so that the hydrogenic approximation for the transition probabilities is expected to be reasonably good. The Sauter relativistic correction[7] would raise the hydrogenic value for transition probabilities at the K-edge 0.32 percent for argon and 0.36 percent for potassium. On the experimental side the absolute absorption coefficients have been measured in the region of the K-absorption limit of argon, the element of next lower atomic number.[8] Relative measurements have been made in the region of the K-edge of potassium in KCl[9] and in metallic potassium.[10]

1. EXPRESSIONS FOR THE RATE OF CHANGE OF THE OSCILLATOR STRENGTH

The rate of change of the oscillator strength may be computed using the expressions for the matrix element in terms of the dipole moment, momentum, and acceleration given by Chandrasekhar.[11]

$$(a|z_j|b)=\int \psi_a^* z_j \psi_b d\tau, \tag{1a}$$

$$(a|z_j|b)=\frac{2}{E_a-E_b}\int \frac{\partial \psi_a^*}{\partial z_j}\psi_b d\tau = -\frac{2}{E_a-E_b}\int \psi_a^* \frac{\partial \psi_b}{\partial z_j} d\tau, \tag{1b}$$

$$(a|z_j|b)=-\frac{4}{(E_a-E_b)^2}\int \psi_a^* \frac{\partial V}{\partial z_j}\psi_b d\tau. \tag{1c}$$

* This research was supported in part by a grant from the National Science Foundation, in part by the U. S. Air Force under a contract monitored by the Office of Scientific Research, Air Research and Development Command.

† Now at Brown University, Providence, Rhode Island.

‡ Now with Remington Rand, Inc., Philadelphia, Pennsylvania.

§ Now at Princeton University, Princeton, New Jersey.

[1] G. R. White, National Bureau of Standards Report, No. 1003, 1952 (unpublished).

[2] D. R. Hartree, Proc. Roy. Soc. (London) **A143**, 506 (1934).

[3] D. R. Hartree and W. Hartree, Proc. Roy. Soc. (London) **A166**, 450 (1938).

[4] W. A. Thatcher, Proc. Roy. Soc. (London) **A172**, 242 (1939).

[5] D. R. Hartree and W. Hartree, Proc. Roy. Soc. (London) **A149**, 210 (1935).

[6] D. R. Hartree and W. Hartree, Proc Roy. Soc. (London) **A164**, 167 (1937).

[7] H. A. Bethe and J. Ashkin, *Passage of Radiation Through Matter. Part II. Experimental Nuclear Physics*, edited by E. Segrè (John Wiley and Sons, Inc., New York, 1953), p. 312.

[8] R. G. Spencer, Phys. Rev. **38**, 1932 (1931); L. G. Parratt, Phys. Rev. **56**, 295 (1939).

[9] J. W. Trischka, Phys. Rev. **67**, 318 (1945).

[10] J. B. Platt, Phys. Rev. **69**, 337 (1946).

[11] S. Chandrasekhar, Astrophys. J. **102**, 223 (1945).

Here z_j is the z-coordinate of the jth electron, measured in units of the radius of the first Bohr orbit for $Z=1$, and E_a and E_b are the energies of the states a and b measured in units of the ionization energy for $Z=1$. If one employs exact ψ's, Eqs. (1) must all give the same value for the matrix element. On the other hand, since the principal contributions to the three matrix elements arise from different ranges of the nuclear distance, approximate ψ's will usually yield different values. Differences in the results of the three methods, therefore, give some measure of the uncertainty of the computed value of $df/d\epsilon$, but it must be remembered that exact agreement of the three results could be obtained from initial and final functions which are exact solutions of the same Schrödinger equation, whether or not that equation contains all the interactions which are physically significant for the problem. As Chandrasekhar has pointed out for two-electron systems,[11] when variationally determined wave functions are employed, the dipole momentum may be expected to give the best results since this expression weights the wave functions most heavily in the region in which they are best determined by the variational procedure. The choice between the dipole moment and momentum expressions has also been discussed by Seaton.[12] With these points in mind the values of $df/d\epsilon$, in what follows, were computed using all three expressions. The ψ's in Eqs. (1) may be constructed from one-electron wave functions of the form $u=(1/\rho)R(\rho)Y(\theta,\varphi)$. At the level of approximation at which one considers one electron moving in a fixed field, Eqs. (1) then lead to the following expressions for $df/d\epsilon$[13]:

$$\frac{df}{d\epsilon}=-\frac{1}{3}\frac{\nu}{R_y}\frac{\max(l,l')}{2l+1}\left\{\int_0^\infty R^N(nl)\rho R^N(\epsilon l')d\rho\right\}^2, \tag{2a}$$

$$\frac{df}{d\epsilon}=-\frac{4}{3}\frac{R_y}{\nu}\frac{\max(l,l')}{2l+1}\left\{\int_0^\infty\left[R^N(nl)\frac{dR^N(\epsilon l')}{d\rho}+\{^{l'}_{-l}\}\frac{R^N(nl)R^N(\epsilon l')}{\rho}\right]d\rho\right\}^2, \tag{2b}$$

$$\frac{df}{d\epsilon}=-\frac{4}{3}\frac{R_y}{\nu}\frac{\max(l,l')}{2l+1}\left\{\int_0^\infty\left[-R^N(\epsilon l')\frac{dR^N(nl)}{d\rho}+\{^{l'}_{-l}\}\frac{R^N(nl)R^N(\epsilon l')}{\rho}\right]d\rho\right\}^2, \tag{2b'}$$

$$\frac{df}{d\epsilon}=-\frac{4}{3}\left(\frac{R_y}{\nu}\right)^3\frac{\max(l,l')}{2l+1}\left\{\int_0^\infty R^N(nl)\frac{dV}{d\rho}R^N(\epsilon l')d\rho\right\}^2. \tag{2c}$$

Here ρ is measured in units of the first Bohr orbit for $Z=1$; ν is the wave-number difference of the final and initial states; R_y is the Rydberg constant expressed in wave numbers, l is the orbital angular momentum quantum number of the electron in the initial state, l' that of the final state; $\max(l,l')$ is the larger of l and l'; $\{^{l'}_{-l}\}$ is l', if l' is greater than l, and $-l$ if l' is less than l, $R^N(nl)/\rho$ is the normalized radial part of the wave function for the electron in the initial state, and $R^N(\epsilon l')/\rho$ that for the final state where ϵ is the energy expressed in rydbergs; and $V=2Z_p/\rho$, where Z_p is the effective nuclear charge for potential. $R^N(\epsilon l)$ is normalized per interval in ϵ by assuring that its amplitude approaches[14]

$$\frac{1}{\sqrt{\pi}}\left[\epsilon+\frac{2Z_p}{\rho}-\frac{l'(l'+1)}{\rho^2}\right]^{-\frac{1}{4}}$$

for large ρ.

If one represents the ψ's as a simple product of one-electron wave functions, each of the expressions in Eqs. (2) must be multiplied by I^2, where

$$I=\int\xi(nl)\xi(\epsilon l')d\tau', \tag{3}$$

and $\xi(nl)$ is the product of the wave functions for the "inactive" electrons in the initial state and $\xi(\epsilon l')$ that for the "inactive" electrons in the final state and $d\tau'$ indicates that the integration is to be carried out over all coordinates except those of the transition electron. For many computations in the optical region the contribution to I of the core electrons may be set equal to one without introducing too large an error. For an x-ray transition which removes an electron from deep in the core of the atom, such a procedure is questionable.

If one represents the ψ's as a determinant or a sum of determinants of one electron wave functions, one must further generalize the products of the I's and the integrals appearing in Eqs. (2) by using a sum of such products over all permutations of the electrons.

2. HYDROGENIC APPROXIMATION

In the hydrogenic approximation,[15] the matrix elements in Eqs. (2) for the various transitions are evaluated using wave functions for a single electron moving in the field of a charge $Z-s$. Here Z is the nuclear charge of the atom concerned and s is the usual sum of Slater shielding constants[16] for those electrons which in the actual atom occupy the same or inner shells. This sum of shielding constants must, in some average sense, take care of the increasing screening of the nuclear charge with its increasing nuclear distance. Since for the computation of the matrix elements one is interested in the behavior of the initial and final wave functions for the same range in electron-nuclear dis-

[12] M. J. Seaton, Proc. Roy. Soc. (London) **A208**, 408 (1951).
[13] L. C. Green and N. E. Weber, Astrophys. J. **111**, 587 (1950).
[14] E. C. Kemble, *Fundamental Principles of Quantum Mechanics* (McGraw-Hill Book Company, Inc., New York, 1937), p. 178.
[15] H. Bethe, *Handbuch der Physik* (Verlag Julius Springer, Berlin, Germany, 1933), second edition, Vol. 24, Part 1, p. 478; J. A. Wheeler and J. A. Bearden, Phys. Rev. **46**, 755 (1934).
[16] J. C. Slater, Phys. Rev. **36**, 57 (1930).

tances, the same s is used for both the discrete and the continuum wave functions. On the other hand, the energy parameter in the equation for the radial hydrogenic functions is chosen in a different manner for the bound and free states. For the former this parameter is taken to be the energy of an electron moving in the field of a charge, $Z-s$, and having the same total quantum number as the electron in the initial state of the atom concerned. For the latter the experimental value of the energy required to remove the electron from the atom is less than the ionization potential computed for the Coulomb field of a charge $Z-s$ by an amount V_0, due to the presence of the outer electrons. It has therefore been customary to take the energy parameter for the free state as the kinetic energy of the electron at infinity reduced by the outer screening constant, V_0. As a result for the low energies of the ejected electron the energy parameters yield wave functions which lie in the energy range of the discrete states. Under these circumstances the wave functions for the free states do not in general have integer quantum numbers or satisfy the proper boundary condition at infinity. However over the limited range of interest these functions may be made to approximate to continuum functions of the proper normalization if they are written in the same form as the ordinary normalized discrete hydrogenic functions multiplied by a spreading factor. The photoelectric transition probability curve may also be extrapolated into this energy region below the Coulomb threshold by using the discrete oscillator strength per unit energy. It should also be noted that for some purposes it may be more convenient to consider the outer screening constant as modifying the potential energy rather than as changing the eigenvalue.

For ionized potassium the rates of change with energy of the oscillator strength, $df/d\epsilon$, in the regions of the K- and L-absorption edges were found for several energies using $Z-s=18.7$ and 14.85 respectively. The experimental threshold energies were found from the wavelengths given by Cauchois and Hulubei[17] to be 265.18 rydbergs for the K-edge and 21.68 rydbergs for the weighted average of the L_{II}- and L_{III}-edges. The results are given in Tables I and V.

For the K-absorption edge one may obtain a comparison with experiment by using Spencer's[8] measurements for argon at two wavelengths 0.002 A on either side of the K-edge, 3.8657 A. From these data the atomic absorption coefficient for the K-shell extrapolated to the absorption limit is 0.875×10^{-19} cm^2. The hydrogenic approximation gives 0.850×10^{-19} cm^2. The experimental value is therefore about 3 percent higher than the hydrogenic calculation for argon, and the situation for the potassium ion may be assumed to be about the same. The value of $df/d\epsilon$ estimated for potassium on this assumption is given in the next to last column of Table I; and, by subtracting the Sauter relativistic correction, an estimated nonrelativistic value has been obtained and recorded in the final column.

[17] Y. Cauchois and H. Hulubei, *Longeurs d'onde des émissions X et des discontinuités d'absorption X* (Herman & Cie, Paris, France, 1947).

3. HARTREE APPROXIMATION

To compute the rate of change with energy of the oscillator strength, $df/d\epsilon$, in the neighborhood of the K-edge using Hartree self-consistent-field wave functions, one must have the wave functions for the various electrons in both the initial and final states of the atom. Fortunately for the potassium ion, Hartree has given the wave functions for the initial state, $K(4s^{-1})$.[2] Wave functions for the bound electrons in the final state, $K(1s^{-1}4s^{-1})$, have been given by Thatcher.[4] It remained to find the wave function for the free electron. Therefore p-continuum wave functions were found by numerical integration of the radial part of the Schrödinger equation for two values of the energy using the $2Z_p$ for $K(1s^{-1}4s^{-1})$ given by Thatcher.[4] In principle the calculation of $df/d\epsilon$ could be entirely theoretical if the ionization energy computed by Thatcher were used. However the experimental value for the threshold energy has been employed since several small inconsistencies in Thatcher's paper raise some doubt as to the correctness of his figure.

The results of the computations are presented in Table I. The quantity ϵ appearing in the second column of Table I is the energy of the free electron expressed in rydbergs. The values of $df/d\epsilon$ given in the third column are obtained by considering the wave functions for the initial and final states to be the Hartree functions of the transition electron alone, that is, Eqs. (2) are employed as they stand. This procedure is an approximation since the Hartree functions are derived on the assumption that the wave function for the atom is a product of the wave functions of the individual electrons. Furthermore, the field in which the transition electron moves when it is in a $1s$ state is different from that in which it moves in an ϵp state. Since Eq. (2c) involves the derivative of a supposedly fixed field, it seemed worth while to find the result using both the initial and final fields. Table I contains the result 0.00463 for the final field. The initial field gives a value 0.36 percent higher. It is also interesting to use Eqs. (2b) and (2b′) to test the accuracy of the various numerical methods used. These two expressions should give the same result regardless of what wave functions are employed. The values from the two equations differed by 0.19 percent. In the fourth column of Table I are given the values obtained from the simple product type wave functions. When the transition electron passes from a $1s$ to an ϵp state, the wave functions of the passive electrons change sufficiently so that the I of Eq. (3) is relatively far from one, in fact $I^2=0.7768$ for the case $\epsilon=0$. Column five shows the improvement in the agreement of the self-consistent field values with the estimated experimental value when the simple product type wave function is replaced by

TABLE I. Values of $df/d\epsilon$ per rydberg per 1s electron in the K-continuum computed with Hartree wave functions.

Matrix element	ϵ	Single-electron approximation ($I=1$)	Simple-product type wave functions	Determinant type wave functions	Hydrogenic approximation	Estimated experimental value	Estimated nonrelativistic experimental value
Moment	0	0.00482	0.00374	0.00446			
Momentum	0	0.00474	0.00368	0.00442	0.00463	0.00476	0.00474
Acceleration	0	0.00463	0.00360	0.00429			
Moment	10	0.00416	0.00323	0.00358			
Momentum	10	0.00408	0.00317	0.00351	0.00420		
Acceleration	10	0.00399	0.00310	0.00341			

the determinant form.[18] The value given by the hydrogenic approximation, the estimated experimental value, and the estimated nonrelativistic experimental value, all of which are discussed in Sec. 2, are given in the last three columns of Table I.

The values of $df/d\epsilon$ were obtained using the three expressions in terms of the dipole moment, momentum, and acceleration. As has been pointed out, the advantage of this procedure is that the principal contributions to the three matrix elements arise from different ranges of the nuclear distance. For the case of the K-absorption edge and the single-electron approximation using Hartree functions, this fact is demonstrated in Table II.

To determine which expression might be expected to give the best value of the oscillator strength in the present case, a plot was made of the integrands both of the three matrix elements and of the eigenvalue integral for the 1s electron. For the free electron of zero energy, the integrand of the eigenvalue integral is everywhere constant and zero, so that no region is preferred. It was clear that the range in nuclear distance which contributed most to the eigenvalue integral for the 1s electron overlapped, roughly equally and to a large extent, the regions which were most important for the momentum and acceleration matrix elements, but that the overlap for the moment matrix element was much smaller. To put this result on a quantitative basis, all four integrals were normalized to one and the area of overlap of each of the integrands of the three matrix elements with the integrand of the eigenvalue integral was determined. These areas were 0.43, 0.93, and 0.86 for the moment, momentum, and acceleration matrix elements respectively. On this basis, therefore, the momentum and acceleration expressions both should give appreciably better values than the moment, and the momentum should be somewhat more reliable than the acceleration.

Inspection of Table I shows a surprising similarity of the values given by the single electron approximation with the hydrogenic and the estimated nonrelativistic experimental values. There is agreement between the hydrogenic and the acceleration matrix element calculations. This might be expected since the acceleration method emphasizes the wave functions near the nucleus where the differences between the Hartree and the hydrogenic wave functions are small and of opposite sign for the 1s and ϵp electrons. However, the agreement of the estimated nonrelativistic experimental value is the best with the momentum method where the wave functions are used over the region where they are best determined.

From Table I it can also be seen that the percentage slopes at the K-edge as given by the different methods vary considerably. Using the momentum expression one finds 1.4, 2.1, and 0.9 percent for the single-electron approximation and the simple-product wave function, the determinant wave function, and the hydrogenic approximation respectively.

4. HARTREE APPROXIMATION USING WAVE FUNCTIONS OF THE ELEMENT OF NEXT HIGHER ATOMIC NUMBER

Thatcher[4] has pointed out that the wave functions for the electrons in the unexcited core of calcium, $Ca(4s^{-2})$, are very similar to the wave functions for potassium ionized in the 1s shell, $K(1s^{-1}4s^{-1})$. It seemed worth while to investigate the extent of such similarity by a quantitative comparison and by the substitution of Ca wave functions for the final states of potassium x-ray K- and L-transitions. If the similarity were sufficiently close, it would suggest that it might be feasible, in general, to use wave functions of the element of the next higher atomic number for the final states of x-ray transitions where more appropriate Hartree calculations were lacking.

A numerical comparison of the wave functions of the x-ray states of potassium, $K(1s^{-1}4s^{-1})$ and $K(2p^{-1}4s^{-1})$, with those of $K(4s^{-1})$ and $Ca(4s^{-2})$ has been made in terms of quantities, δ, which are the differences from

TABLE II. Percentage of the total contribution, without regard to sign, to the matrix element which arises from values of the nuclear distance $r \leq 0.1a_0$ and $\leq 0.3a_0$.[a]

Matrix element	$r \leq 0.1a_0$	$r \leq 0.3a_0$
Moment	15.4	94.0
Momentum	63.9	98.9
Acceleration	77.9	99.9

[a] a_0 is the radius of the first Bohr orbit for $Z=1$.

[18] The possible importance of using the determinant form of the wave function was suggested to us by J. A. Wheeler.

TABLE III. Comparison of K and Ca wave functions.

Electron	With or without exchange	$K(4s^{-1})$ $Ca(4s^{-2})$ δ_Z	$K(1s^{-1}4s^{-1})$ $K(4s^{-1})$ δ_K	$K(1s^{-1}4s^{-1})$ $Ca(4s^{-2})$ $\delta_{K'}$	$K(2p^{-1}4s^{-1})$ $K(4s^{-1})$ δ_L	$K(2p^{-1}4s^{-1})$ $Ca(4s^{-2})$ $\delta_{L'}$
$1s$	o	0.0010	0.0002	0.0004	0.0000	0.0009
	x	0.0010				
$2s$	o	0.0034	0.0016	0.0004	0.0003	0.0020
	x	0.0033	0.0015	0.0003		
$2p$	o	0.0024	0.0025	0.0000	0.0004	0.0008
	x	0.0022	0.0025	0.0000		
$3s$	o	0.0098	0.0064	0.0004	0.0041	0.0015
	x	0.0102	0.0068	0.0005		
$3p$	o	0.0150	0.0157	0.0000	0.0109	0.0006
	x	0.0133	0.0138	0.0001		

one of the integral of the products of the corresponding normalized functions for the two ions,

$$\delta=1-\int_0^\infty R_{nl}{}^N(Z_1)R_{nl}{}^N(Z_2)d\rho.$$

If the wave functions were identical, δ would be zero. The values of δ are presented in Table III both for the nonexchange functions, indicated by an o in the second column, and for the exchange wave functions, indicated by an x. The nonexchange functions are used in this section and the exchange functions will be employed in the next part. The values of δ_Z compare the wave functions of $K(4s^{-1})$ and $Ca(4s^{-2})$, as indicated at the head of the third column. These values measure the similarity of the wave functions of two adjacent elements in this part of the periodic table. There is an uncertainty in all the δ's in Table III roughly of two units in the last figure. The wave functions of potassium ionized in the K-shell, $K(1s^{-1}4s^{-1})$, are first compared to those of $K(4s^{-1})$, δ_K, and then to those of $Ca(4s^{-2})$, $\delta_{K'}$. One sees from the δ_K's that, except for the $1s$ electron, the $K(4s^{-1})$ wave functions are almost as different from the $K(1s^{-1}4s^{-1})$ wave functions as they are from those of the next element. On the other hand, the difference between the $Ca(4s^{-2})$ wave functions and those of $K(1s^{-1}4s^{-1})$ are strikingly small. In the last two columns δ_L and $\delta_{L'}$ give a similar comparison of the $K(2p^{-1}4s^{-1})$ wave functions with those of $K(4s^{-1})$ and $Ca(4s^{-2})$. An examination of Table III shows that in the case of the removal of a $1s$ or a $2p$ electron, the wave functions of the final state for electrons in the same or an inner shell agree more closely with those of the initial state of the potassium ion than with those of calcium. On the other hand, for the wave functions of electrons in the outer shells, the agreement is considerably closer with the calcium wave functions. The dotted line has been inserted in Table III to emphasize this behavior. The agreement improves with increasing orbital momentum, as well as with increasing total quantum number.

In Table IV are given the results of the computation of $df/d\epsilon$ for the K- and L-continua using for the final state the wave functions of $Ca(4s^{-2})$ for all electrons outside the original shell of the transition electron and the wave functions of $K(4s^{-1})$ for all other electrons. The wave functions for the bound electrons of $Ca(4s^{-2})$ were taken from Hartree[2] and those for the free electron in s, p, and d continua at various energies were available.[19]

The results for $df/d\epsilon$ at the K-edge calculated with the substituted calcium functions in Table IV are slightly higher than the corresponding values in Table I. These increases are from 0.0 to 2.6 percent, except for the moment method of obtaining $df/d\epsilon$ from the determinant type wave functions, where the increase is 36 percent. This is probably to be attributed to the bound electron wave functions used for the final state rather than to the continuum function, as will be discussed in the last section. Again we see that the best agreement with the estimated nonrelativistic experimental value is obtained from the single-electron approximation, that is, when I is set equal to one. The values of $df/d\epsilon$ found from the momentum expression for $\epsilon=0$ and $\epsilon=1$ yield values for the percentage slope at the K-edge of 2.5, 2.5, and 1.1 percent for the single electron approximation and the product wave function, the determinant wave function, and the hydrogenic approximation respectively. These values are somewhat higher than those obtained from the more widely separated energies in Table I.

At the L-edge there appears to be no comparable experimental data. The results in Table III indicate that for the L continuum, the ϵd function may give more reliable results than the ϵs function, however, this latter function contributes less than two percent of the total. At the edge the percentage slopes, using the momentum expression, are 17 percent for the single-electron approximation or the product wave function and 10 percent for the hydrogenic approximation.

5. APPROXIMATE HARTREE-FOCK CALCULATION

Finally one may compute $df/d\epsilon$, using for the individual electrons self-consistent-field wave functions

[19] L. C. Green and E. K. Kolchin (unpublished).

TABLE IV. Values of $df/d\epsilon$ in the K- and L-continua using $K(4s^{-1})$ and $Ca(4s^{-2})$ wave functions for the final state.[a]

Continuum	Matrix element	ϵ	Single electron approximation ($l=1$)	Simple product type wave function	Determinant type wave function	Hydrogenic approximation
K	Moment	0	0.00487	0.00374	0.00605	
	Momentum	0	0.00480	0.00369	0.00447	0.00463
	Acceleration	0	0.00475	0.00365	0.00433	
	Moment	1	0.00475	0.00365	0.00591	
	Momentum	1	0.00468	0.00360	0.00436	0.00458
	Acceleration	1	0.00464	0.00356	0.00420	
L	Moment	0	0.0996	0.0799	0.0663	
	Momentum	0	0.0910	0.0730	0.0734	0.1146
	Acceleration	0	0.0790	0.0633	0.0647	
	Moment	1	0.0826	0.0662		
	Momentum	1	0.0756	0.0606		0.1012
	Acceleration	1				

[a] $df/d\epsilon$ is given per Rydberg per $1s$ or per $2p$ electron.

determined with exchange. The functions for $K_x(4s^{-1})$,[20] the initial state of the transition, are given by Hartree and Hartree.[3] On the other hand, no exchange wave functions were available for potassium excited in an x-ray level, but the similarity of the functions of $Ca_o(4s^{-2})$ and $K_o(1s^{-1}4s^{-1})$ in the nonexchange case suggested that the $Ca_x(4s^{-2})$ functions given by Hartree and Hartree[6] might be employed instead. One should not use the $K_0(1s^{-1}4s^{-1})$ wave functions for those of $K_x(1s^{-1}4s^{-1})$ since the inclusion of exchange for both $Ca(4s^{-2})$ and $K(4s^{-1})$ leads to larger differences than those between $Ca_o(4s^{-2})$ and $K_o(1s^{-1}4s^{-1})$. The Hartrees do not give any continuum wave functions, but Bates and Massey have calculated the ϵp function for $Ca_x(4s^{-2})$ using the Hartrees' wave functions for the bound states.[21] Therefore for the K-absorption edge, $df/d\epsilon$ was found using the $K_x(4s^{-1})$ functions for the initial state. For the final state, the $Ca_x(4s^{-2})$ functions for the ϵp and the bound electrons were used, except for the $1s$ electron, for which, in accordance with the discussion in the previous section, the $K_x(4s^{-1})$ function was employed. The results are given in Table V below.

The Bates and Massey $\epsilon p\ ^2P$ wave function mentioned previously, was obtained for the case of a filled $1s$ shell of $Ca_x(4s^{-2})$. Under these circumstances there is an exchange attraction between the $1s$ electrons and the ϵp electron. In the case of $K_x(1s^{-1}4s^{-1})$, the $1s$ shell is not filled and there is now an exchange repulsion between the one remaining $1s$ electron and the ϵp electron for the ^1P continuum function. Accordingly, to obtain a better approximation to the $\epsilon p\ ^1P$ wave function, the Hartree-Fock differential equation for $\epsilon p\ ^1P$ for $K_x(1s^{-1}4s^{-1})$ was solved using known calcium functions to estimate the various integrals which were necessary. For the computation of these integrals, Ca_x wave functions were used for the $2s$, $2p$, $3s$, and $3p$ electrons; but, for the $1s$ and ϵp electrons, Ca_o wave functions were employed since it was thought that these wave functions might more nearly approximate the effects of the exchange repulsion between these two incomplete shells. Later it was found that this repulsion was smaller than anticipated so that the $1s$ and $\epsilon p Ca_x$ functions would have been preferable. However, as appears below, the difference in the $\epsilon p\ ^1P$ function would have been small. The form of the differential equation is given by Bates and Massey.[22] The ϵp function was orthogonalized to the $2p$ and $3p$ functions, and normalized at large values of ρ to the same envelope used in the case of the nonexchange function. No attempt was made to improve the self-consistency of the ϵp wave function by solving the differential equation a second time, using the first solution to compute a better approximation to the integrals. The labor involved seemed unjustified unless the bound state wave functions were also to be made self-consistent. Furthermore, the assumption that the wave functions employed in obtaining the first solution for the ϵp were good approximations to the potassium exchange wave functions was substantiated by a comparison of the present ϵp with that of Bates and Massey. For this comparison both ^3P and ^1P continuum wave functions were obtained by using the positive and negative signs for the $Y_1(1s,\epsilon p)$ exchange integral. The sign used for the $\epsilon p\ ^3P$ function of $K_x(1s^{-1}4s^{-1})$ is the same as that for the $\epsilon p\ ^2P$ of $Ca(4s^{-2})$. The three exchange wave functions were remarkably similar. The significant feature of the three exchange ϵp functions compared to both the nonexchange $K_o(1s^{-1}4s^{-1})$ and $Ca_o(4s^{-2})$ ϵp functions is the decidedly lower first maximum of the exchange functions. The ^1P and ^3P functions were as similar to the ^2P as one would expect on the basis of the similarity of the ϵp functions of $Ca_o(4s^{-2})$ and $K_o(1s^{-1}4s^{-1})$. The

[20] In Secs. 5 and 6, the subscripts x and o following the symbol for the element indicate wave functions calculated with and without exchange respectively.

[21] The authors wish to thank Dr. D. R. Bates for sending them his values for the ϵp wave function.

[22] D. R. Bates and H. S. W. Massey, Proc. Roy. Soc. (London) A177, 329 (1941). It should be noted that the orthogonalization constants in their equation should not be divided by r.

TABLE V. Values of $df/d\epsilon$ for the K-absorption edge calculated with approximate Hartree-Fock functions.[a]

Matrix element	Final state functions: Ca functions	Final state functions: K functions
Moment	0.00793	0.00594
Momentum	0.00468	0.00464
Acceleration	0.00466	0.00445

[a] $df/d\epsilon$ is given per rydberg per 1s electron.

similarity of the ^1P and ^3P functions arises from the fact that the exchange effects of the electrons in complete groups on the ϵp electron are attractive in their results and are larger than either the repulsive or attractive effect of the 1s electron on the ϵp in the ^1P or ^3P continua respectively.

The results of the computations of $df/d\epsilon$ for the K-absorption edge using approximate Hartree-Fock functions are given in Table V. In Table V, the second column gives the values of $df/d\epsilon$ computed using $K_x(4s^{-1})$ functions for the initial state and for the 1s electron of the final state. The remainder of the functions for the final state were those of $Ca_x(4s^{-1})$, including the ϵp function of Bates and Massey. For the third column the $K_x(1s^{-1})$ functions are again employed for the initial state and for the 1s electron of the final state, but the remaining functions of the final state are estimated $K_x(1s^{-1}4s^{-1})$ functions and the ϵp ^1P functions computed as previously described. The estimated $K_x(1s^{-1}4s^{-1})$ functions were found from the $K_o(1s^{-1}4s^{-1})$ functions by adding a quantity which was obtained by weighting the exchange shifts from $K_o(4s^{-1})$ to $K_x(4s^{-1})$ and from $Ca_o(4s^{-2})$ to $Ca_x(4s^{-2})$ roughly in the ratio of 1 to 4.

One would expect the results in the last column of Table V to agree closely with the experimental results, and this is in fact the case for the quantity computed using the momentum matrix element. The acceleration matrix element gives somewhat poorer results, and the moment quite bad ones. It is interesting to note that for the momentum and acceleration cases the matrix elements computed with the substituted calcium functions yield slightly superior results to those obtained with the potassium functions themselves. These results are similar to those given in Tables I and IV for the determinant-type wave functions constructed with one-electron wave functions not involving exchange. The principal difference between the nonexchange and the exchange case is that the exchange values are appreciably higher than the corresponding nonexchange ones.

6. DISCUSSION

As one examines the values presented in Tables I, IV, and V of $df/d\epsilon$ at the K-edge as computed by various procedures, it becomes apparent that in no case has the use of a simple-product-type wave function given results which are at all closely comparable to the estimated experimental value. Relatively good results are obtained with the momentum and the acceleration matrix elements and determinant type wave functions and, in the single electron approximation, with all three matrix elements and either Hartree or hydrogenic functions. Apparently, if one is to go beyond the single electron approximation, it is necessary to include exchange effects at least to the extent of using a determinant-type wave function. Furthermore, a comparison of the results obtained with determinant-type wave functions and with the momentum and acceleration matrix elements indicates that appreciably better values are gotten when the one-electron wave functions employed in the determinants are computed with exchange. Thus the results found with both the Ca_x and the K_x functions are superior to those obtained with Ca_o and K_o functions.

Of the various procedures which have been used above to obtain $df/d\epsilon$ at the K-edge, one would expect that the most reliable would be the one which employs wave functions with exchange for both the initial and final states and the momentum expression for the matrix element. This result is lower by 2.1 percent than the estimated nonrelativistic experimental value. If a determinant-type wave function is employed, but the one-electron wave functions which are used therein are computed without exchange, the result is lower by 6.8 percent for the momentum matrix element. The single-electron approximation using Hartree wave functions and the momentum expression agrees with the estimated nonrelativistic experimental value. If Ca functions are substituted, the corresponding figures are 1.3 and 5.7 percent low and 1.3 percent high respectively. Finally the hydrogenic approximation is 2.3 percent low. If, for the reason suggested above, the results obtained with product-type wave functions are omitted, these relatively small differences between the computed values and the estimated experimental value illustrate the low sensitivity to the choice of wave functions of the quantities computed with the momentum matrix element. The corresponding quantities calculated from the acceleration matrix element show a somewhat wider spread and for the moment matrix element the results are much worse. This situation is considered from a slightly different point of view below.

Further investigation of the substitution of $Ca(4s^{-2})$ functions in the calculations at the K-edge reveal an interesting behavior of the values of $df/d\epsilon$ obtained by the three types of matrix elements. One may take two other combinations of excited state functions besides those employed in Table V. The ϵp function $K_x(1s^{-1}4s^{-1})$ may be used with the substituted $Ca_x(4s^{-2})$ bound state functions, with the usual exception of the 1s electron, and the ϵp function of $Ca_x(4s^{-2})$ may be used with the

estimate $K_x(1s^{-1}4s^{-1})$ bound state functions. This interchanging of the functions of the excited states may also be done for the nonexchange functions used in the determinant form. These results are presented in Table VI.

Table VI has been arranged to emphasize the "pairing" of the results. We see that for the moment method the change from the ϵp function of $K(1s^{-1}4s^{-1})$ to the ϵp function of $Ca(4s^{-2})$ makes only a slight difference in either the exchange or the nonexchange results, but changes in the wave functions of the bound electrons lead to considerable variations. For the acceleration method, as may be seen by comparing similar values in adjacent columns, the results depend upon the ϵp function used and are little affected by the choice of the functions for the bound electrons. For the momentum method all four exchange values are close and show a marked improvement over the nonexchange determinant calculations.

It is interesting to ask why the hydrogenic approximation is so successful in comparison with other methods which treat the physical situation in more detail. The answer lies in part in the fact that the inner and outer screening constants, which were chosen to give the x-ray energies, are successful in producing a rough agreement in the average with the Hartree field over the range in ρ contributing significantly to the matrix elements. As has been previously pointed out, the $1s$ and ϵp hydrogenic wave functions which result from this field are not strikingly similar to the corresponding Hartree functions, but the differences are such as partially to compensate one another over the range of interest. A comparison of the two fields suggests that, as far as the wave functions are concerned, the choice of screening constants is not too critical.

The question as to why the hydrogenic approximation is so successful is also part of the larger question as to why those single-electron approximations which have been tried above are so successful. It is not difficult to show that such approximations are not necessarily good. For example, one may compute $df/d\epsilon$ at the K-edge by employing the $1s$ wave function of $K_o(4s^{-1})$ and an ϵp wave function derived by numerical integration from the $Ca_o(4s^{-2})$ field of the Kramers type given by Zwaan.[23] This choice of functions yields 0.00382 using the moment expression and 0.00406 using the momentum. To understand why these values are so much lower than those obtained from the hydrogenic functions and from both the potassium and the calcium Hartree functions, one may compare the four fields. It appears at once that over the range of interest the absolute value of the differences between Thatcher's field and Zwaan's field are roughly five times as large as those between Thatcher's field and the other two. Furthermore, in the case of Zwaan's field the differences are always in the same direction and such as to make the field stronger. As a result, the first maximum of the ϵp wave function for the Zwaan field is pulled in and lowered with respect to the maxima of the other ϵp functions. The momentum matrix element is correspondingly lowered and the moment matrix element is still further lowered by the increased cancellation of the first negative swing of the ϵp wave function.

TABLE VI. Values of $df/d\epsilon$ at the K-edge showing the effect of the use of different free and bound functions in the final state.

	Bound electrons / Free electrons	With exchange $K(1s^{-1}4s^{-1})$	With exchange $Ca(4s^{-2})$	Without exchange $K(1s^{-1}4s^{-1})$	Without exchange $Ca(4s^{-2})$
Moment	$K(1s^{-1}4s^{-1})$	0.00594	0.00799	0.00446	0.00611
	$Ca(4s^{-2})$	0.00590	0.00793	0.00442	0.00605
Momentum	$K(1s^{-1}4s^{-1})$	0.00464	0.00468	0.00442	0.00448
	$Ca(4s^{-2})$	0.00464	0.00468	0.00441	0.00447
Acceleration	$K(1s^{-1}4s^{-1})$	0.00445	0.00444	0.00429	0.00428
	$Ca(4s^{-2})$	0.00466	0.00466	0.00434	0.00433

In summary, the rates of change of the oscillator strength in certain x-ray continua of K^+ have been calculated using wave functions of different types and the dipole moment, momentum, and the acceleration expressions for the matrix elements. In general it appears that the momentum expression gives results which correspond most closely to the experimental value. The acceleration expression gives the next best values and the moment expression yields relatively poor results. It also appears that the results given by the momentum expression are less sensitive to the choice of the wave functions than are the results obtained with the other expressions. The single-electron approximation gives good results when either Hartree wave functions or those found from the hydrogenic approximation are employed. The remarkable effectiveness of the latter functions is attributed to the fact that the screening constants yield a field which is very similar to the average of the Hartree field in that range in ρ which contributes significantly to the matrix elements. If the single-electron approximation is not employed, it is essential that the exchange effects be included by employing the determinant form of the wave functions. When the determinant form is used, the one-electron functions computed with exchange give considerably better results than those computed without exchange. It has been emphasized that the wave functions of $K(1s^{-1}4s^{-1})$ and $K(2p^{-1}4s^{-1})$ are very similar to those of $K(4s^{-1})$ in the case of $1s$ and $1s$, $2s$, and $2p$ electrons respectively and very similar to the wave functions of $Ca(4s^{-2})$ for all other electrons. Finally, it has been shown that at least in the case of $K^+(1s^{-1}4s^{-1})$ and $Ca^{++}(4s^{-2})$ it is possible to substitute the one electron wave functions of the latter for those of the former with no noticeable deterioration in the results except when the dipole moment expression is

[23] A. Zwaan, "Intensitäten im Ca-Funkenspektrum," Dissertation, Utrecht, 1929 (unpublished).

employed. More generally these results imply that it may be possible to substitute the wave functions of the unexcited ion of the next higher atomic number for the wave functions of the ion of interest excited in an x-ray state when the latter are unknown. However, if such substituted wave functions are to be employed, it would be preferable to use the wave functions of the unexcited ion instead of those of the next atom for all electrons in the same shell as the excited electron and for all inner shells.

The authors wish to thank Miss Cynthia W. Wyeth for her help at several points with the calculations.

PHYSICAL REVIEW VOLUME 98, NUMBER 4 MAY 15, 1955

Experimental Cross Section for Photodetachment of Electrons from H^- and D^-†

LEWIS M. BRANSCOMB AND STEPHEN J. SMITH
National Bureau of Standards, Washington, D. C.

(Received January 3, 1955)

The photodetachment of electrons from atomic hydrogen negative ions has been studied, and the integrated cross section measured by using the radiation from a tungsten filament at 3300°K in a modulated crossed-beam experiment. The wavelength dependence of the cross section is measured from 4000 to about 9000 A by using sharp-cut glass filters. The ratio of the experimental integrated cross section to the value predicted theoretically by Chandrasekhar is 1.01, with a 2 percent reproducibility and 10 percent upper limit to the systematic errors.

I. INTRODUCTION

THE departures of the continuous solar spectrum, in the region between 0.6 and 1.6 microns, from the Planck curve characteristic of a black body were first ascribed by Wildt[1] to the continuous absorption of the H^- ions in the solar photosphere. The electron affinity of H^- is about 0.75 ev and the ion has only one bound state. Hence the absorption of visible and near-infrared radiation leads to photodetachment, described by the equation

$$H^- + h\nu \rightarrow H + e^-. \quad (1)$$

The calculation of the cross section, σ, for this process has been undertaken with great diligence,[2] the most detailed and modern calculations being those of Chandrasekhar.[3] This calculated cross section rises from a threshold at 1.65 microns to a maximum of 4.52×10^{-17} cm^2 at 8275 A. The theoretical values give a basis for consistent agreement between the predicted absorption coefficient of the solar photosphere and the observed solar spectrum.[4]

Until recently[5] negative-ion photodetachment had not been detected in laboratory studies, although Lochte-Holtgreven[6] has reported that the reverse process, radiative attachment, contributes to the continuous emission from a high-current arc discharge. Although one can calculate the cross section for photodetachment from that for radiative attachment by using the principle of detailed balancing,[2] the circumstances of Lochte-Holtgreven's arc measurement do not permit direct evaluation of the cross section. Fite[7] attempted in 1950 to detect photodetachment from H^-. His experiment, although not successful in demonstrating photodetachment, led to the development of the high-current negative ion source[8] used in this experiment, and helped determine the present experimental approach. Photodetachment was observed in this laboratory in 1953.[5] The present paper describes the quantitative results of a crossed-beam experiment yielding the integrated cross section and information about its wavelength dependence in the visible for photodetachment from H^- and D^-.

II. THEORY OF THE EXPERIMENTAL METHOD

When one crosses a beam of H^- ions with a beam of very intense radiant energy of suitable wavelength, photons are absorbed, ions destroyed, and electrons liberated. Since the available concentration of negative ions is very low and since the spectrum is continuous, the study of photodetachment is out of the reach of conventional absorption spectroscopy. When one modulates the light beam, photodetachment may be recognized as a small ripple in the dc ion beam. However,

† For various periods since its inception this research has been sustained by the Harvard University Society of Fellows and the Office of Naval Research, as well as by the National Bureau of Standards.

[1] R. Wildt, Astrophys. J. **89**, 295 (1939).
[2] H. S. W. Massey, *Negative Ions* (Cambridge University Press, London, 1950), second edition.
[3] S. Chandrasekhar, Astrophys. J. **102**, 395, 223 (1945); **100**, 176 (1944).
[4] D. Chalonge and V. Kourganoff, Ann. astrophys. **9**, 69 (1946); **13**, 347 (1950). J. A. Hynek, *Astrophysics; A Topical Symposium* (McGraw-Hill Book Company, Inc., New York, 1951).
[5] L. M. Branscomb and W. L. Fite, Phys. Rev. **93**, 651 (A) (1954).
[6] W. Lochte-Holtgreven, Naturwiss. **38**, 258 (1951).
[7] W. L. Fite, Ph.D. Dissertation, Harvard University, 1951 (unpublished).
[8] W. L. Fite, Phys. Rev. **89**, 411 (1953).

since the noise in a typical high-current ion beam is 1000 times shot noise at low frequencies,[8] we collect the very small alternating current of photodetached electrons produced in the region of intersection of the light and ion beams. In this case the photodetached electron current must be distinguished from the noise within the bandwidth of the amplifier arising from ions scattered in the residual gas, collisional detachment,[9] and noise from the amplifier itself.

The experiment is complicated by the fact that monochromatic light of sufficient intensity was not available, thus necessitating the measurement of integrated cross sections over a wide spectral range.

Consider an H^- ion moving in the x direction with a velocity v. At the point x it is illuminated with a normally incident radiant flux $\phi(x,\lambda)d\lambda$ ergs/cm²-sec of parallel light in the wavelength range λ to $\lambda+d\lambda$. The probability that the ion will lose an electron in the distance dx is

$$P_x dx=(dx/vhc)\int\sigma(\lambda)\phi(x,\lambda)\lambda d\lambda. \quad (2)$$

Let us define $\phi'(\lambda)$ as the normalized radiant flux so that

$$\phi(x,\lambda)=\phi'(\lambda)w(x)/s. \quad (3)$$

Here s is a small distance perpendicular to the ion beam, larger than the ion beam, but small enough so that the light intensity is reasonably constant over this distance, and $w(x)/s$ is the power density at the ion beam. Then the probability of detachment when the ion passes a distance L through the light beam is

$$P=(hcvs)^{-1}\int_\lambda\sigma(\lambda)\phi'(\lambda)\lambda\int_x w(x)dxd\lambda$$

$$=W(hcvs)^{-1}\int_\lambda\sigma(\lambda)\phi'(\lambda)\lambda d\lambda. \quad (4)$$

TABLE I. $P_{\text{theor}}E^{\frac{1}{2}}/\bar{W}$ for nine filters with new[a] tungsten lamps. E is ion energy in ev; $\bar{W}$ is the radiant power in the ion beam; and P_{theor} is the detachment probability [Eq. (5)] calculated from Chandrasekhar's cross section.[b]

Corning filter No.	Approximate cutoff (A)	$P_{\text{theor}}E^{\frac{1}{2}}/\bar{W}\ 10^5$
3389	4200	7.000
3385	4800	7.381
3486	5300	7.287
3482	5500	7.113
2424	5900	7.239
2412	6100	6.798
2030	6600	6.625
2550	~8500	4.671
2540	~9900	3.368

[a] After five to ten hours operation the evaporated tungsten (Fig. 1) causes a ~1 percent decrease from the given values.
[b] See reference 3.

[9] J. B. Hasted, Proc. Roy. Soc. (London) 212, 235 (1952).

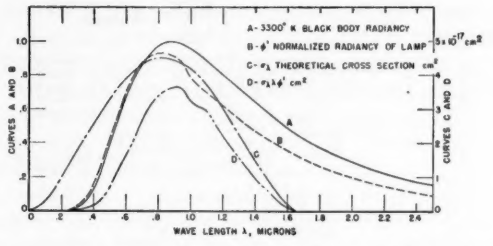
A- 3300° K BLACK BODY RADIANCY
B-φ' NORMALIZED RADIANCY OF LAMP
C-σλ THEORETICAL CROSS SECTION cm²
D-σλφ' cm²
5 x 10¹⁷ cm²
CURVES A AND B
CURVES C AND D
WAVE LENGTH λ, MICRONS

FIG. 1. Wavelength dependent quantities required for calculation of the photodetachment probability in H^- for radiation from the tungsten lamp with no filters. Curve A is normalized to unity at the maximum; curve B is normalized to unit radiant power. Curves B and D show a small dip due to evaporated tungsten and not present in new lamps.

Here $W=\int_0^L w(x)dx$ and is the total power incident on the area sL. This expression is independent of L providing only that $L\geq$ width of the light beam (i.e., $\phi=0$, $x>L$ and $x<0$). In practice s and L are the dimensions of the radiometer with which W is measured.

If a current i of ions and a current j of electrons are drawn from the illuminated region, $P_{\text{exp}}=j/i$. If we use sinusoidally chopped light of time average power $\bar{W}$ in the area sL,

$$P=\bar{j}/i=(\bar{W}/hcvs)\int\sigma(\lambda)\phi'(\lambda)\lambda d\lambda. \quad (5)$$

A measurement of $\bar{j}$ and i gives the experimental probability of detachment per ion (P_{exp}). We can also calculate this probability (P_{theor}) from the theoretical cross section σ, the known spectral distribution of the light ϕ', the measured power $\bar{W}$, ion velocity v, and the vertical dimension s of the rectangular instrument (area sL) used to measure $\bar{W}$. Thus, the experiment consists of a comparison of P_{exp} with P_{theor}. Equation (5) has been written so that the integral can be evaluated numerically and is independent of the parameters which may be varied in the experiment ($\bar{W}$,s,v), provided that a source of sufficient spectral stability is available. Figure 1 shows the form of the wavelength-dependent functions for H^-.

To gain additional information about the wavelength dependence of $\sigma(\lambda)$ we may insert sharp cutoff filters of normalized transmission $T(\lambda)$ in the light beam. For each filter, $\int\sigma\phi'T\lambda d\lambda$ is evaluated, so that the successive ratios $P_{\text{exp}}/P_{\text{theor}}$ for the filters reflect the accuracy of the theoretical cross section in the vicinity of the filter cutoff. Table I gives the values of this integral for nine filters.

III. EXPERIMENTAL METHOD

Figure 2 is a block diagram of the apparatus, a detailed description of which will be published elsewhere.

A. Ion Beam

The ion source is an adaptation of the dc glow discharge source described by Fite,[8] in which electrons and

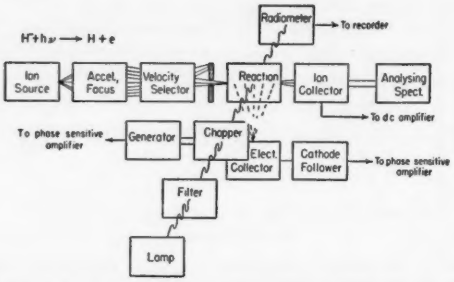

FIG. 2. Diagram of the crossed beam experiment. The generator produces a reference signal of adjustable phase for the phase detector. The electron current is extracted from the illuminated ion beam with weak inhomogeneous electric and magnetic fields in the reaction chamber.

negative ions are extracted from the striated positive column through a 0.015 in.×0.100 in. channel in a conical aluminum anode. A 3-mm aluminum aperture is allowed to float in the positive column immediately in front of the anode cone. The high electron mobility charges this aperture slightly negative with respect to the plasma and assists in increasing the axial concentration of negative ions. The cathode of the discharge is a 1 in.×2 in. Al or Ni cylinder. A dc voltage of 2 to 10 kv is applied across the discharge in series with a 240 000-ohm stabilizing resistance. Typical discharge current is 15 ma.

After emerging from the anode with about 100-ev energy, the negative ions are focussed by an electrostatic coaxial cylinder lens down the axis of the crossed field velocity selector. Helmholtz coils, external to the vacuum system, are available to supply slight corrections to the alignment of the ion beam. Those ions for which the velocity selector produces no transverse displacement pass through three 0.25-in. circular apertures and into the detachment chamber with an energy which may be chosen between 50 and 400 ev.

The apertures permit differential pumping to minimize gas scattering and collisional detachment. The main chamber, containing the velocity selector, is evacuated with a 200-l/sec mercury diffusion pump. The detachment chamber is evacuated with a 50-l/sec pump, whose fore pressure is provided by the main vacuum. The typical operating pressures are 10^{-5} mm in the main chamber and 10^{-6} mm in the detachment chamber.

The detachment chamber is shown schematically in Fig. 3. The ion beam is collected in the Faraday cup at the right. Secondary electron emission is suppressed by a weak transverse magnetic field and on some measurements by a 1.5-volt bias on the collector. A magnetic shutter in the back of the ion collector can permit the ion beam to pass into a 90° sector analyzer for high-resolution mass analysis of the beam. With this aperture closed the time-average ion current is measured with a dc amplifier. For measurements of ion energy an adjustable stopping potential is applied to this collector.

B. Light Beam

A 1-kilowatt projection lamp with a biplane coiled tungsten filament (GE 1 kw T-12 C13D) operating at a color temperature of 3420°K meets the stringent requirement of spectral stability and has a spectral distribution in convenient correspondence with the theoretical cross section (Fig. 1). The manner in which this distribution is determined is described in Part IV.

Radiation from the lamp is focussed by a 6-inch diameter front-aluminized spherical mirror through a 450-cps mechanical chopper and a quartz window, onto the negative ion beam. The image of the filament (which is approximately 1 cm² in area) is somewhat magnified and defocussed by the spherical mirror. Although wasteful of intensity, this defocussing helps meet the requirement that the intensity be homogeneous in the ~0.3-in. diameter of the beam. Of the 1-kw input power to the lamp, approximately 870 watts are radiated, of which about 30 watts are incident on the 0.400 in.×1.5 in. radiometer. A shield of highly polished aluminum foil with a 0.5 in.×1.5 in. aperture, not shown in Fig. 3, is installed inside the vacuum immediately in front of the ion beam. This prevents the radiation coming directly from the lamp filament at wide angles from scattering in the detachment chamber and falling on the back side of the radiometer.

The radiation is incident on the ion beam in a 35° cone and is not parallel, as assumed in the derivation of (5). If one takes proper account of this by replacing the ion velocity in (2) with $v\cos\theta$, where θ is the angle of incidence of a light ray on the ion beam, and writes in place of $\phi(x,\lambda)$ a reasonable angular-dependent function $\phi(x,\lambda,\theta)d\theta$, it can be shown that the error introduced by the assumption of parallelism is negligible. Sources of error due to light beam geometry were investigated by performing the experiment under a wide range of geometrical arrangements.

The radiometer is a copper "V" having a 45° apex angle. The inside surface is blacked with electrolytically deposited platinum. The back surface is covered with polished aluminum foil. Supporting this "V" and conducting the 30 watts of absorbed radiation to a water

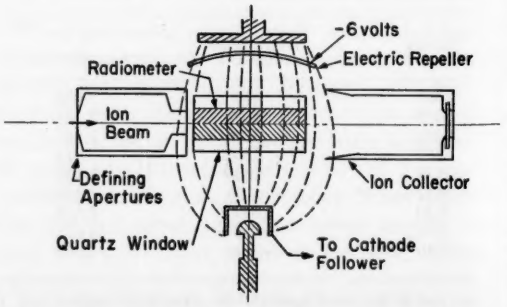

FIG. 3. Schematic of the detachment chamber. The dotted lines indicate the shape of the weak magnetic field used for trapping detached electrons. The electron collector is biased +15 volts.

cooled support, is a precisely machined 0.140-in. diameter bar of oxygen-free high-conductivity, copper. Two constantan wires imbedded in the bar 0.500 in. apart provide two thermocouple junctions, whose temperature difference multiplied by the known heat conductance of the OFHC copper bar provides an absolute measure of the heat energy conducted down the bar. The temperature rise in the radiometer results in radiation losses of about 9 percent. Although exact knowledge of the radiation loss and of the emissivity of the platinum-black would afford a direct measure of the total radiant power incident on the radiometer, the basic calibration is actually performed with standard lamps, as described in Part IV. These two methods of calibration give consistent results.

C. Detached Electron Current

In the region of intersection of the light and ion beams, weak inhomogeneous magnetic and electric fields extract the electrons by causing them to spiral down the magnetic flux lines as shown in Fig. 3. The magnetic field in the ion beam is about 50 gauss. A plate at the top of the detachment chamber is charged 7 volts negative to provide an electric field gradient in the beam. The electron collector, a cap above one pole of the magnet, is biased 15 volts positive. With this geometry, all free electrons generated in the illuminated portion of the ion beam are collected. (See Part V, Sec. D.) The collector is only 0.5-in. in diameter, thus presenting a small target to scattered ions. The predominant noise signal is due to electrons detached in gas collisions.

D. Electron Current Amplifier

With ion currents of 10^{-7} amp and 20 watts of radiation in the beam, modulated currents of photodetached electrons of the order of 10^{-12} amp are to be measured. The unmodulated collisionally-detached electron signal will be of the order of 10^{-11} amp at 10^{-6} mm pressure.[9] The modulated signal is measured by using a modified Baird Associates phase-sensitive detector with a minimum bandwidth of about 1/20 cps. The preamplifier is a 10^8-ohm input cathode follower using a VX-41A tetrode electrometer in triode connection. The chopping frequency of 450 cps is chosen as a compromise between the frequency limitation of the preamp input resistance (with a collector capacitance of about 3 $\mu\mu$f) and the reduction of ion beam noise with frequency.[8]

IV. CALIBRATIONS

A. Spectral Distribution

The projection lamps, after "breaking in," are tested[10] to determine the voltage at which the color temperature is 3420°K. The absolute temperature of the filament is then 3300°K. the reduction depending on the emissivity of tungsten in the visible.[11,12] The Planck curve for 3300°K is then multiplied by the measured transmission of the quartz lamp envelope and by the best available values of the emissivity of tungsten from 3000 A to 4 microns at 3300°K. These data are extrapolated in temperature from the definitive work of DeVos.[13] A partial check on the reliability of this procedure is had by calculating the power attenuation to be expected when each of the nine sharp cutoff filters is interposed in the light beam. This result is compared with the actual attenuation measured by the radiometer. The transmission of each filter is calibrated in the visible[10] and in the infrared.[14] The principal uncertainty in the filter transmissions is caused by the high temperature rise in the glass. The deep red filters usually shatter after a few minutes, in spite of air blast cooling. Systematic errors in $\phi'(\lambda)$ are thought to contribute no more than 2 percent to the error in our results.

B. Radiometer

Several of the projection lamps were calibrated for total radiant power[14] in microwatts/cm² at two meters in the direction perpendicular to the plane of the filament. Each lamp was then placed a known distance from the radiometer, with the mirror removed. The radiation incident on the radiometer was then calculated from the solid angle subtended. Corrections were made for the change in intensity with angle from the lamp, for the reflection from the quartz window, and for the attenuation of two very fine knitted tungsten mesh screens, which prevent the accumulation of static charges on the window. For distances of 2 in. to 12 in. from lamp to radiometer the inverse square law is obeyed, thus demonstrating the linearity of the radiometer and the absence of internal reflections in the detachment chamber. Further demonstration of radiometer linearity is obtained by calibrating a lamp for radiant power at 120 and 105 volts and checking the ratio of these powers with our radiometer.

The reliability of the standardization of the lamp is given as within 2 percent by the Radiometry Section. With 3 percent allowed for the calibration of the radiometer with this lamp, the value of $\overline{W}$ in (5) is thought to have systematic errors no greater than 5 percent.

C. Electron Current Amplifier

The electron current is measured with an amplifier whose gain depends on careful phase-matching and is sensitive to phase shifts. The distributed capacity of the preamplifier input makes it most convenient to calibrate the complete electron current amplifier system by using

[10] Measured by the NBS Photometry and Colorimetry Section.

[11] *Handbook of Chemistry and Physics* (Rubber Publishing Company, Cleveland, 1953), thirty-fifth edition, p. 2466.
[12] D. B. Judd, J. Research Natl. Bur. Standards 44, 1 (1950).
[13] J. C. DeVos, Physica 20, 690 (1954).
[14] Measured by the NBS Radiometry Section.

photoelectrons artificially produced in the detachment chamber. The chopped ultraviolet light from a low-pressure mercury discharge (ozone lamp) produces the photoelectrons. The output of the amplifier is compared with the average photocurrent, measured by floating the entire cathode follower on the 10^4-ohm input of a dc amplifier. This calibration procedure is carried out at about 10-minute intervals during the taking of data. Steady drifts in gain of about 1 percent in each interval are often encountered.

D. Wave Form

Because the amplifier has a very narrow bandwidth, the output detects only that part of the detached electron current or calibrating signal which is in the fundamental frequency. Therefore the wave form of the calibrating signal and of the radiation from the projection lamp must be recorded. This is done while driving the chopper at a very slow rate. Then the first Fourier coefficients of the two wave forms are determined by numerical integration to obtain the corrections for the average electron current, $\bar{j}$, and the light power, $\bar{W}$.

V. APPARATUS PERFORMANCE

A. Operation of the Source

Ion beams of up to 1 μa of H^-, OH^-, O^- and O_2^- have been collected, after mass separation in the velocity selector, with the source discharge operating in the neighborhood of 100 microns pressure and with two or three striations in the positive column. The yield of H^- ions in a dry hydrogen discharge is quite low,[8,15] but the role of the water vapor which must be added for good yields is not clear. In order to find the ratios of H_2 and H_2O concentrations for optimum H^- generation, beams from H_2 wet with D_2O were examined. The results, shown in Table II, are only qualitative, for the striations move with changes in concentration, requiring changes of total pressure and voltage to restore the ion beam. Table II shows that small amounts of D_2O increase the H^- yield, and that D^- ions result directly from water. The largest beams were obtained not in pure water vapor, but in wet hydrogen, as shown in Table II, and as found by Fite.[8] The most abundant ion from pure water discharges is OH^-. H^- and O_2^- yields are about three times smaller, and a trace of O^- is seen. At these relatively low pressures it seems likely that the OH^- is created directly by dissociative attachment,[16] although this seems to be inconsistent with the recent theoretical treatment by Laidler.[17]

TABLE II. Negative ion currents extracted at the anode of a low-pressure glow discharge using mixtures of D_2O and H_2.

Pressure (mm of Hg) at leak to discharge		Ion current (μa)				
D_2O	H_2	H^-	D^-	OD^-	O_2^-	D^-+H^-
20	0	0.001	0.031	0.13	0.01	0.032
20	30	0.008	0.029			0.037
20	85	0.0245	0.017	(not measured)		0.041
~10	85	0.020	0.0065			0.0265
~1	85	0.006	0.00040			0.0064
0	85	0.0051	0.00025	0.0012	0.0009	0.0052

[15] W. H. Bennett and P. F. Darby, Phys. Rev. **49**, 97 (1936).

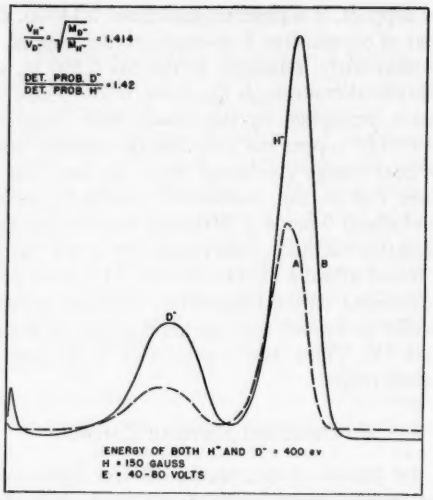

FIG. 4. Velocity selector scan obtained by varying the E-field from 40–80 volts while holding the magnetic field constant. The measured detachment probabilities for H^- and D^- are in the inverse ratio of the ion velocities, as expected since the two isotopes should have the same photodetachment cross sections.

The ions leave the anode of the wet H_2 discharge with about 90-ev energy and a 10–15 ev energy spread. The floating aperture lens described in Part II has very nearly the same potential as the region of the plasma from which the ions originate. Occasionally a second group of ions is observed with energies of about 150 ev, presumably from the second striation from the anode.

B. Velocity Selector

It is necessary to show that the velocity selector has sufficient resolving power to remove OH^- and other ions from the beam, and that the velocity is correctly measured and accounted for in Eq. (5). A mixed D^- and H^- beam of homogeneous energy was generated. With the projection lamp illuminating the beam and the detached electrons being recorded, the velocity selector was scanned across the D^- and H^- beams. Figure 4 shows the result. Within the accuracy of measurement the detachment probabilities are in the ratio of velocities, i.e., 1:1.414. The photodetachment cross sections for the two isotopes are, of course, identical within experimental accuracy.

Because the slower D^- ions give a larger photodetach-

[16] See reference 2, p. 76.
[17] K. J. Laidler, J. Chem. Phys. **22**, 1740 (1954).

ment yield and are less subject to large angle scattering than H^-, they were used for most of the final results quoted in this paper.

C. Phase Adjustment and Photoelectric Effect

The only spurious effect not excluded by modulation is the photoelectric effect. Since the photoelectric effect is independent of ion current, photodetachment is measured by turning on and off the ion beam at constant light intensity, while adjusting the phase for a maximum signal. The photoelectric effect could be eliminated by double modulation, but in our apparatus it usually occurred almost 90° out of phase with the detachment signal, and hence caused no difficulty.

D. Electron Collection Efficiency

The electric and magnetic fields in the detachment chamber were studied both experimentally and analytically to ensure that all slow free electrons in the beam are collected. Figure 5 shows the saturation of photodetached electron current as a function of both the electric and magnetic field. The collection efficiency for electrons is unaffected by applying a 1.5-volt positive potential to the ion collector.

E. Procedure in Obtaining Data

Once the geometry of the optical system is fixed, the wave forms of the chopped light from the projection lamp and the mercury lamp are measured. The ion beam is then turned on and the 90° sector spectrometer verifies the mass spectral purity of the beam. The ion energy is measured. After calibrating the amplifier gain and determining the proper phase adjustments for the synchronous reference signal, a filter is put in place, the projection lamp is turned on, and a set of about 6 photodetachment peaks is recorded. The amplifier gain is again calibrated, the sharp cutoff filter changed and the procedure repeated. At the close of the run the mass spectrum is rechecked and the energy redetermined.

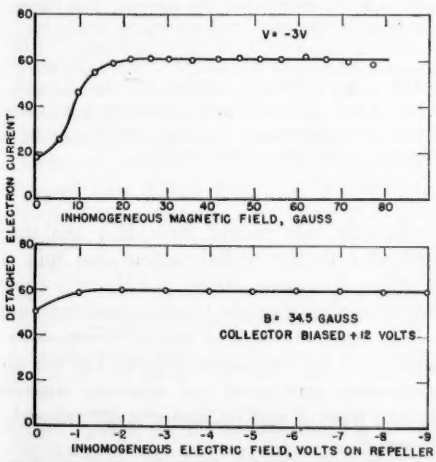

FIG. 5. The current to the electron collector saturates as the magnetic and electric fields in the reaction chamber are separately increased from zero demonstrating that all photodetached electrons are collected.

TABLE III. P_{exp}/P_{theor} averaged over a number of measurements for each of the nine filters, relative to the result obtained for filter 3486.

Corning filter No.	Approximate cutoff (A)	Relative P_{exp}/P_{theor}
3389	4200	0.96
3385	4800	1.02
3486	5300	...
3482	5500	0.97
2424	5900	0.98
2412	6100	1.02
2030	6600	1.00
2550	~8500	0.99
2540	~9900	0.97

VI. RESULTS

Photodetachment from H^- and D^- has been studied with sufficient variation in the parameters to show that Eq. (5) describes correctly the functioning of the apparatus. Data have been taken with variations of a factor of 4 in light power, a factor of 10 in ion current, and a factor of 2 in ion energy. The wave-form corrections have been deliberately exaggerated by masking parts of the optical system until the correction has increased from 3 percent to 15 percent. A wide variety of lamp and mirror geometries were used in an effort to cause lack of homogeneity in the light image to show up as a lack of reproducibility in the data rather than as a systematic error. The intensity distribution $\phi'(\lambda)$ was artificially altered in the visible region of the spectrum by the insertion of the nine sharp cutoff filters.

Under these conditions the reproducibility of the result, P_{exp}/P_{theor}, has a mean deviation of about 2 percent. There are many factors contributing to this scatter: (a) noise in the output signal; (b) gain instability; (c) phase adjustment; (d) spatial variations in ion and light beams; (e) different time constants associated with measurements of $\bar{j}$, i, and $\bar{W}$; (f) spectral distribution (for example, the temperature dependence of the filter transmissions); and (g) ion energy spread and instability.

The systematic errors are difficult to evaluate within definite upper limits. The following systematic errors are considered plausible (some of them having been discussed in Part III): (a) light power $\bar{W}\pm5$ percent; (b) $\int\sigma\phi'\lambda d\lambda\pm2$ percent; (c) ion velocity $v\pm1$ percent; (d) electron current, $\bar{j}$, including wave form, ±1.5 percent; (e) ion current $i\pm1$ percent; (f) radiometer height s, ±0.010 in. out of 0.400 in.$=\pm2.5$ percent. The uncertainty in s results from edge reflection effects. Should all these errors be present and influence the

result in the same direction, an error of 13 percent would be present. As this is rather unlikely, we feel that our determination is reliable to within about 10 percent.

A number of absolute measurements were made under widely differing circumstances regarding the magnitudes of the relevant parameters. These data were taken with filters 3486 and 2412. The average of these values states that

$$P_{\text{exp}}/P_{\text{theor}}=1.01\ (\pm 0.02)\ (\pm 0.10).$$

Here the two figures in parenthesis are taken to describe the reproducibility of the result and to give an estimate of its reliability, respectively.

When the nine filters, with cutoff wavelengths ranging from 4250 to about 9000 A, were placed successively in the beam, the relative ratios of $P_{\text{exp}}/P_{\text{theor}}$ varied as shown in Table III. Filter 3389 has an absorption near the intensity peak, which causes the transmitted energy to be more sensitive to temperature than in the other filters. There is nothing in these data to suggest that the theoretical cross section is in error between 4000 and 9000 A.

VII. CONCLUSIONS

The theoretical value of the cross section for photodetachment of electrons from H^- has been confirmed experimentally, although this cross section could be modified by perhaps 10 percent without being adjudged in conflict with experiment. The method can be applied to other negative ions for the determination of electron affinities and photodetachment cross sections for those ions whose affinities lie in the range from 0.6 to 2.5 ev.

VIII. ACKNOWLEDGMENTS

The suggestions and interest of Professor O. Oldenberg, Professor E. M. Purcell, and Dr. W. L. Fite are gratefully acknowledged. The authors are also indebted to many members of the National Bureau of Standards staff who helped in the construction and calibration of the apparatus, particularly Adolph Huriaux, William McKean, and Victor Grob.

PHYSICAL REVIEW VOLUME 98, NUMBER 4 MAY 15, 1955

Zeeman Effect in the Rotational Spectrum of NO*

MASATAKA MIZUSHIMA, J. T. COX, AND WALTER GORDY
Department of Physics, Duke University, Durham, North Carolina

(Received November 8, 1954; revised manuscript received January 28, 1955)

The Zeeman splitting of the 2-mm wave, $J=1/2\rightarrow 3/2$ rotational transit on of $N^{14}O^{16}$ in the $^2\Pi_{1/2}$ electronic state has been measured with fields of the order of 100 gauss. The observations were made with a wave-guide cell coiled between the poles of a Varian magnet. Magnetic field measurements were made with the electronic resonance of DPPH at frequencies of the order of 300 Mc/sec. A general theory of the Zeeman effect with hfs has been developed and applied specifically to $N^{14}O^{16}$. The g factors for the four states under investigation were found theoretically to be expressed as: $J=1/2$, $g_c=0.0007-\alpha$, $g_d=0.0007+\alpha$; $J=3/2$, $g_c=\vartheta-\frac{2}{3}\alpha$, $g_d=\vartheta+\frac{2}{3}\alpha$, where c and d are the lower and upper components of the Λ-type doublet, respectively. This relation was found to hold experimentally well with the values, $\vartheta=-0.0230$ and $\alpha=+0.0025$. Theoretically, ϑ comes from the mixing of $^2\Pi_{1/2}$ and $^2\Pi_{3/2}$ states and α comes from that of $^2\Pi_{1/2}$ and $^2\Sigma$ states. It was found by the theory, in which the centrifugal force and the spin orbit coupling were taken into account, that the electronic wave function of the two rotational states should be: $J=1/2$, $(^2\Pi_{1/2}|-0.0021\,(^2\Sigma|$; $J=3/2$, $(^2\Pi_{1/2}|-0.0247\,(^2\Pi_{3/2}|-0.0021\,(^2\Sigma|$. These wave functions give ϑ(theor.) $=-0.0229$ and and α(theor.) $=+0.0020$, which agree very well with the observed values. The observed g factor in $J=3/2$ state, $\vartheta=0.0230$ Bohr magnetons, shows that in the supposedly "nonmagnetic" $^2\Pi_{1/2}$ state the NO molecule has a sizeable magnetic moment.

INTRODUCTION

NITRIC oxide is special among all stable molecules, since it has an odd number of electrons whereas all the others have an even number of electrons. This odd electron has an orbital rotational angular momentum $\hbar$ around the molecular axis in the ground state. The spin angular momentum of this electron is also strongly coupled to the molecular axis, resulting in $\Pi_{1/2}$ and $\Pi_{3/2}$ states, where $\Omega=1/2$ and $3/2$, respectively.[1] In the ground state $\Pi_{1/2}$ the magnetic moments due to the orbital motion and spin cancel, while in the $\Pi_{3/2}$ state, which is 121 cm^{-1} above the ground state, they give the resulting magnetic moment of 2 Bohr magnetons. The susceptibility data were explained well by these assumptions. The hfs data in the microwave spectra of this molecule observed by Gordy and Burrus[2] and Gallagher *et al.*[3] showed, how-

* This research was supported by the U. S. Air Force through the Office of Scientific Research of the Air Research and Development Command.

[1] For a review see, J. H. Van Vleck, *The Theory of Electric and Magnetic Susceptibility* (Oxford University Press, London, 1932), p. 269.
[2] C. A. Burrus and W. Gordy, Phys. Rev. **93**, 419 (1954).
[3] Gallagher, Bedard, and Johnson, Phys. Rev. **93**, 729 (1954).

ever, that because of the end-over-end rotation the $\Pi_{1/2}$ and $\Pi_{3/2}$ electronic wave functions mix to a significant extent,[4] so that the ground state may have some amount of magnetic moment. The present study shows that the Zeeman effect of this molecule in the ground state is much larger than that expected by the assumption of pure $^2\Pi_{1/2}$ state. Although to our knowledge no previous investigation of the Zeeman effect of the $^2\Pi_{1/2}$ state has been made, the magnetic $^2\Pi_{3/2}$ state has been investigated through paramagnetic resonance absorption by Beringer and Castle[5] and its magnetic properties have been explained theoretically by Margenau and Henry.[6]

EXPERIMENTAL METHOD

The first rotational transition of NO (the $J=1/2\rightarrow 3/2$) falls at the rather short wavelength of 2 mm. Because of the small dipole moment of the molecule, $\sim$0.07 Debye, and because of the splitting of the transition into several components by internal interaction, the individual lines are extremely weak at normal temperatures. Detection of the individual Zeeman components requires a sensitive 2-mm wave spectrometer having an absorption cell which can be placed in a cooling bath as well as in the magnetic field. Fortunately, NO has a sufficient vapor pressure at 90°K so that the measurements could be made with the cell immersed in liquid air. A considerable increase of the line strength as well as some decrease in cell wall attenuation was thereby achieved.

The absorption cells were made of two-meter length coin silver *I*-band guide (inside cross section 0.180 in. by 0.086 in.), coiled so that it could be placed between the pole pieces (12-in. diameter) of a Varian magnet. The cooling jacket was made of polyfoam lined with copper. Although oversized wave guide was employed, it was found possible to avoid undesirable modes by careful and smooth coiling of the cell. The cell was coiled in the *E* plane so that only the $\Delta M=\pm 1$ components were observed.

The millimeter wave generator and detector employed were those described by King and Gordy.[7] Video-type detection was used with a *p* amplifier and cathode ray display of the lines. The magnetic fields employed were of the order of a hundred gauss. Magnetic field measurements were made with an electronic resonance probe employing the organic radical diphenyl-picryl hydrazyl, which has a very sharp resonance with an accurately known *g* factor[8] of 2.0036 $\pm$0.0002. Frequency measurements for the probe oscillator were made with a Gertsch Meter, Model FM3. Frequency measurements of the Zeeman components were made with the usual secondary frequency standard monitored by station WWV. The Varian magnet was operated from storage batteries.

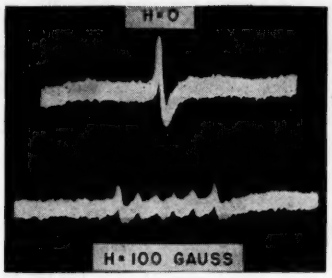

FIG. 1. Zeeman splitting of the $J=1/2\rightarrow 3/2$, $F=3/2\rightarrow 5/2$ transition of $N^{14}O^{16}$ at 1.99-mm wavelength.

EXPERIMENTAL RESULTS

Figure 1 shows a cathode-ray display of one of the hyperfine lines, the $F=3/2\rightarrow 5/2$ transition of the upper frequency component of the Λ doublet, with no externally applied field and with a magnetic field of 100 gauss applied perpendicular to the *E* lines of the microwave radiation. There are actually eight components theoretically predicted for this transition but two pairs are too close to be resolved, so that only six components are apparent. In this type of transition $F\rightarrow F+1$, the intensities of the outer components are the greatest. The component intensities vary according to the formulas:

$$\left.\begin{aligned}\text{Int}(M\rightarrow M+1)&=A(F+M+1)(F+M+2)\\ \text{Int}(M\rightarrow M-1)&=A(F-M+1)(F-M+2)\end{aligned}\right\}F\rightarrow F+1.$$

For an $F\rightarrow F$ line, the outer components are weakest and the relative intensities have the *M* dependence given by the formulas:

$$\left.\begin{aligned}\text{Int}(M\rightarrow M+1)&=B(F-M)(F+M+1)\\ \text{Int}(M\rightarrow M-1)&=B(F+M)(F-M+1)\end{aligned}\right\}F\rightarrow F,$$

where *A* and *B* are constant for a given *J*.

Table I lists the observed frequencies and calculated relative intensities of the Zeeman components of the different $J=1/2\rightarrow 3/2$ lines for the $^2\Pi_{1/2}$ state with an applied field of 97 gauss. These are analyzed below.

ZEEMAN EFFECT OF ROTATING MOLECULES WITH HFS

The theoretical formula for the case of a weak field Zeeman effect with hfs has been discussed by some authors.[9,10] Although our present experiment is done

[4] M. Mizushima, Phys. Rev. **94**, 569 (1954). There were some mistakes in this paper. The errata will be published in this journal.

[5] R. Beringer and J. G. Castle, Phys. Rev. **78**, 581 (1950). Beringer, Rawson, and Henry, Phys. Rev. **94**, 343 (1954).

[6] H. Margenau and A. Henry, Phys. Rev. **78**, 587 (1950).

[7] W. C. King and W. Gordy, Phys. Rev. **90**, 319 (1953); **93**, 407 (1954).

[8] Holden, Kittel, Merritt, and Yager, Phys. Rev. **75**, 1614 (1949); **77**, 147 (1950).

[9] C. K. Jen, Phys. Rev. **74**, 1396 (1948).

[10] Gordy, Smith, and Trambarulo, *Microwave Spectroscopy* (John Wiley and Sons, Inc., New York, 1953).

TABLE I. Zeeman spectrum of NO, $^2\Pi_{1/2}$ state, $J=1/2 \rightarrow 3/2$ transition.

$F \rightarrow F'$	$M_F \rightarrow M_{F'}$	Obs ν in Mc/sec with $H=97.45$ gauss	Calc. rel. int.
	Lower component of Δ doublet		
$3/2 \rightarrow 5/2$	$3/2 \rightarrow 5/2$	150 171.67	25
	$1/2 \rightarrow 3/2$	150 173.52	15
	$3/2 \rightarrow 1/2$		2.5
	$-1/2 \rightarrow 1/2$	150 175.40	7.5
	$1/2 \rightarrow -1/2$	150 177.32	7.5
	$-3/2 \rightarrow -1/2$		2.5
	$-1/2 \rightarrow -3/2$	150 179.40	15
	$-3/2 \rightarrow -5/2$	150 181.29	25
$1/2 \rightarrow 3/2$	$1/2 \rightarrow 3/2$	150 195.15	14
	$-1/2 \rightarrow 1/2$	150 197.49	4.6
	$1/2 \rightarrow -1/2$	150 199.81	4.6
	$-1/2 \rightarrow -3/2$	150 202.48	14
$3/2 \rightarrow 3/2$	$1/2 \rightarrow 3/2$	150 215.29	4.4
	$-1/2 \rightarrow 1/2$	150 217.45	4.4
	$3/2 \rightarrow 1/2$		5.9
	$-3/2 \rightarrow -1/2$	150 219.82	5.9
	$1/2 \rightarrow -1/2$		4.4
	$-1/2 \rightarrow -3/2$	150 228.57	4.4
$1/2 \rightarrow 1/2$	$-1/2 \rightarrow 1/2$	150 223.28	15
	$1/2 \rightarrow -1/2$	150 228.57	15
	Upper component of Δ doublet		
$3/2 \rightarrow 3/2$	$1/2 \rightarrow 3/2$	150 435.83	4.4
	$-1/2 \rightarrow 1/2$	150 438.06	4.4
	$3/2 \rightarrow 1/2$		5.9
	$-3/2 \rightarrow -1/2$	150 440.39	5.9
	$1/2 \rightarrow -1/2$		4.4
	$-1/2 \rightarrow -3/2$	150 442.52	4.4
$3/2 \rightarrow 5/2$	$3/2 \rightarrow 5/2$	150 541.82	25
	$1/2 \rightarrow 3/2$	150 543.81	15
	$3/2 \rightarrow 1/2$		2.5
	$-1/2 \rightarrow 1/2$	150 545.75	7.5
	$1/2 \rightarrow -1/2$	150 547.49	7.5
	$-3/2 \rightarrow -1/2$		2.5
	$-1/2 \rightarrow -3/2$	150 549.35	15
	$-3/2 \rightarrow -5/2$	150 551.27	25
$1/2 \rightarrow 1/2$	$-1/2 \rightarrow 1/2$	150 577.99	15
	$1/2 \rightarrow -1/2$	150 583.13	15
$1/2 \rightarrow 3/2$	$1/2 \rightarrow 3/2$	150 641.19	14
	$-1/2 \rightarrow 1/2$		4.6
	$1/2 \rightarrow -1/2$		4.6
	$-1/2 \rightarrow -3/2$	150 647.68	14

under a rather weak field, it was found that the weak field approximation was not exact enough and the effect of nondiagonal matrix elements was not entirely negligible.

The Hamiltonian of our problem is

$$H=\mathfrak{H}\cdot(-\beta\mathbf{L}-2.002\beta\mathbf{S}+g_n\beta_n\mathbf{N})\equiv\mathfrak{H}\cdot\mathbf{M}\beta\hbar, \quad (1)$$

where $\mathfrak{H}$ is the external magnetic field, β is the Bohr magneton, β_n is the nuclear magneton, **L**, **S**, and **N** are the angular momenta of electronic orbital motion, spin, and the end-over-end rotation, respectively, g_n is the g factor of the nuclear rotation, which is about 1/2, and **M** is a quantity defined by the above formula. The contribution from the nuclear spin magnetic moment[11] was neglected. The matrix element of M (component of **M** along $\mathfrak{H}$) can be obtained by the usual procedure; the result is shown below:

$$(JIFM_F|M|JIFM_F)=gM_F\{J(J+1)+F(F+1)-I(I+1)\}/\{2F(F+1)\}, \quad (2)$$

$$(JIFM_F|M|JI\,F-1\,M_F)=g(F^2-M_F^2)^{\frac{1}{2}}\times\{(I+F+J+1)(I+J-F+1)(I+F-J)(J+F-I)\}^{\frac{1}{2}}/\{4F^2(2F+1)(2F-1)\}^{\frac{1}{2}}, \quad (3)$$

where

$$g=(JJ|M|JJ)/J. \quad (4)$$

It can be shown that in the case of very strong field where hfs is negligible, the eigenvalue of the above matrix gives the strong field solution gM_J. The hfs of the NO molecule has been discussed by one of the present authors.[4] Combining that result with the above formula, we can obtain the solution for any value of field strength. The result for the $J=1/2$ state is shown in Fig. 2 as an example.

CALCULATION OF g FACTOR

The wave function of a rotating NO molecule is, according to the former consideration by one of the present authors,[4]

$$c \text{ state: } \psi_c=(1/\sqrt{2})\{\mu(\Pi_{1/2}J_+M_J|+\mu(\Pi_{1/2}J_-M_J|+\nu(\Pi_{3/2}J_+M_J|+\nu(\Pi_{3/2}J_-M_J|\}, \quad (5)$$

$$d \text{ state: } \psi_d=\sqrt{2}\{\mu(\Pi_{1/2}J_+M_J|-\mu(\Pi_{1/2}J_-M_J|+\nu(\Pi_{3/2}J_+M_J|-\nu(\Pi_{3/2}J_-M_J|\}, \quad (6)$$

where J_+ and J_- mean the same states except that the component of J along the molecular axis has an opposite sign. The quantities μ, ν, are constants which depend on J; $\mu=1$, $\nu=0$ for the $J=1/2$ states, $\mu=0.9998$, $\nu=-0.0247$ for $J=3/2$ states. The symbols c and d designate components of the Ω-type doublet, c being

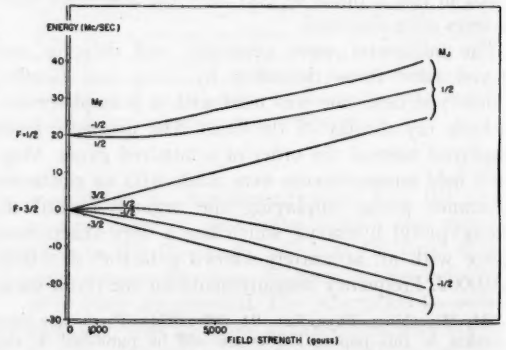

FIG. 2. Energy-field strength diagram for the NO molecule in $^2\Pi_{\frac{1}{2}}$, $J=1/2$, c state.

[11] The fact that the term $0.001\mu^2/(J^2+J)$, which comes from the anomalous magnetic moment of the electronic spin, is small but not entirely negligible was suggested by G. C. Dousmanis (private communication).

the lower component, and $(J_+|L_x+S_x|J_-)$ is defined as positive.

The g factor defined in Eq. (4) is

$$c \text{ state:} \quad g_c=(A+B)/J, \tag{7}$$

$$d \text{ state:} \quad g_d=(A-B)/J, \tag{8}$$

where

$$A=\mu^2\{(\Pi_{1/2}J_+J|M|\Pi_{1/2}J_+J)+(\Pi_{1/2}J_-J|M|\Pi_{1/2}J_-J)\}$$
$$+2\mu\nu\{(\Pi_{1/2}J_+J|M|\Pi_{3/2}J_+J)$$
$$+(\Pi_{1/2}J_-J|M|\Pi_{3/2}J_-J)\}$$
$$+\nu^2\{(\Pi_{3/2}J_+J|M|\Pi_{3/2}J_+J)$$
$$+(\Pi_{3/2}J_-J|M|\Pi_{3/2}J_-J)\}, \tag{9}$$

$$B=\mu^2\{(\Pi_{1/2}J_+J|M|\Pi_{1/2}J_-J)+(\Pi_{1/2}J_-J|M|\Pi_{1/2}J_+J)\}$$
$$+2\mu\nu\{(\Pi_{1/2}J_+J|M|\Pi_{3/2}J_-J)$$
$$+(\Pi_{1/2}J_-J|M|\Pi_{3/2}J_+J)\}$$
$$+\nu^2\{(\Pi_{3/2}J_+J|M|\Pi_{3/2}J_-J)$$
$$+(\Pi_{3/2}J_-J|M|\Pi_{3/2}J_+J)\}. \tag{10}$$

Since M is a linear sum of L, S, and N, we can consider these terms separately.

The matrix elements of L are

$$(\Pi_{1/2}J_+J|L|\Pi_{1/2}J_+J)=\hbar/(J+1)$$
$$=(\Pi_{1/2}J_-J|L|\Pi_{1/2}J_-J)=(\Pi_{3/2}J_+J|L|\Pi_{3/2}J_+J)$$
$$=(\Pi_{3/2}J_-J|L|\Pi_{3/2}J_-J), \tag{11}$$

all the other elements being zero.

The matrix elements of S are

$$(\Pi_{1/2}J_+J|S|\Pi_{1/2}J_+J)=-\hbar/(2J+2)$$
$$=-(\Pi_{3/2}J_-J|S|\Pi_{3/2}J_-J)=(\Pi_{1/2}J_-J|S|\Pi_{1/2}J_-J)$$
$$=-(\Pi_{3/2}J_+J|S|\Pi_{3/2}J_+J), \tag{12}$$

$$(\Pi_{1/2}J_+J|S|\Pi_{3/2}J_+J)=-\hbar\{(J+3/2)(J-1/2)\}^{\frac{1}{2}}/$$
$$(2J+2)=(\Pi_{1/2}J_-J|S|\Pi_{3/2}J_-J), \tag{13}$$

all the other elements being zero. The sign in Eq. (13) is decided by the definition of the wave function.

The matrix elements of N are always zero, since it does not contain the electronic coordinates.

Since no term which contributes to B of Eq. (10) appears so far, all the above matrix elements give the same contribution to the g factors of the c and d states, that is,

$$g_1=\{\mu\nu[(2J+3)(2J-1)]^{\frac{1}{2}}$$
$$+0.001\mu^2-3\nu^2\}/(J^2+J). \tag{14}$$

There exist, however, some small terms which contribute to B. The largest term among them may be the nondiagonal matrix elements caused by the combined effect of $\mathfrak{H}\cdot\beta\mathbf{L}$ and $D\mathbf{L}\cdot\mathbf{S}$, the spin-orbit interaction. Because of the spin-orbit interaction term a small amount of $^2\Sigma_{1/2}$ state, in which the odd π electron is excited to the σ state, is mixed with the ground $\Pi_{1/2}$ state. Thus, in Eqs. (5) and (6), the wave function $(\Pi_{1/2}J_\pm|$ should be replaced by

$$(\Pi_{1/2}'J_\pm|=(\Pi_{1/2}J_\pm|-[D/\sqrt{2}E(^2\Sigma)](^2\Sigma J_\pm| \tag{15}$$

TABLE II. Comparison between observed and calculated Zeeman shift.

$F\to F'$	$M_F\to M_{F'}$	First order theor	Complete theor		Observed
	Lower component of Λ doublet (Mc/sec)				
$3/2\to 3/2$	$+1/2\to+3/2$	−3.53	−3.49		−3.52
	$+3/2\to+1/2$	−1.00	−1.24	−1.33[a]	−1.36
	$-1/2\to+1/2$	−1.26	−1.39		
	$+1/2\to-1/2$	1.26	1.11	1.04[a]	1.01
	$-3/2\to-1/2$	1.0	0.96		
	$-1/2\to-3/2$	3.53	3.61		3.65
$3/2\to 5/2$	$+3/2\to+5/2$	−4.70	−4.79		−4.81
	$+1/2\to+3/2$	−2.87	−2.97		−2.96
	$+3/2\to+1/2$	−0.79	−0.96		···
	$-1/2\to+1/2$	−1.04	−1.11		−1.08
	$+1/2\to-1/2$	1.04	0.93		0.84
	$-3/2\to-1/2$	0.79	0.78		···
	$-1/2\to-3/2$	2.87	2.85		2.92
	$-3/2\to-5/2$	4.70	4.79		4.81
$1/2\to 1/2$	$-1/2\to+1/2$	−2.66	−2.44		−2.41
	$+1/2\to-1/2$	2.66	2.94		2.88
$1/2\to 3/2$	$+1/2\to+3/2$	−3.66	−3.57		−3.61
	$-1/2\to+1/2$	−1.13	−1.31		−1.27
	$+1/2\to-1/2$	1.13	1.03		1.05
	$-1/2\to-3/2$	3.66	3.69		3.72
	Upper component of Λ doublet (Mc/sec)				
$3/2\to 3/2$	$+1/2\to+3/2$	−3.37	−3.38		−3.36
	$+3/2\to+1/2$	−1.30	−1.25	−1.09[a]	−1.13
	$-1/2\to+1/2$	−1.03	−0.98		
	$+1/2\to-1/2$	1.03	1.08	1.19[a]	1.20
	$-3/2\to-1/2$	1.30	1.35		
	$-1/2\to-3/2$	3.37	3.35		3.35
$3/2\to 5/2$	$+3/2\to+5/2$	−4.70	−4.70		−4.73
	$+1/2\to+3/2$	−2.77	−2.75		−2.74
	$+3/2\to+1/2$	−1.10	−1.07		···
	$-1/2\to+1/2$	−0.84	−0.80		−0.80
	$+1/2\to-1/2$	0.84	0.86		0.94
	$-3/2\to-1/2$	1.10	1.13		···
	$-1/2\to-3/2$	2.77	2.78		2.80
	$-3/2\to-5/2$	4.70	4.70		4.72
$1/2\to 1/2$	$-1/2\to+1/2$	−2.57	−2.64		−2.65
	$+1/2\to-1/2$	2.57	2.49		2.49
$1/2\to 3/2$	$+1/2\to+3/2$	−3.24	−3.25		−3.26
	$-1/2\to+1/2$	−1.17	−1.12		···
	$+1/2\to-1/2$	1.17	1.22		···
	$-1/2\to-3/2$	3.24	3.22		3.23

[a] Averaged value of two components taking the intensity as the weight.

(the three upper or the three lower signs must be taken together), where the coefficient $[D/(2)^{\frac{1}{2}}E(^2\Sigma)]$ is calculated by the perturbation method, $E(^2\Sigma)$ is the energy difference between the $^2\Sigma$ state and the ground state. In obtaining this formula the assumption was made that the orbit of the odd electron is a p orbital. Through the $^2\Sigma$ states, we obtain a finite contribution from the $\mathfrak{H}\cdot\beta\mathbf{L}$ term which is effectively

$$(\Pi_{1/2}'J_+J|\mathfrak{H}\cdot\beta\mathbf{L}|\Pi_{1/2}'J_-J)$$
$$=[H\beta D/E(^2\Sigma)]\{(2J+1)/(4J+4)\}, \tag{16}$$

where $(\Pi_{1/2}'|$ means the wave function expressed in Eq. (15). It must be noted that the same effect gives

TABLE III. Zero-field frequency obtained by adjusting the Zeeman components and its comparison with the former values (Mc/sec).

	Lower component		Upper component	
$F \rightarrow F'$	This work	Burrus and Gordy[a]	This work	Burrus and Gordy[a]
$3/2 \rightarrow 3/2$	150 218.88	150 218.89	150 439.19	150 439.22
$3/2 \rightarrow 5/2$	150 176.48	150 176.54	150 546.55	150 546.50
$1/2 \rightarrow 1/2$	150 225.67	150 225.75	150 580.64	150 580.70
$1/2 \rightarrow 3/2$	150 198.76	150 198.85	150 644.44	150 644.37

[a] See reference 2.

a contribution to some other terms, but in the ground state where $|\nu| \ll |\mu|$ they can be neglected.

Summing up all these results, we obtain

$$g_c = (A+B)/J, \quad g_d = (A-B)/J, \tag{17}$$

where

$$A = \{\nu[(2J+3)(2J-1)]^{\frac{1}{2}} + 0.001 - 3\nu^2\}/(J+1),$$
$$B = -[D/E(^2\Sigma)](2J+1)/(4J+4), \tag{18}$$

where we assumed $\mu=1$, $|\nu| \ll 1$. In $J=1/2$ and $J=3/2$ states, they are

$$J=\tfrac{1}{2}\begin{cases} g_c = 0.0007 - [D/E(^2\Sigma)]\tfrac{2}{3} \equiv 0.0007 - \alpha, & (19) \\ g_d = 0.0007 + \alpha, & (20) \end{cases}$$

$$J=\tfrac{3}{2}\begin{cases} g_c = \bar{g} + \tfrac{2}{5}\alpha, & (21) \\ g_d = \bar{g} - \tfrac{2}{5}\alpha, & (22) \end{cases}$$

where

$$\bar{g} = 8\sqrt{3}\nu/15 + 0.0004 - 0.8\nu^2. \tag{23}$$

ANALYSIS OF THE EXPERIMENTAL RESULTS AND COMPARISON WITH THEORY

Using Eqs. (19), (20), (21), (22), (2), and (3), we can obtain a theoretical formula for each Zeeman shift $\Delta\nu$. In Table II, the theoretical values of $\Delta\nu$ are shown for

$$\bar{g}(\text{obs}) = -0.0230, \tag{24a}$$

$$\alpha(\text{obs}) = +0.0025. \tag{24b}$$

In our experiment, zero-field frequencies were not observed. They were observed by Burrus and Gordy,[2] but here we estimated them by fitting the observed shift $\Delta\nu$ with the theoretical one. The values of zero-field frequencies thus obtained are shown in Table III. They agree with the previous value within the experimental error.

The nondiagonal matrix element (3) contributes only 0.002 Mc/sec in the case of the c component of $J=1/2$, and much less for the d component, and is thus negligible for $J=1/2$ states; but it has a rather large effect for $J=3/2$ states. This effect explains the asymmetry of the Zeeman components. The secular equations were solved numerically for $J=3/2$ states. In Table II, the values calculated with all nondiagonal matrix elements neglected are also shown. The difference between these values and those of the complete theory gives the effect of the nondiagonal matrix elements. The effect is small in the upper component since the hfs splitting in this case is large, but in the lower component it is larger than the experimental error.

In our theory $\bar{g}$ is related to ν, the coefficient which gives the extent of the mixing of the $\Pi_{3/2}$ state into the $\Pi_{1/2}$ state, through Eq. (23). The ν was calculated by one of the present authors[4] to be -0.0247, which gives

$$\bar{g}(\text{theor}) = -0.0229 \text{ Bohr magneton.} \tag{25a}$$

This value agrees almost completely with the observed value shown in Eq. (24a). The same value of ν was used successfully in calculating the hfs (ΔW) of this molecule,[4] but the agreement there was not so complete as in the present case. In the hfs case, however, the theoretical results contained not only ν but the p-electron assumption (the assumption that the orbital of the odd electron is a p-atomic orbital), whereas in our case the $\bar{g}$ value comes only from the electronic spin, and no assumption about the orbit is made. Thus the slight deviation in the hfs may be attributed to the incorrectness of the p-electron approximation, as was done before.[4]

The quantity α can be calculated from formula (19). The spin-orbit coupling can be expressed as $D(S_xL_x + S_yL_y) + D'S_z\Lambda$, in which D may be different from D'. If, however, we assume the orbit is nearly atomic, $D \approx D' = 124$ cm^{-1}. The term $E(^2\Sigma)$ is observed spectroscopically[12] to be 44 000 cm^{-1}. Thus the theoretical value of α is

$$\alpha(\text{theor}) = +0.0020 \text{ Bohr magneton.} \tag{25b}$$

The agreement in this case with the observed value $+0.0029$ is good, although not so complete as in the case of $\bar{g}$. Either $D > D'$ or the contribution from the other excited electronic state may not be negligible and could explain the deviation of $+0.0005$.

The quantity α is closely related to what is called the rotational magnetic moment. If we interpret g_n in the formula (1) phenomenologically, forgetting about the electronic structure of the ground state, we shall obtain a term which behaves exactly like the α term. In this case the phenomenological g_n (which is different from the original g_n) is equal to $(3/2)\alpha$. It may be interesting to note that the observed magnetic moment α of 0.0025 Bohr magneton corresponds to the phenomenological g_n of seven nuclear magnetons, which is fairly large as a rotational magnetic moment.

[12] H. Sponer, *Molekuelspektren I* (Verlag Julius Springer, Berlin, 1935).

One-Electron Energies of Atoms, Molecules, and Solids*

J. C. SLATER
Massachusetts Institute of Technology, Cambridge, Massachusetts
(Received January 31, 1955)

In the method of the self-consistent field, the one-electron energies of the occupied orbitals agree closely with ionization energies of the corresponding atom or molecular system. To compare such calculations with experiment, we need a table of ionization energies of the atoms. Such a table is set up in the present paper. For the outer electrons, we use optical data, finding the energy of each configuration as the weighted mean of all the states in that configuration. For the inner electrons, we use x-ray data, and for this purpose present a revised table of x-ray term values. The two sets of values should not agree, for the zero of energy in optical spectra is that for an electron removed an infinite distance from the isolated atom, while in x-ray terms all energies are referred to the Fermi energy in the crystal. For the alkali metals, measurements of both types can be intercompared, and it is shown that for Li the Fermi level lies about 0.8 rydberg, below the zero of energy for the atom, for Na and K about 0.5, and for Rb about 0.4 rydberg. Using this information, appropriate corrections are applied for the other atoms, and a table of ionization energies of the atoms is constructed. The values in this table are compared with experimental information from soft x-ray spectra, and theoretical calculations of energy levels in atoms, molecules, and solids.

IN the method of the self-consistent field, it is known that the energy levels of the one-electron problems of motion of the various electrons in the self-consistent fields agree well with the corresponding ionization energies of the system. The theorem of Koopmans[1] tells us why this should be so. The purpose of the present paper is to set up a reliable table of experimental ionization energies of the isolated atoms, to use in making comparisons with self-consistent field calculations. We discuss the relation of this table to experimental values of energy levels in molecules and solids, and to theoretical values as computed by self-consistent fields. The reason why such a comparison is timely is that we are very recently beginning to get reliable calculations for molecules, made by the MO SCF (molecular orbital self-consistent field) method, and calculations for solids, made by the energy-band method.

For the outer electrons of the atom, we require the data of optical spectroscopy, which are admirable summarized in the tables prepared by the National Bureau of Standards,[2] which at present extend through Nb, with atomic number 41. We do not wish, however, merely to use the atomic ionization potentials, for these refer to the energy required to remove an electron from the lowest energy level of the atom, leaving the ion in its lowest energy level. This lowest energy level, in an atom with a complex spectrum, may be considerably below the properly weighted center of gravity of the configuration of the atom concerned. In making a self-consistent field calculation, however, the multiplet structure is not ordinarily taken into account in the first stage of the calculation, but only later, by solving a secular problem which accounts for the spreading apart of the various levels of the multiplet. This secular problem will leave the average value of the energy levels invariant, on account of the invariance of the trace of a matrix. Consequently the average value of all the experimental terms in a spectrum coming from a given configuration, suitably weighted according to their *a priori* probability, will give a more reliable estimate of the energy of that configuration than will the lowest energy level of the configuration. We can expect that the difference of these weighted mean energies of the atom and ion will be more reliable experimental quantities with which to compare one-electron energies than will the ordinary ionization potentials.

Consequently, we have computed such weighted mean energies of the ground-state configuration of each of the atoms up to Nb, and similar weighted means of the configurations of the singly ionized ions resulting from the neutral atom by removing one of its electrons. The differences between these energies of the atom and ion give ionization energies which may be expected to agree approximately with the one-electron energies in the self-consistent field calculations for the atoms. These values are tabulated in the upper part of Table I. There are some cases, particularly in the iron group, where some of the energy levels of complicated configurations have not been observed. In most such cases, there are other similar spectra of neighboring atoms where such missing terms have been located. By intercomparison, we have estimated the missing terms, which in no case are very important ones. On account of the necessity of making these estimates, some of the ionization energies in the iron group are likely to be in error by several units in the second decimal place.

For the inner electrons, one must use x-ray data. The writer has not been able to find a reliable tabulation of x-ray term values, containing the results of recent measurements, particularly of soft x-ray levels. Consequently, we have prepared such a table, given in Table II. The sources of information are described in

* The work described was assisted by the Office of Naval Research.
[1] T. Koopmans, Physica 1, 104 (1933).
[2] Atomic Energy Levels, Circular 467, National Bureau of Standards; (U. S. Government Printing Office, Washington, D. C.), Vol. 1, H–V, (1949); Vol. 2, Cr–Nb, (1952).

TABLE I. One-electron energies of free atoms (rydbergs).[a]

		1s	2s	2p	3s	3p	3d	4s	4p	4d	5s
H	1	1.00									
He	2	1.81									
Li	3	4.77	0.40								
Be	4	8.9	0.69								
B	5	14.5	1.03	0.42							
C	6	21.6	1.43	0.79							
N	7	30.0	1.88	0.95							
O	8	39.9	2.38	1.17							
F	9	51.2	2.95	1.37							
Ne	10	64.0	3.56	1.59							
Na	11	79.4	5.2	2.80	0.38						
Mg	12	96.5	7.0	4.1	0.56						
Al	13	115.3	9.0	5.8	0.83	0.44					
Si	14	135.9	11.5	7.8	1.10	0.57					
P	15	158.3	14.1	10.1	1.35	0.72					
S	16	182.4	17.0	12.5	1.54	0.86					
Cl	17	208.4	20.3	15.3	1.86	1.01					
A	18	236.2	24.2	18.5	2.15	1.16					
K	19	266.2	28.2	22.2	3.0	1.81		0.32			
Ca	20	297.9	32.8	26.1	3.7	2.4		0.45			
Sc	21	331.1	37.3	30.0	4.2	2.6	0.59	0.55			
Ti	22	366.1	42.0	34.0	4.8	2.9	0.68	0.52			
V	23	402.9	46.9	38.3	5.3	3.2	0.74	0.55			
Cr	24	441.6	51.9	43.0	6.0	3.6	0.75	0.57			
Mn	25	482.0	57.7	47.8	6.6	4.0	0.57	0.50			
Fe	26	524.3	63.0	52.8	7.3	4.4	0.64	0.53			
Co	27	568.3	69.0	58.2	8.0	4.9	0.66	0.53			
Ni	28	614.1	75.3	63.7	8.7	5.4	0.73	0.55			
Cu	29	662.0	81.3	69.6	9.6	6.1	0.79	0.57			
Zn	30	712.0	88.7	76.2	10.5	7.0	1.28	0.69			
Ga	31	764.0	96.4	83.0	11.8	7.9	1.6	0.93	0.44		
Ge	32	818.2	104.6	90.5	13.5	9.4	2.4	1.15	0.55		
As	33	874.5	113.0	98.5	15.4	10.8	3.4	1.30	0.68		
Se	34	932.6	122.1	106.8	17.3	12.2	4.5	1.54	0.80		
Br	35	993.0	131.7	115.6	19.9	13.8	5.6	1.80	0.93		
Kr	36	1055.5	142.0	124.7	22.1	15.9	7.1	2.00	1.03		
Rb	37	1120.1	152.7	134.5	24.3	18.3	8.7	2.7	1.56		0.31
Sr	38	1186.7	163.7	144.6	26.8	20.5	10.4	3.3	2.0		0.42
Y	39	1255.3	175.1	155.0	29.4	22.7	12.0	3.7	2.3	0.48	0.64
Zr	40	1325.9	186.7	165.5	32.0	24.8	13.6	4.1	2.3	0.61	0.54
Nb	41	1398.9	199.3	176.9	35.1	27.6	15.8	5.0	3.1		0.58

[a] Entries above the line are determined from optical data, those below the line from x-ray data. The entries for Li 1s, Na 2p, K 3p, and Rb 4p are determined from both sorts of data. To bring about agreement, as explained in the text, the x-ray levels of Be to C are increased numerically by 0.7 ry with respect to those in Table II, those of the elements from N to F are increased by 0.6, for elements from Na to Zn by 0.5, and those from Ga on by 0.4 ry. The K level of Ne is not modified, since it was determined by an optical transition of the free atom. For A, on the other hand, the K level was determined by absorption of the free atom, and the absorption edge presumably included the broadened transitions to the bound levels 4p, 5p, etc., as well as to the continuum, so that this case corresponds more nearly to that of a solid than of a free atom. The x-ray levels from Table II were used to form properly weighted mean energies for the different j values of the same configuration, before being incorporated in Table I.

In the iron group, there is a discontinuity in our treatment of the optical levels, between Cr and Mn, indicated by a line in the table. At the beginning of the group, the ground-state configuration (as judged by the weighted mean of the term values) is that with two 4s electrons, while at the end of the group it is that with one 4s electron. For the elements up through Cr that with two 4s electrons is definitely lower, for Mn they are very nearly the same, and for the elements from Fe on the lowest configuration is that with one 4s electron. We have assumed as the ground state configuration that with two 4s electrons up through Cr, and that with one 4s from Mn on.

Though energy values for the optical states are listed to two decimal places, there are a number of places in the transition groups where levels had to be estimated from neighboring spectra, and the second decimal place may be uncertain by several units.

the notes to that table. It will be noticed that, in contrast to the existing tables of x-ray term values, we have distinguished sharply between the inner levels, where the separation into such levels as L_1, L_2, L_3 is appropriate, and the outer levels, which as we now know from the theory of solids are broadened into valence or conduction bands. For these outer bands, we have indicated the range of energy in which they are located, as determined by Skinner and other observers of soft x-rays. The writer cannot claim to be an expert on x-rays, or to have been able to make a critical review of the data, but nevertheless he believes that Table II is considerably more reliable than other available tables.

We now notice that the x-ray data are not strictly

TABLE II. X-ray term values (rydbergs).[a]

		K $1s$ $j=1/2$	L_1 $2s$ $1/2$	L_2 $2p$ $1/2$	L_3 $2p$ $3/2$	M_1 $3s$ $1/2$	M_2 $3p$ $1/2$	M_3 $3p$ $3/2$	M_4 $3d$ $3/2$	M_5 $3d$ $5/2$	N_1 $4s$ $1/2$	$N_{2,3}$ $4p$ $1/2, 3/2$
Li	3	4.0		0–0.3								
Be	4	8.2		0–1.0								
B	5	13.8		0–2.2								
C	6	20.9		0–2.3								
N	7	29.4										
O	8	39.3										
F	9	50.6										
Ne	10	64.0	L_1	L_2	L_3							
Na	11	78.9	4.7	2.3	2.3		0–0.2					
Mg	12	96.0	6.5	3.6	3.6		0–0.5					
Al	13	114.8	8.5	5.3	5.3		0–0.9					
Si	14	135.4	11.0	7.4	7.3		0–1.2					
P	15	157.8	13.6	9.7	9.6		0–2.9					
S	16	181.9	16.5	12.1	12.0		0–3.3					
Cl	17	207.9	19.8	14.9	14.8							
A	18	235.7	(23.7)	18.1	19.7	M_1	M_2	M_3				
K	19	265.7	27.7	21.9	21.6	2.5	1.3	1.3	0–0.1			
Ca	20	297.4	32.3	25.8	25.5	3.2	1.9	1.9	0–0.2			
Sc	21	(330.6)	(36.8)	(29.7)	(29.4)	(3.7)	(2.1)	(2.1)				
Ti	22	365.6	41.5	33.9	33.4	4.3	2.4	2.4	0–0.4			
V	23	402.4	46.4	38.2	37.7	4.8	2.7	2.7	0–0.6			
Cr	24	441.1	51.4	43.0	42.3	5.5	3.1	3.1	0–0.5			
Mn	25	481.5	57.2	47.9	47.1	6.1	3.5	3.5	0–0.4			
Fe	26	523.8	62.5	53.1	52.1	6.8	3.9	3.9	0–0.4			
Co	27	567.8	(68.5)	58.5	57.4	7.5	4.4	4.4	0–0.5			
Ni	28	613.6	74.8	64.1	62.9	8.2	4.9	4.9	0–0.4			
Cu	29	661.5	80.8	70.2	68.7	9.1	5.6	5.6	0–0.5			
Zn	30	711.5	88.2	76.9	75.2	10.0	6.5	6.5	0–0.8			
Ga	31	763.6	(96.0)	84.0	82.1	11.4	7.5	7.5	1.2	1.2		
Ge	32	817.8	(104.2)	91.8	89.5	13.1	9.0	9.0	2.0	2.0		
As	33	874.1	112.6	100.1	97.5	15.0	10.4	10.4	3.0	3.0		
Se	34	932.2	(121.7)	108.6	105.6	16.9	11.8	11.8	4.1	4.1		
Br	35	992.6	(131.3)	117.8	114.3	19.5	13.6	13.2	5.3	5.1		
Kr	36	1055.1	(141.6)	127.2	123.4	(21.7)	(16.0)	(15.4)	(6.8)	(6.7)		
Rb	37	1119.7	152.3	137.4	133.0	23.9	18.4	17.7	8.4	8.3	2.3	1.2
Sr	38	1186.3	163.3	147.9	143.0	26.4	20.7	19.9	10.1	9.9	2.9	1.6
Y	39	1254.9	174.7	158.7	153.2	29.0	23.0	22.1	11.7	11.6	3.3	1.9
Zr	40	1325.5	186.3	169.8	163.6	31.6	25.1	24.2	13.3	13.1	3.7	1.9
Nb	41	1398.5	198.9	181.7	174.7	34.7	28.1	26.9	15.5	15.3	4.6	2.7

[a] Most of the data for this table are taken from Landolt-Bornstein's tables (Verlag Julius Springer, Berlin, 1950), eighth edition, Vol. 1, 1. Teil, pp 226–227. That tabulation, unfortunately, was far from up to date at the time of its publication, and therefore the data given there have been corrected in the light of information not included. For Li, Be, B, and C, and the band widths of these elements and those from Na through S, we have used the results of H. W. B. Skinner, Trans. Roy. Soc. (London) **A239**, 95 (1940). For the band widths of K and Ca, we have used R. H. Kingston, Phys. Rev. **84**, 944 (1951), and for the band widths of the elements from Ti to Zn we have used H. W. B. Skinner, Phil. Mag. **45**, 1070 (1954). Results on the elements K to Cu are taken from V. H. Sanner, dissertation, Uppsala, 1941 (unpublished), quoted by H. Niehrs, Ergeb. exakt. Naturwiss. **23**, 359 (1950). That very useful review article contains the best and most up-to-date survey of the soft x-ray levels which the writer has seen, including many references, and the results quoted by Niehrs have been considered in setting up Table II. The K levels of Zn, Ga, and Ge are taken from W. W. Beeman and H. Friedman, Phys. Rev. **56**, 392 (1939), and the other levels of these elements have been corrected, using results quoted in Landolt-Bornstein and in M. Siegbahn, *Spektroskopie der Röntgenstrahlen* (Verlag Julius Springer, Berlin, 1931), second edition, which of course is the authority for work done up to its time of publication. Values given in parentheses are estimated by interpolation. In the case of Sc, in which results are quoted in the tables, we have diminished the tabulated values by 0.6 ry, thereby bringing the values into smooth relationship with the neighboring elements. It seems likely that there is an error in the determination of the K absorption limit for this element, which would account for this discrepancy. A similar discrepancy of 2.0 ry in the levels of Ga exists in all published tables, but the new determination of its K absorption limit by Beeman and Friedman, mentioned above, has removed this discrepancy, so that in Table II the values for Ga fall smoothly in line with neighboring elements.

comparable with the optical data, and cannot immediately be incorporated into Table I. First, of course, we must make a properly weighted average of the two states in a doublet, as L_2 and L_3. But quite aside from this, the values are not comparable because the energies are referred to different zeros of energy. This will be clear from Fig. 1, which illustrates the case of sodium. In Fig. 1, we have illustrated, as accurately as possible, the potential energy felt by an electron in the sodium atom, as determined in a self-consistent field way (in this case, we have used the well-known potential of Prokofjew,[3] which was set up empirically so that the one-electron energies in it would agree as closely as

[3] W. Prokofjew, Z. Physik **58**, 255 (1929).

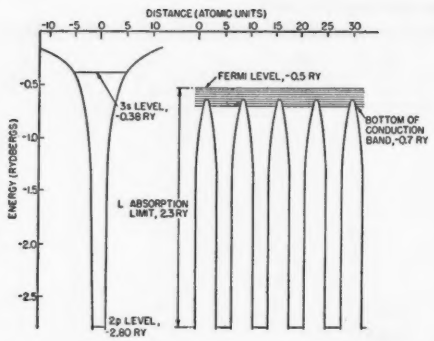

FIG. 1. Energy values in sodium atom and sodium crystal. At left, potential energy of electron in sodium atom, as function of distance from nucleus, going to zero energy at infinite distance, and showing the $3s$ level at -0.38 ry and the $2p$ at -2.80 ry. At right, potential energy in sodium crystal, along a line in 111 direction passing through nearest neighbor atoms. This is drawn so that the potential energy near the nucleus, and the x-ray levels, agree with those of the isolated atom. The conduction band extends downward from the Fermi level, at -0.5 ry, to about -0.7 ry. The L absorption limit is observed when an electron is raised from the $2p$ level to the Fermi level, corresponding to 2.3 ry.

possible with observed term values), and the corresponding potential energy in the sodium crystal, at points along a line in the 111 direction, passing through the centers of nearest-neighbor atoms. For the atom, we have shown the $2p$ and $3s$ energy levels, and for the crystal the conduction band and the $2p$ level. In this case, and in the other alkali metals, we fortunately know all the required energies. The $2p$ level in the atom is at -2.80 rydbergs, the $3s$ at -0.38 ry. In the metal, the $2p$ term value is given as 2.3 ry, and the breadth of the conduction band is about 0.2 ry. Now the x-ray energy levels are set by the absorption limits: the zero of energy is set at the lowest energy level to which an electron can be ejected from an inner level. That is, all x-ray terms are measured from the Fermi level as a zero. If we now adjust the additive constant in the energy for the metal so that the x-ray levels will coincide (that is, so that the potential energy at a point well inside the atom is identical in metal and isolated atom), it is clear that in this case the Fermi level must lie about 0.5 ry below the energy of the atom at infinite distance. Similar arguments show that the depression of the Fermi level for Li is about 0.8 ry, for K about 0.5, and for Rb about 0.4. These are the only elements for which this comparison can be made.

It is clear, then, that in order to find the ionization energies of isolated atoms, using the x-ray term values as a starting point, we must increase the numerical value of each of the x-ray terms by an amount equal to the depression of the Fermi level. Since we do not know this for any elements but the alkali metals, we have done the best we could, and have simply used a smooth interpolation between these elements to deduce an amount by which we should increase the term values. Thus, we have increased the term values of the elements from Be to C by 0.7 ry, those from N to F by 0.6, those from Na to Zn by 0.5, and those from Ga to Nb by 0.4. The only exception is Ne, in which the original measurements[4] represented a K_α emission line of the gaseous atom, so that this value should require no further correction. The energies entered in Table I, for the inner electrons of the atom, are derived from the empirical x-ray term values of Table II by the procedure which we have just described.

In Fig. 2, we show graphically the energy values of Table I. We also show, by black rectangles, the breadths of the outer bands for the various elements, in the cases where they have been measured. Our adjustment of the x-ray levels to take account of the depression of the Fermi level has, of course, determined the height of the top of these black rectangles, which represents the Fermi level. The accuracy of modern determinations of x-ray term values is well shown by the comparative smoothness of the curves. If one uses an older table of x-ray term values, rather than the corrected values of Table II, the curves are much less smooth. Also, if one uses optical ionization potentials rather than the energy differences of weighted mean values for the various configurations, as we have done, the upper parts of the curve are much less smooth.

Before going on to discuss the relation of these energy values to the problem of molecules and solids, let us take up one objection which some persons may well make. For instance, Skinner,[5] in 1932, discussing Li by means of a figure very much like our Fig. 1, on the basis of much less experimental knowledge than we now have, concluded that he could not form a consistent picture of what was going on along the lines we are following in this paper, and therefore sought other interpretations of the situation. He noted that a Li atom which has lost a K electron, as in the initial state of the transition in which a conduction electron falls back into a vacancy in the K shell, is really much like an atom whose atomic number is one unit greater, or a Be atom, as far as its outer structure is concerned. He considered that such a Be atom, introduced into the Li lattice, would have a potential well so much deeper than the ordinary Li atom that it would create a low-lying discrete level, below the bottom of the conduction band, and he thought he was seeing evidence of the existence of such a level. He felt that the simple one-electron picture was quite inadequate to explain what was going on. Various other workers in the field of soft x-ray spectroscopy have made similar remarks at one time or another, and it seems desirable to examine them critically, and see whether they invalidate the simple one-electron picture.

The first part of this discussion can well be a consideration of Koopmans' theorem; the experimenters in the field are not usually aware of its assumptions or its implications. Koopmans considered a Hartree-Fock

[4] J. M. Backovsky, Compt. rend. **202**, 1671 (1936).
[5] H. W. B. Skinner, Proc. Roy. Soc. (London) **A135**, 84 (1932).

solution for an atom (though his results hold equally well for a molecule or solid). From the Hartree-Fock method one can immediately compute the energy of the atom, in its ground state. One can then set up a wave function for the ion, built up out of the same orbitals which are used for the ground state of the atom, but merely omitting the orbital of the electron which has been removed. One can calculate the expectation value of the energy for this wave function, and subtract from it the energy of the ground state of the atom. Koopmans showed that this difference is precisely equal to the one-electron energy parameter for the electron which has been removed.

Now it is obvious to anyone that the wave function for the ionized state, determined in this way, will be less accurate than for the ground state. The wave function for the ground state is determined by varying the one-electron orbitals to minimize its energy, and we have used the same orbitals for the ion, rather than varying them over again to minimize the energy of the ion. The ion really should have more concentrated orbitals, pulled in by the greater nuclear charge. If we correct for this, by solving separately for the ion, or by using second-order perturbation calculations, we shall find that the energy of the ion will be depressed, and the apparent ionization energy will decrease, since the energy of the ground state will not be affected. In other words, we expect to find that the Hartree-Fock one-electron energy parameters give too large values for the x-ray term values. This expectation proves to be generally correct, when we compare atomic calculations with the observations.

The error in the energy arising from this incorrect wave function, however, on account of the perturbation theory, will be a small quantity of the second order, if the error in the wave function is small of the first order. The incorrect wave function, being too extended in space, will have too high a potential energy. On the other hand, since it corresponds to a disturbance of too great effective wavelength, it will have too small a kinetic energy. To the first approximation, these effects will cancel, leaving only a second-order correction to the energy, which may be expected to be small.

We may furthermore expect this type of error in the results of Hartree-Fock calculations to be roughly the same in atom and crystal, so that it should not affect the validity of the type of comparison between the two which we have made. This should be true, at least, if there is not a gross change in the character of the wave function in going from an atom to an ion. If Skinner's hypothesis were true, however, and there were a new discrete level which appeared in the solid, below the level of the continuum, this would be such a decided change in wave function that we might well doubt the applicability of Koopmans' theorem. Let us examine this question, and see if we expect such a level to appear.

We know a good deal more about the nature of impurity levels in solids at present than we did a few

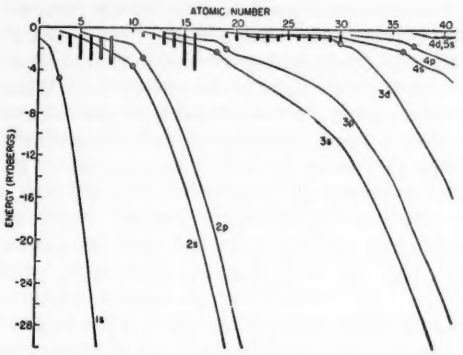

FIG. 2. One-electron energies of atoms, molecules, and solids. The full lines represent the energy values for the atoms, from Table II. The black rectangles represent the filled bands of electrons in the solids. The open rectangles, for the elements oxygen and nitrogen, represent the energy range in which one-electron energies have been calculated for various molecules involving these elements, by the MO SCF method. For carbon, similar calculations on molecules, and on the crystal, give energy levels lying within the range shown by the black rectangle. The circles on each full line indicate the point where the optical and x-ray data join.

years ago, and can now answer this question with considerable assurance. The writer and Koster[6] have shown that when an atom whose atomic number is greater than that of the atoms of the crystal replaces an atom of a metallic crystal, there are two quite different possible things which may happen. If the atomic number is enough greater, it is quite true that a new level will appear below the continuum. If the difference is smaller, however, no new level will appear. The wave functions will be modified, so that the wave functions corresponding to the lower energy levels in the band will become somewhat more concentrated toward the impurity atom, those corresponding to the higher (and generally unoccupied) energy levels will tend to avoid the impurity atom, but unless the difference in atomic number exceeds a critical amount, there will be no discrete level, and no major modification of the wave functions. It seems most likely that a difference of a single unit in atomic number is not enough to result in a discrete level. In a metal, the conduction electrons will tend to shield the crystal from the added Coulomb field resulting from the impurity atom, so that the perturbation produced by this atom is not nearly as great as one would suppose at first sight, and this is why the critical perturbation is not exceeded.

The situation in an insulator or semiconductor of course will be different. There, an impurity atom whose atomic number is one unit greater than the atoms of the lattice (or an atom which has lost an inner electron) will be an ordinary donor atom, and will produce a discrete level, hydrogenic in type and extending rather far out in space, below the conduction band, and another one below the valence band. As far as the valence

[6] G. F. Koster and J. C. Slater, Phys. Rev. **96**, 1208 (1954).

band is concerned, we do not ordinarily consider this discrete level, for the charge which it contains will just balance the compensating decrease in charge density in the other wave functions of the valence band. When the inner electron of the atom is removed, the electrons of the valence band will instantly and automatically rearrange themselves, in such a way as just to fill the revised valence band, including the discrete level, with very small change of charge density. There will in addition be a level appearing just below the conduction band. This will be the familiar donor level, which in principle could be filled with an electron, which would tend to produce electrical neutrality of the atom which has lost its inner electron, but which in practice would not acquire that electron in the short time concerned in the x-ray experiment, or would lose it again immediately on account of thermal excitation. In other words, the net result is a very small change in the charge density in the valence band, as a result of the ionization of the inner electron.

In either of these cases, then, we seem to have the necessary conditions for the application of Koopmans' theorem: the outer electrons will not suffer any large change in wave function when the inner electron is removed. The writer believes, therefore, that a one-electron picture can describe consistently the relations between the levels of the isolated atom and of the crystal of the corresponding element, without the need of introducing any additional discrete levels to complicate the picture. We can expect a self-consistent field calculation, with exchange, to give energy levels for the atom, and the crystal or molecule, which are comparable with each other, though they may be somewhat inaccurate as compared with the experimental values of Table I. To see that the inaccuracies are not very great, however, we may quote the calculated values for the argon atom,[7] almost the only neutral atom for which complete calculations with exchange have been made, and therefore for which we can make direct comparison with the values of Table I. The calculated $1s$ level is 237.2, compared with 236.2 of Table I; for $2s$, 24.6 compared with 24.2; for $2p$, 19.1 compared with 18.5; for $3s$, 2.56 compared with 2.15; and for $3p$, 1.18 compared with 1.16. As we expect, the numbers are all somewhat large, but the agreement in general is remarkable.

Now let us go on to discuss various other aspects of one-electron energies. In calculations of energy bands of solids, very often the potential energy used for the solid has not been comparable with that for the isolated atom, so that a direct comparison is not possible. However, in the calculation of Na by Wigner and Seitz and by the writer,[8] the potential in the solid was taken to be the Prokofjew potential, as it is in the atom, and the depression of the energy band on going from the atom to the solid is in agreement with that shown in Fig. 1, to an accuracy of about 1 ev. In the calculation of Manning and Krutter on Ca,[9] it is indicated how one can adjust the potential used in the crystal to agree with the atom, and they find a band extending from about -0.60 to -0.95 ry, indicating a depression of the Fermi level of about the expected amount, and about the expected width. Herman's calculation[10] on diamond uses a potential which appears as if it might be comparable with the atomic potential. His band, stretching from about -0.9 to -2.4 ry, is roughly in agreement with what we should expect. It is to be emphasized that in future work on energy bands, it would be highly desirable to adjust the potential energy so that its value near the nucleus agrees with that in the isolated atom, so that one can make the sort of comparison of the absolute value of energy levels with the atomic ones which we are discussing here, as well as comparing band widths.

Several molecules have recently been discussed by the molecular orbital method, and their one-electron energies determined. Thus, Mulligan,[11] in his calculation of CO_2, finds L levels running from -11.5 ev to -44.9 ev, or from -0.8 ry to -3.3 ry. The lower levels are largely composed of oxygen wave functions. Similarly for CO, Sahni[12] has levels from -1.0 to -3.2 ry, and Ellison and Shull,[13] in their work on H_2O, find levels from -0.9 to -2.7 ry. These calculations suggest that we are likely to find levels down to about -3.3 ry in molecules containing oxygen, and in Fig. 2 we have shown a rectangle enclosing these energy values. For N_2, Scherr[14] in unpublished calculations finds levels from -1.1 ry to -2.9 ry; we show this energy range as well in Fig. 2. For CH_4, Nesbet[15] in other unpublished work finds the levels to lie between -1.1 ry and -2.0 ry, well within the range shown by the black rectangle in Fig. 2 for carbon. We get the impression, in other words, that the spread of one-electron energy levels in simple molecules will be substantially the same as in solids. This is, of course, what we should expect. It is well known that the splitting of energy levels in a solid is comparable in magnitude with that in a molecule; the only difference is that, as the molecule becomes larger and approaches a solid, more and more energy levels become crowded into the same energy range, and finally become a continuous band.

It seems, then, that the one-electron energies which one can find from ionization energies of atoms and

[7] D. R. Hartree and W. Hartree, Proc. Roy. Soc. (London) **A166**, 450 (1938).
[8] E. Wigner and F. Seitz, Phys. Rev. **43**, 804 (1933); J. C. Slater Phys. Rev. **45**, 794 (1934).
[9] M. F. Manning and H. M. Krutter, Phys. Rev. **51**, 761 (1937).
[10] F. Herman, Phys. Rev. **88**, 1210 (1952).
[11] J. F. Mulligan, J. Chem. Phys. **19**, 347 (1951).
[12] R. C. Sahni, Trans. Faraday Soc. **49**, 1246 (1953).
[13] F. O. Ellison and H. Shull, J. Chem. Phys. **21**, 1420 (1953).
[14] C. W. Sherr, thesis, University of Chicago (unpublished).
Note added in proof.—See also J. Chem. Phys. **23**, 569 (1955).
[15] R. K. Nesbet, thesis, Cambridge University (unpublished).

crystals, and which one can calculate using the self-consistent field method for atoms, molecules, and solids, show a good consistency with each other. Such comparison as we have made here, between the one-electron energies of the atoms and of the other systems, could well be made in the course of future calculations of molecular wave functions or energy bands. In particular, it is interesting to observe the great increase in the width of the bands as we go through the first two periods, adding more electrons and reducing interatomic distances. A particularly interesting thing will be to find just how the *3d* level drops below the valence band, in the elements to the neighborhood of Ge. Interesting deductions regarding molecular binding are of course suggested by the drop of the average value of the one-electron energy in a band, below the atomic levels, but we shall not try to go further into the implications of the results in the present paper.

PHYSICAL REVIEW VOLUME 98, NUMBER 4 MAY 15, 1955

Differential Cross-Section Measurements for Large-Angle Collisions of Helium, Neon, and Argon Ions with Argon Atoms at Energies to 100 kev*

EDGAR EVERHART, R. J. CARBONE, AND GERALD STONE
Physics Department, University of Connecticut, Storrs, Connecticut
(Received January 10, 1955)

The differential cross section for the scattering of positive charge from collisions of noble gas ions with the target gas argon has been measured. The ion beam is passed through a chamber containing the target gas at a pressure of a few microns of mercury, which is low enough to insure that single collisions will predominate. The particles scattered out of the beam are collected and the total positive charge is measured. The collector incorporates collimating holes to select only those particles at a chosen scattering angle with a resolution of about two degrees. The apparatus allows the angle to be varied continuously up to thirty-eight degrees. Data are presented for collisions of singly ionized helium, neon, and argon ions with argon atoms at 25, 50, and 100 kev. The cross sections observed differ from those expected from the Rutherford scattering law and these differences are interpreted in terms of electron screening, ionization, and charge exchange.

1. INTRODUCTION

THE large-angle collisions studied here are those in which ions of helium, neon, and argon with an energy from 25 000 to 100 000 electron volts collide with stationary argon atoms. These collisions can be expected to follow the Rutherford scattering law in the limit of sufficiently high energies, but at the lower energies there will be a modification due to the screening effect of the electrons.

In this energy range the vast majority of the collisions will be small-angle and, in fact, these small-angle collisions account for nearly all of the total cross section. There have been numerous studies of the total cross sections for elastic scattering, charge exchange, and ionization in this energy range.[1-3]

Although the few large-angle collisions which do occur account for a nearly negligible portion of the total cross section, they are interesting, for these are collisions in which the atoms come very close together. Their study gives information regarding the potential energy function between two atoms at very close distances on an atomic (not nuclear) scale. Under some conditions in these experiments, the actual distance of closest approach is less than the radius of the innermost classical electron orbits of either of the colliding atoms. This means that the electron configuration during the collision will be complicated.

In this energy range, the relative velocity of the ion and atom in the collision is of the same order of magnitude as the classical orbital velocity of the atomic electrons. This is the condition under which ionization and charge exchange cross sections are thought to be a maximum.[1]

The scattered particle current into a given solid-angle segment depends on the forces between the atoms during the collision, but the scattered positive charge measured in the experiments described here depends, in addition, on the extent to which the scattered particle was ionized or neutralized during the collision. Specifically, we are measuring in these experiments the differential cross section for scattering of positive charge.

Heydenburg, Hafstad, and Tuve[4] have performed differential cross section measurements for collisions of protons with protons at 600 to 900 kev. Their apparatus is similar in some respects to that to be described here.

* This work was sponsored by the Office of Ordnance Research through the Watertown Arsenal Laboratories and the Springfield Ordnance District.

[1] H. S. W. Massey and E. H. S. Burhop, *Electronic and Ionic Impact Phenomena* (Oxford University Press, London, 1952). Chapter VIII contains an excellent discussion and bibliography of this field.

[2] Niels Bohr, Kgl. Danske Videnskab. Selskab, Mat.-fys. Medd 18, 8 (1948).

[3] S. K. Allison and S. D. Warshaw, Revs. Modern Phys. 25, 779 (1953).

[4] Heydenburg, Hafstad, and Tuve, Phys. Rev. 56, 1078 (1939).

Ramsauer and Kollath[5] have made measurements at large angles of the scattering of protons at energies up to 120 electron volts from several gas targets, and Rouse[6] has made measurements of the large angle scattering of potassium ions from several gases at energies to 360 electron volts. However, there have been, to our knowledge, no previous measurements of large-angle single scattering of ions in the particular energy range of 25 to 100 kev.

2. THEORY OF THE MEASUREMENT

A study of differential cross sections for single collisions requires a suitable thin gas target. This can be realized with an apparatus as shown in Fig. 1. The ion beam enters the chamber, which contains the target gas, through the small defining hole a. At various points along the beam path, there are a few ions scattered out of the beam. If two holes, b and c, are aligned as shown, a small fraction of the scattered ions can pass through them and enter a charge collector. The observed current to this collector is proportional to the differential cross section for scattering of positive charge at the angle in question. Lines drawn from the edges of holes b and c intersect the ion beam and define an effective target volume.

The target gas pressure should be low enough so that the mean free path for elastic scattering, charge exchange, or ionization is at least several centimeters. This is more than adequate to guarantee that multiple large angle collisions within the small target volume are extremely rare, and therefore the scattered beam will be the result of single collisions. This mean free path is also long enough to insure that most of the ions in the beam make no collisions of any sort within the scattering chamber, and that most of those few ions scattered at large angles from the target volume make no further collisions before leaving the chamber through hole b. The test of these statements lies in a measurement of the scattered current at a given angle as a function of the target gas pressure. When this current is found to be proportional to the pressure, the pressure is low enough to insure the aforementioned conditions. In practice, the target gas pressures used in these experiments were of the order of a micron of mercury.

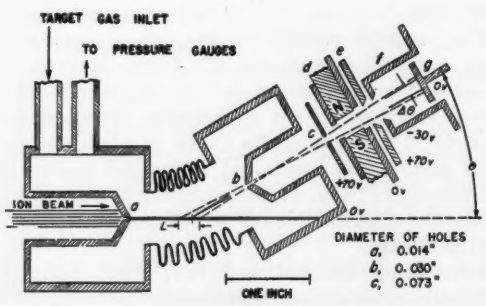

FIG. 1. The scattering apparatus.

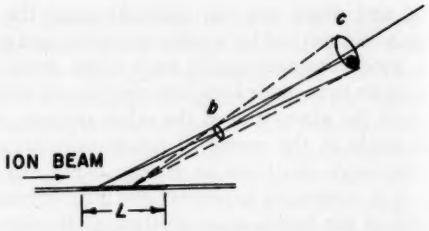

FIG. 2. The solid angle subtended by the charge collector as seen from an arbitrary point in the effective target volume.

There can be no foils across holes a and b at the ion energies used in these experiments. The ratio of the target gas pressure to the pressure in the accelerator is about 200 to 1, and this pressure difference is easily maintained across the two small holes by the accelerator's vacuum system.

The ratio of the scattered current I to the incident ion current N at the angle θ is

$$I/N = n\sigma(\theta)L\Delta\Omega, \tag{1}$$

where n is the number of target particles per unit volume, $\sigma(\theta)$ is the differential cross section for the process in question averaged over the effective solid angle of acceptance $\Delta\Omega$, and L is the length of the target volume measured in the direction of the ion beam.

The value of $L\Delta\Omega$ depends on the location and size of the defining holes. In the apparatus of Fig. 1, holes b and c have diameters s_1 and s_2 which are proportional to their respective distances y_1 and y_2 from the center of the target volume. This defines a cone, as shown in Fig. 2, whose interior angle is

$$\Delta\theta = s_1/y_1 = s_2/y_2. \tag{2}$$

Introducing a new length y_0 defined by

$$y_0 = y_1y_2/(y_2 - y_1), \tag{3}$$

the distance L is found from the geometry of Fig. 1 to be

$$L = 2y_0(\Delta\theta)\csc\theta. \tag{4}$$

An integration must now be performed along length L to find the average solid angle. At the center of the region the solid angle is evidently $\pi(\Delta\theta)^2/4$, and it is zero at each end. At intermediate points the solid angle intersects an area shaped something like the small shaded area in Fig. 2. This integration results in an effective solid angle

$$\Delta\Omega = (\Delta\theta)^2/3. \tag{5}$$

Combining all the aforementioned equations and solving for $\sigma(\theta)$, there results

$$\sigma(\theta) = (3I/N)/[2ny_0(\Delta\theta)^3\csc\theta]. \tag{6}$$

[5] von C. Ramsauer and R. Kollath, Ann. Physik **16**, 570 (1933).
[6] A. G. Rouse, Phys. Rev. **52**, 1238 (1937).

A convenient dimensionless way to plot the measured cross sections is to show $\sigma(\theta)/b^2$ as a function of θ. Here b is a characteristic length defined by

$$b=Z_1Z_2e^2(1+\gamma)/U. \quad (7)$$

In this formula Z_1 and Z_2 are the atomic numbers of the incident particle and the target particle respectively, e is the electronic charge, γ is the ratio of the mass of the incident particle to that of the target particle, and U is the kinetic energy of the incident particle in the laboratory coordinate system. In classical Rutherford scattering theory, b is called the collision diameter and is the distance of closest approach in a "head on" collision.

3. DESCRIPTION OF THE APPARATUS

The University of Connecticut heavy-ion accelerator[7] used in this experiment is of the Cockcroft-Walton type. It produces a focused monoenergetic beam of positive ions at energies continuously variable from 25 to 250 kev. The radio-frequency ion source[8] furnishes 10 to 100 microamperes of singly charged helium, neon, or argon atoms. The ion beam is analyzed by a deflection magnet so that the charge-to-mass ratio of the ions striking the gas target is known. Three sets of electrostatic deflection plates together with the analyzing magnet may be used to line up the beam properly with the axis of the scattering chamber.

The scattering chamber is itself inside a large vacuum box. As shown in Fig. 1, it consists of two parts bridged by a flexible bellows. The first part is rigidly fixed. It contains the hole a, which defines the incoming ion beam, and the connections to the target gas handling system. The flexible bellows allows the second part to rotate through any angle of scattering up to 38° about the center of the effective target volume. This part rotates on a shaft which goes through the vacuum wall by means of an "O"-ring seal. The second part supports the charge collection system and the electrometer.

In the charge collection system, holes b and c define the scattered beam and determine the angular resolution. All other holes are oversize and do not limit the scattered current. The ion current is collected on electrode g which is connected to the electrometer input. Electrode f is maintained 30 volts negative as this was found to be a sufficient potential to prevent secondary electrons from leaving the collector.

At certain angular settings some difficulty was experienced with a background electron current which partially masked the positive current to the collector. This was eliminated by two magnetic fields, the one from a small permanent magnet of 500 gauss behind hole d, and the other from a large Helmholtz coil which immersed the entire scattering apparatus and electrometer in a uniform 10-gauss field. These magnetic fields and potentials have no appreciable effect on the scattered ions, which have a good fraction of the incident energy at these angles. With these extraneous electron currents removed, the observed scattered currents were always positive and were negligibly small when the target gas was removed.

The electrometer circuit is mounted in the vacuum just behind the collector electrode. Various combinations of input resistors and galvanometer shunts give this a useful range of 10^{-6} to 10^{-16} ampere. On the most sensitive current scale the uncertainty was 5×10^{-17} ampere.

The target gas handling system is shown in Fig. 3. The gas leaks from a low-pressure reservoir, passes through a liquid air trap, and enters the scattering chamber. An oil diffusion pump competes with the leak and this shortens the time required to reach equilibrium pressure. A separate closed line leads from the scattering chamber to the pressure measuring gauges. There is no flow of gas in this line and the pressures, which were measured by the McLeod gauge, are therefore the pressures at the scattering chamber.

4. DATA

The value of I/N was found by dividing the current observed at a given angle θ by the main beam current. The value of N was obtained by setting the collector to zero angle and reading the current. The current I at the angle θ would then be measured several times and averaged. Then the apparatus would be returned to zero angle and the beam current N recorded again. If more than a 10 percent change had occurred in N,

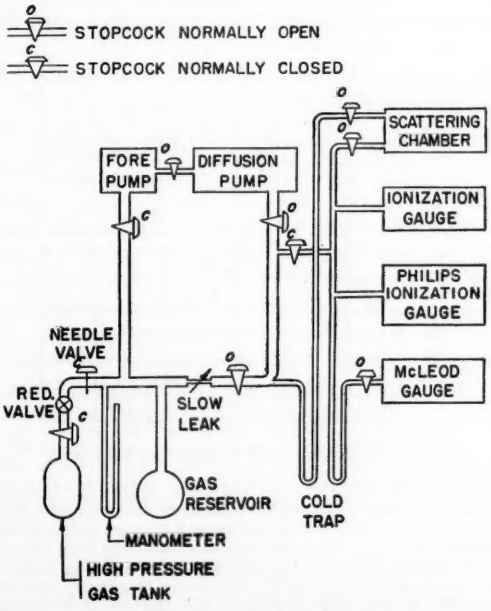

FIG. 3. The target gas handling system.

[7] Everhart, Carbone, and Stone, Technical Report No. 1 to Office of Ordnance Research, January 15, 1954 (unpublished).
[8] Moak, Reese, and Good, Nucleonics 9, 18 (1951).

the point would be repeated. This process was followed for each point or pair of points. The values of N were in the range of 10^{-7} amperes and I was between 10^{-10} and 10^{-16} ampere for most of the points.

The measurements were made on each side of zero angle up to 38° on one side and to 20° on the other. The values of I/N were plotted against θ, and the zero for θ was taken as the angle about which the curves measured on either side of the center were symmetrical. The angular resolution is approximately $\Delta\theta$ which was 0.04 radian, or 2.3°. The lengths y_1 and y_2 were 1.90 and 4.67 cm respectively, so that the geometrical factor $y_0(\Delta\theta)^3$, calculated using Eq. (3), was 2.06×10^{-4} cm.

A measurement of pressure and of temperature allowed the target gas concentration n to be calculated. The pressures were in the range of 0.5 to 3 microns of mercury, measured to an accuracy of 5 percent. The target gas was analyzed with a mass spectrograph and and found to be better than 99.9 percent pure argon.

The values of the cross sections, calculated from the data by using Eqs. (6) and (7), are plotted in Fig. 4 for collisions of singly ionized helium ions with stationary argon atoms at energies of 25, 50, and 100 kev. Figures 5 and 6 are the same except that the incident particles are singly ionized neon ions and argon ions respectively. The cross sections calculated from the data in this way should be independent of target gas pressure if this pressure is low enough. The extent to which this is true is seen on the figures. Each set of points represents data taken at two different pressures as given in the caption.

The differential cross section plotted for each point is the average cross section over the two degree angular resolution. The over-all accuracy assigned to the cross sections is ±30 percent. The curves are so steep that it would be difficult to assign a smaller uncertainty unless the angular resolution were made smaller.

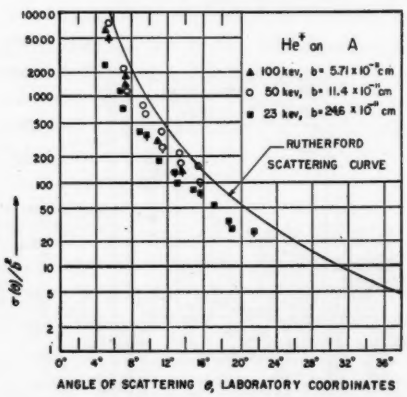
He+ on A
▲ 100 kev, b= 5.71 x 10⁻⁹ cm
○ 50 kev, b= 11.4 x 10⁻⁹ cm
■ 23 kev, b= 24.6 x 10⁻⁹ cm
RUTHERFORD SCATTERING CURVE
σ(θ)/b²
ANGLE OF SCATTERING θ, LABORATORY COORDINATES

FIG. 4. Differential cross-section measurements for scattering of positive charge from single collisions of He^+ ions with argon atoms. The ratio of this cross section to the square of the collision diameter is plotted. Each set of points represents data taken at two pressures, the points for the higher pressure being indicated by a small stem on the symbol. In microns of mercury, the pressures were 2.65 and 0.89 at 100 kev, 2.06 and 0.69 at 50 kev, and 2.65 and 0.89 at 23 kev.

5. DISCUSSION

If the scattering were due only to the Coulomb repulsion between the two colliding nuclei, and if there were no change in charge during the collision, all measured curves of $\sigma(\theta)/b^2$ would lie on top of one another, regardless of the energy. In the center-of-mass coordinate system the theoretical value for this is given by the Rutherford scattering formula $\sigma_0(\theta_0)/b^2=\frac{1}{16}\times\csc^4(\theta_0/2)$, but this must be transformed to the laboratory coordinate system[9] by using the appropriate value of the mass ratio γ. These Rutherford curves have been plotted for comparison on each of the figures.

In Figs. 4, 5, and 6, the curves taken at lower energies generally lie below those taken at higher energies. This effect is most pronounced in the case of argon ions incident on argon atoms and least pronounced in the case of helium ions incident on argon. This departure from Rutherford scattering is interpreted as being due to the electron screening, which should become important when the characteristic length b becomes comparable with atomic dimensions.[2] As seen by inspection of Eq. (7), this length becomes larger at the lower energies and higher atomic numbers. Thus for 100-kev helium ions incident on argon, the calculated value of b is 0.00571×10^{-8} cm, which is much smaller than the dimensions of either atom. At the opposite extreme, for 25-kev argon ions incident on argon, the value of b is 0.373×10^{-8} cm, a size which is comparable with the dimensions of these atoms.

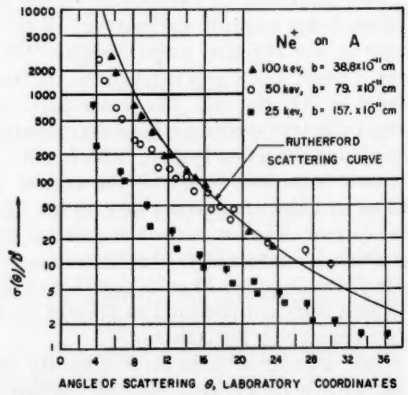
Ne+ on A
▲ 100 kev, b= 38.8x10⁻⁹ cm
○ 50 kev, b= 79. x10⁻⁹ cm
■ 25 kev, b= 157. x10⁻⁹ cm
RUTHERFORD SCATTERING CURVE
σ(θ)/b²
ANGLE OF SCATTERING θ, LABORATORY COORDINATES

FIG. 5. Differential cross-section measurements for scattering of positive charge from single collisions of Ne^+ ions with argon atoms. The ratio of this cross section to the square of the collision diameter is plotted. Each set of points represents data taken at two pressures, the points for the higher pressure being indicated by a small stem on the symbol. In microns of mercury, the pressures were 2.15 and 0.53 at 100 kev, 2.65 and 0.53 at 50 kev, and 2.10 and 0.61 at 25 kev.

[9] See, for example, L. I. Schiff, *Quantum Mechanics* (McGraw-Hill Book Company, Inc., New York, 1949), Chap. V, Sec. 18.

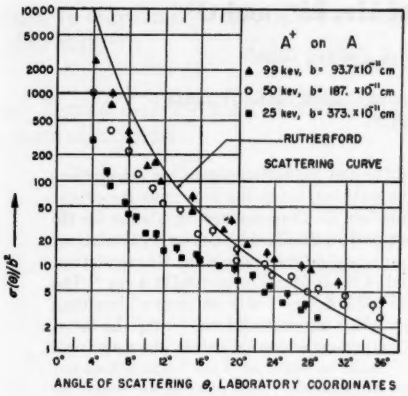

FIG. 6. Differential cross-section measurements for scattering of positive charge from single collisions of A^+ ions with argon atoms. The ratio of this cross section to the square of the collision diameter is plotted. Each set of points represents data taken at two pressures, the points for the higher pressure being indicated by a small stem on the symbol. In microns of mercury, the pressures were 2.94 and 0.67 at 99 kev, 2.64 and 0.69 at 50 kev, and 2.60 and 0.69 at 25 kev.

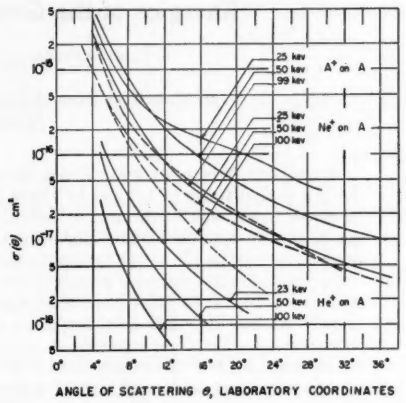

FIG. 7. Differential cross sections in square centimeters for scattering of positive charge from large-angle collisions.

The points in Fig. 4 for the 100-kev helium ions incident on argon lie below the Rutherford curve by a factor of about two. As we have seen above, this cannot be accounted for by electron screening in this case. Although this could be explained by an unsuspected systematic error of a factor of two in our measurements, it is more likely to be accounted for by charge exchange during the collision process. An effect of this magnitude would be observed if about half of the scattered helium atoms were neutral.[10]

There is the criterion, mentioned in Sec. 1, that ionization and charge exchange are most likely when the velocity of the incident ion is comparable with the classical orbital electron velocities.[1] An elementary calculation shows that this is fulfilled in the energy range of these experiments. In Fig. 5, the measured cross section for 50-kev neon ions scattered from argon at large angles is higher than one would expect from the form of the other curves. Possibly there is a maximum in the ionization probability at that energy. The cross section shown in Fig. 6 for scattering charge from the collisions of argon atoms at 100 kev is higher than the Rutherford curve at large angles. This indicates that the average scattered particle is more than singly charged for these particular collisions.

[10] E. Snitzer [Phys. Rev. 89, 1237 (1953)] has indeed observed that a 100-kev helium beam in argon is 53 percent neutral after multiple collisions at zero angle. This may be compared with our data which indicates that a similar ratio may hold for single collisions at large angles.

The scattering apparatus described here would also measure the current due to the recoil target particle if this particle were ionized by the collision. Most of the recoil particles are scattered with low energies at 90°, but there are a few scattered at smaller angles with considerable energy.[1] For Rutherford scattering, the ratio of the cross section for the recoil target particle to that for the scattered incident particle[11] is less than 0.03 for angles less than 30°. This ratio increases until it is unity at about 45°, and as the 90° angle is approached, practically all the current is due to the recoil particles. In our apparatus the maximum angle is 38°, at which angle a small fraction of the current may be due to the recoil particles.

The curves of $\sigma(\theta)/b^2$ do not show easily how the absolute cross section depends on the energy or the kind of ion since the value of b is different for each curve. To show this, the differential cross sections in square centimeters have been plotted in Fig. 7. The scatter of the individual points is not shown, since this was given in the preceding figures. The curves shown are smooth lines drawn through the data. The cross sections for the helium collisions vary about as the inverse square of the energy and as the inverse fourth power of the angle, as would be expected since these data follow the Rutherford law approximately. The other curves are not as regular, although it is seen that generally the cross sections are largest for the heavier ions at the lower energies. The curve for 50-kev neon seems to lie too high and this exception to the rule might be explained, as above, in terms of the dependence of ionization probability on energy.

[11] Everhart, Stone, and Carbone, Technical Report No. 2 to Office of Ordnance Research, April 20, 1954 (unpublished). This is readily calculated from the Rutherford formulas for the scattered and recoil cross sections. See reference 9 also.

Energies of the Ground States of He, Li^+, and O^{6+}

S. CHANDRASEKHAR, *University of Chicago, Chicago, Illinois*
AND
G. HERZBERG, *Division of Physics, National Research Council, Ottawa, Canada*

(Received February 7, 1955)

A complete 14-parameter calculation for the ground state of He and similar 10-parameter calculations for the ground states of Li^+ and O^{6+} have been carried out. In addition, using the four most important of eleven terms, which were tried individually as fifteenth parameters, an 18-parameter calculation for He has been carried out but without minimizing against the scale parameter k. Similar 12-parameter calculations were carried out for Li^+ and O^{6+} using the two most important terms beyond the tenth in the He calculation. As a result, the 18-parameter nonrelativistic ionization potential of He is found to be 198311.4 cm^{-1}. The series of 6, 10, 14, 18 parameter values appears to converge to $198312._2$ cm^{-1} with an error of less than 2 cm^{-1}. Adding the relativistic corrections yields $198310._4$ cm^{-1} which agrees to 0.1 cm^{-1} with the latest experimental value. Considering the uncertainties of the theoretical and experimental values, the magnitude of the Lamb shift of the ground state of He (compared to He^+) must be less than 3 cm^{-1} which does not contradict present theoretical estimates. Similar agreements but within wider limits of error are found for the 12-parameter energy values of the ground states of Li^+ and O^{6+}.

A. INTRODUCTION

HYLLERAAS' well-known method of obtaining the energy of the ground state of helium has recently been carried to a higher (tenth) approximation than previously available.[1] This work showed that Hylleraas' earlier eighth approximation energy contained an error[2] and that the agreement between theory and experiment is not as good as previously believed. By assuming the mass polarization and relativistic corrections of Bethe[3] and Eriksson[4] respectively, a difference between observed and theoretical ionization potential of He of 25 cm^{-1} was found. It was suggested that this discrepancy might be due to an electromagnetic shift (opposite in direction to the Lamb shift) or to incomplete mass polarization or relativistic corrections or to a failure of the tenth approximation in approaching the correct nonrelativistic value. Since the publication of our previous paper, the relativistic corrections have been studied by Sucher and Foley.[5] They found that a term that may be interpreted as a spin-spin interaction had been neglected in the earlier treatments. It amounts to 4 cm^{-1} but is of such a sign that the discrepancy between theory and experiment is increased rather than decreased, i.e., is 29 rather than 25 cm^{-1}. The question of the mass polarization has been studied anew by Wilets[6] who obtained a slightly smaller correction than given by Bethe.[3]

Even before the new relativistic correction was known, work was started to carry the nonrelativistic Hylleraas calculation to still higher orders. When the preliminary results of these calculations were presented at the Rydberg Centennial Symposium at Lund, we learned that Hylleraas[2] had independently carried out similar calculations arriving at very similar results. In view of the importance of the subject and the ever-present possibility of numerical mistakes in the extensive calculations, it appeared worth while to complete and publish our calculations independently of Hylleraas' new work.

B. HYLLERAAS FUNCTIONS AND CORRESPONDING ENERGIES OF THE GROUND STATE OF He

The Hylleraas type of wave function is of the form

$$\psi=\mathfrak{N}e^{-\frac{1}{2}ks}\sum c_{lmn}k^{l+m+n}s^l t^m u^n, \tag{1}$$

where s, t, and u are related to the distances r_1, r_2, and r_{12} (measured in atomic units) of the two electrons from the nucleus and from each other, respectively, by

$$s=r_1+r_2, \quad t=r_2-r_1, \quad u=r_{12}. \tag{2}$$

$\mathfrak{N}$ is a normalization constant and k and the c_{lmn} are constants which are to be adjusted so that the energy

TABLE I. Constants of 14-parameter wave function (14) for the ground state of He.

k (input)	3.85	3.75
E (input)	−2.90370	−2.90370
k from (8)	3.8499301	3.7500555
E from (8)	−2.90370063	−2.90370089
β	+0.39836744	+0.39601198
γ	+0.17742685	+0.17483693
δ	+0.011878857	−0.041079523
ϵ	+0.020414801	+0.024913648
ζ	−0.11994054	−0.11315715
χ_6	+0.077281607	+0.054080045
χ_7	−0.084952179	−0.074771058
χ_8	+0.022483449	+0.021974359
χ_9	+0.014528286	+0.012947629
χ_{10}	+0.042902881	+0.030114033
χ_{11}	+0.0012248967	−0.0012596415
χ_{12}	−0.00010041525	−0.00010267038
χ_{13}	−0.0020615103	−0.0020306527
$\mathfrak{N}$	1.3617172	1.3633714

[1] Chandrasekhar, Elbert, and Herzberg, Phys. Rev. **91**, 1172 (1953), henceforth referred to as I.
[2] See also E. Hylleras, Proc. Rydberg Centennial Conference, Lund, Sweden, July, 1954, p. 83.
[3] H. A. Bethe in Geiger-Scheel's *Handbuch der Physik* (Verlag Julius Springer, Berlin, 1933), second edition, Vol. 24, Part 1.
[4] M. A. S. Eriksson, Z. Physik **109**, 762 (1938).
[5] J. Sucher and H. M. Foley, Phys. Rev. **95**, 966 (1954).
[6] L. Wilets (private communication).

is minimized. In order to be minimized with regard to the c_{lmn}, the energy E must fulfill the determinantal equation (see Bethe[3]):

$$|k^2M_{ij}-kL_{ij}-EN_{ij}|=0. \tag{3}$$

Here i and j stand each for a set of numbers, $l_im_in_i$ and $l_jm_jn_j$ respectively, and M_{ij}, L_{ij}, and N_{ij} are the following sums of integrals:

$$\begin{aligned}M_{ij}=&+(l_il_j-m_im_j+l_in_j+n_il_j-m_in_j-n_im_j)\times[l_i+l_j\ ,\ m_i+m_j\ ,\ n_i+n_j+1]\\&-0.5(l_i+l_j+n_i+n_j)\times[l_i+l_j+1,\ m_i+m_j\ ,\ n_i+n_j+1]\\&-(n_in_j+l_in_j+n_il_j)\times[l_i+l_j\ ,\ m_i+m_j+2,\ n_i+n_j-1]\\&+(n_in_j+m_in_j+n_im_j)\times[l_i+l_j+2,\ m_i+m_j\ ,\ n_i+n_j-1]\\&+0.5(l_i+l_j)\times[l_i+l_j-1,\ m_i+m_j+2,\ n_i+n_j+1]\\&+0.5(n_i+n_j)\times[l_i+l_j+1,\ m_i+m_j+2,\ n_i+n_j-1]\\&-l_il_j\times[l_i+l_j-2,\ m_i+m_j+2,\ n_i+n_j+1]\\&+m_im_j\times[l_i+l_j+2,\ m_i+m_j-2,\ n_i+n_j+1]\\&+0.25\times[l_i+l_j+2,\ m_i+m_j\ ,\ n_i+n_j+1]\\&-0.25\times[l_i+l_j\ ,\ m_i+m_j+2,\ n_i+n_j+1],\end{aligned} \tag{4}$$

$$N_{ij}=[l_i+l_j+2,\ m_i+m_j,\ n_i+n_j+1]-[l_i+l_j,\ m_i+m_j+2,\ n_i+n_j+1], \tag{5}$$

$$\begin{aligned}L_{ij}=&4Z[l_i+l_j+1,\ m_i+m_j,\ n_i+n_j+1]-[l_i+l_j+2,\ m_i+m_j\ ,\ n_i+n_j]\\&+[l_i+l_j\ ,\ m_i+m_j+2,\ n_i+n_j],\end{aligned} \tag{6}$$

where Z is the nuclear charge ($=2$ for He). The brackets $[a,b,c]$ stand for the integrals

$$[a,b,c]=\int\int\int e^{-s}s^at^bu^c\,ds\,du\,dt=\frac{(a+b+c+2)!}{(b+1)(b+c+2)}. \tag{7}$$

The determinantal equation (3) must be solved for several values of k until E is minimized against k also. A check on the correctness of k and E is obtained from the formulas

$$k=L/2M,\quad E=L^2/4MN, \tag{8}$$

where

$$L=2\sum_{i,j}c_ic_jL_{ij},\quad M=2\sum_{i,j}c_ic_jM_{ij},\quad N=2\sum_{i,j}c_ic_jN_{ij}. \tag{9}$$

Here the c_i, c_j are the coefficients c_{lmn} derived from the secular determinant with the best E.

In I, the ten-parameter function

$$\begin{aligned}\psi=\mathfrak{N}e^{-\frac{1}{2}ks}(1+\beta u+\gamma t^2+\delta s+\epsilon s^2+\zeta u^2+\chi_6su\\+\chi_7t^2u+\chi_8u^3+\chi_9t^2u^2)\end{aligned} \tag{10}$$

was used and an energy value for the ground state of He of

$$E=-2.903603 \text{ atomic units} \tag{11}$$

with $k=3.51$ was obtained.[7]

By adding the four terms

$$\chi_{10}t^4+\chi_{11}t^6+\chi_{12}t^4u^2+\chi_{13}t^2u^4 \tag{12}$$

to the bracket in (10), i.e., using a 14-parameter function and minimizing, an energy value of

$$E=-2.903629 \text{ atomic units} \tag{13}$$

was obtained. Here $k=3.53$ was assumed and no minimizing with regard to k was attempted (see, however, below).

In view of the smallness of the decrease of the energy in adding the terms (12), an attempt was made to ascertain whether perhaps other terms might have a larger effect. For this purpose, a fifteenth column was added to the secular determinant in turn corresponding to a term in u^4, or s^3, or t^2u^3, or st^2 and each time the energy was evaluated. The difference of the resulting E values from the value (13) indicated the relative importance of the terms considered. Similarly, the importance of the various terms (12) was ascertained by dropping the particular column of the secular determinant and finding the effect on the energy. In this way, it was found that the contributions of the terms in t^4, t^6, t^4u^2 are small[8] compared to those in t^2u^4, u^4, s^3, and st^2. Therefore, the following 14-parameter function was finally chosen:

$$\begin{aligned}\psi=\mathfrak{N}e^{-\frac{1}{2}ks}(1+\beta u+\gamma t^2+\delta s+\epsilon s^2+\zeta u^2+\chi_6su+\chi_7t^2u\\+\chi_8u^3+\chi_9t^2u^2+\chi_{10}st^2+\chi_{11}s^3+\chi_{12}t^2u^4+\chi_{13}u^4.\end{aligned} \tag{14}$$

With $k=3.53$, this gave an energy value of

$$E=-2.903690 \text{ atomic units.} \tag{15}$$

The test of relation (8) showed that the assumed k value was not yet correct and several further (14×14) determinantal equations with different k values had to be solved. In Table I the coefficients, normalization constants and k and E values obtained from (8) are given for two sets of input values E and k near the

[7] The values for the normalization constant $\mathfrak{N}$ given in the last column of Table I of I are erroneous and should be replaced by 1.359625, 1.359841, and 1.360462.

[8] The term t^2u^3 was also found to be of little importance at this stage. However, later on it was found that a numerical error had occurred in the calculation for t^2u^3 and that actually t^2u^3 is more important than t^2u^4 as shown by the 18-parameter function given below.

TABLE II. Effect of adding various parameters to the 14-parameter Hylleraas function (14) with $k=3.85$.

Term added	E atomic units	ΔE 10^{-6} atomic units
...	−2.9037007	0
s^2u	−2.9037011	−0.4
su^2	−2.9037010	−0.3
s^4	−2.9037076	−6.9
s^3t^2	−2.9037036	−2.9
st^2u	−2.9037032	−2.5
t^4	−2.9037015	−0.8
t^2u^3	−2.9037070	−6.3
u^5	−2.9037076	−6.9
t^6	−2.9037014	−0.7
t^4u^2	−2.9037013	−0.6
$s^{-1}u$	−2.9037025	−1.8
$t^2u^3+u^5$	−2.9037098	−9.1
$s^4+s^3t^2+t^2u^3+u^5$	−2.9037162	−15.5

minimum. By interpolation from the corresponding values of the determinant (3), one obtains for the minimum:

$$k=3.80, \quad E=-2.903701 \text{ atomic units.} \qquad (16)$$

By comparing with (15), it is seen that the effect on the energy of minimizing with respect to k is small.

In order to see what influence on the energy the addition of still higher terms in the series (1) might have, various trial terms were again added in turn to the 14-parameter function (14) as a fifteenth term and the energy determined in each case for $k=3.85$. This envolved only the addition of a single column to the Gaussian algorithm by means of which the 14×14 determinants had been solved for $E=-2.90370$ and $E=-2.90371$. The results are shown in Table II. Only five terms give a noticeably different energy: u^5, s^4, t^2u^3, s^2t^2, and st^2u (in order of decreasing importance). The term $s^{-1}u$ was tried at the suggestion of Professor H. M. James (Purdue University) since he had found it of importance in a low-order approximation; but this term turned out to be unimportant in a 15-parameter function (see Table II).

If the four most important terms of Table II, *viz.*, u^5, s^4, t^2u^3, s^2t^2, are simultaneously added to the 14-parameter function (14), the following 18-parameter energy value is obtained:

$$E=-2.903716 \text{ atomic units.} \qquad (17)$$

It should be noted that this value deviates from the 14-parameter value by much less than the sum of the four individual corrections taken from Table II (−15.5 against -23.0×10^{-6}). This gives one confidence that the other terms of Table II, if they were simultaneously added, would change the energy by less than the sum of the corrections of each term separately, that is, a 25-parameter value including all the terms in Table II would be between the value just given and

$$E=-2.903723 \text{ atomic units.} \qquad (18)$$

It must be emphasized that the 18-parameter value (17) has been obtained with an assumed k-value, which is close to the minimum in the 14-parameter solution (16). From the change of E with k found there, it appears quite safe to conclude that minimizing of the 18-parameter value against k will change it by less than 0.000005. At the present stage, it did not seem worthwhile to carry through this minimizing process.

TABLE III. Constants of an 18-parameter wave function for the ground state of helium:

$$\psi=\mathfrak{N}e^{-\frac{1}{2}ks}(1+\beta u+\gamma t^2+\delta s+\epsilon s^2+\zeta u^2+\chi_6 su+\chi_7 t^2u+\chi_8 u^3+\chi_9 t^2u^2 +\chi_{10}st^2+\chi_{11}s^3+\chi_{12}t^4u+\chi_{13}u^4+\chi_{14}u^5+\chi_{15}t^2u^3+\chi_{16}s^2t^2+\chi_{17}s^4).$$

k (input)	3.85	χ_8	+0.045441323
E (input)	2.90371	χ_9	+0.043516169
k from (8)	3.8499613	χ_{10}	+0.028227870
E from (8)	2.9037063	χ_{11}	+0.0071384413
β	+0.41389641	χ_{12}	+0.00050273143
γ	+0.21197114	χ_{13}	−0.0099342061
δ	+0.029010815	χ_{14}	+0.00093063179
ϵ	+0.0050395758	χ_{15}	−0.0075260852
ζ	−0.14909338	χ_{16}	+0.0030749706
χ_6	+0.079148647	χ_{17}	−0.00080572559
χ_7	−0.12587484	$\mathfrak{N}$	1.3504631

TABLE IV. Constants of 10-parameter wave functions (10) of Li^+ and O^{6+}.

	Li^+		O^{6+}	
k (input)	5.60	5.70	16.40	16.48
k from (8)	5.600055	5.699877	16.400023	16.479994
E (input)	7.279760	7.279770	59.15640	59.156405
E from (8)	7.2797624	7.2797596	59.156413	59.156422
β	+0.3598049	+0.3602588	+0.3771723	+0.3776096
γ	+0.2385639	+0.2569460	+0.6751016	+0.6935819
δ	−0.08864538	−0.04417829	+0.2922311	+0.3283520
ϵ	+0.01678235	+0.01818171	+0.1349207	+0.1569268
ζ	−0.1303588	−0.1370898	−0.5061933	−0.5152307
χ_6	+0.05504580	+0.07733141	+0.3317571	+0.3529975
χ_7	−0.09060980	−0.1066555	−0.7846255	−0.8396899
χ_8	+0.01606871	+0.01499941	+0.1682221	+0.1684930
χ_9	+0.01968222	+0.02688445	+0.4678856	+0.5306426
$\mathfrak{N}$	5.750594	5.756579	141.2470	141.2869

The coefficients of the 18-parameter function nearest to the minimum are given in Table III. It should be noted that the k value from (8) is slightly less than the input value indicating that the best k value is less than 3.85.

C. HYLLERAAS FUNCTIONS AND CORRESPONDING ENERGIES OF THE GROUND STATES OF Li^+ AND O^{6+}

It appears of interest to carry through the Hylleraas calculation for some other two-electron systems. Li^+ and O^{6+} were chosen for this study and a 10-parameter calculation carried out similar to that for He in I. As may be seen from Eqs. (4)–(6), the quantities M_{ij} and N_{ij} in the determinantal equation (3) are the same as for He and only L_{ij} is different. Solving in the same way as for He, the sets of coefficients and corresponding energy values given in Table IV were found. By interpolation one obtains from the E and k values of Table IV and the values of 10×10 determinants

calculated for several other E values:

$$\begin{aligned} &\text{For } Li^+: \quad E=-7.279763, \quad k=5.63, \\ &\text{For } O^{6+}: \quad E=-59.156404, \quad k=16.48. \end{aligned} \tag{19}$$

The k value found for O^{6+} is remarkable since it is larger than $2Z$ which would be the k value in the absence of mutual interaction of the two electrons. It is also noteworthy that for high Z the coefficients $\beta, \gamma, \cdots, \chi_9$ decrease much less rapidly than for low Z.

If the two most important terms beyond the tenth, $s^{\prime 2}$ and s^3, as judged from the He calculation, are added and a 12-parameter calculation carried out for Li^+ with $k=5.60$ and for O^{6+} with 16.4, the following energy values are obtained:

$$\begin{aligned} &Li^+: \quad E=-7.27982_5 \text{ atomic units}, \\ &O^{6+}: \quad E=-59.15648_6 \text{ atomic units}. \end{aligned} \tag{20}$$

Since the energy depends only slightly on k (see Table IV), it would appear that minimizing against k will only very slightly lower the energy values (20) which may therefore be safely considered as 12-parameter values.

After completing these calculations, a paper by Eriksson[9] came to our notice in which the author gives, as a 13-parameter value for Li^+, $E=-7.27984_4$ which agrees most satisfactorily with our value. The terms in (1) used by Eriksson are the same as those used by us except that he has added u^4. He does not give the coefficients in the eigenfunction.

D. DISCUSSION

In going from a Hylleraas wave function with 6 parameters to one with 10, 14, and finally 18 parameters, the nonrelativistic energy of the ground state of He changes from

$$\begin{aligned} &-2.90324_0 \text{ to } -2.903603 \text{ to } -2.903701 \\ &\text{to } -2.903716; \end{aligned} \tag{21}$$

that is, there is a fairly good convergence. It will be remembered that the last four terms added have the largest effect on the energy among a considerable number of terms that have been tried. None of the other terms that have been tried give a contribution greater than 0.000002_5 and most of them much less. To be sure, not all of the fifty terms which are possible up to sixth order have been tried, but only those have not been tried for which a similar *lower* order term gave a contribution of less than 0.00001 to the energy, e.g., since s^2t^2 gives only a contribution of 0.0000029, s^2t^8, s^3t^4, $\cdots$, and s^3t^2, s^4t^2, $\cdots$ were not tried since they would be expected to give a contribution much smaller than s^3t^2. As shown previously, the resultant effect of a number of terms is less than additive. Since the terms that have not been used in the 18-parameter function give individual contributions less than 0.000002_5 and, with one exception, less than 0.0000008, it appears probable, as is also suggested by the series of numbers (21), that the energy of the ground state of He converges to -2.90372 atomic units and is almost certainly not below -2.90373. This assumes, of course, that the variation method does converge. Some doubt has been expressed with regard to this by various authors.[10] Even if these doubts were justified, the value (18) still remains an upper limit to the energy.

The energy value obtained in this way refers to a fixed nucleus. The motion of the nucleus is largely taken into account by multiplying by $2R_{He}$ rather than by $2R_\infty$ when converting to wave number units. A small correction, the mass polarization, first discussed by Bethe, has recently been re-evaluated by Wilets[6] to be $+4.1$ cm^{-1} (compared to Bethe's 5.2 cm^{-1}). In this way, subtracting the energy of the ground state of He^+, one obtains from (18) the following *lower* limit for the nonrelativistic ionization potential of He:

$$\text{I.P.}_{\text{n.r.}} \geqslant 198311.4 \text{ cm}^{-1}. \tag{22}$$

This number is 25.9 cm^{-1} higher than the previous lower limit based on the 10-parameter approximation and the old mass polarization.

Assuming the extrapolated convergence suggested above, the energy value would be

$$\text{I.P.}_{\text{n.r.}}^{(\text{extrapol.})} = 198312._3 \text{ cm}^{-1}, \tag{23}$$

with an error probably not greater than ± 2 cm^{-1} and more likely positive than negative.

If one were to use the old relativity correction of Eriksson, i.e., $+2._2$ cm^{-1}, one would obtain Eriksson:

$$\begin{aligned} &\text{I.P.}_{\text{rel}}(\text{He}) \geqslant 198313.6 \text{ cm}^{-1}, \\ &\text{I.P.}_{\text{rel}}^{(\text{extrapol.})}(\text{He}) = 198314._6 \pm 2 \text{ cm}^{-1}. \end{aligned} \tag{24}$$

However, if Sucher and Foley's relativistic correction is used, i.e., -1.9 cm^{-1}, one obtains[11] Sucher-Foley:

$$\begin{aligned} &\text{I.P.}_{\text{rel}}(\text{He}) \geqslant 198309.5 \text{ cm}^{-1}, \\ &\text{I.P.}_{\text{rel}}^{(\text{extrapol.})}(\text{He}) = 198310._4 \pm 2 \text{ cm}^{-1}. \end{aligned} \tag{25}$$

A provisional experimental value obtained by Zbinden and one of us[12] is

$$\text{I.P.}_{\text{exp}}(\text{He}) = 198310._5 \pm 1 \text{ cm}^{-1}. \tag{26}$$

[9] H. A. S. Eriksson, Arkiv. Mat. Astron. Fysik **B30**, No. 6 (1944).

[10] See, for example, Bartlett, Gibbons, and Dunn, Phys. Rev. **47**, 679 (1935); also V. A. Fock, Izvest. Akad. Nauk. S. S. S. R Ser. Fiz. **18**(2), 161 (1954). The objections of Bartlett *et al.* have been refuted by Coolidge and James [Phys. Rev. **51**, 855 (1937)] who have shown that the Hylleraas method does converge to the correct energy value. However, according to Kato [Trans. Am. Math. Soc. **70**, 212 (1951)], Coolidge and James' proof "is not complete from a mathematical standpoint." Kato has established the convergence of the variation method. He considers it as "highly plausible" but not as proven that it converges to the correct energy value.

[11] Here account has been taken of the note added in proof in Sucher and Foley's paper in which one part of the correction (E_2') is doubled.

[12] G. Herzberg and R. Zbinden (unpublished).

TABLE V. Ionization potentials and Lamb shifts of He and He-like ions.

	Ionization potential (cm^{-1}) nonrelativistic	relativistic	observed	Lamb shift (cm^{-1}) obs	calc
He	$198312._3$	$198310._4$	$198310._5$	$+0.1\pm3$	-1.4
Li^+	610049	610087	610079	-8 ± 25	-8.5
O^{6+}	5959957	5963266	5963000	-266 ± 600	-460

The agreement between the experimental value and the extrapolated theoretical value using the Sucher-Foley relativistic correction is surprisingly close, much closer than one would have expected from the combined uncertainty of the theoretical and experimental values. At any rate, the large discrepancy found in I is entirely due to poor convergence of the tenth approximation.

Since the theoretical value (25) is based on the Dirac theory, the difference between the observed and the calculated value would represent an observed value for the electrodynamic (Lamb) shift of the ground state of He beyond that of He^+. This shift comes out to be

$$-4._0\pm3\ cm^{-1} \quad \text{and} \quad +0.1\pm3\ cm^{-1}$$

for the extrapolated values (24) and (25) based on the Eriksson and Sucher-Foley corrections, respectively. There appears to be general agreement that the Sucher-Foley correction is the correct one. Thus, we conclude that the Lamb shift of the ground state of He lies very probably between $+3\ cm^{-1}$ and $-3\ cm^{-1}$. Günther[13] and Håkansson[14] have made rough theoretical estimates of the Lamb shift of He, obtaining -1.6 and $-1.2\ cm^{-1}$, respectively. It is seen that these values are entirely compatible with the observed value. Conversely, if one considers the theoretical Lamb shift as correct, it would indicate that in extrapolating the convergence of the various approximations to the nonrelativistic energy of the He ground state, the effect of the neglected terms has been slightly underestimated (i.e., by $1.5\ cm^{-1}$ or 0.000007 atomic units), which does not seem unreasonable. The extreme limit suggested above (-2.90373 atomic units) would give an "observed" Lamb shift of $-2._1\ cm^{-1}$, that is, the predicted Lamb shift is well bracketed by the observed values following from the extrapolated and the extreme nonrelativistic energies.

For Li^+, the energy value (20) based on a 12-parameter Hylleraas function together with Bethe's mass polarization leads to a nonrelativistic ionization potential:

$$\text{I.P.}_{\text{n.r.}}(Li^+) \geqslant 610049\ cm^{-1}. \tag{27}$$

Sucher and Foley have not calculated the relativistic correction including the spin-spin interaction and we are dependent on Eriksson's old value[15] of $+38\ cm^{-1}$, yielding

$$\text{I.P.}_{\text{rel}}(Li^+) \geqslant 610087\ cm^{-1}. \tag{28}$$

This value agrees remarkably well with Robinson's[16] experimental value of

$$\text{I.P.}_{\text{exp}}(Li^+) = 610079\pm25\ cm^{-1}. \tag{29}$$

The difference obs-calc of $-8\pm25\ cm^{-1}$ would represent an observed value of the Lamb shift of Li^+ (beyond that of Li^{++}). This value agrees with Håkansson's predicted value of $-8.5\ cm^{-1}$ far better than the accuracy of the data warrants. If one uses Eriksson's[10] 13-parameter value, the observed Lamb shift becomes $-12\pm25\ cm^{-1}$.

For O^{6+}, one finds from the 12-parameter energy value (20) the nonrelativistic ionization potential:

$$\text{I.P.}_{\text{n.r.}}(O^{6+}) \geqslant 5959957\ cm^{-1}. \tag{30}$$

In this case, Sucher and Foley[5] have calculated their relativistic correction, obtaining $+3309\ cm^{-1}$, which may be compared with Eriksson's $+4110\ cm^{-1}$. Using the former yields

$$\text{I.P.}_{\text{rel}}(O^{6+}) \geqslant 5963266\ cm^{-1}. \tag{31}$$

The experimental value of Tyrén[17] is

$$\text{I.P.}_{\text{exp}}(O^{6+}) = 5963000\pm600\ cm^{-1}. \tag{32}$$

From these two figures, an observed shift of $-266\pm600\ cm^{-1}$ results which may be compared with Håkansson's predicted value of $-460\ cm^{-1}$.

The results just presented are summarized in Table V. Neither the theoretical nor the experimental values for the ionization potentials of He, Li^+, and O^{6+} are as yet sufficiently precise to obtain reliable values for the Lamb shifts of the ground states of these systems, but the precision is now approaching that required for such a determination. Preparations are being made for an attempt to increase the accuracy of both theoretical and experimental values still further so that a determination of the Lamb shift will become possible.

The extensive computations underlying the present work, all done by desk machines, were carried out by Miss Alma Marcus, Miss Cecile DeChantigny, and Mrs. Sarah Segall at the National Research Council of Canada. Preparatory computations were done by Miss Donna Elbert at the Yerkes Observatory. We are very much indebted to all of them for their care and perseverance in carrying out these long and tedious calculations.

[13] M. Günther, Physica **15**, 675 (1949).
[14] H. E. V. Håkansson, Arkiv. Fysik **1**, 555 (1950).
[15] *Note added in proof.*—According to E. E. Salpeter (private communication), the Sucher-Foley correction for Li^+ amounts to $+14\ cm^{-1}$ leading to $\text{I.P.}_{\text{rel.}}(Li^+) \geq 610\,063\ cm^{-1}$.
[16] H. A. Robinson, Phys. Rev. **51**, 14 (1937).
[17] F. Tyrén, Nova Acta Reg. Soc. Sci. Ups. **12**, nr 1 (1940).

Electron Broadening and Shift of Spectral Lines of Helium*

BENNETT KIVEL†
Sloane Physics Laboratory, Yale University, New Haven, Connecticut, AND University of California, Los Alamos Scientific Laboratory, Los Alamos, New Mexico

(Received December 9, 1954)

The quantum mechanical treatment of electron broadening as used by Kivel, Bloom, and Margenau is extended to include line shifts and is applied to the He I spectrum. The $3d \rightarrow 2p$ line is anomalous, since it has a small Stark shift and consequently a small Holtsmark broadening. For it the electron effects dominate. Comparison of this line's width and shape with others in the He I spectrum provides a simple experimental check on the theory.

I. THEORY

THE methods for treating electron broadening developed by Kivel, Bloom, and Margenau (KBM)[1] are here extended to include line shifts and applied to He I spectrum. In KBM the broadened line was shown to have a Lorentz shape $1/[(\gamma+\gamma_P+\gamma_U)^2+\omega^2]$, the half-width being the sum of natural (γ), universal (γ_U) and polarization (γ_P) contributions. For practical applications the polarization term dominates the broadening. It corresponds to the lack of rigid quantization in the perturbed atom which, shocked out of its initial state by the passing electron, has a shortened lifetime and more uncertain energy.

In this paper we treat the interaction between atom and free electron as a perturbation and expand the Schrödinger Ψ function with plane wave factors for the free electron. This will give γ_U incorrectly, a shortcoming which is not urgent, since in our applications we neglect γ_U, which was shown to be small compared to γ_P in KBM.

The time rate of change of the expansion amplitude of an initially excited state of the atom, state 2, with no photons present and a free electron with wave number vector $\mathbf{k}_\lambda$, is

$$i\hbar\dot{d}_\lambda=\sum_r J_r e^{i\omega t}b_{r\lambda}+\sum_\mu C_{2\lambda,\,2\mu}e^{i\Omega_{\lambda\mu}t}d_\mu+\sum_{n\neq 2}{}'\sum_\mu C_{2\lambda,\,n\mu}e^{i(\omega_{2n}+\Omega_{\lambda\mu})t}n_\mu. \quad (1)$$

The first sum of matrix elements (J_r), of the interaction between radiation field and atom, coupling atomic state 2 to the ground state 1 and a single photon with energy $\hbar\omega_r$, leads in the usual way to spontaneous emission (γ). The second sum over the diagonal collision matrix elements contributes to γ_U. Although the atomic state is undistorted, an energy exchange between electron and the emitted photon is introduced. The last sum couples state 2 to all others (n), giving rise to polarization broadening (which also includes quenching). Several amplitudes appear on the right side of Eq. (1): $b_{r\lambda}$—atom in state 1, photon with energy $\hbar\omega_r$, free electron in state $\mathbf{k}_\lambda$ (with energy $\epsilon_\lambda=\hbar^2k_\lambda^2/2m$); d_μ—atom in state 2, no photons, electron state $\mathbf{k}_\mu$; and n_μ—atom in state n, no photons, electron state $\mathbf{k}_\mu$. The energies involved are

$$\hbar\omega=E_2-E_1-\hbar\omega_r;\quad \hbar\Omega_{\lambda\mu}=\epsilon_\lambda-\epsilon_\mu;\quad \text{and}\quad \hbar\omega_{2n}=E_2-E_n,$$

where E_n is the energy of the atom in state n.

Similar equations exist for each of the amplitudes. They can be used to reduce Eq. (1) to the form

$$i\hbar\dot{d}_\lambda=\sum_\mu C_{2\lambda,\,2\mu}e^{i\Omega_{\lambda\mu}t}\sum_r\int_0^t\frac{1}{i\hbar}C_{2\mu,\,2r}e^{i\Omega_{\mu r}\tau}d_r d\tau+\cdots. \quad (2)$$

The solution of these coupled differential equations is more easily obtained if all terms on the right of Eq. (2) with amplitudes other than the one on the left (d_λ) can be neglected. This is a valid procedure if one can average over arbitrary phases associated with these amplitudes. Since the electrons come from different sources (i.e., are incoherent), the d_r have factors $\exp(i\phi_r)$ containing unrelated arbitrary phases ϕ_r. An average over these phases leads to the cancellation of all terms on the right of Eq. (2) except the one with d_λ. To see this, consider the simpler example of a similar differential equation:

$$\dot{a}e^{i\phi}=Ae^{i\phi}+Be^{i\phi'}.$$

Assuming this to be true when averaged over ϕ and ϕ', one obtains $\dot{a}=A$.

Thus Eq. (1) becomes

$$\dot{d}_\lambda=-\frac{1}{\hbar^2}\left\{\sum_r|J_r|^2\int_0^t e^{i\omega(t-\tau)}d_\lambda(\tau)d\tau+\sum_\mu|C_{2\lambda,\,2\mu}|^2\int_0^t e^{i\Omega_{\lambda\mu}(t-\tau)}d_\lambda(\tau)d\tau+\sum_n{}'\sum_\mu|C_{2\lambda,\,n\mu}|^2\int_0^t e^{i(\omega_{2n}+\Omega_{\lambda\mu})(t-\tau)}d_\lambda(\tau)d\tau\right\}. \quad (3)$$

The solution,

$$d_\lambda=a_\lambda\exp(-\gamma_2+i\delta_2)t, \quad (4)$$

* Supported under the auspices of the U. S. Atomic Energy Commission. Part II of this paper is contained in a dissertation presented for the degree of Doctor of Philosophy in Yale University.

† Now at the Los Alamos Scientific Laboratory, Los Alamos, New Mexico.

[1] Kivel, Bloom, and Margenau, Phys. Rev. 98, 495 (1955).

of Eq. (3) is sought. The quantity γ_2 contributes to the spectral line width and δ_2 shifts the line center.

The summations over r and μ on the right side of Eq. (3) can be replaced by an integral over energy and a sum over degenerate states. Then using Eq. (4), one obtains the equation for d_λ in the form,

$$\dot{d}_\lambda=\left\{\int_{-\infty}^{+\infty}f(y)\left[\int_0^t e^{[i(y-\delta_2)+\gamma_2](t-\tau)}d\tau\right]dy\right\}d_\lambda$$

$$=\left\{\int_{-\infty}^{+\infty}f(y)\left[\frac{e^{[i(y-\delta_2)+\gamma_2]t}-1}{i(y-\delta_2)+\gamma_2}\right]dy\right\}d_\lambda; \quad (5)$$

$f(y)$ is a sum over degenerate states; e.g., see Eq. (7) where

$$\sum_\mu|C_{2\lambda,n\mu}|^2=\int_{-\infty}^{+\infty}f(y)dy \quad \text{and} \quad y=\omega_{2n}+\Omega_{\lambda\mu}.$$

It is usually assumed that $|J_r|^2$ varies slowly with the photon energy, and that the corresponding $f(y)$ in Eq. (5) can be given its resonance value,[2] i.e.,

$$f_J(\delta_2)\int_{-\infty}^{+\infty}\left\{\frac{e^{[i(y-\delta_2)+\gamma_2]t}-1}{i(y-\delta_2)+\gamma_2}\right\}dyd_\lambda$$

$$=\pi f_J(\delta_2)d_\lambda=-\gamma d_\lambda. \quad (6)$$

Here the factor γ is real, since $f_J(y)$ is real; and radiative decay contributes the natural width γ to γ_2.

In KBM, this same approximation was used for the collision matrix elements. However, it was seen that some matrix elements had logarithmic variations. For these matrix elements a resonance approximation is not strictly valid. The more detailed analysis below shows that in addition to a real part γ_P, there is an imaginary term $i\delta_2$.

Following KBM, we write

$$\sum_\mu|C_{2\lambda,n\mu}|^2=\int\frac{V}{(2\pi)^3}d\mathbf{k}_\mu$$

$$\times\left|\int\int\frac{e^{i\mathbf{K}\cdot\mathbf{R}}}{V}\psi_2^*\psi_n\left(\frac{e^2}{|\mathbf{R}-\mathbf{r}|}-\frac{e^2}{|\mathbf{R}|}\right)d\mathbf{r}d\mathbf{R}\right|^2$$

$$=\frac{V}{(2\pi)^2}\frac{m}{2\hbar k_\lambda}\int_{-\infty}^{+\infty}dy\int_{(k_\lambda-k_\mu)^2}^{(k_\lambda+k_\mu)^2}dK^2$$

$$\times\left|\frac{4\pi e^2}{VK^2}\int(e^{i\mathbf{K}\cdot\mathbf{r}}-1)\psi_2^*\psi_n d\mathbf{r}\right|^2, \quad (7)$$

where $\mathbf{k}_\mu$=final wave number vector of electron, $\mathbf{K}=\mathbf{k}_\mu-\mathbf{k}_\lambda$=momentum transfer vector, V=reciprocal of electron density n, ψ=atomic function, $\mathbf{r}(\mathbf{R})$=position vector of atomic (free) electron from nucleus, and $y=\omega_{2n}+\Omega_{\lambda\mu}$.

[2] G. Wentzel, *Handbuch der Physik* (Verlag Julius Springer, Berlin, 1933), second edition, Vol. 24.1, p. 753.

For small $\mathbf{K}$, we expand

$$e^{i\mathbf{K}\cdot\mathbf{r}}=1+i\mathbf{K}\cdot\mathbf{r}+\cdots.$$

Since the ψ are orthogonal, the leading term survives only in the diagonal elements where it is canceled by the nuclear interaction term. The next term leads to polarization broadening. Retaining this term only, since the K^{-4} factor weights small K heavily,

$$\frac{\sum_\mu|C_{2\lambda,n\mu}|^2}{\hbar^2}\cong\frac{2}{V}\frac{me^4}{\hbar^3k_\lambda}\frac{1}{3}\left|\int\psi_2^*\psi_n r\right.$$

$$\left.\times\cos\theta d\mathbf{r}\right|^2\int_{-\infty}^{+\infty}2\ln\left|\frac{k_\lambda+k_\mu}{k_\lambda-k_\mu}\right|dy$$

$$=\frac{2nv_\lambda\sigma_\lambda}{3\pi}\left(\frac{z_{2n}}{a}\right)^2\int_{-\infty}^{+\infty}2\ln\left|\frac{k_\lambda+k_\mu}{k_\lambda-k_\mu}\right|dy,$$

where

$$z_{2n}\equiv\int\psi_2^*\psi_n r\cos\theta d\mathbf{r},$$

$$\sigma_\lambda=\pi/k_\lambda^2.$$

The factor $\frac{1}{3}$ enters when an average is taken over the random orientation of the atom with respect to the direction of the incident electron.

The coefficient of d_λ on the right side of Eq. (5) is

$$\frac{-2nv_\lambda\sigma_\lambda}{3\pi}\left(\frac{z_{2n}}{a}\right)^2\int_{-\infty}^{+\infty}2\ln\left|\frac{k_\lambda+k_\mu}{k_\lambda-k_\mu}\right|$$

$$\times\left\{\frac{e^{[i(y-\delta_2)+\gamma_2]t}-1}{i(y-\delta_2)+\gamma_2}\right\}dy. \quad (8)$$

We introduce a new variable of integration,

$$Y=(y-\delta_2)/|\omega_{2n}-\delta_2|.$$

Our treatment will be restricted to nondegenerate states where $\omega_{2n}\gg\delta_2$. Then,

$$\frac{k_\lambda+k_\mu}{k_\lambda-k_\mu}=\frac{\hbar(k_\lambda+k_\mu)^2}{2m(Y\mp1)(|\omega_{2n}-\delta_2|)},$$

where the $-(+)$ sign corresponds to $\omega_{2n}-\delta_2>0$ ($\omega_{2n}-\delta_2<0$). The integral in Eq. (8) is simplified by use of a resonance approximation for the slowly varying part of the logarithm, namely,

$$2\pi\ln\left[\frac{\hbar(k_\lambda+k_{\mu'})^2}{2m(|\omega_{2n}-\delta_2|)}\right]$$

$$-\int_{-\infty}^{+\infty}2\left[\frac{e^{[iY+\Gamma]T}-1}{iY+\Gamma}\right]\ln|Y\mp1|dY, \quad (9)$$

provided $k_{\mu'}$ is the resonance value

$$k_{\mu'}{}^2=(2m/\hbar)(\omega_{2n}-\delta_2)+k_\lambda^2,$$

and, by definition,

$$\Gamma\equiv\gamma_2/|\omega_{2n}-\delta_2|$$
$$T\equiv t(|\omega_{2n}-\delta_2|).$$

The resonance approximation is not satisfactory for $2\ln|Y\mp1|$ which diverges at $Y=\pm1$. With this factor the integral in Eq. (9) has an imaginary part. First we evaluate the imaginary part of the first term in the integrand, which is on the order of $\Gamma\ll1$; i.e.,

$$-\mathrm{Im}\int_{-\infty}^{+\infty}\{2\ln|Y\mp1|\exp[(iY+\Gamma)T]\}/(iY+\Gamma)dY=O(\Gamma).$$

To show this we define

$$I(a)\equiv\int_{-\infty}^{+\infty}\{2\ln|Y+a|\exp(iY+\Gamma)T\}/(iY+\Gamma)dY,$$

and use

$$I(a)=\int_{-a}^{+a}\left(\frac{dI}{da}\right)_x dx+I(-a).$$

Since

$$I(a)=[I(-a)]^*,$$

$$2\,\mathrm{Im}I(a)=\int_{-a}^{+a}\left(\frac{dI}{da}\right)_x dx.$$

Now using the semi-circle contour in the positive half of the imaginary plane, we find

$$\frac{dI}{da}=2\int_{-\infty}^{+\infty}\{[e^{(iY+\Gamma)T}]/(Y+a)(iY+\Gamma)\}dY=2\left[\frac{2\pi}{(i\Gamma+a)}+\frac{\pi ie^{(-ia+\Gamma)T}}{-ia+\Gamma}\right];$$

and

$$2\,\mathrm{Im}I(a)\cong-8\pi i\tan^{-1}(a/\Gamma)+4\pi^2 i,$$

since

$$\int_0^{a/\Gamma}\frac{\cos(\Gamma Tx)}{1+x^2}dx\cong\int_0^{\infty}\frac{\cos(\Gamma Tx)}{1+x^2}dx=\frac{\pi}{2}e^{-\Gamma T},$$

and

$$-\frac{d}{d\Gamma T}\int_0^{\infty}\frac{\cos(\Gamma Tx)}{1+x^2}dx=\int_0^{\infty}\frac{x\sin(\Gamma Tx)}{1+x^2}dx=\frac{\pi}{2}e^{-\Gamma T}.$$

Consequently, for $\Gamma\ll1$, we can expand $\tan^{-1}(1/\Gamma)=\frac{1}{2}\pi+O(\Gamma)$, and

$$2\,\mathrm{Im}I(\pm1)\cong O(\Gamma).$$

For the real part of $I(\pm1)$,

$$\mathrm{Re}I(\pm1)=e^{\Gamma T}\int_{-\infty}^{+\infty}2\ln|Y\pm1|\left[\frac{\Gamma\cos(YT)+Y\sin(YT)}{Y^2+\Gamma^2}\right]dY,$$

we lack as neat an evaluation procedure. It is assumed that the resonance approximation of KBM gives γ_P correctly. The method is analogous to Eq. (6) for the radiation field perturbation. To demonstrate its validity we expand $2\ln|Y\pm1|$ in a Taylor series about the resonance value $Y=0$, obtaining $2\ln|Y\pm1|\cong\pm2Y-Y^2$. The slowest variation is the constant resonance value zero, which gives no correction to the term already removed in Eq. (9). The next term in the expansion has an odd integrand and also contributes nothing. The contribution from the neighborhood of the resonance for the Y^2 term is $O(\Gamma^2)$. Hence, the resonance approximation appears to be reasonable in this case and we neglect the real part of $I(\pm1)$.

Second, we write the remaining term in the integral of Eq. (9) as a real and an imaginary part,

$$+\int_{-\infty}^{+\infty}\frac{2\ln|Y\mp1|}{iY+\Gamma}dY=\Gamma\int_{-\infty}^{+\infty}\frac{2\ln|Y\mp1|}{\Gamma^2+Y^2}dY-i\int_{-\infty}^{+\infty}\frac{2Y\ln|Y\mp1|}{\Gamma^2+Y^2}dY.$$

The real part is of the order of Γ^2. To show this we define

$$\Gamma\int_{-\infty}^{+\infty}\frac{2\ln|Y\mp1|}{\Gamma^2+Y^2}dY\equiv\Gamma I_1(\mp1),$$

where

$$I_1(a)\equiv\int_{-\infty}^{+\infty}\frac{2\ln|Y+a|}{\Gamma^2+Y^2}dY=\int_0^a\left(\frac{dI_1}{da}\right)_x dx+I_1(0).$$

Thus,

$$\frac{dI_1}{da}=\frac{2a\pi}{\Gamma(\Gamma^2+a^2)},$$

and

$$I_1(0)=(\pi/\Gamma)\ln(\Gamma^2).$$

Therefore,

$$I_1(a)=(\pi/\Gamma)\ln(\Gamma^2+a^2),$$

and

$$\Gamma I_1(\mp1)=\pi\ln(\Gamma^2+1)\cong\pi\Gamma^2.$$

In a similar manner we evaluate the imaginary part, which leads to the line shift. We define

$$-iI_2(\mp1)\equiv-i\int_{-\infty}^{+\infty}\frac{2Y\ln|Y\mp1|}{\Gamma^2+Y^2}dY,$$

where

$$I_2(a)=\int_{-\infty}^{+\infty}\frac{2Y\ln|Y+a|}{\Gamma^2+Y^2}dY=\int_0^a\left(\frac{dI_2(a)}{da}\right)_x dx+I_2(0).$$

As before,

$$\frac{dI_2}{da}=\frac{2\pi}{\Gamma}-\frac{2a^2\pi}{\Gamma(\Gamma^2+a^2)},$$

and

$$I_2(0)=0,$$

the integrand being an odd function of Y. Finally, we obtain a contribution to δ which is large compared to Γ:

$$-iI_2(\mp1)=-i2\pi\tan^{-1}(\mp1/\Gamma)=\pm i\pi^2+O(\Gamma)\quad\text{for}\quad\Gamma\ll1.\quad(11)$$

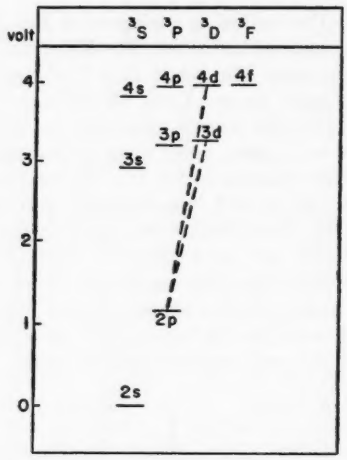

FIG. 1. Partial term scheme for orthohelium. Since broadening depends on near neighbors, the $4d$ level has different properties than $3d$, which lacks a partner corresponding to $4f$.

Collecting the results, we rewrite expression (8), with neglect of terms of order Γ,

$$\frac{-2nv_\lambda\sigma_\lambda}{3\pi}\left(\frac{z_{2n}}{a}\right)^2\left\{2\pi\ln\left[\frac{\hbar(k_\lambda+k_{\mu'})^2}{2m|\omega_{2n}-\delta_2|}\right]\pm i\pi^2\right\} \quad (12)$$
$$\equiv-\gamma_P(2n)+i\delta_{2n},$$

where the $\pm$ sign corresponds to $\omega_{2n}-\delta_2\gtrless 0$.

Consequently,

$$\delta_2=-\left(\frac{2nv_\lambda\sigma_\lambda\pi}{3}\right)\sum_n{}'\left(\frac{z_{2n}}{a}\right)^2\frac{(\omega_{2n}-\delta_2)}{|\omega_{2n}-\delta_2|}=\sum_n{}'\delta_{2n}, \quad (13)$$

where the sum over n includes all states that can be excited by the free electron. Provided ω_{2n} is large in comparison with δ_2, the contributions to the shift are independent of the magnitude of the level separation ω_{2n} and many levels must be considered. The shift δ_{2n}, however, depends on the sign of ω_{2n}. If $\omega_{2n}>0$, then by Eq. (13) $\delta_{2n}<0$ and according to Eq. (14) below $\omega_r>\omega_{21}$. This is consistent with perturbation theory in which coupled levels are mutually repelled. Inversely, if $\omega_{2n}<0$, then $\omega_r<\omega_{21}$, which is also expected. Although for broadening only the near levels need be considered, γ_2 contains the same sum and[3]

$$\gamma_2=\sum_n{}'\gamma_P(2n)+\gamma.$$

This result is the same as KBM under these circumstances.

Since polarization broadening depends on near atomic levels, it is in general smaller for the ground state. Hence, it is reasonable to neglect this broadening contribution. The level shift is not correspondingly small and must be considered. Consequently, we return to Eq. (1) and write

$$i\hbar\dot{b}_{r\lambda}=J_r^*e^{-i\omega t}d_\lambda-(\sum_n{}'\hbar\delta_{1n})b_{r\lambda}.$$

Defining $\delta_1\equiv\sum_n{}'\delta_{1n}$ corresponding to δ_2 in Eq. (13), and substituting $B_{r\lambda}e^{i\delta_1 t}$ for $b_{r\lambda}$, one obtains for an initially excited atom ($d_\lambda=1$ at $t=0$):

$$i\hbar\dot{B}_{r\lambda}=J_r^*e^{[i(\delta_2-\delta_1-\omega)-\gamma_2]t};$$

and the emitted line intensity becomes

$$I(\omega)=\rho_r|b_{r\lambda}(\infty)|^2=\frac{\rho_r|J_r/\hbar|^2}{\gamma_2^2+(\omega+\delta_1-\delta_2)^2}, \quad (14)$$

where ρ_r symbolizes the sum over polarizations and angles of emission as well as the density of final states at ω_r.

II. EXPERIMENTAL VERIFICATION—BROADENING[4]

It is not easy to obtain knowledge of electron or ion densities and temperatures which determine the line broadening. Consequently, an experiment which is independent of these parameters is desired. The comparison of different line widths in a spectrum, of radiators in the same plasma, where all the atoms emit in a given though perhaps uncertain temperature and density, has this property. An especially interesting case is presented by the relative widths of the $nd\,^3D\rightarrow 2p\,^3P$ lines in the helium spectrum (Fig. 1). For example, we will show that the width ratio for lines from the principal quantum levels $n=4$ and $n=3$ is $\sim$150 for Holtsmark ion broadening while it is only $\sim$10 for electron collision broadening. This difference stems from the fact that there is no $3f\,^3F$ level. For the higher principal quantum numbers, the F level is the nearest neighbor of the D level and leads to much larger Stark shifts and consequent Holtsmark broadening than occurs for $n=3$. On the other hand, the collision width receiving a contribution from the more distant P level which is comparable to that from F, remains relatively unchanged with n.

The energy separations of interest are given in Table I (see also reference 5).

TABLE I. Experimental energy separations of some $(1s)(nl)$ and $(1s)(nl+1)$ configurations in triplet helium.[a]

n	$\bar{\nu}_{nf}-\bar{\nu}_{nd}$ (cm^{-1})	$\bar{\nu}_{nd}-\bar{\nu}_{np}$ (cm^{-1})
3		536.8
4	7.78	227.4
5	4.31	116.4
6	2.45	67.16

[a] See reference 5.

[3] This agrees with the results given in an earlier unpublished report by R. Sternheimer.

[4] The author is indebted to Professor G. Breit for the suggestion to consider broadening in the nondegenerate case and to Dr. L. B. Seely for the choice of spectral levels.

[5] C. E. Moore, *Atomic Energy Levels*, National Bureau of Standards Circular 467 (U. S. Government Printing Office, Washington, D. C., 1948), Vol. 1.

The matrix elements which enter both Stark broadening and electron collision broadening are[6]

$$(z_{n,l,0;n,l-1,0})^2=\frac{9n^2}{4}\left[\frac{(n^2-l^2)l^2}{4l^2-1}\right]a^2\equiv z_{nl}^2,$$

when hydrogen wave functions are used for the radiating electron. Table II gives values of z_{nl}^2 for $l=2$ and 3.

A. Estimate of Holtsmark Broadening (Ion Effect)

The component with $m=0$ has the largest Stark shift in a uniform electric field (F). Because the levels of helium are nondegenerate, one obtains in weak fields the quadratic Stark shift. For the D levels with $m=0$ this shift is

$$E_{nd0}^{(2)}=e^2F^2\left(\frac{z_{n3}^2}{E_{nd}-E_{nf}}+\frac{z_{n2}^2}{E_{nd}-E_{np}}\right). \quad (15)$$

With the values in Tables I and II, we find $E_{nd0}^{(2)}$ (Table III). The very small shift for $n=3$ reflects the nonexistence of a $3f^3F$ level. The shift of the ground state $(1s)(2p)$ can be neglected, since $E_{2p0}^{(2)}/(e^2F^2a^2/hc)=0.000975$. To estimate the width we follow Holtsmark

TABLE II. $(z_{n,l,0;n,l-1,0})^2\equiv z_{nl}^2$.

n	z_{n3}^2/a^2	z_{n2}^2/a^2
3	0	27.0
4	64.8	115.2
5	231.4	315.0
6	562.4	691.2

and take

$$F=3.26en^{\frac{4}{3}},$$

and for the ion broadening width (Table IV)

$$\hbar(\gamma_{\text{ion}})_{nd}=4(3.26)^2(e^2/2a)^2n^{4/3}a^4 \times\left|\frac{(z_{n3}^2/a^2)}{E_{nd}-E_{nf}}+\frac{(z_{n2}^2/a^2)}{E_{nd}-E_{np}}\right|. \quad (16)$$

B. Electron Collision Broadening

Neglecting the natural width and considering only the nearest neighbors, one obtains, according to Eq. (12),

$$\gamma_{nl}\cong(2nv_\lambda\sigma_\lambda/3)\sum_{l=l,l+1}\frac{z_{nl}^2}{a^2}2\ln\left|\frac{4\epsilon_\lambda}{E_{nl}-E_{n\,l-1}}\right|, \quad (17)$$

provided we approximate

$$\frac{\hbar^2}{2m}(k_\lambda+k_{\mu'})^2\cong 4\epsilon_\lambda,$$

and

$$\hbar(\omega_{2n}-\delta_n)\cong\hbar\omega_{2n}.$$

Since the broadening depends logarithmically on the energy separation, it is not as sensitive to the principal quantum number as ion broadening.

TABLE III. Stark shifts.

n	3	4	5	6
$\frac{E_{nd0}^{(2)}}{(e^2F^2a^2/hc)}$	0.0503	−7.82	−51.0	−219.3

Table V contains contributions to γ_{nl} from the two near levels, their sum, their successive ratios, and for comparison the corresponding ion ratios (see Table IV). Also included are the wavelengths of the $nd\,^3D\rightarrow 2p\,^3P$ lines. Since the theory used does not correct for the fact that distant electrons are shielded and do not exert a Coulomb field at the atom (plasma cutoff —KBM), the broadening given will be too large. At the density considered, this correction is not serious.

Unlike hydrogen, where there is a large linear Stark effect, helium exhibits an electron broadening that is larger than or comparable to ion broadening. Another advantage in the use of helium is the possible appearance of the forbidden transitions as $4f\,^3F\rightarrow 2p\,^3P$ and $4p\,^3P\rightarrow 2p\,^3P$. Since the uniform field intensity for their appearance is known, this may serve as an indicator of the ion density.

It is likely that our calculation overestimates γ_P. The electrons have been assumed monoenergetic and are represented by plane waves. Actually, the electrons are distributed in energy and our calculation is poor for the slower ones (failure of the Born approximation). If the very slow electrons produce ion-like (Stark) effects, then we may expect that the electron density to be used in γ_P is less than the actual density. This diminution of our calculated γ_P may mean that electron effects are actually less important than ion effects for the lines $nd\,^3D\rightarrow 2p\,^3P$ where $n>3$. Hence, these lines would have contours predictable from Stark shifts.[7] On the other hand, $3d\,^3D\rightarrow 2p\,^3P$ can still have the anomalous electron broadening shape, i.e., the Lorentz shape $[(\gamma+\gamma_P)^2+\omega^2]^{-1}$. Also this line should be broader than expected on comparison with the other members of the series when only ion effects are con-

TABLE IV. Ion broadening width and width ratios for $n=10^{15}$.

n	$(\gamma_{\text{ion}})_{nd}$ (sec^{-1})[a]	$\frac{(\gamma_{\text{ion}})_{n+1,d}}{(\gamma_{\text{ion}})_{n,d}}$
3	$+3.80\times10^{8}$	155.
4	-5.91×10^{10}	6.5
5	-3.85×10^{11}	4.3
6	-1.65×10^{12}	

[a] + indicates blue asymmetry; −, red.

[6] In this section, we use several results given by H. Bethe, *Handbuch der Physik* (Verlag Julius Springer, Berlin, 1933), second edition, Vol. 24, Part 1.

[7] Toshio Takamine, Sci. Papers Inst. Phys. Chem. Research (Tokyo) **5**, 55 (1926).

TABLE V. Electron broadening widths for $n=10^{15}$ and $\epsilon_\lambda=e^2/50a$.

n	$nd\,^3D \rightarrow 2p\,^3P$ Wavelength (A)	Contributions to γ_{nd} from p level (sec^{-1})	f level (sec^{-1})	γ_{nd} Sum (sec^{-1})	$\frac{\gamma_{n+1,d}}{\gamma_{n,d}}$	$\frac{(\gamma_{ion})_{n+1,d}}{(\gamma_{ion})_{n,d}}$
3	5877	1.21×10^{10}	0.	1.21×10^{10}	10.6	155
4	4473	6.43×10^{10}	6.42×10^{10}	1.28×10^{11}	3.50	6.5
5	4027	2.03×10^{11}	2.46×10^{11}	4.49×10^{11}	2.52	4.3
6	3821	4.93×10^{11}	6.40×10^{11}	1.13×10^{12}		

sidered. The ions present may still superpose a slight asymmetry toward the violet. The corresponding singlet line $3d\,^1D \rightarrow 2p\,^1P$ would have the asymmetry to the red side, since unlike the triplet case the energy level $3p$ is greater than $3d$. Thus, electron broadening effects as treated in this report may find a fairly simple experimental verification.

The experimenter must overcome difficulties imposed by the Doppler width,[8] which for the $3d \rightarrow 2p$ line at $\frac{1}{2}$ ev, and $n=10^{15}$ is comparable with the electron broadening. By going to the wings of the line where the Doppler effect is small, the electron "dispersion" width can be determined. This complication in the measurement of the line shape can be avoided by working at higher electron densities. If n is increased by a factor 10 without change in temperature, then electron broadening dominates. Hence, it is suggested that the helium spectrum be studied in an atmosphere of a more easily ionized element, for example, argon for which densities of 10^{17} at 1 ev have been obtained in shock tubes.

III. EXPERIMENTAL VERIFICATION—SPECTRAL LINE SHIFT

Laporte[9] and Kantrowitz[10] have observed large shifts of spectral lines from atoms radiating in shock tubes. Baranger[11] has proposed that these shifts are the result of collisions with electrons. According to the quantum mechanical calculation previously given, there is a line shift. In order to make the result more quantitative, we consider two He I lines: $3d\,^3D \rightarrow 2p\,^3P$ and $4d\,^3D \rightarrow 2p\,^3P$.

For the metastable ground state $2p\,^3P$, only coupling to $2s\,^3S$ shifts the levels. This is because the matrix element to the $1s$ level vanishes (since we have neglected exchange collisions), and the free electrons lack sufficient energy to excite the atom. Thus, for $\epsilon=e^2/50a$ and $n=10^{15}$, $2nv\sigma\pi/3=2.015\times10^8$ sec^{-1}; and the level is shifted according to Eq. (13) by $\delta_{2p}=-1.814\times10^9$ sec^{-1}. The shift of the $3d$ level is found by considering only coupling to $3p$ and $2p$ levels; $\delta_{3d}=-6.650\times10^9$ sec^{-1}. For $4d$, since the atom can be excited, we include $2p$, $3p$, $\cdots$, $6p$ and $4f$, $5f$, $6f$ (a total of 8 levels); $\delta_{4d}=-1.163\times10^9$ sec^{-1}. Consequently, $3d\,^3D \rightarrow 2p\,^3P$ is shifted to the violet 4.836×10^9 sec^{-1} (0.056 A) whereas $4d\,^3D \rightarrow 2p\,^3P$ is shifted to the red by 0.651×10^9 sec^{-1} (0.0043 A). Although these are small shifts, it should be remembered that they are in proportion to the free electron density. If, as reported by Kantrowitz, $n=10^{18}$, then these shifts are increased by a factor 10^3. Thus, sufficiently high electron densities can introduce measurable line shifts.

IV. ACKNOWLEDGMENTS

The author is happy to acknowledge continued guidance and critical suggestions received from Professor Henry Margenau. Thanks are also due to M. M. Gordon (University of Florida), H. Mayer (Los Alamos Scientific Laboratory), and G. Breit (Yale University) for stimulating discussions.

[8] This Doppler complication was brought to our attention by Dr. R. E. Meyerott.
[9] O. Laporte (private communication).
[10] A. Kantrowitz, Phys. Rev. **90**, 368 (1953).
[11] M. Baranger, Phys. Rev. **91**, 436 (1953).

X-Ray-Induced Luminescence from Air*

WILLIAM E. SPICER
Department of Physics, University of Missouri, Columbia, Missouri
(Received December 27, 1954)

The luminescence due to the absorption of x-rays in air has been studied in the range 600 to 250 mμ. Relatively strong peaks were found at 356, 336, and 314 mμ with lesser peaks at 388, 378, and 373 mμ. This luminescence has been associated with argon present in the atmosphere.

A LUMINESCENCE due to absorption of x-rays in air has been observed during a study of the x-ray-induced luminescence from NaCl. As no mention was found in the literature of such an effect, a preliminary study of it has been made.

EXPERIMENTAL TECHNIQUES

Figure 1 is a block diagram of the simple experimental arrangement used in this study. The principle component is a cylindrical brass vacuum tube which contained the gas under study. X-rays enter this tube through a 0.004 inch thick aluminum window. Seventeen centimeters from the face containing this window and inclined at 45° to it was a front surface aluminized mirror by which the luminescence could be directed through a quartz window into the Perkin-Elmer Model 83 monochromator. The x-ray tube, having a tungsten target and a beryllium window, was operated at 10 ma and 35 kv in order to obtain a continuous spectrum. The pressure in the vacuum tube could be reduced by a fore pump and measured with a manometer. By use of the system of stop cocks the tube could be evacuated and filled with various gases. The dispersed luminescent radiation was measured by means of a photon-counter (a 1*P*28 photomultiplier cooled by liquid air and used in conjunction with either a scaler or counting-rate meter). Only the wavelength range from 600 to 250 mμ was studied and in this range the sensitivity is low from 600 to 550 mμ and from 300 to 250 mμ.

To obtain the absolute intensities of the spectra given in this paper, the fraction of the luminescence reaching the monochromator was estimated and the response of the system to the luminescence from air compared with that of a previously calibrated source. The estimate of geometry is probably good to within a factor of 2 whereas the calibration of the source used as a standard may be off by a factor of 4. The spectra as shown have been corrected for the dispersion of the monochromator and spectral sensitivity of the photomultiplier.

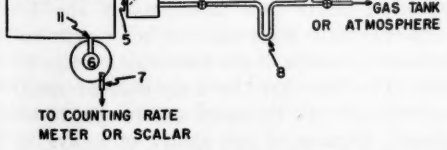

FIG. 1. Block diagram of equipment. (1) X-ray tube. (2) Aluminum window. (3) Vacuum tube. (4) Mirror. (5) Quartz window. (6) Cryostat holding photomultiplier. (7) Pre-amplifier. (8) Liquid air trap. (9) Manometer. (10) Monochromator entrance slit. (11) Monochromator exit slit.

* Supported in part by the Office of Naval Research.

RESULTS

The spectrum of air (Fig. 2) lies in the ultraviolet and consists of relatively strong peaks at 356, 336, and

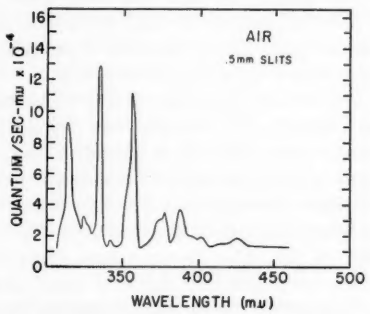

FIG. 2. The luminescent spectrum for air.

314 mμ with lesser peaks at 388, 378, and 373 mμ. The integrated intensity was estimated as 10^6 quantum/sec (6×10^{-13} watt). Quite probably this is a line spectrum, the apparent breadth being due to the lack of resolution of the monochromator. However, no correlation has been found between this spectrum and the arc or spark spectrum of air or of any of the normal components of air.

It seems unlikely that the luminescence is associated with the walls of the tube for it has been observed without the use of any tube. Also, as Fig. 4 illustrates, the luminescence disappears when the tube is evacuated thus establishing that the luminescence is associated with the presence of air.

An attempt was made to determine which component of air was responsible for the luminescence. Since air contains nitrogen, oxygen, argon, hydrogen, carbon dioxide, and water vapor in quantities greater than one part in 10^5, these gases were investigated. The latter two were excluded since the luminescence was not

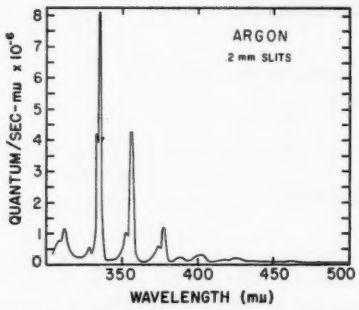

FIG. 3. The luminescent spectrum for argon.

altered by passing the air through a liquid air trap. Samples of the other gases were obtained and examined. The oxygen, nitrogen, and hydrogen were of tank purity, and the argon was 99.6 percent pure. Nitrogen and argon gave positive results whereas oxygen and hydrogen did not. Figure 3 shows the spectrum obtained for argon. The spectral distribution obtained for nitrogen was almost identical with that for argon. Note that the spectral distributions for air and argon are quite similar except for the relatively more intense 314- and 388-mμ peaks in air and the added structure in the case of argon. The latter effect is probably due to the use of narrower monochromator slits.

Table I gives the intensity of the three main luminescent peaks in air, nitrogen, and argon. Since the three spectra were taken in a period of less than 50 minutes and with the same slit openings, it is believed that conditions were identical. The relative strength of the argon spectrum, points to argon as the luminescent component of air. The luminescence observed from nitrogen was very probably due to a small percentage of argon present in the nitrogen cylinder. Additional indication of this was obtained by studying N_2O gas. One might expect x-ray-induced luminescence (as x-ray absorption) to be determined by the element or elements present and not be related to the chemical combination of these elements. However, N_2O gave no luminescence. Thus, it seems probable that the luminescence from air is due to argon.

A measure of the x-ray wavelength effective in producing luminescence was obtained by measuring the intensity of the 336-mμ peak as a function of the thickness of a metal foil (nickel and aluminum were used) placed in the x-ray beam. A straight line was obtained when the logarithm of intensity was plotted against foil thickness. The apparent absorption coefficient of the metal corresponds to an effective wavelength of 1.2 A. The data indicated that about 15 percent of the luminescence resulted from wavelengths between 1.5 and 2.0 A.

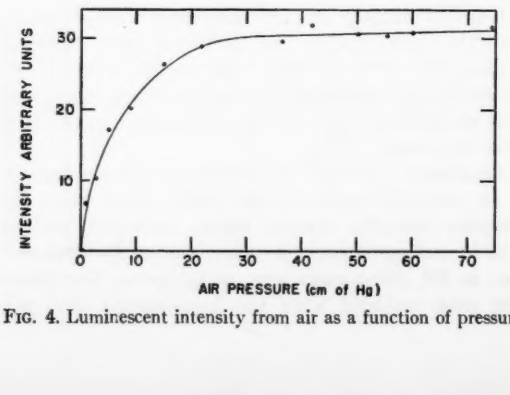

FIG. 4. Luminescent intensity from air as a function of pressure.

The dependence of the luminescent intensity on the pressure of the air is shown in Fig. 4. This data was taken on the 336-mμ peak, however, data was taken on other peaks and similar results were found. The most obvious explanation of this curve is that it is due to a total absorption of the x-rays effective in producing luminescence for pressures higher than 25 cm of Hg and an absorption decreasing with pressure below 25 cm of Hg. This would require a mass absorption coefficient for argon of approximately 600 cm^2/g (corresponding to x-rays of about 6 A); whereas, the luminescence has been found to be due to x-rays of about 1.2 A. Thus the above explanation is ruled out. The absorption of 1.2 A x-rays varies linearly with pressure. Therefore, it does not seem that the luminescence produced is proportional to the x-ray absorption. A more probable explanation is that the curve depends on the electron-ion recombination rates.

TABLE I. Intensities of the principal luminescent peaks of air, nitrogen, and argon.

Wavelength (mμ)	Intensity Air	N_2	A	Ratio of intensities N_2/air	A/air
378	10.8	23.6	865	2.18	80.2
356	30.2	107	2626	3.55	86.8
336	51.1	188	4800	3.67	94.0
			Average	3.13	87

In argon the variation of the luminescent measurements with pressure had the same general form as Fig. 4. However, the break in the curve appeared at 45 cm of Hg and the decrease of luminescence with pressure below the break was not as precipitous.

CONCLUSIONS

This work has been purely of an exploratory nature and is, therefore, somewhat incomplete. It would be desirable to study pure nitrogen for any inherent luminescence. It is likely that the other gases also give luminescence outside of the wavelength range we have studied. The fact that the x-ray-induced spectra are not correlated with the spark or arc spectra must be explained. Because of the ability of x-rays to eject electrons from inner shells of the atoms, a possible explanation may be that the observed luminescence results from optical transitions between levels within these inner shells.

The author is grateful to Professor Eugene B. Hensley and Professor Bernard Goodman for helpful discussions.

Temperature Sensitivities of the Sensitized Fluorescence Spectrum of Thallium†

ROBERT E. SWANSON AND ROBERT H. MCFARLAND
Department of Physics, Kansas State College, Manhattan, Kansas
(Received April 3, 1953; revised manuscript received January 13, 1955)

An investigation of the sensitized fluorescence of thallium and mercury mixtures using a photomultiplier type of detection is discussed. Data are given to indicate the variation of the intensity of the thallium lines as a function of the temperature of the excess mercury. Explanation of results requires the use of Winan's partial selection rule, $\Delta J=0$, in addition to generally accepted ideas concerning energy transfer, emission, and absorption.

INTRODUCTION

COLLISIONS of the second kind were first suggested by Klein and Rosseland.[1] By thermodynamic reasoning it was deduced that excited atoms could collide with slow electrons and transfer their excitation energy to produce unexcited atoms and fast electrons without accompanying radiation. Franck[2] extended this theory to include a system which contained electrons, excited atoms, radiation, and normal atoms of a different element from that excited. From this extension Franck predicted that mercury atoms, excited by light emitted from mercury vapor at a wave length of 2537 A, could transfer their excitation energy during collision with normal atoms of a vapor which does not absorb the mercury radiation. The vapor atoms which are excited by such collisions could then emit their characteristic spectra from all states whose excitation energy is less than the exciting potential corresponding to the mercury 2537 A line. Experimental investigations by Cario and Franck[3] confirmed this prediction with a mixture of mercury and thallium vapors. Franck called the new phenomenon sensitized fluorescence.

Early investigators recognized that metastable mercury atoms probably played an important role in the phenomenon of sensitized fluorescence. Experimental investigations by Donat[4] and Loria[5] seemed to confirm the concept that metastable atoms can enhance thallium lines. Donat and Loria both used argon and nitrogen as foreign gases in mixtures of mercury and thallium and found that both caused enhancement of the thallium lines. It is well known that the presence of nitrogen in mercury vapor being irradiated by mercury 2537 A produces atoms in the metastable mercury 6^3P_0 state. It is interesting to note that Loria found enhancement of thallium lines for small foreign gas pressures; but as the foreign gas pressure was increased, the intensity of thallium lines increased to a maximum and then fell off. The various thallium lines (see Fig. 1) reached their maxima at different foreign gas pressures. Donat did not find maxima for the lines 2768, 3776, and 5350 A.

That inconsistencies such as these could arise is apparent in considering the many difficulties which are encountered in obtaining data concerning sensitized fluorescence by spectrographic methods. A few of these may be listed as (a) obtaining a maximal focus for the ultraviolet light involved, (b) maintaining constant conditions in the gaseous mixture within the specimen tube over the necessarily long exposures, and (c) calibrating the photographic plate in terms of light intensity for the weak lines normally observed.

The purpose of this paper is to describe and discuss the variation of intensity of the sensitized fluorescence of thallium when the temperature controlling the vapor pressure of the mercury present in the mixture is varied. Other parameters are maintained constant by the use of controlled furnaces for heating and the use of electronic detection for maximal focusing and rapid determination of intensities for given temperatures.

APPARATUS AND METHOD

The quartz experimental tubes were similar to those of Winans and co-workers. They were prepared by distilling small amounts of thallium and mercury into the tubes and then sealing them off under a vacuum of the order of 10^{-7} mm or better of mercury. The shape of the experimental tubes is shown in the diagram Fig. 2. The central bulb was about 25 mm in diameter.

The detection apparatus is shown also in the diagram of Fig. 2. The source of the 2537 A radiation was a four-watt General Electric germicidal lamp. This source was focused onto the inner surface of the central bulb of the experimental tube by a pair of quartz lenses. This region, in turn, became the source of the sensitized fluorescence. The visible fluorescent light always appeared in a very thin layer on the inner surface of the tube. It was focused onto the slit of a Bausch and Lomb grating monochromator. The slits of the monochromator were set for a width of 0.4 mm throughout the investigation. The output of the monochromator was received by a 1*P*28 photomultiplier tube. The output current of the photomultiplier tube was passed through a 3-megohm resistor to provide an input voltage for the twin-*t* amplifier. The twin-*t* amplifier was tuned

† An adaptation of a thesis presented by R.E.S. as partial fulfillment of the requirements for the degree Doctor of Philosophy in Physics at Kansas State College.

[1] O. Klein and S. Rosseland, Z. Physik **4**, 46 (1921).
[2] J. Franck, Z. Physik **9**, 259 (1922).
[3] G. Cario and J. Franck, Z. Physik **17**, 202 (1923).
[4] K. Donat, Z. Physik **29**, 345 (1924).
[5] S. Loria, Phys. Rev. **26**, 573 (1925).

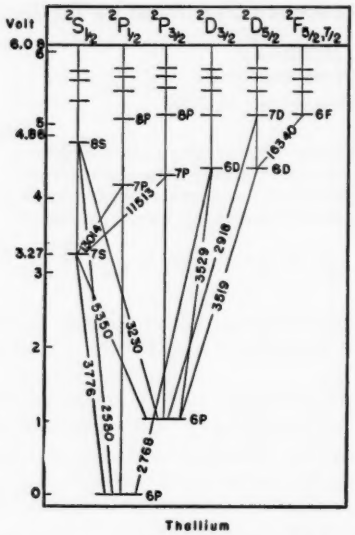

FIG. 1. An energy-level diagram of thallium.

to the 120-cycle signal supplied by the germicidal lamp. Below 80 cps or above 160 cps the output from the amplifier was less than 10 percent of that at 120 cps. The twin-t amplifier circuit was similar to that described by Kessler and Wolfe.[6] The output voltage of the amplifier was read with an RCA audio voltmeter.

Preliminary measurements had indicated that the maximum fluorescence was obtained with the extremity of the tube containing the excess mercury at a temperature between 200°C and 300°C and the central portion of the tube (the region of the thallium bead and source of fluorescence) at a temperature of approximately 900°C. This temperature of 900° was determined by the problem of retaining thallium in this region at higher temperatures rather than by any observed decrease of fluorescence with increasing temperatures. A main oven was designed and built to provide the high-temperature portion of this control. One end of the tube was allowed to protrude from the oven to provide the cool portion. Two quartz windows were installed in this oven to pass the incident and fluorescent light. The angle between the light paths was such as to reduce the effect of reflected light to a minimum. An auxiliary oven was designed to provide the temperature control of the portion of the tube which protruded from the main oven. The temperature of this protrusion will be called the mercury temperature since the mercury condensed in this region. The main oven temperature will be called the thallium temperature since an excess of thallium was maintained in the central bulb. The auxiliary oven could be placed around the protruding tube or removed without disturbing any focusing adjustments. The lower mercury temperatures were obtained by directing a jet of air against the end of the protruding tube.

The temperature of the main oven, the region of the thallium bead and source of fluorescence, determines the temperature of the thallium bead. The temperature of the thallium bead determines the vapor pressure in the immediate vicinity of the bead. The large temperature differential which existed between the central part of the tube and the part which protrudes from the main oven, however, makes it impossible to state precisely what the thallium vapor pressure is at the source of fluorescence. The vapor pressure of the thallium is undoubtedly at some value intermediate to those which would be determined by the two extremes of temperature. Experimental evidence obtained by Loria[5] indicates that the thallium vapor pressure is much closer to that determined by the high temperature of the thallium bead than that determined by the low temperature of the protrusion.

The experimental results to be presented were obtained by observing the intensities of the various thallium lines as the mercury temperature was varied, and the thallium temperature was kept constant. Observations were made at many different thallium temperatures.

EXPERIMENTAL RESULTS

The sensitized fluorescent lines which were observed in this investigation were the thallium lines 2580, 2768, 2918, 3230, 3519, 3529, 3776, and 5350 A. The 3519 and 3529 A lines were not resolved using the photomultiplier tube as a detector so they have been plotted together. Typical data curves are given in Figs. 3, 4, and 5. The relative intensities of the lines are plotted as functions of the mercury temperature. The relative intensity of one line as compared to another may be obtained from the curves. The 5350 A line has been corrected for phototube response since it is the only one with a correction of more than a few percent. Work by Engstrom[7] can be consulted for this photomultiplier

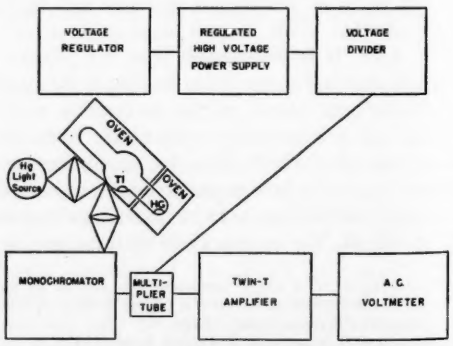

FIG. 2. Apparatus for determination of sensitized fluorescence intensities.

[6] K. G. Kessler and R. A. Wolfe, J. Opt. Soc. Am. 37, 133 (1947).

[7] R. W. Engstrom, J. Opt. Soc. Am. 37, 420 (1947).

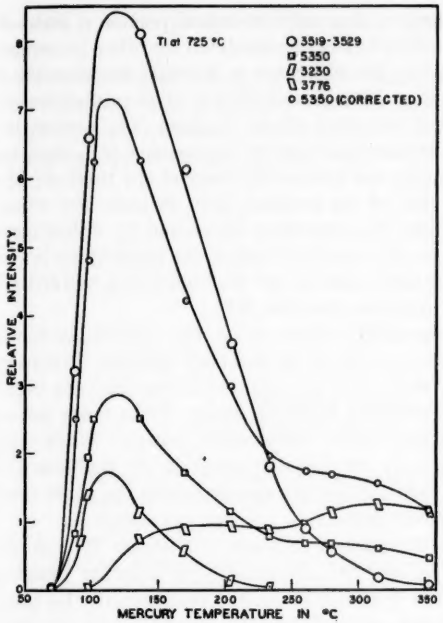

FIG. 3. Sensitized fluorescence intensities as a function of mercury temperatures with the thallium temperature at 725°C. (5350 line corrected for phototube response.)

tube response. Data taken at many different thallium temperatures gave curves having the same general appearance. Therefore, results from only two thallium temperatures are given. The large difference in the intensity scales of Figs. 3 and 4 is due to the difference in the thallium temperatures. Measurements made with transmission screens in an attempt to detect the existence of double absorption, in which an excited mercury atom absorbs a quantum of light, indicated that it was not a detectable process in the excitation of of the thallium levels.

DISCUSSION

The general feature of the results which is most interesting is the variation of line intensities with mercury temperature. Not only does the intensity of a given line vary with mercury temperature, but also the ratio of the intensities of a given pair of lines may vary radically as the mercury temperature changes. Changes in thallium temperature, also, may be seen to cause changes in the intensity of the thallium lines but to a smaller extent and in a more direct fashion.

A feature of the results which warrants close investigation is the way in which the intensities of the thallium lines 5350 A and 3776 A vary. The ratio of their intensities as shown in Fig. 3 can vary widely in value and are dependent upon the mercury temperature.

The general features of these curves can be explained on the basis of a number of related phenomena which are occurring simultaneously within the experimental system. These include (a) an initial expected increase in sensitized fluorescence with increasing mercury vapor pressure, (b) an optimum intensity followed by decreasing intensity due to specular reflection in the mercury vapor and possibly to an unfavorable ratio in number of mercury atoms becoming available to thallium atoms, (c) a probability that metastable mercury states are more highly populated at the higher mercury temperatures and vapor pressures, and (d) the usual dependence of such a system on excitation and transition rules and the reabsorption of the emitted radiation.

It is known that the metastable mercury atom 6^3P_0 is produced by collisions of 6^3P_1 atoms with nitrogen molecules. The number of atoms in the metastable state increases with increasing nitrogen pressures, at least at low nitrogen pressures. It seems probable, therefore, that collisions of the 6^3P_1 atom with other mercury atoms and molecules may produce metastable 6^3P_0 atoms. There are indications in the literature that this does happen.[8–10] Results of the present investigation show an increasing absorption of the 2967 A line in a mercury absorption cell as the vapor pressure is increased and the cell is irradiated with unfiltered mercury light. This implies the presence of 6^3P_0 atoms. Thus it seems reasonable to assume that an increase in the mercury vapor pressure while the vapor is being irradiated by the mercury 2537 A line would bring about an increase in the number of metastable mercury atoms.

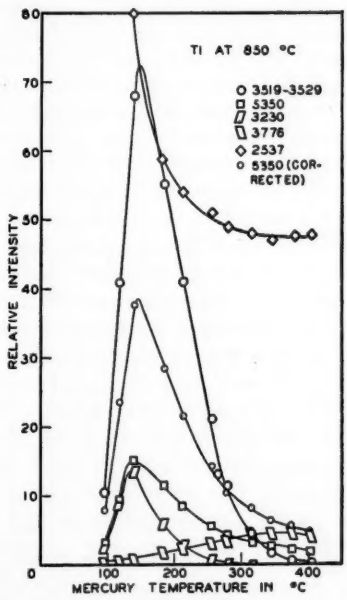

FIG. 4. Sensitized fluorescence intensities as a function of mercury temperatures with the thallium temperature at 850°C. (5350 line corrected for phototube response.)

[8] J. G. Winans, Revs. Modern Phys. **16**, 175 (1944).
[9] W. Orthmann and P. Pringsheim, Z. Physik **35**, 626 (1926).
[10] H. Beutler and B. Josephy, Z. Physik **53**, 747 (1929).

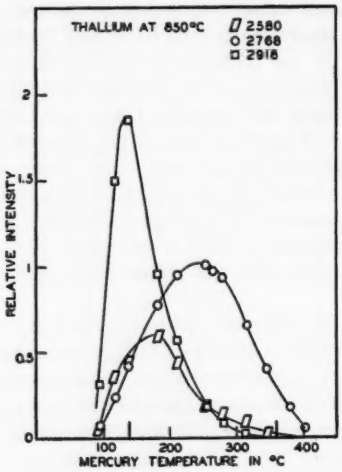

FIG. 5. Sensitized fluorescence intensities of the three least intense lines observed.

The change of intensity of the thallium 3519–3529 A lines is probably the least complex of those observed. Build-up of initial intensity follows the build-up of Hg vapor pressure. Fall-off occurs at approximately the same temperatures as does that for mercury fluorescence and is probably due primarily to specular reflection. A secondary factor contributing to this fall-off must correspond to the dilution effect of the increasing number of mercury atoms present in comparison to a relatively small and constant number of thallium atoms.

The causes of the observed intensities of the thallium 3776 A and 5350 A lines are more complex. If Winan's partial selection rule, $\Delta J=0$,[8] is applied, the most probable transfer of energy at low temperatures and low mercury vapor pressures would be from the 6^3P_1 mercury atom, to leave the thallium atom in the $7^2P_{\frac{1}{2}}$, $8^2P_{\frac{1}{2}}$, and other $j=\frac{3}{2}$ states. These may decay to leave the atom in the $7^2S_{\frac{1}{2}}$ state. Subsequent emission should produce a 3776 A thallium line which should be roughly three times as intense as the 5350 A line. That it does not is an indication of the role that reabsorption plays in determining the intensity of the thallium lines 2580, 2768, and 3776 A which correspond to transitions to the ground state in the thallium atom.

At higher mercury temperatures, an increasingly greater abundance of mercury 6^3P_0 atoms are postulated. Collision of this atom with neutral thallium atoms are most likely to produce excited thallium $7^2S_{\frac{1}{2}}$, $7^2P_{\frac{1}{2}}$, $8^2S_{\frac{1}{2}}$ and other $j=\frac{1}{2}$ atomic states.[8] Thus at higher mercury temperatures, the thallium $7^2S_{\frac{1}{2}}$ state may be excited directly by collision or by transitions from upper states. Under the condition of a direct collision, the colliding atoms must convert to kinetic energy and share the one and four-tenths volt excess excitation energy. The resultant Doppler broadening of the 3776 A thallium line has been observed to be sufficient so that only its central portion is reabsorbed. This effect has been postulated by other investigators[8] to explain the difference in intensity between the thallium lines 2768 A and 3776 A. The postulation of increased excitation of the thallium $7^2S_{\frac{1}{2}}$ level at higher mercury temperatures by the mercury 6^3P_0 atom serves to explain the greater intensity of the thallium 5350 A over that of the thallium 3519–29 lines. For while the thallium $7^2S_{\frac{1}{2}}$ state may be excited by either mercury 6^3P_0 or 6^3P_1 mercury atoms, the probability is greater for an excitation of the thallium $6^2D_{\frac{3}{2},\frac{5}{2}}$ states by 6^3P_1 mercury atom than the 6^3P_0.

A secondary effect which may contribute toward a general increase in the observed thallium 3776 intensity may result from the dilution of the thallium vapor by the increasing mercury vapor. Thus more resonance radiation could conceivably escape. While this is masked by the Doppler effect in the thallium 3776 A line, it becomes more apparent with the other thallium resonance lines.

As evidence of this effect, thallium 2768 A should not be affected appreciably by Doppler broadening. Neither should it be excited preferentially by the mercury 6^3P_0 atom. It may be observed however, that its intensity maximum as compared with thallium 3529 A is shifted toward higher mercury temperatures. Thallium 2580 A arising from an excitation of thallium $8^2S_{\frac{1}{2}}$ state, is, also, observed to exhibit a similar shift. It is probable that this shift is influenced at least in part by the $8^2S_{\frac{1}{2}}$ state being excited by collision with both the mercury 6^3P_0 and 6^3P_1 states due to the $8^2S_{\frac{1}{2}}$ state lying only slightly below the mercury 6^3P_1 state and above the 6^3P_0 state. The intensity variation of thallium 3230 A may be used to indicate the relative extent of the role that these two mercury states play in exciting the thallium $8^2S_{\frac{1}{2}}$ state.

CONCLUSION

The photomultiplier method of detection in the measurement of fluorescence has proved to be sensitive and convenient.

The observations made on the intensity of the sensitized fluorescence of thallium as a function of mercury temperature agree in general with those made by Loria and are in disagreement with those of Donat[4] and Orthmann and Pringsheim.[9] The results given in this paper show that the sensitized fluorescence disappears at sufficiently high mercury pressures. This is to be expected in terms of the dilution of the thallium by the mercury vapor and specular reflection of the mercury vapor. Donat and Orthmann and Pringsheim found a leveling off of the intensity of some lines. The comparison of the results of this investigation with those of Donat and Loria where a foreign gas pressure is the parameter, assumes that collisions of the mercury 6^3P_1 atom with either certain foreign gas molecules or

other mercury atoms produce the metastable mercury 6^3P_0 atom.

An interpretation of the experimental results made with the application of Winan's partial selection rule $\Delta J=0$ gives good explanation of the results. This work seems to give support to this selection rule.

ACKNOWLEDGMENTS

The authors wish to acknowledge the generous help and support given by other members of the Department of Physics. Acknowledgment is, also, due the Office of Ordnance Research for their support of work required to confirm and extend the scope of this paper.

PHYSICAL REVIEW VOLUME 98, NUMBER 4 MAY 15, 1955

Helium Wave Equation

JAMES H. BARTLETT
Department of Physics, University of Illinois, Urbana, Illinois
(Received August 27, 1954; revised manuscript received November 19, 1954)

The wave function for the ground state of helium has been obtained by a method which involves iterating in one direction only, the values of the function in any one plane being made mutually consistent by solving 30 simultaneous equations in 30 unknowns. The local energy value $(H\phi)/\phi$ is approximately constant over most of space, the maximum deviations occurring at large distances between electron and nucleus. The present accuracy is not sufficient to give a good determination of the eigenvalue, but it appears to be at least within 0.5 percent of the experimental value.

DETERMINATION of the form of the wave function for the ground state of the helium atom has been a baffling problem.[1] However, rather powerful methods have now been developed, as a result of which a fairly good wave function has been obtained. It seems, therefore, appropriate to report briefly on the above methods.

The wave equation is

$$\nabla^2\psi+\frac{1}{z}\frac{\partial\psi}{\partial z}+\frac{1}{4r}(E-V)\psi=0, \tag{1}$$

where, if r_1 and r_2 are the electron-nucleus distances and θ is the angle between the corresponding radius vectors, then $4x=2r_1r_2\cos\theta$, $4y=r_1^2-r_2^2$, $4z=2r_1r_2\sin\theta$ and $4r=r_1^2+r_2^2$. The potential energy V is such that

$$-\tfrac{1}{4}V=[2(r+y)]^{-\frac{1}{2}}+[2(r-y)]^{-\frac{1}{2}}-\tfrac{1}{4}(r-x)^{-\frac{1}{2}}. \tag{2}$$

Since the wave function for zero electron interaction is exponential in form, i.e., $\psi=e^{-\frac{1}{2}(r_1+r_2)}$, we make the substitution $\psi=e^F$ and consider the function F. This satisfies the nonlinear equation

$$\nabla^2F+\frac{1}{z}\frac{\partial F}{\partial z}+|\nabla F|^2+\frac{1}{4r}(E-V)=0. \tag{3}$$

The boundary conditions are $F(y)=F(-y)$, $F(z)=F(-z)$, $F\to-\infty$ as $r\to\infty$.

Now the function

$$F^{(0)}=-\tfrac{1}{2}\sqrt{2}[(r+y)^{\frac{1}{2}}+(r-y)^{\frac{1}{2}}]+\tfrac{1}{4}(r-x)^{\frac{1}{2}}$$

satisfies the equation

$$\left(\nabla^2+\frac{1}{z}\frac{\partial}{\partial z}\right)F^{(0)}-\frac{V}{4r}=0. \tag{4}$$

Subtracting (4) from (3), and letting $G=F-F^{(0)}$, the equation for G is

$$\nabla^2G+\frac{1}{z}\frac{\partial G}{\partial z}+|\nabla G|^2+2(\nabla F^{(0)}\cdot\nabla G)+|\nabla F^{(0)}|^2+\frac{E}{4r}=0. \tag{5}$$

Previous work[1] had shown that the Laplacian must be approximated by an adequate difference operator. To this end, we have assumed that G at any point may be represented by a fourth-degree polynomial in x, y, and z. If G be given at five successive mesh points in, say, the x-direction, then the coefficients of the polynomial may be determined. Also, the derivatives of G may be found by differentiating the polynomial.

For the early work, it was necessary to choose a mesh with variable intervals, and this mesh has been retained. At first the boundary was taken to be defined by $|x|=31$, $|y|=31$, $|z|=31$, and G was assumed to be zero there. Later work with the boundary at 63 gives much the same result and this will be reported here. The present mesh points are at $x=\pm63$, ±31, ±15, ±7, ±3, ±1, and 0; $y=0$, 3, 7, 15, 31, and 63; and $z=0$, 1, 3, 7, 15, 31, and 63.

When Eq. (5) is approximated by a difference equation, it relates the value of G at a given point to values at surrounding points. An attempt was made to use

[1] J. H. Bartlett, Phys. Rev. 88, 525 (1952).

TABLE I. Values of the wave function ψ.

z	y	0	3	7	15	31
$x=-31$	0	0.00156	0.00155	0.00151	0.00137	0.00098
	1	0.00156	0.00155	0.00151	0.00137	0.00098
	3	0.00154	0.00153	0.00149	0.00135	0.00096
	7	0.00143	0.00143	0.00139	0.00127	0.00091
	15	0.00109	0.00108	0.00106	0.00098	0.00073
	31	0.00045	0.00045	0.00045	0.00042	0.00034
$x=-15$	0	0.01116	0.01097	0.01021	0.00787	0.00397
	1	0.01110	0.01091	0.01016	0.00783	0.00396
	3	0.01066	0.01048	0.00977	0.00758	0.00386
	7	0.00882	0.00869	0.00817	0.00648	0.00343
	15	0.00462	0.00457	0.00438	0.00371	0.00222
	31	0.00103	0.00102	0.00100	0.00092	0.00069
$x=-7$	0	0.04636	0.04395	0.03627	0.02183	0.00828
	1	0.04562	0.04328	0.03580	0.02162	0.00823
	3	0.04041	0.03855	0.03241	0.02008	0.00782
	7	0.02536	0.02458	0.02172	0.01475	0.00630
	15	0.00839	0.00828	0.00781	0.00625	0.00335
	31	0.00130	0.00130	0.00127	0.00116	0.00084
$x=-3$	0	0.13231	0.11236	0.07581	0.03687	0.01189
	1	0.12508	0.10736	0.07340	0.03607	0.01171
	3	0.08919	0.08039	0.05929	0.03116	0.01060
	7	0.03860	0.03693	0.03131	0.01966	0.00772
	15	0.00982	0.00967	0.00908	0.00716	0.00372
	31	0.00137	0.00136	0.00133	0.00122	0.00087
$x=-1$	0	0.30399	0.19543	0.11035	0.04765	0.01420
	1	0.24117	0.17236	0.10173	0.04512	0.01367
	3	0.11954	0.10362	0.07187	0.03570	0.01165
	7	0.04224	0.04031	0.03388	0.02093	0.00808
	15	0.01004	0.00989	0.00928	0.00731	0.00378
	31	0.00137	0.00136	0.00134	0.00122	0.00087
$x=0$	0	0.91710	0.25696	0.13230	0.05402	0.01550
	1	0.28638	0.19085	0.10913	0.04742	0.01416
	3	0.12243	0.10602	0.07333	0.03629	0.01179
	7	0.04216	0.04027	0.03392	0.02101	0.00811
	15	0.00999	0.00984	0.00924	0.00730	0.00378
	31	0.00137	0.00136	0.00133	0.00122	0.00087
$x=1$	0	0.23527	0.18496	0.10773	0.04718	0.01414
	1	0.21115	0.16341	0.09930	0.04466	0.01362
	3	0.11157	0.09868	0.07001	0.03530	0.01160
	7	0.04066	0.03895	0.03305	0.02067	0.00804
	15	0.00982	0.00968	0.00911	0.00722	0.00376
	31	0.00135	0.00135	0.00132	0.00121	0.00087
$x=3$	0	0.09089	0.09512	0.07000	0.03564	0.01173
	1	0.09390	0.09130	0.06778	0.03487	0.01156
	3	0.07376	0.06967	0.05470	0.03007	0.01045
	7	0.03453	0.03338	0.02907	0.01892	0.00760
	15	0.00921	0.00909	0.00859	0.00689	0.00364
	31	0.00131	0.00131	0.00128	0.00118	0.00085
$x=7$	0	0.02793	0.03147	0.02972	0.01992	0.00798
	1	0.02923	0.03117	0.02935	0.01972	0.00793
	3	0.02838	0.02866	0.02672	0.01830	0.00753
	7	0.01993	0.01966	0.01829	0.01343	0.00604
	15	0.00725	0.00718	0.00687	0.00571	0.00319
	31	0.00119	0.00119	0.00117	0.00108	0.00079
$x=15$	0	0.00578	0.00647	0.00691	0.00630	0.00273
	1	0.00601	0.00647	0.00688	0.00627	0.00357
	3	0.00622	0.00642	0.00669	0.00607	0.00348
	7	0.00575	0.00578	0.00580	0.00522	0.00308
	15	0.00344	0.00343	0.00337	0.00305	0.00198
	31	0.00085	0.00085	0.00084	0.00079	0.00060
$x=31$	0	0.00066	0.00072	0.00079	0.00085	0.00072
	1	0.00068	0.00073	0.00079	0.00085	0.00072
	3	0.00071	0.00074	0.00079	0.00084	0.00071
	7	0.00073	0.00074	0.00077	0.00080	0.00067
	15	0.00064	0.00064	0.00064	0.00064	0.00053
	31	0.00030	0.00030	0.00030	0.00029	0.00024

the Liebmann iteration procedure, advancing one point at a time, and neglecting $|\nabla G|^2$. This was unsuccessful, for the new value of the function at any point was expressible as the quotient of two quantities, where the numerator depended on the neighboring values of G and the denominator depended on the mesh characteristics at the point in question. Since the denominator became small for certain points, and since the correct neighboring values could not be known beforehand, such an iterative procedure results in rapidly increasing values of G at these points. The next method there was to solve a set of six simultaneous equations in six unknowns, the values of G at the mesh points $z=0, \frac{1}{3}, 1, 3, 7, 15$ (x and y constant). This diverged after a time, but was an improvement. Consequently, there was next tried the idea of treating a whole plane ($x=$ constant) at a time, and this, which corresponds to block relaxation, was successful. For any one plane, one uses the values of G on four neighboring planes, so that a large part of space is being correlated at each such step.

As a test to see how well any trial function ϕ satisfies the differential equation, we have calculated the quantity $(H\phi)/\phi=E_{\text{loc}}$ as a function of position. For a true eigenfunction ψ, we would have $(H\psi)/\psi=E=$constant.

We have used $E=-1.4516$ in the iterations, and have started with $G=0$ everywhere. After the sixteenth iteration of G, there were still large differences between E and E_{loc} for large z. At these points $|\nabla G|^2$ is not negligible compared with the other terms. In order to include this term in the calculations, another function was defined as

$$J=F-F^0-G^0,$$

where G^0 was taken to denote the G values from the sixteenth iteration. The equation satisfied by J is

$$\nabla^2 J+\frac{1}{z}\frac{\partial J}{\partial z}+|\nabla J|^2+2(\nabla F^0+\nabla G^0)\cdot\nabla J+\frac{E-E_{\text{loc}}(G^0)}{4r}=0. \quad (6)$$

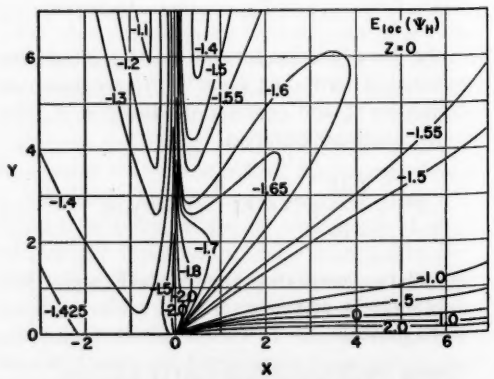

FIG. 1. Contour map of E_{loc}, Hylleraas six-term function ψ_H, for $z=0$.

TABLE II. Values of $|E_{loc}|$.

z	y	0	3	7	15	31
$x=-31$	1	1.4498	1.4503	1.4502	1.4509	1.4528
	3	1.4501	1.4503	1.4501	1.4512	1.4533
	7	1.4500	1.4504	1.4503	1.4515	1.4533
	15	1.4505	1.4505	1.4506	1.4512	1.4530
	31	1.4506	1.4505	1.4502	1.4508	1.4515
$x=-15$	1	1.4490	1.4491	1.4496	1.4514	1.4559
	3	1.4491	1.4492	1.4495	1.4515	1.4552
	7	1.4492	1.4494	1.4498	1.4515	1.4553
	15	1.4500	1.4501	1.4501	1.4513	1.4542
	31	1.4492	1.4498	1.4497	1.4499	1.4520
$x=-7$	1	1.4474	1.4474	1.4482	1.4520	1.4617
	3	1.4476	1.4476	1.4484	1.4520	1.4608
	7	1.4483	1.4484	1.4490	1.4521	1.4597
	15	1.4492	1.4492	1.4498	1.4517	1.4566
	31	1.4472	1.4473	1.4475	1.4488	1.4518
$x=-3$	1	1.4456	1.4450	1.4449	1.4535	1.4784
	3	1.4461	1.4458	1.4461	1.4531	1.4753
	7	1.4466	1.4466	1.4473	1.4530	1.4707
	15	1.4466	1.4467	1.4477	1.4528	1.4667
	31	1.4360	1.4363	1.4373	1.4410	1.4524
$x=-1$	1	1.4447	1.4398	1.4359	1.4566	1.5395
	3	1.4429	1.4407	1.4384	1.4559	1.5299
	7	1.4375	1.4373	1.4383	1.4563	1.5245
	15	1.4299	1.4307	1.4347	1.4546	1.5140
	31	1.3730	1.3743	1.3787	1.3968	1.4480
$x=0$	1	1.4472	1.4379	1.4287	1.4577	1.6065
	3	1.4383	1.4336	1.4276	1.4577	1.6060
	7	1.4233	1.4225	1.4237	1.4590	1.6030
	15	1.4042	1.4059	1.4144	1.4565	1.5850
	31	1.2822	1.2847	1.2946	1.3351	1.4473
$x=1$	1	1.4504	1.4483	1.4457	1.4520	1.4927
	3	1.4481	1.4469	1.4451	1.4518	1.4928
	7	1.4439	1.4436	1.4438	1.4521	1.4929
	15	1.4382	1.4388	1.4408	1.4521	1.4889
	31	1.4081	1.4088	1.4112	1.4226	1.4543
$x=3$	1	1.4512	1.4510	1.4505	1.4514	1.4595
	3	1.4510	1.4508	1.4504	1.4514	1.4597
	7	1.4502	1.4501	1.4500	1.4514	1.4597
	15	1.4491	1.4491	1.4494	1.4516	1.4594
	31	1.4446	1.4447	1.4453	1.4475	1.4538
$x=7$	1	1.4517	1.4516	1.4516	1.4516	1.4531
	3	1.4516	1.4516	1.4515	1.4517	1.4533
	7	1.4515	1.4515	1.4516	1.4514	1.4530
	15	1.4514	1.4513	1.4517	1.4517	1.4531
	31	1.4513	1.4516	1.4518	1.4518	1.4533
$x=15$	1	1.4518	1.4518	1.4517	1.4517	1.4521
	3	1.4519	1.4519	1.4520	1.4517	1.4522
	7	1.4519	1.4518	1.4517	1.4519	1.4520
	15	1.4517	1.4519	1.4518	1.4518	1.4519
	31	1.4520	1.4518	1.4517	1.4522	1.4527
$x=31$	1	1.4516	1.4518	1.4515	1.4519	1.4518
	3	1.4516	1.4520	1.4518	1.4516	1.4518
	7	1.4520	1.4517	1.4520	1.4521	1.4518
	15	1.4518	1.4520	1.4519	1.4521	1.4519
	31	1.4521	1.4520	1.4520	1.4524	1.4516

The same iterative method was used for J as for G. The E_{loc} from the new function showed an immediate improvement over E_{loc} from G^0.

When the E_{loc} for the fourth and fifth iterations of J were calculated, improvement was found in the values at all points of the later iteration compared with the earlier. The improvement was small, however, and it was thought that another value of E might result in faster convergence of E_{loc} toward E. Therefore the two iterations were repeated with $E=-1.444$ and $E=-1.459$. $E=-1.444$ improved E_{loc} at $x=0$, $y=0$, $z=31$ considerably, but at the expense of worse values at $x=0$, $y=31$, $z=1$. The reverse was true for $E=1.459$. These trends continued for a third iteration at each of these eigenvalues. It was concluded that the true eigenvalue must lie between these. Smaller variations in E, within the range -1.450 to -1.453, made no significant changes in E_{loc}. Therefore this process does not limit E more closely than ± 0.5 percent.

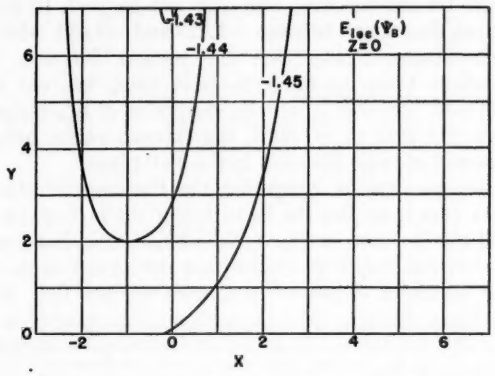

FIG. 2. Contour map of E_{loc}, Bartlett function ψ_B, $z=0$.

After the ninth iteration of J, the E_{loc} values began to oscillate without improving. The values of ψ at this stage are presented in Table I, together with corresponding values of E_{loc} (Table II).

In order that one may appreciate how much better the present function (ψ_B) is than that due to Hylleraas (ψ_H), contour maps of E_{loc} at $z=0$ are given for each function. Figure 1 shows the contours for the Hylleraas six-term function, out as far as $y=7$. Along the $+x$-axis, $E_{loc}\to+\infty$, and along the y-axis, $E_{loc}\to-\infty$. The values of E_{loc} are near to their average value of -1.4516 in only a *small* region of space. Figure 2 shows the con-

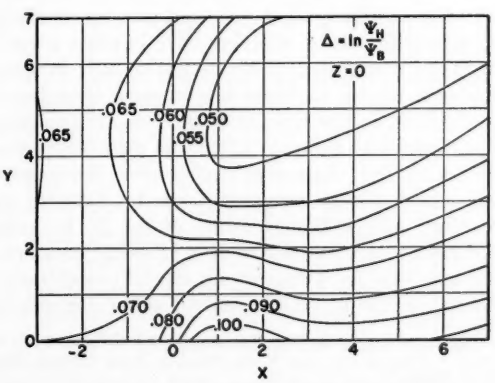

FIG. 3. Contour map of $\ln(\psi_H/\psi_B)$, $z=0$.

tours for our function, also only out to $y=7$. In this region, E_{loc} ranges between -1.429 and -1.452, which demonstrates clearly that the present function is excellent. Over the whole range of space, i.e., out to $|x|=31$, $|y|=31$, $|z|=31$, the value of E_{loc} ranges from -1.2822 to -1.6065, the extreme values being assumed at large distances in the $x=0$ plane.

Another way of comparing the Hylleraas function with ours is to plot the logarithm of the ratio ψ_H/ψ_B, and this is shown in Fig. 3. No normalization has been carried out, but if we assume that the correct value of the logarithm is about 0.07, then we see that the Hylleraas function deviates from ours by roughly ± 3 percent, but this is of course sufficient to cause marked changes in E_{loc}.

Further work may improve ψ and E_{loc} still more, especially at large y and z, and it may also lead to a more precise determination of the eigenvalue.

ACKNOWLEDGMENTS

The author expresses grateful thanks to the University of Illinois Research Board for financial assistance, to Mrs. Marjorie C. Huse, Walter Helly, Mrs. Jean Kellom, and Jerry McCall for help with coding and computations, and to Professor J. W. Nash, Professor J. Robertson, and Miss Ramona J. Russell for their valuable advice and effective cooperation in connection with the programming for and the operation of the ILLIAC.

PHYSICAL REVIEW VOLUME 98, NUMBER 4 MAY 15, 1955

High-Frequency Ionization Coefficients in Neon-Argon Mixtures*

A. D. MacDonald and J. H. Matthews
Dalhousie University, Halifax, Nova Scotia

(Received February 1, 1955)

Breakdown electric fields at 2800-Mc/sec frequency are presented for a number of neon-argon mixtures for a large range of pressure variation. High-frequency ionization coefficients for mixtures varying from pure neon to pure argon have been computed from the breakdown fields. The collision phenomena in the gas mixtures are discussed and a theoretical derivation of breakdown fields is compared with experiment.

IONIZATION coefficients of neon-argon mixtures are of interest chiefly because of the energy exchange which takes place when excited neon atoms collide with argon atoms—the Penning effect.[1,2] The lowest excited state of neon, 2^3S, at 16 volts is metastable, and is about three-tenths of a volt above the ionization potential of argon. A neon atom in this state exists long enough so that it makes many thousands of collisions at moderate gas concentrations. A small amount of argon in the neon will ensure that an excited neon atom will collide with an argon atom. In such a collision there is a very high probability that the neon will return to the ground state and give up its energy in ionizing the argon. We then have in effect a gas in which no energy is lost by excitation and in which ionization results whenever a neon atom is excited at its lowest level. The neon atoms are excited as a result of collisions with electrons which gain their energy from the electric field. Extensive studies of dc discharges in such mixtures have been carried out by Kruithof and Penning,[2] who published tables of the dc ionization coefficient η as a function of E/p (E being the electric field and p the gas pressure), for several concentrations of argon in the neon. The present paper presents the high-frequency ionization coefficient ζ as a function of E/p for a number of different mixtures.

The dc ionization coefficient η is equal to α/E, the Townsend coefficient divided by the electric field. The Townsend coefficient is the number of ions produced by an electron per cm of travel. η is a function of E/p and is perhaps more significant than α. Townsend's α may be written $\nu/\mu E$; ν is the ionization rate per electron and μ the electron mobility so that $\eta=\nu/\mu E^2$. Because diffusion replaces mobility in high-frequency discharges as the controlling electron loss mechanism, the high-frequency ionization coefficient ζ has been defined as ν/DE^2, where D is the diffusion coefficient.[3] The ratio of η to ζ is equal to the ratio of the diffusion coefficient to the mobility, D/μ, which is equal to the average electron energy.

A high-frequency gas discharge is one in which the electric field alternates so rapidly that electrons are not swept out of the field during each cycle. The electrons gain energy from the electric field between elastic collisions and produce ionization by inelastic collisions in the gas. At low ion densities, the probabilities of recombination and attachment are very small and practically all electrons are lost by diffusion to the container walls. Breakdown takes place when the ionization rate equals the electron loss rate. Since the

*Supported by the Defence Research Board of Canada.

[1] M. J. Druyvesteyn and F. M. Penning, Revs. Modern Phys. 12, 87 (1940).

[2] A. A. Kruithof and F. M. Penning, Physica 4, 430 (1937).

[3] M. A. Herlin and S. C. Brown, Phys. Rev. 74, 291 (1948).

number of electrons diffusing out of the container is D/Λ^2, where Λ is the characteristic diffusion length, which under certain limits[4] depends only on the dimensions of the container, the breakdown condition is $D/\Lambda^2=\nu$. Therefore the high-frequency ionization coefficient becomes $1/E^2\Lambda^2$ at breakdown.

EXPERIMENT

The ionization coefficients have been obtained by measuring breakdown electric fields for a large range of pressure variation. The experimental procedure was similar to that described in detail previously.[5,6] A schematic diagram of the equipment is shown in Fig. 1. A known fraction of the 2800-Mc/sec power incident on the resonant cavity is measured by means of a thermistor. The methods of combining cavity Q and power measurements to determine the electric field within the cavity have been described by Rose and Brown.[7,8] The measurements were made in a cylindrical copper cavity of height 0.473 cm, connected through Kovar to a vacuum system capable of maintaining the pressure at less than 2×10^{-7} mm of Hg, with pumps shut off, for a period longer than that necessary to make a series of measurements. Air Reduction Company spectroscopically pure neon and argon were used.

Breakdown electric fields for neon containing three different concentrations of argon are plotted against pressure in Fig. 2. (x percent means x volumes of argon per 100 volumes of neon plus argon.) High-frequency ionization coefficients computed from these and other similar data are presented as functions of E/p in Fig. 3.

DISCUSSION

The breakdown curve of pure neon is approximately parabolic, vertex downward, on a logarithmic graph, and it retains this general shape as argon is added. Both ends of the curve are lowered with increasing percentages of argon, until each attains a minimum before starting to rise. For the high-pressure end, this minimum occurs with about 0.005 percent argon added, and for the low-pressure end with about 1.35 percent argon added (see Fig. 2). However this behavior is to be expected, and agrees with the findings of Kruithof

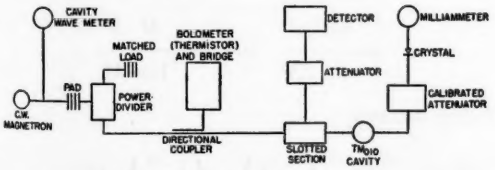

FIG. 1. Block diagram of experimental microwave apparatus.

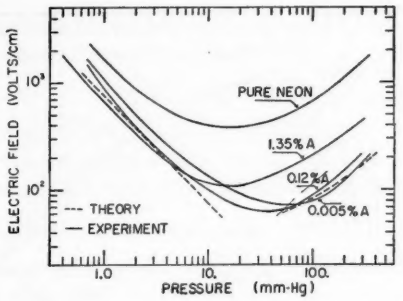

FIG. 2. Breakdown electric fields for pure neon and some neon-argon mixtures. (x percent means x volumes of argon per 100 volumes of neon plus argon). The dashed curve is computed from the theory outlined in the Appendix.

and Penning[2] for the dc case. In the high-pressure region, for example, the number of collisions an atom makes in a given time is proportional to the square of the ratio of the characteristic diffusion length to the mean free path, which means that a neon atom makes many collisions while in its excited state. Thus, a relatively small concentration of argon will ensure that a metastable neon collides with an argon atom, to produce ionization. When the number of argon atoms is increased, some of them are excited directly; consequently they lose energy, which lowers the ionization rate and therefore increases the breakdown field.

At lower pressures, the number of collisions made by a metastable neon atom decreases and therefore the concentration of argon required to produce ionization from each metastable neon is increased.

A theoretical derivation of the electron energy distribution function for neon, with sufficient argon for maximum Penning effect at all pressures, has been made,[9] and is outlined in the Appendix. The theory leads to separate breakdown equations for the cases where (1) the collision frequency is much greater than the angular frequency of the electric field, and (2) where it is much less. The dividing line between the two cases is roughly at the minimum of the breakdown curve. For the low pressure case the breakdown condition yields

$$M(\alpha;1;z_i)=2, \tag{1}$$

where M is the confluent hypergeometric function, $\alpha=30.8/p^2\Lambda^2$, and $z_i=2.07p^2/E^2$; p is the pressure in mm of Hg. For the high-pressure case,

$$M(a;2;w_i)=2, \tag{2}$$

where $a=123/p^2\Lambda^2$, $w_i=25.8\times10^3/E^2\lambda^2$, and λ is the free space wavelength of the electric field in cm.

The theoretically predicted value of the electric field as a function of pressure, computed from Eqs. (1) and (2) is plotted on Fig. 2. It should be compared with the lowest value of the experimentally determined field at

[4] S. C. Brown and A. D. MacDonald, Phys. Rev. **76**, 1629 (1949).
[5] A. D. MacDonald and S. C. Brown, Phys. Rev. **75**, 411 (1949).
[6] A. D. MacDonald and D. D. Betts, Can. J. Phys. **30**, 565 (1952).
[7] S. C. Brown and D. J. Rose, J. Appl. Phys. **23**, 711 (1952).
[8] D. J. Rose and S. C. Brown, J. Appl. Phys. **23**, 719 (1952).
[9] A. D. MacDonald, Ph.D. thesis, Massachusetts Institute of Technology, Cambridge, Massachusetts, 1949 (unpublished).

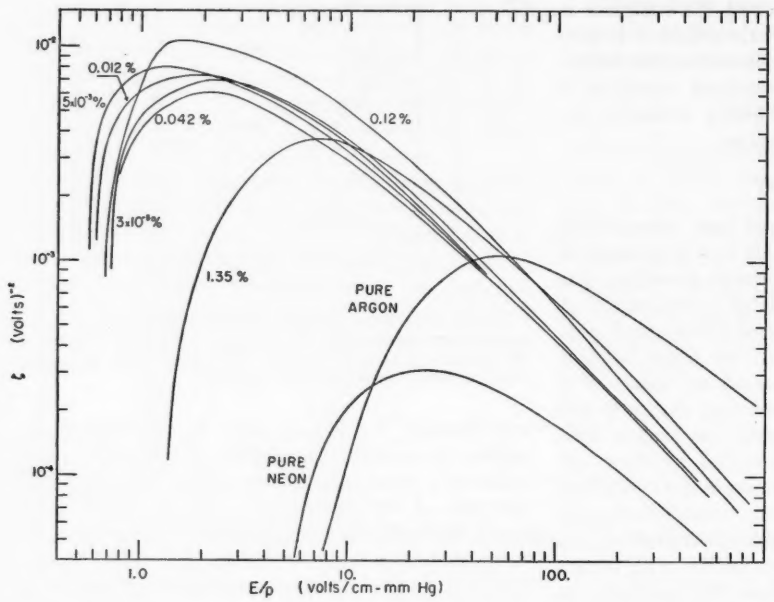

FIG. 3. The high-frequency ionization coefficient, ζ, (volts^{-1}) plotted against the ratio of the electric field to the pressure (volts/cm-mm Hg). The percentages indicated are of argon in the mixture.

any given pressure, because the assumptions of the theory are most nearly fulfilled at these points. The agreement between theory and experiment appears to be good when there is the proper amount of argon required to produce maximum Penning effect with minimum direct excitation of the argon. It should be noted, however, that the approximation of constant electron mean free path is not very accurate at lower electron energies. The effect of this on breakdown fields is being investigated further, and approximate calculations indicate that taking account of the energy dependence of the free path lowers theoretically computed breakdown fields by about 15 percent.

The maximum error in the electric field measurements is less than 5 percent and in pressure measurements less than 2 percent.

ACKNOWLEDGMENTS

We are indebted to Professor W. P. Allis and Professor S. C. Brown of the Massachusetts Institute of Technology for helpful and stimulating discussions. One of the authors (J.H.M.) held a National Research Council of Canada Studentship during the course of the work.

APPENDIX

The differential equation describing the variation of the electron energy distribution function has been derived from the Boltzmann transport equation previously.[5,6,10] If we assume that electrons are accelerated by an electric field $2^{\frac{1}{2}}Ee^{i\omega t}$, that the only electron loss mechanism is diffusion, and that the mean free path is independent of electron energy, the differential equation for the distribution function f is[6]

$$-h_z f+\frac{2m}{Mu}\frac{d}{du}(u^2 f)=\frac{l^2}{3\Lambda^2}f-\frac{E^2l^2}{3u}\frac{d}{du}\left\{\frac{u(v/l)^2}{(v/l)^2+\omega^2}\frac{df}{du}\right\}. \quad (3)$$

In Eq. (3), h_z is the inelastic collision efficiency, m the electronic mass, e the electronic charge, M the atomic mass of neon, l the momentum transfer mean free path, ω the angular frequency of the electric field, v the electron velocity, and $u=mv^2/2e$. The term h_z is zero below the lowest excitation level of 16 volts, and in the proper mixture of neon and argon each metastable neon atom results in an ionization. Therefore, there are no electrons with energies above 16 volts and we need only determine the distribution function for energies less than this value.

Consider first the case where $(v/l)^2$ is much greater than ω^2, i.e., the high-pressure case. The differential equation may be transformed by setting

$$z=\frac{3m}{M}\frac{u^2}{E^2l^2} \quad \text{and} \quad \alpha=\frac{M}{12m}\frac{l^2}{\Lambda^2}.$$

It then becomes

$$\frac{d^2f}{dz^2}+\frac{df}{dz}\left(\frac{1}{z}+1\right)+f\left(1-\frac{\alpha}{z}\right)=0.$$

The solution of this equation is

$$f=e^{-z}[M(\alpha;1;z)+CW(\alpha;1;z)],$$

where M and W are independent solutions of the confluent hypergeometric equation. C is a constant

[10] A. D. MacDonald and S. C. Brown, Phys. Rev. 76, 1634 (1949).

determined by the fact that f goes to zero at a value of $z=z_i$, corresponding to $u=u_i=16$ volts.

Having found the electron energy distribution function, we may find the ionization and diffusion rates by use of the standard formulas. The ionization rate is given by

$$n\nu=8\pi(e/m)^2\int_{u_i}^{\infty}h_i(u/l)f du.$$

This is an improper integral because the distribution function goes to zero at u_i, and we have assumed a very large ionization efficiency h_i, at u_i. The integral may however be evaluated by direct integration of Eq. (3) which yields

$$n\nu=16\pi(e/m)^2E^2(l/3)[zdf/dz]_{z_i}. \tag{4}$$

The diffusion rate is given by

$$nD=(4\pi/9)(M/m)E^2l^3\int_0^{z_i}f dz.$$

The integral involved in the expression for the diffusion rate has been evaluated,[11] and yields the following result:

$$nD=(16\pi/3)lE^2\Lambda^2\{[zdf/dz]_{z_i}+C/\alpha\}. \tag{5}$$

The ratio of (4) to (5) leads, after simplification by use of the Wronskian of the differential equation, to the following:

$$D/\nu=\Lambda^2[M(\alpha;1;z_i)-1].$$

[11] A. D. MacDonald, J. Math. Phys. **28**, 183 (1949).

By use of the breakdown condition $\nu\Lambda^2=D$, referred to in the aforementioned, we obtain

$$M(\alpha;1;z_i)=2, \tag{6}$$

where $\alpha=30.8/(p\Lambda)^2$ and $z_i=2.07(p/E)^2$.

For the low-pressure case, i.e., where $(\nu/l)^2$ is much less than ω^2, Eq. (3) may be transformed by letting

$$(3m/M)(m/e)(\omega/E)^2u=w \quad \text{and} \quad (M/6m)(l/\Lambda)^2=a.$$

With these substitutions, the equation becomes

$$\frac{d^2f}{dw^2}+\frac{df}{dw}\left(\frac{2}{w}+1\right)+f\left(\frac{2-a}{w}\right)=0. \tag{7}$$

The solution of Eq. (7) is

$$f=e^{-w}[M(a;2;w)+BW(a;2;w)],$$

where the arbitrary constant B is again determined by setting $f=0$ at a value of the independent variable corresponding to $u=16$ volts.

The ionization rate and the diffusion coefficient are calculated in the same manner as for the high pressure region. Applications of the breakdown condition leads to

$$M(a;2;w_i)=2, \tag{8}$$

where $a=61.5/(p\Lambda)^2$ and $w_i=26.0\ 10^3/E^2\Lambda^2$.

It should be noted that there are limits to the values of the experimental parameters within which diffusion theory is valid.[4] The data presented in Figs. 2 and 3 are within these limits.

Nuclear Spin Relaxation in Alkali Metals*

D. F. HOLCOMB† AND R. E. NORBERG‡
Department of Physics, University of Illinois, Urbana, Illinois
(Received September 23, 1954)

Nuclear magnetic resonance measurements have been made in metallic lithium, sodium, and rubidium, using pulsed radio-frequency power. The experimental data are values of T_1, the spin-lattice relaxation time, and of T_2, the inverse line width or spin-spin relaxation time. Measurements were made at several Larmor frequencies and at temperatures between −65°C and 250°C. Over a considerable temperature range, T_1 is found to be primarily determined by interaction with the conduction electrons. The magnitudes of T_1 agree fairly well with the Korringa theory in all three metals. The lithium data in particular indicate that $P_f/P_c \cong 0.6$. In lithium and sodium a dependence of T_1 on the resonance frequency is observed, which cannot be explained on the basis of the Korringa theory. Information about the atomic self-diffusion process is also obtained. Portions of the T_1 and T_2 data are interpreted using the theory of Bloembergen, Purcell, and Pound. In addition, some of the T_1 data are interpreted in terms of the lattice diffusion theory of Torrey. These analyses yield values for D, the coefficient of self-diffusion, of $0.24_{-0.10}^{+0.17} \times \exp(-13\,200 \pm 400/RT)$ cm²/sec in lithium and $0.20_{-0.15}^{+0.56} \times \exp(-10\,000 \pm 600/RT)$ cm²/sec in sodium. Although there is some ambiguity in the interpretation of the rubidium data, they indicate $D \cong 0.23 \exp(-9400/RT)$ cm²/sec. Unusual broadenings of the resonance lines are observed at the melting points in all three metals. These broadenings are not presently understood, but some features of the data can be correlated with a mechanism involving magnetic local fields which arise from lattice imperfections.

I. INTRODUCTION

THIS paper reports the results of a series of nuclear magnetic resonance experiments performed on three of the alkali metals, lithium, sodium, and rubidium, using the spin echo and induction decay techniques of Hahn.[1] The quantities which we have measured are the spin-lattice relaxation time T_1 and the spin phase-memory time T_2. ($T_2 \propto 1/\delta H$, where δH is the resonance line width.) These time constants have been observed over a range of temperatures from −65°C to 250°C, which includes the melting points of all three metals. Measurements were made at several values of the Larmor frequency in each metal.

Nuclear magnetic resonance (NMR) and electron spin resonance (ESR) measurements in metals have already yielded results of significance for the description of metallic properties. NMR measurements of the line shape, line width,[2–5] and paramagnetic shift of the resonance frequency[3–6] in metals and alloys have given information about the magnetic dipolar interactions of the metal nuclei among themselves and with the conduction electrons. In noncubic lattices, effects have been observed[5] which arise from interaction of the nuclear quadrupole moments with electric field gradients existing at the lattice sites. From these measurements and others, information can be deduced about the coefficients of self-diffusion, the phase changes, and the electronic distributions in some metals and alloys. Recently, a combination of NMR and ESR measurements[7] in lithium has resulted in the first direct measurement of the electron spin contribution to the bulk susceptibility of a metal.

However, few measurements of T_1 have been reported. The only literature data seem to be some low-temperature measurements on aluminum,[8] copper,[9] and lithium[10] and room temperature data on copper.[11] Without T_1 data, the shift and line width measurements cannot be exploited so as to yield their full information content about the metallic lattice and the conduction electrons. The T_1 data have been lacking primarily because the usual values of T_1 in metals are inconveniently short for measurement by the "steady state" techniques.

In addition, line-width data have not been available for the narrow lines characteristic of cubic metals at temperatures near their melting points. These lines are typically narrower than the smallest easily achievable magnet inhomogeneities.

T_1 and T_2 in the alkalis fall generally between a few hundred microseconds and one second and are thus in a particularly convenient range for measurement with the pulse technique. The alkali metals were chosen for this work primarily because of their theoretical simplicity insofar as electronic properties are concerned. In addition, reported experiments[2,3] had already shown the existence of self-diffusion induced line width transitions in these metals. The low-melting points of the

* Supported by the Office of Naval Research. This paper is based in part upon a thesis submitted by D. F. Holcomb to the University of Illinois in partial fulfillment of the requirements for the Ph.D. degree (January, 1954).
† National Science Foundation Predoctoral Fellow, September, 1952, to August, 1953. Present address: Department of Physics, Cornell University, Ithaca, New York.
‡ Present Address: Department of Physics, Washington University, St. Louis, Missouri.
[1] E. L. Hahn, Phys. Rev. **80**, 580 (1950).
[2] H. S. Gutowsky, Phys. Rev. **83**, 1073 (1951).
[3] H. S. Gutowsky and B. R. McGarvey, J. Chem. Phys. **20**, 1472 (1952).
[4] H. S. Gutowsky and B. R. McGarvey, J. Chem. Phys. **21**, 2114 (1953).
[5] N. Bloembergen and T. J. Rowland, Acta Metallurgica **1**, 731 (1953).
[6] Townes, Herring, and Knight, Phys. Rev. **77**, 852 (1950).
[7] Schumacher, Carver, and Slichter, Phys. Rev. **95**, 1089 (1954).
[8] J. Hatton and B. V. Rollin, Proc. Roy. Soc. (London) **A199**, 222 (1949).
[9] N. Bloembergen, Physica **15**, 588 (1949).
[10] N. J. Poulis, Physica **16**, 373 (1950).
[11] D. F. Abell and W. D. Knight, Phys. Rev. **93**, 940(A) (1954).

alkalis made it possible to work with the molten metals using relatively crude thermal techniques. Measurements were not made in potassium because of its very small nuclear magnetic moment, which would result in prohibitively small nuclear signals with the present experimental arrangement. Measurements in cesium are planned for the future.

Some of the data on sodium which we report here have already appeared in preliminary form.[12]

II. APPARATUS AND MEASUREMENTS

A typical sample consisted of about 0.5 cc of an oil dispersion of metallic spheres sealed into a pyrex vial. The dispersions were produced by violent mechanical agitation of chunks of the metal in a high boiling point oil at a temperature slightly greater than the melting point of the metal. Average particle radii for the samples used were: lithium, 12μ, sodium, 25μ, and rubidium, 50μ. Typical samples contained an actual volume of about 0.1 cc of the metal. Several of the dispersions were prepared by Dr. T. R. Carver, and the rest supplied by Professor H. S. Gutowsky and his group in the chemistry department of the university.

Relaxation measurements were made using radio-frequencies between 3 and 15 Mc/sec. Over this range all but the rubidium samples have an average particle size smaller than the rf skin depth. It proved possible, using any of the samples, to achieve an rf pulse power setting such that there was no induction decay following the rf pulse. We may therefore infer that the rf attenuation arising from skin effects was quite small, since it was possible to produce rf magnetic fields of amplitude H_1 and pulse length t_w for which the magnetic moment nutational angle $\theta_1=\gamma H_1 t_w$ was equal to π uniformly over substantially the entire sample volume. (γ is the nuclear gyromagnetic ratio. μ, the magnetic moment, is equal to $\gamma\hbar I$, where I is the nuclear spin.) Moreover, it can be shown that there will be no spurious effects on T_1 or T_2 of the type suggested by Bloembergen[13] even if the particles are large compared to the skin depth. These effects, for pulsed experiments, depend on the existence of appreciable diffusion of nuclei through the skin depth in times comparable to T_1 or T_2. The time to traverse one skin depth is about δ^2/D, where δ is the skin depth and D the diffusion constant. The largest values of D in the alkalis in the temperature range involved here are perhaps 10^{-5} cm^2/sec (in the liquid phase). At temperatures corresponding to such a value of D, δ is in the vicinity of 50μ. Thus $\delta^2/D=25\times10^{-6}/10^{-5}=2.5$ sec. Since the largest values of T_1 or T_2 in this temperature region of large D are less than 0.1 sec, skin effects should be negligible.

TABLE I. Spectrochemical analyses of the stock materials.

Sample	Percentages for all metallic impurities $\geq$0.01%
Lithium *A*	Na 0.3; Cu, Si 0.05
Lithium *B*	Na 4; Sb, Pb 0.05
Lithium (Li^6-enriched)	Ca, Fe, Ni 0.01
Sodium *A*	Li 0.1; Ca, Mg, Si, Sr 0.05
Sodium *B*	Li 0.4; Ca, Sr 0.1
Rubidium	(Not analyzed)

[12] R. E. Norberg and C. P. Slichter, Phys. Rev. **83**, 1074 (1951).
[13] N. Bloembergen, J. Appl. Phys. **23**, 1383 (1952).

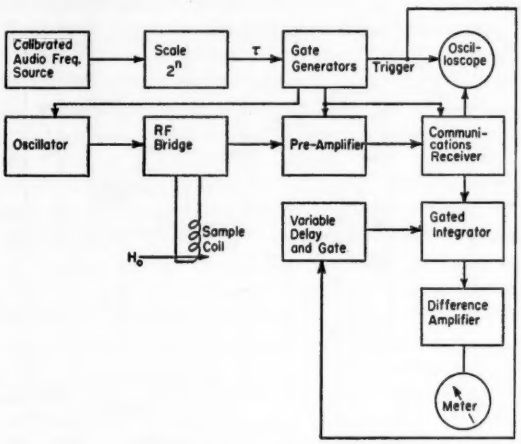

FIG. 1. Block diagram of the apparatus.

The purity of the samples used was not especially good. Table I shows the results of spectrochemical analyses of the stock materials. Most of the lithium and sodium data were obtained with the *A* samples.

A copper-constantan thermocouple was laid against the outside wall of the sample vial and the rf coil then close wound directly onto the vial. For runs above room temperature, a constantan heater was wound noninductively on a card which was then wrapped around the sample. Temperatures below room temperature were attained by immersing the sample coil in a copper trough containing turpentine (whose dielectric constant is relatively insensitive to temperature over the temperature range involved). A coolant mixture of dry ice and acetone flowed through copper tubing soldered to the end walls and bottom of the trough. Temperatures between $-65°$ and 300°C could be maintained and measured to ±1°C with these crude arrangements. The melting points of the lithium and sodium samples were checked calorimetrically by measuring time rate curves of heating and cooling, run with the samples situated in place in the magnet gap. The melting points observed were 97 ± 1°C for sodium (literature value 97.5°C[14]) and 182 ± 1°C for lithium (literature value 180°C[14]). The measured values varied by less than 2°C between rapid-heating and rapid-cooling runs. During most of the T_1 and T_2 measurements, the thermal gradients over the samples were less than 1°C.

The T_1 measurements were made by the application of two rf pulses. As the spacing between these pulses is

[14] C. J. Smithells, *Metals Reference Book* (Butterworth's Scientific Publications, London, 1949).

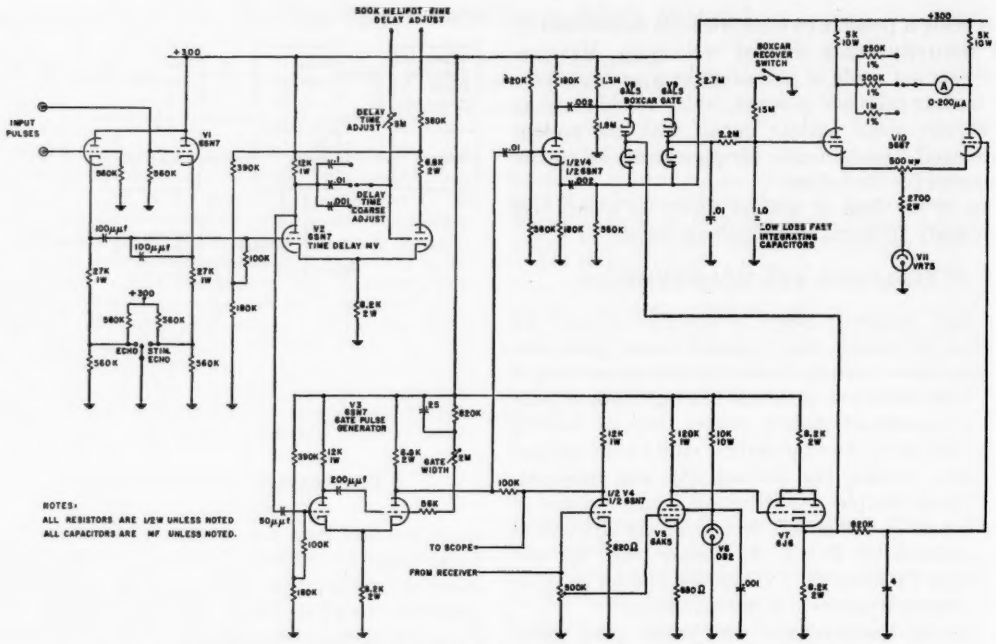

FIG. 2. Boxcar integrating circuit used to improve the signal-to-noise ratio. The necessary gating circuits are also shown in the left part of the figure.

increased, it is found that the initial amplitude of the free induction decay following the second pulse rises along an exponential curve with time constant T_1. The amplitude of the second decay reflects the degree of recovery of the nuclear spin system toward thermal equilibrium in the time interval between the first and second pulses. Most of the T_2 measurements were also made using two rf pulses, following the spin echo technique of Hahn.[1] The amplitude of the echo is observed as a function of the pulse spacing, the resulting exponential decay having time constant T_2. Some T_2 measurements were made using the technique of Carr and Purcell,[15] which is a modification of the Hahn method and involves the application of a series of pulses. The envelope of the echo decay may be observed by the application of a single Carr-Purcell pulse train.

The electromagnet and some of the radio-frequency apparatus have been outlined previously.[16] A block diagram of the experimental arrangement is shown in Fig. 1. A frequency-calibrated audio oscillator provides a basic timing wave which drives a scale of 2^n (where $n=1$ to 5). The interval output of the scaler is used as τ, the separation of the two rf pulses in the Hahn spin echo experiment. The scaler output initiates gate circuits which govern the rf pulses. The variable-frequency pulsed oscillator delivers rf pulses (typically 200 volts, 10 to 50 μsec duration) to a symmetrical twin-T rf bridge, one arm of which contains the sample coil. The output from the bridge is amplified in a preamplifier having about a 100-kc bandpass and a voltage gain of 100. The preamplifier is a modification of the Wallman cascode design.[17] The amplified signal is detected in a communications receiver which has been broad-banded to be 3 db down at ± 15 kc. The preamplifier $B+$ voltage and the suppressor voltage on the first rf amplifier of the receiver are gated downwards during the rf pulse. This switching technique is necessary in order to avoid excessive overdriving of the rf amplifier stages.

The output of the second detector of the receiver is displayed on an oscilloscope and also fed into the electronic measuring circuit shown in Fig. 2. This measuring device is a "boxcar integrator"[18] and is, to a large extent, the work of L. S. Kypta and H. W. Knoebel. The essential operation is that of a cathode follower ($V7$) driving two channels; a reference channel containing a simple RC integrator, and a signal channel containing an electronic switch ($V8$, 9) in the form of a gated diode clamp. This gated diode clamp stage is followed by an RC integrator which utilizes very high leakage impedance condensers (polystyrene insulated). The integrated outputs of the two channels are placed on the input grids of a difference amplifier ($V10$) whose unbalance output is indicated on a meter. At each

[15] H. Y. Carr and E. M. Purcell, Phys. Rev. **94**, 630 (1954).
[16] R. E. Norberg, Phys. Rev. **86**, 745 (1952).
[17] Wallman, Macnee, and Gadsden, Proc. Inst. Radio Engrs. **36**, 700 (1948).
[18] J. L. Lawson and G. E. Uhlenbeck, *Threshold Signals*, Massachusetts Institute of Technology Radiation Laboratory Series (McGraw-Hill Book Company, Inc., New York, 1950), Vol. 24.

repetition of the pulse array, the sampling channel places a charge on the 1.0-μf condenser. The charge is representative of the average signal occurring at $V7$ during the clamp gate. An equilibrium deflection of the output meter is achieved by sampling many pulse repetition intervals. As an example of the use of the circuit consider the method of measuring T_2 with the Hahn two-pulse technique. The two pulses are separated by an interval τ, and the echo occurs at time 2τ. The sampling gate interval is placed on the echo signal at time 2τ and the equilibrium meter deflection recorded. The gate interval is then placed at an arbitrary time on the noise baseline. The difference between the two readings is a measure of the echo amplitude. A plot of such amplitudes as a function of 2τ is exponential with logarithmic slope equal to T_2 if the spin system obeys the Bloch phenomenological equations.[1] Similarly, T_1 is measured by observation of the recovery of the free induction decay following the second rf pulse towards the equilibrium amplitude which corresponds to infinite pulse separation. The relative amplitudes of the decays are measured by automatically keeping the sampling gate at some time $\tau+\epsilon$ on the decay as the time of the second pulse, τ, is varied.

A comparison of the lithium and sodium data presented in Figs. 3 and 6 with those reported earlier[12] from photographic measurements made on similar samples shows the striking improvement of experimental accuracy provided by the gated integrator circuit. The device plays a narrow-banding third detector role for the measurement of transient nuclear resonance signals analogous to that which the familiar "lock-in"[19] plays for the signals of steady state experiments. Full exploitation of the instrument would demand the use of a stable, coherent rf oscillator followed by a gated power amplifier and the use of a phase-sensitive first detector. The difference amplifier could then deliver a center-null output. Our experiments involved amplitude detection of nuclear signals arising from the action of an incoherent pulsed oscillator. The absence of an rf carrier at the time of measurement of the nuclear signals meant that the detector characteristic was non-linear for small nuclear signals. It was necessary to prepare a calibration plot which provided detector corrections to be applied to each measurement.

The T_2 measurements using the technique of Carr and Purcell[15] were made as a check on the possible existence of diffusion-field inhomogeneity effects (Sec. III). For these measurements, R. L. Trogdon designed a pulser which provided the required arrays of pulses with $\theta_1=\pi/2$ and π. The Carr-Purcell T_2 runs were measured by either using the boxcar integrator or by photographing the oscilloscope display.

III. SUMMARY OF THE EXPERIMENTAL RESULTS

A brief outline of some of the experimental results obtained for Li^6, Li^7, Na^{23}, Rb^{85}, and Rb^{87} is given at this point. Detailed analyses of the complete data for each isotope will be made in the subsequent sections. This initial summary is intended to emphasize the major similarities and differences among the data in the various metals.

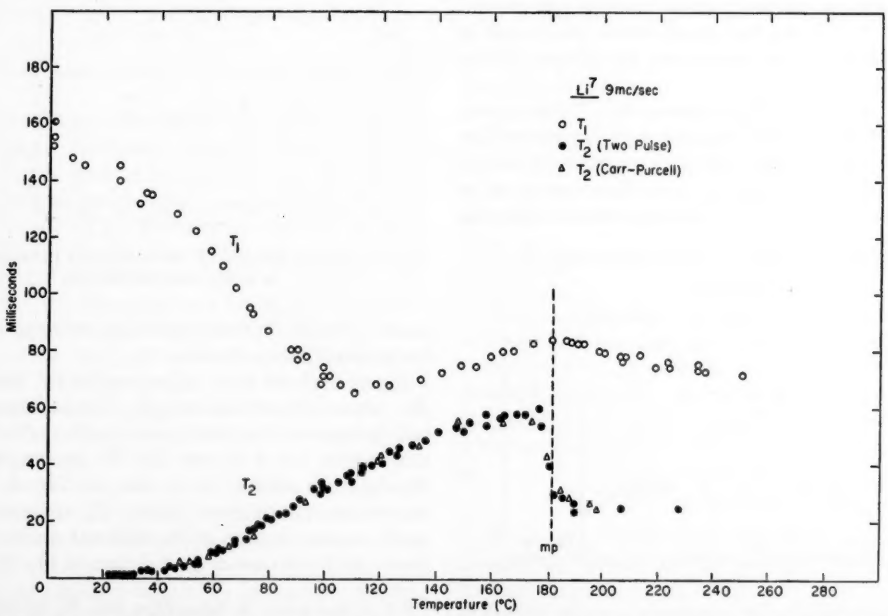

FIG. 3. T_1 and T_2 data for Li^7, measured in a sample of natural abundance, at a Larmor frequency of 9.0 Mc/sec.

[19] Bloembergen, Purcell, and Pound, Phys. Rev. 73, 679 (1948).

Figure 3 shows T_1 and T_2 obtained between 0°C and 250°C for the Li^7 resonance at 9.0 Mc/sec in a sample of natural isotopic abundance (92.1 percent Li^7, 7.9 percent Li^6). T_1 is seen to decrease as the temperature is increased until about 110°C, where a minimum in T_1 occurs. Thereafter T_1 increases until 180°C, then decreases again for higher temperatures. This T_1 behavior will be shown in the next section to result from the superposition of two contributions to the nuclear relaxation. The first relaxation contribution arises from the interaction with the conduction electrons, is designated $(T_1)_e$, and should be inversely proportional to the absolute temperature. The second is a contribution from the direct nuclear dipole-dipole interaction, $(T_1)_d$. $(T_1)_d$ goes through a minimum at the temperature at which the inverse of the mean time which a diffusing nucleus spends at a given lattice site is of the order of ω_0, the Larmor angular frequency. The initial increase of T_2 with increasing temperature is a continuation of the line narrowing observed by Gutowsky and McGarvey[3] to begin near 230°K. The narrowing line width in this region appears to arise entirely from the diffusion-limited nuclear dipolar interaction. T_2 increases until the T_1 contribution to T_2 becomes important [see Eq. (3), Sec. IV]. At the melting point a sharp reduction of T_2 occurs. This corresponds to a surprising broadening of the resonance line upon melting. The broadening is doubly unusual in that it is not accompanied by any associated T_1 decrease. The presence of the T_1 minimum at 110°C indicates that the correlation frequency for the self-diffusive motion has become much greater than the Larmor frequency by the time the melting point is reached, and therefore one would expect $T_1 \cong T_2$,[20] if the high-temperature interaction is able to produce nuclear relaxation. We return to this point in Sec. IV, C.

The complete T_1 and T_2 curves of Fig. 3 were reproducible for both samples A and B with no irreversible effects observed over the indicated temperature range. One possible source of a spurious broadening at a melting point is a suddenly increased rate of diffusion of the nuclei through the static inhomogeneous magnetic field distribution impressed over the sample by the magnet. The effect of such a process can be shown[1,16,21] to be an echo envelope decaying as $\exp(-t/T_2 - kt^3)$, where k is a constant involving the magnetic field gradient and the diffusion coefficient. The additional kt^3 term, if undetected, can result in misinterpretation of the data so as to yield T_2's substantially lower than the true values. Since there was evidence of non-exponential echo envelopes for lithium at high temperatures, check runs of the T_2 data were made by using the method of Carr and Purcell.[15] Their technique removes, in first order, the diffusion-inhomogeneity kt^3 term. The experimental results obtained with the Carr-Purcell technique are plotted as triangles in Fig. 3. The line-broadening at the melting point is shown to be real.

Figure 4 shows the results for Li^6 obtained at 6.0 Mc/sec in a sample enriched to 93.8 percent Li^6, 6.2 percent Li^7.[22] The accuracy of the data obtained from this sample does not approach that for Li^7 in natural abundance, but it is clear that T_1 decreases steadily as the temperature is increased, with no evidence of a minimum. As in Fig. 3, T_2 increases as the nuclear dipolar interaction averages out with increasing diffusion rate, and then levels off rather sooner, with respect to T_1, than in the Li^7 data above. At the melting point T_2 for Li^6 decreases suddenly, although somewhat less markedly than for Li^7.

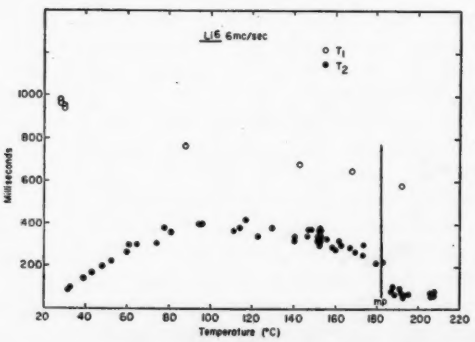

FIG. 4. T_1 and T_2 data for Li^6, measured in a sample enriched to 94 percent Li^6, at 6.0 Mc/sec.

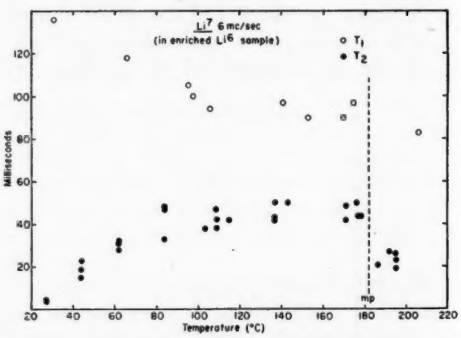

FIG. 5. T_1 and T_2 data for Li^7 in the enriched Li^6 sample referred to in Fig. 4, at 6.0 Mc/sec.

Figure 5 shows data taken on the Li^7 resonance in this same Li^6-enriched sample. The accuracy is very poor because of the small concentration of Li^7 nuclei in this sample, but it is seen that the general features of the data are similar to the data in Fig. 3, with two exceptions. The nuclear dipolar T_1 minimum is very much weaker because of the different nuclear environment. As in the case of the Li^6 data in Fig. 4, T_2 in the

[20] R. K. Wangsness and F. Bloch, Phys. Rev. 89, 728 (1953).

[21] T. P. Das and A. K. Saha, Phys. Rev. 93, 749 (1954).

[22] We are indebted to the Stable Isotope Division of the Oak Ridge National Laboratory (U. S. Atomic Energy Commission) for supplying the enriched metal.

region just below the melting point is appreciably less than T_1.

Figure 6 shows 9.0-Mc/sec data for Na^{23}. Here again, T_1 is in general inversely proportional to the absolute temperature, with a slight decrease occurring at the melting point. This reduction will be interpreted as reflecting the volume dependence of $(T_1)_e$. Most of the low temperature T_2 data in Fig. 6 have been published previously.[12] They extend to higher temperature the line-width transition reported by Gutowsky.[2] T_2 appears to become limited by T_1 near room temperature, and at the melting point displays a broadening similar to that observed in lithium. A few T_2 measurements were made in sodium using the Carr-Purcell technique and verified the T_2 behavior shown in Fig. 6.

Figure 7 shows data obtained for the Rb^{85} and Rb^{87} resonances in a sample of natural abundance (73 percent Rb^{85} and 27 percent Rb^{87}). Few T_2 points were measured because of experimental limitations at the short T_2 values in rubidium and because of rather poor

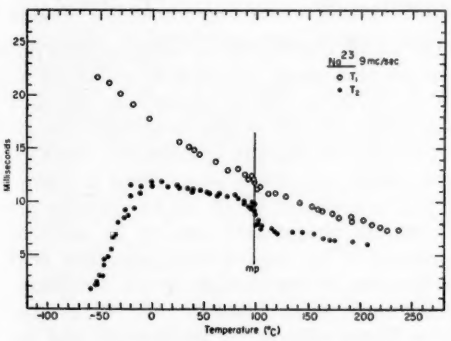

FIG. 6. T_1 and T_2 data for Na^{23} at 9.0 Mc/sec.

signal-to-noise ratios. The data in the two isotopes were taken at about the same magnetic field (7500 oe), corresponding to Larmor frequencies of 3.0 Mc/sec for Rb^{85} and 10.5 Mc/sec for Rb^{87}. The Rb^{87} data show a T_1 minimum near 0°C. The dashed curve indicates T_2 corresponding to the Rb^{87} line width data of Gutowsky and McGarvey[4] and the assumption of a Lorentz line shape, that is, the absorption as a function of frequency is assumed proportional to $1/[1+T_2^2(\omega-\omega_0)^2]$, where ω_0 is the Larmor angular frequency. Above the melting point T_1 is inversely proportional to the absolute temperature within the large experimental scatter. In the liquid, T_2 is equal to T_1 within the error of the observations.

In Rb^{85} the low-temperature T_1 data are qualitatively similar to those in Rb^{87}, with the minimum shifted (as it should be for lower Larmor frequency) towards lower temperature, and lying beyond the range of measurements. T_2 presumably equals T_1 below the melting point, but there are no reliable T_2 data. Again, T_1 decreases with increasing temperature above the melting point, and appears to be entirely $(T_1)_e$. In Rb^{85},

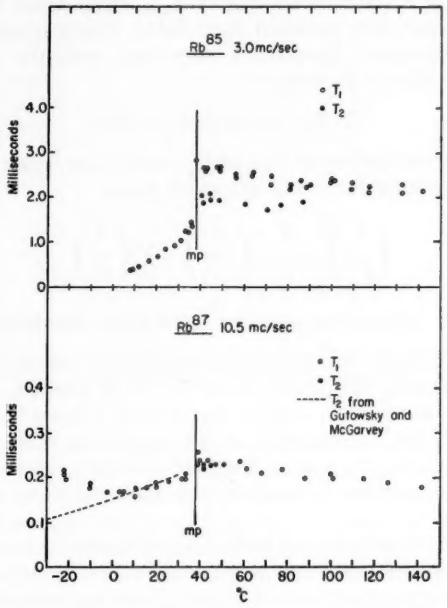

FIG. 7. T_1 and T_2 for a rubidium sample of natural isotopic abundance, 73 percent Rb^{85} and 27 percent Rb^{87}. The Rb^{85} measurements made at 3.0 Mc/sec and the Rb^{87} measurements made at 10.5 Mc/sec correspond to roughly the same value of H_0, the applied static magnetic field.

T_2 in the liquid metal is significantly less than T_1, which indicates the presence of a line broadening similar to that observed in molten lithium and sodium.

Some significant common features of the data in all of the alkalis investigated are a behavior of T_2 near room temperature which reflects a diffusion-induced transition of the dipolar line width, T_1 generally proportional to $1/T$ with several instances of the occurrence of T_1 minima, and an unexpected high-temperature line-width term, very pronounced in lithium, less so in sodium, and visible in rubidium only as an extra broadening in one isotope.

IV. INTERPRETATION OF THE EXPERIMENTAL RESULTS

In the subsequent sections we shall attempt to separate and examine the interactions arising from several sources. In general, we shall assume that an observed spin-lattice relaxation time is the resultant of contributions from a number of lifetime-limiting processes whose effects add as transition probabilities, i.e.

$$1/T_1=\sum_i(1/T_1)_i. \quad (1)$$

If all the interactions which contribute significant line broadenings correspond to the same line shape, then the line widths add and

$$1/T_2=\sum_i(1/T_2)_i. \quad (2)$$

Each line-width term may be further reduced to the

sum of a static broadening $(1/T_2')$, which arises from the essentially constant local fields, and a quantum indeterminacy broadening associated with the spin state lifetime T_1,[19] that is,

$$(1/T_2)_i=(1/T_2')_i+(1/2T_1)_i. \tag{3}$$

The combination of (2) and (3) permits the separation of the individual static line width terms,

$$\left(\frac{1}{T_2'}\right)_i=\frac{1}{T_2}-\left(\frac{1}{2T_1}\right)_i-\sum_{j\neq i}\left(\frac{1}{T_2}\right)_j. \tag{4}$$

A. Interaction with the Conduction Electrons

We begin the detailed examination of the data by considering the interaction of the nuclei with the conduction electrons. Heitler and Teller[23] pointed out in 1936 that there should be a very potent relaxation process for the nuclear magnetic moments in a metal via a spin-spin interaction with the conduction electrons.

The Hamiltonian describing the magnetic interaction of the nucleus with the conduction electrons is discussed by Bloembergen and Rowland.[5] There are three main terms in the interaction, the $\mathbf{I}\cdot\mathbf{S}$ hyperfine nuclear spin-electron spin term which occurs because of the finite value of the electron wave function at the position of the nucleus, the "outside" nuclear spin-electron spin interaction, and a nuclear spin-electron orbit term. The first term is generally by far the largest, and gives rise to a strong relaxation process for the nuclei. Another observable effect of the hyperfine interaction upon the nuclear magnetic resonance in a metal is a paramagnetic shift of the resonance frequency for a nucleus in the metal with respect to the resonance frequency for the same nuclear species in an isolated atom (usually approximated experimentally by a salt).[24] Townes, Herring, and Knight[6] have shown the shift to be a measure of the electron spin contribution to the magnetic susceptibility of the metal, that is,

$$\frac{\Delta H}{H_0}=\frac{8\pi}{3}\chi_a P_f=\frac{I}{2I+1}\frac{\Delta E}{\mu_e\mu_n}\chi_a\frac{P_f}{P_a} \tag{5}$$

in which ΔH is the shift of the resonance frequency and H_0 is the applied static magnetic field. χ_a is the electron spin contribution to the susceptibility per atom, ΔE is the hyperfine splitting of the ground state of the free atom, P_f is the probability density evaluated at the nucleus for an electron in the Fermi surface, and P_a is the probability density at the nucleus for the valence electron in the free atom.

In 1950, Korringa[25] and, independently, Slichter[26] examined the relation between the shift $\Delta H/H_0$ and $(T_1)_e$, the electron contribution to the nuclear spin-lattice relaxation time. Korringa performed a first-order perturbation calculation, using Bloch wave functions for the electrons. The diagonal matrix elements of the Hamiltonian are responsible for the paramagnetic or "Knight" shift, and the off-diagonal terms give the transition probabilities between adjacent m-levels of the nucleus and thus determine $(T_1)_e$.

The nuclear spin-electron orbit term in the Hamiltonian vanishes to first order because of the local electric fields which quench the orbital angular momentum of the electrons in the metal. The quenching should be complete except for a small effect arising from the electron spin-orbit interaction. The spin-spin terms outside the nucleus should be small compared to the hyperfine term, especially so in the alkalis where P_f is rather large. Korringa's result for $(T_1)_e$, considering only the hyperfine interaction, may be written

$$\frac{1}{(T_1)_e}=\frac{4\pi kT}{\hbar}v_0^2\rho^+(\epsilon_0)\rho^-(\epsilon_0)\left(\frac{P_f}{P_a}\frac{\Delta E}{2I+1}\right)^2, \tag{6}$$

where $\rho^{\pm}(\epsilon_0)$ are the densities of electron states per unit volume per unit energy for spins up and down respectively, evaluated at the Fermi surface, and v_0 is the atomic volume. Korringa also considered the outside spin-spin and the nuclear spin-electron orbit contributions, which give rise to small terms in addition to (6). $(T_1)_e$ is predicted by (6) to be inversely proportional to the temperature and to be substantially independent of the applied static magnetic field H_0. These features are not changed by the addition of the aforementioned extra terms to (6). In a magnetic field the Fermi surfaces for electrons of spin up and spin down are separated by an energy $2\gamma_e\hbar H_0$, so there is a small dependence of $\rho^+(\epsilon_0)$ and $\rho^-(\epsilon_0)$ on H_0. However, $\gamma_e\hbar H_0$ is only about 0.01 percent of the Fermi energy ϵ_0, and the effect on $(T_1)_e$ should be very small indeed.

Korringa's result for the Knight shift, also calculated in the free electron approximation, is

$$\frac{\Delta H}{H_0}=\frac{\gamma_e\Delta E}{\gamma_n(2I+1)}v_0\rho^+(\epsilon_0)\frac{P_f}{P_a}. \tag{7}$$

Combination of (6) and (7) leads to what is usually referred to as the "Korringa relation,"[25,26]

$$T_1\left(\frac{\Delta H}{H_0}\right)^2=\frac{\hbar\gamma_e^2}{\pi kT4\gamma_n^2}. \tag{8}$$

It should be noted that Overhauser[27] has derived an expression for $(T_1)_e$ by a slightly different method, and his result agrees exactly with (6).

In addition to the magnetic interactions, there could be a significant coupling between the quadrupole mo-

[23] W. Heitler and E. Teller, Proc. Roy. Soc. (London) **A155**, 629 (1936).
[24] W. D. Knight, Phys. Rev. **76**, 1259 (1949).
[25] J. Korringa, Physica **16**, 601 (1950).
[26] C. P. Slichter (unpublished).
[27] A. W. Overhauser, Phys. Rev. **89**, 689 (1953).

ment of a nucleus with spin $\geqslant 1$ and an electric field gradient at the nucleus arising from the conduction electrons. Such a term has been discussed by Bloembergen and Rowland,[5] but should be negligible for the cubic alkali metals.

Figures 8 through 11 show T_1 data in the various metals, plotted as a function of the reciprocal of the absolute temperature. The plotted points differ slightly from the experimental data given in Sec. III in that T_1 has been corrected for the volume dependence of $(T_1)_e$ as given by (6). The product $v_0^2\rho^2$ is proportional to $v_0^{4/3}$ in the free electron approximation. Because of thermal expansion of the metal, this introduces a small temperature dependence into (6) in addition to the general $1/T$ behavior of $(T_1)_e$. This small additional temperature dependence has been removed, normalizing to the experimental points at 25°C in lithium and sodium and at 40°C in rubidium. Coefficients of thermal expansion were taken from the literature.[28] Equation (8) predicts that the product $T_1(\Delta H/H_0)^2$ should be proportional to $1/T$ with no volume dependence. If the sodium T_1 data of Fig. 6 are so combined with the literature shift values,[4] the results agree with the 9-Mc/sec data of Fig. 10.

The straight lines in the figures are drawn with the inverse temperature dependence predicted by (6), normalized to the experimental points at room temperature in lithium and sodium, and at 40°C in rubidium. It is evident that the major T_1 contributions in these metals are indeed inversely proportional to the absolute temperature. One also notices that in Li^7 and Na^{23} there is a 5 to 10 percent variation of the entire T_1 curve as the magnetic field H_0 is changed by a factor of 3. This point will be considered later in this section.

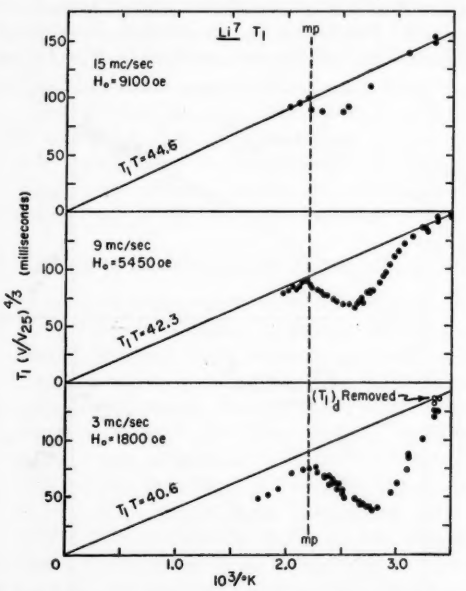

FIG. 8. T_1 data for Li^7, taken at three values of the Larmor frequency and adjusted to remove the $v_0^{-4/3}$ dependence predicted by Eq. (6). The data are plotted against the reciprocal of the absolute temperature in units of $10^3/°K$. The straight lines are drawn with the $1/T$ dependence predicted by Eq. (6) and normalized to the data at 300°K.

[28] *International Critical Tables* (McGraw-Hill Book Company, Inc., New York, 1933).

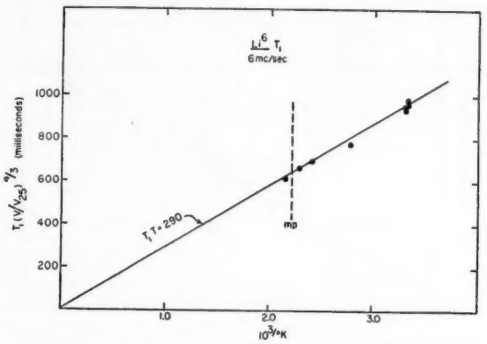

FIG. 9. T_1 data for Li^6, adjusted to remove the $v_0^{-4/3}$ dependence and plotted against reciprocal temperature. The straight line is determined as in Fig. 8.

Table II presents a correlation of the experimental T_1 data with the theoretical expressions (6) and (8). Values for lithium and sodium are taken at 300°K, where the temperature dependence and other considerations indicate that the contribution to the experimental T_1 from interactions other than that with the electrons is small. For the same reason, values for rubidium are taken at 40°C, just above the melting point.

$(T_1)_e$ is calculated from Eq. (6) by using the available theoretical values of m/m^* and P_f/P_a, as indicated in the table. The free electron approximation is modified only to the extent of the use of an effective mass in the evaluation of $v_0\rho$. [$v_0\rho=3/(4\epsilon_0)$ and $\epsilon_0=\hbar(3\pi^2/v_0)^{\frac{1}{3}}/2m^*$.] The general result is that (6) is fairly successful in predicting T_1 when an m^* is used. It should be noted that we have ignored possible effects of correlations among the electrons upon the density of states ρ. A recent calculation by Pines[29] indicates that ρ might be affected to perhaps 10 percent by electron correlation and exchange.

The results for Li^6 and Li^7 are mutually consistent when values at constant ν_0 are compared. [The $(\Delta E/(2I+1))^2$ term in (6) means that $(T_1)_e$ should be proportional to γ_n^{-2}.] The Rb^{85} and Rb^{87} results are also in good mutual agreement.

The value for P_f/P_a in lithium is from a recent recalculation by Kohn with an improved method. The previous value was 1.0.[30] The T_1 data at 15.0 Mc/sec, if taken to represent $(T_1)_e$, indicate that $P_f/P_a\cong 0.6$. The measured T_1's are all somewhat smaller than the values predicted by (6). The consistent discrepancy

[29] D. Pines (private communication).

[30] W. Kohn and N. Bloembergen, Phys. Rev. **80**, 913 (1950); Phys. Rev. **82**, 283 (1951).

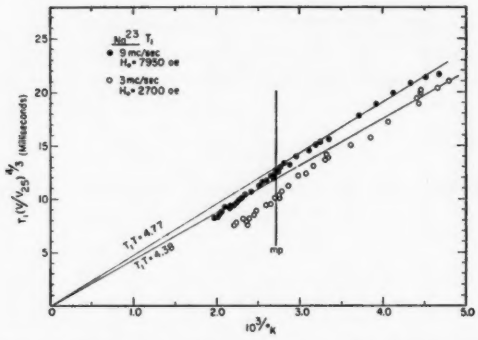

FIG. 10. T_1 data for Na^{23}, taken at two values of the Larmor frequency, adjusted to remove the $\nu_0^{-4/3}$ dependence and plotted against reciprocal temperature. The straight lines are determined as in Fig. 8.

may indicate the presence of an additional relaxation term, and is discussed at the end of this section.

Inspection of the final columns of Table II reveals that the "Korringa relation" (8) yields consistently low T_1's. It should be noted that this discrepancy is in the opposite direction to the effect to be expected if the terms omitted from (6) actually contributed to $(T_1)_e$. If these terms were important, the experimental T_1's would be shorter than those predicted by the Korringa relation. Equation (7), which is more successful, particularly in sodium, is one of the two expressions involved in (8). A check calculation of the shifts predicted by (7) shows that the discrepancy found between experiment and the results of (8) is also present in (7). The measured alkali shifts are all larger than (7) would predict. The Townes, Herring, and Knight expression (5) for the shift is in very good agreement with the measured shifts if current measured[7,31] or theoretical χ_a values are used. In lithium, in particular, the recently measured[7] χ_a agrees with Pines'[32] calculated value and both coincide with χ_a calculated from $\Delta H/H_0$. The failure of (7) seems to arise from the fact that a free electron calculation of the spin susceptibility, even using an effective mass, is not adequate. It should be noted that (7) becomes more successful with increasing Z.

The Li^7 data, Fig. 8, are particularly interesting in that the T_1T product of about 45 is very different from the results of Poulis[10] at low temperatures. He has observed a dependence on ν_0 qualitatively similar to ours, although even more pronounced. However, comparing our 15.0-Mc/sec data with Poulis's results at 15.4 Mc/sec (at which frequencies both sets of data are most nearly proportional to $1/T$) one finds his T_1T at 20°K to be about 25 sec deg as compared with our 45. Although Poulis used the "saturation method"[19] described by Bloembergen, in which there exists the possibility of a calibration error, such an error seems unlikely since Poulis was able to make direct observations of recovery to equilibrium for the longer T_1's as a check on his calibration. The other possibility is a peculiar plateau of the T_1 against T plot between 20°K and 273°K, which seems even more unlikely. Unfortunately, experimental limitations on measurements at short T_2's prevented us from measuring T_1 at liquid nitrogen temperature.

It is difficult to reconcile a significant dependence of $(T_1)_e$ upon the applied static field or the resonance frequency with Eq. (6). As previously pointed out, the only field dependence of $(T_1)_e$ arising from the $\mathbf{I}\cdot\mathbf{S}$ hyperfine term lies in the small effect of H_0 upon the product $\rho^+(\epsilon_0)\rho^-(\epsilon_0)$, and this effect should be completely negligible. Even if the dipole-dipole or spin-orbit contributions to $(T_1)_e$ were appreciable, they should be independent of H_0. It is even more difficult to account for the observed effect in terms of a dependence of $(T_1)_e$ upon ν_0, since the correlation frequency describing the motion of the conduction electrons is much greater than ν_0, and changes in ν_0 should not affect the efficacy of the interaction.

There is one piece of information from the data of Table II which indicates that we are dealing with a dependence of T_1 upon the resonance frequency rather than the applied field, H_0. Consider the relative magnitudes of T_1 measured for Li^6 and Li^7. The results at 300°K are: for Li^6 at 6.0 Mc/sec and 9600 oe, $T_1=965$ msec; for Li^7 at 6.0 Mc/sec and 3600 oe, $T_1=138$ msec; and for Li^7 at 15.0 Mc/sec and 9100 oe, $T_1=150$ msec.

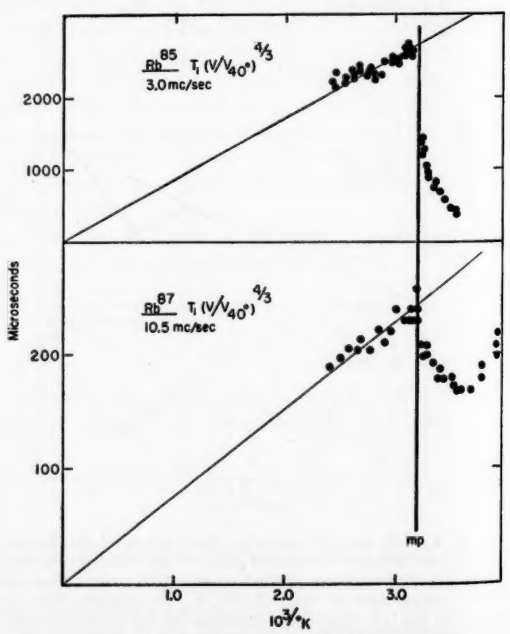

FIG. 11. T_1 data for the rubidium isotopes, with the $\nu_0^{-4/3}$ dependence removed from the data above the melting point, plotted against reciprocal temperature.

[31] S. R. Rao and K. Sarithri, Proc. Indian Acad. Sci. **6**, 207 (1942).
[32] D. Pines, Phys. Rev. **95**, 1090 (1954).

TABLE II. Comparison of experimental and theoretical values of $(T_1)_e$.

	Experiment				Theory				
					Korringa T_1 expression Eq. (6)			"Korringa relation" Eq. (8)	
	ν_0 Mc/sec	H_0 oersteds	T °K	T_1 msec	m/m^*[a]	P_f/P_a	$(T_1)_e$ msec	$\Delta H/H_0$[b]	$(T_1)_e$ msec
Li^6	6.0	9600	300	965±35	0.69	0.5[c]	1590		(616)
Li^7	15.0	9100	300	150±5	0.69	0.5[c]	227	2.61×10^{-4}	88
	9.0	5400		141					
	6.0	3600		138					
	3.0	1800		(136)					
Na^{23}	9.0	8000	300	15.9±0.3	1.02	0.81[d]	16.8	11.2×10^{-4}	10.3
	3.0	2700		13.9					
Rb^{85}	3.0	7300	313	2.75±0.2	1.12	1.0[e]	3.3	65×10^{-4}	2.1
Rb^{87}	10.5	7500	313	0.245±0.02	1.12	1.0[e]	0.29	65×10^{-4}	0.18

[a] H. Brooks (private communication to D. Pines), reference 32.
[b] See reference 3.
[c] W. Kohn, Phys. Rev. 96, 590 (1954). We are indebted to Dr. Kohn for communicating his results to us prior to publication.
[d] See reference 6.
[e] Estimated.

In none of these values does there appear to be a significant $(T_1)_d$ contribution (see Sec. IV, B). From (6), $(T_1)_e$ should be proportional to γ_n^{-2}. $\gamma_7^2/\gamma_6^2=7.0$, therefore the measured Li^6 value predicts a $(T_1)_e$ of 138 msec for Li^7. The γ_n^{-2} dependence seems to hold for constant ν_0 rather than constant H_0. The experimental value for Li^7 at 9100 oe, even assuming the maximum error, corresponds to a minimum value for $(T_1)_e$ of 1020 msec, which is outside the error on the Li^6 T_1 at 9600 oe.

One additional feature of the apparent frequency dependence should be noted. The volume-corrected T_1 curves pass smoothly through the melting point in sodium, and appear to do so in lithium. If the frequency or field dependence arises from any interaction involving the lattice, one would expect a break in the T_1 curve at the melting point. The conduction electrons appear to be the only likely source of an interaction which is insensitive to melting, but the frequency or field dependence probably arises from some interaction other than those which have been mentioned.

B. Effects of Self-Diffusion: Dipolar T_1 and T_2

We now turn to the effects of lattice diffusion on T_1 and T_2 in the alkali metals. A general theory of the T_1's and T_2's which result from interactions of the nuclei with fluctuating local magnetic fields has been given by Bloembergen, Purcell, and Pound[19] and in Bloembergen's thesis.[33] (The Bloembergen, Purcell, and Pound paper will be referred to as BPP in the following.) We will be interested in the BPP theory as it relates to nuclear dipole-dipole interactions and the effects of diffusional motion of the nuclei. The BPP theory was developed in detail for the case of isotropic liquid media, but many of the results are valid for the body-centered cubic lattice of the alkalis. We will also make use of a more complete theory developed by Torrey[34] for T_1 in the case of translational diffusion in a lattice.

[33] N. Bloembergen, *Nuclear Magnetic Relaxation* (Martinus Nijhoff, The Hague, 1948).
[34] H. C. Torrey, Phys. Rev. 92, 962 (1953).

BPP consider the case in which the local magnetic fields at one nuclear site arise from surrounding nuclear dipoles of the same species. The BPP expression for the contribution to the line width from essentially static local fields is

$$\left(\frac{1}{T_2'}\right)_d=\frac{3}{2}\gamma^2\hbar\left(\frac{I(I+1)}{3}\frac{1}{2\pi}\int_{-2/T_2'}^{2/T_2'}J_0(\omega)d\omega\right)^{\frac{1}{2}}, \quad (9)$$

where J_0 is the Fourier transform of the time spectrum of dipolar local fields. The subscript d indicates nuclear dipolar fields as the source of the interaction. For the case of interaction with only one nearest neighbor, Bloembergen[33] obtains

$$\left(\frac{1}{T_2'}\right)_d=\left[\frac{6}{5}\gamma^4\hbar^2\frac{I(I+1)}{b^6}\frac{1}{2\pi}\int_{-2/T_2'}^{2/T_2'}\frac{\tau_c}{1+\omega^2\tau_c^2}d\omega\right]^{\frac{1}{2}}, \quad (10)$$

where τ_c is a correlation time for the relative motion of the nuclei and b is the internuclear distance. The theory has been extended slightly to the case of a homogeneous distribution of nuclear dipoles,[35] and, in this case, one has

$$\left(\frac{1}{T_2'}\right)_d=\frac{3}{2}\gamma^2\hbar\left(\frac{I(I+1)}{3}\frac{1}{2\pi}\times\int_{-2/T_2'}^{2/T_2'}\int_{r=a}^{\infty}\frac{32\pi N}{5r^4}\frac{\tau_c}{1+\omega^2\tau_c^2}drd\omega\right)^{\frac{1}{2}}, \quad (11)$$

where the r-integration is taken from a minimum nuclear impact parameter a. For translational diffusion, the correlation time may be written $\tau_c=r^2/12D$, where D is the diffusion coefficient, $D_0\exp(-E_D/RT)$. N is the number of nuclei per unit volume. Only the low-frequency components of J_0 enter into expression (9) for T_2'. The effective components are those for which $\omega^2\tau_c^2\leqslant(2/T_2')^2\tau_c^2\ll1$. Using this fact, one obtains

[35] R. E. Norberg, thesis, University of Illinois, 1951 (unpublished).

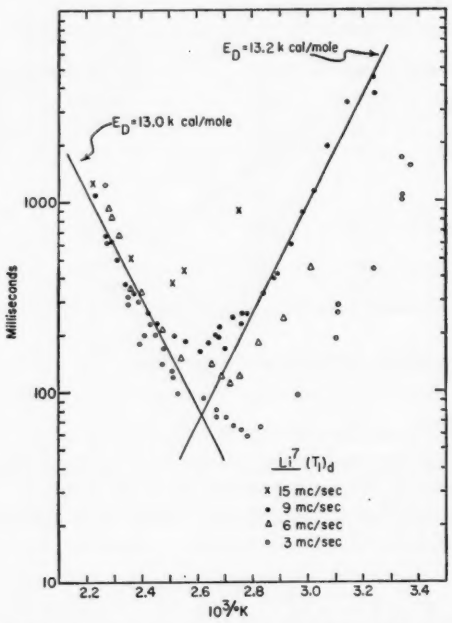

FIG. 12. $(T_1)_d$ for Li^7 at four different frequencies, plotted against reciprocal temperatures, showing the minimum in $(T_1)_d$ and the shift of the minimum with frequency. The straight lines are least-squares fits of those 9-Mc/sec data which lie outside the region of the curved minimum.

$J_0(\omega)=8\pi N/12Da$ and, from (9),

$$(1/T_2')_d=4\gamma^4\hbar^2I(I+1)N/5Da. \tag{12}$$

In the case of the b.c.c. alkali lattices, a will be taken as the nearest neighbor distance.

The fluctuating local fields also produce spin-flipping if the characteristic frequency of the fluctuations is in the vicinity of the Larmor frequency. The flipping provides a spin-lattice relaxation process since magnetic energy is exchanged with the energy of lattice motions. By a method similar to that used in deriving Eq. (11), BPP obtain

$$\left(\frac{1}{T_1}\right)_d=\frac{5\pi}{3}N\gamma^4\hbar^2I(I+1)\int_a^\infty\frac{1}{r^4}\left\{\frac{\tau_c}{1+\omega_0^2\tau_c^2}+\frac{2\tau_c}{1+4\omega_0^2\tau_c^2}\right\}dr. \tag{13}$$

From (13) the important features of the T_1 behavior may be seen. At low temperatures we have the relation $\omega_0^2\tau_c^2\gg1$, therefore $T_1\propto\tau_c$. Again using $\tau_c=r^2/12D$ and integrating (13), we obtain

$$(1/T_1)_d=144\pi\gamma^4\hbar^2I(I+1)ND/25\omega_0^2a^5 \tag{14}$$

for this region of low temperatures. $(T_1)_d$ is inversely proportional to D, and therefore decreases exponentially as the temperature increases. When a temperature is reached such that $\omega_0\tau_c=1/\sqrt{2}$, Eq. (13) gives a minimum value for $(T_1)_d$. At higher temperatures where $\omega_0^2\tau_c^2\ll1$, if we again substitute for τ_c and integrate (13), the result is

$$(1/T_1)_d=2\pi\gamma^4\hbar^2I(I+1)N/5Da, \tag{15}$$

so that $(T_1)_d$ is now proportional to D and increases exponentially as the temperature goes toward ∞.

1. *Lithium*

Let us first examine the Li^7 T_1 minimum. To represent the combination of $(T_1)_e$ and any frequency-dependent $(T_1)_x$ which may exist, we select a smooth curve drawn through the T_1 data at room temperature and those just above the melting point. The curve is nearly proportional to $1/T$ and includes a small decrease at the melting point corresponding to the volume change. The $(T_1)_d$ data resulting from the reciprocal subtraction corresponding to Eq. (1) are shown in Fig. 12. The asymptotic form of the extremes of the minima is seen to be exponential, in agreement with (14) and (15). A least-squares fit of the 9.0-Mc/sec data yields the activation energies indicated. The displacement of the temperatures T_m at which the minima occur as a function of the Larmor frequency ω_0, is well fitted by the relation $\ln\omega_0\propto-E_D/RT_m$, which arises from the condition that $\omega_0\tau_c$ be equal to a constant at the minimum and the assumption that $\tau_c\propto\exp(-E_D/RT)$. A semilog plot of the frequencies against $1/T_m$ is exponential with a slope of about 13 kcal/mole. The minimum $(T_1)_d$'s are proportional to ω_0, which is a general result for motional relaxation, independent of a detailed theory.

In order to determine a diffusion coefficient from the $(T_1)_d$ data, we consider first the high-temperature region, where the relation $\omega_0^2\tau_c^2\ll1$ holds. Here, Eq. (15) is independent of the shape of the cutoff of the spectrum of local fields and is thus unaffected by the particular choice of correlation function. If we take $a=3.02$ A (the nearest-neighbor distance in lithium), $N=4.37\times10^{22}$/cc [from N(b.c.c.)$=2/$(lattice parameter)$^3\times$percent abundance of Li^7], and the measured $(T_1)_d$ of 0.58 sec at $10^3/°K=2.30$, we obtain $D=5.0\times10^{-8}$ cm^2/sec. If we accept 13.2 kcal/mole as the activation energy (see T_2' data below), this result corresponds to $D=0.23\exp(-13\,200/RT)$. The contribution of the 8 percent of Li^6 moments to $(T_1)_d$ and $(T_2')_d$ can be shown to be about 0.3 percent, and it has been neglected in the above considerations. On the low-temperature side of the minimum, (14) fails to yield results consistent with the data. Using $D=0.23\exp(-13\,200/RT)$, Eq. (14) predicts $(T_1)_d=4.3$ sec at $10^3/°K=3.00$ and 9.0 Mc/sec, whereas the observed value is 0.95 sec. It is to be noted that (14) depends upon the choice of correlation function and, because of the a^5 dependence, is very sensitive to a choice of minimum impact parameter.

Torrey[34] has extended the BPP theory to a more precise computation of $(T_1)_d$ for specific cases of trans-

lational lattice diffusion. Assuming that the self-diffusion process consists of a random walk with uniform flight path distance l, his result [reference 34, Eq. (86)] is

$$\left(\frac{1}{T_1}\right)_d = \frac{8\pi}{5}\gamma^4\hbar^2 I(I+1)\frac{n}{k^3 l^3 \omega}\Psi(k,y), \qquad (16)$$

where we take l to be the nearest neighbor distance, and $\Psi(k,y)$ is a function which Torrey has tabulated for a f.c.c. lattice. Using the proper Ψ tabulation for a b.c.c. lattice[36] (for which $k=0.763$), we have applied the theory to the Li^7 data. The method of analysis was to normalize the data of Fig. 12 by forming the ratio $T_1/(T_1)_{\text{minimum}}$ and determine the corresponding $\omega_0\tau/2$ from the tabulated functions. A plot of $\omega_0\tau/2$ against $1/T$ is shown in Fig. 13, corresponding to the 3.0-Mc/sec data of Fig. 12. The analyzed data closely follow an exponential curve, with the indicated activation energy of 13.2 kcal/mole. It should be noted that Torrey uses $\tau=r^2/6D$, so that his τ is equal to twice the τ_c used here.

Torrey's expression, (16), in its low-temperature asymptotic form, provides a better agreement with the observed $(T_1)_d$ than does Eq. (14) from the BPP theory. At $10^3/°K=3.00$, where the 9.0-Mc/sec $(T_1)_d$ is measured to be 0.95 sec, the Torrey expression, with $D=0.24\exp(-13\,200/RT)$, predicts $(T_1)_d=1.2$ sec. As stated previously, Eq. (14) gives 4.3 sec. The BPP and Torrey theories both successfully fit the moderately high temperature $(T_1)_d$ data, for which $\omega_0^2\tau_c^2\ll 1$. Here the effective local fields near ω_0 arise primarily from remote nuclei, since the neighboring nuclei contribute mainly very high frequency terms. On the other hand, the Torrey theory provides a much better fit of the low-temperature T_1 data ($\omega_0^2\tau_c^2\gg 1$) than does the BPP result (14). In this region it is the near neighbors that make the main relaxation contribution, with the remote nuclei providing mainly static terms. The near neighbors are just those for which the distribution of sites deviates most from the BPP assumption of homogeneity, and for which a precise lattice description is most significant.

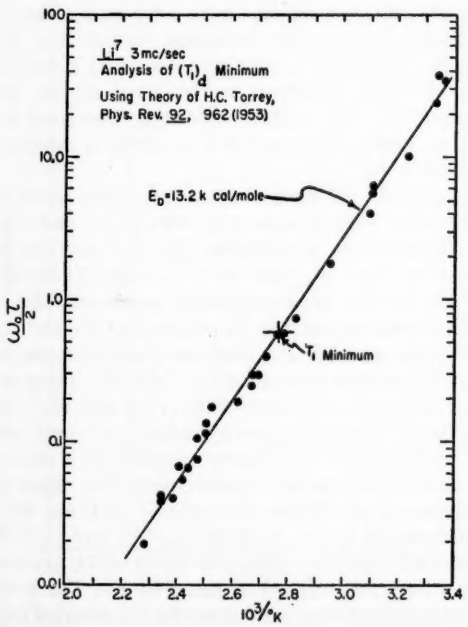

FIG. 13. Plot of $\omega_0\tau/2$ against reciprocal temperature, obtained from analysis of $(T_1)_d$ data for Li^7 at 3 Mc/sec from Fig. 12 using the Torrey theory.

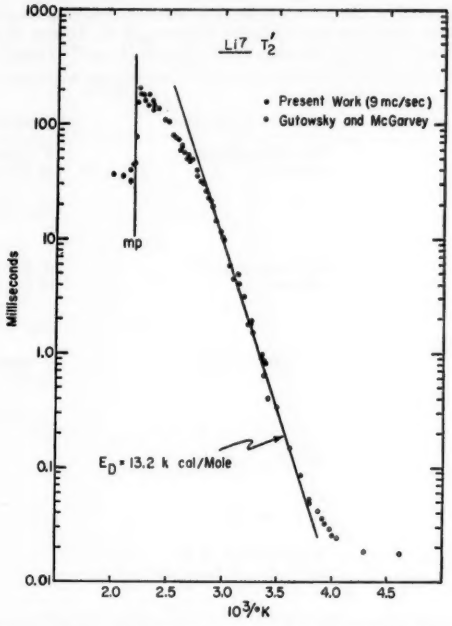

FIG. 14. T_2' for Li^7, calculated from the data of Fig. 3 using Eq. (17) and plotted against reciprocal temperature. The straight line is a best fit of the data in the region of the exponential dependence of T_2' on temperature.

One advantage of Torrey's method is that it facilitates examination of the $(T_1)_d$ data in the immediate vicinity of the minimum, where the corrections for $(T_1)_e$ are smallest. Substitution of the maximum value of Torrey's b.c.c. Ψ function into (16) results in a prediction of $(T_1)_d=225$ msec at the 9.0-Mc/sec T_1 minimum. The observed value (Fig. 12) is about 190 msec.

In order to examine the dipolar T_2 terms in the data, it is necessary to remove the electron line width contributions. Wangsness and Bloch,[20] in examining the range of validity of the Bloch phenomenological equations,[37] show that in an isotropic medium at high temperatures, where the characteristic frequency of the motion of the

[36] H. C. Torrey, Phys. Rev. 96, 690 (1954). We are indebted to Professor Torrey for providing us with the b.c.c. tabulations of his functions in advance of publication.

[37] F. Bloch, Phys. Rev. 70, 460 (1946).

TABLE III. Diffusion coefficients in lithium, resulting from interpretation of the relaxation data with an extension of the theory of BPP and with the lattice diffusion theory of H. C. Torrey. E_D is given in kcal/mole and all D_0's are calculated for $E_D=13.2$ and given in cm²/sec. Indicated average result: $D=(0.24_{-0.10}^{+0.17})\exp[(-13\,200\pm400)/RT]$ cm²/sec.

		BPP theory		Torrey theory	
ν_0	Region of the data	Relation used	Result	Relation used	Result
9.0 Mc/sec	low temperature $\omega_0^2\tau_c^2\gg1$	T dependence of $(T_1)_d$	$E_D=13.2$	T dependence of $\omega_0\tau$	$E_D=13.2$
		Eq. (14)	($D_0=0.05$)	Eq. (16), low T asymptote	$D_0=0.30$
	high temperature $\omega_0^2\tau_c^2\ll1$	T dependence of $(T_1)_d$	$E_D=13.0$	Eq. (16), high T asymptote	$D_0=0.20$
		Eq. (15)	$D_0=0.23$		
	T_2' below 370°K	T dependence of T_2'	$E_D=13.2\pm0.4$		
		Eq. (12)	$D_0=0.25$		
3.0 Mc/sec	all $(T_1)_d$ data			T dependence of $\omega_0\tau$	$E_D=13.2$
	at T_1 minimum			$\omega_0\tau/2=0.592$	$D_0=0.26$
15.0, 9.0 6.0, 3.0 Mc/sec	Temperature of T_1 minimum as function of ω_0		$E_D=13$		

magnetic moment is much greater than the Larmor frequency, one has $T_2'=2T_1$. In this case, Eq. (3) becomes $T_2=T_1$, which agrees with a classical argument that at these high frequencies for the nuclear motion the Larmor precession becomes a small effect and T_1 and T_2 represent the same quantity, since the uniqueness of the z-direction is lost. The motions of the conduction electrons are such that $(\omega_c)_e\gg\omega_0$. Therefore, $(T_1)_e=(T_2)_e$ and Eq. (4) becomes, considering only dipolar and conduction electron terms,

$$\left(\frac{1}{T_2'}\right)_d=\frac{1}{T_2}-\left(\frac{1}{2T_1}\right)_d-\left(\frac{1}{T_1}\right)_e. \qquad (17)$$

Turning to the T_2 data, it was found that in Li^7 near room temperature, where T_1 effects are small, T_2 is independent of the Larmor frequency from 3.0 to 15.0 Mc/sec, as one would expect. In order to inspect the static line width term $(T_2')_d$, we make the reciprocal subtraction described in Eq. (17). We have assumed that any $(T_1)_x$ may be included with the $(T_1)_e$ insofar as line width effects are concerned. The results for the 9.0-Mc/sec data of Fig. 3 are shown in Fig. 14. The line width data of Gutowsky and McGarvey[3] have been converted to T_2' under the assumption of a Lorentz line shape, which is the shape they observed at low temperatures.[38] For this line shape, $T_2=2/(\sqrt{3}\gamma\delta H)$, where δH is measured between the maxima of $d\chi''/dH_0$. The computed T_2's increase from the rigid lattice value and join smoothly onto the low-temperature end of our observations. The data are fitted by an exponential, corresponding to $E_D=13.2$ kcal/mole, from the lowest temperature at which the narrowing has gotten well under way, up through nearly three decades of T_2'. Beyond 100°C, however, T_2' no longer increases at a constant rate, but rather bends down as if either the activation energy were decreasing [which the $(T_1)_d$ data do not indicate] or another line width interaction were becoming important as the direct dipolar term averages out. The sudden broadening associated with melting is seen to correspond to an order of magnitude decrease in T_2'.

Considering the room-temperature region where T_2' seems to be entirely associated with $(T_2')_d$ and where the T_1 correction is negligible, Eq. (12) and the line drawn in Fig. 14 yield $D=0.25\exp(-13\,200/RT)$ cm²/sec. As has been previously mentioned, the Li^6 nuclei contribute less than 0.3 percent to $1/T_2'$ and have been neglected here. The results of the dipolar analyses of the Li^7 data are summarized in Table III. Those data which we have associated with $(T_1)_d$ and $(T_2')_d$ are seen to be in generally good agreement with each other and with the BPP and Torrey theories. As a result of the several independent measurements, we regard the coefficient of self-diffusion for metallic Li^7 below 400°K as determined to be $D=(0.24_{-0.10}^{+0.17})\exp[(-13\,200\pm400)/RT]$ cm²/sec. The error limits on D_0 are those dictated by the assigned accuracy of E_D. The results in Table III indicate that, within the temperature range of the data, D is determined to ±15 percent. The thermodynamical relation of Nachtrieb *et al.*[39] gives $E_D=16.5L_m$, where L_m is the latent heat of melting.

[38] H. S. Gutowsky and B. R. McGarvey (private communication).

[39] Nachtrieb, Weil, Catalano, and Lawson, J. Chem. Phys. 20, 1189 (1952).

This appears to work well in many metals, but predicts E_D for lithium to be 11.34 kcal/mole. The earlier Van Liempt relation,[40] $E_D = 32 \times$ melting temperature, predicts 14.5 kcal/mole.

We now consider the T_2 data for both the Li^6 and Li^7 resonances in the enriched Li^6 sample, from Figs. 4 and 5. Although the enriched sample contains 93.8 percent Li^6 and only 6.2 percent Li^7, the Li^7 moments still make an appreciable contribution to the $(T_2')_d$ observed for Li^6. The expression corresponding to Eq. (12) for the case of two nuclear species in the lattice can be shown to be[41]

$$\left(\frac{1}{T_2'}\right)_a = \frac{4\gamma_a^4\hbar^2 I_a(I_a+1)N_a}{5Da} + \frac{8\gamma_a^2\gamma_b^2\hbar^2 I_b(I_b+1)N_b}{15Da}. \quad (18)$$

Figure 15 shows the Li^6 T_2' data corresponding to the data of Fig. 4. The line which passes through the low-temperature points in Fig. 15 is the theoretical result of Eq. (18), if one uses $D = 0.24 \exp(-13\,200/RT)$. The accuracy of the data does not quite permit us to see the 8 percent difference between D for Li^6 and for Li^7 which should arise from the $(m)^{-\frac{1}{2}}$ dependence of D_0. The high-temperature behavior of the Li^6 T_2' is qualitatively similar to that observed for Li^7 (Fig. 14) and will be discussed in Sec. IV, C.

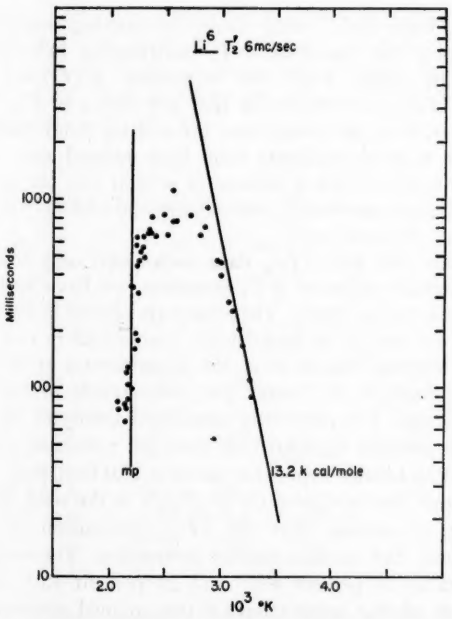

FIG. 15. T_2' for Li^6, calculated from the data of Fig. 4 and plotted against reciprocal temperature. The theoretical line is drawn with the slope determined from the data of Fig. 14 and its position determined by the prediction of Eq. (18).

[40] J. Van Liempt, Z. Phys. **96**, 534 (1935).
[41] D. F. Holcomb, thesis, University of Illinois, 1954 (unpublished).

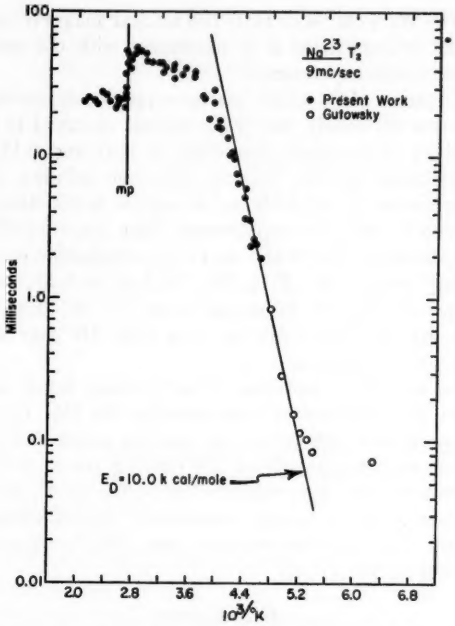

FIG. 16. T_2' for Na^{23}, calculated from the data of Fig. 6 and plotted against reciprocal temperature. The straight line is a best fit of the data in the region of the exponential dependence of T_2' on temperature.

The Li^7 resonance in the enriched Li^6 sample gave the results which have been shown in Fig. 5. Again, as for the Li^6, the low-temperature T_2's for the Li^7 are successfully predicted by Eq. (18). There are only vestigial traces of a weak dipolar T_1 minimum in the Li^7 data for this sample, as should be the case because of the weak nuclear dipolar environment.

2. *Sodium*

The 9.0-Mc/sec sodium data of Fig. 6 have been converted to T_2' by using $1/T_2' = 1/T_2 - 1/T_1$, from Eq. (4). The results are shown in Fig. 16. We have again assumed that any $(T_1)_x$ may be included in $(T_1)_e$ insofar as line-width effects are concerned. As in lithium the relaxation measurements join smoothly onto the T_2' calculated from the line-width data.[2] The exponential section of the data has a slope of 10.0±0.6 kcal/mole. The error here is greater than for the lithium data of Fig. 15 because the exponential region is a decade shorter for the sodium T_2'. Equation (12) and the line drawn in Fig. 16 yield $D = (0.20_{-0.15}^{+0.56}) \times \exp[(-10\,000 \pm 600)/RT]$, where the limits of error on D_0 correspond to those assigned to E_D. Nachtrieb and co-workers[42] have used the radioactive tracer technique in sodium to measure $D = 0.242 \exp[(-10\,450$

[42] Nachtrieb, Catalano, and Weil, J. Chem. Phys. **20**, 1185 (1952).

$\pm 300)/RT]$ cm²/sec. Thus the nuclear magnetic resonance determination is in agreement with the results of the tracer experiments.

Equation (16), which has been previously shown to describe accurately the $(T_1)_d$ minima observed in Li^7, predicts $(T_1)_d$ values in sodium of 0.37 and 0.12 sec respectively at the 9- and 3-Mc/sec minima. The temperature of the 3-Mc/sec minimum is calculated to be 265°K from the requirement that $\omega_0\tau_c=0.5922$ at the minimum. The 9-Mc/sec $(T_1)_d$ contribution is completely masked by $(T_1)_e$ (Fig. 10) but, at 3 Mc/sec, a 10 percent dip in T_1 should occur at $10^3/°K=3.77$. The experimental 3-Mc/sec data (Fig. 10) may show this weak minimum.

As in lithium isotopes, T_2' in sodium bends away from the exponential corresponding to Eq. (12) at temperatures well below the melting point and then decreases precipitously at the melting point. Also, as in lithium, the temperature dependence of T_2' in the molten metal is poorly determined, but is certainly small. The high-temperature data will be discussed further in Sec. IV, C.

3. *Rubidium*

In the rubidium isotopes, we do not have direct T_2 data below the melting point. However, the Rb^{87} line width data reproduced in Fig. 7 and the qualitative similarities to the lithium and sodium data make it fairly certain that in Rb^{87} we have T_1 data which include a diffusion-induced T_1-minimum with $T_2\cong T_1$ on the high-temperature side, and that in Rb^{85} we have just the high-temperature side of a T_1 minimum (and presumably $T_2\cong T_1$). The Rb^{87} minimum at 273°K for 10.5 Mc/sec and the use of $E_D=9$ kcal/mole indicate that the Rb^{85} minimum should occur, for 3.0 Mc/sec, at about 250°K, well below the temperature range of our Rb^{85} measurements. Extending a volume-corrected

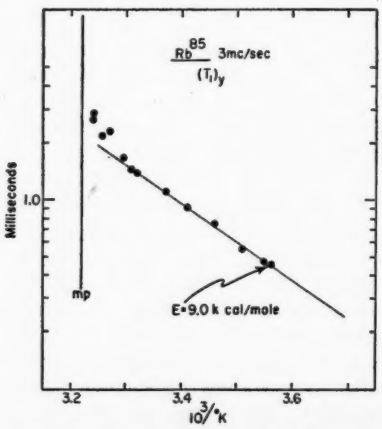

FIG. 17. $(T_1)_y$ for Rb^{85}, calculated from the data of Fig. 7 below the melting point by making a correction for $(T_1)_e$. The straight line is the best line through all data except the four points just below the melting point.

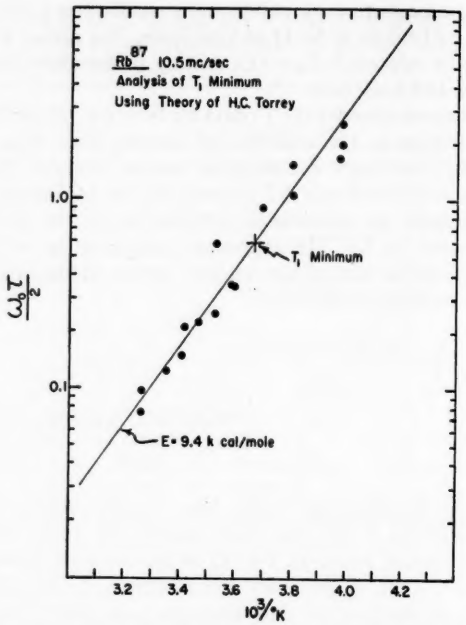

FIG. 18. $(T_1)_y$ for Rb^{87}, calculated from the data of Fig. 7 below the melting point by making a correction for $(T_1)_e$. The data have been analyzed using the Torrey theory in the same fashion as the Li^7 data plotted in Fig. 13.

$(T_1)_e$ from the T_1 data above the melting point, we compute the nonelectron T_1 contribution below the melting point with the expression $1/(T_1)_y=1/T_1-1/(T_1)_e$. The results for Rb^{85} are shown in Fig. 17. Except for a few points near the melting point (rather large thermal gradients may have existed over the sample which had a volume of several cc), the $(T_1)_y$ fall along a reasonably good exponential with activation energy 9.0 kcal/mole.

Since the Rb^{87} $(T_1)_y$ data correspond only to the immediate region of a T_1 minimum, we have applied the method of Torrey. The results are plotted in Fig. 18 and are seen to be surprisingly exponential in view of the obvious limitation of the experimental accuracy. The slope of the Torrey plot corresponds to $E=9.4$ kcal/mole. The previously mentioned theory of Nachtrieb predicts $E_D=8.6$ kcal/mole for rubidium, while the Van Liempt expression predicts 10.0 kcal/mole.

From the isotopic ratio of $(T_1)_y$'s in the solid, however, it appears that the $(T_1)_y$ mechanism is not entirely the nuclear dipolar interaction. The sample contains 73 percent Rb^{85} and 27 percent Rb^{87}. The result of the application of the coupled system T_1 equation analogous to Eq. (18)[41] is that the ratio of $(T_1)_d$ measured in Rb^{85} with respect to that in Rb^{87} is predicted to be 11.2 in the temperature region above the minimum, while the observed ratio near $10^3/°K=3.25$ is about 2. In the next section, we will interpret the T_2 measurements in molten rubidium as indicating

the presence of an additional broadening interaction in Rb^{85}. If we regard the small ratio between the T_1's for the isotopes in the solid phase as the result of a similar reduction of T_1 for Rb^{85} in the solid, then there is the possibility that the Rb^{87} $(T_1)_y$ minimum is entirely dipolar. If so, the Torrey plot (Fig. 18) and Torrey's relation $\omega_0\tau_c=0.5922$ at the minimum, yield $D_0=0.23$ cm²/sec for $E_D=9.4$ kcal/mole. This D_0 value is similar to that previously obtained for lithium and sodium.

C. Anomalous Effects, Mainly T_2 at High Temperatures

In this section we consider several aspects of the data which are not clearly understood. The most striking of these effects are the decrease of T_2 at the melting point in lithium and sodium and the line width contribution, in addition to $1/(T_2)_e$ and $1/(T_2)_d$, which is visible in lithium and sodium over a region of about one hundred degrees centigrade below the melting points.

It was first thought that the high-temperature T_2 effects were associated with an interaction of the nuclear quadrupole moment with electric field gradients caused by imperfections in the b.c.c. metallic lattices.[43] In order to check this hypothesis, measurements were made on the Li^6 and Li^7 resonances in the Li^6-enriched metal obtained from Oak Ridge.[21] For a broadening arising from the postulated quadrupole interaction, there are two possible dependences on the nuclear parameters. If the interaction is subjected to averaging out because of motions in the lattice (as one would expect in the liquid) then[44]

$$1/T_2 \propto Q^2[4I(I+1)-3]/I^2(2I-1)^2.$$

In this case, $(T_2)_{Li^6}/(T_2)_{Li^7}=507$, since $Q_6/Q_7=2.3\times10^{-2}$.[45] If, instead, there is some sort of static, unaveraged interaction, one expects

$$1/T_2 \propto Q[4I(I+1)-3]^{\frac{1}{2}}/I(2I-1),$$

in which case $(T_2)_{Li^6}/(T_2)_{Li^7}=23$. The magnetic moment of Li^6 is also smaller than that of Li^7, but only by a factor of 4, so that magnetic interactions should give rise to smaller T_2 ratios than those given above. As can be seen in Figs. 4 and 5, T_2 above the melting point in Li^6 is less than a factor of 3 longer than T_2 for Li^7 in the same sample. This ratio effectively rules out quadrupolar interactions.

TABLE IV. $(T_2')_x$ in solid and liquid alkali metals near their melting points. The high-temperature static line widths have been calculated in the solids with $(1/T_2')_x=1/T_2'-(1/T_2')_d$. In the liquids, $(T_2')_x=T_2'$.

	ν_0 (Mc/sec)	H_0 (oe)	Liquid T (°K)	Liquid $(T_2')_x$ msec	Solid T (°K)	Solid $(T_2')_x$ msec
In the Li^6-enriched sample:						
Li^6	6	9600	473	81±8	450	480
	3	4800		116±16		
Li^7	6	3600	473	32±4	450	62
In the samples with natural isotopic abundance:						
Li^7	15	9100	473	23±3	450	(250)
	9	5400		35±4		220
	6	3600		47±5		
Na^{23}	9	8000	390	24±2	313	57
	3	2700		23±3		56
Rb^{85}	3	7300	313	7±2		

In order to examine the high-temperature line-width term we calculate $(T_2')_x$ from the T_2' data of Sec. IV, B with the appropriate form of Eq. (4); $1/(T_2')_x=1/T_2'-1/(T_2')_d$. Table IV lists the results of this manipulation of the data for sodium, rubidium, and the two lithium isotopes. Above the melting points the $(T_2')_d$ correction is negligible and $(T_2')_x$ is just T_2', that is, T_2 with the T_1 contribution removed. It should be noted that the high-temperature broadenings are very small compared to rigid lattice dipolar widths. The T_2 of about 25 msec in molten Li^7 corresponds to a resonance line width of about 0.004 gauss.

The temperature dependence of the $(T_2')_x$ data calculated from the 9.0-Mc/sec Li^7 data of Fig. 14 is shown in Fig. 19. Some data taken at other frequencies are also shown. The absolute values of the $(T_2')_x$ points in the solid lithium are certainly suspect, since they are two correction processes removed from the raw data. The line drawn is a least squares fit of the 9.0-Mc/sec data, arbitrarily assuming an exponential temperature dependence. The individual $(T_2')_x$ data in the liquid are more reliable, since the corrections to T_2 are relatively much smaller than in the solid. The temperature dependence of $(T_2')_x$ in the liquid is small. Although

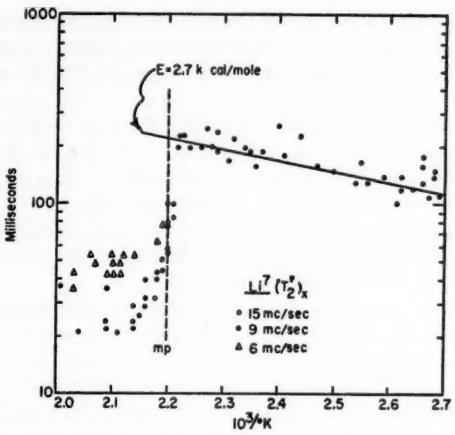

FIG. 19. The high-temperature contribution to T_2 in Li^7 $(T_2')_x$, which has been calculated by removing the dipolar and conduction electron contributions from the T_2 data measured at several Larmor frequencies.

[43] D. F. Holcomb and R. E. Norberg, Phys. Rev. **93**, 919(A) (1954).

[44] R. K. Wangsness and F. Bloch, reference 22, Eq. (5.40).

[45] N. A. Schuster and G. E. Pake, Phys. Rev. **81**, 157 (1951).

the 15.0-Mc/sec data in the solid are in approximate agreement with the 9.0-Mc/sec results, there is a consistent inverse dependence of $(T_2')_x$ in the liquid upon the Larmor frequency.

$(T_2')_x$ obtained from the sodium T_2' data of Fig. 16 shows a temperature dependence in the solid even smaller than that in lithium. Moreover, $(T_2')_x$ drops at the melting point by a factor of only two. The sodium $(T_2')_x$ curves for 9.0 Mc/sec and 3.0 Mc/sec are indistinguishable, with no frequency dependence visible in either the solid or liquid.

The exact mechanisms responsible for the unusual broadenings are not yet understood. However, many of the features of the high-temperature data are consistent with the presence of a magnetic interaction with thermally activated lattice imperfections. We shall list the experimental facts about the broadenings and discuss briefly some of their implications about the nature of the high-temperature interactions.

1. *Decrease in T_2 upon Melting*

The most striking feature of the data is the sudden decrease in T_2 at the melting point in lithium and sodium. The decrease is unaccompanied by a drop in T_1 other than the previously discussed small variation which arises from the volume dependence of $(T_1)_e$. An interaction is indicated which either appears only upon melting or which becomes much stronger in the liquid.

In some metals the self-diffusion coefficient increases by several orders of magnitude upon melting.[46,47] If this is true in the alkalis, the increased D in the liquid should effectively narrow the nuclear dipolar line width $1/(T_2')_d$ to zero. However, if one assumes that the x-interaction arises from magnetic fields associated with the distorted electron cloud near a vacancy, then, by analogy with (12),

$$1/(T_2')_x \propto n/D_v, \tag{19}$$

where $n=n_0\exp(-E_F/RT)$ is the number of vacancies per unit volume. D_v is a diffusion coefficient describing the vacancy motion. If the self-diffusion mechanism is via an atom-vacancy interchange, this D_v is much larger than the atomic self-diffusion coefficient D, and therefore is the determining factor in the narrowing. The activation energy to be associated with D_v is E_M, the barrier or mobility energy. (For the atomic self-diffusion, $E_D=E_F+E_M$.) Thus, (19) becomes

$$(T_2')_x \propto \exp(E_F-E_M/RT). \tag{20}$$

The effect of melting upon a $(T_2')_x$ described by (19) can be a reduction (that is, a line broadening) if the melting produces a larger increase in n than in D_v.

2. *Results in the Solid Metals Near Their Melting Points*

The $(T_2')_x$ terms in solid lithium and sodium have several features in common. The data in Table IV indicate that $(T_2')_x$ in solid lithium and sodium is independent of the Larmor frequency (or of H_0). $(T_2')_x$ first becomes appreciable in lithium and sodium about one hundred degrees centigrade below the melting points (Figs. 14 and 16). This is just the region of temperature in which the resistivities[48] and specific heats[49] become anomalous and where the gradual disintegration of the metallic lattices begins to affect x-ray data.[50] The anomalous resistivity and specific heat terms apparently are associated with the appearance of significant concentrations of thermally activated vacancies in the lattice. Therefore, the explanation of $(T_2')_x$ in this temperature region in terms of a vacancy interaction seems reasonable. However, according to (20), if $E_F>E_M$, which is probably the case, then $(T_2')_x$ should decrease as the temperature rises. Figure 19 shows the opposite to be true. Moreover, crude calculations indicate that a magnetic interaction with the vacancies would not be sufficiently strong to produce the observed effects upon T_2. The situation remains unresolved.

It should be noted that in a solid in which there is vacancy diffusion and in which a vacancy interaction does determine the line width, the temperature dependence indicated by Eq. (20) combined with a knowledge of E_D should permit separate determination of E_F and E_M. Bloembergen[51] has independently recognized this fact.

The unexplained ratios of the T_1's measured in the solid for the two rubidium isotopes (Sec. IV, B) may be connected with the interactions which cause the $(T_2')_x$ effects in all three alkalis, but the point is not clear.

3. *Results in the Liquid Metals*

$(T_2')_x$ in liquid lithium is independent of the isotopic species of the surrounding nuclei (Table IV). The high-temperature T_2 in Fig. 3 for Li^7 in a sample of natural isotopic abundance is approximately the same as T_2 in Fig. 5 for Li^7 in the 93 percent Li^6 sample. Since the local fields caused by the nuclear moments are very different in the two samples, the source of the local fields responsible for the reduced T_2 in the liquid must be external to the nuclear spin system. The similarity of the T_2's in the liquids is surprising in view of the nonequality of the T_2's in the solid samples. In Sec. 4, below, we describe evidence for impurity effects on T_2 in lithium which are important below the melting point but are not evident in the liquid.

$(T_2')_x$ in liquid lithium and sodium is nearly temperature independent. Bloembergen and Rowland[8] have observed the resonance lines in two liquid Hg-Tl alloys to be insensitive to temperat ureand not appreciably narrower than in the solid phases. The $(T_2')_x$ interaction

[46] W. Jost, *Diffusion in Solids, Liquids, Gases* (Academic Press, Inc., New York, 1952), p. 335.
[47] Careri, Paoletti, and Salvetti, Nuovo cimento **11**, 399 (1954).
[48] D. K. C. MacDonald, J. Chem. Phys. **21**, 177 (1953).
[49] L. G. Carpenter, J. Chem. Phys. **21**, 2244 (1953).
[50] C. C. Bidwell, Phys. Rev. **27**, 381 (1926).
[51] N. Bloembergen (to be published).

present in the molten alkalis may be a feature common to many liquid metals and alloys.

From the data presented here and the measurements of Bloembergen and Rowland, it appears that many liquid metals may have T_2 values appreciably less than T_1. Such is not the case for those nonmetallic liquids upon which measurements have been reported. The conduction electrons appear to be the source of the magnetic local fields which determine the line widths in those liquid metals which exhibit T_2 values not determined by T_1. The line widths in liquid lithium and sodium may be the result of anomalous local fields arising from distortion of the electron distribution in the vicinity of imperfections. Since no unusual behavior of T_1 is observed near the melting points, the local magnetic fields in question presumably result from a polarization effect and lie only along the direction of H_0. The alternate explanation for the lack of a T_1 effect would be a low-correlation frequency for the high-temperature interaction, which seems quite unlikely in the liquid metals.

4. *Dependence of the Results upon the Purity of the Samples*

The indications that the high-temperature broadenings arise from interaction with magnetic field sources external to the nuclear spin system lead one to suspect impurities in the metals as a source of some of the anomalous effects. Unfortunately, the total impurity content of our samples is not well known. We do know the metallic impurities in the lithium and sodium samples from spectrographic analyses (Table I). There appears to be little dependence of the data upon these impurities. Lithium samples A and B have sodium as their primary impurity, and differ by a factor of 10 in their sodium contents. Yet the data in Fig. 3 show no difference between the T_2's shown as dots, which were obtained using sample A and those indicated by triangles, which were measured in sample B. It appears more likely that the impurities significant for T_2 might be chemical compounds on the surface or dissolved into the metal particles. Because of the high chemical reactivity of the alkali metals, it is difficult to prevent the occurrence of chemical reactions on the surfaces of the metal particles. There is some evidence that nonmetallic impurities can play a role in the extra broadenings, at least in the region just below the melting points. A comparison of Figs. 3 and 5 shows that, as has been mentioned in Part 3, there are definitely smaller T_2's below the melting point in Fig. 5. A similar reduction of T_2 in the region just below the melting point was produced in lithium sample A by removing most of the oil from the sample (in air) so that there was no protective coating on the particle surfaces. Fortunately, we do have good evidence that at least the major part of the extra broadenings is independent of the surface condition. Dr. T. R. Carver was able to produce, under a helium atmosphere and in a degassed oil, a lithium dispersion in which the particles retained a bright metallic sheen. The T_2 measurements given as triangles in Fig. 3 were made with this sample. They agree with the other T_2 measurements in Fig. 3 which were made in a sample in which the particles were visibly darkened, probably because of the formation of lithium azide at the surfaces.

No differences in T_2 among the various samples was observed above the melting point.

The sodium sample listed as B in Table I gave T_2's lower than those given in Fig. 6. In B, lower T_2's were also observed above the melting point. A small extra decrease of T_1 was observed in the liquid, although T_1 in the solid agrees with the data in Fig. 6. This is the only sample in any of the metals in which a sample dependence of T_1 was observed.

Quantitative investigation of the anomalous effects considered in Sec. IV, particularly in the solid phase in the temperature region just below the melting point, evidently requires more careful control of sample purity than has been achieved in this work.

ACKNOWLEDGMENTS

We would like to thank Professor H. S. Gutowsky and Dr. B. R. McGarvey for communication of some of their results prior to publication. We are indebted to them and to Dr. T. R. Carver for the metallic dispersions used in the experiments. Many of the electronic circuits were designed by H. W. Knoebel and L. S. Kypta. J. Spokas assisted in some of the measurements. Discussions with Professor D. Pines and Professor D. Lazarus were very helpful. Particular thanks are due to Professor C. P. Slichter for his continuing assistance and encouragement throughout the progress of this work.

Molecular Constants and Nuclear-Molecular Interactions of Li^7F^{19} by the Molecular Beam Electric Resonance Method*

R. BRAUNSTEIN† AND J. W. TRISCHKA
Syracuse University, Syracuse, New York
(Received February 4, 1955)

The electric resonance method of molecular beam spectroscopy was used to observe the Li^7F^{19} spectra arising from transitions of the type $(J,m_J) \rightarrow (J,m_J')$. Data were taken for the $(1,0) \rightarrow (1,\pm1)$ and $(2,0) \rightarrow (2,\pm2)$ transitions for the $v=0$ and $v=1$ vibrational states. The latter transitions were observed by a double-quantum process which occurs by the absorption or stimulated emission of two quanta.

From the analysis of the hyperfine structure, the signs and magnitudes of the Li^7 electric quadrupole constant, (eqQ), the F^{19} and Li^7 spin-rotation constant $c_{F^{19}}$ and c_{Li^7} respectively, and the nuclear dipole-dipole interaction, $g_1g_2(\mu_N)^2/r^3h$, were determined. The internuclear distance was determined from the latter constant. (μ^2A) was determined from the strong-field data, where μ is the permanent electric dipole moment and A is the moment of inertia. The dipole moment was then calculated from (μ^2A) and the internuclear distance.

The nuclear-molecular constants are:

	$v=0$	$v=1$
$(eqQ/h)_{Li^7}$ (kc/sec)	$+412.0\pm7.0$	$+412.0\pm7.0$
$(c/h)_F$ (kc/sec)	$+32.9\pm1.0$	$+32.4\pm1.0$
$(c/h)_{Li^7}$ (kc/sec)	$+2.2\pm0.6$	$+1.8\pm0.6$
$g_1g_2(\mu_N)^2/r^3h$ (kc/sec)	$+12.8\pm2.0$	$+11.3\pm2.0$

The molecular constants determined for Li^7F^{19} are:

(μ^2A), 10^{-76} cgs units	837.1 ± 0.9	872.3 ± 1.0
r, A	1.51 ± 0.08	1.57 ± 0.08
μ, Debye units	6.6 ± 0.3	6.4 ± 0.3
ω_e, cm^{-1}	646 ± 32	

The $(2,0) \rightarrow (2,\pm2)$ double-quantum transitions of Li^6F^{19} were also observed, from which the following constants were determined: Li^6F $\omega_e=756\pm38$ cm^{-1}; $(\mu^2A)_0(Li^7F)/(\mu^2A)_0(Li^6F)=1.120\pm0.001$; $(\omega_e)_{Li^6F}/(\omega_e)_{Li^7F}=1.17\pm0.02$.

I. INTRODUCTION

THE radio-frequency spectra of Li^7F^{19} were studied by the molecular beam electric resonance method.[1,2] With this method, transitions within specific rotational and vibrational states were observed. This molecule was previously investigated by the magnetic resonance method,[3] where rotational and vibrational states were not distinguished, and consequently, the analysis of the spectra required a calculation of a statistical average over rotational and vibrational states of the molecules in the beam.

From the analysis of the hyperfine structure of the present spectra, it was possible to determine the constants for the electric quadrupole interaction of Li^7, the Li^7 and F^{19} spin-rotation $(\mathbf{I}\cdot\mathbf{J})$ interactions, and the nuclear dipole-dipole interaction.

Although the F spin-rotation interaction constant in Li^7F^{19} can be calculated from the Li^6F^{19} values obtained by Swartz and Trischka,[4] its direct determination affords a check of Foley's[5] theory and model of this interaction. The Li^7 spin-rotation interaction can be estimated from the magnetic resonance data, but since such a value is obtained from consideration of line widths, the present unambiguous determination is more accurate.

The determination of the nuclear magnetic dipole-dipole interaction constant in this experiment together with a measure of the electric dipole moment squared times the moment of inertia allowed a calculation of the internuclear distance and the electric dipole moment which have not been previously measured. Since Rittner[6] and Trischka[7] have discussed the LiF molecule using a classical model, and Benson and van der Hoff[8] have developed a quantum-mechanical model for this molecule, the molecular constants determined in the present experiment serve as a check on these theories.

The molecular and nuclear-molecular constants were calculated from a study of the $(J,m_J) \rightarrow (J,m_J')$ transitions $(1,0) \rightarrow (1,\pm1)$ and $(2,0) \rightarrow (2,\pm2)$. The latter spectrum was observed by a double-quantum process. Such a transition occurs by the absorption or stimulated emission of two quanta. Hughes and Grabner[9] reported double-quantum transitions in RbF. Whereas the transitions observed by them were between levels which also allow single-quantum transitions to occur, the transitions observed in Li^7F^{19} occurred between levels which forbid a single-quantum transition. Double-quantum transitions similar to those observed in this molecule have been observed by Kusch[10] in magnetic resonance experiments.

II. APPARATUS

The electric resonance apparatus used in this experiment is the same as that used in the experiments of Luce and Trischka[11] with the modifications incorporated by Swartz and Trischka.[4] The reader is referred to the

* This research was supported in part by the Office of Naval Research.
† Now at RCA Laboratories, Princeton, New Jersey.
[1] H. K. Hughes, Phys. Rev. **72**, 614 (1947).
[2] J. W. Trischka, Phys. Rev. **74**, 718 (1948).
[3] P. Kusch, Phys. Rev. **75**, 887 (1949).
[4] J. C. Swartz and J. W. Trischka, Phys. Rev. **88**, 1085 (1952).
[5] J. M. Foley, Phys. Rev. **72**, 504 (1947).
[6] E. S. Rittner, J. Chem. Phys. **19**, 1030 (1951).
[7] J. W. Trischka, J. Chem. Phys. **20**, 1811 (1952).
[8] G. C. Benson and B. M. E. van der Hoff, J. Chem. Phys. **22**, 469 (1954).
[9] V. Hughes and L. Grabner, Phys. Rev. **79**, 314 (1950); **79**, 829 (1950); **82**, 561 (1951).
[10] P. Kusch, Phys. Rev. **93**, 1022 (1954).
[11] R. G. Luce and J. W. Trischka, J. Chem. Phys. **21**, 105 (1953).

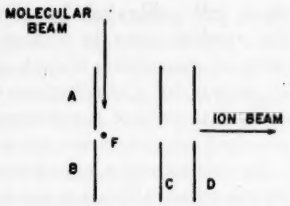

FIG. 1. Cross section of ion gun for mass spectrometer.

aforementioned papers for general information not found in the present description of the modified details of the apparatus. The new features are a new ion gun for the mass spectrometer, a new collimator-buffer field construction, and the use of single crystals for beam material.

A. Ion Gun

A mass spectrometer was used to select Li^7 positive ions produced by surface ionization on a hot oxygenated tungsten wire. The use of a mass spectrometer in these experiments was necessary since positive ion impurities are emitted from the hot wire, and these would have meant a large fluctuating background if the Li^7 ions were collected directly. The separation of Li^6 and Li^7 ions was also especially useful in cases where the spectra of Li^6F^{19} and Li^7F^{19} overlapped.

The geometrical arrangement of the mass spectrometer magnet required that a parallel beam of positive ions be produced normal to the initial direction of the molecular beam. Swartz and Trischka[4] used a gun designed by Thorp[12]; the beam from this ion gun was at times very unstable. The focusing electrodes were at two or three volts with respect to the filament, and consequently, the deposition of a dielectric layer that would become charged might have caused this instability. The positioning of the filament was also very critical in this gun.

The optical analog of electrostatic focusing of charged particles indicates that divergence is produced in a parallel beam of ions on passing through a slit into a field free region. To a first approximation a slit is equivalent to a thin negative lens. However, if there is a field at the point of emergence of the beam from the slit an effective positive lens can be produced and thus a pair of slits can produce a parallel beam of charged particles.

Figure 1 shows a cross section of the two-slit ion gun used in this experiment. The dimensions of the gun were as follows: plates C and D were 0.5 cm apart; plates A and B were 1 cm from C; slits 2.0 cm long and 0.1 cm wide were milled in plates C and D; the filament, F, was placed 0.1 cm from plates A and B which were separated by 0.05 cm. The ratio of F/C potentials was approximately 2 for most of the focusing conditions. Electrodes A and B were approximately 4.5 volts above F with A slightly larger than B. The various electrode potentials were taken off a voltage divider across an electronically stabilized power supply. In this manner, once the gun was focused for one mass peak, other mass peaks could be brought to a focus by changing the accelerating potential while the relative electrode potentials remained the same. With this ion gun, 60 percent of the Li^7 ions formed at the filament arrived at the collector of the mass spectrometer. Although comparable efficiencies were possible with the Thorp gun, the present ion gun gave stable operation.

[12] J. S. Thorp, J. Sci. Instr. **26**, 201 (1949).

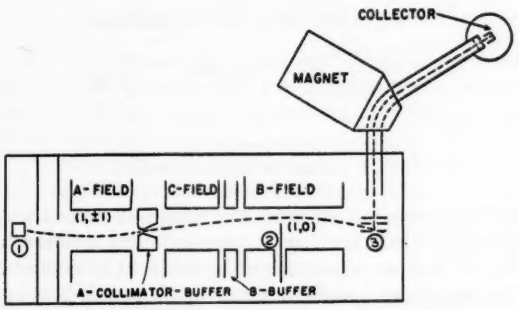

FIG. 2. Schematic diagram of electric resonance apparatus: (1) oven, (2) knife edge for stopping molecules in high rotational states, (3) beam detector and ion gun.

B. Collimator and *A*-Buffer Field

To refocus a beam in the electric resonance apparatus, it is necessary for molecules to maintain their state of space quantization throughout the electric fields. If an electric field of any magnitude is applied in an adiabatic fashion, it is possible for a molecule to maintain its state identity. It will lose its identity, i.e., undergo a nonadiabatic transition, if an electric field changes too rapidly along the beam path. In this apparatus, when observations were made at low Stark fields, difficulties were often experienced with nonadiabatic transitions which presumably occurred in the regions between the uniform Stark field (C-field) and the inhomogeneous deflecting fields (A and B fields). Figure 2 shows a schematic diagram of the apparatus.

To aid in obtaining a slowly varying field along the beam path, Luce and Trischka[11] placed uniform fields called "buffer-fields" on either side of the C-field and adjusted their strength to minimize the number of nonadiabatic transitions produced by the rapid spatial change of field between the large deflecting fields and the Stark field. Despite the use of these fields, the refocused beam showed erratic fluctuations after appreciable beam material was deposited on the glass collimator slits which were placed between the A-buffer field and the C-field. This was due presumably to changes in the accumulation of charge on the insulator surfaces.

To minimize the above difficulties, a metal collimator which combined the function of collimator and A-buffer

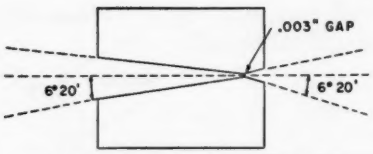

FIG. 3. Collimator and A-buffer field.

field was constructed after the design of Swartz and Trischka.[13] The structure of this component is shown in Fig. 3. A taper was arranged in this field to minimize the electric field gradient along the beam axis between the A- and the C-field region. This structure was mounted from a three point support on the bed plate which supported the A-, B-, and C-fields; this arrangement facilitated the removal of the collimator for cleaning purposes without necessitating the realignment of the collimating slits with respect to the beam path. This collimator-buffer gave satisfactory performance during the weak field runs in this experiment. The weak-field data taken are not reported in this paper. That the buffer fields were effective in controlling nonadiabatic transitions is indicated by the fact that critical settings of the A- and B-buffer fields were necessary in order to observe spectra at very weak fields.

C. Beam Material

The oven charge of LiF was in the form of single crystals in contrast to the powdered crystals usually used in molecular beam techniques with the alkali halides. This allowed a greater amount of beam charge to be loaded in the oven and also resulted in a decrease in the time required for outgassing of a new charge before a data taking run. The single crystals were cleaved from old LiF windows.[14]

D. Measuring Equipment

The radio-frequency source in this experiment was the General Radio signal generator 805-C; frequencies were measured with a General Radio 620-A heterodyne wave meter calibrated against the Bureau of Standard's station WWV. The random error in frequency determination was 2 parts in 10^4 determined by the least count of the wave-meter dial.

The C-field potential was measured using a Leeds and Northrup voltbox a Rubicon potentiometer, and an Eppley standard cell calibrated by the Bureau of Standards. The random error in voltage adjustment during the course of observation of each spectrum was the order of 25 parts in 10^6. Contributions to the uncertainty in the absolute voltage measurements were as follows: the standard cell calibration was known within 1 part in 10^4; the voltbox ratios were known to 2 parts in 10^4; the potentiometer calibration was known within 1 part in 10^4; all contributing to a total possible error in absolute voltage of 4 parts in 10^4. The value of the Stark field was corrected for the residual potential of the C-field structure by means of a direct and a reverse field run and an observation of the consequent shift in a line position.

During the course of some of the measurements it was found that the spectra would undergo random drifts of several kilocycles, which were equivalent to voltage changes of 2 parts in 10^4. It was thought that the increased temperature of the voltbox resistors were a contributing element to this difficulty. Wire wound precision resistors, immersed in an oil bath, were compared to those of the voltbox during the course of a run. However, it was found that the voltbox resistances changed by less than 1 part in 10^4 despite the continued drifts in line positions. Regular checks of the 620-A wave-meter calibration made at this time showed no difficulty from this source. Drifts were finally eliminated by applying the proper operating voltage to the C-field and its associated voltage measuring equipment for a period of 12 hours prior to a run. It should be noted that when specific lines were repeated from time to time, their absolute positions together with their relative separations agreed well within the error that could be ascribed to the limitations in determining a line position due to the errors in measuring changes in beam intensity. That the drift was not due to the transient charging of the gold film with which the glass C-field was coated seems indicated by the observation that when the direction of the Stark field was reversed and the spectra immediately retaken, negligible displacement of a spectral line occurred.

III. THEORY

The Hamiltonian used to explain and to make calculations from the hyperfine structure of the observed spectra of Li^7F^{19} is

$$\mathcal{H}=(\hbar^2/2A)\mathbf{J}^2-\boldsymbol{\mu}\cdot\mathbf{E}-(eqQ)_1\frac{[3(\mathbf{I}_1\cdot\mathbf{J})^2+(3/2)(\mathbf{I}_1\cdot\mathbf{J})-\mathbf{I}_1^2\mathbf{J}^2]}{2I_1(I_1-1)(2J-1)(2J+3)}+c_1(\mathbf{I}_1\cdot\mathbf{J})+c_2(\mathbf{I}_2\cdot\mathbf{J})$$
$$+(g_1g_2\mu_N^2/r^3)\frac{[3(\mathbf{I}_1\cdot\mathbf{J})(\mathbf{I}_2\cdot\mathbf{J})+3(\mathbf{I}_2\cdot\mathbf{J})(\mathbf{I}_1\cdot\mathbf{J})-2(\mathbf{I}_1\cdot\mathbf{I}_2)J(J+1)]}{(2J+3)(2J-1)}. \quad (1)$$

The first term is the rotational energy operator in which A is the moment of inertia of the molecule and $\mathbf{J}$ is the rotational angular momentum. The second term represents the interaction of the external field $\mathbf{E}$ with the permanent electric dipole moment, $\boldsymbol{\mu}$, of the molecule. The third term gives the interaction between the

[13] J. C. Swartz and J. W. Trischka (private communication).
[14] Crystals were supplied through the kindness of Dr. Van Zandt Williams of the Perkin-Elmer Company.

electric quadrupole moment of the alkali nucleus, Q_1, and the gradient of the electric field at the position of the alkali nucleus, q_1, produced by the remaining charges in the molecule; eq_1Q_1 is the quadrupole interaction constant defined by Bardeen and Townes.[15] Subscript 1 refers to the nucleus with the strongest nuclear-molecular coupling, which in this case is the Li^7 nucleus, while subscript 2 refers to the F nucleus. The F nucleus has no quadrupole moment since it has a spin of $\frac{1}{2}$. The fourth and fifth terms are the spin-rotation interactions between the nuclear spins and the rotational angular momentum of the molecule, where c_1 and c_2 are the respective interaction constants for the Li^7 and F^{19} nuclei. The last term is the nuclear magnetic dipole-dipole interaction in which g_1 and g_2 are the nuclear gyromagnetic ratios, μ_N is the nuclear magneton, and r is the internuclear distance.

The energy levels and selection rules are discussed in a paper by Hughes and Grabner.[16] The theory of the double-quantum transitions is also given in the above paper. The theory of this type of transition is presented by them as a second-order time-dependent perturbation calculation. For present purposes, the following conclusions of the theory are pertinent. If the radio-frequency field is sufficiently intense, transitions are predicted to occur at half the frequency given by the Bohr condition. These transitions may be considered as occurring by a double-quantum process whereby two quanta supply the energy. At strong static fields (i.e., fields for which the Stark effect is large compared to all internal-molecular interactions), the selection rules allow a $\Delta m_J=\pm 2$ transition to occur at half the frequency that would be necessary for a single quantum transition, thereby allowing the observation of the $(2,0)\rightarrow(2,\pm 2)$ transition. It also follows from the theory that the line widths of these transitions should be half as wide as the single quantum line widths.

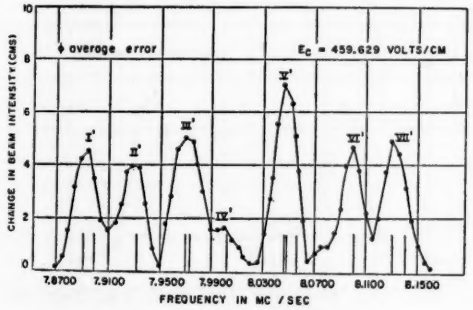

FIG. 4. Single-quantum transitions, $(1,0)\rightarrow(1,\pm 1)$, for the $v=0$ vibrational state of Li^7F^{19}. The predicted line positions are indicated by vertical lines under the observed spectra.

[15] J. Bardeen and C. H. Townes, Phys. Rev. 73, 97 (1948).
[16] V. Hughes and L. Grabner, Phys. Rev. 79, 829 (1950).

IV. SPECTRA AND RESULTS

A consequence of the strong-field theory of the Stark effect for the Hamiltonian, (1), is that to the quadratic term in the field energy, the fine structure produced by terms beyond the second is independent of the value of the electric field; thus the relative separations of the lines are field-independent. By strong field is meant fields where $eq_1Q_1 \ll \mu^2E^2/2A \ll (\hbar^2/2A)J(J+1)$. This is the region where spectra were observed by fixing the C-field voltage and varying the frequency.

Figure 4 shows data for the $(1,0)\rightarrow(1,\pm 1)$ transition for the first vibrational state. A preliminary analysis indicated that there were an insufficient number of resolved lines to enable a determination of the value of the four internal interactions from this spectrum alone. The complexity of the spectra is due to the fact that although the quadrupole interaction is the largest interaction, all the other interactions enter in such a significant fashion that the primary quadrupole structure is no longer dominant. An additional complicating feature in the use of the $(1,0)\rightarrow(1,\pm 1)$ spectra for the determination of the constants is that the lines have a quadratic dependence on the constants.

Consequently, it was decided to search for the $(2,0)\rightarrow(2,\pm 2)$ double-quantum transitions which are allowed at high radio-frequency fields as was previously indicated. This spectrum should be simpler since it is possible to avoid the use of the $m_J=\pm 1$ states, which are always complicated for all J values. Since the direct output voltage of the General Radio signal generator was insufficient, a tuneable resonant circuit, placed in the output of the oscillator, gave as much as 100 volts of rf at resonance. Spectra were found at half the frequency at which the single-quantum $(2,0)\rightarrow(2,\pm 2)$ spectra should have been observed were they not forbidden by the selection rules. Figure 5 shows a typical plot of the first vibrational state of the $(2,0)\rightarrow(2,\pm 2)$ double-quantum transition. The line widths in this spectrum are seen to be half as wide as for the single quantum transitions, which should indeed be the case for the double-quantum transition. The fact that these were double-quantum transitions and were not due to

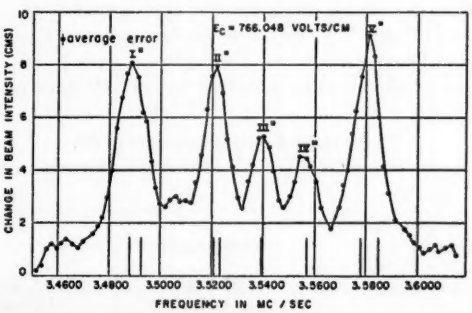

FIG. 5. Double-quantum transitions, $(2,0)\rightarrow(2,\pm 2)$, for the $v=0$ vibrational state of Li^7F^{19}. The predicted line positions are indicated by vertical lines under the observed spectra.

TABLE I. Nuclear-molecular constants of Li^7F^{19}.

Constant	$v=0$	$v=1$
$(eqQ/h)_{Li^7}$ kc/sec	+412.0±7.0	+412.0±7.0
$(c/h)_{F^{19}}$ kc/sec	+32.9±1.0	+32.4±1.0
$(c/h)_{Li^7}$ kc/sec	+2.2±0.6	+1.8±0.6
$g_1g_2(\mu_N)^2/r^3h$ kc/sec	+12.8±2.0	+11.3±2.0

harmonics of the oscillator was shown by the following considerations: (1) A search for spectra at twice the frequency produced negative results. (2) The $(2,0) \rightarrow (2, \pm 2)$ single-quantum transitions were found at intermediate fields and were followed to strong fields where they disappeared. (3) In general, to produce resolved lines for single-quantum transitions in Li^7F^{19}, the rf voltage was of the order of 0.4 volts; 30 volts (which was the voltage necessary to produce spectra at the half frequency) would have caused excessive broadening of the lines.

The previous measurements of the nuclear-molecular constants of Li^7F^{19} and Li^6F^{19} [3,4] were used for a preliminary analysis of the $(2,0) \rightarrow (2, \pm 2)$ structure. The analysis showed that of the five observed lines only two were single; the rest were unresolved doublets. Four equations involving differences between the five observed lines were necessary to calculate the constants (since initially the position of the unperturbed Stark line was not known). Although a satisfactory theory does not exist for the relative intensities of lines observed in electric resonance experiments, the observed relative intensities in this spectrum indicated that equal weight could be given to each transition. Consequently, the approximation was made that the observed position of a line corresponds to the mean position of the theoretical constituent doublets. Of the four difference equations so formed, only three were linearly independent. However, lines II′ and VI′ of the $(1,0) \rightarrow (1, \pm 1)$ spectrum are single and have a linear dependence on the constants so that the required four simultaneous linear equations were formed from a combination of the $J=1$ and $J=2$ spectra. The nuclear-molecular interactions are not expected to vary with rotation for these low rotational states.

The calculated nuclear-molecular interactions are given in Table I. From these constants, the positions of all the lines in $J=1$ and $J=2$ spectra were predicted. These predictions are indicated as vertical lines under the observed spectra in Figs. 4 and 5. The agreement between the observed and predicted line positions justifies the above treatment of the data. It should be noted that giving equal weight to all the possible transitions is not justified in the $J=1$ spectrum since line IV′ which is a single line is much less intense than II′ and VI′ which are also single lines; however, only the single lines II′ and VI′ are used in the calculations of the constants.

TABLE II. Molecular constants of Li^7F^{19}.

Constant	$v=0$	$v=1$
μ^2A, $(J=1)$, 10^{-76} cgs units	836.8 ±1.0	
μ^2A, $(J=2)$, 10^{-76} cgs units	837.1 ±0.9	872.3 ±1.0
r, A	1.51±0.08	1.57±0.08
μ, Debye units	6.6 ±0.3	6.4 ±0.3
ω_e, cm^{-1}	646±32	

After the analysis of the fine structure, the position of the unperturbed Stark line was determined, which together with the measurement of the Stark field and a correction made for the contact potential, allowed the product μ^2A to be calculated. The equation due to Lamb for the energy levels of a rigid rotator in an electric field[1] was used for the calculation. The unperturbed Stark line of the $J=2$ spectrum lies at the mean position of the extreme lines I″ and V″. It can be shown that the Stark line for the $J=1$ spectrum lies at $2c_1$ above the mean position of the extreme lines in this spectrum. The values of μ^2A are shown in Table II.

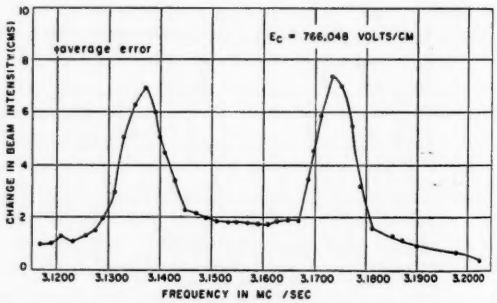

FIG. 6. Double-quantum transitions, $(2,0) \rightarrow (2, \pm 2)$, for the $v=0$ vibrational state of Li^6F^{19}.

The μ^2A values determined from both spectra agree within experimental error, thereby lending further justification for the treatment of the data.

The values of μ and A separately can be obtained in some molecules if the departure from quadratic dependency of the unperturbed Stark frequency can be observed. This method requires excessively large fields in the present case because of the smallness of μ^4A^3 in Li^7F^{19}. However, the calculation of μ and A was made possible in this molecule through the measurement of the magnetic dipole-dipole interaction constant. The value of the internuclear distance obtained from this constant was used to obtain A, which in turn was used together with μ^2A to calculate μ. The calculated values of μ and r are given in Table II.

The line shapes of the $J=2$ double-quantum transitions are not understandable on the basis of the ideal line shape calculated by Torrey.[17] The extreme ends of the spectrum seem to indicate secondary maxima. Between lines I″ and II″ there is further indication of

[17] H. C. Torrey, Phys. Rev. **59**, 293 (1941).

what appears to be an unresolved line which cannot be accounted for since all possible transitions have been considered.

Since no completely isolated line exists in the $(2,0) \rightarrow (2, \pm 2)$ spectra, a study of a line shape was not possible. However, since the spectra of Li^6F^{19} observed by Swartz and Trischka[4] as a single-quantum transition contained only two lines, the double-quantum transitions of this molecule were obtained as a means of comparison. Figure 6 shows the $(2,0) \rightarrow (2, \pm 2)$ spectrum of Li^6F^{19} for $v=0$. This spectrum also shows secondary maxima or at least long tails which are not in keeping with the line shape calculated by Torrey.[17] Figure 7 shows the single-quantum transition observed by Swartz and Trischka[18] for comparison. It should also be noted that the resolution in the $(2,0) \rightarrow (2, \pm 2)$ spectrum of Li^6F is better than in the $(1,0) \rightarrow (1, \pm 1)$ spectrum, permitting a more accurate determination of the F spin-rotation interaction. The prime purpose in obtaining the Li^6F double-quantum transitions was to insure the correct counting of the Li^7F^{19} lines and

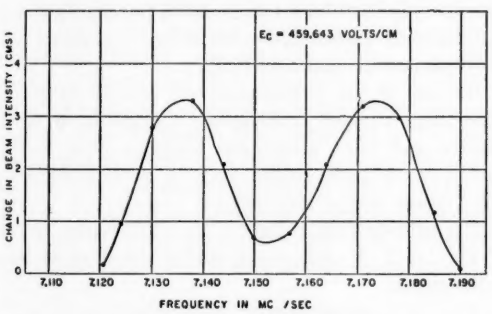

FIG. 7. Single-quantum transitions, $(1,0) \rightarrow (1, \pm 1)$, for the $v=0$ vibrational state of Li^6F^{19}. These line shapes are to be compared with the double-quantum line shapes in Fig. 6.

consequently no further work was done to elucidate the occurrence of these tails.

To provide an additional benefit from the above Li^6F^{19} spectrum, the Li^6F^{19} and Li^7F^{19} spectra were taken at the same field. Consequently, a direct determination of their μ^2A ratio, free from systematic errors in voltage was made. The results are shown in Table III.

From the variation in intensity of corresponding lines in vibrational states, the vibrational constants for Li^6F^{19} and Li^7F^{19} were determined. Since the spectra of Li^6F^{19} and Li^7F^{19} were observed under identical conditions, a direct determination of the ratio of their vibrational constants was possible. In view of the fact that the oven temperature was the same during the course of these runs, the uncertainty in the ratio of ω_e's should be due only to the error in measuring relative intensities of lines. Since the location of the peak intensity is unreliable, the ratios of the areas of corresponding

[18] J. C. Swartz and J. W. Trischka (private communication).

TABLE III. Ratios of Li^6F and Li^7F molecular constants.

Quantity	
$(\mu^2A)_0(Li^7F)/(\mu^2A)_0(Li^6F)$	1.120 ± 0.001
$(\omega_e)_{Li^6F}/(\omega_e)_{Li^7F}$	1.17 ± 0.02

lines of the first three vibrational states of each molecule were determined. In Li^7F^{19}, the ratios of the intensities of successive lines were 0.40 ± 0.01 while in Li^6F^{19}, the ratios were 0.34 ± 0.01. The ratio of the ω_e's are given in Table III. The vibrational constants of Li^7F^{19} and Li^6F^{19} are given in Tables II and IV respectively.

V. DISCUSSION

The present determination of the quadrupole coupling constant $(eqQ/h)_{Li^7} = +412 \pm 7$ kc/sec can be compared with the value $|eqQ/h| = 408 \pm 12$ kc/sec obtained by Kusch[3,19] from molecular beam magnetic resonance data. The agreement may be taken as an indication that this coupling constant does not vary greatly with vibration or rotation. The positive signs obtained for this interaction are in agreement with the result of Logan *et al.*[20] The fluorine spin-rotation constant $c_2/h = +32.9 \pm 1.0$ kc/sec in Li^7F^{19} is consistent with the value $c_2/h = +37.3 \pm 0.3$ kc/sec found in Li^6F^{19} by Swartz and Trischka,[4] when account is taken of the different reduced masses of the molecules in accordance with Foley's[5] model of this interaction. The Li^7 spin-rotation constant $c_1/h = +2.2 \pm 0.6$ kc/sec differs from the value $c/h = 1.4$ kc/sec calculated by us from Kusch's data.[3] The fact that the electric resonance value is larger than the magnetic resonance value is interesting because the fluorine electric resonance value in CsF and LiF is also larger than the values determined by the magnetic resonance method.

The internuclear distances and dipole moments, determined for the first time in the present experiments, are compared in Table V with values obtained in various theoretical calculations. Benson and van der Hoff[8] made use of a quantum mechanical model of LiF, while Rittner[6] and Trischka[7] utilized a semiclassical, polarized-ion model. It will be noted that agreement between theory and experiment exists for all of the results in Table V except for the value of μ found by Rittner. This value is clearly too low. Although results are listed for two vibrational states, the accuracy of the

TABLE IV. Molecular constants of Li^6F.

Constants	
$(\mu^2A)_0(J=2)$, 10^{-76} cgs units	747.6 ± 1.0
ω_e, cm^{-1}	756.0 ± 38

[19] The estimated error in this measurement was kindly supplied to the authors by Professor P. Kusch.

[20] Logan, Cote, and Kusch, Phys. Rev. 86, 280 (1952).

TABLE V. Comparison of experimental and theoretical values of r and μ. The subscripts on r and μ indicate the vibrational state, where r is in angstrom units and μ in Debye units.

Method	r_0	r_1	μ_0	μ_1
Experimental[a]	1.51±0.08	1.57±0.08	6.6±0.3	6.4 ±0.3
Theoretical[b]	1.60	1.62	6.35	6.47
Theoretical[c]	1.53		5.04	
Theoretical[d]	1.44<r<1.65		6.0	

[a] Present experiments.
[b] G. C. Benson and B. M. E. van der Hoff, J. Chem. Phys. 22, 469 (1954).
[c] E. S. Rittner, J. Chem. Phys. 19, 1030 (1951).
[d] J. W. Trischka, J. Chem. Phys. 20, 1811 (1952).

experimental results is not sufficient to determine how r and μ change from one vibrational state to the next.

The $(\mu^2 A)_0$ of Li^6F (listed in Table IV) obtained from the double-quantum transitions agrees with the value obtained by Swartz and Trischka[4] who observed the single-quantum transitions. The observed ratio of $(\mu^2 A)_0$ given in Table III differs beyond experimental error from the ratio 1.12154 of the reduced masses of these isotopes; this difference may be ascribed to the zero point vibrational difference.

The vibrational constant ω_e of Li^7F^{19} is 646±32 cm^{-1} and for Li^6F^{19} ω_e=756±38 cm^{-1}. The absolute values of ω_e are in doubt mainly because of the uncertainty in measuring the temperature of the vapor in the oven, T=1060°K, and the error in measuring relative intensities of lines. By measuring the velocity distribution of molecules from an oven similar to the one used in this experiment, Miller[21] has shown that the error in the temperature determined from a thermocouple reading can be ±50°K. Miller also found that the temperature at the slit may be as much as 50° higher than the temperature near the charge, where the thermocouple was located in the oven used in the present experiments. The temperature given above is the measured temperature plus 50°K. The value of ω_e for different isotopic molecules should vary inversely as the square root of the reduced mass. On this basis the ratio of the ω_e's for Li^6F^{19} and Li^7F^{19} should be 1.06, whereas the observed ratio is 1.17±0.02. The reason for this discrepancy is not clear. An explanation may lie in the value of the radiofrequency field used. The observed intensity of a line depends upon the value of the radiofrequency field. The value of the radiofrequency field was selected to give the narrowest line at a given frequency and this value of field was used throughout a given spectrum; this optimum field may be a function of frequency, being appreciably different even in the brief frequency range from the v=0 spectra to v=2 spectra. It should also be noted that Benson and van der Hoff[5] predicted ω_e=1039 cm^{-1} for Li^6F whereas the observed value is 756±38 cm^{-1}. Rittner[6] predicted that ω_e=773 cm^{-1} for a LiF in which the chemical mass of Li is used. Hence this value is best compared with the experimental result for Li^7F^{19}.

The use of the double-quantum transitions in this experiment enabled considerable simplification of the spectra and their subsequent analysis. This method should prove useful in the study of other molecules if $J \geq 2$ states can be refocused.

The authors wish gratefully to acknowledge the aid of Dr. D. T. F. Marple in taking the data of these experiments.

[21] R. C. Miller and P. Kusch, Quarterly Report, Columbia Radiation Laboratory, August 31, 1953 (unpublished).

Matrix Treatment of Nuclear Induction*

E. T. JAYNES
Department of Physics and W. W. Hansen Laboratories of Physics, Stanford University, Stanford, California
(Received December 20, 1954)

By use of matrix notation, solutions of the Bloch equations may be kept in simple, manageable form even in the case of applied fields that are complicated functions of time. Effects that from the usual standpoint are grossly nonlinear appear as linear relations between matrices, of the same form that one encounters in simple radioactive decay problems. A general property of transients in the case of an arbitrary repetitive applied signal is established, and a formalism is set up in terms of which a large class of special problems may be solved.

I. INTRODUCTION

THE following is an exposition of a method of finding solutions of the Bloch equations[1] making use of matrix theory. It has the advantage that formal solutions are derived in matrix form, with details worked out only at the end of a calculation, the desired result appearing typically as one element of a certain matrix. Although it is undoubtedly true that no solutions can be found by matrix methods which could not have been found without them, the saving of labor due to the condensed notation makes a wider range of calculations feasible. For example, in the companion paper[2] it is shown that Hahn's results[3] on the theory of spin echoes can be rederived in a very simple way and extended to more complicated situations; at the same time certain finer details such as the exact timing and shape of spin-echo signals are readily accounted for. In addition, the matrices correspond to simple geometrical operations so that a great deal of physical information can be read off directly from a matrix expression.

II. GENERAL FORMALISM

The Bloch equation[1] of motion of the nuclear magnetization M due to a magnetic field H will be taken in the form,

$$\frac{\partial \mathbf{M}}{\partial t}+\frac{\mathbf{M}-\chi\mathbf{H}}{T}+\gamma(\mathbf{H}\times\mathbf{M})=0, \tag{1}$$

where χ is the static susceptibility, γ the gyromagnetic ratio, and T the relaxation time. Throughout this paper we make the assumption that the two relaxation times are equal: $T=T_1=T_2$, a condition that is often well satisfied in liquids.[4] As indicated below, the theory is easily extended to the more general case.

In most applications of this theory one will be concerned with a constant magnetic field $\mathbf{H}_0$ in the z direction, with a superimposed alternating field $\mathbf{H}_1$. If the latter oscillates with a single frequency ω, the usual procedure is to transform the problem into an effectively stationary one by passage to a coordinate system rotating about $\mathbf{H}_0$ with angular velocity ω and neglecting the component of $\mathbf{H}_1$ rotating in the opposite direction.[1] Equation (1) remains valid in the rotating system provided we now interpret $\mathbf{H}$ as the "effective" field with components $(H_x, H_y, H_z-\omega/\gamma)$. Our general discussion based on (1) is thus applicable in either the laboratory or the rotating frame.

Equation (1) is cast into matrix form by defining a matrix $\mathfrak{H}(t)$ with the property that $\mathfrak{H}$ operating on any vector has the effect of taking the cross product with $\gamma\mathbf{H}$; symbolically, $\mathfrak{H}=\gamma\mathbf{H}\times$. Thus, in right-handed Cartesian coordinates, $\mathfrak{H}$ takes the form,

$$\mathfrak{H}=\gamma\begin{bmatrix}0 & -H_z & H_y\\ H_z & 0 & -H_x\\ -H_y & H_x & 0\end{bmatrix}. \tag{2}$$

It is often convenient to use the "axial" representation in which a vector M is specified by the components $[M_+=M_x+iM_y, M_-=M_x-iM_y, M_z]$ rather than by the Cartesian $[M_x,M_y,M_z]$. Since the change from one system of representation to another is accomplished by a similarity transformation on all matrices, for example,

$$\mathfrak{H}_{\text{axial}}=\mathbf{S}\mathfrak{H}_{\text{Cartesian}}\mathbf{S}^{-1},$$

with

$$\mathbf{S}=\begin{bmatrix}1 & i & 0\\ 1 & -i & 0\\ 0 & 0 & 1\end{bmatrix},$$

the general relations may be developed without committing ourselves to any particular representation.

The Bloch equations thus appear in matrix form as

$$\frac{\partial \mathbf{M}}{\partial t}+\left[\frac{1}{T}+\mathfrak{H}(t)\right]\mathbf{M}=\mathbf{A}(t), \tag{3}$$

with $\mathbf{A}(t)=\chi\mathbf{H}/T$. If all quantities in (3) were scalars it would reduce to the equation of radioactive decay or of buildup of voltage in an $R-C$ circuit, the general solution of which can be written down immediately; by analogy, we find the solution of the matrix equation. First, we define the time-development matrix $\mathbf{U}(t,t')$,

* Supported in part by the Office of Naval Research.
[1] F. Bloch, Phys. Rev. **70**, 460 (1946): see also Rabi, Ramsey, and Schwinger, Revs. Modern Phys. **26**, 167 (1954).
[2] A. Bloom, following paper [Phys. Rev. **98**, 1104 (1955)].
[3] E. L. Hahn, Phys. Rev. **80**, 580 (1950).
[4] Bloembergen, Purcell, and Pound, Phys. Rev. **70**, 988 (1946).

which satisfies the homogeneous equation,

$$\frac{\partial \mathbf{U}(t,t')}{\partial t}+\left[\frac{1}{T}+\mathfrak{B}(t)\right]\mathbf{U}(t,t')=0, \tag{4}$$

with $\mathbf{U}(t,t)=1$. It is readily verified by substitution that the general solution of (3) is

$$\mathbf{M}(t)=\mathbf{U}(t,0)\mathbf{M}(0)+\int_0^t \mathbf{U}(t,t')\mathbf{A}(t')dt'. \tag{5}$$

To investigate the properties of $\mathbf{U}(t,t')$, note first that the relaxation term may be eliminated from (4) by the transformation,

$$\mathbf{U}(t,t')=\exp[-(t-t')/T]\mathbf{R}(t,t'), \tag{6}$$

and the differential equation satisfied by $\mathbf{R}(t,t')$ is

$$\partial\mathbf{R}(t,t')/\partial t+\mathfrak{B}(t)\mathbf{R}(t,t')=0. \tag{7}$$

According to (7), the value of $\mathbf{R}$ at time $(t+dt)$ is given by

$$\mathbf{R}(t+dt,\,t')=[1-\mathfrak{B}(t)dt]\mathbf{R}(t,t'),$$

and this process can be repeated indefinitely, leading to the following representation of $\mathbf{R}(t,t')$:

$$\mathbf{R}(t,t')=\lim_{n\to\infty}\left[1-\frac{\tau}{n}\mathfrak{B}\left(t-\frac{\tau}{n}\right)\right]\times\left[1-\frac{\tau}{n}\mathfrak{B}\left(t-\frac{2\tau}{n}\right)\right]\cdots\left[1-\frac{\tau}{n}\mathfrak{B}(t')\right], \tag{8}$$

where $\tau=t-t'$. The matrix $[1-\mathfrak{B}(t)dt]$ represents, according to the definition of $\mathfrak{B}$, an infinitesimal rotation about the instantaneous direction of $\mathbf{H}$ through an angle $\gamma|\mathbf{H}|dt$; therefore, the matrix $\mathbf{R}(t,t')$, being the resultant of an infinite number of such rotations, is a finite rotation matrix, representing the total change of $\mathbf{M}$ that would be produced in the time interval $(t'\to t)$ by Larmor precession if the relaxation and static susceptibility terms were absent.

We note in passing that in consequence of (8), $\mathbf{R}(t,t')$ has the group property

$$\mathbf{R}(t,t')\mathbf{R}(t',t'')=\mathbf{R}(t,t''), \tag{9}$$

and that in the case $\mathfrak{B}(t)=\text{const}$, we have

$$\mathbf{R}(t,t')=\exp[-\mathfrak{B}(t-t')]. \tag{10}$$

The matrix (10), when applied to any vector, carries out a rotation about $\mathbf{H}$ as an axis, through an angle $\gamma|\mathbf{H}|(t-t')$.

III. STEADY SIGNAL

As an illustration of the method, we now evaluate (5) for the case where the magnetic field in the laboratory system is given by $H_x=2H_1\cos\omega t$, $H_y=0$, $H_z=H_0$ = const. This is the situation in which use of the rotating coordinate system is useful; in it the matrix $\mathfrak{B}$ is symbolically $\mathbf{B}\times$, where $\mathbf{B}$ is the vector with components $[\gamma H_1,\,0,\,\gamma H_0-\omega]$. We further assume $H_0\gg H_1$, so that the vector $\mathbf{A}$ in (5) is effectively a constant. The time-development matrix is now, from (6) and (10),

$$\mathbf{U}(t,t')=\mathfrak{A}(t-t')=\exp\left[-\left(\frac{1}{T}+\mathfrak{B}\right)(t-t')\right], \tag{11}$$

and the integral in (5) is readily evaluated, since the formula for integration of the exponential function applies to matrices as well as to scalars:

$$\int_0^t \mathfrak{A}(t-t')dt'=[1-\mathfrak{A}(t)]\left(\frac{1}{T}+\mathfrak{B}\right)^{-1}. \tag{12}$$

Thus, the solution (5) reduces to

$$\mathbf{M}(t)=\mathfrak{A}(t)[\mathbf{M}(0)-\mathbf{M}(\infty)]+\mathbf{M}(\infty), \tag{13}$$

with the steady-state magnetization given by

$$\mathbf{M}(\infty)=(1/T+\mathfrak{B})^{-1}\mathbf{A}. \tag{14}$$

The inverse of $(1/T+\mathfrak{B})$ may be evaluated by determinants, giving the result,

$$\mathbf{M}(\infty)=\frac{\chi H_0}{1+b^2T^2}\begin{bmatrix} B_xB_zT^2 \\ B_zT \\ 1+B_z^2T^2\end{bmatrix}, \tag{15}$$

where $b\equiv|\mathbf{B}|$. This agrees with the steady-state solution given by Bloch[1] for the case $T_1=T_2$.

To investigate the transient in (13), we note that $\mathfrak{A}(t)$ represents a rotation about the vector $\mathbf{B}$ through an angle bt, with accompanying exponential decrease in length. Thus, as time goes on, $\mathfrak{A}(t)\mathbf{A}$ is a vector whose tip describes a spiral on the surface of a cone, as illustrated in Fig. 1. This will be called a λ cone; if the initial polarization is taken as the equilibrium value $\mathbf{M}(0)=\chi\mathbf{H}_0$, it opens out into a disk normal to $\mathbf{B}$. Every transient in the presence of a steady signal is one in which the difference between initial and final polarization decays to zero along a λ cone. The frequency of rotation about the λ cone is

$$b=[(\gamma H_1)^2+(\gamma H_0-\omega)^2]^{\frac{1}{2}},$$

which appears in the laboratory frame as a nutation frequency.

Evidently the general nature of the solution can be understood directly from (13). Finding all details requires explicit evaluation of the matrix $\exp(-\mathfrak{B}t)$. This may be done directly, since its geometrical meaning is already understood, or by making use of the Cayley-Hamilton theorem, according to which each matrix satisfies its own characteristic equation. Since the latter method is general, it is described briefly. If $\mathbf{G}$ is any $(n\times n)$ matrix, its characteristic equation is

$$\det(\mathbf{G}-\lambda\mathbf{1})=\sum_{k=0}^{n} C_k\lambda^k=0,$$

and therefore

$$\sum_{k=0}^{n} C_k \mathbf{G}^k = 0.$$

By repeated application of this relation any power series in $\mathbf{G}$ may be reduced to a polynomial of degree not exceeding $(n-1)$; thus we know that $\exp(-\beta t)$ is expressible linearly in terms of β, β^2, and the unit matrix:

$$\exp(-\beta t) = a_0(t)\mathbf{1} + a_1(t)\beta + a_2(t)\beta^2. \tag{16}$$

In the present case the characteristic equation of β reduces to

$$\beta^3 + b^2\beta = 0. \tag{17}$$

From (17) and the requirement,

$$\frac{d}{dt}\exp(-\beta t) = -\beta \exp(-\beta t),$$

we find the system of equations $\dot{a}_0 = 0$, $\dot{a}_1 = b^2 a_2 - a_0$, $\dot{a}_2 = -a_1$ with initial conditions $a_0(0) = -\dot{a}_1(0) = 1$, $a_1(0) = a_2(0) = 0$, whose solution gives

$$\exp(-\beta t) = \mathbf{1} - \frac{\sin bt}{b}\beta + \frac{1-\cos bt}{b^2}\beta^2. \tag{18}$$

Thus, multiplication of any vector $\mathbf{A}$ by $\lambda(t)$ results in the vector

$$\lambda(t)\mathbf{A} = e^{-t/T}\left\{\frac{\mathbf{B}(\mathbf{B}\cdot\mathbf{A})}{b^2} + \left[\mathbf{A} - \frac{\mathbf{B}(\mathbf{B}\cdot\mathbf{A})}{b^2}\right]\cos bt - \frac{\mathbf{B}\times\mathbf{A}}{b}\sin bt\right\}. \tag{19}$$

Using this relation, all details of the solution (13) may now be written down. The result, for the y component of magnetization, as seen in the laboratory system, is

$$M_y(t) = \frac{\chi H_0 \omega_1 T}{1+b^2T^2}[\cos\omega t - \Delta\omega T \sin\omega t] + \frac{\chi H_0\omega_1 T}{b(1+b^2T^2)^{\frac{1}{2}}} \times e^{-t/T}[\Delta\omega \sin(bt+\theta)\sin\omega t - b\cos(bt+\theta)\cos\omega t], \tag{20}$$

where $\omega_1 = \gamma H_1$, $\Delta\omega = \gamma H_0 - \omega$, $\tan\theta = bT$. In the case of resonance ($\Delta\omega = 0$) and strong driving field ($\omega_1 T \gg 1$) the final amplitude is small, but the steady state is well approximated only after many relaxation periods. This problem has previously been treated by Torrey.[5]

It is interesting to note that the form of the general solution (13) corresponds exactly to the solution in simple problems of radioactive decay or buildup of voltage in an $R-C$ circuit. $\lambda(t)$ appears as a matrix analog of the usual exponential damping factor.

[5] H. C. Torrey, Phys. Rev. **76**, 1059 (1949).

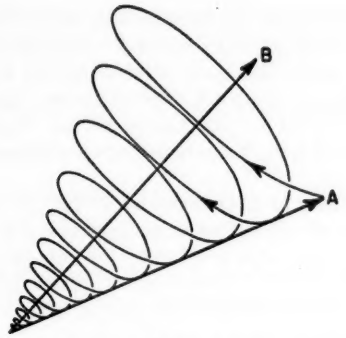

FIG. 1. The λ cone. Locus of the tip of the vector $\lambda(t)\mathbf{A}$ as t varies from 0 to ∞.

IV. GENERAL PERIODIC SIGNAL

To investigate the solution in the case that the magnetic field is an arbitrary periodic function of time, we go back to Eq. (4) and assume β periodic with period τ:

$$\beta(t+\tau) = \beta(t). \tag{21}$$

Then the following relations are consequences of (8)

$$\mathbf{U}(t+n\tau, t'+n\tau) = \mathbf{U}(t,t'), \qquad \mathbf{U}(n\tau,0) = [\mathbf{U}(\tau,0)]^n = \boldsymbol{\alpha}^n(0), \tag{22}$$

where $\boldsymbol{\alpha}(t) = \mathbf{U}(t+\tau, t)$ is the time-development matrix for one period, starting at time t. Writing for brevity, $\mathbf{M}_n(t) = \mathbf{M}(t+n\tau)$, the solution (5) giving the change of M during one period is

$$\mathbf{M}_{n+1}(t) = \mathbf{U}(t+\tau, t)\mathbf{M}_n(t) + \int_{n\tau+t}^{(n+1)\tau+t} \mathbf{U}(t+n\tau+\tau, t')\mathbf{A}(t')dt';$$

or, noting that the integral is independent of n,

$$\mathbf{M}_{n+1}(t) = \boldsymbol{\alpha}(t)\mathbf{M}_n(t) + \mathbf{N}(t), \tag{23}$$

where

$$\mathbf{N}(t) = \int_t^{\tau+t} \mathbf{U}(t+\tau, t')\mathbf{A}(t')dt'. \tag{24}$$

Equation (23) is a simple linear difference equation whose solution is

$$\mathbf{M}_n(t) = \boldsymbol{\alpha}^n[\mathbf{M}_0(t) - \mathbf{M}_\infty(t)] + \mathbf{M}_\infty(t) \tag{25}$$

with the steady-state polarization given by

$$\mathbf{M}_\infty = (1-\boldsymbol{\alpha})^{-1}\mathbf{N}. \tag{26}$$

All eigenvalues of $\boldsymbol{\alpha}$ are less than unity in magnitude, so the term with $\mathbf{M}_0(t)$ in (25) vanishes as $n \to \infty$. Equations (25) and (26) correspond in form to (13) and (14), of which they are a discrete version. Since $\boldsymbol{\alpha}$ is a λ matrix, that is, it represents a combined rotation and exponential shrinking, we see that any transient in the presence of a periodic signal has the following property;

if we look at the polarization only at corresponding instants in each repetition period, we see the difference between initial and final value decaying to zero in discrete jumps along a λ cone. At other times in the repetition period the polarization will not, in general, lie on the same λ cone, but may describe a very complicated path.

The operations represented by α^m and $(1-\alpha)^{-1}$ may be further elucidated by making use of (19). Let the axis of the rotation α be given by the unit vector $\mathbf{n}$, and its magnitude by θ. The matrix α^m applies this rotation m times, so that the result of applying α^m to any vector $\mathbf{A}$ is

$$\alpha^m\mathbf{A}=e^{-mx}\{\mathbf{n}(\mathbf{n}\cdot\mathbf{A})+\sin m\theta(\mathbf{n}\times\mathbf{A}) -\cos m\theta\mathbf{n}\times(\mathbf{n}\times\mathbf{A})\}, \quad (27)$$

where $x\equiv\tau/T$. To get an explicit form for $(1-\alpha)^{-1}$ we use the power series representation,

$$(1-\alpha)^{-1}=1+\alpha+\alpha^2+\cdots,$$

whose convergence is assured by the exponential damping in α. Thus, the result of applying the operation $(1-\alpha)^{-1}$ to any vector $\mathbf{A}$ is the sum of all the individual vectors in (27). The sums are readily evaluated, with the result

$$\frac{1}{1-\alpha}\mathbf{A}=\frac{\mathbf{n}(\mathbf{n}\cdot\mathbf{A})}{1-e^{-x}}+\frac{\sin\theta}{2(\cosh x-\cos\theta)}(\mathbf{n}\times\mathbf{A}) -\frac{e^x-\cos\theta}{2(\cosh x-\cos\theta)}\mathbf{n}\times(\mathbf{n}\times\mathbf{A}). \quad (28)$$

This expression may be approximated as follows in the case that the repetition period is small compared to the relaxation time ($x\ll 1$). The last two terms of (28) are then small, of the order unity, except when θ is near some multiple of 2π, where they become large, of the order $(1/x)$. When θ is near $2n\pi$, the following approximations are valid:

$$\begin{aligned}\frac{\sin\theta}{2(\cosh x-\cos\theta)}&\simeq\frac{\theta-2n\pi}{x^2+(\theta-2n\pi)^2}=\frac{1}{x}\cos\psi\sin\psi,\\ \frac{e^x-\cos\theta}{2(\cosh x-\cos\theta)}&\simeq\frac{x}{x^2+(\theta-2n\pi)^2}=\frac{1}{x}\cos^2\psi,\end{aligned} \quad (29)$$

where $\tan\psi=(\theta-2n\pi)/x$.

In a coordinate system so oriented that its z axis is parallel to $\mathbf{n}$, $(1-\alpha)^{-1}$ therefore takes the form

$$\frac{1}{1-\alpha}=\frac{1}{x}\begin{bmatrix}\cos^2\psi & -\cos\psi\sin\psi & 0\\ \cos\psi\sin\psi & \cos^2\psi & 0\\ 0 & 0 & 1\end{bmatrix}. \quad (30)$$

Thus, apart from the common factor $1/x$, the operator $(1-\alpha)^{-1}$ does not change the component of $\mathbf{A}$ parallel to $\mathbf{n}$, but the perpendicular components are subjected to a rotation through an angle ψ and decrease in magnitude by a factor of $\cos\psi$. Therefore, we have the following picture of the action of $x(1-\alpha)^{-1}$; when θ is far from $2n\pi$, it merely projects an arbitrary vector $\mathbf{A}$ onto the axis of its λ cone; $x(1-\alpha)^{-1}\mathbf{A}=\mathbf{n}(\mathbf{n}\cdot\mathbf{A})$. When θ approaches a resonance, however, $x(1-\alpha)^{-1}\mathbf{A}$ swings out from $\mathbf{n}$, its tip lying on a circle whose diameter is the projection of $\mathbf{A}$ onto the plane normal to $\mathbf{n}$ (Fig. 2a, 2b). In the usual case, where most of the rotation in one period consists of Larmor precession about the steady field $\mathbf{H}_0$, this resonance phenomenon occurs if the applied signal has a spectral line near the Larmor frequency γH_0.

V. COHERENT PULSES

We now specialize the results of the preceding section to the case where the periodic signal consists of pulses of frequency ω, duration t_1, separated by time intervals t_2 during which only the steady field $\mathbf{H}_0$ is present. It is convenient to regard our relations as pertaining to the rotating coordinate system, as the solution may then be pieced together from solutions of the type (13). Using subscripts 1 and 2 to refer to quantities effective during and between pulses, respectively, two time-development matrices are needed:

$$\lambda_1\equiv e^{-t_1/T}\exp(-\beta_1 t_1), \quad \lambda_2\equiv e^{-t_2/T}\exp(-\beta_2 t_2), \quad (31)$$

with

$$\beta_i=\mathbf{B}_i\times, \quad \mathbf{B}_1=[\gamma H_1, 0, \gamma H_0-\omega], \quad \mathbf{B}_2=[0, 0, \gamma H_0-\omega]. \quad (32)$$

Denoting the polarization at the start and end of the nth pulse by $\mathbf{M}_n$, $\mathbf{M}_n'$, respectively, we then use (13) twice:

$$\begin{aligned}\mathbf{M}_n'&=\lambda_1[\mathbf{M}_n-\mathbf{M}_1(\infty)]+\mathbf{M}_1(\infty),\\ \mathbf{M}_{n+1}&=\lambda_2[\mathbf{M}_n'-\mathbf{M}_2(\infty)]+\mathbf{M}_2(\infty),\end{aligned}$$

in which

$$\begin{aligned}\mathbf{M}_1(\infty)&=(1/T+\beta_1)^{-1}\mathbf{A},\\ \mathbf{M}_2(\infty)&=(1/T+\beta_2)^{-1}\mathbf{A}=\chi\mathbf{H}_0\end{aligned} \quad (33)$$

are, respectively, the steady-state polarizations that would be reached if the signal were left on or off indefinitely. Eliminating $\mathbf{M}_n'$ from these equations, we have the difference equation for $\mathbf{M}_n$; comparing with (23) the result is

$$\begin{aligned}\alpha&=\lambda_2\lambda_1=e^{-\tau/T}\exp(-\beta_2 t_2)\exp(-\beta_1 t_1),\\ \mathbf{N}&=\lambda_2(1-\lambda_1)\mathbf{M}_1(\infty)+(1-\lambda_2)\mathbf{M}_2(\infty).\end{aligned} \quad (34)$$

Therefore, after the transient has died out, we find for the steady-state polarization just at the beginning of the pulse:

$$\mathbf{M}_\infty=\mathbf{M}_1(\infty)+\frac{1}{1-\alpha}(1-\lambda_2)[\mathbf{M}_2(\infty)-\mathbf{M}_1(\infty)]. \quad (35)$$

Evidently an analogous, though more complicated, expression for $\mathbf{M}_\infty$ can be found in this way whenever the applied signal has a constant frequency and a stepwise constant amplitude.

VI. TRANSCRIPTION TO SPINOR REPRESENTATION

Calculation of the resultant of several successive rotations, using the above (3×3) matrices rapidly becomes very tedious. In such evaluation it is a practical necessity to use the two-dimensional representation of the rotation group,[6] also called the Cayley-Klein parameters.[7] To each polarization $\mathbf{M}$, oriented with colatitude and azimuth angles θ, φ, i.e., with components in the axial representation

$$M_+ = M\sin\theta e^{i\varphi},$$
$$M_- = M\sin\theta e^{-i\varphi},$$
$$M_z = M\cos\theta,$$

we associate a spinor[8]

$$\psi = \begin{pmatrix} u \\ v \end{pmatrix} = \begin{pmatrix} M^{\frac{1}{2}}\cos(\theta/2)e^{-i(\varphi/2)} \\ M^{\frac{1}{2}}\sin(\theta/2)e^{i(\varphi/2)} \end{pmatrix}, \tag{36}$$

and to every rotation of $\mathbf{M}$ generated by a matrix $\mathbf{R}$:

$$\mathbf{M}' = \mathbf{R}\mathbf{M},$$

there corresponds a unitary transformation of ψ:

$$\psi' = \mathbf{Q}\psi.$$

The relation between the elements of $\mathbf{Q}$ and the axis and magnitude of the corresponding rotation is expressed compactly in terms of the Pauli spin matrices,

$$\sigma_x = \begin{pmatrix} 0 & 1 \\ 1 & 0 \end{pmatrix}, \quad \sigma_y = \begin{pmatrix} 0 & -i \\ i & 0 \end{pmatrix}, \quad \sigma_z = \begin{pmatrix} 1 & 0 \\ 0 & -1 \end{pmatrix},$$

as follows. The rotation through an angle θ about an axis given by a unit vector $\mathbf{n}$ is represented by the matrix

$$Q = \begin{pmatrix} \alpha & \beta \\ -\beta^* & \alpha^* \end{pmatrix} = \exp[-i(\mathbf{n}\cdot\boldsymbol{\sigma})(\theta/2)]$$
$$= \mathbf{1}\cos(\theta/2) - i(\mathbf{n}\cdot\boldsymbol{\sigma})\sin(\theta/2), \tag{37}$$

or the Cayley-Klein parameters for this rotation are

$$\alpha = \cos(\theta/2) - in_z\sin(\theta/2),$$
$$\beta = -in_-\sin(\theta/2). \tag{38}$$

Alternatively, an arbitrary rotation may be specified by three Eulerian angles; if we carry out in succession a rotation through an angle ξ about the z axis; a rotation η about the x axis, and a rotation ζ about the z axis, the Q-matrix of the resultant is

$$\exp[-i\sigma_z(\zeta/2)]\exp[-i\sigma_x(\eta/2)]\exp[-i\sigma_z(\xi/2)],$$

from which we find

$$\alpha = \cos(\eta/2)\exp[-i(\zeta+\xi)/2],$$
$$\beta = -i\sin(\eta/2)\exp[-i(\zeta-\xi)/2]. \tag{39}$$

The $\mathbf{R}$-matrix corresponding to a given $\mathbf{Q}$-matrix assumes the following form in the axial representation

$$\mathbf{R} = \begin{bmatrix} \delta^2 & -\gamma^2 & 2\gamma\delta \\ -\beta^2 & \alpha^2 & -2\alpha\beta \\ \beta\delta & -\alpha\gamma & (\alpha\delta+\beta\gamma) \end{bmatrix}, \tag{40}$$

where $\delta=\alpha^*$, $\gamma=-\beta^*$.

To aid in evaluating the expressions in the preceding section, we wish to find the Cayley-Klein parameters corresponding to the rotation occurring during a pulse. Referring to Eq. (32), this is a rotation about the vector $\mathbf{B}_1$ through an angle $bt=[(\gamma H_1)^2+(\gamma H_0-\omega)^2]^{\frac{1}{2}}t$. Denoting by φ the angle between the x axis and $\mathbf{B}_1$, Eq. (38) thus reduces to

$$\alpha = \cos(bt/2) - i\sin\varphi\sin(bt/2),$$
$$\beta = i\cos\varphi\sin(bt/2). \tag{41}$$

These relations are used in the following paper for treatment of spin echoes. In terms of the Eulerian angles, we see on comparing (38) and (39) that the condition for the axis of the resultant rotation to lie in the x-z plane is $\xi=\zeta$, so that the Eulerian angles corresponding to the rotation (41) are given by

$$\tan\zeta = \sin\varphi\tan(bt/2),$$
$$\sin(\eta/2) = \cos\varphi\sin(bt/2). \tag{42}$$

Upon using the above results, most of the preceding equations have analogs in the two-dimensional representation scheme. The correspondence is determined by that for infinitesimal rotations: if $\beta=\mathbf{B}\times$, we have from (37)

$$[1-\beta dt] \rightarrow [1-\tfrac{1}{2}i(\boldsymbol{\sigma}\cdot\mathbf{B})dt],$$

and therefore a finite rotation matrix is given by

$$\mathbf{Q}(t,t') = \lim_{\tau\to 0}[1-\tfrac{1}{2}i\tau\boldsymbol{\sigma}\cdot\mathbf{B}(t-\tau)]$$
$$\times[1-\tfrac{1}{2}i\tau\boldsymbol{\sigma}\cdot\mathbf{B}(t-2\tau)]\cdots[1-\tfrac{1}{2}i\tau\boldsymbol{\sigma}\cdot\mathbf{B}(t')]. \tag{43}$$

It satisfies the differential equation

$$\partial Q(t,t')/\partial t + \tfrac{1}{2}i\boldsymbol{\sigma}\cdot\mathbf{B}(t)\mathbf{Q}(t,t') = 0, \tag{44}$$

which may also be derived from the fact that in the limit of infinite relaxation time, the spinor (36) satisfies the Schrödinger equation for a particle of spin $\frac{1}{2}$.

[6] E. P. Wigner, *Gruppentheorie und ihre Anwendung auf die Quantenmechanik der Atomspektren* (Friedrick Vieweg, & Sohn, Braunschweig, 1931), Chap. XV.

[7] H. Goldstein, *Classical Mechanics* (Addison-Wesley Press, New York, 1951).

[8] H. A. Kramers, *Quantentheorie des Elektrons und der Strahlung* (Akademische Verlagsgesellschaft, Leipzig, 1938), Chap. 6.

Since the matrix

$$\tfrac{1}{2}i\boldsymbol{\sigma}\cdot\mathbf{B}=\tfrac{1}{2}i\begin{pmatrix}B_z & B_-\\ B_+ & -B_z\end{pmatrix} \tag{45}$$

corresponds to the 3×3 matrix β in all the above relations, it will also be denoted as β in what follows; it will be clear from the context whether we are using the two- or three-dimensional representation. Thus, for example, the rotation matrix (37) may be written as $\exp(-\beta t)$, where $\mathbf{n}\theta=\mathbf{B}t$.

VII. APPROXIMATE SOLUTIONS

In most problems that arise we have a strong constant field $\mathbf{H}_0$, whose direction we choose as the z-axis, plus a weak varying field $\mathbf{H}_1(t)$. Therefore in (7) we write $\beta(t)=\beta_0+\beta_1(t)$, and the major part of the time variation of $\mathbf{R}(t,t')$ or $\mathbf{Q}(t,t')$ is a uniform Larmor precession due to β_0. When we use the two-dimensional representation, this can be removed from the equation of motion (44) by the transformation

$$\mathbf{Q}(t,t')=\exp[-\beta_0 t]\mathbf{Q}'(t,t')\exp[+\beta_0 t'], \tag{46}$$

whereupon $\mathbf{Q}'$ satisfies the relation

$$\partial\mathbf{Q}'(t,t')/\partial t+\beta'(t)\mathbf{Q}'(t,t')=0, \tag{47}$$

with

$$\beta'(t)=\exp[\beta_0 t]\beta_1(t)\exp[-\beta_0 t], \tag{48}$$

and $\mathbf{Q}'(t,t)=1$. This is analogous to passage to the rotating coordinate system discussed in Sec. II, but differs from it in several respects; for example, the rotation frequency is here always $\omega_0=\gamma H_0$ rather than the applied frequency. Since $\mathbf{Q}'$ is only slowly varying if $H_1\ll H_0$, an approximate solution of (47) using a finite number of terms of the expansion

$$\mathbf{Q}'(t,t')=1-\int_{t'}^{t}dt''\beta'(t'')+\int_{t'}^{t}dt''\beta'(t'')\times\int_{t'}^{t''}dt'''\beta'(t''')+\cdots \tag{49}$$

is valid for a much longer time interval than is the corresponding approximate solution of (44). Equation (49) is now used to evaluate $\mathbf{Q}$ for the case that the variable field $\mathbf{H}_1(t)$ lies in the x–y plane. Then, writing $\omega_0=\gamma H_0$, we find $\beta(t)=\mathbf{B}\times$, where $B_\pm(t)=\gamma H_\pm(t)\times\exp(\pm i\omega_0 t)$, $B_z=0$. When we write out (49), the Cayley-Klein parameters for $\mathbf{Q}'$ are

$$\alpha'=1-\tfrac{1}{4}\gamma^2\int_{t'}^{t}dt''\int_{t'}^{t''}dt'''H_-(t'')H_+(t''')\times\exp[i\omega_0(t'''-t'')], \tag{50}$$

$$\beta'=-\tfrac{1}{2}i\gamma\int_{t'}^{t}dt''H_-(t')\exp(-i\omega_0 t''), \tag{51}$$

in which all terms through the second order of β' are retained. From (46), the parameters of $\mathbf{Q}(t,t')$ are

$$\alpha=\alpha'\exp[-i\omega_0(t-t')/2], \tag{52}$$

$$\beta=\beta'\exp[-i\omega_0(t+t')/2]. \tag{53}$$

As shown in the following paper, it is the product of (52) and (53) that is needed for interpretation of experiments in which one observes the effect of a signal which has been impressed for a time short compared to the relaxation time.

For time intervals containing many Larmor periods, the integrals in (50), (51) are well approximated in terms of the Fourier transforms of $H_-(t)$. To fix reasonable orders of magnitude of these terms, we consider the case of protons in water, in a magnetic field such that the Larmor frequency is about 30 megacycles/sec, while a weak signal $H_-(t)$ is applied with a repetition rate of about 1000 sec^{-1}, the relaxation time being of the order of a second. Then we are interested in evaluating (50), (51) for time intervals t_1 for which

$$\begin{aligned}\omega_0 t_1&\sim10^4,\\ \gamma H_- t_1&\sim1,\end{aligned} \tag{54}$$

and there is a wide range of conditions under which the relations $t_1/T\ll\gamma H_- t_1\ll\omega_0 t_1$ are valid. If $H_-(t)$ is represented by a Fourier integral,

$$H_-(t)=\int_{-\infty}^{\infty}G(\omega)\exp(i\omega t)d\omega, \tag{55}$$

we may substitute into (50), (51) and perform the time integrations. Approximations of the form

$$\lim_{t\to\infty}\frac{\exp(i\omega t)-1}{i\omega}=\pi\delta(\omega)$$

will be valid, leading to the simplified expressions:

$$\alpha'=1-\tfrac{1}{8}\pi^2\gamma^2(t-t')^2|G(\omega_0)|^2, \tag{56}$$

$$\beta'=-\tfrac{1}{2}i\pi\gamma(t-t')G(\omega_0). \tag{57}$$

Suppose that after a certain time interval the applied field $H_-(t)$ is turned off. Thereafter, in (52) and (53), α' and β' remain constant at the values fixed by (56), (57), and so the product $\alpha\beta$ continues to oscillate at frequency ω_0 with amplitude $\alpha'\beta'$. If this amplitude contains terms whose phase varies linearly with ω_0, then in an inhomogeneous field where nuclei with all values

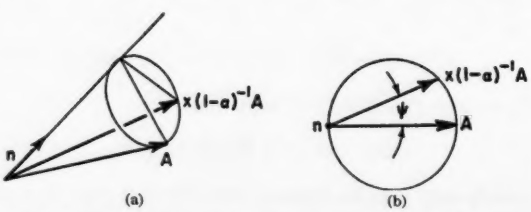

FIG. 2. (a) Circle traversed by $(1-\alpha)^{-1}\mathbf{A}$ as θ sweeps through each resonance. (b) Projection of (a) on a plane normal to $\mathbf{n}$.

of ω_0 are present, one finds "coherences," or "echoes" as described in the following paper.

VIII. GENERALIZATION FOR $T_1 \neq T_2$

The assumption that the two relaxation times are equal has simplified our geometric interpretations, but the analytical expressions in the 3×3 representation remain almost as simple if it is dropped. Thus, the equation of motion (3) remains valid provided we interpret $1/T$ as a diagonal matrix with elements $[1/T_2, 1/T_2, 1/T_1]$. Equations (4), (5), (16) then remain valid although $\mathbf{R}(t,t')$ is no longer a pure rotation matrix. The time-development matrix $\mathbf{U}(t,t')$ is given by an expression of the form (8) in which β is replaced by $(\mathbf{T}^{-1}+\beta)$, and the solution (13) is valid, with $\lambda(t) = \exp[-(\mathbf{T}^{-1}+\beta)t]$. The locus generated by $\lambda(t)$ is now a distorted version of a cone. Similarly, the relations (22)–(26) of Sec. IV still hold, although the geometrical picture is less simple.

PHYSICAL REVIEW VOLUME 98, NUMBER 4 MAY 15, 1955

Nuclear Induction in Inhomogeneous Fields*

ARNOLD L. BLOOM
Varian Associates, Palo Alto, California

(Received December 20, 1954)

The mathematical methods developed by Jaynes are applied to the study of nuclear resonance in inhomogeneous magnetic fields. It is shown that a description of delayed-signal phenomena such as spin echoes is greatly simplified by the use of the spinor representation involving 2×2 transformation matrices. The original results of Hahn on spin echoes are rederived in simplified fashion and more complicated situations are discussed, including large numbers of pulses, exact time dependence in extremely inhomogeneous fields, and continuous pulse trains. Several previously unreported types of delayed-signal phenomena are discussed and illustrated experimentally by oscilloscope traces. The apparatus used to study nuclear induction in very inhomogeneous fields is briefly discussed.

I. INTRODUCTION

THIS report applies the mathematical methods developed in the previous paper[1] to the study of nuclear induction in inhomogeneous magnetic fields, involving a class of phenomena such as spin echoes.[2] In previous papers on spin echoes[2–5] the analysis always involved successive operations in the three-dimensional rotation group, and the use of linear transformation operators was implied even if these operators were not always written in matrix format. It is thus not our intention merely to demonstrate the use of matrices for predicting spin echoes. What we wish to accomplish is the following: (1) to demonstrate the use of Cayley-Klein parameters in spin-echo problems, and (2) to show how the simplicity and generality of the Cayley-Klein formalism makes it possible to study more complicated situations with a minimum of effort.

II. MATHEMATICAL PRELIMINARIES

We shall assume that the reader is familiar with the original spin-echo experiments of Hahn,[2] and with the mathematical and geometrical interpretations presented in the Hahn paper. We shall follow the same general method of attack. Starting with a vector $\mathbf{M}(\Delta\omega)$ which obeys Bloch's[6] equations [Eqs. (1) or (3) of I] and which is initially in the z direction, we perform successive transformations corresponding to discrete time intervals during which a given rf field H_1 is either present or absent. Finally, after all rf signals have been applied, the polarization in the xy plane takes the form,

$$M_{x-iy}(\Delta\omega) = g(\Delta\omega)\textstyle\sum_j G_j(\Delta\omega)\exp[-i\Delta\omega(t-t_j)], \quad (1)$$

where g describes the effect of the magnetic field inhomogeneity and the G's are functions of relaxation, self-diffusion and three-dimensional rotation; it is only the latter variable that is of interest to us. The observed nuclear induction signal depends on the integral of (1) over all values of $\Delta\omega$. In general the integral is zero unless t is in the vicinity of t_j, in which case there is a signal of intensity proportional to G_j. If t_j coincides with an rf pulse the signal is a "free decay," otherwise it is an "echo."

The transformation relations which are of interest to us have been given in Sec. VI of I. During the ith pulse the matrix Q_i is described as

$$Q_i = \begin{pmatrix} \alpha_i & \beta_i \\ -\beta_i^* & \alpha_i^* \end{pmatrix}, \quad (2)$$

* Supported by the Office of Naval Research.

[1] E. T. Jaynes, preceding paper [Phys. Rev. 98, 1099 (1955)], hereafter referred to as I.

[2] E. L. Hahn, Phys. Rev. 80, 580 (1950).

[3] E. L. Hahn and D. E. Maxwell, Phys. Rev. 88, 1070 (1952); D. E. Maxwell, thesis, Stanford University (unpublished).

[4] T. P. Das and A. K. Saha, Phys. Rev. 93, 749 (1954).

[5] H. Y. Carr and E. M. Purcell, Phys. Rev. 94, 630 (1954).

[6] F. Bloch, Phys. Rev. 70, 460 (1946).

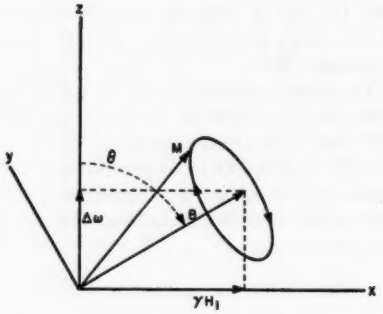

FIG. 1. Diagram of the vectors **M**, **B** and the precession cone in the rotating frame of reference.

in which[7] (omitting subscripts for the moment),

$$\alpha=\cos(\tfrac{1}{2}b\ell)-i\cos\theta\sin(\tfrac{1}{2}b\ell), \qquad (3)$$
$$\beta=-i\sin\theta\sin(\tfrac{1}{2}b\ell),$$

where the asterisk denotes the complex conjugate, and

$$b=|\mathbf{B}|,$$
$$\mathbf{B}=\gamma\mathbf{H}_1+\Delta\omega, \qquad (4)$$
$$\theta=\tan^{-1}(\gamma H_1/\Delta\omega),$$
$$\Delta\omega=\gamma\mathbf{H}_0-\omega.$$

The precession is clockwise for $\gamma>0$ when viewed from in front of the effective field vector **B** (see Fig. 1). In between pulses we have the special case

$$Q=\begin{pmatrix} e^{-\frac{1}{2}i\Delta\omega t} & 0 \\ 0 & e^{\frac{1}{2}i\Delta\omega t}\end{pmatrix}, \qquad (5)$$

corresponding to precession about the z axis with angular frequency $\Delta\omega$. The resultant transformation after n time intervals is then defined as

$$Q=Q_n\cdots Q_1=\begin{pmatrix}\alpha & \beta \\ -\beta^* & \alpha^*\end{pmatrix}. \qquad (6)$$

To convert Q to a three-dimensional representation, we use Eq. (40) of **I**, which we summarize as follows:

$$\begin{pmatrix} M'_{x+iy} \\ M'_{x-iy} \\ M'_z\end{pmatrix}=\begin{pmatrix} \alpha^{*2} & -\beta^{*2} & -2\alpha^*\beta^* \\ -\beta^2 & \alpha^2 & -2\alpha\beta \\ \alpha^*\beta & \alpha\beta^* & (\alpha\alpha^*-\beta\beta^*)\end{pmatrix}\begin{pmatrix} M_{x+iy} \\ M_{x-iy} \\ M_z\end{pmatrix}. \qquad (7)$$

Thus, starting with $M=M_z$ we wish to compute M_{x-iy} at a later time, i.e., the matrix element $(-2\alpha\beta)$ as a function of t. From inspection of Eqs. (2), (5), and (6), we see that $(-2\alpha\beta)$ can be written in the form

$$-2\alpha\beta=\textstyle\sum_j G_j\exp[-i\Delta\omega(t-t_j)], \qquad (8)$$

which is in the form needed to study spin echoes.

[7] All computations in this paper are carried out in the rotating frame of reference, in which H_1 is taken to be always in the x direction. See Rabi, Ramsey, and Schwinger, Revs. Modern Phys. **26**, 167 (1954).

To summarize, we compute α and β by combining the 2×2 Q-matrices and multiply these two parameters together to obtain the required three-dimensional matrix element. This procedure is generally much simpler than that of multiplying 3×3 matrices directly, and many of the results which were laboriously computed in the earlier papers can be determined merely by a visual inspection of the Q-matrices. In addition the generality of the Cayley-Klein parameters allows us to waive the restrictions (nuclei at resonance, short and intense pulses of rf) which were necessary in the earlier work in order to keep the computations to a manageable length.

III. GENERAL ANALYSIS

A. Introduction

In this section, we shall calculate the amplitudes and shapes of signals in an idealized situation in which both T_1 and T_2 (if they are not equal) are very long compared to the times required to do the experiments, and in which self-diffusion effects are absent. For each instant of time we must solve the corresponding Eq. (13) of **I**, which can be written in the form

$$\mathbf{M}(t)=[e^{-t/T}\exp(-\beta t)]\mathbf{M}_1 +[1-e^{-t/T}\exp(-\beta t)]\mathbf{M}_2. \qquad (9)$$

Here $T_1=T_2=T$, $\mathbf{M}_1$ is the polarization at the start of the time interval, $\mathbf{M}_2$ is the steady-state polarization for that interval, and β is the precession matrix.[8] It is customary in treatments of spin echo[2-5] to assume an initial polarization $\mathbf{M}=M_0\mathbf{z}$ prior to the first pulse, and to solve only for the first term in (9), ignoring the effect of $\mathbf{M}_2$. The neglect of this second term during the time between pulses, when it corresponds to a recovery of initial polarization, is justifiable only for long relaxation times; actually the recovery is quite useful for the measurement of T_1. Neglect of $[1-e^{-t/T}\exp(-\beta t)]\mathbf{M}_2$ during a pulse is not so easily justified. In most spin-echo experiments, however, the rf level, if left on continuously, would correspond to a high degree of saturation; in such cases it can be shown that $\mathbf{M}_2$ is either very small or is nearly parallel to **B**, so the total effect of the term is small. We shall follow the usual practice of neglecting the term in $\mathbf{M}_2$; it is nevertheless clear that there are circumstances under which one cannot neglect $\mathbf{M}_2$, even for relatively short pulses and intense rf fields.

We shall make no assumptions in this section about the magnetic field inhomogeneity effect, $g(\Delta\omega)$, except to follow the usual practice in requiring $g(\Delta\omega)=g(-\Delta\omega)$. An inspection of the basic equations of motion and of Fig. 1 shows that if the initial polarization is in the z direction the two vectors for each $|\Delta\omega|$ are at all times symmetrically located about the yz plane, from which it follows that $G_j(\Delta\omega)=-G_j^*(-\Delta\omega)$. Thus if the above restriction on g is fulfilled it is only necessary to use the

[8] In this paper α and β refer to transformation operators as defined in Eqs. (2) and (22) of **I**. The corresponding lightface characters are the Cayley-Klein parameters.

imaginary part of G_f in computing signal amplitudes and shapes.

When the transformation matrices are displayed it is fairly evident how one may modify them to include the effects of relaxation and self-diffusion. These effects have already been calculated in detail for two- and three-pulse systems[4] and it does not appear that their applications to more complex systems will produce much that is physically new or interesting. Exceptions to this latter statement will be discussed qualitatively.

B. One, Two, and Three Pulses

In order to show in a simple manner how our method of calculation works, we shall first rederive Hahn's results[2] for maximum amplitudes of signals following one, two, and three pulses in the absence of relaxation and self-diffusion effects. The notation refers to the time intervals as defined in Fig. 2. Odd numbered subscripts refer to pulses, even numbered subscripts to intervals between pulses. All times are measured from the beginning of the time interval, rather than from the start of the experiment.

1. One pulse.—The term $(-2\alpha\beta)$ in the matrix $Q=Q_2Q_1$ is given by

$$(-2\alpha\beta)=-2\alpha_1\beta_1 e^{-i\Delta\omega t_2}, \tag{10}$$

and substituting Eq. (3) we have

$$(-2\alpha\beta)=[\sin 2\theta \sin^2(\tfrac{1}{2}bt_1)+i\sin\theta \sin bt_1]e^{-i\Delta\omega t_2}. \tag{11}$$

The only signal during this time interval is the free decay following the pulse ($t_2=0$). Near resonance the term $\sin\theta \sin bt_1$ is adequate to describe the free decay amplitude as a function of pulse parameters.

2. Two pulses.—The term $(-2\alpha\beta)$ in the matrix $Q=Q_4\cdots Q_1$ is given by

$$(-2\alpha\beta)=-2(\alpha_1\alpha_3 e^{-2-4}-\beta_1^*\beta_3 e^{+2-4})\times(\beta_1\alpha_3 e^{-2-4}-\alpha_1^*\beta_3 e^{+2-4}), \tag{12}$$

where e^{-2} is short for $\exp(-\frac{1}{2}i\Delta\omega t_2)$, e^{+4} for $\exp(+\frac{1}{2}i\Delta\omega t_4)$, etc. Of the four terms in (12) one of them refers to times which are negative with respect to the second pulse and which we shall disregard. The other two represent coherences at $t_4=0$ (free decay of the second pulse), and at $t_4=t_2$, which is the simple two-pulse echo. Substituting (3) into the coefficient for the free decay, we obtain for the free decay amplitude

$$G_1=-(\alpha_1\alpha_1^*-\beta_1\beta_1^*)(2\alpha_3\beta_3). \tag{13}$$

The amplitude of the echo is given by

$$G_2=2\alpha_1^*\beta_1^*\beta_3^2. \tag{14}$$

For pulses of equal intensity and width, and nuclei near resonance, (14) reduces to

$$G_2=\sin bt_1 \sin^2(\tfrac{1}{2}bt_1), \tag{15}$$

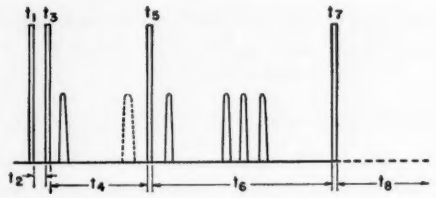

FIG. 2. Timing diagram for up to four unequally spaced pulses.

in agreement with the result calculated by Hahn. Note, however, that Eq. (14) is quite general and with very little extra labor will give the echo amplitude for pulses of different width and intensity, and for nuclei not near resonance. [See for example Eq. (28).]

3. Three pulses with $t_4>t_2$.—In the matrix $Q=Q_6\cdots Q_1$ both α and β consist of four terms with the following exponents:

$$e^{-2-4-6},\ e^{-2+4-6},\ e^{+2-4-6},\ e^{+2+4-6}.$$

When we multiply these together to obtain $(-2\alpha\beta)$, we obtain ten terms (signals) corresponding to the combinations of the above terms taken two at a time. Of these ten terms, two occur at $t_6=0$ and represent the free decay following the third pulse. Of the remaining eight terms, four must occur at negative time t_6, which we temporarily disregard, and four at positive time, which predict echos. The times of the echoes, and the terms which give their intensity, are as follows:

At $t_6=t_2$ (stimulated echo)

$$G_2=4\alpha_1^*\beta_1^*\alpha_3^*\beta_3\alpha_5\beta_5, \tag{16}$$

at $t_6=t_4-t_2$

$$G_3=-2\alpha_1\beta_1\beta_3^{*2}\beta_5^2, \tag{17}$$

at $t_6=t_4$

$$G_4=2(\alpha_1\alpha_1^*-\beta_1\beta_1^*)\alpha_3^*\beta_3^*\beta_5^2, \tag{18}$$

at $t_6=t_4+t_2$

$$G_5=2\alpha_1^*\beta_1^*\alpha_3^{*2}\beta_5^2. \tag{19}$$

By substitution of the definitions, Eqs. (3), one finds that these expressions reduce to the ones given by Hahn for the special case which he considers.

C. Three Equally Spaced Pulses

The numbers of echoes and their amplitudes are also a function of the positions of the pulses. Previously we were careful to state that the third pulse should occur after the simple echo following the first two pulses. Obviously, if the third pulse occurs too soon, certain "echoes of echoes" cannot occur and the amplitudes and the numbers of the echoes following the third pulse will be different. This has been briefly mentioned by Hahn.[2] Here we will discuss a special case, that of three equally spaced pulses ($t_2=t_4$). In this particular case there will be only two echoes following the third pulse and these echoes will be spaced so as to continue the original pulse train.

The details of the calculations are the same as in the preceding cases and we shall merely state the result for

the coefficient of the echo which occurs at a time t_2 (or t_4) following the third pulse, i.e., the first of the two echoes. This coefficient is given by

$$G=2[2\alpha_1{}^*\beta_1{}^*\alpha_3{}^*\beta_3\alpha_5\beta_5+(\alpha_1\alpha_1{}^*-\beta_1\beta_1{}^*)\alpha_3{}^*\beta_3{}^*\beta_5{}^2]. \quad (20)$$

The first term we recognize from (16) to be the coefficient for the three-pulse "stimulated" echo. In the second term, the first section $(\alpha_1\alpha_1{}^*-\beta_1\beta_1{}^*)$ we recognize from (7) to be the matrix element which leaves the z component unchanged; the rest of this term is the formula for the two-pulse echo produced by the second and third pulses. Thus the echo is merely the direct sum of two superimposed echoes. One might think that such a direct sum of echoes would be likely under certain conditions to give an amplitude greater than the original polarization; however, an analysis of the coefficients shows that this is not so.

D. More Than Three Pulses

In his original article, Hahn[2] pointed out the existence of two-pulse and three-pulse (stimulated) echoes. It was of interest in connection with this project to find out if these were the only types of echoes that could be produced, or if there were also echoes that could be understood in terms of four or more pulses. We shall not try to prove the existence of n-pulse echoes for any n but shall investigate the possibility that there exist four-pulse echoes, which will imply that there may exist echoes that could be formed only with $n>4$ pulses.

We suppose that the four pulses are spaced so that all echoes which can be produced by any one set of pulses occur before the next pulse is applied (Fig. 2). In the final transformation the matrix elements α, β each consist of eight terms which, taken two at a time and combining similar exponents, gives a total of 36 terms in the product $-2\alpha\beta$. Of these terms, four occur at $t_8=0$ and represent the free decay following the fourth pulse. The remaining terms are located symmetrically about $t_8=0$ giving 16 terms prior to the fourth pulse, which we disregard, and 16 positive corresponding to echoes. Before going any further, let us return for a moment to the case of three unequally spaced pulses. We noted that there must be four coherence terms for $t_6<0$, symmetric about the third pulse with respect to the four echoes in t_6. However, there are only three actual coherences in the time prior to the third pulse. The extra term, shown by a dotted line in Fig. 2, is therefore a "virtual" echo that does not exist until the third pulse is applied, but following the third pulse the nuclear system behaves in every way as if the virtual echo had actually occurred.

If we include the virtual echo among the sources of two- and three-pulse echoes following the fourth pulse, we get a total of 14 such echoes. This still leaves two echoes unaccounted for, which must be four-pulse or "super-stimulated" echoes.

The analysis can be extended readily to n pulses. If all pulse spacings are unequal, and if

$$t_{2n-2}>t_2+t_4+\cdots+t_{2n-4},$$

as before, then, following the nth pulse there will be 2^{2n-4} echoes. Since the total number of coherences, real and virtual, due to the $(n-1)$st pulse is $2(2^{2n-6})+1$, the nth pulse must create $(2^{2n-5}-1)$ new virtual coherences.

E. Sets of Double Pulses

A special case of four pulses which is of particular interest is that of a two-pulse spin-echo experiment repeated in a time of the order of T_1 or less, so that the sample still has some memory of the previous set of two pulses. In this case one usually observes at least one additional echo, marked S in Fig. 3, following the primary echo. The origin of this echo is as follows: The third pulse (Fig. 3) creates a virtual echo, V, which is mathematically similar to the stimulated echo which would occur at the position occupied by the fourth pulse. The latter pulse, however, transforms V into a two-pulse echo at S. That this analysis is essentially correct can be seen by calculating the coefficient for this echo. The calculation gives

$$G_S=-4\alpha_1{}^*\beta_1{}^*\alpha_3{}^*\beta_3\alpha_5{}^*\beta_5{}^*\beta_7{}^2, \quad (21)$$

which is a stimulated echo transformed by another pulse.

As can be seen from its genesis, this secondary echo has many properties in common with Hahn's stimulated echo. In particular, its amplitude is more nearly dependent on T_1 than on T_2 and is relatively immune to self-diffusion effects. Experimentally, if the signal-to-noise ratio is high, this echo can often be seen even when the time between double pulses is several times T_1.

In the vicinity of resonance, and for pulses of equal length and intensity, Eq. (21) reduces to

$$G_S=\tfrac{1}{2}\sin^3(bt_1)\sin^2(\tfrac{1}{2}bt_1), \quad (22)$$

which has its maximum at $\cos bt_1=-\frac{1}{4}$. If the experimental repetition rate is fast enough, additional echoes can be seen following S which can be explained in terms of virtual echoes of S on pulse three, etc. In some cases real echoes can be seen preceding the pulses as well as following them, but these must be explained by the symmetry property discussed in the section on continuous pulse trains.

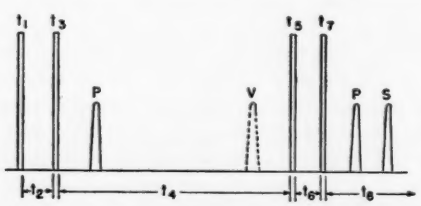

FIG. 3. Diagram for problem of repeated double pulses.

IV. VERY INHOMOGENEOUS FIELDS

A. Introduction

In the original spin-echo experiments[2] performed in fields that were only slightly inhomogeneous, it was shown that: (1) The spacing between second pulse and echo was approximately the same as between first and second pulse. (2) The free decay was the Fourier transform of the moment distribution $g(\Delta\omega)$ in the magnetic field. (3) The echo was shaped like two free decays placed back-to-back.

In this section we shall consider a somewhat different case, that of a magnetic field so inhomogeneous that the total inhomogeneity, $\gamma\Delta H$, is very much greater than the frequency spectrum of the pulses. We shall assume an "infinite flat-topped" distribution [$g(\Delta\omega)$ constant for all $\Delta\omega$], thus the exact locations and shapes of signals will depend on the Fourier transforms of the $G_j(\Delta\omega)$. As explained previously, it is only necessary to compute the imaginary parts of the G's.

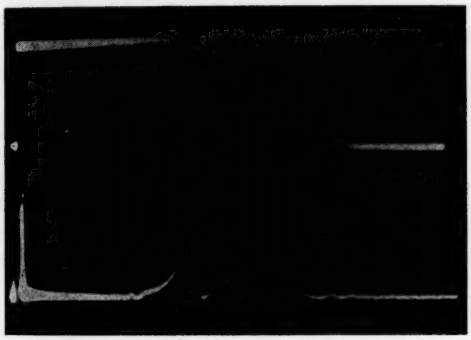

FIG. 4. Free decay (above) and echo (below) when $\gamma H_1 t_1 \approx 4\pi$.

B. Free Decay

The shape of the free decay can be deduced from the imaginary part of Eq. (11):

$$\mathrm{Im}[G(\Delta\omega)] = \sin\theta \sin bt_1 \cos\Delta\omega t_2 - \sin 2\theta \sin^2(\tfrac{1}{2}bt_1) \sin\Delta\omega t_2, \quad (23)$$

where $\theta=\theta(\Delta\omega)$ is given by Eq. (4). The frequency spectrum of the free decay is determined in this case not by the field inhomogeneity but by the rf level. Thus for a given value of $\gamma H_1 t_1$ a long pulse of weak rf amplitude will have a long free decay and a short pulse of strong rf will have a short decay.

It is possible to write (23) in the form

$$\mathrm{Im}G = \cos\Delta\omega t \cos\Delta\omega t_2 + \sin\Delta\omega t \sin\Delta\omega t_2, \quad (24)$$

where the maximum signal presumably occurs at $t_2=t$. A little algebra gives

$$\tan\Delta\omega t = -\cos\theta \tan(\tfrac{1}{2}bt_1). \quad (25)$$

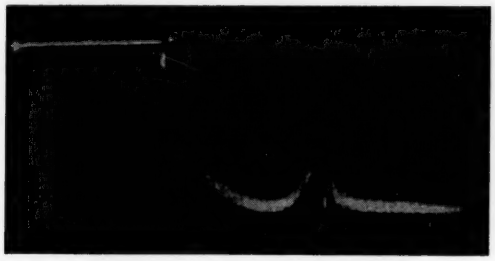

FIG. 5. Free decay and edge echo following single pulse. The pulses were repeated in a time short compared to T_2.

From (25) we see that there is no one instant of time when all components are exactly in phase. However, we can determine a time (prior to the end of the pulse) when the free decay, projected back to this time, would have had its maximum value. If $\gamma H_1 t_1 \leq 1$ and we consider only the components about resonance, we can approximate (25) by

$$\Delta\omega t = -\tfrac{1}{2}bt_1 \cos\theta, \quad (26)$$

and since $\cos\theta=\Delta\omega/b$ we have simply

$$t = -\tfrac{1}{2}t_1. \quad (27)$$

Thus the free decay behaves as if it had started from the midpoint of the pulse. When $\gamma H_1 t_1 \gg 1$, t is different for different groups of values of $\Delta\omega$, with the result that the free decay may show considerable structure. An example of such a free decay is shown in Fig. 4.

C. Edge Echo

The "edge echo" is a phenomenon observable only in a very inhomogeneous magnetic field. If a single square pulse of length t_1 is impressed on the nuclear moment ensemble in such a field, the edge echo appears as a small signal at a time t_1 after the end of the pulse. The effect becomes particularly noticeable for pulses repeated in a time short compared to T_2 and is illustrated in Fig. 5. The structure at the end of the free decay in Fig. 4 can also be considered in part as an edge echo.

The origin of the edge echo can be seen by inspection of Eq. (11). For nuclei far from resonance b is approximately equal to $\Delta\omega$, thus to this approximation (11) contains terms of the form $\exp[-i\Delta\omega(t_2-t_1)]$. A coherence is thus produced by nuclei far from resonance at a time t_1 after the pulse termination. The shape of the edge echo can be inferred by substituting $\Delta\omega$ for b in (23); it has the form $\int \sin[\Delta\omega(t_2-t_1)]d(\Delta\omega)$. The shape of this signal is not the single lobe usually associated with an echo. Instead, if detected by a phase-sensitive detector, it reaches a maximum, goes sharply through zero at $t_2=t_1$, and goes through a maximum in the opposite direction. If the edge echo is viewed only in absolute value, it appears as two maxima separated by a sharp minimum, as shown in Fig. 5.

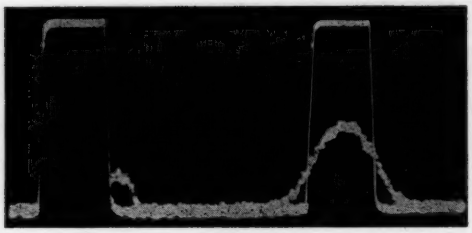

FIG. 6. Superpositions of first pulse, second pulse, and echo showing exact timing of echo maximum.

D. Two-Pulse Echo

For two pulses of equal H_1 the echo signal is obtained by substituting (4) into (14) and taking the imaginary part:

$$\begin{aligned}\mathrm{Im}G_2 = &-\sin^2\theta \sin(bt_1) \sin^2(\tfrac{1}{2}bt_3) \cos[\Delta\omega(t_4-t_2)] \\ &-\sin 2\theta \sin^2\theta \sin^2(\tfrac{1}{2}bt_1) \\ &\times \sin^2(\tfrac{1}{2}bt_3) \sin[\Delta\omega(t_4-t_2)]. \quad (28)\end{aligned}$$

This differs considerably from (23) and the echo is therefore not the same as two free decays placed back-to-back. The common factor $\sin^2\theta$ in (28) cuts down the high-frequency terms in the echo, with the result that the echo is a considerably rounded-off version of the original square pulse. If we write (28) in the form $\cos[\Delta\omega(t_4-t_2-t)]$ we again get (26) and (27) as expressions for t. In other words, if we sweep the oscilloscope with repetition rate $(t_1+t_2)^{-1}$, where t_2 is the time between pulses, and if $\gamma H_1 t_1 = \gamma H_1 t_3 \leq 1$, we will find the echo maximum exactly at the center of the pulse. (See Fig. 6.) For $\gamma H_1 t_1 \gg 1$, the echo shape can get quite complicated (Fig. 4).

V. CONTINUOUS PULSE TRAINS

A. Introduction

In this section, we shall discuss the spin-echo type of solution for continuous trains of pulses. We can assume that the pulse trains start at some initial time $t=0$ and then continue for a time very much longer than the relaxation time T of the substance so that the sample has essentially forgotten when the beginning of the pulse train occurred. We shall follow the same assumptions as in the previous sections with regard to equality of relaxation times and negligible self-diffusion, except that when working with terms that represent infinite series it is necessary to include relaxation time explicitly in the formula in order to insure that the series converge. In what follows, we shall call the repetition time between successive cycles of pulses τ and other definitions shall be as in preceding discussions. We shall, in general, assume that pulse widths are short compared to τ and that $\tau \ll T$.

B. Symmetry with Respect to Time Inversions

One of the more interesting properties of the nuclear system when subjected to continuous pulse trains is the property of time symmetry. Consider the basic equations of motion for the polarization, such as Eq. (1) of I. If we make T large so that the relaxation term is small compared with the other terms in the equation, then reversal of the sign of t is equivalent to a reversal of the sign of the gyromagnetic ratio γ. Thus, if we go backward in time, any solutions which we obtain must also be solutions of Bloch's equations, except for the sign of γ which will make no difference in a system which does not detect phase.[9] If we have an rf driving function which is an even function of time, then after the nuclear system has settled down to steady state it will make no difference whether we take time in the backward or forward direction. Thus the nuclear system must not only produce free decays and edge echoes following the pulses but must anticipate the pulses in exactly the same way. If the driving function consists of double pulses there will be echoes preceding and following the pulses. This property of anticipating the driving function is shown in Fig. 7. Actually, the signal shown in this figure is not perfectly symmetrical owing to self-diffusion effects.

C. End of a Train of Single Pulses

The solution of Bloch's equations for a continuous train of pulses has been given in I. If subscript 1 applies to the pulse, 2 to the interval between pulses, and t is the time following the last pulse, then the solution can be written as

$$\mathbf{M} = \mathbf{M}' \exp(-\beta_2 t), \quad (29)$$

$$\mathbf{M}' = \mathbf{M}_2(\infty) + (1-\alpha)^{-1}(1-\lambda_2)[\mathbf{M}_1(\infty) - \mathbf{M}_2(\infty)], \quad (30)$$

where (30) is just Eq. (35) of I with subscripts interchanged. It is, unfortunately, not possible to add three-dimensional rotation operators by performing any simple operation on the corresponding Q-matrices. Calculation of the solution must therefore be carried out with 3×3 matrices and becomes quite tedious. The solution can be written in the form[8]

$$M_{x-iy} = [\det(1-\alpha)]^{-1}(f + g e^{i\Delta\omega t_2} + h e^{-i\Delta\omega t_2}) e^{-i\Delta\omega t}, \quad (31)$$

where f, g, h are polynomials in α_1, β_1, and $e^{-\tau/T}$. Of interest to us is the effect of the denominator, which can be expanded in a power series as follows:

$$[\det(1-\alpha)]^{-1} \propto \sum_{n=0}^{\infty} \times \left[\frac{(e^{-\tau/T} - e^{-2\tau/T})(\alpha_1^2 e^{-i\Delta\omega t_2} + \mathrm{cc})}{(1-R_{33}e^{-\tau/T})(1-R_{33}e^{-2\tau/T})}\right]^n, \quad (32)$$

[9] This argument is similar to the symmetry property discussed by B. Jacobsohn and R. K. Wangsness, Phys. Rev. 73, 942 (1948). The argument shown there, valid for a weak, frequency-modulated rf signal, requires no assumptions about the magnitude of T_1.

where $R_{33}=\alpha_1\alpha_1^*-\beta_1\beta_1^*$. From (31), (32), and Section IV-D (showing that the center of an echo is related to τ rather that to t_2) we see that the response of the nuclear system is a series of echoes spaced apart a time τ, in essence trying to extend the train of pulses. From (32) we see that the echoes decay exponentially with a decay constant which is a function of $\gamma H_1 t_1$, but not of elapsed time and only indirectly of relaxation time. In other words, the decay takes place in a certain number of pulse repetitions, rather than in a given elapsed time. This is illustrated in Fig. 8, which shows a decay which was independent of time even though τ was varied by a factor of three.

VI. EXPERIMENTAL APPARATUS

Although the spin-echo apparatus used in making the traces shown in Figs. 4–8 and in testing the theory generally was of fairly conventional design, a few words will be said concerning the characteristics and performance of this particular instrument. The apparatus employed a coherent source of 30 megacycles, consisting of a free-running crystal oscillator whose output was keyed after it had passed through several doubler and buffer stages. The rf pulses had a rise time of 10 microseconds and produced a maximum field, $2H_1$ at the sample, of about 10 gauss. Both rf intensity and pulse length were variable. The probe used crossed coils.[10] The proton sample, about 25 cm^3 in volume, was placed in a permanent magnet whose pole faces were shimmed so that the field inhomogeneity across the sample was approximately 50 gauss, corresponding to a "band width"

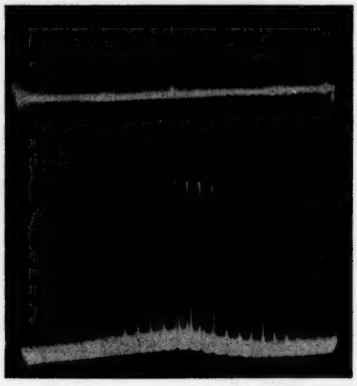

FIG. 7. Double pulses (above) and echoes preceding and following pulses (below). The receiver amplifier limits the amplitude of the stronger echoes. The double pulses were repeated in a time short compared to T_2.

[10] Bloch, Hansen, and Packard, Phys. Rev. 70, 474, (1946).

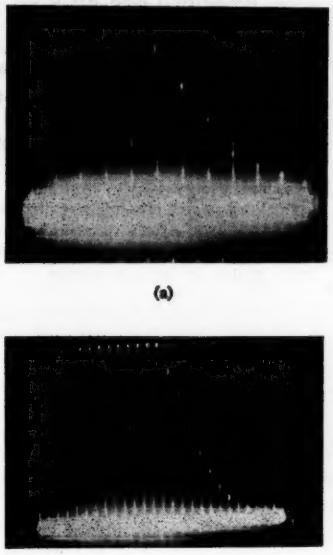

(a)

(b)

FIG. 8. Echoes at the end of a train of single pulses, indicated by the pips that follow an exponentially decaying curve. The repetition times for the pulses are 3 milliseconds (above) and 1 millisecond (below).

of 200 kc. The distribution of nuclei in this field was such that the polarization $g(\Delta\omega)$ was approximately constant over more than half of the total bandwidth. The bandwidths of the transmitter and receiver circuits were likewise about 200 kc. Although the direct coupling between transmitter and receiver in a crossed-coil probe tends to be frequency dependent, it was found possible to reduce the over-all coupling to the point where the rf pulses would not overload the receiver amplifiers.

In a magnetic field as inhomogeneous as the one used here, the effects of self-diffusion severely limit the time in which one can do echo and pulse-train experiments. Experiments involving only a few pulses can be done in ten milliseconds or less; for this a fairly viscous material, such as glycerine or SAE-30 motor oil, is useful. Experiments involving repeated pulses require longer times; for these the best sample material is a relatively nonviscous liquid in a fairly viscous emulsion. Most of the photographs shown here were taken with a sample of water mixed in lanolin, of the type used in cosmetic-cream preparations.[11] Even so, the lifetime for two-pulse echoes before disappearance under self-diffusion effects was only about 60 milliseconds.

[11] S. Fernbach and W. G. Proctor, J. Appl. Phys. 26, 170 (1955).

Energy Loss by 8.86-Mev Deuterons and 4.43-Mev Protons*

J. E. Brolley, Jr., and F. L. Ribe
University of California, Los Alamos Scientific Laboratory, Los Alamos, New Mexico
(Received January 20, 1955)

Using deuterons of average energy 8.86 Mev, the stopping powers relative to air have been measured for the following gases: H_2, He, N_2, O_2, Ne, A, Kr, Xe, CH_4, and CO_2. Absolute stopping cross sections were measured, using 4.43-Mev protons (of equal velocity) for H_2, air, and Kr, and the deuteron results were normalized to give absolute stopping cross sections for all of the gases. Comparison is made with the theoretical results of Aron *et al.*, Walske, and Lindhard and Scharff.

It was found that the NaI(Tl) crystal exhibited a nonlinearity in its response curve of light output *versus* proton or deuteron energy.

INTRODUCTION

In recent years many measurements have been made of the energy loss by fast ions in both solids and gases with the result that dE/dx is well known as a function of proton energy in the low-energy region up to about two Mev[1] and at high energies—18 Mev[2] and 350 Mev.[3] There remains a significant gap in the measurements in the intermediate region where one is particularly concerned with the stopping powers of counter gases and absorbers for reaction products from nuclear disintegration experiments. Here calculations[4] of the stopping cross sections provide the only data on gases.

Aside from their use for practical purposes, further measurements in the intermediate energy region are of physical interest in testing the theories used in attempting to understand the energy-loss process. A recent interesting example of such a theory is that of Lindhard and Scharff[5] in which an attempt is made, on the basis of the statistical model of the atom, to arrive at a universal function which relates the stopping power and energy for all materials and particle energies.

In the present paper, we shall report stopping cross-section measurements at a single ion (deuteron or proton) velocity, corresponding to a proton energy of 4.43 Mev, for the gases H_2, He, N_2, air, O_2, Ne, A, Kr, Xe, CH_4, and CO_2.

APPARATUS AND EXPERIMENTAL ARRANGEMENT

Deuteron Measurements

In the first part of the experiment, the relative stopping powers of the gases were measured by observing the relative amounts of the gases required to give the same energy loss to deuterons of 10-Mev incident energy from the Los Alamos 42-inch cyclotron. The energy-sensitive detector used was a NaI(Tl) crystal whose light response is known to be approximately linear[6,7] in energy for intermediate-energy protons and deuterons. For the deuterons used in this experiment the resolution of the pulse-height groups was approximately 3.3 percent.

A schematic diagram of the apparatus is shown in Fig. 1. The external, electrostatically deflected beam of the cyclotron was brought through a beam tube and scattered through an angle of 90 degrees from a 1.25-mg/cm² gold foil lying in a plane at 45 degrees to the unscattered beam direction. The scattered beam entered a brass absorption cell through a 3.01-mg/cm² Dural

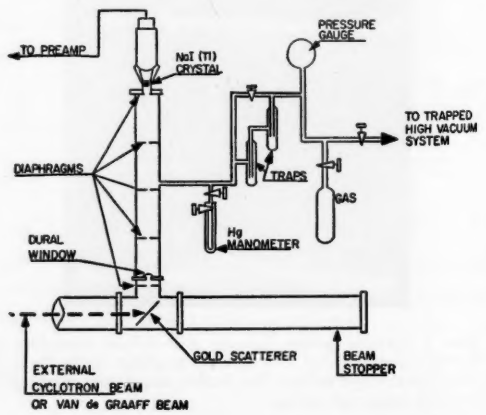

FIG. 1. Schematic diagram of apparatus for measuring stopping cross sections of gases.

* Work done under the auspices of the U. S. Atomic Energy Commission.

[1] Reviews of the low-energy data are given by S. K. Allison and S. D. Warshaw, Revs. Modern Phys. **25**, 779 (1953) and by Ronald Fuchs and W. Whaling of the California Institute of Technology in their unpublished report on stopping cross sections.

[2] D. G. Sachs and J. R. Richardson, Phys. Rev. **83**, 834 (1951); **89**, 1163 (1953).

[3] C. J. Bakker and E. Segrè, Phys. Rev. **81**, 489 (1951); R. Mather and E. Segrè, Phys. Rev. **84**, 191 (1951).

[4] Aron, Hoffman, and Williams, Atomic Energy Commission Report AECU-663 (UCRL-121), 1949 (unpublished). W. A. Aron, University of California Radiation Laboratory Report UCRL-1325, 1951 (unpublished). A more extensive compendium including the earlier work of Aron, Hoffman, and Williams is provided by M. Rich and R. Madey, University of California Radiation Laboratory Report UCRL-2301, 1954 (unpublished).

[5] J. Lindhard and M. Scharff, Kgl. Danske Videnskab. Selskab, Mat.-fys. Medd. **27**, No. 15 (1953).

[6] Taylor, Remley, Jentschke, and Kruger, Phys. Rev. **83**, 169 (1951); Taylor, Jentschke, Remley, Eby, and Kruger, Phys. Rev. **84**, 1034 (1951); F. S. Eby and W. K. Jentschke, Phys. Rev. **96**, 911 (1954); also private communication from Dr. Jentschke.

[7] J. G. Likely and W. Franzen, Phys. Rev. **87**, 666 (1952).

window and was collimated by three antiscattering diaphragms before entering the defining aperture in front of the crystal. The limiting aperture has a diameter of 1.016 cm. The total distance in which energy loss in the absorbing gas could take place between the entrance window and the surface of the scintillator was 90.43 cm. The scintillation crystal had a diameter of 1.25 cm and a thickness of 0.25 cm.

Attached to the absorption cell was a glass filling system followed by a high-vacuum pumping system with a liquid-nitrogen-trapped oil diffusion pump which produced a vacuum of 10^{-5} mm Hg in the absence of absorbing gas. Two glass traps were provided for the gas fillings: one of $Mg(ClO_4)_2$ for removing moisture, and the other of dry ice and acetone. Air could be drawn into the system through a P_2O_5 drying tube, followed by an "ascerite" trap for removing CO_2. All of the compressed gases with the exception of O_2 and CO_2 were of "refined" or "research" grade. Since the gases were stored at considerably more than an atmosphere of pressure, contamination due to air leakage was negligible. Two samples of Xe were used from tanks obtained on dates several years apart, one newly opened and the other previously used for counter fillings and purified by pumping the condensed Xe and subsequently circulating the gas through a hot-calcium purifier. No difference in measured stopping power of the two xenon samples was observed within experimental error.

All of the gas samples were checked for impurities by mass-spectrometric analysis. In this analysis measurements were made at each end of the mass scale corresponding to hydrogen and xenon and continuously between masses 14 and 88 for each gas. No gaseous impurity with molecular weight between one and 131 would have escaped detection. The impurities which occurred in more than "trace" (0.001 percent) amounts are listed for each gas sample in Table I. The last column gives the numerical factors which were applied to the stopping-cross-section results in order to correct for the impurities. The water-vapor impurities were disregarded since they were trapped out in the experiment.

Gas pressures in the absorption cell and filling system were read by means of Wallace and Tiernan absolute pressure gauges which were calibrated by means of an accurate mercury vacuum manometer to within 0.2 percent. The gas temperature was measured by means of a mercury thermometer strapped to the outside of the absorption cell.

The output pulses of the scintillator photomultiplier were amplified by a Los Alamos Model 250 preamplifier and amplifier and fed to the vertical plates of a Tektronix Model 513*D* oscilloscope through its vertical amplifier. Care was taken not to approach saturation of either amplifier. The amplified scintillator pulses were presented on the cathode-ray tube and photographed by means of a camera using 4 in.×5 in. cut film. The linearity of the electronics and optical system was carefully checked by feeding attenuated pulses from a Los Alamos Model 500 mercury-relay pulser through the amplifier system at various times during the runs and photographing the resulting pulses. The model 250 amplifier system was linear to within 0.1 percent, while the oscilloscope amplifier showed a nonlinearity of approximately three percent for which a calibration correction was made.

TABLE I. Measured amounts of impurities in the tank gases used in the stopping-cross-section measurements and correction factors applied to the experimental values to give results corresponding to pure-gas conditions.

Gas	Molecular percent impurity	Correction factor
H_2	0.07 H_2O, 0.19 N_2	0.992
He	0.07 N_2, 0.03 O_2	0.995
N_2	0.06 H_2O	1.000
O_2	0.33 H_2O, 0.61 N_2, 0.28 A	1.001
Ne	0.05 H_2O, 0.11 N_2, 0.02 O_2	0.999
A	0.08 H_2O, 0.31 N_2	1.000
Kr	None	1.000
Xe	0.06 N_2	1.000
CH_4	0.28 N_2, 0.01 O_2, 0.14 C_2H_6	0.999
CO_2	0.11 H_2O, 0.77 N_2, 0.16 O_2	1.003

The experimental procedure consisted of photographing groups of deuteron pulses with gas in the absorption cell and with the cell evacuated to a pressure of 10^{-4} mm Hg. For each exposure about 1000 pulses were used. Preliminary runs were made to determine approximately how much gas was required to provide a 25 percent drop in pulse height, and then final data were taken in a continuous run using a 25 percent fractional drop in pulse height, during which the cyclotron's magnetic field, frequency, and deflection voltage were held as nearly constant as possible. During the measurements the vacuum pulse groups were frequently compared visually with a group from the pulser, and a relative comparison was made of the vacuum pulse heights on the films. The extreme relative variation of the cyclotron energy was thus found to be 0.6 percent throughout the final run.

The energy of the scattered external beam was measured by exposing a 200-micron Ilford C-2 nuclear plate in place of the scintillator with the absorption cell evacuated. We are indebted to Dr. Louis Rosen and his nuclear plate group for making the range analysis and providing us with the result that the deuteron energy was 10.05±0.13 Mev.

Proton Measurements

The deuteron measurements described above provide accurate determinations of the stopping powers of the various gases relative to air, since approximately the same fractional drop in pulse height was used in each case. If one assumes perfect linearity of the light response of the NaI(Tl) crystal to deuteron energy, one can determine the energy loss ΔE in terms of the fractional change $\Delta h/h_0$ in pulse height as $\Delta E = E_0$

$\times(\Delta h/h_0)$, where h_0 is the pulse height corresponding to incident deuteron energy E_0. One can then obtain the absolute rate of energy loss $\Delta E/\Delta x$. However, as will be discussed later, it appears that NaI(Tl) is slightly nonlinear in its light response to protons and deuterons, and this possibility made it desirable to determine the absolute scale for the stopping powers separately.

In order to make absolute measurements of $\Delta E/\Delta x$ a separate experiment was carried out with protons of the same incident velocity as that of the deuterons for the three gases H_2, air, and Kr. Protons of accurately known energy were obtained from the Los Alamos large van de Graaff accelerator, and the experiment was performed as in the deuteron case with the following exception: the lower-energy pulse-height group corresponding to partial absorption of the proton energy in the gas was "bracketed" by means of groups corresponding to protons of known energy from the van de Graaff with the absorption cell evacuated. The van de Graaff energies were very accurately determined by means of a 90-degree magnet whose field was measured with a radio-frequency proton-moment magnetometer. Interpolation in the small interval between the known bracketing energies yielded the energy of the proton group after passing through the gas absorption cell, independent of any slight nonlinearity of the NaI(Tl) crystal response.

In carrying out this part of the experiment, protons of incident energy 5.029 Mev were used. In order to obtain protons of this energy after energy loss in the gold foil, scattering through 90 degrees in the gold foil, and energy loss in the dural window, the van de Graaff voltage was set at 5.309 Mev. The gas pressures used were one-half those used in the deuteron experiment in order to give the same fractional energy loss and mean velocity in the gases.

DATA AND RESULTS

The data were obtained in the form of photographs of groups of pulses which were delay-line clipped to provide almost flat tops approximately one microsecond in duration. A base line was either exposed or drawn on each photograph. In order to make a quantitative analysis of the pulse heights, the photographic negatives were scanned with a Leeds and Northrup microdensitometer, the Brown recorder of which provided a graph of photographic density as a function of displacement from the base line of the negative. A sample microdensitometer trace corresponding to scanning in one direction is shown in Fig. 2. In each case the negative was scanned in both directions, giving mirror-image traces, in order that small instrumental errors should cancel. The background seen in this graph was caused by neutrons and γ rays produced in various parts of the cyclotron external-beam apparatus. Very low-energy background pulses were excluded by the setting of the sweep threshold of the oscilloscope. In scanning, the light spot (of negligible dimensions) moved in the direction perpendicular to the base line and to the flat tops of the scintillator pulse traces.

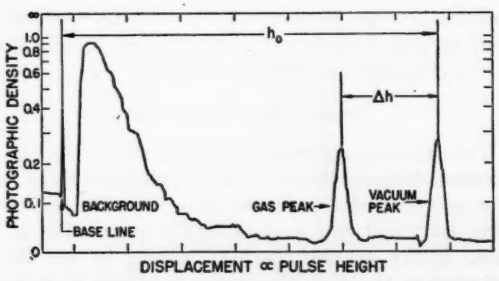

FIG. 2. Microdensitometer trace obtained by scanning the photographic negative of scintillator pulses appearing on the oscilloscope.

The centers of the pulse-height groups corresponding to the most probable pulse-height values were obtained in each case as the locations of the intersections of lines drawn along the sides of the peaks of the densitometer traces. For each gas there were at least two traces corresponding to runs at the same pressure, and it was observed that one could determine the fractional drop in pulse height with an average consistency of about 1.4 percent.

In the case of the deuteron experiment, the fractional decreases in pulse height $\Delta h/h_0$ were not precisely the same but differed by small amounts for different gases. The relative stopping powers were then proportional to $(1/p)\Delta h/h_0$, where p is the absolute pressure of gas in the absorption cell. Values of p, $\Delta h/h_0$, and the stopping power relative to air for the various gases are given in the third, fourth, and fifth columns of Table II.

The results of the proton measurements are given in the sixth, seventh, and eighth columns of Table II. Here the absolute energy loss ΔE was measured, rather than $\Delta h/h_0$. The stopping powers of H_2 and Kr relative to air are seen to agree with those obtained in the deuteron measurements; the value for H_2 is more accurate however, because multiple scattering decreased the intensity of the proton pulse-height group in the case of krypton to a greater extent and made its location somewhat more uncertain.

The ninth column gives the proton energy at which the measurement applies. In the cases of H_2 and air, this is the energy directly measured in the proton experiment, while in the other cases the energies are taken in the ratios of the mean pulse heights $h_0(1-\Delta h/2h_0)$ to that of air. An exception is the case of Kr where the energies found by the two methods were averaged to give the value listed. It can be shown[8] that the error in taking $E_0(1-\Delta E/2E_0)$ as the energy value at which $\Delta E/\Delta x$ is equal to dE/dx is negligible. It is seen that these mean energies are nearly the same for all of the gases, the small variations arising from the fact that

[8] Reference 1, p. 791.

TABLE II. Data and results of stopping cross-section measurements. No correction has been made for impurities in the tank gases.

Gas or element	Atomic number	Pressure, p (mm Hg, 25°C)	$\Delta h/h_0$	Stopping power rel. to air	Pressure, p (mm Hg, 25°C)	ΔE (Mev)	Stopping power rel. to air	Equiv. proton energy (Mev)	Absolute stopping cross section dE/dx (ev-cm²×10⁻¹⁵)
		Deuteron measurements			Proton measurements				
1	2	3	4	5	6	7	8	9	10
½ H_2	1	1175	0.251	0.185±0.003	585.4	1.163	0.186±0.003	4.44	0.338±0.007
He	2	1336	0.248	0.321±0.005				4.45	0.585±0.013
½ N_2	7	233.7	0.261	0.966±0.014				4.42	1.76 ±0.04
½ air		225.8	0.261	1.000	112.9	1.206	1.000	4.42	1.82 ±0.04
½ O_2	8	214.0	0.269	1.088±0.016				4.40	1.98 ±0.04
Ne	10	355.0	0.258	1.258±0.019				4.43	2.29 ±0.05
A	18	219.2	0.258	2.042±0.031				4.43	3.72 ±0.08
Kr	36	138.4	0.271	3.393±0.051	70.0	1.235	3.302±0.082	4.41	6.10 ±0.15
Xe	54	97.6	0.249	4.425±0.075				4.44	8.06 ±0.18
CH_4		285.4	0.263	1.598±0.024				4.43	2.91 ±0.06
CO_2		143.9	0.252	3.037±0.046				4.43	5.53 ±0.12

the pressures were not set for identical energy absorption in all cases.

The last column of Table II gives the absolute stopping cross sections. In the cases of H_2 and air, this is the value directly measured in the proton experiment. The values for the other cases are obtained by multiplying the relative stopping powers of column 5 by the absolute stopping cross section for air. The value for Kr is the average of those obtained by the two methods. None of the results of Table II have been corrected for impurities.

DISCUSSION OF RESULTS

In the absence of other experimental results on gases in the energy range investigated here, a direct comparison of our dE/dx values can be made only with calculated values. In Table III, we present a comparison of our results, corrected for impurities according to Table I, with the calculations of Aron, Hoffman, and Williams[4] and Walske.[9] The stopping cross section of carbon was obtained from those of CH_4, CO_2, H_2, and O_2 by assuming the applicability of Bragg's rule of additivity of stopping powers:

$$CH_4-2H_2=2.91-1.34=1.57,$$
$$CO_2-O_2=5.55-3.96=1.59.$$

The average value for C is 1.58.

In the calculations of UCRL-121,[4] the ionization potential I in the Bethe-Bloch formula was obtained from the Bloch relation, $I=kZ$, using $k=11.5$ ev. For elements in the atomic-number range from carbon to aluminum the K-shell correction, C_K, given by Livingston and Bethe[10] was used. For heavier elements K-, L-, and M-shell corrections were taken somewhat crudely into account by neglecting the stopping power of a shell when the ion energy fell below four times the "critical energy" $(M/m)A_{K,L,M}$. Here M denotes the ion mass, m the electron mass, and $A_{K,L,M}$ the excitation potential of the shell in question. For H and He the theoretical values of Williams[11] for I were used. In the calculations of UCRL-1325,[4] Aron computed values of I to fit the experimental data[3] of Bakker and Segrè and Mather and Segrè, where applicable, preferring the latter for those elements measured by both.

Walske has calculated the L-shell correction C_L, using hydrogen-like wave functions, analogous to his previously calculated K-shell correction C_K. He obtains the average ionization potential I from the measurements of Bakker and Segrè, using their values of the I/Z, normalized at aluminum to the value corresponding to $I=160$ ev. For hydrogen he uses the value $I=16.2$ ev based on Mano's experimental determination.[12]

In Table III, it is seen that the agreement with both sets of calculated values is generally good. An exception is Walske's value for Xe. He estimates however, that the M-shell correction in this case would decrease his stopping cross section by about four percent. This would bring it into agreement with the measured value to within experimental error.

Another theory with which to compare the present results is that of Lindhard and Scharff.[5] By plotting

TABLE III. Comparison of experimentally determined stopping cross sections with the calculated values of Aron *et al.*[a] and Walske.[b] The experimental values have been corrected for impurities in the tank gases.

Element	Experimental dE/dx (ev-cm²×10⁻¹⁵)	UCRL-121[a]	UCRL-1325[a]	Walske[b]
H	0.335±0.007	0.331	0.331	0.341
He	0.582±0.013	0.601	0.601	
C	1.58 ±0.03	1.62	1.59	1.53
N	1.76 ±0.04	1.95		
Air	1.82 ±0.04			
O	1.98 ±0.04	2.09		
Ne	2.29 ±0.05			2.36
A	3.72 ±0.08	3.89	3.94	3.81
Kr	6.10 ±0.15			6.03
Xe	8.06 ±0.18			8.57

[a] See reference 4.
[b] See reference 9.

[9] M. C. Walske, Phys. Rev. **88**, 1283 (1952); also private communication.
[10] M. S. Livingston and H. A. Bethe, Revs. Modern Phys. **9**, 265 (1937).
[11] E. J. Williams, Proc. Cambridge Phil. Soc. **33**, 179 (1937).
[12] Georges Mano, J. phys. radium **5**, 628 (1934).

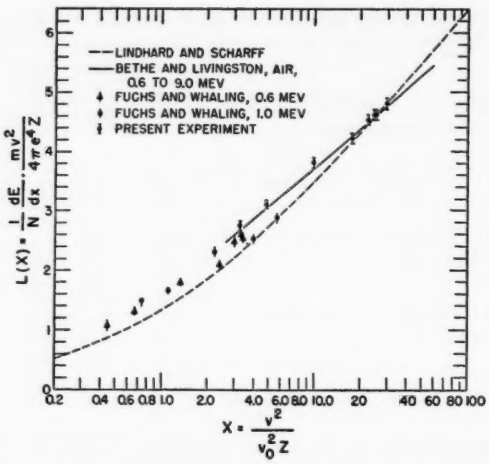
—LINDHARD AND SCHARFF
—BETHE AND LIVINGSTON, AIR, 0.6 TO 9.0 MEV
FUCHS AND WHALING, 0.6 MEV
FUCHS AND WHALING, 1.0 MEV
PRESENT EXPERIMENT
$L(X) = \frac{1}{N}\frac{dE}{dx}\cdot\frac{mv^2}{4\pi e^4 Z}$
$X = \frac{v^2}{v_0^2 Z}$
0.2 0.4 0.6 0.8 1.0 2.0 4.0 6.0 8.0 10.0 20 40 60 80 100

FIG. 3. Plot of stopping cross-section data for protons in gases using the functions $L(dE/dx)$ and $X(E)$. The dashed curve shows the function found by Lindhard and Scharff for protons in solids.

the quantity

$$L(X)=(4\pi e^4 Z/mv^2)^{-1}dE/dx$$

against the quantity

$$X=v^2/Zv_0^2$$

they found that a universal curve could be obtained which approximately brought all of the data for various atomic numbers and proton energies together in a single continuous function. Here dE/dx is the atomic stopping cross section, v the ion velocity, and $v_0=e^2/\hbar$.

In order to compare the curve of Lindhard and Scharff with the present data and other data on the stopping of gases, we have determined the values of X and $L(X)$ both for our results and for the results at proton energies 0.6 and 1.0 Mev for various gases as given by the curves in the compilation of Fuchs and Whaling.[1] These results are plotted in Fig. 3. The points corresponding to the present results run in order of increasing X from Xe to C and those corresponding to the compilation of Fuchs and Whaling from Xe to N. We have also replotted the calculated stopping cross-section curve for air of Livingston and Bethe[10] for proton energies between 0.6 and 9.0 Mev.

The experimental points for gases lie approximately on a continuous curve, with a few exceptions. However a curve fitting the gas data would clearly not coincide with that obtained by Lindhard and Scharff for the data on solids. It is interesting to note that the points corresponding to the present results lie approximately on the replotted air curve of Livingston and Bethe.

RESPONSE OF SODIUM IODIDE TO PROTONS AND DEUTERONS

The measurements of the Illinois group[6] of the response of NaI(Tl) to protons, H_2^+ ions, and deuterons showed that the response curves of light output *versus* ion energy are straight lines in the energy region from one to 11 Mev. In addition, it was shown that for alpha particles saturation and other effects result in a response curve having a knee at about 8 Mev convex downward but tending asymptotically to a straight line, so that for high energies one may consider the curve as a straight line having a negative intercept on the axis of ordinates. In the cases of the singly-charged ions the accuracy of the data (primarily the energy determinations) left some doubt whether or not the straight lines pass through the origin. The accuracy of the data of Likely and Franzen[7] on the response curve for protons from five to 18 Mev likewise leaves some doubt whether or not the high-energy response curve effectively has a small nonzero intercept, due perhaps to a saturation knee at low proton energies.

It was with the possibility of such nonlinearity in mind that the stopping-power measurements for deuterons were performed with approximately the same energy change ΔE in order that the relative stopping-power determinations would not be affected by crystal response. If one formally calculates the energy change in this part of the experiment as $E_0(\Delta h/h_0)$, one should arrive at absolute stopping cross sections which are too great by a factor $(1-\delta h/h_0)^{-1}$, where δh is the magnitude of a negative intercept of the response curve (see Fig. 4). Such calculations were made for the cases of H_2, air, and Kr and the results compared with the stopping cross sections measured absolutely for protons in the manner described earlier, where ΔE was measured directly, independent of crystal response. The resulting values of $\delta h/h_0$ [for deuterons in NaI(Tl)] were 8.2, 8.5, and 11.6 percent respectively, with a weighted average value of 8.5 ± 1.3 percent.

Having thus indirectly measured the amount of nonlinearity of response for deuterons for the crystal used in this experiment, it was interesting to investigate the response curve for protons also. This was done

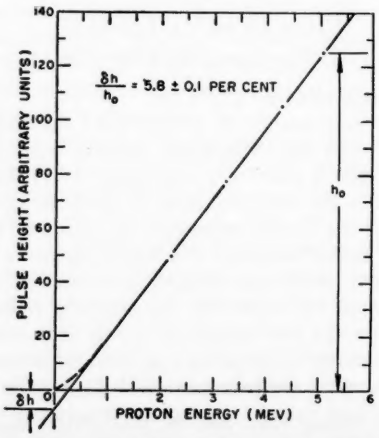

FIG. 4. Response curve of the NaI(Tl) scintillator pulse height (proportional to light output) *versus* proton energy.

directly by setting the van de Graaff energy at known values and measuring scintillator pulse height as a function of proton energy, correcting for 90-degree recoil, energy loss in the gold scatterer, and energy loss in the Dural entrance window. The results are shown in the graph of Fig. 4. It is seen that the proton response curve has an effective negative intercept, presumably due to a nonlinearity in the form of a knee as indicated by the dashed portion of the curve. The value of $\delta h/h_0$ for protons is 5.8 ± 0.1 percent, where h_0 is the pulse height corresponding to a proton energy of 5.03 Mev.

It may be noted that a nonscintillating layer in which energy is lost by the protons or deuterons in entering the crystal would cause the measured response curves to have effective negative intercepts. It should be mentioned that the surface of the crystal on which the ions impinged was cleaved in a dry box and consisted of a single cleavage plane. Transfer to the crystal housing was made in the dry box, and the crystal thereafter was kept sealed under vacuum or in contact with the dry gases used in the experiment. No observable clouding of the glass-like crystal surface occurred during the experiment. The large single crystal from which the disk used in this experiment was cleaved was obtained from the Harshaw Chemical Company and had a thallium activation of 0.2 ± 0.05 percent in content.

The following argument also indicates that the negative intercepts are not due to a nonscintillating surface layer: Since the protons and deuterons at the values of h_0 in question had equal velocities, their energy losses in the layer were the same. The deuterons had twice the energy, and hence approximately twice the pulse height, of the protons. Therefore, if the negative intercepts were due solely to surface energy loss, the quantity $\delta h/h_0$ should have had approximately one-half the value for deuterons that it had for protons. This is not the case since the value eight percent for deuteron is larger than the value six percent for protons.

In this connection the results of der Mateosion and Yuan[13] are of interest. They showed that for Po^{210} alpha particles the surface effect for chemically cleaned NaI crystals was at most five percent.

The present measurements are not inconsistent with those of Allison and Casson[14] who found that the response of NaI(Tl) to protons with energies between 50 and 400 kev is a straight line passing through the origin. A portion of the response curve like the one shown dashed in Fig. 4 would probably be indistinguishable from the straight line determined by their measurements.

We are pleased to acknowledge assistance received in this experiment from Dr. R. L. Henkel who operated the large van de Graaff and assisted in setting up the equipment at that installation; Miss Patricia Fain who performed the mass-spectrometric analysis of our gas samples; Mr. Berlyn Brixner who kindly furnished the plate camera; Mr. Grenfell Boicourt who constructed much of the equipment; and Captain Ralph Speece who instructed us in the use of the microdensitometer.

[13] E. der Mateosian and Luke C. L. Yuan, Phys. Rev. **90**, 868 (1953).
[14] S. K. Allison and H. Casson, Phys. Rev. **90**, 880 (1953).

Special-Relativistic Derivation of Generally Covariant Gravitation Theory*

ROBERT H. KRAICHNAN
Columbia University, New York, New York

(Received November 19, 1954; revised manuscript received February 7, 1955)

The Newtonian gravitation theory is generalized to an inhomogeneous wave equation for a tensor gravitational potential in Euclidean space-time by invoking the special relativity postulates of Lorentz invariance and equivalence of mass and energy. Under the assumption of Lagrangian derivability, this is found to lead uniquely to the generally covariant field theories (including the general relativity theory) augmented by four auxiliary conditions. Appendices treat the general definition of the energy tensor, and an empirically disqualified special relativistic scalar generalization of the Newtonian theory.

INTRODUCTION

THE general theory of relativity has long occupied a position of isolation with respect to the rest of contemporary fundamental physics. The special theory of relativity has been intimately and indispensibly amalgamated with quantum mechanics in evolving current theoretical representations of elementary processes, but the general theory, despite the elegance of its concepts, has not exhibited any real relation whatever to quantum physics. The attempts which have been made to connect general relativity and quantum mechanics have been directed largely at showing to what degree the two disciplines may be *compatible* rather than seeking a basic interdependence. Thus formalisms have been developed in which the fundamental equations of quantum theory are written in generally covariant form, and, on the other hand, both approximate and exact methods for subjecting the Einstein metric field to quantization have been proposed.

There seems a distinct possibility that the wide gap between general relativity theory and quantum mechanics is in part due to a difference in language. In the relativity theory the paths of particles or light rays are defined by invariant geometric properties and the coordinate representation of the paths is secondary and, except in regions where the field is asymptotically Euclidean, ambiguous. The formalism of quantum mechanics, on the other hand, is based on a classical Hamiltonian theory in which fields, potentials, and trajectories have a perfectly explicit coordinate representation, apart from Lorentz transformation. As a prerequisite to making a detailed conceptual translation from one discipline to the other, it would seem necessary to decide what coordinate conditions, so to speak, are implicit in the quantum-mechanical equations of motion at small distances, and there is no clue as to how to do this in the present form of the relativity theory. The question is not resolved by writing the quantum-mechanical wave equations and commutation relations in generally covariant form, for this procedure has no more *a priori* justification than naively rewriting the field equations of pre-Einsteinian gravitation theory in generally covariant form. The latter is easy to do but it does not lead in itself to the correct results, since the essential characteristic of the Einstein theory is not the formal covariance of the equations to coordinate transformation but the relationship of the metric tensor and the gravitational potential.

The present paper is intended as a preliminary step in exploring one possible relationship of the generally covariant theories to the immediate classical basis of quantum theory, and to the quantum formalism itself. It tries to show that there exists a physically logical basis for the generally covariant theories without an *a priori* conceptual identification of the field tensor with the metric of space. The principle of equivalence and the associated geometrical postulates of general relativity are abandoned as a foundation, and, instead, a starting point is taken which employs concepts closer in some respects to those which have been found pertinent to microscopic physics. The Newtonian gravitation theory is generalized in accordance with the special relativity postulates of Lorentz invariance and the equivalence of mass and energy. This amounts to postulating an ordinary Euclidean second-order wave equation for a tensor potential $f_{\mu\lambda}$, in which the source term, however, is the total Lagrangian derived energy-momentum tensor as defined in special relativistic field theories. It is then found that the requirement that such a wave equation be consistent with the Lagrangian field equations leads to a set of four auxiliary conditions and a unique class of Lagrangians which are the Riemannian invariants built on a *single* tensor function $g_{\mu\lambda}$, which is in turn a function of $f_{\mu\lambda}$ and the Euclidean metric tensor $\eta_{\mu\lambda}$. With an appropriate choice of the Riemannian invariant, $g_{\mu\lambda}$ may be identified with the Einstein field tensor. The four auxiliary conditions are not unique, and depend on an arbitrary assignment of covariancy or contravariancy, and of tensor density weight, to $f_{\mu\lambda}$.

In a paper to follow, it is suggested that the generally covariant theories without auxiliary conditions, including the customary Einstein gravitation theory, may possibly allow such a wealth of solutions, in addition to familiar ones, as would permit a basic reinterpretation of the generally covariant theories as a means of kinematical representation comparable in important respects to the classical Hamilton-Jacobi formalism.

* Publication of this paper was assisted by the Ernest Kempton Adams Fund.

THE GRAVITATIONAL LAGRANGIAN

In the Newtonian theory of attraction, the gravitational potential V obeys the equation

$$\nabla^2 V-\lambda\rho=0, \tag{1}$$

where ρ is the density of matter and λ is proportional to the constant of gravitation. We now seek to modify (1) in accordance with the special relativity postulates of Lorentz invariance and equivalence of mass and energy. The obvious Lorentz-invariant generalizations of (1) are the scalar equation

$$\Box^2\phi-\lambda T_{\mu\lambda}\eta^{\mu\lambda}=0, \tag{2}$$

and the tensor equation

$$\Box^2 f_{\mu\lambda}-\lambda T_{\mu\lambda}=0, \tag{3}$$

where ϕ and $f_{\mu\lambda}$ are a scalar and tensor field respectively, $T_{\mu\lambda}$ is the energy-momentum tensor, $\eta_{\mu\lambda}$ is the (Euclidean) metric tensor and $\Box^2$ is the contracted second covariant derivative with respect to $\eta_{\mu\lambda}$. In accordance with the postulate of the equivalence of mass and energy, we now require that $T_{\mu\lambda}$ represent the *total* energy-momentum tensor, *including the contribution associated with the ϕ field or $f_{\mu\lambda}$-field.*[1]

The theory of the scalar equation is treated in Appendix II. This equation does not lead to astronomically correct relativistic corrections to the Newtonian gravitation law. We shall consider here the tensor equation (3). If the "matter variables" are represented formally by u (we do not specify here the number or nature of these variables except to require that they have well-defined covariance properties under coordinate transformation), an invariant Lagrangian leading to the field equations (3) will have the general form

$$L=\int \mathfrak{L}(f,u,\eta)d^4x, \tag{4}$$

where f symbolizes the tensor $f_{\mu\lambda}$ and η the metric tensor $\eta_{\mu\lambda}$. $\mathfrak{L}$ will transform under coordinate transformation as a tensor density of weight $+1$. The field equations for $f_{\mu\lambda}$ resulting from the usual Lagrangian variational procedure are then

$$\delta L/\delta f_{\mu\lambda}=0, \tag{5}$$

and the contravariant energy-momentum tensor-density corresponding to this Lagrangian is

$$\mathfrak{T}^{\mu\lambda}=\delta L/\delta\eta_{\mu\lambda}. \tag{6}$$

When all the field equations for $f_{\mu\lambda}$ and u are satisfied, $\mathfrak{T}^{\mu\lambda}$ obeys the conservation equations[2]

$$\mathfrak{T}^{\mu\lambda}{}_{|\lambda}=0, \tag{7}$$

where $|\lambda$ represents covariant differentiation with respect to $\eta_{\mu\lambda}$.

Multiplying (3) through by $\eta^{\sigma\mu}\eta^{\lambda\tau}|\eta|^{\frac{1}{2}}$ where $|\eta|=\det|\eta_{\mu\lambda}|$, the contravariant density form of the $f_{\mu\lambda}$ equation is

$$\Box^2\mathfrak{f}^{\sigma\tau}-\lambda\mathfrak{T}^{\sigma\tau}=0, \tag{8}$$

where $\mathfrak{f}^{\sigma\tau}$ denotes $\eta^{\sigma\mu}\eta^{\lambda\tau}|\eta|^{\frac{1}{2}}f_{\mu\lambda}$ and we have commuted $\Box^2$ and $\eta^{\alpha\beta}$ since the covariant derivative of a tensor with respect to itself vanishes. In view of (7), any field $\mathfrak{f}^{\sigma\tau}$ which satisfies (8) and obeys customary boundary conditions[3] must also satisfy

$$\mathfrak{f}^{\sigma\tau}{}_{|\tau}=0. \tag{9}$$

It follows that (8) is equivalent to (9) plus the set of equations

$$\mathfrak{D}^{\sigma\tau}(f)-\lambda\mathfrak{T}^{\sigma\tau}=0, \tag{10}$$

where

$$\mathfrak{D}^{\sigma\tau}(f)=|\eta|^{\frac{1}{2}}D^{\sigma\tau}(f)=|\eta|^{\frac{1}{2}}(\Box^2 f^{\sigma\tau}-f^{\sigma\alpha}{}_{|\alpha\beta}\eta^{\beta\tau}-f^{\alpha\tau}{}_{|\alpha\beta}\eta^{\sigma\beta}+f^{\alpha\beta}{}_{|\alpha\beta}\eta^{\sigma\tau}) \tag{11}$$

obeys $[\mathfrak{D}^{\sigma\tau}(f)]_{|\tau}=0$ identically.

Now instead of seeking solutions of the implicit equations (3) directly, we seek the class of Lagrangians leading to the less restrictive field equations (10). The solutions of these equations which obey the auxiliary conditions (9) will then satisfy (3). The requirement that (10) be the Lagrange-Euler equations resulting from variation of the Lagrangian L with respect to $f_{\mu\lambda}$ may be written according to (5) and (6) as

$$\delta L/\delta f_{\sigma\tau}=\mathfrak{D}^{\sigma\tau}(f)-\lambda(\delta L/\delta\eta_{\sigma\tau}). \tag{12}$$

Let $L=L_1+L_2$ where

$$L_2=-(2/\lambda)\int f_{\mu\lambda}\mathfrak{R}^{\mu\lambda}(\eta)d^4x, \tag{13}$$

and $\mathfrak{R}^{\mu\lambda}(\eta)$ is the contracted Riemann-Christoffel tensor density derived from $\eta_{\mu\lambda}$ as fundamental tensor. Since $\mathfrak{R}^{\mu\lambda}(\eta)$ vanishes for the Euclidean $\eta_{\mu\lambda}$, $\delta L_2/\delta f_{\mu\lambda}=0$. It is easily verified that for infinitesimal variations of $\eta_{\sigma\tau}$ from the Euclidean values,

$$\lambda(\delta L_2/\delta\eta_{\sigma\tau})=\mathfrak{D}^{\sigma\tau}(f), \tag{14}$$

so that (12) is equivalent to the following equation for L_1:

$$\delta L_1/\delta f_{\sigma\tau}=-\lambda(\delta L_1/\delta\eta_{\sigma\tau}). \tag{15}$$

It is clear that the general solution of (15) is

$$L_1=L_1(\eta_{\sigma\tau}-\lambda f_{\sigma\tau}, u). \tag{16}$$

That is, L_1 must be a function of the matter variables and the single tensor argument $\eta_{\sigma\tau}-\lambda f_{\sigma\tau}$. Thus, denoting $\eta_{\sigma\tau}-\lambda f_{\sigma\tau}$ by $g_{\sigma\tau}$, the general solution for L in

[1] Some elementary consequences of this requirement on the Euclidean gravitational field equation, and its approximate realization, were treated by the author in a thesis submitted in partial fulfillment of the requirements for the S.B. degree at the Massachusetts Institute of Technology, January 15, 1947, and similarly, but independently, by S. N. Gupta, Phys. Rev. 96, 1683 (1954).

[2] The definition and some properties of the energy tensor are discussed in Appendix I.

[3] We imply the exclusion of the half-advanced, half-retarded solutions of the homogeneous equation $\Box^2\mathfrak{f}^{\sigma\tau}{}_{|\tau}=0$.

empty space is

$$L=\int \mathfrak{K}(g)d^4x-(2/\lambda)\int f_{\mu\lambda}\mathfrak{R}^{\mu\lambda}(\eta)d^4x, \qquad (17)$$

where $\mathfrak{K}(g)$ is a Riemannian invariant-density constructed from $g_{\sigma\tau}$ alone; that is, a "general invariant" in the language of relativity theory. Since the terms in $2/\lambda$ vanish due to the assumption of Euclidean $\eta_{\mu\lambda}$, the field equations for $g_{\sigma\tau}$ are simply those resulting from variation of $\int \mathfrak{K}(g)d^4x$ alone. The simplest nontrivial form $\mathfrak{K}$ is $\mathfrak{K}=\mathfrak{R}^{\mu\lambda}(g)g_{\mu\lambda}$, where $\mathfrak{R}^{\mu\lambda}(g)$ is the contracted contravariant Riemann-Christoffel tensor-density constructed from the fundamental tensor $g_{\mu\lambda}$. This is a form of the Lagrangian for the Einstein gravitational equations so that $g_{\mu\lambda}$ may then be identified with Einstein's metric tensor in empty space. In nonempty regions, $\mathfrak{K}(g)$ will be replaced by some invariant function of both $g_{\mu\lambda}$ and u. Its form will of course depend of the covariance properties of the u variables and on the type of coupling assumed.

NONUNIQUENESS OF THE AUXILIARY CONDITIONS

In the preceding analysis, we have assumed that the tensor $f_{\mu\lambda}$, which is the generalization of the Newtonian potential, is a covariant tensor. There is nothing in the original equation (1) to force this choice, and, we might as well have started with a contravariant tensor, or either a covariant or contravariant tensor density of arbitrary weight. We shall now show that these alternative choices are closely related to the theory already developed, and may be realized by a change in the auxiliary conditions. Since the notation of the tensor calculus requires a definite choice of covariant or contravariant character in an expression, we shall carry through the analysis for a contravariant tensor density of arbitrary weight, and then indicate the minor changes appropriate to the covariant choice.

If we replace L by a new Lagrangian

$$\bar{L}=L_1-(2/\lambda)\int \psi^{\mu\lambda}\mathfrak{R}_{\mu\lambda}(\eta)|\eta|^{-N/2}d^4x, \qquad (18)$$

where $\psi^{\mu\lambda}$ is any tensor density function of $f_{\mu\lambda}$ and $\eta_{\mu\lambda}$ of weight N, connected to $f_{\mu\lambda}$ by an invertible transformation, the field equations for $f_{\mu\lambda}$ are unaltered because of the vanishing of $\mathfrak{R}_{\mu\lambda}(\eta)$. The new energy tensor is

$$\begin{aligned}\delta\bar{L}/\delta\eta_{\sigma\tau}&=\lambda^{-1}|\eta|^{(1-N)/2}D^{\sigma\tau}(\psi)-2\lambda^{-1}\\ &\quad\times\int(\partial\psi^{\mu\lambda}/\partial\eta_{\sigma\tau})\mathfrak{R}_{\mu\lambda}(\eta)|\eta|^{-N/2}d^4x+\delta L_1/\delta\eta_{\sigma\tau}\\ &=\delta L/\delta\eta_{\sigma\tau}-\lambda^{-1}\mathfrak{D}^{\sigma\tau}(f)\\ &\quad+\lambda^{-1}|\eta|^{(1-N)/2}D^{\sigma\tau}(\psi), \qquad (19)\end{aligned}$$

since $\mathfrak{R}_{\mu\lambda}(\eta)=0$. Hence, the field equations (10) may be rewritten

$$|\eta|^{(1-N)/2}D^{\sigma\tau}(\psi)-\lambda(\delta\bar{L}/\delta\eta_{\sigma\tau})=0. \qquad (20)$$

Now let us rewrite the new Lagrangian in terms of $\eta_{\mu\lambda}$ and the new variables $\psi^{\mu\lambda}$. Denoting $\bar{L}$ expressed in this form by $\bar{L}^*$,

$$\frac{\delta\bar{L}^*}{\delta\eta_{\mu\lambda}}=\frac{\delta\bar{L}}{\delta\eta_{\mu\lambda}}+\frac{\delta\bar{L}}{\delta f_{\alpha\beta}}\left(\frac{\partial f_{\alpha\beta}}{\partial\eta_{\mu\lambda}}\right)_{\psi^{\sigma\tau}=\text{const}}=\frac{\delta\bar{L}}{\delta\eta_{\mu\lambda}}, \qquad (21)$$

when the field equations $\delta\bar{L}/\delta f_{\alpha\beta}=0$ are satisfied. Hence, the field equations for $\psi^{\mu\lambda}$ (20) may be written

$$|\eta|^{(1-N)/2}D^{\sigma\tau}(\psi)-\lambda(\delta\bar{L}^*/\delta\eta_{\sigma\tau})=0. \qquad (22)$$

If now we impose the auxiliary conditions

$$\psi^{\mu\lambda}{}_{|\lambda}=0, \qquad (23)$$

(22) becomes

$$\Box^2\psi^{\mu\lambda}-\lambda|\eta|^{(N-1)/2}(\delta\bar{L}^*/\delta\eta_{\sigma\tau})=0, \qquad (24)$$

which is as valid a generalization of (1) as (8). The actual Lagrange-Euler equations resulting from variation of $\bar{L}^*$ with respect to $\psi^{\alpha\beta}$ may be written

$$\frac{\partial f_{\mu\lambda}}{\partial\psi^{\alpha\beta}}\left[D^{\mu\lambda}(\psi)-\lambda|\eta|^{(N-1)/2}\frac{\delta\bar{L}^*}{\delta\eta_{\mu\lambda}}\right]=0, \qquad (25)$$

which although equivalent to (22) are not formally identical as was assumed in the analysis which led to (16). If the analysis is carried through for a covariant tensor density $\psi_{\mu\lambda}$, of weight N, the equations analogous to (23) and (24) are

$$\psi_{\mu\lambda|\sigma}\eta^{\lambda\sigma}=0, \qquad (26)$$

$$\Box^2\psi_{\mu\lambda}-\lambda|\eta|^{(N-1)/2}\eta_{\sigma\mu}\eta_{\tau\lambda}(\delta\bar{L}^*/\delta\eta_{\sigma\tau})=0. \qquad (27)$$

It thus appears that there is associated with any given general invariant a family of Lagrangians leading to equations of the type (10) and differing only by terms which do not affect the field equations but which have the effect of altering the energy tensor by expressions with identically vanishing divergencies. Although the field equations for this family of Lagrangians are all identical in the sense that they can be obtained from each other by variable transformations, the auxiliary conditions (23) or (26) required to satisfy the wave equations of the form (24) or (27) for each choice of variables $\psi(\sigma\tau)$ will not be equivalent in general.

We have thus been led to the result that generalization of the Newtonian potential equation, in accordance with the postulates of special relativity, to the tensor field equation of the form (3) leads uniquely to the class of generally covariant field theories, augmented by auxiliary conditions. There seems to be no way of distinguishing between the various choices of auxiliary conditions on the basis of the assumptions we have made thus far in generalizing the Newtonian law (1). In the usual interpretation of Einstein's gravitation theory as

a law regulating the metric structure of space, auxiliary conditions of the type introduced are considered merely to fix the form of the (arbitrary) coordinate system and are not regarded as having any physical content. In a paper to follow, however, the question of the physical significance of the auxiliary conditions will be reexamined.

ACKNOWLEDGMENT

A part of this work was done while the author was at the Institute for Advanced Study in 1949–1950. He wishes to thank Dr. J. Robert Oppenheimer for the hospitality of the Institute, and Dr. Albert Einstein for the privilege of working with him.

APPENDIX I. DEFINITION OF THE ENERGY TENSOR

The method of constructing the Lagrangian derived energy tensor used in this paper is due to Eddington[4] and been discussed by Chang[5] and others. The general type of Lagrangian considered is of the form

$$L=\int \mathfrak{L}(\eta_{\mu\lambda},w^{(\sigma)})d^4x, \tag{I.1}$$

where $\mathfrak{L}$ is any function of the Euclidean metric tensor $\eta_{\mu\lambda}$, the dynamic variables $w^{(\sigma)}$ and their derivatives of any order, which transforms as an invariant density of weight $+1$ under an arbitrary change of coordinate system. L will then be an invariant. The dynamic variables $w^{(\sigma)}$ are not specified in number or kind except that they have well defined covariance properties under coordinate transformation. Since L is an invariant, the variation

$$\delta L=\int[(\delta L/\delta\eta_{\mu\lambda})\delta\eta_{\mu\lambda}+\textstyle\sum_\sigma(\delta L/\delta w^{(\sigma)})\delta w^{(\sigma)}]d^4x \tag{I.2}$$

will vanish when $\delta\eta_{\mu\lambda}$ and $\delta w^{(\sigma)}$ are variations due to an arbitrary infinitesimal coordinate transformation. The Lagrange equations for the dynamic variables $w^{(\sigma)}$ are

$$\delta L/\delta w^{(\sigma)}=0, \tag{I.3}$$

so that when the field equations are satisfied, (I.2) is simply

$$\int(\delta L/\delta\eta_{\mu\lambda})\delta\eta_{\mu\lambda}d^4x=0. \tag{I.4}$$

Under the infinitesimal coordinate transformation $x'^\mu=x^\mu+\delta x^\mu$, the change in the covariant tensor $\eta_{\mu\lambda}$ is

$$-\delta\eta_{\mu\lambda}=\eta_{\mu\alpha}\delta x^\alpha{}_{,\lambda}+\eta_{\alpha\lambda}\delta x^\alpha{}_{,\mu}-\eta_{\mu\lambda,\alpha}\delta x^\alpha, \tag{I.5}$$

where the $\eta_{\mu\lambda}$ are expressed in terms of the new coordinates. Assuming the δx^μ vanish outside a finite region, (I.4) may be transformed by partial integration to the form

$$\int(\delta L/\delta\eta_{\mu\lambda})_{|\lambda}\eta_{\mu\alpha}\delta x^\alpha=0, \tag{I.6}$$

where $|\lambda$ indicates covariant differentiation with respect to $\eta_{\mu\lambda}$. Since this must hold for arbitrary δx^α,

$$(\delta L/\delta\eta_{\mu\lambda})_{|\lambda}=0, \tag{I.7}$$

and in view of this conservation property the energy tensor density may be identified as

$$\mathfrak{T}^{\mu\lambda}=\delta L/\delta\eta_{\mu\lambda}. \tag{I.8}$$

This definition of the energy tensor is unique to the extent that the form of the Lagrangian leading to given field equations (I.3) is unique. However the Lagrangian may be altered by the formal addition of terms of the form

$$\int A\mathfrak{R}(\eta)d^4x,\quad \int A_{\mu\lambda}\mathfrak{R}^{\mu\lambda}(\eta)d^4x,\quad \text{etc.}, \tag{I.9}$$

(where A, $A_{\mu\lambda}$, $\cdots$ are scalar or tensor functions of the dynamic variables and $\eta_{\mu\lambda}$ and $\mathfrak{R}(\eta)$, $\mathfrak{R}^{\mu\lambda}(\eta)$, $\cdots$ are contractions of the Riemann-Christoffel tensor density built on $\eta_{\mu\lambda}$) without affecting these equations since the Riemann-Christoffel tensor vanishes. Denoting an expression of the form (I.9) by K, since $\delta K/\delta w^{(\sigma)}=0$ for all $w^{(\sigma)}$ values, (I.7) becomes the *identity*

$$(\delta K/\delta\eta_{\mu\lambda})_{|\lambda}\equiv 0. \tag{I.10}$$

Hence the effect of such formal additions to the Lagrangian is to change the energy tensor by an expression whose divergence vanishes identically. This ambiguity is unavoidable since the requirement on an energy tensor is simply that it be conserved when the field equations are satisfied.

A special illustration of the effect of the freedom of definition of the energy tensor is provided by the Lagrangian of the general relativity theory. If the Einstein field tensor $g_{\mu\lambda}$ is regarded as the dynamic variable, the field equations may be obtained from the Lagrangian

$$L=\int\mathfrak{R}(g)d^4x, \tag{I.11}$$

where $\mathfrak{R}(g)$ is the invariant density formed by contraction of the Riemann-Christoffel tensor formed on $g_{\mu\lambda}$. Since this Lagrangian does not contain the metric tensor $\eta_{\mu\lambda}$ at all, the energy tensor as defined above vanishes. However, let us replace each derivative $g_{\mu\lambda,\sigma}$, $g_{\mu\lambda,\sigma\tau}$ occurring in (I.11) by $g_{\mu\lambda|\sigma}$ or $g_{\mu\lambda|\sigma\tau}$ where $|$ indicates covariant differentiation with respect to $\eta_{\mu\lambda}$. This will not destroy the invariance of the Lagrangian to coordinate transformations, and since the form of the Lagrangian will be unaltered in Cartesian coordinates, the field equations will not be affected in any coordinate system. The alteration of the Lagrangian

[4] A. S. Eddington, *Mathematical Theory of Relativity* (The University Press, Cambridge, 1937), second edition, pp. 140–141.
[5] T. S. Chang, Proc. Cambridge Phil. Soc. 44, 76 (1948).

can be represented as the addition of terms of form similar to (I.9). The resultant energy tensor identically obeys the conservation conditions (I.7). A tensor which obeys the conservation conditions only when the field equations are satisfied can be formally derived by changing to new dynamic variables $f_{\mu\lambda}=(g_{\mu\lambda}-\eta_{\mu\lambda})$. The two energy tensors differ only by the expression $\mathfrak{R}^{\mu\lambda}(g)-\frac{1}{2}g^{\mu\lambda}\mathfrak{R}(g)$ and hence are identical when the field equations are satisfied. In that case, they are closely related, in Cartesian coordinates, to the usual "pseudo energy-tensor" as defined, for example, by Eddington.[6]

APPENDIX II. SCALAR THEORY

The scalar gravitation theory corresponding to the field equation

$$\Box^2\phi-\lambda T_{\mu\lambda}\eta^{\mu\lambda}=0 \tag{2}$$

may be developed in close analogy to the treatment of the tensor theory. If the energy tensor $T_{\mu\lambda}$ is derived from a Lagrangian $L(\phi,\eta_{\mu\lambda},u)$, where u represents the matter variables, then (2) is equivalent to the Lagrange-Euler equation if

$$\delta L/\delta\phi=|\eta|^{\frac{1}{2}}\Box^2\phi-\lambda(\delta L/\delta\eta_{\mu\lambda})\eta_{\mu\lambda}. \tag{II.1}$$

Let $L=L_1+L_2$, where

$$L_2=-(3\lambda)^{-1}\int\phi\mathfrak{R}(\eta)d^4x, \tag{II.2}$$

where $\mathfrak{R}(\eta)$ is the Riemannian curvature invariant. For Euclidean $\eta_{\mu\lambda}$, $\delta L_2/\delta\phi$ then vanishes and

$$\lambda(\delta L_2/\delta\eta_{\mu\lambda})\eta_{\mu\lambda}=|\eta|^{\frac{1}{2}}\Box^2\phi. \tag{II.3}$$

Hence the resulting equation for L_1 is

$$\delta L_1/\delta\phi+\lambda\eta_{\mu\lambda}(\delta L_1/\delta\eta_{\mu\lambda})=0. \tag{II.4}$$

Now make the transformation $\gamma_{\mu\lambda}=\epsilon^{-\lambda\phi}\eta_{\mu\lambda}$, so that

$$L_1(\phi,\eta_{\mu\lambda},u)=L_1^*(\phi,\gamma_{\mu\lambda},u). \tag{II.5}$$

Then, (II.4) may be written

$$0=\frac{\delta L_1^*}{\delta\phi}+\frac{\delta L_1^*}{\delta\gamma_{\mu\lambda}}\frac{\partial\gamma_{\mu\lambda}}{\partial\phi}+\lambda\frac{\delta L_1^*}{\delta\gamma_{\alpha\beta}}\frac{\partial\gamma_{\alpha\beta}}{\partial\eta_{\mu\lambda}}\eta_{\mu\lambda}=\frac{\delta L_1^*}{\delta\phi}, \tag{II.6}$$

which shows that L_1^* must be a function of u and the tensor $\gamma_{\mu\lambda}$ alone. Hence, Eq. (2) leads to the general Lagrangian,

$$L=\int\mathfrak{K}(\epsilon^{-\lambda\phi}\eta_{\mu\lambda})d^4x+\int\mathfrak{J}(\epsilon^{-\lambda\phi}\eta_{\mu\lambda},u)d^4x-(3\lambda)^{-1}\int\phi\mathfrak{R}(\eta)d^4x, \tag{II.7}$$

where $\mathfrak{K}$ and $\mathfrak{J}$ are any general invariant densities built on the fundamental tensor $\epsilon^{-\lambda\phi}\eta_{\mu\lambda}$. Since the last term vanishes for Euclidean $\eta_{\mu\lambda}$, the equations of motion will be unaltered by dropping it and hence, making the change of variable $\psi=\epsilon^{-\lambda\phi}$, the field equations may be obtained by variation of the Lagrangian

$$L=\int\mathfrak{K}(\psi\eta_{\mu\lambda})d^4x+\int\mathfrak{J}(\psi\eta_{\mu\lambda},u)d^4x. \tag{II.8}$$

It will be noted that if $g_{\mu\lambda}=\psi\eta_{\mu\lambda}$, this is the general Lagrangian for the tensor theory, and it follows then that if there do exist solutions of the tensor theory of this form, then ψ must obey the field equation of the scalar theory.

If $\mathfrak{K}(\psi\eta_{\mu\lambda})=\mathfrak{R}(\psi\eta_{\mu\lambda})$, it may be verified that for Euclidean $\eta_{\mu\lambda}$, (II.8) reduces to

$$L=\int\psi^{-1}\psi_{,\alpha}\psi_{,\beta}\eta^{\alpha\beta}|\eta|^{\frac{1}{2}}d^4x+\int\mathfrak{J}(\psi\eta_{\mu\lambda},u)d^4x. \tag{II.9}$$

This form bears an interesting resemblance to the Lagrangian of the general relativity theory, which Eddington[7] has pointed out can be written as an expression homogeneous of order 2 in the quantities $\mathfrak{g}^{\mu\lambda}{}_{,\alpha}$ and homogeneous of order -1 in the $\mathfrak{g}^{\mu\lambda}$. However, in distinction to the general relativity case, a simple variable transformation renders this scalar theory linear.

It is readily seen that the class of scalar theories just developed can give no bending of light by a gravitational field. In the absence of gravitational field, the Lagrangian of the electromagnetic field may be written

$$L_{\text{e.m.}}=\int(A_{\mu,\lambda}-A_{\lambda,\mu})(A_{\sigma,\tau}-A_{\tau,\sigma})\eta^{\mu\sigma}\eta^{\lambda\tau}|\eta|^{\frac{1}{2}}d^4x. \tag{II.10}$$

This expression is homogeneous of degree 0 in the $\eta_{\mu\lambda}$, and hence it is apparent that it will be unaltered if $\eta_{\mu\lambda}$ is replaced by $\psi\eta_{\mu\lambda}$.

The Lagrangian (II.9) leads in first approximation to the Newtonian law of gravitation, but it predicts a motion of the perihelion of Mercury different from the observed advance. The motion can be obtained exactly.

[6] A. S. Eddington, reference 4, pp. 134–137.

[7] A. S. Eddington, reference 4, pp. 131–134.

Relativistic Cosmology. I

AMALKUMAR RAYCHAUDHURI
Theoretical Physics Department, Indian Association for the Cultivation of Science, Jadavpur, Calcutta, India
(Received December 28, 1953)

The paper presents some general relations obtaining in relativistic cosmology. It appears from these that a simple change over to anisotropy without the introduction of spin does not solve any of the outstanding difficulties of isotropic cosmological models.

I. INTRODUCTION

PERHAPS the only point in which all the current theories of cosmology are found to be in agreement is the time-dependent nature of the spatial geometry. It therefore seems of considerable interest to investigate the temporal behavior of a gravitating system as observed by a member of the system itself in its neighborhood. It is true that there exists a fairly large amount of literature where a study has been made on similar problems; however they all depend on some additional assumptions of which homogeneity and (or) some symmetry postulates seem to be very common ones. While there may indeed be some great aesthetic appeal in favor of such assumptions, yet they seem nevertheless open to serious doubts even on a smoothed-out scale and very definitely do not provide an exact picture of the universe when one considers the finer details. Further, the introduction of such assumptions lead to rather ambiguous situations when one runs into some difficulties, e.g., the well-known difficulties regarding the time-scale[1] and the original singularity (a creation in the finite past?) of the isotropic cosmologic models of general relativity have been variously attributed to the assumption of homogeneity and isotropy on the one hand[2–4] and to a failure of the general theory of relativity on the other.[5]

In this paper, an attempt is therefore made to study the temporal behavior of a gravitating cloud on the basis of the Einstein gravitational equations under very general conditions. This would presumably give one an idea about the potentialities and limitations of the general theory of relativity in providing a satisfactory solution to the cosmological problem.

[1] Recent researches have led to a doubling of the nebular distances and thus the "age" of the universe has been correspondingly increased. However, it seems doubtful whether even this revised time scale would be consistent with the estimates of the age of the earth by A. Holmes, Nature **163**, 453 (1949) and some of the astrophysical estimates [F. Hoyle, Nature **163**, 196 (1949)].
[2] A. S. Eddington, Science Progr. **34**, 225 (1939).
[3] R. C. Tolman, Revs. Modern Phys. **21**, 374 (1949); G. Omer, Jr., Astrophys. J. **109**, 164 (1949).
[4] R. C. Tolman, *Relativity, Thermodynamics and Cosmology* Clarendon Press, Oxford, 1934), pp. 438–39.
[5] For a concise review of these theories, see H. Bondi, *Cosmology* Cambridge University Press, Cambridge, 1952).

II. THE DIFFERENTIAL EQUATION GOVERNING THE SPATIAL EXPANSION (OR CONTRACTION)

We shall assume that there is no interaction except through the Einstein gravitational equations

$$-8\pi T^{\mu}{}_{\nu}=R^{\mu}{}_{\nu}-\tfrac{1}{2}R\delta^{\mu}{}_{\nu}+\Lambda\delta^{\mu}{}_{\nu}, \tag{1}$$

where the symbols have their usual significance. Under this circumstance the world lines of matter will be time-like geodesics. Further, we shall consider that there is no chaotic motion. We may now take the world lines of matter as our t-lines and if the coordinate along these lines measures the proper interval, the line element can be written in the form[6]

$$ds^2=dt^2+2g_{4i}dtdx^i+g_{ik}dx^idx^k, \tag{2}$$

where the three-space metric $d\sigma^2=g_{ik}dx^idx^k$ is negative definite. Without loss of generality we can take $g_{4k}=0$ at a particular point (say $t=x^1=x^2=x^3=0$), i.e., the $(x^1x^2x^3)$ space is orthogonal to the world line at this point. The condition that the t-lines are geodesics gives

$$g_{4k,4}=0, \tag{3}$$

so that g_{4k}'s vanish everywhere on the t-axis. We shall take this t-axis as the world line of our observer.

It may be noted that we are not taking $g_{4k}=0$ everywhere, i.e., we are not assuming that the geodesic congruence of the world lines is normal. This, according to Gödel,[7] corresponds to the existence of a spin relative to the compass of inertia. Our considerations therefore include the spinning cosmological models as well.

The energy momentum tensor is given by

$$T^{\mu}{}_{\nu}=\rho\frac{dx^{\mu}}{ds}\frac{dx_{\nu}}{ds}=g_{\nu\alpha}\rho\frac{dx^{\mu}}{ds}\frac{dx^{\alpha}}{ds}, \tag{4}$$

so that for our cosmic fluid whose world lines are the t-lines (i.e., $dx^4/ds=1$, $dx^i/ds=0$), $T^{\mu}{}_{\nu}$ has only one nonvanishing component at points on the t-axis (where $g_{4k}=0$), namely

$$T^4{}_4=\rho.$$

It is now easy to deduce the following relation from the field equations (1):

$$R^4{}_4=\Lambda-4\pi\rho. \tag{5}$$

[6] In this paper, Greek indices run from 1 to 4 while Latin indices run from 1 to 3.
[7] K. Gödel, Revs. Modern Phys. **21**, 447 (1949).

A direct calculation of $R^4{}_4$ gives at any point on the t-axis,

$$R^4{}_4=\frac{\partial^2}{\partial t^2}[\log\sqrt{(-g)}]+\tfrac{1}{4}g^{ik}\dot{g}_{kl}g^{lm}\dot{g}_{mi}+\tfrac{1}{4}g^{ik}g^{lm}(g_{l4,k}-g_{k4,l})(g_{i4,m}-g_{m4,i}), \quad (6)$$

where dots indicate differentiation with respect to time and $g_{ik,l}$ stands for $(\partial/\partial x^l)g_{ik}$.

We can show that $\frac{1}{4}g^{ik}\dot{g}_{kl}g^{lm}\dot{g}_{mi}-\frac{1}{3}[(\partial/\partial t)\log\sqrt{(-g)}]^2$ vanishes in case of isotropic expansion (or contraction) and is positive otherwise. For, at the particular point we can diagonalize the (3×3) matrix g_{ik} by a transformation of the form

$$\bar{x}^i=f^i(x^1,x^2,x^3), \quad \bar{t}=t, \quad (7)$$

where f^i is a function of its arguments, analytic at points on the t-axis. Such a transformation does not however disturb the value of any of the terms in (6). Hence, without loss of generality we can assume g_{ik} to be diagonalized, so that

$$\begin{aligned}&\tfrac{1}{4}g^{ik}\dot{g}_{kl}g^{lm}\dot{g}_{mi}-\tfrac{1}{3}\left(\frac{\partial}{\partial t}\log\sqrt{(-g)}\right)^2\\&=\tfrac{1}{4}[g^{ik}\dot{g}_{kl}g^{lm}\dot{g}_{mi}-\tfrac{1}{3}g^{ik}\dot{g}_{ik}g^{lm}\dot{g}_{lm}]\\&=\tfrac{1}{2}[g^{11}g^{22}\dot{g}_{12}{}^2+g^{11}g^{33}\dot{g}_{13}{}^2+g^{22}g^{33}\dot{g}_{23}{}^2]\\&\quad+\frac{1}{12}\left[\left(\frac{\dot{g}_{11}}{g_{11}}-\frac{\dot{g}_{22}}{g_{22}}\right)^2+\left(\frac{\dot{g}_{22}}{g_{22}}-\frac{\dot{g}_{33}}{g_{33}}\right)^2+\left(\frac{\dot{g}_{33}}{g_{33}}-\frac{\dot{g}_{11}}{g_{11}}\right)^2\right]\\&=\phi^2(\text{say}),\end{aligned} \quad (8)$$

where ϕ vanishes if and only if $\dot{g}_{ik}=\alpha g_{ik}$ at the point under consideration, α being independent of the pairs of indices i and k, i.e., ϕ vanishes if the expansion (or contraction) at the point be isotropic. We note, further, that the relation $\dot{g}_{ik}=\alpha g_{ik}$ is invariant under transformation (7).

If v^μ be the velocity vector of matter, then with our choice of coordinate system it is simply the unit vector along the t-line at the point and hence $v^i=0$ and $v^4=1$ so that

$$\omega_{ik}\equiv\tfrac{1}{2}(v_{i;k}-v_{k;i})\equiv\tfrac{1}{2}(v_{i,k}-v_{k,i})=\tfrac{1}{2}(g_{i4,k}-g_{k4,i}). \quad (9)$$

The vanishing of the tensor ω_{ik} is the necessary and sufficient condition for the geodesic congruence of the world lines to be normal.[8] We shall identify the antisymmetric tensor ω_{ik} with spin, as seems natural from the classical relation $\omega=\frac{1}{2}\,\text{curl}\,v$.[9] Using (9), we can write,

$$\tfrac{1}{4}g^{ik}g^{lm}(g_{i4,m}-g_{m4,i})(g_{l4,k}-g_{k4,l})=g^{ik}g^{lm}\omega_{im}\omega_{lk},$$

and this expression is easily seen to be negative definite. Writing this as $-2\omega^2$ as is consistent with the classical analogy, we get from (6) and (8),

$$R^4{}_4=\frac{\partial^2}{\partial t^2}[\log\sqrt{(-g)}]+\frac{1}{3}\left[\frac{\partial}{\partial t}\log\sqrt{(-g)}\right]^2+\phi^2-2\omega^2, \quad (10)$$

so that substitution in (5) gives

$$(1/G)(\partial^2G/\partial t^2)=(\Lambda-4\pi\rho-\phi^2+2\omega^2)/3, \quad (11)$$

where we have put $G^6=-g$.

In the ordinary isotropic case, the corresponding equation is

$$(1/G)(\partial^2G/\partial t^2)=(\Lambda-4\pi\rho)/3. \quad (12)$$

Further, one can deduce an equation formally exactly similar to (12) on the basis of Newtonian mechanics,[10] where Λ corresponds to a repulsive force proportional to distance and the term involving density arises from Newtonian gravitational attraction. Considering Eq. (11), therefore, one may say that on the classical analogy the spin gives rise to a repulsive force (the centrifugal repulsion) while any anisotropy in the local expansion effectively increases the gravitational attraction.

From the divergence relation $T^\mu{}_{4;\mu}=0$, we get

$$\rho G^3=C(\text{const}). \quad (13)$$

However, the dependence of ϕ^2 and ω^2 on G remains in general arbitrary, and thus it does not seem possible to integrate (11) without introducing further assumptions.

III. THE CASE OF A NONSPINNING GRAVITATING SYSTEM

In case the spin vanishes, $\omega^2=0$ and Eq. (11) becomes

$$(1/G)(\partial^2G/\partial t^2)=(\Lambda-4\pi\rho-\phi^2)/3. \quad (14)$$

It follows at once that a necessary condition for a completely static behavior in the neighborhood is

$$\rho=\Lambda/4\pi,$$

i.e., the local density must satisfy the relation obtaining in the Einstein static universe. It is to be noted that this condition is arrived at without any assumption regarding symmetry or conditions obtaining in the distant parts of the universe. It is now easy to see that if the whole universe is static the relation must be satisfied everywhere. It therefore follows that no nonspinning nonhomogeneous universe can be static and the only static nonspinning universe is the Einstein universe.[11]

[8] L. P. Eisenhart, *Riemannian Geometry* (Princeton University Press, Princeton, 1949), p. 115.

[9] This definition of spin is slightly different from that of Gödel. While we consider an antisymmetric tensor, Gödel defines the spin as a vector constructed from this tensor, the velocity vector and the Levi-Civita tensor ϵ^{iklm}. However, so long as the field is purely gravitational, so that the velocity field forms a geodesic congruence, physical conclusions from either definition are very similar.

[10] See reference 5, Chap. IX.

[11] The empty de Sitter universe is also sometimes regarded as static. However, in the coordinate system in which this universe is static, the t-lines are not geodesics and thus the static nature is only apparent due to the absence of matter.

We note further that Eq. (14) shows that, in the absence of spin, with a given value of ρ and $\dot{G}/G$ (determinable in principle from local observations) at a certain instant, the time behavior in the locality is identical for all locally isotropically expanding systems and is given by Eq. (12).[12] Further, in general, we have as the first integral of (14):

$$\dot{\phi}^2-\dot{G}_A^2=\frac{\Lambda}{3}(G^2-G_A^2)+\frac{8\pi C}{3}\left(\frac{1}{G}-\frac{1}{G_A}\right)+\frac{2}{3}\int_t^{t_A}\phi^2 G dG, \quad (15)$$

where we have used Eq. (13) and the subscript A indicates the values corresponding to an assigned state. Hence, finally, the time interval between two states A and B is given by

$$\tau_{AB}=\int_{Q_B}^{1}\frac{dQ}{\left[\frac{\Lambda}{3}(Q^2-1)+\frac{8\pi\rho_A}{3Q}(1-Q)+\left(\frac{\dot{G}}{G}\right)_A^2+\Theta\right]^{\frac{1}{2}}}, \quad (16)$$

where we have written Q for G/G_A and $\Theta\equiv\frac{2}{3}\int_Q^1\phi^2 Q dQ$; hence, if $G_A>G_B$, then over the whole range of integration $Q\leqslant 1$ and therefore $\Theta\geqslant 0$, the equality sign occurring only if ϕ^2 vanishes (i.e., isotropic expansion or contraction). We may hence enunciate the theorem that in the absence of spin, the time interval between a state A of given ρ and $\dot{G}/G$ and another state B of specified volume ratio (i.e., G_B/G_A given) is a maximum in case of isotropic expansion (or contraction) if $G_A>G_B$ and there is no zero of $\dot{G}$ in the interval considered. In particular, in the cosmological problem in the absence of spin, among models which start from the singular state $G=0$, the time scale to the present state is a maximum for the isotropic models.

It may appear therefore that so far as the difficulty regarding the short time scale of relativistic isotropic models is concerned, nothing would be gained by simply changing over to nonisotropic models without introducing spin. However, the actual situation is slightly different. The cosmological constant Λ is not independently known. For the isotropic models, the necessity of a good fit with data of second order (e.g., the departure of the velocity-distance relation from linearity and the plausible bounds to the value of pressure) sets an upper bound to Λ which proves insufficient to give a long time scale. When, however, one gives up the assumption of isotropy, the second-order data do not set any precise bound on Λ as some other arbitrary parameters come into the picture. One can thus allow much higher values of Λ and obtain correspondingly longer time scales. Thus the longer time scales are due to an increased freedom in the choice of Λ rather than to anisotropy itself.[13] However, it should be noted that the introduction of such an arbitrary parameter robs the theory of much of its appeal and indeed if one sets $\Lambda=0$, then the theorem we have just proved shows that a simple change-over to anisotropy would only decrease the time scale.

Further, Eq. (14) shows that if $\Lambda=0$, then G cannot have any minimum, so that one has to start from a singularity at a finite time in the past as in isotropic models. Thus a simple change-over to anisotropy does not solve any of the difficulties.

IV. SOME IMPORTANT RELATIONS

In this section, we shall prove some interesting relations. By direct calculations we have, at any point on the t-axis, for the contracted Riemann-Christoffel tensor components,

$$R^i{}_k=R^{*i}{}_k+\tfrac{1}{2}g^{li}\partial^2/\partial t^2 g_{lk}+g^{li}\Gamma_{lp}{}^4\Gamma_{4k}{}^p-\tfrac{1}{2}g^{li}g^{pm}\dot{g}_{pm}\Gamma_{lk}{}^4+g^{li}\Gamma_{kp}{}^4\Gamma_{4l}{}^p-g^{li}g_{4p,k}\Gamma_{4l}{}^p, \quad (17)$$

where $R^{*i}{}_k$ are the corresponding tensor components for the three-space $d\sigma^2=g_{ik}dx^i dx^k$, and the Γ's are the Christoffel 3-index symbols. Contracting Eq. (17), we get, after some simplifications (the contraction here is from 1 to 3),

$$R^i{}_i=R^{*i}{}_i+\frac{\partial^2}{\partial t^2}[\log\sqrt{(-g)}]+\left[\frac{\partial}{\partial t}\log\sqrt{(-g)}\right]^2+g^{ik}g^{lm}g_{lA,i}\dot{g}_{km}-\tfrac{1}{2}g^{lm}g_{lA,m}g^{ik}\dot{g}_{ik}-g^{li}g_{4p,i}\Gamma_{4l}{}^p. \quad (18)$$

A very great simplification in the above relation can be attained by making a further specification of the coordinate system. So far, the three-space has been taken to be only orthogonal to the t-axis. If now we make a transformation,

$$\bar{x}^i=x^i, \quad \bar{t}=t+\phi(x^i),$$

where the function ϕ satisfies the following conditions,

$$(\phi,_i)_0=0, \quad (\phi,_{ik})_0=\tfrac{1}{2}(g_{4k,i}+g_{4i,k}),$$

the suffix 0 indicating the value at $x^i=0$. Then in the new coordinate system $(\bar{g}_{4i,k})_0$ will be antisymmetric, i.e.,

$$(\bar{g}_{4i,k})_0=-(\bar{g}_{4k,i})_0.$$

Such a coordinate transformation, however, does not affect any of the results so far obtained and (18) now

[12] Equation 12 has been shown to be valid by R. C. Tolman [Proc. Natl. Acad. Sci. **20**, 169 (1934)] at the center of symmetry in a spherically symmetric system. J. L. Synge [Proc. Natl. Acad. Sci. **20**, 635 (1934)] has obtained the same equation on the assumption of "symmetry" about the world line at the point.

[13] See, in this connection, the papers cited in reference 3.

becomes (on dropping bars)

$$R^i{}_i = R^{*i}{}_i + \frac{\partial^2}{\partial t^2}[\log\sqrt{(-g)}] + \left[\frac{\partial}{\partial t}\log\sqrt{(-g)}\right]^2 - 2\omega^2; \quad (19)$$

so that using (1), (4), and (10), we get

$$8\pi\rho = \tfrac{1}{2}R - R^4{}_4 - \Lambda = \frac{R^{*i}{}_i - \phi^2}{2} + \frac{1}{3}\left[\frac{\partial}{\partial t}\log\sqrt{(-g)}\right]^2 - \Lambda. \quad (20)$$

Differentiating (20) with respect to t and using (13), and comparing with (11), we get the interesting relation

$$\frac{\partial}{\partial t}(R^{*i}{}_i - \phi^2) = (6\phi^2 - 2R^{*i}{}_i - 8\omega^2)\frac{\dot{G}}{G}. \quad (21)$$

If the spin vanishes and the expansion also be locally isotropic, then from (17), (4), and (1), we find that $R^{*i}{}_k$ is of the form $K\delta^i{}_k$. It is easy to see that a three-space whose contracted Riemann-Christoffel tensor is of this form is locally isotropic. Hence we have the theorem that if spin be absent and if the expansion be locally isotropic, then the space is locally isotropic. Thus local spatial isotropy follows from the restricted assumption of locally isotropic expansion (or contraction) in case of vanishing spin.

Letters to the Editor

PUBLICATION of brief reports of important discoveries in physics may be secured by addressing them to this department. The closing date for this department is five weeks prior to the date of issue. No proof will be sent to the authors. The Board of Editors does not hold itself responsible for the opinions expressed by the correspondents. Communications should not exceed 600 words in length and should be submitted in duplicate.

Electron Affinity of Atomic Oxygen

LEWIS M. BRANSCOMB AND STEPHEN J. SMITH
National Bureau of Standards, Washington D. C.
(Received March 3, 1955)

THE electron affinity of atomic oxygen has been deduced experimentally by other investigators from the study of electron attachment at a hot filament[1,2] and from dissociative attachment in a mass spectrometer.[3–6] These methods have yielded consistent results: 2.33±0.03 ev,[2] 2.2±0.2 ev,[3] 2.0±0.5 ev,[4] 2.09 ±0.4 ev,[5] and 2.2±0.2 ev.[6] Theoretical calculations using a self-consistent field can give only a lower limit of 0.5 ev.[7] Recent empirical isoelectronic extrapolations by Moiseiwitsch[8] and Bates and Moiseiwitsch[9] predict 1.12 ev and 2.0 ev, respectively.

We have made a direct determination of the O^- affinity by observing the threshold and measuring the cross section for photodetachment of an electron from the O^- ion. First applied to H^-,[10,11] this method uses a beam of mass-separated negative ions illuminated by a beam of radiation of measured intensity and spectral distribution, $\phi(\lambda)$. A current of free electrons, detached from the ions in the region of intersection of the photon and ion beams, is collected and measured.

The wavelength dependence of the cross section $\sigma(\lambda)$ is tested with water-cooled glass filters, whose transmissions $T_n(\lambda)$ are shown in Fig. 1. The probabilities per ion photodetachment, averaged from 23 experiments,

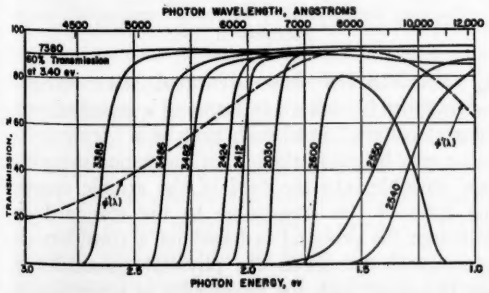

FIG. 1. Transmissions of filters used to determine wavelength dependence of O^- photodetachment cross section. The dashed curve is the normalized spectral distribution of the radiation source with the ordinate taken as 1 (micron)$^{-1}$=100 percent.

TABLE I. Experimental photodetachment probability, P_{exp}, for O^- with 9 glass filters; and P_{calc} using Eq. (1) and the $\sigma(\lambda)$ given in Fig. 2 for a 1.45-ev affinity.

Corning filter No.	$P_{exp}\times10^5$ [a]	$P_{calc}\times10^5$	$(P_{exp}-P_{calc})\times10^5$
7380	1.66 ±0.02	1.686	−0.02
3385	1.50 ±0.04	1.502	0.00
3486	1.35 ±0.03	1.350	0.00
3482	1.25 ±0.04	1.243	0.01
2424	1.08 ±0.05	1.100	−0.02
2412	0.948±0.07	0.985	−0.04
2030	0.820±0.03	0.790	0.03
2600	0.377±0.04	0.375	0.002
2550	0.074±0.016	0.0811	−0.007
2540	<0.02	0.0	<0.02

[a] Each datum is the mean value from 23 experiments, and the average deviation of these measurements from the mean.

are given in Table I. For the nth filter, the experimental probability is related to $\sigma(\lambda)$ by

$$P_n=1.703\times10^{13}\int\sigma(\lambda)\phi'(\lambda)T_n(\lambda)\lambda d\lambda. \quad (1)$$

Here $\phi'(\lambda)$ is normalized $[\int\phi'(\lambda)d\lambda=1]$, and λ is in microns. The filters with cutoffs above 1.9 ev were used in pairs to give the circled points of Fig. 2, each point corresponding to the difference of two P's, $\sigma(\lambda)$ being assumed slowly varying. The average deviation of these points is quite large because of the noise level and the temperature dependence of the filter transmissions, but the points are not independent, as shown by (1).

The large detachment signal with filter 2600 shows that the threshold lies substantially below 1.75 ev. With filter 2540 no signal is observed $[\sigma(\lambda)<1\times10^{-19}\ \text{cm}^2]$, giving a threshold above 1.35 ev. A monotonic function, nearly parabolic, has been fitted to the data of Table I. The upper limit to the affinity for a monotonic function is about 1.52 ev. If the threshold is to lie above 1.52 ev, a narrow resonance peak followed by a minimum seems to be required so that (1) and Table I can be satisfied.

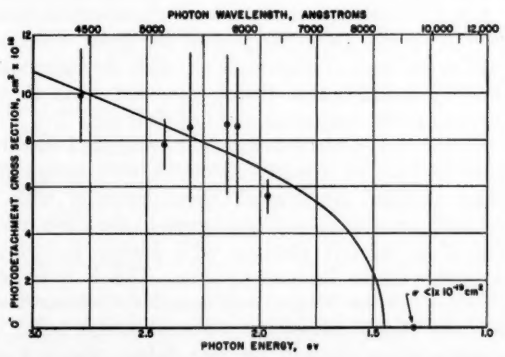

FIG. 2. Cross section for photodetachment of electrons from O^-. The solid curve is not extrapolated, but is the best fit to the data of Table I for a monotonic function and is thus not uniquely determined.

There is no evidence of a maximum near the threshold, although this possibility is not excluded.

The resolution of the mass separator was sufficient to exclude O_2^-, which has a detachment threshold below 1 volt and a cross section of about 0.4×10^{-18} cm² at 8000 A. Mass peaks of impurities at 17 and 19 amu were about 0.2 percent of the $(O^{16})^-$ peak, and thus comparable with the $(O^{18})^-$ peak, as determined with a high-resolution analyzer after the detachment chamber.

The O^- affinity given by our data is 1.45 ± 0.15 ev, the estimated uncertainty being related to the shape of $\sigma(\lambda)$ very near the threshold. This result is in unresolved conflict with previous experiments,[1–6] although not inconsistent with theoretical extrapolations.

[1] D. T. Vier and J. E. Mayer, J. Chem. Phys. **12**, 28 (1944).
[2] M. Metlay and G. E. Kimball, J. Chem. Phys. **16**, 744 (1948).
[3] W. W. Lozier, Phys. Rev. **46**, 268 (1934).
[4] G. Hanson, Phys. Rev. **48**, 476(A) (1935).
[5] H. D. Hagstrum and J. T. Tate, Phys. Rev. **59**, 354 (1941).
[6] H. D. Hagstrum, Revs. Modern Phys. **23**, 185 (1951).
[7] Hartree, Hartree, and Swirles, Trans. Roy. Soc. (London) A238, 229 (1939).
[8] B. L. Moiseiwitsch, Proc. Phys. Soc. (London) **A67**, 25 (1954).
[9] D. R. Bates and B. L. Moiseiwitsch, Proc. Phys. Soc. (London) (to be published).
[10] L. M. Branscomb and W. L. Fite, Phys. Rev. **93**, 651(A) (1954).
[11] L. M. Branscomb and S. J. Smith, Phys. Rev. **98**, 1126 (1955).

Orthogonality of the Furry-Sommerfeld-Maue Wave Functions and their Use in Perturbation Theory

ROBERT T. SHARP AND J. DAVID JACKSON
Department of Mathematics, McGill University, Montreal, Canada
(Received January 13, 1955; revised manuscript received March 15, 1955)

IN a recent paper on internal pair formation, Horton and Phibbs[1] assert that the Furry-Sommerfeld-Maue wave functions[2–4] for a Dirac particle in a Coulomb field are not orthogonal, and that for any process calculated by perturbation theory using these wave functions, the interaction matrix element must be modified accordingly.

It is our contention that the Furry-Sommerfeld-Maue wave functions are orthogonal in the usual sense, at least to the order of magnitude to which they are valid, and that perturbation theory does not need to be modified in any way on account of their use.

Horton and Phibbs prove in their Appendix I that the wave function of a positive electron with energy E_+ which satisfies the iterated Dirac equation with a Coulomb potential is not orthogonal to the wave function of a negative electron with energy E_- which satisfies a similar iterated equation. This is to be expected, since the positive and negative electrons have different Hamiltonians, the Coulomb terms being of opposite signs. As will be seen below, the lack of orthogonality of wave functions appropriate to different Hamiltonians is irrelevant to the problem.

In their Sec. III Horton and Phibbs go through the standard derivation of time-dependent perturbation theory, but because of the assumed applicability of their Appendix I, end up with a modified interaction matrix element [their Eqs. (16) and (18)]. The results of their Appendix I are not applicable, however, because, as is customary, they use as their unperturbed wave functions the various eigenfunctions of a *single* Hamiltonian. In the pair production problem, this demands interpreting the initial state as that of a negative electron with negative energy and the final state as that of a negative electron of positive energy.[5] Horton and Phibbs make the error of identifying the initial state wave function with that of a positive electron of positive energy satisfying the iterated Dirac equation, and so are led to use the irrelevant Appendix I to alter perturbation theory.

It is a straightforward matter to show that for a given sign of the electronic charge, wave functions satisfying both the ordinary and iterated Dirac equations of two different energies are orthogonal in the usual sense. Since the Furry-Sommerfeld-Maue wave functions are approximate solutions of these equations, they will be orthogonal to the same order of approximation. Consequently no modification of perturbation theory is necessary when these wave functions are used.

It should be mentioned that the main conclusions of Horton and Phibbs on the validity of the Born approximation in internal pair production are unaffected.

[1] G. K. Horton and E. Phibbs, Phys. Rev. **96**, 1066 (1954).
[2] W. H. Furry, Phys. Rev. **46**, 391 (1934).
[3] A. Sommerfeld and A. W. Maue, Ann. Physik **22**, 629 (1935).
[4] H. A. Bethe and L. C. Maximon, Phys. Rev. **93**, 768 (1954).
[5] See Sec. V of reference 4 for this argument applied directly to the Furry-Sommerfeld-Maue wave functions.

Comments on Straumanis' Concepts Regarding Avogadro's Number*

E. RICHARD COHEN, *North American Aviation, Inc., Downey, California*
AND
J. W. M. DUMOND, *California Institute of Technology, Pasadena, California*
(Received December 10, 1954; revised manuscript received February 21, 1955)

STRAUMANIS[1] has advocated that Avogadro's number be defined in terms of a standard crystal, "purest calcite," until such time as a "truly reliable" value may be established. This suggestion introduces a new variable into the field of the atomic constants: the ratio of the true value to the standard value. Although his proposal is based on a consideration of operational definitions for physical quantities, it is not in accord with the philosophy of simplification of concepts. It is, however, strongly influenced by the existence of discrepancies in the values obtained for Avogadro's number (both by direct measurement and

by indirect inference from least-squares adjustments, such as those of DuMond and Cohen[2]). We have pointed out[3] that, in contradiction to Straumanis, there are several experimental methods which yield values of Avogadro's number more accurate than the direct crystal density method. In a rebuttal[4] Straumanis countered with the argument that the crystallographer was concerned primarily with the quantity which we might call the Siegbahn-Avogadro number rather than with N itself. The Siegbahn-Avogadro number is defined here as $N_s' = N(\lambda_g/\lambda_s)^3$, and is the actual quantity which results from the direct crystal density x-ray method.[5] It is N_s', and not N, which relates macroscopic density, molecular weight, and lattice spacing in x-units. The crystallographer, using these units, is therefore interested in finding the experimental procedure which gives N_s' with highest accuracy, rather than the one which gives the most accurate value of N. Although DC 54[3] showed that the indirect methods can give the most accurate value of N, it is also true that, in general, they give N_s' with lesser accuracy. It is therefore useful to compare the direct value of N_s' with the indirect values computed from measurements of other physical constants.

We shall use the data given in DC 54 and shall use essentially the same notation as that paper. The equations of DC 54, each identified by a description of the experiments which it represents, are

$$
\begin{aligned}
x_3 + x_4 &= 84.2 \pm 10.9 = a_1 && \text{(Faraday constant)},\\
-3x_1 + 2x_3 + x_4 &= 145.0 \pm 10.5 = a_2 && \text{(proton cyclotron resonance)},\\
3x_1 - x_3 &= -23.0 \pm 22.9 = a_3 && \text{(proton magnetic resonance)},\\
x_5 &= 0.0 \pm 30.1 = a_4 && \text{(grating wavelengths)},\\
-x_1 + x_3 - x_5 &= -65.4 \pm 29.5 = a_5 && \text{(short-wavelength limit)},\\
x_4 + 3x_5 &= 34.0 \pm 37.8 = a_6 && \text{(x-ray crystal density)},\\
x_1 &= 40.0 \pm 4.5 = a_7 && \text{(hydrogen fine structure)}.
\end{aligned}
$$

We now introduce into these equations the substitution $y = x_4 + 3x_5$; so that y is the linearized variable corresponding to $N(\lambda_g/\lambda_s)^3$. In addition to the direct value, a_6, the other six equations can be combined into eleven distinct just-determinate solutions. Listed in the order of their accuracy, the complete set of solutions is

$$
\begin{aligned}
a_6 &\quad N(\lambda_g/\lambda_s)^3 = (0.606179 \pm 0.000023) \times 10^{24}\\
a_1 + 2a_4 - a_5 - a_7 &\quad N(\lambda_g/\lambda_s)^3 = (0.606225 \pm 0.000023) \times 10^{24}\\
a_2 + a_4 - 2a_5 + a_7 &\quad N(\lambda_g/\lambda_s)^3 = (0.606350 \pm 0.000036) \times 10^{24}\\
\tfrac{1}{2}(a_1 - a_2 + 3a_4 - 3a_5) &\quad N(\lambda_g/\lambda_s)^3 = (0.606276 \pm 0.000039) \times 10^{24}\\
\tfrac{1}{2}(a_1 + a_2 + 3a_4 - 3a_5) &\quad N(\lambda_g/\lambda_s)^3 = (0.606287 \pm 0.000039) \times 10^{24}\\
\tfrac{1}{2}(2a_2 + a_3 + 3a_4 - 3a_5) &\quad N(\lambda_g/\lambda_s)^3 = (0.606299 \pm 0.000040) \times 10^{24}\\
-a_1 + 2a_2 - 3a_5 + 3a_7 &\quad N(\lambda_g/\lambda_s)^3 = (0.606475 \pm 0.000056) \times 10^{24}\\
a_2 - a_3 - 3a_5 + 3a_7 &\quad N(\lambda_g/\lambda_s)^3 = (0.606452 \pm 0.000057) \times 10^{24}\\
a_1 + a_3 + 3a_4 - 3a_7 &\quad N(\lambda_g/\lambda_s)^3 = (0.606122 \pm 0.000058) \times 10^{24}\\
2a_1 - a_2 + 3a_4 - 3a_7 &\quad N(\lambda_g/\lambda_s)^3 = (0.606099 \pm 0.000058) \times 10^{24}\\
a_1 - 2a_3 - 3a_5 + 3a_7 &\quad N(\lambda_g/\lambda_s)^3 = (0.606428 \pm 0.000061) \times 10^{24}\\
a_2 + 2a_3 + 3a_4 - 3a_7 &\quad N(\lambda_g/\lambda_s)^3 = (0.606145 \pm 0.000062) \times 10^{24}
\end{aligned}
$$

The least-squares solution is 0.606208 ± 0.000020 (the error is the standard deviation by internal consistency; it becomes 0.000050 by external consistency). We see that the solutions range from a high 0.606475 to a low of 0.606099, whereas the direct value (which is the most accurate solution of the set) is 0.606179 ± 0.000023. The second solution of the set is statistically as accurate as the direct measurement, yet the two values disagree by approximately 1.5 times the error of the difference. The failure of the standard deviation spread of the direct value to contain a single one of the set of the other (indirect) values, whereas one would expect it to contain on the order of half of them, is indicative of the type of discrepancy with which we are faced.

Straumanis is therefore correct in stating that the crystal density x-ray diffraction method gives the best single determination of N_s', although a least-squares adjusted value which is based on an evaluation of *all* the pertinent data is presumably more accurate still.

* Jointly supported by the Office of Naval Research and the U. S. Atomic Energy Commission.

[1] M. E. Straumanis, Phys. Rev. **92**, 1155 (1953).

[2] J. W. M. DuMond and E. R. Cohen, Revs. Modern Phys. **25**, 691 (1952).

[3] J. W. M. DuMond and E. R. Cohen, Phys. Rev. **94**, 1790 (1954), referred to as DC 54.

[4] M. E. Straumanis, Phys. Rev. **95**, 566 (1954).

[5] The quantity N_s' is a physical constant like N or e, whose value is to be determined by experiment, either directly or indirectly. It is to be distinguished from the number $N_s = 0.60594 \times 10^{24}$ (a specific numerical value) which was deduced by Siegbahn from the Faraday constant and the early (incorrect) "oil drop" value of the electron charge. Siegbahn used N_s as the value of Avogadro's number in a calculation which was originally intended to give the grating space of calcite in centimeters. This value is now regarded instead as *arbitrarily* establishing an *exact* value in x-units. The statement that the effective grating space of calcite for first-order reflection at 18°C is 3029.04 x-units defines this unit. Since Siegbahn's work, the values of the chemical atomic weights have changed slightly, and the perturbing effects of crystal purity have been pointed out by Straumanis and others; the experimental value N_s' is therefore no longer in agreement with the number N_s.

Domain Patterns on Rolled Single Crystal of Ni_3Fe

SŌSHIN CHIKAZUMI AND KENZŌ SUZUKI

Department of Physics and Chemistry, Gakushuin University, Mejiro, Tokyo, Japan

(Received October 4, 1954)

IT is well known that iron-nickel alloys acquire a strong magnetic anisotropy when they are cold-rolled.[1] Isoperm is a magnetic material prepared in this manner. Recently, Néel,[2] and independently Taniguchi and Yamamoto,[3] tried to interpret the origin of this anisotropy in terms of directional order[4] or an orientational superlattice. They supposed that such an arrangement of atoms may be induced by mechanical stresses, where plastic deformation may play a role in carrying the atoms to their equilibrium positions.

By studying this effect with single crystals of Ni_3Fe, we have obtained distinct domain patterns on the rolled crystal and here propose a new mechanism for the origin of the directional order.

Experimental results:

(1) Distinct domain patterns were obtained when the crystal was rolled in the (110) plane (Fig. 1). The direction of domain magnetization appears always along the $[1\bar{1}0]$ direction, irrespective of the rolling direction.

(2) The final shape of the specimen depends upon the rolling direction. In any case the preferred elongation takes place along the [001] direction. [Roll plane: (110).]

(3) Many slip bands were observed on the rolled surface, most of which are parallel to the $[1\bar{1}0]$ direction. [Roll plane: (110).]

(4) The magnitude of anisotropy increases at first almost proportionally to the rolling reduction. It reaches a maximum value of 2.5×10^5 ergs/cc at $r=70$ percent and decreases when rolled further. (Roll: (110), [001].) The specimen was previously annealed for 1 hour at 490°C.

(5) When the alloy is perfectly ordered, it develops the anisotropy more slowly. For instance, the anisotropy amounts to 1.2×10^5 ergs/cc at $r=70$ percent.

(6) Even when the specimen is quenched from 700°C, its anisotropy appears in just the same way as (4).

The following mechanism is proposed: When dislocations travel in the material in which short-range order exists, they may destroy the order between neighboring atomic planes which are parallel to the slip plane. The order, however, may not be altered in these atomic planes. If, therefore, the slip takes place at the same time along another slip plane, the order will remain only in the direction which is common to both the slip planes. This is a directionally ordered arrangement.

This idea is verified experimentally in several respects. When the crystal is rolled in the (110) plane, slip can take place exclusively in the (111) and $(11\bar{1})$ planes, for

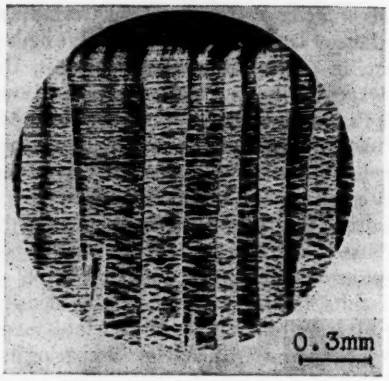

FIG. 1. Domain pattern on rolled (110) plate of Ni_3Fe. Edge of crystal is parallel to roll direction [001].

the other two equivalent planes are normal to the surface and slips in them will make no contribution in reducing the thickness. This is confirmed by (2) and (3). In this case, therefore, the order may remain only in the $[1\bar{1}0]$ direction, which is common to the (111) and $(11\bar{1})$ planes. Accordingly this may become the direction of easy magnetization. This agrees with (1).

In this mechanism, some degree of order is prerequisite. When, however, the order is perfect, the dislocation may travel in pairs so as to conserve the ordered state[5] and accordingly make less contribution in destroying the order. The result (5) may be interpretable along this line. Further, the experimental result (6) can be interpreted by assuming that the alloy does not completely lose its short-range order even when it is quenched from 700°C.

[1] G. W. Rathenau and J. L. Snoek, Physica **8**, 555 (1941).
[2] L. Néel, Compt. rend. **238**, 305 (1954); J. phys. radium **15**, 225 (1954).
[3] S. Taniguchi and M. Yamamoto, Sci. Repts. Research Inst. Tôhoku Univ. **A6**, 330 (1954).
[4] S. Chikazumi, J. Phys. Soc. Japan **5**, 327, 333 (1950); Phys. Rev. **85**, 918 (1952).
[5] J. C. Fisher, Acta Metallurgica **2**, 9 (1954).

Auxiliary Conditions in the Bohm-Pines Theory of the Electron Gas

E. N. ADAMS

Westinghouse Research Laboratories, East Pittsburgh, Pennsylvania

(Received November 1, 1954; revised manuscript received February 14, 1955)

BOHM and Pines[1] (BP), in their quantum theory of a hypothetical electron gas, described a procedure for completely solving the many-body Schrödinger equation, at least so far as the long-range part of the interelectron interaction is concerned. In carrying through their program, they met with a certain difficulty, *viz.*, that their equations required that any state

vector for describing a physically realizable state of the system must satisfy a number of auxiliary conditions of the form

$$(p_k-\Lambda_k)\psi\equiv\Omega_{-k}\psi=0, \quad (1)$$

whereas they were unable to find any simple way of ensuring compliance by state vectors which they constructed as approximations to state vectors for physical states. BP deferred any detailed treatment of this difficulty for a later publication, but gave arguments designed to show that their equations were substantially correct, even though their approximate wave functions failed to satisfy the auxiliary conditions (1). They apparently felt that a treatment which takes account of the auxiliary conditions would involve no really major modifications of the treatment which they have given.

We have studied the implications of the auxiliary conditions and have come to a different opinion. We conclude that, if consideration is restricted to the part of function space containing functions which satisfy the auxiliary conditions, there are no states for which the BP basic approximation is valid, even as a rough approximation. While we have reached the conclusion only after a detailed examination, we can describe the basis for our conclusion very simply. The fundamental approximation of BP is to neglect a term U in the Hamiltonian, given by

$$U=(2\pi e^2/m)\textstyle\sum_{k,\,l(k\neq l)}q_kq_l{}^+\sum_\mu\exp[i(k-l)\cdot x_\mu]. \quad (2)$$

The argument used to drop U assumed that (a) the sum of phase factors must give a small number since the electrons are rather evenly distributed and (b) the oscillators for which q_k, q_l are the quantized amplitudes are with high probability in their ground states, so that U is not large on account of the factor $q_kq_l{}^+$.

The assumption (b) can be proved incorrect for any physically realizable state, and it can be shown that U diverges quadratically for such a state. We first observe that every state can be written in the form

$$\psi=\exp(iS/\hbar)\chi, \quad (3)$$

where

$$S=\textstyle\sum_k q_k\Lambda_k. \quad (4)$$

Since the Λ_k are functions of the electron coordinates only, the condition that ψ satisfy the set of Eqs. (1) is that χ satisfy the equations

$$p_k\chi=0. \quad (5)$$

The set of solutions of (5) is just the set of all functions which are independent of q_k, and thus depend on the electron coordinates alone. Therefore all physically admissable states are of the form (3) with

$$\chi\equiv\chi(x_\mu).$$

It is now easy to see that the wave function for any physically admissible state is very different from an oscillator ground state wave function. The expectation value of $q_kq_k{}^+$ for the oscillator ground state is $(\hbar/2\omega)$, whereas the expectation value of $q_kq_k{}^+$ for the state (3) diverges quadratically. It can be verified that the manner of divergence of $\langle q_kq_k{}^+\rangle$ is precisely what we expect in a state for which p_k has a sharp value.

If the state (3) is expanded in the excitation number representation of the oscillator, it is found that when Λ_k is equal to zero, each state of excitation occurs with equal probability. For $\Lambda_k\neq0$ the average of the oscillator energy is

$$\hbar\omega\langle N_k+\tfrac{1}{2}\rangle=\tfrac{1}{2}|\Lambda_k|^2+\omega^2\langle q_k{}^2\rangle, \quad (6)$$

where $\langle q_k{}^2\rangle$ is exactly the same as it was for the state with $\Lambda_k=0$. While it is no longer true that each excitation state occurs with equal probability, Eq. (6) shows that the average excitation is actually greater still. We see that for states which satisfy Eq. (3), $\langle N_k\rangle$ always diverges at least as badly as though each excitation state were occupied with equal probability.

The existence of the aforementioned divergence shows that it is wrong to identify the q_k with the amplitudes of (physical) plasma oscillations, which would surely not be very highly excited. Thus in the original BP representation the true wave function must be in an essential way more complicated than BP supposed, and the true (finite) eigenvalue is the resultant of several actually infinite terms, of which U is one, the zero-order oscillator Hamiltonian another.

We believe that the fundamental physical idea of BP is a sound one, and that their work can lead to valuable insights into the electron gas problem. However, on the basis of the preceding discussion, we conclude that a proper founding of their theory on the many-body Schrödinger theory remains to be given.

The writer is grateful to Professor Gregor Wentzel for an illuminating discussion of this problem.

[1] D. Bohm and D. Pines, Phys. Rev. **92**, 609 (1953).

Attempt to Detect High Mobility Holes in Germanium Using the Drift Mobility Technique

N. J. Harrick

Philips Laboratories, Irvington on Hudson, New York

(Received March 24, 1955)

THE discovery of a second set of holes in germanium[1] has made it of interest to search carefully for an indication of their presence in the drift mobility experiment.[2] Such a search has been carried out at room temperature on n-type, 5 ohm-cm germanium. The sensitivity of the drift mobility technique has been improved by using alloyed indium dots as emitters and collectors rather than point contacts and by the use of a transverse magnetic field which served to concentrate the holes in the vicinity of the collector. Further gain

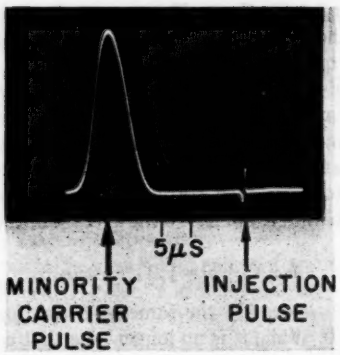

FIG. 1. Typical drift mobility trace for *n*-type germanium. The pulse on the left represents the arrival at the collector of the hole packet and the pulse on the right is caused by the injection pulse.

using a magnetic field was obtained when the emitter and collector were on opposite surfaces of the bar because the holes were then guided through the bulk of the germanium and the effects of surface recombination were thereby decreased. By thus increasing the sensitivity of the drift mobility experiment, many signals were observed which were attributable to phenomena other than a second set of holes. The areas of some of the secondary narrow pulses were as low as 0.02 percent of the main minority carrier pulse.

Figure 1 is a photograph of a typical drift mobility trace where the ohmic sweeping pulse has been balanced out. The width of the injection pulse which appears on the right, is about one-half of a microsecond. Note that some differentiation of the injection pulse occurs due to the capacitance of the junctions. The photograph was taken at an insufficient gain for the secondary signals to be visible.

There was no signal observed which could be attributed to a second set of holes. As an example of one observation where the drift time was 50 microseconds and the emitter-collector separation was 10.5 mm, an estimate for the sensitivity of detection of a signal from

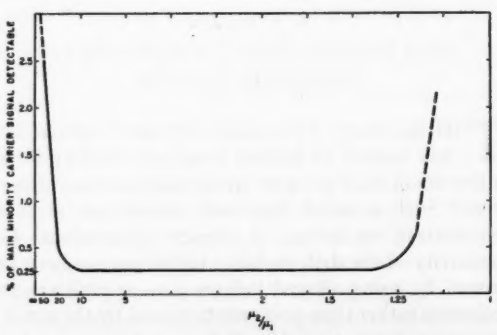

FIG. 2. Estimate of the magnitude of signals from holes of low mass which would have been observed had any been present.

holes of low mass assuming a line width comparable to that of the main minority carrier pulse is shown by the curve of Fig. 2. The abscissas are given in terms of mobility ratios and the ordinates represent signals as percentages of the main minority carrier pulse which could have been detected. Thus, over a mobility ratio range of 10 to 1.4, a signal of $\frac{1}{4}$ percent would have been observed; while at a mobility ratio of 50, 2.5 percent would have been observed. Careful observations were made for higher mobility ratios than those indicated by the curve in Fig. 2 and no signal was observed. The accuracy of observation was difficult to estimate in this case.

Measurements were made of the width of the hole packet, for a low injection level, to see if undue broadening occurs reflecting the possible presence of holes of low mass. The measured line widths *versus* drift time, for various emitter-collector separations, are plotted in

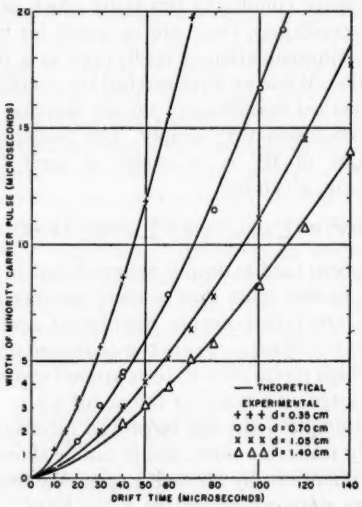
WIDTH OF MINORITY CARRIER PULSE (MICROSECONDS)
DRIFT TIME (MICROSECONDS)
0 10 20 30 40 50 60 80 100 120 140
0 1 2 3 4 5 10 15 20
THEORETICAL
EXPERIMENTAL
+ + + d = 0.35 cm
○ ○ ○ d = 0.70 cm
× × × d = 1.05 cm
△ △ △ d = 1.40 cm

FIG. 3. Plot of the half-width of the minority carrier pulse at half-amplitude *versus* drift time for *n*-type germanium.

Fig. 3 where the solid curves represent the theoretical relation

$$\Delta t_{\frac{1}{2}} = 1.66 D^{\frac{1}{2}} t_d^{\frac{1}{2}}/d.$$

Here $\Delta t_{\frac{1}{2}}$ is one-half of the time width of the packet at half-amplitude, D is the ambipolar diffusion constant of the added minority carriers, t_d is the drift time, and d is the emitter-collector separation. This relation is readily derived from Brooks' formula[3] describing the motion in a filament of an injected pulse of carriers, originally infinitesimally narrow, subject to drift, diffusion, and recombination. As may be seen in Fig. 3, there is excellent agreement between experiment and theory. An additional point of interest is the slight asymmetry in the minority carrier pulse which may be seen in Fig. 1. This asymmetry may be accounted for on the

basis of carrier loss by recombination which, for large pulse widths, is not negligible over the time spread of the packet. Thus these measurements on the observed minority carrier pulse can be adequately accounted for in terms of a single set of holes.

Holes of high mobility have not been detected by utilizing the more sensitive drift mobility technique. This, however, does not imply that they do not exist.

The author wishes to thank the members of the Transistor Group at Philips Laboratories for their assistance in preparing the samples and Mr. T. R. Kohler for help with the circuitry. He is indebted to Dr. P. H. Dowling, Dr. F. K. du Pré, and Dr. E. S. Rittner for critical discussions and helpful suggestions.

[1] Dresselhaus, Kip, and Kittel, Phys. Rev. **92**, 827 (1953).
[2] J. R. Haynes and W. Shockley, Phys. Rev. **81**, 835 (1951).
[3] Harvey Brooks, Phys. Rev. **90**, 336(A) (1953).

Voltage-Dependence of Electroluminescent Brightness. I. Dielectric-Imbedded Phosphors

F. A. Schwertz, J. J. Mazenko, and E. R. Michalik
Mellon Institute, Pittsburgh, Pennsylvania*
(Received March 4, 1955)

THE brightness of seven different electroluminescent phosphors has been measured as a function of voltage and frequency. The measurements were made on conventional test cells in which the dielectric-imbedded phosphor is sandwiched between a transparent, conducting electrode (on glass) and a vacuum-deposited aluminum electrode. The electrode spacing was about 60 microns in all cases, and the electrode area about 8 cm². The space between the electrodes was filled by a uniformly distributed suspension of phosphor in plasticized polyvinyl chloride, the phosphor occupying about 30 percent of the total volume.

For all phosphors, the root mean square of the alternating voltage, V, and the time average of the electroluminescent brightness, L, conformed quite accurately to the equation

$$L=aV\exp(-b/V^{\frac{1}{2}}), \qquad (1)$$

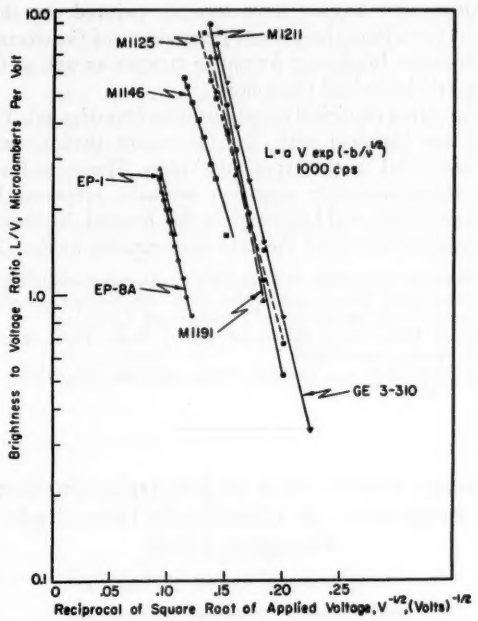

FIG. 1. Voltage dependence of electroluminescent brightness.

where a and b are arbitrary parameters. This statement is affirmed, for example, by the data depicted in Fig. 1, where a plot of $\ln(L/V)$ *versus* $(1/V^{\frac{1}{2}})$ yields straight lines in agreement with the above equation.

The values of the parameters a and b are listed in Table I. These data indicate that a increases linearly with the frequency; however, a few of the phosphors show saturation effects in the neighborhood of 1000 cycles per second. The parameter, b, on the other hand, is independent of the frequency; furthermore, all values of b lie in the limited range from 30 to 45 (volts)$^{\frac{1}{2}}$.

The linear dependence of the parameter a on the frequency indicates that it is proportional to the available number of optically active centers. Accordingly $(1/e)$ of the optically active centers are excited when $V=b^2$. The most desirable phosphors are therefore characterized by large values of a and small values of b.

TABLE I. a and b values in the range 60–1000 cps.

Phosphor number	Phosphor type	a, microlamberts per volt				b, (volt)$^{\frac{1}{2}}$			
		60 cps	360 cps	750 cps	1000 cps	60 cps	360 cps	750 cps	1000 cps
M 1191[a]	Zn(Al)S:Cu	78.7	742	1240	1760	35.5	40.3	39.8	41.1
M 1125[a]	ZnS:Cu	64.2	301	647	734	30.3	34.1	35.7	35.0
M 1211[a]	ZnS:Cu	352	2110	3090	3140	41.9	44.8	44.5	43.6
GE 3-310[a]	ZnS(Se):Cu	60.4	438	1290	1709	31.5	34.8	38.3	39.0
M 1146[a]	ZnS:(Cu, Mn)	44.1	132	166	207	32.0	32.6	31.0	31.7
EP-1[b]	ZnS:(Cu, Pb)	7.9	51.3	88.4	92.9	38.0	40.9	39.9	38.5
EP-8*A*[b]	ZnS:Cu	12.7	43.8	70.8	89.7	39.8	39.2	38.5	39.0

[a] These phosphors were kindly supplied by Dr. H. C. Froelich of the General Electric Company, Cleveland, Ohio.
[b] Phosphors purchased from Derby & Company Ltd., London, England.

Alfrey and Taylor[1] have recently pointed out that Eq. (1) describes the voltage dependence of the electroluminescent brightness for single crystals as well as for dielectric-imbedded phosphors.

Two other empirical equations were investigated. The first was identical with Eq. (1) except that $V^{\frac{1}{2}}$ was replaced by V in the exponential term. The second was the three-parameter equation recently proposed by Howard, Ivey, and Lehmann[2] in this Journal. Neither of these equations fitted the data as accurately as Eq. (1).

* Multiple Fellowship on Computer Components sustained by the Electronics Directorate of the U. S. Air Force Cambridge Research Center, Research and Development Command.

[1] G. F. Alfrey and J. B. Taylor, Brit. J. Appl. Phys. Supplement No. 4, p. S44 (1955).

[2] Howard, Ivey, and Lehmann, Phys. Rev. **96**, 799 (1954).

Voltage Dependence of Electroluminescent Brightness. II. Chemically Deposited Phosphor Films

F. A. Schwertz and R. E. Freund

Mellon Institute, Pittsburgh, Pennsylvania*

(Received March 4, 1955)

THE voltage dependence of the brightness of an electroluminescent ZnS:Mn film prepared according to the method of Studer, Cusano, and Young[1] and Halsted and Koller[2] has been examined at 60 cps and found to conform to the empirical equation[3]

$$L = aV \exp(-b/V^{\frac{1}{2}}). \quad (1)$$

This statement is supported by the data shown in Fig. 1, where the logarithm of (L/V) is plotted against $(1/V^{\frac{1}{2}})$. As predicted by Eq. (1), the data so represented yield a straight line.

It now appears that any electroluminescent light source (at least of the ZnS class), be it of the single crystal,[4] chemically deposited, or dielectric-imbedded[3] phosphor type, displays the voltage dependence of electroluminescent brightness predicted by Eq. (1).

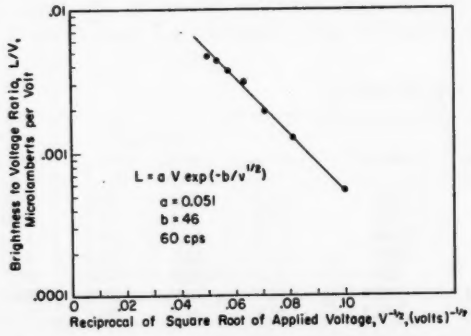

FIG. 1. Brightness-voltage characteristics for chemically deposited electroluminescent ZnS:Mn film.

A number of the chemically deposited ZnS:Mn films prepared in this Laboratory have also exhibited dc electroluminescence.

* Multiple Fellowship on Computer Components sustained by the Electronics Directorate of the U. S. Air Force Cambridge Research Center, Research and Development Command.

[1] Studer, Cusano, and Young, J. Opt. Soc. Am. **41**, 559 (1951).

[2] R. E. Halsted and L. R. Koller, Phys. Rev. **93**, 349 (1954).

[3] See accompanying Letter for definition of symbols [Schwertz, Mazenko, and Michalik, Phys.Rev. **98**, 1132 (1955)].

[4] Data of W. W. Piper and F. E. Williams, Brit. J. Appl. Phys., Supplement No. 4, p. S45 (1955).

Ring Diffusion as the Mechanism of Self-Diffusion in Germanium

Sumner Mayburg

Physics Laboratory, Sylvania Electric Products, Inc., Bayside, New York

(Received April 1, 1955)

PORTNOY, Letaw, and Slifkin[1] have measured the self-diffusion of germanium and found that it is given by the relation

$$D_{\text{self Ge}} = 7.8e^{-68\,500/RT} \text{ cm}^2/\text{sec}. \quad (1)$$

Previously we had measured the number of vacancies and interstitials[2] quenched into a germanium sample when the sample is radiation-cooled from temperatures near the melting point. From these quenching experiments, we deduce that the equilibrium defects are Frenkel defects with a concentration given by the equation

$$n_e/N = 6.7e^{-46\,100/RT}. \quad (2)$$

Furthermore, we have evidence[3] that the interstitial is more mobile than the vacancy, at least at temperatures below 585°C. If we were to conclude that self-diffusion in germanium is determined by interstitial diffusion, the diffusion constant for interstitials is

$$D_i = \frac{D_{\text{self}}}{(n_e/N)} = D_0 e^{-E/RT} = 1.2e^{-(22\,400)/RT} \text{ cm}^2/\text{sec}. \quad (3)$$

Zener[3] has shown that the D_0 for interstitial diffusion should be much less than 1 cm^2/sec. Fuller *et al.*[4] estimated D_0 for interstitial copper in germanium to be 0.00019 using Zener's theory. If we use Zener's theory to calculate D_0 for interstitial Ge in Ge, we find $D_0 \sim 0.001$.[4] The large D_0 in Eq. (3) raises a doubt that self-diffusion in germanium is really by interstitial diffusion.

There is a stronger argument against diffusion by a defect mechanism in germanium. From the diffusion constant for germanium interstitials it is simple to calculate the jump time, τ, for interstitials from the random walk equation[4]

$$D_i = 4a^2/6\tau, \quad (4)$$

where a, the jump distance between interstitial positions, is 2.4 A. Since the jump time as a function of temperature is known, the number of jumps, J, an interstitial might take during the quenching of a germanium sample from high temperature is given by the expression

$$J=\int\frac{dt}{\tau}\equiv\int\frac{dT}{\tau}\frac{dt}{dT}. \tag{5}$$

The cooling rate during the quenching process is governed by the radiation law. Therefore,

$$\frac{dT}{dt}=\left(\frac{dT}{dt}\right)_Q\frac{T^4}{T_Q{}^4}, \tag{6}$$

where T_Q is the temperature near the melting point from which the sample is quenched and $(dT/dt)_Q$ is determined at the temperature near the melting point by measuring the power required to maintain the sample at that temperature.

By use of Eqs. (3), (4), and (6), Eq. (5) yields

$$J=-\frac{3}{2}\frac{D_0}{a^2}T_Q{}^4\left(\frac{dt}{dT}\right)_Q\int_{T_Q}^{300^\circ\mathrm{K}}e^{-E/RT}\frac{dT}{T^4},$$

where $T_Q\sim1200^\circ$K and $(dT/dt)_Q\sim-100^\circ$K/sec for the particular samples used in our quenching experiments. The result is that $J=2\times10^{12}$.

Thus, the total number of jumps that an interstitial can take during the quenching process is 10^{12}. This is an extremely high number of jumps; so high in fact that it is impossible to see how we could have quenched in any vacancies or interstitials during the quenching process. From Eq. (2) we see that there is at most one vacancy and interstitial in 10^8 atoms in a quenched sample. If the interstitials jump 10^{12} times during the quenching process, interstitials will have had occasion to jump close to vacancies and recombine with them. Therefore, it is impossible to envision how we are able to observe any concentration at all of quenched-in Frenkel defects.

If we had assumed that the vacancies were more mobile, and hence the mechanism of self-diffusion was vacancy diffusion, then the number of jumps which a vacancy would undergo in the cooling process would be about the same as the number of jumps calculated above for interstitials. In this case we would have also been led to the conclusion that no defects could be quenched into the sample.

A simple way of explaining the anomaly is to invoke ring diffusion as the mechanism for the self-diffusion in germanium. Zener[5] has studied ring diffusion extensively in copper and has shown that the simultaneous interchange of several atoms in a ring requires less energy than the direct interchange of two atoms. The complexity of the covalent bonding in germanium makes it difficult to estimate the activation energy of ring diffusion for comparison with experiment. However, since all atoms of the crystal can participate in ring diffusion, the atomic jump rates required for ring diffusion to explain the self-diffusion are slower by a factor of 10^8 than the jump rates of the defects if a defect mechanism were the correct mechanism of self-diffusion.

Another piece of evidence against defect diffusion explaining the self-diffusion comes from the work of Brown, Fletcher, and Wright[6] who studied the annealing of bombardment damage in germanium. They find that the activation energy for the fastest-moving defect is 41 600 cal/mole. If we combine this energy of motion with the activation energy for production of defects, Eq. (2), we find the activation energy for self-diffusion by a defect mechanism to be 87 700 cal/mole which is 30 percent higher than the measured energy of self-diffusion.

[1] Portnoy, Letaw, and Slifkin, Bull. Am. Phys. Soc. **30**, No. 2, 13 (1955).
[2] S. Mayburg, Phys. Rev. **95**, 38 (1954).
[3] C. Zener, J. Appl. Phys. **22**, 373 (1951).
[4] Fuller, Struthers, Ditzenberger, and Wolfstern, Phys. Rev. **93**, 1182 (1954).
[5] C. Zener, Acta Cryst. **3**, 346 (1950).
[6] Brown, Fletcher, and Wright, Phys. Rev. **92**, 592 (1953).

Thermal Bleaching of Color Centers

A. Halperin and A. Braner
Department of Physics, The Hebrew University, Jerusalem, Israel
(Received March 21, 1955)

RECENTLY Hesketh and Schneider[1] have reported results of observations on the thermal bleaching of F-centers in KCl crystals colored by x-rays. Their bleaching curves showed peaks at about 170°K, which they have interpreted as due to a large scale restoration of F-centers. It was later suggested by Halperin and Garlick[2] that these absorption peaks, as well as similar peaks which appear on warming other crystals from low temperatures, are caused by vapor films which condense on the surfaces of the crystals.

We have now been able to eliminate completely these peaks by introducing an efficient liquid-air trap into the

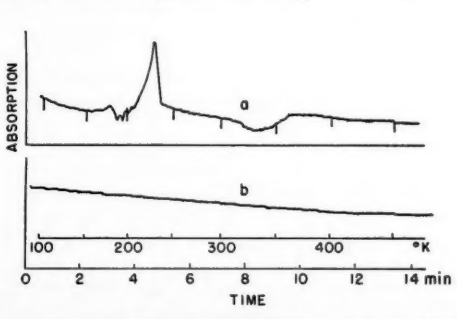

FIG. 1. Absorption of an uncolored KCl crystal on warming from 90°K: (a) showing the effects of condensed vapor films; (b) showing elimination of these effects by an effective trap.

evacuated cryostat near the crystal. Thus it was proved definitely that the peaks are due to condensed films and should not be related in any way to the color centers in the crystal.

The effect of this trap is illustrated in Fig. 1, which is a photocopy of two independent records of the absorption of an uncolored KCl crystal *vs* temperature, on warming the crystal from 90°K to about 500°K. Curve *a* was obtained with the aforementioned trap made ineffective by keeping it at room temperature. It shows the peaks due to condensed vapor films. The main peak at about 225°K corresponds to about 20 percent absorption in this case. (The small regular marks to the lower side of the curve are temperature indictions from 100 to 450°K, every 50°K.)

Curve *b* shows the results of the same measurement repeated but this time with the trap kept at 90°K during warming. No traces are now left of the peaks which appeared in curve *a*. The small slope in the curve seems to be due to a slight increase in the transparency of the crystal with increase in temperature.

The undisturbed curve of the thermal bleaching of *F*-centers in a KCl crystal colored by x-rays at 90°K was now measured with the new arrangement. The trap was kept at 90°K during the time of x-irradiation and during warming after the irradiation, when the absorption of the crystal at 5500 A was continuously recorded as function of time of warming. The rate of heating was kept nearly constant (about 25 deg/min for the range 120–600°K) by suitable adjustment of the power of the heater. A plot of the optical density *vs* temperature, as obtained from this record is given in Fig. 2. No restoration of *F*-centers takes place. The shape of the curve, however, shows that the trapped electrons leave the *F*-centers mainly at several fixed temperature regions, which indicates the existence of several activation energies. These measurements were repeated several times and found to be reproducible. Hesketh and Schneider claim that in their measurements the "peaks" appeared only after *F*-irradiation at 90°K before warming. To check this, a crystal colored at 90°K was partially bleached optically by *F*-light before warming. However, the thermal bleaching curve obtained in this case was essentially the same as in Fig. 2.

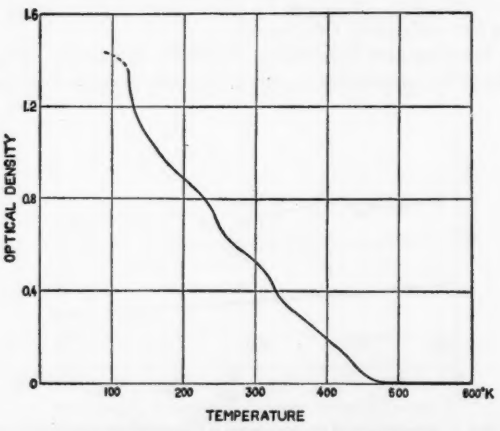

FIG. 2. Thermal bleaching curve of *F*-centers in a colored KCl crystal.

The thermoluminescence of the same crystal colored similarly by x-rays at 90°K was also measured; once with a phototube sensitive in the ultraviolet-blue region as detector, and then with one of maximum sensitivity at about 9000 A. Several luminescence peaks were recorded in these measurements and were found to fit well the temperatures at which *F*-centers are released, as obtained from Fig. 2. Thus, with the "blue" detector the main thermoluminescence peaks were at 220°K and 315°K (in addition to a few minor peaks). With the "red" detector a strong peak was obtained at 450°K and minor peaks at 220 and 350°K.

The existence of several activation energies for *F*-centers in KCl crystals was already reported from thermoluminescence experiments[3,4] and from "current glow curves."[5] The temperatures of the peaks correspond fairly well to those obtained in the present work.

Investigation is being carried on and a fuller account will be published later.

[1] R. V. Hesketh and E. E. Schneider, Phys. Rev. **94**, 494 (1954).
[2] A. Halperin and G. F. J. Garlick, Phys. Rev. **95**, 1098 (1954).
[3] J. A. Ghormley and H. A. Levy, J. Phys. Chem. **56**, 548 (1952).
[4] J. Sharma, Phys. Rev. **85**, 692 (1952).
[5] D. Dutton and R. J. Maurer, Phys. Rev. **90**, 126 (1953).

Dislocation Relaxations at Low Temperatures and the Determination of the Limiting Shearing Stress of a Metal

W. P. MASON
Bell Telephone Laboratories, Murray Hill, New Jersey
(Received March 7, 1955)

RECENTLY, Bordoni[1] has measured attenuation peaks at low temperatures in lead, aluminum, copper, and silver which indicate relaxation effects. Measurements of Bömmel[2] on lead single crystals whose Q^{-1} values are shown by Fig. 1 verify that this is a relaxation effect. Plotting the log of the frequency against the inverse of the absolute temperature, Fig. 2, one determines an activation energy U of 790 calories per mole with a constant $C=2.9\times10^9$ in the equation $\omega_0=Ce^{-U/RT}$.

It is shown that the values obtained agree with a displacement of a dislocation from a minimum energy position in a close-packed glide plane by one atomic spacing against the limiting shearing stress of the crystal. The model considered is one used by Koehler.[3] Dislocations are tied down at irregular intervals by impurity atoms, giving loops of average length l.

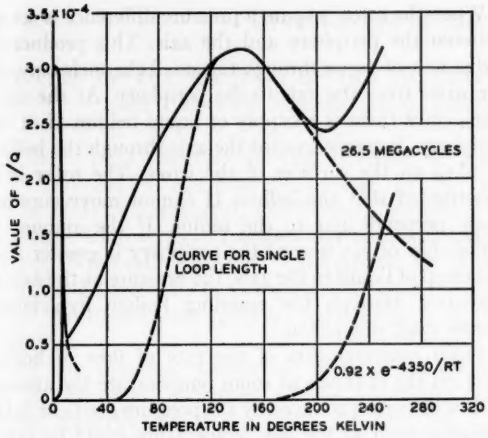

FIG. 1. Internal friction for single-crystal lead at 26.5 Mc/sec. Dot-dash line, theoretical curve for one loop length. Dashed curve —high-temperature attenuation due to breakaways.

Thermal agitation causes loops to be displaced to adjacent minimum energy positions against the limiting shearing stress and the force to stretch dislocations. The model, Fig. 3(b), is a straight section connected to the pinning points by "kinks." Direct calculations show that the model results in the potential well arrangement of Fig. 3(c), with the energies

$$H=(T_{13})_0 b^2 l/\pi; \quad A=2b^3[(T_{13})_0\mu/2\pi]^{\frac{1}{2}} \text{ in ergs}, \quad (1)$$

where b is the atomic spacing along the glide plane, l the average loop length, μ the shear elastic constant along the glide plane, and $(T_{13})_0$ the limiting shearing stress. From reaction rate theory, one can show that there is a

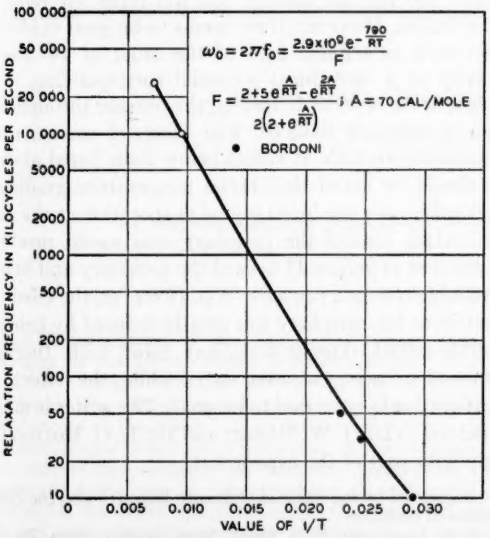

FIG. 2. Semilogarithmic plot of f_0 *versus* $1/T$.

TABLE I. Ratio of limiting shearing stress to elastic shear moduli for four face-centered metals.

Metal	Temp. of max. atten.	Act. energy $H-A$ in cal/mole	b in cm $\times10^8$	μ dynes/cm²	$(T_{13})_0$ dynes/cm²	$(T_{13})_0/\mu$
Pb	35°K	790	3.5	7.0×10^{10}	3.9×10^5	5.5×10^{-6}
Cu	85°K	1910	2.55	4.6×10^{11}	1.75×10^6	3.8×10^{-6}
Al	100°K	2260	2.86	2.5×10^{11}	1.6×10^6	6.4×10^{-6}
Ag	70°K	1580	2.88	2.7×10^{11}	1.1×10^6	4.1×10^{-6}

relaxation having a Q^{-1} given by

$$\frac{1}{Q}=\frac{2e^{-A/RT}}{1+2e^{-A/RT}}\left[\frac{N_0(1-p)b^4l^2\mu}{kT}\right]\left[\frac{\omega/\omega_0}{1+(\omega/\omega_0)^2}\right], \quad (2)$$

where $\omega_0=Ce^{-(H-A)/RT}$, N_0 is the number of loops per cc, and p the percentage of the total loop covered by one "kink." C is 2π times the frequency that the dislocation attacks the barrier H. This should be comparable to the resonant frequency of a dislocation in the potential well given by

$$C=2\pi f=(1/b)[(T_{13})_0/\rho]^{\frac{1}{2}}, \quad (3)$$

which is within a factor of 2.5 of C determined experimentally.

A single-sized loop results in an attenuation curve shown by the dot-dash line of Fig. 1. A distribution of lengths centered around the mean value gives the form of the measured curve. Numerically, using the high temperature attenuation of Fig. 1,

$$l\doteq4\times10^{-4};$$
$$N_0 l=\text{number of dislocations per sq cm}\doteq4\times10^6. \quad (4)$$

Table I shows the limiting shearing stress determined from the four measurements of Bordoni using the activation energy determined here for lead, and Eq. (1) for $(H-A)$.

The higher-temperature attenuation whose equation is shown by Fig. 1 results from the temporary unpinning of the pinned points. This allows mechanical energy to interchange between loops and makes the mechanical energy abstracted from the vibration by the loops incoherent. It is readily shown that this results in a loss independent of frequency equal to

$$1/Q=[2(T_{13})_0/\mu]^{\frac{1}{2}}N_0 l b V_s e^{-U/RT}/2\pi, \quad (5)$$

where $N_0e^{-U/RT}$ is the number of unpinned dislocation loops per cc and V_s the shear velocity. Using $N_0l=4$

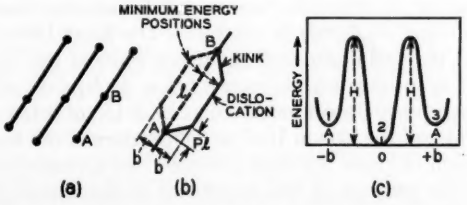

FIG. 3. Proposed model for dislocation relaxation.

$\times 10^6$, $U=4350$ cal/mole, $V_s=8\times 10^4$ cm/sec, a good agreement is obtained with the data. 4350 cal/mole is in good agreement with the binding energy of an impurity atom,[4]

$$U=\tfrac{2}{3}[(1+\sigma)/(1-\sigma)]\mu b^3\epsilon \text{ ergs}, \quad (6)$$

where σ is Poisson's ratio and $\epsilon=(r'-r)/r$ represents the increase in radius of the impurity atom over the normal atom.

It is a pleasure to acknowledge a number of helpful discussions with W. T. Read on dislocation theory.

[1] P. C. Bordoni, J. Acoust. Soc. Am. **26**, 495–503 (1954).
[2] H. E. Bömmel, Phys. Rev. **96**, 220–221 (1954).
[3] C. Zener, *Theory of Diffusion, Imperfections in Nearly Perfect Crystals* (John Wiley and Sons, Inc., New York, 1952), Chap. 7.
[4] See A. H. Cottrell, *Dislocations and Plastic Flow in Crystals* (Oxford University Press, London, 1953), p. 57.

Effect of a Centrifugal Field upon the Rate of Transfer through a Helium II Film*

J. W. Beams
University of Virginia, Charlottesville, Virginia
(Received March 28, 1955)

THE rate of transfer of liquid in helium II films over surfaces is believed[1] to be slightly dependent upon the difference in height between the two levels of liquid helium II. This effect should be greatly magnified if the helium II film is acted upon by a centrifugal field which can be made many times larger than the gravitational field of the earth. An attempt has been made to investigate this effect by observing the transfer through a helium II film creeping from the periphery to the axis in a spinning rotor. The results, while complicated by rotor heating, are believed to be of sufficient interest to report at this time.

The rotor is spun on the lower end of a 60-cm long stainless steel 0.08-cm i.d. thin-walled hypodermic needle tube by an air turbine situated above the apparatus. The rotor contains two radial tubes tightly packed with radial one-mil nichrome wires and is so constructed that the only connection between the axis and periphery is through the channels between the wires. The rotor is surrounded by two concentric cylindrical Dewar flasks. The outer Dewar contains liquid nitrogen, while the inner contains liquid helium. The inner one is so arranged that it can be evacuated. A measured amount of helium slightly above atmospheric pressure is admitted through the hypodermic needle shaft and condenses in the rotor. The inner Dewar is next pumped down until the temperature of the liquid helium surrounding the rotor is below the lambda point. The rotor is always immersed at least 15 cm below the surface of the helium II. The temperature of the liquid helium II inside the rotor is determined approximately by the pressure at the upper end of the hypodermic needle shaft.

When the rotor is spun, a pressure difference is set up between the periphery and the axis. This produces a radial flow of vapor through the small channels between the wires from the axis to the periphery. At the same time, since there is a supply of liquid helium II at the periphery, it creeps toward the axis through the helium II films on the surfaces of the wires. The rotor is so constructed that the helium II cannot move continuously perpendicular to the radius. If the amount of radial flow of gas toward the periphery is greater than the creep of liquid to the axis, the pressure at the axis as measured through the spinning hollow hypodermic needle shaft should fall.

From measurements of the rate of flow of helium through the channels at room temperature the amount of flow of vapor produced by the pressure gradient in the spinning rotor at the low temperature could be calculated. Also the amount of transfer of helium II over the surfaces of the small wires to the axis could be reliably estimated when the rotor was not spinning. It was found that when the rotor (3.5 cm i.d. and 4.45 cm o.d.) was quickly accelerated to a speed between 100 and 140 rps, the pressure at the axis first dropped and then started rising. At these rotor speeds, the mass transfer through the helium II film to the axis should be over 10 times that of the gas flowing from the axis to periphery through the channels, provided that the amount transferred through the film was independent of the centrifugal field. Therefore, the drop in pressure at the axis indicated that the rate of transfer through the helium II film was reduced by the centrifugal field. The later rise in pressure was shown to be due to the heating of the rotor by surface friction produced by the surrounding helium II. At rotor speeds very much below 100 rps the calculated pressure drops produced by the centrifugal fields were too small to measure with precision, while above 140 rps the heating was too rapid for reliable observation. However, there seems to be good evidence that in a centrifugal field of the order of 10^3 times gravity or a centrifugal potential corresponding to a height of the order of 10 meters, the transfer through the film is definitely reduced. The effect, of course, may become appreciable at values below those listed above. It should be noted that radial temperature gradients inside the rotor produced say by evaporation at the axis or heating around the periphery also would produce radial flow of helium II toward the periphery and hence possibly produce a pressure drop. However, the effect of heating at the periphery was greatly reduced by using a double-walled (Dewar-flask-like) rotor with thermal connection near the axis only, while the effect of evaporation is estimated to be small. The writer is much indebted to Dr. J. W. Stewart and Dr. L. G. Hoxton for help with part of the experiment.

* Supported by the Office of Ordnance Research and the Navy Bureau of Ordnance.
[1] J. G. Daunt and R. S. Smith, Revs. Modern Phys. **26**, 172 (1954).

Proceedings of the American Physical Society

Minutes of the Meeting of the Division of Fluid Dynamics Held at Old Point Comfort and Langley Aeronautical Laboratory, Virginia, November 22–24, 1954

THE 1954 Meeting of the Division of Fluid Dynamics was held November 22, 23, and 24 in Hotel Chamberlin, Old Point Comfort, Fort Monroe, Virginia, and Langley Aeronautical Laboratory, National Advisory Committee for Aeronautics, Langley Field, Virginia. About a hundred fifty members and guests participated in the meeting.

At the opening session on Monday afternoon, F. N. Frenkiel, chairman of the Division, made some remarks on the present meaning of fluid dynamics and then introduced H. J. E. Reid, director of the Langley Aeronautical Laboratory, who welcomed the participants. After the opening session, three scientific sessions were held in Hotel Chamberlin and a fourth one, on Wednesday morning, was held at the Langley Aeronautical Laboratory. During these sessions, four invited papers and twenty-three contributed papers were presented. The banquet of the Division was followed by an after-dinner address given by H. L. Dryden, director of the National Advisory Committee for Aeronautics and past chairman of the Division of Fluid Dynamics. Informal discussions and contacts between the participants, which are the main characteristic of the divisional meetings, appeared to be most profitable.

A visit to the Langley Field Gas Dynamics Laboratory followed the regular sessions. The participants were received by M. C. Ellis, Jr., head of the Gas Dynamics Branch, who summarized the research activity of the Gas Dynamics Laboratory. The most recent research contributions to fluid dynamics and some of the future plans were described by several members of the National Advisory Committee for Aeronautics staff: P. W. Huber described some unsteady-flow research and a theory for predicting the flow of real gases in shock tubes was discussed by R. L. Trimpi. R. V. Hess talked on the interaction of a shock with a heated boundary layer. W. H. Michael, Jr., discussed some supersonic flow studies on flat-plate delta wings, and G. P. Wood described experimental investigations of supersonic flow around lifting symmetrical double-wedge airfoils. Some studies on the applications of a transient technique to heat-transfer measurements of blunt bodies were reported by I. E. Beckwith, and experiments relating to the use of the thermal decomposition of nitrous oxide in hypersonic wind tunnels were described by A. P. Sabol. A discussion and exchange of views between the visiting participants and the scientific staff of the Langley Aeronautical Laboratory followed.

The local organizing committee, headed by John Stack, was largely responsible for a very interesting and pleasant meeting. The programme of the 1954 meeting of the Division including the abstracts of contributed papers follows.

François N. Frenkiel
Applied Physics Laboratory
The Johns Hopkins University
Silver Spring, Maryland

Aerodynamics (Including Transonic and Supersonic Flow)

(Adolph Busemann, presiding)

Invited Paper

A1. Physical Concepts Relating to Transonic Wind Tunnels. Ray H. Wright, *Langley Aeronautical Laboratory.* (30 min.)

Contributed Papers

A2. Determination of the Transonic Pressure Drag on Wedges by the Throat Station Method.* Robert Wesley Truitt, *Virginia Polytechnic Institute* (introduced by R. A. Alpher).—The throat station concept of Tsien and Fejer, combined with the principle of stationarity of the local Mach number, is used to find the pressure drag on the front face of a two-dimensional wedge in the transonic speed range. The pressure distribution is determined by the Karman-Tsien method in the entire subcritical range; the pressure distribution at the critical Mach number establishes the location of the throat station at the wedge shoulder. The local Mach number distribution, corresponding to the critical Mach number, remains constant with any further increase in the subsonic free-stream Mach number. Then, by the principle of stationarity, the local Mach number distribution remains stationary in the supersonic range if the detached shock is normal. The method is applied to the theoretical incompressible pressure distribution of a simple two-dimensional wedge up to the critical Mach number. The constant p_L/p^* distribution, corresponding to the critical Mach number, is used in the Maccoll-Codd method to determine the pressure drag coefficient in the transonic range ($-0.69 \leqq \xi_0 \leqq 1.1$). The

results of the present method are presented in transonic similarity form and compared with existing theoretical and experimental results. The agreement of the present method with other findings is good.

* This work has been supported by the U. S. Air Force, Air Research and Development Command.

A3. Minimum Drag Bodies of Revolution in a Nonuniform Supersonic Flow Field. CONRAD RENNEMANN, JR., *NACA Langley Aeronautical Laboratory* (introduced by H. L. Dryden).—The aerodynamic characteristics of airplanes designed for supersonic flight speeds are influenced by the interference effects between the various components of the configuration. One of the simpler problems involving interference effects is the determination of the shape of satellite bodies, such as external fuel tanks, for low wave drag. For problems of this type the interference pressure field can be approximately represented by a disturbance to a uniform pressure field. An expression for the wave drag of a slender body of revolution in such a flow has been derived on the basis of linear theory. Using this equation, the minimum drag body of revolution in nonuniform flow was determined by standard variational procedures for the isoperimetric conditions of given volume and length. The resulting body shape is a Sears-Haack body of revolution plus a correction term dependent on the nonuniformity of the flow field considered. A sample calculation is presented for the minimum drag body of revolution of given volume and length located in the flow field of a parabolic body of revolution.

A4. Mach Number and Yaw Angle Determination for Conical Flow Regimes Using Two Surface-Flow Angle Indicators.* H. S. SICINSKI AND H. F. SCHULTE, *University of Michigan.*—In the search for principles applicable to measuring upper air environments (i.e., temperature, density, wind vectors, etc.) from supersonic missiles in the regions above 30 kilometers altitude, it became evident that knowledge of the angle of surface flow on a right circular cone coupled with body-coordinate rotational parameters would permit calculation of the free stream Mach number and the yaw angle. An instrumentation was developed for measuring the surface flow angle utilizing a rectangular metal plate $\frac{3}{4}\times\frac{1}{8}\times 0.003$ inches driving a capacitive transducer. The electronic version of the instrument requires a minimum force of 60 dynes at the plate's center of pressure for accurate alignment with the stream. Correlation of the theory with experiment was provided in a series of wind tunnel experiments with the subsequent realization that the vane angle as measured by an external optical system would provide a reliable "Machmeter" for wind tunnel instrumentations, particularly low density tunnels where conventional Pitot tubes become complicated by having to measure very low pressures. Such an optical transducer for the vane angle would require a lower actuating force than the electronic version of the instrument. (However the electronic version is better suited to recording dynamic conditions such as encountered in free flights.) The discussion will concern the governing relations, the solution of the resulting transcendental equations, experimental results, and the possible applications.

* The research reported in this paper has been sponsored by the Geophysics Research Directorate of the Air Force Cambridge Research Center, Air Research and Development Command.

A5. Laminar Free Convection from a Vertical Surface for Prescribed Variations of (1) Wall Heat Transfer Rate, or (2) of Wall Temperature. E. M. SPARROW, *NACA Lewis Flight Propulsion Laboratory* (introduced by S. L. Simon).—Laminar free convection from a vertical plate with nonuniform thermal conditions at the surface is studied. Prescribed variations have been considered for (1) the wall heat transfer rate and (2) the wall temperature. The flow is taken to be of the boundary layer type. The problem of determining the temperature and velocity profiles in the boundary layer is formulated by the Kármán-Pohlhausen method. The solution of the resulting equations is achieved by expansion of the dependent variables in Maclaurin series in terms of ξ, the parameter by which the nonuniform surface thermal condition is specified. The first five terms of these series have been computed. Formulas are presented for calculating the heat transfer moduli for fluids in the Prandtl number range 0.01 to 1000. These formulas contain truncated series. The magnitude of the truncation error has been estimated wherever possible. Results for the important special case of uniform wall heat transfer rate are given.

Shock Waves

(G. N. Patterson, presiding)

Invited Paper

B1. Determination of Flows behind Stationary and Pseudo-Stationary Shocks. A. H. TAUB, *University of Illinois.* (30 min.)

Contributed Papers

B2. Difference Solution of Shock Diffraction Problem. H. F. LUDLOFF AND M. B. FRIEDMAN, *New York University.*—The time dependent, nonlinear equations of motion and the appropriate boundary condition have been formulated, in order to obtain a solution describing reflection and diffraction of a strong shock from an arbitrary corner. A difference procedure was used, which had the following characteristics: Although the problem is conical, the equations are formulated in x-, y-, t-coordinates, in which they are hyperbolic. The equations are written in "divergence form." The difference form of the equations supplies automatically a certain amount of viscosity which is necessary for the creation of new entropy values. The developing field has been computed by means of the IBM 701. The results of the compression produced by the shock at the corner can be seen from the plot of the isopycnics at three subsequent time cycles $t=3$, 19, 87, and are in satisfactory agreement with the interferograms. The way in which the machine evolves the final field, guided by the hyperbolic equations of motion, corresponds to the actual happenings in nature, except for an artificial slowdown of the sequence of events.

B3. Vortex Created by a Shock Passing over a Vertical Wall.* DAVID L. MATTHEWS, *Princeton University* (introduced by Walker Bleakney).—Interferograms and shadowgrams are shown, depicting the conditions near a sharp vertical wedge of 5° angle, after a weak shock has been incident normally. Over a wide time interval the configuration remains similar to itself. The density distribution is compared with the theory described by Howard in the paper which follows. The effect of

varying shock strength is shown, and there are other interesting features.

* This work has been supported by the Office of Naval Research.

B4. On the Vortices Produced by Shocks.* LOUIS N. HOWARD, *Princeton University* (introduced by Walker Bleakney).—Assuming isentropic flow, it is possible to formulate a relatively simple theory of a symmetrical pseudo-stationary vortex—like motion in a gas. After making certain approximations, one can solve the equations and find the density and velocity fields. The density is approximately given (for $\gamma=7/5$) by

$$\rho=\rho_0[1+(r/r_0)^{\mu}]^{5/2},$$

where r_0 and μ are constants and r is the radial pseudo-stationary coordinate. This is in quite good agreement with experiments on the vortices produced in the diffraction of a shock striking a wedge.

* This work has been supported by the Office of Naval Research.

Invited Paper

B5. Approach to Equilibrium Ionization Following Strong Shock Waves in Argon. ARTHUR KANTROWITZ AND HARRY PETSCHECK, *Cornell University* (30 min.)

Contributed Papers (continued)

B6. Pressure Variation in Shock Tube Flow.* RAYMOND J. EMRICH AND ROBERT L. PETERSON, *Lehigh University.*—The elementary, idealized theory of flow in the shock tube predicts a region of constant pressure between the shock and the tail of the rarefaction. While several workers have observed deviations from this idealized behavior, the deviations have not been reported in the literature, probably because the response of individual gauge elements is not sufficiently well understood. Measurements have been made with a piezoelectric and a mechanical gauge mounted next to each other and recording the same flow by essentially different electronic procedures. These separate indications agree sufficiently to demonstrate that the pressure continues to rise with time after the jump associated with shock passage. With an initial pressure ratio of 10 across the diaphragm and using nitrogen throughout, a pressure rise to twice the jump across the shock was recorded during the first 30 msec after shock passage. This pressure rise, observed at 85 tube diameters from the diaphragm, was recorded before the arrival of any reflected wave. A shock would travel 450 tube diameters in an endless tube during this time. So large a pressure rise would not be expected during flow times ordinarily used in shock tube studies.

* Supported by the Office of Naval Research.

B7. Schlieren Studies of the Flow Behind Strong Shocks.* W. SMITH, H. GLICK, A. HERTZBERG, AND W. SQUIRE, *Cornell Aeronautical Laboratory, Inc., Buffalo, New York.*—A modified Beams-type spark of approximately 10^{-7} sec duration is used for schlieren studies of the flow of air or argon behind a strong shock wave ($5<M<15$). The flow Mach number, density, and speed of sound behind the moving shock are measured by examining the wave pattern produced by small perturbations at the flow boundary. Agreement with theoretical calculations is good. A relaxation region is indicated by a density gradient immediately behind a strong shock and by the perturbation-wave pattern. Preliminary measurements indicate a relaxation time of the order of 10^{-5} sec. Luminosity studies of the flow illustrate the high degree of luminosity which occurs in the boundary layer. Sharply defined boundary-layer transition is observed in the flow at a Reynolds number of the order of 5×10^{6}. Also pictured are multiple, similarly directed, strong shock waves in various stages of interaction.

* This work was sponsored by the U. S. Air Force under contract.

B8. Refraction of Shock Waves at a Gaseous Interface.* ROBERT G. JAHN, *Princeton University* (introducted by Walker Bleakney).—Parallel-fringe interferograms have been obtained of the refraction patterns produced by shock waves of strength $\xi=0.85$ and $\xi=0.30$, impinging on boundaries between air $-CO_2$ and air $-CH_4$. The observed patterns agree well with the Polachek and Seeger theory of regular refraction [Phys. Rev. **84**, 922 (1951)]. In addition to verifying the qualitative predictions of the theory, such as the existence of certain limiting angles and the nature of the reflected wave for various initial conditions, the experiments yield values for the reflected wave strength and the angle of the refracted wave which are in agreement with Polachek and Seeger's numerical calculations of these quantities. Experiments performed at angles of incidence greater than the limiting angles of the theory produce "irregular" refraction patterns of considerable interest and complexity. The experimental technique involves a special 1-in. wide test section for the main shock tube, which holds a rotable cylindrical cell, in which the two gases of interest are separated by a Zapon film $<10^{-5}$ cm thick. The refraction process is observed to be quite sensitive to the purity of the gases involved, thereby suggesting a possible method for the measurement of the γ of the gas.

* This work was supported in part by the Office of Naval Research.

Fluid Dynamics (Including Turbulence)

(G. B. Schubauer, presiding)

Invited Paper

C1. Structure of the Solutions of the Navier-Stokes Equation for the High and Low Reynolds Numbers. P. LAGERSTROM, *California Institute of Technology.* (30 min.)

Contributed Papers

C2. An Experimental Study of Shock Wave Turbulence Interaction.* LESLIE S. G. KOVASZNAY, *The Johns Hopkins University* (introduced by Francis H. Clauser).—Small perturbation theory indicates[1] that fluctuations in a compressible, viscous, heat-conductive medium have three distinct "modes": vorticity mode (turbulence); pressure mode (sound waves);

entropy mode (temperature spottiness). As long as each of these fields is weak, there is no interaction between them within the fluid away from solid boundaries. When one or more of the three modes is intense, nonlinear interaction takes place and energy is converted from one mode into another. Weak turbulence passing through a stationary strong shock wave has been treated theoretically by Ribner.[2,3] A simple experiment was carried out by the author in a supersonic wind tunnel. An axisymmetric turbulent wake was produced by a cylindrical body and a wedge created a strong oblique shock wave. The resulting flow field was explored by a hot-wire anemometer and the detailed fluctuation fields have been studied in the light of existing theories.

* This work was performed under the joint sponsorship of U. S. Navy Bureau of Ordnance and Project SQUID.
[1] L. S. G. Kovasznay, J. Aeronaut. Sci. **20**, 657 (1953).
[2] H. S. Ribner, Natl. Advisory Comm. Aeronaut. Tech. Notes 2864 (1953).
[3] H. S. Ribner, Natl. Advisory Comm. Aeronaut. Tech. Notes 3255 (1954).

C3. On the Production of Vorticity in Isotropic Turbulence. R. BETCHOV, *The George Washington University.*—The mean rate of production of vorticity in isotropic, homogeneous, and incompressible turbulence is proportional to a nondimensional factor S defined as a mean cube of the normalized local acceleration. Measurements with various methods of producing turbulence and various Reynolds numbers confirmed the earlier results of Townsend: $S=0.4$. At every point and instant we can define the 3 eigenvalues a, b, c, and the 3 eigenvectors of the strain tensor $(\partial U_i/\partial x_j)+(\partial U_j/\partial x_i)$. Let us choose $a^2 \geq b^2 \geq c^2$ and let L, M, N be the vorticity components along the principal axes. Then one can demonstrate: $-\langle abc\rangle = \langle aL^2+bM^2+cN^2\rangle = \alpha S$ where $\langle\ \rangle$ indicates the average and α is constant. Furthermore, we have $-0.7 \leq S \leq 0.7$ and the limit is reached if $b=c=-a/2$. If we assume that abc is always negative and if we properly randomize a, we obtain $S=0.44$. This indicates that the flow has, in the average, the configuration of a jet impinging on an obstacle and forming an elliptical sheet. The vorticity is nearly perpendicular to this jet. It is amplified by the radial stretching action of the sheet and it tends to deflect the jet away from the obstacle.

C4. On the Relations Between One- and Three-Dimensional Functions in Isotropic Turbulence and the Direct Measurement of Energy Transfer Function. FRANCIS R. HAMA, *University of Maryland* (introduced by F. N. Frenkiel).—In the study of turbulence, one can only measure one-dimensional quantities directly, in spite of the physical importance of three-dimensional ones, such as spectrum and transfer function. In order to obtain the three-dimensional functions, one has to differentiate twice the one-dimensional functions with respect to the wave number. The purpose of this paper is to give first the relations in which a single differentiation is sufficient, so that the experimental error might be considerably reduced. Second, an instrument which measures a spectral equivalent of double correlation between any two fluctuating quantities and which is particularly suitable for the direct measurement of the energy transfer function is proposed.

C5. Measurements of Velocity and Temperature Fluctuations Behind a Hot Grid.* S. CORRSIN, A. L. KISTLER, AND V. O'BRIEN, *The Johns Hopkins University.*—The longitudinal velocity and temperature correlations in the (approximately) isotropic fields downstream of a heated grid are roughly the same. Far downstream, the temperature fluctuations die out slower than the velocity fluctuations, as predicted by simple theoretical conditions.[1] The triple mixed correlation function, $[\langle u_1\theta_1\theta_2\rangle_M/(\langle u^2\rangle_M)^{\frac{1}{2}}\langle\theta^2\rangle_M]$ occurring in the temperature correlation equation is of the same order as the triple velocity correlation function.

* Supported by the National Advisory Committee for Aeronautics.
[1] S. Corrsin, J. Aeronaut. Sci. **18**, 417 (1951).

C6. Momentum Transfer and Heat Diffusion in the Mixing of Coaxial Turbulent Jets. Y. V. G. ACHARYA,* *Laboratorium voor Aero-en Hydro-dynamica der Technische Hoogeschool, Delft* (introduced by S. Corrsin).—Mean velocity and temperature measurements were carried out in coaxial turbulent jets.[1] The profiles at the various sections were reduced to a common profile, and it was found that irrespective of the ratio of the velocities of the primary and secondary streams, the reduced profiles could be represented by one Gaussian curve for the velocity and another for the temperature. An analysis of some of the turbulence theories indicated that the best theory, which was applicable to such profiles, was Prandtl's theory of a constant mixing coefficient[2] ε across a normal section, where $\varepsilon=Kb(U_{\max}-U_{\min})$. Using momentum and heat equations, formulas were derived to determine the value of K from the experimental data, for the case of momentum transfer and a similar coefficient EK, for the case of heat diffusion. The main conclusions of the investigation are: (a) the value of K increases, along the axis of the flow, with the distance from the nozzle exit of the primary stream. It also increases with the absolute value of the difference in velocities between the primary and secondary streams; (b) EK behaves in a manner similar to K; and (c) E is dependent on the various characteristics of the flow and is not always greater than unity, as it is found to be in the case of free jets.[3]

* Now at the Department of Aeronautics, The Johns Hopkins University.
[1] Y. V. G. Acharya, doctoral dissertation. The library of The Technical University, Delft, Holland.
[2] L. Prandtl, ZAAM **22**, 241 (1942).
[3] W. Szablawski, Natl. Advisory Comm. Aeronaut., Tech. Mem. 1288 (1950).

C7. Equilibrium Turbulent Flow in a Slightly Divergent Channel.* J. R. RUETENIK† AND S. CORRSIN, *The Johns Hopkins University.*—Hot-wire measurements have been made of some mean flow and turbulence properties of fully developed, plane diffuser flow at a divergence half-angle of 1°. Comparison with parallel wall channel flow at the same Reynolds number shows large increases in turbulent energy level and average shear level, some reduction in skin friction and in mean velocity ratio near the walls.

* Supported by the Office of Naval Research.
† Now at the Massachusetts Institute of Technology.

C8. The Stability of Vortex Streets with Consideration of the Diffusion of the Vorticity of the Individual Vortices. ULRICH DOMM AND HERMANN FOETTINGER, *Fluid Dynamics Institute Technical University, West Berlin* (introduced by J. R. Weske).—An investigation is presented of the stability of straight twin-row vortex streets with staggered arrangements of real vortices of equal age, whose vorticity diffuses into the ambient fluid. The velocity distribution of the vortex field is introduced by the Rayleigh relation for the azimuthal component

$$V_\varphi=(\Gamma_0/2\pi r)[1-\exp(-r^2/4\nu t)].$$

The equations of motion are established for displacements of the vortex centers which are small compared with the pitch of the street, such that linearization is permissible. Stability characteristics are derived by analysis of the properties of the resulting matrices. The results show that, for the stable arrangement, the ratio of centerline width h and pitch l of the vortex sheet is a function of the nondimensional time $\tau=4\nu t/l^2$. For vanishing viscosity ν and also for time t approaching zero, the width-pitch ratio has the value computed by von Kármán: $K=h/l=0.281$.

Banquet Of the Division Of Fluid Dynamics

(Clark B. Millikan, presiding)

Invited Paper

D1. Fifty Years of Boundary Layer Theory and Experiment. HUGH L. DRYDEN, *National Advisory Committee for Aeronautics.*

Fluid Dynamics (Including Boundary Layer)

(Stanley Corrsin presiding)

Contributed Papers

E1. Motion in the Boundary Layer Over a Flat Plate with a Sudden Change of Speed. C. C. LIN,* *Massachusetts Institute of Technology.*—Solutions of problems of unsteady motion in the boundary layer often deal with cases of impulsive start, uniformly accelerated motion, or some special situations of periodic motion. The problem under consideration deals with the response of an existing steady basic flow to a sudden change in the free stream. By the introduction of suitable combination of the variables, the problem is reduced to one involving two independent variables. The earlier part of the motion has been worked out in full. The settlement of the motion into a new Blasius regime is examined somewhat more extensively than that done by Stewartson.[1]

* This work is done while the writer is on a sabbatical leave from Massachusetts Institute of Technology with a Guggenheim Fellowship working at the Graduate School of Aeronautical Engineering at Cornell University. It is partly sponsored by the Office of Naval Research.

[1] Stewartson, Quart. J. Mech. Appl. Math. 4, 182 (1951).

E2. Thermal Expansion and Aerodynamic Stability of Open Flames. HANS M. CASSEL, *U. S. Bureau of Mines, Pittsburgh.*—In a simplified treatment of flame stability the one-dimensional relation $U_b/U_u = D_u/D_b = \epsilon$ (where U is velocity, D is density, and subscripts u and b refer to unburned and burned masses) is replaced by the assumption of isotropic expansion. Therefore the continuity equation becomes: $UD^{\frac{1}{3}} = U_u D_u^{\frac{1}{3}}$. Streamlines rising through a horizontal plane flame are considered as diverging conically, forming angles α with the normal to the flame front. The radial velocity component U_R rises from zero to $U_m = S_u \epsilon^{\frac{1}{3}} \sin\alpha$ (where S_u is burning velocity) over the thickness of the flame L. Owing to viscosity η, this velocity gradient sets up a shearing force, parallel to the flame front, acting upon any circular segment in radial direction: $f = 2\pi\eta\epsilon^{\frac{1}{3}} S_u \int_0^R R \sin\alpha dR/L$. The tendency to stretch the flame front is opposed by the flame surface tension, whose existence follows from the curvature dependence of the burning velocity, and is given by $\sigma = 2S_u k\epsilon^{\frac{1}{3}}(\epsilon^{\frac{1}{3}}-1)c_p$, where k is thermal conductivity and c_p specific heat. The balance of forces f and σ determines the maximum radius a stable flat flame may attain: $R_m = 4L(\epsilon^{\frac{1}{3}}-1)\epsilon^{\frac{1}{3}}/\gamma$ with $\gamma = c_p/c_v$. This is of the same order of magnitude as cellular flame radii derived from different arguments by Markstein.[1] In a qualitative way the present picture checks with experience to the same extent as Markstein's theory.

[1] Fourth Symposium (International) on Combustion, Baltimore, p. 47 (1953).

E3. Diffusion Analogy for Shocks Interacting with Thermal Boundary Layers.* WAYLAND GRIFFITH AND WALKER BLEAKNEY, *Princeton University.*—Experiments have been performed in the Princeton shock tube on the interaction of a plane shock wave with a layer of variable gas concentration as an analogy to a very hot thermal layer. Previous experiments in which a heated plate was slid into the test section just before arrival of the shock have established the validity of a linearized theory for small amounts of heating.[1] One of the authors (W. B.) suggested that many of the experimental difficulties involved in studying very hot layers and strong shocks could be sidestepped by letting a light gas with a high velocity of sound diffuse through the surface into the adjacent air. Helium leaking through a large number of holes drilled in a solid plate serves to create a layer in which the local sound speed is more than double that in air, corresponding to a thermal layer of 1200°K. Hess[2] has pointed out that above certain limits the steady interaction expected, and observed, thus far should be replaced by one in which a bubble of nearly stagnant air accumulates behind the compression. The formation of such a bubble, observed with a Mach-Zehnder interferometer, will be described.

* This work has been supported by the Office of Naval Research.

[1] W. Griffith, *Interaction of a Shock Wave with a Thermal Boundary Layer* (to be published).

[2] R. V. Hess, private communication.

E4. Transverse Curvature Effect in Compressible Axially Symmetric Laminar Boundary Layer Flow.* RONALD F. PROBSTEIN AND DAVID ELLIOTT, *Brown University and Princeton University* (introduced by F. N. Frenkiel).—The viscous transverse curvature effect in compressible axially symmetric laminar boundary layer flow has been investigated, and it is found that it is characterized by the parameter Δ/r_0 which is essentially the ratio of the boundary layer thickness to the body radius. It is shown that the Busemann and Crocco integrals of the two-dimensional energy equation for $Pr=1$, are still valid for axially symmetric flow in which the transverse curvature effects are considered. By a generalization of Mangler's transformation, the boundary layer equations are reduced to an almost two-dimensional form, making the analysis simpler for two asymptotic flow regions characterized by $\Delta/r_0 \gg 1$ and Δ/r_0 less than or of the order of unity. It is with the latter region that the present paper is primarily concerned, and for this case it is shown that the additional term in the momentum and energy equations which differentiates them from the two-dimensional form behaves like an axial pressure gradient. Asymptotic solutions can be found for (1) the velocity and temperature distributions for the compressible zero pressure gradient case when the body shapes are given by $r_0 = ax^n$ and $r_0 = ae^{bz}$, and (2) the velocity distribution for incompressible flow with an external velocity of the form $u_e = bx^m$ past a body given by $r_0 = ax^n$. The zeroth approximation is the Mangler result. It is also shown that similar exact solutions exist whenever $2n+m=1$ is identically satisfied. In the case of the cone and cylinder with zero pressure gradient where the equations have been numerically integrated for $Pr=1$, the first-order correction to the Mangler

formulation shows that the effect on both the skin friction and heat transfer coefficients can become appreciable.

* This work has been supported by the Office of Naval Research and Office of Scientific Research of the U. S. Air Force.

E5. Study of the Behavior of the Boundary Layer in the Region of Transition from Laminar to Turbulent Flows. JEROME PERSH, *U. S. Naval Ordnance Laboratory* (introduced by Eva M. Winkler).—A study has been conducted of a large amount of boundary layer velocity profile data in the region of transition from laminar to turbulent flow. These data have been collected from a number of experimental investigations of boundary layer flows on flat plates, hollow cylinder models, and airfoils in both incompressible and compressible flows. As a result of this study, a new criterion for determining the beginning of transition is proposed. This criterion is dependent on the variation in the transition region of a parameter which defines the profile shape. It is shown that transition region boundary layer velocity profiles form a single parameter family of curves which differ in shape from turbulent boundary layer velocity profiles, particularly in the region near the wall.

E6. Unsteady Viscous Flow in the Vicinity of a Stagnation Point. N. ROTT, *Cornell University* (introduced by A. Kantrowitz).—Consider viscous incompressible "stagnation-point" flow, two- or three-dimensional, in the infinite half-space. Let the limiting plane perform rigid translatory oscillations, in any direction in its plane, while the flow at infinity remains steady. The corresponding unsteady boundary layer is found as an exact solution of the Navier-Stokes equations. The solution joins smoothly the quasi-steady behavior at low frequencies with the Stokes-Rayleigh type of flow at high frequencies. It is characteristic of the unsteady part of the solution that its velocity component perpendicular to the wall is zero. Thus, it leaves the development of the steady part of the "stagnation-point" boundary layer unaffected; it also has no influence on the heat transfer, if the wall temperature is constant. If the wall is at rest and the free stream oscillates[1] the behavior of the flow is quite different; solutions with harmonic time dependence can be found only to a linearized approximation.

[1] M. J. Lighthill, Proc. Roy. Soc. (London) **A224** (1954).

E7. Internal Finite Gravity Waves in a Stratified Fluid.* ROBERT R. LONG, *Civil Engineering Department, The Johns Hopkins University* (introduced by S. Corrsin).—A discussion is given of the steady-state flow of a fluid with a certain basic density and velocity distribution over a finite obstacle. The type of motion depends primarily on an "internal" Froude number F_i. If this number exceeds a certain critical value, a steady flow exists and resembles potential motion. If F_i is very small, no solution exists unless the obstacle is very small. For intermediate values of F_i, a steady state ceases to be possible when the obstacle exceeds a certain height. If the height is moderate the solution exists, but instability is indicated. An experimental investigation reveals very close agreement when the steady flow exists theoretically. Nonexistence is associated with a progressive alteration of the upstream distribution of velocity and density, and the instability is manifested by the development of turbulent eddies over the barrier and downstream.

* Supported by the U. S. Weather Bureau.

MINUTES OF THE 1955 ANNUAL MEETING HELD AT NEW YORK CITY, JANUARY 27–29, 1955

(Corresponding to *Bulletin of the American Physical Society*, Volume 30, No. 1)

THE 1955 Annual Meeting of the American Physical Society was notable in being the first Annual Meeting ever held in New York City but not in the buildings of Columbia University. We had our scientific sessions in the Hotel New Yorker, the Hotel McAlpin, Manhattan Center, and Vanderbilt Hall of the Washington Square Campus of New York University. This dispersion of our sessions was regrettable but inevitable at this our first "hotel" meeting in New York; we hope to be able to concentrate them better in years to come. Not all of the halls were adequate, but one had the impression from a very slight sampling that our members, by an large, were not dissatisfied with the downtown locale, imposed on us by the fact that our meetings are now too large for our generous former host to receive. The arrangements for this meeting were initiated by Wallace Waterfall of the American Institute of Physics, and completed and mainly conducted by S. A. Korff, to whom we owe an enormous debt of gratitude. Among his collaborators were Arthur Beiser, Morris Shamos, M. W. Zemansky; Mrs. M. A. Lee, and many others of the staff of the American Institute of Physics who served at the registration; and Mrs. S. A. Korff and Mrs. Mariette Kuper, to whom the ladies of the meeting are indebted for a lavish programme of entertainment which they arranged.

The registration at this meeting was 1987. As usual, we do not know how this should be distributed between our Society and the American Association of Physics Teachers, nor do we know how many omitted to register (nor at the moment of this writing do we know whether the registration fees of those who did register sufficed to cover the costs of the meeting). The registration was lower by about 5 percent than that of the previous Annual Meeting, but the number of contributed papers (330) was about ten percent higher; yet the Annual Meeting remains inferior to the Washington meeting in this regard. Our divisions of Electron Physics and of Fluid Dynamics provided symposia. The retiring Presidential Address of H. A. Bethe—"Pi-Mesons and Nucleons"—was given in the great theatre of Manhattan Center, so that for the first time in several years no one had to be turned away from this ceremony.

The Banquet of the Society and the AAPT was held on the Friday evening in the Grand Ballroom of the Hotel New Yorker. The Oliver E. Buckley

Solid-State Physics Prize was conferred on LeRoy Apker. H. D. Smyth was the after-dinner speaker, and the evening was concluded with a delightful film-and-speech presentation of the 1954 expedition up the Himalayan peak known as K-2, by George Bell who is both mountain climber and member of the Society. The attendance was 377. It is always regretted that those who speak at our Annual Meeting banquet must lose so many of their potential audience to the other attractions of New York.

The Business Meeting of the Society was held on the Friday morning at nine in Vanderbilt Hall. At this meeting were formally announced the names of those Fellows of the Society who had just been elected to office and were to commence their terms the day after. R. T. Birge became President at the end of the meeting; E. P. Wigner became Vice-President; F. Seitz and A. M. Weinberg entered upon four-year terms on the Council; G. J. Dienes, R. G. Herb, K. G. McKay, J. R. Pellam, L. Tonks, G. Wentzel, E. M. McMillan, and J. W. M. DuMond entered upon three-year terms on the Board of Editors, the first six of these being assigned to *The Physical Review* and the last two to *Reviews of Modern Physics*. K. K. Darrow and G. B. Pegram were re-elected Secretary and Treasurer, respectively, and S. A. Goudsmit continues as Managing Editor.

The Council had met on the previous Wednesday afternoon. It elected to Membership 191 candidates and to Fellowship 6 candidates; their names are appended. It chose a Nominating Committee consisting of H. A. Bethe (Chairman), Harvey Brooks, S. A. Goudsmit, S. A. Korff, R. E. Marshak, Leona Marshall, W. A. Nierenberg, G. B. B. M. Sutherland, and L. S. Taylor; this committee is to convene at the Washington meeting. It nominated H. A. Bethe and H. D. Smyth to three-year terms on the Governing Board of the American Institute of Physics (they have subsequently been elected by the member Societies at the Annual Meeting of the Institute). The question whether to split *The Physical Review* (see the back cover page of our New York Bulletin) was deferred to the Washington meeting.

Elected to Fellowship: R. A. Charpie, C. L. Cowan, Jr.,* David Feldman, R. D. Huntoon, J. R. MacDonald, D. J. Montgomery.

Elected to membership: *Norman Manvel Abramson, Rex G. Alexander, Elizabeth Dux Anderson, Norman C. Anderson, Andre Jean Bassompierre, *Boris William Batterman, *Henry S. Belson, *August Gehard Berger, Jr., George Harold Bloom, *Gregory Louis Boisvert, *Donald Lee Bowers, *Arnold Sander Boxer, John Brunn, *Solomon J. Buchsbaum, *Murray Bullis, Ronald E. Burgess, *Gerald Burns, *Chris D. Calsoyas, *Arnold Jules Cantor, *Donald Cohen, *George Rolland Cole, Franklyn M. Collins, John Charles Connor, John Michael Coogan, Henry Howland Crapo, *Robert Kyran Curran, *Peter Cziffra, *William Paul Dumke, John Robert Eklundi *Jassim Mohammed El-Hussaini, *Guy Trask Emery, Shinj, Endo, *Julius W. Enig, *Albert R. Erwin, Jr., *Rafael Fessel, Vincent Carmine Forte, H. P. R. Frederikse, Robert Elmer Freund, Arnold Marvin Friedman, Charles Geoffrey Blythe Garrett, *Solomon Gartenhaus, Tino Gaumann, Charles James Goebel, Stanley Arthur Golden, Martin Goldstein, John B. Goodenough, *Oscar Wallace Greenberg, Suraj N. Gupta, Gunter Hagen, Bernard George Harvey, *Yoshio Hashimoto, *Theodore Higier, *Henry Allen Hill, *John Feynman Hirshberg, *Jay Leonard Hirshfield, *Kazuo Hisatake, John Peter Hobson, Charles Stanley Hollander, *Louis Philip Howland, Dennis Howard Howling, Sister M. Ignatia, Tsutumu Imamura, Everett Byron Ireland, Jr., Bernard Jacobs, *Robert George Jahn, *Charles P. Jamieson, *Theodore Paul Janusz, Harald C. Jensen, *Hugh Freeborn Johnston, *John Paul Jones, Peter Kafalas, *Sheldon Lee Kahalas, Tadashi Kaneno, *David M. Kaplan, *Louis Katz, *Terence James Kennett, Vahe Keshishian, Robert James Keyes, *Roger P. Kohin, Jan Korringa, *George Donald Kramer, Stanley Kronenberg, *Peter Dale Kunz, *Chris E. Kuyatt, *Alfred Landman, *Jay T. Last, Bernard Mathew Leadon, Ernest Anton Lederer, *Robert Weir Lee, Harris Benjamin Levy, Robert Humphrey Lewis, *Andrew David Liehr, *Norman E. Linson, *James Duane Livingston, *Donald C. Lorents, *William Alfred Love, Frances Lytle Lummis, Kenneth Robert MacKenzie, Robert Smith Macmillan, Theodore Harold Maiman, James Merrill Martin, John Alfred Martin, Chester Charles McCabe, Alice Lorena McCrea, Leon Robert McNarry, Hans W. Meissner, Norman Menyuk, Louis Meyerhoff, *Salvatore Milani, Sidney N. Milford, Charles Fredric Miller, Jr., Gottfried Irving Moller, *Alfred James Morency, Susumu Morita, Preston Perry Morris, Jr., Erwin Wilhelm Mueller, Karl Alex Muller, Tuvia Nadel, Salwa C. Nassar, Marcus Howard Norwood, Rudolf Hans Nussbaum, *Donald Eugene O'Reilly, *William John O'Sullivan, James Donald Ozzello, Thomas Oliver Passell, *Brian David Pate, *George Theodore Paulissen, *Douglas Campbell Pearce, Victor Paul Peterson, Heinz Gerhard Pfeiffer, *William Lewis Pillinger, John Worth Pitzenberger, Ralph Edward Pixley, *Lee Girard Pondrom, Boris Pregel, *Glen Anderson Rebka, Jr., *Howard Robert Reiss, *Henry Leopold Richter, Jr., Oswald Paul Riedel, *Marion Colburn Rinehart, Edwin Kirk Roberts, *Leonard Sidney Rodberg, George Allendorph Rogers, *Gerald Morris Rothberg, *John Lynn Russell, Jr., Aaron Perry Sanders, *Alden Robert Sayers, *Paul Otto Schissel, Christof Schmelzer, George William Series, Koichi Shimoda, *Rex Hawkins Shudde, *Geoffrey Gay Shute, *George Andrew Sinnott, Stanley Carl Skirvin, Jack Coss Slattery, Richard Pearson Smith, *Herman Hershel Smotrich, *Power Bunmei Sogo, Alfred H. Sommer, *George Baugh Spence, *Glenn Howard Spencer, Jr., *Ralph Edward Stajdohar, Stanley Sterling Strong, Robert W. Swain, *Donald Adolph Swenson, John Joseph Taylor, Richard Edward Taylor, Chan Mou Tchen, Hans H. Theissing, Ronald F. Tucker, William Eric Tucker, *Frank Turkot, *Walter Vali, *Charles Colburn Vogler, Oscar Roger Vogt, James Vollmer, *Roger Hilburn Walmsley, Julian Wallace Webster, Herman Harry Wieder, William Charles Wiley, *George Abiah Williams, III, William Stanley Cossom Williams, *John Herbert Wood, *Walter H. Wurster, *Taketora Yamagata, *Leonard Yarmus, *Ernest Arthur Young, Jr., *Russell Dawson Young, Clayton Donald Zerby, *Robert C. Ziegler.

*—Student.

KARL K. DARROW, *Secretary*,
American Physical Society
Columbia University
New York 27, New York

Errata Pertaining to Abstracts B6, C3, C7, E10, G2, HA10, RA14, S9, S10, and V9

B6, by P. M. Stier, C. F. Barnett, R. A. Howard, and W. Bugg. The fifth and sixth sentences should be combined to read: The present results join smoothly the curves obtained[1] at higher energies and for hydrogen as the target gas, the agreement with the results of Whittier[2] is excellent.

C3, by E. L. Jossem and L. G. Parratt. In lines 7, 16, 20, and 23, instead of β_5 read β^{VI}.

C7, by B. E. K. Alter and C. W. Curtis. A footnote should be added to the title, reading: Work supported in part by the Office of Ordnance Research, U. S. Army.

E10, by R. M. Sternheimer. In lines 11 and 13, instead of *A*1 read aluminum.

G2, by M. G. Inghram. The byline should read *University of Chicago and Argonne National Laboratory.*

HA10, by R. C. Block and H. W. Newson. In line 9, the value 229 should be deleted.

RA14, by A. Rubin, F. Ajzenberg, and J. B. Reynolds. In the title, instead of P^{13}, read P^{31}. In line 9, instead of S^{21}, read P^{31}.

S9, by S. Raboy, T. B. Novey, and V. E. Krohn. In line 10, instead of $A_2=0.14\pm0.03$ and $\lambda_2=(14\pm3)\times10^6$, read $A_2=-0.18\pm0.02$ and $\lambda_2=(19\pm3)\times10^6$.

S10, by V. E. Krohn, T. B. Novey, and S. Raboy. In the last line, instead of $+0.8\pm0.2$, read $+1.4\pm0.2$.

V9, by L. J. Neuringer. In line 14, instead of $\sim2\times10^{-4}$ ev/°C, read 0.7×10^{-4} ev/°C. In line 16, instead of $-2.3\sim\times10^{-4}$ ev/°C, read -3.7×10^{-5} ev/°C.

PROGRAMME

THURSDAY MORNING AT 10:00

Manhattan Center, Masonic Room

(W. W. HAVENS, JR., presiding)

Neutron Physics, I

A1. Neutron Inelastic Scattering. JANET B. GUERNSEY,* AND A. WATTENBERG, *M. I. T.*—Low-energy gamma-rays (between 100 and 350 kev) have been observed from the inelastic scattering of neutrons by several heavy nuclides. The Rockefeller electrostatic generator was used as a source of neutrons from 0.2 to 2 Mev, from the reaction $H^3(p,n)$. A ten-channel analyzer and a thin NaI(Tl) crystal were used as the detecting system. The crystal thickness was determined experimentally to minimize neutron background effects and retain sufficient resolution for the detection of the gamma rays. Yield curves will be presented for the following elements: tantalum, platinum, gold, hafnium.

* On leave from Wellesley College.

A2. Gamma Radiation from Interaction of 4.4 Mev Neutrons with Fe^{54} and Fe^{56}.* ROLF M. SINCLAIR, *Westinghouse Research Laboratories.*—A 32-gram scatterer enriched to 35 percent Fe^{54} was bombarded with 4.4-Mev neutrons, and the resultant gamma radiation detected with a NaI(Tl) crystal. Comparison with the results from similar scatterers of normal iron shows that a 1.37- ±0.02-Mev gamma ray comes from Fe^{54}, and that the well-known 850-kev gamma ray comes from Fe^{56}. The cross section for production of the former gamma ray is 0.60±0.08 that of the latter. The 1.37 Mev gamma ray is tentatively assigned to the reaction $Fe^{54}(n,n')Fe^{54*}(\gamma)Fe^{54}$, from the first excited state. This energy value, together with that of the first level in Fe^{56}, is consistent with similar energies for other sets of isotopes in the vicinity of magic neutron numbers.[1,2]

* Supported in part by the joint program of the Office of Naval Research and the U. S. Atomic Energy Commission.
[1] G. Scharff-Goldhaber, Phys. Rev. 90, 587 (1953).
[2] P. Stähelin and P. Preiswerk, Nuovo cimento 10, 1219 (1953).

A3. Differential Elastic Scattering of 14-Mev Neutrons. J. O. ELLIOT, *Naval Research Laboratory and University of Maryland.*—The differential elastic scattering cross sections of Bi, Ta, In, Fe, and S for 14-Mev neutrons were measured at laboratory scattering angles between 5° and 55° with an angular resolution varying from ±1° to ±3° using the $T(d,n)He^4$ reaction as a source of primary neutrons. Measurements were performed at 90° to the deuteron beam using cylindrical scatterers with wall thicknesses designed to scatter elastically approximately 10 percent of the incident beam. The neutron detector consisted of a stilbene crystal 1 cm in diameter by 1 cm long mounted on a Dumont 6292 photomultiplier, the output pulses were biased in such a way as to retain only those corresponding to a neutron energy of at least 12 Mev. Corrections to the measured cross-section values for the presence of twice-scattered neutrons and for the effect of the angular resolution have been calculated. An estimate of the contribution from inelastically scattered gamma rays has been made.

A4. Cloudy Crystal Ball Analysis of 14 Mev Elastic Neutron Scattering Data. W. R. FAUST, R. C. O'ROURKE, AND J. O. ELLIOT, *Naval Research Laboratory.*—Calculations have been made of the differential elastic cross section for bismuth by use of an interaction potential of the form $Vo(1+i\zeta)$. The parameters Vo, ζ, and R, the nuclear radius, were all varied to obtain the best fit to the experimental data[1] according to the following criteria: (a) a least squares fit which perhaps weighs unduly the portion of the experimental curve prior to the first minimum; (b) the best fit as determined by eye for small angles as well as those near the first maximum. The latter procedure was used because of the relatively large experimental error near the first minimum. Preliminary values obtained by the least squares method, yield $Vo=18.6$ Mev, $\zeta=0.01$ and $R=(1.16 \text{ to } 1.26)\times A^{\frac{1}{3}}\times 10^{13}$.

[1] J. O. Elliot, "Differential elastic scattering of 14-Mev neutrons," Bull. Am. Phys. Soc. (unpublished).

A5. Determination of Nuclear Level Density. S. E. DARDEN, A. OKAZAKI, AND R. L. BECKER, *University of Wisconsin.**—The attenuation of a neutron beam deviates from exponential dependence on sample thickness when the total cross section varies over the energy spectrum of the incident beam, an effect which gives rise to the hardening of a beam passing through an absorber in the $1/v$ region. For neutron energies near 100 kev, where only S-wave neutrons should interact appreciably, the magnitude of such deivations depends on the average ratio of width to spacing of the levels of the compound nucleus, providing the energy spread of the neutron beam is large compared to the level spacing. The transmission of a thin sample was measured to one-half percent statistical accuracy, after which the neutron beam was filtered through a thick sample of the same material and the transmission of the thin sample remeasured. The increase in transmission with the filtered neutrons can be related to $\bar{\Gamma}_n/\bar{D}$. Eleven elements were investigated for neutron energies between 100 and 200 kev. The results indicate variations in $\bar{\Gamma}_n/\bar{D}$ as a function of atomic weight in qualitative agreement with the predictions of the complex square well model of nuclear scattering.[1]

* Work supported by the U. S. Atomic Energy Commission and the Wisconsin Alumni Research Foundation.
[1] Feshbach, Porter, and Weisskopf, Phys. Rev. 96, 448 (1954).

A6. An Analysis of Neutron Self-Indication Transmission Cross Sections. J. E. MONAHAN AND A. LANGSDORF, JR., *Argonne National Laboratory.*—If all neutrons interacting with a "detector" sample are detected equally, transmission measurements determine a mean exponential, $e^{-N\sigma'}=\int Re^{-N\sigma}\times(1-e^{-M\sigma})\,dE/\int R(1-e^{-M\sigma})dE$, where $R(E)$ is the neutron spectrum; $\sigma(E)$ and $\sigma'(N,M)$ are microscopic and measured cross sections, respectively; and N, M, atoms per cm² of transmission and detector sample, respectively. Defining $\sigma(E)=\bar{\sigma}(1+\delta(E))$, the moments of δ are $\langle\delta^i\rangle=\int R\delta^i dE/\int R dE$. The condition, $\langle\delta\rangle=0$, defines $\bar{\sigma}$. Expansion of the exponential gives

$$\sigma'=\bar{\sigma}-\left[\frac{N}{2}-\frac{M}{\exp(M\bar{\sigma})-1}\right]\bar{\sigma}^2\langle\delta^2\rangle+\left[\frac{N^2}{6}-\frac{M(N+M)}{2[\exp(M\bar{\sigma})-1]}\right]\bar{\sigma}^3\langle\delta^3\rangle+\cdots.$$

In the limit $M\to\infty$, this becomes the simpler expression for ordinary "flat" detection $\sigma''(N)$. The series for σ'', $d\sigma''/dN$, σ', and $d\sigma'/dM$ converge in the limits $N\to 0$ and $M\to 0$. The convergence of $d\sigma'/dN$ as $N\to 0$ is conditional upon the

behavior of all $\langle\delta^l\rangle$; thus extrapolation of σ' to $N=0$ from practical sample thicknesses is not always possible.

A7. Measurement of Neutron Transmission Cross Sections by a Self-Indication Technique. A. LANGSDORF, J. E. MONAHAN, AND F. PAUL MOORING, *Argonne National Laboratory.*—The simplest application of the analysis of the preceding abstract to self-indication data yields values of $\bar{\sigma}$ and $\langle\delta^2\rangle$ over the energy band ΔE in which $R\neq 0$. This value of $\bar{\sigma}$ is more accurate than that obtained by measuring the ordinary "flat" detected transmission cross section at several sample thicknesses. Data of $\bar{\sigma}$ *versus* E, then, give the resonance area $\sigma_0\Gamma$ for an isolated resonance that is not too poorly resolved. If experimental conditions permit the evaluation of $\langle\delta^2\rangle$, and if $R(E)$ is known adequately, all the resonance parameters can be evaluated for an isolated resonance even though it is poorly resolved. Another application is the detection of structure in $\sigma(E)$ within the band ΔE, even if this be made up of many resonances, unresolved or even overlapping. In this case, $\langle\delta^2\rangle$ and $\langle\delta^1\rangle$ may be interpreted, perhaps not unambiguously, in terms of suitable models, involving, for example, the concept of a mean resonance height and a mean width-to-spacing ratio. Experimental data of these types obtained using the Argonne electrostatic generator neutron source will be presented.

A8. Neutron Cross Sections in the 4 Mev Range.* W. S. EMMERICH, *Westinghouse Research Laboratories.*—Total cross sections and angular distributions for elastic scattering of 4.0- and 4.4-Mev neutrons have been calculated using the model of Feshbach, Porter, and Weisskopf[1] with $V_0=36$ and 40 Mev and $\zeta=0.05$. The results have been compared to experimental data between 3.7 and 4.7 Mev. Agreement for total cross sections has been improved by using $R=r_0A^{\frac{1}{3}}+a_0$ as the radius of the potential well with tentative values of $r_0=1.26\times10^{-13}$ cm and $a_0=0.70\times10^{-13}$ cm. Experimental differential elastic cross sections have been plotted as a function of R for comparison purposes and, except for light elements where strong individual resonances appear, agree with the general features of the theory. The calculated compound nucleus formation appears too low, however, for the observed nonelastic cross sections, and the use of other values of V_0 and ζ will be discussed in this energy range.

* Supported in part by the U. S. Atomic Energy Commission and the Office of Naval Research.
[1] Feshbach, Porter, and Weisskopf, Phys. Rev. 90, 166 (1953).

A9. Interaction of High-Energy Neutrons with Molybdenum. R. W. WANIEK, R. FOX, L. GARRIDO, AND E. G. SILVER.*—Molybdenum wires (14μ radius) embedded in Ilford G5 emulsions were exposed under good geometry conditions to the neutron beam of the Harvard 95-in. synchrocyclotron.[1,2] Runs were taken at neutron energies of 40, 70, and 110 Mev by changing the location of the Be-target and the collimation channels. The plates were scanned for events along the wires, and the spatial angle as well as the range were determined for each outcoming prong. The energy spectra as well as the angular distributions of the secondaries (only protons and alphas being considered) will be presented. The proton spectra produced by the neutrons at the three different energies exhibit similar peaks around 3.5 Mev. The angular distributions of these low energy particles is anisotropic.

* Now at Oak Ridge School of Reactor Technology.
[1] E. G. Silver and R. W. Waniek, Phys. Rev. 95, 586 (1954).
[2] E. G. Silver and R. W. Waniek, Rev. Sci. Instr. 25, 119 (1954).

A10. More Experimental Evidence for the Optical Model for Neutrons between 60 and 110 Mev.* VAUGHN CULLER AND R. W. WANIEK, *Harvard University.*—Results from the measurements of total cross sections for neutrons between 60 and 110 Mev made at the Harvard 95-inch synchrocyclotron[1] have been analyzed using optical models.[2,3] As expected, reasonably good agreement was obtained for the higher energies, whereas at the lower energies the fit could be reached only for very improbable values of the parameters involved. From the 97-Mev data the analysis by Fernbach's model[2] yields a nuclear radius of $1.40\ A^{\frac{1}{3}}\times10^{-13}$ cm; at 81 Mev the radius becomes $1.46\ A^{\frac{1}{3}}\times10^{-13}$ cm.

* Supported by the joint program of the Office of Naval Research and the U. S. Atomic Energy Commission.
[1] V. Culler and R. W. Waniek, Phys. Rev. 95, 585 (1954).
[2] Fernbach, Serber, and Taylor, Phys. Rev. 75, 1352 (1949).
[3] W. Heckrotte, Phys. Rev. 95, 1279 (1954).

THURSDAY MORNING AT 10:00

McAlpin, Colonial Room

(L. H. FISHER, presiding)

Discharges and Ions in Gases

B1. An Analysis of the Plasma of Fluorescent Lamps, I. F. BITTER, *M. I. T.*, AND J. F. WAYMOUTH, *Sylvania Electric Products Inc.*—An attempt has been made to explain the properties of the "plasma" of fluorescent lamps in considerable detail, using the ambipolar diffusion theory of Schottky,[1] modified to include ionization by multiple electron impacts. A significant factor in the electrical behavior of the plasma is the concentration of mercury atoms in the excited state ($^3P_1$) and in the metastable state (we consider only one, which may be thought of as a combination of $^3p_0$ and $^3p_2$ metastable states). These concentrations are calculated as functions of lamp parameters and operating conditions. Ionization is assumed to occur by electron collisions with excited and metastable atoms. The cross section for this process is one of two inaccurately known parameters, which we treat as adjustable constants, occurring in the calculations. The other is the average absorption coefficient for quanta of the resonance line, which has a complicated hyperfine structure. A comparison of theoretical prediction with experimental data is undertaken in the following communication.

[1] W. Schottky, Physik Z. 25, 635 (1924).

B2. An Analysis of the Plasma of Fluorescent Lamps. II. J. F. WAYMOUTH, *Sylvania Electric Products, Inc.*, AND F. BITTER, *M. I. T.*—Qualitative agreement of the theory outlined above with experiment is demonstrated for all the derived quantities as functions of the several parameters of the discharge. The magnitudes of the calculated electron temperature, electric field, total light output, and efficiency are also in sufficiently good agreement with experimental values for the lamps of greatest commercial interest to permit extrapolations to lamps of hitherto-untried dimensions and pressures to be

made with a good deal of confidence. Optimum agreement of theory with experiment is obtained using a mean life time of ultraviolet photons in the discharge 3.6 times that employed by Kenty,[1] and with a value 3.3 for the ratio of cross section for ionization of excited state to that of the ground state, as compared to the "order of magnitude" quoted by Klarfeld.[2]

[1] C. Kenty, J. Appl. Phys. 21, 1304 (1950).
[2] B. Klarfeld, Tech. Phys. U.S.S.R. 5, 913 (1939).

B3. Spectroscopic Study of the Discharge and Afterglow Produced in Nitrogen by Pulsed Microwaves. GEORGES DÉJARDIN, JOSEPH JANIN, AND IVAN EYRAUD, *Université de Lyon.*—The luminous discharge and afterglow excited in pure nitrogen by pulsed microwaves (3.2 cm) have been studied by means of a monochromator behind which is a multiplier phototube connected with an oscilloscope. A suitable electronic arrangement enables this device to give the two curves representing the pulse modulation (width: 2 microseconds) and the variation in intensity of the isolated radiation. The results so obtained have been confirmed by using a spectrograph equipped with a stroboscopic disk. At relatively high pressures (25 mm), the emission of the second positive system, which reaches generally its maximum *before* the end of a pulse, can be essentially attributed to electron collisions. On the contrary, the recombination between ions N_2^+ and electrons is probably dominant in the generation of the first positive system, for which the maximum occurs *at* the end of a pulse and the afterglow is much more persistent. Electron collisions and recombination of ions N_2^{++} seem to take part simultaneously in the emission of the negative bands. The same assumptions explain the phenomena observed at low pressures (0.5 mm). The variations displayed on the oscilloscope screen are then widely different, but the negative bands can also be detected a long time after the second positive system has vanished. Moreover, the emission of the first positive bands, which is relatively weak during the discharge, is the strongest in the beginning of an afterglow decaying much more slowly than for the other systems.

B4. Secondary Electron Resonance Discharge Mechanism. I. R. K. SMITHER, *Yale University*, AND C. W. HOOVER, JR., *Bell Telephone Laboratories.*—The secondary electron resonance discharge mechanism has been shown to be responsible for severe current loading of a cavity resonator intended for use as a rf accelerating section. Studies of this mechanism, using the resonator as a tool, have revealed additional features of the mechanism. In particular, several breakdown regions have been observed at different accelerating voltages with discontinuous transitions taking place between these levels under certain conditions as the power input to the resonator is increased. The breakdown voltage levels exhibit widely different power sensitivities. A "spike" or surge of rf voltage across the accelerating gap precedes breakdown in all cases. The effect on the operation of the resonator and the experimental method used to verify that the discharge observed was due to this mechanism will be described. The method used in studying the mechamism and the new features revealed will be discussed Finally, the various means used to suppress the build-up of current through this mechanism will be given.

B5. Secondary Electron Resonance Discharge Mechanism. II. C. W. HOOVER, JR., *Bell Telephone Laboratories*, AND R. K. SMITHER, *Yale University.*—The simple theory of the secondary electron resonance discharge mechanism is extended to account for the experimental results described in Part I. Multiple breakdown levels are explained on the basis of dynamic and energetic limitations on the process. A phase stability criterion is developed which shows which of the breakdown modes dynamically and energetically possible, will build up. This same criterion is also applied to explain the varying power sensitivity of the breakdown levels, the conditions for discontinuous transitions between levels, and the "spike" effect. An expression for current build up in the breakdown region is derived to within a constant x the current amplitude. Finally a criterion is developed which can be applied in the design of any resonator to show whether breakdown through this mechanism will result in serious loading. Possible means for suppressing this mechanism suggested by this study are given.

B6. Charge States of Hydrogen Ions in Gases. P. M. STIER, C. F. BARNETT, R. A. HOWARD,* AND W. BUGG,† *Oak Ridge National Laboratory.*—Measurements of charge exchange cross sections for hydrogen ions passing through gases have been extended to the energy region 3 to 30 kev. The present experiment determines the fraction of the hydrogen beam in each charge state (+1, 0, and −1) after passage through a "thick" gas target, i.e., sufficient gas for equilibrium to be established between competing electron capture and loss reactions. Also, a determination is made of the cross section for a neutral atom to gain or lose an electron, i.e., become a positive or negative ion. The target gases used were hydrogen, helium, nitrogen, oxygen, neon, and argon. The present results join smoothly the curves obtained[1] at higher energies and for hydrogen as the target gas. The agreement with the results of Whittier[2] is excellent. At low energies, the average charge of the hydrogen beam is different for the various gases. In helium it is nearly +1, but approaches 0 in the more easily ionized gases. This behavior is equivalent to that observed for the heavier ions (e.g., A^+) at much higher energies.

* Permanent address: University of Oklahoma.
† Present address: University of Tennessee.
[1] Stier, Barnett, and Evans, Phys. Rev. (to be published).
[2] A. Charles Whittier, Can. J. Phys. 32, 275–290 (1954).

B7. Electron Loss Cross Sections of Moving Helium Atoms. SOL KRASNER, *University of Chicago*, AND J. CUEVAS, *University of Chicago and Junta de Energia Nuclear, Madrid, Spain* (introduced by S. K. Allison).—When helium atoms with velocities comparable to or greater than e^2/h (2.19×10^8 cm/sec; 100 kev) traverse matter they may be ionized through the loss of one or both electrons in a single atomic encounter. In our experiments a unidirectional beam in charge equilibrium is produced by admitting gas to a chamber through which He^+ ions pass after acceleration in a Cockcroft-Walton circuit. The attenuation of the He^0 component is observed as gas is admitted to a subsequent compartment, in the presence of a transverse magnetic field so adjusted as to impose a radius of curvature of 23.7 cm on any He^+ ions formed by electron loss. The sum of the loss cross sections for the removal of one or both electrons has been measured in H_2, He, and air for He atoms of kinetic energies 100 to 450 kev. These cross sections are somewhat larger than those measured by our group[1] for hydrogen atoms and show, in the region investigated, an increase rather than a decrease, with increasing energy.

[1] J. H. Montague, Phys. Rev. 81, 1026 (1951).

B8. Double Electron Capture by Alpha Particles in Helium.* D. D. BETTS AND J. D. JACKSON, *McGill University.*—Using the adiabatic impact parameter of Kohn,[1] the double electron capture cross section for slow α particles in helium has been calculated. Evaluating the appropriate molecular energy curves for the He_2^{++} molecule ion presented the chief difficulty. Results show that the cross section can be represented approximately by $[9.9-1.3\log E(ev)]\pi a_0^2$ for energies between 1 and 10^4 ev. An approximation method, based on the validity of a first-order perturbation calculation for large impact parameters combined with the known qualitative behavior of the capture probability at small impact parameters, has been developed for resonance capture processes. Application of this method to the foregoing double-capture problem, as well as to the capture of a single electron by H^+ in H and He^+ in He, yields results in fair agreement with the more exact calcula-

tions.[2,3] The possibility of using the approximation technique in more complicated resonance capture processes will be discussed.

* Supported by the National Research Council of Canada.
[1] W. Kohn, Phys. Rev. 90, 383A (1953).
[2] A. Dalgarno and H. N. Yadav, Proc. Phys. Soc. (London) A66, 173 (1953).
[3] J. D. Jackson, Can. J. Phys. 32, 60 (1954).

B9. Cross Sections for Electron Capture and Loss by 26-Mev Nitrogen Ions. A. ZUCKER, H. L. REYNOLDS, AND L. D. WYLY, *Oak Ridge National Laboratory.*—Electron capture and loss cross sections in zapon for 26-Mev nitrogen ions have been measured. N^{7+}, N^{6+}, and N^{5+} charge groups separated by the fringing magnetic field of the cyclotron were passed through zapon foils varying in thickness from about $3\mu g/cm^2$ to 6 $\mu g/cm^2$. These foils were sufficiently thin so that charge equilibrium was not achieved. The relative intensities of the non-equilibrium charge distributions were analyzed by graphical methods to determine the following ratios of the cross sections $\sigma_{56}/\sigma_{67}=2.6$, $\sigma_{56}/\sigma_{65}=3.8$, and $\sigma_{67}/\sigma_{76}=0.78$. Assuming that an average atom in zapon has a mass of 14, the cross sections for electron capture and loss per atom for 26-Mev nitrogen ions are: $\sigma_{65}=2.0\times10^{-18}$ cm², $\sigma_{76}=3.8\times10^{-18}$ cm², $\sigma_{56}=7.7\times10^{-18}$ cm², and $\sigma_{67}=3.0\times10^{-18}$ cm². The probable errors in these values are approximately 20 percent. Nonequilibrium charge distributions as a function of foil thickness will be presented for initial beams consisting entirely of any one of the ion groups N^{7+}, N^{6+}, or N^{5+}.

B10. Validity Criteria for Calculating the Differential Cross Section for Collisions of Kev Ions with Atoms.* GERALD STONE, ROBERT CARBONE, AND EDGAR EVERHART, *University of Connecticut.*—For a classical determination of the differential cross section for single collisions of kev ions with atoms to be valid there are two necessary conditions. The first is that the de Broglie wavelength λ of the incident particle be small compared with any significant dimension x of the scattering center. It is shown that this condition is satisfied for a 100-kev helium ion colliding with an argon atom when the wavelength of the helium ion is compared with the distance of closest approach for a Coulomb potential. The condition is also fulfilled when this wavelength is compared with other significant dimensions of the argon atom. The second condition for the validity of the classical solution is that the deflection due to the collision must be well defined with respect to the uncertainty relationship. It is shown that this condition is satisfied for 100 kev ion-atom scattering when the electron screening is neglected. If the potential is screened, the condition is also fulfilled for ions deflected greater than about 7×10^{-5} radian. The quantum-mechanical Born approximation is valid for deflections less than this angle. Thus there is a large region of validity for classical calculations of kilovolt energy ion-atom scattering.

* Supported by the Office of Ordnance Research.

B11. Cross Section Measurements for Large Angle Collisions of He, Ne, and A Ions with Argon Gas Atoms at Energies from 25–100 kev.* ROBERT J. CARBONE, GERALD STONE, AND EDGAR EVERHART, *University of Connecticut.*—The differential cross section for the scattering of positive charge from collisions of noble gas ions with the target gas argon has been investigated. The ion beam is passed through a chamber containing the target gas at a pressure of a few microns of Hg which is low enough to insure that single collisions will predominate. The particles scattered out of this beam are collected in a Faraday cage which measures the total positive charge. This cage incorporates collimating slits to select only those particles at a chosen scattering angle θ within a 2° resolution. The apparatus allows the angle θ to be varied continuously up to 40°. Data is presented for collision of singly ionized helium, neon, and argon with argon atoms at 25, 50, and 100 kev. The experimental points are compared to the classical Rutherford differential cross section and to a differential cross section which allows for screening by the atomic electrons.

* Supported by the Office of Ordnance Research.

B12. A Comparison of the Energy to Make an Ion-Pair in Various Gases for Alpha and Beta-Particles. WILLIAM P. JESSE AND JOHN SADAUSKIS, *Argonne National Laboratory.*—A series of measurements has been made of the relative currents produced in different gases by beta-particles from Ni_{63} and from tritium sources in an ionization chamber. In all cases only relative current measurements with argon as a standard gas have as yet been made. The value of W, the average energy to make an ion-pair for each of the different gases computed relative to argon as a standard, is found to be the same for the Ni_{63} and tritium sources. If these relative W_β values are plotted against previously determined W_α values for polonium alpha-particles, a marked difference is observed in the gases investigated. For hydrogen and the noble gases the plotted points lie closely on a 45° straight line through the origin. Thus for these gases the ratio W_β/W_α is constant. This constant may well be unity, but this is not proved as yet by these results. For all other gases so far investigated the plotted points lie below the 45° line, indicating a higher efficiency of ionization (and a lower W) for the beta-particles than for the polonium alpha-particles. The apparent significance of these results will be discussed.

THURSDAY MORNING AT 10:00

New Yorker, Panel Room

(S. L. QUIMBY, presiding)

Metals

C1. Electron Band Structure of Iron. JOSEPH CALLAWAY, *University of Miami.*—The electron band structure of the body-centered cubic form of iron has been calculated by the orthogonalized plane wave (OPW) method. The crystal potential is determined from the superposition of charge densities, obtained from a Hartree field for the d^6s^2 configuration of the free atom. Exchange effects are studied using Slater's free electron approximation to the exchange potential. Since the Hartree wave functions for the core states do not include exchange, the OPW method fails for states of predominately S symmetry. These are treated by the cellular method. The OPW method has been modified to improve convergence of the wave function for states of D symmetry. The bands formed from the atomic d electrons are narrow, about

2 volts wide. The splitting of the d bands at the center of the Brillouin zone is much smaller than at the corners and faces of the zone, with maximum separation occuring at the point N. The problem of determining the relative position of the S and D levels will be discussed.

C2. Thermal Scattering of Electrons between Bands in a Metal.* JOHN B. GIBSON, *Iowa State College* (introduced by J. M. Keller).—The method of deformation potentials[1] has been extended to apply to the case of multi-band metals. All terms to first order in the strain have been retained. The theory involves energies for homogeneously strained crystals. These are expanded by perturbation theory in terms of wave functions of the unstrained crystal. This is particularly simple if one assumes a "rubber potential" that deforms with the lattice, and if one makes a corresponding change of variable. The dependence of energy on strain can then be expressed directly in terms of the effective mass tensor and the velocity vector. The scattering amplitude is, as usual, proportional to the integral over one cell $\int u_{k'l'}^* u_{kl} d\tau$, where the Bloch wave function for the lth band is $\psi_{kl}=i^{ik\cdot r}u_{kl}$. For small angle scattering this integral is constant for transitions within the same band, while it is proportional to q, the phonon propagation vector, for transitions between bands.

*Work was performed in the Ames Laboratory of the U. S. Atomic Energy Commission.

[1] J. Bardeen and W. Shockley, Phys. Rev. **80**, 72 (1950).

C3. Energy Levels in Metallic Potassium.* E. L. JOSSEM AND L. G. PARRATT, *Cornell University*.—Information about electron energy levels in metallic potassium has been obtained from the x-ray K emission and absorption spectra. The emission lines were studied with a bent crystal focusing vacuum spectrometer with a proportional counter detection system. Of the several lines in this region, the β_1 and β_5 are of principal present interest. The β_1 line, the strongest in the region, represents the transition to the $1s$ level of an electron associated with the $3p$ band. This line is observed to have the same energy position, width and shape in metallic potassium as in chemical compounds of potassium (e.g., KCl). It is tentatively concluded that the $3p$ band in potassium, some 18.4 ev below the Fermi surface in the metal, is narrow (about 0.22 ev wide) and is but little affected by the nature of the surrounding atoms. The β_5 line, a very weak line which appears just at the long wavelength side of the K-absorption edge, presumably involves the transition of an electron in the conduction band to the $1s$ level. However, since the conduction band is nominally $4s$, selection rules require that β_5 represent that fraction of the conduction electrons having p-type symmetry. Discussion will be given of the width and shape of the β_5 line.

*Supported by the United States Air Force through the Office of Scientific Research of the Air Research and Development Command.

C4. Interpretation of Optical Properties of Metal Surfaces. S. ROBERTS, *General Electric Research Laboratory*.—Reflection of light from a metal is governed by the surface impedance which in turn defines a complex surface dielectric constant. It is shown that the observed surface dielectric constants of the metals Ag, Au, Cu, Pt, Ir, and Ni obey an equation derived on the premise that surface dielectric constant is an analytic function of frequency. The surface properties of each of these metals, except possibly Au, are characterized by at least two relaxation rates which are related to the relaxation rates for conduction in the interior. An explanation for the existence of two relaxation rates, instead of one as previously assumed, is based on the band theory of metals. Theory indicates that there will be two types of conduction processes, each with its own relaxation rate whenever the Fermi level falls in a region of overlapping allowed energy bands. It has long been recognized[1] that both s and d bands are of importance for the conductivity of transition metals; however, this interpretation does not appear to have been extended to optical properties. It is now shown that even some nontransition metals may have two types of conduction electrons.

[1] N. F. Mott, Proc. Roy. Soc. (London) **A153**, 699–717 (1936).

C5. Disordering of Polyatomic Solids by Neutrons. E. G. HARRIS, *Naval Research Laboratory*.—A method is outlined for calculating the number of vacant lattice sites or interstitial atoms produced in a polyatomic solid by neutron radiation. It is assumed that the colliding atoms are in the energy range for which the orbital picture is valid and that the kinetic energy of the atoms is sufficiently low that no appreciable fraction of the energy loss occurs in inelastic collisions. Integral equations are derived which relate the number of interstitial atoms of each atomic species with the energy of the neutron which caused them. The asymptotic behavior of the solutions of these equations is examined. It is found that for high neutron energies the number of displaced atoms of each species is a linear function of the energy of the incident neutron. The equations are solved numerically for the interesting case of diatomic solids. A rigid sphere interaction between atoms is assumed. It is found that a high-energy neutron uses approximately one-half of its energy in the production of displaced atoms. For monoatomic solids the results agree with those of Snyder and Neufeld.[1]

[1] W. S. Snyder and Jacob Neufeld, Phys. Rev. **94**, 760(A) (1954).

C6. Relationship Between Small Angle Dislocation Boundaries and Creep. BETSY ANCKER, THOMAS H. HAZLETT, AND EARL R. PARKER, *University of California, Berkeley*.—Small angle dislocation boundaries of controlled nature (sharp or diffuse) and density were introduced into high-purity polycrystalline nickel prior to creep. By this method, the shape of the creep curve was varied drastically. The initial density of sub-boundaries ranged from an average of nearly zero per grain to a large number which was limited by the occurrence of recrystallization. X-ray microscopic examination showed that the dislocation networks developed during creep were nearly identical and were independent of the initial density and nature. They were characterized by a multitude of generally parallel, very small angle boundaries (a few minutes) as well as some larger ones of the type developed by cold-work and recovery. The density of sub-boundaries developed during creep is also independent of the creep strain within the limits of 1 percent and 7.5 percent, the strain at which the most ductile specimens fractured. The near identity of the substructures developed during creep, irrespective of the initial sub-boundary density and the amount of creep strain, was further verified by the substantial equality of the specimens' tensile strengths after creep. The only detectable difference in the sub-structures was an increase of the average sub-boundary angle with increasing total strain.

C7. Propagation of Plastic Strain along Lead Bars. B. E. K. ALTER AND C. W. CURTIS, *Lehigh University*.—The progress of a compressive pulse, produced by suddenly applying pressure to one end of a lead bar, has been followed by measuring strain in the bar as a function of time with circumferentially wound resistance gauges spaced at $\frac{1}{2}$-inch intervals. With sufficient pressure to produce plastic deformation in an initially unstrained bar, the pulse develops a small elastic head which can easily be distinguished from a more slowly moving plastic wave. The elastic head maintains an essentially constant magnitude and shape, whereas the plastic component spreads out rapidly. By using a double pulse technique to prestress the bar, it has been shown that the dispersion of the plastic wave cannot be accounted for by the von Karman-Taylor-White theory, neglecting rate of strain. The applicability of the

strain rate theory,[1-3] which has recently been proposed to explain results obtained with copper,[4] will be discussed.

[1] L. E. Malvern, J. Appl. Mech. 18, 203 (1951).
[2] R. J. Rubin, J. Appl. Phys. 25, 528 (1954).
[3] C. Riparbelli, J. Aeronaut. Sci. 21 (February, 1954).
[4] E. J. Sternglass and D. A. Stuart, J. Appl. Mech. 20, 427 (1953).

C8. Anomalous Behavior of Cu_3Au Quenched from above 600°C. R. FEDER AND A. S. NOWICK,* *Frankford Arsenal.*—The lattice parameter (at 25°C of Cu_3Au in the ordered state is about 0.15 percent lower than in the disordered state. This fact is the basis of a method for studying ordering kinetics at temperatures below 385°C (the critical temperature) by means of lattice parameter measurements on powdered specimens. A study of the change in parameter with time of anneal (annealing temperatures in the range 210°C to 275°C) was carried out as a function of quenching temperature from 400°C to 700°C. For specimens quenched in the range 400°C to 600°C, essentially the same ordering rate was observed independently of quenching temperature. Specimens quenched from above 600°C and annealed at 210°C quickly develop a broadening of all normal lattice lines on the side toward larger Bragg angles, although no broadening exists in the as-quenched condition. Because of this effect, the mean lattice parameter is changing far more rapidly than in those specimens quenched from below 600°C. This anomalous behavior may be interpreted by assuming that nuclei for order are relatively rare in specimens quenched from above 600°C.

* Permanent address: Yale University.

C9. Critical Temperature for Self-Induced Ordering in Ag-Zn Solid Solutions.* CHI YAO LI† AND A. S. NOWICK, *Yale University.*—The thermodynamics of stress-induced ordering in substitutional solid solutions has been shown[1] to follow in close analogy to the Weiss theory of paramagnetism. Specifically, the relaxation strength Δ for stress-induced ordering varies inversely as $T-T_c$. The quantity T_c may be interpreted as a critical temperature for self-induced ordering, i.e., below this temperature the lattice would order spontaneously (without the presence of an applied stress) if atoms were sufficiently mobile. To investigate this phenomenon experimentally, values of relaxation strength have been obtained over a wide range of temperatures, for wire specimens of α-Ag-Zn alloys, by measurement of relaxed rigidity modulus, internal friction, and strain relaxation. The results show that the reciprocal of Δ plots against T in a straight line, as predicted by the theory. From the intercepts, values of T_c of of 185°K, 153°K, and 131°K are obtained for alloys of 33.5, 30.2, and 24.2 atomic percent zinc, respectively.

* Work supported by the U. S. Army Office of Ordnance Research.
† Now at Lehigh University, Bethlehem, Pennsylvania.
[1] C. Zener, *Elasticity and Anelasticity of Metals* (University of Chicago Press, Chicago, 1948), p. 111.

C10. Effects of Heat Treatment and Ion-Bombardment Cleaning on the Catalytic Activity of a Pure Nickel Surface. R. F. WOODCOCK* AND H. E. FARNSWORTH, *Brown University.*—Investigations on surface catalysis for hydrogenation of ethylene at a clean nickel surface as a function of outgassing by heat treatment in high vacuum[1] have been continued. Improvements have been made in reaction chamber design to eliminate spurious effects, and the heat treatment has been supplemented by positive ion-bombardment cleaning, followed by annealing.[2] The activity increases enormously with outgassing up to 800° to 900°C in vacuum. In the present procedure, the surface is heated at 800°C for 30 minutes and further cleaned by ion-bombardment and subsequent annealing. The reaction chamber, and nickel specimen of about 4 cm^2 area, are held at a constant temperature in the range 60°C to 135°C during the reaction, with a total pressure of reactants of 12 mm Hg. A mass spectrometer is used for detection. Immediately after bombardment the activity is greater than after heat treatment alone. However, after low-temperature annealing at approximately 600°C for 1 minute, the activity approaches zero. Possible interpretations of these results will be discussed.

* Fellow, Sylvania Electric Products, Inc.
[1] R. K. Sherburne and H. E. Farnsworth, J. Chem. Phys. 19, 387 (1951).
[2] Farnsworth, Schlier, and Burger, Bull. Am. Phys. Soc. 29, No. 7, 35 (1954).

THURSDAY MORNING AT 10:00

Manhattan Center, Gold Room

(G. F. TAPE, presiding)

Apparatus of Nuclear Physics

D1. Betatron Orbit Stability Studies. G. C. BALDWIN, *General Electric Research Laboratory.*—Experiments are described which are a continuation of work reported previously with a pulsed betatron in which the field index is controllable in the interval $0.5<n<0.9$.[1] Capture of electrons scattered from the target into epitrochoidal orbits has been observed. Near $n=\frac{3}{4}$ the beam is found to be radially unstable if the guide field contains a first harmonic azimuthal variation exceeding a predictable critical magnitude. Excitation of radial oscillation by changing n to $\frac{3}{4}$ is demonstrated to be an advantageous method of rapidly bringing the beam to the target at a desired azimuth, requiring relatively little stored energy. Resonant damping of radial injection oscillations[2] is indicated by the increased output produced by transient first harmonic perturbation of the guide field applied at 90° to injector azimuth.

[1] Baldwin, Elder, and Westendorp, Phys. Rev. 95, 600(A) (1954).
[2] S. E. Barden, Proc. Roy. Soc. (London) B64, 579 (1951).

D2. Fixed Field Alternating Gradient Accelerators.* KEITH R. SYMON, *Wayne University and Midwestern Universities Research Association.*—It is possible, using alternating gradient focussing, to design circular accelerators with dc magnets, having almost any desired radial dependence of energy. One can construct a static magnetic field distribution in which stable proton orbits between 0.5 Mev and 20 Bev will all lie inside a single doughnut of 1-meter radial aperture. The required magnet cross sections are not significantly greater than in conventional AG synchrotrons. In the simplest FFAG designs with some reverse field sectors, the over-all orbit radius is greater by a factor of 3 to 5 than that for a conventional AG sychrotron. A number of ways of reducing this factor are being studied. The use of dc magnets simplifies the magnet power supply, eliminates remanent field problems, simplifies saturation problems, and permits dc trimming for imperfections. If rf acceleration is used, accurate frequency tracking is unnecessary, and high repetition rates are practical. In many

designs, there is no transition energy. The vertical aperture can be made large at the injection orbit and small at the high energy orbit, with consequent saving in iron and relaxing of injection tolerances. Very low injection energies can be used with negligible increase in magnet cost.

* Supported by the National Science Foundation.

D3. Synchrotron Application of Reverse Field Types of Fixed Field Alternating Gradient Magnets.* L. W. JONES, K. R. SYMON, K. M. TERWILLIGER, AND D. W. KERST, *Midwestern Universities Research Association.*—Details of the use of Symon's fixed field alternating gradient magnets in synchrotron construction will be described. The possibility of decreasing the large circumference due to the presence of reverse field sectors by making these sectors very short but with a correspondingly greater field gradient brings in important edge effects as a result of the strong taper of the sector edges. This edge effect is not important if the same gradient is used in forward and reverse field sectors. FFAG synchrotrons designed with the high energy orbit at the inner radius (negative momentum compaction) have no transition energy. Typical parameters for multibillion volt FFAG proton synchrotrons with equal absolute values of gradients but different forward and reverse field sector lengths, with equal sector lengths but different gradients, and with short reverse field sectors will be shown. Transition energies are nonexistent or greater than the maximum particle energy. Possible pole structures having the field shaped by iron and copper, rf simplifications, and injection simplifications will be discussed.

* Supported by the National Science Foundation.

D4. Application of the Fixed Field Alternating Gradient Principle to Betratrons and Cyclotrons.* K. M. TERWILLIGER, L. W. JONES, D. W. KERST, AND K. R. SYMON, *Midwestern Universities Research Association.*—The essential idea in FFGA designs presented in accompanying papers is to provide stability of betatron oscillations while having a spacial change in guide field sufficient to accommodate all particle energies. A betatron constructed or modified to become a FFAG accelerator would have an injection duty cycle and beam duty cycle of order $\frac{1}{2}(1-\Delta\phi/\phi)$, where $\Delta\phi$ is the change in flux through the betatron accelerating core necessary to accelerate the electrons to full energy, and ϕ is the total possible change in core flux. This would allow acceptance times and possibly electron currents to be 10^4 times that of present accelerators. The spiral ridged pole design would allow 3 to 5 times more energy than the reverse field designs. If feasible, spiral ridges could convert synchrocyclotrons to constant frequency cyclotrons. The average field can be made to match the relativistic increase of mass. The vertical defocusing produced by the radial increase of field is compensated by the alternate gradient effect of the spiral ripples in the field.

* Supported by the National Science Foundation.

D5. Fixed Field Alternating Gradient Accelerator with Spirally Ridged Poles.* D. W. KERST, K. M. TERWILLIGER, K. R. SYMON, AND L. W. JONES, *Midwestern Universities Research Association.*—If the magnetic field in the median plane of an accelerator is made to vary according to

$$H=H_0(r/r_0)^k[1+f\sin(\{r-r_0\}/\lambda-N\theta)]$$

it is shown that for suitable parameters radial and vertical focusing result, the field is unidirectional, and the momentum spread held by such a machine is great enough to contain simultaneously the injected particles at the low field radius and the full energy particles at the high field radius. The application of these spirally ridged magnet poles to the design of a multibillion volt accelerator will be discussed. The advantages are the same as those described by K. R. Symon in an accompanying abstract, but the circumference is less. The radial aperture required for this ridged field is considerably greater than that for the usual A.G. synchrotron if we use field gradients of the same magnitude. Possibilities of constructing this ridged field will be discussed. Ridged fields might also be applied to betatrons, synchrotrons, and synchrocyclotrons of lower energy to increase output.

* Supported by the National Science Foundation.

D6. Analysis of Angular Distribution Data by Electronic Computers. L. C. BIEDENHARN* AND A. SIMON, *Oak Ridge National Laboratory.*—The analysis of nuclear reaction and scattering angular distribution data has become a routine task, with extensive numerical tables available for applying standard theoretical results.[1] The task is, nevertheless, time consuming, even aside from the question of interfering levels, and testing all possible spin and parity assignments may be a sizeable problem. In such a situation the application of electronic computers is clearly indicated. A general technique for the computation of Racah and Clebsch-Gordan coefficients already exists and has been used in preparing numerical tables.[2] Combining this with an automatic least squares fitting of the S-matrix parameters, such as is done by Fermi[3] for the meson scattering problem, we have a completely automatic routing for assigning spin parameters. We have coded for the ORACLE the general angular distribution solution for reactions as given in reference 1. For the present, only a single level was assumed, but this restriction will be removed in time. Sample problems have been analyzed, in from 10 to 15 minutes, involving tests of several hundred possible assignments of spins and angular momenta.

* Now at Rice Institute.

[1] J. M. Blatt and L. C. Biedenharn, Revs. Modern Phys. **24**, 258 (1952). References to the extensive literature on this subject may be found here.
[2] A. Simon, Phys. Rev. **95**, 657(A) (1954); Oak Ridge National Laboratories reports 1679 and 1718.
[3] E. Fermi, LA-1492.

D7. On the Bilateral Development of Thick Nuclear Emulsions. RAYMOND FOX AND R. W. WANIEK, *Harvard University.*—The major limitation in the use of thick nuclear emulsions lies in the development process. To achieve a gain factor of 2 or more in facilitating this processing we resorted to a bilateral development technique which yielded satisfactory results for emulsions up to 2000 microns thickness. To surmount the difficulties encountered in processing the stripped emulsions the following procedure was adopted: The two surfaces of the dry pellicule are confined by a gauze which is rendered adhesive by soaking in a solution of acetone and Duco cement. The emulsion is thereby restrained from lateral expansion but possesses complete freedom in the direction of its thickness. The gauze is attached to a polyethylene frame to inhibit contractions and to ease handling. The pellicule secured in this way is then processed according to a low temperature technique used at this laboratory (unpublished). After the washing stage the emulsion is mounted on a treated glass backing and carefully allowed to dry at high humidity. High energy tracks in the plate were scanned with a Koristka MS-2 scattering microscope to test for distortions and the results obtained will be presented.

D8. Response of Anthracene to Low-Energy Protons and Helium Ions.* E. J. ZIMMERMAN, *University of Nebraska.*—Photomultiplier pulse amplitudes produced by light from anthracene crystals bombarded by protons and helium ions

from 25 to 375 kev have been measured. Both curves of pulse height *vs* energy are nonlinear, that for protons curving away from the energy axis while that for helium ions bends towards it. Since, over most of this energy range, dE/dx for protons decreases while dE/dx for alphas increases, part, but probably not all, of the non-linearity may be due to high density of excitation along the particle path as suggested by Birks.[1] If one plots the specific fluorescence (slope of pulse amplitude *vs* total range) against dE/dx, it appears that the parameters in Birks' theory[1] cannot be the same for both protons and helium ions. Both response curves extrapolate smoothly to the origin, indicating an absence of any non-scintillating surface layer more than a few Kev thick.

* Supported in part by the U. S. Atomic Energy Commission and in part by a Summer grant by the Nebraska University Research Council.
[1] J. B. Birks, *Scintillation Counters* (McGraw-Hill Book Company, Inc., New York, 1953), Chap. 6.

D9. Cobalt-60 Field Distributions Using Silver Activated Phosphate Glass. HERBERT RABIN AND WILLIAM E. PRICE, *U. S. Naval Research Laboratory.*—The measurement of high doses of gamma rays by absorption changes in silver activated phosphate glass has been previously reported for cobalt-60[1] and fuel element[2] radiation. The base glass by weight is 50 percent $Al(PO_3)_3$, 25 percent $Ba(PO_3)_2$, and 25 percent KPO_3 to which is added approximately 8 percent by weight of $AgPO_3$. The sensitivity of this glass is sufficiently great to permit satisfactory measurement of dose to 2 by 10^6 rep and dose rate independence has been established to over 10^7 rep/hour. Small plates of this glass lend themselves to the point by point mapping of field distributions of x-rays, gamma rays, and high energy electron beams. Glass plates 1 cm square and approximately 3 mm thick have been utilized in mapping the gamma field of the two and one-half kilocurie NRL cobalt-60 source and results are in good agreement with theoretical calculations of field distribution based on line source computations. Absolute dose determinations throughout the field depend on the accuracy of the standard on which the glass is initially calibrated; silver activated glass measurements calibrated with ceric-sulfate agree to within 12 percent of direct ion chamber measurements.

[1] J. H. Schulman, NRL Memorandum Report 266 (February, 1954).
[2] H. Rabin, NRL Memorandum Report 309 (June, 1954).

D10. Ionization of Air by Gamma Rays.* E. L. BURKHARD AND J. H. LEWIS, *Convair, A Division of General Dynamics Corporation (Fort Worth).*—The absorption of energy from gamma rays by air is calculated by using a linear absorption coefficient that varies with the initial energy of the photon and the distance from the source. The dependence upon distance arises from degradation of the photon energy in the Compton scattering process. A point source of gamma rays is assumed to radiate a spectrum of energies in the range 0.1 to 10 Mev. The number of gamma rays of any energy is assumed to be a decreasing exponential function of energy.[1] The equilibrium distribution of free electron density is calculated from the rate of energy absorption and the rate at which the free electrons are removed by attachment and recombination.

* This work was supported by contract with Wright Air Development Center.
[1] J. W. Motz, Phys. Rev. **86**, 753 (1952).

D11. Photographic Amplification in Alpha-Particle Auto-Radiography. K. H. SUN, P. R. MALMBERG, AND P. SZYDLIK, *Westinghouse Research Laboratories.*—The detection of alpha particles in photographic plates or films is usually carried out either by microscopic observation of alpha-tracks in an emulsion or by visual examination of the photographic blackening. In the latter case, the number of alpha particles required to give a barely visible photographic image is about $10^5/cm^2$ in Kodak Tri-X film. In autoradiography, the energetically charged particles may come directly from an alpha source, or from the passage of neutrons through nuclear processes such as (n,α) or (n,f). If a thin layer of powdered ZnS-Ag, about 10 microns thick, is placed between the alpha-particle source and the photographic film, the optical density of the developed photographic image is considerably higher than that without the ZnS-Ag. For equal optical densities, the use of the ZnS-Ag layer reduces the exposure time by a factor of 60 to 140, depending on the region of the optical density. The number of polonium-alpha particles required to give a barely visible image in Tri-X film is reduced to about $800/cm^2$. Optical density *vs* log exposure curves are given for Tri-X film exposed to polonium alphas with and without a ZnS-Ag layer.

D12. Forty-Channel Pulse Height Analyzer. E. J. COOK* AND G. F. PIEPER, *Yale University.*—A 40-channel pulse height analyzer employing the amplitude to time conversion technique and delay line information storage has been constructed. The unit consists of two chassis with a total of 56 tubes exclusive of power supplies. The first chassis produces an output pulse whose time delay after a master trigger is proportional to the original input amplitude. The second chassis stores all information delivered to it in this delayed pulse form in circulating binary codes of pulses in each of its 40 channels. The memory element is a 240-microsecond quartz delay line operated at a carrier frequency of 40 megacycles. Each six-microsecond channel has positions for 14 pulses of 0.2 microsecond duration, giving a channel capacity of 16 383 counts. The dead time of the instrument is fixed at 500 microseconds. Information is currently read out by displaying individual channels on an oscilloscope with a delayed sweep. A digital to analog converter for automatic data presentation is under construction. This will require 51 more tubes and will cause a chart recorder to plot number of counts per channel *versus* channel number in histogram form.

* Now at Research Laboratory, General Electric Company.

D13. A Fast Coincidence System with Amplitude Discrimination. G. S. STANFORD AND G. F. PIEPER, *Yale University.*—A system has been devised for the recording of coincident protons and gamma rays for (x,p,γ) correlation studies. Pulse-height analysis is carried out on those gamma rays which are coincident with a certain group of portons. The protons are detected in a thin NaI crystal and a particular group is selected with a single channel pulse height analyzer. The time delay between the input signal and the firing of the single channel analyzer is sufficiently dependent upon pulse height and analyzer settings to require the use of a "self-coincident" gating system to make the input to the $p-\gamma$ coincidence circuit independent of this effect. The gamma-ray channel employs a similar self-coincident arrangement to compensate for the variability in the firing time of a low-level discriminator. 6BN6's are used for coincidence circuits and EFP-60's are employed as generators of short pulses with sharp edges. A resolving time of 0.1 microsecond can be used when the range of gamma ray pulse heights to be investigated is 6–80 volts. The final coincidence between proton and gamma-ray pulses operates a linear gating circuit. The gamma pulses are then analyzed in the Yale 40 channel pulse height analyzer.

THURSDAY MORNING AT 10:00

McAlpin, Red Room

(H. P. Noyes, presiding)

Meson and High-Energy Theory

E1. A *D*-Wave Solution to Pion-Proton Scattering Data.* JAY OREAR, *Columbia University.*—An attempt has been made to see how much a small *d*-wave component can influence the *s*-wave solutions to the π^+ and π^- scattering data in the energy region 100 to 220 Mev. In this region the *s*-wave solutions depart appreciably from their best fit low energy curves: ($\alpha_3=-0.11\eta$) and $\alpha_1=0.16\eta$).[1] Preliminary investigations show that these low-energy recipes may be used up to 220 Mev if a *d*-wave phase shift ($T=3/2$, $J=5/2$) is used which goes as $-0.013\eta^5$. Then one is able to fit all data including the recent Chicago 165 and 189 Mev π^+ angular distributions within experimental errors using $\alpha_{31}=\alpha_{13}=\alpha_{11}=0$ and an α_{33} which passes through 90° at about 190 Mev. Since other choices of the *d* waves should permit equally large shifts in the *s* waves, the present data is not adequate to give definite values for any of the phase shifts except α_{33} in the region above 100 Mev.

*Supported by the joint program of the Office of Naval Research and the U. S. Atomic Energy Commission.
[1] Jay Orear, Phys. Rev. **96**, 176 (1954).

E2. Evidence for Pion-Pion Interaction.* W. G. HOLLADAY† AND R. G. SACHS, *University of Wisconsin.*—It has been shown by Sachs[1] that a large no-pion, two-pion cross term and the neglect of pion kinetic energy made it possible to calculate the nucleon magnetic moments on the basis of a no-recoil, core-pion model of the nucleon, the one-pion probability being zero and the two-pion $L=1$ state appearing with probability 9 percent, the maximum allowed by the sum of the moments. However, reasonable values of pion kinetic energy lower the moments sufficiently that some mechanism is needed to increase them again to the correct values. Core recoil, interaction currents, and excited cores are found to decrease the calculated moments. However, the assumption of a reasonably strong pion-pion attraction, which increases the contribution from the no-pion, two-pion cross term, is capable of giving large enough moments, provided the two-pion state is more probable than the one-pion state, just the situation that a pion-pion attraction would tend to produce. The correct $n-p$ mass difference follows in a natural way from these considerations.

*Work supported in part by U. S. Atomic Energy Commission.
†National Science Foundation Predoctoral Fellow. Now at Vanderbilt University.
[1] R. G. Sachs, Phys. Rev. **87**, 1100 (1952).

E3. Radiative Corrections to Muon Decay. R. J. FINKELSTEIN AND R. E. BEHRENDS, *University of California, Los Angeles.*—To compare the Fermi constants of neutron and muon decay one ought to take into account mesic and electromagnetic corrections. We have calculated electromagnetic radiative corrections, including inner bremsstrahlung, to the decay spectrum of the muon and find a change in lifetime of a few percent, depending on the assumed nature of the β interaction. Since this correction is energy dependent, it could conceivably distort the shape of the μ spectrum and mislead one about the β interaction, which is inferred from just this shape. That turns out not to be the case for the shape is not distorted in a significant way. However, it is important to correct the total lifetime, which may be altered by as much as 5 percent.

E4. Deuteron Model for π-Meson and Photon Capture by Complex Nuclei.* B. T. FELD, *M. I. T.*—We consider the model of π-meson capture in complex nuclei in which the interaction is with a pair of nucleons.[1] From the properties of meson production in nucleon-nucleon collisions, it may be concluded that the dominant interaction for mesons of moderate energies is with a deuteron-like pair. Similar considerations may be applied to the capture of high energy photons by nuclei if we assume that the photons interact through excitation of the nucleon "isobar." Data on the high energy photodisintegration of the deuteron lend support to this assumption, and also give an experimental measure of its limitations. The deuteron model (first proposed by Levinger) in this form is in reasonable agreement with observations on high energy neutrons and protons when proper account is taken of the internal motion of the nucleons.

*This work was supported in part by the joint program of the Office of Naval Research and the U. S. Atomic Energy Commission.
[1] S. Tamor, Phys. Rev. **77**, 412 (1950); Brueckner, Serber, and Watson, Phys. Rev. **84**, 258 (1951).

E5. Meson Pair Theory. BRUCE H. MCCORMICK AND ABRAHAM KLEIN,* *Harvard University.*—In connection with a program to investigate the *S*-wave part of the meson-nucleon interaction, we have carried through a re-examination of the meson pair theory of Wentzel, which has yielded some new results. The solution of the field equations provides the linear transformations between "in" and "out" variables, which defines the *S* matrix, and between "in" and Heisenberg variables, which defines the transformation $U(O, -\infty)$. The *S* matrix is well-known to consist of one channel-meson scattering. The matrix elements of $U(O, -\infty)$ yield all possible Fock space amplitudes. A generating function for the latter is easily constructed by means of Schwinger's dynamical principle. One can then obtain and exhibit explicitly (a) the renormalization constant associated with the true to free vacuum transition, (b) the proper mesic field of the source, and (c) the integral equation for meson scattering with correct asymptotic solution. As a further result, the self-energy of the sources can be obtained by comparing the vacuum states at different times. We are currently studying the extension of these methods to the isotopic spin-orbit coupling term, $\tau\cdot\pi\times\phi$.

*Society of Fellows.

E6. Exchange Current Effects in the Two-Nucleon System. J. BERNSTEIN AND ABRAHAM KLEIN,* *Harvard University.*—The program of calculation of exchange current effects in the deuteron[1] has been continued and extended to the investigation of photodisintegration. Further work has been confined to the Tamm-Dancoff method. To date, numerical computations have been completed for the quadrupole moment, correct to fourth order in the coupling constant. The adiabatic approximation and hard core wave functions were used. The results, to be presented, indicate a rate of convergence for electromagnetic effects, considerably more favorable than that for the nuclear potential itself, the total exchange contribution amounting to about five percent. The interaction current operator effective for transitions has been found to be composed of the meson current, obtained in the past by many authors, and a nucleon current part with matrix elements of the same order of magnitude. The latter has not been found previously because of intrinsic differences between Tamm-Dancoff and approximation schemes employed hitherto. Application to the high-energy photoeffect is in progress.

*Society of Fellows.
[1] J. Bernstein and A. Klein, Phys. Rev. **95**, 655A (1954).

E7. Production of K Mesons by Protons of Cosmotron Energy. MARTIN M. BLOCK,* *Naval Research Laboratory.*—The energy spectrum of K particles (970 m_e) produced by 2.9 Bev protons bombarding a heavy nucleus has been calculated for a laboratory observation angle of 90°. We have assumed that all K particles are produced in nucleon-nucleon collisions of the type $p+p \rightarrow K^+ + \Lambda^+ + N$,[1] where Λ^+ is a hyperon (2350 m_e). The proton-heavy nucleus collision is replaced by a proton-nucleon collision, where the target nucleons have an internal momentum distribution given by the Fermi degenerate gas model. The relativistic phase space is calculated in the appropriate center of mass system, as a function of target momentum. Two types of matrix elements have been employed, both giving isotropic angular distributions in the center of mass system; I constant, II proportional to K-particle momentum at low energies and falling off as the total energy for high energies. The resultant differential cross sections are transformed to 90° laboratory cross sections and then averaged over the internal momentum distribution. For matrix element I, the spectrum exhibits a peak at ~30 Mev and extends to ~150 Mev. Calculations are currently being made for other momentum distributions and laboratory angles.

* On military leave from Duke University, Durham, North Carolina.
[1] Block, Harth, Fowler, Shutt, Thorndike, and Whittemore, Bull. Am. Phys. Soc. **29**, No. 7, 33 (1954), abstract W10.

E8. Integral Equations of the Meson-Nucleon System.* R. L. MILLS, *Brookhaven National Laboratory.*—A formal study has been made of the covariant system of coupled integral equations describing one nucleon and an unlimited number of mesons. It is found to be possible to uncouple the unrenormalized equations; that is, the amplitudes thus defined can be expressed in terms of the solutions of an infinite sequence of uncoupled linear integral equations. Renormalization of the nucleon propagator and the vertex operator can be carried out and the resulting equations, which are coupled only through involving these renormalized quantities, become a finite, uncoupled sequence of equations when an upper limit is put on the number of mesons present in the intermediate states considered, and the lower order approximations are assumed to be already solved.

* Work performed under the auspices of the U. S. Atomic Energy Commission.

E9. Theory of Pion Photoproduction.* M. ROSS, *Brookhaven National Laboratory.*—Photoproduction of mesons from nucleons has been calculated using a pseudoscalar theory without cut off. Scattering of the meson after the photon vertex is considered in a Tamm-Dancoff approximation. Approximation from a gauge invariant expression is used to determine which diagrams should be considered. Two types of processes, the anomalous moment type of interaction and the ordinary electromagnetic scattering of mesons and nucleons, are both found to contribute large magnetic dipole matrix elements to the $p3/2$, $T=3/2$ state as called for by experiment. The former process cannot be adequately treated in the present framework. A Pauli moment interaction, for instance, yields unrealistic results. It is found for the second process that high momenta intermediate mesons make a surprisingly large contribution to the electric quadrapole matrix element. A detailed study has been made of the physical processes determining the ratio of the magnetic dipole and electric quadrapole interactions. The expressions will be compared with the well known nonrelativistic forms of these interactions.

* Work performed under the auspices of the U. S. Atomic Energy Commission.

E10. Polarization of Nucleons Elastically Scattered from Nuclei.* R. M. STERNHEIMER, *Brookhaven National Laboratory.*—The polarization P of nucleons elastically scattered from nuclei has been calculated for a complex nuclear potential V having the radial dependence $1/\{1+\exp[(r-r_0)/a]\}$, where r_0 is the nuclear radius and a determines the length of the exponential tail. The spin-orbit coupling was taken as $U\mathbf{l}\cdot\boldsymbol{\sigma}$, where $U \propto (1/r)(dV/dr)$. The WKB method was used in the calculations. The variation of P with the optical parameter k_1/K and the strength of the spin-orbit coupling was investigated for $A1$. In general, P remains positive throughout the first diffraction minimum. For the Berkeley data[1] for the polarization of 300 Mev protons scattered from $A1$, a reasonable fit has been obtained inside the first diffraction peak. The values of the parameters are: $k_1 \sim 1.2\times10^{12}$ cm^{-1}, $K \sim 3\times10^{13}$ cm^{-1}, with $r_0 \sim 3.2\times10^{-13}$ cm, $a \sim 0.5\times10^{-13}$ cm. The required U has a maximum of ~0.7 Mev near $r=r_0$. The effect of changing the shape of the central potential and the spin-orbit coupling will be discussed. The functions β and R, introduced by Wolfenstein to describe the asymmetry in a triple scattering experiment, have been evaluated for several cases.

* Work performed under the auspices of the U. S. Atomic Energy Commission.
[1] Chamberlain, Segrè, Tripp, Wiegand, and Ypsilantis, Phys. Rev. **95**, 1105 (1954).

E11. Asymmetry in Deuteron Pickup by High-Energy Polarized Protons.* B. J. MALENKA, *Washington University.*—The recent availability of strongly polarized beams of high-energy protons suggests their application to the deuteron pickup problem.[1] A preliminary examination of the direct pickup process in a heavy nucleus can be made by means of a classical argument of the type considered by Newns.[2] This model leads us to expect a right-left asymmetry for the emerging deuteron beam in the plane perpendicular to the original direction of polarization as a consequence of the difference in scattering of the proton and the pickup deuteron inside the nucleus. An estimate of the maximum asymmetry expected has been made assuming a small probability of the deuteron being elastically scattered inside the nucleus and assuming that the neutron is picked up from a definite $j=l\pm\frac{1}{2}$ state. Further approximations will be discussed.

* Partially supported by the Office of Naval Research.
[1] Such experiments also have been suggested by P. Hillman, Harwell (private communication).
[2] H. C. Newns, Proc. Phys. Soc. (London) **66A**, 477 (1953).

E12. Limitations of the Stripping Theory in Inelastic Deuteron Scattering.* JAMES W. HAFFNER, *M. I. T.*—The angular distributions of inelastic deuterons from light nuclei have been investigated using 15-Mev dueterons from the M. I. T. cyclotron and a particle selective technique developed in this laboratory.[1] The shapes of the resulting distributions indicate that the nuclear interaction theory,[2] which is analogous to a stripping-recombination process, holds fairly well for most angles. However, the nuclear theory fails at small angles and a Coulomb interaction theory[3] fits the data better. The significance of this fact relative to the stripping process in general is considered.

* Supported in part by the Office of Naval Research and the U. S. Atomic Energy Commission.
[1] F. A. Aschenbrenner, Phys. Rev. **95**, 600(A) (1954).
[2] Huby and Newns, Phil. Mag. **42**, 1442 (1951).
[3] Mullins and Guth, Phys. Rev. **82**, 141 (1951).

E13. Proton Bremsstrahlung. BEHRAM KURSUNOGLU, *University of Miami.*—Bombardment of several nuclei by protons with energies below threshold π^0-production energy gives rise to a continuous γ-ray spectrum arising from proton bremsstrahlung in the nucleus. A detailed experiment carried out at Berkeley[1] for Cu, Al, C, and Be yield bremsstrahlung curves that diverge at the low-energy region of the γ-radiation. The fact that the magnitude of the photon-cross section should be

proportional to fine structure constant times the elastic scattering cross section of the protons suggests the use of an interaction Hamiltonian describing the nucleon-nucleus interaction in terms of an optical potential. The inelastic part of the interaction being due entirely to the coupling of the protons to the radiation field. A semi-phenomenological investigation of the proton-bremsstrahlung based on the above model has been carried out. Numerical results will be given at the meeting.

[1] D. Cohen (private communication).

THURSDAY MORNING AT 10:00

McAlpin, Green Room

(F. N. FRENKIEL, presiding)

Liquid State: Fluid Dynamics

EA1. Structure of Liquid Tellurium. R. BUSCHERT, I. G. GEIB, AND K. LARK-HOROVITZ, *Purdue University.**—Monochromatic copper $K\alpha$ and Molybdenum $K\alpha$ radiation is incident on the free surface of molten Te (465°C) in a helium atmosphere. Jets of pure helium and baffles are used to retard deposition of Te on the windows and in the slits of the spectrometer. Argon and krypton Geiger counters with aluminum filters to absorb fluorescent L radiation are used to measure the scattered intensity as a function of $\sin\theta/\lambda$. The incident intensity is monitored with a Geiger counter set at a fixed position. The intensity curves for CuKα and MoKα after corrections for absorption, polarization, and background are analyzed.[1] The radial distribution curve shows peaks at 2.9A, 3.7A, 4.3A, and 6.4A. The area under the first peak corresponds to approximately two nearest neighbors. Since the bond distance along the chain in the solid is 2.86A, these results indicate the presence of similar chains in the liquid as predicted by Lark-Horovitz from electrical measurements.[2]

* Work supported by a Signal Corps contract.
[1] G. C. Danielson and C. Lanczos, J. Franklin Inst. **233**, 365, 435 (1942).
[2] A. Epstein and H. Fritzsche, Phys. Rev. **93**, 922(A) (1954); **94**, 1426(A) (1954).

EA2. Dislocation Model of Liquids. JEROME ROTHSTEIN, *Signal Corps Engineering Laboratories.*—It is suggested that defects in general, and vacancies in particular, can cooperate to form dislocations as the melting point is approached from below. Melting would then occur when dislocation density is sufficiently high to cause resistance to shear to vanish. Low defect densities should increase with temperature through a Boltzmann factor. Sufficiently large defect density should result in cooperative lowering of the activation energy for defect formation, thereby leading to a sharp melting point. The reason for the lowering can be seen from the fact that fewer broken bonds are required to form a single multiple vacancy than the same free volume in the form of individual separated vacancies. A brief discussion is given of the relation of this model to hole and crystallite theories of liquid, to cooperative theories of melting, and to some experimental results in the literature on pre-transition phenomena, crystallization, and liquid structure.

EA3. Secondary Recrystallization Analogy in a Heterogeneous Liquid System. JOHN P. NIELSEN, *New York University.*—General grain growth is somewhat analogous to foam cell growth because of the similar nature of the driving force in the two cases, namely, interfacial or surface free energy. Secondary recrystallization is a special type of grain growth which appears to be nucleated by a "geometrical coalescence" phenomenon.[1] In this phenomenon two suitably oriented grains on first encountering each other create a new low energy common boundary resulting in a highly unstable boundary geometry at the point of encounter. The instability results in the development of a complex grain statistically nine times larger than the neighboring grains which, because of this size advantage, proceeds to "consume" its neighbors. A striking physical analogy for the nucleation of this secondary recrystallization can be produced in a liquid-liquid system. A stirred oil-water mixture, with surface tension adjusted by alcohol, will produce a mass of uniformly sized oil globules. An occasional pair of globules in mutual contact will coalesce producing a globule twice as large as neighbor globules, which by virtue of this size advantage "consumes" its neighbors. The analogy can be improved by having globules that also increase in size by diffusion from the continuum.

[1] John P. Nielsen, Trans. Am. Inst. Mining Met. Engrs. **6**, 1084.

EA4. Wave Propagation in Elastic Tubes Filled with Streaming, Viscous Liquid.* G. W. MORGAN, *Brown University* (introduced by R. B. Lindsay).—A previous analysis by Morgan[1] and Kiely of wave propagation in a system at rest is extended to determine the influence of tube inertia and of a steady stream upon which waves are superposed on the phase velocity and damping. The investigation is restricted to thin-walled tubes, to waves whose amplitude is small, and whose length is great compared with the tube radius R. The magnitude of the kinematic viscosity ν is limited by the condition $\omega R^2/\nu \gg 1$, where ω is the frequency of the disturbance. An approximate solution is obtained by boundary layer analysis. It is found that the phase velocity is equal to the sum of the phase velocity in a system at rest and the average velocity of the steady stream, provided the latter is so small that a linear correction is sufficiently accurate. For larger velocities a more complicated situation exists. The results for the limiting case of vanishing velocity are compared with those for $\nu=0$.

* This research was supported by the Office of Naval Research.
[1] G. W. Morgan and J. P. Kiely, J. Acoust. Soc. Am. **26**, 3, 323 (1954).

EA5. Investigation of a Quantitative Phase Contrast Method for Examining Nonhomogeneous Media. G. C. KRUEGER, *University of Maine.*—Of the optical methods generally used in studying the phenomena associated with fluid flow fields, *viz.*, the shadowgraph and schlieren methods and the Mach-Zehnder interferometer,[1] only the interferometer appears to be suitable for quantitative investigation. Minor modifications of these optical systems effectively transforms them into a phase microscope.[2] The final image in a phase microscope may be considered as being formed by light diffracted by the object superposed on a coherent background of undiffracted light. The optical properties of the object can be inferred by varying the phase and amplitude of the coherent background, these being determined by the optical properties of the phase plate. The progress of our investigation will be reported. This investigation has been supported in part by the University of Main Coe Research Fund and more recently by the National Science Foundation.

[1] N. F. Barnes and S. L. Bellinger, J. Opt. Soc. Am. **35**, 497–509 (1945).
[2] F. Zernike, Physica **5**, 785–795 (1938); **9**, 686–698, 974–986 (1942); Proc. Phys. Soc. (London) **61**, 158–164 (1948).

EA6. On Statistical Theory of Shear Turbulence in a Parallel Flow. C. M. TCHEN, *National Bureau of Standards.*—We assume that the mean motion is steady and has only a horizontal component which is a function of the vertical coordinate. The turbulent motion is statistically steady but inhomogeneous. However, the scale of inhomogeneity is assumed to be much larger than the wavelengths of the turbulent motion considered. From the Reynolds equation, the equation for the propagation of correlation can be derived. We are interested in the variation of the correlation function with the length interval. For very large intervals the correlation is controlled by very big eddies, not governed by statistics, but by the geometry of the system. For very small intervals the correlation is controlled by eddies in the viscous region. Between those two extreme regions the correlation will be controlled mainly by eddies active in transferring the energy from the mean flow into big eddies, and through nonlinear mechanism, from big eddies into smaller ones. For such an intermediate range of length intervals and for a strong mean velocity gradient, the correlation function is found independent of the length interval, in contrast with the Kolmogoroff theory of locally isotropic turbulence. But it agrees with the law of spectral function, as found earlier to be inversely proportional to the wave number.

EA7. The Blast from a Sphere of High-Pressure Gas. HAROLD L. BRODE, *The RAND Corporation.*—The gas dynamics resulting from the release of an isothermal sphere of gas initially at rest and at a high pressure are described by the numerical solution of the differential equations which represent an ideal gas in radial motion. The resulting outward shock and the inward rarefactions and shocks are described in some detail and are compared with the gas dynamics of the point-source solution.[1] The existence of the inward moving shocks has been discussed in several places[2–4] and in one instance the early phase has been numerically calculated.[5] This phenomenon is observed in the present calculations to occur repeatedly, subjecting the origin to several compressive waves which are reflected there and which move out to overtake the main shock.

[1] H. L. Brode, Phys. Rev. **95**, 658(A) (1954).
[2] F. Wecken, Z. angew, Math. Mech. **30**, 270 (1950).
[3] J. A. McFadden, J. Appl. Phys. **23**, 1269 (1952).
[4] H. Schardin, Communications on Pure and Applied Mathematics (Inst. of Mathematical Sciences, New York University, (1954), Vol. VIII, p. 223.
[5] T. S. Walton, Phys. Rev. **87**, 910(A) (1952).

EA8. A Method for Numerical Solution of Transient Hydrodynamic Shock Problems in Two Space Dimensions. HARWOOD G. KOLSKY, *Los Alamos Sceintific Laboratory.*—A method for numerically solving hydrodynamic problems involving two space dimensions and time has been developed based on the von Neumann-Richtmyer method of treating shocks.[1] Finite difference equations for the system are constructed from the basic differential equations of compressible hydrodynamics. Difference formulas are also given for checking the stability of the numerical space-time mesh, and for checking the total energy of the system. The results of several check problems done on the Los Alamos IBM 701 Computer are compared to known solutions. The check problems include a plane shock, supersonic flow past a wedge, and a diverging blast wave interacting with the ground. The requirements imposed on electronic computers by problems of this type and possible extensions of the method to other types of physical problems will be discussed briefly.

[1] J. von Neumann and R. D. Richtmyer, J. Appl. Phys. **21**, 232 (1950).

EA9. A Method for the Observation of the Ionization Profile Behind Explosive Produced Shocks in Air. JACOB SAVITT, *U. S. Naval Ordnance Laboratory.*—In many types of explosive experiments, the ionization produced by the detonation of chemical explosives is used to start and stop electrical circuits by shorting ionization probes. In these systems, current flows through the ionized region produced at and behind shock fronts in air. A method for the observation of the ionization profiles behind such shocks is described. Preliminary measurements of a qualitative nature of the shocks produced by the detonation of small quantities of lead azide are presented and discussed. It is found that the region of maximum ionization for these shocks is at some distance behind the shock front.

EA10. Mass Flow in the Shock Tube.* ALBERT C. WILLIAMS AND RAYMOND J. EMRICH, *Lehigh University.*—The measurements made by Mack[1] of density as a function of time and distance throughout the flow in a 3.5-cm-diameter shock tube permit the calculation of mass flow as a function of time and distance. The one-dimensional continuity equation is $\partial\rho/\partial t+\partial m/\partial x=0$ where $m=\rho u$ is the mass flow; the corresponding difference equation is $\Delta m=-(\Delta\rho/\Delta t)(\Delta x)$. Lines of constant density, determined experimentally, are plotted on an $x-t$ diagram. The difference equation is applied point by point throughout the flow region, using the boundary conditions at the rarefaction head and at the shock front, to yield the mass flow. The two boundary conditions overdetermine the problem so that an estimate of overall accuracy is possible. For starting pressure ratios $P_{41}=9.8$ and 49.2, the mass flow has been found to deviate significantly from that of the ideal shock tube theory, except near the rarefaction head.

* Supported by the Office of Naval Research.
[1] John E. Mack, Lehigh University Institute of Research, Technical Report 4 (April 1954); Emrich, Mack, and Shunk, Phys. Rev. **90**, 375(A) (1953).

Business Meeting of the Division of Fluid Dynamics

THURSDAY AFTERNOON AT 2:00

Manhattan Center, Gold Room

(A. KANTROWITZ, presiding)

Symposium of the Division of Fluid Dynamics

Fluid-Dynamics Problems in Astrophysics

F1. A Theory of Turbulence. S. CHANDRASEKHAR, *Yerkes Observatory.* (40 min.)

F2. Gas-Dynamics Effects of Star Formation. MALCOLM SAVEDOFF, *University of Rochester.* (30 min.)

F3. The Formation of Galaxies. DENNIS SCIAMA, *Institute for Advanced Study.* (30 min.)

F4. Turbulence in Stellar Atmospheres. MARTIN SCHWARZSCHILD, *Princeton University.* (40 min.)

THURSDAY AFTERNOON AT 2:00

New Yorker, North Ballroom

(G. E. MOORE, presiding)

Symposium of the Division of Electron Physics

G1. Precision Measurements of Ionization Probabilities of Monoenergetic Electrons. R. E. FOX, *Westinghouse Research Laboratories.* (30 min.)

G2. Mass-Spectrometric Analysis of Ions Produced in the Field Ion Microscope. M. G. INGHRAM, *University of Chicago.* (30 min.)

G3. Upper-Atmospheric Studies during the International Geophysical Year. J. KAPLAN, *University of California, Los Angeles.* (30 min.)

Business Meeting of the Division of Electron Physics

THURSDAY AFTERNOON AT 2:00

McAlpin, Colonial Room

(YARDLEY BEERS, presiding)

Invited Paper

H1. Molecular Amplification and Generation of Microwaves with Applications to Spectroscopy and to Time Standards. J. P. GORDON, *Columbia University.* (30 min.)

Microwaves

H2. Pure Rotational Spectra of the Thallium Halides.* M. MANDEL AND A. H. BARRETT, *Columbia University.*—The pure rotational spectra of the thallium halides have been observed using a high-temperature microwave spectrometer.[1] Internuclear distances, vibration-rotation interactions, and mass ratios of the chlorine and bromine isotopes have been determined.

Molecule	$r_e(A)$	α_e(Mc/sec)
$Tl^{205}F$	2.0844 ±0.0001	44.98 ±0.05
$Tl^{205}Cl^{35}$	2.4848 ±0.0001	11.90 ±0.01
$Tl^{205}Br^{79}$	2.6181 ±0.0001	3.927 ±0.005
$Tl^{205}I$	2.8136 ±0.0001	1.985 ±0.005

The thallium chloride results revealed a discrepancy in the previous work on TlCl[2] where the isotope identified as $Tl^{205}Cl^{35}$ is in reality $Tl^{203}Cl^{37}$. The electric quadrupole coupling constants of $Tl^{205}Br^{79}$ and $Tl^{205}I$ in the $v=0$ state were found to be $+130\pm5$ Mc and -550 ± 20 Mc, respectively, and the electric dipole moment of $Tl^{205}F$ to be approximately 7 debye units. The results give evidence about the ionic character of these molecules and the electronegativity of Tl.

*Work supported jointly by the Signal Corps, the Office of Naval Research, and the Air Research and Development Command.
[1] Stitch, Honig, and Townes, Rev. Sci. Instr. 25, 759 (1954).
[2] Carlson, Lee, and Fabricand, Phys. Rev. 85, 784 (1952).

H3. The Microwave Spectrum of Nitrosyl Bromide.* QUITMAN WILLIAMS AND T. L. WEATHERLY, *Georgia Institute of Technology.*—The microwave spectrum of NOBr has been investigated in the region 20 000 to 40 000 Mc. The molecule is an almost symmetric top, and its spectrum in this region consists of three separate groups of lines for the transitions $J=2\rightarrow3$, $3\rightarrow4$, and $4\rightarrow5$. Each transition, $J\rightarrow J+1$, produces a large number of lines as a result of the slight asymmetry, the large bromine quadrupole coupling, and the presence of two bromine isotopes. A preliminary analysis of the $J=2\rightarrow3$ transition yields the following values for quadrupole couplings, rotational constants, and asymmetry parameters:

	$NOBr^{79}$	$NOBr^{81}$
$(eQ\partial^2V/\partial z^2)$	429.5 ±2.6 Mc	358.9 ±2.2 Mc
A	83 728. ±178 Mc	83 456. ±178 Mc
B	3746.78 ±0.25 Mc	3722.26 ±0.25 Mc
C	3586.29 ±0.25 Mc	3563.34 ±0.25 Mc
b	−0.0010023	−0.0009956

The rotational constant A was determined from the relation $I_C=I_A+I_B$. The quadrupole coupling was calculated assuming the electronic distribution near the bromine nucleus to be symmetric about the z axis which extends along the N−Br bond. The interatomic distances and bond angle are in the process of calculation.

*Sponsored by the Office of Ordnance Research, U. S. Army.

H4. Zeeman Effect in the Rotational Spectrum of NO.* MASATAKA MIZUSHIMA, J. T. COX, AND WALTER GORDY, *Duke University.*—The Zeeman splitting of the 2 mm wave, $J=1/2\rightarrow3/2$ rotational transition of $N^{14}O^{16}$ in the $^2\Pi_{\frac{1}{2}}$ electronic state has been measured with fields of the order of 100 gauss. The observations were made with a waveguide cell coiled between the poles of a Varian magnet. Magnetic field measurements were made with the electronic resonance of DPPH at frequencies of the order of 300 Mc. A general theory of the Zeeman effect with h.f.s. has been developed and applied specifically to $N^{14}O^{16}$. The g factors for the four states under investigation were found theoretically to be expressed as: $J=1/2$, $g_c=\alpha$, $g_d=-\alpha$; $J=3/2$, $g_c=\beta+(2/5)\alpha$, $g_d=\beta-(2/5)\alpha$, where c and d are the lower and upper components of the

Λ-type doublet, respectively. This relation was found to hold experimentally with the values, $g=+0.0232$ and $\alpha=+0.0029$. Theoretically, g comes from the mixing of $^2\Pi_{\frac{1}{2}}$ and $^2\Pi_{\frac{3}{2}}$ states and α comes from that of $^2\Pi_{\frac{1}{2}}$ and $^2\Sigma$ states. It was found by the theory, in which the molecular rotation and the spin orbit coupling were taken into account, that the electronic wave function of the two rotational states should be: $J=1/2$, $(^2\Pi_{\frac{1}{2}}|-0.0021(^2\Sigma|$; $J=3/2$, $(^2\Pi_{\frac{1}{2}}|-0.0247(^2\Pi_{\frac{3}{2}}-0.0021(^2\Sigma|$. These wave functions give g (theo.) $=+0.0228$ and α (theo.) $=+0.0020$. which agree very well with the observed values.

* This research was supported by The United States Air Force through the Office of Scienctific Research of the Air Research and Development Command.

H5. Reduction of Doppler Width of Microwave Lines.* R. H. ROMER† AND R. H. DICKE, *Princeton University.*—A new method for reducing the Doppler width of microwave lines has been developed, which depends on the properties of a specially shaped resonant cavity. Ammonia at low pressure is contained in a TE_{111} cylindrical cavity, with diameter large compared to height. An intense pulse of 1.25 cm power excites the gas to states from which it emits coherent spontaneous radiation.[1] The radiation following the pulse is damped, as molecules colliding with the walls are removed from the coherently radiating system. In a short time, the only molecules still contributing have velocities nearly parallel to the large faces of the cavity. These molecules travel for a long time, giving the line a width determined by the cavity diameter. Calculations based on a 5.75 cm diameter cavity predict a line of nearly Lorentz shape, 16 kc in width, about $\frac{1}{4}$ of the Doppler width. Experimentally observed lines are in good agreement with this.

* Research supported by the Signal Corps.
† National Science Foundation Predoctoral Fellow.
[1] R. H. Dicke, Phys. Rev. **93**, 99 (1954).

H6. The Microwave Spectrum of NO_2.* GEORGE R. BIRD, *The Rice Institute.*—The microwave spectrum of NO_2 was first observed by McAfee,[1] who found a group of eight absorption lines ranging from 26 695.08 mc to 26 563.23 mc and tentatively assigned these to the rotational transition $J_{K-1K+1}=6_{06}\rightleftarrows5_{15}$ on the basis of electron diffraction data and Zeeman effect measurements. Muller[2] examined an isotopic mixture for another $N^{14}O_2$ line or an $N^{15}O_2$ line predicted from McAfee's assignment, but found neither. Recent infrared observations by Moore[3] yield precise rotational constants inconsistent with McAfee's assignment. Four new groups of absorption lines have now been predicted from the infrared data and found. A group of ten lines ranging from 15 653.98 mc to 14 929.90 mc has been assigned $8_{08}\rightarrow7_{17}$ and Zeeman shifts of individual lines have been measured. A combination rule for the fine structure frequency differences has been discovered and used to identify the ten lines in detail. An analysis of the fine structure is now being performed by Lin and the author, and it may be expected that magnetic interaction constants differing widely from those previously reported will be obtained.

* Work done at Mallinckrodt Laboratories, Harvard University, and supported in part by the Office of Naval Research.
[1] K. B. McAfee, Jr., Phys. Rev. **78**, 340(A) (1950), Phys. Rev. **82**, 971 (1951).
[2] N. Muller, "The Spectrum of Chlorofluoromethane," Doctoral thesis, Harvard University, 1952.
[3] G. E. Moore, J. Opt. Soc. Am. **43**, 1045 (1953).

H7. Microwave Spectrum of Methylamine. KOICHI SHIMODA,* TETSUJI NISHIKAWA, AND TAKASHI ITOH, *University of Tokyo* (introduced by C. H. Townes).—The molecule is a slightly asymmetric rotor with hindered rotation and inversion; the spectrum consists of more than two hundred lines between 7 and 30 kMc/sec. Several reports of lines have already appeared[1–4] but none of them has given consistent assignments. We have assigned seven series of $\Delta J=0$ lines which are characteristic of the asymmetric molecule with internal rotation. The rotational transitions ($\Delta J=\pm1$) are also affected by K-type doubling, inversion, and internal rotation. From their Stark patterns and frequencies we have obtained decisive assignments of more than 30 lines and determined the five rotational constants required to describe the molecule. The height of the hindering potential has been determined to be 685 ± 10 cm^{-1} assuming a sinusoidal form. The magnitude of inversion doubling changes from 5 kMc/sec to more than 30 kMc/sec depending upon the rotational and vibrational states and in agreement with theoretical expectation. Transitions between K-type doublets have also been identified.

* Carbide and Carbon Fellow, Columbia University, 1954–1955.
[1] D. R. Lide, Journ. Chem. Phys. **20**, 1812 (1952).
[2] K. Shimoda and T. Nishikawa, J. Phys. Soc. Japan **8**, 133 and 425 (1953).
[3] K. Shimoda, T. Nishikawa and T. Itoh, J. Chem. Phys. **22**, 1456 (1954); J. Phys. Soc. Japan **9**, Nr6 (1954).
[4] D. R. Lide, J. Chem. Soc. **22**, Nr9 (1954).

H8. Molecular Distortion Caused by Hindered Rotation.* HENRY T. MINDEN, *Chicago Midway Laboratories.*—If there is a force hindering internal rotation of ethane about its figure axis, there ought to be a force tending to distort the hydrogen tetrahedra. The tumbling moment of inertia should increase as the molecule assumes higher torsional states. Assuming a cosine hindering potential there ought to be a term proportional to $\langle\frac{1}{2}V_0(1-\cos3\alpha)\rangle A_y$ in the expression for the perpendicular rotational constant. The variation of this quantity with barrier height for the first twelve torsional states (for $K=0$) has been computed and a theoretical microwave spectrum deduced for the ethane-like molecule CH_3SiF_3.

* This research was supported in whole by the United States Air Force.

H9. Magnetic Hyperfine Effects and Electronic Structure of NO.* G. C. DOUSMANIS, *Columbia University.*—The theory[1] of magnetic hfs in diatomic molecules has been re-examined and the Hamiltonian is obtained as $H=a(I_{x'}L_{x'}+I_{y'}L_{y'}+I_{z'}L_{z'})+(b+c)I_{z'}S_{z'}+b(I^+S^-+I^-S^+)/2+d(e^{2i\varphi}I^-S^-+e^{-2i\varphi}I^+S^+)/4+e[e^{i\varphi}(S^-I_{z'}+I^-S_{z'})+e^{-i\varphi}(S^+I_{z'}+I^+S_{z'})]$. This H is the same as the one of reference 1, except for the constants d and e which differ by a factor of two with the ones given there. The expressions presently obtained are $d=3g_l\mu_0\mu_N(\sin^2\chi/r^3)_{Av}$. $e=3g_l\mu_0\mu_N(\sin\chi\times\cos\chi/r^3)_{Av}$. The corrected expressions are applied to the observed[2] hyperfine effects in the $N^{14}O^{16}$ molecule and the magnetic constants thereby determined. The values in Mc/sec are $a=83.4$, $b=69.2$, $c=-87.6$, $d=112.6$, $16\pi g_l\mu_0\mu_N\psi^2(0)/3=39.9$. These several experimental parameters, as well as the observed quadrupole interaction, give considerable information on the molecular wave functions, and are interpreted in terms of an electronic structure consisting of about 65 percent $N=0$ and 35 percent $^-N=0^+$. The unpaired electron is shown to be essentially in a $2p\pi$ orbital, but with 2 percent s-character. Values of the magnetic constants calculated from atomic wave function approximations agree with the experimental ones to about 8 percent.

* Work supported jointly by the Signal Corps, the Office of Naval Research, and the Air Research and Development Command.
[1] Frosch and Foley, Phys. Rev. **88**, 1437 (1952).
[2] Beringer *et al.*, Phys. Rev. **78**, 581 (1950); **94**, 343 (1954); Gordy and Burrus, Phys. Rev. **93**, 419 (1954); Gallagher, Bedard, and Johnson, Phys. Rev. **94**, 729 (1954).

THURSDAY AFTERNOON AT 2:00

Manhattan Center, Masonic Room

(D. J. HUGHES, presiding)

Neutrons, II

HA1. Slow Neutron Resonant Scattering.* H. L. FOOTE, JR., *Brookhaven National Laboratory*, AND J. MOORE, *Brookhaven National Laboratory and Columbia University.*—A new experimental technique is being developed for the observation of low-energy resonance scattering as a function of energy. A thin scattering sample is placed at a glancing angle to an incident monochromatic neutron beam. This geometry allows a maximum number of neutrons to be scattered and to be detected, thus giving practical counting rates. A single BF_3 counter placed to one side of the sample and at right angles to the incident beam is used to detect the scattered neutron. The observed counting rate is proportional to the ratio (σ_s/α_t). This arrangement also permits a simplified analysis. The experimental apparatus will be described and results obtained presented.

* Research performed under the auspices of the U. S. Atomic Energy Commission.

HA2. Slow Neutron Velocity Spectrometer Using the Nevis Synchrocyclotron.* G. GRIMM, L. J. RAINWATER, AND W. W. HAVENS, JR., *Columbia University.*—The high energy beam of a synchrocyclotron deflected into a target in about one cycle of rotation of the proton beam (~0.05 μsec) should supply an extremely intense neutron source because of the high excitation of the compound nucleus. The feasibility of this procedure has been successfully demonstrated using the Nevis cyclotron. At the proper time in the frequency modulation cycle the total internal proton beam is deflected vertically to strike a tungsten target at the base of an internal moderator box containing nylon. The neutrons are collimated by a 6×6 in. opening in the 8 foot thick lead and iron cyclotron shield and by additional boron loaded concrete and B_4C shields. The counters are shielded from gamma rays and fast neutrons by 24 inches of lead placed below the slow neutron path. The initial studies have used a bank of fourteen BF_3 counters 20 cm long, 2½ in. diameter filled to a pressure of 20 cm and a source detector distance of 34.85 meters. The open beam counting rate is about 2000 counts/hour for a 2 μsec detection channel in the 100–1000 ev region. Many resonances have been observed ranging from the 20-kev group in Ti to the 5.2-ev level in Ag.

* Supported by the U. S. Atomic Energy Commission and the Joint U. S. Atomic Energy Commission and Office of Naval Research program.

HA3. Recent Mechanical Improvements in the Brookhaven Fast Chopper.* F. G. P. SEIDL, *Brookhaven National Laboratory.*—A new structurally improved 30-inch rotor for the Brookhaven fast chopper[1] or neutron shutter is in operation at 10 000 rpm. The first rotor was run at 6000 rpm. To eliminate air drag rotors are spun *in vacua* of 10^{-4} mm or better. During spin tests the second rotor was held at various speeds up to 12 030 rpm for 3 hr and 12 150 rpm for 1.5 hr. For continuous operation at 12 000 rpm still greater strength is needed in the parts containing the narrowest portions of the neutron slits; these travel 1571 ft sec at 12 000 rpm. Following a design modification of these parts, a third rotor is under construction. Moreover, it will be possible to hold steel pieces in the third rotor near its rotation axis; they should reduce γ-ray background by 50 times. Because of the faster rotor speed now available and the use of an improved neutron detector which is due to H. Palevsky, the over-all time uncertainty in the time-of-flight setup has been *observed* to be 1 μsec corresponding to a total resolution width at half-maximum of 0.05 μsec/*m* for a 20 *m* flight path.

* Work carried out under contract with U. S. Atomic Energy Commission.
[1] Seidl, Hughes *et al.*, Phys. Rev. 95, 476 (1954).

HA4. Radiation Widths of Nuclear Energy Levels.* J. S. LEVIN AND D. J. HUGHES, *Brookhaven National Laboratory.*—The experimental data on radiation widths of slow neutron resonances, primarily from the Brookhaven slow chopper, have been investigated for dependence on excitation energy, nuclear spin, atomic weight, and nuclear level spacing. In a single nuclide the radiation widths seem to be relatively constant from level to level as is expected if many final states are available for the gamma-ray transition. However, there is also some evidence that radiation widths in a given nuclide are somewhat different for levels of different spins. Among the many nuclides for which measurements have been made there seems to be little or no dependence of the radiation widths on the spin of the target nuclide. Radiation widths show a tendency to decrease with increasing atomic weight, however they increase just before a closed nuclear shell and decrease after the shell closing; a discontinuity of a factor of 30 is observed near an atomic weight of 208. This behavior of radiation widths has been investigated in light of the theoretical formulas given by Blatt and Weisskopf, and it appears to be explainable in terms of the observed binding energies and nuclear level spacings.

* Work carried out under contract with U. S. Atomic Energy Commission.

HA5. Resonance Parameters in U^{238}.* R. S. CARTER, *Brookhaven National Laboratory.*—The resonance structure in the total neutron cross section of U^{238} has been studied using the Brookhaven fast chopper. The energy interval studied extended up to 7000 ev. The complete sets of Breit-Wigner level parameters have been determined for the four lowest energy resonances using the "thick-thin" method of area analysis. The parameters E_0 and the neutron width Γ_n have been determined for the remainder of the resonances observed. The individual parameters were used to determine the average level spacing $\bar{D}$, the average reduced neutron width $\langle\Gamma_n^0\rangle$, and the ratio $\langle\Gamma_n^0\rangle/\bar{D}$. The resonance absorption integral has been calculated.

* Work carried out under contract with U. S. Atomic Energy Commission.

HA6. Neutron Widths of Nuclear Energy Levels.* D. J. HUGHES, *Brookhaven National Laboratory.*—The parameters of many neutron resonances for heavy elements have been measured recently with the Brookhaven fast chopper.[1] In this work, it was possible to obtain neutron widths even in the poor resolution region by taking advantage of the relative constancy of radiation widths from level to level in a single nuclide. Sufficiently many neutron widths were obtained for individual nuclides to investigate the distribution in size of the reduced neutron widths, which exhibit a wide range in size, typically extending over a factor of about 100 in a single nuclide. Within the present experimental accuracy the size distributions observed in about ten nuclides are exponential. There seems to be no correlation between the neutrons widths of specific levels and the spacings to adjacent levels, as might be expected from the simplified theory of the relationship of neutron width to spacing. The *average* reduced neutron width, however, bears a simple relationship to the *average*

spacing, being about 10^{-4} of the latter, the exact value depending on the atomic weight.

* Work carried out under contract with U. S. Atomic Energy Commission.
[1] Carter, Harvey, Hughes, and Pilcher, Phys. Rev. **96**, 113 (1954).

HA7. Level Spacings of Heavy Nuclei.* JOHN A. HARVEY, *Brookhaven National Laboratory.*—The variation with atomic weight of the level density at neutron binding energy for heavy nuclei has been studied with the Brookhaven fast chopper. The level spacing for *s*-wave neutrons for odd Z nuclei around the magic numbers of 50, 82, and 126 neutrons is about a hundred times greater than that between shells. The level spacing increases as the neutron closed shells are approached and then drops rapidly above the shells in contrast to the 1-Mev neutron capture results.[1] Even after adjusting the level spacings to the same excitation energy, the same characteristics are present. The spacing of the levels for $l=0$ neutrons in a particular nuclide appears more uniform than would be expected if the levels were distributed randomly. The variations of the level spacing between odd Z and even Z nuclei and between odd and even isotopes for even Z nuclei will be discussed.

* Work carried out under contract with U. S. Atomic Energy Commission.
[1] Hughes, Garth, and Levin, Phys. Rev. **91**, 1423 (1953).

HA8. $\bar{\Gamma}_n^0/\bar{D}$ for Slow Neutron Resonances. R. COTE AND L. M. BOLLINGER, *Argonne National Laboratory.*—Neutron resonances in elements whose masses are near 55 have been studied by means of the Argonne neutron velocity selector. A collection of these data has been made in order to obtain some additional evidence to aid in establishing the most nearly correct nuclear model. The "cloudy crystal ball" model of the nucleus proposed by Feshbach, Porter, and Weisskopf[1] predicts that the ratio of the average reduced neutron width to the average level spacing, $\bar{\Gamma}_n^0/\bar{D}$, may exhibit maxima for several mass values. Carter, Harvey, Hughes, and Pilcher[2] have presented data on nuclei whose masses are near 155. Their data reveal a maximum in $\bar{\Gamma}_n^0/\bar{D}$ near 155 and if a 42-Mev well depth, which satisfies these data, is inserted into the theory additonal maxima are predicted at 11 and 55. The present collection consisting of new data on Va, Cr, Co, Cu, and As and earlier data on Mn, Zn, and Ga[3] show a maximum at about 55.

[1] Feshbach, Porter, and Weisskopf, Phys. Rev. **90**, 166 (1953).
[2] Carter, Harvey, Hughes, and Pilcher, Phys. Rev. **96**, 113 (1954).
[3] Bollinger, Dahlberg, and Palmer, private communication.

HA9. Total Neutron Cross Sections in the Kilovolt Region: Sc, V, Mn, and Co.* H. MARSHAK AND H. W. NEWSON, *Duke University.*—The total neutron cross sections of Sc, V, Mn, and Co between 2 and 100 kev were measured simultaneously by the method previously used.[1] The samples were about the same thickness; so that comparison with the same resolution and self absorption could be made. Thinner samples were used for measuring the peak cross sections when feasible. The V sample showed particularly strong resonances at 4.1, 6.6, 11.5, 16.6, 22.2, 69.1, and 87.1 kev. The 69.1 and 87.1 kev appear to be resolved. Their measured peak cross sections implied $J=4$, and $J=3$ respectively for *S*-wave scattering. Area analysis of the other resonances (based on two samples of different thicknesses) yielded J value assignments in certain cases. There were other weaker resonances from 22 to 70 kev. The Mn sample showed strong resonances at 2.4, 7.3, 9.0, 21.2, 27.3, and 35.1 kev. The 35.1-kev resonances appeared to be resolved and its J value is 3. Area analysis on the 2.4-kev resonance yielded a J value of 3, consistent with the Argonne Fast Chopper data[2] on Mn. There were other weak resonances in Mn. The Co sample showed only three appreciable resonances. They were at 5.4, 7.8, and 28.3 kev.

* Work supported by the U. S. Atomic Energy Commission.
[1] J. H. Gibbons, Phys. Rev. **94**, 773 (1954).
[2] Bollinger, Palmer, and Dahlberg, Phys. Rev. **95**, 645 (1954).

HA10. Total Neutron Cross Sections in the Kilovolt Region: Separated Isotopes of Nickel and Cerium.* R. C. BLOCK AND H. W. NEWSON, *Duke University.*—Transmission cross sections of Ni^{58}, Ni^{60}, Ce^{140}, and Ce^{142} (obtained as oxides from the Oak Ridge National Laboratories) were investigated with the neutron collimation-detection equipment previously reported.[1] The nickel isotopes were examined over an energy region from 2 to 270 kev. Ni^{58} exhibits resonances at 5, 17, 65, 109, 124, 142, 162, 192, 211, 229, and 236 kev, the high peaks occurring at 17, 65, 142, 162, and 211 kev. Ni^{60} has peaks at 15, 30, 67, 88, 99, 109, 140, 162, 188, 200, and 257 kev with prominent peaks at 15, 30, 67, 188, and 200 kev. The cerium isotopes were run over two energy regions: 0.5 to 60 kev and 80 to 125 kev (the latter range with a thicker than usual target). In the 0.5 to 60 kev range Ce^{140} has resonances at 2.8, 6.7, 10, 22, and 43 kev, the strong peaks at 10, 22, and 43 kev. Ce^{142} resonances are at 1.6, 3.2, 4.2, 9, 16, 26, and 44 kev. There is a very strong peak at 1.6 kev, a weak peak at 9 kev, and the others are comparable in strength to the strong Ce^{140} peaks. In the 80 to 125 kev region no peaks in Ce^{140} were resolved. A partially resolved peak at 95 kev was observed in Ce^{142}.

* Work supported by the U. S. Atomic Energy Commission.
[1] J. H. Gibbons, Phys. Rev. **94**, 773 (1954).

HA11. Total Neutron Cross Section of Eu in the 0.001 to 0.01 ev Region. N. HOLT,* *Joint Establishment for Nuclear Energy Research, Kjeller, Norway.*—The cross section was measured using a mechanical neutron-monochromator.[1] The sample used was spectroscopically pure Eu_2O_3 dissolved in dilute DNO_3. By subtracting the contribution of the resonances at 0.327, 0.461, and 1.055 ev observed with the BNL crystal spectometer[2] and fitting the difference to the Breit-Wigner formula by means of the method of least squares, the following preliminary Breit-Wigner constants were found: $\sigma_0=8.4\times10^4$ barn, $E_0=-6\times10^{-4}$ ev, and $\tau=0.067$ ev. These values give a higher and somewhat narrower resonance than previously published.[3] The radiation width which results is in agreement with the width associated with the first positive resonance.[4] These two resonances are known to populate the 9.3 hr isomeric activity in the same amount.[5]

* Now at Brookhaven National Laboratory.
[1] N. Holt, JENER Publication No. 7, p. 169 (1953).
[2] Sailor, Landon, and Foote, Phys. Rev. **93**, 1292 (1954).
[3] W. J. Sturm, Phys. Rev. **71**, 757 (1947).
[4] H. H. Landon and V. L. Sailor, Bull. Am. Phys. Soc. **29**, No. 7, 10 (1954).
[5] R. E. Wood, Phys. Rev. **95**, 453 (1954).

HA12. Inelastic Scattering of Cold Neutrons by Aluminum.* R. L. ZIMMERMAN AND H. PALEVSKY, *Brookhaven National Laboratory.*—The transmission of cold neutrons through aluminum has been measured as a function of neutron wavelength and sample temperature, for temperatures varying between 100 and 900°K. The neutron wavelengths were determined by a time of flight method using the Brookhaven slow chopper. The wavelength region investigated extended from 5 to 12A. The transmission is a measure of the total neutron cross section and for wavelengths greater than the Bragg cutoff ($\lambda>4.7$A) the cross section consists of capture, inelastic and incoherent scattering. At the highest temperature investigated (880°K) the inelastic scattering is about $\frac{1}{2}$ of the total cross section and at this temperature the experimental value is about 10 percent higher than the prediction of the theory based on the incoherent approximation.[1] A calculation by Singwi,[2] which takes account of the coherent effects is in poorer agreement (20 percent) with experiment. In both theories the Debye model for the solid is used. The discrepancies between experiment and theory may be an indication of the failure of the Debye approximation.

* Work carried out under contract with U. S. Atomic Energy Commission.
[1] G. Placzek, Phys. Rev. **93**, 895 (1954).
[2] Private communication.

THURSDAY AFTERNOON AT 2:00

McAlpin, Green Room

(R. B. BRODE, presiding)

Cosmic Rays

I1. Velocity Spectrum of Cosmic-Ray Particles at Twelve-Grams Atmospheric Depth.* E. N. MITCHELL, *University of Minnesota* (introduced by J. R. Winckler).—Two balloon flights have been made at $\lambda = 55°$ carrying a Čerenkov detector whose mean pulse height is energy dependent and is thus capable of providing an independent check on the minimum velocity at this latitude. The Čerenkov detector was operated in coincidence with a GM telescope and surrounded by a ring of guard counters. An experimental measurement of the dependence of the pulse height distribution on velocity of this detector made in the π-meson beam of the University of Chicago synchrotron has been used to calibrate the detector. The response of the detector to relativistic particles was gotten by measurements made with sea level relativistic mesons. Of 9000 particles recorded at altitude about 6000 of these may be accounted for by the integral spectrum $N(>E) = 0.42/(E+1)$ using the cutoff predicted at this latitude by the geomagnetic theory. About 2000 of the particles have energies for protons between 100 and 300 Mev, and about 1000 have energies between 300 and 900 Mev. If these last two groups are attributed to secondaries and albedo particles, then the experiment is consistent with geomagnetic theory. This is now being examined. It was found that the total flux was 30 percent higher than that found by investigators using GM telescopes.

* This research was supported in part by the Office of Naval Research and the U. S. Atomic Energy Commission.

I2. Momentum Distribution of Low-Energy Cosmic-Ray Particles. A. SNYDER AND DEL CASTILLO, *Purdue University.* (introduced by W. Y. Chang).—In the pictures taken from the twin cloud chamber setup[1] (see another abstract) we have observed a large number (roughly 6500) of single particle tracks through the two chambers. About 250 of these particles have suffered observable multiple scattering in the Pb plates of the bottom chamber. Using the method developed by the M.I.T. group,[2] we have obtained the values of $pc\beta$ in Mev by measuring the angles of multiple scattering in the Pb plates. In the measurable range of 100 to 1000 Mev the distribution of $pc\beta$ has a broad maximum around 250 Mev with a half-width roughly equal to 300 Mev. The ξ values used for identifying particles are also obtained for those (30), which have stopped at least in the fourth Pb plate.

[1] Under roughly 30-inch cement forming the roofs of the building.
[2] S. Olbert, Phys. Rev. **87**, 319 (1952); Annis, Bridge, and Olbert, Phys. Rev. **89**, 1216 (1953).

I3. Nuclear Interaction of Sea-Level, Cosmic-Ray Particles with Carbon and Lead. DEL CASTILLO, A. SNYDER, L. GRODZINS, AND W. Y. CHANG, *Purdue University.*—Two cloud chambers, 16×16×14 in. each, were placed one above the other. The top chamber contained three carbon plates (10×7×1 in. each) and four Pb plates (11×10×$\frac{1}{4}$ in. each) intended for producing the nuclear events, while the bottom chamber had nine Pb plates (11×10×$\frac{1}{4}$ in. each) to suggest the nature and properties of the shower particles. An event with at least two particles coming out of the bottom of either chamber was recorded. About 209 nuclear events were obtained from about 12 000 pairs of pictures for the two chambers. 134 of these events have less than 10 particles and are suitable for analysis; the rest either are large mixed showers or small ones having difficulties for analysis. Results have been obtained for the distributions of multiplicity, angle, and momentum of the charged particles; for the missing link showers (π^0 mesons), and for the ξ values[1] of those particles stopped after traversing at least 4 Pb plates in the bottom chamber. This last distribution shows that roughly $\frac{1}{3}$ of the charged particles are charged mesons. The angular and multiplicity distributions are about the same for carbon and lead. Our present results indicates multiple production of mesons supporting our previous conclusions.[2]

[1] Annis, Bridge, and Olbert, Phys. Rev. **89**, 1216 (1953).
[2] Phys. Rev. **84**, 582, 584 (1951); **89**, 408 (1953).

I4. Origin of the Charge Spectrum of Primaries. S. F. SINGER, *University of Maryland.*—Does the cosmic-ray charge spectrum necessarily reflect the abundance of elements? Or can we assume that the protons and alpha particles in the "primary" radiation (near the earth) are produced largely by the fragmentation in interstellar hydrogen of an original radiation which consists mainly of iron? It is possible to reproduce the observed charge distribution of the primaries, including the iron "peak." "Protons" also include neutrons and deuterons; "alpha particles" include He^3 and H^3. We have used evaporation theory, cosmic-ray data, and helium analyses of meteorites. The required mean path length is 6 g/cm^2. Points for the fragmentation hypothesis are: It leads to the same velocity spectrum for all components. Certain injection mechanisms favor heavy nuclei. Crucial tests are: The presence of Li, Be, B in the primary radiation, as well as He^3 and H^3.[1] Enhancement of heavy primaries during solar flare increases.

[1] S. F. Singer, Duke University Cosmic Ray Conference, November 1953.

I5. World-Wide Variations in Cosmic-Ray Intensity 1937–1952. SCOTT E. FORBUSH, *DTM, Carnegie Institution of Washington.*—Results from continuous registration of cosmic-ray ionization at four stations, from 1937–1952, show an eleven-year variation of about four percent which is similar at all stations. This variation is negatively correlated with that in sunspot numbers. The variation is about the same whether the annual means are based on results: (a) for all days, (b) for the five magnetically disturbed days of each month, or (c) for the five magnetically quiet days of each month. This indicates that the variation with sunspot number does not result from large world-wide decreases in intensity which occur on some magnetically disturbed days. Good reliability of changes in ionization data over long periods of time is indicated through a comparison of results with Neher's data from balloon-borne ionization chambers. The variability of daily means is a minimum near sunspot minimum. Evidence indicates a connection between the mechanism responsible for cosmic-ray changes and that for magnetic variations. Some details of this study will appear in the *Journal of Geophysical Research.*

I6. Diffusion of Cosmic Rays in the Earth-Sun Region. P. MORRISON, *Cornell University.*—Not only the nonrecurring world-wide cr (cosmic ray) decreases of Forbush type, but also the 27-day periodic intensity changes, have been ascribed to the transient presence of a diffusing medium (turbulent magnetized clouds emanating from the sun) in the region of the earth's orbit.[1] Physical evidence for such clouds has been sought in this way: The solar flares are known to produce large short-time cr increases within certain target zones on the earth's surface. Hourly cr neutron counts during a number of smaller flares (data generously supplied by J. Simpson) show that the target zones are spread, and the flare pulse widened greatly in time, whenever the flare occurs during an intensity *maximum* of the 27-day cycle. This

indicates presence of a diffusing cloud at such times of maxima. The small flare pulses yield rather poor statistics. The Forbush-type events, on the contrary, are times of minimal intensity occurring during the earth's immersion in a diffusing cloud. This difference implies an appreciable injection of cr from the sun into the stream of clouds responsible for the 27-day period during their emission.

[1] P. Morrison, Phys. Rev. 95, 646(A) (1954).

I7. Preliminary Studies with a High-Energy Photon Spectrometer.* C. E. SWARTZ AND J. W. DEWIRE,† *Brookhaven National Laboratory.*—A high-energy photon spectrometer employing a large Čerenkov shower detector has been constructed and has been put into use in studies with the Cosmotron. The photons are materialized in a lead radiator and are detected by a coincidence-anticoincidence telescope which gates a ten channel discriminator in which the shower pulses are analyzed. The shower development takes place in a stack of lead glass plates of specific gravity 5.0, which are viewed end on by a DuMont 6394 photomultiplier tube. The glass occupies a cylindrical volume 10 cm in diameter and 18 cm long. The radiation length in the glass is 1.76 cm. The spectrometer has been calibrated with monoenergetic electrons of 160 and 390 Mev. The energy resolution is better than 30 percent at both energies. Photon spectra taken at 90° to a carbon target bombarded by protons of 1, 2, and 3 Bev will be shown and discussed.

* Work performed under the auspices of the U. S. Atomic Energy Commission.
† On leave from Cornell University.

Invited Papers

I8. Abundance of Lithium, Beryllium, and Boron in the Primary Cosmic Radiation. M. F. KAPLON, *University of Rochester.* (30 min.)

THURSDAY AFTERNOON AT 2:00

New York University, Vanderbilt Hall

(H. A. BETHE, presiding)

Invited Papers

IA1. Angular Correlation of Aligned Nuclei. P. S. JASTRAM, *Washington University.* (30 min.)

IA2. Coupling in Nuclear Beta-Decay. O. KOFOED-HANSEN, *University of Copenhagen and Columbia University.* (30 min.)

IA3. The Universal Fermi Interaction. L. MICHEL, *Ecole Polytechnique and Institute for Advanced Study.* (30 min.)

IA4. The Giant Resonances of Nuclear Photodisintegration. D. H. WILKINSON, *Cambridge University and Brookhaven National Laboratory.* (30 min.)

THURSDAY AFTERNOON AT 2:00

McAlpin, Red Room

(A. PAIS, presiding)

Statistical Theory

J1. A New Extension of Collective Coordinates for the Many Body Problem. JEROME K. PERCUS, *New York City,* AND GEORGE J. YEVICK, *Stevens Institute of Technology.*—In previous work,[1] we have employed the collective coordinate approach to describe the general problem of the dynamical behavior of N interacting particles. This work was characterized by a set of harmonic oscillators for the collective coordinates. In the comparison of the collective coordinate Lagrangian with the physical Lagrangian, we have found it necessary to alter the physical Lagrangian in a manner which does not affect the equations of motion. Moreover coupling between oscillators which is the dominant mechanism for irreversibility (the decay of orderly mechanical motion into chaotic thermal motion) was omitted. This coupling has now been achieved by an improved expression for the kinetic energy term in the collective coordinate Lagrangian which eliminates the velocity dependent potentials. Moreover new types of collective coordinates are suggested by an approximate diagonalization of the kinetic energy. These coordinates represent an intermediate stage in the transition from the individual to the collective. The new coordinates and their time derivatives bear a close relation to the density, velocity, and force in a hydrodynamical system.

[1] See Phys. Rev. 94, 787(A) (1954) (detailed analyses have recently been submitted to Phys. Rev.).

J2. Some Comments on Feynman's Atomic Theory of Liquid Helium. GEORGE J. YEVICK, *Stevens Institute of Technology,* AND JEROME K. PERCUS, *New York City.*—In a very interesting paper, Feynman[1] has presented strong plausibility arguments as to the nature of the quantum-mechanical wave functions for the many body problem of the super-fluid, liquid helium. We shall first briefly indicate how these wave functions can be gotten by the use of collective coordinates as a zero-order approximation to our theory. Next, we shall show how Feynman's energy spectrum may be obtained from the zero-order theory in terms of the two body potentials. The principal weakness in

Feynman's theory is the lack of coupling between the "phonon" and "roton" oscillators. This is the mechanism for irreversible processes, e.g., the transfer of energy from the low wave number phonons to the rotons. Another serious difficulty is that the 3N number of degrees of freedom are not built into the theory. This can be shown to be quite troublesome for very high wave numbers (roton states) which in some sense describe closeup effects. In this connection, we have succeeded in expressing very high rotons which are not independent coordinates as nonlinear combinations of both phonons and rotons.

[1] R. P. Feynman, Phys. Rev. **94**, 262 (1954).

J3. Remarks on the Fluctuation Dissipation Theorem.* J. WEBER, *University of Maryland.*—The integral[1] form of the fluctuation dissipation theorem is commonly employed to calculate the results of precise measurements of the mean squared values of fluctuating quantities, in terms of the generalized resistance. The resistance function is a measure of the response of a system to harmonic driving forces which have been applied for a long time. We imagine that measurements are made on one system, at intervals which are large enough apart so that the system can return to equilibrium between measurements. Single measurements are necessarily averages over small time intervals and under these conditions the coupling of the measuring apparatus to the modes of a system will be different from the infinite time coupling implied by the resistance function. The measured fluctuations will depend in a detailed way on the method of measurement. Such effects can be taken into account by regarding the differential form[2] of the fluctuation dissipation theorem as fundamental rather than the integral form, and then introducing suitable coupling constants for the different modes before integration over all frequencies is carried out. Examples will be discussed.

* Supported by the Office of Naval Research.
[1] H. B. Callen and T. A. Welton, Phys. Rev. **83**, 1, 34 (1951).
[2] J. Weber, Phys. Rev. **96**, 556 (1954).

J4. Variational Principles in Irreversible Thermodynamics. IRWIN MANNING AND LASZLO TISZA, *M.I.T.*—A systematic presentation of the irreversible thermodynamics of steady state processes has been developed. The discussion is based on a variational principle in close formal analogy with Gibbsian thermostatics. The role of the fundamental equation is played by a generalized dissipation function. In analogy to the equations of state, the variational principle yields the relations between the currents and forces which in general need not be linear. Legendre transformations lead to other potentials which play a role parallel to the Gibbs, Helmholtz, etc. potentials in thermostatics, and provide the same flexibility in the choice of independent parameters. The analogs of the Maxwell relations are reciprocity conditions which in case of linear processes reduce to the well-known Onsager relations. The relationship of the variational principle to some of those suggested in the past will be discussed.

J5. Statistical Ensemble Representing Stationary Non-equilibrium States.* JOEL LEBOWITZ AND PETER G. BERGMANN, *Syracuse University.*—If a system is to be capable of approaching thermodynamic equilibrium or a nonequilibrium stationary state, it must be in thermal contact with one or several inexhaustible reservoirs. We are assuming that the reservoir consists of an infinite number of independent components and that the system interacts with each component impulsively and but once in its history. The corresponding ensemble in gamma space will then obey an integro-differential equation which contains stochastic terms in addition to the usual Liouville terms. If there is only one reservoir at a definite temperature, the distribution function of the system will approach the canonical form asymptotically, with the Helmholtz potential decreasing monotonically with time. For certain types of interaction kernels, we have shown that in the presence of several reservoirs at different temperatures the distribution also approaches asymptotically a stationary state. Though we have not as yet succeeded in constructing this stationary state explicitly, some of its properties have been deduced.

* Supported by Office of Scientific Research, U. S. Air Force.

J6. Invariant Characteristics of One-Dimensional Binary Lattices. EDWARD H. KERNER AND JOSEPH G. LOGAN, *University of Buffalo.*—The periodic lattice of A and B atoms $\cdots[(n_1B)(n_2A)(n_3B)\cdots(n_rA)]\cdots$ has certain properties which are invariant to the ordering of the sequence. From the eigenvalue equation $\cos kl=\frac{1}{2}Tr H_B^{n_1}H_A^{n_2}\cdots H_A^{n_r}$ where (for square well A and B for example) the H matrices are those recently introduced by one of us[1] for A and B cells, it follows that whenever H_B and H_A commute the Trace is insensible to the structure of the sequence, becoming equal to $Tr H_B^{n_B}H_A^{n_A}$, n_B and n_A being the total numbers of B and A atoms. The conditions for commutability may be easily expressed in a pair of equations connecting the energy with the A and B lattice parameters. For energy levels satisfying these equations the Trace may be evaluated from that of the simple diatomic lattice $\cdots[(n_BB)(n_AA)]\cdots$ and the levels classified as "super-forbidden" or "super-allowed" in view of the invariance of their character to the ordering of the sequence. Such super-*levels* would seem to imply the existence of super-*bands* surrounding them of greater or smaller width as the ordering of the lattice is altered.

[1] E. H. Kerner, Phys. Rev. **95**, 687 (1954).

J7. Thermal Diffusion in Multiple Component Isotopic Mixtures.* J. W. CORBETT† AND W. W. WATSON, *Yale University.*—The general equation for thermal diffusion in a mixture of several gases simplifies in the case of isotopic mixtures to allow one to write [to the first order of $(m_i-m_j)/\bar{m}$] for the equilibrium state

$$\nabla \ln c_i = -\sum_j c_j \frac{m_i-m_j}{\bar{m}}\alpha_0 \nabla \ln T,$$

where the α_0 is characteristic of the molecular species. These equations can be linearized by the approximation that the product of the concentrations (c_ic_j) changes so little in the process that it may be considered constant. Thus, the general matrix solution of the simultaneous equations can be used. Since the matrix involved is (by the reciprocity conditions) antisymmetric, this method of solution may be applied only to mixtures with an even number of isotopes. Two-bulb experiments, analyzed by this method, give an inversion point for $R_T[\equiv\alpha_0(\text{expt})/\alpha_0$ (rigid elastic spheres)] for krypton (six components) close to room temperature.

* Supported in part by the U. S. Atomic Energy Commission.
† General Electric Coffin Fellow.

J8. The Collective Description of an Electron Gas. M. DRESDEN, *University of Kansas.*—It has been shown by Bohm and Pines[1] that for many phenomena, in which a dense electron gas is involved, the collective description is more appropriate, than a description following the detailed motion of individual electrons. A study has been made of the mathematical and physical relationship between the conventional and the collective mode of description. The collective description can be expressed best in terms of a splitting of the density fluctuations of the electron gas. One therefore seeks a transformation, which starting from the Hamiltonian of the electron gas, will effect this separation. For this purpose it has been found useful to employ the analogue of a transformation due to Kramers. (See Welton[2] and van Kampen[3]). This type of transformation allows one to show, that the coupling between an electron and an electromagnetic field may be described in terms of the addition of a fluctuating term to the position of the electron, in the potential energy. It will be shown, that an appro-

priate modification of this transformation allows one to obtain the transformation to the collective description in this fashion.

[1] Bohm and Pines, Phys. Rev. **85**, 338 (1952).
[2] Welton, Phys. Rev. **74**, 1157 (1948).
[3] van Kampen, Dan. Mat. Fys. Medd. **26**, No. 15 (1951).

J9. Stark Fields from Ions in a Plasma. ARTHUR BROYLES, *The RAND Corporation.*—An investigation has been made of the problem of determining the probability that a radiating ion in a plasma will experience an electric field of a given magnitude from other ions. All the ions are assumed to have the same charge and to move in a sea of uniform negative charge. Formulas resulting from various approximations will be presented along with calculations for certain specific cases. One approximation uses collective waves as suggested by Pines and Bohm.[1] For iron at one kilovolt temperature and normal density (7.83 g/cm^3), the broadening of K to L lines is such that the line intensity equals the continuum intensity at a frequency displacement from the line center of about 1/30th that of the Holtsmark distribution.[3]

[1] D. Pines and D. Bohm, Phys. Rev. **85**, 338 (1952).
[3] Holtsmark, Ann. Physik **58**, 577 (1919); Physik Z. **20**, 162 (1919); Physik Z. **25**, 73 (1924).

J10. Magnetic Moment of a Fermi-Dirac Gas. A. W. SÁENZ AND R. C. O'ROURKE, *Naval Research Laboratory.*—This investigation consists of two parts. In the first one, we deal with the computation of the density of states of an assembly in statistical equilibrium by means of two perturbation-theoretic methods, I and II. In both I and II, we employ Laplace transform techniques, but while I is based on the Schwinger trace formula, II rests on a new procedure for expanding exponential operators, and can be shown to be better term by term than I, in a suitable sense. A preliminary report will be given on the second part of our study, not yet completed, which deals with the application of I and II to the magnetic susceptibility of metals.

Invited Paper

J11. (Title to be announced.) R. E. PEIERLS, *University of Birmingham.* (30 min.)

THURSDAY AFTERNOON AT 3:00

New Yorker, Mosaic Room

(R. T. BIRGE, presiding)

Post-Deadline Papers, if Any

FRIDAY MORNING AT 9:00

New York University, Vanderbilt Hall

(H. A. BETHE, presiding)

Business Meeting of the American Physical Society

Invited Papers Beginning at 10:00

Hyperons and Heavy Mesons

K1. Investigations of the Bristol School. M. G. K. MENON, *Bristol University, England.* (40 min.)
K2. Investigations of the Indian School. YASH PAL, *Tata Research Institute, Bombay, India.* (30 min.)
K3. Investigations of the Italian School. N. DALLAPORTA, *University of Padua, Italy.* (30 min.)
K4. Heavy Mesons Produced in the Interaction of 2-3 Bev Particles. E. O. SALANT, *Brookhaven.* (30 min.)

FRIDAY MORNING AT 10:15

McAlpin, Colonial Room

(GREGORY BREIT, presiding)

Scattering of Elementary Particles

L1. Absolute Cross Sections for the Coulomb Scattering of 1.75 Mev Electrons.* T. F. RUANE,† B. WALDMAN, AND W. C. MILLER, *University of Notre Dame.*—Electrons from our electrostatic generator were scattered from thin foils of aluminum, nickel, and gold. The scattered electrons were analyzed by means of a 90° magnetic spectrometer using a scintillation detector. The cross sections were measured at 30°, 60°, and 90° with an estimated error of ±2 percent and at 120° and 150° with an estimated error of ±5 percent. A comparison of these results with the Mott theory as evaluated by McKinley and Feshbach,

and Bartlett and Watson, shows deviations of 5 percent to 10 percent, the experimental results being low. Corrections for nuclear size and screening, and the radiative correction of Schwinger, seem to be needed to remove this discrepancy.

* Assisted by the joint program of the Office of Naval Research and the U. S. Atomic Energy Commission.
† Now at Knolls Atomic Power Laboratory, Schenectady, New York.

L2. Elastic Scattering of Protons from Li^7.* PHILIP R. MALMBERG,† *State University of Iowa.*—The yield curves for the elastic scattering of protons from Li^7 were measured in the energy range 1350–3000 kev at the center of mass angles 70°, 90°, 110°, 130°, 150°, and 167.1°. The State University of Iowa statitron supplied the incident proton beam. The various proton groups scattered from different elements in the target were separated by a magnetic analyzer. The 167.1° data agreed well with the earlier work of Wisconsin[1] at 166.3°. At all six angles the curves showed a peak at about 2000 kev (peak position varied between 1950 kev at 70° to 2050 kev at 167.1°), a dip at 2230 kev and an anomaly near the 1882 kev $Li^7(p,n)Be^7$ threshold. At the more forward angles this anomaly appears as a spike closely coincident in energy with the position of the neutron threshold. A behavior of this nature has been predicted by Wigner.[2]

* This work supported in part by the U. S. Atomic Energy Commission.
† Now at the Naval Research Laboratory.
[1] S. Bashkin and H. T. Richards, Phys. Rev. **84**, 1124 (1951).
[2] E. P. Wigner, Phys. Rev. **73**, 1002 (1948).

L3. Scattering of 9.76 Mev Protons by He^4. JOHN H. WILLIAMS AND STANLEY W. RASMUSSEN,* *University of Minnesota.*—Protons accelerated by the first section of the Minnesota linear accelerator have been scattered from purified helium gas at 10-cm pressure. The Los Alamos multiple-plate scattering chamber[1] defined the scattering angles to ±1 degree. A *single* exposure recorded the scattered protons at 26 laboratory angles from 35° to 172.5° and the recoil α particles at 6 angles from 22.5° to 35°. Absolute cross sections were obtained by counting 400 or more tracks in C-2 emulsions for each angle. The results are in good agreement with those of Putnam[2] at 9.48 Mev, considering the difference in proton energy. The results of Cork and Hartsough[3] are not confirmed in the angular range 115° to 155° in the C. of M. system. Recent Birmingham[4] results are confirmed in the general form of the curve from 50° to 150°, C. of M., but not in absolute cross section where the Birmingham results are 85 percent of the present cross sections over the above angular range.

* Supported by the U. S. Atomic Energy Commission.
[1] Allred, Rosen, Tallmadge, and Williams, Rev. Sci. Instr. **22**, 191 (1951).
[2] T. M. Putnam, Phys. Rev. **87**, 932 (1952).
[3] B. Cork and W. Hartsough, Phys. Rev. **96**, 859 (1954).
[4] R. G. Freemantle *et al.*, Phil. Mag. **45**, 1090 (1954).

L4. Proton-Proton Scattering Experiments at 170 and 260 Mev.* OWEN CHAMBERLAIN AND JOHN D. GARRISON,† *University of California, Berkeley.*—The differential proton-proton scattering cross section has been measured at 170 and 260 Mev for laboratory angles of 4.4° to 30°. The proton beam was obtained by reducing the energy of the 345-Mev beam of the Berkeley cyclotron. A liquid-hydrogen target was used. Counting was done using a telescope of two liquid scintillation counters. A Faraday cup served as a standard for beam calibration. The results indicate a cross section, in the center-of-mass system, independent of energy, and rather independent of angle, outside of the Coulomb region. The level of the differential cross section is close to 3.6 millibarns per steradian.

* This work was performed under the auspices of the U. S. Atomic Energy Commission.
† Now at Sloane Physics Laboratory, Yale University, New Haven, Connecticut.

L5. Proton-Proton Scattering at 900 Mev.* T. W. MORRIS, J. D. GARRISON, AND E. C. FOWLER, *Yale University*, AND W. B. FOWLER, R. P. SHUTT, A. M. THRONDIKE, AND W. L. WHITTEMORE, *Brookhaven National Laboratory.*—900 Mev protons incident on a diffusion cloud chamber containing hydrogen at 20 atmospheres are being studied. More than 160 scattering events have been located, of which 75 have been identified as elastic and 73 as inelastic with only one meson being produced. Though no cases have yet been identified, multiple meson production is not ruled out. The elastic scatterings are distributed in center-of-mass angle as follows:

0°–10°	1
10°–20°	13
20°–30°	17
30°–40°	11
40°–50°	7
50°–60°	6
60°–70°	7
70°–80°	4
80°–90°	4

Results of a complete analysis of the inelastic events will be presented including the angle and energy distributions of the particles and the ratio of charged to neutral meson production.

* Work performed under the auspices of the U. S. Atomic Energy Commission.

L6. Elastic p-p Angular Distributions from 440 to 1000 Mev. L. W. SMITH, A. W. MCREYNOLDS, AND G. A. SNOW, *Brookhaven National Laboratory.**—Preliminary results on the angular distribution of elastic p-p scattering have been obtained at 440, 600, 800, and 1000 Mev incident proton energies. The proton energy spread is $<\pm 5$ percent. The circulating beam of the Cosmotron strikes an internal target of CH_2 or C in a straight section having thin walls. Elastic p-p events are detected by coincidences in two scintillation counter telescopes set at the correct kinematic angles and with appropriate relative time delays. The measurements extend from ~30° to 90° in the CM system. The CH_2 accidental coincidence rate is held to <10 percent, and the quasielastic contribution from C is negligible. Auxiliary beam intensity monitors permit determination of angular distributions at each energy to 5 percent accuracy and cross sections as a function of energy to 20 percent accuracy. The 440-Mev results are in essential agreement with those of Sutton *et al.*[1] At higher energies the angular distributions become sharply peaked forward. The ratios $[d\sigma_{cm}(\theta=35°)/d\omega]/[d\sigma_{cm}(\theta=90°)/d\omega]$ are 1.1, 2.3, 6.3, and 10.5 at 440, 600, 800, and 1000 Mev, respectively. The total elastic cross section remains roughly the same from 440 to 1000 Mev.

* Under the auspices of the U. S. Atomic Energy Commission.
[1] Sutton, Fields, Fox, Kane, Mott, and Stallwood, Phys. Rev. **95**, 663 (1954).

L7. Proposed Method for Obtaining a High-Energy Polarized Proton Beam. R. TRIPP, *University of California, Berkeley.*—Recent experiments[1] indicate that at 32 Mev the asymmetries obtained in double-scattering experiments are small and their interpretation in terms of polarization becomes uncertain. A proposal to enhance the ability to detect the expected small polarization involves performing the first scattering in an energy region where some highly polarizing elastic resonances should exist and then accelerating this polarized beam to 32 Mev. The Berkeley Linear Accelerator acceptance energy is 4±0.04 Mev. It uses for an injector a Van de Graaff accelerator capable to producing 4.7-Mev protons. The suggestion is then to scatter the protons upon emerging from the Van de Graaff, bring a portion of the scattered beam to parallelism by means of a strong focusing lens and then inject it into the linear accelerator. For this machine it appears that an oxygen resonance can be utilized, although further investigation may reveal a more suitable element. With a 1 mg/cm² target and a solid angle of 0.02 steradian, a beam greater than 10^5 protons/sec should be obtainable. This work was done under the auspices of the U. S. Atomic Energy Commission.

[1] Bradner and Iloff, UCRL-2691; Simmons (private communication).

L8. *n-p* Scattering at 17.9 Mev. A. GALONSKY AND J. JUDISH, *Oak Ridge National Laboratory.*—The yield of recoil protons from 17.9±0.1-Mev neutrons was measured every 5° from 0° to 45° in the laboratory system. Neutrons were produced by bombarding a tritium gas target with 1.70-Mev deuterons from an electrostatic generator. Proton recoils from a thin CH_2 radiator were counted by a triple coincidence spectrometer consisting of two argon-CO_2 proportional counters followed by a NaI(Tl) crystal which was thick enough to stop the protons. The coincidence spectrum of proton energies in the crystal was measured at each of the above angles. Spectrum widths were kept under 25 percent by using progressively thinner radiators as the angle of observation was increased. Part of the width is introduced by the angular resolution, which was ±3°. The statistical accuracy of the measurements varied from 2 percent to 3 percent. The ratio of neutron scattering cross sections at 180° and 90° in the CM system is 1.08±0.03. Corrections on the proton spectra will be made for Coulomb scattering effects in the radiator, the argon-CO_2, the walls of the proportional counters, and the angle-defining slit over the NaI crystal.

L9. Multiple Scattering of Low-Energy Alpha-Particles in a Gas. G. ALLEN, R. WEBELER, AND S. BARILE, *NACA.*—Alpha particles from a polonium source were slowed down and allowed to enter a cloud chamber containing a mixture of hydrogen, water, and ethyl alcohol at pressures of 12.25 cm, 1.5 cm, and 2.24 cm, respectively, before expansion. Eighty-four sharp tracks of particles which stopped in the illuminated part of the chamber and which did not show any sharp bends due to single scattering were selected for study. Starting at the termini of the projected tracks, the angles between successive chords of three millimeters length were measured, the energies at the first three intersections of the chords being approximately 18, 45, and 85 kev. Contrary to the situation at higher energies we were unable to represent the distribution of the 84 angles corresponding to each energy as a gaussian distribution plus a well separated single and plural scattering "tail." The rms values of the distribution were found to be 11.3°, 5.6°, and 3.5° for 18, 45, and 85 kev, respectively. Because of the non-Gaussian nature of the distribution no procedure is available for correcting these results for the experimental error which was determined to be between 2.5° and 1.5° depending on the magnitude of the angle.

L10. Scattering of 100-Mev γ Rays from Carbon.* D. M. RITSON, A. PEVSNER, AND R. L. ZIMMERMAN, *M.I.T.*—The scattered γ rays from a carbon target exposed to the 130-Mev M.I.T. Synchrotron beam were detected by their materialization in a 1.5-mm lead plate placed inside a magnetic cloud chamber. The cloud chamber could be rotated to observe γ's scattered at 45°, 90°, and 135° from the target. The cloud chamber was triggered by the loose requirement of one particle passing through a threefold scintillation telescope at the back of the chamber. Charged particles originating from the target were generally swept out by the magnetic field and did not trigger the chamber. The differential cross sections at 97 Mev and 77 Mev obtained from the analysis of four thousand pictures are given in the table below. The errors quoted in the table are statistical. In addition, the absolute efficiencies are probably known only to ±20 percent. The significance of the results will be discussed at the meeting.

	45°	90°	135°
94 Mev	$3.1\pm0.5\ 10^{-28}$ cm²/sterad	$1.4\pm0.3\ 10^{-28}$ cm²/sterad	$2.2\pm0.5\ 10^{-28}$ cm²/sterad
77 Mev	$2.9\pm0.5\ 10^{-28}$ cm²/sterad	$1.5\pm0.3\ 10^{-28}$ cm²/sterad	$1.8\pm0.4\ 10^{-28}$ cm²/sterad

* This work was supported in part by the joint program of the U. S. Atomic Energy Commission and the Office of Naval Research.

Invited Paper

L11. Elastic Scattering of Protons. K. STRAUCH, *Harvard University.* (30 min.)

FRIDAY MORNING AT 10:15

McAlpin, Green Room

(H. G. HAGSTRUM, presiding)

Electron Physics

LA1. Scattering of 20-Kev Electrons in Thin Films.* H. MENDLOWITZ AND L. MARTON, *National Bureau of Standards.*—The energy and angular distributions of electrons scattered from thin films indicate that there is a large probability for a two stage process which includes (1) an inelastic scattering and (2) an elastic scattering from the crystal lattice. This is found even for crystals of about thirty layers of atoms. The angular distributions of the elastically scattered electrons and those suffering the characteristic energy losses are found to depend on whether the material is a single crystal or polycrystalline. The manner in which the cross sections vary is consistent with the above mentioned collision mechanism. These data can be utilized to interpret electron diffraction patterns from polycrystalline materials, and sheds doubt on the assumption[1] that the lattice spacings in single crystals differ from those in polycrystalline materials.

* Supported by Office of Naval Research.

[1] Z. G. Pinsker, *Electron Diffraction* (Butterworth Scientific Publications, London 1953), p. 209.

LA2. Single Scattering of 20-Kev Electrons in Solids.* L. MARTON, J. AROL SIMPSON, AND T. F. MCCRAW, *National Bureau of Standards.*—The energy distribution of 20-kev electrons scattered from metallic foils has been measured with equipment[1] giving an energy resolution of 15 volts and an angular resolution better than 6×10^{-4} radian. The measurements extend to a maximum loss of 150 ev, a maximum angle of 4×10^{-2} radian, and over an intensity range exceeding 10^3. Several materials were investigated. Sample thickness was varied from about 100A to about 800A. Also the amount of crystal alignment was varied from single crystals giving sharp Laue spots to polycrystalline materials giving Debye-Scherrer ring diffraction patterns. The cross section of the characteristic energy losses[2] relative to the elastic cross section is found to be a function of angle and the above mentioned crystal parameters. Some of these results will be discussed in the following paper.

* This work supported by the Office of Naval Research.

[1] Marton, McCraw, Simpson, Phys. Rev. 95, 634(A) (1954).

[2] Marton and Leder, Phys. Rev. 94, 203 (1954). Leder and Marton, Phys. Rev. 95, 1345 (1954).

LA3. Field Emission from Titanium Single Crystals. E. G. BROCK AND J. E. TAYLOR, *General Electric Research Laboratory.*—Field emission microscope patterns from single crystals of titanium have been observed. At room temperature titanium has a hexagonal-close-packed crystal structure. This low-temperature alpha phase transforms at 882°C to a body-centered-cubic beta structure.[1] Electron emission patterns from titanium single crystals held in the two temperature regions show the symmetry of their respective stable crystal structures. The orientation relation between the two phases is similar to that reported for zirconium.[2]

[1] C. J. Smithells, *Metals Reference Book* (Interscience Publishers, Inc., New York, 1949).
[2] W. G. Burgers, Physica 1, 561 (1933–34).

LA4. On the Magnification and Resolution of the Field Emission Electron Microscope. D. J. ROSE, *Bell Telephone Laboratories.*—The resolution of the field emission electron microscope is expressed as a function of its magnification. It is shown that a resolution of about 3A is possible provided the magnification is much greater than that computed for an atomically smooth emission tip. Further analysis shows that irregular projections on the surface of the tip can provide local areas of such increased magnification. Some atomic detail of these irregularities should therefore be observable.

LA5. Light Output from Dielectric-Imbedded Electroluminescent Phosphors. F. A. SCHWERTZ AND J. J. MAZENKO, *Mellon Institute.*—The time-average light output from a number of plastic-imbedded electroluminescent phosphor powders was studied as a function of frequency and field strength using sine and square voltage waves. For both types of stimulation the time-average light output was measured in the frequency range from 0.1 to 50 kilocycles per second. For square waves the light output increased more rapidly with frequency than with sine waves, but peak light output was obtained at approximately 20 kilocycles per second in both cases. For sine waves the time-average light output increased as the n'th power of the applied field, n ranging from approximately 2 to approximately 4 for nine different electroluminescent phosphor samples. The results were generally in agreement with those reported by Nudelman and Matossi.*

* S. Nudelman and F. Matossi, Phys. Rev. (to be published).

LA6. Field Enhanced Solid-State Luminescence. D. A. CUSANO, *General Electric Research Laboratory.*—Large increases in the luminescent brightness of ultraviolet excited or x-ray excited zinc sulfide layers have been observed when these phosphors are subjected to electric fields. The application of 100 volts dc across vapor-deposited ZnS:Mn films approximately 10 microns thick (10^5 v/cm) has been observed to increase the brightness 50 times. This occurs for excitation by either x-rays or ultraviolet. Smaller changes of brightness by ac fields on powder cells with x-ray excitation have been earlier reported.[1] In the present work, however, some 10-fold true light amplification has been realized with low ultraviolet intensity. Ten or more visible photons are emitted per incident ultraviolet photon. For a given value of dc field, the brightness increases monotonically with excitation intensity. Therefore, the single phosphor layer acts as an image intensifying screen. The structure consists solely of a phosphor film between plane parallel electrodes, one of which is transparent. Although this phosphor exhibits negligible emission under the action of an electric field alone, this enhancement phenomenon may be regarded as "electroluminescence," the magnitude of which is dependent on excitation intensity. In this sense, the exciting radiation "controls" the emission of light.

[1] G. Destriau, Electrochemical Society Meeting, May 2–6, 1954.

LA7. Edge Electroluminescence from CdS Crystals at Low dc Fields. R. W. SMITH, *RCA Laboratories.*—The wavelength of the electroluminescence from certain CdS crystals[1] is very close to the optical absorption edge of the crystal and follows the shift of the absorption edge from 77 to 300°K. The green radiation extends completely between the electrodes and is apparently generated throughout the volume of the crystal at dc electric fields E as low as 10^3 volts/cm. The radiated power is essentially proportional to the current density, J, and is approximately 10^{-8} times the input power. $J \alpha E^{10}$. The decay time of the radiation is $<10^{-6}$ sec. While electroluminescence in insulators has usually been interpreted in terms of high field effects, such a model apparently does not fit in this case. In view of the low value of the field E it is not reasonable that impact ionization or field excitation can excite carriers in the body of the crystal to edge emission, where $h\nu = 2.4$ ev. The generation of light uniformly throughout the volume between the electrodes precludes any simple assumptions of high local fields. A more reasonable mechanism, suggested by A. Rose and H. S. Sommers of these Laboratories, is that excess holes and electrons are injected at opposite electrodes and recombine radiatively in the body of the crystal.

[1] R. W. Smith, Phys. Rev. 93, 347 (1954).

LA8. Photoelectric Mixing of Incoherent Light.* A. THEODORE FORRESTER,† RICHARD A. GUDMUNDSEN,‡ AND PHILIP O. JOHNSON,§ *University of Southern California*, Los Angeles.—As previously proposed[1] beats have been obtained between incoherent light sources by mixing Zeeman components of a visible spectral line at a photosurface. Periodicity in emission was observed through the excitation of a 3-cm cavity. Because of incoherence between the spectral lines and incoherence between the beats from different cathode areas, signal/shot noise at the cavity is only 10^{-4} but the beats were modulated, optically, while maintaining constant intensity, and our receiver was able to yield a signal/noise of two at the indicator. The basic idea is that, in the photoelectric process, the emission probability for electrons is proportional to the square of the resultant electric field amplitude. This appears to be a point of view that is not so directly tested in any other experiment involving quantum effects. The experiment also demonstrates that any time delay between photon absorption and electron release must be significantly less than 10^{-10} second.

* Supported in part by the U. S. Office of Naval Research.
† On sabbatical leave at the University of Pittsburgh.
‡ Now at Hughes Aircraft Company.
§ Now at North American Aviation.
[1] Forrester, Parkins, and Gerjuoy, Phys. Rev. 72, 728 (1947); Gerjuoy, Forrester, and Parkins, Phys. Rev. 73, 922 (1948).

LA9. A More General Theory of Magnetic Self-Focusing. WILLARD H. BENNETT, *Naval Research Laboratory.*—Almost electrically neutral, mixed ion and electron streams of low density can be magnetically self-focusing in the absence of an applied electromotive force, only if the current in the stream exceeds a calculable minimum critical current, whether the velocity distributions are Maxwellian or non-Maxwellian. In the evolution of such a stream, the first things to happen are the permanent loss of some of the charged particles from the stream and the rapid attainment of cylindrical symmetry by the remainder. Such streams are not subject to Kruskal and Schwarzschild* instability. The theory is developed in a relativistically invariant form and is applicable to solar proton streams in the interplanetary plasma.

* Proc. Roy. Soc. (London) 223, 348 (1954).

LA10. The Magnistor, a Solid-State Electronic Valve. MILTON GREEN, *Signal Corps Engineering Laboratory.*—The property of magnetoresistivity can be employed to produce tuned amplifiers[1] and oscillators principally for the subaudio

and the audio range. To accomplish this, a strip or a coil of a magnetoresistive material, generally bismuth, is placed in the magnetic circuit of a laminated or a ferrite core of an inductor* and appropriately wired into an electric circuit containing a dc power supply. The circuitry is simple and the device can be constructed to match almost any given combination of input and output impedances. Magnetoresistive materials, until now, have been such that the amplifier gives useful power gains only at very low temperatures[2] (−190°C and lower). There is hope for raising the limit to within room temperature by recent semiconductor developments. The only internal source of noise of such an amplifier is Johnson temperature noise. Consequently, operating as it does at low temperatures, low impedances and narrow band pass, it should exceed any of the existing types of amplifiers in the detection of weak signals. Experimental results will be shown for magnistors designed in these laboratories.

[1] U. S. Patent No. 1596558, Vol. 29, 9, 22 and No. 1810539, Vol. 16, 8, 26 by B. N. Sakoloff.
* This combination as described is referred to as a magnistor.
[2] E. Justi and H. J. Thuny, Z. Naturforsch. **90**, 183 (1954).

LA11. Photomultiplier Transit Time Measurements.* R. V. SMITH, *Westinghouse Research Laboratories.*—A spark discharge has been used to illuminate simultaneously a 935 phototube and selected small areas on the photocathode of various photomultipliers. The two output pulses were displayed on the same oscilloscope sweep and the time difference measured by reference to a superposed 700 m.c. sine wave. The table shows the over-all photomultiplier voltage (v) on a divider chosen for maximum gain (except that the 6342 shield was at first dynode potential), transit time (t) for illumination of the photocathode center only, and the difference (δt) between edge and center transit times.

Tube	v (volts)	t (sec $\times 10^9$)	δt (sec $\times 10^9$)
5819 No. 1	1100	33.7	4.3
	1400	30.9	2.9
5819 No. 2	950	32.4	3.8
	1300	27.8	2.5
6342 No. 1	1050	32.8	5.2
	1700	26.7	2.9
6342 No. 2	1500	29.5	4.4
	1800	26.8	2.8

* Assisted by the joint program of the Office of Naval Research and U. S. Atomic Energy Commission.

FRIDAY MORNING AT 10:15

Manhattan Center, Masonic Room

(K. G. McKAY, presiding)

Various Topics in Solid-State Physics

M1. Molecular Orientation Produced in Polymethyl Methacrylate by Hot Stretching. MARY J. KRAMER, *Naval Research Laboratory.*—A commercially produced sample of hot-stretched polymethyl methacrylate was examined for evidence of molecular orientation. The sample chosen had a high value of birefringence and an appreciably enhanced resistance to crack propagation, as compared to as-cast polymethyl methacrylate. The x-ray diffraction halos obtained with the flat-film transmission technique were scanned circumferentially with a microphotometer. The preferred orientation thus detected was interpreted with the aid of Coumoulos'[1] analysis, as showing that hot-stretching tends to align the polymer chains with the stretching direction. A halo not recorded by Coumoulos, but reported by Robinson, *et al.*[2] was found in these patterns. As calculated by the modified Bragg equation, this halo corresponds to a spacing of about 17A. The preferred orientation of this halo in the pattern of the hot-stretched material revealed the 17A spacing to be along the length of the chain.

[1] G. D. Coumoulos, Proc. Roy. Soc. (London) **A182**, 166 (1943).
[2] Robinson, Ruggy, and Slantz, J. Appl. Phys. **15**, 343 (1944).

M2. (Abstract withdrawn.)

M3. Localized Energy States in Crystalline Alkali Chlorides.* C. F. HEMPSTEAD AND L. G. PARRATT, *Cornell University.*—The absorption fine structure in the vicinity of the K edge of chlorine in alkali chlorides has been carefully recorded. Correction by a new method has been made for the resolving power of the x-ray spectrometer. (The magnitude of the correction depends upon the absorber thickness.) The corrected structure is more complex than has been heretofore realized. The inner electron vacancy that results when the K-electron is photoejected causes a significant perturbation of the normal periodic potential in the neighborhood of the excited ion containing the vacancy. This ion of atomic number Z appears to a first approximation as an impurity atom of $Z+1$ in the solid. Consequent localized exciton-type energy states are invoked to explain the observed spectra. For KCl, the lowest absorption "line" (farthest below the conduction continuum) is at least a doublet with a separation of about 0.8 ev and having a doublet peak intensity ratio of about 1 to 3.3. A "reasonable" resolution of the observed contour into component absorption lines, each of Lorentzian shape, indicates in a range of about 6 ev at least six components for KCl and six for NaCl. The pattern of component lines or exciton-type states is markedly different for different chlorides.

* Supported by the United States Air Force through the Office of Scientific Research of the Air Research and Development Command.

M4. Direction Breakdown in Alkali Halide Crystals. M. E. CASPARI, *M. I. T.**—Room temperature experiments on NaCl and KBr under homogeneous and inhomogeneous field

conditions revealed the existence of three types of breakdown paths. These are anodic, cathodic, and homogeneous field paths. The formation of anodic paths was always initiated by prebreakdown discharges through the insulating medium surrounding the anode. Cathodic paths originated directly from the cathode when cathodic point-plane electrode systems were employed. Both anodic and cathodic paths were orientated with respect to the crystal structure; paths produced by homogeneous fields, however, followed the direction of the applied field. The temperature dependence of the anodic breakdown path directions in several alkali halide crystals was investigated from −160°C to 350°C under reproducible field conditions. In general, the results agree with those of Davisson.[1] In potassium and rubidium salts the temperature at which the path orientations changed from the [100] to the [110] direction could be determined to within ±10°C. The mechanism of the formation of the various breakdown paths and the theoretical implications of the results will be discussed.

* Sponsored by the Office of Naval Research, the Army Signal Corps, and the Air Force.
[1] J. W. Davisson, Phys. Rev. **70**, 685 (1946).

M5. Dislocation Line Energy and Slip in NaCl and AgCl Crystals.* ROBB THOMSON, *University of Illinois.*—Calculations of the elastic energy of dislocations in NaCl and AgCl have been made which include the effects due to the elastic anisotropy of the crystals. At low temperatures the calculations give some evidence in NaCl for the choice of (110) slip planes over (100) slip planes. However, the calculations do not predict the large difference in the yield stress experimentally observed.[1] This result suggests that other mechanisms such as a differential pinning of edge dislocations in different slip planes are also important. At high temperatures the preference for (110) slip planes due to crystal anisotropy disappears, in agreement with suggestions by early experimenters[2] that other slip planes become active at high temperatures. The calculations for AgCl do not predict any marked preference for (110) slip planes over (100) slip planes in agreement with the observed pencil glide in AgCl.[3]

* Supported by the United States Air Force.
[1] S. Dommerich, Z. Physik **90**, 189 (1934).
[2] E. Schmid and W. Boas, *Plasticity of Crystals* (F. Hughes and Company, London, 1950).
[3] J. F. Nye, Proc. Roy. Soc. (London) **198**, 190 (1949).

M6. Model for the Room Temperature Bleaching of *F* Centers by *F* Light in X-Rayed NaCl.* ROBERT HERMAN AND R. F. WALLIS, *The Johns Hopkins University.*—During the optical bleaching of *F* centers it is assumed that *F* center electrons are elevated to the conduction band on absorption of *F* light leaving negative ion vacancies. Conduction electrons may be captured by holes and by negative ion vacancies. It is assumed that the cross sections for the latter two processes are equal and that the conduction electron concentration is small and stationary. During the bleaching process the nonuniformity of the local light intensity I produces gradients in the local F-center concentration n. Under the above conditions the equations specifying I and n reduce to $\partial n/\partial t = -bIn^2$ and $\partial I/\partial x = -\mu In$, where b and μ are constants. These equations have been integrated numerically for the case of a uniform initial F-center distribution. The results are compared with quantitative measurements of the F-center concentration as a function of F-light irradiation time in x-rayed NaCl. It is found that the behavior of the model is consistent with experimental data for lightly x-rayed crystals in which no appreciable growth of M and R bands occurs during bleaching. In heavily x-rayed crystals in which appreciable growth of M and R bands occurs, deviations from the behavior of the model are observed.

* This work was supported by the Bureau of Ordnance, Department of the Navy.

M7. Slow Neutron Spectrometry—A New Tool for the Study of Energy Levels in Condensed Systems. B. N. BROCKHOUSE, *Chalk River Laboratories.*—It has long been realized that energy distributions of initially monoenergetic neutrons scattered by molecules or condensed systems would yield important information not otherwise easily accessible to experiment. With high reactor flux and suitable spectrometer design such measurements are now feasible. Monoenergetic neutrons, selected from the *NRX* reactor spectrum by a crystal, are scattered by the specimen and the energy distribution of the scattered neutrons is analyzed by another crystal. A survey of the field has been made and more detailed studies are in progress. The sharp division of incoherent scattering into elastic and inelastic components predicted by theory has been verified with vanadium. In liquid lead, light water, and heavy water a similar division into a "quasi-elastic" component, and an inelastic component which increases with increasing angle, can be made. For coherent scattering the "elastic" component is associated with the peaks in the liquid diffraction pattern. In liquid lead the inelastic component is similar to that of the solid at about the same temperature and angle of scattering. Diffuse magnetic scattering, studied with MnO and Mn_2O_3, and with Cr_2O_3 above and below its Néel temperature, is largely inelastic, the mean energy changes being of the order of the Néel temperatures.

Invited Paper

M8. Study of Energy Levels in Solids, Liquids, and Magnetic Materials by Scattered Slow Neutrons. B. N. BROCKHOUSE, *Chalk River Laboratories.* (30 min.)

FRIDAY MORNING AT 10:15

New Yorker, Panel Room

(M. GOLDHABER, presiding)

Beta and Gamma Emitters, I

MA1. The Decay of Cr^{48}.† R. VAN LIESHOUT,* D. H. GREENBERG, AND C. S. WU, *Columbia University.*—The nuclide Cr^{48} has been reported as a spallation product[1] decaying with a half-life of 1 day, presumably by electron capture only. However, gamma rays can be expected in view of the large spin difference between the two ground states involved. We have found gamma rays of 116 and 305 kev decaying with a 23-hr period over 6 half-lives. The characteristic gamma rays

of V^{48} were shown to grow in at a rate compatible with this period. No positrons were found in the decay of Cr^{48} (<2 percent). Further work employing coincidence techniques is in progress. Cr^{48} was produced by spallation of Ni with 380-Mev protons in the Nevis cyclotron. Ni was chosen as target to produce Cr^{48} efficiently with respect to other Cr activities.[2] The completeness of the chemical separations was evidenced by the absence of positron emitting impurities.

† Partially supported by the U. S. Atomic Energy Commission.
* On leave from the Institute for Nuclear Research, Amsterdam, The Netherlands.
[1] Rudstam, Stevenson, and Folger, Phys. Rev. 87, 358 (1952).
[2] E. Belmont and J. M. Miller, Phys. Rev. 95, 1554 (1954).

MA2. The Disintegration of Selenium-73. R. W. HAYWARD AND D. D. HOPPES, *National Bureau of Standards.*—The radiations from the 7.1 hour selenium-73 activity have been investigated using magnetic lens, scintillation pulse height, and coincidence counting techniques. Two gamma rays of 361- and 67-kev energy and of nearly equal intensity were observed to be in prompt coincidence with each other and in delayed coincidence with the annihilation radiation resulting from the positron decay. The reported[1] 860- and 1310-kev gamma rays appear to be less than 1 percent of the total intensity. Energy and intensity measurements of the positrons indicate that the main group (1.32 Mev, log $ft=5.3$) excites the gamma cascade, while a weaker group (1.68 mev, log $ft \approx 8.4$) excites the 67-kev transition only. These data coupled with internal conversion information lead to a level scheme in As^{73} as follows: ground level, $p_{3/2}$; 67-kev level, $f_{7/2}$; and 428-kev level, $g_{9/2}$, $\tau_{1/2}=6\mu$ sec. The positron decaying Se^{73} is in a $g_{9/2}$ state.

[1] F. R. Scott, Phys. Rev. 84, 659 (1951).

MA3. Decay and Fast Neutron Excitation of Zr^{90m}. E. C. CAMPBELL, R. W. PEELLE, F. C. MAIENSCHEIN, AND P. H. STELSON, *Oak Ridge National Laboratory.*—Evidence is presented for a new isomer in Zr^{90} ($N=50$, $Z=40$) with a half-life of 0.83 ± 0.03 sec and a gamma energy of 2.30 ± 0.02 Mev. The isomer is found in pile neutron bombardment of electromagnetically enriched (98.7 percent) Zr^{90}. Gamma measurements were made with a NaI spectrometer and multichannel analyzer. The isomer was also produced by monoenergetic neutrons from the $T(p,n)$ reaction. An electronic timer and an electrostatic proton beam deflector provided a repetitive cycle for short neutron bombardment and gamma counting. The yield curve exhibits a threshold at 2.3-Mev neutron energy. This is taken as evidence that the isomer is produced by inelastic neutron scattering, i.e., $Zr^{90}(n,n')Zr^{90m}$. The complicated structure of the yield curve, which was measured up to 4.4 Mev, gives evidence on the existence of excited states of Zr^{90} which feed the isomeric level. The energy and half-life are consistent with an $E5$ assignment for the isomeric transition. It is suggested that the 5-level might arise from the promotion of a $p_{1/2}$ proton into a $g_{9/2}$ state.

MA4. The Decay of Ru^{103}. H. H. FORSTER AND A. ROSEN, *University of Southern California.*—The beta- and gamma-ray spectra of (42*d*) Ru^{103} were investigated with a double thin lens beta-ray spectrometer of about 2 percent resolution. Source materials were obtained from Oak Ridge and Chalk River. An analysis of the beta spectrum showed two distinct beta groups with maximum energies of 680 and 205 kev and evidence of a third beta group of about 140 kev max energy, the possible existence of which has been suggested.[1] Gamma lines, obtained through internal conversion and through the photoelectron spectrum of a 40 mg/cm² Pb radiator had energies of 37.5, 307, 490, and 600 kev. Details of the spectrum will be presented and a possible decay scheme will be discussed.

[1] Cork, Le Blanc, Stumpf, and Nester, Phys. Rev. 86, 575 (1952).

MA5. The Disintegration of 5.8-Day Sb^{120}. C. L. MCGINNIS, *National Bureau of Standards and National Research Council.*—The assignment of a six-day activity[1] to Sb^{120} has been confirmed. The activity was produced by 15-Mev deuteron bombardment of enriched Sn^{119} and by 50-Mev bremsstrahlung bombardment of Sb. It decays by electron capture followed by a cascade of four γ rays, 0.090, 0.200, 1.035, and 1.180-Mev. The conversion electron intensities are in the ratio 1770:1000:10.4:7.8, respectively. The $\gamma\gamma$ angular correlation for the $0.09\gamma-0.20\gamma$ is dipole-quadrupole of the 3, 2, 0 type, and quadrupole-quadrupole of the 4, 2, 0 type for the $0.20\gamma-(1.04\gamma+1.18\gamma)$ and the $1.04\gamma-1.18\gamma$ cascades. From these data it is inferred that the 0.090γ is $E1$ and the other three γ's are $E2$. The 1.180γ was also observed in the decay of the 16.6^m Sb^{120}. In this activity the ratio of the 1.180γ to total β^+ was 0.03.

[1] M. Lindner and I. Perlman, Phys. Rev. 23, 1124 (1948).

MA6. Radiations of Sb^{122}.* B. FARRELLY, L. KOERTS, R. VAN LIESHOUT, N. BENCZER, AND C. S. WU, *Columbia University.*—The radiations of Sb^{122} have been investigated and a decay scheme together with spin and parity assignments proposed. Analysis of the β spectrum revealed the presence of three different energy groups with end points 1.98 Mev, 1.40 Mev, and 740 kev and relative intensities (29.4:61.7:8.9), respectively. Four γ radiations of energies 566 kev, 686 kev, 1137 kev, and 1258 kev have been investigated with a single channel and a selective coincidence scintillation spectrometer. The 566 kev and 686 kev γ lines are in cascade and the 1258 kev γ line is the cross over radiation. All three of them are on the β^- branch. The 1137 kev γ line is associated with the K capture which is only a few percent of the total disintegration. An accurate energy determination of these radiations and their K and L internal conversion coefficients were obtained from the external and internal conversion electron spectra. The ratio of β^+/β^- is less than 10^{-3}. The shape of the spectra and the ft-values of the various groups are consistent with the spin and parity assignment of 2^- for the ground state of Sb^{122}.

* This work was partially supported by the U. S. Atomic Energy Commission.

MA7. The Radioactive Decay of 65 Hour Sb^{122}.* MICHAEL J. GLAUBMAN, *Princeton University.*—Sixty-five Sb^{122} was investigated using Sb^{121} (97.7 percent–99.4 percent) bombarded with thermal neutrons for 70 hours. Spectrometer measurements show three beta groups with end-point energies: 1.987-, 1.423-, and 0.734 Mev, and log ft values: 8.6 (log ft (w^2-mc^2) $=10.0$, p^2+q^2 shape), 7.6 (allowed shape), and 7.7, and four gamma rays with energies: 0.563-, 0.693-, 1.152-, and 1.256 Mev, and intensities: 73 percent, 3.5 percent, 0.75 percent, and 0.8 percent. From gamma-gamma and beta-gamma coincidences the excited states of Te^{122} were found at 0.563- and 1.256 Mev. X-gamma coincidences and x-ray critical absorption showed 2 percent and 0.75 percent K capture transitions to the ground state and to a 1.152-Mev level of Sn^{122}. Annihilation radiation was not observed setting an upper limit of 0.005 percent for positrons. The directional correlation of the 0.693- and the 0.563-Mev gammas indicated a $2(L=2\ 91\pm5$ percent) 2 0 cascade. We conclude, therefore, that the ground state of Sb^{122} is $2-$ ($g_{7/2}$, $h_{11/2}$), the first two excited states of Te^{122} are $2+$, and the first excited state of Sn^{122} may also be $2+$.

* Supported by the Office of Naval Research, the U. S. Atomic Energy Commission, and the Higgins Scientific Trust Fund.

MA8. Radiations of I^{126}* L. KOERTS, P. MACKLIN,† B. FARRELLY, R. VAN LIESHOUT, AND C. S. WU, *Columbia University.*—The β and γ radiations and the electron capture process of I^{126} have geen thoroughly investigated. The β^- branch consists of three groups of maximum energies 1.25,

0.865, and 0.385 Mev. The relative intensities of these three β^- groups are 1:3.1:0.03, respectively. The shape of the highest energy β^- group identifies the ground-to-ground transition to be a unique first forbidden one of $\Delta J=2$, yes. The spectrum of the middle β^- group as measured by the magnetic coincidence spectrometer has an allowed shape. The number of β^+ emission is only 2.8 percent of that of the β^- emission. Two groups of maximum energies 1.11 and 0.46 Mev were found with an intensity ratio of 3.5:1. The shape of the β^+ spectrum of the ground-to-ground transition is also the unique first forbidden type. The correlations among the various γ lines and χ line and their relative intensities are determined by a selective coincidence scintillation spectrometer. In conclusion, the spin and parity of the I^{136} ground state is definitely 2^- and its decay scheme is in general agreement with that of Perlman and Welker.[1]

* This work partially supported by the U. S. Atomic Energy Commission.
† Now at Miami University.
[1] M. L. Perlman and J. P. Welker, Phys. Rev. 95, 133 (1954).

MA9. Coincidence Studies of the Disintegration of Pm^{151} and Nd^{147}.† H. S. Hans,* Babulal Saraf,‡ and C. E. Mandeville, *Bartol Research Foundation.*—Chemically pure Nd_2O_3 was irradiated by slow neutrons on five successive occasions in the Brookhaven pile. The 27.5-hour Pm^{151} was found to emit gamma rays of 64, 100, 163, 177, 240, 275, 340, 440, 650, and 700 kev. The 11-day Nd^{147} was shown to emit quanta of energies 92, 165, 280, 320, 410, 440, 530, and 690 kev. The relative intensities of the various quantum radiations have been determined, and coincidence measurements have been performed to ascertain the various sequential relationships between pairs of gamma rays. Partial decay schemes of both radionuclides will be discussed.

† Assisted by the joint program of the Office of Naval Research and the U. S. Atomic Energy Commission.
* Fulbright Fellow from The Muslim University of Aligarh, India.
‡ On leave of absence from Agra College, Agra, India; at present at the Nobel Institute for Physics, Stockholm, Sweden.

MA10. The Gamma-Gamma Directional Correlation in Er^{166}. J. S. Fraser and J. C. D. Milton, *Chalk River Laboratories.*—The directional correlation of the 1380- and 81-kev gamma rays excited in the beta decay of 27-hr Ho^{166} shows unambiguously that the spins of the 1460- and 81-kev levels of Er^{166} are 0 and 2, respectively. The observed directional correlation of the 1600- and 81-kev gamma rays is consistent with a spin of one or two for the 1680-kev level. The severe attenuation of the correlation produced by the large quadrupole moment and relatively long lifetime of the 81-kev state has been partially removed in a source of $Ho(NO_3)_3$ maintained above the melting point. The results, corrected for angular resolution, are fitted by the distribution $W(\theta)=1\pm(0.137\pm0.006)P_2(\cos\theta)+(0.560\pm0.019)P_4(\cos\theta)$ yielding for the attenuation coefficients $G_2=0.384\pm0.011$ and $G_4=0.490\pm0.017$. The 1460-kev spin 0 level and the 81-kev spin 2 level may correspond to the β-vibrational and first rotational levels respectively predicted by the strong coupling approximation of the Bohr-Mottelson[1] theory.

[1] A. Bohr and B. R. Mottelson, Dan. Mat. Fys. Medd. 27, No. 16 (1953).

MA11. Disintegration of 27-hr Ho^{166}. R. L. Graham, J. L. Wolfson, and M. A. Clark, *Chalk River Laboratories.*—A magnetic spectrometer study of the β-ray spectrum from 27-hr Ho^{166} shows two main components with end-points of 1771 ± 7 and 1854 ± 5 kev. The 1771 kev β-ray spectrum was examined in coincidence with L conversion electrons of the 80 kev γ transition and was found to have a predominantly α shape. From the measured $\gamma80$ conversion line intensities and known K conversion coefficient this β component has an intensity of 48 ± 4 percent. Subtraction shows that the 1854 kev component has approximately allowed shape. The angular correlations between $\gamma80$ and energetic β rays and between $\gamma80$ and $\gamma1380$ have been compared to obtain the ratio of the $g_2A_2P_2(\cos\theta)$ terms in the correlation $1+g_2A_2P_2(\cos\theta)+g_4A_4P_4\times(\cos\theta)$. Taking the $\gamma-\gamma$ cascade as $0-2-0$ (see preceding abstract) the theoretical ratio for $g_2A_2(\beta-\gamma)/g_2A_2(\gamma-\gamma)$ is 1.37 or $\leqslant0.68$ for Ho^{166} assignments of $0-$ or $1-$, respectively. The observed ratio, 1.37 ± 0.17, together with the shapes of the β components indicate an assignment of $0-$ for Ho^{166} (27 hr).

MA12. The Long-Lived Isomer of Ho^{166}. J. C. D. Milton, J. S. Fraser, and G. M. Milton. *Chalk River Laboratories.*—A holmium sample was highly purified by ion exchange methods both before and after a 5-week irradiation at a neutron flux of $\sim5\times10^{13}$ cm^{-2} sec^{-1} in the N. R. X. reactor. A long-lived activity of about 1 μC/mg was obtained which may be identified with the Ho^{166} activity reported by Butement.[1] A careful comparison of the low energy spectrum with that of the 27-hr activity indicated that the energies and relative intensities of the 80.2 ± 0.5 kev γ ray and 49-kev KX rays were identical in both isomers. In addition, γ rays with energies 188 ± 5, 283 ± 10, 725 ± 20, and 845 ± 20 kev were observed. Coincidence measurements showed that all five γ rays were in cascade. No lifetime greater than 2×10^{-9} sec was observed in $\beta-\gamma$ coincidence measurements. Assuming the three lowest energy γ rays arise from rotational levels on the ground state, the first 3 excited states may then be fitted to the Bohr-Mottelson formula[2] $E_I=AI(I+1)-BI^2(I+1)^2$ where $A=13.6$ kev, $B=0.013$ kev, $I=0$, 2, 4, 6.

[1] F. D. S. Butement, Proc. Phys. Soc. (London) A65, 254 (1952).
[2] A. Bohr and B. Mottelson Dan. Mat. Fys. Medd. 27, No. 16 (1953).

Friday Morning at 10:15

Manhattan Center, Gold Room

(L. B. Borst, presiding)

General Nuclear Physics

N1. U L_I X-Ray Transition from Separated Isotopes.* G. L. Rogosa, *Florida State University,* and W. F. Peed, *Oak Ridge National Laboratory.*—An experimental search for isotope shift in the x-ray levels of heavy elements has been continued with the examination of the $2s_{\frac{1}{2}}$ state of U. The $L\beta_3\times(L_I\rightarrow M_{III})$ x-ray transition from separated isotopes of U^{238}, U^{235}, and U^{233} was measured, using a double crystal x-ray spectrometer. Special target pellets were fabricated and placed inside a demountable and continuously pumped x-ray tube. No evidence for an isotope shift, to within 1 ev, on the L_I level was found in the measurement of the x-ray transition. Theory[1] now predicts an effect smaller than our detectable limit.

* Supported by the U. S. Atomic Energy Commission.
[1] G. Igo and M. S. Wertheim, Phys. Rev. 95, 1097 (1954).

N2. Effect of a Static Electric Field on Positronium Formation.* S. Marder, W. Bennett, C. S. Wu, *Columbia University,* and V. W. Hughes, *Columbia University and Yale University.*—The effect of an rf electric field on the formation

of positronium was first reported by Deutsch and Brown in their Zeeman effect measurement.[1] The effect of a static electric field on the formation of positronium in the gases He, A, and SF_6 has been studied. The experimental arrangement consisted of a positron source (Cu^{64}) in a cavity filled with the gas at a pressure of about 2 atmospheres. Both electric and magnetic fields could be applied. The energy spectrum of the annihilation radiation was observed with a NaI(Tl) scintillation spectrometer. An analysis of this spectrum leads to a value for the fraction of positrons which form positronium. In He and A the fraction begins to increase at fields of about 60 and 250 volts/cm respectively, and rises to a saturation value by fields of about 150 and 500 volts/cm. The fraction increased by a factor of about 1.5 in He and 2.5 in A. No effect of the electric field was observed in SF_6. The theory of the effect of the electric field on formation is discussed in the following abstract.

* This work partially supported by the U. S. Atomic Energy Commission.
[1] Deutsch and Brown, Phys. Rev. 85, 1047 (1952); also M. Deutsch (private communication on his observation of static field effect in A).

N3. Theory of Effect of a Static Electric Field on Positronium Formation.* W. B. TEUTSCH,† *University of Pennsylvania*, AND V. W. HUGHES, *Yale University*.—In the absence of an electric field those positrons which fail to form positronium as they are slowed down in a gas to energies below the threshold energy for formation will thermalize and undergo what we call "free annihilation." In the presence of an electric field E, these positrons will attain a velocity distribution which depends principally upon E, pressure, and σ_{elastic} for slow positrons in the gas. The fraction of these positrons which form positronium can be computed from appropriate averages over the distribution, these averages involving the cross sections for formation of positronium and for free annihilation. The cross section σ_{elastic} for S-wave positrons in He (much smaller than for electrons) has been computed by a variational procedure for several approximate potentials, and $\sigma_{\text{formation}}$ in He has been computed in the Born approximation. It is predicted that E will have no observable effect on formation until the mean energy of the distribution is $\sim\frac{1}{10}$ of the threshold energy and that formation will then increase rapidly with E to a saturation value, in agreement with the experimental data of the preceding abstract.

* This research has been supported in part by the Office of Naval Research.
† National Science Foundation predoctoral fellow.

N4. Mass Spectrometric Search for Naturally Occurring Isotopes of Low Abundance. F. A. WHITE, T. L. COLLINS, AND F. M. ROURKE, *Knolls Atomic Power Laboratory*.*—A two-stage magnetic mass analyzer[1] has been used to search for isotopes which occur in nature in very low abundance. This instrument minimizes the effect of small angle elastic scattering of positive ions which, in many instances, limits the resolution of isotopes differing by only one mass unit, but having relative abundance ratios of 10^4 to 1 or greater. A new naturally occurring isotope, Ta-180, has been found and the Ta-180/Ta-181 ratio has been measured to be 0.000123 $\pm$0.000003. New upper limits for the percentage abundances of other isotopes of this element are: Ta-177, Ta-178, Ta-179, 0.0003; Ta-182, Ta-183, 0.0002. In addition, tungsten and niobium have been investigated for new isotopes. None have been found, but the following new upper limits are: W-185, 0.0002; W-187, 0.0001; Nb, "all other," 0.0002.

* Operated by the General Electric Company for the U. S. Atomic Energy Commission.
[1] F. A. White and T. L. Collins, Appl. Spectroscopy 8, 17 (1954); November (1954).

N5. Nuclear Orbital Assignments for Ta^{180}. P. F. ZWEIFEL, *Knolls Atomic Power Laboratory*.*—Assuming natural tantalum contained $\sim$50 percent Ta^{180} at the origin of the earth ($t=0$), the recently measured[1] isotopic abundance of Ta^{180} yields a beta-decay half life of $>3\times10^8$ years. The beta energy, obtained from Stehn's nuclear mass parabolas[2] for isobars, is 0.6 Mev [to the $(2,+)$ first excited state of W^{180}]. This half life and energy lead to a log ft value of 17.4, which is associated with a third-forbidden decay, meaning the ground state of Ta^{180} should be a $(5,-)$ or $(6,-)$ state. On this basis the probable orbital assignments for the ground state appear to be $Z=g_{7/2}$, $N=f_{5/2}$. The eight-hour excited state of Ta^{180} will be discussed also. It is hoped that experimental work on other quasi-stable odd-odd nuclei will lead to more information concerning nuclear orbital assignments. The spin assignments are not sensitive to changes in the assumed isotopic abundances at $t=0$; the limits for a third-forbidden decay of this energy are approximately 2×10^7 years $<T_{1/2}<2\times10^{11}$ years.

* Operated for the U. S. Atomic Energy Commission by the General Electric Company.
[1] See preceding abstract.
[2] J. R. Stehn, Phys. Rev. 93, 932 (1954).

N6. Magnetic and Electric Deflection Spectrometry of Neutrino Recoils in Argon-37. ARTHUR H. SNELL AND FRANCES PLEASONTON, *Oak Ridge National Laboratory*.—Chlorine-37 ions which recoil as the result of neutrino emission in the electron capture transformation of argon-37 emerge in a collimated beam from a field-free volume. The energies, momenta, and e/m values of the recoils are studied by electric and magnetic deflection, followed by post-deflection acceleration through 5 kv and registration with an electron multiplier. Auger electron emission leaves the ions charged, the doubly and quadruply charged states being about half as abundant as the triply charged state. The singly charged state is weakly represented, and the quintuply charged state has not yet been sought. The recoil energy of the ions is 9.6$\pm$0.5 ev, in agreement with that to be expected from the emission of a neutrino of the known transition energy 816 kev. Instrumental resolution is small compared with the natural widths of the lines. The observed line widths are in agreement with predictions based upon thermal motion and recoil from Auger electron emission.

N7. Apparent Importance of $(7/2)^6$ in the Representation of Nuclear Masses as Multiples of the Electron Mass. ENOS E. WITMER, *University of Pennsylvania*.—The mass of any nucleus in any state may be represented by Mm, where m is the rest mass of the electron. Many $M-$ values appear to be integers and the writer[1] has surmised that M is in general a certain type of rational number. This work gave $m=0.000\,548\,770\,285\,9$ amu. The writer[1] has also pointed out that the $M-$ values for the lightest nuclei in the ground state are given to a very high degree of accuracy by an approximate formula, of which the main term is $(7/2)^6\,A$, where A is the number of nucleons in the nucleus. In abbreviated form this formula may be written as $M=(7/2)^6\,A-B$. The values of B for the ground states of U^{238} and U^{239} are respectively 3673.35 and 3682.51. Since $2(7/2)^6$ lies between these two values we conclude that $B\leqslant 2(7/2)^6$ for all stable nuclei. It also seems probable that $B\leqslant 18A$ with Ni^{60} at the upper limit. A regularity in certain excited nuclear energy levels is noted. The apparent importance of $(7/2)^6$ indicated here may be related to the three dimensionality of space, since $7/2=3+\frac{1}{2}$.

[1] E. E. Witmer, Phys. Rev. 95, 667 (1954); 95, 610 (1954).

Invited Papers

N8. A Focusing Atomic-Beam Apparatus. D. R. HAMILTON, *Princeton University*. (30 min.)

N9. Spins and Moments of Radioactive Nuclei. V. W. COHEN, *Brookhaven*. (30 min.)

FRIDAY MORNING AT 10:15

McAlpin, Red Room

(S. BOROWITZ, presiding)

General Theory

OA1. Emission of Negative-Energy Gravitons by Matter. F. J. BELINFANTE, *Purdue University.*—Will the lack of positive definiteness of the gravitational energy density T_g^{00} make matter raise its energy by emission of negative-energy gravity radiation? We postulate absence of "incident" gravitons.[1] Classically this means that all gravitational fields are retarded fields. Double stars are most effective gravity radiators. Their gravitational radiation can be calculated classically. In the "wave zone" (field $\propto r^{-1}$), the outward radial component of the energy flux equals cT_g^{00}. Superimposed on positive definite terms in T_g^{00} are much larger oscillating terms causing regions of negative energy density. If, however, at a fixed time t, at a fixed distance r from the double star and fixed angle θ with z-axis perpendicular to its orbital plane, these oscillating terms are integrated over φ around this z-axis they average zero. Therefore, due to the positive definite terms, there is at all times a slight excess of emission of positive-energy over negative-energy gravitons. Thus, fears for radiative energy gain by matter seem ungrounded. In fact, e.g., Capella would lose half its orbital energy in 9.2×10^{16} years.

[1] J. C. Swihart and F. J. Belinfante, Phys. Rev. 95, 630 (1954).

OA2. A New Approximation Method for the Gravitational Field Equations. J. N. GOLDBERG, *Armour Research Foundation.*—For certain applications (e.g., radiation) it is desirable to drop the restriction to small velocities which is essential to the approximation method developed by Einstein, Infeld, and Hoffmann.[1] Since the radius of the Schwarzchild singularity is much smaller than the radius of all known bodies, the gravitational potentials may be expanded in terms of the ratio of the Schwarzchild radius to the interparticle distance. With the coordinate conditions $\gamma_{\mu\nu,\nu}=0$, in each order the field equations are inhomogeneous wave equations, with known right-hand side. From the Bianchi identities and the relationship between the field equations and the super-potentials for the strong conservation laws[2] one can show that the four-dimensional ordinary divergence of the inhomogeneous terms vanishes. Therefore, in principle the solutions of the field equations consistent with the coordinate conditions may be written down explicitly. Furthermore, the surface integrals corresponding to those used by EIH may be shown to be empty. Hence, differential equations of motion cannot be obtained by this approximations method. The integrated equations of motion may be obtained by examining the singularities of the field.

[1] Einstein, Infeld, and Hoffmann, Ann. of Math. 39, 66 (1938).
[2] J. N. Goldberg, Phys. Rev. 89, 263 (1953).

OA3. On the Possible Convergence of the Mass Renormalization. T. A. WELTON, *Oak Ridge National Laboratory.*—The question of the possible convergence of the formally infinite mass renormalization has been attacked as follows. First, it is shown that quantum electrodynamics (at least for all processes not involving closed loops) is completely equivalent to the wave mechanics of a particle moving in a space of four equivalent dimensions, subject to the action of a classical force field, with random phases but known power spectrum. The analysis of the behavior of this system can then be carried through in considerably simplified form. It is shown that perturbation theory is inadequate for the calculation of the mass correction, and that the appropriate dimensionless expansion parameter is not α, but rather the usual fractional mass correction with definite upper cutoff. The perturbation series must certainly fail if this parameter is infinite, and apparently the radius of convergence is roughly unity. A numerical, non-perturbation analysis of the simplified problem is being performed. Preliminary results have been obtained for a very much idealized problem, which, however, contains the essential features of the real problem. It is found that the mass correction actually approaches a finite limit as the perturbation value diverges. Similar arguments fail completely for the infinite charge renormalization.

OA4. Transformations in Phase Space and Dirac Brackets.* PETER G. BERGMANN AND IRWIN GOLDBERG, *Syracuse University.*—A set of constraints, constants of the motion, will restrict the physically meaningful portions of a classical phase space to a hypersurface in such widely diversified cases as when the original Lagrangian is invariant under a transformation group depending on arbitrary functions or when the Lagrangian is linear in the time derivatives. We have studied the group of transformations in phase space that maintain the Hamiltonian form of the equations of motion and which maintain the exact form of the constraints. This group may be characterized without recourse to Dirac's separation into first-class and second-class constraints. However, if there are any first-class constraints, then the group of transformations contains an invariant subgroup, those transformations having a vanishing generator. The factor group of this subgroup has a one-to-one relationship to the "permissible" generators, and the group-theoretical commutators are generated by the (generalized) Dirac brackets. The quantized theory will have to deal only with the permissible observables. Commutators with all constraints vanish outright.

* Supported by Office of Naval Research.

OA5. Spin Models. DAVID FINKELSTEIN, *Stevens Institute of Technology and New York University.*—Covariant models are presented for particles or systems in which integer or half-integer intrinsic spin results from an actual rotation. The models are restricted to be rigid in a definite sense, and with the requirement of covariance this considerably limits the possible kinematic structures. Some of the possibilities are similar to covariant models which have already been investigated (Yukawa, Bopp, Pias, *et al.*) but others appear to be new. In all cases the wave-function is scalar and the spin-states, of course, result from decomposition into "internal" spherical harmonics. Each model possesses a spin-mass spectrum, but only some models exhibit half-integer spins. With each kinematic structure is associated a simplest possible Lagrangian, and several are presented with their spectra. Since interactions are not included a comparison with nature would be premature. Quantization of the free fields is complicated by the

fact that one particle may possess both half-integer and integer spins.

OA6. A New Interpretation of the Dirac Equation. RALPH SCHILLER, *Stevens Institute of Technology.*—In recent publications by different authors, various new interpretations have been given the Schrödinger and Pauli equations. These interpretations differ from the usual one accorded these equations in quantum nechanics in that the existence of a continuous particle trajectory is assumed, and the uncertainties associated with these trajectories are attributed to some background field or fluid. We try to extend this point of view to the Dirac equation, and we show that the Dirac equation may be interpreted as a special kind of fluid of spinning bodies. The electrons can be considered as vortex singularities of this fluid. The equations of motion which the electrons satisfy are similar to the equations of motion of a spinning charge which were proposed by Frenkel in 1926 in the early days of quantum mechanics. The several respects in which our equations differ from his will be discussed.

OA7. On the Foundation of a Wave-Mechanical Theory of the Electron. WALTER GLASER, *Farrand Optical Company, Inc.* —A new covariant formulation of a theory of electrons is given. It is a natural generalization of the Maxwell Lorentz theory with the basic hypothesis that the vacuum supports a magnetization as well as a magnetic field strength. The magnetization in the vacuum and a corresponding electric polarization are so determined that they do not become apparent in the macroscopic Lorentz equations of motion. This is the very root of the electron spin. On this basis the electron exhibits finite self-energy and a definite "electron radius." Further, the electron possesses a magnetic moment and angular momentum which are proportional with their ratio given by the "anomalous" factor $e/m.c$ characteristic of the electron spin. The theory yields a small additional magnetic moment of the electron equal to the product of the electron charge and the electron radius, or of the Bohr magneton and fine structure constant. The relation to the Dirac wave equation is pointed out.

OA8. A Connection Between Recent Theories of Bohm, De Broglie, Dirac, and Schrödinger. HANS FREISTADT, *Newark College of Engineering.*—Utilizing a connection, pointed out by Schrödinger,[1] between the so-called Klein-Gordon equation and Dirac's new theory of electrons,[2] one obtains the causal interpretation of quantum mechanics proposed by Bohm[3] and De Broglie[4] as a slight generalization of Dirac's new theory. The formulation thus obtained is of simpler axiomatic structure than the formulation of Bohm and De Broglie; in particular, the Hamilton-Jacobi action function S is not introduced explicitly into the axioms, but appears naturally, as in Dirac's new theory. The treatment is confined to particles obeying the Klein-Gordon equation.

[1] E. Schrödinger, Nature **169**, 538 (1952).
[2] P. A. M. Dirac, Proc. Roy. Soc. (London) **A209**, 291 (1951).
[3] D. Bohm, Phys. Rev. **85**, 166, 180 (1952).
[4] L. de Broglie and J.-P. Vigier, *La Physique Quantique Restera-t-elle Indeterministe?* (Gauthier-Villars, Paris, 1953).

OA9. Lagrangians Linear in the "Velocities."* EZRA NEWMAN AND PETER G. BERGMANN, *Syracuse University.*—Lagrangians linear in the first time derivatives are of sufficient importance in physics (particle fields, general relativity in the Palatini formulation, Einstein-Strauss type unified field theory, etc.) to warrant special consideration. Our treatment is patterned after Dirac's[1] more general exploration of Lagrangians leading to algebraic relations between the canonical variables. In our case the number of such constraints is at least as large as the number of configuration coordinates. The secondary constraints are free of canonical momentum densities. We have examined all the possibilities that may arise, —incompatibility of the field equations, proper Cauchy-Kowalewski problems, and the appearance of arbitrary functions in the solutions. Quantization schemes for the compatible cases will be described.

* Supported by Office of Naval Research.
[1] Can. J. Math. **2**, 129 (1950); **3**, 1 (1951).

OA10. (Abstract withdrawn.)

OA11. Force—Its Nature, Structure, and Generation (Creation) (As Disclosed by $f\times t=m$). LUCIEN V. ALEXIS, SR., *School of Post Modern Science.*—To AB, an opened or closed curve as a static or dynamic space-time event, this paper applies ($f\times t=m$) revised, and extracts the separate mathematical expressions for the curve in pure space and in pure time. Obtaining thereby 0 and 1 as the limits of the form and content of the ultimate unit of each of the two continua, we identify time, the substance, as force, the substance, in inverse action; it identifies both units as units of duration, the physical ultimate. From the symbol for physical form and content, thus obtained, of duration, the paper then separates the general mathematical symbol for form alone and, using the symbol, arrives at the structure, nature, and generation (creation) of force.

OA12. Simple, Empirical Mass Spectrum of Fundamental Particles. LEO BANET, *Naval Material Laboratory* (introduced by H. Korbel).—There are two series (π,μ) which express the empirical mass values of fundamental particles:

$$m_I = 276n = n\sum_{i=1}^{8} 2^{(x)}, \quad m_{II} = \tfrac{3}{4}S_n\sum_{i=1}^{8} 2^{(x)}$$

$$(n=1,2,3\cdots), \quad (S_n=(1+2+\cdots n)^2), \quad (m_e=1)$$

where $x=2^i$.

Replacing the mass factor 276 by 272 for P and α, the only stable particles of this group, one obtains masses 276, 552, 828, 1104, 1380 and 207, 1836, 7344, in good agreement with observed values; they are particularly close where accurate measurements are available. Two additional masses, obtained by simple combinations of the values listed (2×1104 and $2(276+207)$) also show good agreement with observed values. Another mass obtained from a similar combination, gives 1242 which approximates a recently reported particle. The accuracy of all calculated values can be determined as soon as more accurate mass values are available. A relationship between the fine structure constant and the mass spectrum seems to be present.[1] The reason for the presence of the five smallest integers in the above series is thought to be connected with the geometry of the particle configuration.

[1] Y. Nambu, Progr. Theoret. Phys. (Japan), **17**, 595 (1952). The author assumes the sole responsibility for the above statements.

FRIDAY AFTERNOON AT 2:00

Manhattan Center, Promenade Ballroom

(R. T. BIRGE AND M. W. WHITE, presiding)

Joint Ceremonial Session of the APS and the AAPT

Retiring Presidential Address of the American Physical Society

P1. Pi-Mesons and Nucleons. H. A. BETHE, *Cornell University.*

Presentation of the Oersted Medal of the AAPT

Response of the Oersted Medallist

P2. Physics Is an Art. V. E. EATON, *Wesleyan University.*

Thirteenth Richtmyer Memorial Lecture of the AAPT

P3. On the Development of the Compound-Nucleus Model. E. P. WIGNER, *Princeton University.*

FRIDAY EVENING AT 7:00

Grand Ballroom, Hotel New Yorker

(H. A. BETHE AND M. W. WHITE, presiding)

Banquet of the American Physical Society and the AAPT

After-dinner speakers: H. D. Smyth and G. E. Bell.

Presentation of the third Oliver E. Buckley Solid-State Physics Prize to LeRoy Apker.

SATURDAY MORNING AT 9:30

Manhattan Center, Masonic Room

(W. C. DUNLAP, presiding)

Semiconductors, I

Q1. Short-Time Polarization in Thorium Oxide.* W. E. DANFORTH, *Bartol Research Foundation.*—When a continuous current of several microamperes per square centimeter is passed through a single crystal of oxygen-poor thorium oxide in vacuum, the potential difference across the crystal rises abruptly at first and then continues to increase in time. Observations between 900°C and 1300°C show that, immediately after the initial rise, the rate of rise of polarization is so rapid as to require oscillographic examination. The time required for final equilibrium to be established is, however, several hours. Measurements of the initial rise have been made as a function of temperature. Values of resistivity vary from 5700 ohm-cm at 900°C to 400 ohm-cm at 1280°C. The plot of $\log\sigma$ *vs* $1/T$ is linear and yields an activation energy (u) of 2.2 ev assuming the form $\log\sigma = u/2kT$. Ultraviolet absorption spectra of low-oxygen thoria show a maximum at 3.0 ev. The observed conductivities result from the motion of ions as well as electrons. If, as appears probable, the electronic conductivity predominates, the activation energy and the absorption peak may be related to the same band of donor centers.

*Assisted by the U. S. Navy, Bureau of Ships, and by the Office of Ordnance Research.

Q2. Lattice Defects in Silicon. SUMNER MAYBURG, *Sylvania Electric Products, Inc.*—Heat treatment studies on silicon near the melting point have produced no *reversible* changes in room temperature resistivity which can be ascribed to an equilibrium solubility of vacancies or interstitials in the silicon. Certain *irreversible* changes in room temperature resistivity produced by the heat treatment can be explained by assuming that interstitial silicon is introduced into the crystal during the growing process and can be diffused out of the crystal only by heating the specimen for long periods of time. The presence of frozen-in interstitials and the lack of Frenkel defects in silicon is correlated with the lack of frozen-in interstitials and the presence of Frenkel defects[1] in germanium. This correlation arises because the time for the diffusion of a non-

equilibrium concentration of interstitials out of a crystal which has no Frenkel defects is to the time needed when an appreciable equilibrium number of Frenkel defects is present as π^2a^2/L^2f where a is the average jump distance for an interstitial, L is the smallest crystal dimension, and f is the ratio of Frenkel defects to the number of atoms in the crystal. For germanium, the extra interstitials can diffuse out 10^6 times faster than indicated by the normal diffusion time.

[1] S. Mayburg, Phys. Rev. 95, 38 (1954).

Q3. Theory of the Energy Levels of Donor Electrons in Silicon.* W. KOHN, *Department of Physics, Carnegie Institute of Technology* AND J. M. LUTTINGER, *University of Michigan.*—Conduction electrons in Si are described by two different effective mass values.[1] We have obtained approximate solutions of the resulting "effective mass" Schroedinger equation for a number of low-lying states. The solutions could be checked in the limits where the mass ratio is 1 and ∞, respectively. We have also ascertained those linear combinations of degenerate solutions which are appropriate to the tetrahedral symmetry about the donor atom. Oscillator strengths for a number of optical transitions from the ground state have been estimated. Finally, empirical information about ground-state energies and hyperfine structure of electrons in donor states was used to estimate the deviations from the effective mass theory. For some states these deviations should be small and correlations between a number of absorption lines, associated with different impurity atoms, are predicted.

* This work was begun while the authors were summer visitors at the Bell Telephone Laboratories.
[1] Dexter, Lax, Kip, and Dresselhaus, Phys. Rev. 96, 222 (1954).

Q4. Impurity Band Conduction in Germanium and Silicon. E. M. CONWELL, *Sylvania Electric Products, Inc.*—Germanium and silicon samples of high impurity content are characterized by maxima in the curves of Hall constant R *vs* temperature T. This has been attributed by Hung[1] to conduction in impurity states. In the present study it is also observed for highly impure samples that: (1) In the degenerate region, characterized by R and ζ independent of temperature, the mobility increases with impurity concentration; (2) Before the onset of degeneracy the slope of mobility *vs* T may be much steeper than can be accounted for by the known scattering processes. These features are also explainable on the basis of conduction in impurity states. Estimates are made of the lowest concentrations for which overlapping of impurities should be adequate to give impurity band conduction. In the case of n-type germanium this estimate is considerably higher than the lowest concentration for which the effect was reported by Hung and Gliessman.[2]

[1] C. S. Hung, Phys. Rev. 79, 727 (1950).
[2] C. S. Hung and J. R. Gliessman, Phys. Rev. 79, 726 (1950).

Q5. Optical and Impact Recombination in Impurity Photoconductivity in Germanium and Silicon. N. SCLAR AND E. BURSTEIN, *United States Naval Research Laboratory.*—The impact (three body) recombination and optical recombination coefficients have been calculated for hydrogen-like impurity centers in extrinsic germanium and silicon. These coefficients have been compared with the phonon recombination coefficient calculated by Gummel and Lax[1] for a similar model. For the temperature range of interest, it is found that the optical coefficient is smaller than the phonon coefficient by a factor of approximately 10^3 and 10^4 in germanium and silicon, respectively. The impact recombination coefficient, however, may be comparable with the phonon coefficient at 4.2°K in the presence of background radiation and definitely exceeds it above certain temperatures even in the dark. These temperatures are approximately 6°K and 30°K for germanium and silicon. Under these conditions, the time constant for impurity photoconductivity is determined by the impact recombination coefficient.

[1] Gummel and Lax, Phys. Rev. (to be published).

Q6. Germanium Surface Conductivity and the Effects of Water Vapor. EDWARD N. CLARKE, *Sylvania Electric Products, Inc.*—It has recently been shown[1] that the effect of water vapor on a freshly etched germanium surface is to produce ionic conduction in a thin surface film of water. This conductance is much smaller than the effect usually associated with water vapor on germanium. It has also been suggested[2] that a surface oxide is required for the much larger "channel" effect of water. The results to be presented show that the surface oxide can be altered in such a way as to reduce greatly the effect of water vapor on surface conductivity. Evidence will be presented for the interpretation that (1) the large "channel" effect of water vapor is to be associated with the presence on the surface of the water soluble form of GeO_2 (amorphous or hexagonal), and (2) that if the water soluble form of GeO_2 is converted to the insoluble form (tetragonal) the "channel" effect is much reduced.

[1] J. T. Law, Proc. Inst. Radio Engrs. 42, 1367 (1954).
[2] A. L. McWhorter and R. H. Kingston, Proc. Inst. Radio Engrs. 42, 1376 (1954).

Q7. Ultraviolet Light Induced Surface Channel and Carrier Lifetime Effects in Germanium. H. CHRISTENSEN, *Bell Telephone Laboratories.*—Surface conduction channels[1] and minority carrier lifetime effects have been produced by ultraviolet irradiation of a reverse biased $n-p$ junction bar of germanium in suitable gaseous ambients. These effects have been studied by the chopped light spot method.[2] A channel forms on the p-type conductivity side in a vacuum of 10^{-4} mm when the bar is irradiated with 2537-angstrom mercury light. This channel formation is ascribed to excitation of surface atoms which tend to act as electron donors when the reverse bias field is applied. A channel on the n-type conductivity side forms when the gaseous ambient is a mixture of mercury vapor at about 0.001 mm and N_2 at atmospheric pressure and the surface is irradiated by 2537-angstrom light. This channel is ascribed to the formation of metastable $Hg(^3P_0)$ atoms at the surface which tend to act as electron acceptors when the reverse bias field is applied. When the uv light is incident upon the ambient gas mixture and shielded from the bar, a drastic increase of surface recombination rate is noted.

[1] W. L. Brown, Phys. Rev. 91, 518 (1953).
[2] H. Christensen, Phys. Rev. 96, 827(A) (1954).

Q8. Electrical Breakdown in Germanium at Low Temperatures.* F. J. DARNELL AND S. A. FRIEDBERG, *Carnegie Institute of Technology.*—Electrical breakdown[1–4] has been studied in single crystal and polycrystalline germanium of varying impurity concentration (n and p type) between 0.15°K and 20°K by a dc method. Down to 4°K, the values of the critical electric field required for breakdown, E_c, agree with those already reported. At the lowest temperature, E_c is relatively independent of temperature. Hall coefficients have been measured with specimens in the prebreakdown and breakdown conditions. The carrier concentration is observed to increase upon breakdown in roughly the same ratio as the current density, as expected for carrier multiplication by impact ionization.[3,4] A small mobility change could account for the discrepancy in these ratios. The transverse magnetic field is observed to suppress breakdown and from the ratio $E_c \times (H=H)/E_c(H=O)$ reasonable relaxation times may be estimated.

* Supported in part by the Office of Naval Research and the National Science Foundation.
[1] Estermann, Foner, and Zimmerman, Phys. Rev. 75, 1631 (1949).
[2] A. W. Gerritsan, Physica 15, 427 (1949).
[3] Sclar, Burstein, Turner, and Davisson, Phys. Rev. 91, 215 (1953); 92, 858 (1953).
[4] Ryder, Ross, and Kleinman, Phys. Rev. 95, 1342 (1954).

Q9. Effect of Ion-Bombardment Cleaning of Germanium on Point Contact Rectification.* R. B. ALLEN AND H. E. FARNSWORTH, *Brown University.*—The apparatus, described previously,[1] allows the cleaning of contact surfaces by vacuum techniques and measurement *in vacuo* of the diode characteristics of a tungsten and a columbium cat whisker against the same crystal of germanium. Prolonged vacuum heating of the germanium at 800°C followed by annealing yields a slight difference in activation potential between the tungsten-germanium diode and the columbium-germanium diode. The activation potential is computed from the temperature dependence of the low level diode resistance.[2] Ion bombardment is now being used to clean the germanium surface.[3] Preliminary results indicate that ion bombardment lowers both the forward and reverse current for low applied potentials. Subsequent annealing restores the forward characteristic to a greater extent than the reverse characteristic. Hence, the net result of ion bombardment, followed by annealing, is an improvement of the rectification ratio.

* Supported by the International Business Machines Corporation.
[1] R. B. Allen and H. E. Farnsworth, New England Section, Am. Phys. Soc. (October, 1954).
[2] W. E. Meyerhof, Phys. Rev. **71**, 727 (1947).
[3] Farnsworth, Schlier, and Burger, Bull. Am. Phys. Soc. **29**, No. 7, 35 (1954).

Q10. Forward Characteristic of a Point Contact Rectifier.* KURT LEHOVEC, ALMA MARCUS, AND KURT SCHOENI, *Sprague Electric Company.*—When a forward current flows through a rectifier, formed by a semiconductor and a metal point contact, a large number of minority carriers are injected into the semiconductor. The concentration of injected minority carriers decreases with the distance from the metal semiconductor boundary (1) because of spreading of the current, and (2) because of the finite lifetime of the injected minority carriers. The current-voltage characteristic in the forward direction has been calculated, neglecting the effects of recombination. The calculations are an extension of those of Banbury[1] to cases where the injection factor (ratio of minority carrier current to total current) differs from unity. The dependence of the injection factor on current magnitude has been investigated. For relatively large currents, the injection factor approaches the value $(1+b)^{-1}$, where b is the ratio of majority-to-minority carrier mobility. This may be one of the factors causing the observed decrease in current amplification factor in point contact transistors at high emitter currents.

* Work supported by contract with the U. S. Army Signal Corps.
[1] P. C. Banbury, Proc. Phys. Soc. (London) **B66**, 833 (1953).

Q11. Adsorption of Hydrogen and Oxygen on Germanium.* R. M. BURGER, H. E. FARNSWORTH, AND R. E. SCHLIER, *Brown University.*—Adsorption of hydrogen and oxygen has been observed on the (100) face of a Ge crystal using the low-energy (below 250 ev) electron diffraction technique. The crystal was outgassed up to 750°C by prolonged heating in a high vacuum and the surface was cleaned by argon ion bombardment.[1] The diffraction pattern obtained in the two principal azimuths after annealing the surface was observed before and after exposure to hydrogen and oxygen at pressures up to 1 mm. Where both even and odd order diffraction beams were observed at about the same wavelength, the intensity of the odd surface order beams decreased relative to the intensity of the even order beams in both azimuths after adsorption of either gas at the lower pressures. This indicates that both gases adsorb interstitially in the surface plane of atoms of Ge along the (001) face diagonals. At the higher pressures the diffraction pattern indicates the formation of an amorphous layer of gas on the surface, for both gases. The diffraction pattern from the Ge lattice was present after exposure to oxygen and hydrogen at the above maximum pressures. However, the intensity of the pattern after exposure to oxygen was less than that after exposure to hydrogen.

* Assisted by a Joint Service's Contract with the Massachusetts Institute of Technology, and a subcontract with Brown University.
[1] Farnsworth, Schlier, and Burger, Bull. Am. Phys. Soc. **29**, No. 7, 35 (1954).

Q12. Adsorption of Oxygen and Nitrogen by Titanium.* T. H. GEORGE, H. E. FARNSWORTH, AND R. E. SCHLIER, *Brown University.*—Adsorption of oxygen and nitrogen on the (0001) face of a Ti single crystal has been measured by the low-energy (below 250 ev) electron diffraction technique. The crystal was outgassed for many hours at 750°C and then cleaned by argon ion bombardment.[1] After annealing the diffraction pattern of the Ti structure was observed. Adsorption was allowed to take place in ten-minute intervals at several pressures. The surface was cleaned immediately preceding each exposure. Oxygen at 2×10^{-8} mm Hg and nitrogen at 10^{-5} mm Hg showed no observable adsorption. Oxygen was adsorbed at 5×10^{-7} mm Hg, and nitrogen at 10^{-2} mm Hg. Subsequent exposures at pressures of 10^{-5} mm Hg for oxygen and 10^{-1} mm Hg for nitrogen produced no appreciable change. Both gases are adsorbed in a monolayer having hexagonal structure with the same spacing as that of a (0001) Ti plane. However, the distances between the Ti surface and the adsorbed monolayers are not the same, and also differ from the distance between two adjacent (0001) Ti planes.

* Assisted by Office of Ordnance Research, U. S. Army.
[1] Schlier, Farnsworth, and George, Bull. Am. Phys. Soc. **29**, No. 7, 35 (1954).

Q13. Study of Electrical Characteristics of Grain Boundaries. H. F. MATARE, H. KEDESDY, A. MACDONALD, AND A. PETERSEN, *Signal Corps Engineering Laboratory.*—The different forms of crystal imperfections of the "grain-boundary type" give rise to interesting electrical properties. Three-probe measurements have been started on Ge and Si crystals in coordination with x-ray diffraction studies. Electrical and structural measurements were made on boundaries of polycrystalline material and on materials obtained by the double-seed method.* While ideal twinning seems to have no bearing on the fundamental electronic constant, disturbed interfaces with locked lattice points in the boundary zone have specific characteristics (gate effect in three-probe measurements). While in one case the boundary stress field might set as potential-energy source with a high trap density and corresponding multiplication effect,[1] another type reveals pentode-like saturation characteristics when the boundary stress field is subject to polarization. Electrical characteristics show correlation between boundary structure and electronic behaivor. Relation to boundary stress field is discussed with respect to lifetime and mobility.

* The authors are indebted to P. H. Keck who put at their disposal purified Si and helped in the preparation of double-seed crystals in a floating-zone apparatus.
[1] H. F. Matare, Z. Naturforsch. 9a, H.7/5 (1954).

Q14. Relationship among Hardness, Energy Gap, and Melting Point of Diamond-Type and Related Structures. G. WOLFF, L. TOMAN, AND J. CLARK, *Signal Corps Engineering Laboratory.*—The Knoop micro-hardness values of the Group IV *B* elements, of SiC, the III–V compounds and of some II–VI compounds follow Goldschmidt's relation $H=\text{const}\,r^{-n}$, where H is the Knoop number, r the interatomic distance, and n is a constant. For the elements and SiC, n is close to 5 and for the III–V compounds, n is about 9. Similar relationships have been found for the melting point and for the optical gap width of these materials. The results will be discussed in terms of the character of the chemical bonds.

SATURDAY MORNING AT 9:30

McAlpin, Green Room

(B. T. MATTHIAS, presiding)

Cryogenics, I

QA1. Magnetic and Thermal Properties of UI_3 at Liquid Helium Temperatures. L. D. ROBERTS AND R. B. MURRAY,* *Oak Ridge National Laboratory.*—Previous measurements[1] of the magnetic susceptibility of UI_3 reveal a susceptibility maximum near 3.2°K of antiferromagnetic character, and a second susceptibility maximum at 1.5°K which is strongly depressed by an applied magnetic field of only 5–10 oersteds. The specific heat of UI_3 has now been measured from 1.2° to 4.2°K. These measurements show a λ-type anomaly of magnitude 10 joules/deg-mole at 2.61°K which is interpreted as arising from the onset of long range antiferromagnetic order. No indication of a specific heat anomaly was observed near 1.5°K. Above 2.61° the specific heat falls rapidly to a value of 4 joules/deg-mole at 3.0°K and remains almost constant to 4.2°K. Intgration of the specific heat shows that only 20 percent of the total spin entropy, assumed to be $R \ln 2$, has been achieved at 2.61°K. Examination of the field dependence of the susceptibility indicates that the susceptibility maximum at 1.5°K is due to a type of ferromagnetism involving about one electron in 10^4. This latter behavior is tentatively interpreted as an antiferromagnetic domain boundary effect.

* Fellow of the Oak Ridge Institute of Nuclear Studies from the University of Tennessee.

[1] Roberts, Lavalle, and Erickson, J. Chem. Phys. **22**, 1145 (1954).

QA2. Magnetic and Thermal Properties of $MnCl_2$ at Liquid Helium Temperatures. R. B. MURRAY* AND L. D. ROBERTS, *Oak Ridge National Laboratory.*—Measurements of the magnetic susceptibility of polycrystalline and single crystal samples of anhydrous $MnCl_2$ have been carried out† from 1.1° to 4.2°K using an ac mutual inductance bridge. The susceptibility was found to be independent of an applied magnetic field up to 500 oersteds throughout this region and displays anomalous behavior near 2°K, suggesting a magnetic ordering transition. In view of the field independence of the susceptibility, this transition is interpreted as one of an antiferromagnetic nature, although both χ_{ab} and χ_c continue to rise slowly with decreasing temperature below the transition region. Specific heat measurements on polycrystalline $MnCl_2$ in the same temperature region reveal *two* well-defined λ-type anomalies of magnitude 12 joules/deg-mole, located at 1.81° and 1.96°K. This behavior is tentatively interpreted as arising first from a transition from the paramagnetic to an antiferromagnetic state at 1.96°K, followed by a re-orientation of the electron spin system to a second type of antiferromagnetism at 1.81°K. This interpretation is suggested by a molecular field calculation, and is consistent with the observed susceptibility behavior.

* Fellow of the Oak Ridge Institute of Nuclear Studies from the University of Tennessee.

† In conjunction with Dr. R. A. Erickson, now at the Ohio State University.

QA3. Thermal Magnetoresistance of Zinc at Liquid Helium Temperatures. P. B. ALERS, *United States Naval Research Laboratory.*—The behavior of the thermal resistance of zinc monocrystals in a magnetic field has been investigated at liquid helium temperatures. In measurements in fields up to 25 kilogauss both the thermal and electric magnetoresistive effects were observed, and the variation of the Lorenz ratio with field has been calculated. From this a crude estimate can be made of the lattice conductivity as a function of field. In addition, small oscillations in the thermal magnetoresistance have been observed which are similar to oscillations in the electric magnetoresistance, and which can be linked to the oscillations of the de Haas-van Alphen effect. In contrast to the behavior of bismuth, both the electric and the thermal oscillations are in phase, indicating that the thermal conduction process is primarily electronic even in fairly large fields, although the number of participating electrons per atom is probably small. In measurements employing fields up to 60 kilogauss the thermal magnetoresistance continues to increase but is strongly dependent on the relative orientations of crystal and field. Saturation is not observed, although for some orientations the slope of the curve of the relative thermal resistance, $\Delta W/W_0$ *vs* $\bar{B}$ decrease with increasing field. The effect of the magnetic field on the thermal resistance is nearly independent of temperature in the range in which data were taken (2.7°K to 3.5°K).

QA4. Pressure Dependence of de Haas-van Alphen Parameters in a Bismuth Crystal at 4.2°K. WILLIAM C. OVERTON, JR., AND TED G. BERLINCOURT, *U. S. Naval Research Laboratory.*—An effect due to hydrostatic pressure on the de Haas-van Alphen parameters, the period β/E_0 and phase, has been observed in a bismuth single crystal at 4.2°K. The pressure dependence was seen by measurement of the Hall coefficient and magnetoresistance in fields up to 12 000 gauss under liquid helium pressures up to 1800 psi. With the magnetic field parallel to a trigonal axis (within about 5°), the Hall voltage probes parallel to a binary axis and the current vector perpendicular to both of these axes a normal (negative sign) Hall coefficient was observed to oscillate with a single period in reciprocal field in agreement with previous work.[1] The observed period, β/E_0, of the oscillations, is in fair agreement with the period of the susceptibility oscillations (de Haas-van Alphen effect) for the corresponding orientation. β/E_0 was found to change from 1.572×10^{-5} gauss^{-1} at 100 psi to 1.593×10^{-5} gauss^{-1} at 1680 psi. This 1.3 percent change in β/E_0 due to pressure is about 8 times the sum of the probable errors involved. The change in the phase and in other field dependent quantities due to pressure will be discussed.

[1] J. M. Reynolds and D. D. Triantos, Bull. Am. Phys. Soc. **29**, No. 5, 11 (1954).

QA5. Hall Effect and Magnetoresistance Oscillations of Antimony Single Crystals in Magnetic Fields at Liquid Helium Temperatures. M. C. STEELE, *United States Naval Research Laboratory.*—Measurements on antimony single crystals in the temperature range 1.5°K–4.2°K and fields up to 25 kilogauss have revealed an oscillatory dependence of both the Hall coefficient and the magnetoresistance upon magnetic field. For both properties the oscillations are periodic in reciprocal field. With the magnetic field parallel to the trigonal axis, while the electric current was parallel to a binary axis, the observed period, β/E_0, was 9.8×10^{-7} gauss^{-1}. This is in good agreement with the period observed in the de Haas-van Alphen effect measurements on antimony[1] for very nearly the same orientation. The amplitude of the oscillating component of the Hall coefficient was 0.6 percent of the mean value ($+2.35\times10^{-2}$ cm^3/coulomb) at 1.55°K and 25 kilogauss. For the same conditions the resistance oscillation amplitude was also about 0.6 percent of its mean value. The oscillations in

both properties were still readily observable at 4.2°K and 25 kilogauss.

[1] D. Shoenberg, Trans. Roy. Soc. (London) **A245**, 1 (1952).

QA6. The Electronic Specific Heat of α-Mn.* G. GUTHRIE, S. A. FRIEDBERG, AND J. E. GOLDMAN, *Carnegie Institute of Technology.*—Previous measurements of the specific heat of Mn[1] show extremely high values for γ, the coefficient of the linear term. These measurements were made at liquid hydrogen temperatures. The importance of this quantity relative to the understanding of the *d* bands in transition metals suggested the desirability of measuring the specific heat at liquid helium temperatures. The calorimetric technique is similar to that previously described.[2] Carbon resistors were used as thermometers and measurements were made between 1.8 and 4.2°K. Two samples of manganese were measured. One was in the form of electrolytic flakes that had been treated to remove contaminant gases.[3] The other was cut from a cast ingot[4] completely in the α phase. The results yield a value for γ of 0.00329 ± 0.00015 cal/mole°K[2] which compares with the previous value of 0.00441. The results for the two different types of manganese metal yield values within experimental error of each other.

* Supported by the U. S. Office of Naval Research.
[1] L. D. Armstrong and H. Grayson-Smith, Can. J. Research **A27**, 9 (1949).
[2] Estermann, Friedberg, and Goldman, Phys. Rev. **87**, 582 (1952).
[3] Kindly provided by Dr. C. G. Shull of Oak Ridge and is the same sample on which he had made neutron diffraction measurements revealing a very feeble antiferromagnetism.
[4] The cast ingot was obtained from Dr. Moore of the National Research Corporation through the kind cooperation of Professor J. G. Daunt.

QA7. Vibration Spectra and Specific Heats of Cubic Metals, Part II. Application to Silver. A. B. BHATIA, *National Research Council of Canada,* AND G. K. Horton, *University of Alberta.*—From the secular equation derived in Part I[1] the frequency spectrum of silver, and hence its specific heat C_v at constant volume as a function of temperature T, is calculated. The calculations are made with two sets of elastic constants, namely with their values at $T=0$°K and at room temperature. The calculated C_v are compared with experimental data and with calculations of Leighton[2] based on a two force-constant model (in contrast to the three appearing in our secular equation) by plotting corresponding effective Debye Θ's against T. Above 5°K, the agreement between present calculations and experiment is more satisfactory than obtained by Leighton. The discrepancy below 5°K is similar to that found in Part I for Na and it is not unlikely that these discrepancies are the result of an inadequate evaluation of the contribution to the observed C_v from the quasi-free electrons in a metal.

[1] Phys. Rev. (to be published).
[2] R. B. Leighton, Revs. Modern Phys. **20**, 165 (1948).

QA8. Electron Transfer Mechanism for Ultrasonic Attenuation in Metals. C. KITTEL, *University of California, Berkeley.*—The measurements by Bömmel[1] of ultrasonic attenuation in lead crystals in the superconducting and normal states are discussed in the light of phonon-electron interactions. Thermal conductivity studies by Hulm suggest that phonon-electron attenuation is turned off in the superconducting state. We suggest that part of the phonon-electron attenuation in the normal state is caused by electron transfer processes in the Brillouin zone. It is likely as suggested by Leigh that there are substantial contributions to the elastic compliance of polyvalent metals from the deformation of the form of the Fermi surface under stress. The deformation compliance s_t is characterized by a relaxation time τ of the same order as the electrical conductivity relaxation time. The energy attenuation coefficient is given by $\alpha=\omega^2\tau v\rho s_t$, for $\omega\tau \ll 1$; here ω is the angular frequency, v the sound velocity, and ρ the density. This expression is not inconsistent with the experimental measurements. A full account has been submitted to *Acta Metallurgica.*

[1] H. E. Bömmel, Phys. Rev. **96**, 220 (1954).

QA9. The Absorption of 10 Mc/sec Sound Pulses by a Superconducting Polycrystalline Tin Rod.* L. MACKINNON,† *Brown University.*—The absorption of 10 Mc/sec sound pulses in a cylindrical polycrystalline tin rod has been studied over the temperature range 1.5−4.2°K by the following method. A constant amplitude pulse was fed into one end of the rod and the magnitude of the envelope of the rectified pulse received at the other end was measured. Relative, not absolute, absorptions were, of course, studied in this way. It was found that the absorption in the range 3.73°K to 4.20°K was considerable but that below 3.73°K it dropped off steadily, the magnitude of the received pulse at 2°K being some fifty times that received above the transition temperature. The significance of this change in absorption is discussed in terms of the "two-fluid" model of superconductivity and the possibility of calculating from the observations the temperature dependence of the ratio of "superconducting" to "normal" electrons is considered.

* Supported by the U. S. Office of Naval Research.
† On leave of absence from Charterhouse, Godalming, Surrey, England.

Invited Paper

QA10. The Surface Tension of Liquid Helium 4 and Liquid Helium 3. K. R. ATKINS, *University of Pennsylvania.* (30 min.)

SATURDAY MORNING AT 9:30

Manhattan Center, Gold Room

(E. M. PURCELL, presiding)

Quadrupole and Magnetic Resonance

R1. Paramagnetic Resonance of Atomic Phosphorus.* H. G. DEHMELT, *Duke University.*—Paramagnetic resonance due to phosphorus atoms in the gaseous state has been observed in the microwave region near 9200 Mc/sec. A spectrometer similar to that described by Beringer and Heald and a proton resonance controlled field near 3300 gauss were employed. The thermal dissociation of the P_4 molecules was achieved by pumping a helium-argon mixture at a pressure of 20 to 40 mm Hg which was charged with P_4 vapor of a partial pressure around 0.01 mm Hg through a high temperature dc arc. The inert gas carrier allowed the maintenance of the arc and prevented diffusion of the P atoms to the walls, where they

would have recombined before reaching the spectrometer cavity. The resonance consisted of a doublet symmetrically spaced around a field corresponding to the free electron g value. The doublet separation was 20.0±0.5 gauss and is easily explained as a magnetic hfs-splitting caused by the P^{31} nucleus. Of the order of 1 percent admixture of the excited $3s3p^24s\ ^4S_{\frac{1}{2}}$ state to the symmetrical $3s^23p^3\ ^4S_{\frac{1}{2}}$ ground state, which itself could not couple to the nucleus, is sufficient to explain a splitting of this magnitude. The width of the lines of about 1 gauss was entirely due to field inhomgeneity. As expected for these S-state atoms no pressure broadening due to the inert gas carrier was observed.

* Supported by the Office of Ordnance Research, U. S. Army.

R2. Nuclear Magnetic Resonance in Semiconductors: GaSb and InSb. J. M. MAYS, R. G. SHULMAN, AND D. W. MCCALL, *Bell Telephone Laboratories.*—Nuclear magnetic resonances have been observed in the semiconductors GaSb and InSb (Ga^{69}, Ga^{71}, Sb^{121}, and Sb^{123} resonances in GaSb and In^{115} and Sb^{121} in InSb). The samples, kindly supplied by Dr. H. J. Hrostowski, were p-type with 10^{17} holes/cc. Line widths and shapes were remarkably resistant to alteration, exhibiting no variation with orientation in single crystals, no change in going from single crystals to powder samples nor in going from liquid nitrogen to room temperature, nor, finally, in going from Ga^{69} to Ga^{71} or Sb^{121} to Sb^{123} in GaSb. Relative intensities show that resonances are split by quadrupole coupling, and saturation behavior varies from isotope to isotope in a way that indicates the quadrupole interaction is also the dominant relaxation mechanism. Widths and shapes of the lines are determined by the internuclear exchange interaction described in the following paper.

R3. Nuclear Magnetic Resonance in Semiconductors: Exchange Broadening and Line Shapes. R. G. SHULMAN, J. M. MAYS, AND D. W. MCCALL, *Bell Telephone Laboratories.*—Ramsey's[1] theory of exchange interaction between valence electrons provides an explanation of the experimental facts presented in the preceding paper. This theory has been used previously[2] to explain multiplet structure observed in liquids but the present work represents the first observation of such effects in non-metallic solids. If, in applying the theory to InSb and GaSb, we consider only nearest neighbor interactions, equal line widths are predicted for different isotopes of the same element in the same compound. The line shapes have been computed as the envelope of hundreds of components and are found to be very nearly Gaussian, in agreement with experiment. The line width ratios $\delta H(\mathrm{Ga})/\delta H(\mathrm{Sb})$ and $\delta H(\mathrm{Sb})/\delta H(\mathrm{In})$ have been calculated from theory alone and are in exact agreement with experiment (values are 1.15 and 1.74, respectively). Second nearest neighbor interactions explain the slight differences in the line widths observed for the isotopic pairs in GaSb. Further discussion of the relation of the electronic structure to resonance widths will be given.

[1] N. F. Ramsey, Phys. Rev. 91, 303 (1953). This interpretation was suggested to us by N. Bloembergen in private conversation.
[2] Gutowsky, McCall, and Slichter, J. Chem. Phys. 21, 279 (1953).

R4. Nuclear Resonance Saturation in Solids.* ALFRED G. REDFIELD,† *Harvard University.*—The real part of the rf nuclear magnetic susceptibility in metallic Cu and Al (at 300°K, 6800 gauss) does not decrease at the same rf level (0.25 gauss) as the imaginary part, but remains roughly constant under conditions of slow passage out to $H_1 \cong 2.0$ gauss, beyond which it decreases. This behavior is in conflict with the predictions of the Bloch equations and the theory of Bloembergen, Purcell, and Pound. The evidently erroneous assumptions in these theories as applied to solids will be discussed. A general theory of magnetic resonance in solids has been developed which is applicable at rf levels greater than the absorption saturation level and is in agreement with experiment. The entire spin Hamiltonian is transformed to a rotating coordinate system, and resulting non-secular time dependent terms are ignored. The spin system is described by a canonical distribution of states with respect to the transformed Hamiltonian. The spin-lattice interaction determines the expectation value of the transformed Hamiltonian and the nuclear magnetization.

* Supported in part by the Office of Naval Research.
† National Science Foundation Postdoctoral Fellow 1953–1954.

R5. Nuclear Magnetic Relaxation of Nonuniform Systems. S. BROERSMA, *Northwestern University.*—The relaxation of a hydrocarbon mixed with copper sulfate crystals as a function of time shows for large crystals the behavior of the pure liquid. For crystals of a size of about 50 microns the liquid gives a relaxation pattern analogous to that of two coaxial samples placed together in the nuclear induction coils. In that case the diffusion distance during the relaxation time is of the order of the distance between the crystals; we have the coexistence of two phases. For smaller cavities the behavior again is more like that of a uniform liquid but of shorter relaxation time; T is determined by a $1/T$ average. The electric charges on (nonmagnetic) ions dissolved in water cause large local increases in the viscosity if not the formation of aggregates. The viscosity coefficient entering into the proton-proton interaction then is in part an inverse viscosity average, weighted by the relative dimensions of the moving parts. The motion of the electric ions, creating a fluctuating magnetic field, provides an additional relaxation mechanism for the water. Theoretically, the increase in the relaxation due to either effect is of the order of the relaxation of pure water. For 20 percent solutions of Na, Mg, and Al salts T_1 is found to be lower by a factor of 1.5 to 4 as compared with pure water.

R6. As^{75} Pure Quadrupole Resonances. P. J. BRAY, *Rensselaer Polytechnic Institute,** AND R. G. BARNES, *University of Delaware.*†—The As^{75} pure quadrupole resonance (first measured in arsenic trioxide[1]) has been detected with superregenerative spectrometers in several trihalides and in the triphenyl. The frequencies for the chloride, bromide, and iodide at 77°K are respectively 78.950, 61.180, and 116.860 Mcps with an accuracy of approximately 20 kcps. A doublet structure with frequencies of 98.900 and 98.500 Mcps at 77°K is shown by the triphenyl. The temperature dependence of the As^{75} resonance in the trihalides is small. Explanations based on the molecular and crystalline structures will be advanced and illustrated with the aid of such similar compounds as antimony trichloride.

* Research supported by a grant from the National Science Foundation.
† Research supported by the Office of Ordnance Research and the Research Corporation.
[1] H. Krüger and U. Meyer-Berkhout, Z. Physik 132, 221 (1952).

R7. Pure Quadrupole Resonances in Sb and Bi Compounds. R. G. BARNES, *University of Delaware,** AND P. J. BRAY, *Rensselaer Polytechnic Institute.*†—The pure quadrupole spectra of Sb^{121} and Sb^{123} have been measured in the triphenyl and trioxide. The triphenyl lines show a doublet structure. At 77°K the six highest frequencies in this compound are 156.200 and 152.471 Mcps, 142.174 and 138.859 Mcps, 95.741 and 92.267 Mcps with an accuracy of approximately 50 kcps. The remaining resonances have also been observed and accurate values will be given. Quadrupole coupling constants and asymmetry parameters as a function of temperature will be given for both compounds and compared with the results for antimony trichloride. Room temperature measurements supplementing the original 83°K data[1] for the latter compound have been made and the results thereof will be presented. Two lines of frequencies 111.320±0.070 and 201.380±0.070 Mcps at 77°K have been found in BII_3. The identification and tem-

perature dependence of these resonances will be discussed on the basis of the known layer structure of this compound.

* Research supported by the Research Corporation and the Office of Ordnance Research.
† Research supported by a grant from the National Science Foundation.
[1] H. G. Dehmelt and H. Krüger, Z. Physik 130, 385 (1951).

R8. Impurity Effects on Nuclear Quadrupole Spectrum of Cl^{35}. S. L. SEGEL AND B. C. LUTZ, *University of Delaware.**—It has been previously reported,[1] that small amounts of para-dibromobenzene added to para-dichlorobenzene greatly affects the nuclear quadrupole resonance line of Cl^{35}. Additional investigations into the effects of other impurities such as para-bromochlorobenzene and para-diiodobenzene have been made. The table shows the decrease in relative line heights of the Cl^{35} quadrupole line as a result of the introduction of these impurities.

Mole % impurity	0.05	0.10	0.40	1.2	2.5
p-brchl	0.88	0.82	0.60	0.40	0.33
p-dibr	0.86	0.75	0.48	0.24	0.15
p-diiodo	0.51	0.45	0.39	0.27	0.20

The integrated intensity of the line remains approximately constant. It should be noted that *p*-dichloro-, *p*-bromochloro-, and para-dibromobenzene have the same crystal structure, monoclinic, and approximately the same lattice constants; whereas, *p*-diiodobenzene has a rhombic crystal structure.

* Work supported by the Office of Ordnance Research and the Research Corporation.
[1] Duchesne and Monfils, Compt. rend. 238, 1801 (1954).

Invited Papers

R9. Theory of the Indirect Nuclear-Exchange Interaction in Metals. M. A. RUDERMAN, *University of California, Berkeley.* (20 min.)

R10. Nuclear Spin Exchange in Solids. N. BLOEMBERGEN, *Harvard University.* (30 min.)

SATURDAY MORNING AT 9:30

McAlpin, Colonial Room

(E. C. POLLARD, presiding)

Reactions of Transmutation and Nuclear Energy Levels, I

RA1. Gamma Rays from Proton Capture in Li^7.* C. P. SWANN, M. A. ROTHMAN, W. C. PORTER, AND C. E. MANDEVILLE, *Bartol Research Foundation.*—Thin targets of metallic lithium have been irradiated by protons supplied by the ONR-Bartol Van de Graaff generator. The excitation function for production of gamma rays of energies greater than ~10 Mev has been determined for 1.5 Mev $\leqslant E_p \leqslant$ 5 Mev. At 2.1 Mev, a broad resonance of half-width 0.4 Mev is superposed upon a slowly rising continuum. At an angle of observation of 90° with the incident beam, the resonance is pronounced, corresponding to a level in Be^8 at 19.1 Mev. Only a portion of the increased yield at 5 Mev over that at 2.5 Mev can be attributed to the use of a fixed discriminator setting inobserving the gamma rays.

* Assisted by the joint program of the Office of Naval Research and the U. S. Atomic Energy Commission.

RA2. Excitation Curve of the Reaction $B^{10}(p,\gamma)C^{11}$.* T. M. HAHN, JR.,† B. D. KERN, AND G. K. FARNEY,‡ *Department of Physics, University of Kentucky, Lexington, Kentucky.*—Protons in the energy range from 0.78- to 1.72-Mev have been used to bombard a thin B^{10}-enriched target and the spectrum of the emitted gamma-rays has been observed as a function of proton energy. The spectra, which were obtained with a scintillation counter and a twenty-channel differential pulse-height analyzer, consist of radiation due to both B^{10} and B^{11}; a graphical analysis of the spectrum at each proton energy determined the contribution of the radiative transition to the ground state of C^{11}. The resulting excitation curve exhibits a broad resonance with its peak at proton energy 1.18±0.04 Mev and with a breadth at half-maximum of 0.57±0.02 Mev. These results are in agreement with those of Day and Huus[1] who find a resonance at 1.21-Mev, but the resonances reported in this energy range by Krone and Seagondollar[2] were not observed.

* Sponsored by the Office of Ordnance Research, U. S. Army.
† Now at Virginia Polytechnic Institute.
‡ Now at Bell Telephone Laboratories.
[1] R. B. Day and T. Huus, Phys. Rev. 95, 1003 (1954).
[2] R. W. Krone and L. W. Seagondollar, Phys. Rev. 92, 935 (1953).

RA3. Angular Distributions of Resolved Neutron Groups from the $B^{11}(d,n)C^{12}$ Reaction.* J. R. RISSER, J. PRICE, AND C. M. CLASS, *The Rice Institute.*—The neutrons from the two highest *Q* groups (13.7 and 9.3 Mev) of the $B^{11}(d,n)C^{12}$ reaction have been resolved with a counter which consists of a thin polyethelene radiator from which recoil protons are detected in coincidence by a gas proportional counter and a NaI scintillator. The coincidence pulse gates a multichannel analyzer which examines the pulse-height distribution produced by the protons in the crystal. The angular distributions with respect to the beam of the two groups were taken at five bombarding energies between 1 and 5 Mev. For some energies, the angular distributions show strong peaking in the forward and backward directions, while at others the distributions are isotropic. These results are compatible with the existence of several broad states of the compound nucleus, but the possibility that part of the structure is due to the stripping reaction is not excluded. An excitation curve taken at 0° to the beam for these groups over the same energy range shows resonances which also suggest compound nucleus formation.

* Supported by the U. S. Atomic Energy Commission.

RA4. The 7.68-Mev Level in C^{12} and Stellar Energy Production. E. E. SALPETER, *Cornell University.*—In some types of red giant stars, found in globular clusters, central temperatures of over 10^8°K are predicted theoretically.[1] The conversion of 3 alpha particles into one C^{12} nucleus takes place in the interior of such stars and affects their structure greatly. The individual steps of this conversion are

$$2\alpha + 0.10 \text{ Mev} \rightarrow Be^8; \quad Be^8 + \alpha + 0.31 \text{ Mev} \rightarrow C^{12*};$$
$$C^{12*} \rightarrow C^{12} + 2\gamma + 7.68 \text{ Mev}.$$

A formula will be presented for the rate of this reaction as a function of temperature and density. The numerical results depend critically on the exact resonance energy and the spin-parity assignment of the "7.68 Mev" level in C^{12}. The experi-

mental information[2] on this level will be discussed and theoretical estimates of its various partial widths given.

[1] M. Schwarzschild and F. Hoyle (private communication).
[2] T. Lauritsen and F. Ajzenberg, Revs. Modern Phys. (to be published).

RA5. Differential Cross Sections for the Scattering of Protons by Carbon as a Function of Incident Proton Energy.* ROBERT PEELLE,† *Princeton University.*—Absolute angular distributions were measured for protons scattered by the carbon contained in hydrocarbon foils. The external proton beam of the Princeton University synchrocyclotron was used covering the range of energy 14 to 19 Mev. The energy resolution of the beam was somewhat better than 0.3 Mev and the angular resolution of the NaI(Tl) scintillation detector was usually about two degrees. The range of the proton beam was measured in aluminum within 3 mg/cm² by a differential range spectrometer. Cross sections for the ground state and the level at 4.43 Mev were measured with about 4 percent accuracy at many angles between 20 and 170 degrees for eleven bombarding energies spaced at intervals of about 0.5 Mev. For three of these beam energies the 7.7 and 9.6 Mev levels were included and the data extended to smaller angles. Accuracy was poorer for the more negative Q values. Cross sections for the scattering of protons on hydrogen were measured at each energy used, and the results are in agreement with published data. The results of these measurements will be discussed.

* This work was supported by the U. S. Atomic Energy Commission and the Higgins Scientific Trust Fund.
† Now at Oak Ridge National Laboratory.

RA6. Inelastic Electron Scattering from Carbon at 188 Mev.* J. H. FREGEAU AND R. HOFSTADTER, *Stanford University.*—The elastic scattering peak in carbon-12 is accompanied by a number of additional peaks corresponding to inelastic scattering of electrons from the excited levels of carbon. Those peaks which have been carefully investigated correspond to energies (A) 4.43 Mev, (B) 7.68 Mev, and (C) 9.70 Mev. The angular distributions of inelastically scattered electrons have been studied in the range 45° to 80°. Experimental comparisons have been made between the inelastic peaks of carbon and the elastic scattering from hydrogen. Using a theoretical cross section for hydrogen the "absolute" cross sections for inelastic scattering can be obtained. For example, at 50° the 4.43-Mev peak has an approximate cross section of 1.3×10^{-30} cm²/sterad. The peak at 7.68-Mev corresponds approximately to 4.3×10^{-31} cm²/sterad, the 9.70-Mev peak to 2.9×10^{-31} cm²/sterad. The angular distributions of the inelastic peaks fall off less violently with increasing angle than the elastic carbon peak. The angular distributions will be presented.

* This research was supported jointly by the U. S. Navy (Office of Naval Research) and the U. S. Atomic Energy Commission, and by the U. S. Air Force (Office of Scientific Research, Air Research and Development Command). It was also aided by a grant from the Research Corporation.

RA7. The $C^{13}(p,\gamma)N^{14}$ Reaction. H. B. WILLARD, J. D. KINGTON, AND J. K. BAIR, *Oak Ridge National Laboratory.*—Thin carbon targets, enriched to 61 percent with C^{13}, were prepared by cracking methyl iodide vapor on platinum. Capture gamma rays produced by proton bombardment were detected with a 3×3 in. NaI crystal located about 9 in. from the target (the latter mounted at 45° with respect to the proton beam). One new resonance at $E_p=3.11$ Mev, width $\Gamma=30$ kev (resolution 5 kev), was observed in extending previous data[1] to the (p,n) threshold 3.236 Mev. This level in N^{14} at 10.43 Mev decays mainly to the ground state, although a small percentage of cascade radiation has been observed. Angular distributions of the 10.43-Mev gamma ray can be fitted to the expansion $\omega(\theta)=1-0.40\pm0.02P_2(\cos\theta)$. These results are consistent with the assumption that this level in N^{14} is formed in a $J=2^-$ state by the capture of d-wave protons, followed by electric dipole radiator to the ground state (1^+). The mixing ratio of channel spin 0 to channel spin 1 is 3 to 2, in agreement with either $j-j$ or Russell-Saunders coupling.[2]

[1] J. D. Seagrave, Phys. Rev. **85**, 197 (1952).
[2] R. F. Christy, Phys. Rev. **89**, 839 (1953).

RA8. Energy Levels in N^{14} by Inelastic α-Scattering. D. W. MILLER, U. C. GUPTA, V. K. RASMUSSEN, AND M. B. SAMPSON,* *Indiana University.*—Previous work[1] on the inelastic scattering of alpha particles by a nitrogen gas target gave excitation energies which agreed with other observers in the region below 7 Mev. The present work was undertaken to investigate discrepancies at higher excitation energies. 22-Mev α particles were scattered by a thin melamine target and inelastic groups were observed at angles of 12.5°, 79°, and 90°. Levels were located in N^{14} at 7.01±0.06, 7.94±0.07, 8.45 ±0.07, and 10.05±0.07 Mev. This observation of new levels in a previously well-explored region may be explained by the higher angular momentum states accessible in this experiment. The widths of the observed peaks are such that close levels would not be separated; in particular, the known levels from 8.6 to 9.17 Mev were not resolved. Previously-reported levels which were not observed are those at 7.4, 7.7, 8.06, and 9.49 Mev. The 8.06 level has previously been assigned isotopic spin $T=1$.[2] Such an assignment is also indicated by the present experiment for the 9.49-Mev level. The status of the 7.4- and 7.7-Mev states is uncertain.

* Supported by the joint program of the U. S. Office of Naval Research and the U. S. Atomic Energy Commission.
[1] Carmichael, Sampson, and Johnson, Phys. Rev. **91**, 473A (1953). Carmichael, Indiana University Ph.D. thesis (1953).
[2] Clegg and Wilkinson, Phil. Mag. **44**, 1269 (1953).

RA9. Radiative Capture of Protons by N^{14}.* S. BASHKIN, R. R. CARLSON, AND E. B. NELSON. *State University of Iowa.*—The 277-kev resonance for production of O^{15} in its 7.61-Mev state was excited by 300-kev proton bombardment of a thick TiN target. A three-crystal pair spectrometer resolved gamma rays of 5.25±0.1 Mev, 6.1±0.1 Mev, and 6.6±0.1 Mev, agreeing with previous work.[1] Relative intensities are 0.25, 1.00, and 0.40, respectively, to within 25 percent. Direct ground state transitions have an intensity less than 5 percent of the 6.1-Mev transitions. The yield of 6.1-Mev gamma radiation is $(3.8\pm1.0)\times10^{-12}$ γ/p by comparison with the known yield of 6.13-Mev gamma rays from $F^{19}(p,\alpha\gamma)O^{16}$. Correcting for energy loss in the target and assuming the above transitions end in the $\frac{1}{2}^-O^{15}$ ground state, the total radiative capture yield in nitrogen is $(0.23\pm0.06)\times10^{-10}\gamma/p$. Duncan and Perry[2] obtained $(0.35\pm0.03)\times10^{-10}$ β^+/p. The intensity ratio of 6.1-Mev radiation to 5.25-Mev radiation, measured with a single crystal spectrometer, was (10±3) percent higher at 0° to the beam than at 90°. The present data require $1_p>0$, in disagreement with the suggestion of Duncan and Perry.[2] A $5/2^-$ assignment to the capture state is consistent with the present data.

* Supported in part by the U. S. Atomic Energy Commission.
[1] Johnson, Robinson, and Moak, Phys. Rev. **85**, 931 (1952).
[2] D. B. Duncan and J. E. Perry, Phys. Rev. **82**, 809 (1951).

RA10. Upper Limit to the Lifetime of a Compound Nucleus. H. G. GRAETZER* AND E. C. POLLARD, *Yale University.*—The reaction $N^{14}+\alpha\rightarrow F^{18}\rightarrow O^{17}+p$ was studied in order to determine directly by experimental means an upper limit on the lifetime of a compound nucleus. In Bohr's compound nucleus model, the lifetime is estimated to be less than 10^{-15} second, which is too short by several orders of magnitude to be measured by electronic coincidence techniques. The proposed method was to study the shape of a particular resonance peak, using the same target nucleus, first in a gaseous state and then in a solid state. Any broadening of the solid state peak will be due to atomic collisions made by the compound nucleus before it decays in flight. Using the analyzed 8-Mev alpha beam from the Yale cyclotron and a highly peaked propor-

tional counter detector, a sharp and reproducible proton peak was observed. Within an experimental error of 30 kev, no broadening due to solid target was observed. From the range-energy relation for the compound nucleus, and the stopping power of the solid target, an upper limit of 5.0×10^{-14} second is reported.

* Supported by Office of Naval Research.

RA11. Energy Levels in F^{17} and Al^{26}.* W. T. DOYLE† AND A. B. ROBBINS.—Energy levels in F^{17} and Al^{26} have been obtained by means of (α,n) reactions on N^{14} and Na^{23}, using a proportional counter telescope and a slow neutron threshold technique. Precision measurements were not possible with these methods because of the low neutron yields available with the cyclotron alpha particles. The Q values for the reaction $N^{14}(\alpha,n)F^{17}$ are -4.8 and -5.3 Mev and for the $Na^{23}(\alpha,n)Al^{26}$ reaction are -5.4, -4.6, -3.6, and -2.9 Mev. Good agreement has been obtained between the two methods.

* Supported in part by the Office of Naval Research.
† National Science Foundation Predoctoral Fellow.

RA12. Energy Levels of Al^{26}.* R. SHERR,† R. W. KAVANAGH, AND W. R. MILLS, *California Institute of Technology.*—The energy levels of Al^{26} have been investigated through observations on the $Mg^{25}(p,\gamma)Al^{26}$ reaction. The ratio of capture cross section to positron yield at various resonances was found to vary over a range of 20, indicating the existence of a state whose lifetime is much longer than that of the 6.7-sec positron emitting state. Energy and coincidence measurements of the capture γ rays were combined with Browne's[1] results on the $T=0$ states to give the following energy levels: ground state, 219, 416, 1052, 1750, 1846, 2064, and 2074 kev. Spin and parity assignments consistent with the observed γ rays are $5+$, $0+$, $3+$, and $1+$ for the first four states. Measurements of the positron spectrum of the 6.7-sec activity with a lens spectrometer gave $E_{max}=3.20\pm0.05$ Mev, in agreement with the value expected for decay from the 219-kev state. The ft value (3120 ± 90) and energy support identification of this state as the lowest $T=1$ state. The assignment of spin 5 to the ground state would account for its apparently long lifetime.

* Supported by the joint program of the Office of Naval Research and the U. S. Atomic Energy Commission.
† Present address: Princeton University, Princeton, New Jersey.
[1] C. P. Browne, Phys. Rev. **95**, 860 (1954).

RA13. (α,p) Reaction Studies. G. F. PIEPER, G. S. STANFORD, AND P. VON HERRMANN, *Yale University.*—Several (α,p) reactions are under investigation using the 8.1-Mev alpha-particle beam of the Yale cyclotron. Protons are detected in a thin NaI crystal and the resulting pulse amplitudes are analyzed in the Yale 40-channel analyzer. The $Al^{27}(\alpha,p)Si^{30}$ reaction is used as a standard for calibration purposes; the ground-state Q is known from the masses and the level values are accurately known from the work of Van Patter and Buechner* on $Si^{29}(d,p)Si.^{30}$ The following preliminary data has been obtained: (1) $P^{31}(\alpha,p)S^{34}$,—ground-state Q value $+0.5$ Mev, a definite level at 2.1 Mev, and some evidence for levels at 0.7, 3.0, and 3.6 Mev. (2) $S^{33}(\alpha,p)Cl^{35}$, —ground-state Q value -2.3 Mev, a definite level at 1.1 Mev, and some evidence for levels at 0.7 and 1.7 Mev. (3) $B^{10}(\alpha,p)C^{13}$ —Q values of $+0.1$ Mev, -0.5 Mev, and -1.4 Mev appear to correspond to well-known levels in C^{13}. The ground-state Q value of 3.8 Mev so far obtained may correspond to an unresolved overlap of the true ground-state group and a group from the questioned level at 0.7 Mev in C^{13}.

* D. M. Van Patter and W. W. Beuchner, Phys. Rev. **87**, 51 (1952).

RA14. Neutrons from the Proton Bombardment of P^{31}.* A. RUBIN AND F. AJZENBERG, *Boston University*, AND J. B. REYNOLDS, *Princeton University.*—A phosphorus target, 100 kev thick, has been bombarded with 17.5-Mev protons from the Princeton cyclotron. The resultant neutrons have been studied by means of Ilford C-2 emulsions, 400 microns thick, placed at five angles to the incident proton beam and 4.5 inches from the target. In this experiment only long tracks, corresponding to low states of P^{31}, have been measured. Preliminary measurements at 30, 90, and 150 degrees (1963 tracks) indicate a ground-state Q value of -6.03 ± 0.2 Mev which corresponds to a mass defect for S^{31} of -10.07 ± 0.2 Mev. This result is in good agreement with the value adopted by Endt and Kluyver.[1] Neutron groups have also been observed corresponding to excited state(s) of S^{31} at 1.13 ± 0.2, 2.23 ± 0.15, 3.29 ± 0.15, 4.60 ± 0.15, and 6.20 ± 0.2 Mev above the ground state. Neutrons from the ground-state group were found to be peaked in the forward direction.

* This work has been supported in part by the U. S. Air Force through the Office of Scientific Research and in part by the Atomic Energy Commission.
[1] Endt and Kluyver, Revs. Modern Phys. **26**, 95 (1954).

SATURDAY MORNING AT 9:30

New Yorker, Panel Room

(C. S. WU, presiding)

Beta and Gamma Emitters II; Angular Correlation

S1. Evidence for a Mixed M3+E4 Isomeric Transition. JOHN W. MIHELICH* AND M. GOLDHABER, *Brookhaven National Laboratory.*†—An improved determination of the L subshell conversion ratios of the 74.2 kev isomeric transition in Os^{191m} (14 hr) leads to $L_I:L_{II}:L_{III}=55\pm7:16\pm4:100$. This result, taken together with recently available theoretical conversion coefficients by Rose, Swift, and Goertzel,[1] leads to the conclusion that we are dealing here with an M3 transition with a small admixture of an E4 transition. The exact percentage of the admixture depends on a more detailed knowledge of the Z dependence of conversion coefficients than is at present available. Previously[2] this transition was believed to be E3+M4. From the new assignment of the character of the isomeric transition and from the ft value of the β decay of Os^{191} (16 day) to Ir^{191m} (5.6 sec)[3] the most plausible level assignments are: Os^{191} $(9/2-)$ and Os^{191m} $(\frac{3}{2}-)$.

* Now at Notre Dame University.
† Under the auspices of the U. S. Atomic Energy Commission.
[1] Privately circulated tables.
[2] R. D. Hill and J. W. Mihelich, Phys. Rev. **89**, 323 (1953).
[3] Mihelich, McKeown, and Goldhaber, Phys. Rev. **96**, 1450(L) (1954) R. A. Nauman and J. B. Gerhart, Phys. Rev. **96**, 1452(L) (1954).

S2. Iridium-194.† C. E. MANDEVILLE, JAGDISH VARMA,* AND BABULAL SARAF,‡ *Bartol Research Foundation.*—Electromagnetically enriched quantities of Ir^{193} were exposed for time intervals ranging from 0.5 to 2.0 hr on five successive occasions in the Brookhaven pile. The 19-hour Ir^{194} was found to emit gamma rays of energies 0.295, 0.325, 0.635, 0.640,

0.93, 1.14, 1.28, 1.45, 1.58, 1.77, and ~2.00 Mev. By coincidence studies, sequential relationships were established between ten pairs of gamma rays. The first and second excited states of the residual nucleus were located at 325 and 620 kev. The angular correlation function of the 0.295 Mev–0.325 Mev cascade was measured and found to correspond to a $2\rightarrow2\rightarrow0$ distribution, thus giving the spins of the first two excited states of Pt^{194}.

† Assisted by the joint program of the Office of Naval Research and the U. S. Atomic Energy Commission.
* Research Fellow, Bartol; at present at the University of Glasgow, Scotland.
‡ Research Fellow, Bartol; at present at the Nobel Institute of Physics, Stockholm, Sweden.

S3. The Decay of Bi^{207}. N. H. LAZAR AND E. D. KLEMA, *Oak Ridge National Laboratory.*—The gamma rays following electron capture by Bi^{207} have been studied using the 3 in. by 3 in. cylindrical single-crystal NaI spectrometer and by means of coincidence spectroscopy. The intensity of the 0.579, 1.067, and 1.77 Mev gamma rays were determined with an expected error of ~8 percent. No indication of gamma rays reported at 1.46 or 2.45 Mev[1] were found. The proposed decay scheme is confirmed, quantitatively, through the number of coincidences found between the K x-rays and the various gamma rays. From the data, it appears the 2.34 Mev level is excited by L capture only, in agreement with other recent work.[2] There appears to be ~3 percent K capture to the 0.570 Mev level. An angular correlation experiment was performed between the 1.77–0.570 Mev cascade. The possible spins of the 2.34 Mev level based on these results will be discussed.

[1] J. R. Prescott, Proc. Phys. Soc. (London) **A67**, 530 (1954).
[2] D. E. Alburger and A. W. Sunyar, Abstract to the 1954 Berkeley Meeting of the American Physical Society.

S4. The Beta Decay of RaE.* L. LIDOFSKY, N. BENCZER, P. MACKLIN,† AND C. S. WU, *Columbia University.*—A summary of recent investigations made on the genetic chain Ra(D→E→F) will be presented. The main discussion will be on the fitting of the β spectrum in which a measurement, made with a vacuum evaporated source of low surface density, was used. Since the spin of the ground state of RaE has been recently determined as $J=1$, only a $J=1\rightarrow J=0$; (yes) transition and a linear combination of the S and T interactions will be considered. A fitting is possible for $\epsilon_0=3.29\ mc^2$; $i(G_S/G_T)(\int\beta r/\int\beta\sigma xr)=0.22$ and $(\alpha Z/2R)^{-1}(\int\beta\alpha/\int\beta\sigma xr)=1.51$. The sensitivity of the fitting to a variation of these parameters will be illustrated. Finally, the influence of this fitting on the choice of the relative algebraic sign of the S and T interactions in β decay will be discussed.

* This work was partially supported by the U. S. Atomic Energy Commission.
† Now at Miami University, Oxford, Ohio.

S5. Rotational States of Excitation in U^{234}. E. L. CHURCH* AND A. W. SUNYAR, *Argonne National Laboratory and Brookhaven National Laboratory.*—The levels in U^{234} excited by alpha decay of Pu^{238} have been studied by conversion-electron spectroscopy. Transitions of 43.6±0.3 and 100.0±0.4 kev have been observed converting in the L, M, N, and O shells. The relative conversion in the L and M subshells corresponds to that expected for electric-quadrupole transitions.[1] Delayed coincidence experiments indicate the lifetime of the 43.6-kev transition to be $<5\times10^{-10}$ second, corresponding to a gamma transition probability >30 times the single-particle estimate.[2] Alpha energies indicate that these transitions form a cascade leading to the ground state,[3] while the branching ratios favor a 0, 2, 4 spin sequence. The spins, parities, and spacings of the observed levels are characteristic of "rotational" states of excitation,[4] as is the observed enhancement of the ground-state transition probability. The magnitudes of the rotation-vibration parameters, $\hbar^2/2\Im=7.30\pm0.06$ kev and $\hbar\omega_{\beta,\gamma}=1.0\pm0.2$ Mev, are in agreement with independent estimates of these quantities.[4]

* On loan from Frankford Arsenal, Philadelphia, Pennsylvania.
[1] E. L. Church and J. E. Monahan, Phys. Rev. **94**, 762 (1954).
[2] V. F. Weisskopf, Phys. Rev. **83**, 1073 (1951).
[3] F. Asaro and I. Perlman, Phys. Rev. **94**, 381 (1954).
[4] A. Bohr and B. Mottelson, Kgl. Danske Videnskab. Selskab Mat. fys. Medd., **27**, 16 (1953).

S6. Higher Excited States of Even-Even Nuclei. GERTRUDE SCHARFF-GOLDHABER AND JOSEPH WENESER, *Brookhaven National Laboratory.**—Some empirical regularities and their tentative theoretical interpretations are presented. For $60<A<150$ the ratio of the energy of the second excited state, E_2, to the energy of the first excited state, E_1, is about 2.2 with few exceptions. The majority of these second excited states are 2+, the remainder being 4+ or 0+ with few exceptions. Near $A=150$, as A decreases, E_1 increases steeply and there is apparently an abrupt transition from a Bohr-Mottelson rotational level pattern to the one described above. The Kraushaar-Goldhaber empirical rules [(a) weak $2+\rightarrow0+$ crossover, (b) $E2$, $M1$ comparable in the $2+\rightarrow2+$ transition] are extended. From a modified Bohr-Mottelson Hamiltonian with weak to moderate coupling the observed energy ratio follows naturally; the selection rules arise (a) from the unfavored nature of two-phonon transitions and (b) from the speed-up of $E2$ and absence of $M1$ in one-phonon transitions. On this basis a 0+, 2+, 4+ triplet would be expected in the region around $2E_1$. $E2$ matrix elements will be discussed. The extended shell model also yields some of these results (seniority rules).

* Under the auspices of the U. S. Atomic Energy Commission.

S7. Magnetic Moment of the 0.247-Mev Excited State of Cd^{111}.† W. ZOBEL* AND R. M. STEFFEN, *Purdue University.*—Using dilute aqueous solutions of the parent In^{111} the prompt and delayed directional correlation of the 0.173–0.247 Mev gamma-gamma cascade of Cd^{111} has been measured with external magnetic fields up to 8000 gauss applied perpendicularly to the correlation plane. From the observed azimuthal shift of the correlation pattern, owing to the Larmor precession of the Cd^{111} nucleus in its intermediate state, and from the attenuation of the directional correlation in the magnetic field the magnetic moment of the 0.247-Mev Cd^{111} level was determined as $\mu=-(0.78\pm0.03)\mu_0$. The error is mainly due to the error in the lifetime of the nuclear state and due to the uncertainty in the time-dependent quadrupole interaction in the liquid sources.[1] The new value of μ is within the limits of error of the previous determination by the Swiss group ($\mu=-(0.70\pm0.12)\mu_0$) and agrees with recent measurements done by the same group. It shows conclusively, however, that the first excited state of Cd^{111} has a considerably larger magnetic moment than the ground state ($\mu_G=-0.5949\mu_0$). From the extreme single-particle model one would expect that the magnetic moment is that of the odd neutron, i.e., $-1.91\ \mu_0$ both in the ground state and in the excited state.

† Supported in part by the U. S. Atomic Energy Commission.
* Now at Oak Ridge National Laboratory.
[1] P. B. Hemmig and R. M. Steffen, Phys. Rev. **92**, 832 (1953).

S8. Angular Distribution of the Resonance Fluorescence Radiation from the 411-kev Level in Hg^{198}.† FRANZ R. METZGER, *Bartol Research Foundation.*—Using the resonance fluorescence effect obtained by heating a source of Au^{198} to 1125°C, the angular distribution of the resonance radiation from the 411-kev level in Hg^{198} has been measured. The experimental distribution has the form $1+(0.37\pm0.06)P_2(\cos\theta)+(1.07\pm0.08)P_4(\cos\theta)$. It agrees very well with the distribution expected for an excited state of spin 2 and a ground state of spin 0.

† Assisted by the joint program of the Office of Naval Research and the U. S. Atomic Energy Commission.

S9. Attenuation of α-γ Angular Correlation of Am^{241} in Liquid-Film Sources.* S. RABOY, T. B. NOVEY, AND V. E. KROHN, *Argonne National Laboratory.*—The anisotropy, $[W(180°)/W(90°)]-1$, of the delayed coincidences from Am^{241} has been measured in $1N HClO_4$ liquid-film sources[1] as a function of the time delay between the emission of the alpha particle and the 60-kev gamma ray. The results show a time-dependent attenuation consistent with the theory of random fluctuations of the electric quadrupole interaction in liquid media, and indicate $A_2=0.14\pm0.03$ and $\lambda_2=(14\pm3)\times10^6$ sec^{-1} in the theoretical formula,[2,3] $w(\theta,t)=[1+A_2\exp(-\lambda_2 t)P_2(\cos\theta)]\exp(-t/\tau_N)$.

*Work performed under the auspices of the U. S. Atomic Energy Commission.

[1] T. B. Novey, Phys. Rev. **96**, 547 (1954).
[2] A. Abragam and R. V. Pond, Phys. Rev. **92**, 943 (1953).
[3] F. Coester, Phys. Rev. **93**, 1304 (1954).

S10. Gyromagnetic Ratio of 6×10^{-8} sec Np^{237} by Angular-Correlation Techniques.* V. E. KROHN, T. B. NOVEY, AND S. RABOY, *Argonne National Laboratory.*—The gyromagnetic ratio of the 6×10^{-8} sec state of Np^{237} has been obtained from measurement of the Am^{241} α−γ angular-correlation pattern as a function of a magnetic field applied perpendicularly to the plane defined by the detectors and the $HClO_4$ liquid-film sources. The result obtained was $g=+0.8\pm0.2$ nuclear units.

*Work performed under the auspices of the U. S. Atomic Energy Commission.

S11. Angular Correlation in the Decay of Co^{56}.† J. P. HURLEY, S. W. RUDMAN, AND P. S. JASTRAM, *Washington University.*—The angular correlation distribution has been measured for the cascaded 1.25- and 0.84-Mev gamma rays which follow the decay of Co^{56}, by use of a coincidence spectrometer which combines short resolving time with energy selection, and which permits the coincidence rates corresponding to three different angles to be measured concurrently. Besides the 1.25-Mev photon, four other gamma rays, all of higher energy, are known to be in coincidence with the 0.84-Mev branch. Their contribution to the angular correlation is collectively determined by comparing coincidence rates with the discriminator window set alternately on and just above the 1.25-Mev line. Upon subtraction of the competing rates, the net angular correlation is found to be in good agreement with that computed on the basis of spin assignments of 0–2–4 for the ground state, 0.84- and 2.09-Mev levels in Fe^{56}, with both gamma rays quadrupole.

† Supported in part by the joint program of the Office of Naval Research and the Atomic Energy Commission.

S12. Polarization Correlation in the Decay of Co^{56}.† G. T. WOOD* AND P. S. JASTRAM, *Washington University.*—The polarization-direction correlation has been measured for the 1.25–0.84 Mev gamma-ray cascade which follows the decay of Co^{56}, employing Compton scattering from a liquid scintillator for the polarization detector. A sodium iodide crystal was used for the scintillator in the polarization-insensitive channel in order to provide energy resolution. By setting the discriminator in this channel to select the 1.25-Mev photon, and accepting only those pulses in the scattering counter which corresponded in height to approximately 90-degree deflection of the 0.84-Mev quantum, contributions to the prompt coincidence rates due to competing branches in the Co^{56} decay and other modes of counter-to-counter scattering were effectively eliminated. Using the angular correlation coefficients indicated by the results of the preceding paper, we found the polarization of the 0.84-Mev photon to conform, both in magnitude and direction, with electric quadripole radiation, and, accordingly to lead to an assignment of even parity for the first excited state in Fe^{56}. Similar measurements on other gamma rays in the decay scheme are in progress.

† Supported in part by the joint program of the Office of Naval Research and the U. S. Atomic Energy Commission.
* University Fellow in Physics.

SATURDAY MORNING AT 9:30

New Yorker, North Ballroom

(G. T. REYNOLDS, presiding)

Mesons

T1. Electron Spectrum from Muon Decay. H. J. BRAMSON, *Hughes Aircraft Corporation.*—Work is in progress on bringing into consistent form the results of the many experiments to ascertain the decay spectrum of the mu meson. Using the parameter ρ of the Michel theory to characterize the electron spectrum and adopting the recent value of the mu meson mass reported by Birnbaum and Barkas, a statistically "best" value of ρ from experiments based on the range, momentum, and scattering of the electron will be presented.

T2. Pion-Pair Production in a Nuclear Emulsion. HERMAN YAGODA, *National Institutes of Health.*—The tracks of a π^+ and π^- meson are observed to diverge from a common origin without any other associated tracks. Both particles terminate their range within the confines of a single 1500-micron thick emulsion exposed to cosmic radiation in the stratosphere, and exhibit typical $\pi-\mu$ decay and σ-star formation. The energies of the mesons are 18.0 and 18.7 Mev, respectively, and the angle between the tracks is 120°. The Q value of the event, computed as a two-body decay, is 27.9 Mev. This is not consistent with the decay of neutral theta or zeta mesons. The event may have originated from the decay of a neutral tau meson, $\tau^0\rightarrow\pi^0+\pi^+\pi^-$ for which the Q could vary between 0 and 80 Mev. Other possibilities are the materialization of a pion-pair by photon-Coulomb field interaction, or the collision of a high-energy neutron with a surface neutron of one of the emulsion nuclei.

T3. Photoproduction of Neutral Mesons in H and D.* H. H. BINGHAM, J. C. KECK, AND A. V. TOLLESTRUP, *California Institute of Technology.*—The production of neutral mesons by photons on hydrogen and deuterium is being investigated using the technique of counting the decay photons. A low-temperature high-pressure gas target is exposed to bremsstrahlung from the Caltech synchrotron. The decay photons from neutral mesons are detected in a telescope of three liquid scintillation counters of which the first is in anticoincidence and the second and third in coincidence. A 3/16 in. lead converter is placed alternately before or behind the anticoincidence counter; the difference in counting rate is assumed due to neutral particles, primarily photons, converted in the lead. Counts due to low-energy

photons and neutrons are suppressed by placing an aluminum absorber between the second and third counters. The coincidence resolving time is 10^{-8} sec and both accidental counts and deadtime losses are carefully monitored with a view to obtaining precise results. Measurements are being made at laboratory angles of 30°, 73°, and 140° for synchrotron energies of 300, 400, and 500 Mev. Except at 30°, backgrounds run with the target evacuated are less than three percent. A preliminary reduction of the 73° data gives D to H yield ratios of 1.79 ±0.09, 1.80±0.09, 1.70±0.09 at synchrotron energies of 500, 400, and 300 Mev, respectively.

* This work was supported in part by the U. S. Atomic Energy Commission.

T4. Photoproduction of π^+ Mesons from Hydrogen near Threshold.* J. E. Leiss,† S. Penner, and C. S. Robinson, *University of Illinois.*—A preliminary experiment[1] has been repeated using a liquid hydrogen target and improved counter geometry. Mesons produced in hydrogen are stopped in a carbon absorber surrounding the target, and the resulting decay positrons counted. The activation curves obtained have been analyzed for the total cross section at 2-Mev intervals from threshold to 180 Mev. The absolute counting efficiency was calculated using a Monte Carlo method and the Illiac digital computer. The maximum uncertainty in this calculated efficiency is believed less than 10 percent. The total cross section σ_T is well fitted by $\sigma T/4\pi\chi=[(1.60\pm0.1)+(1.20\pm0.56)\eta^2]\times10^{-29}$ cm² where the notation is that of Bernardini and Goldwasser.[2] The 90° center-of-mass cross section[3] is well fitted by $\sigma 90°/\chi=[(1.56\pm0.06)+(1.48\pm0.19)\eta^2]\times10^{-29}$ cm²/sterad. The renormalized symmetric coupling constant g and the coupling constant of the Chew cut-off theory f are determined to be $g^2=11.7\pm0.7$ and $f^2=0.069\pm0.004$. The connection with the s-wave scattering phase shifts will be discussed.

* Supported in part by U. S. Office of Naval Research, U. S. Atomic Energy Commission, and National Science Foundation.
† Now at National Bureau of Standards, Washington, D. C.
[1] C. S. Robinson and J. E. Leiss, Phys. Rev. 95, 638(A) (1954).
[2] G. Bernardini and E. L. Goldwasser, Phys. Rev. 95, 857 (1954).
[3] J. E. Leiss and C. S. Robinson, Phys. Rev. 95, 638(A) (1954).

T5. Negative Pions from Neutron Bombardment of Deuterons. Myron W. Knapp and Wilson M. Powell, *University of California, Berkeley.*—In order to obtain information on the neutron-neutron interaction, a cloud chamber filled with deuterium gas was bombarded with the neutron beam of the Berkeley 184-inch synchrocyclotron. The spectrum[1] of the neutron beam, which is produced by 340-Mev protons on a 2½ inch lithium deuteride target, is peaked at 300 Mev and extends to 340 Mev. The three reactions $d(n,\pi^-p)d$, $d(n,\pi^-pn)p$, and $d(n,\pi^-)\mathrm{He}^3$ were studied. A total of 310 events was examined; the three reactions contributed 208, 80, and 22 events, respectively. Laboratory system angular distributions and energy spectra of the mesons will be presented. This work was performed under the auspices of the United States Atomic Energy Commission.

[1] John De Pangher, Jr., Phys. Rev. 95, 578 (1954).

T6. Elastic Scattering of Pi Mesons from Nuclei. I.* Ross Williams,† Winslow Baker, Aihud Pevsner,‡ and James Rainwater, *Columbia University.*—The elastic scattering of 78±4 Mev π^- and π^+ mesons from copper has been measured between 20° and 170° with an angular resolution varying from 4° to 10°. A multiple system of double and triple coincidences between four scintillation counters was used to reduce background to a low level. These experimental results, as well as results for the angular distribution of the elastic scattering of 80 and 130-Mev mesons by lithium,[1] will be compared with the shapes predicted by various theories.

* Supported by the joint program of the U. S. Atomic Energy Commission and U. S. Office of Naval Research.
† Now at Paul Rosenberg Associates.
‡ Now at Massachusetts Institute of Technology.
[1] Williams, Pevsner, Rainwater, and Lindenbaum, Phys. Rev. 94, 765(A) (1954).

T7. Elastic Scattering of Pi Mesons from Nuclei. II.* W. F. Baker, R. E. Williams,† and J. Rainwater, *Columbia University.*—In order to obtain a quick survey of some of the main features of the elastic (plus near elastic) scattering of ~78-Mev π^+ and π^- mesons for $\theta\geq\sim75°$, the differential scattering cross sections of a number of elements have been measured at a few selected angles. The elements range in Z from 3 to 82 to test the gross dependence on nuclear size. A few different angles were used to see if the dependence of the cross section on A and on the sign of the meson charge varies in a regular or an anomalous manner as the angle of scattering is varied. The results will be presented and their significance discussed.

* Supported by the joint program of the U. S. Atomic Energy Commission and the U. S. Office of Naval Research.
† Now at Paul Rosenberg Associates.

T8. Positive Pion Scattering by Hydrogen at 189 Mev.* U. Kruse, H. L. Anderson, W. C. Davidon, and M. Glicksman, *The University of Chicago.*—Measurements of the angular distribution of positive pions scattered by liquid hydrogen have been carried out at energy 189 Mev. These were for the purpose of making a phase shift analysis carried out to complement the negative pion measurements by Glicksman[1] at 187 Mev. The differential cross sections in millibarns per steradian in the center of mass system were as follows:

Center of mass angle χ (degrees)	Differential cross section (mb/sterad)
40.3	23.3±1.6
75.7	9.0±0.9
106.6	8.9±1.0
133.4	15.7±1.5
157.1	25.6±2.7

Numerical integration of these results gave 195.0±10.8 mb for the total cross section. The same cross section was determined in an independent way by means of a transmission measurement, with the result, 194.1±5.2 mb.

* Research supported by a joint program of the U. S. Office of Naval Research and the U. S. Atomic Energy Commission.
[1] M. Glicksman, Phys. Rev. 95, 1045 (1954).

T9. Absorption of Pions in Carbon and Nitrogen.* P. Ammiraju, M. Rinehart, K. C. Rogers, and L. M. Lederman, *Columbia University.*—Negative pions were moderated and brought to rest in the gas of the Nevis diffusion cloud chamber, filled consecutively with 2 atmos of ethylene (C_2H_4) and 2 atmos of nitrogen. Using residual range *vs* curvature as criteria for distinguishing stopping π^- and μ^- mesons, we find 88±2 percent of the muon stopping in C_2H_4 undergo β decay. Fifty (±20) percent of the muon absorptions lead to charged particle emission. The star prong distribution of the observed pion stars in ethylene and nitrogen are

Light Nucleus \ No. of Prongs	0	1	2	3	4	5
Carbon (386 stars)	11.7	15.0	24.9	38.8	9.1	0.5
Nitrogen (255 stars)	13.3	17.7	18.8	32.9	14.9	2.4

In carbon, the dominant 3-prong reaction is $\pi^-+C^{12}\rightarrow2\alpha+1p+3n$, while the 4-prong stars predominantly follow the reaction: $\pi^-+C^{12}\rightarrow1\alpha+3p+5n$. The 3-prong stars are

analyzed and compared with the theory of Clark and Ruddelsden.[1] Energy distribution of the α particles give evidence for a specific absorption mechanism rather than for a statistical distribution of the meson rest energy. Evidence is obtained for the formation of an intermediate state in the 3-prong reaction: $\pi^- + C^{12} \rightarrow (Be^8)^* + 1p + 3n$; $(Be^8)^* \rightarrow 2\alpha$. Additional details will be presented.

* Supported by the joint program of the U. S. Atomic Energy Commission and U. S. Office of Naval Research.

[1] A. C. Clark and S. N. Ruddelsden, Proc. Phys. Soc. **A44**, 1064 (1951).

SATURDAY MORNING AT 9:30

McAlpin, Red Room

(N. M. KROLL, presiding)

Theoretical Physics, Including S-Matrix, Atomic Theory

TA1. A Variational Principle for the Total Scattering Amplitude. J. MAYO GREENBERG, *Rensselaer Polytechnic Institute.*—There has recently been developed[1] a new variational principle for the total scattering amplitude. By a suitable modification, the formulation divides the scattering amplitude into its real and imaginary parts and, in fact, exhibits the Born approximation as the first approximation to the real part. In those cases where it is important to know the phase of the scattering amplitude as well as its magnitude this is a very convenient separation. The type of trial functions to be used are those involving the difference between the wave function and its asymptotic form. This makes it unanalytically possible, in some cases, to use the soft sphere[2] wave functions to obtain a result which is probably better than the second and perhaps the third Born approximation.

[1] S. I. Rubinow, Phys. Rev. **96**, 218 (1954).
[2] E. W. Montroll and J. M. Greenberg, Phys. Rev. **86**, 889 (1952).

TA2. Variational Expressions for *N*-Channel Collision Parameters. J. L. MCHALE AND R. M. THALER,* *Los Alamos Scientific Laboratory.*—The formulation described earlier[1] to calculate the scattering matrix for two coupled states has been extended to treat schematically the reaction $a+Y \rightarrow b+Z$ with N exit channels including the incident channel. Following Wheeler,[2] we assume that the radial channel functions satisfy a system of N simultaneous integro-differential equations. One set of N independent vectors $\mathbf{u}^i$ satisfying these equations has the asymptotic form: $u_j{}^i \sim F_j\delta_{ij} + X_j{}^i G_j$, where F_j and G_j are the regular and irregular solutions of the homogeneous equation in channel j with $i,j \leq N$. Here $X_j{}^i = k_j{}^{-1} \int_0^\infty dr' F_j(r') \times \int_0^\infty dr'' \sum_1{}^N V_{jk}(r',r'') u_k{}^i(r'')$, where $V_{jk}(r',r'') = V_{kj}{}^*(r'',r')$ is Wheeler's generalized potential[2] coupling channels j and k. In principle V_{jk} is determined by the potentials and internal wave functions. Time reversal or flux conservation show that $X_j{}^i$ is symmetric. The $\frac{1}{2}N(N+1)$ collision parameters $X_j{}^i$ completely characterized the collision. Schwinger-type variational expressions for $X_j{}^i$ are presented which are stationary to first order variations of $u_j{}^i$.

* Work done under the auspices of the U. S. Atomic Energy Commission
[1] J. L. McHale and R. M. Thaler, Bull. Am. Phys. Soc. **29**, 25 (1954), abstract O8.
[2] John A. Wheeler, Phys. Rev. **52**, 1107 (1937).

TA3. *S*-Matrix in Terms of Phenomenological Collision Parameters. R. M. THALER AND J. L. MCHALE,* *Los Alamos Scientific Laboratory.*—Formally, the scattering matrix and the collision parameters discussed in the preceding abstract are easily related. The solution of the collision complex is a linear combination of the N vectors $\mathbf{u}^i$ such that

$$\sum_{i=1}^N \eta_i u_j{}^i \sim \eta_j F_j + G_j \sum_{i=1}^N \eta_i X_j{}^i \equiv \eta_j (F_j + G_j \tan\delta_j), \quad (1)$$

where δ_j is the phase shift in channel j. Diagonalization[1] of the S-matrix requires that all components of the wave-function have the same phase shift δ^μ which implies the eigenvalue problem $\mathbf{X}\eta = \eta \tan\delta^\mu$. The N eigenphase shifts δ^μ are then given by the roots of the secular determinant, $\|X_j{}^i - \delta_{ij} \tan\delta^\mu\| = 0$. Since $X_j{}^i$ is real and symmetric, the roots of the secular determinant are real, and for nondegenerate roots, the mixture parameter eigenvectors are orthogonal, i.e., $\sum_i \eta_j{}^\alpha \eta_j{}^\beta = 0$. Therefore, the components of the N eigenvectors η^μ are the elements, row by row, of the orthogonal matrix which diagonalizes $X_j{}^i$. The eigenphase shifts δ^μ and the matrix of mixture parameters $\eta_j{}^\mu$ thus completely determine the S-matrix.

* Work done under the auspices of the U. S. Atomic Energy Commission.
[1] J. M. Blatt and L. C. Biedenharn, Revs. Modern Phys. **24**, 258 (1952).

TA4. On the Construction of Noncentral Potentials from the *S*-Matrix. ROGER G. NEWTON* AND RES JOST, *Institute for Advanced Study.*—The procedure[1] of obtaining the potential from the knowledge of the bound states and the phase shift or the S-matrix as a function of the energy has been generalized to systems of differential equations. The purpose of this work is the application to certain restricted kinds of noncentral potentials and specifically to that of the tensor force and spin-orbit coupling. It was found that some of the previous procedures, in the scalar case, do not admit of a simple extension to the present case. In particular, the problem of obtaining the value at the origin of the wave function whose asymptotic value at infinity is exp(ikr), from the S-matrix, is significantly more involved than in the one-dimensional case. As a result, not every unitary S-matrix, however well behaved at high energies, leads to a potential with finite first and second absolute moment. The introduction of the centrifugal barrier with its r^{-2} singularity at the origin also leads to difficulties more severe than in the scalar case.

* Frank B. Jewett Fellow.
[1] See Res Jost and Walter Kohn, Kgl. Danske Videnskab. Selskab, Mat.-fys. Medd. **27**, No. 9 (1953) and references therein.

TA5. On the Decomposition of the Generalized Duffin-Kemmer Algebra. K. M. CASE, *University of Michigan.*—The decomposition of the generalized Duffin-Kemmer algebra, defined as the enveloping algebra of n abstract quantities $\beta_1, \beta_2, \ldots \beta_n$ which satisfy the relations

$$\beta_\mu\beta_\lambda\beta_\nu + \beta_\nu\beta_\lambda\beta_\mu = \delta_{\mu\lambda}\beta_\nu + \delta_{\nu\lambda}\beta_\mu,$$

has been given by Kemmer and others.[1] These authors stress the analogy with the Dirac algebra. This connection is shown to lie deeper on the basis of an elementary derivation of the decomposition using only properties of the Dirac algebra. This treatment, which has much in common with the simple decompositions which have been given for $n=4$,[2] shows that all the Kemmer results, for example the occurrence of "twin algebras," are the result of corresponding spinor properties. The formulas for the decomposition are simplified by this approach and permit some useful generalizations. Transformation properties of irreducible constituents may be obtained

by inspection. Some applications to wave equations in higher dimensional spaces are indicated.

[1] N. Kemmer, Proc. Cambridge Phil. Soc. **39**, 189 (1943).
[2] A. Klein, Phys. Rev. **82**, 639 (1951).

TA6. The Nonrelativistic Limit of Spin $k+\frac{1}{2}$ Particle Wave Equations. P. A. MOLDAUER AND K. M. CASE, *University of Michigan.*—The Dirac-Pauli-Fierz theory for half-integral spin particles is investigated in the nonrelativistic limit. Starting from the Rarita-Schwinger[1] formulation of the theory, the wave function $\psi_{\mu_1\mu_2}\ldots_{\mu_k}$ (symmetric) which describes a particle of spin $k+\frac{1}{2}$ is reduced with respect to the three-dimensional rotation group and the superfluous components are eliminated. The Hamiltonian is calculated to order $1/m^2$ and the intrinsic magnetic dipole and electric quadrupole moments are found. In addition the spin-orbit coupling and Darwin type terms are obtained.

[1] Rarita and Schwinger, Phys. Rev. **60**, 61 (1941).

TA7. Joint Probabilities and Transition Probabilities in Differential-Space Quantum Theory. NORBERT WIENER, *Massachusetts Institute of Technology,* AND ARMAND SIEGEL,* *Boston University.*—In our theory of quantum systems[1] the statistical predictions ordinarily obtained from the wave function are obtained from an ensemble of deterministic systems each of which has a sharp value for every observable. The values over this ensemble for two observables corresponding to two noncommuting operators in ordinary quantum mechanics are, necessarily, imperfectly correlated, and it is of interest to find their joint probability distribution. Suppose they correspond to quantum-mechanical operators $\mathbf{R}$ and $\mathbf{S}=\exp(-i\mathbf{K}\lambda)\mathbf{R}\exp(i\mathbf{K}\lambda)$; $\mathbf{K}$ is Hermitian. We have obtained the joint probability to first order in λ, i.e. valid for $\mathbf{S}$ close to $\mathbf{R}$: given a wave function $\psi(x)=\Sigma a_i\varphi_i(x)=\Sigma a_i'\varphi_i'(x)$, $\varphi_i(x)$ and $\varphi_i'(x)$ eigenfunctions of $\mathbf{R}$ and $\mathbf{S}$, respectively. Then for the ensemble corresponding to $\psi(x)$, prob.$\{R=R_i, S=S_j\}=[|a_i|^2|a_j'|^2-|a_j|^2|a_j'|^2]_+$ for $i\neq j$; $[\ldots]_+$ means the positive part of the quantity inside brackets. If $\mathbf{K}$ is the Hamiltonian and λ the time, this expression is $|a_i|^2$ times the probability that a system (of the ensemble corresponding to ψ) having $R=R_i$ at time zero will make a transition after a (small) interval λ to $R=R_j$.

* Work of this author supported by Office of Naval Research.
[1] N. Wiener and A. Siegel, Phys. Rev. **91**, 1551 (1953); also a forthcoming article "The differential-space theory of quantum systems."

TA8. The Determination of the Scattering Potential from the Spectral Weight Function.* I. KAY AND H. E. MOSES, *New York University.*—By generalizing the method of Gelfand and Levitan[1] it is shown that in many cases the potential can be obtained uniquely from the spectral measure function, if we specify the asymptotic behavior in some representation of the eigenstates of the total Hamiltonian H associated with the measure function. In contrast to earlier treatments where one restricts oneself to an unperturbed Hamiltonian H_0 and a representation such that the H_0 is a second derivative operator and the potential is diagonal, the procedure described is quite general: H_0 may have almost any character, and the potential need not be diagonal in the representation in which the asymptotic description of the eigenfunctions is specified. The transformation U which maps the eigenfunctions of H_0 into these of H and U^{-1} are given triangular properties in the specified representation. U and U^{-1} then satisfy a Wiener-Hopf equation which involves the spectral measure function. In many cases the solution for U, U^{-1} can be obtained explicitly in terms of the spectral measure function. The potential can then be obtained from these operators.

* The research reported in this article was done at The Institute of Mathematical Sciences, New York University, and has been made possible through support and sponsorship extended by the U. S. Air Force, Air Force Cambridge Research Center.
[1] I. M. Gelf and B. M. Levitan, Izvest. Akad. Nauk S.S.S.R. Ser. Math. **15**, 309 (1951).

TA9. Vacuum Polarization and Proton-Proton Scattering.* L. L. FOLDY,† *Case Institute of Technology,* AND E. ERIKSEN, *University of Oslo.*—An attempt has been made to detect the presence of effects of vacuum polarization in currently available experimental data on proton-proton scattering. In spite of the smallness of these effects and relatively large errors in the data, it appears that the data substantiate the predicted vacuum polarization effects in the electrostatic interaction of heavy charged particles, if one assumes the nuclear potential has a Yukawa shape. By correcting the available data for these effects, new values are obtained for the zero energy scattering length and effective range of the specifically nuclear interaction between two protons.

* Supported by the National Science Foundation, European Council for Nuclear Research, and Norges Naturvitenskapelige Forskningsrad.
† Fulbright and Guggenheim Fellow during portion of this research.

TA10. A Covariant Formalism Describing the Polarization of Spin One-Half Particles. L. MICHEL, *Institute for Advanced Study,* AND A. S. WIGHTMAN, *Princeton University.*—We denote by $u(p,s)$, the state of a spin $\frac{1}{2}$ particle of four momentum p and mass $m\neq 0$, whose spin is polarized along a space like four pseudo-vector s, such that $s\cdot p=0$, $s^2=-1$. Then the projection operator onto $u(p,s)$ may be written

$$P_{\alpha\beta}(p,s)=[\bar{u}u]^{-1}u_\alpha\bar{u}_\beta=[4m]^{-1}[1-\gamma_5\mathbf{s}][m+\mathbf{p}]$$

(We use Feynman notation.) s_μ is the generalization of the Stokes pseudo-vector and is the expectation value of $\gamma_5\gamma_\mu$. For a mixture, the degree of polarization is $(-s^2)^{\frac{1}{2}}$. For $m=0$, we have

$$P_{\alpha\beta}'=[u^*u]^{-1}u_\alpha u_\beta^*=(4p_0)^{-1}[1-\gamma_5\mathbf{s}(\tau+\xi)]\mathbf{p}\gamma_0$$

where $\mathbf{s}_\tau$ is a transverse polarization vector and ξ is the amplitude for circular polarization. These formulas permit one to make covariant polarization calculations in terms of traces.

TA11. A Problem in Shower Theory—"Approximation A." R. C. O'ROURKE, *Naval Research Laboratory.*—The Bhabha-Heitler method of solving the shower equations in "approximation A" has been applied to the situation in which a beam of photons with a prescribed spectrum is incident upon a thick target. The mathematical aspects of the work are an immediate and direct extension of the classic work of Bhabha Heitler[1] and N. Arley,[2] who treated primary monoenergetic electrons and photons respectively. The contribution of the present work lies perhaps more in the numerical results which have been obtained on the Naval Research Laboratory electronic digital computer. The numerical work completed so far is for the ideal primary spectrum $kN(o,k)$ equals a constant, i.e., the high energy Bremstrahlung shape. The results can be usefully employed in the calculation of photonuclear yields in thick targets.

[1] H. J. Bhabha and W. Heitler, Proc. Roy. Soc. (London) **A159**, 432 (1937).
[2] N. Arley and B. Eriksen, Kgl. Danske Videnskab. Selskab, Mat.-fys. Medd. 17, No. 11 (1940).

TA12. Wave Functions and Transition Probabilities for Light Atoms.* HUSEYIN YILMAZ,† *M.I.T.*—(Introduced by Philip M. Morse).—A new method of taking electronic correlations into account is presented. This method differs from conventional configuration methods in its generality, simplicity, and interpretation. However, due to the particular choice of perturbation series, there are substantial similarities. The computation is based on a function, the S-function, which was tabulated beforehand. This function is a bilinear Laplace transform of the Green's function and has various useful properties. The method is applied to the $(1s^22s^22p^2)$ configuration of C_I, N_{II}, O_{III}, and F_{IV}. A few significant terms are identified which take care of 60–80 percent of the discrepancy between experimental and theoretical values of multiplet separations. The spin-orbit separations and nebular transitions are calculated. With a slight modification of the $2p$ wave

function it is seen that substantial agreement with experiment can be obtained.

* Work supported by the Office of Naval Research.
† Now at Stevens Institute of Technology.

TA13. Theoretical Evaluation of the Binding Energy of HEH.* A. A. EVETT, *Yale University*.—The variational method developed by Coolidge and James for molecular hydrogen has been applied to the helium hydride ion, extending the earlier work of Coulson and Duncanson[1] and of Toh.[2] Several terms not considered previously in the power series expansion of the wave function in elliptical coordinates were found to be very effective in increasing the binding energy. Wave functions with 23 terms are being considered and the results will be presented. A 10-term function gives a binding energy, uncorrected for zero-point energy, of 1.56 ev; this is to be compared with 1.28 ev reported by Toh for a 12-term function. The inclusion of additional terms shifts the equilibrium interatomic separation to values larger than that found by Toh, thereby bringing the potential energy curve more in accord with that obtained by the use of refinement of the electron pair and molecular orbital procedures.[1]

[1] Coulson and Duncanson, Proc. Roy. Soc. (London) **A165**, 104 (1938).
[2] Toh, Proc. Phys. Math. Soc. Japan **22**, 119 (1940).

TA14. Inertial Effects and Dielectric Relaxation. E. P. GROSS, *Syracuse University*.—We study the dielectric response of a dilute solution of polar molecules in nonpolar compressed gases. As the pressure is lowered to several hundred atmospheres, the collision frequency decreases; the dipoles' inertial response causes large deviations from the absorption and dispersion predicted by the Debye equations. We assume collisions are instantaneous and formulate kinetic equations with a variety of collision kernels. One model is a soft impact theory which extends Debye's Brownian motion theory to include inertial effects. Other cases involve strong collisions and partial specular reflection. A common feature is that the Debye shape is found at high pressures. Inertial corrections are important between one and a few hundred atmospheres; they depend on the model. Another common feature is the connection of Debye spectrum with the discrete rotation lines. The collision frequency $1/t$ increases with increasing gas pressure; at low pressures it is proportional to the width of a rotation line. At high pressures when the Debye shape is found, the relaxation time t^* is given by $t^*=1/t(I/kT)$. Here I is the moment of inertia of the dipole, k is Boltzmann's constant, and T is the temperature of the non-polar gas.

SATURDAY MORNING AT 9:30

New York University, Vanderbilt Hall

(G. R. COLLINS, presiding)

Invited Papers on Nuclear Polarization

U1. Experiments on High-Energy Polarized Protons. EMILIO SEGRÈ, *University of California, Berkeley*. (30 min.)

U2. Recent Work with Polarized Protons at Harwell. BASIL ROSE, *Atomic Energy Research Establishment, Harwell, England*. (30 min.)

Invited Papers on Nuclear Instrumentation

U3. Plans of CERN for its Laboratories. C. J. BAKKER, *University of Amsterdam, Holland*. (30 min.)

U4. Beam Extraction of the Liverpool Synchrocyclotron. A. V. CREWE, *University of Liverpool, England*. (30 min.)

U5. Bubble Chambers for Experiments in High-Energy Nuclear Physics. D. A. GLASER, *University of Michigan*. (30 min.)

SATURDAY AFTERNOON AT 2:00

Manhattan Center, Masonic Room

(G. L. PEARSON, presiding)

Semiconductors, II

V1. Relaxation Effects in Field-Induced Surface Conductance.* R. H. KINGSTON AND A. L. MCWHORTER, *M. I. T.*—The modulation of the surface conductance of germanium by an external field[1] has been found by Morrison[2] to exhibit a transient behavior. Upon application of an electric field normal to the surface of a thin single crystal of germanium, the conductance changes abruptly and then relaxes to its original value in a time of the order of 0.1 to 10 seconds. To obtain a more quantitative picture of the surface behavior this effect was studied by measuring the conductance variation with a sinusoidal signal applied to the field electrode. The frequency response, which was constant above a frequency between 100 and 1000 cps, decreased as log$f$ such that the extrapolated response fell to zero at frequencies from 10^{-6} to 10^{-1} cps. This logarithmic behavior was observed over several decades and actual measurements were made down to 10^{-3} cps. This behavior may be explained by postulating traps in or on the surface oxide layer, having relaxation times, τ, such that the number of traps per unit relaxation time is proportional to $1/\tau$.

* The research in this document was supported jointly by the U. S. Army, Navy, and Air Force under contract with the Massachusetts Institute of Technology.
[1] W. Shockley and G. L. Pearson, Phys. Rev. **74**, 232 (1948).
[2] S. R. Morrison, provate communication.

V2. Surface Traps and $1/f$ Noise in Germanium.* A. L. MCWHORTER, *M.I.T.*—The distribution of trapping time

constants found in the preceding paper can also explain $1/f$ noise in germanium filaments. The wide range of time constants, which seem to require that the traps be in the oxide layer, could arise from a distribution of trap energy levels, but not a uniform one as has sometimes been proposed. However, if the traps are filled by tunneling from the germanium, then an approximately uniform distribution of either barrier heights or widths leads to the desired result. Such a variation in barrier widths would naturally result if the traps were homogeneously distributed throughout the oxide layer. On the other hand, if the traps arise from absorbed ions, fluctuations of the oxide thickness over the surface would give the required variation of barrier width. The lack of a strong temperature dependence of $1/f$ noise seems to favor the tunneling hypothesis.

* The research in this document was supported jointly by the U. S. Army, Navy, and Air Force under contract with the Massachusetts Institute of Technology.

V3. Carrier Effective Masses in Germanium.* JAMES M. GOLDEY† AND SANBORN C. BROWN, *M.I.T.*—Current carriers in a medium make a contribution to its dielectric coefficient. An experiment, similar to those of Benedict and Shockley,[1] which utilizes this effect has been performed to determine the effective masses of electrons and holes in germanium[2] by measuring its microwave dielectric coefficient at several temperatures. The dielectric coefficient was determined by measuring the complex transmission coefficient for 24.15 kilomegacycle radiation through a thin slab of germanium. The values obtained for the effective masses were $M^*=(0.09\pm0.05)M_0$ for electrons and $M^*=(0.30\pm0.05)M_0$ for holes. These results are in agreement with those obtained by cyclotron resonance[3] and magnetic susceptibility measurements,[4] but disagree with those of Benedict and Shockley.[1]

* This work has been supported in part by the Signal Corps; the Office of Scientific Research, Air Research and Development Command; and the Office of Naval Research.
† Now at Bell Telephone Laboratories.
[1] T. S. Benedict and W. Shockley, Phys. Rev. 79, 1152 (1953); T. S. Benedict, Phys. Rev. 91, 1565 (1953).
[2] The germanium was kindly supplied by Dr. J. A. Hornbeck of the Bell Telephone Laboratories and Professor J. E. Thomas of the Lincoln Laboratory, M.I.T.
[3] Lax, Zeiger, Dexter, and Rosenblum, Phys. Rev. 93, 1418 (1954); Dexter, Zeiger, and Lax, Phys. Rev. 95, 557 (1954).
[4] J. H. Crawford and D. K. Stevens, Phys. Rev. 94, 1415(A) (1954).

V4. Hall Mobility of Optically Excited Carriers in Germanium. W. W. TYLER AND R. NEWMAN, *General Electric Research Laboratory.*—Hall mobility measurements of optically induced carriers have been made in high-resistivity Au,[1,2] Fe,[2] induced carriers have been made in high-resistivity Au-,[1,2] Fe-,[3] Co-,[3] and Ni-doped[3] Ge crystals in the temperature region from 200°K to 77°K. Preliminary studies yield the following results. In the spectral region of impurity absorption ($h\nu<0.7$ ev) where sensitivity permitted measurement, carriers generated in p-type material (Au-doped sample) were observed to be holes; carriers generated in n-type material (Au-, Fe-doped samples) were observed to be electrons. In the region of intrinsic absorption, although electrons and holes are generated in pairs, Hall mobility measurements indicate that the photoconduction is due primarily to electrons in both n- and p-type high-resistivity samples. This suggests that in the materials studied hole trapping is the important photoconductive process, consistent with the double acceptor model. In contrast, for a high-lifetime, n-type, undoped crystal containing about 2×10^{13} low ionization energy donor atoms per cm^3, results indicated normal mobility for optically excited electrons and holes.

[1] W. C. Dunlap, Jr., Phys. Rev. 91, 1282 (1953).
[2] R. Newman, Phys. Rev. 94, 278 (1954).
[3] W. W. Tyler, R. Newman, and H. H. Woodbury, Phys. Rev. (papers to be published).

V5. Hall Effect in p-Type Germanium. COLMAN GOLDBERG AND R. E. DAVIS, *Westinghouse Research Laboratories.*—The Hall coefficient has been measured for samples of p-type germanium as a function of temperature from 77°K to 310°K and as a function of field from 15 gauss to 3500 gauss. The Hall coefficient decreases with increasing field, R_0 being as much as 30 percent higher than $R_{3000}(R_0=\lim_{H\to0}R_H)$. This difference is important since it is R_0 that must be used for comparing experimental results with low field theory. At 77°K the Hall coefficient "saturates," being constant above about 1500 gauss. At higher temperatures the Hall coefficient does not saturate with the magnetic fields used here. R_0 decreases with decreasing temperature but is less temperature-dependent than R_{3000} so that while $R_{3000}\sigma_0$ has a temperature dependence of approximately $T^{-1.8}$ (in agreement with previously reported results[1]) $R_0\sigma_0$ has a temperature dependence of approximately $T^{-2.0}$. The temperature dependence of the conductivity mobility is found to be approximately $T^{-2.8}$. The value of the ratio $R_0\sigma_0/\mu$ is higher than the ratio μ_H/μ reported by Morin.[2]

[1] P. P. Debye, Phys. Rev. 91, 208 (1953).
[2] F. J. Morin, Phys. Rev. 93, 62 (1954).

V6. Studies of Crystal Growth, and Electrical and Optical Properties of Gray Tin. J. H. BECKER, *National Bureau of Standards.*—Smooth, coherent films of gray tin have been prepared by transforming films of white tin bonded to a substrate material. Increased grain size results from increasing the grain size of the white tin crystals, decreasing the speed of transformation, and choosing combinations of sample thickness and bonding agents. This technique involves some features similar to those reported by Ewald[1] and Groen and Burgers,[2] through initiated independently of them. For an n-type sample (5×10^{16}/cc), investigations at 5°K with light 1–40 μ show a photoresponse corresponding to a forbidden energy gap 0.075 ± 0.005 ev, but no transmission at 78° or 5°K (i.e. $<10^{-4}$ at 10μ and $<10^{-3}$ at 20μ, sample 30μ thick). Hall, magneto Hall, resistivity, and magnetoresistance effects observed on similar samples from 286°K to 2.5°K give a forbidden energy gap at 0°K of 0.085 ± 0.005 ev and mobility of electrons of about 2000, 30 000, and 13 000 cm^2/volt-sec at 273°, 78°, and 5°K, respectively.[1,3]

[1] A. W. Ewald, Phys. Rev. 94, 1428(A) (1954).
[2] L. J. Groen and W. G. Burgers, Koninkl. Nederl. Akad. V. Wetensch. B57, 79 (1954).
[3] G. Busch and E. Mooser, Helv. Phys. Acta 26, 697 (1953); J. T. Kendall, Phil. Mag. 45 (1954).

V7. Optical Absorption in Single Crystals of Ge and Si. W. C. DASH, R. NEWMAN, AND E. A. TAFT, *General Electric Research Laboratory.*—Optical absorption measurements were made on polished single crystals of high-purity silicon and germanium ranging in thickness from 5 mm to less than 1 micron. Absorption constants up to 10^5 cm^{-1} were measured. For silicon, the absorption constant was found to be considerably lower in the range from 1.2 ev to 3.3 ev than is indicated by published data.[1] For germanium, our results differ from evaporated film data[2] ($h\rho>0.8$ ev). In each absorption constant *vs* photon energy curve a marked change in slope occurs. For silicon it occurs at about 1.5 ev (absorption constant is $\sim10^3$ cm^{-1}) and for germanium at about 0.8 ev (absorption constant $\sim5\times10^3$ cm^{-1}). Such a break is consistent with the theoretical analysis of Hall *et al.*[3] Absorption measurements on evaporated films of silicon in sealed tubes were made for comparison with the single-crystal data.

[1] See T. S. Moss, *Photoconductivity in the Elements* (Academic Press, Inc., New York, 1952).
[2] W. H. Brattain and H. B. Briggs, Phys. Rev. 77, 1705 (1949).
[3] Hall, Bardeen and Blatt, Atlantic City Photoconductivity Conference (to be published). See also Hall, Bardeen, and Blatt, Phys. Rev. 95, 559 (1954).

V8. Effect of Pressure on the Electrical Properties of InSb.* DONALD LONG AND PARK H. MILLER, JR., *University of*

Pennsylvania.—The pressure dependence of the resistivity of InSb was measured up to 2000 atmospheres at 24.3°C and 47.3°C. The sample† was intrinsic in the range of interest. The resistivity is an exponential function of pressure and increases by a factor of 2 for 2000 atmospheres at 24.3°C. If it is assumed that this change in resistivity is caused by an increase in energy gap and that the behavior of InSb with pressure approximates that of a classical semiconductor, these measurements lead to a value for the increase in energy gap of about 18×10^{-6} ev/atmos. Preliminary experiments indicate that the Hall constant increases with pressure in a similar manner.

* This work supported by U. S. Navy contract.
† InSb sample was provided by Dr. R. G. Breckenridge of the National Bureau of Standards.

V9. Effect of Pressure on the Absorption Edges of Tellurium. L. J. NEURINGER, *University of Pennsylvania.**—Tellurium has two separate absorption edges[1] depending on the angle between the polarization of the incident radiation and the crystallographic axis. A single crystal of tellurium was placed in a high-pressure chamber equipped with sapphire windows and freon-113 as hydrostatic fluid. The radiation from the monochromator was polarized by means of selenium films mounted at the Brewster angle. For radiation polarized parallel to the C axis of the crystal the energy gap shifts by $\sim-1.9\times10^{-6}$ ev/atmos. Loferski[1] has measured the shift of the absorption edge with temperature and found it to be $\sim-3\times10^{-6}$ ev/°C. The observed pressure shift corresponds to a lattice dilation effect of $\sim2\times10^{-4}$ ev/°C. Consequently the interaction between the electrons and the new phonon spectrum should account for a shift of $\sim-2.3\times10^{-4}$ ev/°C. Preliminary measurements show that for the E vector perpendicular to the C axis the energy gap also decreases to an extent which has not yet been accurately determined.

* Work supported by a U. S. Navy contract.
[1] J. J. Loferski, Phys. Rev. 93, 707 (1954).

V10. Effect of Pressure on the Optical Absorption Edge in Silicon and Germanium.† D. M. WARSCHAUER, *M.I.T.* AND W. PAUL AND H. BROOKS, *Harvard University.*—The effect of pressure on the optical absorption edges of germanium and silicon has been measured in the pressure range 1 to 8000 atmospheres. The result of isoabsorption plots for germanium ($\alpha=10$ to 70 cm^{-1}) is a change of optical energy gap with pressure $=(8.9\pm0.5)\times10^{-12}$ ev dyne^{-1} cm^2, in agreement with the findings of Spitzer *et al.* at lower pressures. However, if an attempt is made to extrapolate from the measured absorption coefficients to find the minimum energy gap, assuming the form of transition probability used by Hall, Bardeen, and Blatt, it is possible to obtain a shift in closer agreement with the conductivity gap shift of 5.5×10^{-12} ev dyne^{-1} cm^2. Although the proper form for the absorption coefficient due to indirect transitions, to which the energy gap and shift with pressure are quite sensitive, is in some doubt, fitting the experimental results to any of several possible forms brings the deduced shift closer to the electrical values than the isoabsorption plots. In silicon, although our value of the gap shift determined from isoabsorption plots (approximately -2×10^{-12} ev dyne^{-1} cm^2) is at present less precise than that for germanium, the energy gap decreases with pressure contrary to the results of Spitzer.

† This research was supported jointly by the U. S. Army, Navy, and Air Force, under contract with the Massachusetts Institute of Technology, and by Harvard University.

V11. The Pressure Dependence of the Resistivity, Hall Effect, and Magnetoresistance in Germanium.* G. B. BENEDEK, *M.I.T.*, AND W. PAUL AND H. BROOKS, *Harvard University.*—Measurements of the electrical resistance, Hall constant, and longitudinal and transverse magnetoresistance have been made at 0°C as a function of pressure in the range 1–10 000 kgs/cm^2 on samples of n- and p-type germanium in each of which the carriers are of one type and their concentration is independent of pressure. In n-type Ge, the increase in pressure to 10 000 kgs/cm^2 at 0°C produces a 4.25 percent increase in the Hall constant and a 7.68 percent increase in the electrical resistivity. The percentage changes in the magnetoresistive coefficients $\Delta\rho/\rho\equiv M$ produced by 10 000 kgs/cm^2 are as follows:

M_{100}, -9.5 percent; $M_{100^{010}}$, -7 percent;
$M_{110^{1\bar{1}0}}$, -7 percent; M_{110}, -12 percent.

No correction for the much smaller dimensional changes has been made for either n or p type. In p-type material it was found that for fields down to 600 gauss fourth-order terms in the magnetic field contribute appreciably to the magnetoresistance, while the Hall constant is independent of the magnitude of the field for fields below $\sim$2000 gauss. A pressure change of 10 000 kgs/cm^2 at 0°C in the p-type material causes a 2.26 percent decrease in the electrical resistivity and a 4.91 percent decrease in the Hall constant. The pressure changes in the magnetoresistive coefficients in p-type Ge have been measured but their interpretation is complicated by the contribution of terms higher than the second order in the magnetic field strength.

* The research in this document was supported jointly by the U. S. Army, Navy and Air Force, under contract with the Massachusetts Institute of Technology, and by Harvard University.

V12. (Abstract withdrawn.)

V13. Electronic States in a Perturbed Periodic Lattice. PAULA FEUER, *Purdue University.*—Solutions of the one-dimensional Schroedinger equation for a periodic potential modified by a perturbing potential are expressed as $\psi(x)=\Sigma\phi(x_k)a(x-x_k)$. $a(x-x_k)$ is a Wannier function localized around the kth atom of the crystal and associated with a particular permitted band; the coefficients ϕ must satisfy a differential equation of infinite order.[1] W, B, K, solutions of the equation for ϕ have now been obtained; in a permitted band

$$\phi(x)=\frac{1}{[v(x)]^{\frac{1}{2}}}\left\{c_1\exp\left[\frac{i}{\hbar}\int p(x)dx\right]+c_2\exp\left[-\frac{i}{\hbar}\int p(x)dx\right]\right\},$$

where $p(x)=p(E-V(x))$ is the local effective momentum and $v(x)$ is the velocity of a wave packet constructed from Bloch waves with effective momenta in the neighborhood of $p(x)$. In the neighboring forbidden bands $\phi(x)$ decreases exponentially with distance from a band edge. Various types of perturbing potentials have been considered and quantum conditions have been derived for impurity states and for states in which the permitted band is crossed.

[1] J. C. Slater, Phys. Rev. 76, 1592 (1949).

V14. An Interpolation Scheme for Energy Bands in Solids.* L. C. ALLEN, *M.I.T.*—The orthogonalized plane wave method is formulated as an interpolation scheme for use in conjunction

with calculations made at symmetry points in the Brillouin zone. The Fourier coefficients of the crystal potential and the matrix components of the Hamiltonian between core functions are treated as parameters to be fitted to other calculations made at symmetry points by such methods as the cellular, orthogonalized plane wave, and augmented plane wave. The interpolation scheme then provides a method for making calculations at a general point in the Brillouin zone. The scheme is most useful for the case of valence and excited states where the wave function on one center overlaps many of its neighbors.

* Supported in part by the Office of Naval Research.

SATURDAY AFTERNOON AT 2:00

New Yorker, Panel Room

(P. KUSCH, presiding)

Molecular-Beam, Optical, Biological Physics

VA1. New Method for Investigating the hfs of a Metastable State.* J. HEBERLE, H. REICH, AND P. KUSCH, *Columbia University.*—An atomic-beam method has been developed for measurement of the hfs of the metastable $2^2S_{\frac{1}{2}}$ state of hydrogen. The Zeeman levels of the $2^2S_{\frac{1}{2}}$ state are classified as $\alpha(m_s=+\frac{1}{2})$ or $\beta(m_s=-\frac{1}{2})$ according to the high-field value of m_s. Molecules of H_2 or D_2 are dissociated in a hot tungsten oven. An 11-ev electron beam excites the atoms to the α and β states in a field of approximately 580 gauss. The β atoms are quenched immediately after formation because their lifetime in such a field is only about 5×10^{-8} sec.[1] The remaining α atoms pass through two successive regions of rf magnetic field of variable frequency where transitions to a β state are induced. The atoms pass on into a second field of 580 gauss where the newly formed β atoms are quenched. The α atoms that remain strike a metal detector plate. Electrons ejected from the detector plate are collected. A resonance is observed as a decrease in detector current.

* Work supported jointly by the Signal Corps, the Office of Naval Research, and the Air Research and Development Command.
[1] Lamb and Retherford, Phys. Rev. **79**, 549 (1950).

VA2. Hyperfine Structure of Metastable Hydrogen.* H. REICH, J. HEBERLE, AND P. KUSCH, *Columbia University.*—The hfs $\Delta\nu(2S)$ of the $2^2S_{\frac{1}{2}}$ state has been measured by the method described in the preceding abstract. The frequency ν_{14} of the transition $F=m_F=1\rightarrow F=m_F=0$ is given by $\Delta\nu+1.40$ Mc sec^{-1} gauss^{-1}; the frequency ν_{24} of the transition $F=1$, $m_F=0\rightarrow F=m_F=0$ is given by $\Delta\nu+0.022\ 2$ Mc sec^{-1} gauss^{-2}. To determine $\Delta\nu(2S)$ both ν_{14} and ν_{24} were measured in a field of 0.19 gauss. The line width $W\approx v/2L$ (v is the average velocity of the atoms) was reduced to 5.5 kc/sec by making the separation L between the two rf region[1] as large as 40 cm. It has been found that $\Delta\nu(2S)_{\text{exp}}=177\ 556.6\pm0.3$ kc/sec. Theoretically[2] $\Delta\nu(2S)$ is related to $\Delta\nu(1S)$ of the ground state by $\Delta\nu(2S)=\Delta\nu(1S)/(8-5\alpha^2)$. From the two existing values[3,4] of $\Delta\nu(1S)$ one obtains $\Delta\nu(2S)_{\text{theoret}}=177\ 556.55\pm0.03$ and $177\ 556.634\pm0.007$ kc/sec, respectively. Additional measurements are being made to investigate possible systematic errors and to improve the accuracy to 3 parts in 10^7.

* Work supported jointly by the Signal Corps, the Office of Naval Research, and the Air Research and Development Command.
[1] N. F. Ramsey, Phys. Rev. **78**, 695 (1950).
[2] G. Breit, Phys. Rev. **35**, 1447 (1930).
[3] A. G. Prodell and P. Kusch, Phys. Rev. **88**, 184 (1952).
[4] J. P. Wittke and R. H. Dicke, Phys. Rev. **96**, 530(L) (1954).

VA3. The Nuclear Spin and h.f.s. Interaction in 3.1-hr Cs^{134m}*. D. A. GILBERT AND VICTOR W. COHEN, *Brookhaven National Laboratory.*—An atomic beam magnetic resonance experiment has been performed on the 3.1-hr isomer of Cs^{134} giving the results $I=8\hbar$ and $\Delta\nu=3684.594\pm0.020$ Mc/sec. The beam was detected by allowing it to deposit for an arbitrary time on a tungsten target which was then removed and its activity counted by a proportional counter. The spin was determined from a study of the $\Delta F=0$ transitions in a range of frequencies from a few Mc/sec to about 150 Mc/sec. The value of $\Delta\nu$ was determined from a study of the $\Delta F=\pm1$ transitions in a magnetic field of about 1 gauss. The nuclear magnetic moment computed from our data is $\mu=1.10\pm0.01$ n.m. with a positive sign.

* Work performed under the auspices of the U. S. Atomic Energy Commission.

VA4. The g Factor of the Electron in the $2S$ State of Hydrogen.*† L. D. WHITE,‡ *Princeton University.*—Measurements have been made of the resonances corresponding to turning the electron over in the $2S$ state of hydrogen. The method is similar to that of Lamb and Retherford[1]—a beam of $2S$ atoms passes through a microwave cavity and is detected by the electrons ejected from a tungsten plate. Atoms with electron spins antiparallel to the magnetic field are removed from the $2S$ state by suitable electric fields. The present preliminary result is $g_e/g_p=658.231\pm0.008$, where g_e is the g factor of the free electron and g_p is the g factor of the proton in a spherical sample of mineral oil (Nujol). About 90 percent of the stated uncertainty is in the amount of correction to be made for the slight shifts in the energy levels caused by the velocity dependent electric field seen by the atoms in moving through the magnetic field. The origin of this uncertainty lies in insufficient knowledge of the velocity distribution. It is expected that further work will decrease this uncertainty.

* Supported by the U. S. Atomic Energy Commission and The Higgins Scientific Trust Fund.
† Dr. R. H. Dicke suggested the problem and acted as general adviser for the research.
‡ U. S. Atomic Energy Commission Predoctoral Fellow 1951–1953.
[1] Lamb and Retherford, Phys. Rev. **79**, 549 (1950) and **81**, 222 (1951).

VA5. Triplet Fine Structure of Helium.* T. H. MAIMAN AND W. E. LAMB, JR., *Stanford University.*—The fine structure of helium levels $1snp(n^3P_J,\ J=0,\ 1,\ 2)$ is being studied by a microwave method. Helium atoms are excited to n^3P_J by electron bombardment and the optical radiation $n^3P_J\rightarrow2^3S_1$ is observed with a photomultiplier tube. The intensity of this radiation changes when radio waves induce transitions between the fine structure levels. Thus, the separation $3^3P_1-3^3P_2$ is found to be 658 ± 1 Mc/sec in contrast to the most recent optical measurements which indicated a separation of 750 ± 300 Mc/sec.

* Research supported by the joint program of the Office of Naval Research and the U. S. Atomic Energy Commission.

VA6. Oxygen Gas Continuous Absorption in the Extreme Ultraviolet. WILLIAM A. RENSE AND R. MERCURE, *University of Colorado.*—Measurements of the absorption of oxygen gas in the wavelength ranges 1300 A to 1700 A and 100 A to 900 A were made by means of a multiplier phototube technique involving the use of a modified grazing-incidence spectrograph as a monochromator. The source for the first range (Schumann-Runge dissociation continuum) was a hydrogen-filled Geissler tube discharged continuously at 600 volts. Twenty-two coefficients were measured in this region with probable errors mostly of about 10 percent or less. An oscillator strength (f-value) of 0.177 was found for the continuum. A Lyman-type capillary (discontinuous discharge at 11 kv) was employed for measurements of twenty-one coefficients in the region 100 A to 900 A where very strong continuous absorption occurs. An f-value of 6.9 was computed. Coefficients beyond 200 A were very small. Maximum continuous absorption occurs at about 590 A where coefficients of about 900 cm^{-1} were obtained. Absorption increases abruptly between 800 A and 700 A .Near 700 A where structure is superimposed on the continuum, coefficients as high as 1080 cm^{-1} were measured.

VA7. Investigation of a Quantitative Phase Contrast Method for Examining Nonhomogeneous Media. G. C. KRUEGER, *University of Maine.*—Of the optical methods generally used in studying the phenomena associated with fluid flow fields, *viz.*, the shadowgraph and schlieren methods and the Mach-Zehnder interferometer,[1] only the interferometer appears to be suitable for quantitative investigation. Minor modifications of these optical systems effectively transforms them into a phase microscope.[2] The final image in a phase microscope may be considered as being formed by light diffracted by the object superposed on a coherent background of undiffracted light. The optical properties of the object can be inferred by varying the phase and amplitude of the coherent background, these being determined by the optical properties of the phase plate. The progress of our investigation will be reported. This investigation has been supported in part by the University of Maine Coe Research Fund and more recently by the National Science Foundation.

[1] N. F. Barnes and S. L. Bellinger, J. Opt. Soc. Am. 35, 497–509 (1945).
[2] F. Zernike, Physica 5, 785–795 (1938); 686–698, 974–986 (1942); Proc. Phys. Soc. (London) 61, 158–164 (1948).

VA8. Electron Effects in Spectral Line Broadening.* HENRY MARGENAU, *Yale University.*—The widths of the lines of atomic hydrogen emitted in the sun are fairly well explained as ionic Stark effects. The broadening by electrons, which are as numerous as the ions, is small because they "behave like waves." We here ask and answer: When do the charged constituents of a plasma take on particle characteristics? The constituents are represented as wave packets whose minimum half width is determined by the energy fluctuations of the thermal ensemble. This half width is shown to be $\lambda\hbar/=(2mkT)^{\frac{1}{2}}$. Particle behavior results when $\lambda \leq a$, a being the linear size of the atoms with which the charge collides. For the solar chromosphere ($kT \approx 1$ ev) this criterion results in a condition upon the mass of the charge: It behaves like a particle when $m > \hbar^2/2a^2kT = 10^{-26}$ g. This is satisfied by H ions, but not by electrons.

* Work supported by the Office of Naval Research.

VA9. Electron Impact Broadening of Spectral Lines of Helium.* BENNETT KIVEL, *Los Alamos Scientific Laboratory.*—Electron broadening has been calculated quantum-mechanically by extending the treatment of Weisskopf and Wigner for the natural width. In accord with the uncertainty principle the width of a spectral line is increased compared to the natural width when electron collisions decrease the lifetime of the initial and final atomic states. Its shape is the same as that of the natural line. Using the Born approximation, the probability of this electron collision effect is found to depend logarithmically on the atomic energy separations between these atomic states and their neighbors. This is to be compared with Holtsmark ion broadening, which is inversely proportional to the same separations. Hence, in a plasma the HeI line $3d \rightarrow 2p$ will be characterized by electron broadening having a Lorentz shape $(\gamma^2+\omega^2)^{-1}$, since there is no near atomic level to cause large Stark shifts. This is probably not so for $4d \rightarrow 2p$ because of the near $4f$ level. In addition to broadening, the theory predicts that the electrons introduce line shifts.

* Part of this work is contained in a dissertation presented for the degree of Doctor of Philosophy in Yale University.

VA10. Line Broadening by Electrons: The Validity of Simple Theories. ROLAND E. MEYEROTT, *The RAND Corporation,* AND HENRY MARGENAU, *Yale University.*—The simple theories of line broadening by electron impact are compared with the detailed computations of Kivel, Bloom, and Margenau, and are found to be in surprisingly good agreement over the range of temperatures and densities of interest in most applications.

VA11. A New Method of Microelectrophoresis. ALEXANDER KOLIN, *University of Chicago.*—Electrophoresis is carried out in a column of nonuniform electrolyte concentration. The speed of the ions is a function of the electrolyte conductivity, being a maximum in the region of minimum conductivity. The mixture of proteins to be separated is introduced so as to form a layer of minimum conductivity. When entering the region of high conductivity, the migrating protein ions, which formed originally a wide belt, are contracted into a narrow line. This line contains a mixture of ions which separate rapidly into several sharp lines containing the different protein components. Combining a pH gradient with the conductivity gradient makes it possible to accomplish the separation within a path length of a few millimeters. The isoelectric points of the proteins lie within the range of the pH variation. Stability against thermal convection is achieved by a sharp density gradient maintained along the protein ion path. Ions other than proteins may also be separated by means of this method.

VA12. Monte Carlo Methods in the Study of Cell Growth. JOSEPH G. HOFFMAN, *Roswell Park Memorial Institute,* AND N. METROPOLIS AND V. GARDINER, *Los Alamos Scientific Laboratories.**—The time of incidence and duration of mitosis in cells of transplantable Dba mouse tumors are assumed to be result of random processes. The shape of the frequency distribution of intermitotic times is determined by the number of random events in a cell that lead to mitosis and whether the events occur serially in time or simultaneously. Models of cellular events and their effect on intermitotic time will be discussed. Monte Carlo calculations on the digital computer (Maniac) were made to study the effect of the distribution of intermitotic times on: distribution of population sizes as a function of time, age distribution in the population, incidence of mitosis, and latent periods in growth of single cells. Results show the distribution of population sizes ir tumors to be sensitive to the intermitotic time distribution. Data on Dba tumor cells grown subcutaneously in Dba mouse and in hen embryo yolk-sac have Poisson incidence of mitosis in the cell population. This is corroborated in the calculations. Subcutaneous growth of Dba has a cell number doubling time of 24 hours and behaves as if 18 random serial events in the cell determined mitosis.

* This work supported by the U. S. Atomic Energy Commission.

SATURDAY AFTERNOON AT 2:00

Manhattan Center, Gold Room

(H. A. BOORSE, presiding)

Invited Paper

W1. The Role of Substrate, Surface-Finish, Film-Height, and Temperature in Helium II Film Transport. BERNARD SMITH, *Columbia University.* (30 min.)

Cryogenics, II

W2. Surface Tension of He^3. D. R. LOVEJOY, *University of Toronto.**—The surface tension of He^3 has been measured by a capillary rise method between 1.08 and 2.32°K. A decrease of more than 50 percent was observed in this range and this supports the ideas on which Atkins' theory, of the surface tension of liquid helium, is based. On the basis of this theory the surface tension has been extrapolated to 0°K, where it has the value 0.154 ± 0.005 erg cm^{-2}. Above 2.3°K it was extrapolated linearly to zero at the critical temperature. The Eötvös constant was calculated to be about 0.8.

* Now at the National Research Council of Canada.

W3. Second Sound Attenuation in Rotating Helium II.* C. T. LANE, R. G. WHEELER, AND C. H. BLAKEWOOD, *Yale University.*—Evidence is presented to show that the attenuation of second sound is increased by imparting to the normal component of the fluid a constant angular rotation about an axis parallel to the direction of sound propagation. Measurements at 1.32°K, using a pulse technique, are reported for various fluid velocities in the range 4 to 33.6 radians per second corresponding to linear fluid velocities from 4.4 to 36 cm/sec. It is found that the relative pulse height (fluid in rotation compared to fluid at rest) is a linear function of the angular velocity of the fluid; the ratio being approximately 0.87 at 4 rad/sec and 0.31 at 33.6 rad/sec. If there exists any effect of rotation on the second sound velocity, it appears to be very small.

* Research assisted by a grant from the National Science Foundation.

W4. Heat Transport and Boundary Layer Resistance in He II below 1°K. HENRY A. FAIRBANK* AND J. WILKS, *Oxford University.*—Our investigation of the thermal conductivity of liquid helium in the magnetic temperature range[1] has been extended to a larger tube diameter of 0.80 mm. The thermal conductivity increases proportionally with tube diameter below 0.6°K. The results are consistent with a heat transport in the liquid due entirely to thermal waves or phonons with sufficiently long mean free paths that boundary scattering alone limits the conductivity. The Kapitza boundary layer heat resistance has been measured from 0.2 to 1°K. For heat flowing across a copper-liquid helium interface the heat flux per unit temperature drop was found to be proportional to T^3.

* On leave during 1954–1955 from Yale University.
[1] H. A. Fairbank and J. Wilks, Phys. Rev. **95**, 277 (1954).

W5. The Dependence of Transfer Rates of the Helium II Film on Film Length.* P. J. FLEMING,† J. H. WERNTZ, JR., AND J. R. DILLINGER, *University of Wisconsin.*—Measurements have been made of the rate at which liquid helium is transferred by the He II film out of Pyrex glass capillaries at a temperature of about 1.5°K. Precision bore capillaries with an inside diameter of about one millimeter were used. At constant H_0 the volume flow rate was found to decrease with increasing H, and at constant H the volume flow rate increased with increasing H_0. H is taken as the distance from the liquid level inside the capillary to the top of the capillary. H_0 is the distance from the top of the capillary to the place at which the helium bath was in contact with the capillary. Values of H and H_0 up to 16 cm were used. The results are discussed in terms of the existing phenomenological theories.[1–3]

* This work was supported in part by the Wisconsin Alumni Research Foundation and in part by the U. S. Atomic Energy Commission.
† Now at Wellesley College.
[1] K. R. Atkins, Proc. Roy. Soc. (London) **203A**, 240 (1950).
[2] T. Kasuya, Progr. Theoret. Phys. **9**, 87 (1953).
[3] J. G. Dash, Phys. Rev. **94**, 1091 (1954).

W6. The "Closed" Fountain Effect and Compressibility of Helium II.* H. FORSTAT AND C. A. REYNOLDS, *University of Connecticut.*—Previously we have reported[1] finding a sudden rise in the height of the liquid level in a closed system of helium II through which a heat current was passing. The major portion of the liquid was in the spaces between tightly packed rouge particles. An average size of the spaces has been determined by flow measurements and, using the measured surface tension of helium, the underpressure necessary to form a bubble of this radius has been calculated. This value is in agreement with the underpressure calculated on the basis of H. London's thermomechanical pressure equation. The calculated underpressure at which the upward break occurs is reproducible when the apparatus is agitated. However, when the apparatus is undisturbed the break occurs at much greater underpressure, sometimes at such great ones that the liquid is calculated to be under negative pressure. In a new apparatus the direction of the heat current has been reversed so that the liquid has been subjected to pressure. The compressibility has been measured and will be compared to the values obtained by other methods.

* Work partially supported by the Research Corporation, the National Science Foundation, and the Office of Naval Research.
[1] C. A. Reynolds, Phys. Rev. **93**, 1118 (1954).

W7. Effect of the Superconducting Transition on the Internal Friction of Tin. BENJAMIN WELBER, *NACA.*—It was recently reported that the attenuation of a 20 Mc pulse in a lead single crystal is decreased by about 40 percent in the transition from the normal to the superconducting state.[1] In the present experiment the change of the mechanical properties of tin during the transition was investigated. For this purpose use was made of a 50-kc composite oscillator[2] consisting of a quartz crystal cemented to a matched polycrystalline specimen of tin. At a temperature of 2.77°K it was observed that the coefficient of internal friction as determined from the electrical impedance of the quartz oscillator increases by 1.5 percent when the superconducting state is destroyed by the application of a magnetic field. In addition, an increase in Young's modulus of the order of one part in 10^5 appears to

occur at the same time. Increasing the magnetic field to several times the critical value produces no further change in the aforementioned properties of the metal.

[1] H. E. Bommel, Phys. Rev. **96**, 220 (1954).
[2] S. L. Quimby, Phys. Rev. **25**, 558 (1925).

W8. Superconducting Winding for Electromagnet.* G. B. YNTEMA, *Cornell University.*—Superconducting niobium wire constitutes the winding of an electromagnet for use in a liquid helium bath. The model built has 4296 turns of 0.002 inch diam unannealed wire carrying 1.8 ampere and produces 7.1 kilogauss in a small gap. The wire remains superconducting while carrying a large current only so long as no segment of it is converted to the normal-conducting state; presumably such a resistive segment, when once started, grows because of the rapid production of heat within it. To avoid regions of concentrated heat production at the junctions of the Nb wire to copper leads, these junctions were spread out by spot welding the Nb at close intervals along several centimeters of its length to nickel foil, which was soldered to the copper. Particular samples of 0.0011 inch diam unannealed Nb at 4.2°K carried up to 9 ampere; 0.002 inch diam, 10 ampere; and 0.005 inch diam, 29 ampere. In an externally applied transverse magnetic field of 5 kilogauss at 1.7°K, 0.002 inch wire carried 1.5 ampere. Solenoids and iron-core magnets with such windings should be useful in various cryogenic experiments.

* Research done at the University of Illinois with support from the U. S. Atomic Energy Commission.

W9. On the Rotational Transition in Solid Hydrogen. K. TOMITA,* *Harvard University.*—Cooperative appearance of the rotation of hydrogen molecules, which is indicated both by proton resonance[1] and by specific heat,[2] is described by a semi-classical theory. The order of magnitude of the restriction to the rotation which is experienced by a molecule is estimated to be 4°K. The results derived from several different types of experiments, *vis.*, line shape of proton resonance, spin-lattice relaxation-time, and transition temperature of specific heat, are in reasonable agreement with each other. For the case of pure ortho-hydrogen, a calculation of the potential energy and the anisotropy based on intermolecular forces is carried out.

* On leave from the University of Kyoto.
[1] J. Hatton and B. V. Rollin, Proc. Roy. Soc. (London) **A199**, 222 (1949); R. Reif and E. M. Purcell, Phys. Rev. **91**, 631 (1953).
[2] R. W. Hill and B. W. A. Ricketson, Phil. Mag. **45**, 377 (1954).

SATURDAY AFTERNOON AT 2:00

McAlpin, Colonial Room

(W. W. BUECHNER, presiding)

Reactions of Transmutation and Nuclear Energy Levels, II

X1. Competition between (α,pn) and $(\alpha,2n)$ Reactions on Cr^{50}.* J. M. MILLER, *Columbia University and Brookhaven National Laboratory,* AND G. FRIEDLANDER AND S. MARKOWITZ, *Brookhaven National Laboratory.*—The large ratios of the formation cross sections of Mn^{52} to those of Fe^{52} observed in several high energy nuclear reactions may be interpreted in terms of the evaporation of nucleons from excited nuclei. This hypothesis has been examined by the investigation of the relative probability of the loss of a proton and a neutron as compared with the loss of two neutrons from excited Fe^{54} nuclei. Chromium was bombarded with 33-Mev alpha particles; deuteron contamination of the beam was shown to be less than 0.05 percent by means of a $Cu^{63}(d,2n)Zn^{63}$ monitoring reaction. The relative formation cross sections of $Mn^{52}/Mn^{52m}/Fe^{52}$ are 18/8/1, compared with corresponding ratios of 19/−/1 resulting from 340-Mev proton irradiation of iron.[1] The fact that, in spite of the Coulomb barrier, the probability of evaporating a neutron and a proton is so large compared to that of evaporating two neutrons, indicates a level density of Mn^{52} (odd-odd, $T_f=1$) substantially larger than that of Fe^{52} (even-even, $T_f=0$) at a given excitation above the ground state.

* Research performed under the auspices of the U. S. Atomic Energy Commission.
[1] Rudstam, Stevenson, and Folger, Phys. Rev. **87**, 358 (1952).

X2. Excitation Functions for Reactions of Copper with High-Energy Protons.* J. A. MISKEL, M. L. PERLMAN, AND G. FRIEDLANDER, *Brookhaven National Laboratory,* AND J. M. MILLER, *Columbia University and Brookhaven National Laboratory.*—Spallation of copper with 2.2-Bev protons[1] gives rise to a yield *versus* mass curve markedly different from that observed with 340-Mev protons.[2] We have now measured excitation functions for the production of Na^{24}, A^{37}, A^{41}, Mn^{52}, and Mn^{56} from copper over a range of proton energies from about 0.5 to 3.0 Bev. All irradiations were monitored by the $Al^{27}(p,3pn)Na^{24}$ reaction.[3] The argon activities were counted in the gas phase inside proportional counters; the manganese and sodium activities were counted as MnO_2 and NaCl, respectively, with end window proportional counters. The excitation functions show some systematic trends. The Mn^{52} cross section is practically constant over the entire energy range, both argon excitation functions rise rather steeply to a maximum near 1 Bev and then drop slowly, whereas the Na^{24} cross section increases with energy up to about 2 Bev and then remains almost constant.

* Research performed under the auspices of the U. S. Atomic Energy Commission.
[1] Friedlander, Miller, Wolfgang, Hudis, and Baker, Phys. Rev. **94**, 727 (1954).
[2] Batzel, Miller, and Seaborg, Phys. Rev. **84**, 671 (1951).
[3] Hudis, Wolfgang, Sugarman, and Friedlander, Phys. Rev. **94**, 775 (1954).

X3. (γ,n) Cross Sections in Zr^{90} and Zr^{91}. R. NATHANS AND P. F. YERGIN, *University of Pennsylvania.*—The (γ,n) thresholds of these isotopes are widely separated (12.1 and 7.2 Mev respectively) because Zr^{90} has a "magic number" (50) of neutrons. By direct neutron detection, using separated isotopes from ORNL, we find that despite this the location and magnitude of the peak of the giant resonance is the same for each isotope and agrees well with the previously reported photoneutron systematics.[1] The half-widths of the Zr^{90}, Zr^{91} and the previously measured Nb^{93} resonances increase progressively with the neutron numbers (50, 51, and 52 respectively) but all are narrower than expected from the systematics. This reinforces the previous observation that nuclides at or near the magic neutron numbers 28, 50, 82, and 126 have unusually narrow giant resonances.

[1] R. Nathans and J. Halpern, Phys. Rev. **93**, 437 (1954).

X4. (γ,n) Cross Sections in Mg^{24} and Mg^{25}. P. F. YERGIN AND R. NATHANS, *University of Pennsylvania.*—We have measured these cross sections by neutron detection using separated isotope targets form ORNL (1.77 and 0.50 g of isotope, respectively). Both "giant resonance" peaks occur at about 20 Mev, as does the previously reported[1,2] $Mg^{25}(\gamma,p)$ peak. An unusual feature of our results is that both the peak and integrated (to 24 Mev) cross sections for $Mg^{25}(\gamma,n)$ are about twice those for $Mg^{24}(\gamma,n)$. About $\frac{1}{4}$ of the integrated cross section for $Mg^{24}(\gamma,n)$ is between threshold and the onset of the giant resonance. Our results are in contardiction to the report[1] that the peak of the giant resonance for $Mg^{25}(\gamma,n)$ is at about 13 Mev, which would result in far more protons than neutrons being emitted at the higher energies. These observations were described to threshold differences. The thresholds involved are: $Mg^{24}(\gamma,n)$16.6 Mev; $Mg^{25}(\gamma,p)$12.1 Mev; $Mg^{25}(\gamma,n)$7.3 Mev. We find no such threshold effect.

[1] Katz, Baker, and Montalbeth, Can. J. Phys. **32**, 580 (1954).
[2] Toms and Stephens, Phys. Rev. **82**, 709 (1951).

X5. Multipolarity of Gamma Transitions in F^{19} and Na^{23} by Coulomb Excitation. G. M. TEMMER AND N. P. HEYDENBURG, *Department of Terrestrial Magnetism, Carnegie Institution of Washington.*—Using the comparison method of Bjerregaard and Huss[1] we have determined the multipolarity of the transition to the 198-kev (second-excited) state in F^{19} and the 446-kev (first-excited) state in Na^{23} to be $E2$. A series of pairs of thin-target yields for corresponding proton and alpha-particle energies at equal $\xi=(Z_1Z_2e^2/\hbar)[(1/v_f)(1/v_i)]$ were obtained, making sure that no significant *resonant* contribution was made by the protons. The energy intervals for F^{19} where this was achieved were: 0.71–0.76 Mev (protons) and 1.72–1.92 Mev (alphas). For Na^{23} the intervals were: 0.90–0.98 Mev (protons) and 2.00–2.22 Mev (alphas). At least six independent pairs of yields were obtained for each nucleus. We were able to show (a) that between the well-known, strong resonances for the (p,γ), $(p,\alpha\gamma)$, and $(p,p'\gamma)$ reactions on F^{19} and Na^{23} the predicted amount of Coulomb excitation occurs, and (b) that the yield ratios are appropriate for $E2$ transitions ($Y_\alpha/Y_p\sim11$). Our reported transition probability for Na^{23} is therefore correct.[2] Any excess gamma yield (with protons) from resonances, target backing, etc. would have tended toward the ratio predicted for $E1$ transitions ($Y_\alpha/Y_p\sim7$). Background and low yield have prevented us from applying this test to the 114-kev (first-excited) state of F^{19} which is presumably reached by $E1$ transition.[3]

[1] J. H. Bjerregaard and T. Huus, Phys. Rev. **94**, 204 (1954).
[2] G. M. Temmer and N. P. Heydenburg, Phys. Rev. **96**, 426 (1954).
[3] Sherr, Li, and Christy, Phys. Rev. **94**, 1076 (1954).

X6. Assignment of Energy Levels by Coulomb Excitation with 5.7-Mev Alpha Particles. N. P. HEYDENBURG AND G. M. TEMMER, *Department of Terrestrial Magnetism, Carnegie Institution of Washington.*—We have observed Coulomb excitation of nuclei in the rare earth region using enriched isotopes (supplied by Oak Ridge), and 5.7-Mev He^{++} ions. The following gamma rays were observed in the odd A isotopes (energies in kev): Nd^{145}70, Gd^{155}146, Gd^{157}131, Hf^{177}113 and 250, Hf^{179}119. No gamma rays were found in Nd^{143}, Sm^{147}, and Sm^{149}, in contrast with our earlier supposition.[1] Except for Hf^{177} and Hf^{179} the intensities are much weaker than the quadrupole transitions in the even A isotopes of these elements The following gamma rays (some previously known) were identified in the even A isotopes: Nd^{148}300, Nd^{150}128, Sm^{150}337, Sm^{152}122, Sm^{154}82, Gd^{154}123. These are strongly excited quadrupole transitions to the first excited 2^+ states. Furthermore Gd and Hf show strong unresolved gamma rays at 85 and 90 kev respectively, associated with known 2^+ states in the even A isotopes. We have also observed gamma rays up to 1.2 Mev in Ti, V, Fe, Cu, Zn, Ge, Se, Nb, Mo, Ru, Pd, and Cd. Some gamma lines could be identified with known 2^+ states in even-even isotopes, while others must await assignment with enriched isotopes.

[1] G. M. Temmer and N. P. Heydenburg, Phys. Rev. **94**, 1399 (1954).

X7. Anomalous Dependence of F_p/F_n on Bombarding Energy. B. L. COHEN AND E. NEWMAN, *Oak Ridge National Laboratory.*—The quantity F_p/F_n, the ratio of probabilities for proton and neutron emission from nuclear reactions in the statistical region, is determined from measurements of (p,pn) and $(p,2n)$ cross sections induced by 21.5 Mev protons bombarding elements of mass 48 to 71. The results are then compared with determinations of F_p/F_n at lower energies. In all cases, data for various differences in energy available for proton and neutron emission are extrapolated to zero energy difference. It is found that F_p/F_n increases by well over an order of magnitude within a few Mev, reaching values considerably larger than unity. This is not accompanied by any very drastic change in the energy distributions or angular distributions of the emitted protons. It is shown that this behavior cannot be explained by any existing theories, or modifications of them. It is further proven that any model in which energy exchange is pictured as taking place by successive intenucleon elastic collisions—all commonly used models are special cases of this—cannot explain the data. Measurements of $(p,pn)+(p,2n)$ and $(p,2p)$ cross sections in lighter elements indicate that values of F_p/F_n considerably larger than unity are quite general up to mass 66 at this bombarding energy.

X8. Survey of (p,n) Reactions at 11.7 Mev. H. G. BLOSSER, T. H. HANDLEY, AND M. K. HULLINGS, *Oak Ridge National Laboratory.*—A survey of (p,n) reactions at 11.7 Mev has been undertaken on middle Z elements ranging from scandium to cerium using the internal beam of the ORNL 86-in. cyclotron. Ratios of some 25 cross sections to $Cu^{63}(p,n)Zn^{63}$ have been measured using an activation technique. Cross sections were computed from ratios of activities by using known decay scheme information and the previously measured $Cu^{63}(p,n)Zn^{63}$ cross section. For $Z\gtrsim28$, (p,n) cross sections become essentially equal to total reaction cross sections and using Shapiro's calculation[1] of total cross sections one finds $Ro\approx1.5\times10^{-13}$ cm. This is the same value obtained by Blaser *et al.*[2] at 6.7 Mev by the same method. Cross sections on Ni^{60} and Zr^{90} (which were anomalously low at 6.7 Mev) were found to be of order of 50 percent of the neighboring cross sections indicating that the 6.7-Mev measurements of reference 2 were below threshold. Cross sections for Sc^{45} and Cr^{52} fall well below calculated total cross sections indicating probable substantial competition from other reactions.

[1] M. M. Shapiro, Phys. Rev. **90**, 171 (1953).
[2] Blaser, Boehm, Marmier, and Scherrer, Helv. Phys. Acta **24**, 441 (1951).

X9. Nuclear Pairs from the Proton Bombardment of Ca^{40}.* T. W. BONNER, R. D. BENT, AND J. H. MCCRARY, *The Rice Institute.*—A thick calcium metal target was bombarded with 4.84-Mev protons and a search was made with a magnetic lens pair spectrometer for pairs which might originate from the 3.35-Mev state of Ca^{40}. A pair line was observed at 3.46 ± 0.1 Mev. With 1 mm of Al absorber between the target and a 2-mil lead converter, no external pair line was observed at this energy indicating that the pairs observed in the first case were nuclear pairs and not internally converted gamma-ray pairs. The existence of pairs and the absence of gamma radiation establish the angular momentum of the first excited state of Ca^{40} as zero.

* Supported by the U. S. Atomic Energy Commission.

X10. Gamma Radiation from the Deuteron Bombardment of N^{14}.* R. D. BENT, T. W. BONNER, J. H. MCCRARY, AND R. F. SIPPEL, *The Rice Institute.*—The gamma radiation from

the bombardment of a thick CrN target with 4.0-Mev deuterons has been measured with a magnetic lens pair spectrometer. The internal pair spectrum was observed between 5.0 and 9.3 Mev with 2.5 percent resolution. Gamma-ray lines were observed at 5.26±0.04, 6.12±0.06, 6.33±0.05, 6.81±0.04, 7.31±0.04, 8.33±0.04, and 9.13±0.06 Mev, corrected for doppler shifts. The internal pair spectrum from the bombardment of a thick ZrN target with 4.25 Mev deuterons was observed between 9.1 and 11.4 Mev with 3.6 percent resolution. Lines with about equal intensities were observed at 9.13 and 10.04±0.04 Mev. Weak higher energy radiation may also be present. The 6.33-, 7.31-, 8.33-, 9.13-, and 10.04-Mev gamma rays are assigned to the $N^{14}(d,p)^*N^{15}$ reaction. The 6.12- and 6.81-Mev lines are assigned to the $N^{14}(d,n)^*O^{15}$ reaction. The 5.26-Mev line may be from both N^{15} and O^{15}.

* Supported by the U. S. Atomic Energy Commission.

X11. Angular Distribution of Fragments from 450-Mev Proton Fission of Bi.* R. L. WOLKE, *University of Chicago.*—The angular distribution of fission fragment nuclei escaping from a Bi target bombarded with 450-Mev protons has been measured. The target is a $\frac{3}{32}$-in. brass ball, electroplated with about 15 mg/cm² of Bi, and situated at the center of the base of a recoil "catcher" cone of pure Al foil, whose axis is aligned along the proton direction. The foil is cut into pieces corresponding to various emission angles and processed radiochemically. Forward asymmetries have been observed for the fission products Ba, Cd, and Sr. The number of Sr fragments caught in the interval 0–30° (lab) divided by the number caught in the entire forward hemisphere is 1.20±0.04 times the value predicted by isotropy. For 30–60° and 60–90°, the corresponding numbers are 1.03±0.02 and 0.92±0.01, respectively. The application of these and other results to the calculation of certain parameters of the fission mechanism will be discussed.

* Research supported in part by a grant from the U. S. Atomic Energy Commission.

X12. The Neutron Multiplicity Spectrum from Spontaneous Fission. JOHN ISE, JR., DONALD A. HICKS, AND ROBERT V. PYLE. *University of California, Berkeley.*—The distribution in number of neutrons emitted from the spontaneous fission of several transuranic elements has been measured, using a large liquid scintillator tank similar to that described by Cowan *et al.* at Los Alamos.[1] Samples of the various unstable actinides of atomic number greater than 96 were plated on a metal disk inside a small fission chamber which was placed at the center of the scintillator tank. The fission pulse was made to trigger the sweep of an oscilloscope and the pulses arising from neutron capture in the cadmium contained in the scintillator solution were displayed on the sweep and photographed. Results of the observed number distributions will be given, together with the real distribution calculated from the over-all efficiency of the tank for recording a pulse from a neutron starting at the center of the tank. This work was performed under the auspices of the U. S. Atomic Energy Commission.

[1] Cowan, Reines, Harrison, Anderson, and Hayes, Phys. Rev. 90, 493 (1953).

X13. Photodisintegration of Carbon, Oxygen, and Nitrogen in Nuclear Emulsions.* RAYMOND D. COOPER AND DAN J. ZAFFARANO, *Iowa State College.*—Lithium loaded Ilford 200-μ B-2 plates were exposed to the direct beam from the Iowa State 70 Mev synchrotron and then developed by a modified grain gradation process so that singly charged particles could be easily discriminated from multiply charged ones. Identification of the stars found in the plates was made by computing momentum unbalances assuming various identities for the particles involved. Of a total of 2291 stars of three or four prongs measured in two plates, 647 were found to be due to the reaction $C^{12}(\gamma,3\alpha)$; 348 were identified as due to $O^{16}(\gamma,4\alpha)$; and the reactions $N^{14}(\gamma,2\alpha)Li^6$ and $N^{14}(\gamma,np)3\alpha$ were represented by 190 and 182 events respectively. Cross section histograms for the first three of these reactions were obtained after making corrections for the stars which were not entirely within the emulsion and for the shape of the bremsstrahlung spectrum. In about one-fifth of the events due to the last reaction, $N^{14}\times(\gamma,np)3\alpha$, the momentum unbalance method indicates that the neutron and proton probably came off together as a deuteron. An attempt was also made to determine whether the reaction $N^{14}(\gamma,2\alpha)Li^6$ went through an excited or the ground state of Be^8 or through an excited state of B^{10}, and these results will be given.

* Work was performed in the Ames Laboratory of the U. S. Atomic Energy Commission.

SATURDAY AFTERNOON AT 2:00

McAlpin, Green Room

(J. E. GOLDMAN, presiding)

Ferromagnetics and Ferroelectrics

Y1. Ferromagnetic Hall Effect of Nickel Alloys. ALBERT I. SCHINDLER, *Naval Research Laboratory.*—Recently Karplus and Luttinger[1] have shown that the extraordinary Hall constant of ferromagnetic materials is proportional to the square of the electrical resistivity. $R_1=A\rho^2$ For experimental verification they have cited the data of Jan and Gijsman[2] on the temperature dependence of the Hall constants of pure Ni and Fe. In the case of Fe the exponent of ρ is 1.94, in the case of Ni, it is 1.42. In addition, Kooi[3] has shown that R_1, for alloys of Fe containing small additions of Si, exhibits the same temperature dependence as pure Fe. An examination of published Hall constant data of alloys of Ni with Cu, Al, Si, and Sn[4] also shows that the Karplus-Luttinger theory is roughly obeyed by these systems. In all of these alloys there seems to be no change in the exponent of ρ due to alloying. Additions of Al, Si, or Sn do alter the coefficient A, whereas additions of up to 30 atomic percent of Cu leave A essentially unchanged. Contrary to theory, there seems to be no correlation of the change in A with the filling of the 3-d band caused by alloying.

[1] R. Karplus and J. M. Luttinger, Phys. Rev. 95, 1154 (1954).
[2] J.-P. Jan, Helv. Phys. Acta 25, 677 (1952); J.-P. Jan and J. M. Gijsman, Physica 18, 339 (1952).
[3] C. Kooi, Phys. Rev. 95, 843 (1954).
[4] A. I. Schindler and E. M. Pugh, Phys. Rev. 89, 295 (1953); J. Smit and J. Volger, Phys. Rev. 92, 1576 (1953).

Y2. The Magnetic Transformation in MnBi. R. R. HEIKES, *Westinghouse Research Laboratories.*—It is well known that MnBi undergoes an abrupt change in magnetization at a temperature of 360°C. In addition, there is a drastic change

in lattice constants; c changes by approximately 3 percent, while a changes by almost 1.5 percent. Guillaud interpreted this transition in terms of change from a ferromagnetic state at low temperatures to an antiferromagnetic state at high temperatures. This interpretation appears inconsistent with the extremely large change in lattice constant. Susceptibility measurements have been performed above 360°C on a sample of MnBi whose x-ray diffraction pattern shows only lines due to MnBi. The measurements indicate that the high-temperature phase is actually ferromagnetic with a Curie point of 170°C. The material was then quenched from 380°C, retaining the high-temperature phase. Saturation magnetization measurements on this material indicated a Curie temperature of approximately 200°C. Because of the inaccuracies involved in the measurements, particularly in the case of the quenched phase, the two values of the Curie point are considered to be in good agreement. The present work elaborates and confirms the unpublished suggestion of L. Himmel and K. Jack of our Laboratories that the high-temperature phase of MnBi is ferromagnetic.

Y3. Rapid Remagnetization of Thin Molybdenum Permalloy Tapes. T. L. GILBERT, J. M. KELLY, AND H. EKSTEIN, *Armour Research Foundation.*—The time derivative of the magnetization in ½ to 2 mil thick, ½ inch wide, 4–79 Molybdenum Permalloy tapes wound on small bobbins has been measured as a function of the time for the following applied field schedule. The tape is first saturated in one direction and allowed to return to its remanent state. The time rate of magnetization parallel to the tape length is then observed as reverse fields of 0.1 up to 5 oersted are switched on, (the rise time being under 0.1 μsec). In ½ and ¼ mil tapes, the primary features of this observed "switching pulse" correspond closely to predictions based on a model wherein the magnetization is assumed to rotate uniformly in the plane of the tape, subject only to the forces exerted by the external field and the eddy current field and an anomalous force which gives rise to a local dissipation proportional everywhere to the square of the time derivative of the local magnetization. With thicker tapes the magnetization cannot be uniform throughout the thickness and two domain walls moving inward from the surfaces may be expected to form, particularly at high fields, as described previously.[1]

[1] H. Ekstein and J. Kelly, Phys. Rev. **94**, 1440(A) (1954).

Y4. Saturation Magnetization and Remanence of Beta Uranium Hydride. WARREN E. HENRY, *U. S. Naval Research Laboratory,* AND DIETER M. GRUEN, *Argonne National Laboratory.*—The occurrence of a ferromagnetic transition for beta-uranium hydride has been confirmed by Gruen. In the present investigation, the saturation magnetization (M_s) and remanence of $\beta-UH_3$ have been measured as a function of temperature between 1.3°K and 295°K and in magnetic fields up to 50 000 gauss. M_s shows a sluggish onset of an anomaly at above 200°K indicating short range order. On the other hand, a sharp transition is indicated from the zero field remanence and occurs at about 175°K. Saturation is nearly complete at 11 000 gauss where a high precision is possible. At 1.3°K the remanence is about 70 percent of the saturation moment. In the liquid nitrogen range, there is some indication of another anomaly in $M_s(T)$. This second anomaly, being further studied, does not show in the remanence, which is perhaps a better measure of the cooperative behavior. The magnetization was measured both in high and zero magnetic fields by a ballistic method[1] in which a spherical container, with powdered sample, is moved relative to a double coil system.

[1] W. E. Henry, Phys. Rev. **88**, 559 (1952).

Y5. Diffuse Magnetic Neutron Diffraction. A. W. MCREYNOLDS, *Brookhaven National Laboratory.**—It was previously shown[1] that superposed on the nuclear and elastic magnetic Bragg diffraction peaks in magnetic crystals is a weaker diffuse magnetic peak arising from short range correlation of spins. In order to separate out this diffuse component a more detailed study has been made of the space distribution and temperature dependence of scattering around the (111) and (113) reciprocal lattice points in ferrimagnetic Fe_3O_4. The principal effect is around the Curie temperature 580°C. There a diffuse peak symmetrical in reciprocal space around the (111) lattice point reaches a maximum intensity, decreasing over a 50–100°C range above and below. From its width and temperature dependence may be deduced the spin correlation as a function of distance and temperature. At all temperatures magnetic inelastic scattering is indicated by presence in the magnetic peaks of a small asymmetric component independent of applied fields.

* Under the auspices of the U. S. Atomic Energy Commission.
[1] A. W. McReynolds and T. Riste, Phys. Rev. **95**, 1161 (1954).

Y6. Domain Configuration and Crystallographic Orientation in Grain-Oriented Fe-Si Alloy. T. G. NILAN AND W. S. PAXTON, *U. S. Steel Corporation.*—The magnetic domain structure in grain-oriented 3-½ percent silicon-iron alloy has been investigated by the powder pattern technique.[1] The patterns observed can be classified into five different types depending on the orientation of the particular grains. A large number of such grains were examined and their orientation determined by means of an optical goniometer and in some cases by x-rays. It is found that the pattern depends on the angle ϕ made by the [100] direction nearest the rolling direction with the plane of the sheet. When neighboring grains differ by only a small angle, the domains will often be continuous across the grain boundary, as observed by Williams, Dijkstra,[2] and others. Photographs of several unusual patterns will be shown. For small deviations ($\phi<10°$) from the perfect cube-on-edge orientation, the method may be used to determine the orientation of the grains.

[1] Williams, Bozoeth, and Shockley, Phys. Rev. **75**, 155 (1949).
[2] L. J. Dijkstra and U. M. Martius, Revs. Modern Physics **25**, 146 (1953).

Y7. Magnetic Resonance in a Ferrimagnetic Containing an Arbitrary Number of Sublattices. ROALD K. WANGSNESS, *U. S. Naval Ordnance Laboratory.*—The method of finding the equations of motion for the components of the net magnetization from the equations of motion for the individual sublattices, which has been briefly used before,[1] has been extended to include the cynamic demagnetizing and anisotropy fields as well as molecular fields. Each sublattice is characterized by a magnetization, gyromagnetic ratio, and anisotropy constant; one need not assume the same molecular field coefficient for each pair of sublattices. In the limit of very large molecular fields, the resultant equations of motion turn out to have the same form and lead to the same resonance frequency as for the ferromagnetic case except that they involve the usual effective gyromagnetic ratio and an anisotropy constant which is the sum of the sublattice anisotropy constants. These results agree with those found for the two-sublattice case by a different method.[2]

[1] R. K. Wangsness, Phys. Rev. **95**, 339 (1954).
[2] R. K. Wangsness, Phys. Rev. **93**, 68 (1954).

Y8. Specific Heats of Zinc Ferrite and Zinc Chromite at Low Temperatures.* S. A. FRIEDBERG AND D. L. BURK, *Carnegie Institute of Technology.*—Neutron diffraction studies[1] indicate that in $ZnOFe_2O_3$, a normal spinel, long range antiferromagnetic ordering of Fe^{+++} moments due to $B-B$ interaction sets in below about 10°K. We have measured the specific heat of a specimen[2] of $ZnOFe_2O_3$ between 1.3° and 200°K and observed the specific heat anomaly associated with this transition. The maximum at ~9.5°K is not particularly sharp. A large short range order "tail" is still apparent at 20°K. The

analogous spinel $ZnOCr_2O_3$ has also been studied.[3] A sharp λ-shaped anomaly was found, C_p rising to ~14 cal/mole°K at 11.8°K. Subsequent neutron diffraction investigation[4] shows $ZnOCr_2O_3$ to be antiferromagnetic below this temperature. Details of these anomalies will be discussed.

* Supported by the Office of Naval Research.
[1] L. M. Corliss and J. M. Hastings, Proceedings, International Conference on crystallography, Paris (July, 1954).
[2] Kindly supplied by Dr. V. C. Wilson of the General Electric Company.
[3] Specimen generously provided by Dr. T. McGuire of the Naval Ordnance Laboratory.
[4] Hastings, Corliss, and Goldman, Pittsburgh Diffraction Conference, (November, 1954).

Y9. Magnetic Susceptibility in Zinc Ferrite.* A. ARROTT AND J. E. GOLDMAN, *Carnegie Institute of Technology.*—The appearance of new lines in the neutron diffraction spectrum of zinc ferrite[1] and zinc chromite[2] and the specific heat anomalies[3] suggest that the interaction between magnetic ions on octahedral sites in spinel lattices (B−B interaction) is: (a) antiferromagnetic, (b) considerably weaker than at first supposed, and (c) gives rise to long range effects which are relatively complex. Measurements have been made of the magnetic susceptibility of zinc ferrite[4] over a range of temperatures extending from 2°K to room temperature. The susceptibility is constant at low temperatures and begins to decrease at approximately 30°K with a Curie-Weiss behavior. The high-temperature behavior is that of an ideal paramagnet containing two Fe^{+3} ions per molecule and an extrapolated θ of −40°K. This behavior suggests persisting short range effects above the temperature of the peak in the specific heat where the antiferromagnetic neutron diffraction lines have already diminished in intensity.

* Supported by the Office of Naval Research.
[1] L. M. Corliss and J. M. Hastings, Proceedings, International Conference on Crystallography, Paris (July, 1954).
[2] Hastings, Corliss, and Goldman, Pittsburgh Diffraction Conference (1954).
[3] S. A. Friedberg and D. Burk, previous abstract.
[4] Kindly supplied by Dr. V. C. Wilson of the General Electric Comapny. Measurements of the specific heat (previous abstract) and susceptibility were made on the same sample.

Y10. Temperature Effects in Ferrites at Microwave Frequencies. B. J. DUNCAN AND L. SWERN, *Sperry Gyroscope Company.*—The microwave properties of ferrites in waveguide depend upon several parameters; one of the most important is the temperature of the ferrite. Studies have been made of the effect of ferrite temperature upon Faraday rotation, ferrite loss, phase shift, reflection coefficient and the ellipticity of microwaves propagated through the ferrite medium. These temperature effects were studied at *X*-band frequencies with the ferrites located in both rectangular and circular waveguide; in the latter case both linearly and circularly polarized waves were used. The ferrites studied are those which are commercially available; in particular, ferramics *D*, *G*, and 1331 were investigated most thoroughly. In each case, the temperature was varied from 25°C to the Curie temperature. For ferrites in circular waveguide near the Curie temperature the rotation and phase shift approach zero, the axial ratio approaches infinity, and the absorption loss increases at a rapid rate to some large value. For ferrites in rectangular wave guide, with frequency held constant, the magnetic field required for resonance decreases by over 30 percent as the temperature is increased from 25°C to the Curie temperature. This is due to a change in the effective *g* factor in the ferrite. These and other effects will be discussed.

Y11. Optical Properties and Twinning of $PbZrO_3$ Single Crystals.* F. JONA, G. SHIRANE, AND R. PEPINSKY, *The Pennsylvania State University.*—Single crystals of $PbZrO_3$ were grown by using PbF_2 as a flux. The twinning was studied, and essential differences between this twinning and the domain structure of ferroelectric $BaTiO_3$ have been observed. It is shown that orthorhombic phase of $PbZrO_3$ is optically negative and the refractive index is smallest along the *a* axis, along which axis the main antiparallel shifts of Pb have been reported.[1] The birefringence has been measured as a function of the temperature up to the transition temperature 230°C, and compared with the temperature dependence of the spontaneous strain.

* Research supported by Wright Air Development Center and Signal Corps Engineering Laboratories.
[1] Sawaguchi, Maniwa, and Hoshino, Phys. Rev. **83**, 1078 (1951).

Y12. Anomalous Optical Properties of Ferroelectric $PbTiO_3$.† GEN SHIRANE AND RAY PEPINSKY, *The Pennsylvania State University.*—The birefringence of the tetragonal phase of $PbTiO_3$ has been reported as 0.011 for sodium light at room temperature.[1] This value diminishes when the crystals are cooled below room temperature.[2] With increasing temperature, the birefringence increases gradually, reaches a maximum value of 0.018 at 400°C, and decreases again to 0.012 at the Curie temperature, 490°C. It is not possible to explain this temperature dependence by a combination of the linear and square terms of the spontaneous strain. This situation is in contrast with the case of $BaTiO_3$, in which the birefringence decreases with increasing temperature, in a linear relation to the spontaneous strain. It is confirmed that $PbTiO_3$ is optically negative as in the case of $BaTiO_3$. Preliminary results of a structural study of $PbTiO_3$ at room temperature are presented.

† Research supported by Wright Air Development Center and Signal Corps Engineering Laboratory.
[1] H. H. Rogers, Tech. Rept. 56, Lab. Inst. Research, M.I.T. (1952).
[2] P. W. Forsbergh, Jr., Progr. Rept. XI, p. 51, Lab. Inst. Research, M.I.T. (1952).

Y13. Ferroelectric Behavior of Solid Solutions of $KNbO_3$ and $KTaO_3$. SOL TRIEBWASSER AND FREDERIC HOLTZBERG, *IBM Watson Laboratory.*—$KNbO_3$ and $KTaO_3$ are ferroelectrics of the perovskite type with Curie temperatures at 707°K[1] and 13.2°K,[2] respectively. Differential thermal analysis and x-ray studies of the system $K_2CO_3+(1-x)Nb_2O_5+xTa_2O_5$ have been made. Comparisons of x-ray spectrometer traces of powder samples of quenched material with similar traces of pure $KNbO_3$ and $KTaO_3$ indicate that solid solution between the two components exist. Differential thermal analysis yields a simple two component solid solution phase diagram. Studies of ceramics of the composition from $X=0$ to 0.20 indicate that the Curie temperature of $KNbO_3$ is depressed approximately 7°C per percent of $KTaO_3$. The tetragonal to orthorhombic transition in $KNbO_3$ at 224°C[1] is lowered in a similar manner.

[1] B. T. Matthias and J. P. Remeika, Phys. Rev. **82**, 727 (1951).
[2] Hulm, Matthias, and Long, Phys. Rev. **79**, 885 (1950).

Y14. Low Temperature Dielectric Measurements. J. F. YOUNGBLOOD, *General Electric Research Laboratory.*—Measurements have been made at low temperatures on the dielectric constant and loss factor of several ferroelectric materials and strontium titanate. The latter is of particular interest as the dielectric constant for single crystals reaches values near 10°K of 17 000 to 18 000, about 58 times the room temperature values, and is strongly voltage sensitive. Near the low temperature maximum in dielectric constant the loss factor shows a strong peak. Such behavior is suggestive of a ferroelectric Curie temperature with domain formation. However, hysteresis measurements do not show such a transition conclusively.

Y15. Dynamic Behavior of Domain Walls in Barium Titanate. ELIZABETH A. LITTLE, *M. I. T.* (introduced by A. V. Hippel).—The nucleation and growth of 90° and 180° domains in barium titanate single crystals have been measured with optical techniques. Both types of domains nucleate as long thin wedges with an initial velocity of about 10^4 cm/sec for $E=5$ kv/cm. For 90° domains, measurements of

the nucleation rate as a function of time and field strength are given. After a domain has been introduced into a crystal, its growth may be described in terms of wall motion. 90° wall motion depends strongly on strains and any clamping of the crystal, and appears to cease for frequencies in the megacycle range, where the piezoelectric resonances of the crystal set in. For 180° wedges, the availability of neutralizing electric charges appears to determine the growth rate. The interaction of 180° and 90° domains, which leads to head-to-head and tail-to-tail 90° walls and long relaxation times, is described.

SATURDAY AFTERNOON AT 2:00

New Yorker, North Ballroom

(L. M. LEDERMAN, presiding)

Heavy Mesons and Hyperons

Z1. Some Results on K Particles.* W. B. FRETTER, E. W. FRIESEN, G. E. KEPLER, AND A. LAGARRIGUE, *University of California, Berkeley.*—Several K particles have been identified using measurements of ionization and momentum. The ionization measurements are made by counting droplets in tracks in a cloud chamber containing helium. The chamber is placed in a magnetic field of 7500 gauss. One group of five particles all positive, non-decaying and of average mass 900 ± 30 electron masses suggests the presence of K_μ particles.[1] A positive particle of mass 1330 ± 80, and a negative particle of mass 1190 ±70, have also been observed. A positive τ meson has been observed to decay in our chamber with a Q value of 78 ± 20 Mev. The measurements and errors of mass determinations have been checked by comparison with the measurements on 22 particles believed to be protons.

* Assisted by the joint program of the U. S. Office of Naval Research and the U. S. Atomic Energy Commission.
[1] B. P. Gregory *et al.*, Nuovo cimento II, 292 (1954).

Z2. Cosmic-Ray Observations of $K^\pm$ Mesons. N. SEEMAN, M. M. SHAPIRO, AND B. STILLER, *Naval Research Laboratory.*—Tracks of 15 stopped $K^\pm$ mesons have been observed in Ilford G.5 emulsions flown at an altitude of ~30 km. Thirteen of these were found in large (15×12.5 cm) stripped emulsion stacks flown near the geomagnetic equator. Eight of the 13 originate in observable stars. Two also terminate in stars, and are interpreted as due to negative K mesons. Two others have one L meson (π or μ) secondary of ~20 Mev each and are attributable to $\tau^\pm$ decaying by the alternate scheme $\tau^\pm\rightarrow\pi^\pm+\pi^0+\pi^0$. In 11 of the 15 cases there is a single charged-secondary track having a grain density close to the ionization plateau. Most of the primaries are sufficiently long so that two or more of the following methods of mass determination could be applied: constant-sagitta scattering *vs* range, constant-cell scattering *vs* grain density, and mean gap length *vs* range. Protons and pions are employed for calibration. Preliminary results indicate masses of ~1000 m_e for the primaries. The secondaries thus far identified in the decay events are all L mesons.

Z3. K Mesons Produced by 2.2 and 3 Bev Protons.* G. G. HARRIS, *Columbia University.*—Stacks of Ilford G5 stripped emulsions have been exposed at the Brookhaven Cosmotron. Two types of exposure were made. The plates were exposed: (a) directly to the beam of protons inside the vacuum chamber (3 Bev), (b) about 3 inches away from a small graphite target and 90° to the beam direction (2.2 and 3 Bev). These plates are being searched for K mesons by examining the end of all stopping tracks. To date 28 K type particles have been found coming to rest in the emulsion, one τ meson has also been found. None of the K particles has an associated Auger electron or recoil blob which would indicate a negatively charged meson. Mass measurements on the primary tracks by range *vs* scattering which are consistent with the τ meson mass will be discussed. About one-fourth of the secondary tracks are long enough for scattering-blob density measurements. The information from these measurements may be summarized: There is no evidence for low-energy μ-meson secondaries. There is no definite evidence for a π-meson secondary of $P\beta=166$ Mev/c. There is a spread of $P\beta$ from 130–230 Mev/c and a blob density spread of $b/bp=0.94-1.08$.

* Supported by a joint program of the U. S. Office of Naval Research and the U. S. Atomic Energy Commission.

Z4. Heavy Unstable Particles from Captured K^- Mesons.* J. HORNBOSTEL AND E. O. SALANT, *Brookhaven National Laboratory.*—The previously reported arrangement for magnetically selecting negative particles from a target in the Cosmotron[1] was improved. Using 2.8-Bev protons, eight more K^- mesons have been identified in G5 emulsions. Momentum-range and grain count-range measurements both gave K masses about 1000 m_e. All K mesons stopped (ranges 35–45 mm) giving stars with 2–5 outgoing tracks; in five stars, one track is less than 1.5 minimum. In four stars, a charged, heavy (1–4 times proton mass), unstable particle emerges. In three events it stops (ranges 0.4, 0.5, 1.7 mm) and gives a light track. One of latter is due to a 20-Mev σ meson; its parent is evidently a hyperon, possibly bound in triton. The fourth heavy particle has thrice-minimum track for its entire path, at end of which is seen only a backward light particle (1.08 ± 0.05 minimum, $p\beta>100$ Mev/c). If latter is pion from free decay, $Q>180$ Mev, too large for known charged hyperon decay; if muon or electron, such decay is likewise unknown.

* Work done under the auspices of the U. S. Atomic Energy Commission.
[1] J. Hornbostel and E. O. Salant, Phys. Rev. 93, 902 (1954).

Z5. Observations of K^+ Mesons. HARRY H. HECKMAN, S. GOLDHABER, AND F. M. SMITH, *University of California, Berkeley.*—A stack of 600μ Ilford G5 emulsions has been exposed to the secondary particles from a target bombarded by 4.8-Bev protons of the Bevatron. The stack was placed in a re-entrant well ten inches from the target at 90° to the beam direction. The observed numbers of particles stopping in the range interval 1.7 to 5.0 cm in the emulsion are $K^+:\pi^+:\pi^-:p=3:59:25:100$. Mass measurements of the K^+ mesons are being made by residual range and ionization. The percent transparency of the track is taken to be a measure of the ionization. Of the three secondaries from the K^+ mesons (924 ± 122 m_e), only one has sufficient range (10.25 mm) to enable one to make an estimate of the mass by multiple scattering *vs* ionization. The characteristics of this secondary particle are (a) the ratio of ionization to that of calibration electrons (of about 100 Mev) is 1.032 ± 0.028, (b) the average $p\beta c$ over the entire range is 102 ± 14 Mev, and (c) an approximate 25 precent loss in $p\beta c$ between the ranges of 1.25 and

10.25 mm. The expected ionization of a μ meson of this $p\beta c$ would be 33 percent above minimum. The secondary particle has, therefore, properties characteristic of an electron. Further results will be reported. This work is being done under the auspices of the U. S. Atomic Energy Commission.

Z6. Measurements on K Particles and Their Decay Products. GERSON GOLDHABER AND STEPHEN J. GOLDSACK, *University of California, Berkeley.*—Stacks of nuclear emulsions have been exposed at 90° to the proton beam of the Bevatron at 4.8-Bev maximum energy. The stacks were at a distance of 10 inches from the target with 0.1-in. aluminum as intervening material. The scanning of the emulsions was carried out in a region 5 to 6 cm from the leading edge. The alignment of the stack was such that a secondary from the target runs its entire length (5 to 6 cm) in only 2 to 5 of the emulsions in the stack. To date nine K particles have been found in the above stacks. Preliminary mass measurements on five of them give mass values consistent with the 950 m_e value. In four cases the decay products are sufficiently flat in the emulsion to allow good measurements. In three of the cases preliminary multiple scattering measurements give $p\beta = 185 \pm 25$, 200 ± 25, and 150 ± 40 Mev/c. In the fourth case (K_3) the decay particle gives $p\beta = 60 \pm 12$ Mev/c over the first 4 mm and decreases gradually to $p\beta = 30 \pm 6$ Mev/c after 15 mm. The track goes for 9 mm in the first emulsion and has been followed for 8 mm in the next five emulsions. The grain density remains constant over the entire length and equal to the plateau value to good accuracy. Preliminary scattering measurements on K_3 give a mass of 980 ± 260 m_e by constant sagitta method and 1170 ± 270 m_e by the constant cell method. This work was done under the auspices of the U. S. Atomic Energy Commission.

Z7. Heavy Mesons and Hyperons from Targets Bombarded by 4,8- and 5.7-Bev Protons. S. GOLDHABER, GERSON GOLDHABER, H. H. HECKMAN, AND F. M. SMITH, *University of California, Berkeley.*—A target assembly with emulsion stacks mounted on a plunging probe was injected directly into the vacuum chamber of the Bevatron. The timing of the injection was such that the leading target intercepted the beam at full energy. A thin lip target damped radial oscillation of the beam and brought the full energy protons onto the target. In this manner three emulsion stacks were exposed: 1. The emulsions were placed at a distance of 1 cm from a tantalum target so as to detect secondaries in an angular interval between 50°–130° to the beam direction. 2. Geometry as in case 1, but for a carbon target. The beam energy for these two exposures was 4.8 Bev. 3. The emulsion stack itself served as a target with a bombarding energy of 5.7 Bev. To date the systematic area scanning of the emulsions exposed with the tantalum target has given 370 protons, $56\pi^+$, $53\pi^-$, $6\mu^+$, $3K$ particles, and $1\Lambda^0$. The following back of π mseons in the 5.7-Bev exposure has yielded one-τ meson. Preliminary mass measurements on the K particles are in good agreement with the 920–960 m_e mass values. Results on careful mass measurements and Q values will be presented. This work was done under the auspices of the U. S. Atomic Energy Commission.

Z8. Production of Unstable Particles in Carbon and Lead by 2-Bev Pions.* H. BLUMENFELD, E. T. BOOTH, AND L. M. LEDERMAN, *Columbia University*, AND W. CHINOWSKY, *Brookhaven National Laboratory.*—A 36-in. expansion cloud chamber in a magnetic field of 10 000 gauss was exposed to the 2-Bev negative pion beam of the Brookhaven Cosmotron. The chamber contained two $\frac{1}{4}$-in. thick lead plates and two $\frac{1}{8}$-in. thick carbon plates. In a systematic scanning of about 800 photographs, 14 cases of the production of unstable particles by incident pions were observed. Of these, 7 events occurred in lead and 6 in carbon, giving a ratio of mean free paths in g/cm², lead to carbon of ~3. Absolute cross-sections for production are approximately 1 percent of geometric for both lead and carbon. Preliminary analysis of the decay events establishes that the ratio of observed Λ^0 to θ^0 events is 4:1. One charged V track was observed but not identified. A single clear case of associated production in carbon, of a $\Lambda^0 - \theta^0$ pair was observed in a test strip. This event will be discussed. The average Q value for the Λ^0 decays was determined to be 35 ± 3 Mev.

* Assisted by the U. S. Atomic Energy Commission and the joint Office of Naval Research–U. S. Atomic Energy Commission program.

Z9. Nuclear Absorption of a Fast Charged Hyperon. D. T. KING AND M. M. BLOCK,* *Naval Research Laboratory.*—In a collection of "fundamental" collisions found in G5 emulsions exposed to the cosmic radiation we have observed a star consisting of a gray primary (a), and two emergent gray tracks, (b and c); there was no evidence of residual nuclear recoil or β decay. The three tracks were not coplanar, and therefore the emission of a neutral secondary was considered. The measured masses of a, b, and c were 2600 ± 670, 1680 ± 450, and 920 ± 320 m_e, respectively. b and c are identified as proton and K particle; if a is considered to be a proton there is insufficient energy for the secondaries. If a is assumed to be a hyperon of 2600 m_e, the neutral has a calculated mass of 1780 ± 80 m_e and is identified as a neutron. We tentatively suggest the absorption scheme $\Lambda^\pm + P \rightarrow P + K^\pm + N$, and compare this mode of absorption with the recently observed[1] production scheme $P + P \rightarrow \Lambda^+ + K^+ + N$. Both reactions are compatible with the hypothesis[2] of Pais and Gell-Mann that heavy unstable particles are produced and absorbed in pairs, and indicate that the observed K particles are bosons.

* On military leave of absence from Duke University, Durham, North Carolina.
[1] Block, Harth, Fowler, Shutt, Thorndike, and Whittemore, Bull. Am. Phys. Soc. **29**, 33 (1954).
[2] A. Pais, Phys. Rev. **86**, 663 (1952); M. Gell-Mann, Phys. Rev. **92**, 833 (1953).

Z10. Correlation of Planes in V Particle Decay Events.* V. A. J. VAN LINT, GEORGE T. REYNOLDS, S. B. TREIMAN, AND F. H. TENNY, *Princeton University.*—Measurements have been made on the angles between the plane containing the decay products of a V particle and (1) the plane containing the lines of flight of the two V particles in the case of double V events,[1,2] or (2) the plane containing the producing particle and the line of flight of the V particle in the case of single V events where the producing particle could be determined. To date the limited statistics indicate anisotropic distributions in both types of correlation. This is a continuing measurement program, and latest results will be described.

* Supported by the joint program of the Office of Naval Research and the U. S. Atomic Energy Commission.
[1] Treiman, Reynolds, and Hodson, Phys. Rev. (to be published).
[2] Ballam, Hodson, Martin, Rau, Reynolds, and Treiman, Phys. Rev. (to be published).

Z11. Production of Neutral V Events in Lead by Neutrons from the Cosmotron.* R. M. WALKER,† R. S. PRESTON, E. C. FOWLER, AND H. L. KRAYBILL.—Eight events interpreted as the decay of neutral V-particles have been observed in approximately 2000 pictures taken of the interactions of the Cosmotron neutron beam with a lead plate placed inside a cloud chamber. Under the assumption that the nucleons in lead are free, one event may be interpreted by the raection $\pi^- + P \rightarrow \Lambda^0 + \theta^0$, and another by the reaction $N + N \rightarrow \Lambda^0 + \theta^0 + N$. There are a total of 166 interactions observed in the argon filling gas and these are used to deduce a production cross section for Λ^0 particles in lead, by neutrons with energies probably >1 Bev, of <3 mb. A calculation[1] converting nuclear cross sections to nucleon values indicates that the cross sections for the elementary reactions, nucleon+nucleon→Λ^0 +nucleon (threshold~500 Mev) and nucleon+nucleon→Λ^0 +Λ^0 (threshold ~900 Mev) are <0.2 mb. The low value deduced for the latter reaction may be due to a strong energy

dependence, but the results are consistent with the hypothesis that the reaction is forbidden.

* Supported in part by the U. S. Atomic Energy Commission.
† Now at General Electric Research Laboratories.
[1] R. Jastrow, Phys. Rev. (to be published).

Z12. Analysis of Charged *V* Events.* W. H. ARNOLD AND J. BALLAM, *Princeton University.*—Measurements on charged *V*'s observed in the Princeton double cloud chamber experiment at Echo Lake, Colorado have so far yielded sixteen cases in which both primary and secondary momenta are measurable. Of the six negatives, four have p^* values consistent with the two-body decay of a particle of mass ~1000; the other two are consistent with the assumed alternate decay mode of the τ. There is also a negative whose primary is unmeasurable, but which has a $p_\tau > 190$ and whose secondary undergoes what is probably $\pi - \mu$ decay. Of the ten positives, one is consistent with the τ, one is probably a hyperon, and the others are all consistent with $p^* \sim 200$–240. One τ^+ has been observed in the normal decay mode.

* Supported by the joint program of the Office of Naval Research and the U. S. Atomic Energy Commission.

SATURDAY AFTERNOON AT 2:00

McAlpin, Red Room

(E. P. WIGNER, presiding)

Nuclear Theory

ZA1. Energy Levels of Pb^{208}*. G. E. TAUBER, *Western Reserve University.*—Recent experimental work indicates that the excited states of Pb^{208} do not follow the simple $I = 0, 2, 4$ rule, but have spins ranging between 3 and 5 and odd parity. According to the shell model Pb^{208} is a doubly "magic" nucleus and its lowest excited levels would arise from the excitation of either a proton or neutron and could be treated in terms of particle-hole configurations. A general particle-particle interaction of the form $V = (mP + nQ)V(|r_1 - r_2|)$, where P denotes Majorana and Q Bartlett forces, has been assumed and the energy levels in the $j-j$ limit obtained for all possible configurations. The energy levels have been calculated for both a delta-type and a Gaussian potential, with various ranges. It has been found possible to explain the energy levels by postulating certain configurations and relative strengths of the interactions.

ZA2. Matrix Elements of a Nuclear p^3 Configuration. S. MESHKOV, *University of Delaware* AND C. W. UFFORD, *University of Pennsylvania.*—In an attempt to apply the Bacher and Goudsmit[1-3] method to the calculation of nuclear energy levels in terms of experimentally observed energies of other nuclei, we have calculated the matrix elements of a nuclear p^3 configuration in terms of the matrix elements derived from experimental observations of the p^2 configuration.[4] The only assumption regarding the nature of the nuclear force is that it be a 2-particle one. If we assume, in particular, spin-orbit or tensor forces, our matrix elements reduce to the corrected elements of Elliot.[5] We have used *ls* coupling, although the calculation proceeds in the same way if *jj* coupling is used. A general method for the calculation of the matrix elements of any configuration l^n from those of l^{n-1} will be discussed.

[1] R. F. Bacher and S. Goudsmit, Phys. Rev. **46**, 948 (1934).
[2] S. Meshkov and C. W. Ufford, Phys. Rev. **94**, 75 (1954).
[3] R. E. Trees, J. Research Natl. Bur. Standards **53**, 35 (1954).
[4] S. Meshkov, Phys. Rev. **91**, 871 (1953).
[5] J. P. Elliot, Proc. Roy. Soc. (London) **218**, 345 (1953).

ZA3. The 3-Body Exchange Magnetic Moments of H^3 and He^3.† ANDREW M. LOCKETT,* *Massachusetts Institute of Technology.*—The contribution of 3-body exchange currents to the magnetic moments of H^3 and He^3 is calculated using symmetric $PS(PS)$ meson theory. The 3-body moment of lowest order in G is found to be considerably smaller than the lowest order 2-body moment, the latter being identical to that calculated by Villars[1] using (PV) coupling, which itself is too small to explain the observed moments of H^3 and He^3. The next lowest order 2-body and 3-body moments are estimated and found to be an order of magnitude smaller than the lowest order 3-body moment. The nucleons are treated nonrelativistically with neglect of recoil.

† Work supported by Shell Oil Company Fellowship in Physics at Massachusetts Institute of Technology.
* Now at Stevens Institute of Technology, Hoboken, New Jersey.
[1] F. Villars, Helv. Phys. Acta **20**, 476 (1947).

ZA4. Polarized Neutrons on Li^6. M. PESHKIN AND J. H. ROBERTS, *Northwestern University* AND V. L. TELEGDI, *University of Chicago.*—Measurements of the angular distributions of tritons from the reaction $Li^6(n,\alpha)H^3$ using unpolarized neutrons near the 0.25 Mev P-wave resonance have been reported by Roberts *et al.* The $\cos^2\theta$ term in the angular distribution provides the level parameters without the necessity for subtracting the estimated S-wave contribution. The results approximate the one-level dispersion formula only poorly, with widths near $\Gamma_\alpha = 0.07$, $\Gamma_n = 0.14$ Mev at resonance. The $\cos\theta$ term depends on the phase relation between S and P contributions, as does the left-right asymmetric term if the neutrons are polarized. We have calculated the angular distribution for polarized neutrons in terms of the unknown reaction amplitudes. Using relations provided by the results with unpolarized neutrons, we obtain limits on the asymmetric term, which may be as large as one third of the total cross section. The one-level formula shows that the effect cannot vanish at all energies and is probably greatest just off the peak, but the poor fit does not allow a detailed prediction. Preliminary measurements in Li^6 glass speck loaded emulsions give small and uncertain asymmetries.

ZA5. The P-He^3 Interaction. R. M. FRANK AND J. L. GAMMEL, *University of California.*—Phase shift analyses of elastic scattering data involving unlike particles having spin one-half are made using an IBM 701 calculator. The phase shifts (δ's) for a given l are allowed to depend upon S and J tensor coupling is omitted. In applying this to the Minnesota[1] P–He^3 data only S and P waves were included. With the δ's independent of S and J we find Lowen's[2] solution and two others, which have unreasonable energy dependences. If the δ's depend upon S and J we find three more solutions. For one of these the $^1S-\delta$ has an unreasonable energy dependence. For the others the ^3S and $^3P\delta$'s are like Lowen's. One has a $^1P-\delta$ which is zero at all energies, and a negative $^1S-\delta$ which passes through $-90°$ at 3.5 Mev. Another has a negative $^1P-\delta$ (-15 at 3.52 Mev) and a positive $^1S-\delta$ (60° at 3.5 Mev) Born's approximation predicts a solution like Lowen's except

that the triplet δ's are about 1.2 times the singlet δ's. No definite J dependence of the δ's could be established.

[1] Famularo, Brown, Holmgren, and Stratton, Phys. Rev. 93, 928(A) (1954).
[2] H. R. Lowen, Bull. Am. Phys. Soc., Vol. 29, No. 5, 15 (1954).

ZA6. Nuclear Configuration Interaction with Singlet Two-Body Forces.* CARL A. LEVINSON, *Indiana University.*—If one assumes that only two-body singlet forces act between nucleons then the effects of configuration interaction in *jj* coupling can be computed quiet simply for two-body configurations. This is done by algebraic manipulation of the Schroedinger equation rather then setting up the matrix of the Hamiltonian. The three particle configuration matrix elements can then readily be computed using the two particle matrix elements. If one is given all experimental energies for a two particle configuration, then the techniques mentioned above allow one to compute the three particle configuration energies and wave functions including configuration interaction. The nuclei Ca^{42} and Ca^{43} with $f_{7/2}^2$ and $f_{7/2}^3$ configurations are being studied. The effect of the $f_{5/2}$, $p_{3/2}$, and $p_{1/2}$ states is included. The results show that considerable configuration interaction occurs in these nuclei and gives a fairly good fit to their level spacings and the magnetic moment of Ca^{43}.

* This work was done in part while the author was a visitor at the Brookhaven National Laboratory, and was supported by a grant from the National Science Foundation.

ZA7. Alpha Decay of Spheroidal Nuclei.* R. F. CHRISTY, *California Institute of Technology.*—The calculation of the relative population of low rotational states of residual nuclei of α decay is complicated by two features. The nuclear boundary is a nonspherical surface, and the orbital angular momentum of the outgoing alpha is not constant in the nonspherical Coulomb field. A new form of the W. K. B. method has been found which is suitable for treating such problems in three dimensions. The wave function from each point on the nuclear surface can be considered as progressing radially out through the barrier and diffusing transversely in angle. The diffusion in angle, when folded with a spherical harmonic ψ, leads to the usual reduction associated with the centrifugal barrier. The wave function at large distances is found by integrating over the nuclear surface with the diffusion kernel and multiplying by the radial barrier integral (which is a function of angle). Approximate results have been found which are consistent with experiment and show large and comparable probabilities for $l=0$ and $l=2$ for $\psi=$constant on the nuclear surface. The probability for $l=4$ is then fairly small but is sensitive to deviations from $\psi=$constant and may vanish if ψ is smaller at the ends of the nucleus.

* Assisted by the joint program of the U. S. Office of Naval Research and the U. S. Atomic Energy Commission.

ZA8. Velocity-Dependent Nuclear Potential.* J. S. LEVINGER, *Louisiana State University.*—Both experiments[1] and two different calculations (phenomenological[2] and dispersion-theoretic[3]) give an integrated cross section σ_{int} for photonuclear absorption about 50 percent larger than that for the dipole sum rule. This suggests that the common nuclear potential for the independent-particle model should have an appreciable commutator with the position: for example, the nuclear potential might be velocity-dependent. (The resulting increase in σ_{int} would be a reinterpretation of that calculated phenomenologically for two-body exchange forces.) We shall present numerical results for σ_{int} for the velocity-dependent potentials of Van Vleck[4] and Brueckner,[5] and compare with experiment.

* Supported by the National Science Foundation.
[1] For example, R. Nathans and J. Halpern, Phys. Rev. 93, 437 (1954).
[2] J. S. Levinger and H. A. Bethe, Phys. Rev. 78, 115 (1950) and J. S. Levinger, Phys. Rev. 97, 122 (1955).
[3] Gell-Mann, Goldberger, and Thirring, Phys. Rev. 95, 1612 (1954).
[4] J. H. Van Vleck, Phys. Rev. 48, 367 (1935).
[5] K. A. Brueckner, Phys. Rev. 96, 508 (1954).

ZA9. Particle Motion in an Anisotropic Harmonic Oscillator Well.* MARTIN L. GURSKY, *Los Alamos Scientific Laboratory.*—A major contribution to the total nuclear energy in the collective model is due to the sum of the individual energies of the constituent nucleons in a distorted potential field.[1] As a first attempt to treat a nucleus of ellipsoidal shape it is possible to consider a potential of the form: $V=V_0\sum_{i=1}^{3}x_i^2/a_i^2$. The energy of a particle in this anisotropic oscillator well is familiar: $E(n_1,n_2,n_3;\ a_1,a_2,a_3)=(2\hbar^2V_0/m)^{\frac{1}{2}}\sum_{i=1}^{3}(n_i+\frac{1}{2})/a_i$. After introducing the volume preserving parameters α, γ, and R_0,[1] one may represent the individual particle energy defined by a particular choice of the quantum triplet (n_1,n_2,n_3) as a surface in the cylindrical space α, γ, E. Application of the Pauli principle enables one to construct a total energy surface corresponding to any arbitrary ensemble of Z protons and N neutrons. Preferred (minimum energy) shapes are seen to deviate further from the spherical as one studies nucleon numbers more remote from oscillator closed shells.

* Work done under the auspices of the Atomic Energy Commission.
[1] D. L. Hill and J. A. Wheeler, Phys. Rev. 89, 1102 (1953).

ZA10. The IPM Mass Surface.* A. E. S. GREEN AND KIUCK LEE, *The Florida State University.*—An analytic expression has been found which represents the sum of the energy eigenvalues for a spherical well rather accurately for the range of well radii, well depths, and occupancy numbers of interest in nuclear physics. Using this expression we have derived an analytical mass surface according to the independent particle model (IPM) which contains only a radius constant parameter r_0 and a well depth parameter V_0. With reasonable choices of V_0 and r_0 it is possible to account approximately for total nuclear binding energies throughout the range of mass numbers, however, it appears impossible to account for the line of beta stability. The IMP mass surface is altered appreciably if one appends a "tail" to the spherical well. These modified results and the relationship of this work to earlier investigations of the IPM mass surface as well as the Wigner mass surface will be discussed.

* Supported by a grant from the U. S. Atomic Energy Commission.

ZA11. A Modification of the One-Particle Model for Nuclear Radiative Transitions. P. R. WALLACE, *McGill University.*—The one-particle theory of isomeric transitions in nuclei is modified to account for the following anomalies: (a) that most lifetimes are longer than predicted by the one-particle model, (b) that odd-proton magnetic transitions tend to be less probable than the corresponding odd-neutron ones, despite the greater magnetic moment of the proton. In those cases where cooperative effects are minimized, and the transitions are "almost" one-particle ones, the model may be modified to take account of the small difference between the final and initial states of the *other* particles, due to the alteration of nuclear potential caused by the change of state of the nucleon *primarily* involved in the transition. The transition probability is modified by a factor $\int\phi_f^*\phi_i d_i$ for each nonparticipating particle; these factors are each slightly less than unity, but their cumulative effect is to lengthen the lifetime perceptibly. This effect will be greater for odd-proton than for odd-neutron transitions. For, because of the Coulomb force, proton transitions will affect the nuclear potential over a greater distance than will the nuclear force. Thus, odd-proton lifetimes will be lengthened more than odd-neutron ones.

ZA12. Nuclear Models. R. J. EDEN AND N. C. FRANCIS, *Indiana University.**—If it is assumed that internucleon forces are due to singular potentials of the type deduced in scattering theory it follows that the wave function of a nucleus will contain strong correlations and cannot be approximately equal to product wave functions of the type used in

nuclear models. We consider the properties of "model operators" which transform a model wave function into the actual nuclear wave function. Our method considers (1) the properties and conditions on model operators for ideal nuclear models, (2) how far these conditions are satisfied in practice, (3) approximate expressions for model operators and applications to various observables connected with atomic nuclei.

* Support by a grant from the National Science Foundation.

SUPPLEMENTARY PROGRAMME

SP1. Radiations from Y^{90}, Zr^{97}, Pr^{142}, and Pr^{143}.* B. SARAF,† J. VARMA,‡ AND C. E. MANDEVILLE,§ *Bartol Research Foundation.*—The radiations of the previously listed radionuclides have been investigated with the aid of scintillation spectrometers employing crystals of NaI(Tl). A pure sample of Y^{90}, obtained from Oak Ridge, was found to emit gamma rays in an amount of at most 10^{-6} photon per disintegration. Zr^{97} was produced at Brookhaven by slow neutrons on isotopic Zr^{96}. The gamma rays of the 17-hr $Zr^{97} \xrightarrow{\beta} Nb^{97} \xrightarrow{\beta} Mo^{97}$ are of energies 0.67, 0.75, and 1.6 Mev, the hardest quantum[1] appearing in only two percent of the disintegrations. A sample of praseodymium oxide (99.98 percent pure) was irradiated by neutrons to produce Pr^{142} which was found to decay with emission of a single gamma ray at 1.6 Mev. No gamma rays were detected in the disintegration of Pr^{143}. Any present were estimated to have an intensity of upper limit 10^{-5} photon per disintegration.

* Assisted by the joint program of the Office of Naval Research and the U. S. Atomic Energy Commission.

† Research Fellow, Bartol; on leave of absence from Agra College, Agra, India.

‡ Research Fellow, Bartol; at present at the University of Glasgow, Scotland.

§ To be given at the end of Session S if chairman rules that time permits.

[1] Previously reported at 1.42 Mev by Mandeville, Shapiro, Mandenhall, Zucker, and Conklin, J. Franklin Inst. **254**, 381 (1952).

SP2. Angular Distributions of Neutrons from (p,n) Reactions. BERNARD L. COHEN, *Oak Ridge National Laboratory.**—Angular distributions of neutrons from (p,n) reactions on Mg, Al, Cu, Mo, Ag, Ta, Au, Th, and U were measured using 23 Mev protons from the Oak Ridge National Laboratory 86-inch cyclotron incident on thick targets. Neutrons were detected by silver and aluminum threshold detectors, which give data for about 13 Mev and 6 Mev neutrons respectively. An extensive series of tests and calculations was made to assure that the method was valid and that background was properly taken into account. All angular distributions are characterized by large peaks in the forward direction. The 0°/180° intensity ratios vary from 3 to 15 for 13-Mev neutrons, and from 1.3 to 5 for 6-Mev neutrons. The Mg and Al high energy data show minima at about 25° and secondary maxima (as high as the 0° peak) at about 40°. Yield determinations indicate that the number of neutron per nuclear reaction increases with atomic number from ~0.25 for Mg and Al, to ~2.0 for heavy elements, and ~4.2 for Th and U (due to fission). Temperatures of the neutron energy distributions are estimated. All evidence indicates that direct interactions (as opposed to compound nucleus formation) is of considerable importance in these reactions.

* To be given at the end of Session X, if the Chairman rules that time permits.

Author Index to Papers Presented at the 1955 Annual Meeting

Ancker, Betsy, Thomas H. Hazlett, and Earl R. Parker—C6
Alers, P. B.—QA3
Alexis, Lucien V., Sr.—OA11
Allen, G., R. Webeler, and S. Barile—L9
Allen, L. C.—V14
Allen, R. B. and H. E. Farnsworth—Q9
Alter, B. E. K. and C. W. Curtis—C7
Ammiraju, P., M. Rinehart, K. C. Rogers, and L. M. Lederman—T9
Arnold, W. H. and J. Ballam—Z12
Arrott, A. and J. E. Goldman—Y9
Atkins, K. R.—QA10
Banet, Leo—OA12
Baker, W. F., R. E. Williams, and J. Rainwater—T7
Bakker, C. J.—U3
Baldwin, G. C.—D1
Barnes, R. G. and P. J. Bray—R7
Bashkin, S., R. R. Carlson, and E. B. Nelson—RA9
Becker, J. H.—V6
Belinfante, F. J.—OA1
Benedek, G. B., W. Paul, and H. Brooks—V11
Bennett, Willard H.—LA9
Bent, R. D., T. W. Bonner, J. H. McCrary, and R. F. Sippel—X10
Bergmann, Peter G. and Irwin Goldberg—OA4
Bernstein, J. and Abraham Klein—E6
Bethe, H. A.—P1
Betts, D. D. and J. D. Jackson—B8
Bhatia, A. B. and G. K. Horton—QA7
Biedenharn, L. C. and A. Simon—D6
Bingham, H. H., J. C. Keck, and A. V. Tollestrup—T3
Bird, George R.—H6
Bitter, F. and J. F. Waymouth—B1
Block, Martin M.—E7
Block, R. C. and H. W. Newson—HA10
Bloembergen, N.—R10
Blosser, H. G., T. H. Handley, and M. K. Hullings—X8
Blumenfeld, H., E. T. Booth, and L. M. Lederman—Z8
Bonner, T. W., R. D. Bent, and J. H. McCrary—X9
Bramson, H. J.—T1
Bray, P. J. and R. G. Barnes—R6
Brock, E. G. and J. E. Taylor—LA3
Brockhouse, B. N.—M7, M8
Brode, Harold L.—EA7
Broersma, S.—R5
Broyles, Arthur—J9
Burger, R. M., H. E. Farnsworth, and R. E. Schlier—Q11
Burkhard, E. L. and J. H. Lewis—D10
Buschert, R., I. G. Geib, and K. Lark-Horovitz—EA1
Callaway, Joseph—C1
Campbell, E. C., R. W. Peelle, F. C. Maienschein, and P. H. Stelson—MA3
Carbone, Robert J., Gerald Stone, and Edgar Everhart—B11
Carter, R. S.—HA5
Case, K. M.—TA5
Caspari, M. E.—M4
Castillo, Del, A. Snyder, L. Grodzins, and W. Y. Chang—I3
Chamberlain, Owen and John D. Garrison—L4
Chandrasekhar, S.—F1
Christensen, H.—Q7
Christy, R. F.—ZA7
Church, E. L. and A. W. Sunyar—S5
Clarke, Edward N.—Q6
Cohen, Bernard L.—SP2
— and E. Newman—X7
Cohen, V. W.—N9
Conwell, E. M.—Q4
Cook, E. J. and G. F. Pieper—D12
Cooper, Raymond D. and Dan J. Zaffarano—X13
Corbett, J. W. and W. W. Watson—J7
Cote, R. and L. M. Bollinger—HA8
Crewe, A. V.—U4
Culler, Vaughn and R. W. Waniek—A10
Cusano, D. A.—LA6
Dallaporta, N.—K3
Danforth, W. E.—Q1
Darden, S. E., A. Okazaki, and R. L. Becker—A5
Darnell, F. J. and S. A. Friedberg—Q8
Dash, W. C., R. Newman, and E. A. Taft—V7
Dehmelt, H. G.—R1
Déjardin, Georges, Joseph Janin, and Ivan Eyraud—B3
Dousmanis, G. C.—H9
Doyle, W. T. and A. B. Robbins—RA11
Dresden, M.—J8
Duncan, B. J. and L. Swern—Y10
Eaton, V. E.—P2
Eden, R. J. and N. C. Francis—ZA12
Elliot, J. O.—A3
Emmerich, W. S.—A8
Evett, A. A.—TA13
Fairbank, Henry A. and J. Wilks—W4
Farrelly, B., L. Koerts, R. van Lieshout, N. Benczer, and C. S. Wu—MA6
Faust, W. R., R. C. O'Rourke, and J. O. Elliot—A4
Feder, R. and A. S. Nowick—C8
Feld, B. T.—E4
Feuer, Paula—V13
Finkelstein, David—OA5
Finkelstein, R. J. and R. E. Behrends—E3
Fleming, P. J., J. H. Werntz, Jr. and J. R. Dillinger—W5
Foldy, L. L. and E. Eriksen—TA9
Foote, H. L., Jr., and J. Moore—HA1
Forbush, Scott E.—I5
Forrester, A. Theodore, Richard A. Gudmundsen, and Philip O. Johnson—LA8
Forstat, H. and C. A. Reynolds—W6
Forster, H. H. and A. Rosen—MA4
Fox, Raymond and R. W. Waniek—D7
Fox, R. E.—G1
Frank, R. M. and J. L. Gammel—ZA5
Fraser, J. S. and J. C. D. Milton—MA10
Fregeau, J. H. and R. Hofstadter—RA6
Freistadt, Hans—OA8
Fretter, W. B., E. W. Friesen, G. E. Kepler, and A. Lagarrigue—Z1
Friedberg, S. A. and D. L. Burk—Y8
Galonsky, A. and J. Judish—L8
George, T. H., H. E. Farnsworth, and R. E. Schlier—Q12
Gibson, John B.—C2
Gilbert, D. A. and Victor W. Cohen—VA3
Gilbert, T. L., J. M. Kelly, and H. Ekstein—Y3
Glaser, D. A.—U5
Glaser, Walter—OA7
Glaubman, Michael J.—MA7
Goldberg, Coleman and R. E. Davis—V5
Goldberg, J. N.—OA2
Goldey, James M. and Sanborn C. Brown—V3
Goldhaber, Gerson and Stephen J. Goldsack—Z6
Goldhaber, S., Gerson Goldhaber, H. H. Heckman, and F. M. Smith—Z7
Gordon, J. P.—H1
Graetzer, H. G. and E. C. Pollard—RA10
Graham, R. L., J. L. Wolfson, and M. A. Clark—MA11
Green, A. E. S. and Kiuck Lee—ZA10
Green, Milton—LA10
Greenberg, J. Mayo—TA1

Grimm, G., L. J. Rainwater, and W. W. Havens, Jr.—HA2
Gross, E. P.—TA14
Guernsey, Janet B. and A. Wattenberg—A1
Gursky, Martin L.—ZA9
Guthrie, G., S. A. Friedberg, and J. E. Goldman—QA6
Haffner, James W.—E12
Hahn, Jr., T. M., B. D. Kern, and G. K. Farney—RA2
Hamilton, D. R.—N8
Hans, H. S., Babulal Saraf, and C. E. Mandeville—MA9
Harris, E. G.—C5
Harris, G. G.—Z3
Harvey, John A.—HA7
Hayward, R. W. and D. D. Hoppes—MA2
Heberle, J., H. Reich, and P. Kusch—VA1
Heckman, Harry H., S. Goldhaber, and F. M. Smith—Z5
Heikes, R. R.—Y2
Hempstead, C. F. and L. G. Parratt—M3
Henry, Warren E. and Dieter M. Gruen—Y4
Herman, Robert and R. F. Wallis—M6
Heydenburg, N. P. and G. M. Temmer—X6
Hoffman, Joseph G., N. Metropolis, and V. Gardiner—VA12
Holladay, W. G. and R. G. Sachs—E2
Holt, N.—HA11
Hoover, C. W., Jr. and R. K. Smither—B5
Hornbostel, J. and E. O. Salant—Z4
Hughes, D. J.—HA6
Hurley, J. P., S. W. Rudman, and P. S. Jastram—S11
Inghram, M. G.—G2
Ise, John, Jr., Donald A. Hicks, and—X12
Jastram, P. S.—IA1
Jesse, William P. and John Sadauskis—B12
Jona, F., G. Shirane, and R. Pepinsky—Y11
Jones, L. W., K. R. Symon, K. M. Terwilliger, and D. W. Kerst—D3
Jossem, E. L. and L. G. Parratt—C3
Kaplan, J.—G3
Kaplon, M. F.—I8
Kay, I. and H. E. Moses—TA8
Kerner, Edward H. and Joseph G. Logan—J6
Kerst, D. W., K. M. Terwilliger, K. R. Symon, and L. W. Jones—D5
King, D. T. and M. M. Block—Z9
Kingston, R. H. and A. L. McWhorter—V1
Kittel, C.—QA8
Kivel, Bennett—VA9
Knapp, Myron W. and Wilson M. Powell—T5
Koerts, L., P. Macklin, B. Farrelly, R. van Lieshout, and C. S. Wu—MA8
Kofoed-Hansen, O.—IA2
Kohn, W.—Q3
Kolin, Alexander—VA11
Kolsky, Harwood G.—EA8
Kramer, Mary J.—M1
Krasner, Sol and J. Cuevas—B7
Krohn, V. E., T. B. Novey, and S. Raboy—S10
Krueger, G. C.—EA5, VA7
Kruse, U., H. L. Anderson, W. C. Davidon, and M. Glicksman—T8
Kursunoglu, Behram—E13
Lane, C. T., R. G. Wheeler, and C. H. Blakewood—W3
Langsdorf, A., J. E. Monahan, and F. Paul Mooring—A7
Lazar, N. H. and E. D. Klema—S3
Lebowitz, Joel and Peter G. Bergmann—J5
Lehovec, Kurt, Alma Marcus, and Kurt Schoeni—Q10
Leiss, J. E., S. Penner, and C. S. Robinson—T4
Levin, J. S. and D. J. Hughes—HA4
Levinger, J. S.—ZA8
Levinson, Carl A.—ZA6
Li, Chi Yao and A. S. Nowick—C9
Lidofsky, L., N. Benczer, P. Macklin, and C. S. Wu—S4
Little, Elizabeth A.—Y15
Lockett, Andrew M.—ZA3
Long, Donald and Park H. Miller, Jr.—V8
Lovejoy, D. R.—W2
Mackinnon, L.—QA9
Maiman, T. H. and W. E. Lamb, Jr.—VA5
Malenka, B. J.—E11
Malmberg, Philip R.—L2
Mandel, M. and A. H. Barrett—H2
Mandeville, C. E., Jagdish Varma, and Babulal Saraf—S2
Manning, Irwin and Laszlo Tisza—J4
Marder, S., W. Bennett, C. S. Wu, and V. W. Hughes—N2
Margenau, Henry—VA8
Marshak, H. and H. W. Newson—HA9
Marton, L., J. Arol Simpson, and T. F. McCraw—LA2
Matare, H. F., H. Kedesdy, A. MacDonald, and A. Petersen—Q13
Mayburg, Sumner—Q2
Mays, J. M., R. G. Shulman, and D. W. McCall—R2
McCormick, Bruce H. and Abraham Klein—E5
McGinnis, C. L.—MA5
McHale, J. L. and R. M. Thaler—TA2
McReynolds, A. W.—Y5
McWhorter, A. L.—V2
Mendlowitz, H. and L. Marton—LA1
Menon, M. G. K.—K1
Meshkov, S. and C. W. Ufford—ZA2
Metzger, Franz R.—S8
Meyerott, Roland E. and Henry Margenau—VA10
Michel, L.—IA3
Michel, L. and A. S. Wightman—TA10
Mihelich, John W. and M. Goldhaber—S1
Miller, D. W., U. C. Gupta, V. K. Rasmussen, and M. B. Sampson—RA8
Miller, J. M., G. Friedlander, and S. Markowitz—X1
Mills, R. L.—E8
Milton, J. C. D., J. S. Fraser, and G. M. Milton—MA12
Minden, Henry T.—H8
Miskel, J. A., M. L. Perlman, G. Friedlander, and J. M. Miller—X2
Mitchell, E. N.—I1
Mizushima, Masataka, J. T. Cox, and Walter Gordy—H4
Moldauer, P. A. and K. M. Case—TA6
Monahan, J. E. and A. Langsdorf, Jr.—A6
Morgan, G. W.—EA4
Morris, T. W., J. D. Garrison, and E. C. Fowler—L5
Morrison, P.—I6
Murray, R. B. and L. D. Roberts—QA2
Nathans, R. and P. F. Yergin—X3
Neuringer, L. J.—V9
Newman, Ezra and Peter G. Bergmann—OA9
Newton, Roger G. and Res Jost—TA4
Nielsen, John P.—EA3
Nilan, T. G. and W. S. Paxton—Y6
Orear, Jay—E1
O'Rourke, R. C.—TA11
Overton, William C. Jr., and Ted G. Berlincourt—QA4
Pal, Yash—K2
Peelle, Robert—RA5
Peierls, R. E.—J11
Percus, Jerome K. and George J. Yevick—J1
Peshkin, M., J. H. Roberts, and V. L. Telegdi—ZA4
Pieper, G. F., G. S. Stanford, and P. von Herrmann—RA13
Rabin, Herbert and William E. Price—D9
Raboy, S., T. B. Novey, and V. E. Krohn—S9
Redfield, Alfred G.—R4
Reich, H., J. Heberle, and P. Kusch—VA2
Rense, William A. and R. Mercure—VA6
Risser, J. R., J. Price, and C. M. Class—RA3
Ritson, D. M., A. Pevsner, and R. L. Zimmerman—L10
Roberts, L. D. and R. B. Murray—QA1
Roberts, S.—C4

Rogosa, G. L. and W. F. Peed—N1
Romer, R. H. and R. H. Dicke—H5
Rose, Basil—U2
Rose, D. J.—LA4
Ross, M.—E9
Rothstein, Jerome—EA2
Ruane, T. F., B. Waldman, and W. C. Miller—L1
Ruderman, M. A.—R9
Rubin, A., F. Ajzenberg, and J. B. Reynolds—RA14
Sáenz, A. W. and R. C. O'Rourke—J10
Salant, E. O.—K4
Salpeter, E. E.—RA4
Saraf, B., J. Varma, and C. E. Mandeville—SP1
Savedoff, Malcolm—F2
Savitt, Jacob—EA9
Scharff-Goldhaber, Gertrude and Joseph Weneser—S6
Schiller, Ralph—OA6
Schindler, Albert I.—Y1
Schwarzschild, Martin—F4
Schwertz, F. A. and J. J. Mazenko—LA5
Sciama, Dennis—F3
Sclar, N. and E. Burstein—Q5
Seeman, N., M. M. Shapiro, and B. Stiller—Z2
Segel, S. L. and B. C. Lutz—R8
Segrè, Emilio—U1
Seidl, F. G. P.—HA3
Sherr, R., R. W. Kavanagh, and W. R. Mills—RA12
Shimoda, Koichi, Tetsuji Nishakawa, and Takashi Itoh—H7
Shirane, Gen and Ray Pepinsky—Y12
Shulman, R. G., J. M. Mays, and D. W. McCall—R3
Sinclair, Rolf M.—A2
Singer, S. F.—I4
Smith, Bernard—W1
Smith, L. W., A. W. McReynolds, and G. A. Snow—L6
Smith, R. V.—LA11
Smith, R. W.—LA7
Smither, R. K. and C. W. Hoover, Jr.—B4
Snell, Arthur H. and Frances Pleasonton—N6
Snyder, A. and Del Castillo—I2
Stanford, G. S. and G. F. Pieper—D13
Steele, M. C.—QA5
Sternheimer, R. M.—E10
Stier, P. M., C. F. Barnett, R. A. Howard, and W. Bugg—B6
Stone, Gerald, Robert Carbone, and Edgar Everhart—B10
Strauch, K.—L11
Sun, K. H., P. R. Malmberg, and P. Szydlik—D11
Swann, C. P., M. A. Rothman, W. C. Porter, and C. E. Mandeville—RA1
Swartz, C. E. and J. W. DeWire—I7
Symon, Keith R.—D2
Tauber, G. E.—ZA1
Tchen, C. M.—EA6
Temmer, G. M. and N. P. Heydenburg—X5
Terwilliger, K. M., L. W. Jones, D. W. Kerst, and K. R. Symon—D4
Teutsch, W. B. and V. W. Hughes—N3
Thaler, R. M. and J. L. McHale—TA3
Thomson, Robb—M5
Tomita, K.—W9
Triebwasser, Sol and Frederic Holtzberg—Y13
Tripp, R.—L7
Tyler, W. W. and R. Newman—V4
van Lieshout, R., D. H. Greenberg, and C. S. Wu—MA1
van Lint, V. A. J., George T. Reynolds, S. B. Treiman, and F. H. Tenny—Z10
Walker, R. M., R. S. Preston, E. C. Fowler, and H. L. Kraybill—Z11
Wallace, P. R.—ZA11
Wangsness, Roald K.—Y7
Waniek, R. W., R. Fox, L. Garrido, and E. G. Silver—A9
Warschauer, D. M., W. Paul, and H. Brooks—V10
Waymouth, J. F. and F. Bitter—B2
Weber, J.—J3
Welber, Benjamin—W7
Welton, T. A.—OA3
White, F. A., T. L. Collins, and F. M. Rourke—N4
White, L. D.—VA4
Wiener, Norbert and Armand Siegel—TA7
Wigner, E. P.—P3
Wilkinson, D. H.—IA4
Willard, H. B., J. D. Kington, and J. K. Bair—RA7
Williams, Albert C. and Raymond J. Emrich—EA10
Williams, John H. and Stanley W. Rasmussen—L3
Williams, Quitman and T. L. Weatherly—H3
Williams, Ross, Winslow Baker, Aihud Pevsner, and James Rainwater—T6
Witmer, Enos E.—N7
Wolff, G., L. Toman, and J. Clark—Q14
Wolke, R. L.—X11
Wood, G. T. and P. S. Jastram—S12
Woodcock, R. F. and H. E. Farnsworth—C10
Yagoda, Herman—T2
Yergin, P. F. and R. Nathans—X4
Yevick, George J. and Jerome K. Percus—J2
Yilmaz, Huseyin—TA12
Yntema, G. B.—W8
Youngblood, J. F.—Y14
Zimmerman, E. J.—D8
Zimmerman, R. L. and H. Palevsky—HA12
Zobel, W. and R. M. Steffen—S7
Zucker, A., H. L. Reynolds, and L. D. Wyly—B9
Zweifel, P. F.—N5

MINUTES OF THE SPRING MEETING OF THE NEW ENGLAND SECTION AT BROWN UNIVERSITY, PROVIDENCE, RHODE ISLAND, ON APRIL 2, 1955

THE New England Section of the American Physical Society held its annual Spring Meeting on Saturday, April 2, at Brown University, Providence, Rhode Island. Four invited papers were heard at the morning session: "Nuclear Reaction Studies with a Small Accelerator," Russell A. Peck, Jr., Brown University. "Acoustics Research in the Physics Department of Brown University," Robert T. Beyer, Brown University. "Some Recent Experiments in Surface Physics at Brown University," H. E. Farnsworth, Brown University. "The Yale Neutron Velocity Selector System," Howard L. Schultz, Yale University.

Following a luncheon at the Refectory, the laboratories of the Physics Department were open for inspection. At the afternoon session, in Wilson Hall, ten contributed papers were presented.

W. M. Preston, *Secretary-Treasurer*
New England Section
Harvard University
Cambridge, Massachusetts

1. Neutron Cross Sections for Zirconium. JANET B. GUERNSEY, *M. I. T. and Wellsley College.*—The total neutron cross section for natural zirconium has been measured for neutrons with energies between 700 and 1200 kev, using a hydrogen recoil counter in a good geometry transmission experiment. The inelastic cross section for the excitation of the 930-kev level in zirconium has been measured as a function of neutron energy from its onset at about 950 kev to 2.2 Mev. The de-excitation gamma radiation has been observed with a single-crystal NaI(Tl) spectrometer. The cross section for the production of these gamma rays in the natural element is about 0.8 barn at 1.5 Mev. Isotopic assignment is still uncertain. Some correlation between inelastic and elastic cross sections has been observed.

2. Background Tracks in Nuclear Emulsions. S. YAMAMOTO AND F. E. STEIGERT, *Yale University.*—A series of 50-μ Ilford C-2 emulsions were exposed to a flux of neutrons from the $Be^9(d,n)$ reactions, moderated by 30 cm of paraffin both with and without cadmium shielding. Control plates were similarly exposed in the absence of the neutron flux. Two types of spectra were observed. The first, present on all plates, was apparently the result of a natural contamination of radio nuclides in the emulsions. Much of this data is immediately explained by the expected thorium series alpha emitters. The second group appeared to be the result of thermal neutron induced reactions. Some evidence was found for neutron capture by Th-232 leading to U-233 and thereby to alpha emitters of the neptunium series. The reaction $N^{14}(n,p)C^{14}$ was also observed.[1] All groups have not as yet been identified.

[1] Yagoda, *Radioactive Measurements with Nuclear Emulsions* (John Wiley and Sons, Inc., New York, 1949).

3. Calibration of Linear Amplifiers with a Mercury Relay Pulse Generator. J. K. MAJOR, *Yale University.*—A simple circuit to simulate pulses from proportional counters and other detectors has been developed for calibrating linear amplifiers, pulse amplitude analyzers, and other equipment. A mercury contact relay is used to charge a capacitor from a calibrated dc source and to discharge it through a pulse-forming network with the desired rise and decay times[1–3] into a characteristic impedance of 100 ohms; no vacuum tubes are used. Positive or negative output pulses are continuously variable in amplitude up to 10 v, using a 10-turn helical potentiometer of 0.1 percent linearity and precision attenuators, with rise times from $<7m\mu s$ to 10 μs and exponential decay times from 1 to 100 μs. A single pulse repetition frequency of 60 cps is used, not only because circuitry is simplified but also because higher rates are precluded by the capacitor charging time and the mechanical design of the relay, while performance of the relay may be unstable at lower rates.[2,3] The pulse generator is small, simple, stable, and reliable, and pulse amplitudes are believed accurate to several percent.

[1] R. L. Garwin, Rev. Sci. Instr. **21**, 903–904 (1950).
[2] O. L. Stone, LA-1330 (1953).
[3] C. E. Harper, ISC-455 (1954).

4. The Absorption of 10-Mc/sec Sound in a Polycrystalline Magnesium Rod between 1.5 and 4.2°K.* L. MACKINNON,† *Brown University.*—By a method previously described,[1] the relative absorption of 10-Mc/sec sound has been studied in magnesium over the temperature range 1.5–4.2°K and compared with the absorption at liquid nitrogen temperatures. The absorption has been found to be considerably greater in the liquid helium temperature range than at the liquid nitrogen boiling point, but to decrease steadily as the temperature is lowered from 4.2 to 1.5°K. This result is consistent with theoretical predictions[2–4] that absorption and electrical conductivity are mutually proportional (since the liquid helium range is below the resistance minimum usually associated with magnesium), but the nature of the observations can lead to no more than a qualitative comparison between theory and experiment.

* Supported by the Office of Naval Research.
† On leave of absence from Charterhouse, Godalming, Surrey, England.
[1] L. Mackinnon, Bull. Am. Phys. Soc. **30**, No. 1, 42 (1955).
[2] W. P. Mason, Phys. Rev. **97**, 557 (1955).
[3] C. Kittel, Bull. Am. Phys. Soc. **30**, No. 1, 42 (1955).
[4] R. W. Morse (to be published).

5. Small-Angle X-Ray Scattering by the System Iso-Octane-*n*-Heptforane.* T. E. BRACKETT, R. D. DUNLAP, AND J. BISCOE, *University of Maine.*—Curves of small-angle scattering have been obtained for mixtures of iso-octane and *n*-heptforane (C_7F_{16}) with compositions ranging from zero to 100 percent of each component. Samples containing 100 percent of either component show little if any small-angle scattering. With the addition of the second component, the small-angle scattering increases in intensity to a maximum of about 50 mole percent. The experiments were made at temperatures slightly above the unmixing temperature of 22°C. When Guinier plots of the data are made, straight lines do not result, but from the measurement of the slopes at various points on the curves, radii of 5 to 20 A are obtained.

* This research supported by University of Maine Coe Fund and Division of Industrial Cooperation.

6. Computed Transition Probabilities for the X-Ray *K*-edge of Potassium.* MARGARET N. LEWIS,† LOUIS C. GREEN, MARJORIE M. MULDER,‡ AND PAUL C. MILLER,§ *Haverford College,* AND ELEANOR K. KOLCHIN, *Columbia University.*—

The rate of change of the oscillator strength at the K-edge of ionized potassium has been computed in a number of ways. Both hydrogenic and Hartree wave functions have been used in the single electron approximation, and Hartree and Hartree-Fock wave functions in the many electron case. Calcium wave functions both with and without exchange have also been employed. The moment, momentum, and acceleration matrix elements have been computed. The momentum matrix element gives values most closely in agreement with experiment and is most stable with respect to changes in the wave functions. It is followed by the acceleration and the moment in that order. The single electron approximation gives good results. If the single-electron approximation is not used, it is essential that exchange effects be included by employing the determinant form of the wave functions, and the Hartree-Fock one-electron wave functions then give considerably better results than the ordinary Hartree functions. It also proves to be possible to substitute the wave functions of the unexcited ion of next higher atomic number, calcium, for the wave functions of potassium excited in an x-ray level without noticeable deterioration in the results.

* This research was supported in part by a grant from the National Science Foundation, in part by the U. S. Air Force under a contract monitored by the Office of Scientific Research, Air Research and Development Command.
† Now at Brown University, Providence, Rhode Island.
‡ Now with Remington Rand, Inc., Philadelphia, Pennsylvania.
§ Now at Princeton University, Princeton, New Jersey.

7. The Open Screen Technique in Electron Microscopy.* GEORGE A. FARRALL AND CHARLES R. MINGINS, *Tufts University.*—The open screen technique is a method by which a given submicroscopic area of a solid surface can be viewed with successive replicas. Standard procedure for making and dry-stripping replicas is followed with a few changes. Instead of a standard screen, a Lektromesh screen with a hole 40/1000 inch in diameter in its center is used. This hole can be easily centered with the eye over a selected surface area. It is common practice to scribe an "X" on the specimen surface to supply reference axes under the microscope. Because of the hole, a small paper disk must be used between the Scotch tape and the screen to prevent the film and tape from adhering. Since the film is spread over a much greater nonsupporting area than usual, thicker films must be used. This obviously places limitations on the applications of the technique. The method, however, has been developed to study granular distortion in barium titanate ceramic due to heating and electrostriction, and seems to be well adapted to this purpose. No special equipment other than a punch for the screens is required, and the process calls for approximately the same amount of time as the standard replication procedure.

* Sponsored by the Office of Ordnance Research, U. S. Army.

8. The Raman and Fluorescence Spectra of Allyl Diglycol Carbonate.* MYRON A. JEPPESEN, *Bowdoin College.*—The Raman and the fluorescence spectra of allyl diglycol carbonate (CR-39) have been photographed in the visible region. The spectra of the monomer (liquid) and of the polymer (solid) are compared. When the sample is irradiated by unfiltered light from a mercury arc, a continuous fluorescence spectrum appears in the region from 4200 A to 5000 A. This spectrum is particularly intense in the scattered light from the polymer. A filter which cuts out from the incident light wavelengths below 4300 A eliminates the fluorescence and thus permits the Raman spectrum to be observed. Probable assignments of some lines in the spectra to vibrational modes of the molecules are made. Almost, complete polymerization of the aliphatic double bonds is indicated by the spectrum of the polymer.

* Supported by the National Science Foundation.

9. Fundamental Research in the United States. J. L. B. BLIZARD, *New England Institute for Medical Research.*—With the largest educated population in the world, the United States ranks third in the number of Nobel Prize winners in physics, second in chemistry, and first in physiology. Recent trends in American high school science enrollment should be considered. From 1890 to 1950, enrollment in physics dropped from 23 percent to 4 percent, in chemistry from 10 percent to 7.5 percent, and in biology rose from 7 percent to 20 percent.[1] If the three countries leading in Nobel Prize winners are compared (Germany, England, and the United States), it is seen that, with 56 percent of the populations of the 3 combined countries, and with 91 percent of the college educated population,[2] the United States has contributed only 35 percent of the Nobel Prize winners in science.[3] Only 28 percent of the physics Nobel Prize winners of the three countries are residents of the United States. The activity of worldwide and American research in physics, chemistry, and biology is compared on the basis of publications, manpower, and Nobel Prize winners.

[1] Phys. Today **8**, No. 3, p. 12 (March, 1955).
[2] Statistical Yearbook of the United Nations, New York, 1952.
[3] World Almanac, 1955.

10. Origins of Papers Presented at Regular Meetings of the American Physical, Acoustical, and Optical Societies in 1954. J. A. DILLON, JR., *Brown University,* AND M. L. DILLON.—The major contributors are listed according to the total numbers of papers presented at the meetings of the three societies, and the results are compared with those of previous years. The distribution of papers according to regions is discussed, and the number of papers listing government support is indicated.

CONTENTS—Continued

... Oxygen ... Lewis ... and Stephen J. Smith 1127

... Their Use in Perturba-
... and J. David Jackson 1128

... Concepts Regarding Avogadro ...
... E. ... and J. W. M. DuMond 1128

... Single Crystal of Fe_3O_4 ... Kenzō Suzuki 1130

... E. N. Adams 1130

... High Mobility Holes in Germanium ... Drift Mobility Technique ...
... N. J. Harrick 1131

... Electroluminescent Brightness ... -Imbedded Phosphors ...
... F. A. Schwertz, ... and E. R. Michalik 1133

... Electroluminescent Brightness ... Chemically Deposited Phosphor
... Schwertz and R. E. Freund 1134

... the Mechanics of Self-Diffusion in ... Sumner Mayburg 1134

... of Color Centers ... A. Halperin and A. Braner 1135

... of Low Temperatures and the Dissociation of the Limiting Shearing
... W. P. Mason 1136

... Fluid Upon the Rate of Transfer Through a Helium II Film ...
... J. W. Beams 1138

... Physical Society:

... of the Division of Fluid Dynamics Held at Old Point Comfort and
... Aerodynamical Laboratory, Virginia, November 22–24, 1954 ... 1139

... Annual Meeting Held at New York City, January 27–29, 1955 (Corre-
... *Bulletin of the American Physical Society*, Volume 30, No. 1) ... 1144

... Meeting of the New England Section at Brown University, Providence,
... on April 2, 1955 ... 1210

... Indexes for 1893–1920 and 1921–1950 are available.
... front cover for prices. Orders should be sent to the
... Institute of Physics, 57 East 55th Street, New York 22,

Contents

Some Corrections Required . . . . . Second Series

Comparison of the Boiling Temperatures in Liquid He[3] and
Stability of a Plane Boundary Inside a Superconductor
Spatial Distribution of Atoms in Liquid He[3]
Results of Limitations on Space Current Densities in Ga
Quantum Effects in the Interaction between Electrons a
Rosenfeld's Red-Shift Formula
Entropy of Radiation
Velocity Analysis of Thermionic Emission from Single-C
Density of States Curve for Nickel
Dielectric, X-Ray, and Optical Study of Ferroelectric Cd
Model for Luminescence and Photoconductivity in the
Theory of Donor States in Silicon
Electron Capture Probability of the Upper Copper Acce

Ferromagnetic Resonance in Ferrosilicon
Magnetic Resonance for Arbitrary Field Strengths
Change in KCl Lattice by Soft X-Rays
Magnetic Susceptibility of Rubidium and Manganese
Paramagnetism Observed at the Superconducting Transi
Seebeck Effect in Silicon
Plasma Oscillations in Metals
Low-Temperature Luminescence and Absorption of CdS
Oscillatory Hall Effect, Magnetoresistance, and Magnet

Hall Mobility of Optically Excited Carriers in Germaniu
Infrared Absorption of Indium Antimonide
Temperature Variation of the Elastic Constants of Cubic

Dynamic Behavior of Domain Walls in Barium Titanate
Recombination Processes in Cadmium Sulfide
Interpolation Scheme for Energy Bands in Solids
Response of Anthracene and Stilbene to Low-Energy Pro
Specific Directions of Longitudinal Wave Propagation in
Electrical Resistance of Copper-Gold Alloys at Low Tem
Dielectric Behavior of Barium Titanate in the Paraelectric

Magnetic Properties of Zinc Sulfide and Cadmium Sulfid
Computed Transition Probabilities for X-Ray Continua an
Margaret N. Lewis, Louis C. Green, Marjorie M. Muller
Experimental Cross Section for Photodetachment of Electrons

Zeeman Effect in the Rotational Spectrum of NO
One-Electron Energies of Atoms, Molecules, and Solids
Differential Cross-Section Measurements for Large-Angle
Argon Atoms at Energies to 100 kev
Energies of the Ground States of He, Li+, and O++
Electron Broadening and Shift of Spectral Lines of Helium
X-Ray-Induced Luminescence from Air
Temperature Susceptibilities of the Sensitized Fluorescence

Helium Wave Equation
High-Frequency Ionization Coefficients in Neon-Argon
Nuclear Spin Relaxation in Alkali Metals
Molecular Constants and Nuclear-Molecular Interactions
nance Method
Matrix Treatment of Nuclear Induction
Nuclear Induction in Inhomogeneous Fields
Energy Loss by 5.85-Mev Deuterons and 4.45-Mev Pro
Special-Relativistic Derivation of Generally Covariant
Relativistic Cosmology. I

(continued on cover)